NUCLEAR PHYSICS

JOURNAL DEVOTED TO THE EXPERIMENTAL AND THEORETICAL STUDY OF THE FUNDAMENTAL CONSTITUENTS OF MATTER AND THEIR INTERACTIONS

EDITOR: L. ROSENFELD - COPENHAGEN
ASSOCIATE EDITOR: O. NATHAN - COPENHAGEN

VOLUME XXV

NORTH-HOLLAND PUBLISHING COMPANY - AMSTERDAM

NUCLEAR PHYSICS

EDITORIAL BOARD

AUSTRALIA & NEW ZEALAND:	H. Messel (Sydney), M. L. Oliphant (Canberra)
AUSTRIA:	B. Karlik (Vienna), H. Thirring (Vienna)
BELGIUM:	M. de Hemptinne (Louvain), J. Verhaeghe (Ghent)
CANADA:	G. Volkoff (Vancouver)
DENMARK:	C. Møller (Copenhagen), S. Rozental (Copenhagen), G. E. Brown (Copenhagen)
FINLAND:	L. Simons (Helsinki)
FRANCE:	A. Berthelot (Saclay), S. Gorodetzky (Strasbourg)
GERMANY (DEM. REP.):	G. Hertz (Leipzig)
GERMANY (FED. REP.):	W. Gentner (Freiburg i. B.), J. H. D. Jensen (Heidelberg)
GREAT BRITAIN:	W. E. Burcham (Birmingham), T. H. R. Skyrme (Harwell)
HUNGARY:	L. Janossy (Budapest)
INDIA:	H. Bhabha (Bombay), R. Ramanna (Trombay)
IRISH REPUBLIC:	J. McConnell (Maynooth)
ISRAEL:	G. Racah (Jerusalem)
ITALY:	E. Amaldi (Rome)
JAPAN:	S. Kikuchi (Tokai), S. Tomonaga (Tokyo)
MEXICO:	M. Moshinsky (Mexico)
NETHERLANDS:	H. Brinkman (Groningen), S. R. de Groot (Leiden)
NORWAY:	E. Hylleraas (Oslo), A. Lundby (Oslo), H. Wergeland (Trondheim)
POLAND:	L. Infeld (Warsaw), J. Werle (Warsaw)
PORTUGAL:	J. M. Araújo (Porto), J. R. de Almeida Santos (Coimbra)
SOUTH AMERICA:	G. Beck (Saõ Paulo), J. Leite Lopes (Rio de Janeiro)
SPAIN:	J. M. Otero (Madrid), C. Sanchez del Rio (Madrid)
SWEDEN:	O. Klein (Stockholm), K. Siegbahn (Uppsala), I. Waller (Uppsala)
SWITZERLAND:	P. Huber (Basel), P. Scherrer (Zürich)
U.A.R. & ARAB COUNTRIES:	F. El Bedewi (Cairo), M. G. Nooh (Cairo)
U.S.A.:	H. H. Barschall (Madison, Wisconsin), S. Devons (New York), V. F. Weisskopf (Cambridge, Mass.)
U.S.S.R.:	M. A. Markov (Moscow), I. S. Shapiro (Moscow), D. V. Skobeltzyn (Moscow)
YUGOSLAVIA:	I. Supek (Zagreb)

NUCLEAR PHYSICS

JOURNAL DEVOTED TO THE EXPERIMENTAL AND THEORETICAL STUDY OF THE FUNDAMENTAL CONSTITUENTS OF MATTER AND THEIR INTERACTIONS

EDITOR: L. ROSENFELD - COPENHAGEN

VOLUME XXV

MAY 1961 — JUNE 1961

NORTH-HOLLAND PUBLISHING COMPANY - AMSTERDAM

PRINTED IN THE NETHERLANDS

1.E.3:
6.D

Nuclear Physics **25** (1961) 1—135; © *North-Holland Publishing Co., Amsterdam*
Not to be reproduced by photoprint or microfilm without written permission from the publisher

SEMIEMPIRICAL ATOMIC MASS LAW

PHILIP A. SEEGER

California Institute of Technology, Pasadena, California

and

Los Alamos Scientific Laboratory, University of California, Los Alamos, New Mexico †

Received 30 January 1961

Abstract: New terms are proposed for the atomic mass law which incorporate effects of nuclear deformation and shell structure including interference effects between unfilled neutron and proton shells. In addition, a surface-symmetry term is included. Coulomb terms are fixed by recent radii determinations in electron scattering. The standard deviation of calculated masses is reduced by the addition of the new terms as is the error in extrapolating from one side of the valley of beta stability to the other. The usefulness of the law for calculating the mass and binding energy of atoms with large neutron excess is discussed. A table giving mass excess, neutron, proton and alpha-particle binding energies, and beta decay transition energies is appended.

1. Introduction

An improved expression for atomic masses as a function of position in the NZ-plane has been sought for the purpose of studying in detail the process of nucleosynthesis by rapid neutron capture [1, 2]). For this purpose, it must be possible to extrapolate the mass law to atoms with high neutron excess, but there exists no means of directly testing the law in this region of the NZ-plane. Criteria for testing the law in the valley of beta stability are listed in sect. 2.

The familiar Weizsäcker semiemperical mass law [3, 4]) consists of terms whose forms follow from the statistical model of the nucleus, each multiplied by a coefficient to be determined empirically. The mass excess of the atom with Z protons and N neutrons was taken to be

$$\Delta M_{\mathrm{W}}(Z, A) = NM_{\mathrm{n}}+ZM_{\mathrm{H}}-A-\alpha A+\beta I^2/A+\gamma A^{\frac{2}{3}}+(3e^2/5R_0)Z^2/A^{\frac{1}{3}}, \quad (1)$$

where M_{n} and M_{H} are the neutron and hydrogen atom masses, $A = N+Z$, and $I = N-Z$. Modifications of this original form will be discussed in sects. 3 and 4.

The free coefficients, such as α, β, and γ in eq. (1) and similar quantities appearing in modified forms of the mass law, are found from least squares analysis by fitting either to the mass excess M–A or to the packing fraction $(M$–$A)/A$. Fitting to the packing fraction is equivalent to using a weighting factor of $1/A^2$ in the mass excess, and since A varies over a wide range, the results here reported were determined by fitting to the mass excess. In many

† Work supported in part by the joint program of the Office of Naval Research and the U. S. Atomic Energy Commission.

past treatments of the problem, a limited number of masses for the atoms nearest the line of beta stability have been used. In this study, however, all available odd mass atoms were used, all data being weighted inversely as the first power of the estimated error. The principal source was the table of Everling *et al.* [5]); masses omitted from that table but estimated in the earlier work of Huizenga [6]) were corrected to the later value of Pb^{208} by addition of 1.123 mMU and used with the quoted errors doubled. Thus a total of 488 odd-mass atoms with $A \geqq 19$ were used to determine a mass law for odd-mass atoms. The calculation of atomic masses for even mass nuclei from the law is discussed in sect. 5. All computations were made on an IBM 704 at Los Alamos Scientific Laboratory.

2. Criteria for Testing of Mass Laws

Three criteria for testing the mass laws have been considered. First, the errors δ_i of the masses calculated by the law compared to the input data were plotted, and the standard deviation calculated by

$$\sigma = \left(\frac{n}{n-k}\right)^{\frac{1}{2}} \left(\frac{\sum w_i \delta_i^2}{\sum w_i}\right)^{\frac{1}{2}}, \tag{2}$$

where n is the number of input masses, k the number of free coefficients, and w_i the weight of the input datum. This is a measure of the ability of the law to fit known masses; it is to be made as small as possible. A standard deviation $\sigma \lesssim 1\ \mathrm{MeV}/c^2 \approx 1$ mMU is considered to be satisfactory.

As another test, called the "interpolation" test, the 488 odd-mass atoms were divided at random into two groups. This was done by ascertaining whether the last bit in the binary expression for the mass excess was even or odd. The first group, consisting of 232 masses, was used to determine the coefficients of a mass law of the same form as the law in question, and then that law was used to "predict" the masses of the 256 atoms in the second group. The standard deviation σ_1 of the first group was calculated by eq. (2), and that of the second group by

$$\sigma_2 = \left(\frac{\sum w_i \delta_i^2}{\sum w_i}\right)^{\frac{1}{2}}. \tag{3}$$

The ratio $(\sigma_2/\sigma_1)_{\mathrm{int}}$ is taken as a measure of the ability of the particular form of mass law to interpolate; σ_1 should be approximately the same as σ, and the ratio $(\sigma_2/\sigma_1)_{\mathrm{int}}$ should be less than, say, 1.05.

For our purposes the most significant criterion was a third test called the "extrapolation" test. The 488 odd mass atoms were again divided into two groups: the first containing those atoms on the line of beta stability plus those on the neutron poor side of the valley of beta stability, the second containing atoms only from the neutron rich side of beta stability. The first group had 282

atoms and the second had 206. The standard deviations σ_1 and σ_2 and the ratio $(\sigma_2/\sigma_1)_{\text{ext}}$ were calculated as in the interpolation test. Once again σ_1 should be similar to σ, and the ratio $(\sigma_2/\sigma_1)_{\text{ext}}$ should be close to unity. It is difficult to estimate an acceptable value for this ratio, but we might hope to make $(\sigma_2/\sigma_1)^2_{\text{ext}} \lesssim 2$ or $(\sigma_2/\sigma_1)^2_{\text{ext}} \lesssim 1.4$.

3. Standard Form of the Mass Law

For our "standard" form of the mass law, the symmetry term was modified to include $|I|$ as well as I^2 as suggested by Wigner [7, 8]) and the coefficient β was modified to include composition dependence of the surface effects [9]). The factor 2 in $2|I|$ was suggested by E. E. Salpeter [10]). Following Mozer [11]), the Coulomb term was modified to trapezoidal charge distribution and exchange effects. The coefficients $3e^2/5R_0 = 0.8076$ MeV/c^2 and $\frac{7}{24}(t/R_0)^2 = 2.29$ were determined using $R_0 = 1.07$ fm, $t = 2.8$ fm from scattering experiments with high energy electrons [12]). Then in MeV/c^2 on the O^{16} scale the mass excess becomes

$$\Delta M_{\text{stan}}(Z, A) = 8.3674N + 7.5848Z - \alpha A + \left(\beta - \frac{n}{A^{\frac{1}{3}}}\right)\left(\frac{I^2 + 2|I|}{A}\right) + \gamma A^{\frac{2}{3}} + 0.8076\,\frac{Z^2}{A^{\frac{1}{3}}}\left(1 - \frac{0.7636}{Z^{\frac{2}{3}}} - \frac{2.29}{A^{\frac{2}{3}}}\right). \tag{4}$$

The coefficients as determined by least squares are

$$\begin{aligned} \alpha &= 16.11 \text{ MeV}/c^2, & \gamma &= 20.21 \text{ MeV}/c^2, \\ \beta &= 20.65 \text{ MeV}/c^2, & \eta &= 48.00 \text{ MeV}/c^2. \end{aligned} \tag{4a}$$

The errors in the calculated mass excesses are shown in fig. 1, and the three evaluation tests yield

Standard deviation: $\sigma = 2.61$ MeV/c^2;
Interpolation: $\sigma_1 = 2.87$ MeV/c^2, $(\sigma_2/\sigma_1)_{\text{int}} = 0.84$;
Extrapolation: $\sigma_1 = 2.19$ MeV/c^2, $(\sigma_2/\sigma_1)_{\text{ext}} = 1.75$.

It will be noted that the standard form fails in the two most crucial tests: the standard deviation σ and the extrapolation ratio $(\sigma_2/\sigma_1)_{\text{ext}}$ are too large.

4. Additional Terms in the Mass Law

In the attempt to find a mass law which would extrapolate more successfully than the standard form (4), a function $S(N, Z)$, representing the increase in nuclear binding energy both at closed shells due to magic numbers of N or Z and between closed shells due to the deformation of the nucleus, was subtracted from ΔM_{stan} to give ΔM_0, the mass excess for odd-mass atoms. Thus $\Delta M_0 = \Delta M_{\text{stan}} - S(N, Z)$. We may now write

$$S(N, Z) = k_s C_0 + k_d(C_1\eta - C_2\eta^2), \tag{5}$$

where k_s and k_d are shell and deformation coefficients which may vary from shell to shell, $C_0(N, Z)$ is the functional representation of the excess binding energy due to shell effects, and the extra energy due to deformation is approxi-

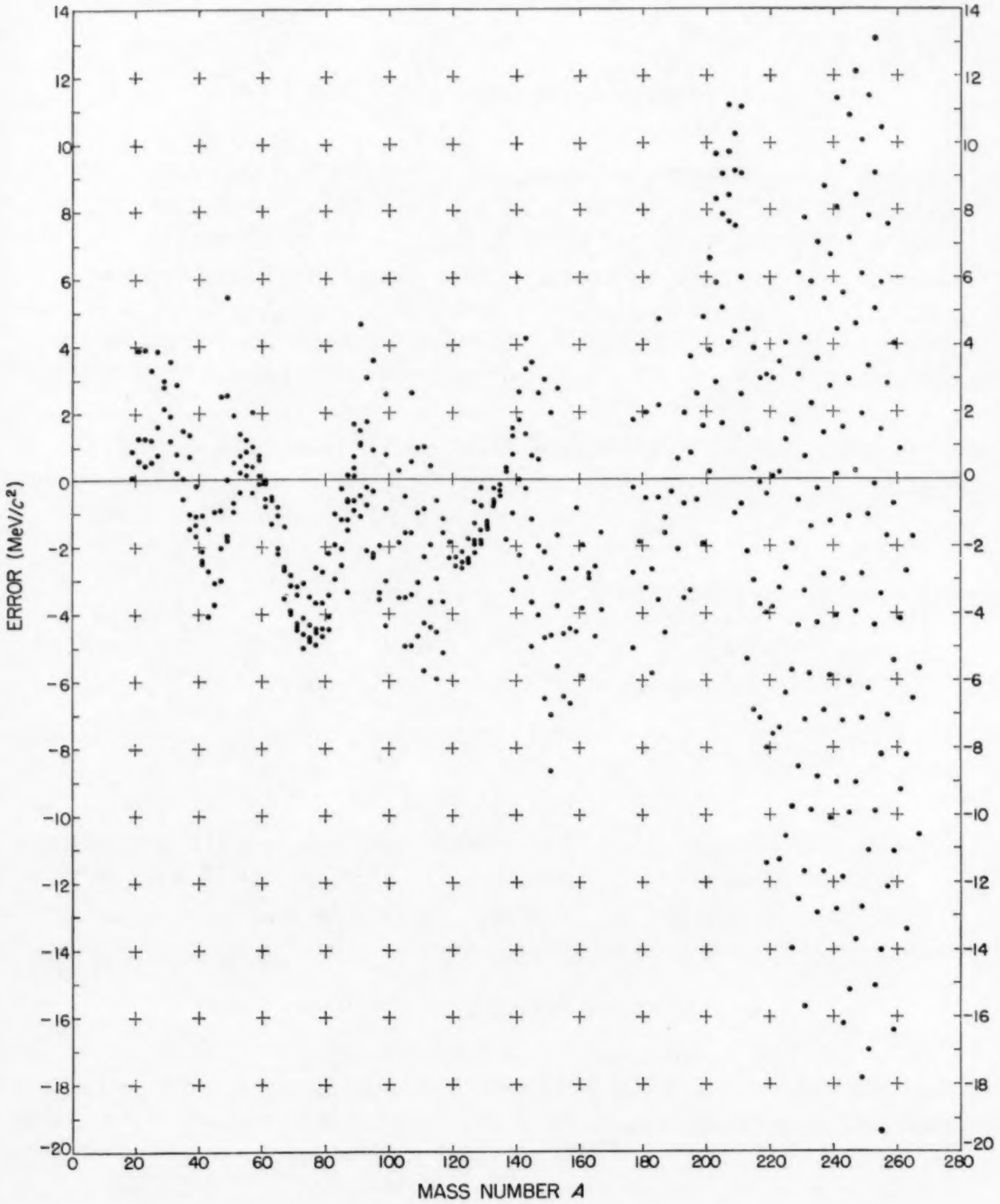

Fig. 1. Errors δ_i of 488 atomic mass excesses for odd-mass atoms calculated by the standard mass law (4) with coefficients (4a), plotted versus atomic mass number A. Note the large systematic shell effects.

mated by $C_1\eta - C_2\eta^2$. In this last expression $\eta = \Delta R/\bar{R}$ is the spheroidal eccentricity, $C_1\eta$ is the excess nuclear binding energy due to deformation and $C_2\eta^2$ is the change in Coulomb and surface energies in deforming a uniformly charged sphere into a spheroid. By the usual argument that the nucleus takes that deformation η_0 such that the deformation energy is a maximum,

$$\frac{\mathrm{d}}{\mathrm{d}\eta}\,(C_1\eta - C_2\eta^2)\,\Big|_0 = C_1 - 2C_2\eta_0 = 0,$$

$$\eta_0 = \frac{C_1}{2C_2}, \quad C_1\eta_0 - C_2\eta_0^2 = \frac{C_1^2}{4C_2}.$$

The coefficient C_2 can be expressed as [13])

$$C_2 \approx 8A^{\frac{2}{3}}\left(1 - 0.005\,\frac{Z^2}{A}\right) \qquad \mathrm{MeV}/c^2.$$

In this study, C_2 has been considered constant over the range of A included within any one shell of N or Z.

The function $C_1\eta$ can be calculated as a sum over all nucleons outside a closed shell. Each such nucleon is in a spheroidal rather than spherical potential, and the excess binding energy can be calculated by the methods of Rainwater [14]) or Nilsson [15]). It is to be expected that C_1 is zero at a nucleus for which both Z and N are magic, and has a maximum near the middle of each shell of Z or N. This behaviour makes it possible to approximate C_1 with sine functions.

The term C_0 must be a maximum at closed shells and reach a minimum near the middle of the shell. It has therefore been assumed that $C_0 = K - C_1$, where K is a constant.

With these assumptions, (5) becomes

$$S = k_s K - k_s C_1 + k_d C_1^2/4C_2, \tag{6}$$

where $k_s K$, k_s and $k_d/4C_2$ are constants within any given shell. For the nucleus with N neutrons and Z protons, let N' and Z' be the fractional occupations of the last shells,

$$N' = \frac{N - N_j}{N_{j+1} - N_j}, \qquad Z' = \frac{Z - Z_k}{Z_{k+1} - Z_k}, \tag{7}$$

where the magic closed shell numbers are

$$N_j,\, Z_k = 8,\, 20,\, 50,\, 82,\, 126,\, 184,$$

and

$$N_j \leqq N < N_{j+1}, \qquad Z_k \leqq Z < Z_{k+1}.$$

Consider eq. (6) if C_1 is expanded in a Fourier sine series,

$$C_1 = A_1 \sin N'\pi + A_2 \sin 2N'\pi + \ldots + B_1 \sin Z'\pi + B_2 \sin 2Z'\pi + \ldots .$$

Since the square of the sine has the same qualitative properties as the sine itself, that is, goes to zero at magic numbers and has its maximum halfway in between, such terms in C_1^2 add nothing essentially new to our approximation for S which is not already included in the linear terms in C_1. The cross-products in C_1^2, such as $(\sin N'\pi)(\sin Z'\pi)$, are unlike any terms in C_1 itself, and must be included in S. Previous attempts [11, 16–18]) to include shell structure have used $S = f(N)+g(Z)$, which neglects cross product terms. We feel it is essential to include these terms in order to have some representation of the effects of the proton shell structure on the neutron shell structure and vice versa. Thus, the final approximate form adopted for S was

$$S_{jk}(N', Z') = \zeta_j \sin N'\pi+\zeta_k \sin Z'\pi+\nu_j \sin 2N'\pi \\ +\nu_k \sin 2Z'\pi+(\phi_j+\phi_k)(\sin N'\pi)(\sin Z'\pi)+\chi, \qquad (8)$$

where indices j and k refer to the shells of N and Z respectively, and the ζ_i, ν_i, ϕ_i, and χ are constants approximately related to the constants in eq. (6). Note that S_{jk} is symmetric in N and Z, so that it is charge independent. Also note that the constant term χ does not vary from shell to shell, in order to make S_{jk} a continuous function. Then the mass law for odd mass atoms is

$$\Delta M_0(Z, A) = \Delta M_{\text{stan}}(Z, A)-S_{jk}(N', Z'). \qquad (9)$$

The coefficients α, β, γ and η as determined by least squares are, in MeV/c^2,

$$\alpha = 17.06, \quad \beta = 33.61, \quad \gamma = 25.00, \quad \eta = 59.54. \qquad (9a)$$

The coefficients ζ, ν, ϕ and χ as determined by least squares are given in table 1.

TABLE 1

The coefficients ς, ν, ϕ and χ (in MeV/c^2)

≦ Z or N <	ς	ν	ϕ	χ
8, 20	4.008	−0.428	−1.389	13.51
20, 50	− 0.508	2.331	−0.463	13.51
50, 82	− 7.636	0.496	1.950	13.51
82, 126	−15.63	−2.284	10.67	13.51
126, 184	−27.59	2.660	26.99	13.51

A representation of the function S_{jk} versus N and Z is given in fig. 2. Fig. 3 is a plot of the error of the calculated mass excess versus A. The three evaluation tests give

Standard deviation: $\sigma = 0.75$ MeV/c^2;
Interpolation: $\sigma_1 = 0.83$ MeV/c^2, $(\sigma_2/\sigma_1)_{\text{int}} = 1.01$;
Extrapolation: $\sigma_1 = 0.96$ MeV/c^2, $(\sigma_2/\sigma_1)_{\text{ext}} = 1.35$.

Note that the standard deviation is reduced to less than a third of the previous value, and that the ratio $(\sigma_2/\sigma_1)_{\text{ext}}$ is substantially reduced from that for the

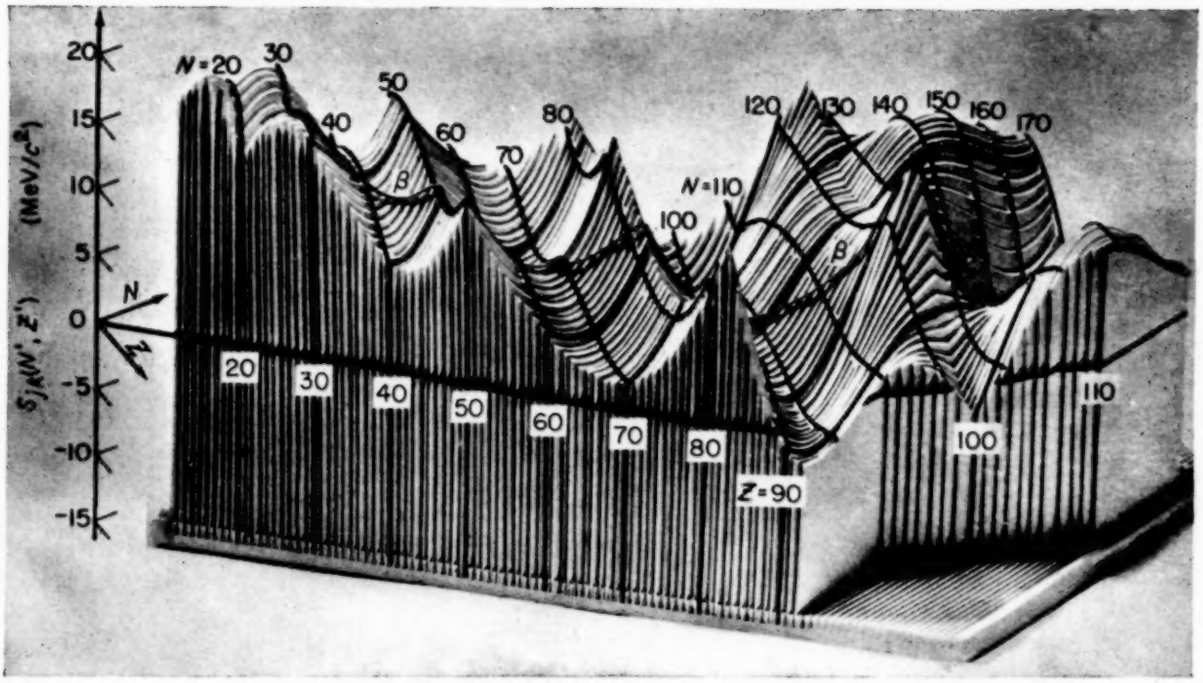

Fig. 2. Excess binding energy $S_{jk}(N', Z')$ due to nuclear shell structure and deformation, plotted versus N and Z. Each strip of the model is a constant Z, and every tenth value of Z is indicated along the front of the figure. The lines of constant N are perpendicular to those of constant Z, and are numbered along the top of the figure. Magic numbers of N or Z appear as discontinuous derivatives of S, and double magic number atoms appear as peaks. Positive values of S correspond to lower masses. The path of the line of beta stability is indicated by the line β–β.

standard form. Other forms for S were tried, but only the function S_{jk} as given in eq. (8) gave this improved result for the extrapolation test †. Thus we have $\sigma < 1$ MeV/c^2, $(\sigma_2/\sigma_1)_{\text{int}} \approx 1$ and $(\sigma_2/\sigma_1)_{\text{ext}}$ within the proposed criterion of 1.4.

5. Table of Masses

The mass law (9) with least square determined coefficients yields the masses of odd-mass atoms directly. In order to calculate masses of even-mass atoms, it was necessary to consider the pairing energy term δ_A, given by

$$\Delta M(Z, A) = \Delta M_0(Z, A) + \begin{cases} +\frac{1}{2}\delta_A \text{ for odd atoms,} \\ +0 \text{ for odd mass atoms,} \\ -\frac{1}{2}\delta_A \text{ for even atoms.} \end{cases} \tag{10}$$

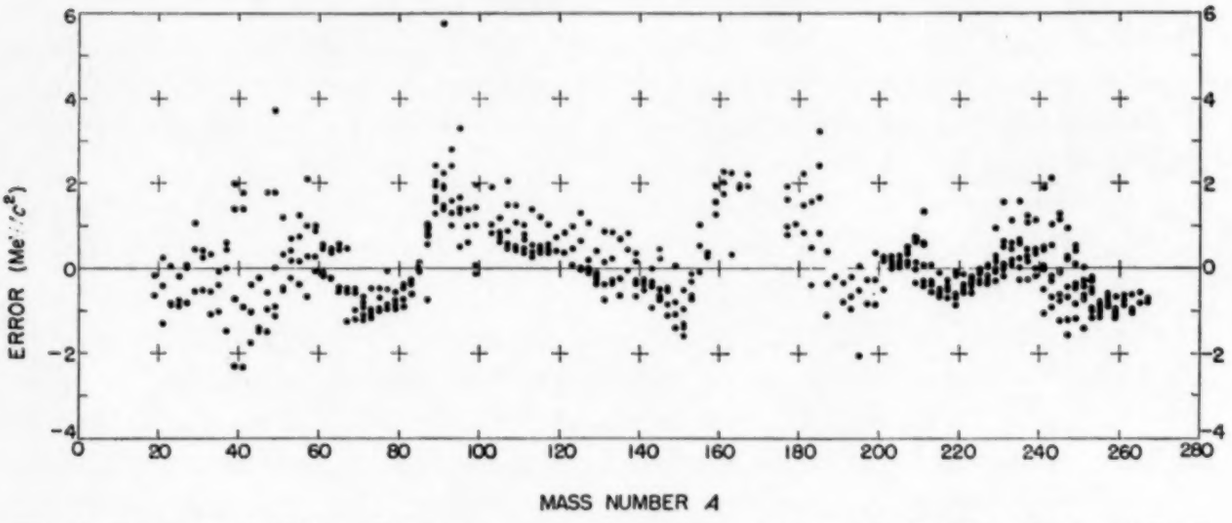

Fig. 3. Errors δ_i of 488 atomic mass excesses for odd mass atoms calculated by the generalized mass law (9) with the coefficients of (9a) and table 1 plotted versus atomic mass number A. Compare with fig. 1; note that systematic effects remain, but are small.

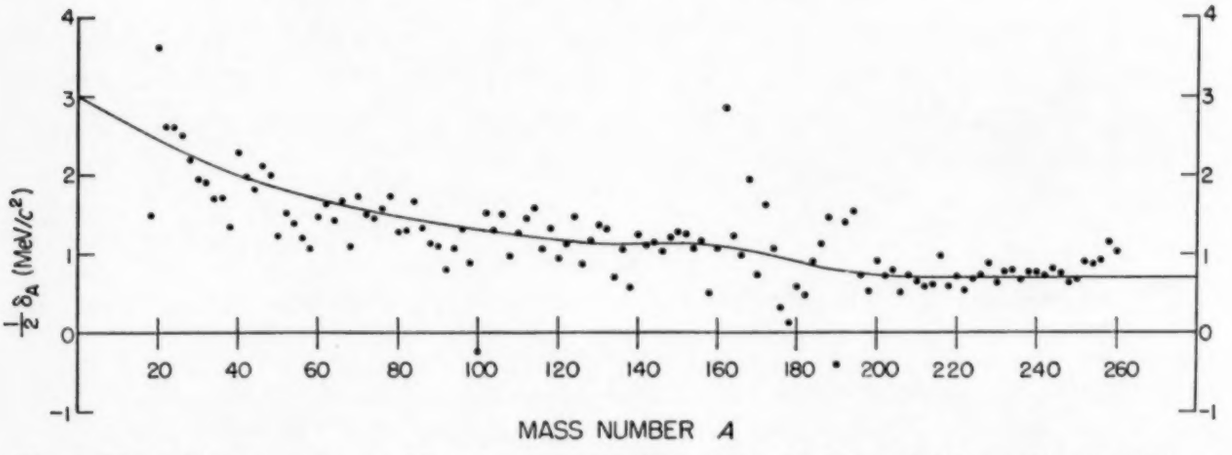

Fig. 4. The pairing energy term $\frac{1}{2}\delta_A$ taken as a function of A only. The point for each even A is an average of $\pm[\Delta M_{\text{exp}}(Z, A) - \Delta M_0(Z, A)]$ over those values of Z for which masses are known, taking the $+$sign if Z is odd and the $-$sign if Z is even. A total of 511 even masses were calculated.

† For example, the result of using the form for S in ref. [16]) was $(\sigma_2/\sigma_1)_{\text{ext}} = 1.58$.

The function δ_A was estimated by calculating ΔM_0 from eq. (9) for all known even-mass atoms. For each even value of A, the difference between ΔM_0 and the experimental mass excess averaged over Z was plotted as $\pm\frac{1}{2}\delta_A$. The rough curve fitted to these points (fig. 4) was used as $\frac{1}{2}\delta_A$.

A table of mass excesses (on the O^{16} scale) and binding energies of 7479 atoms was calculated using eq. (10). Listed in table 2 (on pp. 9—135) as functions of Z and A are the mass excess in MeV/c^2, the binding energies of the last neutron, of the last proton, of the last alpha particle, and the energies available for negaton and positon decay. All energies are given in MeV.

6. Conclusions

It is hoped that by simultaneously determining the S_{jk} function and the standard mass law terms, the interference of shell effects in the determination of α, β, γ, and η has been reduced. A comparison of the coefficients of the standard form (4a) with those of the modified form (9a) shows that all of the major coefficients, α, β, γ, and η, are increased when S_{jk} is included.

A comparison of fig. 3 with fig. 1 shows that a function of the form (8) is capable of representing the extra binding energy of a nucleus due to effects not included in the standard mass law (4), at least in the region of beta stability in the NZ-plane. Whether our generalized mass law (9) or any other is capable of being extrapolated to atoms with high neutron excess remains a moot question, but the results of the extrapolation test near the region of beta stability tend to indicate that of various forms tested, the form here reported should extrapolate with least error. Furthermore, the cross product term in N and Z included in (8) is felt to be a necessary result of elementary theoretical considerations.

I am deeply grateful to Dr. William A. Fowler for his suggestions and help in preparing this paper, to Dr. Arthur N. Cox and Los Alamos Scientific Laboratory for help and use of the computer, and to Dr. Robert A. Becker for his useful discussions.

References

1) E. M. Burbidge, G. R. Burbidge, W. A. Fowler and F. Hoyle, Revs. Mod. Phys. **29** (1957) 547
2) Robert A. Becker and William A. Fowler, Phys. Rev. **115** (1959) 1410
3) C. F. Von Weizsäcker, Z. f. Physik **96** (1935) 431
4) H. A. Bethe and R. F. Bacher, Revs. Mod. Phys. **8** (1935) 367
5) Everling, König, Mattauch and Wapstra, Nuclear Physics **18** (1960) 529
6) J. R. Huizenga, Physica **21** (1955) 410
7) E. Feenberg, Revs. Mod. Phys. **19** (1947) 239
8) J. M. Blatt and V. F. Weisskopf, Theoretical Nuclear Physics, (Wiley New York, 1952), p. 225 ff.
9) Brandt, Werner, Wakano, Fuller and Wheeler, Proc. Intern. Conf. on Nucleidic Masses (University of Toronto Press, 1960)

U·M·I

COMPUTER PRINT-OUTS, PAGES 9-135,
DO NOT PHOTOGRAPH WELL. THIS
REPRODUCTION IS MADE FROM THE BEST
COPY AVAILABLE.

10) E. E. Salpeter, private communication
11) F. S. Mozer, Phys. Rev. **116** (1959) 970
12) Hall, Ravenhall and Hofstadter, Phys. Rev. **101** (1956) 1131
13) W. J. Swiatecki, Phys. Rev. **104** (1956) 993
14) James Rainwater, Phys. Rev. **79** (1950) 432
15) S. G. Nilsson, Mat. Fys. Medd. Dan. Vid. Selsk. **29**, No. 16 (1955)
16) P. A. Seeger, Bull. Amer. Phys. Soc. **4** (1959) 461
17) A. G. W. Cameron, Can. Jour. Phys. **35** (1957) 1021
18) A. E. S. Green, Phys. Rev. **95** (1954) 1006

TABLE 2

Table of atomic mass excesses and nuclear binding energies for 7479 isotopes. The mass excesses were calculated by eq. (10), and the binding energies by taking appropriate differences. The first three columns give the atomic number Z, the chemical symbol and the mass number A. Column 4 gives the atomic mass excess $\Delta M = M - A$ (in MeV/c^2). Column 5 gives the binding energy of the last neutron (in MeV). Column 6 gives the binding energy of the last proton (in MeV). Column 7 gives the binding energy of the last alpha particle (in MeV). Column 8 gives the energy available for negaton decay (in MeV). Finally, column 9 gives the energy available for positon decay (in MeV); this is the energy released in electron capture, or about 1 MeV greater than the kinetic energy in positon decay

ATOM			M - A	NEUTRON	PROTON	ALPHA	Q BETA -	Q BETA +
11	NA	22	1.085	10.878	7.233	10.348	-3.142	2.971
11	NA	23	-2.672	12.124	8.371	10.579	-3.247	-3.607
11	NA	24	-1.047	6.743	9.567	11.068	5.419	-1.314
11	NA	25	-2.868	10.189	10.720	11.364	3.107	-7.818
11	NA	26	.598	4.901	11.937	11.876	9.476	-5.669
11	NA	27	.740	8.225	13.111	12.184	7.292	-12.069
11	NA	28	6.048	3.060	14.346	12.749	13.545	-9.968
11	NA	29	8.073	6.342	15.527	13.189	11.405	-16.120
11	NA	30	14.984	1.456	16.793	14.033	17.336	-13.984
11	NA	31	18.601	4.750	17.951	14.785	15.169	-18.443
11	NA	32	25.681	1.288	18.948	17.094	19.689	-16.035
11	NA	33	29.435	4.614	19.867	19.218	17.303	-21.352
ATOM			M - A	NEUTRON	PROTON	ALPHA	Q BETA -	Q BETA +
12	MG	23	.575	12.019	8.095	9.798	-10.101	3.247
12	MG	24	-6.466	15.409	11.379	9.840	-12.289	-5.419

(continued on pp. 10—135)

TABLE 2

Atomic mass excesses and nuclear binding energies

12	MG	25	-5.975	7.876	12.513	10.318	-3.620	-3.107
12	MG	26	-8.878	11.271	13.595	10.602	-3.714	-9.476
12	MG	27	-6.552	6.041	14.734	11.096	2.636	-7.292
12	MG	28	-7.497	9.313	15.822	11.373	.532	-13.545
12	MG	29	-3.332	4.202	16.964	11.891	6.751	-11.405
12	MG	30	-2.352	7.387	18.009	12.227	4.757	-17.336
12	MG	31	3.432	2.584	19.137	12.986	10.649	-15.169
12	MG	32	5.993	5.807	20.194	13.632	8.553	-19.689
12	MG	33	12.131	2.229	21.135	15.671	13.187	-17.303
12	MG	34	15.018	5.481	22.001	17.559	10.927	-22.541
12	MG	35	22.247	1.139	22.897	18.407	16.188	-20.189
12	MG	36	26.299	4.315	23.722	19.026	13.958	-25.263
	ATOM		M - A	NEUTRON	PROTON	ALPHA	Q BETA -	Q BETA +
13	AL	24	5.823	13.221	2.337	9.530	-8.186	12.289
13	AL	25	-2.355	16.545	3.473	9.560	-10.348	3.620
13	AL	26	-5.164	11.176	6.774	9.858	-3.892	3.714
13	AL	27	-9.188	12.391	7.894	10.125	-3.984	-2.636
13	AL	28	-8.029	7.209	9.063	10.592	4.288	-.532
13	AL	29	-10.082	10.420	10.170	10.824	2.165	-6.751
13	AL	30	-7.108	5.393	11.361	11.315	8.172	-4.757
13	AL	31	-7.217	8.476	12.450	11.566	6.143	-10.649
13	AL	32	-2.561	3.711	13.577	12.217	11.888	-8.553
13	AL	33	-1.055	6.862	14.633	12.738	9.753	-13.187
13	AL	34	4.091	3.221	15.625	14.502	14.338	-10.927
13	AL	35	6.059	6.400	16.544	16.152	12.102	-16.188
13	AL	36	12.341	2.085	17.490	16.949	17.289	-13.958
13	AL	37	15.517	5.191	18.367	17.526	15.083	-19.055
13	AL	38	22.887	.997	19.269	18.280	20.111	-16.850
13	AL	39	27.215	4.039	20.106	18.830	17.929	-21.784
	ATOM		M - A	NEUTRON	PROTON	ALPHA	Q BETA -	Q BETA +
14	SI	25	7.993	14.382	5.414	9.091	-15.063	10.348
14	SI	26	-1.272	17.633	6.502	9.108	-17.084	3.892
14	SI	27	-5.204	12.299	7.625	9.388	-10.604	3.984
14	SI	28	-12.317	15.481	10.715	9.461	-12.612	-4.288
14	SI	29	-12.248	8.298	11.803	9.882	-4.338	-2.165
14	SI	30	-15.280	11.399	12.782	10.011	-4.323	-8.172
14	SI	31	-13.359	6.447	13.836	10.417	1.664	-6.143
14	SI	32	-14.449	9.457	14.817	10.561	-.285	-11.888
14	SI	33	-10.809	4.727	15.833	11.086	5.425	-9.753
14	SI	34	-10.247	7.806	16.777	11.505	3.354	-14.338
14	SI	35	-6.044	4.163	17.719	13.085	7.930	-12.102
14	SI	36	-4.948	7.272	18.592	14.550	5.814	-17.289
14	SI	37	.434	2.985	19.492	15.306	11.024	-15.083
14	SI	38	2.776	6.025	20.326	15.851	8.933	-20.111
14	SI	39	9.286	1.858	21.186	16.570	13.984	-17.929
14	SI	40	12.816	4.837	21.984	17.092	11.913	-22.800
14	SI	41	20.394	.790	22.807	17.787	16.806	-20.632
14	SI	42	25.041	3.721	23.570	18.306	14.743	-25.342
14	SI	43	33.609	-.201	24.358	19.000	19.475	-23.174
	ATOM		M - A	NEUTRON	PROTON	ALPHA	Q BETA -	Q BETA +
15	P	26	15.812	15.611	-.234	8.889	-13.280	17.084
15	P	27	5.400	18.780	.913	8.886	-15.262	10.604
15	P	28	.295	13.473	2.086	9.137	-8.858	12.612
15	P	29	-7.910	16.572	3.177	9.164	-10.843	4.338
15	P	30	-10.957	11.415	6.294	9.403	-4.703	4.323
15	P	31	-15.024	12.434	7.329	9.445	-4.685	-1.664

TABLE 2

Atomic mass excesses and nuclear binding energies

15	P	32	-14.164	7.507	8.389	9.744	3.077	.285
15	P	33	-16.234	10.438	9.370	9.761	1.108	-5.425
15	P	34	-13.601	5.734	10.377	10.102	6.687	-3.354
15	P	35	-13.973	8.739	11.310	10.366	4.580	-7.930
15	P	36	-10.762	5.156	12.303	11.810	8.987	-5.814
15	P	37	-10.590	8.195	13.226	13.143	6.893	-11.024
15	P	38	-6.157	3.935	14.176	13.857	12.032	-8.933
15	P	39	-4.698	6.909	15.060	14.366	9.964	-13.984
15	P	40	.903	2.766	15.968	15.048	14.949	-11.913
15	P	41	3.588	5.683	16.813	15.539	12.900	-16.806
15	P	42	10.297	1.658	17.682	16.199	17.733	-14.743
15	P	43	14.135	4.530	18.491	16.690	15.691	-19.475
15	P	44	21.873	.629	19.321	17.352	20.366	-17.405
15	P	45	26.769	3.472	20.095	17.867	18.317	-21.970
15	P	46	35.435	-.299	20.888	18.556	22.828	-19.879
	ATOM		M - A	NEUTRON	PROTON	ALPHA	Q BETA -	Q BETA +
16	S	27	20.662	16.798	2.735	8.502	-20.044	15.262
16	S	28	9.153	19.877	3.832	8.465	-21.874	8.858
16	S	29	2.933	14.587	4.947	8.669	-15.430	10.843
16	S	30	-6.255	17.555	5.930	8.592	-17.198	4.703
16	S	31	-10.339	12.452	6.966	8.744	-11.035	4.685
16	S	32	-17.241	15.269	9.802	8.532	-12.788	-3.077
16	S	33	-17.342	8.469	10.763	8.703	-5.024	-1.108
16	S	34	-20.288	11.314	11.639	8.618	-5.076	-6.687
16	S	35	-18.553	6.632	12.537	8.803	.484	-4.580
16	S	36	-19.749	9.564	13.361	8.909	-1.555	-8.987
16	S	37	-17.482	6.100	14.305	10.283	2.725	-6.893
16	S	38	-18.189	9.074	15.184	11.551	.742	-12.032
16	S	39	-14.662	4.840	16.090	12.228	5.901	-9.964
16	S	40	-14.046	7.752	16.933	12.708	3.940	-14.949
16	S	41	-9.313	3.634	17.800	13.356	8.946	-12.900
16	S	42	-7.436	6.490	18.608	13.821	7.000	-17.733
16	S	43	-1.557	2.488	19.439	14.452	11.852	-15.691
16	S	44	1.507	5.303	20.212	14.918	9.909	-20.366
16	S	45	8.452	1.423	21.006	15.551	14.603	-18.317
16	S	46	12.607	4.212	21.746	16.043	12.646	-22.828
16	S	47	20.515	.460	22.505	16.704	17.176	-20.756
16	S	48	25.642	3.240	23.214	17.245	15.190	-25.101
16	S	49	34.390	-.380	23.939	17.958	19.552	-22.995
	ATOM		M - A	NEUTRON	PROTON	ALPHA	Q BETA -	Q BETA +
17	CL	28	31.026	18.047	-2.779	8.388	-18.301	21.874
17	CL	29	18.363	21.030	-1.626	8.302	-20.088	15.430
17	CL	30	10.943	15.787	-.426	8.478	-13.786	17.198
17	CL	31	.696	18.615	.634	8.314	-15.515	11.035
17	CL	32	-4.453	13.516	1.699	8.357	-9.427	12.788
17	CL	33	-12.318	16.232	2.662	8.017	-11.156	5.024
17	CL	34	-15.212	11.262	5.455	7.864	-5.306	5.076
17	CL	35	-19.037	12.192	6.333	7.622	-5.356	-.484
17	CL	36	-18.194	7.525	7.226	7.639	1.857	1.555
17	CL	37	-20.207	10.381	8.043	7.583	-.202	-2.725
17	CL	38	-18.931	7.090	9.033	8.939	3.812	-.742
17	CL	39	-20.562	9.999	9.958	10.199	1.844	-5.901
17	CL	40	-17.986	5.791	10.909	10.833	6.931	-3.940
17	CL	41	-18.258	8.640	11.797	11.278	4.988	-8.946
17	CL	42	-14.435	4.544	12.707	11.888	9.929	-7.000
17	CL	43	-13.409	7.341	13.558	12.320	8.001	-11.852
17	CL	44	-8.401	3.360	14.429	12.913	12.794	-9.909
17	CL	45	-6.151	6.117	15.243	13.348	10.869	-14.603

TABLE 2

Atomic mass excesses and nuclear binding energies

17	CL	46	-.039	2.255	16.076	13.945	15.509	-12.646
17	CL	47	3.338	4.990	16.853	14.405	13.570	-17.176
17	CL	48	10.453	1.253	17.647	15.030	18.051	-15.190
17	CL	49	14.838	3.982	18.389	15.540	16.081	-19.552
17	CL	50	22.836	.370	19.139	16.209	20.410	-17.512
17	CL	51	28.085	3.118	19.847	16.795	18.386	-21.719
17	CL	52	36.822	-.370	20.567	17.531	22.550	-19.631
	ATOM		M - A	NEUTRON	PROTON	ALPHA	Q BETA -	Q BETA +
18	AR	29	38.451	19.244	.160	8.165	-24.808	20.088
18	AR	30	24.729	22.089	1.219	7.973	-26.369	13.786
18	AR	31	16.211	16.886	2.317	8.061	-20.024	15.515
18	AR	32	4.974	19.604	3.307	7.788	-21.603	9.427
18	AR	33	-1.161	14.503	4.293	7.704	-15.476	11.156
18	AR	34	-9.906	17.112	5.173	7.261	-17.070	5.306
18	AR	35	-13.680	12.142	6.053	6.951	-11.197	5.356
18	AR	36	-20.051	14.738	8.599	6.420	-12.898	-1.857
18	AR	37	-20.006	8.322	9.396	6.273	-5.683	.202
18	AR	38	-22.742	11.104	10.120	6.063	-5.957	-3.812
18	AR	39	-22.406	8.031	11.060	7.462	-2.153	-1.844
18	AR	40	-24.917	10.879	11.940	8.777	-4.021	-6.931
18	AR	41	-23.246	6.696	12.845	9.373	1.079	-4.988
18	AR	42	-24.364	9.486	13.691	9.784	-.768	-9.929
18	AR	43	-21.410	5.413	14.560	10.357	4.187	-8.001
18	AR	44	-21.196	8.153	15.371	10.759	2.352	-12.794
18	AR	45	-17.020	4.192	16.204	11.317	7.161	-10.869
18	AR	46	-15.548	6.895	16.982	11.722	5.324	-15.509
18	AR	47	-10.232	3.051	17.778	12.284	9.980	-13.570
18	AR	48	-7.598	5.734	18.521	12.715	8.125	-18.051
18	AR	49	-1.244	2.013	19.281	13.305	12.621	-16.081
18	AR	50	2.425	4.699	19.997	13.791	10.718	-20.410
18	AR	51	9.699	1.093	20.721	14.425	15.062	-18.386
18	AR	52	14.272	3.795	21.398	14.979	13.111	-22.550
18	AR	53	22.320	.319	22.087	15.679	17.290	-20.477
18	AR	54	27.651	3.037	22.731	16.306	15.286	-24.482
18	AR	55	36.332	-.313	23.386	17.082	19.304	-22.361
	ATOM		M - A	NEUTRON	PROTON	ALPHA	Q BETA -	Q BETA +
19	K	32	26.577	18.026	-2.781	8.059	-18.271	21.603
19	K	33	14.314	20.630	-1.756	7.658	-19.806	15.476
19	K	34	7.165	15.517	-.741	7.388	-13.739	17.070
19	K	35	-2.483	18.015	.162	6.788	-15.295	11.197
19	K	36	-7.153	13.038	1.058	6.310	-9.486	12.898
19	K	37	-14.323	15.537	1.857	5.615	-11.164	5.683
19	K	38	-16.785	10.830	4.364	5.182	-5.730	5.957
19	K	39	-20.253	11.835	5.096	4.826	-6.003	2.153
19	K	40	-20.896	9.010	6.074	6.311	-.870	4.021
19	K	41	-24.325	11.797	6.992	7.727	-2.731	-1.079
19	K	42	-23.596	7.638	7.935	8.274	2.296	.768
19	K	43	-25.597	10.369	8.818	8.644	.459	-4.187
19	K	44	-23.548	6.318	9.723	9.171	5.348	-2.352
19	K	45	-24.181	9.001	10.570	9.532	3.524	-7.161
19	K	46	-20.872	5.058	11.437	10.046	8.273	-5.324
19	K	47	-20.212	7.707	12.248	10.412	6.449	-9.980
19	K	48	-15.723	3.878	13.076	10.931	11.051	-8.125
19	K	49	-13.865	6.509	13.851	11.323	9.209	-12.621
19	K	50	-8.293	2.795	14.634	11.863	13.670	-10.718
19	K	51	-5.363	5.438	15.373	12.311	11.780	-15.062
19	K	52	1.161	1.844	16.123	12.901	16.081	-13.111
19	K	53	5.030	4.498	16.827	13.417	14.144	-17.290

TABLE 2

Atomic mass excesses and nuclear binding energies

19	K	54	12.366	1.032	17.540	14.079	18.283	-15.286
19	K	55	17.028	3.705	18.208	14.667	16.293	-19.304
19	K	56	25.032	.363	18.885	15.400	20.275	-17.247
19	K	57	30.344	3.056	19.520	16.063	18.231	-21.118
19	K	58	38.885	-.174	20.161	16.857	22.069	-19.015
19	K	59	44.721	2.531	20.764	17.581	19.979	-22.758
19	K	60	53.691	-.603	21.373	18.417	23.692	-20.625
ATOM			M - A	NEUTRON	PROTON	ALPHA	Q BETA -	Q BETA +
20	CA	33	34.121	19.094	.041	7.940	-23.243	19.806
20	CA	34	20.903	21.585	.996	7.435	-24.727	13.739
20	CA	35	12.812	16.459	1.938	7.008	-18.647	15.295
20	CA	36	2.333	18.846	2.769	6.250	-20.031	9.486
20	CA	37	-3.159	13.860	3.591	5.607	-14.092	11.164
20	CA	38	-11.055	16.263	4.317	4.759	-15.499	5.730
20	CA	39	-14.250	11.562	5.050	4.179	-9.853	6.003
20	CA	40	-20.026	14.143	7.357	3.584	-11.452	.870
20	CA	41	-21.594	9.936	8.283	5.198	-6.318	2.731
20	CA	42	-25.892	12.665	9.152	6.759	-6.559	-2.296
20	CA	43	-26.056	8.531	10.045	7.259	-1.587	-.459
20	CA	44	-28.895	11.207	10.883	7.587	-3.399	-5.348
20	CA	45	-27.705	7.177	11.742	8.069	1.440	-3.524
20	CA	46	-29.145	9.807	12.548	8.390	-.357	-8.273
20	CA	47	-26.661	5.883	13.373	8.860	4.350	-6.449
20	CA	48	-26.774	8.480	14.146	9.187	2.556	-11.051
20	CA	49	-23.074	4.667	14.936	9.663	7.126	-9.209
20	CA	50	-21.962	7.256	15.682	10.023	5.307	-13.670
20	CA	51	-17.143	3.549	16.435	10.521	9.747	-11.780
20	CA	52	-14.920	6.144	17.142	10.931	7.900	-16.081
20	CA	53	-9.114	2.561	17.860	11.480	12.192	-14.144
20	CA	54	-5.918	5.171	18.533	11.952	10.306	-18.283
20	CA	55	.735	1.714	19.215	12.574	14.449	-16.293
20	CA	56	4.757	4.346	19.856	13.125	12.519	-20.275
20	CA	57	12.113	1.011	20.504	13.817	16.518	-18.231
20	CA	58	16.816	3.664	21.112	14.444	14.543	-22.069
20	CA	59	24.742	.442	21.728	15.199	18.410	-19.979
20	CA	60	29.999	3.110	22.307	15.889	16.397	-23.692
20	CA	61	38.385	-.018	22.891	16.686	20.151	-21.571
20	CA	62	44.099	2.654	23.442	17.411	18.113	-25.182
20	CA	63	52.868	-.402	23.997	18.220	21.775	-23.046
ATOM			M - A	NEUTRON	PROTON	ALPHA	Q BETA -	Q BETA +
21	SC	35	31.458	22.539	-2.970	8.386	-22.823	18.647
21	SC	36	22.364	17.462	-1.968	7.822	-16.860	20.031
21	SC	37	10.933	19.798	-1.015	6.991	-18.262	14.092
21	SC	38	4.444	14.856	-.019	6.330	-12.431	15.499
21	SC	39	-4.397	17.209	.927	5.523	-13.851	9.853
21	SC	40	-8.574	12.544	1.908	5.030	-8.301	11.452
21	SC	41	-15.276	15.070	2.835	4.563	-9.905	6.318
21	SC	42	-19.333	12.424	5.324	6.157	-6.388	6.559
21	SC	43	-24.469	13.503	6.162	7.825	-6.628	1.587
21	SC	44	-25.496	9.394	7.025	8.209	-.185	3.399
21	SC	45	-29.145	12.017	7.835	8.430	-1.995	-1.440
21	SC	46	-28.788	8.010	8.668	8.802	2.776	.357
21	SC	47	-31.011	10.590	9.450	9.023	.983	-4.350
21	SC	48	-29.330	6.686	10.254	9.391	5.627	-2.556
21	SC	49	-30.200	9.237	11.011	9.628	3.837	-7.126
21	SC	50	-27.269	5.437	11.780	10.006	8.362	-5.307
21	SC	51	-26.890	7.988	12.513	10.287	6.548	-9.747
21	SC	52	-22.820	4.298	13.262	10.707	10.935	-7.900

TABLE 2

Atomic mass excesses and nuclear binding energies

21	SC	53	-21.306	6.853	13.971	11.050	9.094	-12.192
21	SC	54	-16.224	3.286	14.695	11.541	13.338	-10.306
21	SC	55	-13.714	5.857	15.381	11.960	11.459	-14.449
21	SC	56	-7.762	2.415	16.082	12.532	15.558	-12.519
21	SC	57	-4.405	5.010	16.747	13.044	13.633	-16.518
21	SC	58	2.273	1.689	17.424	13.701	17.593	-14.543
21	SC	59	6.332	4.309	18.069	14.305	15.624	-18.410
21	SC	60	13.602	1.097	18.724	15.039	19.456	-16.397
21	SC	61	18.234	3.735	19.350	15.718	17.451	-20.151
21	SC	62	25.986	.616	19.984	16.508	21.173	-18.113
21	SC	63	31.093	3.260	20.590	17.237	19.143	-21.775
21	SC	64	39.249	.212	21.204	18.052	22.778	-19.728
21	SC	65	44.769	2.847	21.792	18.796	20.739	-23.324
21	SC	66	53.291	-.154	22.387	19.599	24.312	-21.284
	ATOM		M - A	NEUTRON	PROTON	ALPHA	Q BETA -	Q BETA +
22	TI	36	39.224	23.425	-.181	9.233	-28.339	16.860
22	TI	37	29.195	18.397	.754	8.535	-22.396	18.262
22	TI	38	16.875	20.687	1.642	7.637	-23.724	12.431
22	TI	39	9.454	15.789	2.575	6.967	-17.910	13.851
22	TI	40	-.272	18.094	3.460	6.215	-19.256	8.301
22	TI	41	-5.371	13.466	4.382	5.821	-13.716	9.905
22	TI	42	-12.945	15.941	5.254	5.499	-15.243	6.388
22	TI	43	-17.842	13.264	6.093	7.200	-11.669	6.628
22	TI	44	-25.311	15.837	8.426	8.894	-13.376	.185
22	TI	45	-27.151	10.207	9.240	9.166	-6.933	1.995
22	TI	46	-31.564	12.781	10.003	9.281	-7.168	-2.776
22	TI	47	-31.993	8.797	10.790	9.547	-2.395	-.983
22	TI	48	-34.956	11.330	11.530	9.670	-4.117	-5.627
22	TI	49	-34.037	7.448	12.292	9.941	.531	-3.837
22	TI	50	-35.631	9.962	13.016	10.096	-1.205	-8.362
22	TI	51	-33.438	6.174	13.754	10.387	3.324	-6.548
22	TI	52	-33.756	8.685	14.450	10.591	1.573	-10.935
22	TI	53	-30.400	5.012	15.165	10.936	5.965	-9.094
22	TI	54	-29.562	7.529	15.841	11.209	4.183	-13.338
22	TI	55	-25.173	3.978	16.533	11.639	8.432	-11.459
22	TI	56	-23.319	6.514	17.190	12.008	6.607	-15.558
22	TI	57	-18.038	3.086	17.861	12.533	10.712	-13.633
22	TI	58	-15.320	5.649	18.499	13.011	8.840	-17.593
22	TI	59	-9.292	2.340	19.151	13.637	12.805	-15.624
22	TI	60	-5.854	4.929	19.771	14.220	10.884	-19.456
22	TI	61	.784	1.729	20.403	14.938	14.723	-17.451
22	TI	62	4.813	4.339	21.007	15.613	12.761	-21.173
22	TI	63	11.950	1.230	21.620	16.401	16.490	-19.143
22	TI	64	16.470	3.847	22.207	17.138	14.500	-22.778
22	TI	65	24.030	.807	22.803	17.964	18.142	-20.739
22	TI	66	28.979	3.419	23.375	18.729	16.140	-24.312
22	TI	67	36.923	.424	23.953	19.555	19.719	-22.280
22	TI	68	42.278	3.012	24.509	20.308	17.720	-25.813
22	TI	69	50.605	.040	25.071	21.097	21.261	-23.802
	ATOM		M - A	NEUTRON	PROTON	ALPHA	Q BETA -	Q BETA +
23	V	38	40.599	19.359	-3.820	8.640	-20.629	23.724
23	V	39	27.364	21.603	-2.904	7.704	-21.976	17.910
23	V	40	18.983	16.748	-1.945	6.900	-16.266	19.256
23	V	41	8.345	19.006	-1.032	6.107	-17.626	13.716
23	V	42	2.298	14.414	-.085	5.765	-12.180	15.243
23	V	43	-6.173	16.839	.812	5.385	-13.715	11.669
23	V	44	-11.935	14.129	1.678	6.970	-10.163	13.376
23	V	45	-20.218	16.651	2.492	8.551	-11.871	6.933

TABLE 2

Atomic mass excesses and nuclear binding energies

23	V	46	-24.396	12.545	4.830	8.672	-6.999	7.168
23	V	47	-29.599	13.570	5.620	8.739	-7.233	2.395
23	V	48	-30.840	9.608	6.431	8.953	-1.069	4.117
23	V	49	-34.568	12.095	7.196	9.031	-2.789	-.531
23	V	50	-34.427	8.226	7.974	9.248	1.812	1.205
23	V	51	-36.763	10.703	8.716	9.361	.080	-3.324
23	V	52	-35.329	6.933	9.475	9.608	4.554	-1.573
23	V	53	-36.365	9.404	10.194	9.775	2.807	-5.965
23	V	54	-33.745	5.747	10.929	10.085	7.149	-4.183
23	V	55	-33.604	8.227	11.627	10.324	5.371	-8.432
23	V	56	-29.927	4.690	12.339	10.716	9.575	-6.607
23	V	57	-28.750	7.191	13.016	11.054	7.755	-10.712
23	V	58	-24.159	3.776	13.706	11.544	11.819	-8.840
23	V	59	-22.097	6.306	14.363	11.992	9.951	-12.805
23	V	60	-16.739	3.009	15.031	12.586	13.880	-10.884
23	V	61	-13.939	5.567	15.669	13.143	11.965	-14.723
23	V	62	-7.948	2.377	16.317	13.831	15.771	-12.761
23	V	63	-4.540	4.958	16.937	14.481	13.815	-16.490
23	V	64	1.970	1.857	17.565	15.241	17.515	-14.500
23	V	65	5.888	4.450	18.167	15.955	15.531	-18.142
23	V	66	12.840	1.416	18.775	16.755	19.150	-16.140
23	V	67	17.203	4.004	19.360	17.499	17.153	-19.719
23	V	68	24.557	1.013	19.950	18.300	20.713	-17.720
23	V	69	29.344	3.581	20.518	19.034	18.721	-21.261
23	V	70	37.128	.584	21.062	19.772	22.300	-19.225
23	V	71	42.323	3.172	21.614	20.489	20.271	-22.800
23	V	72	50.539	.151	22.168	21.161	23.832	-20.791
	ATOM		M - A	NEUTRON	PROTON	ALPHA	Q BETA -	Q BETA +
24	CR	40	35.249	22.457	-.301	7.584	-27.279	16.266
24	CR	41	25.971	17.646	.597	6.833	-21.587	17.626
24	CR	42	14.478	19.860	1.451	6.006	-22.879	12.180
24	CR	43	7.542	15.304	2.341	5.521	-17.445	13.715
24	CR	44	-1.772	17.681	3.184	5.109	-18.911	10.163
24	CR	45	-8.348	14.943	3.998	6.585	-15.306	11.871
24	CR	46	-17.397	17.417	4.764	8.061	-16.943	6.999
24	CR	47	-22.366	13.336	5.555	8.134	-12.072	7.233
24	CR	48	-29.771	15.772	7.756	8.069	-13.695	1.069
24	CR	49	-31.779	10.376	8.524	8.237	-7.529	2.789
24	CR	50	-36.238	12.827	9.255	8.284	-7.782	-1.812
24	CR	51	-36.842	8.971	10.000	8.458	-3.179	-.080
24	CR	52	-39.883	11.408	10.705	8.536	-4.850	-4.554
24	CR	53	-39.172	7.656	11.428	8.744	-.373	-2.807
24	CR	54	-40.894	10.089	12.114	8.872	-2.063	-7.149
24	CR	55	-38.976	6.449	12.815	9.147	2.283	-5.371
24	CR	56	-39.502	8.893	13.482	9.355	.559	-9.575
24	CR	57	-36.506	5.372	14.164	9.715	4.766	-7.755
24	CR	58	-35.978	7.840	14.812	10.025	2.997	-11.819
24	CR	59	-32.049	4.438	15.475	10.485	7.065	-9.951
24	CR	60	-30.619	6.937	16.106	10.909	5.244	-13.880
24	CR	61	-25.904	3.652	16.750	11.475	9.178	-11.965
24	CR	62	-23.719	6.183	17.365	12.009	7.305	-15.771
24	CR	63	-18.354	3.003	17.991	12.671	11.116	-13.815
24	CR	64	-15.545	5.558	18.590	13.300	9.199	-17.515
24	CR	65	-9.643	2.466	19.198	14.036	12.905	-15.531
24	CR	66	-6.310	5.034	19.783	14.732	10.956	-19.150
24	CR	67	.050	2.007	20.374	15.509	14.580	-17.153
24	CR	68	3.844	4.573	20.944	16.235	12.615	-20.713
24	CR	69	10.624	1.588	21.519	17.016	16.181	-18.721
24	CR	70	14.828	4.163	22.101	17.761	14.162	-22.300
24	CR	71	22.052	1.143	22.660	18.480	17.747	-20.271

TABLE 2

Atomic mass excesses and nuclear binding energies

24	CR	72	26.707	3.713	23.201	19.180	15.744	-23.832
24	CR	73	34.381	.694	23.743	19.834	19.312	-21.831
24	CR	74	39.528	3.220	24.268	20.434	17.337	-26.557
24	CR	75	48.870	-.975	24.800	19.862	22.066	-24.569
24	CR	76	55.710	1.528	25.314	19.230	20.105	-28.069
	ATOM		M - A	NEUTRON	PROTON	ALPHA	Q BETA -	Q BETA +
25	MN	42	37.358	18.567	-3.802	6.851	-19.953	22.879
25	MN	43	24.987	20.738	-2.924	5.986	-21.261	17.445
25	MN	44	17.139	16.216	-2.012	5.454	-15.917	18.911
25	MN	45	6.959	18.547	-1.146	4.995	-17.392	15.306
25	MN	46	-.454	15.780	-.309	6.361	-13.812	16.943
25	MN	47	-10.294	18.207	.482	7.730	-15.450	12.072
25	MN	48	-16.076	14.149	1.295	7.751	-10.647	13.695
25	MN	49	-24.250	16.541	2.064	7.641	-12.270	7.529
25	MN	50	-28.456	12.574	4.262	7.670	-7.570	7.782
25	MN	51	-33.663	13.574	5.010	7.673	-7.822	3.179
25	MN	52	-35.033	9.737	5.775	7.803	-1.898	4.850
25	MN	53	-38.800	12.134	6.501	7.841	-3.567	.373
25	MN	54	-38.831	8.399	7.244	8.014	.859	2.063
25	MN	55	-41.259	10.795	7.949	8.105	-.828	-2.283
25	MN	56	-40.061	7.170	8.670	8.341	3.470	-.559
25	MN	57	-41.272	9.579	9.355	8.516	1.750	-4.766
25	MN	58	-38.975	6.071	10.054	8.840	5.915	-2.997
25	MN	59	-39.114	8.506	10.721	9.119	4.149	-7.065
25	MN	60	-35.863	5.116	11.399	9.546	8.179	-5.244
25	MN	61	-35.081	7.586	12.047	9.940	6.362	-9.178
25	MN	62	-31.024	4.310	12.705	10.475	10.262	-7.305
25	MN	63	-29.470	6.813	13.336	10.982	8.394	-11.116
25	MN	64	-24.744	3.641	13.975	11.615	12.175	-9.199
25	MN	65	-22.548	6.171	14.588	12.219	10.262	-12.905
25	MN	66	-17.266	3.085	15.208	12.927	13.943	-10.956
25	MN	67	-14.530	5.631	15.804	13.599	11.999	-14.580
25	MN	68	-8.771	2.609	16.406	14.350	15.602	-12.615
25	MN	69	-5.557	5.154	16.986	15.055	13.642	-16.181
25	MN	70	.666	2.144	17.543	15.783	17.245	-14.162
25	MN	71	4.305	4.728	18.107	16.508	15.231	-17.747
25	MN	72	10.963	1.709	18.674	17.204	18.802	-15.744
25	MN	73	15.069	4.262	19.223	17.885	16.805	-19.312
25	MN	74	22.191	1.245	19.775	18.546	20.357	-17.337
25	MN	75	26.804	3.754	20.309	19.128	18.389	-22.066
25	MN	76	35.605	-.433	20.850	18.543	23.098	-20.105
25	MN	77	41.922	2.051	21.373	17.899	21.142	-23.611
25	MN	78	51.219	-.929	21.899	18.476	24.634	-21.635
25	MN	79	58.032	1.554	22.407	19.016	22.664	-25.085
	ATOM		M - A	NEUTRON	PROTON	ALPHA	Q BETA -	Q BETA +
26	FE	44	33.056	21.560	-.484	5.803	-26.362	15.917
26	FE	45	24.350	17.072	.373	5.230	-21.031	17.392
26	FE	46	13.358	19.360	1.186	4.730	-22.443	13.812
26	FE	47	5.156	16.569	1.975	5.995	-18.819	15.450
26	FE	48	-5.429	18.952	2.720	7.266	-20.392	10.647
26	FE	49	-11.979	14.918	3.488	7.241	-15.590	12.270
26	FE	50	-20.886	17.274	4.221	7.098	-17.164	7.570
26	FE	51	-25.842	13.323	4.970	7.085	-12.464	7.822
26	FE	52	-33.134	15.660	7.056	6.973	-14.034	1.898
26	FE	53	-35.232	10.465	7.784	7.063	-8.110	3.567
26	FE	54	-39.690	12.825	8.475	7.061	-8.383	-.859
26	FE	55	-40.430	9.107	9.184	7.197	-3.955	.828
26	FE	56	-43.531	11.468	9.857	7.257	-5.590	-3.470

TABLE 2

Atomic mass excesses and nuclear binding energies

26	FE	57	-43.022	7.858	10.546	7.459	-1.289	-1.750
26	FE	58	-44.890	10.235	11.203	7.605	-2.960	-5.915
26	FE	59	-43.263	6.741	11.873	7.897	1.208	-4.149
26	FE	60	-44.042	9.146	12.513	8.150	-.512	-8.179
26	FE	61	-41.444	5.769	13.165	8.547	3.521	-6.362
26	FE	62	-41.286	8.210	13.789	8.917	1.745	-10.262
26	FE	63	-37.864	4.945	14.424	9.424	5.649	-8.394
26	FE	64	-36.919	7.422	15.033	9.909	3.818	-12.175
26	FE	65	-32.811	4.259	15.651	10.516	7.603	-10.262
26	FE	66	-31.209	6.766	16.246	11.099	5.725	-13.943
26	FE	67	-26.529	3.687	16.847	11.784	9.410	-11.999
26	FE	68	-24.373	6.211	17.428	12.437	7.496	-15.602
26	FE	69	-19.199	3.194	18.013	13.165	11.103	-13.642
26	FE	70	-16.579	5.748	18.607	13.879	9.116	-17.245
26	FE	71	-10.926	2.714	19.177	14.586	12.724	-15.231
26	FE	72	-7.839	5.280	19.729	15.293	10.735	-18.802
26	FE	73	-1.736	2.264	20.283	15.969	14.311	-16.805
26	FE	74	1.833	4.798	20.820	16.604	12.339	-20.357
26	FE	75	8.416	1.785	21.360	17.246	15.897	-18.389
26	FE	76	12.508	4.275	21.881	17.809	13.954	-23.098
26	FE	77	20.780	.095	22.410	17.210	18.664	-21.142
26	FE	78	26.585	2.562	22.921	16.552	16.736	-24.634
26	FE	79	35.368	-.415	23.436	17.111	20.232	-22.664
26	FE	80	41.685	2.050	23.932	17.634	18.290	-26.099
26	FE	81	50.937	-.885	24.431	18.205	21.730	-24.115
26	FE	82	57.724	1.580	24.913	18.739	19.775	-27.493
	ATOM		M - A	NEUTRON	PROTON	ALPHA	Q BETA -	Q BETA +
27	CO	46	35.800	17.948	-3.865	5.167	-19.496	22.443
27	CO	47	23.975	20.193	-3.032	4.622	-20.919	18.819
27	CO	48	14.963	17.379	-2.222	5.785	-17.323	20.392
27	CO	49	3.611	19.719	-1.455	6.957	-18.898	15.590
27	CO	50	-3.722	15.700	-.672	6.877	-14.149	17.164
27	CO	51	-13.377	18.022	.076	6.692	-15.724	12.464
27	CO	52	-19.100	14.090	.843	6.633	-11.083	14.034
27	CO	53	-27.122	16.390	1.573	6.482	-12.653	8.110
27	CO	54	-31.307	12.552	3.659	6.460	-8.123	8.383
27	CO	55	-36.476	13.536	4.370	6.422	-8.395	3.955
27	CO	56	-37.941	9.833	5.096	6.518	-2.710	5.590
27	CO	57	-41.734	12.160	5.787	6.543	-4.342	1.289
27	CO	58	-41.930	8.564	6.493	6.708	-.085	2.960
27	CO	59	-44.471	10.909	7.166	6.822	-1.754	-1.208
27	CO	60	-43.530	7.426	7.851	7.078	2.374	.512
27	CO	61	-44.964	9.802	8.507	7.301	.657	-3.521
27	CO	62	-43.031	6.435	9.173	7.665	4.655	-1.745
27	CO	63	-43.512	8.848	9.811	8.007	2.883	-5.649
27	CO	64	-40.737	5.592	10.458	8.483	6.755	-3.818
27	CO	65	-40.414	8.044	11.080	8.942	4.928	-7.603
27	CO	66	-36.934	4.888	11.708	9.519	8.687	-5.725
27	CO	67	-35.939	7.372	12.314	10.078	6.812	-9.410
27	CO	68	-31.869	4.298	12.925	10.734	10.475	-7.496
27	CO	69	-30.303	6.801	13.515	11.364	8.565	-11.103
27	CO	70	-25.695	3.760	14.081	12.038	12.209	-9.116
27	CO	71	-23.650	6.322	14.656	12.730	10.225	-12.724
27	CO	72	-18.574	3.291	15.233	13.413	13.817	-10.735
27	CO	73	-16.047	5.840	15.792	14.098	11.833	-14.311
27	CO	74	-10.506	2.826	16.355	14.780	15.392	-12.339
27	CO	75	-7.481	5.343	16.899	15.395	13.425	-15.897
27	CO	76	-1.447	2.333	17.447	16.019	16.967	-13.954
27	CO	77	2.115	4.806	17.977	16.563	15.029	-18.664
27	CO	78	9.850	.633	18.515	15.950	19.719	-16.736

TABLE 2

Atomic mass excesses and nuclear binding energies

27	CO	79	15.136	3.081	19.034	15.278	17.795	-20.232
27	CO	80	23.395	.108	19.558	15.819	21.275	-18.290
27	CO	81	29.207	2.556	20.063	16.324	19.338	-21.730
27	CO	82	37.950	-.375	20.572	16.878	22.762	-19.775
27	CO	83	44.246	2.071	21.063	17.395	20.812	-23.158
27	CO	84	53.431	-.817	21.558	17.962	24.179	-21.190
27	CO	85	60.171	1.628	22.035	18.491	22.216	-24.517
27	CO	86	69.756	-1.218	22.516	19.071	25.526	-22.536
27	CO	87	76.897	1.226	22.979	19.612	23.552	-25.805
	ATOM		M - A	NEUTRON	PROTON	ALPHA	Q BETA -	Q BETA +
28	NI	48	32.286	20.975	-.726	4.379	-25.819	17.323
28	NI	49	22.509	18.144	.038	5.451	-22.189	18.898
28	NI	50	10.427	20.450	.769	6.540	-23.717	14.149
28	NI	51	2.347	16.447	1.516	6.418	-18.970	15.724
28	NI	52	-8.017	18.731	2.225	6.198	-20.489	11.083
28	NI	53	-14.469	14.819	2.954	6.099	-15.849	12.653
28	NI	54	-23.184	17.083	3.647	5.907	-17.366	8.123
28	NI	55	-28.081	13.264	4.358	5.848	-12.835	8.395
28	NI	56	-35.232	15.519	6.341	5.707	-14.363	2.710
28	NI	57	-37.391	10.527	7.035	5.768	-8.676	4.342
28	NI	58	-41.845	12.821	7.696	5.764	-8.989	.085
28	NI	59	-42.717	9.239	8.372	5.896	-4.730	1.754
28	NI	60	-45.904	11.554	9.018	5.982	-6.355	-2.374
28	NI	61	-45.621	8.084	9.676	6.208	-2.224	-.657
28	NI	62	-47.686	10.433	10.307	6.405	-3.901	-4.655
28	NI	63	-46.395	7.076	10.948	6.741	.099	-2.883
28	NI	64	-47.492	9.465	11.565	7.059	-1.636	-6.755
28	NI	65	-45.342	6.217	12.190	7.508	2.239	-4.928
28	NI	66	-45.621	8.646	12.792	7.944	.445	-8.687
28	NI	67	-42.751	5.497	13.401	8.496	4.207	-6.812
28	NI	68	-42.344	7.960	13.990	9.034	2.362	-10.475
28	NI	69	-38.868	4.891	14.584	9.667	6.028	-8.565
28	NI	70	-37.904	7.403	15.186	10.304	4.089	-12.209
28	NI	71	-33.876	4.339	15.765	10.956	7.736	-10.225
28	NI	72	-32.391	6.883	16.326	11.628	5.777	-13.817
28	NI	73	-27.879	3.855	16.890	12.289	9.372	-11.833
28	NI	74	-25.898	6.386	17.436	12.928	7.412	-15.392
28	NI	75	-20.906	3.376	17.985	13.589	10.976	-13.425
28	NI	76	-18.414	5.875	18.517	14.184	9.034	-16.967
28	NI	77	-12.914	2.868	19.052	14.787	12.580	-15.029
28	NI	78	-9.869	5.323	19.569	15.312	10.668	-19.719
28	NI	79	-2.659	1.157	20.094	14.684	15.358	-17.795
28	NI	80	2.120	3.588	20.601	13.997	13.460	-21.275
28	NI	81	9.869	.618	21.111	14.520	16.945	-19.338
28	NI	82	15.188	3.048	21.604	15.006	15.034	-22.762
28	NI	83	23.434	.121	22.100	15.543	18.462	-20.812
28	NI	84	29.252	2.549	22.579	16.042	16.539	-24.179
28	NI	85	37.954	-.335	23.061	16.592	19.912	-22.216
28	NI	86	44.230	2.092	23.526	17.104	17.977	-25.526
28	NI	87	53.346	-.749	23.995	17.668	21.292	-23.552
28	NI	88	60.037	1.677	24.445	18.194	19.346	-26.804
28	NI	89	69.524	-1.120	24.901	18.772	22.604	-24.817
28	NI	90	76.589	1.303	25.338	19.313	20.647	-28.012
	ATOM		M - A	NEUTRON	PROTON	ALPHA	Q BETA -	Q BETA +
29	CU	49	44.698	21.774	-4.828	4.293	-24.274	22.189
29	CU	50	34.144	18.922	-4.050	5.266	-20.664	23.717
29	CU	51	21.316	21.195	-3.305	6.267	-22.195	18.970
29	CU	52	12.471	17.212	-2.540	6.101	-17.508	20.489

TABLE 2

Atomic mass excesses and nuclear binding energies

29	CU	53	1.380	19.459	-1.812	5.841	-19.029	15.849
29	CU	54	-5.819	15.566	-1.065	5.706	-14.445	17.366
29	CU	55	-15.245	17.794	-.354	5.477	-15.963	12.835
29	CU	56	-20.869	13.991	.373	5.378	-11.483	14.363
29	CU	57	-28.715	16.213	1.068	5.202	-13.011	8.676
29	CU	58	-32.856	12.508	3.049	5.158	-8.643	8.989
29	CU	59	-37.987	13.499	3.727	5.121	-8.955	4.730
29	CU	60	-39.549	9.929	4.417	5.217	-3.495	6.355
29	CU	61	-43.397	12.215	5.077	5.272	-5.118	2.224
29	CU	62	-43.785	8.756	5.749	5.464	-1.023	3.901
29	CU	63	-46.494	11.077	6.393	5.632	-2.698	-.099
29	CU	64	-45.856	7.729	7.046	5.935	1.271	1.636
29	CU	65	-47.581	10.093	7.674	6.226	-.462	-2.239
29	CU	66	-46.067	6.853	8.309	6.644	3.385	-.445
29	CU	67	-46.958	9.259	8.922	7.055	1.594	-4.207
29	CU	68	-44.706	6.115	9.539	7.578	5.333	-2.362
29	CU	69	-44.896	8.557	10.136	8.091	3.490	-6.028
29	CU	70	-41.993	5.465	10.710	8.668	7.191	-4.089
29	CU	71	-41.612	7.986	11.292	9.282	5.256	-7.736
29	CU	72	-38.168	4.924	11.877	9.908	8.886	-5.777
29	CU	73	-37.252	7.451	12.445	10.558	6.930	-9.372
29	CU	74	-33.310	4.426	13.016	11.224	10.508	-7.412
29	CU	75	-31.882	6.939	13.569	11.841	8.552	-10.976
29	CU	76	-27.447	3.932	14.126	12.482	12.098	-9.034
29	CU	77	-25.494	6.414	14.665	13.057	10.160	-12.580
29	CU	78	-20.537	3.411	15.208	13.641	13.689	-10.668
29	CU	79	-18.018	5.848	15.733	14.146	11.780	-15.358
29	CU	80	-11.340	1.690	16.266	13.503	16.451	-13.460
29	CU	81	-7.076	4.103	16.781	12.800	14.556	-16.945
29	CU	82	.154	1.137	17.300	13.305	18.023	-15.034
29	CU	83	4.972	3.549	17.801	13.773	16.116	-18.462
29	CU	84	12.713	.627	18.306	14.292	19.527	-16.539
29	CU	85	18.043	3.037	18.794	14.773	17.608	-19.912
29	CU	86	26.253	.157	19.286	15.306	20.962	-17.977
29	CU	87	32.054	2.566	19.761	15.801	19.033	-21.292
29	CU	88	40.691	-.270	20.240	16.349	22.330	-19.346
29	CU	89	46.920	2.138	20.701	16.859	20.389	-22.604
29	CU	90	55.942	-.654	21.167	17.423	23.629	-20.647
29	CU	91	62.558	1.751	21.615	17.949	21.677	-23.847
29	CU	92	71.921	-.996	22.069	18.529	24.860	-21.880
29	CU	93	78.882	1.407	22.504	19.069	22.898	-25.024
	ATOM		M - A	NEUTRON	PROTON	ALPHA	Q BETA -	Q BETA +
30	ZN	52	29.980	21.899	-1.079	5.915	-26.872	17.508
30	ZN	53	20.409	17.938	-.353	5.710	-22.188	19.029
30	ZN	54	8.626	20.150	.338	5.410	-23.657	14.445
30	ZN	55	.718	16.276	1.048	5.239	-19.075	15.963
30	ZN	56	-9.386	18.471	1.726	4.978	-20.544	11.483
30	ZN	57	-15.704	14.685	2.420	4.844	-16.065	13.011
30	ZN	58	-24.213	16.876	3.083	4.638	-17.547	8.643
30	ZN	59	-29.032	13.187	3.761	4.561	-13.179	8.955
30	ZN	60	-36.054	15.389	5.652	4.432	-14.691	3.495
30	ZN	61	-38.279	10.592	6.314	4.497	-9.230	5.118
30	ZN	62	-42.762	12.850	6.950	4.526	-9.602	1.023
30	ZN	63	-43.796	9.402	7.596	4.688	-5.506	2.698
30	ZN	64	-47.127	11.698	8.217	4.832	-7.145	-1.271
30	ZN	65	-47.119	8.360	8.848	5.107	-3.174	.462
30	ZN	66	-49.452	10.700	9.455	5.375	-4.875	-3.385
30	ZN	67	-48.552	7.468	10.070	5.766	-1.025	-1.594
30	ZN	68	-50.038	9.853	10.665	6.155	-2.788	-5.333
30	ZN	69	-48.386	6.715	11.265	6.653	.953	-3.490

TABLE 2

Atomic mass excesses and nuclear binding energies

30	ZN	70	-49.184	9.166	11.874	7.172	-.919	-7.191
30	ZN	71	-46.868	6.050	12.459	7.726	2.785	-5.256
30	ZN	72	-47.054	8.554	13.027	8.319	.872	-8.886
30	ZN	73	-44.181	5.495	13.598	8.923	4.505	-6.930
30	ZN	74	-43.819	8.005	14.152	9.524	2.572	-10.508
30	ZN	75	-40.434	4.983	14.709	10.168	6.154	-8.552
30	ZN	76	-39.546	7.479	15.248	10.763	4.222	-12.098
30	ZN	77	-35.653	4.475	15.791	11.383	7.771	-10.160
30	ZN	78	-34.226	6.940	16.317	11.937	5.857	-13.689
30	ZN	79	-29.798	3.940	16.846	12.501	9.390	-11.780
30	ZN	80	-27.791	6.360	17.358	12.986	7.506	-16.451
30	ZN	81	-21.632	2.209	17.877	12.327	12.178	-14.556
30	ZN	82	-17.869	4.604	18.378	11.609	10.308	-18.023
30	ZN	83	-11.144	1.643	18.883	12.094	13.779	-16.116
30	ZN	84	-6.814	4.037	19.371	12.543	11.898	-19.527
30	ZN	85	.435	1.119	19.863	13.044	15.312	-17.608
30	ZN	86	5.290	3.512	20.337	13.507	13.420	-20.962
30	ZN	87	13.021	.637	20.816	14.023	16.779	-19.033
30	ZN	88	18.361	3.028	21.278	14.501	14.876	-22.330
30	ZN	89	26.531	.197	21.744	15.032	18.178	-20.389
30	ZN	90	32.313	2.586	22.192	15.526	16.265	-23.629
30	ZN	91	40.881	-.201	22.646	16.074	19.510	-21.677
30	ZN	92	47.061	2.187	23.082	16.585	17.586	-24.860
30	ZN	93	55.983	-.555	23.523	17.150	20.774	-22.898
30	ZN	94	62.521	1.830	23.946	17.677	18.842	-26.025
30	ZN	95	71.756	-.868	24.375	18.259	21.974	-24.055
30	ZN	96	78.610	1.513	24.785	18.800	20.034	-27.127
30	ZN	97	88.120	-1.142	25.202	19.395	23.112	-25.153
	ATOM		M - A	NEUTRON	PROTON	ALPHA	Q BETA -	Q BETA +
31	GA	53	42.597	22.622	-5.033	5.710	-25.320	22.188
31	GA	54	32.283	18.681	-4.290	5.469	-20.693	23.657
31	GA	55	19.792	20.859	-3.581	5.133	-22.165	19.075
31	GA	56	11.158	17.002	-2.856	4.923	-17.634	20.544
31	GA	57	.361	19.164	-2.162	4.628	-19.105	16.065
31	GA	58	-6.666	15.394	-1.454	4.456	-14.673	17.547
31	GA	59	-15.853	17.555	-.775	4.217	-16.156	13.179
31	GA	60	-21.364	13.878	-.084	4.104	-11.830	14.691
31	GA	61	-29.049	16.053	.579	3.943	-13.342	9.230
31	GA	62	-33.160	12.478	2.466	3.913	-9.130	9.602
31	GA	63	-38.290	13.498	3.114	3.913	-9.502	5.506
31	GA	64	-39.982	10.059	3.771	4.042	-4.255	7.145
31	GA	65	-43.945	12.330	4.403	4.157	-5.892	3.174
31	GA	66	-44.577	8.999	5.043	4.401	-1.950	4.875
31	GA	67	-47.527	11.318	5.660	4.642	-3.649	1.025
31	GA	68	-47.250	8.090	6.283	5.003	.177	2.788
31	GA	69	-49.339	10.456	6.885	5.367	-1.584	-.953
31	GA	70	-48.266	7.294	7.465	5.808	2.191	.919
31	GA	71	-49.652	9.754	8.053	6.304	.321	-2.785
31	GA	72	-47.926	6.641	8.644	6.830	4.007	-.872
31	GA	73	-48.687	9.128	9.217	7.400	2.097	-4.505
31	GA	74	-46.391	6.072	9.794	8.007	5.712	-2.572
31	GA	75	-46.588	8.565	10.354	8.586	3.782	-6.154
31	GA	76	-43.767	5.546	10.918	9.208	7.346	-4.222
31	GA	77	-43.425	8.025	11.464	9.782	5.416	-7.771
31	GA	78	-40.083	5.025	12.014	10.382	8.948	-5.857
31	GA	79	-39.188	7.472	12.547	10.915	7.036	-9.390
31	GA	80	-35.297	4.477	13.084	11.459	10.550	-7.506
31	GA	81	-33.810	6.880	13.603	11.925	8.671	-12.178
31	GA	82	-28.177	2.735	14.130	11.249	13.321	-10.308
31	GA	83	-24.923	5.113	14.639	10.514	11.455	-13.779

TABLE 2

Atomic mass excesses and nuclear binding energies

31	GA	84	-18.712	2.156	15.152	10.981	14.906	-11.898
31	GA	85	-14.878	4.533	15.648	11.411	13.028	-15.312
31	GA	86	-8.130	1.620	16.149	11.893	16.423	-13.420
31	GA	87	-3.758	3.995	16.633	12.339	14.535	-16.779
31	GA	88	3.485	1.125	17.121	12.837	17.874	-14.876
31	GA	89	8.354	3.498	17.592	13.298	15.976	-18.178
31	GA	90	16.048	.673	18.068	13.814	19.259	-16.265
31	GA	91	21.371	3.044	18.526	14.292	17.350	-19.510
31	GA	92	29.475	.264	18.991	14.825	20.575	-17.586
31	GA	93	35.209	2.633	19.437	15.321	18.657	-20.774
31	GA	94	43.679	-.103	19.889	15.872	21.826	-18.842
31	GA	95	49.782	2.264	20.323	16.385	19.898	-21.974
31	GA	96	58.576	-.427	20.764	16.954	23.011	-20.034
31	GA	97	65.008	1.936	21.187	17.483	21.076	-23.112
31	GA	98	74.088	-.713	21.616	18.066	24.135	-21.168
31	GA	99	80.813	1.642	22.028	18.607	22.197	-24.194
31	GA	100	90.119	-.938	22.473	19.228	25.150	-22.305
	ATOM		M - A	NEUTRON	PROTON	ALPHA	Q BETA -	Q BETA +
32	GE	55	41.957	19.387	-2.089	5.164	-25.226	22.165
32	GE	56	28.792	21.532	-1.415	4.797	-26.651	17.634
32	GE	57	19.466	17.693	-.723	4.552	-22.122	19.105
32	GE	58	8.007	19.826	-.061	4.228	-23.549	14.673
32	GE	59	.303	16.072	.616	4.024	-19.119	16.156
32	GE	60	-9.533	18.204	1.265	3.757	-20.561	11.830
32	GE	61	-15.707	14.541	1.928	3.613	-16.236	13.342
32	GE	62	-24.029	16.689	2.565	3.426	-17.709	9.130
32	GE	63	-28.789	13.127	3.214	3.365	-13.498	9.502
32	GE	64	-35.727	15.306	5.022	3.282	-15.019	4.255
32	GE	65	-38.053	10.693	5.655	3.383	-9.771	5.892
32	GE	66	-42.627	12.942	6.267	3.475	-10.221	1.950
32	GE	67	-43.878	9.618	6.886	3.691	-6.277	3.649
32	GE	68	-47.427	11.916	7.485	3.910	-7.948	-.177
32	GE	69	-47.755	8.695	8.089	4.245	-4.121	1.584
32	GE	70	-50.457	11.069	8.703	4.614	-5.912	-2.191
32	GE	71	-49.974	7.884	9.293	5.031	-2.135	-.321
32	GE	72	-51.934	10.327	9.866	5.505	-3.983	-4.007
32	GE	73	-50.784	7.218	10.442	6.007	-.295	-2.097
32	GE	74	-52.103	9.687	11.002	6.528	-2.182	-5.712
32	GE	75	-50.370	6.635	11.564	7.112	1.435	-3.782
32	GE	76	-51.113	9.110	12.109	7.668	-.472	-7.346
32	GE	77	-48.841	6.095	12.659	8.269	3.094	-5.416
32	GE	78	-49.030	8.557	13.190	8.821	1.188	-8.948
32	GE	79	-46.224	5.561	13.726	9.399	4.722	-7.036
32	GE	80	-45.848	7.991	14.245	9.912	2.835	-10.550
32	GE	81	-42.480	5.000	14.768	10.436	6.352	-8.671
32	GE	82	-41.498	7.385	15.273	10.881	4.497	-13.321
32	GE	83	-36.377	3.247	15.785	10.188	9.148	-11.455
32	GE	84	-33.617	5.607	16.279	9.436	7.307	-14.906
32	GE	85	-27.906	2.656	16.779	9.883	10.761	-13.028
32	GE	86	-24.553	5.015	17.261	10.294	8.909	-16.423
32	GE	87	-18.293	2.107	17.748	10.758	12.307	-14.535
32	GE	88	-14.390	4.464	18.217	11.185	10.445	-17.874
32	GE	89	-7.622	1.600	18.692	11.666	13.787	-15.976
32	GE	90	-3.210	3.956	19.149	12.110	11.915	-19.259
32	GE	91	4.021	1.135	19.611	12.609	15.202	-17.350
32	GE	92	8.899	3.489	20.056	13.070	13.320	-20.575
32	GE	93	16.552	.714	20.507	13.588	16.550	-18.657
32	GE	94	21.853	3.066	20.940	14.069	14.659	-21.826
32	GE	95	29.884	.337	21.380	14.606	17.833	-19.898
32	GE	96	35.565	2.686	21.801	15.105	15.934	-23.011

TABLE 2

Atomic mass excesses and nuclear binding energies

32	GE	97	43.932	.001	22.229	15.661	19.051	-21.076
32	GE	98	49.953	2.346	22.640	16.177	17.146	-24.135
32	GE	99	58.616	-.296	23.057	16.749	20.210	-22.197
32	GE	100	64.969	2.015	23.429	17.250	18.356	-25.150
32	GE	101	73.868	-.532	23.835	17.860	21.314	-23.266
32	GE	102	80.495	1.740	24.224	18.370	19.461	-26.173
32	GE	103	89.632	-.770	24.620	18.984	22.373	-24.294
	ATOM		M - A	NEUTRON	PROTON	ALPHA	Q BETA -	Q BETA +
33	AS	57	41.588	22.222	-5.212	4.618	-25.113	22.122
33	AS	58	31.556	18.399	-4.506	4.337	-20.633	23.549
33	AS	59	19.422	20.502	-3.830	3.980	-22.061	19.119
33	AS	60	11.027	16.762	-3.139	3.740	-17.675	20.561
33	AS	61	.528	18.866	-2.477	3.442	-19.118	16.236
33	AS	62	-6.320	15.216	-1.802	3.264	-14.832	17.709
33	AS	63	-15.291	17.338	-1.154	3.047	-16.306	13.498
33	AS	64	-20.708	13.785	-.495	2.954	-12.129	15.019
33	AS	65	-28.282	15.941	.139	2.842	-13.650	9.771
33	AS	66	-32.406	12.492	1.939	2.856	-9.588	10.221
33	AS	67	-37.601	13.562	2.559	2.920	-10.037	6.277
33	AS	68	-39.479	10.245	3.185	3.106	-4.987	7.948
33	AS	69	-43.634	12.523	3.792	3.298	-6.658	4.121
33	AS	70	-44.545	9.278	4.375	3.577	-2.796	5.912
33	AS	71	-47.839	11.661	4.967	3.921	-4.586	2.135
33	AS	72	-47.951	8.480	5.562	4.310	-.828	3.983
33	AS	73	-50.489	10.906	6.140	4.760	-2.673	.295
33	AS	74	-49.921	7.799	6.722	5.265	.996	2.182
33	AS	75	-51.806	10.252	7.287	5.762	-.890	-1.435
33	AS	76	-50.641	7.203	7.856	6.324	2.709	.472
33	AS	77	-51.935	9.661	8.407	6.858	.804	-3.094
33	AS	78	-50.219	6.651	8.963	7.437	4.351	-1.188
33	AS	79	-50.947	9.095	9.501	7.967	2.447	-4.722
33	AS	80	-48.683	6.104	10.044	8.525	5.962	-2.835
33	AS	81	-48.832	8.517	10.569	9.017	4.077	-6.352
33	AS	82	-45.995	5.530	11.100	9.521	7.575	-4.497
33	AS	83	-45.526	7.898	11.613	9.947	5.722	-9.148
33	AS	84	-40.924	3.766	12.132	9.236	10.353	-7.307
33	AS	85	-38.667	6.110	12.634	8.466	8.514	-10.761
33	AS	86	-33.462	3.163	13.141	8.894	11.948	-8.909
33	AS	87	-30.600	5.505	13.631	9.286	10.098	-12.307
33	AS	88	-24.834	2.602	14.126	9.732	13.476	-10.445
33	AS	89	-21.410	4.942	14.605	10.141	11.617	-13.787
33	AS	90	-15.126	2.084	15.088	10.605	14.939	-11.915
33	AS	91	-11.180	4.422	15.555	11.032	13.070	-15.202
33	AS	92	-4.421	1.608	16.027	11.515	16.336	-13.320
33	AS	93	.002	3.944	16.482	11.960	14.458	-16.550
33	AS	94	7.194	1.176	16.943	12.463	17.668	-14.659
33	AS	95	12.051	3.510	17.387	12.929	15.781	-17.833
33	AS	96	19.632	.787	17.837	13.452	18.934	-15.934
33	AS	97	24.880	3.119	18.270	13.938	17.039	-19.051
33	AS	98	32.807	.441	18.709	14.481	20.136	-17.146
33	AS	99	38.407	2.768	19.131	14.985	18.236	-20.210
33	AS	100	46.613	.161	19.588	15.572	21.225	-18.356
33	AS	101	52.554	2.426	20.000	16.063	19.376	-21.314
33	AS	102	61.035	-.113	20.419	16.663	22.315	-19.461
33	AS	103	67.260	2.142	20.820	17.162	20.466	-22.373
33	AS	104	75.988	-.361	21.229	17.740	23.360	-20.524
33	AS	105	82.476	1.880	21.621	18.268	21.516	-23.395
33	AS	106	91.435	-.592	22.020	18.842	24.370	-21.555
33	AS	107	98.173	1.630	22.403	19.363	22.535	-24.392
33	AS	108	107.357	-.817	22.792	19.923	25.356	-22.566

TABLE 2

Atomic mass excesses and nuclear binding energies

ATOM			M - A	NEUTRON	PROTON	ALPHA	Q BETA -	Q BETA +
34	SE	59	41.483	19.073	-2.342	4.083	-24.979	22.061
34	SE	60	28.702	21.149	-1.695	3.699	-26.367	17.675
34	SE	61	19.646	17.423	-1.034	3.429	-21.983	19.118
34	SE	62	8.512	19.502	-.399	3.105	-23.389	14.832
34	SE	63	1.015	15.864	.249	2.897	-19.104	16.306
34	SE	64	-8.579	17.962	.874	2.655	-20.545	12.129
34	SE	65	-14.632	14.420	1.508	2.534	-16.369	13.650
34	SE	66	-22.818	16.553	2.121	2.398	-17.860	9.588
34	SE	67	-27.564	13.113	2.742	2.385	-13.798	10.037
34	SE	68	-34.491	15.295	4.475	2.373	-15.352	4.987
34	SE	69	-36.976	10.852	5.082	2.533	-10.301	6.658
34	SE	70	-41.748	13.139	5.699	2.730	-10.896	2.796
34	SE	71	-43.253	9.872	6.293	2.984	-7.034	4.586
34	SE	72	-47.123	12.238	6.869	3.305	-8.802	.828
34	SE	73	-47.816	9.060	7.450	3.670	-5.042	2.673
34	SE	74	-50.917	11.469	8.013	4.070	-6.866	-.996
34	SE	75	-50.916	8.366	8.579	4.551	-3.195	.890
34	SE	76	-53.350	10.801	9.129	5.025	-5.058	-2.709
34	SE	77	-52.739	7.757	9.683	5.564	-1.458	-.804
34	SE	78	-54.570	10.198	10.219	6.076	-3.339	-4.351
34	SE	79	-53.394	7.192	10.760	6.633	.209	-2.447
34	SE	80	-54.645	9.619	11.283	7.141	-1.671	-5.962
34	SE	81	-52.910	6.632	11.811	7.678	1.846	-4.077
34	SE	82	-53.570	9.027	12.322	8.149	-.014	-7.575
34	SE	83	-51.248	6.046	12.838	8.633	3.485	-5.722
34	SE	84	-51.277	8.397	13.336	9.039	1.657	-10.353
34	SE	85	-47.180	4.270	13.841	8.309	6.289	-8.514
34	SE	86	-45.410	6.597	14.328	7.521	4.475	-11.948
34	SE	87	-40.698	3.655	14.820	7.929	7.910	-10.098
34	SE	88	-38.310	5.980	15.295	8.302	6.086	-13.476
34	SE	89	-33.026	3.083	15.776	8.730	9.466	-11.617
34	SE	90	-30.065	5.406	16.240	9.120	7.632	-14.939
34	SE	91	-24.250	2.553	16.709	9.567	10.957	-13.070
34	SE	92	-20.757	4.874	17.161	9.976	9.115	-16.336
34	SE	93	-14.456	2.066	17.620	10.443	12.384	-14.458
34	SE	94	-10.474	4.385	18.061	10.872	10.533	-17.668
34	SE	95	-3.729	1.623	18.508	11.360	13.745	-15.781
34	SE	96	.698	3.940	18.938	11.811	11.886	-18.934
34	SE	97	7.841	1.224	19.375	12.320	15.043	-17.039
34	SE	98	12.671	3.538	19.795	12.792	13.176	-20.136
34	SE	99	20.171	.867	20.221	13.323	16.278	-18.236
34	SE	100	25.388	3.150	20.603	13.787	14.460	-21.225
34	SE	101	33.178	.577	21.020	14.363	17.454	-19.376
34	SE	102	38.720	2.826	21.419	14.843	15.634	-22.315
34	SE	103	46.794	.294	21.826	15.432	18.577	-20.466
34	SE	104	52.629	2.532	22.216	15.950	16.757	-23.360
34	SE	105	60.960	.036	22.613	16.518	19.655	-21.516
34	SE	106	67.066	2.261	22.995	17.039	17.840	-24.370
34	SE	107	75.637	-.204	23.383	17.604	20.699	-22.535
34	SE	108	82.002	2.003	23.756	18.119	18.892	-25.356
34	SE	109	90.807	-.438	24.135	18.673	21.718	-23.535
34	SE	110	97.427	1.747	24.500	19.172	19.925	-26.328
34	SE	111	106.470	-.675	24.871	19.704	22.723	-24.526
ATOM			M - A	NEUTRON	PROTON	ALPHA	Q BETA -	Q BETA +
35	BR	60	55.069	19.760	-6.002	3.983	-23.434	26.367
35	BR	61	41.629	21.808	-5.342	3.569	-24.826	21.983
35	BR	62	31.901	18.095	-4.670	3.265	-20.481	23.389
35	BR	63	20.119	20.149	-4.023	2.911	-21.889	19.104

TABLE 2

Atomic mass excesses and nuclear binding energies

35	BR	64	11.966	16.521	-3.366	2.671	-17.639	20.545
35	BR	65	1.737	18.596	-2.731	2.401	-19.081	16.369
35	BR	66	-4.958	15.062	-2.089	2.247	-14.935	17.860
35	BR	67	-13.766	17.175	-1.467	2.084	-16.426	13.798
35	BR	68	-19.139	13.741	-.840	2.040	-12.391	15.352
35	BR	69	-26.675	15.903	-.232	2.003	-13.945	10.301
35	BR	70	-30.852	12.544	1.461	2.055	-9.968	10.896
35	BR	71	-36.219	13.734	2.055	2.227	-10.563	7.034
35	BR	72	-38.322	10.470	2.654	2.452	-5.636	8.802
35	BR	73	-42.774	12.820	3.235	2.749	-7.403	5.042
35	BR	74	-44.052	9.645	3.820	3.116	-3.662	6.866
35	BR	75	-47.721	12.037	4.389	3.492	-5.485	3.195
35	BR	76	-48.292	8.938	4.961	3.950	-1.833	5.058
35	BR	77	-51.281	11.356	5.516	4.401	-3.695	1.458
35	BR	78	-51.230	8.316	6.076	4.918	-.114	3.339
35	BR	79	-53.603	10.740	6.618	5.407	-1.994	-.209
35	BR	80	-52.974	7.739	7.165	5.942	1.535	1.671
35	BR	81	-54.756	10.149	7.696	6.430	-.344	-1.846
35	BR	82	-53.555	7.167	8.230	6.946	3.153	.014
35	BR	83	-54.733	9.545	8.748	7.396	1.294	-3.485
35	BR	84	-52.934	6.568	9.271	7.860	4.774	-1.657
35	BR	85	-53.470	8.903	9.777	8.247	2.948	-6.289
35	BR	86	-49.884	4.782	10.289	7.499	7.559	-4.475
35	BR	87	-48.608	7.091	10.783	6.692	5.746	-7.910
35	BR	88	-44.396	4.156	11.283	7.081	9.161	-6.086
35	BR	89	-42.492	6.463	11.767	7.435	7.338	-9.466
35	BR	90	-37.697	3.572	12.256	7.844	10.698	-7.632
35	BR	91	-35.208	5.878	12.728	8.217	8.866	-10.957
35	BR	92	-29.872	3.031	13.206	8.646	12.170	-9.115
35	BR	93	-26.840	5.335	13.667	9.039	10.329	-12.384
35	BR	94	-21.006	2.534	14.135	9.490	13.577	-10.533
35	BR	95	-17.475	4.836	14.586	9.904	11.729	-13.745
35	BR	96	-11.188	2.081	15.044	10.377	14.920	-11.886
35	BR	97	-7.201	4.381	15.484	10.813	13.064	-15.043
35	BR	98	-.506	1.672	15.932	11.309	16.199	-13.176
35	BR	99	3.893	3.969	16.362	11.768	14.336	-16.278
35	BR	100	10.928	1.332	16.827	12.313	17.362	-14.460
35	BR	101	15.725	3.571	17.248	12.765	15.548	-17.454
35	BR	102	23.086	1.006	17.677	13.330	18.521	-15.634
35	BR	103	28.217	3.237	18.088	13.799	16.705	-18.577
35	BR	104	35.871	.713	18.507	14.351	19.629	-16.757
35	BR	105	41.304	2.935	18.909	14.859	17.814	-19.655
35	BR	106	49.226	.446	19.319	15.418	20.693	-17.840
35	BR	107	54.938	2.655	19.712	15.931	18.883	-20.699
35	BR	108	63.110	.196	20.112	16.488	21.724	-18.892
35	BR	109	69.089	2.388	20.497	16.996	19.922	-21.718
35	BR	110	77.503	-.046	20.889	17.542	22.731	-19.925
35	BR	111	83.747	2.124	21.265	18.035	20.943	-22.723
35	BR	112	92.406	-.292	21.648	18.561	23.726	-20.947
35	BR	113	98.921	1.852	22.017	19.030	21.956	-23.724
35	BR	114	107.838	-.549	22.392	19.527	24.718	-21.970
	ATOM		M - A	NEUTRON	PROTON	ALPHA	Q BETA -	Q BETA +
36	KR	63	42.008	18.741	-2.523	3.084	-24.656	21.889
36	KR	64	29.605	20.771	-1.900	2.706	-26.032	17.639
36	KR	65	20.817	17.155	-1.267	2.438	-21.783	19.081
36	KR	66	9.976	19.208	-.655	2.144	-23.196	14.935
36	KR	67	2.661	15.683	-.034	1.964	-19.051	16.426
36	KR	68	-6.748	17.776	.567	1.778	-20.517	12.391
36	KR	69	-12.730	14.349	1.176	1.708	-16.482	13.945
36	KR	70	-20.884	16.521	1.794	1.675	-18.068	9.968

TABLE 2

Atomic mass excesses and nuclear binding energies

36	KR	71	-25.656	13.140	2.389	1.702	-14.092	10.563
36	KR	72	-32.686	15.397	4.051	1.803	-15.749	5.636
36	KR	73	-35.371	11.053	4.634	2.004	-10.821	7.403
36	KR	74	-40.389	13.386	5.200	2.250	-11.506	3.662
36	KR	75	-42.236	10.215	5.770	2.593	-7.764	5.485
36	KR	76	-46.459	12.590	6.322	2.945	-9.565	1.833
36	KR	77	-47.587	9.495	6.879	3.380	-5.912	3.695
36	KR	78	-51.116	11.896	7.419	3.808	-7.751	.114
36	KR	79	-51.609	8.860	7.963	4.302	-4.169	1.994
36	KR	80	-54.509	11.268	8.491	4.768	-6.026	-1.535
36	KR	81	-54.412	8.270	9.022	5.282	-2.496	.344
36	KR	82	-56.708	10.664	9.537	5.748	-4.351	-3.153
36	KR	83	-56.028	7.687	10.057	6.243	-.852	-1.294
36	KR	84	-57.708	10.048	10.560	6.672	-2.687	-4.774
36	KR	85	-56.417	7.076	11.068	7.117	.794	-2.948
36	KR	86	-57.444	9.394	11.559	7.483	-1.008	-7.559
36	KR	87	-54.354	5.278	12.055	6.716	3.606	-5.746
36	KR	88	-53.557	7.570	12.534	5.889	1.817	-9.161
36	KR	89	-49.831	4.641	13.019	6.259	5.233	-7.338
36	KR	90	-48.395	6.931	13.487	6.594	3.435	-10.698
36	KR	91	-44.073	4.046	13.961	6.985	6.796	-8.866
36	KR	92	-42.041	6.335	14.418	7.340	4.990	-12.170
36	KR	93	-37.169	3.495	14.882	7.752	8.296	-10.329
36	KR	94	-34.583	5.782	15.329	8.128	6.481	-13.577
36	KR	95	-29.204	2.987	15.782	8.562	9.732	-11.729
36	KR	96	-26.108	5.272	16.218	8.961	7.910	-14.920
36	KR	97	-20.265	2.524	16.662	9.419	11.104	-13.064
36	KR	98	-16.705	4.807	17.088	9.841	9.274	-16.199
36	KR	99	-10.443	2.106	17.522	10.323	12.413	-14.336
36	KR	100	-6.434	4.358	17.912	10.741	10.632	-17.362
36	KR	101	.176	1.757	18.337	11.274	13.661	-15.548
36	KR	102	4.565	3.978	18.744	11.715	11.875	-18.521
36	KR	103	11.511	1.421	19.160	12.268	14.851	-16.705
36	KR	104	16.242	3.636	19.559	12.755	13.063	-19.629
36	KR	105	23.491	1.119	19.966	13.297	15.991	-17.814
36	KR	106	28.532	3.325	20.357	13.797	14.203	-20.693
36	KR	107	36.056	.844	20.755	14.347	17.087	-18.883
36	KR	108	41.386	3.038	21.138	14.852	15.303	-21.724
36	KR	109	49.167	.586	21.527	15.402	18.149	-19.922
36	KR	110	54.771	2.763	21.903	15.903	16.373	-22.731
36	KR	111	62.803	.336	22.284	16.443	19.187	-20.943
36	KR	112	68.680	2.491	22.652	16.931	17.425	-23.726
36	KR	113	76.965	.082	23.026	17.451	20.213	-21.956
36	KR	114	83.120	2.212	23.386	17.917	18.468	-24.718
36	KR	115	91.670	-.183	23.752	18.409	21.235	-22.969
	ATOM		M - A	NEUTRON	PROTON	ALPHA	Q BETA -	Q BETA +
37	RB	64	55.636	19.395	-6.043	3.042	-23.096	26.032
37	RB	65	42.601	21.403	-5.411	2.637	-24.474	21.783
37	RB	66	33.173	17.796	-4.770	2.337	-20.257	23.196
37	RB	67	21.712	19.828	-4.150	2.017	-21.671	19.051
37	RB	68	13.769	16.310	-3.523	1.806	-17.553	20.517
37	RB	69	3.752	18.384	-2.915	1.594	-19.020	16.482
37	RB	70	-2.816	14.935	-2.330	1.466	-14.953	18.068
37	RB	71	-11.565	17.117	-1.734	1.408	-16.539	14.092
37	RB	72	-16.937	13.740	-1.135	1.407	-12.583	15.749
37	RB	73	-24.550	15.980	-.551	1.484	-14.240	10.821
37	RB	74	-28.883	12.701	1.097	1.640	-10.394	11.506
37	RB	75	-34.472	13.956	1.668	1.862	-11.078	7.764
37	RB	76	-36.894	10.789	2.242	2.182	-6.317	9.565
37	RB	77	-41.675	13.148	2.800	2.510	-8.116	5.912

TABLE 2

Atomic mass excesses and nuclear binding energies

37	RB	78	-43.365	10.058	3.363	2.923	-4.483	7.751
37	RB	79	-47.439	12.442	3.908	3.327	-6.321	4.169
37	RB	80	-48.483	9.410	4.459	3.800	-2.760	6.026
37	RB	81	-51.916	11.801	4.992	4.244	-4.616	2.496
37	RB	82	-52.358	8.809	5.530	4.737	-1.106	4.351
37	RB	83	-55.175	11.185	6.052	5.181	-2.959	.852
37	RB	84	-55.021	8.213	6.578	5.656	.518	2.687
37	RB	85	-57.211	10.558	7.088	6.065	-1.315	-.794
37	RB	86	-56.436	7.592	7.603	6.490	2.145	1.008
37	RB	87	-57.960	9.892	8.101	6.836	.345	-3.606
37	RB	88	-55.375	5.782	8.605	6.049	4.939	-1.817
37	RB	89	-55.064	8.057	9.091	5.204	3.151	-5.233
37	RB	90	-51.830	5.133	9.584	5.555	6.546	-3.435
37	RB	91	-50.870	7.407	10.060	5.871	4.749	-6.796
37	RB	92	-47.031	4.529	10.543	6.244	8.088	-4.990
37	RB	93	-45.465	6.801	11.008	6.582	6.283	-8.296
37	RB	94	-41.065	3.968	11.481	6.977	9.567	-6.481
37	RB	95	-38.935	6.238	11.936	7.337	7.754	-9.732
37	RB	96	-34.018	3.450	12.399	7.756	10.982	-7.910
37	RB	97	-31.369	5.718	12.845	8.139	9.162	-11.104
37	RB	98	-25.979	2.978	13.299	8.583	12.334	-9.274
37	RB	99	-22.856	5.244	13.736	8.990	10.507	-12.413
37	RB	100	-17.066	2.577	14.207	9.487	13.569	-10.632
37	RB	101	-13.485	4.786	14.635	9.892	11.790	-13.661
37	RB	102	-7.310	2.193	15.071	10.413	14.798	-11.875
37	RB	103	-3.340	4.398	15.490	10.842	13.015	-14.851
37	RB	104	3.179	1.848	15.917	11.358	15.971	-13.063
37	RB	105	7.500	4.047	16.327	11.834	14.186	-15.991
37	RB	106	14.330	1.537	16.746	12.366	17.094	-14.203
37	RB	107	18.969	3.728	17.148	12.857	15.310	-17.087
37	RB	108	26.083	1.254	17.558	13.398	18.175	-15.303
37	RB	109	31.018	3.432	17.952	13.895	16.395	-18.149
37	RB	110	38.398	.988	18.353	14.437	19.224	-16.373
37	RB	111	43.616	3.149	18.740	14.932	17.453	-19.187
37	RB	112	51.255	.729	19.133	15.464	20.250	-17.425
37	RB	113	56.752	2.870	19.513	15.947	18.493	-20.213
37	RB	114	64.652	.468	19.898	16.461	21.265	-18.468
37	RB	115	70.435	2.584	20.270	16.921	19.526	-21.235
37	RB	116	78.608	.195	20.647	17.407	22.278	-19.511
37	RB	117	84.692	2.283	21.011	17.838	20.559	-22.262
37	RB	118	93.157	-.098	21.381	18.290	23.296	-20.560
37	RB	119	99.564	1.961	21.738	18.685	21.600	-24.714
37	RB	120	109.776	-1.844	22.087	17.667	25.755	-23.003
37	RB	121	117.941	.202	22.422	16.611	24.040	-25.678
	ATOM		M - A	NEUTRON	PROTON	ALPHA	Q BETA -	Q BETA +
38	SR	67	43.383	18.414	-2.625	2.235	-24.285	21.671
38	SR	68	31.322	20.428	-2.025	1.892	-25.675	17.553
38	SR	69	22.772	16.918	-1.418	1.655	-21.558	19.020
38	SR	70	12.137	19.002	-.801	1.448	-23.057	14.953
38	SR	71	4.974	15.530	-.205	1.295	-18.991	16.539
38	SR	72	-4.354	17.696	.374	1.215	-20.558	12.583
38	SR	73	-10.310	14.323	.957	1.189	-16.601	14.240
38	SR	74	-18.489	16.547	1.525	1.215	-18.238	10.394
38	SR	75	-23.394	13.272	2.096	1.347	-14.391	11.078
38	SR	76	-30.577	15.551	3.690	1.501	-16.094	6.317
38	SR	77	-33.559	11.348	4.249	1.797	-11.332	8.116
38	SR	78	-38.881	13.690	4.791	2.101	-12.091	4.483
38	SR	79	-41.118	10.604	5.338	2.491	-8.457	6.321
38	SR	80	-45.723	12.972	5.868	2.873	-10.272	2.760
38	SR	81	-47.301	9.945	6.403	3.323	-6.710	4.616

TABLE 2

Atomic mass excesses and nuclear binding energies

38	SR	82	-51.252	12.319	6.920	3.745	-8.543	1.106
38	SR	83	-52.216	9.331	7.443	4.217	-5.032	2.959
38	SR	84	-55.540	11.691	7.949	4.640	-6.862	-.518
38	SR	85	-55.897	8.724	8.460	5.094	-3.383	1.315
38	SR	86	-58.581	11.052	8.955	5.482	-5.192	-2.145
38	SR	87	-58.306	8.092	9.455	5.887	-1.731	-.345
38	SR	88	-60.313	10.375	9.938	6.214	-3.507	-4.939
38	SR	89	-58.215	6.269	10.425	5.407	1.090	-3.151
38	SR	90	-58.376	8.528	10.896	4.541	-.674	-6.546
38	SR	91	-55.619	5.611	11.374	4.874	2.722	-4.749
38	SR	92	-55.119	7.868	11.834	5.171	.950	-8.088
38	SR	93	-51.748	4.996	12.301	5.526	4.290	-6.283
38	SR	94	-50.631	7.251	12.751	5.846	2.510	-9.567
38	SR	95	-46.689	4.425	13.209	6.225	5.795	-7.754
38	SR	96	-45.000	6.678	13.650	6.568	4.008	-10.982
38	SR	97	-40.531	3.898	14.098	6.971	7.238	-9.162
38	SR	98	-38.313	6.150	14.529	7.339	5.444	-12.334
38	SR	99	-33.363	3.417	14.968	7.769	8.618	-10.507
38	SR	100	-30.635	5.639	15.363	8.135	6.872	-13.569
38	SR	101	-25.275	3.008	15.794	8.619	9.936	-11.790
38	SR	102	-22.108	5.200	16.208	9.012	8.185	-14.798
38	SR	103	-16.355	2.615	16.630	9.521	11.195	-13.015
38	SR	104	-12.791	4.804	17.036	9.966	9.439	-15.971
38	SR	105	-6.686	2.262	17.450	10.471	12.397	-14.186
38	SR	106	-2.764	4.445	17.849	10.939	10.638	-17.094
38	SR	107	3.660	1.944	18.255	11.461	13.550	-15.310
38	SR	108	7.908	4.119	18.646	11.944	11.791	-18.175
38	SR	109	14.623	1.652	19.045	12.477	14.660	-16.395
38	SR	110	19.175	3.816	19.429	12.967	12.906	-19.224
38	SR	111	26.163	1.379	19.820	13.502	15.738	-17.453
38	SR	112	31.004	3.526	20.197	13.991	13.992	-20.250
38	SR	113	38.259	1.113	20.580	14.517	16.794	-18.493
38	SR	114	43.386	3.240	20.950	14.995	15.061	-21.265
38	SR	115	50.909	.844	21.327	15.503	17.838	-19.526
38	SR	116	56.330	2.947	21.690	15.959	16.122	-22.278
38	SR	117	64.133	.564	22.060	16.441	18.880	-20.559
38	SR	118	69.861	2.639	22.416	16.868	17.184	-23.296
38	SR	119	77.964	.265	22.778	17.316	19.926	-21.600
38	SR	120	84.021	2.311	23.128	17.708	18.253	-25.755
38	SR	121	93.901	-1.513	23.460	16.662	22.437	-24.040
38	SR	122	101.747	.522	23.779	15.580	20.735	-26.693
38	SR	123	111.920	-1.806	24.104	15.966	23.384	-24.966
38	SR	124	120.053	.235	24.418	16.335	21.669	-27.575
38	SR	125	130.475	-2.055	24.737	16.753	24.273	-25.837
38	SR	126	138.851	-.008	25.046	17.153	22.546	-28.404
	ATOM		M - A	NEUTRON	PROTON	ALPHA	Q BETA -	Q BETA +
39	Y	68	56.996	19.039	-6.029	2.249	-22.705	25.675
39	Y	69	44.329	21.035	-5.423	1.881	-24.096	21.558
39	Y	70	35.195	17.502	-4.838	1.587	-19.948	23.057
39	Y	71	23.965	19.596	-4.243	1.355	-21.448	18.991
39	Y	72	16.203	16.130	-3.644	1.175	-17.403	20.558
39	Y	73	6.291	18.279	-3.061	1.070	-18.970	16.601
39	Y	74	-.252	14.911	-2.473	1.045	-15.035	18.238
39	Y	75	-9.003	17.118	-1.902	1.047	-16.671	14.391
39	Y	76	-14.484	13.848	-1.326	1.156	-12.846	16.094
39	Y	77	-22.226	16.110	-.766	1.286	-14.548	11.332
39	Y	78	-26.791	12.931	.817	1.517	-10.826	12.091
39	Y	79	-32.661	14.238	1.364	1.798	-11.584	8.457
39	Y	80	-35.450	11.157	1.917	2.166	-6.972	10.272
39	Y	81	-40.591	13.508	2.453	2.525	-8.786	6.710

TABLE 2

Atomic mass excesses and nuclear binding energies

39	Y	82	-42.709	10.486	2.993	2.953	-5.245	8.543
39	Y	83	-47.184	12.843	3.517	3.354	-7.077	5.032
39	Y	84	-48.678	9.861	4.047	3.804	-3.587	6.862
39	Y	85	-52.514	12.203	4.559	4.207	-5.416	3.383
39	Y	86	-53.389	9.243	5.077	4.641	-1.958	5.192
39	Y	87	-56.575	11.553	5.578	5.009	-3.766	1.731
39	Y	88	-56.807	8.599	6.086	5.395	-.326	3.507
39	Y	89	-59.305	10.866	6.576	5.703	-2.101	-1.090
39	Y	90	-57.702	6.764	7.071	4.875	2.475	.674
39	Y	91	-58.341	9.006	7.550	3.989	.713	-2.722
39	Y	92	-56.069	6.096	8.035	4.304	4.085	-.950
39	Y	93	-56.038	8.336	8.503	4.583	2.314	-4.290
39	Y	94	-53.142	5.471	8.979	4.921	5.632	-2.510
39	Y	95	-52.484	7.710	9.438	5.223	3.853	-5.795
39	Y	96	-49.008	4.891	9.904	5.586	7.115	-4.008
39	Y	97	-47.769	7.128	10.354	5.913	5.330	-7.238
39	Y	98	-43.757	4.356	10.811	6.302	8.536	-5.444
39	Y	99	-41.981	6.591	11.252	6.655	6.744	-8.618
39	Y	100	-37.507	3.893	11.729	7.098	9.840	-6.872
39	Y	101	-35.211	6.072	12.161	7.451	8.096	-9.936
39	Y	102	-30.292	3.449	12.602	7.922	11.138	-8.185
39	Y	103	-27.550	5.625	13.027	8.303	9.388	-11.195
39	Y	104	-22.230	3.048	13.460	8.773	12.376	-9.439
39	Y	105	-19.083	5.221	13.877	9.208	10.623	-12.397
39	Y	106	-13.403	2.687	14.301	9.702	13.561	-10.638
39	Y	107	-9.890	4.855	14.711	10.159	11.805	-13.550
39	Y	108	-3.883	2.361	15.128	10.672	14.697	-11.791
39	Y	109	-.037	4.521	15.530	11.146	12.941	-14.660
39	Y	110	6.269	2.062	15.939	11.670	15.792	-12.906
39	Y	111	10.425	4.211	16.334	12.153	14.041	-15.738
39	Y	112	17.012	1.781	16.736	12.680	16.856	-13.992
39	Y	113	21.465	3.914	17.124	13.163	15.114	-16.794
39	Y	114	28.325	1.507	17.519	13.682	17.900	-15.061
39	Y	115	33.071	3.621	17.900	14.154	16.171	-17.838
39	Y	116	40.207	1.231	18.287	14.657	18.933	-16.122
39	Y	117	45.253	3.321	18.661	15.108	17.221	-18.880
39	Y	118	52.677	.944	19.041	15.584	19.964	-17.184
39	Y	119	58.037	3.007	19.408	16.007	18.273	-19.926
39	Y	120	65.768	.637	19.781	16.449	21.002	-18.253
39	Y	121	71.464	2.671	20.141	16.837	19.334	-22.437
39	Y	122	81.012	-1.180	20.474	15.755	23.538	-20.735
39	Y	123	88.537	.842	20.795	14.637	21.832	-23.384
39	Y	124	98.385	-1.481	21.121	15.000	24.460	-21.669
39	Y	125	106.203	.549	21.435	15.348	22.741	-24.273
39	Y	126	116.305	-1.735	21.755	15.744	25.325	-22.546
39	Y	127	124.371	.301	22.065	16.125	23.595	-25.110
39	Y	128	134.686	-1.948	22.379	16.551	26.139	-23.375
39	Y	129	142.961	.092	22.684	16.960	24.400	-25.902
	ATOM		M - A	NEUTRON	PROTON	ALPHA	Q BETA -	Q BETA +
40	ZR	70	55.142	21.650	-3.228	1.897	-28.059	19.948
40	ZR	71	45.414	18.096	-2.635	1.578	-23.913	21.448
40	ZR	72	33.607	20.175	-2.056	1.324	-25.394	17.403
40	ZR	73	25.262	16.712	-1.474	1.119	-21.350	18.970
40	ZR	74	14.783	18.846	-.907	.964	-22.897	15.035
40	ZR	75	7.668	15.482	-.335	.915	-18.962	16.671
40	ZR	76	-1.638	17.674	.220	.893	-20.578	12.846
40	ZR	77	-7.678	14.408	.780	.978	-16.752	14.548
40	ZR	78	-15.965	16.654	1.323	1.084	-18.433	10.826
40	ZR	79	-21.077	13.480	1.871	1.292	-14.711	11.584
40	ZR	80	-28.478	15.769	3.402	1.510	-16.446	6.972

TABLE 2

Atomic mass excesses and nuclear binding energies

40	ZR	81	-31.804	11.693	3.939	1.855	-11.834	8.786
40	ZR	82	-37.464	14.027	4.458	2.192	-12.646	5.245
40	ZR	83	-40.108	11.011	4.983	2.599	-9.103	7.077
40	ZR	84	-45.091	13.351	5.491	2.978	-10.912	3.587
40	ZR	85	-47.098	10.374	6.005	3.407	-7.421	5.416
40	ZR	86	-51.431	12.700	6.502	3.788	-9.227	1.958
40	ZR	87	-52.809	9.745	7.004	4.202	-5.768	3.766
40	ZR	88	-56.480	12.039	7.490	4.550	-7.552	.326
40	ZR	89	-57.204	9.091	7.982	4.916	-4.111	2.101
40	ZR	90	-60.177	11.341	8.457	5.205	-5.862	-2.475
40	ZR	91	-59.053	7.244	8.936	4.357	-1.282	-.713
40	ZR	92	-60.154	9.469	9.398	3.450	-3.020	-4.085
40	ZR	93	-58.352	6.565	9.868	3.746	.353	-2.314
40	ZR	94	-58.773	8.789	10.321	4.007	-1.393	-5.632
40	ZR	95	-56.337	5.931	10.780	4.328	1.925	-3.853
40	ZR	96	-56.123	8.153	11.224	4.613	.171	-7.115
40	ZR	97	-53.098	5.342	11.675	4.960	3.434	-5.330
40	ZR	98	-52.293	7.562	12.109	5.271	1.674	-8.536
40	ZR	99	-48.725	4.799	12.552	5.645	4.882	-6.744
40	ZR	100	-47.347	6.990	12.951	5.956	3.170	-9.840
40	ZR	101	-43.307	4.328	13.385	6.386	6.268	-8.096
40	ZR	102	-41.430	6.490	13.804	6.726	4.550	-11.138
40	ZR	103	-36.938	3.875	14.230	7.184	7.593	-9.388
40	ZR	104	-34.606	6.036	14.641	7.581	5.869	-12.376
40	ZR	105	-29.706	3.467	15.061	8.040	8.859	-10.623
40	ZR	106	-26.963	5.625	15.465	8.465	7.131	-13.561
40	ZR	107	-21.695	3.099	15.877	8.949	10.071	-11.805
40	ZR	108	-18.580	5.252	16.275	9.398	8.340	-14.697
40	ZR	109	-12.978	2.766	16.680	9.902	11.235	-12.941
40	ZR	110	-9.523	4.912	17.071	10.368	9.504	-15.792
40	ZR	111	-3.616	2.460	17.469	10.885	12.357	-14.041
40	ZR	112	.156	4.596	17.854	11.361	10.630	-16.856
40	ZR	113	6.351	2.172	18.246	11.881	13.449	-15.114
40	ZR	114	10.426	4.293	18.624	12.358	11.730	-17.900
40	ZR	115	16.901	1.892	19.009	12.872	14.519	-16.171
40	ZR	116	21.275	3.993	19.381	13.339	12.814	-18.933
40	ZR	117	28.032	1.610	19.760	13.836	15.579	-17.221
40	ZR	118	32.712	3.687	20.126	14.283	13.891	-19.964
40	ZR	119	39.764	1.316	20.497	14.754	16.638	-18.273
40	ZR	120	44.765	3.366	20.857	15.173	14.969	-21.002
40	ZR	121	52.130	1.002	21.222	15.612	17.703	-19.334
40	ZR	122	57.474	3.024	21.575	15.996	16.056	-23.538
40	ZR	123	66.705	-.863	21.892	14.868	20.306	-21.832
40	ZR	124	73.924	1.148	22.197	13.706	18.613	-24.460
40	ZR	125	83.462	-1.170	22.508	14.048	21.237	-22.741
40	ZR	126	90.980	.849	22.808	14.376	19.529	-25.325
40	ZR	127	100.776	-1.429	23.113	14.753	22.109	-23.595
40	ZR	128	108.547	.597	23.409	15.115	20.390	-26.139
40	ZR	129	118.561	-1.647	23.710	15.523	22.930	-24.400
40	ZR	130	126.545	.384	24.001	15.916	21.201	-26.909
40	ZR	131	136.740	-1.828	24.299	16.350	23.706	-25.166
40	ZR	132	144.903	.204	24.588	16.767	21.972	-27.646
	ATOM		M - A	NEUTRON	PROTON	ALPHA	Q BETA -	Q BETA +
41	NB	72	59.001	18.693	-6.002	1.605	-22.260	25.394
41	NB	73	46.612	20.757	-5.420	1.327	-23.743	21.350
41	NB	74	37.680	17.299	-4.833	1.124	-19.720	22.897
41	NB	75	26.630	19.417	-4.263	.944	-21.268	18.962
41	NB	76	18.940	16.058	-3.687	.873	-17.354	20.578
41	NB	77	9.074	18.233	-3.127	.827	-18.970	16.752
41	NB	78	2.469	14.973	-2.562	.889	-15.166	18.433

TABLE 2

Atomic mass excesses and nuclear binding energies

41	NB	79	-6.366	17.202	-2.014	.972	-16.847	14.711
41	NB	80	-12.032	14.033	-1.460	1.157	-13.146	16.446
41	NB	81	-19.970	16.306	-.923	1.353	-14.882	11.834
41	NB	82	-24.819	13.216	.599	1.637	-11.271	12.646
41	NB	83	-31.004	14.553	1.125	1.953	-12.082	9.103
41	NB	84	-34.179	11.542	1.656	2.338	-7.599	10.912
41	NB	85	-39.677	13.865	2.171	2.696	-9.407	7.421
41	NB	86	-42.204	10.894	2.691	3.104	-5.938	9.227
41	NB	87	-47.040	13.204	3.194	3.465	-7.742	5.768
41	NB	88	-48.928	10.255	3.704	3.859	-4.306	7.552
41	NB	89	-53.092	12.532	4.197	4.188	-6.089	4.111
41	NB	90	-54.315	9.590	4.696	4.535	-2.670	5.862
41	NB	91	-57.771	11.823	5.179	4.805	-4.420	1.282
41	NB	92	-57.134	7.730	5.666	3.936	.140	3.020
41	NB	93	-58.705	9.939	6.136	3.010	-1.598	-.353
41	NB	94	-57.380	7.042	6.613	3.287	1.753	1.393
41	NB	95	-58.262	9.250	7.074	3.531	.007	-1.925
41	NB	96	-56.295	6.400	7.542	3.835	3.302	-.171
41	NB	97	-56.533	8.605	7.994	4.104	1.549	-3.434
41	NB	98	-53.968	5.802	8.454	4.435	4.788	-1.674
41	NB	99	-53.606	8.006	8.898	4.732	3.029	-4.882
41	NB	100	-50.517	5.278	9.377	5.118	6.159	-3.170
41	NB	101	-49.575	7.426	9.813	5.416	4.448	-6.268
41	NB	102	-45.980	4.772	10.257	5.832	7.522	-4.550
41	NB	103	-44.531	6.918	10.686	6.159	5.806	-7.593
41	NB	104	-40.476	4.312	11.123	6.578	8.826	-5.869
41	NB	105	-38.565	6.457	11.544	6.964	7.104	-8.859
41	NB	106	-34.094	3.896	11.973	7.411	10.073	-7.131
41	NB	107	-31.766	6.039	12.388	7.826	8.346	-10.071
41	NB	108	-26.920	3.521	12.810	8.299	11.266	-8.340
41	NB	109	-24.213	5.660	13.218	8.739	9.537	-11.235
41	NB	110	-19.027	3.181	13.633	9.233	12.412	-9.504
41	NB	111	-15.973	5.314	14.035	9.692	10.683	-12.357
41	NB	112	-10.474	2.869	14.443	10.200	13.519	-10.630
41	NB	113	-7.098	4.991	14.838	10.670	11.794	-13.449
41	NB	114	-1.305	2.574	15.240	11.182	14.596	-11.730
41	NB	115	2.381	4.682	15.629	11.653	12.880	-14.519
41	NB	116	8.461	2.288	16.024	12.160	15.654	-12.814
41	NB	117	12.453	4.376	16.407	12.621	13.951	-15.579
41	NB	118	18.822	1.998	16.795	13.112	16.702	-13.891
41	NB	119	23.126	4.063	17.171	13.554	15.017	-16.638
41	NB	120	29.796	1.697	17.553	14.020	17.751	-14.969
41	NB	121	34.428	3.736	17.922	14.435	16.086	-17.703
41	NB	122	41.418	1.377	18.297	14.868	18.807	-16.056
41	NB	123	46.399	3.387	18.660	15.248	17.164	-20.306
41	NB	124	55.311	-.546	18.978	14.065	21.452	-18.613
41	NB	125	62.224	1.454	19.285	12.849	19.755	-21.237
41	NB	126	71.450	-.858	19.596	13.171	22.360	-19.529
41	NB	127	78.667	1.151	19.897	13.479	20.649	-22.109
41	NB	128	88.158	-1.123	20.204	13.836	23.210	-20.390
41	NB	129	95.632	.893	20.500	14.180	21.486	-22.930
41	NB	130	105.344	-1.345	20.802	14.570	24.008	-21.201
41	NB	131	113.034	.677	21.095	14.946	22.275	-23.706
41	NB	132	122.931	-1.529	21.394	15.365	24.763	-21.972
41	NB	133	130.803	.495	21.685	15.767	23.025	-24.448
41	NB	134	140.856	-1.685	21.980	16.207	25.485	-22.714
41	NB	135	148.886	.338	22.269	16.629	23.747	-25.167
41	NB	136	159.074	-1.821	22.563	17.084	26.184	-23.437
	ATOM		M - A	NEUTRON	PROTON	ALPHA	Q BETA -	Q BETA +
42	MO	74	57.400	21.322	-3.204	1.352	-27.615	19.720

TABLE 2

Atomic mass excesses and nuclear binding energies

42	MO	75	47.898	17.869	-2.633	1.125	-23.593	21.268
42	MO	76	36.294	19.971	-2.079	.922	-25.121	17.354
42	MO	77	28.044	16.617	-1.520	.827	-21.208	18.970
42	MO	78	17.635	18.777	-.976	.757	-22.803	15.166
42	MO	79	10.481	15.521	-.428	.796	-19.000	16.847
42	MO	80	1.115	17.734	.104	.857	-20.659	13.146
42	MO	81	-5.089	14.571	.642	1.019	-16.958	14.882
42	MO	82	-13.548	16.827	1.162	1.192	-18.672	11.271
42	MO	83	-18.923	13.742	1.689	1.455	-15.061	12.082
42	MO	84	-26.580	16.025	3.160	1.711	-16.811	7.599
42	MO	85	-30.270	12.057	3.676	2.075	-12.328	9.407
42	MO	86	-36.266	14.364	4.174	2.411	-13.168	5.938
42	MO	87	-39.298	11.399	4.679	2.800	-9.698	7.742
42	MO	88	-44.622	13.691	5.166	3.140	-11.479	4.306
42	MO	89	-47.003	10.748	5.660	3.514	-8.042	6.089
42	MO	90	-51.645	13.009	6.137	3.823	-9.801	2.670
42	MO	91	-53.351	10.074	6.621	4.152	-6.382	4.420
42	MO	92	-57.274	12.290	7.088	4.403	-8.107	-.140
42	MO	93	-57.108	8.201	7.558	3.513	-3.543	1.598
42	MO	94	-59.133	10.393	8.013	2.565	-5.256	-1.753
42	MO	95	-58.269	7.504	8.474	2.825	-1.905	-.007
42	MO	96	-59.596	9.695	8.919	3.051	-3.626	-3.302
42	MO	97	-58.082	6.853	9.372	3.339	-.331	-1.549
42	MO	98	-58.756	9.042	9.808	3.592	-2.058	-4.788
42	MO	99	-56.636	6.247	10.253	3.908	1.182	-3.029
42	MO	100	-56.676	8.407	10.654	4.162	-.498	-6.159
42	MO	101	-54.023	5.715	11.091	4.534	2.632	-4.448
42	MO	102	-53.502	7.846	11.512	4.818	.947	-7.522
42	MO	103	-50.337	5.202	11.941	5.221	4.022	-5.806
42	MO	104	-49.302	7.333	12.356	5.564	2.331	-8.826
42	MO	105	-45.669	4.735	12.778	5.971	5.352	-7.104
42	MO	106	-44.167	6.865	13.186	6.346	3.654	-10.073
42	MO	107	-40.112	4.313	13.602	6.783	6.625	-8.346
42	MO	108	-38.186	6.441	14.004	7.189	4.922	-11.266
42	MO	109	-33.750	3.931	14.414	7.653	7.843	-9.537
42	MO	110	-31.439	6.056	14.810	8.084	6.138	-12.412
42	MO	111	-26.656	3.585	15.214	8.571	9.015	-10.683
42	MO	112	-23.993	5.704	15.605	9.022	7.309	-13.519
42	MO	113	-18.892	3.267	16.003	9.523	10.147	-11.794
42	MO	114	-15.900	5.376	16.387	9.986	8.446	-14.596
42	MO	115	-10.499	2.966	16.779	10.492	11.250	-12.880
42	MO	116	-7.192	5.061	17.158	10.957	9.556	-15.654
42	MO	117	-1.498	2.673	17.544	11.459	12.333	-13.951
42	MO	118	2.120	4.749	17.918	11.915	10.652	-16.702
42	MO	119	8.109	2.378	18.298	12.401	13.406	-15.017
42	MO	120	12.045	4.431	18.666	12.839	11.743	-17.751
42	MO	121	18.342	2.071	19.039	13.300	14.480	-16.086
42	MO	122	22.612	4.098	19.401	13.710	12.836	-18.807
42	MO	123	29.235	1.744	19.768	14.139	15.561	-17.164
42	MO	124	33.859	3.743	20.124	14.515	13.938	-21.452
42	MO	125	42.469	-.242	20.427	13.270	18.288	-19.755
42	MO	126	49.090	1.747	20.719	11.993	16.604	-22.360
42	MO	127	58.018	-.561	21.017	12.296	19.206	-20.649
42	MO	128	64.948	1.438	21.304	12.586	17.505	-23.210
42	MO	129	74.146	-.831	21.597	12.925	20.063	-21.486
42	MO	130	81.336	1.177	21.880	13.253	18.349	-24.008
42	MO	131	90.759	-1.056	22.170	13.627	20.867	-22.275
42	MO	132	98.168	.958	22.451	13.988	19.144	-24.763
42	MO	133	107.778	-1.243	22.737	14.392	21.628	-23.025
42	MO	134	115.371	.774	23.017	14.782	19.899	-25.485
42	MO	135	125.139	-1.400	23.302	15.210	22.354	-23.747
42	MO	136	132.890	.616	23.580	15.622	20.625	-26.184

TABLE 2

Atomic mass excesses and nuclear binding energies

42	MO	137	142.794	-1.537	23.865	16.066	23.059	-24.451
42	MO	138	150.687	.475	24.144	16.493	21.333	-26.872
42	MO	139	160.716	-1.662	24.428	16.946	23.751	-25.148
	ATOM		M - A	NEUTRON	PROTON	ALPHA	Q BETA -	Q BETA +
43	TC	76	61.415	18.444	-5.932	1.195	-21.942	25.121
43	TC	77	49.252	20.530	-5.373	.968	-23.470	21.208
43	TC	78	40.438	17.181	-4.809	.851	-19.579	22.803
43	TC	79	29.481	19.325	-4.261	.758	-21.175	19.000
43	TC	80	21.774	16.075	-3.708	.775	-17.393	20.659
43	TC	81	11.870	18.272	-3.170	.813	-19.053	16.958
43	TC	82	5.124	15.113	-2.628	.954	-15.374	18.672
43	TC	83	-3.862	17.353	-2.101	1.105	-17.087	15.061
43	TC	84	-9.769	14.274	-1.569	1.346	-13.498	16.811
43	TC	85	-17.942	16.541	-1.053	1.581	-15.248	12.328
43	TC	86	-23.098	13.523	.413	1.889	-11.731	13.168
43	TC	87	-29.600	14.869	.918	2.205	-12.572	9.698
43	TC	88	-33.143	11.910	1.429	2.573	-8.196	11.479
43	TC	89	-38.961	14.186	1.924	2.893	-9.977	8.042
43	TC	90	-41.843	11.250	2.425	3.248	-6.562	9.801
43	TC	91	-46.970	13.494	2.910	3.538	-8.320	6.382
43	TC	92	-49.167	10.565	3.401	3.849	-4.923	8.107
43	TC	93	-53.565	12.765	3.876	4.082	-6.648	3.543
43	TC	94	-53.877	8.679	4.354	3.171	-2.103	5.256
43	TC	95	-56.364	10.855	4.816	2.203	-3.816	1.905
43	TC	96	-55.970	7.973	5.286	2.446	-.489	3.626
43	TC	97	-57.751	10.148	5.739	2.655	-2.209	.331
43	TC	98	-56.698	7.314	6.201	2.927	1.062	2.058
43	TC	99	-57.817	9.487	6.646	3.164	-.665	-1.182
43	TC	100	-56.178	6.728	7.127	3.492	2.496	.498
43	TC	101	-56.655	8.845	7.564	3.732	.817	-2.632
43	TC	102	-54.449	6.161	8.011	4.091	3.924	-.947
43	TC	103	-54.359	8.277	8.441	4.361	2.239	-4.022
43	TC	104	-51.632	5.641	8.881	4.725	5.291	-2.331
43	TC	105	-51.022	7.757	9.305	5.056	3.600	-5.352
43	TC	106	-47.821	5.167	9.737	5.451	6.600	-3.654
43	TC	107	-46.737	7.283	10.154	5.815	4.903	-6.625
43	TC	108	-43.108	4.738	10.580	6.241	7.852	-4.922
43	TC	109	-41.593	6.853	10.992	6.637	6.150	-7.843
43	TC	110	-37.576	4.351	11.412	7.091	9.052	-6.138
43	TC	111	-35.671	6.462	11.817	7.514	7.348	-9.015
43	TC	112	-31.302	3.999	12.231	7.992	10.206	-7.309
43	TC	113	-29.039	6.104	12.631	8.436	8.502	-10.147
43	TC	114	-24.346	3.674	13.038	8.928	11.322	-8.446
43	TC	115	-21.749	5.770	13.433	9.385	9.622	-11.250
43	TC	116	-16.749	3.368	13.834	9.884	12.409	-9.556
43	TC	117	-13.831	5.450	14.223	10.343	10.719	-12.333
43	TC	118	-8.532	3.069	14.619	10.837	13.479	-10.652
43	TC	119	-5.297	5.132	15.002	11.288	11.802	-13.406
43	TC	120	.303	2.767	15.391	11.768	14.541	-11.743
43	TC	121	3.862	4.808	15.768	12.200	12.881	-14.480
43	TC	122	9.775	2.454	16.151	12.656	15.604	-12.836
43	TC	123	13.674	4.469	16.522	13.061	13.964	-15.561
43	TC	124	19.921	2.121	16.899	13.484	16.676	-13.938
43	TC	125	24.181	4.107	17.263	13.856	15.057	-18.288
43	TC	126	32.486	.062	17.568	12.541	19.460	-16.604
43	TC	127	38.813	2.041	17.862	11.195	17.773	-19.206
43	TC	128	47.442	-.262	18.161	11.478	20.357	-17.505
43	TC	129	54.083	1.727	18.450	11.751	18.653	-20.063
43	TC	130	62.987	-.537	18.744	12.073	21.193	-18.349
43	TC	131	69.892	1.462	19.029	12.384	19.476	-20.867

TABLE 2

Atomic mass excesses and nuclear binding energies

43	TC	132	79.024	-.765	19.319	12.743	21.977	-19.144
43	TC	133	86.151	1.241	19.602	13.090	20.250	-21.628
43	TC	134	95.473	-.955	19.890	13.480	22.717	-19.899
43	TC	135	102.785	1.055	20.171	13.858	20.985	-22.354
43	TC	136	112.266	-1.114	20.458	14.274	23.425	-20.625
43	TC	137	119.736	.897	20.739	14.677	21.691	-23.059
43	TC	138	129.354	-1.251	21.025	15.111	24.110	-21.333
43	TC	139	136.965	.756	21.307	15.530	22.381	-23.751
43	TC	140	146.751	-1.419	21.550	15.933	24.873	-21.946
43	TC	141	154.450	.668	21.832	16.404	23.065	-24.443
43	TC	142	164.357	-1.540	22.120	16.811	25.548	-22.652
43	TC	143	172.189	.536	22.405	17.284	23.754	-25.142
43	TC	144	182.220	-1.664	22.696	17.733	26.231	-23.370
	ATOM		M - A	NEUTRON	PROTON	ALPHA	Q BETA -	Q BETA +
44	RU	78	60.018	21.072	-3.181	.992	-27.270	19.579
44	RU	79	50.656	17.729	-2.633	.851	-23.380	21.175
44	RU	80	39.167	19.856	-2.101	.736	-24.955	17.393
44	RU	81	30.923	16.612	-1.564	.731	-21.173	19.053
44	RU	82	20.498	18.792	-1.043	.747	-22.812	15.374
44	RU	83	13.225	15.640	-.517	.866	-19.133	17.087
44	RU	84	3.729	17.863	-.006	.995	-20.824	13.498
44	RU	85	-2.694	14.790	.510	1.214	-17.235	15.248
44	RU	86	-11.367	17.040	1.009	1.428	-18.962	11.731
44	RU	87	-17.028	14.029	1.515	1.715	-15.445	12.572
44	RU	88	-24.946	16.285	2.931	1.975	-17.189	8.196
44	RU	89	-28.984	12.406	3.427	2.324	-12.814	9.977
44	RU	90	-35.282	14.665	3.905	2.624	-13.659	6.562
44	RU	91	-38.649	11.735	4.391	2.960	-10.244	8.320
44	RU	92	-44.244	13.962	4.859	3.231	-11.978	4.923
44	RU	93	-46.917	11.041	5.335	3.524	-8.580	6.648
44	RU	94	-51.774	13.224	5.794	3.739	-10.280	2.103
44	RU	95	-52.549	9.142	6.256	2.807	-5.731	3.816
44	RU	96	-55.482	11.301	6.702	1.817	-7.419	.489
44	RU	97	-55.542	8.427	7.156	2.043	-4.091	2.209
44	RU	98	-57.760	10.585	7.593	2.236	-5.787	-1.062
44	RU	99	-57.152	7.760	8.039	2.492	-2.516	.665
44	RU	100	-58.674	9.889	8.441	2.687	-4.163	-2.496
44	RU	101	-57.473	7.166	8.880	3.000	-1.001	-.817
44	RU	102	-58.373	9.267	9.302	3.226	-2.655	-3.924
44	RU	103	-56.598	6.592	9.733	3.571	.451	-2.239
44	RU	104	-56.923	8.693	10.149	3.857	-1.209	-5.291
44	RU	105	-54.622	6.066	10.574	4.208	1.844	-3.600
44	RU	106	-54.421	8.167	10.984	4.528	.177	-6.600
44	RU	107	-51.640	5.586	11.403	4.912	3.177	-4.903
44	RU	108	-50.960	7.687	11.808	5.267	1.504	-7.852
44	RU	109	-47.743	5.151	12.221	5.683	4.453	-6.150
44	RU	110	-46.628	7.252	12.620	6.070	2.775	-9.052
44	RU	111	-43.019	4.758	13.027	6.516	5.677	-7.348
44	RU	112	-41.508	6.857	13.422	6.931	3.995	-10.206
44	RU	113	-37.541	4.401	13.824	7.401	6.855	-8.502
44	RU	114	-35.668	6.494	14.213	7.838	5.173	-11.322
44	RU	115	-31.371	4.071	14.610	8.324	7.994	-9.622
44	RU	116	-29.158	6.155	14.994	8.774	6.316	-12.409
44	RU	117	-24.550	3.759	15.386	9.267	9.105	-10.719
44	RU	118	-22.012	5.829	15.765	9.720	7.436	-13.479
44	RU	119	-17.099	3.455	16.151	10.209	10.198	-11.802
44	RU	120	-14.238	5.507	16.526	10.655	8.541	-14.541
44	RU	121	-9.019	3.148	16.906	11.130	11.284	-12.881
44	RU	122	-5.829	5.177	17.275	11.558	9.643	-15.604
44	RU	123	-.290	2.828	17.650	12.008	12.370	-13.964

TABLE 2

Atomic mass excesses and nuclear binding energies

44	RU	124	3.245	4.832	18.013	12.409	10.749	-16.676
44	RU	125	9.124	2.489	18.382	12.827	13.464	-15.057
44	RU	126	13.026	4.465	18.740	13.195	11.865	-19.460
44	RU	127	21.040	.353	19.031	11.804	16.343	-17.773
44	RU	128	27.086	2.321	19.312	10.383	14.668	-20.357
44	RU	129	35.430	.023	19.598	10.649	17.250	-18.653
44	RU	130	41.793	2.003	19.874	10.906	15.558	-21.193
44	RU	131	50.416	-.255	20.156	11.212	18.095	-19.476
44	RU	132	57.047	1.736	20.429	11.510	16.388	-21.977
44	RU	133	65.901	-.486	20.708	11.854	18.885	-20.250
44	RU	134	72.755	1.513	20.980	12.190	17.167	-22.717
44	RU	135	81.800	-.677	21.258	12.568	19.631	-20.985
44	RU	136	88.841	1.327	21.529	12.936	17.907	-23.425
44	RU	137	98.045	-.837	21.806	13.343	20.343	-21.691
44	RU	138	105.243	1.169	22.077	13.737	18.617	-24.110
44	RU	139	114.584	-.973	22.355	14.165	21.033	-22.381
44	RU	140	121.878	1.073	22.672	14.622	19.223	-24.873
44	RU	141	131.385	-1.140	22.951	15.019	21.712	-23.065
44	RU	142	138.809	.943	23.226	15.487	19.911	-25.548
44	RU	143	148.435	-1.258	23.507	15.890	22.391	-23.754
44	RU	144	155.989	.813	23.784	16.317	20.605	-26.231
44	RU	145	165.737	-1.380	24.069	16.765	23.079	-24.456
44	RU	146	173.430	.674	24.348	17.188	21.315	-26.930
44	RU	147	183.309	-1.512	24.636	17.632	23.786	-25.179
ATOM			M - A	NEUTRON	PROTON	ALPHA	Q BETA -	Q BETA +
45	RH	80	64.122	18.281	-5.881	.902	-21.751	24.955
45	RH	81	52.096	20.393	-5.344	.765	-23.326	21.173
45	RH	82	43.309	17.154	-4.802	.738	-19.567	22.812
45	RH	83	32.358	19.319	-4.275	.732	-21.206	19.133
45	RH	84	24.553	16.172	-3.743	.830	-17.549	20.824
45	RH	85	14.541	18.380	-3.227	.938	-19.240	17.235
45	RH	86	7.596	15.313	-2.705	1.137	-15.674	18.962
45	RH	87	-1.583	17.546	-2.199	1.330	-17.401	15.445
45	RH	88	-7.757	14.541	-1.687	1.597	-13.907	17.189
45	RH	89	-16.171	16.781	-1.191	1.838	-15.651	12.814
45	RH	90	-21.622	13.819	.223	2.133	-12.209	13.659
45	RH	91	-28.406	15.151	.709	2.415	-13.054	10.244
45	RH	92	-32.266	12.228	1.201	2.732	-8.766	11.978
45	RH	93	-38.337	14.439	1.678	2.985	-10.500	8.580
45	RH	94	-41.494	11.524	2.161	3.260	-7.125	10.280
45	RH	95	-46.818	13.691	2.628	3.457	-8.824	5.731
45	RH	96	-48.063	9.612	3.099	2.505	-4.294	7.419
45	RH	97	-51.450	11.755	3.553	1.494	-5.982	4.091
45	RH	98	-51.972	8.890	4.016	1.705	-2.679	5.787
45	RH	99	-54.636	11.031	4.462	1.881	-4.374	2.516
45	RH	100	-54.511	8.242	4.943	2.149	-1.181	4.163
45	RH	101	-56.471	10.328	5.382	2.329	-2.828	1.001
45	RH	102	-55.717	7.614	5.829	2.629	.309	2.655
45	RH	103	-57.049	9.699	6.261	2.841	-1.344	-.451
45	RH	104	-55.715	7.033	6.702	3.146	1.739	1.209
45	RH	105	-56.466	9.118	7.127	3.420	.079	-1.844
45	RH	106	-54.598	6.500	7.561	3.758	3.109	-.177
45	RH	107	-54.817	8.586	7.980	4.067	1.443	-3.177
45	RH	108	-52.463	6.014	8.408	4.440	4.421	-1.504
45	RH	109	-52.197	8.101	8.822	4.785	2.748	-4.453
45	RH	110	-49.403	5.573	9.244	5.191	5.677	-2.775
45	RH	111	-48.696	7.661	9.653	5.569	3.999	-5.677
45	RH	112	-45.503	5.175	10.069	6.005	6.882	-3.995
45	RH	113	-44.396	7.260	10.473	6.412	5.201	-6.855
45	RH	114	-40.840	4.812	10.884	6.873	8.042	-5.173

TABLE 2

Atomic mass excesses and nuclear binding energies

45	RH	115	-39.365	6.892	11.282	7.303	6.361	-7.994
45	RH	116	-35.474	4.477	11.688	7.781	9.165	-6.316
45	RH	117	-33.655	6.548	12.082	8.225	7.488	-9.105
45	RH	118	-29.447	4.159	12.482	8.711	10.261	-7.436
45	RH	119	-27.297	6.218	12.871	9.158	8.593	-10.198
45	RH	120	-22.780	3.850	13.266	9.640	11.340	-8.541
45	RH	121	-20.302	5.890	13.649	10.081	9.685	-11.284
45	RH	122	-15.472	3.537	14.038	10.549	12.413	-9.643
45	RH	123	-12.660	5.555	14.416	10.971	10.775	-12.370
45	RH	124	-7.504	3.212	14.799	11.416	13.488	-10.749
45	RH	125	-4.341	5.204	15.171	11.812	11.870	-13.464
45	RH	126	1.161	2.866	15.548	12.224	14.573	-11.865
45	RH	127	4.697	4.831	15.914	12.586	12.977	-16.343
45	RH	128	12.417	.647	16.207	11.113	17.520	-14.668
45	RH	129	18.180	2.605	16.490	9.610	15.844	-17.250
45	RH	130	26.236	.311	16.778	9.859	18.409	-15.558
45	RH	131	32.321	2.282	17.057	10.101	16.715	-18.095
45	RH	132	40.659	.029	17.341	10.392	19.236	-16.388
45	RH	133	47.015	2.012	17.617	10.677	17.526	-18.885
45	RH	134	55.588	-.205	17.898	11.008	20.008	-17.167
45	RH	135	62.169	1.787	18.171	11.332	18.287	-19.631
45	RH	136	70.934	-.398	18.451	11.700	20.736	-17.907
45	RH	137	77.701	1.600	18.724	12.059	19.009	-20.343
45	RH	138	86.626	-.557	19.003	12.456	21.431	-18.617
45	RH	139	93.551	1.443	19.277	12.843	19.701	-21.033
45	RH	140	102.655	-.737	19.514	13.220	22.190	-19.223
45	RH	141	109.673	1.349	19.789	13.672	20.377	-21.712
45	RH	142	118.898	-.858	20.071	14.065	22.852	-19.911
45	RH	143	126.044	1.221	20.350	14.530	21.048	-22.391
45	RH	144	135.384	-.973	20.635	14.976	23.512	-20.605
45	RH	145	142.657	1.094	20.917	15.402	21.724	-23.079
45	RH	146	152.115	-1.090	21.206	15.851	24.183	-21.315
45	RH	147	159.523	.960	21.492	16.275	22.415	-23.786
45	RH	148	169.108	-1.218	21.786	16.722	24.871	-22.046
45	RH	149	176.664	.812	22.075	17.139	23.128	-24.517
45	RH	150	186.391	-1.360	22.374	17.578	25.582	-22.804
45	RH	151	194.112	.646	22.668	17.984	23.868	-25.274
	ATOM		M - A	NEUTRON	PROTON	ALPHA	Q BETA -	Q BETA +
46	PD	82	62.877	20.913	-3.196	.750	-27.072	19.567
46	PD	83	53.564	17.680	-2.669	.702	-23.313	21.206
46	PD	84	42.102	19.829	-2.159	.674	-24.930	17.549
46	PD	85	33.781	16.688	-1.643	.751	-21.274	19.240
46	PD	86	23.269	18.879	-1.144	.838	-22.943	15.674
46	PD	87	15.818	15.819	-.638	1.016	-19.376	17.401
46	PD	88	6.150	18.036	-.148	1.188	-21.080	13.907
46	PD	89	-.520	15.037	.348	1.435	-17.586	15.651
46	PD	90	-9.413	17.261	.828	1.656	-19.307	12.209
46	PD	91	-15.352	14.305	1.314	1.933	-15.864	13.054
46	PD	92	-23.500	16.516	2.679	2.163	-17.581	8.766
46	PD	93	-27.837	12.705	3.156	2.462	-13.293	10.500
46	PD	94	-34.369	14.899	3.617	2.696	-14.122	7.125
46	PD	95	-37.994	11.992	4.084	2.954	-10.747	8.824
46	PD	96	-43.769	14.142	4.536	3.134	-12.421	4.294
46	PD	97	-45.468	10.067	4.990	2.160	-7.886	5.982
46	PD	98	-49.294	12.193	5.428	1.129	-9.549	2.679
46	PD	99	-50.262	9.336	5.875	1.323	-6.245	4.374
46	PD	100	-53.330	11.434	6.278	1.457	-7.861	1.181
46	PD	101	-53.643	8.681	6.717	1.710	-4.668	2.828
46	PD	102	-56.026	10.751	7.140	1.876	-6.290	-.309
46	PD	103	-55.705	8.046	7.572	2.162	-3.152	1.344

TABLE 2

Atomic mass excesses and nuclear binding energies

46	PD	104	-57.453	10.116	7.989	2.389	-4.782	-1.739
46	PD	105	-56.545	7.459	8.415	2.681	-1.698	-.079
46	PD	106	-57.707	9.530	8.826	2.944	-3.335	-3.109
46	PD	107	-56.259	6.920	9.246	3.271	-.304	-1.443
46	PD	108	-56.884	8.992	9.652	3.570	-1.948	-4.421
46	PD	109	-54.945	6.428	10.067	3.932	1.031	-2.748
46	PD	110	-55.080	8.502	10.468	4.268	-.620	-5.677
46	PD	111	-52.695	5.983	10.877	4.665	2.310	-3.999
46	PD	112	-52.385	8.057	11.274	5.035	.653	-6.882
46	PD	113	-49.597	5.579	11.678	5.463	3.537	-5.201
46	PD	114	-48.882	7.652	12.071	5.863	1.877	-8.042
46	PD	115	-45.726	5.212	12.471	6.317	4.718	-6.361
46	PD	116	-44.639	7.280	12.858	6.740	3.058	-9.165
46	PD	117	-41.143	4.872	13.254	7.211	5.863	-7.488
46	PD	118	-39.708	6.932	13.637	7.649	4.207	-10.261
46	PD	119	-35.890	4.550	14.028	8.128	6.981	-8.593
46	PD	120	-34.120	6.597	14.407	8.571	5.332	-11.340
46	PD	121	-29.987	4.235	14.792	9.047	8.081	-9.685
46	PD	122	-27.885	6.265	15.167	9.482	6.446	-12.413
46	PD	123	-23.435	3.917	15.547	9.945	9.176	-10.775
46	PD	124	-20.992	5.925	15.917	10.363	7.557	-13.488
46	PD	125	-16.211	3.587	16.292	10.802	10.272	-11.870
46	PD	126	-13.412	5.569	16.656	11.193	8.673	-14.573
46	PD	127	-8.280	3.235	17.026	11.600	11.378	-12.977
46	PD	128	-5.103	5.190	17.384	11.957	9.801	-17.520
46	PD	129	2.336	.929	17.666	10.397	14.428	-15.844
46	PD	130	7.827	2.877	17.938	8.808	12.765	-18.409
46	PD	131	15.606	.588	18.214	9.043	15.329	-16.715
46	PD	132	21.424	2.550	18.482	9.271	13.646	-19.236
46	PD	133	29.489	.302	18.755	9.550	16.165	-17.526
46	PD	134	35.579	2.277	19.021	9.823	14.466	-20.008
46	PD	135	43.881	.066	19.292	10.144	16.946	-18.287
46	PD	136	50.198	2.051	19.556	10.459	15.234	-20.736
46	PD	137	58.693	-.128	19.826	10.817	17.680	-19.009
46	PD	138	65.196	1.865	20.091	11.169	15.961	-21.431
46	PD	139	73.850	-.287	20.361	11.560	18.379	-19.701
46	PD	140	80.464	1.753	20.671	11.986	16.570	-22.190
46	PD	141	89.296	-.464	20.943	12.358	19.056	-20.377
46	PD	142	96.046	1.617	21.211	12.806	17.249	-22.852
46	PD	143	104.996	-.583	21.486	13.196	19.721	-21.048
46	PD	144	111.872	1.492	21.757	13.615	17.925	-23.512
46	PD	145	120.933	-.694	22.036	14.061	20.387	-21.724
46	PD	146	127.932	1.368	22.310	14.486	18.607	-24.183
46	PD	147	137.108	-.808	22.592	14.936	21.063	-22.415
46	PD	148	144.237	1.238	22.870	15.361	19.306	-24.871
46	PD	149	153.535	-.931	23.158	15.811	21.759	-23.128
46	PD	150	160.809	1.094	23.440	16.230	20.029	-25.582
46	PD	151	170.244	-1.068	23.732	16.674	22.480	-23.868
46	PD	152	177.679	.933	24.019	17.085	20.780	-26.321
46	PD	153	187.269	-1.223	24.315	17.520	23.231	-24.638
46	PD	154	194.885	.752	24.607	17.920	21.562	-27.088
46	PD	155	204.650	-1.398	24.908	18.346	24.011	-25.435
	ATOM		M - A	NEUTRON	PROTON	ALPHA	Q BETA -	Q BETA +
47	AG	84	67.032	18.212	-5.884	.699	-21.725	24.930
47	AG	85	55.055	20.345	-5.368	.650	-23.343	21.274
47	AG	86	46.212	17.210	-4.846	.707	-19.709	22.943
47	AG	87	35.194	19.385	-4.340	.773	-21.378	19.376
47	AG	88	27.230	16.331	-3.828	.932	-17.834	21.080
47	AG	89	17.066	18.532	-3.331	1.084	-19.539	17.586
47	AG	90	9.893	15.540	-2.828	1.312	-16.067	19.307

TABLE 2

Atomic mass excesses and nuclear binding energies

47	AG	91	.513	17.748	-2.342	1.513	-17.788	15.864
47	AG	92	-5.919	14.799	-1.848	1.771	-14.369	17.581
47	AG	93	-14.545	16.993	-1.371	1.983	-16.085	13.293
47	AG	94	-20.247	14.070	-.006	2.234	-12.700	14.122
47	AG	95	-27.247	15.367	.463	2.451	-13.529	10.747
47	AG	96	-31.348	12.468	.939	2.691	-9.312	12.421
47	AG	97	-37.583	14.602	1.399	2.855	-10.986	7.886
47	AG	98	-39.745	10.530	1.862	1.860	-6.470	9.549
47	AG	99	-44.018	12.640	2.308	.809	-8.132	6.245
47	AG	100	-45.469	9.818	2.791	1.015	-4.907	7.861
47	AG	101	-48.975	11.874	3.230	1.134	-6.523	4.668
47	AG	102	-49.736	9.129	3.678	1.373	-3.354	6.290
47	AG	103	-52.552	11.183	4.111	1.525	-4.977	3.152
47	AG	104	-52.672	8.487	4.552	1.770	-1.862	4.782
47	AG	105	-54.846	10.542	4.978	1.984	-3.491	1.698
47	AG	106	-54.372	7.893	5.412	2.264	-.431	3.335
47	AG	107	-55.955	9.950	5.833	2.515	-2.067	.304
47	AG	108	-54.936	7.348	6.261	2.831	.941	1.948
47	AG	109	-55.976	9.407	6.676	3.119	-.702	-1.031
47	AG	110	-54.460	6.852	7.100	3.471	2.255	.620
47	AG	111	-55.005	8.912	7.510	3.797	.605	-2.310
47	AG	112	-53.039	6.401	7.928	4.185	3.514	-.653
47	AG	113	-53.134	8.463	8.333	4.546	1.858	-3.537
47	AG	114	-50.759	5.992	8.746	4.965	4.722	-1.877
47	AG	115	-50.445	8.053	9.147	5.358	3.063	-4.718
47	AG	116	-47.697	5.620	9.556	5.803	5.886	-3.058
47	AG	117	-47.007	7.677	9.952	6.220	4.227	-5.863
47	AG	118	-43.914	5.275	10.356	6.683	7.014	-4.207
47	AG	119	-42.871	7.324	10.748	7.115	5.359	-6.981
47	AG	120	-39.452	4.949	11.147	7.587	8.116	-5.332
47	AG	121	-38.069	6.984	11.534	8.023	6.469	-8.081
47	AG	122	-34.330	4.629	11.928	8.493	9.203	-6.446
47	AG	123	-32.610	6.647	12.310	8.922	7.569	-9.176
47	AG	124	-28.549	4.306	12.699	9.378	10.284	-7.557
47	AG	125	-26.483	6.302	13.076	9.790	8.667	-10.272
47	AG	126	-22.085	3.969	13.459	10.223	11.370	-8.673
47	AG	127	-19.659	5.941	13.831	10.608	9.773	-11.378
47	AG	128	-14.903	3.612	14.208	11.009	12.466	-9.801
47	AG	129	-12.092	5.556	14.574	11.360	10.891	-14.428
47	AG	130	-4.938	1.214	14.859	9.708	15.592	-12.765
47	AG	131	.277	3.152	15.134	8.029	13.929	-15.329
47	AG	132	7.777	.868	15.414	8.249	16.479	-13.646
47	AG	133	13.324	2.821	15.685	8.466	14.795	-16.165
47	AG	134	21.113	.578	15.961	8.732	17.300	-14.466
47	AG	135	26.935	2.545	16.229	8.995	15.599	-16.946
47	AG	136	34.963	.339	16.503	9.305	18.065	-15.234
47	AG	137	41.013	2.318	16.770	9.612	16.351	-17.680
47	AG	138	49.235	.145	17.043	9.962	18.784	-15.961
47	AG	139	55.470	2.132	17.310	10.308	17.062	-18.379
47	AG	140	63.895	-.057	17.540	10.648	19.555	-16.570
47	AG	141	70.241	2.022	17.809	11.070	17.742	-19.056
47	AG	142	78.797	-.189	18.084	11.438	20.215	-17.249
47	AG	143	85.276	1.889	18.356	11.884	18.405	-19.721
47	AG	144	93.947	-.304	18.635	12.317	20.862	-17.925
47	AG	145	100.547	1.767	18.910	12.736	19.063	-20.387
47	AG	146	109.325	-.411	19.193	13.182	21.509	-18.607
47	AG	147	116.044	1.648	19.473	13.609	19.727	-21.063
47	AG	148	124.931	-.519	19.761	14.062	22.166	-19.306
47	AG	149	131.776	1.522	20.046	14.490	20.406	-21.759
47	AG	150	140.780	-.636	20.340	14.944	22.841	-20.029
47	AG	151	147.764	1.384	20.630	15.368	21.108	-22.480
47	AG	152	156.899	-.768	20.930	15.818	23.541	-20.780

TABLE 2

Atomic mass excesses and nuclear binding energies

47	AG	153	164.039	1.228	21.225	16.234	21.838	-23.231
47	AG	154	173.323	-.917	21.531	16.677	24.271	-21.562
47	AG	155	180.638	1.052	21.831	17.083	22.600	-24.011
47	AG	156	190.091	-1.086	22.143	17.518	25.030	-22.375
47	AG	157	197.602	.856	22.449	17.914	23.392	-24.821
47	AG	158	207.242	-1.273	22.766	18.340	25.819	-23.217
47	AG	159	214.967	.642	23.076	18.727	24.213	-25.657
	ATOM		M - A	NEUTRON	PROTON	ALPHA	Q BETA -	Q BETA +
48	CD	86	65.921	20.844	-3.281	.565	-27.048	19.709
48	CD	87	56.572	17.716	-2.775	.601	-23.415	21.378
48	CD	88	45.065	19.875	-2.286	.647	-25.061	17.834
48	CD	89	36.605	16.827	-1.790	.786	-21.517	19.539
48	CD	90	25.960	19.012	-1.310	.918	-23.199	16.067
48	CD	91	18.301	16.027	-.823	1.127	-19.727	17.788
48	CD	92	8.450	18.218	-.352	1.309	-21.424	14.369
48	CD	93	1.541	15.277	.125	1.549	-18.005	16.085
48	CD	94	-7.546	17.455	.587	1.742	-19.697	12.700
48	CD	95	-13.718	14.538	1.055	1.975	-16.312	13.529
48	CD	96	-22.036	16.685	2.373	2.145	-17.982	9.312
48	CD	97	-26.597	12.929	2.834	2.369	-13.765	10.986
48	CD	98	-33.275	15.046	3.278	2.516	-14.562	6.470
48	CD	99	-35.885	10.977	3.725	1.501	-10.040	8.132
48	CD	100	-40.561	13.044	4.128	.402	-11.623	4.907
48	CD	101	-42.452	10.258	4.568	.593	-8.398	6.523
48	CD	102	-46.382	12.297	4.992	.697	-9.989	3.354
48	CD	103	-47.576	9.561	5.424	.923	-6.820	4.977
48	CD	104	-50.809	11.601	5.842	1.089	-8.418	1.862
48	CD	105	-51.355	8.913	6.268	1.322	-5.303	3.491
48	CD	106	-53.942	10.954	6.680	1.524	-6.909	.431
48	CD	107	-53.888	8.314	7.100	1.792	-3.848	2.067
48	CD	108	-55.877	10.357	7.507	2.033	-5.462	-.941
48	CD	109	-55.273	7.764	7.922	2.338	-2.454	.702
48	CD	110	-56.715	9.809	8.324	2.617	-4.075	-2.255
48	CD	111	-55.610	7.262	8.735	2.960	-1.118	-.605
48	CD	112	-56.552	9.310	9.132	3.278	-2.747	-3.514
48	CD	113	-54.992	6.807	9.538	3.656	.162	-1.858
48	CD	114	-55.481	8.856	9.932	4.010	-1.473	-4.722
48	CD	115	-53.508	6.394	10.333	4.421	1.391	-3.063
48	CD	116	-53.583	8.443	10.723	4.807	-.248	-5.886
48	CD	117	-51.233	6.017	11.121	5.245	2.576	-4.227
48	CD	118	-50.928	8.063	11.507	5.656	.936	-7.014
48	CD	119	-48.230	5.669	11.900	6.112	3.724	-5.359
48	CD	120	-47.568	7.706	12.282	6.538	2.087	-8.116
48	CD	121	-44.538	5.337	12.671	7.004	4.846	-6.469
48	CD	122	-43.533	7.362	13.049	7.435	3.217	-9.203
48	CD	123	-40.179	5.013	13.433	7.898	5.952	-7.569
48	CD	124	-38.833	7.021	13.807	8.322	4.336	-10.284
48	CD	125	-35.151	4.685	14.187	8.773	7.053	-8.667
48	CD	126	-33.455	6.672	14.556	9.180	5.454	-11.370
48	CD	127	-29.431	4.344	14.931	9.606	8.158	-9.773
48	CD	128	-27.369	6.305	15.295	9.986	6.578	-12.466
48	CD	129	-22.983	3.981	15.664	10.381	9.274	-10.891
48	CD	130	-20.531	5.915	16.023	10.727	7.715	-15.592
48	CD	131	-13.651	1.488	16.298	8.980	12.508	-13.929
48	CD	132	-8.701	3.417	16.564	7.208	10.858	-16.479
48	CD	133	-1.471	1.138	16.834	7.417	13.408	-14.795
48	CD	134	3.813	3.083	17.095	7.623	11.736	-17.300
48	CD	135	11.336	.845	17.362	7.880	14.241	-15.599
48	CD	136	16.898	2.805	17.622	8.135	12.551	-18.065
48	CD	137	24.661	.604	17.887	8.437	15.015	-16.351

TABLE 2

Atomic mass excesses and nuclear binding energies

48	CD	138	30.451	2.578	18.146	8.738	13.311	-18.784
48	CD	139	38.408	.410	18.411	9.082	15.742	-17.062
48	CD	140	44.340	2.436	18.715	9.467	13.940	-19.555
48	CD	141	52.498	.209	18.981	9.804	16.431	-17.742
48	CD	142	58.582	2.283	19.243	10.223	14.627	-20.215
48	CD	143	66.870	.079	19.512	10.589	17.096	-18.405
48	CD	144	73.084	2.153	19.776	10.989	15.296	-20.862
48	CD	145	81.483	-.032	20.048	11.422	17.750	-19.063
48	CD	146	87.816	2.035	20.316	11.840	15.960	-21.509
48	CD	147	96.318	-.134	20.592	12.288	18.403	-19.727
48	CD	148	102.765	1.920	20.864	12.716	16.631	-22.166
48	CD	149	111.370	-.238	21.145	13.172	19.067	-20.406
48	CD	150	117.939	1.799	21.422	13.603	17.318	-22.841
48	CD	151	126.656	-.350	21.709	14.061	19.750	-21.108
48	CD	152	133.358	1.666	21.991	14.489	18.030	-23.541
48	CD	153	142.200	-.475	22.284	14.944	20.460	-21.838
48	CD	154	149.052	1.515	22.571	15.365	18.771	-24.271
48	CD	155	158.039	-.619	22.869	15.815	21.201	-22.600
48	CD	156	165.061	1.345	23.162	16.227	19.545	-25.030
48	CD	157	174.210	-.782	23.466	16.668	21.973	-23.392
48	CD	158	181.423	1.154	23.764	17.071	20.352	-25.819
48	CD	159	190.754	-.963	24.073	17.505	22.777	-24.213
48	CD	160	198.177	.945	24.375	17.899	21.189	-26.633
48	CD	161	207.706	-1.161	24.689	18.327	23.608	-25.059
48	CD	162	215.354	.719	24.995	18.714	22.053	-27.468
	ATOM		M - A	NEUTRON	PROTON	ALPHA	Q BETA -	Q BETA +
49	IN	88	70.126	18.228	-5.969	.516	-21.882	25.061
49	IN	89	58.122	20.371	-5.473	.542	-23.528	21.517
49	IN	90	49.159	17.330	-4.970	.662	-20.008	23.199
49	IN	91	38.028	19.499	-4.483	.775	-21.689	19.727
49	IN	92	29.874	16.521	-3.989	.965	-18.241	21.424
49	IN	93	19.546	18.696	-3.511	1.130	-19.938	18.005
49	IN	94	12.151	15.762	-3.025	1.352	-16.543	19.697
49	IN	95	2.595	17.924	-2.556	1.528	-18.235	16.312
49	IN	96	-4.053	15.015	-2.079	1.744	-14.874	17.982
49	IN	97	-12.832	17.146	-1.619	1.897	-16.543	13.765
49	IN	98	-18.714	14.249	-.298	2.076	-13.201	14.562
49	IN	99	-25.845	15.499	.154	2.207	-13.998	10.040
49	IN	100	-28.938	11.460	.637	1.199	-8.712	11.623
49	IN	101	-34.054	13.483	1.077	.081	-10.295	8.398
49	IN	102	-36.393	10.707	1.526	.257	-7.094	9.989
49	IN	103	-40.756	12.730	1.959	.348	-8.684	6.820
49	IN	104	-42.392	10.003	2.401	.532	-5.539	8.418
49	IN	105	-46.052	12.027	2.827	.686	-7.137	5.303
49	IN	106	-47.032	9.348	3.262	.905	-4.045	6.909
49	IN	107	-50.040	11.375	3.683	1.096	-5.651	3.848
49	IN	108	-50.415	8.743	4.112	1.353	-2.612	5.462
49	IN	109	-52.820	10.772	4.527	1.583	-4.226	2.454
49	IN	110	-52.640	8.187	4.951	1.877	-1.239	4.075
49	IN	111	-54.492	10.220	5.362	2.146	-2.860	1.118
49	IN	112	-53.806	7.681	5.781	2.479	.077	2.747
49	IN	113	-55.154	9.716	6.187	2.788	-1.552	-.162
49	IN	114	-54.008	7.221	6.601	3.157	1.337	1.473
49	IN	115	-54.899	9.258	7.003	3.503	-.298	-1.391
49	IN	116	-53.335	6.804	7.412	3.906	2.547	.248
49	IN	117	-53.809	8.841	7.810	4.284	.908	-2.576
49	IN	118	-51.864	6.423	8.216	4.715	3.713	-.936
49	IN	119	-51.953	8.457	8.610	5.118	2.074	-3.724
49	IN	120	-49.656	6.069	9.011	5.567	4.845	-2.087
49	IN	121	-49.384	8.096	9.401	5.987	3.209	-4.846

TABLE 2

Atomic mass excesses and nuclear binding energies

49	IN	122	-46.751	5.734	9.797	6.445	5.951	-3.217
49	IN	123	-46.131	7.748	10.183	6.870	4.324	-5.952
49	IN	124	-43.169	5.405	10.575	7.326	7.043	-4.336
49	IN	125	-42.204	7.402	10.956	7.744	5.429	-7.053
49	IN	126	-38.909	5.072	11.343	8.188	8.131	-5.454
49	IN	127	-37.590	7.048	11.719	8.589	6.533	-8.158
49	IN	128	-33.947	4.725	12.101	9.008	9.225	-6.578
49	IN	129	-32.257	6.676	12.472	9.382	7.647	-9.274
49	IN	130	-28.246	4.357	12.848	9.770	10.330	-7.715
49	IN	131	-26.159	6.281	13.214	10.110	8.774	-12.508
49	IN	132	-19.559	1.767	13.493	8.265	13.646	-10.858
49	IN	133	-14.879	3.687	13.763	6.396	11.997	-13.408
49	IN	134	-7.923	1.412	14.037	6.595	14.535	-11.736
49	IN	135	-2.905	3.349	14.303	6.792	12.863	-14.241
49	IN	136	4.347	1.115	14.573	7.039	15.356	-12.551
49	IN	137	9.646	3.069	14.837	7.287	13.666	-15.015
49	IN	138	17.140	.873	15.106	7.583	16.119	-13.311
49	IN	139	22.667	2.841	15.369	7.878	14.413	-15.742
49	IN	140	30.399	.635	15.594	8.173	16.920	-13.940
49	IN	141	36.067	2.700	15.857	8.555	15.117	-16.431
49	IN	142	43.956	.479	16.127	8.888	17.595	-14.627
49	IN	143	49.774	2.549	16.393	9.306	15.788	-17.096
49	IN	144	57.789	.352	16.666	9.715	18.244	-15.296
49	IN	145	63.734	2.422	16.935	10.116	16.441	-17.750
49	IN	146	71.856	.246	17.212	10.551	18.880	-15.960
49	IN	147	77.915	2.308	17.486	10.970	17.088	-18.403
49	IN	148	86.134	.148	17.768	11.422	19.514	-16.631
49	IN	149	92.304	2.198	18.046	11.852	17.739	-19.067
49	IN	150	100.621	.050	18.334	12.313	20.157	-17.318
49	IN	151	106.905	2.083	18.618	12.748	18.406	-19.750
49	IN	152	115.328	-.055	18.913	13.212	20.819	-18.030
49	IN	153	121.740	1.955	19.202	13.646	19.096	-20.460
49	IN	154	130.281	-.174	19.503	14.108	21.507	-18.771
49	IN	155	136.838	1.811	19.799	14.535	19.814	-21.201
49	IN	156	145.516	-.311	20.107	14.992	22.224	-19.545
49	IN	157	152.237	1.647	20.409	15.411	20.565	-21.973
49	IN	158	161.072	-.467	20.723	15.860	22.972	-20.352
49	IN	159	167.977	1.462	21.031	16.270	21.348	-22.777
49	IN	160	176.988	-.643	21.351	16.713	23.752	-21.189
49	IN	161	184.098	1.258	21.664	17.114	22.162	-23.608
49	IN	162	193.301	-.836	21.990	17.551	24.559	-22.053
49	IN	163	200.631	1.037	22.307	17.945	23.002	-24.462
49	IN	164	210.040	-1.042	22.638	18.379	25.388	-22.937
49	IN	165	217.603	.804	22.959	18.770	23.863	-25.332
49	IN	166	227.227	-1.256	23.293	19.204	26.235	-23.835
	ATOM		M - A	NEUTRON	PROTON	ALPHA	Q BETA -	Q BETA +
50	SN	91	59.717	17.817	-2.973	.464	-24.828	21.689
50	SN	92	48.115	19.969	-2.503	.559	-26.488	18.241
50	SN	93	39.484	16.999	-2.025	.730	-23.044	19.938
50	SN	94	28.693	19.158	-1.563	.876	-24.720	16.543
50	SN	95	20.829	16.232	-1.094	1.081	-21.329	18.235
50	SN	96	10.820	18.377	-.641	1.239	-23.001	14.874
50	SN	97	3.711	15.476	-.180	1.439	-19.644	16.543
50	SN	98	-5.512	17.591	.265	1.575	-21.293	13.201
50	SN	99	-11.847	14.702	.718	1.739	-17.956	13.998
50	SN	100	-20.226	16.746	1.966	1.799	-19.516	8.712
50	SN	101	-23.759	11.901	2.406	.772	-14.230	10.295
50	SN	102	-29.299	13.908	2.830	-.367	-14.911	7.094
50	SN	103	-32.072	11.140	3.263	-.204	-11.657	8.684
50	SN	104	-36.853	13.148	3.681	-.099	-13.172	5.539

TABLE 2

Atomic mass excesses and nuclear binding energies

50	SN	105	-38.915	10.429	4.108	.072	-9.976	7.137
50	SN	106	-42.987	12.440	4.520	.214	-11.503	4.045
50	SN	107	-44.389	9.769	4.941	.422	-8.366	5.651
50	SN	108	-47.803	11.782	5.348	.603	-9.907	2.612
50	SN	109	-48.594	9.159	5.764	.848	-6.829	4.226
50	SN	110	-51.401	11.174	6.166	1.069	-8.385	1.239
50	SN	111	-51.632	8.598	6.577	1.353	-5.367	2.860
50	SN	112	-53.882	10.618	6.975	1.614	-6.941	-.077
50	SN	113	-53.602	8.087	7.381	1.938	-3.981	1.552
50	SN	114	-55.345	10.110	7.775	2.239	-5.572	-1.337
50	SN	115	-54.601	7.623	8.177	2.600	-2.670	.298
50	SN	116	-55.882	9.649	8.568	2.939	-4.278	-2.547
50	SN	117	-54.717	7.202	8.966	3.334	-1.430	-.908
50	SN	118	-55.578	9.228	9.353	3.706	-3.052	-3.713
50	SN	119	-54.027	6.817	9.748	4.129	-.255	-2.074
50	SN	120	-54.500	8.840	10.132	4.526	-1.889	-4.845
50	SN	121	-52.593	6.460	10.522	4.969	.865	-3.209
50	SN	122	-52.702	8.476	10.903	5.383	-.776	-5.951
50	SN	123	-50.455	6.121	11.289	5.835	1.940	-4.324
50	SN	124	-50.212	8.125	11.666	6.253	.298	-7.043
50	SN	125	-47.633	5.788	12.048	6.704	2.983	-5.429
50	SN	126	-47.040	7.775	12.421	7.116	1.346	-8.131
50	SN	127	-44.123	5.450	12.799	7.553	4.008	-6.533
50	SN	128	-43.172	7.416	13.167	7.949	2.381	-9.225
50	SN	129	-39.903	5.098	13.541	8.362	5.026	-7.647
50	SN	130	-38.576	7.040	13.904	8.730	3.414	-10.330
50	SN	131	-34.933	4.725	14.272	9.111	6.048	-8.774
50	SN	132	-33.205	6.639	14.631	9.445	4.455	-13.646
50	SN	133	-26.876	2.038	14.902	7.503	9.367	-11.997
50	SN	134	-22.458	3.949	15.164	5.537	7.897	-14.535
50	SN	135	-15.769	1.678	15.430	5.726	10.600	-12.863
50	SN	136	-11.009	3.608	15.689	5.917	9.103	-15.356
50	SN	137	-4.020	1.379	15.952	6.158	11.756	-13.666
50	SN	138	1.021	3.326	16.209	6.401	10.233	-16.119
50	SN	139	8.254	1.135	16.471	6.691	12.838	-14.413
50	SN	140	13.480	3.141	16.772	7.027	11.202	-16.920
50	SN	141	20.950	.897	17.034	7.320	13.849	-15.117
50	SN	142	26.360	2.957	17.291	7.700	12.190	-17.595
50	SN	143	33.985	.742	17.555	8.032	14.796	-15.788
50	SN	144	39.544	2.808	17.814	8.405	13.119	-18.244
50	SN	145	47.293	.619	18.081	8.815	15.685	-16.441
50	SN	146	52.976	2.684	18.343	9.216	13.996	-18.880
50	SN	147	60.827	.516	18.613	9.652	16.526	-17.088
50	SN	148	66.620	2.574	18.879	10.073	14.828	-19.514
50	SN	149	74.565	.423	19.154	10.528	17.326	-17.739
50	SN	150	80.463	2.469	19.425	10.962	15.625	-20.157
50	SN	151	88.500	.331	19.706	11.427	18.093	-18.406
50	SN	152	94.509	2.359	19.982	11.866	16.394	-20.819
50	SN	153	102.644	.232	20.268	12.335	18.834	-19.096
50	SN	154	108.775	2.237	20.550	12.773	17.141	-21.507
50	SN	155	117.024	.119	20.843	13.241	19.555	-19.814
50	SN	156	123.293	2.098	21.130	13.674	17.871	-22.224
50	SN	157	131.672	-.012	21.429	14.137	20.260	-20.565
50	SN	158	138.100	1.940	21.722	14.562	18.587	-22.972
50	SN	159	146.629	-.162	22.027	15.019	20.951	-21.348
50	SN	160	153.236	1.760	22.326	15.434	19.292	-23.752
50	SN	161	161.936	-.332	22.637	15.884	21.629	-22.162
50	SN	162	168.742	1.561	22.940	16.291	19.984	-24.559
50	SN	163	177.629	-.519	23.257	16.734	22.295	-23.002
50	SN	164	184.652	1.345	23.564	17.134	20.664	-25.388
50	SN	165	193.740	-.721	23.885	17.575	22.945	-23.863
50	SN	166	200.992	1.115	24.196	17.971	21.329	-26.235

TABLE 2

Atomic mass excesses and nuclear binding energies

50	SN	167	210.292	-.932	24.520	18.410	23.579	-24.738
50	SN	168	217.782	.878	24.833	18.805	21.976	-27.090
50	SN	169	227.298	-1.148	25.159	19.247	24.193	-25.619
50	SN	170	235.028	.637	25.473	19.644	22.604	-27.947
50	SN	171	244.759	-1.364	25.801	20.091	24.786	-26.499
	ATOM		M - A	NEUTRON	PROTON	ALPHA	Q BETA -	Q BETA +
51	SB	92	74.604	18.308	-7.302	-.869	-23.329	26.488
51	SB	93	62.527	20.444	-6.827	-.796	-24.989	23.044
51	SB	94	53.413	17.481	-6.345	-.645	-21.568	24.720
51	SB	95	42.158	19.623	-5.880	-.521	-23.244	21.329
51	SB	96	33.821	16.705	-5.407	-.337	-19.876	23.001
51	SB	97	23.355	18.833	-4.950	-.200	-21.548	19.644
51	SB	98	15.781	15.941	-4.485	-.021	-18.215	21.293
51	SB	99	6.109	18.039	-4.037	.095	-19.864	17.956
51	SB	100	-.709	15.186	-3.553	.265	-16.605	19.516
51	SB	101	-9.529	17.187	-3.112	.306	-18.165	14.230
51	SB	102	-14.389	13.227	-1.785	-.716	-13.780	14.911
51	SB	103	-20.415	14.394	-1.299	-1.821	-14.461	11.657
51	SB	104	-23.681	11.633	-.806	-1.648	-10.418	13.172
51	SB	105	-28.939	13.625	-.329	-1.506	-11.932	9.976
51	SB	106	-31.484	10.913	.154	-1.300	-8.757	11.503
51	SB	107	-36.023	12.906	.620	-1.124	-10.282	8.366
51	SB	108	-37.896	10.241	1.092	-.886	-7.165	9.907
51	SB	109	-41.765	12.236	1.547	-.677	-8.702	6.829
51	SB	110	-43.016	9.618	2.006	-.408	-5.643	8.385
51	SB	111	-46.265	11.617	2.448	-.166	-7.195	5.367
51	SB	112	-46.942	9.044	2.895	.136	-4.194	6.941
51	SB	113	-49.621	11.047	3.324	.410	-5.763	3.981
51	SB	114	-49.773	8.519	3.756	.742	-2.819	5.572
51	SB	115	-51.931	10.525	4.171	1.048	-4.405	2.670
51	SB	116	-51.605	8.041	4.589	1.408	-1.517	4.278
51	SB	117	-53.287	10.050	4.990	1.742	-3.120	1.430
51	SB	118	-52.525	7.605	5.393	2.126	-.286	3.052
51	SB	119	-53.773	9.615	5.780	2.483	-1.903	.255
51	SB	120	-52.612	7.206	6.169	2.886	.882	1.889
51	SB	121	-53.458	9.214	6.542	3.258	-.746	-.865
51	SB	122	-51.926	6.835	6.918	3.671	1.995	.776
51	SB	123	-52.395	8.836	7.278	4.051	.360	-1.940
51	SB	124	-50.510	6.483	7.640	4.464	3.064	-.298
51	SB	125	-50.616	8.473	7.988	4.841	1.427	-2.983
51	SB	126	-48.386	6.138	8.338	5.245	4.101	-1.346
51	SB	127	-48.131	8.112	8.675	5.609	2.468	-4.008
51	SB	128	-45.553	5.790	9.014	5.993	5.119	-2.381
51	SB	129	-44.929	7.743	9.341	6.334	3.496	-5.026
51	SB	130	-41.990	5.428	9.671	6.690	6.131	-3.414
51	SB	131	-40.981	7.359	9.990	7.001	4.522	-6.048
51	SB	132	-37.660	5.046	10.311	7.321	7.146	-4.455
51	SB	133	-36.243	6.951	10.623	7.596	5.556	-9.367
51	SB	134	-30.355	2.479	11.064	5.719	10.333	-7.897
51	SB	135	-26.368	4.380	11.495	3.818	8.864	-10.600
51	SB	136	-20.112	2.111	11.928	4.162	11.557	-9.103
51	SB	137	-15.776	4.031	12.352	4.506	10.063	-11.756
51	SB	138	-9.212	1.803	12.776	4.897	12.707	-10.233
51	SB	139	-4.584	3.740	13.190	5.288	11.188	-12.838
51	SB	140	2.278	1.505	13.560	5.678	13.874	-11.202
51	SB	141	7.102	3.544	13.963	6.153	12.242	-13.849
51	SB	142	14.170	1.299	14.365	6.579	14.884	-12.190
51	SB	143	19.190	3.348	14.755	7.086	13.230	-14.796
51	SB	144	26.425	1.132	15.145	7.583	15.830	-13.119
51	SB	145	31.607	3.185	15.522	8.069	14.159	-15.685

TABLE 2

Atomic mass excesses and nuclear binding energies

51	SB	146	38.980	.995	15.897	8.585	16.719	-13.996
51	SB	147	44.301	3.046	16.259	9.082	15.036	-16.526
51	SB	148	51.792	.877	16.620	9.606	17.560	-14.828
51	SB	149	57.239	2.920	16.966	10.104	15.870	-17.326
51	SB	150	64.838	.768	17.311	10.627	18.360	-15.625
51	SB	151	70.407	2.798	17.641	11.117	16.668	-18.093
51	SB	152	78.114	.660	17.970	11.629	19.128	-16.394
51	SB	153	83.811	2.671	18.283	12.102	17.437	-18.834
51	SB	154	91.634	.544	18.595	12.596	19.869	-17.141
51	SB	155	97.469	2.532	18.891	13.046	18.184	-19.555
51	SB	156	105.422	.414	19.187	13.515	20.589	-17.871
51	SB	157	111.412	2.377	19.465	13.937	18.914	-20.260
51	SB	158	119.512	.267	19.744	14.378	21.292	-18.587
51	SB	159	125.678	2.201	20.006	14.769	19.629	-20.951
51	SB	160	133.945	.101	20.269	15.181	21.981	-19.292
51	SB	161	140.306	2.006	20.515	15.540	20.330	-21.629
51	SB	162	148.758	-.084	20.763	15.923	22.656	-19.984
51	SB	163	155.334	1.791	20.993	16.252	21.019	-22.295
51	SB	164	163.988	-.286	21.226	16.609	23.316	-20.664
51	SB	165	170.795	1.560	21.441	16.912	21.693	-22.945
51	SB	166	179.664	-.501	21.661	17.246	23.959	-21.329
51	SB	167	186.714	1.317	21.863	17.527	22.350	-23.579
51	SB	168	195.806	-.725	22.071	17.844	24.583	-21.976
51	SB	169	203.105	1.068	22.262	18.108	22.987	-24.193
51	SB	170	212.423	-.951	22.459	18.413	25.186	-22.604
51	SB	171	219.974	.817	22.639	18.666	23.603	-24.786
51	SB	172	229.517	-1.176	22.827	18.964	25.765	-23.212
51	SB	173	237.315	.569	22.999	19.211	24.196	-25.357
51	SB	174	247.076	-1.394	23.180	19.508	26.319	-23.798
	ATOM		M - A	NEUTRON	PROTON	ALPHA	Q BETA -	Q BETA +
52	TE	95	65.402	17.947	-4.403	-2.075	-25.155	23.244
52	TE	96	53.697	20.072	-3.954	-1.972	-26.807	19.876
52	TE	97	44.902	17.162	-3.497	-1.809	-23.439	21.548
52	TE	98	33.996	19.274	-3.056	-1.693	-25.085	18.215
52	TE	99	25.973	16.390	-2.607	-1.535	-21.752	19.864
52	TE	100	15.896	18.445	-2.202	-1.467	-23.322	16.605
52	TE	101	8.636	15.627	-1.761	-1.316	-20.062	18.165
52	TE	102	-.608	17.612	-1.336	-1.295	-21.597	13.780
52	TE	103	-5.955	13.714	-.849	-2.283	-17.264	14.461
52	TE	104	-13.263	15.676	.433	-3.353	-18.733	10.418
52	TE	105	-17.007	12.111	.911	-3.143	-14.689	11.932
52	TE	106	-22.727	14.087	1.373	-2.963	-15.380	8.757
52	TE	107	-25.741	11.381	1.841	-2.722	-12.204	10.292
52	TE	108	-30.731	13.358	2.294	-2.512	-13.704	7.165
52	TE	109	-33.063	10.699	2.751	-2.243	-10.585	8.702
52	TE	110	-37.373	12.678	3.193	-2.005	-12.098	5.643
52	TE	111	-39.069	10.064	3.639	-1.710	-9.036	7.195
52	TE	112	-42.748	12.046	4.068	-1.446	-10.564	4.194
52	TE	113	-43.858	9.478	4.501	-1.127	-7.559	5.763
52	TE	114	-46.954	11.463	4.918	-.838	-9.104	2.819
52	TE	115	-47.526	8.939	5.338	-.497	-6.156	4.405
52	TE	116	-50.087	10.929	5.741	-.186	-7.718	1.517
52	TE	117	-50.167	8.447	6.147	.174	-4.825	3.120
52	TE	118	-52.240	10.440	6.537	.504	-6.405	.286
52	TE	119	-51.870	7.998	6.930	.878	-3.585	1.903
52	TE	120	-53.494	9.992	7.306	1.221	-5.159	-.882
52	TE	121	-52.712	7.585	7.685	1.604	-2.369	.746
52	TE	122	-53.921	9.577	8.048	1.953	-3.975	-1.995
52	TE	123	-52.755	7.201	8.413	2.336	-1.229	-.360
52	TE	124	-53.574	9.187	8.764	2.683	-2.842	-3.064

TABLE 2

Atomic mass excesses and nuclear binding energies

52	TE	125	-52.043	6.836	9.117	3.059	-.133	-1.427
52	TE	126	-52.487	8.812	9.456	3.395	-1.749	-4.101
52	TE	127	-50.599	6.479	9.798	3.753	.929	-2.468
52	TE	128	-50.672	8.440	10.126	4.069	-.684	-5.119
52	TE	129	-48.425	6.120	10.457	4.402	1.972	-3.496
52	TE	130	-48.121	8.063	10.777	4.690	.367	-6.131
52	TE	131	-45.503	5.750	11.099	4.990	3.005	-4.522
52	TE	132	-44.806	7.670	11.410	5.243	1.414	-7.146
52	TE	133	-41.799	5.361	11.724	5.505	4.041	-5.556
52	TE	134	-40.688	7.256	12.029	5.721	2.466	-10.333
52	TE	135	-35.232	2.912	12.462	3.909	7.121	-8.864
52	TE	136	-31.669	4.804	12.886	2.073	5.665	-11.557
52	TE	137	-25.839	2.537	13.311	2.572	8.359	-10.063
52	TE	138	-21.919	4.447	13.728	3.070	6.878	-12.707
52	TE	139	-15.772	2.220	14.145	3.613	9.525	-11.188
52	TE	140	-11.595	4.191	14.596	4.196	7.931	-13.874
52	TE	141	-5.140	1.912	15.003	4.730	10.619	-12.242
52	TE	142	-.713	3.940	15.400	5.344	9.002	-14.884
52	TE	143	5.959	1.695	15.796	5.903	11.647	-13.230
52	TE	144	10.595	3.731	16.179	6.494	10.010	-15.830
52	TE	145	17.448	1.515	16.562	7.112	12.614	-14.159
52	TE	146	22.261	3.555	16.931	7.709	10.961	-16.719
52	TE	147	29.265	1.363	17.300	8.330	13.527	-15.036
52	TE	148	34.232	3.400	17.654	8.922	11.864	-17.560
52	TE	149	41.369	1.230	18.008	9.533	14.394	-15.870
52	TE	150	46.476	3.259	18.346	10.107	12.725	-18.360
52	TE	151	53.739	1.106	18.683	10.697	15.222	-16.668
52	TE	152	58.987	3.120	19.005	11.242	13.553	-19.128
52	TE	153	66.373	.981	19.326	11.800	16.020	-17.437
52	TE	154	71.765	2.976	19.630	12.307	14.354	-19.869
52	TE	155	79.285	.848	19.934	12.824	16.793	-18.184
52	TE	156	84.833	2.819	20.221	13.285	15.135	-20.589
52	TE	157	92.499	.702	20.508	13.755	17.548	-18.914
52	TE	158	98.220	2.646	20.777	14.164	15.899	-21.292
52	TE	159	106.050	.538	21.047	14.583	18.286	-19.629
52	TE	160	111.963	2.454	21.300	14.938	16.651	-21.981
52	TE	161	119.976	.355	21.553	15.305	19.012	-20.330
52	TE	162	126.102	2.241	21.789	15.607	17.390	-22.656
52	TE	163	134.315	.154	22.027	15.923	19.724	-21.019
52	TE	164	140.672	2.011	22.247	16.173	18.117	-23.316
52	TE	165	149.103	-.063	22.470	16.442	20.422	-21.693
52	TE	166	155.705	1.765	22.675	16.646	18.830	-23.959
52	TE	167	164.364	-.292	22.884	16.874	21.104	-22.350
52	TE	168	171.223	1.509	23.076	17.038	19.526	-24.583
52	TE	169	180.118	-.528	23.273	17.232	21.767	-22.987
52	TE	170	187.238	1.247	23.452	17.364	20.202	-25.186
52	TE	171	196.370	-.765	23.638	17.531	22.408	-23.603
52	TE	172	203.752	.985	23.806	17.639	20.857	-25.765
52	TE	173	213.119	-.999	23.983	17.788	23.025	-24.196
52	TE	174	220.758	.729	24.142	17.880	21.489	-26.319
52	TE	175	230.350	-1.225	24.311	18.018	23.617	-24.765
52	TE	176	238.237	.481	24.463	18.101	22.096	-26.849
52	TE	177	248.044	-1.440	24.626	18.237	24.184	-25.311
52	TE	178	256.167	.244	24.773	18.317	22.679	-29.110
	ATØM		M - A	NEUTRØN	PRØTØN	ALPHA	Q BETA -	Q BETA +
53	I	96	80.503	18.421	-7.517	-2.291	-23.670	26.807
53	I	97	68.341	20.530	-7.059	-2.204	-25.321	23.439
53	I	98	59.081	17.627	-6.594	-2.058	-21.977	25.085
53	I	99	47.725	19.723	-6.144	-1.958	-23.623	21.752
53	I	100	39.217	16.875	-5.660	-1.788	-20.368	23.322

TABLE 2

Atomic mass excesses and nuclear binding energies

53	I	101	28.699	18.886	-5.218	-1.735	-21.938	20.062
53	I	102	20.989	16.077	-4.768	-1.599	-18.702	21.597
53	I	103	11.310	18.047	-4.333	-1.591	-20.237	17.264
53	I	104	5.469	14.208	-3.839	-2.569	-15.979	18.733
53	I	105	-2.318	16.154	-3.361	-3.602	-17.447	14.689
53	I	106	-7.347	13.397	-2.075	-3.433	-14.227	15.380
53	I	107	-13.537	14.557	-1.605	-3.269	-14.917	12.204
53	I	108	-17.027	11.858	-1.129	-3.045	-10.975	13.704
53	I	109	-22.478	13.818	-.669	-2.852	-12.474	10.585
53	I	110	-25.275	11.164	-.203	-2.600	-9.375	12.098
53	I	111	-30.034	13.127	.246	-2.380	-10.886	9.036
53	I	112	-32.184	10.517	.699	-2.103	-7.842	10.564
53	I	113	-36.299	12.483	1.136	-1.856	-9.367	7.559
53	I	114	-37.850	9.918	1.577	-1.556	-6.379	9.104
53	I	115	-41.370	11.887	2.001	-1.285	-7.920	6.156
53	I	116	-42.369	9.366	2.428	-.963	-4.987	7.718
53	I	117	-45.342	11.340	2.839	-.670	-6.545	4.825
53	I	118	-45.835	8.861	3.253	-.329	-3.667	6.405
53	I	119	-48.305	10.837	3.650	-.017	-5.241	3.565
53	I	120	-48.335	8.397	4.050	.339	-2.415	5.159
53	I	121	-50.343	10.375	4.433	.665	-4.004	2.369
53	I	122	-49.946	7.971	4.819	1.030	-1.226	3.975
53	I	123	-51.526	9.948	5.190	1.362	-2.827	1.229
53	I	124	-50.732	7.573	5.562	1.729	-.091	2.842
53	I	125	-51.910	9.545	5.920	2.061	-1.700	.133
53	I	126	-50.738	7.196	6.280	2.421	.999	1.749
53	I	127	-51.529	9.158	6.626	2.743	-.613	-.929
53	I	128	-49.988	6.827	6.974	3.087	2.056	.684
53	I	129	-50.397	8.776	7.309	3.390	.448	-1.972
53	I	130	-48.488	6.458	7.647	3.711	3.094	-.367
53	I	131	-48.509	8.389	7.973	3.987	1.493	-3.005
53	I	132	-46.220	6.078	8.301	4.276	4.122	-1.414
53	I	133	-45.840	7.988	8.619	4.520	2.535	-4.041
53	I	134	-43.154	5.681	8.939	4.773	5.153	-2.466
53	I	135	-42.353	7.567	9.250	4.982	3.581	-7.121
53	I	136	-37.334	3.348	9.687	3.284	8.105	-5.665
53	I	137	-34.198	5.231	10.114	1.564	6.649	-8.359
53	I	138	-28.797	2.966	10.543	2.051	9.332	-6.878
53	I	139	-25.297	4.867	10.962	2.537	7.852	-9.525
53	I	140	-19.526	2.597	11.339	3.023	10.577	-7.931
53	I	141	-15.760	4.601	11.749	3.593	8.984	-10.619
53	I	142	-9.715	2.323	12.160	4.113	11.665	-9.002
53	I	143	-5.688	4.340	12.559	4.713	10.050	-11.647
53	I	144	.586	2.094	12.959	5.302	12.687	-10.010
53	I	145	4.834	4.119	13.346	5.877	11.053	-12.614
53	I	146	11.299	1.902	13.733	6.480	13.649	-10.961
53	I	147	15.738	3.929	14.108	7.061	12.001	-13.527
53	I	148	22.368	1.737	14.482	7.666	14.558	-11.864
53	I	149	26.975	3.760	14.841	8.241	12.900	-14.394
53	I	150	33.753	1.590	15.201	8.836	15.421	-12.725
53	I	151	38.517	3.603	15.545	9.393	13.758	-15.222
53	I	152	45.434	1.450	15.890	9.967	16.247	-13.553
53	I	153	50.354	3.448	16.218	10.494	14.584	-16.020
53	I	154	57.412	1.309	16.547	11.036	17.042	-14.354
53	I	155	62.491	3.288	16.859	11.525	15.383	-16.793
53	I	156	69.698	1.160	17.171	12.025	17.813	-15.135
53	I	157	74.951	3.115	17.467	12.469	16.162	-17.548
53	I	158	82.321	.998	17.763	12.922	18.565	-15.899
53	I	159	87.763	2.925	18.042	13.315	16.925	-18.286
53	I	160	95.313	.818	18.322	13.718	19.301	-16.651
53	I	161	100.964	2.716	18.584	14.058	17.673	-19.012
53	I	162	108.712	.620	18.849	14.410	20.023	-17.390

TABLE 2

Atomic mass excesses and nuclear binding energies

53	I	163	114.591	2.488	19.095	14.696	18.409	-19.724
53	I	164	122.555	.404	19.345	14.998	20.730	-18.117
53	I	165	128.680	2.242	19.576	15.235	19.132	-20.422
53	I	166	136.875	.173	19.812	15.492	21.423	-18.830
53	I	167	143.260	1.982	20.029	15.683	19.839	-21.104
53	I	168	151.697	-.069	20.252	15.900	22.098	-19.526
53	I	169	158.351	1.713	20.456	16.053	20.528	-21.767
53	I	170	167.035	-.317	20.667	16.238	22.752	-20.202
53	I	171	173.963	1.440	20.860	16.360	21.196	-22.408
53	I	172	182.895	-.565	21.060	16.520	23.383	-20.857
53	I	173	190.094	1.168	21.243	16.620	21.840	-23.025
53	I	174	199.269	-.808	21.435	16.764	23.988	-21.489
53	I	175	206.733	.903	21.609	16.850	22.458	-23.617
53	I	176	216.141	-1.041	21.794	16.985	24.565	-22.096
53	I	177	223.860	.649	21.962	17.064	23.050	-24.184
53	I	178	233.488	-1.260	22.141	17.198	25.115	-22.679
53	I	179	241.448	.407	22.304	17.277	23.615	-26.242
53	I	180	252.498	-2.683	22.777	16.197	26.794	-25.118
53	I	181	262.029	-1.164	23.171	14.934	25.667	-27.240
ATOM			M - A	NEUTRON	PROTON	ALPHA	Q BETA -	Q BETA +
54	XE	99	71.348	18.077	-4.682	-2.337	-25.482	23.623
54	XE	100	59.586	20.130	-4.276	-2.280	-27.049	20.368
54	XE	101	50.636	17.317	-3.834	-2.125	-23.793	21.938
54	XE	102	39.691	19.312	-3.408	-2.086	-25.337	18.702
54	XE	103	31.547	16.512	-2.973	-1.964	-22.102	20.237
54	XE	104	21.448	18.466	-2.554	-1.943	-23.612	15.979
54	XE	105	15.130	14.686	-2.076	-2.884	-19.403	17.447
54	XE	106	6.880	16.617	-1.613	-3.879	-20.850	14.227
54	XE	107	1.380	13.867	-1.143	-3.726	-17.630	14.917
54	XE	108	-6.052	15.799	.100	-3.602	-19.085	10.975
54	XE	109	-10.003	12.319	.561	-3.395	-15.143	12.474
54	XE	110	-15.900	14.264	1.007	-3.218	-15.844	9.375
54	XE	111	-19.148	11.615	1.458	-2.984	-12.743	10.886
54	XE	112	-24.342	13.562	1.893	-2.780	-14.231	7.842
54	XE	113	-26.932	10.957	2.333	-2.521	-11.185	9.367
54	XE	114	-31.472	12.907	2.757	-2.292	-12.688	6.379
54	XE	115	-33.450	10.346	3.185	-2.010	-9.696	7.920
54	XE	116	-37.382	12.299	3.597	-1.756	-11.215	4.987
54	XE	117	-38.797	9.782	4.012	-1.452	-8.278	6.545
54	XE	118	-42.168	11.739	4.411	-1.177	-9.814	3.667
54	XE	119	-43.064	9.263	4.813	-.853	-6.931	5.241
54	XE	120	-45.920	11.224	5.200	-.558	-8.484	2.415
54	XE	121	-46.338	8.786	5.589	-.219	-5.652	4.004
54	XE	122	-48.720	10.749	5.962	.090	-7.220	1.226
54	XE	123	-48.699	8.346	6.338	.439	-4.436	2.827
54	XE	124	-50.641	10.309	6.699	.756	-6.016	.091
54	XE	125	-50.210	7.936	7.062	1.107	-3.276	1.700
54	XE	126	-51.737	9.894	7.412	1.425	-4.864	-.999
54	XE	127	-50.916	7.547	7.763	1.771	-2.160	.613
54	XE	128	-52.045	9.496	8.101	2.080	-3.751	-2.056
54	XE	129	-50.845	7.167	8.441	2.411	-1.077	-.448
54	XE	130	-51.581	9.104	8.769	2.703	-2.667	-3.094
54	XE	131	-50.002	6.788	9.099	3.012	-.016	-1.493
54	XE	132	-50.342	8.708	9.418	3.279	-1.599	-4.122
54	XE	133	-48.375	6.400	9.740	3.559	1.035	-2.535
54	XE	134	-48.307	8.299	10.051	3.795	-.536	-5.153
54	XE	135	-45.934	5.995	10.365	4.040	2.085	-3.581
54	XE	136	-45.439	7.872	10.671	4.243	.529	-8.105
54	XE	137	-40.847	3.775	11.098	2.657	4.938	-6.649
54	XE	138	-38.129	5.649	11.516	1.051	3.492	-9.332

TABLE 2

Atomic mass excesses and nuclear binding energies

54	XE	139	-33.148	3.387	11.936	1.525	6.174	-7.852
54	XE	140	-30.103	5.322	12.391	2.043	4.616	-10.577
54	XE	141	-24.744	3.009	12.803	2.514	7.342	-8.984
54	XE	142	-21.380	5.003	13.205	3.070	5.761	-11.665
54	XE	143	-15.738	2.725	13.607	3.575	8.442	-10.050
54	XE	144	-12.101	4.731	13.998	4.115	6.841	-12.687
54	XE	145	-6.219	2.485	14.389	4.688	9.480	-11.053
54	XE	146	-2.350	4.498	14.768	5.245	7.862	-13.649
54	XE	147	3.737	2.281	15.147	5.832	10.461	-12.001
54	XE	148	7.810	4.294	15.512	6.394	8.829	-14.558
54	XE	149	14.075	2.102	15.877	6.982	11.391	-12.900
54	XE	150	18.332	4.111	16.228	7.538	9.752	-15.421
54	XE	151	24.759	1.940	16.579	8.115	12.278	-13.758
54	XE	152	29.188	3.938	16.914	8.653	10.636	-16.247
54	XE	153	35.770	1.785	17.249	9.208	13.131	-14.584
54	XE	154	40.370	3.767	17.569	9.717	11.491	-17.042
54	XE	155	47.108	1.629	17.888	10.240	13.955	-15.383
54	XE	156	51.885	3.590	18.191	10.711	12.321	-17.813
54	XE	157	58.789	1.464	18.494	11.194	14.758	-16.162
54	XE	158	63.756	3.400	18.780	11.618	13.133	-18.565
54	XE	159	70.839	1.285	19.067	12.055	15.544	-16.925
54	XE	160	76.012	3.194	19.336	12.430	13.931	-19.301
54	XE	161	83.291	1.089	19.607	12.817	16.316	-17.673
54	XE	162	88.689	2.969	19.859	13.140	14.717	-20.023
54	XE	163	96.182	.875	20.115	13.477	17.075	-18.409
54	XE	164	101.825	2.725	20.351	13.748	15.492	-20.730
54	XE	165	109.549	.644	20.591	14.036	17.822	-19.132
54	XE	166	115.452	2.464	20.813	14.259	16.254	-21.423
54	XE	167	123.421	.398	21.039	14.503	18.554	-19.839
54	XE	168	129.599	2.190	21.246	14.682	17.002	-22.098
54	XE	169	137.823	.143	21.459	14.889	19.270	-20.528
54	XE	170	144.283	1.907	21.653	15.031	17.733	-22.752
54	XE	171	152.767	-.116	21.853	15.206	19.965	-21.196
54	XE	172	159.512	1.622	22.036	15.320	18.443	-23.383
54	XE	173	168.254	-.375	22.226	15.473	20.638	-21.840
54	XE	174	175.281	1.340	22.398	15.566	19.129	-23.988
54	XE	175	184.275	-.627	22.579	15.705	21.284	-22.458
54	XE	176	191.576	1.066	22.742	15.786	19.789	-24.565
54	XE	177	200.810	-.867	22.916	15.918	21.903	-23.050
54	XE	178	208.373	.805	23.072	15.994	20.423	-25.115
54	XE	179	217.833	-1.093	23.240	16.127	22.494	-23.615
54	XE	180	225.704	.496	23.328	16.142	21.154	-26.794
54	XE	181	236.362	-2.291	23.720	15.291	24.110	-25.667
54	XE	182	245.519	-.789	24.095	14.257	23.010	-27.758
54	XE	183	256.380	-2.493	24.482	14.920	25.098	-26.654
54	XE	184	265.766	-1.019	24.853	15.459	24.019	-28.709
54	XE	185	276.826	-2.693	25.234	16.052	26.072	-27.624
54	XE	186	286.438	-1.244	25.598	16.585	25.012	-29.643
	ATOM		M - A	NEUTRON	PROTON	ALPHA	Q BETA -	Q BETA +
55	CS	100	86.634	18.563	-7.702	-2.522	-24.067	27.049
55	CS	101	74.429	20.572	-7.259	-2.479	-25.633	23.793
55	CS	102	65.029	17.768	-6.808	-2.339	-22.402	25.337
55	CS	103	53.649	19.748	-6.372	-2.314	-23.945	22.102
55	CS	104	45.060	16.956	-5.929	-2.233	-20.733	23.612
55	CS	105	34.533	18.895	-5.500	-2.225	-22.243	19.403
55	CS	106	27.730	15.170	-5.015	-3.132	-18.104	20.850
55	CS	107	19.010	17.087	-4.546	-4.091	-19.552	17.630
55	CS	108	13.033	14.344	-4.068	-3.955	-16.356	19.085
55	CS	109	5.140	16.261	-3.607	-3.848	-17.812	15.143
55	CS	110	-.056	13.563	-2.363	-3.682	-14.667	15.844

TABLE 2

Atomic mass excesses and nuclear binding energies

55	CS	111	-6.405	14.716	-1.910	-3.523	-15.368	12.743
55	CS	112	-10.111	12.073	-1.452	-3.307	-11.522	14.231
55	CS	113	-15.747	14.004	-1.010	-3.121	-13.010	11.185
55	CS	114	-18.784	11.404	-.563	-2.881	-9.981	12.688
55	CS	115	-23.754	13.338	-.133	-2.670	-11.482	9.696
55	CS	116	-26.168	10.781	.302	-2.407	-8.507	11.215
55	CS	117	-30.518	12.718	.721	-2.172	-10.023	8.278
55	CS	118	-32.354	10.203	1.143	-1.887	-7.102	9.814
55	CS	119	-36.132	12.145	1.549	-1.629	-8.634	6.931
55	CS	120	-37.436	9.671	1.958	-1.324	-5.765	8.484
55	CS	121	-40.686	11.617	2.351	-1.046	-7.313	5.652
55	CS	122	-41.500	9.182	2.747	-.725	-4.495	7.220
55	CS	123	-44.263	11.130	3.127	-.433	-6.058	4.436
55	CS	124	-44.625	8.729	3.510	-.101	-3.286	6.016
55	CS	125	-46.934	10.677	3.878	.201	-4.861	3.276
55	CS	126	-46.873	8.306	4.248	.536	-2.131	4.864
55	CS	127	-48.756	10.251	4.604	.840	-3.714	2.160
55	CS	128	-48.294	7.905	4.963	1.171	-1.020	3.751
55	CS	129	-49.768	9.841	5.308	1.467	-2.606	1.077
55	CS	130	-48.915	7.514	5.654	1.786	.059	2.667
55	CS	131	-49.986	9.439	5.989	2.066	-1.526	.016
55	CS	132	-48.744	7.125	6.326	2.364	1.116	1.599
55	CS	133	-49.410	9.033	6.652	2.622	-.462	-1.035
55	CS	134	-47.770	6.728	6.980	2.892	2.163	.536
55	CS	135	-48.020	8.617	7.298	3.120	.596	-2.085
55	CS	136	-45.968	6.316	7.619	3.358	3.210	-.529
55	CS	137	-45.785	8.184	7.930	3.554	1.658	-4.938
55	CS	138	-41.621	4.203	8.359	2.076	5.945	-3.492
55	CS	139	-39.322	6.069	8.778	.578	4.497	-6.174
55	CS	140	-34.719	3.764	9.156	.994	7.255	-4.616
55	CS	141	-32.086	5.734	9.568	1.497	5.696	-7.342
55	CS	142	-27.141	3.422	9.981	1.953	8.410	-5.761
55	CS	143	-24.180	5.407	10.385	2.493	6.829	-8.442
55	CS	144	-18.942	3.129	10.789	3.025	9.500	-6.841
55	CS	145	-15.699	5.124	11.183	3.549	7.899	-9.480
55	CS	146	-10.211	2.879	11.577	4.105	10.527	-7.862
55	CS	147	-6.723	4.880	11.959	4.645	8.911	-10.461
55	CS	148	-1.019	2.663	12.341	5.214	11.498	-8.829
55	CS	149	2.685	4.664	12.710	5.759	9.870	-11.391
55	CS	150	8.580	2.472	13.080	6.329	12.420	-9.752
55	CS	151	12.481	4.467	13.436	6.866	10.785	-12.278
55	CS	152	18.551	2.297	13.792	7.426	13.301	-10.636
55	CS	153	22.639	4.280	14.133	7.945	11.664	-13.131
55	CS	154	28.879	2.127	14.475	8.483	14.147	-11.491
55	CS	155	33.153	4.093	14.801	8.973	12.512	-13.955
55	CS	156	39.565	1.956	15.129	9.479	14.965	-12.321
55	CS	157	44.031	3.901	15.439	9.932	13.338	-14.758
55	CS	158	50.623	1.776	15.751	10.398	15.763	-13.133
55	CS	159	55.295	3.695	16.046	10.806	14.145	-15.544
55	CS	160	62.081	1.582	16.343	11.227	16.544	-13.931
55	CS	161	66.975	3.473	16.622	11.585	14.939	-16.316
55	CS	162	73.972	1.370	16.903	11.958	17.311	-14.717
55	CS	163	79.107	3.232	17.167	12.265	15.721	-17.075
55	CS	164	86.333	1.142	17.434	12.589	18.066	-15.492
55	CS	165	91.727	2.973	17.683	12.846	16.491	-17.822
55	CS	166	99.198	.896	17.935	13.123	18.807	-16.254
55	CS	167	104.867	2.698	18.170	13.333	17.249	-18.554
55	CS	168	112.597	.638	18.409	13.568	19.534	-17.002
55	CS	169	118.553	2.411	18.630	13.736	17.991	-19.270
55	CS	170	126.550	.370	18.858	13.934	20.243	-17.733
55	CS	171	132.801	2.116	19.067	14.068	18.714	-19.965
55	CS	172	141.069	.100	19.283	14.237	20.930	-18.443

TABLE 2

Atomic mass excesses and nuclear binding energies

55	CS	173	147.616	1.820	19.481	14.344	19.416	-20.638
55	CS	174	156.152	-.169	19.687	14.493	21.593	-19.129
55	CS	175	162.990	1.529	19.875	14.582	20.092	-21.284
55	CS	176	171.786	-.429	20.073	14.718	22.228	-19.789
55	CS	177	178.907	1.247	20.254	14.796	20.741	-21.903
55	CS	178	187.950	-.676	20.445	14.928	22.834	-20.423
55	CS	179	195.339	.979	20.619	15.004	21.360	-22.494
55	CS	180	204.550	-.844	20.867	15.200	23.284	-21.154
55	CS	181	212.252	.665	21.037	15.217	21.951	-24.110
55	CS	182	222.509	-1.890	21.438	14.587	24.665	-23.010
55	CS	183	231.282	-.405	21.822	13.775	23.559	-25.098
55	CS	184	241.747	-2.098	22.218	14.360	25.615	-24.019
55	CS	185	250.754	-.640	22.596	14.885	24.532	-26.072
55	CS	186	261.426	-2.305	22.985	15.461	26.556	-25.012
55	CS	187	270.665	-.872	23.357	15.978	25.493	-27.030
55	CS	188	281.543	-2.510	23.737	16.542	27.484	-25.984
55	CS	189	291.010	-1.101	24.101	17.049	26.436	-27.966
	ATOM		M - A	NEUTRON	PROTON	ALPHA	Q BETA -	Q BETA +
56	BA	103	77.594	18.204	-4.980	-2.637	-25.770	23.945
56	BA	104	65.793	20.168	-4.560	-2.598	-27.289	20.733
56	BA	105	56.776	17.385	-4.131	-2.530	-24.076	22.243
56	BA	106	45.834	19.309	-3.716	-2.533	-25.562	18.104
56	BA	107	38.563	15.638	-3.248	-3.407	-21.468	19.552
56	BA	108	29.390	17.540	-2.795	-4.332	-22.896	16.356
56	BA	109	22.952	14.805	-2.333	-4.213	-19.701	17.812
56	BA	110	14.612	16.707	-1.887	-4.122	-21.137	14.667
56	BA	111	8.963	14.016	-1.434	-3.973	-17.993	15.368
56	BA	112	1.412	15.919	-.232	-3.854	-19.437	11.522
56	BA	113	-2.738	12.517	.212	-3.656	-15.591	13.010
56	BA	114	-8.803	14.432	.640	-3.488	-16.304	9.981
56	BA	115	-12.272	11.837	1.073	-3.266	-13.274	11.482
56	BA	116	-17.660	13.755	1.491	-3.073	-14.754	8.507
56	BA	117	-20.495	11.202	1.912	-2.828	-11.777	10.023
56	BA	118	-25.252	13.125	2.319	-2.610	-13.272	7.102
56	BA	119	-27.498	10.613	2.729	-2.343	-10.348	8.634
56	BA	120	-31.671	12.540	3.124	-2.102	-11.859	5.765
56	BA	121	-33.373	10.069	3.521	-1.815	-8.986	7.313
56	BA	122	-37.005	12.000	3.904	-1.554	-10.514	4.495
56	BA	123	-38.205	9.567	4.289	-1.249	-7.691	6.058
56	BA	124	-41.338	11.501	4.660	-.972	-9.233	3.286
56	BA	125	-42.073	9.102	5.033	-.656	-6.457	4.861
56	BA	126	-44.742	11.036	5.393	-.369	-8.011	2.131
56	BA	127	-45.042	8.668	5.754	-.048	-5.276	3.714
56	BA	128	-47.274	10.599	6.102	.243	-6.840	1.020
56	BA	129	-47.161	8.255	6.452	.561	-4.141	2.606
56	BA	130	-48.973	10.179	6.790	.846	-5.708	-.059
56	BA	131	-48.460	7.854	7.130	1.153	-3.038	1.526
56	BA	132	-49.859	9.767	7.458	1.424	-4.604	-1.116
56	BA	133	-48.948	7.456	7.789	1.712	-1.958	.462
56	BA	134	-49.933	9.353	8.109	1.961	-3.518	-2.163
56	BA	135	-48.616	7.050	8.431	2.223	-.888	-.596
56	BA	136	-49.179	8.930	8.744	2.446	-2.439	-3.210
56	BA	137	-47.442	6.631	9.059	2.677	.179	-1.658
56	BA	138	-47.566	8.491	9.366	2.868	-1.358	-5.945
56	BA	139	-43.819	4.621	9.783	1.494	2.825	-4.497
56	BA	140	-41.974	6.522	10.236	.144	1.297	-7.255
56	BA	141	-37.782	4.175	10.648	.544	4.052	-5.696
56	BA	142	-35.551	6.136	11.050	1.031	2.502	-8.410
56	BA	143	-31.009	3.826	11.453	1.470	5.215	-6.829
56	BA	144	-28.442	5.800	11.847	1.948	3.644	-9.500

TABLE 2

Atomic mass excesses and nuclear binding energies

56	BA	145	-23.598	3.524	12.241	2.463	6.314	-7.899
56	BA	146	-20.738	5.507	12.624	2.967	4.726	-10.527
56	BA	147	-15.634	3.263	13.008	3.505	7.355	-8.911
56	BA	148	-12.518	5.251	13.379	4.025	5.753	-11.498
56	BA	149	-7.186	3.035	13.751	4.576	8.342	-9.870
56	BA	150	-3.841	5.022	14.110	5.100	6.730	-12.420
56	BA	151	1.695	2.832	14.469	5.651	9.283	-10.785
56	BA	152	5.251	4.812	14.815	6.169	7.667	-13.301
56	BA	153	10.976	2.643	15.161	6.709	10.186	-11.664
56	BA	154	14.733	4.610	15.491	7.208	8.569	-14.147
56	BA	155	20.641	2.459	15.823	7.727	11.057	-12.512
56	BA	156	24.599	4.409	16.139	8.198	9.445	-14.965
56	BA	157	30.693	2.273	16.456	8.686	11.904	-13.338
56	BA	158	34.860	4.201	16.756	9.119	10.301	-15.763
56	BA	159	41.149	2.078	17.058	9.568	12.732	-14.145
56	BA	160	45.537	3.980	17.343	9.958	11.141	-16.544
56	BA	161	52.036	1.868	17.630	10.362	13.546	-14.939
56	BA	162	56.661	3.742	17.899	10.704	11.970	-17.311
56	BA	163	63.386	1.642	18.171	11.062	14.349	-15.721
56	BA	164	68.267	3.486	18.425	11.354	12.789	-18.066
56	BA	165	75.236	1.399	18.682	11.664	15.142	-16.491
56	BA	166	80.391	3.212	18.921	11.908	13.598	-18.807
56	BA	167	87.619	1.140	19.164	12.173	15.923	-17.249
56	BA	168	93.063	2.923	19.389	12.371	14.397	-19.534
56	BA	169	100.563	.868	19.619	12.595	16.691	-17.991
56	BA	170	106.308	2.622	19.830	12.754	15.181	-20.243
56	BA	171	114.087	.588	20.048	12.944	17.442	-18.714
56	BA	172	120.139	2.316	20.247	13.069	15.948	-20.930
56	BA	173	128.200	.306	20.454	13.232	18.173	-19.416
56	BA	174	134.559	2.009	20.642	13.334	16.694	-21.593
56	BA	175	142.898	.028	20.839	13.478	18.880	-20.092
56	BA	176	149.558	1.707	21.017	13.563	17.416	-22.228
56	BA	177	158.166	-.240	21.205	13.697	19.560	-20.741
56	BA	178	165.116	1.417	21.375	13.774	18.109	-22.834
56	BA	179	173.978	-.495	21.556	13.906	20.210	-21.360
56	BA	180	181.266	1.080	21.657	13.919	18.899	-23.284
56	BA	181	190.302	-.668	21.833	14.118	20.830	-21.951
56	BA	182	197.845	.824	21.992	14.137	19.533	-24.665
56	BA	183	207.723	-1.510	22.372	13.719	22.046	-23.559
56	BA	184	216.132	-.042	22.735	13.182	20.962	-25.615
56	BA	185	226.222	-1.723	23.110	13.750	23.013	-24.532
56	BA	186	234.870	-.281	23.469	14.259	21.951	-26.556
56	BA	187	245.173	-1.936	23.838	14.816	23.970	-25.493
56	BA	188	254.059	-.519	24.191	15.316	22.927	-27.484
56	BA	189	264.575	-2.148	24.553	15.861	24.914	-26.436
56	BA	190	273.697	-.755	24.899	16.350	23.886	-28.393
56	BA	191	284.424	-2.360	25.251	16.880	25.841	-27.358
56	BA	192	293.779	-.987	25.588	17.357	24.824	-29.281
56	BA	193	304.715	-2.568	25.930	17.871	26.746	-28.254
	ATOM		M - A	NEUTRON	PROTON	ALPHA	Q BETA -	Q BETA +
57	LA	105	80.852	20.598	-7.474	-2.813	-25.889	24.076
57	LA	106	71.396	17.823	-7.036	-2.758	-22.699	25.562
57	LA	107	60.031	19.733	-6.612	-2.773	-24.184	21.468
57	LA	108	52.286	16.113	-6.138	-3.617	-20.154	22.896
57	LA	109	42.653	18.000	-5.679	-4.511	-21.584	19.701
57	LA	110	35.748	15.272	-5.212	-4.409	-18.413	21.137
57	LA	111	26.956	17.160	-4.760	-4.336	-19.850	17.993
57	LA	112	20.849	14.475	-4.301	-4.206	-16.728	19.437
57	LA	113	12.853	16.363	-3.857	-4.104	-18.173	15.591
57	LA	114	7.501	13.720	-2.654	-3.948	-15.101	16.304

TABLE 2

Atomic mass excesses and nuclear binding energies

57	LA	115	1.002	14.866	-2.220	-3.798	-15.813	13.274
57	LA	116	-2.906	12.276	-1.781	-3.595	-12.059	14.754
57	LA	117	-8.718	14.179	-1.357	-3.420	-13.538	11.777
57	LA	118	-11.981	11.630	-.930	-3.194	-10.578	13.272
57	LA	119	-17.151	13.537	-.517	-2.994	-12.070	10.348
57	LA	120	-19.813	11.029	-.101	-2.746	-9.162	11.859
57	LA	121	-24.386	12.941	.300	-2.523	-10.670	8.986
57	LA	122	-26.492	10.473	.704	-2.253	-7.811	10.514
57	LA	123	-30.514	12.389	1.093	-2.009	-9.335	7.691
57	LA	124	-32.105	9.959	1.485	-1.722	-6.525	9.233
57	LA	125	-35.616	11.878	1.863	-1.460	-8.063	6.457
57	LA	126	-36.731	9.482	2.242	-1.160	-5.298	8.011
57	LA	127	-39.766	11.403	2.609	-.888	-6.848	5.276
57	LA	128	-40.434	9.036	2.977	-.581	-4.123	6.840
57	LA	129	-43.021	10.954	3.332	-.304	-5.682	4.141
57	LA	130	-43.265	8.612	3.689	.001	-2.992	5.708
57	LA	131	-45.422	10.524	4.033	.275	-4.554	3.038
57	LA	132	-45.255	8.201	4.380	.571	-1.893	4.604
57	LA	133	-46.990	10.102	4.715	.832	-3.454	1.958
57	LA	134	-46.415	7.793	5.053	1.110	-.815	3.518
57	LA	135	-47.728	9.680	5.379	1.351	-2.371	.888
57	LA	136	-46.740	7.379	5.708	1.605	.252	2.439
57	LA	137	-47.622	9.249	6.028	1.821	-1.294	-.179
57	LA	138	-46.207	6.953	6.350	2.046	1.317	1.358
57	LA	139	-46.644	8.804	6.663	2.233	-.217	-2.825
57	LA	140	-43.270	4.994	7.036	.911	3.946	-1.297
57	LA	141	-41.834	6.931	7.445	-.342	2.415	-4.052
57	LA	142	-38.053	4.586	7.856	.041	5.157	-2.502
57	LA	143	-36.224	6.538	8.258	.511	3.604	-5.215
57	LA	144	-32.086	4.229	8.662	.976	6.303	-3.644
57	LA	145	-29.912	6.194	9.055	1.436	4.730	-6.314
57	LA	146	-25.464	3.919	9.451	1.933	7.386	-4.726
57	LA	147	-22.989	5.892	9.835	2.418	5.797	-7.355
57	LA	148	-18.270	3.649	10.221	2.937	8.412	-5.753
57	LA	149	-15.528	5.625	10.595	3.438	6.810	-8.342
57	LA	150	-10.571	3.411	10.970	3.969	9.386	-6.730
57	LA	151	-7.588	5.384	11.332	4.474	7.776	-9.283
57	LA	152	-2.416	3.195	11.696	5.006	10.315	-7.667
57	LA	153	.790	5.161	12.046	5.504	8.701	-10.186
57	LA	154	6.163	2.994	12.397	6.026	11.206	-8.569
57	LA	155	9.584	4.947	12.733	6.506	9.593	-11.057
57	LA	156	15.154	2.797	13.072	7.007	12.067	-9.445
57	LA	157	18.790	4.732	13.394	7.459	10.460	-11.904
57	LA	158	24.559	2.598	13.719	7.929	12.905	-10.301
57	LA	159	28.417	4.509	14.027	8.345	11.307	-12.732
57	LA	160	34.396	2.389	14.338	8.778	13.725	-11.141
57	LA	161	38.489	4.274	14.632	9.151	12.140	-13.546
57	LA	162	44.691	2.165	14.929	9.541	14.532	-11.970
57	LA	163	49.037	4.022	15.209	9.867	12.962	-14.349
57	LA	164	55.478	1.926	15.492	10.212	15.327	-12.789
57	LA	165	60.094	3.752	15.758	10.490	13.775	-15.142
57	LA	166	66.793	1.669	16.028	10.789	16.113	-13.598
57	LA	167	71.696	3.464	16.280	11.021	14.578	-15.923
57	LA	168	78.666	1.397	16.537	11.276	16.888	-14.397
57	LA	169	83.872	3.162	16.776	11.464	15.370	-16.691
57	LA	170	91.126	1.113	17.021	11.681	17.649	-15.181
57	LA	171	96.645	2.849	17.248	11.832	16.148	-17.442
57	LA	172	104.190	.822	17.481	12.016	18.393	-15.948
57	LA	173	110.027	2.531	17.697	12.136	16.908	-18.173
57	LA	174	117.864	.530	17.920	12.295	19.116	-16.694
57	LA	175	124.018	2.214	18.126	12.393	17.646	-18.880
57	LA	176	132.142	.243	18.340	12.536	19.814	-17.416

TABLE 2

Atomic mass excesses and nuclear binding energies

57	LA	177	138.606	1.904	18.537	12.619	18.358	-19.560
57	LA	178	147.007	-.034	18.744	12.754	20.483	-18.109
57	LA	179	153.768	1.606	18.933	12.831	19.041	-20.210
57	LA	180	162.367	-.231	19.196	13.029	20.996	-18.899
57	LA	181	169.472	1.263	19.379	13.045	19.693	-20.830
57	LA	182	178.312	-.473	19.574	13.247	21.602	-19.533
57	LA	183	185.677	1.003	19.753	13.271	20.313	-22.046
57	LA	184	195.169	-1.125	20.138	12.990	22.611	-20.962
57	LA	185	203.209	.328	20.507	12.653	21.520	-23.013
57	LA	186	212.919	-1.343	20.887	13.200	23.537	-21.951
57	LA	187	221.203	.083	21.252	13.688	22.469	-23.970
57	LA	188	231.132	-1.562	21.625	14.224	24.457	-22.927
57	LA	189	239.661	-.161	21.983	14.702	23.408	-24.914
57	LA	190	249.811	-1.783	22.348	15.224	25.367	-23.886
57	LA	191	258.584	-.405	22.698	15.691	24.334	-25.841
57	LA	192	268.955	-2.004	23.054	16.197	26.263	-24.824
57	LA	193	277.969	-.647	23.395	16.651	25.243	-26.746
57	LA	194	288.558	-2.223	23.741	17.141	27.142	-25.738
57	LA	195	297.810	-.884	24.072	17.581	26.131	-27.627
57	LA	196	308.615	-2.438	24.406	18.055	27.999	-26.623
57	LA	197	318.097	-1.115	24.725	18.481	26.994	-28.477
57	LA	198	329.112	-2.647	25.047	18.937	28.830	-27.474
	ATOM		M - A	NEUTRON	PROTON	ALPHA	Q BETA -	Q BETA +
58	CE	107	84.215	18.247	-5.234	-3.012	-25.987	24.184
58	CE	108	72.440	20.142	-4.824	-3.038	-27.449	20.154
58	CE	109	64.238	16.570	-4.367	-3.853	-23.458	21.584
58	CE	110	54.161	18.443	-3.924	-4.718	-24.869	18.413
58	CE	111	46.806	15.723	-3.473	-4.634	-21.700	19.850
58	CE	112	37.577	17.596	-3.036	-4.578	-23.118	16.728
58	CE	113	31.026	14.918	-2.593	-4.466	-19.998	18.173
58	CE	114	22.602	16.792	-2.164	-4.382	-21.424	15.101
58	CE	115	16.816	14.154	-1.729	-4.243	-18.352	15.813
58	CE	116	9.153	16.030	-.566	-4.132	-19.788	12.059
58	CE	117	4.820	12.701	-.141	-3.948	-16.034	13.538
58	CE	118	-1.403	14.590	.270	-3.790	-16.760	10.578
58	CE	119	-5.080	12.045	.684	-3.583	-13.799	12.070
58	CE	120	-10.651	13.938	1.085	-3.400	-15.272	9.162
58	CE	121	-13.717	11.433	1.489	-3.169	-12.361	10.670
58	CE	122	-18.681	13.331	1.879	-2.963	-13.850	7.811
58	CE	123	-21.179	10.866	2.272	-2.710	-10.989	9.335
58	CE	124	-25.580	12.769	2.651	-2.482	-12.493	6.525
58	CE	125	-27.553	10.340	3.033	-2.210	-9.679	8.063
58	CE	126	-31.433	12.247	3.401	-1.963	-11.198	5.298
58	CE	127	-32.918	9.853	3.772	-1.678	-8.429	6.848
58	CE	128	-36.311	11.760	4.130	-1.418	-9.960	4.123
58	CE	129	-37.339	9.396	4.490	-1.125	-7.230	5.682
58	CE	130	-40.273	11.302	4.837	-.860	-8.770	2.992
58	CE	131	-40.868	8.962	5.187	-.566	-6.075	4.554
58	CE	132	-43.362	10.862	5.525	-.303	-7.619	1.893
58	CE	133	-43.536	8.541	5.865	-.017	-4.953	3.454
58	CE	134	-45.600	10.432	6.195	.236	-6.497	.815
58	CE	135	-45.357	8.124	6.527	.506	-3.853	2.371
58	CE	136	-46.991	10.002	6.848	.741	-5.392	-.252
58	CE	137	-46.327	7.703	7.172	.989	-2.765	1.294
58	CE	138	-47.524	9.564	7.487	1.200	-4.295	-1.317
58	CE	139	-46.427	7.270	7.805	1.420	-1.680	.217
58	CE	140	-47.217	9.157	8.158	1.647	-3.286	-3.946
58	CE	141	-44.249	5.399	8.563	.415	.788	-2.415
58	CE	142	-43.209	7.328	8.960	-.747	-.737	-5.157
58	CE	143	-39.828	4.985	9.359	-.382	2.001	-3.604

TABLE 2

Atomic mass excesses and nuclear binding energies

58	CE	144	-38.388	6.928	9.749	.024	.456	-6.303
58	CE	145	-34.642	4.621	10.141	.470	3.151	-4.730
58	CE	146	-32.851	6.575	10.523	.909	1.589	-7.386
58	CE	147	-28.786	4.303	10.907	1.386	4.243	-5.797
58	CE	148	-26.683	6.264	11.279	1.850	2.666	-8.412
58	CE	149	-22.338	4.023	11.653	2.349	5.280	-6.810
58	CE	150	-19.957	5.986	12.014	2.828	3.692	-9.386
58	CE	151	-15.364	3.774	12.378	3.339	6.267	-7.776
58	CE	152	-12.731	5.734	12.728	3.823	4.673	-10.315
58	CE	153	-7.911	3.547	13.080	4.335	7.213	-8.701
58	CE	154	-5.043	5.499	13.417	4.811	5.617	-11.206
58	CE	155	-.009	3.334	13.757	5.313	8.124	-9.593
58	CE	156	3.087	5.271	14.082	5.773	6.531	-12.067
58	CE	157	8.330	3.124	14.409	6.255	9.009	-10.460
58	CE	158	11.654	5.043	14.720	6.687	7.423	-12.905
58	CE	159	17.110	2.911	15.034	7.140	9.873	-11.307
58	CE	160	20.671	4.807	15.331	7.537	8.299	-13.725
58	CE	161	26.350	2.689	15.631	7.953	10.723	-12.140
58	CE	162	30.160	4.557	15.915	8.309	9.164	-14.532
58	CE	163	36.075	2.452	16.201	8.684	11.562	-12.962
58	CE	164	40.151	4.291	16.471	8.995	10.020	-15.327
58	CE	165	46.319	2.199	16.744	9.326	12.393	-13.775
58	CE	166	50.679	4.007	16.999	9.591	10.870	-16.113
58	CE	167	57.118	1.929	17.260	9.878	13.216	-14.578
58	CE	168	61.779	3.706	17.502	10.098	11.713	-16.888
58	CE	169	68.502	1.644	17.749	10.343	14.031	-15.370
58	CE	170	73.478	3.391	17.979	10.522	12.546	-17.649
58	CE	171	80.497	1.348	18.215	10.731	14.834	-16.148
58	CE	172	85.798	3.066	18.432	10.874	13.368	-18.393
58	CE	173	93.119	1.047	18.657	11.053	15.621	-16.908
58	CE	174	98.749	2.737	18.863	11.168	14.173	-19.116
58	CE	175	106.372	.744	19.077	11.324	16.389	-17.646
58	CE	176	112.329	2.410	19.274	11.419	14.957	-19.814
58	CE	177	120.248	.448	19.479	11.561	17.134	-18.358
58	CE	178	126.524	2.091	19.666	11.644	15.716	-20.483
58	CE	179	134.727	.164	19.864	11.780	17.850	-19.041
58	CE	180	141.371	1.723	19.982	11.796	16.571	-20.996
58	CE	181	149.779	-.040	20.173	11.996	18.535	-19.693
58	CE	182	156.709	1.437	20.347	12.016	17.270	-21.602
58	CE	183	165.364	-.287	20.533	12.224	19.188	-20.313
58	CE	184	172.558	1.173	20.703	12.317	17.935	-22.611
58	CE	185	181.689	-.763	21.065	12.222	20.062	-21.520
58	CE	186	189.382	.674	21.412	12.072	18.988	-23.537
58	CE	187	198.734	-.985	21.770	12.598	20.997	-22.469
58	CE	188	206.676	.426	22.112	13.065	19.946	-24.457
58	CE	189	216.253	-1.210	22.464	13.578	21.927	-23.408
58	CE	190	224.445	.176	22.801	14.034	20.894	-25.367
58	CE	191	234.250	-1.438	23.146	14.532	22.846	-24.334
58	CE	192	242.692	-.075	23.477	14.977	21.829	-26.263
58	CE	193	252.725	-1.666	23.814	15.459	23.753	-25.243
58	CE	194	261.417	-.324	24.137	15.890	22.748	-27.142
58	CE	195	271.679	-1.895	24.465	16.355	24.643	-26.131
58	CE	196	280.616	-.570	24.778	16.772	23.647	-27.999
58	CE	197	291.104	-2.120	25.096	17.220	25.512	-26.994
58	CE	198	300.282	-.811	25.400	17.623	24.521	-28.830
58	CE	199	310.991	-2.341	25.706	18.055	26.355	-27.827
58	CE	200	320.403	-1.045	25.999	18.444	25.367	-29.631
58	CE	201	331.325	-2.554	26.294	18.859	27.170	-28.626
	ATOM		M - A	NEUTRON	PROTON	ALPHA	Q BETA -	Q BETA +
59	PR	109	87.695	20.561	-7.671	-3.234	-26.062	23.458

TABLE 2

Atomic mass excesses and nuclear binding energies

59	PR	110	79.031	17.032	-7.208	-4.025	-22.127	24.869
59	PR	111	68.506	18.892	-6.760	-4.866	-23.541	21.700
59	PR	112	60.695	16.179	-6.304	-4.800	-20.396	23.118
59	PR	113	51.024	18.038	-5.863	-4.762	-21.816	19.998
59	PR	114	44.026	15.366	-5.415	-4.668	-18.718	21.424
59	PR	115	35.168	17.225	-4.981	-4.603	-20.145	18.352
59	PR	116	28.941	14.594	-4.541	-4.484	-17.094	19.788
59	PR	117	20.854	16.455	-4.116	-4.391	-18.531	16.034
59	PR	118	15.357	13.864	-2.953	-4.247	-15.528	16.760
59	PR	119	8.719	15.006	-2.537	-4.107	-16.254	13.799
59	PR	120	4.621	12.465	-2.117	-3.918	-12.587	15.272
59	PR	121	-1.355	14.344	-1.711	-3.753	-14.059	12.361
59	PR	122	-4.831	11.843	-1.301	-3.541	-11.163	13.850
59	PR	123	-10.190	13.727	-.905	-3.351	-12.650	10.989
59	PR	124	-13.088	11.265	-.507	-3.116	-9.803	12.493
59	PR	125	-17.874	13.154	-.121	-2.903	-11.304	9.679
59	PR	126	-20.235	10.728	.266	-2.648	-8.503	11.198
59	PR	127	-24.489	12.622	.641	-2.416	-10.018	8.429
59	PR	128	-26.351	10.229	1.018	-2.145	-7.260	9.960
59	PR	129	-30.109	12.125	1.383	-1.899	-8.787	7.230
59	PR	130	-31.503	9.762	1.749	-1.618	-6.068	8.770
59	PR	131	-34.792	11.656	2.103	-1.365	-7.603	6.075
59	PR	132	-35.743	9.318	2.460	-1.082	-4.917	7.619
59	PR	133	-38.582	11.207	2.805	-.829	-6.456	4.953
59	PR	134	-39.103	8.888	3.152	-.553	-3.798	6.497
59	PR	135	-41.504	10.768	3.489	-.309	-5.337	3.853
59	PR	136	-41.599	8.463	3.827	-.047	-2.700	5.392
59	PR	137	-43.562	10.330	4.156	.182	-4.234	2.765
59	PR	138	-43.229	8.034	4.486	.423	-1.613	4.295
59	PR	139	-44.747	9.886	4.808	.629	-3.139	1.680
59	PR	140	-43.931	7.551	5.089	.800	-.441	3.286
59	PR	141	-45.037	9.473	5.405	1.024	-2.043	.788
59	PR	142	-42.472	5.803	5.808	-.126	1.940	.737
59	PR	143	-41.828	7.723	6.203	-1.206	.409	-2.001
59	PR	144	-38.844	5.383	6.601	-.817	3.131	-.456
59	PR	145	-37.794	7.317	6.990	-.431	1.582	-3.151
59	PR	146	-34.439	5.013	7.382	-.004	4.262	-1.589
59	PR	147	-33.029	6.957	7.763	.414	2.696	-4.243
59	PR	148	-29.348	4.687	8.147	.872	5.333	-2.666
59	PR	149	-27.618	6.637	8.520	1.315	3.754	-5.280
59	PR	150	-23.649	4.398	8.895	1.794	6.351	-3.692
59	PR	151	-21.631	6.350	9.259	2.252	4.762	-6.267
59	PR	152	-17.404	4.140	9.625	2.743	7.321	-4.673
59	PR	153	-15.124	6.087	9.978	3.205	5.726	-7.213
59	PR	154	-10.660	3.903	10.333	3.698	8.250	-5.617
59	PR	155	-8.133	5.841	10.675	4.154	6.655	-8.124
59	PR	156	-3.444	3.679	11.020	4.638	9.146	-6.531
59	PR	157	-.679	5.602	11.350	5.078	7.555	-9.009
59	PR	158	4.231	3.458	11.684	5.541	10.016	-7.423
59	PR	159	7.237	5.361	12.002	5.956	8.434	-9.873
59	PR	160	12.372	3.233	12.323	6.391	10.868	-8.299
59	PR	161	15.627	5.112	12.629	6.772	9.298	-10.723
59	PR	162	20.996	2.998	12.938	7.173	11.706	-9.164
59	PR	163	24.513	4.850	13.231	7.513	10.152	-11.562
59	PR	164	30.131	2.750	13.529	7.874	12.534	-10.020
59	PR	165	33.927	4.572	13.809	8.172	10.999	-12.393
59	PR	166	39.809	2.484	14.095	8.491	13.356	-10.870
59	PR	167	43.902	4.275	14.363	8.744	11.840	-13.216
59	PR	168	50.066	2.203	14.636	9.022	14.170	-11.713
59	PR	169	54.471	3.962	14.892	9.232	12.674	-14.031
59	PR	170	60.931	1.907	15.155	9.470	14.976	-12.546
59	PR	171	65.663	3.636	15.400	9.642	13.500	-14.834

TABLE 2

Atomic mass excesses and nuclear binding energies

59	PR	172	72.430	1.600	15.651	9.846	15.771	-13.368
59	PR	173	77.497	3.300	15.885	9.984	14.313	-15.621
59	PR	174	84.576	1.289	16.127	10.160	16.550	-14.173
59	PR	175	89.982	2.961	16.351	10.272	15.110	-16.389
59	PR	176	97.372	.977	16.584	10.427	17.309	-14.957
59	PR	177	103.114	2.625	16.799	10.522	15.886	-17.134
59	PR	178	110.808	.673	17.024	10.665	18.044	-15.716
59	PR	179	116.878	2.298	17.231	10.749	16.636	-17.850
59	PR	180	124.800	.445	17.512	10.952	18.625	-16.571
59	PR	181	131.244	1.924	17.712	10.971	17.356	-18.535
59	PR	182	139.439	.172	17.924	11.177	19.299	-17.270
59	PR	183	146.175	1.632	18.119	11.202	18.044	-19.188
59	PR	184	154.623	-.080	18.325	11.353	19.943	-17.935
59	PR	185	161.627	1.363	18.516	11.454	18.698	-20.062
59	PR	186	170.393	-.399	18.880	11.528	20.645	-18.988
59	PR	187	177.737	1.024	19.230	11.549	19.562	-20.997
59	PR	188	186.730	-.626	19.589	12.049	21.537	-19.946
59	PR	189	194.326	.770	19.934	12.492	20.476	-21.927
59	PR	190	203.551	-.857	20.287	12.978	22.425	-20.894
59	PR	191	211.403	.515	20.626	13.409	21.385	-22.846
59	PR	192	220.862	-1.091	20.972	13.879	23.307	-21.829
59	PR	193	228.972	.257	21.304	14.298	22.283	-23.753
59	PR	194	238.668	-1.328	21.642	14.752	24.180	-22.748
59	PR	195	247.036	-.000	21.966	15.157	23.169	-24.643
59	PR	196	256.969	-1.566	22.294	15.595	25.039	-23.647
59	PR	197	265.592	-.256	22.609	15.986	24.039	-25.512
59	PR	198	275.761	-1.802	22.927	16.406	25.882	-24.521
59	PR	199	284.635	-.507	23.232	16.784	24.888	-26.355
59	PR	200	295.036	-2.034	23.539	17.188	26.703	-25.367
59	PR	201	304.155	-.751	23.833	17.552	25.712	-27.170
59	PR	202	314.781	-2.259	24.128	17.940	27.499	-26.179
59	PR	203	324.135	-.986	24.410	18.292	26.507	-27.951
59	PR	204	334.978	-2.476	24.693	18.665	28.266	-26.955
59	PR	205	344.555	-1.210	24.963	19.005	27.270	-28.696
	ATOM		M - A	NEUTRON	PROTON	ALPHA	Q BETA -	Q BETA +
60	ND	112	81.091	19.324	-5.000	-5.041	-26.767	20.396
60	ND	113	72.840	16.618	-4.560	-4.993	-23.624	21.816
60	ND	114	62.743	18.464	-4.134	-4.973	-25.027	18.718
60	ND	115	55.313	15.798	-3.702	-4.898	-21.931	20.145
60	ND	116	46.035	17.645	-3.283	-4.849	-23.341	17.094
60	ND	117	39.384	15.018	-2.858	-4.749	-20.291	18.531
60	ND	118	30.885	16.867	-2.447	-4.674	-21.710	15.528
60	ND	119	24.972	14.280	-2.030	-4.548	-18.708	16.254
60	ND	120	17.208	16.132	-.905	-4.446	-20.139	12.587
60	ND	121	12.703	12.872	-.497	-4.274	-16.472	14.059
60	ND	122	6.332	14.738	-.103	-4.126	-17.213	11.163
60	ND	123	2.459	12.241	.295	-3.930	-14.316	12.650
60	ND	124	-3.285	14.112	.679	-3.756	-15.785	9.803
60	ND	125	-6.570	11.653	1.067	-3.537	-12.935	11.304
60	ND	126	-11.732	13.529	1.443	-3.339	-14.419	8.503
60	ND	127	-14.471	11.106	1.821	-3.099	-11.615	10.018
60	ND	128	-19.091	12.987	2.187	-2.880	-13.112	7.260
60	ND	129	-21.322	10.598	2.555	-2.622	-10.351	8.787
60	ND	130	-25.436	12.481	2.912	-2.388	-11.860	6.068
60	ND	131	-27.189	10.121	3.271	-2.119	-9.136	7.603
60	ND	132	-30.826	12.004	3.618	-1.876	-10.654	4.917
60	ND	133	-32.126	9.668	3.968	-1.604	-7.964	6.456
60	ND	134	-35.305	11.546	4.307	-1.359	-9.486	3.798
60	ND	135	-36.167	9.229	4.649	-1.091	-6.823	5.337
60	ND	136	-38.899	11.100	4.980	-.854	-8.345	2.700

TABLE 2

Atomic mass excesses and nuclear binding energies

60	ND	137	-39.328	8.796	5.314	-.598	-5.703	4.234
60	ND	138	-41.616	10.655	5.638	-.375	-7.222	1.613
60	ND	139	-41.609	8.360	5.965	-.139	-4.596	3.139
60	ND	140	-43.490	10.248	6.327	.107	-6.194	.441
60	ND	141	-42.993	7.871	6.647	.275	-3.492	2.043
60	ND	142	-44.412	9.786	6.960	.497	-5.079	-1.940
60	ND	143	-42.237	6.193	7.350	-.580	-1.166	-.409
60	ND	144	-41.975	8.105	7.732	-1.632	-2.691	-3.131
60	ND	145	-39.376	5.768	8.117	-1.264	.026	-1.582
60	ND	146	-38.701	7.692	8.492	-.899	-1.516	-4.262
60	ND	147	-35.724	5.391	8.870	-.494	1.159	-2.696
60	ND	148	-34.681	7.324	9.237	-.098	-.397	-5.333
60	ND	149	-31.371	5.057	9.608	.338	2.237	-3.754
60	ND	150	-30.000	6.996	9.967	.758	.668	-6.351
60	ND	151	-26.393	4.760	10.329	1.216	3.263	-4.762
60	ND	152	-24.725	6.699	10.678	1.651	1.687	-7.321
60	ND	153	-20.850	4.493	11.031	2.121	4.245	-5.726
60	ND	154	-18.910	6.427	11.370	2.562	2.665	-8.250
60	ND	155	-14.788	4.246	11.713	3.033	5.189	-6.655
60	ND	156	-12.590	6.170	12.042	3.469	3.611	-9.146
60	ND	157	-8.234	4.011	12.374	3.932	6.103	-7.555
60	ND	158	-5.785	5.919	12.691	4.352	4.531	-10.016
60	ND	159	-1.197	3.779	13.012	4.797	6.995	-8.434
60	ND	160	1.504	5.667	13.318	5.192	5.434	-10.868
60	ND	161	6.329	3.543	13.628	5.611	7.871	-9.298
60	ND	162	9.290	5.406	13.922	5.974	6.325	-11.706
60	ND	163	14.361	3.297	14.220	6.359	8.737	-10.152
60	ND	164	17.596	5.132	14.501	6.684	7.209	-12.534
60	ND	165	22.928	3.036	14.788	7.031	9.597	-10.999
60	ND	166	26.454	4.841	15.057	7.315	8.089	-13.356
60	ND	167	32.062	2.760	15.332	7.622	10.452	-11.840
60	ND	168	35.896	4.533	15.590	7.864	8.966	-14.170
60	ND	169	41.797	2.467	15.854	8.132	11.304	-12.674
60	ND	170	45.956	4.209	16.100	8.333	9.840	-14.976
60	ND	171	52.163	2.160	16.353	8.564	12.149	-13.500
60	ND	172	56.659	3.871	16.588	8.728	10.707	-15.771
60	ND	173	63.184	1.843	16.831	8.927	12.986	-14.313
60	ND	174	68.026	3.525	17.056	9.061	11.565	-16.550
60	ND	175	74.872	1.522	17.289	9.234	13.810	-15.110
60	ND	176	80.063	3.176	17.504	9.344	12.407	-17.309
60	ND	177	87.228	1.202	17.728	9.499	14.616	-15.886
60	ND	178	92.765	2.831	17.935	9.593	13.230	-18.044
60	ND	179	100.242	.890	18.151	9.739	15.398	-16.636
60	ND	180	106.175	2.434	18.287	9.763	14.154	-18.625
60	ND	181	113.888	.655	18.497	9.969	16.152	-17.356
60	ND	182	120.140	2.116	18.689	9.994	14.923	-19.299
60	ND	183	128.132	.376	18.893	10.205	16.876	-18.044
60	ND	184	134.680	1.819	19.080	10.301	15.657	-19.943
60	ND	185	142.928	.119	19.279	10.460	17.566	-18.698
60	ND	186	149.748	1.547	19.463	10.570	16.357	-20.645
60	ND	187	158.175	-.059	19.803	10.798	18.168	-19.562
60	ND	188	165.193	1.349	20.129	10.974	17.099	-21.537
60	ND	189	173.850	-.290	20.464	11.448	19.064	-20.476
60	ND	190	181.125	1.092	20.786	11.865	18.017	-22.425
60	ND	191	190.019	-.526	21.117	12.325	19.956	-21.385
60	ND	192	197.555	.831	21.433	12.730	18.928	-23.307
60	ND	193	206.689	-.767	21.758	13.173	20.842	-22.283
60	ND	194	214.488	.568	22.069	13.566	19.830	-24.180
60	ND	195	223.866	-1.011	22.387	13.992	21.719	-23.169
60	ND	196	231.930	.304	22.691	14.371	20.720	-25.039
60	ND	197	241.553	-1.256	23.001	14.781	22.583	-24.039
60	ND	198	249.879	.041	23.297	15.146	21.594	-25.882

TABLE 2

Atomic mass excesses and nuclear binding energies

60	ND	199	259.748	-1.501	23.598	15.540	23.431	-24.888
60	ND	200	268.333	-.218	23.887	15.892	22.448	-26.703
60	ND	201	278.443	-1.742	24.178	16.270	24.259	-25.712
60	ND	202	287.282	-.472	24.457	16.609	23.278	-27.499
60	ND	203	297.628	-1.978	24.738	16.972	25.063	-26.507
60	ND	204	306.712	-.717	25.008	17.300	24.081	-28.266
60	ND	205	317.284	-2.205	25.278	17.649	25.839	-27.270
60	ND	206	326.602	-.951	25.537	17.967	24.853	-29.000
60	ND	207	337.392	-2.422	25.796	18.304	26.583	-27.998
60	ND	208	346.930	-1.171	26.044	18.612	25.591	-29.699
60	ND	209	357.923	-2.626	26.291	18.936	27.294	-28.687
60	ND	210	367.667	-1.376	26.528	19.237	26.292	-30.360
	ATOM		M - A	NEUTRON	PROTON	ALPHA	Q BETA -	Q BETA +
61	PM	113	96.464	19.760	-7.789	-5.160	-25.421	23.624
61	PM	114	87.770	17.061	-7.345	-5.130	-22.302	25.027
61	PM	115	77.243	18.894	-6.915	-5.128	-23.707	21.931
61	PM	116	69.376	16.235	-6.479	-5.072	-20.633	23.341
61	PM	117	59.675	18.068	-6.055	-5.042	-22.045	20.291
61	PM	118	52.595	15.447	-5.626	-4.960	-19.017	21.710
61	PM	119	43.681	17.282	-5.211	-4.904	-20.437	18.708
61	PM	120	37.347	14.701	-4.790	-4.796	-17.454	20.139
61	PM	121	29.175	16.539	-4.382	-4.712	-18.885	16.472
61	PM	122	23.545	13.997	-3.257	-4.579	-15.949	17.213
61	PM	123	16.776	15.137	-2.858	-4.448	-16.689	14.316
61	PM	124	12.499	12.643	-2.455	-4.269	-13.105	15.785
61	PM	125	6.365	14.502	-2.065	-4.111	-14.572	12.935
61	PM	126	2.686	12.046	-1.672	-3.908	-11.737	14.419
61	PM	127	-2.856	13.910	-1.291	-3.725	-13.218	11.615
61	PM	128	-5.979	11.490	-.907	-3.499	-10.426	13.112
61	PM	129	-10.971	13.359	-.535	-3.294	-11.921	10.351
61	PM	130	-13.576	10.972	-.161	-3.050	-9.171	11.860
61	PM	131	-18.053	12.844	.202	-2.827	-10.676	9.136
61	PM	132	-20.172	10.486	.567	-2.570	-7.963	10.654
61	PM	133	-24.162	12.358	.921	-2.337	-9.476	7.964
61	PM	134	-25.819	10.024	1.278	-2.075	-6.794	9.486
61	PM	135	-29.344	11.892	1.624	-1.839	-8.312	6.823
61	PM	136	-30.554	9.577	1.972	-1.579	-5.657	8.345
61	PM	137	-33.625	11.438	2.310	-1.349	-7.174	5.703
61	PM	138	-34.394	9.137	2.651	-1.100	-4.539	7.222
61	PM	139	-37.013	10.986	2.982	-.882	-6.052	4.596
61	PM	140	-37.296	8.650	3.272	-.694	-3.345	6.194
61	PM	141	-39.502	10.573	3.597	-.451	-4.938	3.492
61	PM	142	-39.333	8.199	3.924	-.286	-2.241	5.079
61	PM	143	-41.071	10.105	4.244	-.067	-3.824	1.166
61	PM	144	-39.285	6.581	4.632	-1.037	.017	2.691
61	PM	145	-39.402	8.485	5.011	-2.026	-1.514	-.026
61	PM	146	-37.185	6.151	5.394	-1.678	1.185	1.516
61	PM	147	-36.884	8.066	5.768	-1.335	-.362	-1.159
61	PM	148	-34.284	5.768	6.144	-.951	2.294	.397
61	PM	149	-33.608	7.691	6.511	-.577	.732	-2.237
61	PM	150	-30.668	5.427	6.881	-.162	3.348	-.668
61	PM	151	-29.656	7.355	7.241	.236	1.775	-3.263
61	PM	152	-26.412	5.123	7.604	.673	4.351	-1.687
61	PM	153	-25.095	7.050	7.955	1.086	2.772	-4.245
61	PM	154	-21.575	4.848	8.310	1.535	5.311	-2.665
61	PM	155	-19.977	6.769	8.652	1.955	3.730	-5.189
61	PM	156	-16.201	4.592	8.998	2.407	6.234	-3.611
61	PM	157	-14.336	6.502	9.331	2.822	4.656	-6.103
61	PM	158	-10.317	4.348	9.668	3.266	7.129	-4.531
61	PM	159	-8.191	6.242	9.991	3.667	5.558	-6.995

TABLE 2

Atomic mass excesses and nuclear binding energies

61	PM	160	-3.930	4.106	10.318	4.095	8.003	-5.434
61	PM	161	-1.542	5.979	10.631	4.473	6.444	-7.871
61	PM	162	2.965	3.860	10.949	4.875	8.862	-6.325
61	PM	163	5.624	5.708	11.251	5.223	7.320	-8.737
61	PM	164	10.387	3.604	11.558	5.594	9.713	-7.209
61	PM	165	13.331	5.423	11.850	5.905	8.190	-9.597
61	PM	166	18.365	3.334	12.148	6.241	10.559	-8.089
61	PM	167	21.610	5.122	12.429	6.513	9.057	-10.452
61	PM	168	26.930	3.047	12.717	6.810	11.402	-8.966
61	PM	169	30.493	4.804	12.988	7.043	9.922	-11.304
61	PM	170	36.116	2.745	13.266	7.303	12.242	-9.840
61	PM	171	40.014	4.469	13.527	7.497	10.785	-12.149
61	PM	172	45.952	2.429	13.796	7.723	13.076	-10.707
61	PM	173	50.197	4.122	14.047	7.883	11.642	-12.986
61	PM	174	56.462	2.103	14.307	8.079	13.903	-11.565
61	PM	175	61.062	3.767	14.549	8.210	12.490	-13.810
61	PM	176	67.656	1.774	14.801	8.384	14.717	-12.407
61	PM	177	72.613	3.410	15.035	8.493	13.323	-14.616
61	PM	178	79.534	1.446	15.279	8.651	15.512	-13.230
61	PM	179	84.844	3.057	15.505	8.747	14.137	-15.398
61	PM	180	92.022	1.190	15.805	8.960	16.159	-14.154
61	PM	181	97.736	2.653	16.025	8.988	14.925	-16.152
61	PM	182	105.217	.886	16.256	9.200	16.904	-14.923
61	PM	183	111.256	2.329	16.469	9.231	15.684	-16.876
61	PM	184	119.023	.600	16.694	9.387	17.620	-15.657
61	PM	185	125.362	2.028	16.902	9.491	16.411	-17.566
61	PM	186	133.392	.338	17.122	9.657	18.303	-16.357
61	PM	187	140.007	1.752	17.326	9.777	17.103	-18.168
61	PM	188	148.094	.281	17.666	10.138	18.774	-17.099
61	PM	189	154.786	1.675	17.991	10.450	17.694	-19.064
61	PM	190	163.109	.045	18.326	10.894	19.624	-18.017
61	PM	191	170.063	1.413	18.647	11.283	18.567	-19.956
61	PM	192	178.627	-.197	18.977	11.712	20.474	-18.928
61	PM	193	185.847	1.147	19.293	12.089	19.435	-20.842
61	PM	194	194.658	-.444	19.616	12.502	21.320	-19.830
61	PM	195	202.147	.878	19.925	12.865	20.298	-21.719
61	PM	196	211.210	-.695	20.241	13.262	22.160	-20.720
61	PM	197	218.970	.607	20.544	13.612	21.152	-22.583
61	PM	198	228.286	-.948	20.852	13.992	22.991	-21.594
61	PM	199	236.317	.337	21.148	14.328	21.994	-23.431
61	PM	200	245.886	-1.202	21.447	14.693	23.809	-22.448
61	PM	201	254.184	.069	21.734	15.017	22.820	-24.259
61	PM	202	264.004	-1.452	22.024	15.366	24.611	-23.278
61	PM	203	272.565	-.194	22.302	15.680	23.626	-25.063
61	PM	204	282.630	-1.698	22.582	16.015	25.394	-24.081
61	PM	205	291.446	-.448	22.851	16.318	24.409	-25.839
61	PM	206	301.749	-1.936	23.120	16.641	26.152	-24.853
61	PM	207	310.808	-.692	23.379	16.936	25.165	-26.583
61	PM	208	321.339	-2.163	23.637	17.248	26.884	-25.591
61	PM	209	330.629	-.923	23.886	17.534	25.892	-27.294
61	PM	210	341.375	-2.378	24.133	17.837	27.587	-26.292
61	PM	211	350.881	-1.139	24.370	18.117	26.586	-27.968
61	PM	212	361.828	-2.579	24.606	18.411	28.257	-26.954
61	PM	213	371.534	-1.338	24.833	18.686	27.245	-28.604
	ATOM		M - A	NEUTRON	PROTON	ALPHA	Q BETA -	Q BETA +
62	SM	116	90.009	19.309	-5.181	-5.309	-26.862	20.633
62	SM	117	81.721	16.656	-4.760	-5.272	-23.791	22.045
62	SM	118	71.612	18.476	-4.352	-5.259	-25.187	19.017
62	SM	119	64.118	15.862	-3.937	-5.196	-22.160	20.437
62	SM	120	54.801	17.684	-3.536	-5.156	-23.564	17.454

TABLE 2

Atomic mass excesses and nuclear binding energies

62	SM	121	48.060	15.108	-3.129	-5.067	-20.583	18.885
62	SM	122	39.494	16.934	-2.734	-4.999	-21.998	15.949
62	SM	123	33.465	14.397	-2.335	-4.883	-19.062	16.689
62	SM	124	25.604	16.228	-1.244	-4.787	-20.490	13.105
62	SM	125	20.937	13.035	-.853	-4.624	-16.905	14.572
62	SM	126	14.423	14.881	-.473	-4.481	-17.661	11.737
62	SM	127	10.361	12.429	-.090	-4.293	-14.825	13.218
62	SM	128	4.447	14.282	.281	-4.123	-16.290	10.426
62	SM	129	.950	11.865	.656	-3.911	-13.496	11.921
62	SM	130	-4.405	13.723	1.019	-3.718	-14.974	9.171
62	SM	131	-7.377	11.339	1.385	-3.485	-12.221	10.676
62	SM	132	-12.209	13.200	1.741	-3.273	-13.710	7.963
62	SM	133	-14.686	10.844	2.099	-3.027	-10.994	9.476
62	SM	134	-19.025	12.706	2.447	-2.802	-12.491	6.794
62	SM	135	-21.032	10.375	2.798	-2.548	-9.805	8.312
62	SM	136	-24.898	12.233	3.138	-2.319	-11.307	5.657
62	SM	137	-26.451	9.920	3.481	-2.066	-8.647	7.174
62	SM	138	-29.855	11.772	3.815	-1.841	-10.149	4.539
62	SM	139	-30.961	9.473	4.151	-1.597	-7.509	6.052
62	SM	140	-33.951	11.358	4.523	-1.339	-9.095	3.345
62	SM	141	-34.564	8.980	4.853	-1.155	-6.382	4.938
62	SM	142	-37.092	10.895	5.175	-.915	-7.960	2.241
62	SM	143	-37.247	8.523	5.499	-.752	-5.259	3.824
62	SM	144	-39.301	10.421	5.815	-.579	-6.825	-.017
62	SM	145	-37.888	6.954	6.188	-1.496	-3.034	1.514
62	SM	146	-38.370	8.849	6.553	-2.433	-4.559	-1.185
62	SM	147	-36.521	6.519	6.921	-2.107	-1.867	.362
62	SM	148	-36.578	8.424	7.279	-1.788	-3.406	-2.294
62	SM	149	-34.340	6.130	7.641	-1.426	-.756	-.732
62	SM	150	-34.016	8.043	7.992	-1.076	-2.308	-3.348
62	SM	151	-31.431	5.783	8.348	-.684	.302	-1.775
62	SM	152	-30.763	7.699	8.692	-.310	-1.259	-4.351
62	SM	153	-27.867	5.471	9.040	.105	1.313	-2.772
62	SM	154	-26.886	7.386	9.376	.495	-.253	-5.311
62	SM	155	-23.706	5.188	9.716	.923	2.282	-3.730
62	SM	156	-22.436	7.097	10.044	1.320	.716	-6.234
62	SM	157	-18.992	4.924	10.376	1.751	3.218	-4.656
62	SM	158	-17.446	6.821	10.694	2.145	1.657	-7.129
62	SM	159	-13.749	4.671	11.018	2.571	4.129	-5.558
62	SM	160	-11.933	6.551	11.327	2.952	2.578	-8.003
62	SM	161	-7.986	4.421	11.641	3.362	5.023	-6.444
62	SM	162	-5.898	6.279	11.940	3.721	3.486	-8.862
62	SM	163	-1.696	4.166	12.245	4.108	5.905	-7.320
62	SM	164	.674	5.998	12.535	4.439	4.386	-9.713
62	SM	165	5.141	3.900	12.831	4.797	6.783	-8.190
62	SM	166	7.805	5.703	13.110	5.094	5.285	-10.559
62	SM	167	12.553	3.620	13.397	5.417	7.658	-9.057
62	SM	168	15.528	5.392	13.667	5.678	6.184	-11.402
62	SM	169	20.571	3.324	13.944	5.966	8.534	-9.922
62	SM	170	23.874	5.064	14.204	6.189	7.085	-12.242
62	SM	171	29.229	3.013	14.472	6.442	9.410	-10.785
62	SM	172	32.876	4.720	14.723	6.630	7.986	-13.076
62	SM	173	38.555	2.688	14.982	6.851	10.284	-11.642
62	SM	174	42.559	4.364	15.224	7.006	8.884	-13.903
62	SM	175	48.572	2.354	15.474	7.200	11.153	-12.490
62	SM	176	52.939	4.000	15.708	7.330	9.775	-14.717
62	SM	177	59.290	2.017	15.951	7.503	12.011	-13.323
62	SM	178	64.022	3.635	16.176	7.613	10.655	-15.512
62	SM	179	70.708	1.682	16.411	7.773	12.853	-14.137
62	SM	180	75.862	3.213	16.567	7.810	11.641	-16.159
62	SM	181	82.811	1.419	16.796	8.027	13.674	-14.925
62	SM	182	88.313	2.865	17.007	8.061	12.478	-16.904

TABLE 2

Atomic mass excesses and nuclear binding energies

62	SM	183	95.572	1.109	17.231	8.280	14.468	-15.684
62	SM	184	101.403	2.536	17.437	8.382	13.285	-17.620
62	SM	185	108.952	.819	17.656	8.546	15.231	-16.411
62	SM	186	115.089	2.230	17.859	8.661	14.058	-18.303
62	SM	187	122.904	.552	18.073	8.837	15.960	-17.103
62	SM	188	129.319	1.952	18.272	8.970	14.795	-18.774
62	SM	189	137.092	.595	18.586	9.446	16.372	-17.694
62	SM	190	143.484	1.975	18.887	9.873	15.303	-19.624
62	SM	191	151.496	.355	19.197	10.288	17.221	-18.567
62	SM	192	158.153	1.710	19.494	10.649	16.173	-20.474
62	SM	193	166.412	.109	19.800	11.048	18.069	-19.435
62	SM	194	173.339	1.440	20.093	11.396	17.040	-21.320
62	SM	195	181.849	-.143	20.394	11.779	18.914	-20.298
62	SM	196	189.050	1.166	20.682	12.114	17.901	-22.160
62	SM	197	197.818	-.400	20.977	12.480	19.753	-21.152
62	SM	198	205.295	.890	21.260	12.802	18.754	-22.991
62	SM	199	214.323	-.660	21.548	13.153	20.583	-21.994
62	SM	200	222.077	.613	21.825	13.462	19.594	-23.809
62	SM	201	231.364	-.920	22.106	13.798	21.402	-22.820
62	SM	202	239.393	.339	22.376	14.096	20.420	-24.611
62	SM	203	248.939	-1.179	22.650	14.418	22.205	-23.626
62	SM	204	257.237	.070	22.913	14.706	21.227	-25.394
62	SM	205	267.037	-1.433	23.178	15.016	22.989	-24.409
62	SM	206	275.597	-.192	23.434	15.295	22.012	-26.152
62	SM	207	285.643	-1.679	23.691	15.594	23.751	-25.165
62	SM	208	294.455	-.444	23.938	15.866	22.771	-26.884
62	SM	209	304.738	-1.916	24.186	16.156	24.488	-25.892
62	SM	210	313.789	-.684	24.426	16.423	23.502	-27.587
62	SM	211	324.296	-2.140	24.664	16.705	25.197	-26.586
62	SM	212	333.571	-.908	24.895	16.968	24.203	-28.257
62	SM	213	344.289	-2.350	25.124	17.244	25.875	-27.245
62	SM	214	353.772	-1.116	25.346	17.504	24.870	-28.893
62	SM	215	364.684	-2.545	25.566	17.774	26.520	-27.868
62	SM	216	374.359	-1.307	25.779	18.032	25.503	-29.494
62	SM	217	385.449	-2.723	25.989	18.298	27.133	-28.455
	ATOM		M - A	NEUTRON	PROTON	ALPHA	Q BETA -	Q BETA +
63	EU	118	96.799	17.080	-7.493	-5.419	-22.475	25.187
63	EU	119	86.278	18.888	-7.081	-5.425	-23.874	22.160
63	EU	120	78.365	16.280	-6.663	-5.380	-20.868	23.564
63	EU	121	68.643	18.090	-6.257	-5.358	-22.275	20.583
63	EU	122	61.492	15.519	-5.847	-5.287	-19.312	21.998
63	EU	123	52.526	17.333	-5.448	-5.237	-20.728	19.062
63	EU	124	46.094	14.800	-5.044	-5.138	-17.810	20.490
63	EU	125	37.842	16.619	-4.653	-5.057	-19.238	16.905
63	EU	126	32.084	14.125	-3.563	-4.930	-16.364	17.661
63	EU	127	25.186	15.265	-3.179	-4.802	-17.120	14.825
63	EU	128	20.737	12.817	-2.791	-4.628	-13.612	16.290
63	EU	129	14.446	14.658	-2.414	-4.472	-15.076	13.496
63	EU	130	10.569	12.245	-2.034	-4.273	-12.295	14.974
63	EU	131	4.845	14.092	-1.665	-4.092	-13.771	12.221
63	EU	132	1.501	11.711	-1.293	-3.871	-11.029	13.710
63	EU	133	-3.692	13.561	-.932	-3.669	-12.515	10.994
63	EU	134	-6.534	11.209	-.568	-3.433	-9.808	12.491
63	EU	135	-11.227	13.060	-.213	-3.217	-11.302	9.805
63	EU	136	-13.591	10.731	.144	-2.972	-8.624	11.307
63	EU	137	-17.804	12.580	.491	-2.749	-10.122	8.647
63	EU	138	-19.706	10.270	.841	-2.504	-7.469	10.149
63	EU	139	-23.452	12.113	1.181	-2.283	-8.967	7.509
63	EU	140	-24.857	9.772	1.481	-2.088	-6.245	9.095
63	EU	141	-28.182	11.693	1.815	-1.834	-7.827	6.382

TABLE 2

Atomic mass excesses and nuclear binding energies

63	EU	142	-29.131	9.317	2.152	-1.653	-5.120	7.960
63	EU	143	-31.988	11.224	2.481	-1.416	-6.693	5.259
63	EU	144	-32.476	8.855	2.814	-1.210	-3.999	6.825
63	EU	145	-34.854	10.745	3.138	-1.038	-5.560	3.034
63	EU	146	-33.811	7.324	3.508	-1.913	-1.819	4.559
63	EU	147	-34.654	9.211	3.869	-2.807	-3.351	1.867
63	EU	148	-33.172	6.884	4.235	-2.504	-.679	3.406
63	EU	149	-33.585	8.780	4.591	-2.208	-2.225	.756
63	EU	150	-31.708	6.490	4.952	-1.868	.404	2.308
63	EU	151	-31.733	8.393	5.302	-1.541	-1.154	-.302
63	EU	152	-29.504	6.138	5.657	-1.171	1.435	1.259
63	EU	153	-29.179	8.043	6.001	-.819	-.131	-1.313
63	EU	154	-26.632	5.820	6.350	-.426	2.419	.253
63	EU	155	-25.988	7.724	6.688	-.058	.849	-2.282
63	EU	156	-23.152	5.530	7.030	.349	3.364	-.716
63	EU	157	-22.211	7.427	7.360	.725	1.794	-3.218
63	EU	158	-19.103	5.260	7.695	1.137	4.275	-1.657
63	EU	159	-17.879	7.143	8.018	1.512	2.712	-4.129
63	EU	160	-14.511	4.999	8.346	1.919	5.163	-2.578
63	EU	161	-13.009	6.866	8.661	2.282	3.611	-5.023
63	EU	162	-9.383	4.741	8.982	2.676	6.035	-3.486
63	EU	163	-7.601	6.585	9.288	3.019	4.498	-5.905
63	EU	164	-3.712	4.479	9.602	3.392	6.897	-4.386
63	EU	165	-1.641	6.296	9.900	3.708	5.379	-6.783
63	EU	166	2.520	4.206	10.206	4.054	7.755	-5.285
63	EU	167	4.894	5.993	10.496	4.339	6.260	-7.658
63	EU	168	9.344	3.918	10.794	4.653	8.613	-6.184
63	EU	169	12.037	5.674	11.076	4.904	7.143	-8.534
63	EU	170	16.789	3.615	11.366	5.184	9.473	-7.085
63	EU	171	19.818	5.338	11.640	5.400	8.029	-9.410
63	EU	172	24.890	3.296	11.923	5.649	10.334	-7.986
63	EU	173	28.271	4.987	12.190	5.831	8.916	-10.284
63	EU	174	33.675	2.964	12.465	6.050	11.195	-8.884
63	EU	175	37.419	4.623	12.724	6.204	9.801	-11.153
63	EU	176	43.164	2.623	12.993	6.398	12.050	-9.775
63	EU	177	47.279	4.252	13.245	6.527	10.681	-12.011
63	EU	178	53.367	2.279	13.507	6.703	12.896	-10.655
63	EU	179	57.855	3.880	13.752	6.816	11.549	-12.853
63	EU	180	64.221	2.001	14.071	7.044	13.602	-11.641
63	EU	181	69.137	3.451	14.310	7.085	12.399	-13.674
63	EU	182	75.835	1.670	14.561	7.309	14.412	-12.478
63	EU	183	81.104	3.098	14.794	7.349	13.226	-14.468
63	EU	184	88.118	1.354	15.038	7.513	15.197	-13.285
63	EU	185	93.721	2.764	15.267	7.624	14.025	-15.231
63	EU	186	101.031	1.058	15.506	7.796	15.954	-14.058
63	EU	187	106.944	2.454	15.730	7.921	14.792	-15.960
63	EU	188	114.525	.786	15.964	8.107	16.679	-14.795
63	EU	189	120.720	2.172	16.184	8.251	15.524	-16.372
63	EU	190	128.181	.906	16.496	8.819	17.006	-15.303
63	EU	191	134.275	2.274	16.794	9.341	15.924	-17.221
63	EU	192	141.980	.663	17.101	9.723	17.808	-16.173
63	EU	193	148.342	2.005	17.396	10.053	16.748	-18.069
63	EU	194	156.298	.412	17.698	10.420	18.612	-17.040
63	EU	195	162.935	1.730	17.988	10.737	17.571	-18.914
63	EU	196	171.149	.154	18.285	11.087	19.415	-17.901
63	EU	197	178.065	1.451	18.570	11.391	18.391	-19.753
63	EU	198	186.541	-.109	18.861	11.726	20.215	-18.754
63	EU	199	193.739	1.169	19.140	12.017	19.206	-20.583
63	EU	200	202.482	-.376	19.425	12.337	21.010	-19.594
63	EU	201	209.963	.887	19.699	12.617	20.012	-21.402
63	EU	202	218.973	-.643	19.976	12.922	21.797	-20.420
63	EU	203	226.734	.606	20.243	13.192	20.807	-22.205

TABLE 2

Atomic mass excesses and nuclear binding energies

63	EU	204	236.010	-.909	20.514	13.485	22.572	-21.227
63	EU	205	244.048	.330	20.774	13.746	21.587	-22.989
63	EU	206	253.585	-1.170	21.037	14.028	23.332	-22.012
63	EU	207	261.892	.061	21.290	14.283	22.350	-23.751
63	EU	208	271.684	-1.425	21.544	14.556	24.075	-22.771
63	EU	209	280.249	-.199	21.790	14.806	23.091	-24.488
63	EU	210	290.286	-1.669	22.036	15.072	24.797	-23.502
63	EU	211	299.099	-.446	22.274	15.318	23.809	-25.197
63	EU	212	309.369	-1.902	22.512	15.580	25.495	-24.203
63	EU	213	318.414	-.678	22.742	15.825	24.500	-25.875
63	EU	214	328.903	-2.121	22.971	16.082	26.166	-24.870
63	EU	215	338.164	-.894	23.193	16.327	25.162	-26.520
63	EU	216	348.856	-2.325	23.413	16.581	26.811	-25.503
63	EU	217	358.316	-1.093	23.627	16.827	25.796	-27.133
63	EU	218	369.195	-2.512	23.838	17.079	27.426	-26.100
63	EU	219	378.836	-1.273	24.044	17.326	26.398	-27.711
63	EU	220	389.923	-2.720	24.209	17.539	28.088	-26.588
63	EU	221	399.689	-1.398	24.407	17.825	26.970	-28.257
63	EU	222	410.929	-2.873	24.601	18.036	28.645	-27.117
	ATOM		M - A	NEUTRON	PROTON	ALPHA	Q BETA -	Q BETA +
64	GD	120	99.233	19.286	-5.371	-5.615	-26.961	20.868
64	GD	121	90.918	16.683	-4.967	-5.588	-23.958	22.275
64	GD	122	80.804	18.481	-4.576	-5.582	-25.350	19.312
64	GD	123	73.255	15.916	-4.178	-5.528	-22.390	20.728
64	GD	124	63.904	17.719	-3.792	-5.493	-23.792	17.810
64	GD	125	57.080	15.191	-3.401	-5.410	-20.875	19.238
64	GD	126	48.448	16.999	-3.021	-5.345	-22.289	16.364
64	GD	127	42.306	14.509	-2.637	-5.232	-19.415	17.120
64	GD	128	34.349	16.324	-1.578	-5.136	-20.841	13.612
64	GD	129	29.522	13.195	-1.200	-4.976	-17.333	15.076
64	GD	130	22.864	15.025	-.833	-4.832	-18.105	12.295
64	GD	131	18.616	12.616	-.462	-4.645	-15.324	13.771
64	GD	132	12.530	14.453	-.101	-4.474	-16.785	11.029
64	GD	133	8.823	12.075	.263	-4.264	-14.041	12.515
64	GD	134	3.274	13.916	.618	-4.070	-15.512	9.808
64	GD	135	.075	11.566	.976	-3.843	-12.802	11.302
64	GD	136	-4.966	13.409	1.324	-3.634	-14.281	8.624
64	GD	137	-7.681	11.083	1.676	-3.395	-11.600	10.122
64	GD	138	-12.237	12.923	2.018	-3.178	-13.083	7.469
64	GD	139	-14.485	10.615	2.363	-2.938	-10.427	8.967
64	GD	140	-18.611	12.494	2.744	-2.677	-11.997	6.245
64	GD	141	-20.355	10.111	3.083	-2.486	-9.271	7.827
64	GD	142	-24.011	12.024	3.415	-2.235	-10.838	5.120
64	GD	143	-25.295	9.651	3.748	-2.057	-8.127	6.693
64	GD	144	-28.477	11.550	4.074	-1.865	-9.684	3.999
64	GD	145	-29.294	9.184	4.402	-1.661	-6.985	5.560
64	GD	146	-31.992	11.065	4.723	-1.490	-8.529	1.819
64	GD	147	-31.304	7.679	5.077	-2.335	-4.814	3.351
64	GD	148	-32.492	9.556	5.423	-3.200	-6.339	.679
64	GD	149	-31.359	7.234	5.772	-2.920	-3.675	2.225
64	GD	150	-32.112	9.120	6.112	-2.649	-5.213	-.404
64	GD	151	-30.579	6.835	6.457	-2.333	-2.590	1.154
64	GD	152	-30.939	8.727	6.791	-2.030	-4.139	-1.435
64	GD	153	-29.048	6.477	7.129	-1.683	-1.556	.131
64	GD	154	-29.052	8.371	7.457	-1.355	-3.111	-2.419
64	GD	155	-26.838	6.153	7.790	-.984	-.566	-.849
64	GD	156	-26.515	8.045	8.111	-.638	-2.124	-3.364
64	GD	157	-24.005	5.857	8.438	-.253	.386	-1.794
64	GD	158	-23.378	7.741	8.752	.102	-1.169	-4.275
64	GD	159	-20.591	5.580	9.073	.494	1.309	-2.712

TABLE 2

Atomic mass excesses and nuclear binding energies

64	GD	160	-19.674	7.451	9.380	.848	-.237	-5.163
64	GD	161	-16.620	5.313	9.694	1.237	2.212	-3.611
64	GD	162	-15.418	7.166	9.994	1.581	.678	-6.035
64	GD	163	-12.099	5.048	10.301	1.959	3.101	-4.498
64	GD	164	-10.609	6.878	10.593	2.286	1.585	-6.897
64	GD	165	-7.021	4.779	10.893	2.644	3.984	-5.379
64	GD	166	-5.235	6.581	11.178	2.946	2.490	-7.755
64	GD	167	-1.366	4.499	11.471	3.279	4.867	-6.260
64	GD	168	.730	6.271	11.749	3.553	3.398	-8.613
64	GD	169	4.894	4.204	12.035	3.857	5.754	-7.143
64	GD	170	7.316	5.945	12.305	4.098	4.311	-9.473
64	GD	171	11.790	3.894	12.584	4.372	6.645	-8.029
64	GD	172	14.556	5.601	12.847	4.581	5.231	-10.334
64	GD	173	19.355	3.568	13.120	4.825	7.541	-8.916
64	GD	174	22.480	5.242	13.376	5.003	6.155	-11.195
64	GD	175	27.618	3.230	13.642	5.220	8.440	-9.801
64	GD	176	31.113	4.872	13.890	5.371	7.081	-12.050
64	GD	177	36.598	2.883	14.150	5.566	9.336	-10.681
64	GD	178	40.471	4.494	14.393	5.696	8.003	-12.896
64	GD	179	46.306	2.533	14.646	5.875	10.226	-11.549
64	GD	180	50.620	4.054	14.820	5.929	9.042	-13.602
64	GD	181	56.738	2.249	15.068	6.161	11.103	-12.399
64	GD	182	61.423	3.682	15.299	6.208	9.939	-14.412
64	GD	183	67.878	1.913	15.542	6.439	11.961	-13.226
64	GD	184	72.920	3.325	15.768	6.551	10.813	-15.197
64	GD	185	79.696	1.592	16.007	6.724	12.794	-14.025
64	GD	186	85.076	2.987	16.229	6.846	11.658	-15.954
64	GD	187	92.152	1.292	16.463	7.029	13.597	-14.792
64	GD	188	97.846	2.674	16.683	7.167	12.469	-16.679
64	GD	189	105.197	1.017	16.913	7.364	14.367	-15.524
64	GD	190	111.175	2.389	17.130	7.522	13.245	-17.006
64	GD	191	118.351	1.192	17.415	8.162	14.678	-15.924
64	GD	192	124.171	2.547	17.688	8.757	13.605	-17.808
64	GD	193	131.594	.945	17.970	9.107	15.476	-16.748
64	GD	194	137.686	2.275	18.241	9.407	14.424	-18.612
64	GD	195	145.364	.690	18.519	9.741	16.274	-17.571
64	GD	196	151.734	1.997	18.786	10.028	15.240	-19.415
64	GD	197	159.674	.428	19.060	10.347	17.072	-18.391
64	GD	198	166.327	1.715	19.323	10.621	16.054	-20.215
64	GD	199	174.534	.160	19.592	10.924	17.867	-19.206
64	GD	200	181.472	1.429	19.852	11.187	16.862	-21.010
64	GD	201	189.951	-.111	20.116	11.476	18.656	-20.012
64	GD	202	197.176	1.142	20.371	11.728	17.663	-21.797
64	GD	203	205.927	-.384	20.630	12.004	19.438	-20.807
64	GD	204	213.438	.856	20.881	12.248	18.452	-22.572
64	GD	205	222.461	-.655	21.134	12.513	20.209	-21.587
64	GD	206	230.253	.575	21.380	12.749	19.228	-23.332
64	GD	207	239.542	-.922	21.628	13.006	20.967	-22.350
64	GD	208	247.609	.301	21.868	13.237	19.987	-24.075
64	GD	209	257.159	-1.183	22.110	13.488	21.708	-23.091
64	GD	210	265.490	.036	22.345	13.716	20.727	-24.797
64	GD	211	275.291	-1.434	22.580	13.962	22.429	-23.809
64	GD	212	283.874	-.216	22.810	14.190	21.444	-25.495
64	GD	213	293.914	-1.673	23.039	14.433	23.128	-24.500
64	GD	214	302.736	-.454	23.263	14.662	22.136	-26.166
64	GD	215	313.002	-1.898	23.486	14.903	23.802	-25.162
64	GD	216	322.045	-.676	23.704	15.135	22.802	-26.811
64	GD	217	332.521	-2.108	23.920	15.377	24.451	-25.796
64	GD	218	341.769	-.881	24.132	15.613	23.440	-27.426
64	GD	219	352.438	-2.302	24.342	15.856	25.073	-26.398
64	GD	220	361.835	-1.030	24.586	16.133	23.973	-28.088
64	GD	221	372.719	-2.516	24.789	16.340	25.667	-26.970

TABLE 2

Atomic mass excesses and nuclear binding energies

64	GD	222	382.284	-1.198	24.990	16.621	24.554	-28.645
64	GD	223	393.328	-2.676	25.186	16.829	26.234	-27.513
64	GD	224	403.045	-1.350	25.380	17.076	25.108	-29.173
64	GD	225	414.232	-2.820	25.571	17.323	26.776	-28.027
	ATOM		M - A	NEUTRON	PROTON	ALPHA	Q BETA -	Q BETA +
65	TB	122	106.154	17.089	-7.651	-5.746	-22.649	25.350
65	TB	123	95.645	18.877	-7.256	-5.758	-24.044	22.390
65	TB	124	87.696	16.317	-6.856	-5.721	-21.102	23.792
65	TB	125	77.955	18.108	-6.466	-5.702	-22.506	20.875
65	TB	126	70.737	15.586	-6.072	-5.636	-19.607	22.289
65	TB	127	61.721	17.383	-5.688	-5.585	-21.022	19.415
65	TB	128	55.190	14.898	-5.300	-5.487	-18.164	20.841
65	TB	129	46.855	16.702	-4.921	-5.404	-19.591	17.333
65	TB	130	40.969	14.253	-3.863	-5.276	-16.774	18.105
65	TB	131	33.939	15.398	-3.490	-5.143	-17.546	15.324
65	TB	132	29.315	12.992	-3.115	-4.969	-14.109	16.785
65	TB	133	22.863	14.819	-2.748	-4.808	-15.568	14.041
65	TB	134	18.786	12.444	-2.379	-4.608	-12.835	15.512
65	TB	135	12.877	14.276	-2.018	-4.423	-14.305	12.802
65	TB	136	9.315	11.930	-1.655	-4.204	-11.605	14.281
65	TB	137	3.919	13.763	-1.300	-4.002	-13.081	11.600
65	TB	138	.846	11.440	-.943	-3.771	-10.408	13.083
65	TB	139	-4.058	13.272	-.594	-3.559	-11.888	10.427
65	TB	140	-6.614	10.923	-.286	-3.368	-9.150	11.997
65	TB	141	-11.084	12.837	.057	-3.111	-10.717	9.271
65	TB	142	-13.174	10.458	.403	-2.923	-7.998	10.838
65	TB	143	-17.168	12.362	.742	-2.674	-9.560	8.127
65	TB	144	-18.794	9.993	1.083	-2.454	-6.856	9.684
65	TB	145	-22.309	11.883	1.417	-2.263	-8.408	6.985
65	TB	146	-23.463	9.521	1.754	-2.059	-5.717	8.529
65	TB	147	-26.490	11.394	2.083	-1.889	-7.257	4.814
65	TB	148	-26.153	8.031	2.434	-2.714	-3.569	6.339
65	TB	149	-27.684	9.899	2.777	-3.561	-5.102	3.675
65	TB	150	-26.899	7.582	3.124	-3.303	-2.459	5.213
65	TB	151	-27.989	9.458	3.462	-3.056	-4.005	2.590
65	TB	152	-26.800	7.178	3.805	-2.762	-1.405	4.139
65	TB	153	-27.492	9.060	4.138	-2.483	-2.960	1.556
65	TB	154	-25.940	6.815	4.477	-2.158	-.400	3.111
65	TB	155	-26.271	8.698	4.804	-1.853	-1.962	.566
65	TB	156	-24.391	6.487	5.138	-1.503	.560	2.124
65	TB	157	-24.391	8.367	5.461	-1.179	-1.003	-.386
65	TB	158	-22.210	6.186	5.790	-.813	1.484	1.169
65	TB	159	-21.900	8.058	6.107	-.479	-.075	-1.309
65	TB	160	-19.437	5.904	6.431	-.106	2.379	.237
65	TB	161	-18.831	7.762	6.742	.230	.829	-2.212
65	TB	162	-16.096	5.632	7.061	.602	3.255	-.678
65	TB	163	-15.200	7.471	7.367	.930	1.719	-3.101
65	TB	164	-12.194	5.362	7.680	1.293	4.118	-1.585
65	TB	165	-11.005	7.178	7.980	1.605	2.601	-3.984
65	TB	166	-7.725	5.087	8.289	1.951	4.978	-2.490
65	TB	167	-6.233	6.876	8.583	2.241	3.484	-4.867
65	TB	168	-2.668	4.802	8.887	2.564	5.838	-3.398
65	TB	169	-.860	6.560	9.175	2.828	4.370	-5.754
65	TB	170	3.005	4.502	9.473	3.125	6.703	-4.311
65	TB	171	5.145	6.228	9.756	3.359	5.263	-6.645
65	TB	172	9.325	4.187	10.049	3.627	7.575	-5.231
65	TB	173	11.814	5.879	10.327	3.832	6.164	-7.541
65	TB	174	16.325	3.856	10.615	4.073	8.453	-6.155
65	TB	175	19.178	5.514	10.887	4.249	7.071	-8.440
65	TB	176	24.033	3.513	11.170	4.466	9.334	-7.081

TABLE 2

Atomic mass excesses and nuclear binding energies

65	TB	177	27.262	5.139	11.436	4.618	7.981	-9.336
65	TB	178	32.468	3.161	11.715	4.816	10.215	-8.003
65	TB	179	36.079	4.756	11.977	4.949	8.889	-10.226
65	TB	180	41.578	2.869	12.313	5.195	10.966	-9.042
65	TB	181	45.634	4.311	12.570	5.254	9.789	-11.103
65	TB	182	51.484	2.518	12.839	5.493	11.830	-9.939
65	TB	183	55.916	3.935	13.091	5.547	10.674	-11.961
65	TB	184	62.107	2.177	13.355	5.723	12.678	-10.813
65	TB	185	66.902	3.573	13.603	5.844	11.539	-12.794
65	TB	186	73.419	1.851	13.862	6.025	13.503	-11.658
65	TB	187	78.555	3.231	14.106	6.158	12.377	-13.597
65	TB	188	85.376	1.546	14.361	6.351	14.301	-12.469
65	TB	189	90.830	2.914	14.601	6.501	13.183	-14.367
65	TB	190	97.930	1.267	14.851	6.709	15.068	-13.245
65	TB	191	103.672	2.625	15.088	6.881	13.956	-14.678
65	TB	192	110.566	1.474	15.369	7.568	15.342	-13.605
65	TB	193	116.118	2.816	15.638	8.212	14.255	-15.476
65	TB	194	123.263	1.222	15.916	8.528	16.093	-14.424
65	TB	195	129.090	2.541	16.182	8.795	15.027	-16.274
65	TB	196	136.494	.963	16.455	9.095	16.846	-15.240
65	TB	197	142.602	2.259	16.717	9.350	15.799	-17.072
65	TB	198	150.273	.697	16.986	9.635	17.601	-16.054
65	TB	199	156.667	1.973	17.244	9.877	16.571	-17.867
65	TB	200	164.610	.424	17.508	10.148	18.356	-16.862
65	TB	201	171.295	1.683	17.763	10.379	17.340	-18.656
65	TB	202	179.514	.148	18.022	10.637	19.109	-17.663
65	TB	203	186.489	1.392	18.272	10.859	18.105	-19.438
65	TB	204	194.986	-.129	18.526	11.106	19.858	-18.452
65	TB	205	202.251	1.102	18.772	11.321	18.863	-20.209
65	TB	206	211.024	-.406	19.021	11.558	20.599	19.228
65	TB	207	218.575	.816	19.262	11.768	19.610	20.967
65	TB	208	227.621	-.678	19.506	11.998	21.331	-19.987
65	TB	209	235.451	.537	19.742	12.206	20.345	-21.708
65	TB	210	244.763	-.944	19.981	12.432	22.051	-20.727
65	TB	211	252.862	.268	20.212	12.639	21.065	-22.429
65	TB	212	262.430	-1.201	20.445	12.863	22.755	-21.444
65	TB	213	270.787	.011	20.672	13.072	21.766	-23.128
65	TB	214	280.600	-1.446	20.899	13.296	23.441	-22.136
65	TB	215	289.199	-.232	21.122	13.509	22.447	-23.802
65	TB	216	299.243	-1.677	21.343	13.735	24.108	-22.802
65	TB	217	308.070	-.459	21.560	13.953	23.106	-24.451
65	TB	218	318.329	-1.892	21.776	14.182	24.753	-23.440
65	TB	219	327.365	-.669	21.988	14.408	23.742	-25.073
65	TB	220	337.862	-2.129	22.161	14.603	25.451	-23.973
65	TB	221	347.052	-.822	22.368	14.874	24.354	-25.667
65	TB	222	357.730	-2.311	22.573	15.074	26.051	-24.554
65	TB	223	367.093	-.996	22.776	15.352	24.942	-26.234
65	TB	224	377.936	-2.476	22.976	15.596	26.627	-25.108
65	TB	225	387.456	-1.152	23.174	15.842	25.506	-26.776
65	TB	226	398.447	-2.624	23.369	16.091	27.180	-25.637
65	TB	227	408.107	-1.293	23.562	16.342	26.048	-27.293
65	TB	228	419.232	-2.757	23.753	16.595	27.711	-26.143
65	TB	229	429.018	-1.419	23.941	16.850	26.570	-27.787
	ATOM		M - A	NEUTRON	PROTON	ALPHA	Q BETA -	Q BETA +
66	DY	124	108.798	19.258	-5.568	-5.955	-27.070	21.102
66	DY	125	100.461	16.704	-5.181	-5.934	-24.131	22.506
66	DY	126	90.343	18.485	-4.804	-5.930	-25.523	19.607
66	DY	127	82.743	15.968	-4.421	-5.878	-22.625	21.022
66	DY	128	73.354	17.756	-4.049	-5.842	-24.027	18.164
66	DY	129	66.447	15.275	-3.671	-5.757	-21.171	19.591

TABLE 2

Atomic mass excesses and nuclear binding energies

66	DY	130	57.744	17.070	-3.303	-5.686	-22.585	16.774
66	DY	131	51.485	14.626	-2.931	-5.570	-19.768	17.546
66	DY	132	43.423	16.429	-1.900	-5.465	-21.195	14.109
66	DY	133	38.432	13.359	-1.532	-5.301	-17.757	15.568
66	DY	134	31.622	15.177	-1.174	-5.149	-18.544	12.835
66	DY	135	27.182	12.807	-.811	-4.958	-15.810	14.305
66	DY	136	20.919	14.630	-.457	-4.780	-17.266	11.605
66	DY	137	17.000	12.287	-.100	-4.568	-14.564	13.081
66	DY	138	11.255	14.113	.249	-4.371	-16.027	10.408
66	DY	139	7.830	11.792	.601	-4.145	-13.351	11.888
66	DY	140	2.537	13.660	.990	-3.894	-14.905	9.150
66	DY	141	-.366	11.270	1.337	-3.706	-12.164	10.717
66	DY	142	-5.176	13.177	1.677	-3.452	-13.717	7.998
66	DY	143	-7.609	10.800	2.020	-3.267	-10.994	9.560
66	DY	144	-11.938	12.697	2.354	-3.064	-12.541	6.856
66	DY	145	-13.901	10.330	2.692	-2.845	-9.832	8.408
66	DY	146	-17.746	12.212	3.021	-2.656	-11.368	5.717
66	DY	147	-19.233	9.855	3.355	-2.453	-8.672	7.257
66	DY	148	-22.584	11.718	3.679	-2.284	-10.194	3.569
66	DY	149	-22.582	8.366	4.014	-3.102	-6.507	5.102
66	DY	150	-24.439	10.224	4.340	-3.944	-8.034	2.459
66	DY	151	-23.984	7.912	4.670	-3.710	-5.399	4.005
66	DY	152	-25.395	9.779	4.991	-3.488	-6.936	1.405
66	DY	153	-24.532	7.504	5.317	-3.218	-4.343	2.960
66	DY	154	-25.540	9.375	5.632	-2.963	-5.889	.400
66	DY	155	-24.310	7.137	5.954	-2.661	-3.336	1.962
66	DY	156	-24.951	9.009	6.265	-2.378	-4.887	-.560
66	DY	157	-23.388	6.804	6.582	-2.051	-2.371	1.003
66	DY	158	-23.694	8.673	6.887	-1.749	-3.921	-1.484
66	DY	159	-21.825	6.499	7.200	-1.404	-1.440	.075
66	DY	160	-21.816	8.358	7.500	-1.090	-2.985	-2.379
66	DY	161	-19.660	6.212	7.808	-.735	-.534	-.829
66	DY	162	-19.351	8.058	8.104	-.419	-2.068	-3.255
66	DY	163	-16.919	5.935	8.407	-.063	.354	-1.719
66	DY	164	-16.313	7.762	8.698	.248	-1.163	-4.118
66	DY	165	-13.606	5.661	8.997	.596	1.234	-2.601
66	DY	166	-12.703	7.463	9.282	.894	-.262	-4.978
66	DY	167	-9.717	5.382	9.577	1.227	2.113	-3.484
66	DY	168	-8.506	7.156	9.857	1.505	.642	-5.838
66	DY	169	-5.230	5.092	10.147	1.819	2.996	-4.370
66	DY	170	-3.698	6.835	10.423	2.073	1.553	-6.703
66	DY	171	-.119	4.788	10.708	2.362	3.888	-5.263
66	DY	172	1.750	6.498	10.979	2.589	2.476	-7.575
66	DY	173	5.650	4.468	11.260	2.853	4.790	-6.164
66	DY	174	7.873	6.145	11.526	3.053	3.409	-8.453
66	DY	175	12.107	4.133	11.803	3.292	5.701	-7.071
66	DY	176	14.699	5.776	12.064	3.467	4.352	-9.334
66	DY	177	19.280	3.786	12.337	3.684	6.620	-7.981
66	DY	178	22.253	5.395	12.594	3.837	5.301	-10.215
66	DY	179	27.190	3.430	12.863	4.037	7.541	-8.889
66	DY	180	30.612	4.946	13.052	4.111	6.376	-10.966
66	DY	181	35.845	3.134	13.317	4.362	8.459	-9.789
66	DY	182	39.654	4.559	13.565	4.427	7.319	-11.830
66	DY	183	45.242	2.779	13.826	4.673	9.368	-10.674
66	DY	184	49.430	4.180	14.072	4.799	8.249	-12.678
66	DY	185	55.363	2.434	14.329	4.984	10.261	-11.539
66	DY	186	59.916	3.815	14.571	5.117	9.157	-13.503
66	DY	187	66.179	2.104	14.825	5.308	11.131	-12.377
66	DY	188	71.076	3.470	15.064	5.454	10.038	-14.301
66	DY	189	77.647	1.796	15.315	5.659	11.973	-13.183
66	DY	190	82.863	3.151	15.552	5.823	10.888	-15.068
66	DY	191	89.717	1.514	15.799	6.045	12.782	-13.956

TABLE 2

Atomic mass excesses and nuclear binding energies

66	DY	192	95.224	2.860	16.033	6.231	11.702	-15.342
66	DY	193	101.862	1.729	16.289	6.943	13.087	-14.255
66	DY	194	107.170	3.060	16.533	7.615	12.007	-16.093
66	DY	195	114.063	1.475	16.785	7.897	13.831	-15.027
66	DY	196	119.648	2.782	17.027	8.133	12.770	-16.846
66	DY	197	126.803	1.212	17.276	8.401	14.576	-15.799
66	DY	198	132.672	2.498	17.515	8.624	13.533	-17.601
66	DY	199	140.096	.943	17.761	8.877	15.322	-16.571
66	DY	200	146.254	2.209	17.998	9.089	14.296	-18.356
66	DY	201	153.954	.667	18.241	9.329	16.068	-17.340
66	DY	202	160.405	1.917	18.475	9.531	15.055	-19.109
66	DY	203	168.384	.388	18.714	9.759	16.812	-18.105
66	DY	204	175.128	1.623	18.946	9.953	15.810	-19.858
66	DY	205	183.389	.107	19.182	10.171	17.552	-18.863
66	DY	206	190.425	1.331	19.411	10.361	16.558	-20.599
66	DY	207	198.965	-.173	19.644	10.571	18.286	-19.610
66	DY	208	206.290	1.043	19.870	10.758	17.297	-21.331
66	DY	209	215.106	-.449	20.100	10.964	19.010	-20.345
66	DY	210	222.712	.761	20.324	11.150	18.024	-22.051
66	DY	211	231.797	-.718	20.550	11.354	19.723	-21.065
66	DY	212	239.675	.489	20.771	11.542	18.737	-22.755
66	DY	213	249.021	-.978	20.994	11.747	20.422	-21.766
66	DY	214	257.159	.229	21.213	11.940	19.433	-23.441
66	DY	215	266.752	-1.226	21.432	12.148	21.104	-22.447
66	DY	216	275.136	-.016	21.648	12.348	20.111	-24.108
66	DY	217	284.964	-1.460	21.865	12.560	21.768	-23.106
66	DY	218	293.577	-.246	22.078	12.769	20.768	-24.753
66	DY	219	303.623	-1.679	22.291	12.987	22.413	-23.742
66	DY	220	312.411	-.420	22.539	13.244	21.328	-25.451
66	DY	221	322.698	-1.919	22.749	13.432	23.037	-24.354
66	DY	222	331.679	-.614	22.957	13.699	21.942	-26.051
66	DY	223	342.152	-2.105	23.163	13.896	23.641	-24.942
66	DY	224	351.310	-.791	23.368	14.135	22.535	-26.627
66	DY	225	361.950	-2.273	23.571	14.378	24.224	-25.506
66	DY	226	371.268	-.950	23.773	14.626	23.108	-27.180
66	DY	227	382.059	-2.424	23.973	14.878	24.787	-26.048
66	DY	228	391.521	-1.094	24.171	15.133	23.662	-27.711
66	DY	229	402.448	-2.560	24.368	15.393	25.332	-26.570
66	DY	230	412.039	-1.223	24.564	15.655	24.198	-28.224
66	DY	231	423.090	-2.683	24.758	15.920	25.861	-27.074
66	DY	232	432.798	-1.340	24.950	16.186	24.719	-28.719
66	DY	233	443.960	-2.795	25.142	16.455	26.375	-27.562
66	DY	234	453.776	-1.448	25.331	16.724	25.228	-29.201
	ATOM		M - A	NEUTRON	PROTON	ALPHA	Q BETA -	Q BETA +
67	HO	127	105.368	18.866	-7.440	-6.114	-24.222	22.625
67	HO	128	97.381	16.353	-7.054	-6.077	-21.342	24.027
67	HO	129	87.617	18.132	-6.678	-6.053	-22.746	21.171
67	HO	130	80.328	15.656	-6.297	-5.983	-19.905	22.585
67	HO	131	71.253	17.442	-5.925	-5.924	-21.321	19.768
67	HO	132	64.619	15.002	-5.549	-5.819	-18.519	21.195
67	HO	133	56.189	16.797	-5.181	-5.725	-19.947	17.757
67	HO	134	50.166	14.391	-4.149	-5.587	-17.181	18.544
67	HO	135	42.992	15.541	-3.786	-5.444	-17.968	15.810
67	HO	136	38.186	13.174	-3.419	-5.261	-14.593	17.266
67	HO	137	31.564	14.989	-3.059	-5.091	-16.048	14.564
67	HO	138	27.281	12.650	-2.697	-4.886	-13.355	16.027
67	HO	139	21.181	14.468	-2.342	-4.695	-14.816	13.351
67	HO	140	17.442	12.107	-2.027	-4.518	-12.062	14.905
67	HO	141	11.798	14.011	-1.677	-4.270	-13.613	12.164
67	HO	142	8.541	11.624	-1.323	-4.086	-10.880	13.717

TABLE 2

Atomic mass excesses and nuclear binding energies

67	HO	143	3.386	13.523	-.977	-3.835	-12.429	10.994
67	HO	144	.603	11.150	-.627	-3.607	-9.714	12.541
67	HO	145	-4.069	13.039	-.284	-3.406	-11.257	9.832
67	HO	146	-6.378	10.677	.062	-3.187	-8.557	11.368
67	HO	147	-10.561	12.550	400	-2.999	-10.088	8.672
67	HO	148	-12.390	10.197	.742	-2.794	-7.402	10.194
67	HO	149	-16.075	12.052	1.076	-2.625	-8.919	6.507
67	HO	150	-16.405	8.698	1 408	-3.448	-5.236	8.034
67	HO	151	-18.585	10.547	1.731	-4.295	-6.770	5.399
67	HO	152	-18.459	8.241	2.060	-4.085	-4.158	6.936
67	HO	153	-20.189	10.097	2.378	-3.886	-5.704	4.343
67	HO	154	-19.651	7.829	2.703	-3.639	-3.134	5.889
67	HO	155	-20.974	9.690	3.018	-3.406	-4.688	3.336
67	HO	156	-20.065	7.458	3.340	-3.126	-2.159	4.887
67	HO	157	-21.017	9.320	3.651	-2.866	-3.717	2.371
67	HO	158	-19.772	7.122	3.969	-2.559	-1.226	3.921
67	HO	159	-20.385	8.980	4.276	-2.277	-2.782	1.440
67	HO	160	-18.831	6.814	4.591	-1.951	-.326	2.985
67	HO	161	-19.126	8.662	4.895	-1.656	-1.876	.534
67	HO	162	-17.282	6.524	5.207	-1.318	.548	2.068
67	HO	163	-17.273	8.358	5.507	-1.018	-.990	-.354
67	HO	164	-15.150	6.244	5.816	-.678	1.407	1.163
67	HO	165	-14.841	8.058	6.112	-.382	-.114	-1.234
67	HO	166	-12.440	5.967	6.419	-.046	2.258	.262
67	HO	167	-11.830	7.757	6.712	.239	.759	-2.113
67	HO	168	-9.147	5.685	7.015	.562	3.109	-.642
67	HO	169	-8.226	7.446	7.305	.831	1.637	-2.996
67	HO	170	-5.252	5.393	7.606	1.136	3.966	-1.553
67	HO	171	-4.007	7.122	7.893	1.383	2.523	-3.888
67	HO	172	-.725	5.086	8.191	1.667	4.833	-2.476
67	HO	173	.860	6.782	8.475	1.889	3.422	-4.790
67	HO	174	4.464	4.764	8.771	2.150	5.711	-3.409
67	HO	175	6.406	6.425	9.052	2.348	4.333	-5.701
67	HO	176	10.347	4.426	9.345	2.588	6.601	-4.352
67	HO	177	12.661	6.053	9.623	2.762	5.255	-6.620
67	HO	178	16.952	4.076	9.913	2.983	7.499	-5.301
67	HO	179	19.649	5.670	10.188	3.138	6.185	-7.541
67	HO	180	24.236	3.780	10.539	3.406	8.276	-6.376
67	HO	181	27.386	5.217	10.810	3.485	7.117	-8.459
67	HO	182	32.335	3.419	11.096	3.743	9.178	-7.319
67	HO	183	35.874	4.828	11.364	3.815	8.045	-9.368
67	HO	184	41.181	3.061	11.646	4.006	10.073	-8.249
67	HO	185	45.103	4.446	11.912	4.141	8.962	-10.261
67	HO	186	50.759	2.711	12.189	4.334	10.956	-9.157
67	HO	187	55.048	4.078	12.452	4.478	9.861	-11.131
67	HO	188	61.037	2.378	12.726	4.679	11.819	-10.038
67	HO	189	65.674	3.730	12.986	4.837	10.736	-11.973
67	HO	190	71.975	2.066	13.256	5.053	12.656	-10.888
67	HO	191	76.934	3.408	13.513	5.230	11.581	-12.782
67	HO	192	83.522	1.780	13.780	5.464	13.464	-11.702
67	HO	193	88.775	3.114	14.034	5.663	12.394	-13.087
67	HO	194	95.163	1.980	14.284	6.377	13.780	-12.007
67	HO	195	100.232	3.299	14.523	7.050	12.687	-13.831
67	HO	196	106.877	1.722	14.770	7.298	14.478	-12.770
67	HO	197	112.226	3.018	15.006	7.501	13.404	-14.576
67	HO	198	119.138	1.456	15.249	7.734	15.179	-13.533
67	HO	199	124.774	2.732	15.482	7.925	14.123	-15.322
67	HO	200	131.959	1.182	15.722	8.144	15.883	-14.296
67	HO	201	137.886	2.440	15.953	8.325	14.844	-16.068
67	HO	202	145.350	.904	16.189	8.532	16.590	-15.055
67	HO	203	151.572	2.145	16.417	8.704	15.564	-16.812
67	HO	204	159.318	.621	16.651	8.901	17.297	-15.810

TABLE 2

Atomic mass excesses and nuclear binding energies

67	HO	205	165.837	1.849	16.876	9.067	16.283	-17.552
67	HO	206	173.867	.337	17.107	9.256	18.003	-16.558
67	HO	207	180.680	1.555	17.330	9.419	16.998	-18.286
67	HO	208	188.993	.054	17.557	9.603	18.706	-17.297
67	HO	209	196.096	1.264	17.779	9.765	17.708	-19.010
67	HO	210	204.688	-.224	18.003	9.946	19.404	-18.024
67	HO	211	212.074	.981	18.222	10.110	18.410	-19.723
67	HO	212	220.938	-.496	18.444	10.292	20.094	-18.737
67	HO	213	228.599	.707	18.661	10.461	19.101	-20.422
67	HO	214	237.725	-.759	18.880	10.646	20.774	-19.433
67	HO	215	245.648	.445	19.095	10.823	19.780	-21.104
67	HO	216	255.025	-1.010	19.312	11.014	21.442	-20.111
67	HO	217	263.195	.197	19.525	11.201	20.444	-21.768
67	HO	218	272.809	-1.247	19.739	11.400	22.097	-20.768
67	HO	219	281.210	-.034	19.951	11.598	21.093	-22.413
67	HO	220	291.083	-1.505	20.125	11.770	22.811	-21.328
67	HO	221	299.660	-.210	20.335	12.019	21.725	-23.037
67	HO	222	309.738	-1.710	20.545	12.201	23.434	-21.942
67	HO	223	318.511	-.406	20.753	12.464	22.339	-23.641
67	HO	224	328.775	-1.897	20.961	12.696	24.040	-22.535
67	HO	225	337.726	-.584	21.168	12.935	22.936	-24.224
67	HO	226	348.160	-2.066	21.375	13.179	24.628	-23.108
67	HO	227	357.272	-.745	21.580	13.430	23.516	-24.787
67	HO	228	367.859	-2.219	21.785	13.687	25.199	-23.662
67	HO	229	377.116	-.890	21.989	13.949	24.079	-25.332
67	HO	230	387.841	-2.357	22.192	14.216	25.756	-24.198
67	HO	231	397.229	-1.021	22.395	14.487	24.629	-25.861
67	HO	232	408.078	-2.482	22.596	14.763	26.299	-24.719
67	HO	233	417.585	-1.139	22.797	15.043	25.166	-26.375
67	HO	234	428.547	-2.595	22.998	15.325	26.831	-25.228
67	HO	235	438.163	-1.249	23.197	15.609	25.694	-26.879
67	HO	236	449.231	-2.700	23.396	15.895	27.355	-25.727
67	HO	237	458.949	-1.351	23.593	16.182	26.214	-27.373
67	HO	238	470.117	-2.800	23.791	16.469	27.873	-26.219
	ATOM		M - A	NEUTRON	PROTON	ALPHA	Q BETA -	Q BETA +
68	ER	128	118.723	19.234	-5.771	-6.316	-27.194	21.342
68	ER	129	110.363	16.727	-5.397	-6.293	-24.317	22.746
68	ER	130	100.234	18.497	-5.032	-6.282	-25.710	19.905
68	ER	131	92.575	16.027	-4.662	-6.223	-22.871	21.321
68	ER	132	83.138	17.804	-4.300	-6.174	-24.275	18.519
68	ER	133	76.136	15.369	-3.932	-6.080	-21.475	19.947
68	ER	134	67.347	17.156	-3.573	-5.995	-22.890	17.181
68	ER	135	60.960	14.755	-3.210	-5.866	-20.126	17.968
68	ER	136	52.779	16.549	-2.202	-5.746	-21.552	14.593
68	ER	137	47.612	13.534	-1.841	-5.571	-18.177	16.048
68	ER	138	40.637	15.342	-1.488	-5.406	-18.976	13.355
68	ER	139	35.997	13.007	-1.131	-5.206	-16.283	14.816
68	ER	140	29.504	14.861	-.738	-4.975	-17.819	12.062
68	ER	141	25.411	12.460	-.384	-4.802	-15.063	13.613
68	ER	142	19.421	14.357	-.038	-4.557	-16.601	10.880
68	ER	143	15.815	11.974	.312	-4.376	-13.865	12.429
68	ER	144	10.317	13.865	.654	-4.171	-15.400	9.714
68	ER	145	7.188	11.496	1.000	-3.945	-12.682	11.257
68	ER	146	2.179	13.376	1.337	-3.745	-14.208	8.557
68	ER	147	-.472	11.019	1.679	-3.527	-11.505	10.088
68	ER	148	-4.988	12.883	2.013	-3.340	-13.019	7.402
68	ER	149	-7.156	10.535	2.351	-3.136	-10.328	8.919
68	ER	150	-11.169	12.381	2.679	-2.967	-11.826	5.236
68	ER	151	-11.815	9.013	2.994	-3.809	-8.121	6.770
68	ER	152	-14.300	10.853	3.300	-4.674	-9.647	4.158

TABLE 2

Atomic mass excesses and nuclear binding energies

68	ER	153	-14.485	8.552	3.611	-4.488	-7.043	5.704
68	ER	154	-16.516	10.399	3.912	-4.314	-8.580	3.134
68	ER	155	-16.286	8.137	4.220	-4.089	-6.018	4.688
68	ER	156	-17.906	9.987	4.517	-3.881	-7.561	2.159
68	ER	157	-17.301	7.763	4.821	-3.622	-5.040	3.717
68	ER	158	-18.547	9.613	5.114	-3.384	-6.586	1.226
68	ER	159	-17.603	7.423	5.415	-3.098	-4.102	2.782
68	ER	160	-18.505	9.270	5.705	-2.837	-5.645	.326
68	ER	161	-17.250	7.112	6.003	-2.529	-3.195	1.876
68	ER	162	-17.831	8.948	6.289	-2.254	-4.731	- 548
68	ER	163	-16.283	6.819	6.585	-1.933	-2.312	.990
68	ER	164	-16.556	8.641	6.868	-1.650	-3.833	-1.407
68	ER	165	-14.726	6.537	7.162	-1.325	-1.441	.114
68	ER	166	-14.698	8.339	7.442	-1.043	-2.943	-2.258
68	ER	167	-12.589	6.258	7.733	-.720	-.575	-.759
68	ER	168	-12.256	8.035	8.011	-.447	-2.053	-3.109
68	ER	169	-9.863	5.974	8.300	-.134	.294	-1.637
68	ER	170	-9.218	7.722	8.576	.124	-1.155	-3.966
68	ER	171	-6.530	5.680	8.863	.422	1.173	-2.523
68	ER	172	-5.558	7.396	9.136	.662	-.245	-4.833
68	ER	173	-2.562	5.371	9.421	.941	2.065	-3.422
68	ER	174	-1.248	7.053	9.692	1.159	.681	-5.711
68	ER	175	2.073	5.047	9.976	1.418	2.972	-4.333
68	ER	176	3.746	6.694	10.244	1.614	1.623	-6.601
68	ER	177	7.406	4.708	10.526	1.853	3.893	-5.255
68	ER	178	9.453	6.320	10.793	2.029	2.579	-7.499
68	ER	179	13.464	4.356	11.072	2.252	4.826	-6.185
68	ER	180	15.960	5.872	11.274	2.348	3.671	-8.276
68	ER	181	20.269	4.058	11.552	2.620	5.767	-7.117
68	ER	182	23.157	5.480	11.814	2.705	4.643	-9.178
68	ER	183	27.829	3.695	12.090	2.970	6.709	-8.045
68	ER	184	31.108	5.089	12.351	3.114	5.611	-10.073
68	ER	185	36.141	3.334	12.625	3.314	7.646	-8.962
68	ER	186	39.803	4.705	12.885	3.461	6.568	-10.956
68	ER	187	45.187	2.983	13.156	3.664	8.570	-9.861
68	ER	188	49.218	4.336	13.415	3.821	7.508	-11.819
68	ER	189	54.938	2.648	13.684	4.034	9.475	-10.736
68	ER	190	59.319	3.987	13.940	4.206	8.424	-12.656
68	ER	191	65.353	2.333	14.207	4.435	10.353	-11.581
68	ER	192	70.058	3.662	14.461	4.627	9.310	-13.464
68	ER	193	76.382	2.044	14.725	4.874	11.202	-12.394
68	ER	194	81.383	3.366	14.977	5.089	10.162	-13.780
68	ER	195	87.545	2.205	15.203	5.781	11.593	-12.687
68	ER	196	92.399	3.513	15.417	6.434	10.505	-14.478
68	ER	197	98.822	1.944	15.640	6.649	12.283	-13.404
68	ER	198	103.959	3.231	15.852	6.820	11.213	-15.179
68	ER	199	110.651	1.676	16.072	7.021	12.974	-14.123
68	ER	200	116.076	2.943	16.283	7.181	11.921	-15.883
68	ER	201	123.043	1.400	16.501	7.369	13.668	-14.844
68	ER	202	128.760	2.650	16.711	7.521	12.629	-16.590
68	ER	203	136.008	1.120	16.926	7.697	14.363	-15.564
68	ER	204	142.022	2.354	17.135	7.842	13.337	-17.297
68	ER	205	149.554	.835	17.349	8.010	15.058	-16.283
68	ER	206	155.864	2.057	17.557	8.150	14.043	-18.003
68	ER	207	163.681	.550	17.770	8.312	15.752	-16.998
68	ER	208	170.287	1.762	17.978	8.451	14.746	-18.706
68	ER	209	178.388	.266	18.189	8.610	16.443	-17.708
68	ER	210	185.284	1.471	18.397	8.750	15.444	-19.404
68	ER	211	193.665	-.014	18.607	8.909	17.130	-18.410
68	ER	212	200.845	1.188	18.815	9.054	16.134	-20.094
68	ER	213	209.498	-.286	19.025	9.217	17.810	-19.101
68	ER	214	216.952	.914	19.232	9.369	16.815	-20.774

TABLE 2

Atomic mass excesses and nuclear binding energies

68	ER	215	225.868	-.549	19.442	9.538	18.481	-19.780
68	ER	216	233.583	.652	19.650	9.702	17.484	-21.442
68	ER	217	242.751	-.800	19.859	9.879	19.141	-20.444
68	ER	218	250.712	.406	20.067	10.056	18.140	-22.097
68	ER	219	260.117	-1.037	20.277	10.244	19.788	-21.093
68	ER	220	268.272	.213	20.523	10.473	18.707	-22.811
68	ER	221	277.935	-1.296	20.732	10.637	20.423	-21.725
68	ER	222	286.303	-.001	20.942	10.882	19.335	-23.434
68	ER	223	296.172	-1.501	21.151	11.061	21.043	-22.339
68	ER	224	304.735	-.196	21.360	11.285	19.947	-24.040
68	ER	225	314.790	-1.688	21.569	11.517	21.649	-22.936
68	ER	226	323.532	-.375	21.779	11.756	20.546	-24.628
68	ER	227	333.757	-1.857	21.988	12.004	22.240	-23.516
68	ER	228	342.660	-.536	22.197	12.259	21.131	-25.199
68	ER	229	353.037	-2.010	22.407	12.522	22.818	-24.079
68	ER	230	362.085	-.681	22.616	12.792	21.703	-25.756
68	ER	231	372.600	-2.148	22.826	13.068	23.385	-24.629
68	ER	232	381.779	-.811	23.035	13.351	22.264	-26.299
68	ER	233	392.418	-2.272	23.244	13.639	23.941	-25.166
68	ER	234	401.716	-.930	23.454	13.932	22.816	-26.831
68	ER	235	412.469	-2.386	23.663	14.230	24.489	-25.694
68	ER	236	421.876	-1.039	23.872	14.531	23.361	-27.355
68	ER	237	432.735	-2.491	24.081	14.835	25.032	-26.214
68	ER	238	442.244	-1.142	24.290	15.141	23.901	-27.873
68	ER	239	453.203	-2.592	24.498	15.448	25.571	-26.730
68	ER	240	462.812	-1.241	24.707	15.756	24.440	-28.387
68	ER	241	473.869	-2.690	24.915	16.063	26.109	-27.244
	ATOM		M - A	NEUTRON	PROTON	ALPHA	Q BETA -	Q BETA +
69	TM	131	115.446	18.865	-7.627	-6.469	-24.416	22.871
69	TM	132	107.413	16.400	-7.253	-6.422	-21.594	24.275
69	TM	133	97.610	18.170	-6.888	-6.384	-23.000	21.475
69	TM	134	90.238	15.740	-6.517	-6.300	-20.214	22.890
69	TM	135	81.086	17.519	-6.154	-6.223	-21.631	20.126
69	TM	136	74.331	15.122	-5.786	-6.103	-18.879	21.552
69	TM	137	65.789	16.909	-5.425	-5.990	-20.306	18.177
69	TM	138	59.613	14.543	-4.417	-5.838	-17.587	18.976
69	TM	139	52.280	15.700	-4.059	-5.678	-18.386	16.283
69	TM	140	47.323	13.325	-3.741	-5.528	-14.978	17.819
69	TM	141	40.474	15.216	-3.385	-5.301	-16.513	15.063
69	TM	142	36.022	12.819	-3.026	-5.132	-13.766	16.601
69	TM	143	29.680	14.710	-2.674	-4.890	-15.302	13.865
69	TM	144	25.717	12.330	-2.318	-4.666	-12.575	15.400
69	TM	145	19.870	14.215	-1.968	-4.462	-14.108	12.682
69	TM	146	16.387	11.850	-1.615	-4.237	-11.399	14.208
69	TM	147	11.032	13.722	-1.269	-4.038	-12.922	11.505
69	TM	148	8.030	11.369	-.918	-3.818	-10.229	13.019
69	TM	149	3.172	13.226	-.576	-3.632	-11.739	10.328
69	TM	150	.657	10.882	-.228	-3.426	-9.059	11.826
69	TM	151	-3.694	12.719	.110	-3.257	-10.553	8.121
69	TM	152	-4.653	9.327	.423	-4.128	-6.828	9.647
69	TM	153	-7.442	11.156	.727	-5.023	-8.362	7.043
69	TM	154	-7.937	8.862	1.036	-4.859	-5.782	8.580
69	TM	155	-10.268	10.699	1.336	-4.708	-7.326	6.018
69	TM	156	-10.344	8.444	1.643	-4.505	-4.789	7.561
69	TM	157	-12.261	10.284	1.940	-4.319	-6.340	5.040
69	TM	158	-11.961	8.067	2.245	-4.081	-3.845	6.586
69	TM	159	-13.501	9.907	2.539	-3.863	-5.398	4.102
69	TM	160	-12.860	7.726	2.842	-3.596	-2.940	5.645
69	TM	161	-14.054	9.562	3.134	-3.354	-4.491	3.195
69	TM	162	-13.100	7.413	3.435	-3.063	-2.068	4.731

TABLE 2

Atomic mass excesses and nuclear binding energies

69	TM	163	-13.971	9.239	3.725	-2.805	-3.609	2.312
69	TM	164	-12.723	7.119	4.025	-2.499	-1.217	3.833
69	TM	165	-13.286	8.930	4.314	-2.231	-2.744	1.441
69	TM	166	-11.755	6.837	4.613	-1.918	-.380	2.943
69	TM	167	-12.014	8.627	4.901	-1.649	-1.887	.575
69	TM	168	-10.203	6.557	5.199	-1.337	.454	2.053
69	TM	169	-10.157	8.321	5.486	-1.074	-1.027	-.294
69	TM	170	-8.062	6.272	5.784	-.769	1.293	1.155
69	TM	171	-7.703	8.008	6.070	-.518	-.159	-1.173
69	TM	172	-5.313	5.978	6.368	-.225	2.142	.245
69	TM	173	-4.626	7.681	6.653	.009	.722	-2.065
69	TM	174	-1.928	5.669	6.951	.286	3.005	-.681
69	TM	175	-.899	7.338	7.236	.501	1.621	-2.972
69	TM	176	2.123	5.345	7.534	.761	3.885	-1.623
69	TM	177	3.513	6.978	7.818	.957	2.537	-3.893
69	TM	178	6.874	5.006	8.116	1.199	4.781	-2.579
69	TM	179	8.638	6.603	8.400	1.377	3.469	-4.826
69	TM	180	12.289	4.716	8.760	1.667	5.565	-3.671
69	TM	181	14.502	6.154	9.043	1.768	4.413	-5.767
69	TM	182	18.514	4.355	9.340	2.047	6.484	-4.643
69	TM	183	21.120	5.762	9.622	2.139	5.365	-6.709
69	TM	184	25.497	3.990	9.917	2.349	7.409	-5.611
69	TM	185	28.495	5.370	10.198	2.501	6.316	-7.646
69	TM	186	33.234	3.628	10.491	2.710	8.332	-6.568
69	TM	187	36.617	4.985	10.771	2.867	7.261	-8.570
69	TM	188	41.710	3.274	11.062	3.080	9.245	-7.508
69	TM	189	45.463	4.614	11.340	3.249	8.191	-9.475
69	TM	190	50.895	2.936	11.628	3.473	10.142	-8.424
69	TM	191	54.999	4.263	11.904	3.658	9.100	-10.353
69	TM	192	60.748	2.619	12.189	3.898	11.016	-9.310
69	TM	193	65.180	3.936	12.463	4.103	9.982	-11.202
69	TM	194	71.221	2.326	12.745	4.363	11.863	-10.162
69	TM	195	75.952	3.637	13.016	4.592	10.832	-11.593
69	TM	196	81.894	2.425	13.236	5.237	12.313	-10.505
69	TM	197	86.540	3.722	13.445	5.845	11.212	-12.283
69	TM	198	92.746	2.161	13.661	6.026	12.959	-11.213
69	TM	199	97.676	3.437	13.867	6.165	11.876	-12.974
69	TM	200	104.155	1.889	14.081	6.332	13.608	-11.921
69	TM	201	109.375	3.147	14.285	6.461	12.542	-13.668
69	TM	202	116.131	1.611	14.496	6.616	14.261	-12.629
69	TM	203	121.646	2.853	14.700	6.738	13.210	-14.363
69	TM	204	128.684	1.328	14.908	6.884	14.918	-13.337
69	TM	205	134.496	2.556	15.111	6.999	13.880	-15.058
69	TM	206	141.821	1.043	15.318	7.138	15.577	-14.043
69	TM	207	147.929	2.259	15.519	7.252	14.550	-15.752
69	TM	208	155.541	.756	15.726	7.387	16.238	-14.746
69	TM	209	161.945	1.963	15.927	7.501	15.221	-16.443
69	TM	210	169.840	.472	16.132	7.636	16.899	-15.444
69	TM	211	176.535	1.673	16.334	7.754	15.889	-17.130
69	TM	212	184.711	.192	16.539	7.891	17.558	-16.134
69	TM	213	191.688	1.390	16.741	8.017	16.553	-17.810
69	TM	214	200.137	-.081	16.946	8.160	18.215	-16.815
69	TM	215	207.388	1.117	17.149	8.296	17.212	-18.481
69	TM	216	216.099	-.344	17.354	8.448	18.866	-17.484
69	TM	217	223.610	.856	17.558	8.598	17.863	-19.141
69	TM	218	232.572	-.595	17.763	8.763	19.511	-18.140
69	TM	219	240.329	.611	17.969	8.929	18.505	-19.788
69	TM	220	249.564	-.869	18.137	9.070	20.223	-18.707
69	TM	221	257.513	.419	18.344	9.292	19.137	-20.423
69	TM	222	266.969	-1.089	18.551	9.449	20.849	-19.335
69	TM	223	275.129	.207	18.759	9.691	19.759	-21.043
69	TM	224	284.788	-1.292	18.968	9.904	21.465	-19.947

TABLE 2

Atomic mass excesses and nuclear binding energies

69	TM	225	293.142	.013	19.178	10.128	20.369	-21.649
69	TM	226	302.986	-1.477	19.389	10.361	22.069	-20.546
69	TM	227	311.517	-.163	19.600	10.603	20.967	-22.240
69	TM	228	321.529	-1.645	19.813	10.855	22.663	-21.131
69	TM	229	330.219	-.322	20.026	11.117	21.556	-22.818
69	TM	230	340.382	-1.796	20.240	11.387	23.246	-21.703
69	TM	231	349.215	-.466'	20.455	11.666	22.134	-23.385
69	TM	232	359.515	-1.932	20.670	11.954	23.821	-22.264
69	TM	233	368.477	-.595	20.886	12.248	22.705	-23.941
69	TM	234	378.900	-2.055	21.103	12.550	24.388	-22.816
69	TM	235	387.980	-.713	21.321	12.858	23.270	-24.489
69	TM	236	398.515	-2.168	21.539	13.172	24.950	-23.361
69	TM	237	407.703	-.821	21.758	13.491	23.830	-25.032
69	TM	238	418.343	-2.272	21.977	13.814	25.509	-23.901
69	TM	239	427.633	-.923	22.196	14.140	24.389	-25.571
69	TM	240	438.372	-2.372	22.416	14.468	26.068	-24.440
69	TM	241	447.760	-1.021	22.636	14.798	24.948	-26.109
69	TM	242	458.597	-2.470	22.857	15.129	26.628	-24.978
69	TM	243	468.083	-1.119	23.077	15.460	25.510	-26.648
69	TM	244	479.018	-2.568	23.298	15.790	27.192	-25.519
69	TM	245	488.604	-1.219	23.518	16.118	26.076	-27.191
69	TM	246	499.642	-2.671	23.738	16.443	27.761	-26.065
	ATOM		M - A	NEUTRON	PROTON	ALPHA	Q BETA -	Q BETA +
70	YB	133	120.610	16.764	-5.613	-6.638	-24.522	23.000
70	YB	134	110.451	18.526	-5.256	-6.608	-25.918	20.214
70	YB	135	102.717	16.102	-4.895	-6.533	-23.134	21.631
70	YB	136	93.210	17.874	-4.540	-6.463	-24.541	18.879
70	YB	137	86.095	15.482	-4.180	-6.350	-21.791	20.306
70	YB	138	77.200	17.263	-3.826	-6.243	-23.208	17.587
70	YB	139	70.666	14.902	-3.468	-6.096	-20.489	18.386
70	YB	140	62.300	16.733	-2.436	-5.912	-22.001	14.978
70	YB	141	56.987	13.681	-2.079	-5.766	-18.593	16.513
70	YB	142	49.788	15.566	-1.729	-5.542	-19.489	13.766
70	YB	143	44.982	13.173	-1.375	-5.375	-16.740	15.302
70	YB	144	38.292	15.057	-1.028	-5.180	-18.263	12.575
70	YB	145	33.978	12.682	-.676	-4.957	-15.535	14.108
70	YB	146	27.786	14.559	-.332	-4.756	-17.053	11.399
70	YB	147	23.955	12.199	.017	-4.531	-14.341	12.922
70	YB	148	18.259	14.063	.358	-4.333	-15.848	10.229
70	YB	149	14.911	11.715	.704	-4.114	-13.151	11.739
70	YB	150	9.716	13.562	1.041	-3.928	-14.644	9.059
70	YB	151	6.859	11.225	1.383	-3.722	-11.960	10.553
70	YB	152	2.175	13.051	1.716	-3.554	-13.434	6.828
70	YB	153	.920	9.622	2.012	-4.467	-9.663	8.362
70	YB	154	-2.155	11.442	2.297	-5.405	-11.188	5.782
70	YB	155	-2.942	9.154	2.590	-5.264	-8.615	7.326
70	YB	156	-5.555	10.981	2.872	-5.136	-10.149	4.789
70	YB	157	-5.921	8.733	3.161	-4.955	-7.620	6.340
70	YB	158	-8.116	10.563	3.440	-4.791	-9.160	3.845
70	YB	159	-8.103	8.354	3.727	-4.573	-6.672	5.398
70	YB	160	-9.920	10.184	4.003	-4.377	-8.213	2.940
70	YB	161	-9.564	8.011	4.288	-4.128	-5.763	4.491
70	YB	162	-11.032	9.836	4.563	-3.905	-7.299	2.068
70	YB	163	-10.362	7.697	4.847	-3.632	-4.883	3.609
70	YB	164	-11.506	9.511	5.119	-3.390	-6.409	1.217
70	YB	165	-10.541	7.403	5.403	-3.099	-4.024	2.744
70	YB	166	-11.375	9.202	5.674	-2.846	-5.534	.380
70	YB	167	-10.128	7.120	5.957	-2.546	-3.174	1.887
70	YB	168	-10.658	8.898	6.229	-2.289	-4.663	-.454
70	YB	169	-9.130	6.840	6.512	-1.987	-2.326	1.027

TABLE 2

Atomic mass excesses and nuclear binding energies

70	YB	170	-9.355	8.592	6.782	-1.734	-3.787	-1.293
70	YB	171	-7.543	6.556	7.066	-1.436	-1.471	.159
70	YB	172	-7.455	8.279	7.337	-1.193	-2.900	-2.142
70	YB	173	-5.349	6.262	7.621	-.905	-.602	-.722
70	YB	174	-4.933	7.952	7.892	-.675	-1.996	-3.005
70	YB	175	-2.520	5.954	8.176	-.401	.285	-1.621
70	YB	176	-1.761	7.609	8.447	-.187	-1.072	-3.885
70	YB	177	.976	5.630	8.733	.072	1.192	-2.537
70	YB	178	2.094	7.250	9.004	.268	-.127	-4.781
70	YB	179	5.169	5.292	9.290	.513	2.118	-3.469
70	YB	180	6.724	6.812	9.499	.631	.962	-5.565
70	YB	181	10.089	5.003	9.785	.926	3.060	-4.413
70	YB	182	12.030	6.426	10.057	1.032	1.941	-6.484
70	YB	183	15.755	4.642	10.344	1.319	4.016	-5.365
70	YB	184	18.088	6.035	10.617	1.482	2.928	-7.409
70	YB	185	22.178	4.277	10.903	1.700	4.977	-6.316
70	YB	186	24.903	5.643	11.177	1.863	3.915	-8.332
70	YB	187	29.356	3.914	11.463	2.082	5.936	-7.261
70	YB	188	32.465	5.258	11.737	2.252	4.897	-9.245
70	YB	189	37.272	3.560	12.022	2.477	6.888	-8.191
70	YB	190	40.753	4.887	12.295	2.659	5.864	-10.142
70	YB	191	45.900	3.220	12.580	2.896	7.823	-9.100
70	YB	192	49.732	4.535	12.852	3.095	6.810	-11.016
70	YB	193	55.198	2.901	13.135	3.349	8.735	-9.982
70	YB	194	59.358	4.207	13.406	3.569	7.729	-11.863
70	YB	195	65.120	2.606	13.686	3.842	9.619	-10.832
70	YB	196	69.581	3.906	13.956	4.086	8.616	-12.313
70	YB	197	75.328	2.621	14.151	4.663	10.188	-11.212
70	YB	198	79.787	3.908	14.337	5.205	9.091	-12.959
70	YB	199	85.801	2.354	14.531	5.354	10.826	-11.876
70	YB	200	90.546	3.622	14.715	5.462	9.745	-13.608
70	YB	201	96.833	2.080	14.906	5.599	11.465	-12.542
70	YB	202	101.870	3.331	15.090	5.698	10.399	-14.261
70	YB	203	108.436	1.801	15.280	5.824	12.106	-13.210
70	YB	204	113.767	3.036	15.463	5.918	11.054	-14.918
70	YB	205	120.616	1.518	15.653	6.036	12.749	-13.880
70	YB	206	126.244	2.740	15.837	6.126	11.710	-15.577
70	YB	207	133.379	1.232	16.026	6.238	13.395	-14.550
70	YB	208	139.303	2.443	16.211	6.328	12.366	-16.238
70	YB	209	146.724	.946	16.401	6.439	14.042	-15.221
70	YB	210	152.941	2.150	16.588	6.532	13.022	-16.899
70	YB	211	160.646	.663	16.779	6.645	14.689	-15.889
70	YB	212	167.152	1.861	16.967	6.744	13.675	-17.558
70	YB	213	175.135	.384	17.160	6.862	15.335	-16.553
70	YB	214	181.922	1.581	17.351	6.971	14.325	-18.215
70	YB	215	190.176	.113	17.546	7.098	15.978	-17.212
70	YB	216	197.233	1.311	17.740	7.221	14.970	-18.866
70	YB	217	205.747	-.147	17.937	7.360	16.616	-17.863
70	YB	218	213.061	1.053	18.134	7.500	15.607	-19.511
70	YB	219	221.823	-.395	18.333	7.654	17.249	-18.505
70	YB	220	229.342	.849	18.571	7.850	16.163	-20.223
70	YB	221	238.375	-.666	18.774	7.984	17.875	-19.137
70	YB	222	246.119	.623	18.978	8.202	16.785	-20.849
70	YB	223	255.370	-.883	19.183	8.356	18.492	-19.759
70	YB	224	263.323	.415	19.391	8.558	17.398	-21.465
70	YB	225	272.773	-1.083	19.599	8.771	19.102	-20.369
70	YB	226	280.917	.224	19.810	8.996	18.004	-22.069
70	YB	227	290.549	-1.265	20.022	9.232	19.703	-20.967
70	YB	228	298.866	.051	20.235	9.479	18.601	-22.663
70	YB	229	308.663	-1.429	20.451	9.737	20.297	-21.556
70	YB	230	317.136	-.106	20.667	10.006	19.191	-23.246
70	YB	231	327.081	-1.578	20.886	10.285	20.883	-22.134

TABLE 2

Atomic mass excesses and nuclear binding energies

70	YB	232	335.694	-.246	21.106	10.575	19.774	-23.821
70	YB	233	345.772	-1.711	21.327	10.874	21.464	-22.705
70	YB	234	354.512	-.372	21.550	11.182	20.353	-24.388
70	YB	235	364.710	-1.831	21.774	11.499	22.041	-23.270
70	YB	236	373.565	-.487	22.000	11.823	20.928	-24.950
70	YB	237	383.873	-1.941	22.227	12.155	22.615	-23.830
70	YB	238	392.833	-.593	22.455	12.492	21.502	-25.509
70	YB	239	403.244	-2.043	22.684	12.835	23.190	-24.389
70	YB	240	412.304	-.692	22.914	13.181	22.078	-26.068
70	YB	241	422.812	-2.141	23.145	13.532	23.766	-24.948
70	YB	242	431.969	-.789	23.376	13.885	22.656	-26.628
70	YB	243	442.573	-2.237	23.609	14.239	24.347	-25.510
70	YB	244	451.826	-.886	23.841	14.595	23.239	-27.192
70	YB	245	462.528	-2.335	24.075	14.950	24.933	-26.076
70	YB	246	471.881	-.985	24.308	15.304	23.829	-27.761
70	YB	247	482.685	-2.437	24.542	15.655	25.527	-26.649
70	YB	248	492.142	-1.090	24.776	16.005	24.427	-28.338
70	YB	249	503.055	-2.545	25.010	16.350	26.130	-27.229
70	YB	250	512.625	-1.203	25.243	16.691	25.035	-28.922
	ATOM		M - A	NEUTRON	PROTON	ALPHA	Q BETA -	Q BETA +
71	LU	136	117.751	16.467	-7.450	-6.729	-21.865	24.541
71	LU	137	107.886	18.232	-7.091	-6.667	-23.274	21.791
71	LU	138	100.408	15.846	-6.727	-6.561	-20.537	23.208
71	LU	139	91.154	17.621	-6.370	-6.459	-21.955	20.489
71	LU	140	84.302	15.220	-6.051	-6.361	-19.160	22.001
71	LU	141	75.580	17.089	-5.695	-6.182	-20.673	18.593
71	LU	142	69.276	14.671	-4.705	-6.054	-17.904	19.489
71	LU	143	61.722	15.922	-4.349	-5.833	-18.799	16.740
71	LU	144	56.556	13.533	-3.989	-5.624	-15.440	18.263
71	LU	145	49.513	15.411	-3.635	-5.430	-16.962	15.535
71	LU	146	44.839	13.041	-3.277	-5.208	-14.245	17.053
71	LU	147	38.296	14.910	-2.925	-5.007	-15.761	14.341
71	LU	148	34.107	12.556	-2.568	-4.781	-13.061	15.848
71	LU	149	28.063	14.412	-2.219	-4.584	-14.565	13.151
71	LU	150	24.360	12.070	-1.864	-4.363	-11.880	14.644
71	LU	151	18.819	13.908	-1.518	-4.177	-13.369	11.960
71	LU	152	15.609	11.577	-1.166	-3.970	-10.697	13.434
71	LU	153	10.583	13.394	-.823	-3.801	-12.168	9.663
71	LU	154	9.033	9.917	-.528	-4.766	-8.355	11.188
71	LU	155	5.673	11.727	-.243	-5.758	-9.887	8.615
71	LU	156	4.594	9.446	.049	-5.638	-7.339	10.149
71	LU	157	1.699	11.262	.330	-5.532	-8.881	7.620
71	LU	158	1.044	9.023	.620	-5.371	-6.378	9.160
71	LU	159	-1.431	10.843	.900	-5.227	-7.925	6.672
71	LU	160	-1.707	8.643	1.188	-5.029	-5.464	8.213
71	LU	161	-3.801	10.462	1.466	-4.851	-7.012	5.763
71	LU	162	-3.733	8.299	1.754	-4.619	-4.589	7.299
71	LU	163	-5.479	10.113	2.032	-4.413	-6.133	4.883
71	LU	164	-5.096	7.985	2.319	-4.154	-3.745	6.409
71	LU	165	-6.518	9.789	2.597	-3.927	-5.278	4.024
71	LU	166	-5.842	7.691	2.885	-3.649	-2.921	5.534
71	LU	167	-6.953	9.479	3.163	-3.409	-4.437	3.174
71	LU	168	-5.995	7.409	3.453	-3.119	-2.107	4.663
71	LU	169	-6.804	9.176	3.731	-2.872	-3.600	2.326
71	LU	170	-5.568	7.131	4.023	-2.578	-1.293	3.787
71	LU	171	-6.073	8.872	4.302	-2.332	-2.759	1.471
71	LU	172	-4.554	6.849	4.596	-2.040	-.472	2.900
71	LU	173	-4.747	8.560	4.877	-1.801	-1.905	.602
71	LU	174	-2.937	6.557	5.173	-1.516	.364	1.996
71	LU	175	-2.805	8.235	5.456	-1.289	-1.033	-.285

TABLE 2

Atomic mass excesses and nuclear binding energies

71	LU	176	-.689	6.252	5.754	-1.015	1.219	1.072
71	LU	177	-.216	7.894	6.039	-.801	-.139	-1.192
71	LU	178	2.221	5.931	6.340	-.540	2.095	.127
71	LU	179	3.052	7.537	6.627	-.341	.776	-2.118
71	LU	180	5.762	5.657	6.992	-.029	2.867	-.962
71	LU	181	7.028	7.101	7.281	.094	1.713	-3.060
71	LU	182	10.089	5.307	7.585	.395	3.783	-1.941
71	LU	183	11.740	6.717	7.875	.508	2.666	-4.016
71	LU	184	15.160	4.947	8.180	.738	4.716	-2.928
71	LU	185	17.202	6.326	8.471	.910	3.631	-4.977
71	LU	186	20.987	4.582	8.776	1.136	5.658	-3.915
71	LU	187	23.419	5.935	9.068	1.310	4.601	-5.936
71	LU	188	27.568	4.219	9.373	1.538	6.603	-4.897
71	LU	189	30.385	5.551	9.665	1.719	5.568	-6.888
71	LU	190	34.889	3.863	9.968	1.955	7.542	-5.864
71	LU	191	38.077	5.179	10.260	2.149	6.525	-7.823
71	LU	192	42.922	3.522	10.562	2.397	8.469	-6.810
71	LU	193	46.463	4.826	10.853	2.609	7.463	-8.735
71	LU	194	51.630	3.201	11.153	2.874	9.376	-7.729
71	LU	195	55.501	4.496	11.442	3.108	8.378	-9.619
71	LU	196	60.965	2.903	11.740	3.393	10.258	-8.616
71	LU	197	65.139	4.193	12.026	3.650	9.264	-10.188
71	LU	198	70.696	2.811	12.217	4.135	10.931	-9.091
71	LU	199	74.975	4.088	12.397	4.586	9.822	-10.826
71	LU	200	80.801	2.541	12.584	4.702	11.528	-9.745
71	LU	201	85.368	3.800	12.763	4.780	10.435	-11.465
71	LU	202	91.471	2.265	12.947	4.885	12.128	-10.399
71	LU	203	96.330	3.508	13.125	4.956	11.049	-12.106
71	LU	204	102.712	1.985	13.308	5.051	12.731	-11.054
71	LU	205	107.867	3.213	13.485	5.117	11.667	-12.749
71	LU	206	114.534	1.701	13.667	5.207	13.338	-11.710
71	LU	207	119.984	2.917	13.845	5.271	12.287	-13.395
71	LU	208	126.936	1.415	14.027	5.357	13.950	-12.366
71	LU	209	132.682	2.622	14.206	5.423	12.909	-14.042
71	LU	210	139.920	1.130	14.389	5.510	14.565	-13.022
71	LU	211	145.957	2.330	14.569	5.582	13.533	-14.689
71	LU	212	153.477	.847	14.754	5.673	15.182	-13.675
71	LU	213	159.801	2.044	14.936	5.753	14.158	-15.335
71	LU	214	167.597	.571	15.123	5.852	15.802	-14.325
71	LU	215	174.198	1.766	15.308	5.946	14.782	-15.978
71	LU	216	182.263	.302	15.497	6.057	16.422	-14.970
71	LU	217	189.131	1.500	15.686	6.167	15.405	-16.616
71	LU	218	197.454	.045	15.878	6.293	17.041	-15.607
71	LU	219	204.575	1.246	16.071	6.422	16.024	-17.249
71	LU	220	213.179	-.237	16.229	6.529	17.732	-16.163
71	LU	221	220.501	1.046	16.426	6.718	16.639	-17.875
71	LU	222	229.335	-.467	16.625	6.846	18.345	-16.785
71	LU	223	236.878	.825	16.827	7.060	17.250	-18.492
71	LU	224	245.925	-.679	17.030	7.249	18.953	-17.398
71	LU	225	253.671	.621	17.236	7.451	17.855	-19.102
71	LU	226	262.913	-.874	17.445	7.665	19.555	-18.004
71	LU	227	270.846	.435	17.656	7.892	18.455	-19.703
71	LU	228	280.265	-1.052	17.869	8.132	20.152	-18.601
71	LU	229	288.366	.266	18.085	8.385	19.049	-20.297
71	LU	230	297.945	-1.212	18.303	8.651	20.744	-19.191
71	LU	231	306.197	.115	18.523	8.928	19.639	-20.883
71	LU	232	315.920	-1.355	18.746	9.218	21.332	-19.774
71	LU	233	324.308	-.021	18.971	9.520	20.225	-21.464
71	LU	234	334.159	-1.484	19.198	9.832	21.917	-20.353
71	LU	235	342.670	-.143	19.427	10.155	20.809	-22.041
71	LU	236	352.637	-1.600	19.659	10.487	22.501	-20.928
71	LU	237	361.258	-.254	19.892	10.829	21.393	-22.615

TABLE 2

Atomic mass excesses and nuclear binding energies

71	LU	238	371.331	-1.706	20.127	11.178	23.086	-21.502
71	LU	239	380.054	-.356	20.364	11.535	21.979	-23.190
71	LU	240	390.226	-1.805	20.603	11.898	23.673	-22.078
71	LU	241	399.046	-.452	20.843	12.267	22.569	-23.766
71	LU	242	409.313	-1.899	21.084	12.639	24.266	-22.656
71	LU	243	418.226	-.546	21.327	13.015	23.164	-24.347
71	LU	244	428.587	-1.993	21.571	13.394	24.864	-23.239
71	LU	245	437.595	-.641	21.816	13.774	23.767	-24.933
71	LU	246	448.052	-2.089	22.061	14.154	25.472	-23.829
71	LU	247	457.158	-.739	22.308	14.534	24.379	-25.527
71	LU	248	467.715	-2.190	22.555	14.913	26.088	-24.427
71	LU	249	476.925	-.843	22.802	15.289	25.001	-26.130
71	LU	250	487.590	-2.298	23.049	15.661	26.716	-25.035
71	LU	251	496.913	-.955	23.297	16.030	25.634	-26.742
71	LU	252	507.695	-2.415	23.544	16.394	27.354	-25.651
71	LU	253	517.141	-1.078	23.791	16.752	26.277	-27.363
71	LU	254	528.052	-2.543	24.037	17.104	28.003	-26.277
	ATOM		M - A	NEUTRON	PROTON	ALPHA	Q BETA -	Q BETA +
72	HF	138	120.944	18.583	-5.473	-6.884	-26.155	20.537
72	HF	139	113.109	16.202	-5.117	-6.783	-23.420	21.955
72	HF	140	103.461	18.015	-4.722	-6.642	-24.917	19.160
72	HF	141	96.253	15.576	-4.366	-6.548	-22.124	20.673
72	HF	142	87.180	17.440	-4.016	-6.371	-23.627	17.904
72	HF	143	80.521	15.027	-3.660	-6.246	-20.859	18.799
72	HF	144	71.996	16.893	-2.689	-6.086	-22.365	15.440
72	HF	145	66.475	13.888	-2.334	-5.879	-19.005	16.962
72	HF	146	59.084	15.758	-1.987	-5.687	-19.900	14.245
72	HF	147	54.057	13.394	-1.633	-5.466	-17.181	15.761
72	HF	148	47.168	15.256	-1.287	-5.266	-18.682	13.061
72	HF	149	42.628	12.908	-.936	-5.041	-15.980	14.565
72	HF	150	36.240	14.755	-.592	-4.844	-17.468	11.880
72	HF	151	32.188	12.419	-.243	-4.624	-14.780	13.369
72	HF	152	26.306	14.249	.097	-4.438	-16.251	10.697
72	HF	153	22.751	11.923	.443	-4.230	-13.576	12.168
72	HF	154	17.388	13.730	.779	-4.063	-15.027	8.355
72	HF	155	15.561	10.195	1.057	-5.092	-11.146	9.887
72	HF	156	11.934	11.994	1.324	-6.150	-12.667	7.339
72	HF	157	10.580	9.721	1.599	-6.051	-10.126	8.881
72	HF	158	7.421	11.526	1.863	-5.967	-11.656	6.378
72	HF	159	6.494	9.295	2.135	-5.826	-9.160	7.925
72	HF	160	3.757	11.104	2.396	-5.703	-10.695	5.464
72	HF	161	3.211	8.914	2.667	-5.522	-8.241	7.012
72	HF	162	.856	10.722	2.927	-5.363	-9.776	4.589
72	HF	163	.654	8.570	3.198	-5.148	-7.360	6.133
72	HF	164	-1.351	10.373	3.457	-4.959	-8.889	3.745
72	HF	165	-1.240	8.256	3.728	-4.715	-6.508	5.278
72	HF	166	-2.921	10.048	3.988	-4.502	-8.025	2.921
72	HF	167	-2.516	7.963	4.259	-4.236	-5.675	4.437
72	HF	168	-3.889	9.740	4.520	-4.008	-7.174	2.107
72	HF	169	-3.204	7.683	4.793	-3.728	-4.849	3.600
72	HF	170	-4.275	9.438	5.055	-3.491	-6.324	1.293
72	HF	171	-3.314	7.407	5.331	-3.204	-4.022	2.759
72	HF	172	-4.083	9.136	5.595	-2.966	-5.467	.472
72	HF	173	-2.843	7.127	5.873	-2.679	-3.184	1.905
72	HF	174	-3.301	8.826	6.139	-2.445	-4.595	-.364
72	HF	175	-1.772	6.838	6.420	-2.162	-2.329	1.033
72	HF	176	-1.908	8.504	6.688	-1.937	-3.701	-1.219
72	HF	177	-.077	6.536	6.972	-1.663	-1.452	.139
72	HF	178	.125	8.165	7.243	-1.449	-2.784	-2.095
72	HF	179	2.275	6.218	7.530	-1.186	-.551	-.776

TABLE 2

Atomic mass excesses and nuclear binding energies

72	HF	180	2.895	7.748	7.741	-1.047	-1.716	-2.867
72	HF	181	5.316	5.947	8.031	-.731	.375	-1.713
72	HF	182	6.305	7.378	8.308	-.603	-.750	-3.783
72	HF	183	9.073	5.599	8.600	-.295	1.321	-2.666
72	HF	184	10.444	6.996	8.880	-.111	.233	-4.716
72	HF	185	13.570	5.241	9.175	.128	2.285	-3.631
72	HF	186	15.329	6.608	9.457	.310	1.230	-5.658
72	HF	187	18.818	4.878	9.754	.546	3.259	-4.601
72	HF	188	20.966	6.220	10.039	.732	2.231	-6.603
72	HF	189	24.817	4.516	10.336	.971	4.237	-5.568
72	HF	190	27.347	5.837	10.623	1.165	3.231	-7.542
72	HF	191	31.552	4.162	10.921	1.413	5.210	-6.525
72	HF	192	34.453	5.466	11.209	1.621	4.220	-8.469
72	HF	193	39.000	3.821	11.507	1.882	6.170	-7.463
72	HF	194	42.254	5.114	11.794	2.108	5.192	-9.376
72	HF	195	47.123	3.498	12.091	2.386	7.111	-8.378
72	HF	196	50.707	4.783	12.378	2.634	6.140	-10.258
72	HF	197	55.876	3.199	12.674	2.932	8.027	-9.264
72	HF	198	59.765	4.478	12.959	3.203	7.059	-10.931
72	HF	199	65.153	2.979	13.127	3.576	8.859	-9.822
72	HF	200	69.273	4.247	13.286	3.917	7.754	-11.528
72	HF	201	74.934	2.707	13.452	4.003	9.448	-10.435
72	HF	202	79.343	3.958	13.610	4.053	8.358	-12.128
72	HF	203	85.280	2.430	13.775	4.129	10.038	-11.049
72	HF	204	89.982	3.666	13.933	4.174	8.961	-12.731
72	HF	205	96.200	2.149	14.097	4.242	10.630	-11.667
72	HF	206	101.195	3.372	14.256	4.283	9.565	-13.338
72	HF	207	107.697	1.866	14.421	4.348	11.225	-12.287
72	HF	208	112.987	3.078	14.582	4.389	10.171	-13.950
72	HF	209	119.773	1.581	14.748	4.452	11.822	-12.909
72	HF	210	125.355	2.785	14.912	4.498	10.778	-14.565
72	HF	211	132.424	1.298	15.080	4.564	12.422	-13.533
72	HF	212	138.295	2.497	15.247	4.617	11.386	-15.182
72	HF	213	145.643	1.019	15.419	4.690	13.024	-14.158
72	HF	214	151.795	2.215	15.590	4.755	11.994	-15.802
72	HF	215	159.416	.746	15.766	4.839	13.628	-14.782
72	HF	216	165.842	1.942	15.941	4.920	12.602	-16.422
72	HF	217	173.726	.483	16.122	5.018	14.232	-15.405
72	HF	218	180.413	1.681	16.303	5.118	13.208	-17.041
72	HF	219	188.551	.230	16.488	5.235	14.835	-16.024
72	HF	220	195.447	1.471	16.712	5.395	13.736	-17.732
72	HF	221	203.861	-.047	16.903	5.495	15.437	-16.639
72	HF	222	210.990	1.239	17.096	5.681	14.337	-18.345
72	HF	223	219.628	-.271	17.292	5.805	16.036	-17.250
72	HF	224	226.971	1.024	17.491	5.980	14.935	-18.953
72	HF	225	235.816	-.477	17.693	6.168	16.632	-17.855
72	HF	226	243.358	.826	17.898	6.371	15.530	-19.555
72	HF	227	252.391	-.666	18.107	6.588	17.226	-18.455
72	HF	228	260.113	.646	18.318	6.819	16.122	-20.152
72	HF	229	269.317	-.837	18.532	7.065	17.817	-19.049
72	HF	230	277.201	.484	18.750	7.325	16.711	-20.744
72	HF	231	286.559	-.991	18.971	7.600	18.405	-19.639
72	HF	232	294.588	.339	19.194	7.888	17.299	-21.332
72	HF	233	304.083	-1.128	19.421	8.189	18.993	-20.225
72	HF	234	312.242	.209	19.651	8.503	17.887	-21.917
72	HF	235	321.860	-1.251	19.883	8.830	19.580	-20.809
72	HF	236	330.135	.092	20.119	9.168	18.475	-22.501
72	HF	237	339.865	-1.362	20.357	9.517	20.170	-21.393
72	HF	238	348.245	-.013	20.597	9.876	19.066	-23.086
72	HF	239	358.075	-1.463	20.841	10.245	20.763	-21.979
72	HF	240	366.553	-.110	21.086	10.621	19.661	-23.673
72	HF	241	376.477	-1.557	21.334	11.005	21.361	-22.569

TABLE 2

Atomic mass excesses and nuclear binding energies

72	HF	242	385.047	-.203	21.583	11.395	20.263	-24.266
72	HF	243	395.062	-1.648	21.835	11.791	21.967	-23.164
72	HF	244	403.723	-.293	22.089	12.190	20.873	-24.864
72	HF	245	413.828	-1.738	22.344	12.593	22.582	-23.767
72	HF	246	422.580	-.384	22.600	12.998	21.494	-25.472
72	HF	247	432.779	-1.832	22.857	13.403	23.208	-24.379
72	HF	248	441.626	-.480	23.116	13.809	22.125	-26.088
72	HF	249	451.924	-1.930	23.375	14.213	23.846	-25.001
72	HF	250	460.874	-.583	23.635	14.616	22.769	-26.716
72	HF	251	471.279	-2.037	23.896	15.015	24.496	-25.634
72	HF	252	480.341	-.695	24.156	15.410	23.426	-27.354
72	HF	253	490.863	-2.155	24.417	15.801	25.159	-26.277
72	HF	254	500.048	-.818	24.677	16.186	24.095	-28.003
72	HF	255	510.700	-2.284	24.937	16.564	25.834	-26.931
	ATOM		M - A	NEUTRON	PROTON	ALPHA	Q BETA -	Q BETA +
73	TA	140	128.379	16.518	-7.685	-7.018	-22.074	24.917
73	TA	141	118.376	18.370	-7.330	-6.881	-23.573	22.124
73	TA	142	110.807	15.936	-6.970	-6.791	-20.792	23.627
73	TA	143	101.380	17.795	-6.615	-6.617	-22.297	20.859
73	TA	144	94.360	15.387	-6.254	-6.449	-19.541	22.365
73	TA	145	85.480	17.248	-5.899	-6.291	-21.047	19.005
73	TA	146	78.984	14.864	-4.924	-6.098	-18.315	19.900
73	TA	147	71.238	16.113	-4.569	-5.907	-19.209	17.181
73	TA	148	65.850	13.755	-4.208	-5.685	-15.896	18.682
73	TA	149	58.608	15.610	-3.855	-5.486	-17.396	15.980
73	TA	150	53.707	13.268	-3.495	-5.259	-14.707	17.468
73	TA	151	46.968	15.107	-3.143	-5.062	-16.193	14.780
73	TA	152	42.557	12.778	-2.785	-4.840	-13.518	16.251
73	TA	153	36.327	14.598	-2.435	-4.655	-14.986	13.576
73	TA	154	32.415	12.279	-2.079	-4.446	-12.325	15.027
73	TA	155	26.706	14.076	-1.733	-4.278	-13.773	11.146
73	TA	156	24.601	10.473	-1.455	-5.382	-9.831	12.667
73	TA	157	20.706	12.262	-1.188	-6.514	-11.358	10.126
73	TA	158	19.078	9.996	-.912	-6.436	-8.843	11.656
73	TA	159	15.654	11.791	-.647	-6.371	-10.380	9.160
73	TA	160	14.452	9.569	-.373	-6.248	-7.910	10.695
73	TA	161	11.452	11.368	-.110	-6.143	-9.452	8.241
73	TA	162	10.632	9.187	.164	-5.979	-7.025	9.776
73	TA	163	8.014	10.985	.427	-5.836	-8.567	7.360
73	TA	164	7.538	8.844	.701	-5.635	-6.180	8.889
73	TA	165	5.269	10.637	.965	-5.460	-7.716	6.508
73	TA	166	5.105	8.531	1.240	-5.229	-5.364	8.025
73	TA	167	3.159	10.313	1.505	-5.028	-6.888	5.675
73	TA	168	3.285	8.241	1.783	-4.772	-4.568	7.174
73	TA	169	1.645	10.007	2.051	-4.554	-6.073	4.849
73	TA	170	2.049	7.964	2.332	-4.281	-3.779	6.324
73	TA	171	.708	9.709	2.602	-4.052	-5.260	4.022
73	TA	172	1.384	7.691	2.887	-3.770	-2.989	5.467
73	TA	173	.342	9.410	3.160	-3.537	-4.439	3.184
73	TA	174	1.293	7.416	3.449	-3.252	-2.187	4.595
73	TA	175	.557	9.104	3.726	-3.020	-3.602	2.329
73	TA	176	1.793	7.131	4.020	-2.738	-1.368	3.701
73	TA	177	1.375	8.785	4.301	-2.513	-2.744	1.452
73	TA	178	2.909	6.833	4.599	-2.237	-.526	2.784
73	TA	179	2.826	8.451	4.884	-2.021	-1.860	.551
73	TA	180	4.611	6.582	5.249	-1.691	.217	1.716
73	TA	181	4.941	8.037	5.539	-1.548	-.950	-.375
73	TA	182	7.056	6.253	5.845	-1.226	1.110	.750
73	TA	183	7.752	7.671	6.138	-1.091	-.015	-1.321
73	TA	184	10.211	5.908	6.447	-.840	2.029	-.233

TABLE 2

Atomic mass excesses and nuclear binding energies

73	TA	185	11.285	7.293	6.744	-.648	.942	-2.285
73	TA	186	14.100	5.553	7.055	-.402	2.969	-1.230
73	TA	187	15.559	6.908	7.355	-.210	1.915	-3.259
73	TA	188	18.734	5.192	7.669	.035	3.923	-2.231
73	TA	189	20.580	6.522	7.971	.231	2.898	-4.237
73	TA	190	24.116	4.831	8.285	.480	4.884	-3.231
73	TA	191	26.343	6.141	8.589	.686	3.882	-5.210
73	TA	192	30.233	4.477	8.904	.944	5.844	-4.220
73	TA	193	32.830	5.771	9.208	1.164	4.859	-6.170
73	TA	194	37.062	4.135	9.523	1.436	6.795	-5.192
73	TA	195	40.011	5.418	9.827	1.675	5.822	-7.111
73	TA	196	44.567	3.812	10.140	1.964	7.729	-6.140
73	TA	197	47.848	5.086	10.444	2.224	6.765	-8.027
73	TA	198	52.706	3.510	10.754	2.533	8.642	-7.059
73	TA	199	56.294	4.779	11.055	2.816	7.681	-8.859
73	TA	200	61.519	3.142	11.219	3.054	9.618	-7.754
73	TA	201	65.485	4.402	11.373	3.263	8.502	-9.448
73	TA	202	70.985	2.867	11.533	3.319	10.171	-8.358
73	TA	203	75.242	4.111	11.686	3.342	9.069	-10.038
73	TA	204	81.021	2.589	11.844	3.390	10.726	-8.961
73	TA	205	85.570	3.818	11.997	3.408	9.637	-10.630
73	TA	206	91.630	2.307	12.155	3.450	11.283	-9.565
73	TA	207	96.473	3.525	12.308	3.466	10.207	-11.225
73	TA	208	102.816	2.024	12.466	3.506	11.845	-10.171
73	TA	209	107.951	3.232	12.621	3.525	10.780	-11.822
73	TA	210	114.577	1.741	12.780	3.566	12.411	-10.778
73	TA	211	120.002	2.942	12.938	3.591	11.356	-12.422
73	TA	212	126.909	1.461	13.100	3.637	12.982	-11.386
73	TA	213	132.619	2.658	13.261	3.672	11.934	-13.024
73	TA	214	139.801	1.185	13.426	3.728	13.557	-11.994
73	TA	215	145.789	2.380	13.592	3.778	12.516	-13.628
73	TA	216	153.240	.916	13.761	3.846	14.135	-12.602
73	TA	217	159.495	2.112	13.932	3.915	13.099	-14.232
73	TA	218	167.205	.657	14.106	4.001	14.717	-13.208
73	TA	219	173.716	1.857	14.282	4.092	13.684	-14.835
73	TA	220	181.711	.372	14.424	4.162	15.377	-13.736
73	TA	221	188.425	1.654	14.607	4.316	14.269	-15.437
73	TA	222	196.653	.139	14.793	4.410	15.962	-14.337
73	TA	223	203.592	1.429	14.983	4.592	14.855	-16.036
73	TA	224	212.037	-.078	15.176	4.752	16.547	-14.935
73	TA	225	219.184	1.220	15.372	4.926	15.439	-16.632
73	TA	226	227.828	-.277	15.573	5.116	17.131	-15.530
73	TA	227	235.165	1.030	15.777	5.322	16.023	-17.226
73	TA	228	243.991	-.458	15.985	5.543	17.715	-16.122
73	TA	229	251.500	.858	16.197	5.780	16.606	-17.817
73	TA	230	260.489	-.622	16.412	6.033	18.298	-16.711
73	TA	231	268.154	.703	16.632	6.301	17.190	-18.405
73	TA	232	277.289	-.768	16.855	6.586	18.882	-17.299
73	TA	233	285.090	.565	17.082	6.885	17.774	-18.993
73	TA	234	294.355	-.898	17.313	7.199	19.467	-17.887
73	TA	235	302.280	.443	17.547	7.527	18.361	-19.580
73	TA	236	311.661	-1.013	17.784	7.868	20.055	-18.475
73	TA	237	319.695	.333	18.025	8.223	18.951	-20.170
73	TA	238	329.179	-1.117	18.270	8.589	20.648	-19.066
73	TA	239	337.312	.234	18.517	8.966	19.547	-20.763
73	TA	240	346.892	-1.212	18.768	9.354	21.247	-19.661
73	TA	241	355.116	.143	19.022	9.751	20.149	-21.361
73	TA	242	364.784	-1.301	19.278	10.156	21.854	-20.263
73	TA	243	373.095	.056	19.537	10.568	20.762	-21.967
73	TA	244	382.849	-1.387	19.798	10.986	22.472	-20.873
73	TA	245	391.246	-.029	20.061	11.409	21.385	-22.582
73	TA	246	401.086	-1.473	20.327	11.836	23.101	-21.494

TABLE 2

Atomic mass excesses and nuclear binding energies

73	TA	247	409.571	-.117	20.594	12.265	22.020	-23.208
73	TA	248	419.501	-1.563	20.863	12.695	23.743	-22.125
73	TA	249	428.079	-.210	21.133	13.126	22.669	-23.846
73	TA	250	438.105	-1.659	21.404	13.556	24.399	-22.769
73	TA	251	446.783	-.311	21.676	13.984	23.333	-24.496
73	TA	252	456.916	-1.765	21.948	14.408	25.070	-23.426
73	TA	253	465.705	-.422	22.221	14.830	24.011	-25.159
73	TA	254	475.954	-1.882	22.495	15.246	25.755	-24.095
73	TA	255	484.866	-.545	22.767	15.656	24.703	-25.834
73	TA	256	495.244	-2.011	23.040	16.060	26.454	-24.776
	ATOM		M - A	NEUTRON	PROTON	ALPHA	Q BETA -	Q BETA +
74	W	142	131.599	18.718	-5.638	-7.046	-26.513	20.792
74	W	143	123.677	16.290	-5.285	-6.958	-23.734	22.297
74	W	144	113.901	18.143	-4.936	-6.831	-25.229	19.541
74	W	145	106.527	15.742	-4.582	-6.665	-22.475	21.047
74	W	146	97.298	17.596	-4.234	-6.509	-23.970	18.315
74	W	147	90.447	15.218	-3.879	-6.317	-21.238	19.209
74	W	148	81.746	17.069	-2.923	-6.141	-22.726	15.896
74	W	149	76.004	14.110	-2.569	-5.919	-19.413	17.396
74	W	150	68.414	15.957	-2.222	-5.721	-20.297	14.707
74	W	151	63.160	13.621	-1.868	-5.494	-17.607	16.193
74	W	152	56.075	15.452	-1.523	-5.298	-19.076	13.518
74	W	153	51.313	13.130	-1.171	-5.076	-16.399	14.986
74	W	154	44.740	14.940	-.829	-4.891	-17.849	12.325
74	W	155	40.479	12.628	-.479	-4.682	-15.185	13.773
74	W	156	34.432	14.415	-.141	-4.516	-16.613	9.831
74	W	157	32.065	10.734	.121	-5.705	-12.583	11.358
74	W	158	27.920	12.512	.371	-6.923	-14.098	8.843
74	W	159	26.033	10.254	.629	-6.863	-11.588	10.380
74	W	160	22.362	12.039	.877	-6.819	-13.112	7.910
74	W	161	20.903	9.826	1.133	-6.714	-10.648	9.452
74	W	162	17.657	11.614	1.379	-6.626	-12.177	7.025
74	W	163	16.581	9.443	1.635	-6.478	-9.757	8.567
74	W	164	13.718	11.231	1.881	-6.352	-11.284	6.180
74	W	165	12.985	9.100	2.138	-6.165	-8.904	7.716
74	W	166	10.469	10.883	2.384	-6.004	-10.424	5.364
74	W	167	10.047	8.790	2.643	-5.784	-8.079	6.888
74	W	168	7.853	10.561	2.890	-5.595	-9.586	4.568
74	W	169	7.718	8.502	3.151	-5.349	-7.272	6.073
74	W	170	5.828	10.258	3.402	-5.140	-8.759	3.779
74	W	171	5.967	8.228	3.666	-4.874	-6.472	5.260
74	W	172	4.373	9.962	3.920	-4.652	-7.933	2.989
74	W	173	4.780	7.960	4.189	-4.375	-5.667	4.439
74	W	174	3.480	9.667	4.446	-4.146	-7.096	2.187
74	W	175	4.159	7.689	4.719	-3.864	-4.850	3.602
74	W	176	3.161	9.365	4.981	-3.635	-6.242	1.368
74	W	177	4.119	7.409	5.259	-3.352	-4.012	2.744
74	W	178	3.435	9.051	5.525	-3.127	-5.363	.526
74	W	179	4.686	7.116	5.808	-2.849	-3.149	1.860
74	W	180	4.394	8.659	6.016	-2.693	-4.332	-.217
74	W	181	5.891	6.871	6.304	-2.359	-2.258	.950
74	W	182	5.945	8.313	6.580	-2.211	-3.397	-1.110
74	W	183	7.767	6.546	6.873	-1.882	-1.338	.015
74	W	184	8.182	7.952	7.155	-1.678	-2.437	-2.029
74	W	185	10.343	6.206	7.453	-1.418	-.393	-.942
74	W	186	11.131	7.580	7.739	-1.216	-1.454	-2.969
74	W	187	13.644	5.855	8.041	-.961	.574	-1.915
74	W	188	14.812	7.199	8.332	-.758	-.454	-3.923
74	W	189	17.682	5.497	8.637	-.502	1.555	-2.898
74	W	190	19.232	6.817	8.932	-.294	.556	-4.884

TABLE 2

Atomic mass excesses and nuclear binding energies

74	W	191	22.461	5.139	9.240	-.034	2.544	-3.882
74	W	192	24.390	6.439	9.538	.185	1.567	-5.844
74	W	193	27.971	4.786	9.847	.455	3.533	-4.859
74	W	194	30.267	6.071	10.147	.689	2.573	-6.795
74	W	195	34.189	4.445	10.457	.972	4.514	-5.822
74	W	196	36.838	5.719	10.758	1.225	3.565	-7.729
74	W	197	41.084	4.122	11.068	1.526	5.478	-6.765
74	W	198	44.064	5.387	11.369	1.799	4.537	-8.642
74	W	199	48.613	3.818	11.678	2.119	6.421	-7.681
74	W	200	51.902	5.079	11.977	2.415	5.483	-9.618
74	W	201	56.983	3.286	12.121	2.501	7.589	-8.502
74	W	202	60.814	4.537	12.256	2.560	6.478	-10.171
74	W	203	66.173	3.009	12.397	2.590	8.137	-9.069
74	W	204	70.295	4.245	12.532	2.588	7.037	-10.726
74	W	205	75.933	2.729	12.673	2.610	8.684	-9.637
74	W	206	80.347	3.953	12.808	2.606	7.595	-11.283
74	W	207	86.266	2.448	12.949	2.624	9.231	-10.207
74	W	208	90.971	3.662	13.086	2.620	8.153	-11.845
74	W	209	97.171	2.167	13.229	2.638	9.780	-10.780
74	W	210	102.166	3.373	13.370	2.638	8.712	-12.411
74	W	211	108.647	1.887	13.515	2.660	10.333	-11.356
74	W	212	113.927	3.087	13.660	2.669	9.273	-12.982
74	W	213	120.684	1.610	13.809	2.698	10.888	-11.934
74	W	214	126.245	2.807	13.959	2.720	9.835	-13.557
74	W	215	133.273	1.339	14.113	2.761	11.447	-12.516
74	W	216	139.104	2.536	14.269	2.799	10.400	-14.135
74	W	217	146.395	1.076	14.429	2.857	12.009	-13.099
74	W	218	152.488	2.275	14.592	2.917	10.965	-14.717
74	W	219	160.031	.824	14.759	2.994	12.574	-13.684
74	W	220	166.334	2.065	14.966	3.117	11.457	-15.377
74	W	221	174.155	.546	15.140	3.180	13.140	-14.269
74	W	222	180.691	1.832	15.318	3.331	12.024	-15.962
74	W	223	188.737	.321	15.500	3.422	13.709	-14.855
74	W	224	195.490	1.615	15.687	3.566	12.594	-16.547
74	W	225	203.745	.113	15.877	3.726	14.279	-15.439
74	W	226	210.697	1.415	16.072	3.902	13.164	-17.131
74	W	227	219.142	-.078	16.270	4.095	14.850	-16.023
74	W	228	226.276	1.233	16.474	4.304	13.736	-17.715
74	W	229	234.894	-.250	16.682	4.531	15.422	-16.606
74	W	230	242.191	1.070	16.894	4.775	14.309	-18.298
74	W	231	250.964	-.405	17.110	5.037	15.997	-17.190
74	W	232	258.407	.924	17.331	5.315	14.885	-18.882
74	W	233	267.316	-.542	17.557	5.610	16.574	-17.774
74	W	234	274.888	.795	17.787	5.921	15.464	-19.467
74	W	235	283.919	-.664	18.021	6.249	17.156	-18.361
74	W	236	291.606	.681	18.259	6.591	16.048	-20.055
74	W	237	300.744	-.771	18.502	6.949	17.742	-18.951
74	W	238	308.531	.580	18.748	7.320	16.638	-20.648
74	W	239	317.766	-.867	18.998	7.704	18.336	-19.547
74	W	240	325.645	.488	19.252	8.100	17.237	-21.247
74	W	241	334.967	-.954	19.510	8.507	18.940	-20.149
74	W	242	342.930	.404	19.771	8.924	17.845	-21.854
74	W	243	352.334	-1.036	20.035	9.351	19.553	-20.762
74	W	244	360.378	.323	20.302	9.784	18.465	-22.472
74	W	245	369.861	-1.117	20.573	10.225	20.180	-21.385
74	W	246	377.986	.243	20.845	10.671	19.098	-23.101
74	W	247	387.551	-1.198	21.120	11.121	20.821	-22.020
74	W	248	395.758	.160	21.397	11.574	19.747	-23.743
74	W	249	405.409	-1.284	21.677	12.028	21.477	-22.669
74	W	250	413.706	.071	21.957	12.483	20.411	-24.399
74	W	251	423.451	-1.377	22.239	12.938	22.149	-23.333
74	W	252	431.846	-.028	22.523	13.390	21.092	-25.070

TABLE 2

Atomic mass excesses and nuclear binding energies

74	W	253	441.694	-1.481	22.806	13.840	22.839	-24.011
74	W	254	450.198	-.137	23.091	14.285	21.789	-25.755
74	W	255	460.162	-1.597	23.376	14.726	23.544	-24.703
74	W	256	468.790	-.260	23.661	15.161	22.503	-26.454
74	W	257	478.884	-1.727	23.945	15.589	24.265	-25.409
	ATOM		M - A	NEUTRON	PROTON	ALPHA	Q BETA -	Q BETA +
75	RE	144	139.131	16.648	-7.869	-7.143	-22.405	25.229
75	RE	145	129.002	18.496	-7.516	-7.017	-23.902	22.475
75	RE	146	121.268	16.102	-7.156	-6.851	-21.162	23.970
75	RE	147	111.685	17.950	6.802	-6.696	-22.658	21.238
75	RE	148	104.473	15.580	-6.440	-6.503	-19.940	22.726
75	RE	149	95.417	17.423	-6.086	-6.327	-21.430	19.413
75	RE	150	88.711	15.073	-5.123	-6.118	-18.732	20.297
75	RE	151	80.767	16.311	-4.768	-5.920	-19.616	17.607
75	RE	152	75.151	13.983	-4.406	-5.692	-16.346	19.076
75	RE	153	67.713	15.806	-4.052	-5.496	-17.814	16.399
75	RE	154	62.589	13.491	-3.691	-5.272	-15.153	17.849
75	RE	155	55.664	15.292	-3.339	-5.087	-16.601	15.185
75	RE	156	51.044	12.988	-2.980	-4.878	-13.952	16.613
75	RE	157	44.648	14.764	-2.631	-4.712	-15.377	12.593
75	RE	158	42.018	10.997	-2.368	-5.994	-11.270	14.098
75	RE	159	37.621	12.764	-2.116	-7.306	-12.790	11.588
75	RE	160	35.473	10.515	-1.855	-7.264	-10.305	13.112
75	RE	161	31.552	12.289	-1.605	-7.236	-11.835	10.648
75	RE	162	29.834	10.086	-1.345	-7.147	-9.398	12.177
75	RE	163	26.338	11.863	-1.096	-7.075	-10.932	9.757
75	RE	164	25.002	9.703	-.836	-6.941	-8.540	11.284
75	RE	165	21.888	11.481	-.586	-6.828	-10.074	8.904
75	RE	166	20.893	9.362	-.324	-6.652	-7.723	10.424
75	RE	167	18.126	11.135	-.072	-6.503	-9.250	8.079
75	RE	168	17.439	9.054	.193	-6.292	-6.935	9.586
75	RE	169	14.991	10.816	.447	-6.113	-8.449	7.272
75	RE	170	14.588	8.770	.716	-5.874	-6.166	8.759
75	RE	171	12.439	10.516	.974	-5.671	-7.659	6.472
75	RE	172	12.305	8.501	1.247	-5.411	-5.403	7.933
75	RE	173	10.448	10.225	1.510	-5.193	-6.870	5.667
75	RE	174	10.577	8.238	1.788	-4.918	-4.637	7.096
75	RE	175	9.009	9.935	2.056	-4.692	-6.072	4.850
75	RE	176	9.403	7.973	2.341	-4.410	-3.858	6.242
75	RE	177	8.131	9.639	2.614	-4.180	-5.256	4.012
75	RE	178	8.799	7.700	2.905	-3.896	-3.059	5.363
75	RE	179	7.835	9.331	3.185	-3.669	-4.415	3.149
75	RE	180	8.726	7.476	3.545	-3.324	-2.358	4.332
75	RE	181	8.149	8.945	3.830	-3.164	-3.545	2.258
75	RE	182	9.342	7.174	4.133	-2.824	-1.503	3.397
75	RE	183	9.105	8.605	4.425	-2.670	-2.645	1.338
75	RE	184	10.618	6.854	4.733	-2.398	-.616	2.437
75	RE	185	10.736	8.250	5.030	-2.186	-1.716	.393
75	RE	186	12.585	6.519	5.343	-1.920	.300	1.454
75	RE	187	13.070	7.882	5.646	-1.709	-.761	-.574
75	RE	188	15.266	6.172	5.963	-1.446	1.241	.454
75	RE	189	16.127	7.506	6.269	-1.232	.214	-1.555
75	RE	190	18.677	5.817	6.590	-.968	2.201	-.556
75	RE	191	19.917	7.128	6.901	-.749	1.203	-2.544
75	RE	192	22.822	5.462	7.223	-.479	3.172	-1.567
75	RE	193	24.438	6.752	7.537	-.249	2.197	-3.533
75	RE	194	27.694	5.111	7.861	.031	4.146	-2.573
75	RE	195	29.675	6.386	8.177	.276	3.190	-4.514
75	RE	196	33.272	4.771	8.502	.570	5.115	-3.565
75	RE	197	35.605	6.034	8.817	.834	4.172	-5.478

TABLE 2

Atomic mass excesses and nuclear binding energies

75	RE	198	39.527	4.446	9.142	1.144	6.072	-4.537
75	RE	199	42.192	5.702	9.457	1.429	5.137	-6.421
75	RE	200	46.419	4.140	9.779	1.757	7.011	-5.483
75	RE	201	49.394	5.392	10.092	2.063	6.079	-7.589
75	RE	202	54.336	3.425	10.232	1.979	8.357	-6.478
75	RE	203	58.036	4.668	10.363	1.868	7.237	-8.137
75	RE	204	63.257	3.146	10.500	1.871	8.874	-7.037
75	RE	205	67.249	4.376	10.630	1.845	7.765	-8.684
75	RE	206	72.751	2.865	10.766	1.843	9.390	-7.595
75	RE	207	77.035	4.084	10.897	1.817	8.292	-9.231
75	RE	208	82.818	2.584	11.033	1.812	9.908	-8.153
75	RE	209	87.391	3.794	11.165	1.788	8.820	-9.780
75	RE	210	93.454	2.304	11.302	1.785	10.429	-8.712
75	RE	211	98.314	3.507	11.437	1.768	9.351	-10.333
75	RE	212	104.654	2.027	11.577	1.771	10.954	-9.273
75	RE	213	109.796	3.226	11.716	1.764	9.884	-10.888
75	RE	214	116.409	1.754	11.860	1.777	11.483	-9.835
75	RE	215	121.826	2.951	12.004	1.786	10.420	-11.447
75	RE	216	128.705	1.488	12.153	1.813	12.018	-10.400
75	RE	217	134.386	2.686	12.303	1.842	10.961	-12.009
75	RE	218	141.523	1.231	12.458	1.888	12.558	-10.965
75	RE	219	147.458	2.432	12.615	1.940	11.504	-12.574
75	RE	220	154.877	.948	12.739	1.972	13.177	-11.457
75	RE	221	161.015	2.230	12.904	2.089	12.051	-13.140
75	RE	222	168.667	.716	13.074	2.148	13.726	-12.024
75	RE	223	175.028	2.005	13.247	2.296	12.601	-13.709
75	RE	224	182.896	.500	13.426	2.424	14.277	-12.594
75	RE	225	189.466	1.798	13.609	2.568	13.154	-14.279
75	RE	226	197.533	.300	13.796	2.729	14.831	-13.164
75	RE	227	204.293	1.608	13.989	2.908	13.710	-14.850
75	RE	228	212.541	.119	14.187	3.105	15.389	-13.736
75	RE	229	219.472	1.436	14.389	3.321	14.268	-15.422
75	RE	230	227.882	-.043	14.597	3.555	15.949	-14.309
75	RE	231	234.967	1.283	14.809	3.807	14.831	-15.997
75	RE	232	243.522	-.187	15.027	4.078	16.514	-14.885
75	RE	233	250.742	1.147	15.249	4.367	15.398	-16.574
75	RE	234	259.424	-.315	15.477	4.674	17.083	-15.464
75	RE	235	266.764	1.028	15.709	4.999	15.970	-17.156
75	RE	236	275.557	-.426	15.947	5.340	17.659	-16.048
75	RE	237	283.001	.923	16.189	5.698	16.550	-17.742
75	RE	238	291.893	-.524	16.436	6.072	18.243	-16.638
75	RE	239	299.429	.831	16.687	6.460	17.138	-18.336
75	RE	240	308.408	-.611	16.943	6.862	18.836	-17.237
75	RE	241	316.027	.748	17.202	7.277	17.737	-18.940
75	RE	242	325.085	-.690	17.466	7.704	19.441	-17.845
75	RE	243	332.780	.672	17.734	8.141	18.349	-19.553
75	RE	244	341.913	-.765	18.006	8.588	20.059	-18.465
75	RE	245	349.682	.598	18.281	9.044	18.974	-20.180
75	RE	246	358.887	-.838	18.559	9.506	20.693	-19.098
75	RE	247	366.730	.524	18.840	9.974	19.616	-20.821
75	RE	248	376.012	-.914	19.124	10.447	21.343	-19.747
75	RE	249	383.933	.446	19.410	10.923	20.274	-21.477
75	RE	250	393.295	-.995	19.699	11.401	22.010	-20.411
75	RE	251	401.301	.361	19.990	11.879	20.951	-22.149
75	RE	252	410.754	-1.085	20.282	12.357	22.697	-21.092
75	RE	253	418.855	.266	20.575	12.833	21.647	-22.839
75	RE	254	428.409	-1.186	20.870	13.305	23.402	-21.789
75	RE	255	436.618	.158	21.165	13.774	22.361	-23.544
75	RE	256	446.287	-1.301	21.460	14.238	24.125	-22.503
75	RE	257	454.619	.036	21.756	14.695	23.093	-24.265
75	RE	258	464.417	-1.431	22.051	15.145	24.865	-23.231

ATOM	M - A	NEUTRON	PROTON	ALPHA	Q BETA -	Q BETA +

TABLE 2

Atomic mass excesses and nuclear binding energies

76	OS	147	134.343	16.454	5.490	-7.057	24.078	22.658
76	OS	148	124.413	18.297	-5.143	-6.902	25.562	19.940
76	OS	149	116.846	15.934	-4.789	-6.710	-22.846	21.430
76	OS	150	107.443	17.771	4.442	-6.536	-24.322	19.732
76	OS	151	100.383	15.428	4.087	-6.326	21.624	19.616
76	OS	152	91.498	17.253	-3.146	-6.142	23.087	16.346
76	OS	153	85.527	14.338	-2.791	-5.914	-19.817	17.814
76	OS	154	77.742	16.152	-2.445	-5.718	-20.680	15.153
76	OS	155	72.265	13.845	-2.091	-5.495	-18.018	16.601
76	OS	156	64.996	15.636	-1.747	-5.312	19.447	13.952
76	OS	157	60.025	13.339	-1.396	-5.102	-16.797	15.377
76	OS	158	53.288	15.104	-1.055	-4.938	18.201	11.270
76	OS	159	50.411	11.244	-.808	-6.323	-13.990	12.790
76	OS	160	45.779	13.000	-.573	-7.738	-15.495	10.305
76	OS	161	43.387	10.760	-.328	-7.713	-13.016	11.835
76	OS	162	39.232	12.522	-.095	-7.702	-14.530	9.398
76	OS	163	37.270	10.329	.148	-7.628	-12.099	10.932
76	OS	164	33.542	12.096	.380	-7.571	-13.617	8.540
76	OS	165	31.963	9.947	.624	-7.450	-11.231	10.074
76	OS	166	28.616	11.714	.857	-7.350	-12.749	7.723
76	OS	167	27.376	9.608	1.102	-7.186	-10.404	9.250
76	OS	168	24.374	11.369	1.337	-7.047	-11.914	6.935
76	OS	169	23.439	9.302	1.584	-6.846	-9.605	8.449
76	OS	170	20.753	11.053	1.822	-6.675	-11.101	6.166
76	OS	171	20.099	9.022	2.074	-6.442	-8.824	7.659
76	OS	172	17.709	10.757	2.315	-6.247	-10.298	5.403
76	OS	173	17.318	8.758	2.572	-5.990	-8.049	6.870
76	OS	174	15.214	10.471	2.818	-5.777	-9.495	4.637
76	OS	175	15.081	8.501	3.081	-5.504	-7.268	6.072
76	OS	176	13.261	10.187	3.332	-5.279	-8.681	3.858
76	OS	177	13.387	8.242	3.601	-4.997	-6.473	5.256
76	OS	178	11.857	9.897	3.858	-4.768	-7.847	3.059
76	OS	179	12.250	7.975	4.134	-4.481	-5.655	4.415
76	OS	180	11.085	9.532	4.335	-4.315	-6.861	2.358
76	OS	181	11.694	7.758	4.617	-3.965	-4.809	3.545
76	OS	182	10.845	9.216	4.888	-3.801	-5.971	1.503
76	OS	183	11.750	7.463	5.177	-3.455	-3.932	2.645
76	OS	184	11.235	8.883	5.455	-3.231	-5.050	.616
76	OS	185	12.452	7.150	5.751	-2.952	-3.023	1.716
76	OS	186	12.285	8.535	6.036	-2.730	-4.100	-.300
76	OS	187	13.831	6.821	6.338	-2.455	-2.085	.761
76	OS	188	14.025	8.174	6.630	-2.234	-3.123	-1.241
76	OS	189	15.913	6.479	6.937	-1.961	-1.121	-.214
76	OS	190	16.476	7.804	7.236	-1.736	-2.126	-2.201
76	OS	191	18.714	6.130	7.548	-1.461	-.139	-1.203
76	OS	192	19.650	7.431	7.851	-1.230	-1.114	-3.172
76	OS	193	22.240	5.778	8.167	-.949	.856	-2.197
76	OS	194	23.548	7.060	8.474	-.706	-.096	-4.146
76	OS	195	26.486	5.430	8.793	-.416	1.855	-3.190
76	OS	196	28.157	6.696	9.103	-.158	.920	-5.115
76	OS	197	31.434	5.091	9.424	.146	2.849	-4.172
76	OS	198	33.454	6.347	9.736	.422	1.926	-6.072
76	OS	199	37.055	4.766	10.056	.743	3.831	-5.137
76	OS	200	39.408	6.015	10.369	1.039	2.916	-7.011
76	OS	201	43.316	4.460	10.688	1.377	4.795	-6.079
76	OS	202	45.980	5.703	10.999	1.693	3.882	-8.357
76	OS	203	50.799	3.548	11.122	1.423	6.361	-7.237
76	OS	204	54.383	4.783	11.237	1.128	5.246	-8.874
76	OS	205	59.484	3.267	11.358	1.109	6.875	-7.765
76	OS	206	63.361	4.491	11.473	1.063	5.769	-9.390
76	OS	207	68.742	2.986	11.594	1.040	7.386	-8.292

TABLE 2

Atomic mass excesses and nuclear binding energies

76	OS	208	72.909	4.200	11.710	.995	6.289	-9.908
76	OS	209	78.571	2.706	11.832	.971	7.896	-8.820
76	OS	210	83.025	3.913	11.951	.931	6.807	-10.429
76	OS	211	88.963	2.429	12.075	.912	8.406	-9.351
76	OS	212	93.700	3.630	12.198	.880	7.325	-10.954
76	OS	213	99.912	2.156	12.327	.868	8.919	-9.884
76	OS	214	104.926	3.354	12.455	.850	7.844	-11.483
76	OS	215	111.405	1.888	12.589	.851	9.434	-10.420
76	OS	216	116.687	3.086	12.724	.850	8.365	-12.018
76	OS	217	123.426	1.628	12.864	.868	9.953	-10.961
76	OS	218	128.965	2.828	13.006	.889	8.888	-12.558
76	OS	219	135.954	1.379	13.154	.928	10.476	-11.504
76	OS	220	141.700	2.621	13.343	1.014	9.339	-13.177
76	OS	221	148.964	1.104	13.498	1.041	11.002	-12.051
76	OS	222	154.941	2.390	13.659	1.156	9.867	-13.726
76	OS	223	162.427	.881	13.824	1.213	11.533	-12.601
76	OS	224	168.619	2.176	13.994	1.324	10.400	-14.277
76	OS	225	176.312	.674	14.169	1.452	12.067	-13.154
76	OS	226	182.702	1.978	14.349	1.599	10.936	-14.831
76	OS	227	190.583	.486	14.535	1.763	12.606	-13.710
76	OS	228	197.152	1.798	14.726	1.947	11.476	-15.389
76	OS	229	205.203	.316	14.922	2.150	13.148	-14.268
76	OS	230	211.933	1.638	15.124	2.373	12.021	-15.949
76	OS	231	220.136	.164	15.331	2.615	13.696	-14.831
76	OS	232	227.008	1.495	15.544	2.877	12.572	-16.514
76	OS	233	235.344	.031	15.762	3.159	14.250	-15.398
76	OS	234	242.341	1.371	15.986	3.460	13.129	-17.083
76	OS	235	250.793	-.085	16.216	3.780	14.810	-15.970
76	OS	236	257.898	1.263	16.450	4.118	13.693	-17.659
76	OS	237	266.451	-.186	16.691	4.474	15.379	-16.550
76	OS	238	273.650	1.169	16.936	4.848	14.267	-18.243
76	OS	239	282.291	-.274	17.187	5.238	15.958	-17.138
76	OS	240	289.572	1.087	17.442	5.643	14.851	-18.836
76	OS	241	298.290	-.351	17.703	6.063	16.548	-17.737
76	OS	242	305.644	1.013	17.968	6.497	15.449	-19.441
76	OS	243	314.432	-.421	18.238	6.943	17.153	-18.349
76	OS	244	321.853	.946	18.512	7.401	16.061	-20.059
76	OS	245	330.708	-.487	18.790	7.868	17.773	-18.974
76	OS	246	338.195	.880	19.072	8.344	16.690	-20.693
76	OS	247	347.115	-.553	19.357	8.828	18.411	-19.616
76	OS	248	354.669	.813	19.646	9.318	17.337	-21.343
76	OS	249	363.658	-.622	19.938	9.812	19.067	-20.274
76	OS	250	371.285	.741	20.233	10.310	18.003	-22.010
76	OS	251	380.350	-.698	20.530	10.810	19.744	-20.951
76	OS	252	388.057	.660	20.829	11.310	18.690	-22.697
76	OS	253	397.209	-.784	21.130	11.810	20.441	-21.647
76	OS	254	405.007	.569	21.433	12.308	19.398	-23.402
76	OS	255	414.257	-.883	21.736	12.802	21.160	-22.361
76	OS	256	422.162	.463	22.041	13.293	20.126	-24.125
76	OS	257	431.526	-.996	22.346	13.777	21.898	-23.093
76	OS	258	439.552	.341	22.651	14.255	20.875	-24.865
76	OS	259	449.046	-1.126	22.957	14.726	22.656	-23.842
	ATOM		M - A	NEUTRON	PROTON	ALPHA	Q BETA -	Q BETA +
77	IR	149	139.692	18.650	-7.695	-7.081	-24.261	22.846
77	IR	150	131.765	16.295	-7.334	-6.888	-21.561	24.322
77	IR	151	122.007	18.125	-6.979	-6.713	-23.038	21.624
77	IR	152	114.584	15.790	-6.617	-6.503	-20.357	23.087
77	IR	153	105.344	17.608	-6.262	-6.318	-21.820	19.817
77	IR	154	98.422	15.289	-5.311	-6.102	-19.155	20.680
77	IR	155	90.283	16.507	-4.956	-5.907	-20.018	18.018

TABLE 2

Atomic mass excesses and nuclear binding energies

77	IR	156	84.443	14.207	-4.594	-5.683	-16.792	19.447
77	IR	157	76.821	15.989	-4.240	-5.500	-18.219	16.797
77	IR	158	71.489	13.700	-3.879	-5.290	-15.586	18.201
77	IR	159	64.401	15.455	-3.529	-5.128	-16.988	13.990
77	IR	160	61.274	11.494	-3.278	-6.621	-12.687	15.495
77	IR	161	56.402	13.239	-3.039	-8.146	-14.196	13.016
77	IR	162	53.762	11.008	-2.790	-8.135	-11.742	14.530
77	IR	163	49.369	12.760	-2.553	-8.139	-13.261	12.099
77	IR	164	47.160	10.577	-2.305	-8.077	-10.856	13.617
77	IR	165	43.194	12.333	-2.067	-8.033	-12.380	11.231
77	IR	166	41.365	10.196	-1.818	-7.922	-10.021	12.749
77	IR	167	37.780	11.952	-1.579	-7.833	-11.545	10.404
77	IR	168	36.288	9.859	-1.327	-7.677	-9.229	11.914
77	IR	169	33.045	11.611	-1.085	-7.547	-10.745	9.605
77	IR	170	31.854	9.558	-.830	-7.351	-8.467	11.101
77	IR	171	28.923	11.299	-.584	-7.187	-9.968	8.824
77	IR	172	28.007	9.283	-.324	-6.959	-7.723	10.298
77	IR	173	25.367	11.008	-.073	-6.767	-9.204	8.049
77	IR	174	24.709	9.025	.193	-6.513	-6.987	9.495
77	IR	175	22.349	10.728	.450	-6.301	-8.440	7.268
77	IR	176	21.942	8.774	.723	-6.028	-6.246	8.681
77	IR	177	19.860	10.450	.986	-5.803	-7.665	6.473
77	IR	178	19.704	8.523	1.267	-5.519	-5.491	7.847
77	IR	179	17.905	10.167	1.537	-5.287	-6.870	5.655
77	IR	180	17.946	8.327	1.889	-4.934	-4.838	6.861
77	IR	181	16.503	9.810	2.166	-4.763	-6.049	4.809
77	IR	182	16.816	8.054	2.462	-4.408	-4.031	5.971
77	IR	183	15.682	9.501	2.748	-4.238	-5.197	3.932
77	IR	184	16.284	7.766	3.051	-3.949	-3.190	5.050
77	IR	185	15.476	9.176	3.343	-3.718	-4.312	3.023
77	IR	186	16.384	7.459	3.653	-3.433	-2.315	4.100
77	IR	187	15.917	8.835	3.953	-3.202	-3.394	2.085
77	IR	188	17.148	7.136	4.269	-2.920	-1.406	3.123
77	IR	189	17.034	8.481	4.575	-2.689	-2.446	1.121
77	IR	190	18.602	6.800	4.896	-2.408	-.470	2.126
77	IR	191	18.852	8.117	5.208	-2.173	-1.475	.139
77	IR	192	20.765	6.455	5.534	-1.890	.490	1.114
77	IR	193	21.384	7.748	5.851	-1.648	-.486	-.856
77	IR	194	23.644	6.107	6.181	-1.358	1.465	.096
77	IR	195	24.631	7.380	6.502	-1.105	.513	-1.855
77	IR	196	27.237	5.761	6.833	-.806	2.447	-.920
77	IR	197	28.585	7.020	7.157	-.538	1.514	-2.849
77	IR	198	31.528	5.424	7.490	-.225	3.428	-1.926
77	IR	199	33.224	6.671	7.815	.060	2.508	-3.831
77	IR	200	36.493	5.099	8.147	.389	4.401	-2.916
77	IR	201	38.521	6.339	8.472	.694	3.489	-4.795
77	IR	202	42.097	4.791	8.803	1.039	5.359	-3.882
77	IR	203	44.438	6.026	9.126	1.363	4.451	-6.361
77	IR	204	49.138	3.668	9.246	.891	7.130	-5.246
77	IR	205	52.609	4.896	9.359	.395	6.008	-6.875
77	IR	206	57.592	3.385	9.477	.354	7.620	-5.769
77	IR	207	61.356	4.603	9.589	.289	6.506	-7.386
77	IR	208	66.620	3.103	9.707	.246	8.106	-6.289
77	IR	209	70.675	4.313	9.819	.184	7.001	-7.896
77	IR	210	76.218	2.824	9.937	.143	8.592	-6.807
77	IR	211	80.557	4.028	10.053	.087	7.495	-8.406
77	IR	212	86.375	2.549	10.173	.052	9.079	-7.325
77	IR	213	90.994	3.749	10.292	.007	7.989	-8.919
77	IR	214	97.082	2.279	10.415	-.018	9.568	-7.844
77	IR	215	101.971	3.478	10.539	-.048	8.485	-9.434
77	IR	216	108.322	2.017	10.668	-.058	10.062	-8.365
77	IR	217	113.473	3.216	10.799	-.067	8.984	-9.953

TABLE 2

Atomic mass excesses and nuclear binding energies

77	IR	218	120.077	1.763	10.934	-.058	10.561	-8.888
77	IR	219	125.478	2.966	11.072	-.043	9.487	-10.476
77	IR	220	132.361	1.484	11.177	-.047	11.140	-9.339
77	IR	221	137.961	2.767	11.323	.034	9.993	-11.002
77	IR	222	145.074	1.255	11.475	.058	11.648	-9.867
77	IR	223	150.894	2.546	11.631	.173	10.504	-11.533
77	IR	224	158.220	1.042	11.792	.267	12.161	-10.400
77	IR	225	164.245	2.342	11.959	.379	11.019	-12.067
77	IR	226	171.766	.847	12.131	.510	12.679	-10.936
77	IR	227	177.977	2.156	12.309	.660	11.539	-12.606
77	IR	228	185.676	.669	12.492	.830	13.201	-11.476
77	IR	229	192.055	1.988	12.682	1.020	12.064	-13.148
77	IR	230	199.912	.511	12.877	1.231	13.729	-12.021
77	IR	231	206.440	1.839	13.078	1.462	12.595	-13.696
77	IR	232	214.436	.371	13.285	1.714	14.263	-12.572
77	IR	233	221.095	1.709	13.498	1.986	13.133	-14.250
77	IR	234	229.212	.250	13.717	2.279	14.805	-13.129
77	IR	235	235.984	1.596	13.942	2.593	13.678	-14.810
77	IR	236	244.205	.146	14.173	2.926	15.355	-13.693
77	IR	237	251.073	1.500	14.410	3.279	14.233	-15.379
77	IR	238	259.383	.057	14.653	3.650	15.915	-14.267
77	IR	239	266.333	1.417	14.901	4.040	14.799	-15.958
77	IR	240	274.720	-.020	15.156	4.446	16.487	-14.851
77	IR	241	281.741	1.346	15.415	4.869	15.378	-16.548
77	IR	242	290.195	-.086	15.680	5.307	17.073	-15.449
77	IR	243	297.279	1.283	15.950	5.760	15.972	-17.153
77	IR	244	305.792	-.146	16.224	6.225	17.675	-16.061
77	IR	245	312.934	1.225	16.504	6.702	16.583	-17.773
77	IR	246	321.505	-.203	16.787	7.189	18.295	-16.690
77	IR	247	328.704	1.168	17.075	7.685	17.213	-18.411
77	IR	248	337.332	-.261	17.367	8.189	18.935	-17.337
77	IR	249	344.591	1.109	17.663	8.700	17.863	-19.067
77	IR	250	353.282	-.323	17.961	9.215	19.596	-18.003
77	IR	251	360.606	1.043	18.263	9.733	18.534	-19.744
77	IR	252	369.367	-.393	18.568	10.254	20.279	-18.690
77	IR	253	376.767	.967	18.875	10.775	19.229	-20.441
77	IR	254	385.610	-.475	19.184	11.295	20.984	-19.398
77	IR	255	393.098	.879	19.494	11.813	19.946	-21.160
77	IR	256	402.036	-.571	19.806	12.327	21.713	-20.126
77	IR	257	409.627	.776	20.119	12.837	20.686	-21.898
77	IR	258	418.677	-.683	20.433	13.341	22.464	-20.875
77	IR	259	426.390	.655	20.747	13.838	21.448	-22.656
77	IR	260	435.570	-.813	21.060	14.326	23.236	-21.641
	ATOM		M - A	NEUTRON	PROTON	ALPHA	Q BETA -	Q BETA +
78	PT	152	134.942	18.471	-5.350	-6.919	-25.915	20.357
78	PT	153	127.165	16.145	-4.995	-6.709	-23.235	21.820
78	PT	154	117.578	17.954	-4.649	-6.525	-24.683	19.155
78	PT	155	110.301	15.644	-4.294	-6.309	-22.018	20.018
78	PT	156	101.235	17.434	-3.367	-6.128	-23.445	16.792
78	PT	157	95.041	14.561	-3.013	-5.905	-20.218	18.219
78	PT	158	87.075	16.333	-2.669	-5.724	-21.052	15.586
78	PT	159	81.390	14.052	-2.316	-5.516	-18.418	16.988
78	PT	160	73.961	15.796	-1.975	-5.356	-19.799	12.687
78	PT	161	70.599	11.730	-1.740	-6.965	-15.382	14.196
78	PT	162	65.503	13.463	-1.516	-8.606	-16.874	11.742
78	PT	163	62.630	11.241	-1.283	-8.609	-14.423	13.261
78	PT	164	58.015	12.982	-1.062	-8.627	-15.925	10.856
78	PT	165	55.574	10.809	-.829	-8.578	-13.524	12.380
78	PT	166	51.386	12.554	-.608	-8.546	-15.030	10.021
78	PT	167	49.324	10.429	-.375	-8.445	-12.677	11.545

TABLE 2

Atomic mass excesses and nuclear binding energies

78	PT	168	45.517	12.175	-.152	-8.365	-14.182	9.229
78	PT	169	43.789	10.095	.083	-8.217	-11.871	10.745
78	PT	170	40.321	11.836	.309	-8.095	-13.368	8.467
78	PT	171	38.891	9.797	.548	-7.906	-11.096	9.968
78	PT	172	35.730	11.528	.777	-7.747	-12.578	7.723
78	PT	173	34.571	9.527	1.021	-7.522	-10.339	9.204
78	PT	174	31.696	11.242	1.255	-7.334	-11.799	6.987
78	PT	175	30.789	9.275	1.505	-7.081	-9.588	8.440
78	PT	176	28.189	10.968	1.745	-6.871	-11.019	6.246
78	PT	177	27.525	9.031	2.003	-6.597	-8.831	7.665
78	PT	178	25.195	10.697	2.249	-6.372	-10.227	5.491
78	PT	179	24.775	8.788	2.514	-6.085	-8.059	6.870
78	PT	180	22.784	10.358	2.706	-5.914	-9.290	4.838
78	PT	181	22.552	8.599	2.978	-5.556	-7.263	6.049
78	PT	182	20.847	10.072	3.240	-5.381	-8.450	4.031
78	PT	183	20.879	8.335	3.521	-5.021	-6.437	5.197
78	PT	184	19.475	9.772	3.793	-4.781	-7.580	3.190
78	PT	185	19.787	8.055	4.082	-4.484	-5.578	4.312
78	PT	186	18.699	9.456	4.362	-4.244	-6.677	2.315
78	PT	187	19.310	7.756	4.659	-3.951	-4.684	3.394
78	PT	188	18.554	9.123	4.947	-3.710	-5.741	1.406
78	PT	189	19.481	7.441	5.252	-3.419	-3.757	2.446
78	PT	190	19.071	8.777	5.548	-3.177	-4.776	.470
78	PT	191	20.327	7.111	5.859	-2.887	-2.802	1.475
78	PT	192	20.275	8.420	6.163	-2.641	-3.787	-.490
78	PT	193	21.870	6.772	6.480	-2.347	-1.823	.486
78	PT	194	22.179	8.058	6.789	-2.094	-2.780	-1.465
78	PT	195	24.118	6.429	7.111	-1.795	-.829	-.513
78	PT	196	24.790	7.695	7.426	-1.531	-1.762	-2.447
78	PT	197	27.071	6.087	7.751	-1.221	.172	-1.514
78	PT	198	28.100	7.338	8.069	-.943	-.742	-3.428
78	PT	199	30.716	5.751	8.397	-.621	1.173	-2.508
78	PT	200	32.092	6.992	8.718	-.326	.271	-4.401
78	PT	201	35.031	5.428	9.046	.011	2.167	-3.489
78	PT	202	36.738	6.660	9.367	.325	1.272	-5.359
78	PT	203	39.987	5.119	9.695	.677	3.145	-4.451
78	PT	204	42.008	6.347	10.015	1.009	2.254	-7.130
78	PT	205	46.601	3.775	10.122	.324	5.156	-6.008
78	PT	206	49.972	4.996	10.222	-.383	4.040	-7.620
78	PT	207	54.850	3.490	10.326	-.441	5.646	-6.506
78	PT	208	58.514	4.703	10.426	-.522	4.537	-8.106
78	PT	209	63.674	3.208	10.532	-.580	6.130	-7.001
78	PT	210	67.626	4.415	10.633	-.656	5.027	-8.592
78	PT	211	73.062	2.931	10.740	-.711	6.611	-7.495
78	PT	212	77.297	4.133	10.845	-.778	5.513	-9.079
78	PT	213	83.005	2.659	10.955	-.825	7.090	-7.989
78	PT	214	87.513	3.859	11.065	-.879	5.998	-9.568
78	PT	215	93.486	2.394	11.180	-.913	7.569	-8.485
78	PT	216	98.259	3.594	11.296	-.950	6.482	-10.062
78	PT	217	104.489	2.138	11.418	-.967	8.051	-8.984
78	PT	218	109.516	3.340	11.542	-.981	6.967	-10.561
78	PT	219	115.991	1.892	11.670	-.977	8.535	-9.487
78	PT	220	121.222	3.136	11.841	-.926	7.378	-11.140
78	PT	221	127.968	1.621	11.978	-.933	9.023	-9.993
78	PT	222	133.425	2.910	12.121	-.851	7.868	-11.648
78	PT	223	140.390	1.402	12.268	-.828	9.514	-10.504
78	PT	224	146.058	2.699	12.421	-.749	8.362	-12.161
78	PT	225	153.226	1.200	12.579	-.653	10.010	-11.019
78	PT	226	159.087	2.506	12.743	-.537	8.860	-12.679
78	PT	227	166.438	1.016	12.912	-.402	10.511	-11.539
78	PT	228	172.475	2.331	13.088	-.246	9.364	-13.201
78	PT	229	179.991	.851	13.269	-.070	11.018	-12.064

TABLE 2

Atomic mass excesses and nuclear binding energies

78	PT	230	186.183	2.176	13.457	.128	9.873	-13.729
78	PT	231	193.845	.705	13.651	.347	11.531	-12.595
78	PT	232	200.173	2.039	13.852	.588	10.390	-14.263
78	PT	233	207.962	.578	14.059	.851	12.051	-13.133
78	PT	234	214.408	1.922	14.272	1.135	10.914	-14.805
78	PT	235	222.305	.470	14.492	1.440	12.579	-13.678
78	PT	236	228.850	1.822	14.718	1.767	11.447	-15.355
78	PT	237	236.839	.378	14.950	2.114	13.118	-14.233
78	PT	238	243.468	1.738	15.189	2.482	11.991	-15.915
78	PT	239	251.534	.302	15.434	2.869	13.668	-14.795
78	PT	240	258.233	1.668	15.685	3.274	12.548	-16.487
78	PT	241	266.363	.237	15.942	3.698	14.232	-15.378
78	PT	242	273.122	1.609	16.205	4.138	13.120	-17.073
78	PT	243	281.307	.182	16.473	4.594	14.812	-15.972
78	PT	244	288.117	1.557	16.747	5.064	13.708	-17.675
78	PT	245	296.351	.133	17.026	5.548	15.410	-16.583
78	PT	246	303.210	1.509	17.310	6.043	14.316	-18.295
78	PT	247	311.492	.085	17.598	6.549	16.027	-17.213
78	PT	248	318.398	1.461	17.891	7.065	14.944	-18.935
78	PT	249	326.729	.036	18.189	7.588	16.666	-17.863
78	PT	250	333.686	1.410	18.490	8.118	15.594	-19.596
78	PT	251	342.072	-.018	18.795	8.652	17.328	-18.534
78	PT	252	349.089	1.351	19.102	9.190	16.268	-20.279
78	PT	253	357.539	-.083	19.413	9.729	18.015	-19.229
78	PT	254	364.625	1.281	19.727	10.269	16.967	-20.984
78	PT	255	373.152	-.159	20.043	10.808	18.726	-19.946
78	PT	256	380.322	1.197	20.360	11.344	17.692	-21.713
78	PT	257	388.941	-.252	20.679	11.876	19.463	-20.686
78	PT	258	396.213	1.096	20.999	12.403	18.440	-22.464
78	PT	259	404.942	-.362	21.320	12.924	20.224	-21.448
78	PT	260	412.334	.976	21.641	13.437	19.213	-23.236
78	PT	261	421.193	-.492	21.962	13.942	21.007	-22.229
	ATOM		M - A	NEUTRON	PROTON	ALPHA	Q BETA -	Q BETA +
79	AU	153	150.400	18.824	-7.873	-7.098	-24.648	23.235
79	AU	154	142.260	16.507	-7.511	-6.886	-21.987	24.683
79	AU	155	132.319	18.308	-7.157	-6.703	-23.436	22.018
79	AU	156	124.680	16.007	-6.794	-6.486	-20.790	23.445
79	AU	157	115.259	17.788	-6.439	-6.306	-22.217	20.218
79	AU	158	108.126	15.500	-5.501	-6.095	-19.584	21.052
79	AU	159	99.807	16.687	-5.148	-5.915	-20.417	18.418
79	AU	160	93.760	14.414	-4.786	-5.708	-17.233	19.799
79	AU	161	85.981	16.147	-4.435	-5.550	-18.614	15.382
79	AU	162	82.378	11.971	-4.194	-7.280	-14.097	16.874
79	AU	163	77.053	13.692	-3.965	-9.042	-15.592	14.423
79	AU	164	73.940	11.480	-3.726	-9.057	-13.165	15.925
79	AU	165	69.098	13.210	-3.498	-9.086	-14.670	13.524
79	AU	166	66.417	11.048	-3.258	-9.046	-12.296	15.030
79	AU	167	62.001	12.783	-3.030	-9.023	-13.806	12.677
79	AU	168	59.698	10.670	-2.789	-8.930	-11.480	14.182
79	AU	169	55.660	12.405	-2.559	-8.857	-12.990	11.871
79	AU	170	53.689	10.339	-2.315	-8.715	-10.709	13.368
79	AU	171	49.987	12.069	-2.081	-8.598	-12.210	11.096
79	AU	172	48.308	10.046	-1.833	-8.411	-9.969	12.578
79	AU	173	44.909	11.766	-1.594	-8.256	-11.456	10.339
79	AU	174	43.495	9.782	-1.340	-8.032	-9.249	11.799
79	AU	175	40.376	11.486	-1.095	-7.845	-10.715	9.588
79	AU	176	39.207	9.536	-.834	-7.591	-8.537	11.019
79	AU	177	36.356	11.219	-.583	-7.380	-9.974	8.831
79	AU	178	35.423	9.301	-.313	-7.104	-7.821	10.227
79	AU	179	32.834	10.956	-.054	-6.876	-9.223	8.059

TABLE 2

Atomic mass excesses and nuclear binding energies

79	AU	180	32.074	9.128	.286	-6.522	-7.215	9.290
79	AU	181	29.816	10.626	.553	-6.346	-8.451	7.263
79	AU	182	29.297	8.886	.840	-5.984	-6.460	8.450
79	AU	183	27.317	10.348	1.116	-5.803	-7.652	6.437
79	AU	184	27.054	8.630	1.410	-5.499	-5.672	7.580
79	AU	185	25.365	10.057	1.694	-5.253	-6.819	5.578
79	AU	186	25.376	8.357	1.997	-4.950	-4.848	6.677
79	AU	187	23.994	9.749	2.290	-4.702	-5.952	4.684
79	AU	188	24.295	8.066	2.600	-4.402	-3.988	5.741
79	AU	189	23.238	9.425	2.901	-4.153	-5.049	3.757
79	AU	190	23.847	7.758	3.218	-3.854	-3.092	4.776
79	AU	191	23.129	9.086	3.527	-3.603	-4.115	2.802
79	AU	192	24.061	7.435	3.851	-3.305	-2.164	3.787
79	AU	193	23.693	8.736	4.166	-3.049	-3.152	1.823
79	AU	194	24.959	7.101	4.495	-2.748	-1.211	2.780
79	AU	195	24.947	8.379	4.817	-2.486	-2.169	.829
79	AU	196	26.552	6.762	5.150	-2.178	-.238	1.762
79	AU	197	26.899	8.021	5.476	-1.905	-1.172	-.172
79	AU	198	28.842	6.423	5.813	-1.589	.745	.742
79	AU	199	29.543	7.667	6.142	-1.302	-.169	-1.173
79	AU	200	31.820	6.090	6.480	-.974	1.732	-.271
79	AU	201	32.865	7.323	6.812	-.671	.831	-2.167
79	AU	202	35.466	5.766	7.150	-.329	2.713	-1.272
79	AU	203	36.842	6.992	7.481	-.008	1.821	-3.145
79	AU	204	39.754	5.456	7.818	.348	3.684	-2.254
79	AU	205	41.445	6.676	8.148	.685	2.796	-5.156
79	AU	206	45.932	3.881	8.254	-.225	5.918	-4.040
79	AU	207	49.204	5.096	8.353	-1.156	4.799	-5.646
79	AU	208	53.978	3.593	8.457	-1.231	6.391	-4.537
79	AU	209	57.543	4.802	8.556	-1.325	5.277	-6.130
79	AU	210	62.599	3.312	8.659	-1.398	6.857	-5.027
79	AU	211	66.452	4.515	8.759	-1.486	5.748	-6.611
79	AU	212	71.783	3.036	8.864	-1.554	7.320	-5.513
79	AU	213	75.915	4.236	8.967	-1.631	6.216	-7.090
79	AU	214	81.515	2.767	9.074	-1.688	7.781	-5.998
79	AU	215	85.917	3.966	9.181	-1.750	6.683	-7.569
79	AU	216	91.778	2.506	9.293	-1.793	8.244	-6.482
79	AU	217	96.438	3.707	9.406	-1.835	7.149	-8.051
79	AU	218	102.549	2.256	9.524	-1.858	8.708	-6.967
79	AU	219	107.456	3.461	9.645	-1.876	7.617	-8.535
79	AU	220	113.844	1.980	9.732	-1.913	9.252	-7.378
79	AU	221	118.945	3.266	9.861	-1.864	8.087	-9.023
79	AU	222	125.558	1.755	9.995	-1.872	9.724	-7.868
79	AU	223	130.876	3.049	10.134	-1.789	8.561	-9.514
79	AU	224	137.697	1.547	10.278	-1.726	10.199	-8.362
79	AU	225	143.215	2.849	10.428	-1.645	9.039	-10.010
79	AU	226	150.227	1.356	10.583	-1.544	10.679	-8.860
79	AU	227	155.927	2.667	10.745	-1.423	9.521	-10.511
79	AU	228	163.111	1.184	10.912	-1.282	11.165	-9.364
79	AU	229	168.973	2.505	11.086	-1.119	10.009	-11.018
79	AU	230	176.309	1.031	11.266	-.935	11.655	-9.873
79	AU	231	182.315	2.362	11.453	-.728	10.503	-11.531
79	AU	232	189.784	.898	11.646	-.499	12.153	-10.390
79	AU	233	195.912	2.239	11.846	-.247	11.005	-12.051
79	AU	234	203.494	.785	12.053	.027	12.659	-10.914
79	AU	235	209.726	2.135	12.267	.324	11.515	-12.579
79	AU	236	217.403	.690	12.487	.642	13.174	-11.447
79	AU	237	223.721	2.049	12.714	.983	12.035	-13.118
79	AU	238	231.477	.612	12.947	1.345	13.700	-11.991
79	AU	239	237.866	1.979	13.187	1.727	12.568	-13.668
79	AU	240	245.685	.548	13.434	2.129	14.239	-12.548
79	AU	241	252.131	1.921	13.687	2.551	13.114	-14.232

TABLE 2

Atomic mass excesses and nuclear binding energies

79	AU	242	260.001	.497	13.946	2.991	14.793	-13.120
79	AU	243	266.495	1.874	14.212	3.448	13.677	-14.812
79	AU	244	274.409	.453	14.483	3.921	15.365	-13.708
79	AU	245	280.942	1.834	14.760	4.409	14.258	-15.410
79	AU	246	288.894	.415	15.042	4.910	15.956	-14.316
79	AU	247	295.465	1.797	15.330	5.423	14.860	-16.027
79	AU	248	303.454	.378	15.622	5.948	16.569	-14.944
79	AU	249	310.063	1.759	15.920	6.481	15.484	-16.666
79	AU	250	318.092	.338	16.221	7.022	17.205	-15.594
79	AU	251	324.744	1.716	16.527	7.569	16.132	-17.328
79	AU	252	332.820	.291	16.837	8.122	17.866	-16.268
79	AU	253	339.524	1.664	17.150	8.677	16.807	-18.015
79	AU	254	347.658	.233	17.466	9.233	18.554	-16.967
79	AU	255	354.425	1.600	17.784	9.790	17.507	-18.726
79	AU	256	362.631	.162	18.106	10.345	19.268	-17.692
79	AU	257	369.479	1.520	18.429	10.898	18.235	-19.463
79	AU	258	377.773	.073	18.753	11.446	20.009	-18.440
79	AU	259	384.719	1.422	19.079	11.988	18.990	-20.224
79	AU	260	393.121	-.035	19.406	12.524	20.777	-19.213
79	AU	261	400.186	1.303	19.733	13.051	19.770	-21.007
79	AU	262	408.718	-.165	20.060	13.568	21.569	-20.006
	ATOM		M - A	NEUTRON	PROTON	ALPHA	Q BETA -	Q BETA +
80	HG	156	145.470	18.653	-5.565	-6.919	-26.285	20.790
80	HG	157	137.476	16.361	-5.212	-6.702	-23.640	22.217
80	HG	158	127.711	18.133	-4.867	-6.524	-25.050	19.584
80	HG	159	120.225	15.853	-4.513	-6.314	-22.417	20.417
80	HG	160	110.993	17.599	-3.601	-6.150	-23.800	17.233
80	HG	161	104.595	14.766	-3.250	-5.945	-20.616	18.614
80	HG	162	96.475	16.487	-2.909	-5.791	-21.412	14.097
80	HG	163	92.645	12.197	-2.682	-7.646	-16.773	15.592
80	HG	164	87.105	13.907	-2.468	-9.535	-18.248	13.165
80	HG	165	83.768	11.705	-2.243	-9.560	-15.823	14.670
80	HG	166	78.712	13.423	-2.030	-9.600	-17.308	12.296
80	HG	167	75.807	11.273	-1.806	-9.568	-14.937	13.806
80	HG	168	71.179	12.996	-1.593	-9.554	-16.427	11.480
80	HG	169	68.650	10.896	-1.367	-9.467	-14.105	12.990
80	HG	170	64.397	12.620	-1.152	-9.402	-15.593	10.709
80	HG	171	62.197	10.568	-.924	-9.264	-13.317	12.210
80	HG	172	58.277	12.287	-.706	-9.151	-14.798	9.969
80	HG	173	56.366	10.279	-.473	-8.967	-12.561	11.456
80	HG	174	52.745	11.989	-.250	-8.815	-14.027	9.249
80	HG	175	51.092	10.020	-.012	-8.591	-11.825	10.715
80	HG	176	47.745	11.714	.216	-8.405	-13.268	8.537
80	HG	177	46.330	9.782	.462	-8.150	-11.096	9.974
80	HG	178	43.244	11.454	.697	-7.938	-12.510	7.821
80	HG	179	42.057	9.554	.950	-7.659	-10.363	9.223
80	HG	180	39.289	11.136	1.130	-7.491	-11.616	7.215
80	HG	181	38.267	9.390	1.392	-7.133	-9.614	8.451
80	HG	182	35.757	10.877	1.643	-6.952	-10.826	6.460
80	HG	183	34.968	9.156	1.914	-6.584	-8.840	7.652
80	HG	184	32.726	10.609	2.175	-6.333	-10.010	5.672
80	HG	185	32.184	8.909	2.455	-6.023	-8.036	6.819
80	HG	186	30.224	10.328	2.726	-5.767	-9.162	4.848
80	HG	187	29.946	8.646	3.015	-5.457	-7.196	5.952
80	HG	188	28.283	10.030	3.295	-5.199	-8.280	3.988
80	HG	189	28.287	8.363	3.593	-4.891	-6.321	5.049
80	HG	190	26.939	9.715	3.883	-4.631	-7.363	3.092
80	HG	191	27.243	8.064	4.189	-4.324	-5.410	4.115
80	HG	192	26.226	9.385	4.488	-4.062	-6.414	2.164
80	HG	193	26.845	7.748	4.801	-3.755	-4.468	3.152

TABLE 2

Atomic mass excesses and nuclear binding energies

80	HG	194	26.170	9.043	5.108	-3.489	-5.438	1.211
80	HG	195	27.116	7.421	5.428	-3.179	-3.500	2.169
80	HG	196	26.791	8.693	5.741	-2.907	-4.441	.238
80	HG	197	28.070	7.088	6.067	-2.591	-2.513	1.172
80	HG	198	28.097	8.340	6.386	-2.309	-3.430	-.745
80	HG	199	29.712	6.753	6.715	-1.985	-1.514	.169
80	HG	200	30.089	7.990	7.039	-1.689	-2.413	-1.732
80	HG	201	32.034	6.422	7.371	-1.354	-.513	-.831
80	HG	202	32.753	7.649	7.697	-1.044	-1.399	-2.713
80	HG	203	35.021	6.099	8.030	-.696	.485	-1.821
80	HG	204	36.070	7.318	8.357	-.369	-.394	-3.684
80	HG	205	38.649	5.788	8.690	-.008	1.471	-2.796
80	HG	206	40.014	7.002	9.016	.334	.596	-5.918
80	HG	207	44.405	3.976	9.112	-.809	3.956	-4.799
80	HG	208	47.587	5.185	9.201	-1.970	2.844	-6.391
80	HG	209	52.267	3.688	9.296	-2.057	4.433	-5.277
80	HG	210	55.742	4.892	9.386	-2.161	3.324	-6.857
80	HG	211	60.703	3.406	9.480	-2.244	4.901	-5.748
80	HG	212	64.464	4.607	9.573	-2.340	3.795	-7.320
80	HG	213	69.699	3.133	9.670	-2.416	5.362	-6.216
80	HG	214	73.734	4.332	9.765	-2.499	4.259	-7.781
80	HG	215	79.234	2.868	9.866	-2.562	5.819	-6.683
80	HG	216	83.534	4.067	9.967	-2.628	4.718	-8.244
80	HG	217	89.289	2.613	10.074	-2.675	6.274	-7.149
80	HG	218	93.841	3.815	10.182	-2.718	5.175	-8.708
80	HG	219	99.839	2.369	10.295	-2.744	6.728	-7.617
80	HG	220	104.592	3.615	10.449	-2.723	5.556	-9.252
80	HG	221	110.858	2.101	10.570	-2.760	7.184	-8.087
80	HG	222	115.834	3.392	10.696	-2.709	6.013	-9.724
80	HG	223	122.315	1.886	10.827	-2.715	7.642	-8.561
80	HG	224	127.498	3.185	10.963	-2.666	6.472	-10.199
80	HG	225	134.177	1.688	11.105	-2.599	8.103	-9.039
80	HG	226	139.548	2.996	11.253	-2.513	6.935	-10.679
80	HG	227	146.406	1.509	11.406	-2.406	8.568	-9.521
80	HG	228	151.946	2.827	11.566	-2.279	7.403	-11.165
80	HG	229	158.964	1.350	11.732	-2.129	9.038	-10.009
80	HG	230	164.654	2.677	11.904	-1.958	7.875	-11.655
80	HG	231	171.811	1.210	12.083	-1.764	9.514	-10.503
80	HG	232	177.630	2.548	12.269	-1.547	8.354	-12.153
80	HG	233	184.907	1.091	12.462	-1.307	9.997	-11.005
80	HG	234	190.835	2.439	12.661	-1.043	8.841	-12.659
80	HG	235	198.211	.992	12.868	-.757	10.488	-11.515
80	HG	236	204.229	2.349	13.081	-.447	9.337	-13.174
80	HG	237	211.686	.911	13.302	-.115	10.989	-12.035
80	HG	238	217.777	2.277	13.529	.240	9.844	-13.700
80	HG	239	225.298	.846	13.764	.617	11.502	-12.568
80	HG	240	231.445	2.220	14.005	1.014	10.363	-14.239
80	HG	241	239.016	.796	14.253	1.432	12.028	-13.114
80	HG	242	245.208	2.176	14.508	1.869	10.898	-14.793
80	HG	243	252.818	.758	14.769	2.325	12.572	-13.677
80	HG	244	259.043	2.142	15.036	2.799	11.450	-15.365
80	HG	245	266.684	.727	15.309	3.288	13.133	-14.258
80	HG	246	272.938	2.113	15.589	3.793	12.022	-15.956
80	HG	247	280.605	.700	15.874	4.311	13.716	-14.860
80	HG	248	286.885	2.087	16.164	4.841	12.616	-16.569
80	HG	249	294.579	.674	16.460	5.382	14.321	-15.484
80	HG	250	300.887	2.059	16.760	5.932	13.234	-17.205
80	HG	251	308.612	.643	17.065	6.489	14.952	-16.132
80	HG	252	314.954	2.025	17.375	7.053	13.878	-17.866
80	HG	253	322.717	.604	17.688	7.621	15.610	-16.807
80	HG	254	329.104	1.981	18.005	8.191	14.549	-18.554
80	HG	255	336.918	.553	18.325	8.763	16.296	-17.507

TABLE 2

Atomic mass excesses and nuclear binding energies

80	HG	256	343.363	1.922	18.647	9.335	15.250	-19.268
80	HG	257	351.243	.487	18.973	9.905	17.011	-18.235
80	HG	258	357.763	1.847	19.300	10.471	15.979	-20.009
80	HG	259	365.729	.402	19.629	11.032	17.754	-18.990
80	HG	260	372.344	1.752	19.959	11.587	16.736	-20.777
80	HG	261	380.416	.296	20.290	12.135	18.525	-19.770
80	HG	262	387.149	1.634	20.622	12.673	17.521	-21.569
80	HG	263	395.350	.167	20.953	13.202	19.323	-20.574
	ATOM		M - A	NEUTRON	PROTON	ALPHA	Q BETA -	Q BETA +
81	TL	158	152.760	16.723	-7.700	-6.891	-22.435	25.050
81	TL	159	142.642	18.486	-7.347	-6.713	-23.846	22.417
81	TL	160	134.794	16.216	-6.984	-6.505	-21.234	23.800
81	TL	161	125.210	17.951	-6.632	-6.342	-22.618	20.616
81	TL	162	117.887	15.691	-5.708	-6.151	-20.017	21.412
81	TL	163	109.418	16.837	-5.358	-6.001	-20.813	16.773
81	TL	164	105.353	12.432	-5.123	-7.984	-15.513	18.248
81	TL	165	99.591	14.129	-4.901	-10.001	-16.989	15.823
81	TL	166	96.021	11.938	-4.668	-10.034	-14.589	17.308
81	TL	167	90.744	13.644	-4.447	-10.082	-16.075	14.937
81	TL	168	87.605	11.506	-4.213	-10.056	-13.730	16.427
81	TL	169	82.755	13.218	-3.991	-10.048	-15.222	14.105
81	TL	170	79.991	11.131	-3.756	-9.965	-12.928	15.593
81	TL	171	75.514	12.844	-3.532	-9.903	-14.420	13.317
81	TL	172	73.075	10.806	-3.293	-9.767	-12.172	14.798
81	TL	173	68.927	12.515	-3.065	-9.657	-13.657	12.561
81	TL	174	66.771	10.523	-2.821	-9.473	-11.451	14.027
81	TL	175	62.917	12.222	-2.587	-9.321	-12.921	11.825
81	TL	176	61.013	10.271	-2.337	-9.096	-10.752	13.268
81	TL	177	57.426	11.954	-2.097	-8.908	-12.200	11.096
81	TL	178	55.754	10.040	-1.839	-8.650	-10.061	12.510
81	TL	179	52.420	11.701	-1.591	-8.434	-11.481	10.363
81	TL	180	50.905	9.883	-1.263	-8.088	-9.493	11.616
81	TL	181	47.880	11.392	-1.007	-7.915	-10.752	9.614
81	TL	182	46.583	9.665	-.732	-7.551	-8.784	10.826
81	TL	183	43.808	11.142	-.467	-7.365	-10.003	8.840
81	TL	184	42.736	9.439	-.183	-7.053	-8.050	10.010
81	TL	185	40.220	10.884	.091	-6.795	-9.226	8.036
81	TL	186	39.386	9.201	.383	-6.480	-7.283	9.162
81	TL	187	37.142	10.611	.667	-6.216	-8.415	7.196
81	TL	188	36.563	8.946	.967	-5.900	-6.479	8.280
81	TL	189	34.608	10.323	1.260	-5.633	-7.568	6.321
81	TL	190	34.303	8.672	1.569	-5.318	-5.637	7.363
81	TL	191	32.653	10.017	1.871	-5.050	-6.684	5.410
81	TL	192	32.640	8.380	2.188	-4.736	-4.757	6.414
81	TL	193	31.313	9.695	2.498	-4.466	-5.766	4.468
81	TL	194	31.608	8.072	2.822	-4.151	-3.843	5.438
81	TL	195	30.615	9.360	3.139	-3.877	-4.818	3.500
81	TL	196	31.231	7.751	3.469	-3.561	-2.901	4.441
81	TL	197	30.583	9.016	3.793	-3.281	-3.845	2.513
81	TL	198	31.527	7.423	4.128	-2.959	-1.937	3.430
81	TL	199	31.226	8.669	4.456	-2.670	-2.857	1.514
81	TL	200	32.502	7.091	4.795	-2.341	-.958	2.413
81	TL	201	32.547	8.323	5.127	-2.039	-1.859	.513
81	TL	202	34.152	6.762	5.467	-1.700	.027	1.399
81	TL	203	34.536	7.983	5.801	-1.384	-.860	-.485
81	TL	204	36.463	6.440	6.142	-1.034	1.011	.394
81	TL	205	37.178	7.653	6.477	-.704	.133	-1.471
81	TL	206	39.417	6.128	6.816	-.342	1.987	-.596
81	TL	207	40.449	7.336	7.149	.002	1.114	-3.956
81	TL	208	44.743	4.073	7.247	-1.380	4.705	-2.844

TABLE 2

Atomic mass excesses and nuclear binding energies

81	TL	209	47.834	5.277	7.338	-2.779	3.592	-4.433
81	TL	210	52.418	3.783	7.433	-2.877	5.171	-3.324
81	TL	211	55.803	4.983	7.524	-2.990	4.060	-4.901
81	TL	212	60.669	3.501	7.619	-3.082	5.628	-3.795
81	TL	213	64.337	4.699	7.712	-3.184	4.519	-5.362
81	TL	214	69.475	3.229	7.808	-3.267	6.078	-4.259
81	TL	215	73.415	4.427	7.904	-3.354	4.972	-5.819
81	TL	216	78.816	2.967	8.003	-3.423	6.524	-4.718
81	TL	217	83.015	4.168	8.104	-3.491	5.419	-6.274
81	TL	218	88.665	2.717	8.208	-3.541	6.968	-5.175
81	TL	219	93.111	3.922	8.315	-3.585	5.865	-6.728
81	TL	220	99.036	2.442	8.388	-3.649	7.487	-5.556
81	TL	221	103.674	3.729	8.503	-3.627	6.309	-7.184
81	TL	222	109.821	2.220	8.622	-3.663	7.932	-6.013
81	TL	223	114.673	3.515	8.746	-3.608	6.754	-7.642
81	TL	224	121.025	2.015	8.875	-3.572	8.377	-6.472
81	TL	225	126.073	3.319	9.009	-3.519	7.201	-8.103
81	TL	226	132.612	1.828	9.149	-3.445	8.825	-6.935
81	TL	227	137.837	3.142	9.295	-3.352	7.650	-8.568
81	TL	228	144.544	1.661	9.447	-3.238	9.276	-7.403
81	TL	229	149.926	2.985	9.605	-3.101	8.103	-9.038
81	TL	230	156.779	1.514	9.770	-2.943	9.732	-7.875
81	TL	231	162.297	2.849	9.942	-2.761	8.562	-9.514
81	TL	232	169.276	1.389	10.120	-2.556	10.193	-8.354
81	TL	233	174.910	2.733	10.305	-2.328	9.026	-9.997
81	TL	234	181.994	1.283	10.497	-2.075	10.661	-8.841
81	TL	235	187.723	2.638	10.697	-1.800	9.498	-10.488
81	TL	236	194.893	1.198	10.903	-1.500	11.137	-9.337
81	TL	237	200.697	2.563	11.117	-1.177	9.979	-10.989
81	TL	238	207.933	1.131	11.337	-.830	11.624	-9.844
81	TL	239	213.796	2.504	11.565	-.461	10.472	-11.502
81	TL	240	221.082	1.081	11.800	-.070	12.123	-10.363
81	TL	241	226.988	2.462	12.042	.343	10.978	-12.028
81	TL	242	234.310	1.045	12.291	.776	12.636	-10.898
81	TL	243	240.246	2.431	12.547	1.229	11.499	-12.572
81	TL	244	247.594	1.020	12.809	1.700	13.167	-11.450
81	TL	245	253.551	2.410	13.077	2.189	12.040	-13.133
81	TL	246	260.916	1.002	13.352	2.694	13.717	-12.022
81	TL	247	266.889	2.394	13.633	3.214	12.600	-13.716
81	TL	248	274.270	.987	13.920	3.748	14.289	-12.616
81	TL	249	280.258	2.379	14.212	4.293	13.185	-14.321
81	TL	250	287.654	.971	14.510	4.850	14.886	-13.234
81	TL	251	293.659	2.362	14.813	5.415	13.794	-14.952
81	TL	252	301.076	.950	15.120	5.987	15.510	-13.878
81	TL	253	307.107	2.337	15.432	6.565	14.432	-15.610
81	TL	254	314.555	.920	15.747	7.147	16.161	-14.549
81	TL	255	320.622	2.300	16.067	7.731	15.098	-16.296
81	TL	256	328.113	.876	16.389	8.316	16.843	-15.250
81	TL	257	334.233	2.248	16.715	8.900	15.795	-17.011
81	TL	258	341.785	.815	17.043	9.482	17.555	-15.979
81	TL	259	347.975	2.177	17.373	10.060	16.522	-17.754
81	TL	260	355.608	.734	17.705	10.632	18.297	-16.736
81	TL	261	361.891	2.085	18.039	11.197	17.280	-18.525
81	TL	262	369.628	.630	18.373	11.754	19.070	-17.521
81	TL	263	376.027	1.969	18.707	12.301	18.066	-19.323
81	TL	264	383.893	.501	19.041	12.838	19.870	-18.331
	ATOM		M - A	NEUTRON	PROTON	ALPHA	Q BETA -	Q BETA +
82	PB	160	156.028	18.828	-5.801	-6.949	-28.346	21.234
82	PB	161	147.828	16.567	-5.450	-6.743	-25.849	22.618
82	PB	162	137.904	18.291	-5.109	-6.585	-27.332	20.017

TABLE 2

Atomic mass excesses and nuclear binding energies

82	PB	163	130.231	16.041	-4.759	-6.397	-24.854	20.813
82	PB	164	120.866	17.732	-3.864	-6.264	-26.310	15.513
82	PB	165	116.580	12.653	-3.642	-8.377	-21.010	16.989
82	PB	166	110.609	14.338	-3.433	-10.525	-21.715	14.589
82	PB	167	106.819	12.158	-3.214	-10.565	-19.120	16.075
82	PB	168	101.335	13.852	-3.006	-10.620	-20.390	13.730
82	PB	169	97.977	11.726	-2.787	-10.600	-17.855	15.222
82	PB	170	92.918	13.426	-2.579	-10.597	-19.138	12.928
82	PB	171	89.933	11.352	-2.358	-10.517	-16.664	14.420
82	PB	172	85.247	13.054	-2.148	-10.459	-17.957	12.172
82	PB	173	82.584	11.031	-1.924	-10.324	-15.543	13.657
82	PB	174	78.222	12.729	-1.711	-10.216	-16.843	11.451
82	PB	175	75.838	10.752	-1.482	-10.031	-14.487	12.921
82	PB	176	71.765	12.440	-1.264	-9.878	-15.790	10.752
82	PB	177	69.627	10.506	-1.029	-9.651	-13.490	12.200
82	PB	178	65.815	12.178	-.804	-9.462	-14.791	10.061
82	PB	179	63.901	10.282	-.562	-9.200	-12.545	11.481
82	PB	180	60.398	11.870	-.393	-9.044	-13.714	9.493
82	PB	181	58.632	10.133	-.143	-8.693	-11.643	10.752
82	PB	182	55.367	11.632	.098	-8.515	-12.803	8.784
82	PB	183	53.811	9.924	.357	-8.145	-10.779	10.003
82	PB	184	50.786	11.392	.607	-7.888	-11.926	8.050
82	PB	185	49.446	9.708	.875	-7.570	-9.944	9.226
82	PB	186	46.669	11.144	1.136	-7.303	-11.078	7.283
82	PB	187	45.557	9.480	1.414	-6.979	-9.134	8.415
82	PB	188	43.042	10.882	1.685	-6.707	-10.254	6.479
82	PB	189	42.176	9.234	1.972	-6.382	-8.344	7.568
82	PB	190	39.939	10.604	2.253	-6.106	-9.450	5.637
82	PB	191	39.337	8.969	2.550	-5.782	-7.573	6.684
82	PB	192	37.397	10.307	2.841	-5.505	-8.666	4.757
82	PB	193	37.079	8.686	3.146	-5.182	-6.819	5.766
82	PB	194	35.451	9.995	3.446	-4.903	-7.901	3.843
82	PB	195	35.433	8.386	3.760	-4.581	-6.083	4.818
82	PB	196	34.133	9.668	4.068	-4.298	-7.155	2.901
82	PB	197	34.428	8.072	4.388	-3.974	-5.366	3.845
82	PB	198	33.464	9.331	4.703	-3.685	-6.431	1.937
82	PB	199	34.083	7.749	5.029	-3.358	-4.670	2.857
82	PB	200	33.460	8.990	5.350	-3.061	-5.730	.958
82	PB	201	34.406	7.422	5.681	-2.726	-3.996	1.859
82	PB	202	34.125	8.648	6.006	-2.419	-5.054	-.027
82	PB	203	35.396	7.096	6.340	-2.075	-3.346	.860
82	PB	204	35.453	8.311	6.668	-1.755	-4.404	-1.011
82	PB	205	37.045	6.775	7.003	-1.402	-2.721	-.133
82	PB	206	37.430	7.982	7.332	-1.068	-3.778	-1.987
82	PB	207	39.335	6.463	7.667	-.705	-2.118	-1.114
82	PB	208	40.038	7.664	7.996	-.359	-3.177	-4.705
82	PB	209	44.242	4.164	8.086	-1.984	.460	-3.592
82	PB	210	47.247	5.362	8.171	-3.624	-.345	-5.171
82	PB	211	51.742	3.872	8.261	-3.728	1.532	-4.060
82	PB	212	55.041	5.069	8.347	-3.845	.724	-5.628
82	PB	213	59.817	3.591	8.436	-3.942	2.585	-4.519
82	PB	214	63.397	4.788	8.524	-4.046	1.771	-6.078
82	PB	215	68.444	3.321	8.617	-4.131	3.613	-4.972
82	PB	216	72.292	4.519	8.709	-4.219	2.789	-6.524
82	PB	217	77.596	3.063	8.805	-4.288	4.614	-5.419
82	PB	218	81.697	4.266	8.902	-4.354	3.777	-6.968
82	PB	219	87.246	2.819	9.004	-4.403	5.582	-5.865
82	PB	220	91.549	4.065	9.147	-4.406	4.653	-7.487
82	PB	221	97.365	2.551	9.256	-4.467	6.514	-6.309
82	PB	222	101.889	3.843	9.369	-4.439	5.565	-7.932
82	PB	223	107.919	2.338	9.487	-4.470	7.405	-6.754
82	PB	224	112.648	3.638	9.610	-4.447	6.434	-8.377

TABLE 2

Atomic mass excesses and nuclear binding energies

82	PB	225	118.872	2.143	9.738	-4.405	8.252	-7.201
82	PB	226	123.787	3.453	9.871	-4.344	7.257	-8.825
82	PB	227	130.187	1.967	10.010	-4.263	9.050	-7.650
82	PB	228	135.267	3.287	10.155	-4.161	8.030	-9.276
82	PB	229	141.822	1.812	10.306	-4.037	9.797	-8.103
82	PB	230	147.047	3.143	10.464	-3.890	8.751	-9.732
82	PB	231	153.736	1.679	10.628	-3.721	10.491	-8.562
82	PB	232	159.083	3.020	10.799	-3.528	9.417	-10.193
82	PB	233	165.884	1.566	10.977	-3.311	11.129	-9.026
82	PB	234	171.333	2.918	11.161	-3.070	10.027	-10.661
82	PB	235	178.225	1.475	11.353	-2.805	11.711	-9.498
82	PB	236	183.755	2.837	11.553	-2.516	10.581	-11.137
82	PB	237	190.718	1.404	11.759	-2.202	12.237	-9.979
82	PB	238	196.310	2.776	11.973	-1.865	11.080	-11.624
82	PB	239	203.325	1.352	12.193	-1.505	12.709	-10.472
82	PB	240	208.960	2.732	12.421	-1.121	11.526	-12.123
82	PB	241	216.010	1.316	12.657	-.715	13.129	-10.978
82	PB	242	221.674	2.704	12.899	-.288	11.920	-12.636
82	PB	243	228.747	1.294	13.148	.160	13.500	-11.499
82	PB	244	234.427	2.688	13.404	.628	12.268	-13.167
82	PB	245	241.511	1.283	13.667	1.114	13.826	-12.040
82	PB	246	247.199	2.679	13.936	1.618	12.574	-13.717
82	PB	247	254.289	1.277	14.212	2.138	14.112	-12.600
82	PB	248	259.980	2.676	14.494	2.672	12.842	-14.289
82	PB	249	267.073	1.275	14.782	3.220	14.364	-13.185
82	PB	250	272.768	2.673	15.075	3.780	13.079	-14.886
82	PB	251	279.865	1.270	15.374	4.349	14.588	-13.794
82	PB	252	285.567	2.666	15.677	4.928	13.292	-15.510
82	PB	253	292.675	1.259	15.986	5.513	14.791	-14.432
82	PB	254	298.393	2.650	16.299	6.103	13.486	-16.161
82	PB	255	305.524	1.237	16.616	6.697	14.978	-15.098
82	PB	256	311.270	2.621	16.936	7.293	13.668	-16.843
82	PB	257	318.438	1.200	17.260	7.889	15.158	-15.795
82	PB	258	324.230	2.575	17.587	8.483	13.847	-17.555
82	PB	259	331.453	1.145	17.917	9.075	15.336	-16.522
82	PB	260	337.311	2.509	18.249	9.661	14.026	-18.297
82	PB	261	344.611	1.067	18.582	10.241	15.519	-17.280
82	PB	262	350.559	2.420	18.917	10.814	14.214	-19.070
82	PB	263	357.960	.966	19.252	11.378	15.713	-18.066
82	PB	264	364.023	2.305	19.589	11.931	14.416	-19.870
82	PB	265	371.553	.837	19.925	12.472	15.923	-18.880
	ATOM		M - A	NEUTRON	PROTON	ALPHA	Q BETA -	Q BETA +
83	BI	163	155.085	18.519	-9.596	-8.834	-26.035	24.854
83	BI	164	147.177	16.276	-9.361	-8.774	-23.576	26.310
83	BI	165	137.590	17.954	-9.139	-8.771	-25.031	21.010
83	BI	166	132.325	13.633	-8.160	-10.828	-20.501	21.715
83	BI	167	125.939	14.753	-7.745	-12.912	-21.206	19.120
83	BI	168	121.725	12.581	-7.321	-12.762	-18.087	20.390
83	BI	169	115.832	14.261	-6.912	-12.631	-19.356	17.855
83	BI	170	112.056	12.143	-6.495	-12.426	-16.843	19.138
83	BI	171	106.597	13.826	-6.094	-12.244	-18.124	16.664
83	BI	172	103.204	11.761	-5.685	-11.989	-15.672	17.957
83	BI	173	98.126	13.445	-5.295	-11.762	-16.961	15.543
83	BI	174	95.065	11.429	-4.897	-11.465	-14.570	16.843
83	BI	175	90.325	13.107	-4.518	-11.202	-15.865	14.487
83	BI	176	87.555	11.138	-4.132	-10.871	-13.532	15.790
83	BI	177	83.117	12.805	-3.767	-10.581	-14.829	13.490
83	BI	178	80.607	10.878	-3.395	-10.226	-12.552	14.791
83	BI	179	76.446	12.528	-3.045	-9.920	-13.847	12.545
83	BI	180	74.112	10.701	-2.626	-9.489	-11.748	13.714

TABLE 2

Atomic mass excesses and nuclear binding energies

83	BI	181	70.275	12.204	-2.293	-9.240	-12.910	11.643
83	BI	182	68.170	10.473	-1.953	-8.807	-10.861	12.803
83	BI	183	64.590	11.948	-1.637	-8.561	-12.013	10.789
83	BI	184	62.712	10.245	-1.316	-8.198	-10.009	11.926
83	BI	185	59.389	11.690	-1.018	-7.900	-11.148	9.944
83	BI	186	57.747	10.010	-.716	-7.555	-9.184	11.078
83	BI	187	54.691	11.424	-.437	-7.273	-10.310	9.134
83	BI	188	53.296	9.762	-.154	-6.950	-8.382	10.254
83	BI	189	50.520	11.143	.107	-6.690	-9.493	8.344
83	BI	190	49.390	9.498	.371	-6.394	-7.599	9.450
83	BI	191	46.910	10.847	.614	-6.159	-8.696	7.573
83	BI	192	46.063	9.214	.859	-5.891	-6.833	8.666
83	BI	193	43.898	10.533	1.084	-5.681	-7.918	6.819
83	BI	194	43.352	8.913	1.311	-5.440	-6.083	7.901
83	BI	195	41.516	10.203	1.520	-5.254	-7.157	6.083
83	BI	196	41.288	8.596	1.730	-5.039	-5.350	7.155
83	BI	197	39.794	9.861	1.923	-4.873	-6.415	5.366
83	BI	198	39.895	8.266	2.117	-4.678	-4.636	6.431
83	BI	199	38.753	9.510	2.296	-4.528	-5.695	4.670
83	BI	200	39.191	7.929	2.477	-4.350	-3.943	5.730
83	BI	201	38.402	9.156	2.643	-4.210	-4.997	3.996
83	BI	202	39.179	7.590	2.811	-4.043	-3.272	5.054
83	BI	203	38.743	8.804	2.967	-3.908	-4.325	3.346
83	BI	204	39.857	7.254	3.125	-3.745	-2.625	4.404
83	BI	205	39.766	8.458	3.272	-3.610	-3.679	2.721
83	BI	206	41.209	6.924	3.421	-3.448	-2.003	3.778
83	BI	207	41.454	8.123	3.562	-3.308	-3.058	2.118
83	BI	208	43.215	6.606	3.705	-3.143	-1.405	3.177
83	BI	209	43.782	7.801	3.841	-2.995	-2.462	-.460
83	BI	210	47.592	4.557	4.234	-4.566	.914	.345
83	BI	211	50.210	5.750	4.622	-6.152	.110	-1.532
83	BI	212	54.317	4.261	5.010	-5.964	1.982	-.724
83	BI	213	57.233	5.451	5.393	-5.790	1.175	-2.585
83	BI	214	61.627	3.973	5.775	-5.599	3.032	-1.771
83	BI	215	64.830	5.164	6.152	-5.418	2.220	-3.613
83	BI	216	69.502	3.695	6.526	-5.224	4.062	-2.789
83	BI	217	72.982	4.888	6.895	-5.036	3.241	-4.614
83	BI	218	77.921	3.428	7.260	-4.836	5.067	-3.777
83	BI	219	81.664	4.625	7.619	-4.639	4.234	-5.582
83	BI	220	86.896	3.135	7.935	-4.471	6.118	-4.653
83	BI	221	90.850	4.413	8.283	-4.226	5.193	-6.514
83	BI	222	96.324	2.894	8.625	-4.050	7.060	-5.565
83	BI	223	100.513	4.178	8.961	-3.793	6.116	-7.405
83	BI	224	106.213	2.667	9.290	-3.568	7.962	-6.434
83	BI	225	110.620	3.960	9.612	-3.337	6.997	-8.252
83	BI	226	116.530	2.458	9.927	-3.100	8.821	-7.257
83	BI	227	121.137	3.760	10.235	-2.855	7.833	-9.050
83	BI	228	127.237	2.267	10.535	-2.603	9.633	-8.030
83	BI	229	132.025	3.579	10.827	-2.343	8.621	-9.797
83	BI	230	138.296	2.096	11.111	-2.075	10.395	-8.751
83	BI	231	143.245	3.418	11.387	-1.798	9.357	-10.491
83	BI	232	149.667	1.946	11.654	-1.514	11.104	-9.417
83	BI	233	154.756	3.278	11.912	-1.221	10.039	-11.129
83	BI	234	161.307	1.816	12.162	-.919	11.759	-10.027
83	BI	235	166.515	3.159	12.403	-.608	10.666	-11.711
83	BI	236	173.174	1.708	12.636	-.289	12.358	-10.581
83	BI	237	178.481	3.061	12.859	.038	11.237	-12.237
83	BI	238	185.230	1.619	13.073	.374	12.902	-11.080
83	BI	239	190.615	2.982	13.279	.717	11.754	-12.709
83	BI	240	197.434	1.549	13.475	1.068	13.392	-11.526
83	BI	241	202.881	2.920	13.663	1.425	12.217	-13.129
83	BI	242	209.753	1.495	13.842	1.789	13.830	-11.920

TABLE 2

Atomic mass excesses and nuclear binding energies

83	BI	243	215.247	2.874	14.012	2.159	12.630	-13.500
83	BI	244	222.158	1.456	14.173	2.533	14.218	-12.268
83	BI	245	227.685	2.840	14.326	2.912	12.995	-13.826
83	BI	246	234.625	1.427	14.471	3.294	14.561	-12.574
83	BI	247	240.177	2.816	14.607	3.679	13.318	-14.112
83	BI	248	247.138	1.406	14.736	4.065	14.864	-12.842
83	BI	249	252.709	2.797	14.856	4.451	13.602	-14.364
83	BI	250	259.688	1.388	14.970	4.837	15.132	-13.079
83	BI	251	265.277	2.779	15.076	5.222	13.855	-14.588
83	BI	252	272.275	1.369	15.175	5.604	15.371	-13.292
83	BI	253	277.885	2.758	15.267	5.982	14.082	-14.791
83	BI	254	284.908	1.345	15.353	6.355	15.588	-13.486
83	BI	255	290.546	2.729	15.432	6.723	14.290	-14.978
83	BI	256	297.602	1.311	15.507	7.084	15.788	-13.668
83	BI	257	303.280	2.689	15.575	7.436	14.485	-15.158
83	BI	258	310.383	1.264	15.639	7.780	15.980	-13.847
83	BI	259	316.117	2.634	15.698	8.114	14.674	-15.336
83	BI	260	323.285	1.200	15.753	8.438	16.168	-14.026
83	BI	261	329.092	2.560	15.804	8.750	14.863	-15.519
83	BI	262	336.344	1.115	15.852	9.050	16.360	-14.214
83	BI	263	342.247	2.464	15.896	9.337	15.059	-15.713
83	BI	264	349.607	1.007	15.938	9.610	16.562	-14.416
83	BI	265	355.630	2.345	15.978	9.870	15.267	-15.923
83	BI	266	363.122	.875	16.016	10.116	16.777	-14.636
	ATOM		M - A	NEUTRON	PROTON	ALPHA	Q BETA -	Q BETA +
84	PO	165	162.621	16.499	-7.860	-11.184	-26.197	25.031
84	PO	166	152.825	18.163	-7.650	-11.312	-27.628	20.501
84	PO	167	147.145	14.048	-7.235	-13.305	-23.292	21.206
84	PO	168	139.812	15.700	-6.288	-15.336	-24.520	18.087
84	PO	169	135.188	12.992	-5.878	-14.998	-21.401	19.356
84	PO	170	128.900	14.655	-5.483	-14.681	-22.104	16.843
84	PO	171	124.721	12.546	-5.080	-14.293	-19.590	18.124
84	PO	172	118.876	14.213	-4.694	-13.932	-20.843	15.672
84	PO	173	115.088	12.155	-4.299	-13.502	-18.389	16.961
84	PO	174	109.635	13.820	-3.924	-13.107	-19.649	14.570
84	PO	175	106.190	11.812	-3.540	-12.647	-17.254	15.865
84	PO	176	101.087	13.471	-3.177	-12.230	-18.517	13.532
84	PO	177	97.946	11.508	-2.806	-11.753	-16.179	14.829
84	PO	178	93.159	13.155	-2.457	-11.327	-17.443	12.552
84	PO	179	90.292	11.234	-2.101	-10.845	-15.160	13.847
84	PO	180	85.860	12.800	-1.830	-10.486	-16.294	11.748
84	PO	181	83.186	11.042	-1.489	-9.950	-14.190	12.910
84	PO	182	79.032	12.521	-1.171	-9.607	-15.316	10.861
84	PO	183	76.603	10.796	-.848	-9.093	-13.260	12.013
84	PO	184	72.721	12.249	-.547	-8.714	-14.376	10.009
84	PO	185	70.538	10.551	-.241	-8.296	-12.365	11.148
84	PO	186	66.931	11.974	.043	-7.954	-13.470	9.184
84	PO	187	65.000	10.298	.331	-7.580	-11.498	10.310
84	PO	188	61.678	11.690	.598	-7.282	-12.590	8.382
84	PO	189	60.013	10.032	.867	-6.958	-10.654	9.493
84	PO	190	56.988	11.392	1.116	-6.710	-11.734	7.599
84	PO	191	55.607	9.749	1.368	-6.441	-9.831	8.696
84	PO	192	52.896	11.078	1.599	-6.245	-10.899	6.833
84	PO	193	51.815	9.448	1.833	-6.031	-9.027	7.918
84	PO	194	49.435	10.748	2.047	-5.887	-10.083	6.083
84	PO	195	48.673	9.130	2.264	-5.727	-8.240	7.157
84	PO	196	46.638	10.402	2.463	-5.632	-9.287	5.350
84	PO	197	46.210	8.796	2.663	-5.522	-7.473	6.415
84	PO	198	44.532	10.045	2.847	-5.471	-8.513	4.636
84	PO	199	44.447	8.452	3.033	-5.405	-6.727	5.695

TABLE 2

Atomic mass excesses and nuclear binding energies

84	PO	200	43.134	9.681	3.204	-5.392	-7.762	3.943
84	PO	201	43.399	8.102	3.376	-5.362	-6.004	4.997
84	PO	202	42.451	9.315	3.535	-5.378	-7.038	3.272
84	PO	203	43.068	7.751	3.696	-5.376	-5.307	4.325
84	PO	204	42.482	8.953	3.846	-5.412	-6.341	2.625
84	PO	205	43.444	7.405	3.997	-5.430	-4.637	3.679
84	PO	206	43.212	8.600	4.138	-5.478	-5.674	2.003
84	PO	207	44.512	7.068	4.282	-5.506	-3.995	3.058
84	PO	208	44.620	8.259	4.418	-5.558	-5.036	1.405
84	PO	209	46.244	6.744	4.556	-5.589	-3.380	2.462
84	PO	210	46.678	7.933	4.689	-5.638	-4.426	-.914
84	PO	211	50.100	4.945	5.077	-7.156	-1.301	-.110
84	PO	212	52.335	6.133	5.460	-8.687	-2.099	-1.982
84	PO	213	56.058	4.645	5.844	-8.207	-.227	-1.175
84	PO	214	58.595	5.830	6.223	-7.739	-1.028	-3.032
84	PO	215	62.610	4.352	6.601	-7.259	.831	-2.220
84	PO	216	65.440	5.537	6.975	-6.790	.024	-4.062
84	PO	217	69.741	4.067	7.346	-6.314	1.868	-3.241
84	PO	218	72.854	5.254	7.713	-5.847	1.052	-5.067
84	PO	219	77.430	3.791	8.076	-5.377	2.880	-4.234
84	PO	220	80.778	5.020	8.471	-4.877	1.976	-6.118
84	PO	221	85.657	3.488	8.823	-4.452	3.864	-5.193
84	PO	222	89.265	4.760	9.171	-3.958	2.943	-7.060
84	PO	223	94.397	3.235	9.512	-3.542	4.814	-6.116
84	PO	224	98.251	4.513	9.847	-3.093	3.875	-7.962
84	PO	225	103.623	2.996	10.175	-2.649	5.727	-6.997
84	PO	226	107.708	4.282	10.497	-2.210	4.767	-8.821
84	PO	227	113.303	2.772	10.811	-1.776	6.597	-7.833
84	PO	228	117.604	4.067	11.118	-1.347	5.616	-9.633
84	PO	229	123.404	2.567	11.417	-.923	7.422	-8.621
84	PO	230	127.901	3.871	11.709	-.505	6.416	-10.395
84	PO	231	133.889	2.380	11.992	-.092	8.198	-9.357
84	PO	232	138.562	3.694	12.268	.314	7.167	-11.104
84	PO	233	144.717	2.213	12.534	.715	8.922	-10.039
84	PO	234	149.548	3.537	12.793	1.108	7.864	-11.759
84	PO	235	155.849	2.066	13.042	1.496	9.593	-10.666
84	PO	236	160.816	3.400	13.283	1.876	8.508	-12.358
84	PO	237	167.244	1.940	13.515	2.249	10.209	-11.237
84	PO	238	172.327	3.284	13.738	2.615	9.096	-12.902
84	PO	239	178.862	1.833	13.953	2.973	10.770	-11.754
84	PO	240	184.042	3.187	14.158	3.323	9.630	-13.392
84	PO	241	190.664	1.745	14.355	3.663	11.277	-12.217
84	PO	242	195.924	3.108	14.542	3.995	10.111	-13.830
84	PO	243	202.617	1.674	14.721	4.317	11.733	-12.630
84	PO	244	207.940	3.044	14.891	4.629	10.542	-14.218
84	PO	245	214.690	1.617	15.053	4.930	12.139	-12.995
84	PO	246	220.064	2.994	15.206	5.219	10.925	-14.561
84	PO	247	226.859	1.572	15.351	5.497	12.500	-13.318
84	PO	248	232.274	2.953	15.488	5.762	11.265	-14.864
84	PO	249	239.106	1.535	15.616	6.014	12.820	-13.602
84	PO	250	244.556	2.918	15.738	6.253	11.566	-15.132
84	PO	251	251.422	1.501	15.851	6.477	13.105	-13.855
84	PO	252	256.904	2.885	15.958	6.686	11.836	-15.371
84	PO	253	263.803	1.468	16.057	6.879	13.360	-14.082
84	PO	254	269.320	2.851	16.150	7.057	12.078	-15.588
84	PO	255	276.256	1.431	16.236	7.218	13.591	-14.290
84	PO	256	281.814	2.810	16.317	7.362	12.300	-15.788
84	PO	257	288.795	1.386	16.391	7.489	13.806	-14.485
84	PO	258	294.404	2.759	16.461	7.599	12.509	-15.980
84	PO	259	301.443	1.328	16.525	7.690	14.010	-14.674
84	PO	260	307.116	2.694	16.585	7.763	12.710	-16.168
84	PO	261	314.228	1.255	16.641	7.818	14.210	-14.863

TABLE 2

Atomic mass excesses and nuclear binding energies

84	PO	262	319.984	2.612	16.693	7.855	12.910	-16.360
84	PO	263	327.188	1.163	16.741	7.874	14.412	-15.059
84	PO	264	333.046	2.510	16.786	7.875	13.116	-16.562
84	PO	265	340.363	1.050	16.829	7.858	14.622	-15.267
84	PO	266	346.345	2.385	16.870	7.823	13.331	-16.777
84	PO	267	353.798	.914	16.909	7.772	14.845	-15.492
	ATOM		M - A	NEUTRON	PROTON	ALPHA	Q BETA -	Q BETA +
85	AT	168	164.332	14.472	-9.603	-13.546	-22.217	24.520
85	AT	169	156.589	16.111	-9.192	15.389	-23.446	21.401
85	AT	170	151.004	13.952	-8.232	-15.070	-20.892	22.104
85	AT	171	144.311	15.060	-7.827	-14.763	-21.595	19.590
85	AT	172	139.719	12.960	-7.413	-14.385	-18.571	20.843
85	AT	173	133.477	14.610	-7.016	-14.036	-19.823	18.389
85	AT	174	129.284	12.561	-6.611	-13.618	-17.393	19.649
85	AT	175	123.444	14.207	-6.224	-13.237	-18.650	17.254
85	AT	176	119.604	12.207	-5.829	-12.791	-16.279	18.517
85	AT	177	114.125	13.846	-5.454	-12.390	-17.539	16.179
85	AT	178	110.602	11.891	-5.071	-11.927	-15.226	17.443
85	AT	179	105.453	13.516	-4.709	-11.519	-16.485	15.160
85	AT	180	102.154	11.666	-4.278	-10.991	-14.352	16.294
85	AT	181	97.375	13.146	-3.931	-10.649	-15.480	14.190
85	AT	182	94.348	11.395	-3.577	-10.132	-13.399	15.316
85	AT	183	89.863	12.852	-3.246	-9.808	-14.519	13.260
85	AT	184	87.098	11.133	-2.910	-9.376	-12.484	14.376
85	AT	185	82.902	12.563	-2.596	-9.018	-13.593	12.365
85	AT	186	80.401	10.869	-2.278	-8.621	-11.600	13.470
85	AT	187	76.498	12.270	-1.982	-8.299	-12.698	11.498
85	AT	188	74.268	10.597	-1.683	-7.947	-10.743	12.590
85	AT	189	70.668	11.968	-1.405	-7.669	-11.827	10.654
85	AT	190	68.723	10.312	-1.125	-7.367	-9.906	11.734
85	AT	191	65.438	11.652	-.865	-7.138	-10.978	9.831
85	AT	192	63.795	10.011	-.603	-6.890	-9.088	10.899
85	AT	193	60.842	11.320	-.361	-6.713	-10.147	9.027
85	AT	194	59.518	9.691	-.118	-6.519	-8.287	10.083
85	AT	195	56.913	10.972	.107	-6.394	-9.335	8.240
85	AT	196	55.925	9.355	.332	-6.253	-7.503	9.287
85	AT	197	53.683	10.610	.541	-6.175	-8.542	7.473
85	AT	198	53.045	9.005	.750	-6.083	-6.737	8.513
85	AT	199	51.174	10.238	.942	-6.049	-7.769	6.727
85	AT	200	50.896	8.646	1.136	-5.999	-5.991	7.762
85	AT	201	49.403	9.860	1.315	-6.000	-7.019	6.004
85	AT	202	49.489	8.281	1.495	-5.985	-5.268	7.038
85	AT	203	48.375	9.482	1.662	-6.013	-6.296	5.307
85	AT	204	48.823	7.919	1.829	-6.024	-4.571	6.341
85	AT	205	48.081	9.109	1.985	-6.070	-5.600	4.637
85	AT	206	48.886	7.562	2.143	-6.098	-3.901	5.674
85	AT	207	48.507	8.747	2.291	-6.154	-4.933	3.995
85	AT	208	49.657	7.217	2.440	-6.191	-3.259	5.036
85	AT	209	49.624	8.400	2.581	-6.249	-4.297	3.380
85	AT	210	51.104	6.887	2.724	-6.286	-2.645	4.426
85	AT	211	51.401	8.070	2.861	-6.338	-3.688	1.301
85	AT	212	54.434	5.335	3.251	-7.610	-.818	2.099
85	AT	213	56.285	6.517	3.635	-8.893	-1.617	.227
85	AT	214	59.622	5.030	4.020	-8.421	.250	1.028
85	AT	215	61.780	6.210	4.400	-7.961	-.551	-.831
85	AT	216	65.416	4.731	4.779	-7.491	1.304	-.024
85	AT	217	67.873	5.911	5.152	-7.031	.498	-1.868
85	AT	218	71.802	4.438	5.523	-6.566	2.341	-1.052
85	AT	219	74.550	5.620	5.889	-6.110	1.526	-2.880
85	AT	220	78.802	4.115	6.213	-5.690	3.431	-1.976

TABLE 2

Atomic mass excesses and nuclear binding energies

85	AT	221	81.793	5.376	6.569	-5.202	2.529	-3.864
85	AT	222	86.321	3.839	6.921	-4.791	4.420	-2.943
85	AT	223	89.583	5.105	7.266	-4.310	3.503	-4.814
85	AT	224	94.376	3.575	7.606	-3.871	5.378	-3.875
85	AT	225	97.896	4.847	7.940	-3.437	4.443	-5.727
85	AT	226	102.941	3.323	8.267	-3.008	6.299	-4.767
85	AT	227	106.706	4.602	8.587	-2.584	5.345	-6.597
85	AT	228	111.988	3.086	8.900	-2.165	7.180	-5.616
85	AT	229	115.982	4.373	9.206	-1.753	6.204	-7.422
85	AT	230	121.484	2.865	9.505	-1.346	8.017	-6.416
85	AT	231	125.690	4.161	9.795	-.944	7.017	-8.198
85	AT	232	131.396	2.662	10.078	-.549	8.806	-7.167
85	AT	233	135.795	3.968	10.352	-.160	7.781	-8.922
85	AT	234	141.683	2.479	10.618	.222	9.544	-7.864
85	AT	235	146.256	3.794	10.876	.598	8.494	-9.593
85	AT	236	152.309	2.315	11.125	.967	10.230	-8.508
85	AT	237	157.035	3.641	11.366	1.330	9.153	-10.209
85	AT	238	163.231	2.171	11.598	1.685	10.862	-9.096
85	AT	239	168.092	3.507	11.820	2.032	9.758	-10.770
85	AT	240	174.412	2.047	12.035	2.372	11.440	-9.630
85	AT	241	179.387	3.392	12.240	2.703	10.309	-11.277
85	AT	242	185.813	1.942	12.436	3.026	11.965	-10.111
85	AT	243	190.884	3.296	12.624	3.340	10.808	-11.733
85	AT	244	197.398	1.853	12.803	3.645	12.438	-10.542
85	AT	245	202.551	3.215	12.974	3.939	11.256	-12.139
85	AT	246	209.139	1.779	13.136	4.224	12.862	-10.925
85	AT	247	214.359	3.147	13.289	4.497	11.657	-12.500
85	AT	248	221.009	1.718	13.435	4.758	13.241	-11.265
85	AT	249	226.286	3.090	13.572	5.008	12.015	-12.820
85	AT	250	232.989	1.664	13.702	5.245	13.579	-11.566
85	AT	251	238.317	3.040	13.824	5.469	12.334	-13.105
85	AT	252	245.068	1.616	13.938	5.679	13.881	-11.836
85	AT	253	250.443	2.992	14.045	5.875	12.620	-13.360
85	AT	254	257.242	1.569	14.146	6.056	14.152	-12.078
85	AT	255	262.665	2.944	14.240	6.221	12.879	-13.591
85	AT	256	269.513	1.519	14.327	6.371	14.400	-12.300
85	AT	257	274.989	2.891	14.409	6.505	13.117	-13.806
85	AT	258	281.895	1.462	14.485	6.622	14.629	-12.509
85	AT	259	287.433	2.829	14.556	6.722	13.340	-14.010
85	AT	260	294.406	1.394	14.621	6.805	14.848	-12.710
85	AT	261	300.018	2.755	14.683	6.871	13.554	-14.210
85	AT	262	307.073	1.312	14.740	6.919	15.060	-12.910
85	AT	263	312.776	2.665	14.793	6.950	13.767	-14.412
85	AT	264	319.930	1.213	14.843	6.964	15.274	-13.116
85	AT	265	325.741	2.557	14.890	6.960	13.983	-14.622
85	AT	266	333.013	1.095	14.934	6.940	15.493	-13.331
85	AT	267	338.953	2.427	14.976	6.903	14.207	-14.845
85	AT	268	346.366	.955	15.017	6.851	15.725	-13.562
	ATOM		M - A	NEUTRON	PROTON	ALPHA	Q BETA -	Q BETA +
86	RN	170	171.896	16.506	-7.723	-15.462	-26.153	20.892
86	RN	171	165.907	14.357	-7.318	-15.153	-23.601	21.595
86	RN	172	158.290	15.984	-6.394	-14.869	-24.814	18.571
86	RN	173	153.299	13.358	-5.996	-14.502	-21.789	19.823
86	RN	174	146.676	14.990	-5.615	-14.167	-22.483	17.393
86	RN	175	142.094	12.950	-5.225	-13.764	-20.052	18.650
86	RN	176	135.883	14.578	-4.855	-13.398	-21.280	16.279
86	RN	177	131.665	12.586	-4.476	-12.968	-18.907	17.539
86	RN	178	125.828	14.204	-4.118	-12.584	-20.135	15.226
86	RN	179	121.938	12.257	-3.751	-12.138	-17.818	16.485
86	RN	180	116.506	13.799	-3.469	-11.811	-18.919	14.352

TABLE 2

Atomic mass excesses and nuclear binding energies

86	RN	181	112.856	12.018	-3.117	-11.301	-16.781	15.480
86	RN	182	107.746	13.477	-2.786	-10.979	-17.875	13.399
86	RN	183	104.381	11.732	-2.449	-10.480	-15.788	14.519
86	RN	184	99.581	13.167	-2.134	-10.112	-16.874	12.484
86	RN	185	96.495	11.453	-1.813	-9.701	-14.833	13.593
86	RN	186	92.001	12.862	-1.514	-9.360	-15.910	11.600
86	RN	187	89.196	11.173	-1.210	-8.984	-13.910	12.698
86	RN	188	85.011	12.552	-.928	-8.680	-14.975	10.743
86	RN	189	82.495	10.883	-.642	-8.348	-13.012	11.827
86	RN	190	78.629	12.233	-.377	-8.089	-14.066	9.906
86	RN	191	76.416	10.580	-.108	-7.806	-12.137	10.978
86	RN	192	72.883	11.900	.140	-7.596	-13.178	9.088
86	RN	193	70.989	10.261	.390	-7.367	-11.281	10.147
86	RN	194	67.805	11.552	.622	-7.208	-12.311	8.287
86	RN	195	66.248	9.924	.854	-7.032	-10.442	9.335
86	RN	196	63.428	11.187	1.070	-6.923	-11.463	7.503
86	RN	197	62.224	9.572	1.286	-6.800	-9.623	8.542
86	RN	198	59.782	10.810	1.486	-6.737	-10.636	6.737
86	RN	199	58.943	9.206	1.686	-6.661	-8.823	7.769
86	RN	200	56.887	10.423	1.872	-6.640	-9.831	5.991
86	RN	201	56.423	8.832	2.058	-6.604	-8.046	7.019
86	RN	202	54.758	10.032	2.230	-6.617	-9.052	5.268
86	RN	203	54.670	8.455	2.404	-6.614	-7.294	6.296
86	RN	204	53.394	9.643	2.565	-6.652	-8.302	4.571
86	RN	205	53.681	8.081	2.727	-6.673	-6.570	5.600
86	RN	206	52.788	9.261	2.879	-6.727	-7.582	3.901
86	RN	207	53.440	7.715	3.031	-6.763	-5.877	4.933
86	RN	208	52.916	8.891	3.175	-6.825	-6.894	3.259
86	RN	209	53.921	7.363	3.321	-6.867	-5.215	4.297
86	RN	210	53.750	8.538	3.459	-6.928	-6.240	2.645
86	RN	211	55.090	7.027	3.599	-6.969	-4.585	3.688
86	RN	212	55.252	8.205	3.734	-7.022	-5.617	.818
86	RN	213	57.901	5.718	4.118	-8.048	-2.990	1.617
86	RN	214	59.373	6.896	4.497	-9.085	-3.785	-.250
86	RN	215	62.331	5.409	4.877	-8.621	-1.920	.551
86	RN	216	64.113	6.585	5.252	-8.168	-2.718	-1.304
86	RN	217	67.375	5.105	5.626	-7.708	-.864	-.498
86	RN	218	69.462	6.281	5.996	-7.258	-1.667	-2.341
86	RN	219	73.024	4.805	6.363	-6.804	.176	-1.526
86	RN	220	75.371	6.020	6.764	-6.321	-.712	-3.431
86	RN	221	79.264	4.474	7.123	-5.914	1.195	-2.529
86	RN	222	81.901	5.730	7.477	-5.438	.295	-4.420
86	RN	223	86.080	4.188	7.826	-5.041	2.188	-3.503
86	RN	224	88.998	5.449	8.170	-4.611	1.273	-5.378
86	RN	225	93.453	3.912	8.508	-4.187	3.151	-4.443
86	RN	226	96.642	5.179	8.839	-3.768	2.220	-6.299
86	RN	227	101.361	3.648	9.165	-3.355	4.080	-5.345
86	RN	228	104.808	4.921	9.483	-2.947	3.130	-7.180
86	RN	229	109.778	3.397	9.795	-2.546	4.970	-6.204
86	RN	230	113.468	4.678	10.099	-2.150	3.999	-8.017
86	RN	231	118.673	3.162	10.396	-1.760	5.817	-7.017
86	RN	232	122.590	4.451	10.686	-1.377	4.824	-8.806
86	RN	233	128.013	2.944	10.967	-1.000	6.618	-7.781
86	RN	234	132.139	4.241	11.240	.629	5.601	-9.544
86	RN	235	137.763	2.744	11.506	.265	7.370	-8.494
86	RN	236	142.079	4.051	11.763	.093	6.327	-10.230
86	RN	237	147.882	2.564	12.011	.444	8.071	-9.153
86	RN	238	152.369	3.881	12.251	.788	7.001	-10.862
86	RN	239	158.334	2.403	12.482	1.125	8.718	-9.758
86	RN	240	162.972	3.730	12.705	1.454	7.622	-11.440
86	RN	241	169.078	2.261	12.919	1.775	9.313	-10.309
86	RN	242	173.848	3.598	13.124	2.089	8.190	-11.965

TABLE 2

Atomic mass excesses and nuclear binding energies

86	RN	243	180.077	2.138	13.321	2.394	9.855	-10.808
86	RN	244	184.960	3.484	13.509	2.691	8.706	-12.438
86	RN	245	191.295	2.033	13.688	2.978	10.345	-11.256
86	RN	246	196.277	3.386	13.859	3.256	9.172	-12.862
86	RN	247	202.702	1.942	14.022	3.524	10.787	-11.657
86	RN	248	207.768	3.302	14.176	3.781	9.591	-13.241
86	RN	249	214.272	1.864	14.322	4.028	11.184	-12.015
86	RN	250	219.410	3.228	14.461	4.263	9.967	-13.579
86	RN	251	225.983	1.795	14.591	4.485	11.540	-12.334
86	RN	252	231.188	3.163	14.714	4.695	10.304	-13.881
86	RN	253	237.823	1.732	14.830	4.892	11.860	-12.620
86	RN	254	243.089	3.101	14.939	5.076	10.608	-14.152
86	RN	255	249.786	1.671	15.041	5.245	12.149	-12.879
86	RN	256	255.113	3.040	15.136	5.400	10.884	-14.400
86	RN	257	261.873	1.608	15.225	5.539	12.413	-13.117
86	RN	258	267.266	2.975	15.309	5.663	11.138	-14.629
86	RN	259	274.093	1.540	15.386	5.772	12.658	-13.340
86	RN	260	279.559	2.902	15.459	5.864	11.376	-14.848
86	RN	261	286.464	1.462	15.527	5.940	12.891	-13.554
86	RN	262	292.013	2.818	15.590	6.000	11.605	-15.060
86	RN	263	299.009	1.371	15.649	6.043	13.118	-13.767
86	RN	264	304.656	2.720	15.704	6.069	11.831	-15.274
86	RN	265	311.758	1.265	15.757	6.080	13.344	-13.983
86	RN	266	317.520	2.606	15.806	6.073	12.059	-15.493
86	RN	267	324.746	1.141	15.852	6.051	13.575	-14.207
86	RN	268	330.641	2.472	15.897	6.014	12.294	-15.725
86	RN	269	338.011	.998	15.940	5.961	13.816	-14.446
	ATOM		M - A	NEUTRON	PROTON	ALPHA	Q BETA -	Q BETA +
87	FR	172	183.104	14.771	-9.612	-15.162	-22.542	24.814
87	FR	173	175.088	16.383	-9.214	-14.890	-23.756	21.789
87	FR	174	169.160	14.296	-8.276	-14.547	-21.288	22.483
87	FR	175	162.146	15.381	-7.885	-14.225	-21.982	20.052
87	FR	176	157.163	13.350	-7.485	-13.835	-19.053	21.280
87	FR	177	150.572	14.959	-7.104	-13.486	-20.279	18.907
87	FR	178	145.963	12.976	-6.714	-13.070	-17.933	20.135
87	FR	179	139.756	14.574	-6.344	-12.703	-19.159	17.818
87	FR	180	135.425	12.698	-5.903	-12.212	-16.993	18.919
87	FR	181	129.637	14.156	-5.546	-11.902	-18.090	16.781
87	FR	182	125.622	12.383	-5.181	-11.411	-15.977	17.875
87	FR	183	120.170	13.819	-4.838	-11.108	-17.067	15.788
87	FR	184	116.456	12.081	-4.489	-10.692	-15.002	16.874
87	FR	185	111.329	13.494	-4.162	-10.344	-16.083	14.833
87	FR	186	107.911	11.785	-3.830	-9.954	-14.062	15.910
87	FR	187	103.105	13.173	-3.520	-9.633	-15.132	13.910
87	FR	188	99.986	11.487	-3.205	-9.279	-13.151	14.975
87	FR	189	95.507	12.846	-2.912	-8.996	-14.209	13.012
87	FR	190	92.695	11.180	-2.615	-8.685	-12.262	14.066
87	FR	191	88.553	12.509	-2.339	-8.445	-13.308	12.137
87	FR	192	86.061	10.859	-2.061	-8.184	-11.393	13.178
87	FR	193	82.270	12.159	-1.802	-7.993	-12.427	11.281
87	FR	194	80.116	10.521	-1.542	-7.784	-10.541	12.311
87	FR	195	76.691	11.793	-1.301	-7.644	-11.563	10.442
87	FR	196	74.892	10.167	-1.058	-7.488	-9.705	11.463
87	FR	197	71.847	11.412	-.834	-7.396	-10.717	9.623
87	FR	198	70.418	9.797	-.609	-7.290	-8.886	10.636
87	FR	199	67.766	11.019	-.400	-7.244	-9.891	8.823
87	FR	200	66.719	9.415	-.191	-7.184	-8.085	9.831
87	FR	201	64.469	10.617	.003	-7.177	-9.085	8.046
87	FR	202	63.810	9.026	.198	-7.156	-7.306	9.052
87	FR	203	61.964	10.213	.378	-7.181	-8.305	7.294

TABLE 2

Atomic mass excesses and nuclear binding energies

87	FR	204	61.696	8.636	.559	-7.191	-6.552	8.302
87	FR	205	60.252	9.812	.728	-7.239	-7.552	6.570
87	FR	206	60.369	8.250	.897	-7.271	-5.825	7.582
87	FR	207	59.317	9.420	1.055	-7.333	-6.830	5.877
87	FR	208	59.810	7.874	1.214	-7.378	-5.129	6.894
87	FR	209	59.136	9.042	1.365	-7.445	-6.140	5.215
87	FR	210	59.989	7.514	1.516	-7.494	-4.464	6.240
87	FR	211	59.674	8.683	1.660	-7.558	-5.484	4.585
87	FR	212	60.869	7.173	1.805	-7.603	-3.831	5.617
87	FR	213	60.891	8.345	1.945	-7.658	-4.859	2.990
87	FR	214	63.158	6.101	2.328	-8.444	-2.475	3.785
87	FR	215	64.251	7.274	2.707	-9.240	-3.273	1.920
87	FR	216	66.831	5.787	3.085	-8.787	-1.413	2.718
87	FR	217	68.239	6.959	3.459	-8.345	-2.213	.864
87	FR	218	71.129	5.477	3.831	-7.897	-.362	1.667
87	FR	219	72.848	6.649	4.199	-7.459	-1.166	-.176
87	FR	220	76.082	5.133	4.526	-7.057	.751	.712
87	FR	221	78.069	6.381	4.886	-6.587	-.137	-1.195
87	FR	222	81.606	4.830	5.242	-6.195	1.770	-.295
87	FR	223	83.892	6.082	5.594	-5.733	.871	-2.188
87	FR	224	87.725	4.535	5.940	-5.313	2.766	-1.273
87	FR	225	90.302	5.790	6.281	-4.900	1.854	-3.151
87	FR	226	94.422	4.248	6.616	-4.491	3.734	-2.220
87	FR	227	97.281	5.508	6.945	-4.089	2.806	-4.080
87	FR	228	101.678	3.971	7.268	-3.693	4.669	-3.130
87	FR	229	104.808	5.237	7.585	-3.302	3.723	-4.970
87	FR	230	109.468	3.707	7.894	-2.918	5.567	-3.999
87	FR	231	112.856	4.980	8.197	-2.540	4.601	-5.817
87	FR	232	117.766	3.457	8.492	-2.169	6.424	-4.824
87	FR	233	121.395	4.738	8.780	-1.804	5.435	-6.618
87	FR	234	126.539	3.224	9.059	-1.445	7.236	-5.601
87	FR	235	130.392	4.514	9.332	-1.093	6.224	-7.370
87	FR	236	135.752	3.008	9.596	-.747	8.000	-6.327
87	FR	237	139.812	4.307	9.851	-.408	6.963	-8.071
87	FR	238	145.368	2.811	10.099	-.076	8.714	-7.001
87	FR	239	149.616	4.120	10.338	.250	7.652	-8.718
87	FR	240	155.350	2.633	10.569	.568	9.377	-7.622
87	FR	241	159.765	3.952	10.791	.879	8.288	-9.313
87	FR	242	165.657	2.475	11.005	1.183	9.987	-8.190
87	FR	243	170.222	3.803	11.210	1.479	8.873	-9.855
87	FR	244	176.254	2.335	11.407	1.767	10.546	-8.706
87	FR	245	180.950	3.672	11.595	2.046	9.406	-10.345
87	FR	246	187.105	2.213	11.775	2.317	11.054	-9.172
87	FR	247	191.915	3.557	11.947	2.579	9.890	-10.787
87	FR	248	198.177	2.105	12.110	2.831	11.514	-9.591
87	FR	249	203.087	3.457	12.265	3.073	10.327	-11.184
87	FR	250	209.444	2.011	12.413	3.305	11.929	-9.967
87	FR	251	214.443	3.368	12.552	3.525	10.721	-11.540
87	FR	252	220.883	1.927	12.684	3.735	12.303	-10.304
87	FR	253	225.963	3.287	12.809	3.932	11.076	-11.860
87	FR	254	232.482	1.849	12.926	4.117	12.641	-10.608
87	FR	255	237.637	3.212	13.037	4.289	11.398	-12.149
87	FR	256	244.230	1.775	13.141	4.448	12.948	-10.884
87	FR	257	249.460	3.137	13.238	4.592	11.691	-12.413
87	FR	258	256.128	1.699	13.330	4.723	13.229	-11.138
87	FR	259	261.435	3.060	13.415	4.839	11.962	-12.658
87	FR	260	268.183	1.620	13.495	4.940	13.491	-11.376
87	FR	261	273.573	2.977	13.571	5.026	12.217	-12.891
87	FR	262	280.408	1.532	13.641	5.096	13.740	-11.605
87	FR	263	285.891	2.884	13.707	5.151	12.462	-13.118
87	FR	264	292.825	1.433	13.769	5.190	13.982	-11.831
87	FR	265	298.414	2.779	13.827	5.214	12.702	-13.344

TABLE 2

Atomic mass excesses and nuclear binding energies

87	FR	266	305.461	1.320	13.882	5.222	14.222	-12.059
87	FR	267	311.171	2.658	13.934	5.214	12.943	-13.575
87	FR	268	318.347	1.191	13.983	5.192	14.465	-12.294
87	FR	269	324.195	2.519	14.031	5.155	13.190	-13.816
87	FR	270	331.519	1.043	14.076	5.103	14.717	-12.541
	ATOM		M - A	NEUTRON	PROTON	ALPHA	Q BETA -	Q BETA +
88	RA	175	184.128	14.687	-7.383	-14.612	-23.912	21.982
88	RA	176	176.216	16.279	-6.485	-14.317	-25.103	19.053
88	RA	177	170.851	13.733	-6.103	-13.942	-22.174	20.279
88	RA	178	163.896	15.323	-5.739	-13.610	-22.851	17.933
88	RA	179	158.915	13.348	-5.367	-13.212	-20.503	19.159
88	RA	180	152.418	14.864	-5.077	-12.926	-21.573	16.993
88	RA	181	147.727	13.059	-4.717	-12.453	-19.405	18.090
88	RA	182	141.599	14.495	-4.377	-12.162	-20.469	15.977
88	RA	183	137.236	12.730	-4.030	-11.690	-18.353	17.067
88	RA	184	131.458	14.146	-3.704	-11.343	-19.411	15.002
88	RA	185	127.412	12.414	-3.371	-10.947	-17.342	16.083
88	RA	186	121.973	13.806	-3.059	-10.617	-18.392	14.062
88	RA	187	118.238	12.102	-2.742	-10.247	-16.365	15.132
88	RA	188	113.136	13.469	-2.446	-9.946	-17.405	13.151
88	RA	189	109.716	11.788	-2.145	-9.611	-15.416	14.209
88	RA	190	104.957	13.127	-1.865	-9.346	-16.445	12.262
88	RA	191	101.861	11.463	-1.581	-9.056	-14.491	13.308
88	RA	192	97.454	12.774	-1.317	-8.834	-15.508	11.393
88	RA	193	94.696	11.125	-1.050	-8.592	-13.585	12.427
88	RA	194	90.657	12.407	-.802	-8.419	-14.591	10.541
88	RA	195	88.254	10.771	-.553	-8.229	-12.697	11.563
88	RA	196	84.596	12.025	-.321	-8.104	-13.692	9.705
88	RA	197	82.564	10.400	-.088	-7.966	-11.826	10.717
88	RA	198	79.303	11.628	.129	-7.889	-12.813	8.886
88	RA	199	77.657	10.014	.346	-7.799	-10.973	9.891
88	RA	200	74.804	11.220	.547	-7.766	-11.954	8.085
88	RA	201	73.554	9.617	.749	-7.721	-10.140	9.085
88	RA	202	71.116	10.805	.937	-7.725	-11.118	7.306
88	RA	203	70.269	9.214	1.126	-7.717	-9.330	8.305
88	RA	204	68.248	10.389	1.301	-7.752	-10.308	6.552
88	RA	205	67.804	8.812	1.477	-7.772	-8.548	7.552
88	RA	206	66.195	9.977	1.642	-7.828	-9.529	5.825
88	RA	207	66.147	8.415	1.807	-7.868	-7.795	6.830
88	RA	208	64.939	9.575	1.963	-7.936	-8.783	5.129
88	RA	209	65.276	8.030	2.119	-7.986	-7.076	6.140
88	RA	210	64.454	9.190	2.267	-8.057	-8.072	4.464
88	RA	211	65.158	7.663	2.416	-8.109	-6.391	5.484
88	RA	212	64.700	8.826	2.559	-8.175	-7.398	3.831
88	RA	213	65.750	7.317	2.703	-8.221	-5.740	4.859
88	RA	214	65.633	8.485	2.843	-8.274	-6.759	2.475
88	RA	215	67.524	6.477	3.219	-8.825	-4.605	3.273
88	RA	216	68.244	7.647	3.591	-9.383	-5.403	1.413
88	RA	217	70.452	6.160	3.964	-8.941	-3.546	2.213
88	RA	218	71.491	7.328	4.333	-8.509	-4.346	.362
88	RA	219	74.014	5.844	4.700	-8.074	-2.497	1.166
88	RA	220	75.331	7.050	5.101	-7.610	-3.377	-.751
88	RA	221	78.206	5.493	5.461	-7.222	-1.460	.137
88	RA	222	79.836	6.737	5.818	-6.765	-2.348	-1.770
88	RA	223	83.020	5.183	6.170	-6.388	-.442	-.871
88	RA	224	84.958	6.429	6.518	-5.979	-1.340	-2.766
88	RA	225	88.448	4.878	6.861	-5.575	.555	-1.854
88	RA	226	90.688	6.128	7.199	-5.178	-.356	-3.734
88	RA	227	94.476	4.580	7.531	-4.787	1.526	-2.806
88	RA	228	97.009	5.834	7.857	-4.402	.600	-4.669

TABLE 2

Atomic mass excesses and nuclear binding energies

88	RA	229	101.085	4.291	8.177	-4.023	2.466	-3.723
88	RA	230	103.902	5.551	8.491	-3.651	1.523	-5.567
88	RA	231	108.255	4.014	8.798	-3.285	3.370	-4.601
88	RA	232	111.342	5.280	9.098	-2.925	2.408	-6.424
88	RA	233	115.960	3.750	9.391	-2.572	4.236	-5.435
88	RA	234	119.303	5.024	9.677	-2.226	3.252	-7.236
88	RA	235	124.168	3.502	9.955	-1.886	5.058	-6.224
88	RA	236	127.752	4.784	10.225	-1.553	4.051	-8.000
88	RA	237	132.848	3.271	10.488	-1.226	5.833	-6.963
88	RA	238	136.654	4.562	10.743	-.906	4.803	-8.714
88	RA	239	141.964	3.058	10.989	-.592	6.560	-7.652
88	RA	240	145.973	4.358	11.227	-.285	5.505	-9.377
88	RA	241	151.477	2.864	11.458	.015	7.237	-8.288
88	RA	242	155.670	4.174	11.679	.308	6.156	-9.987
88	RA	243	161.349	2.689	11.893	.594	7.863	-8.873
88	RA	244	165.709	4.008	12.098	.872	6.757	-10.546
88	RA	245	171.544	2.532	12.295	1.143	8.438	-9.406
88	RA	246	176.051	3.860	12.484	1.406	7.306	-11.054
88	RA	247	182.025	2.393	12.664	1.661	8.963	-9.890
88	RA	248	186.663	3.730	12.837	1.907	7.808	-11.514
88	RA	249	192.761	2.270	13.001	2.144	9.441	-10.327
88	RA	250	197.515	3.613	13.157	2.371	8.263	-11.929
88	RA	251	203.722	2.160	13.306	2.589	9.874	-10.721
88	RA	252	208.580	3.509	13.447	2.797	8.675	-12.303
88	RA	253	214.887	2.060	13.581	2.993	10.267	-11.076
88	RA	254	219.841	3.414	13.707	3.179	9.049	-12.641
88	RA	255	226.239	1.969	13.827	3.353	10.623	-11.398
88	RA	256	231.282	3.325	13.940	3.515	9.389	-12.948
88	RA	257	237.769	1.881	14.046	3.664	10.948	-11.691
88	RA	258	242.899	3.237	14.146	3.800	9.701	-13.229
88	RA	259	249.473	1.794	14.240	3.923	11.248	-11.962
88	RA	260	254.691	3.149	14.329	4.031	9.990	-13.491
88	RA	261	261.356	1.703	14.412	4.126	11.527	-12.217
88	RA	262	266.668	3.055	14.490	4.207	10.262	-13.740
88	RA	263	273.430	1.606	14.563	4.273	11.793	-12.462
88	RA	264	278.844	2.953	14.632	4.324	10.523	-13.982
88	RA	265	285.712	1.498	14.698	4.361	12.051	-12.702
88	RA	266	291.239	2.840	14.759	4.383	10.778	-14.222
88	RA	267	298.228	1.379	14.818	4.390	12.305	-12.943
88	RA	268	303.882	2.713	14.873	4.383	11.033	-14.465
88	RA	269	311.006	1.244	14.926	4.362	12.562	-13.190
88	RA	270	316.802	2.571	14.978	4.326	11.293	-14.717
88	RA	271	324.077	1.093	15.027	4.278	12.826	-13.447
	ATOM		M - A	NEUTRON	PROTON	ALPHA	Q BETA -	Q BETA +
89	AC	177	193.025	16.662	-9.224	-14.327	-24.069	22.174
89	AC	178	186.747	14.645	-8.311	-13.978	-21.688	22.851
89	AC	179	179.418	15.696	-7.938	-13.663	-22.366	20.503
89	AC	180	173.991	13.794	-7.492	-13.218	-19.656	21.573
89	AC	181	167.131	15.227	-7.129	-12.951	-20.724	19.405
89	AC	182	162.068	13.431	-6.757	-12.496	-18.584	20.469
89	AC	183	155.590	14.846	-6.406	-12.225	-19.646	18.353
89	AC	184	150.869	13.088	-6.048	-11.835	-17.554	19.411
89	AC	185	144.754	14.483	-5.711	-11.508	-18.609	17.342
89	AC	186	140.364	12.757	-5.368	-11.134	-16.562	18.392
89	AC	187	134.603	14.129	-5.045	-10.824	-17.607	16.365
89	AC	188	130.541	12.430	-4.718	-10.476	-15.600	17.405
89	AC	189	125.132	13.776	-4.411	-10.194	-16.634	15.416
89	AC	190	121.401	12.098	-4.101	-9.882	14.663	16.445
89	AC	191	116.351	13.417	-3.810	-9.637	-15.685	14.491
89	AC	192	112.962	11.757	3.517	-9.367	-13.746	15.508

TABLE 2

Atomic mass excesses and nuclear binding energies

89	AC	193	108.282	13.048	-3.243	-9.165	-14.756	13.585
89	AC	194	105.248	11.401	-2.967	-8.944	-12.847	14.591
89	AC	195	100.951	12.664	-2.709	-8.789	-13.844	12.697
89	AC	196	98.289	11.029	-2.450	-8.618	-11.962	13.692
89	AC	197	94.390	12.266	-2.209	-8.511	-12.949	11.826
89	AC	198	92.116	10.642	-1.967	-8.390	-11.092	12.813
89	AC	199	88.629	11.854	-1.742	-8.329	-12.070	10.973
89	AC	200	86.757	10.240	-1.516	-8.257	-10.238	11.954
89	AC	201	83.694	11.431	-1.305	-8.238	-11.210	10.140
89	AC	202	82.234	9.827	-1.095	-8.207	-9.403	11.118
89	AC	203	79.599	11.002	-.899	-8.224	-10.372	9.330
89	AC	204	78.556	9.411	-.702	-8.229	-8.589	10.308
89	AC	205	76.351	10.572	-.519	-8.274	-9.559	8.548
89	AC	206	75.724	8.995	-.335	-8.305	-7.802	9.529
89	AC	207	73.942	10.149	-.163	-8.369	-8.776	7.795
89	AC	208	73.722	8.587	.009	-8.417	-7.044	8.783
89	AC	209	72.352	9.738	.172	-8.491	-8.025	7.076
89	AC	210	72.526	8.193	.335	-8.548	-6.319	8.072
89	AC	211	71.549	9.345	.490	-8.622	-7.309	6.391
89	AC	212	72.098	7.818	.645	-8.678	-5.628	7.398
89	AC	213	71.491	8.975	.794	-8.745	-6.629	5.740
89	AC	214	72.392	7.466	.943	-8.793	-4.971	6.759
89	AC	215	72.129	8.630	1.089	-8.845	-5.985	4.605
89	AC	216	73.647	6.850	1.462	-9.169	-4.058	5.403
89	AC	217	73.998	8.017	1.831	-9.497	-4.859	3.546
89	AC	218	75.836	6.529	2.200	-9.069	-3.008	4.346
89	AC	219	76.510	7.693	2.565	-8.650	-3.811	2.497
89	AC	220	78.708	6.170	2.891	-8.268	-1.890	3.377
89	AC	221	79.666	7.409	3.250	-7.818	-2.772	1.460
89	AC	222	82.184	5.849	3.606	-7.446	-.858	2.348
89	AC	223	83.462	7.090	3.958	-7.005	-1.747	.442
89	AC	224	86.298	5.531	4.307	-6.607	.159	1.340
89	AC	225	87.893	6.773	4.650	-6.214	-.740	-.555
89	AC	226	91.044	5.217	4.989	-5.828	1.155	.356
89	AC	227	92.949	6.461	5.323	-5.448	.245	-1.526
89	AC	228	96.409	4.908	5.652	-5.075	2.128	-.600
89	AC	229	98.619	6.157	5.974	-4.708	1.203	-2.466
89	AC	230	102.379	4.608	6.291	-4.348	3.071	-1.523
89	AC	231	104.885	5.861	6.602	-3.994	2.130	-3.370
89	AC	232	108.934	4.318	6.906	-3.647	3.981	-2.408
89	AC	233	111.724	5.578	7.203	-3.307	3.022	-4.236
89	AC	234	116.051	4.041	7.493	-2.973	4.853	-3.252
89	AC	235	119.111	5.307	7.777	-2.646	3.874	-5.058
89	AC	236	123.700	3.778	8.053	-2.325	5.684	-4.051
89	AC	237	127.015	5.053	8.321	-2.011	4.683	-5.833
89	AC	238	131.851	3.532	8.582	-1.703	6.470	-4.803
89	AC	239	135.404	4.815	8.835	-1.402	5.445	-6.560
89	AC	240	140.468	3.303	9.081	-1.107	7.209	-5.505
89	AC	241	144.240	4.596	9.318	-.819	6.160	-7.237
89	AC	242	149.514	3.093	9.547	-.537	7.899	-6.156
89	AC	243	153.487	4.395	9.769	-.262	6.825	-7.863
89	AC	244	158.952	2.902	9.982	.007	8.539	-6.757
89	AC	245	163.106	4.213	10.187	.268	7.441	-8.438
89	AC	246	168.744	2.729	10.384	.522	9.130	-7.306
89	AC	247	173.062	4.050	10.573	.769	8.007	-8.963
89	AC	248	178.855	2.574	10.755	1.008	9.672	-7.808
89	AC	249	183.320	3.903	10.928	1.239	8.526	-9.441
89	AC	250	189.252	2.435	11.093	1.462	10.168	-8.263
89	AC	251	193.848	3.771	11.251	1.676	8.999	-9.874
89	AC	252	199.905	2.310	11.402	1.881	10.619	-8.675
89	AC	253	204.621	3.652	11.544	2.076	9.429	-10.267
89	AC	254	210.792	2.196	11.680	2.261	11.030	-9.049

TABLE 2

Atomic mass excesses and nuclear binding energies

89	AC	255	215.616	3.543	11.809	2.436	9.822	-10.623
89	AC	256	221.893	2.091	11.931	2.600	11.405	-9.389
89	AC	257	226.821	3.440	12.046	2.752	10.181	-10.948
89	AC	258	233.198	1.990	12.156	2.893	11.749	-9.701
89	AC	259	238.225	3.340	12.259	3.022	10.511	-11.248
89	AC	260	244.701	1.891	12.356	3.138	12.067	-9.990
89	AC	261	249.828	3.241	12.448	3.241	10.819	-11.527
89	AC	262	256.406	1.790	12.534	3.331	12.365	-10.262
89	AC	263	261.636	3.137	12.616	3.408	11.108	-11.793
89	AC	264	268.321	1.683	12.693	3.471	12.649	-10.523
89	AC	265	273.662	3.026	12.766	3.520	11.387	-12.051
89	AC	266	280.462	1.568	12.836	3.556	12.923	-10.778
89	AC	267	285.923	2.906	12.901	3.577	11.658	-12.305
89	AC	268	292.849	1.441	12.964	3.585	13.193	-11.033
89	AC	269	298.443	2.773	13.024	3.580	11.929	-12.562
89	AC	270	305.509	1.301	13.081	3.561	13.465	-11.293
89	AC	271	311.251	2.626	13.136	3.529	12.203	-12.826
89	AC	272	318.472	1.147	13.190	3.485	13.743	-11.562
	ATOM		M - A	NEUTRON	PROTON	ALPHA	Q BETA -	Q BETA +
90	TH	180	193.647	16.504	-6.645	-13.822	-25.266	19.656
90	TH	181	187.856	14.159	-6.280	-13.396	-22.556	20.724
90	TH	182	180.652	15.571	-5.936	-13.147	-23.084	18.584
90	TH	183	175.235	13.784	-5.582	-12.712	-20.942	19.646
90	TH	184	168.424	15.179	-5.249	-12.396	-21.975	17.554
90	TH	185	163.362	13.429	-4.908	-12.027	-19.881	18.609
90	TH	186	156.926	14.804	-4.587	-11.718	-20.906	16.562
90	TH	187	152.209	13.084	-4.260	-11.364	-18.855	17.607
90	TH	188	146.141	14.436	-3.953	-11.073	-19.871	15.600
90	TH	189	141.766	12.742	-3.641	-10.745	-17.860	16.634
90	TH	190	136.064	14.069	-3.347	-10.482	-18.866	14.663
90	TH	191	132.037	12.395	-3.050	-10.190	-16.889	15.685
90	TH	192	126.708	13.696	-2.772	-9.963	-17.884	13.746
90	TH	193	123.038	12.038	-2.491	-9.713	-15.939	14.756
90	TH	194	118.094	13.311	-2.228	-9.528	-16.922	12.847
90	TH	195	114.795	11.666	-1.963	-9.325	-15.005	13.844
90	TH	196	110.250	12.912	-1.715	-9.187	-15.977	11.962
90	TH	197	107.339	11.279	-1.466	-9.033	-14.087	12.949
90	TH	198	103.208	12.499	-1.233	-8.941	-15.049	11.092
90	TH	199	100.700	10.875	-.999	-8.837	-13.184	12.070
90	TH	200	96.995	12.072	-.781	-8.790	-14.138	10.238
90	TH	201	94.904	10.458	-.562	-8.731	-12.298	11.210
90	TH	202	91.636	11.635	-.358	-8.724	-13.248	9.403
90	TH	203	89.972	10.032	-.153	-8.706	-11.431	10.372
90	TH	204	87.146	11.193	.039	-8.733	-12.380	8.589
90	TH	205	85.911	9.602	.230	-8.747	-10.589	9.559
90	TH	206	83.526	10.752	.411	-8.800	-11.539	7.802
90	TH	207	82.718	9.175	.591	-8.840	-9.774	8.776
90	TH	208	80.766	10.319	.761	-8.909	-10.730	7.044
90	TH	209	80.377	8.757	.931	-8.964	-8.991	8.025
90	TH	210	78.845	9.899	1.092	-9.041	-9.956	6.319
90	TH	211	78.858	8.355	1.253	-9.101	-8.242	7.309
90	TH	212	77.725	9.500	1.408	-9.177	-9.219	5.628
90	TH	213	78.120	7.973	1.563	-9.234	-7.531	6.629
90	TH	214	77.363	9.124	1.712	-9.300	-8.522	4.971
90	TH	215	78.114	7.616	1.862	-9.347	-6.858	5.985
90	TH	216	77.705	8.777	2.009	-9.396	-7.863	4.058
90	TH	217	78.857	7.215	2.375	-9.497	-6.149	4.859
90	TH	218	78.845	8.380	2.738	-9.603	-6.953	3.008
90	TH	219	80.321	6.891	3.100	-9.188	-5.106	3.811
90	TH	220	80.598	8.090	3.497	-8.745	-5.986	1.890

TABLE 2

Atomic mass excesses and nuclear binding energies

90	TH	221	82.438	6.527	3.854	-8.378	-4.069	2.772
90	TH	222	83.042	7.764	4.209	-7.942	-4.954	.858
90	TH	223	85.209	6.200	4.560	-7.586	-3.042	1.747
90	TH	224	86.140	7.437	4.907	-7.199	-3.934	-.159
90	TH	225	88.633	5.874	5.250	-6.818	-2.029	.740
90	TH	226	89.888	7.112	5.589	-6.443	-2.929	-1.155
90	TH	227	92.705	5.551	5.924	-6.075	-1.034	-.245
90	TH	228	94.281	6.791	6.253	-5.713	-1.945	-2.128
90	TH	229	97.416	5.232	6.577	-5.359	-.062	-1.203
90	TH	230	99.308	6.476	6.896	-5.011	-.985	-3.071
90	TH	231	102.754	4.921	7.209	-4.670	.884	-2.130
90	TH	232	104.953	6.168	7.516	-4.335	-.055	-3.981
90	TH	233	108.702	4.619	7.817	-4.008	1.797	-3.022
90	TH	234	111.198	5.872	8.111	-3.687	.841	-4.853
90	TH	235	115.237	4.328	8.398	-3.373	2.675	-3.874
90	TH	236	118.017	5.588	8.679	-3.065	1.700	-5.684
90	TH	237	122.333	4.051	8.952	-2.764	3.514	-4.683
90	TH	238	125.381	5.319	9.219	-2.469	2.517	-6.470
90	TH	239	129.958	3.790	9.478	-2.180	4.309	-5.445
90	TH	240	133.259	5.066	9.729	-1.898	3.290	-7.209
90	TH	241	138.080	3.547	9.973	-1.622	5.059	-6.160
90	TH	242	141.615	4.832	10.209	-1.352	4.017	-7.899
90	TH	243	146.661	3.321	10.438	-1.088	5.762	-6.825
90	TH	244	150.413	4.616	10.659	-.830	4.695	-8.539
90	TH	245	155.665	3.115	10.872	-.579	6.416	-7.441
90	TH	246	159.614	4.418	11.077	-.334	5.325	-9.130
90	TH	247	165.055	2.927	11.274	-.096	7.022	-8.007
90	TH	248	169.183	4.239	11.464	.135	5.908	-9.672
90	TH	249	174.794	2.756	11.646	.359	7.581	-8.526
90	TH	250	179.084	4.077	11.820	.576	6.443	-10.168
90	TH	251	184.850	2.602	11.987	.785	8.093	-8.999
90	TH	252	189.286	3.931	12.147	.986	6.933	-10.619
90	TH	253	195.191	2.462	12.299	1.178	8.563	-9.429
90	TH	254	199.762	3.797	12.444	1.362	7.382	-11.030
90	TH	255	205.795	2.334	12.582	1.537	8.993	-9.822
90	TH	256	210.488	3.674	12.713	1.702	7.794	-11.405
90	TH	257	216.640	2.215	12.838	1.857	9.387	-10.181
90	TH	258	221.449	3.558	12.957	2.001	8.172	-11.749
90	TH	259	227.714	2.102	13.069	2.135	9.750	-10.511
90	TH	260	232.634	3.447	13.176	2.257	8.521	-12.067
90	TH	261	239.010	1.992	13.277	2.368	10.087	-10.819
90	TH	262	244.041	3.336	13.372	2.467	8.848	-12.365
90	TH	263	250.528	1.880	13.463	2.554	10.404	-11.108
90	TH	264	255.672	3.223	13.549	2.628	9.156	-12.649
90	TH	265	262.275	1.764	13.630	2.690	10.705	-11.387
90	TH	266	267.539	3.104	13.708	2.738	9.452	-12.923
90	TH	267	274.265	1.641	13.782	2.774	10.997	-11.658
90	TH	268	279.656	2.976	13.852	2.797	9.741	-13.193
90	TH	269	286.515	1.509	13.919	2.807	11.285	-11.929
90	TH	270	292.044	2.838	13.984	2.805	10.028	-13.465
90	TH	271	299.048	1.364	14.046	2.790	11.572	-12.203
90	TH	272	304.729	2.686	14.107	2.763	10.317	-13.743
90	TH	273	311.891	1.205	14.166	2.724	11.864	-12.485
	ATOM		M - A	NEUTRON	PROTON	ALPHA	Q BETA -	Q BETA +
91	PA	182	203.736	15.043	-8.296	-13.380	-22.218	23.084
91	PA	183	196.178	15.926	-7.941	-13.151	-22.746	20.942
91	PA	184	190.398	14.147	-7.578	-12.798	-20.126	21.975
91	PA	185	183.243	15.522	-7.235	-12.502	-21.157	19.881
91	PA	186	177.832	13.779	-6.885	-12.154	-19.087	20.906
91	PA	187	171.065	15.134	-6.554	-11.866	-20.110	18.855

TABLE 2

Atomic mass excesses and nuclear binding energies

91	PA	188	166.012	13.420	-6.218	-11.534	-18.081	19.871
91	PA	189	159.626	14.753	-5.901	-11.263	-19.094	17.860
91	PA	190	154.930	13.063	-5.579	-10.957	-17.102	18.866
91	PA	191	148.926	14.372	-5.277	-10.714	-18.103	16.889
91	PA	192	144.592	12.701	-4.971	-10.442	-16.143	17.884
91	PA	193	138.977	13.983	-4.683	-10.235	-17.132	15.939
91	PA	194	135.016	12.328	-4.393	-10.005	-15.201	16.922
91	PA	195	129.800	13.583	-4.121	-9.840	-16.178	15.005
91	PA	196	126.227	11.940	-3.847	-9.656	-14.273	15.977
91	PA	197	121.426	13.169	-3.591	-9.535	-15.238	14.087
91	PA	198	118.257	11.537	-3.333	-9.400	-13.358	15.049
91	PA	199	113.883	12.740	-3.091	-9.324	-14.313	13.184
91	PA	200	111.134	11.117	-2.849	-9.236	-12.455	14.138
91	PA	201	107.202	12.299	-2.622	-9.203	-13.402	12.298
91	PA	202	104.884	10.685	-2.395	-9.159	-11.568	13.248
91	PA	203	101.403	11.848	-2.182	-9.164	-12.509	11.431
91	PA	204	99.526	10.245	-1.969	-9.159	-10.698	12.380
91	PA	205	96.500	11.393	-1.769	-9.196	-11.638	10.589
91	PA	206	95.065	9.802	-1.570	-9.222	-9.850	11.539
91	PA	207	92.492	10.941	-1.382	-9.283	-10.792	9.774
91	PA	208	91.497	9.363	-1.194	-9.331	-9.028	10.730
91	PA	209	89.367	10.496	-1.016	-9.407	-9.976	8.991
91	PA	210	88.801	8.934	-.839	-9.468	-8.237	9.956
91	PA	211	87.100	10.068	-.670	-9.549	-9.195	8.242
91	PA	212	86.945	8.523	-.502	-9.613	-7.481	9.219
91	PA	213	85.651	9.661	-.341	-9.690	-8.450	7.531
91	PA	214	85.884	8.134	-.180	-9.749	-6.761	8.522
91	PA	215	84.972	9.280	-.024	-9.814	-7.744	6.858
91	PA	216	85.567	7.772	.131	-9.860	-6.078	7.863
91	PA	217	85.006	8.929	.284	-9.906	-7.077	6.149
91	PA	218	85.797	7.576	.644	-9.796	-5.570	6.953
91	PA	219	85.427	8.738	1.002	-9.689	-6.378	5.106
91	PA	220	86.585	7.210	1.321	-9.329	-4.462	5.986
91	PA	221	86.508	8.444	1.675	-8.901	-5.347	4.069
91	PA	222	87.996	6.879	2.027	-8.551	-3.434	4.954
91	PA	223	88.252	8.112	2.375	-8.132	-4.322	3.042
91	PA	224	90.073	6.546	2.721	-7.756	-2.413	3.934
91	PA	225	90.662	7.779	3.062	-7.387	-3.308	2.029
91	PA	226	92.817	6.212	3.400	-7.024	-1.405	2.929
91	PA	227	93.739	7.446	3.734	-6.667	-2.307	1.034
91	PA	228	96.226	5.880	4.063	-6.318	-.413	1.945
91	PA	229	97.478	7.116	4.388	-5.976	-1.325	.062
91	PA	230	100.293	5.552	4.708	-5.640	.558	.985
91	PA	231	101.871	6.790	5.022	-5.312	-.366	-.884
91	PA	232	105.009	5.229	5.331	-4.991	1.504	.055
91	PA	233	106.905	6.471	5.633	-4.676	.566	-1.797
91	PA	234	110.357	4.915	5.930	-4.369	2.420	-.841
91	PA	235	112.562	6.162	6.221	-4.068	1.466	-2.675
91	PA	236	116.317	4.612	6.505	-3.774	3.303	-1.700
91	PA	237	118.819	5.865	6.783	-3.486	2.330	-3.514
91	PA	238	122.864	4.322	7.053	-3.204	4.148	-2.517
91	PA	239	125.649	5.583	7.317	-2.929	3.155	-4.309
91	PA	240	129.969	4.047	7.574	-2.659	4.951	-3.290
91	PA	241	133.020	5.316	7.824	-2.396	3.937	-5.059
91	PA	242	137.598	3.789	8.066	-2.138	5.711	-4.017
91	PA	243	140.899	5.067	8.301	-1.886	4.674	-5.762
91	PA	244	145.717	3.549	8.529	-1.640	6.426	-4.695
91	PA	245	149.249	4.836	8.749	-1.400	5.365	-6.416
91	PA	246	154.289	3.327	8.961	-1.165	7.093	-5.325
91	PA	247	158.032	4.624	9.166	-.937	6.009	-7.022
91	PA	248	163.275	3.124	9.364	-.714	7.714	-5.908
91	PA	249	167.213	4.430	9.554	-.498	6.607	-7.581

TABLE 2

Atomic mass excesses and nuclear binding energies

91	PA	250	172.642	2.939	9.737	-.288	8.288	-6.443
91	PA	251	176.756	4.253	9.913	-.085	7.158	-8.093
91	PA	252	182.353	2.771	10.081	.112	8.818	-6.933
91	PA	253	186.628	4.092	10.243	.301	7.666	-8.563
91	PA	254	192.379	2.617	10.397	.482	9.305	-7.382
91	PA	255	196.802	3.945	10.544	.655	8.134	-8.993
91	PA	256	202.694	2.475	10.685	.820	9.753	-7.794
91	PA	257	207.253	3.808	10.820	.977	8.564	-9.387
91	PA	258	213.277	2.344	10.948	1.124	10.166	-8.172
91	PA	259	217.964	3.680	11.070	1.262	8.961	-9.750
91	PA	260	224.113	2.218	11.186	1.390	10.549	-8.521
91	PA	261	228.923	3.557	11.296	1.507	9.330	-10.087
91	PA	262	235.193	2.097	11.401	1.614	10.905	-8.848
91	PA	263	240.124	3.436	11.501	1.710	9.675	-10.404
91	PA	264	246.516	1.975	11.596	1.794	11.241	-9.156
91	PA	265	251.570	3.314	11.687	1.867	10.003	-10.705
91	PA	266	258.087	1.851	11.773	1.929	11.562	-9.452
91	PA	267	263.268	3.186	11.856	1.978	10.318	-10.997
91	PA	268	269.915	1.720	11.935	2.016	11.872	-9.741
91	PA	269	275.230	3.052	12.010	2.041	10.625	-11.285
91	PA	270	282.016	1.581	12.083	2.055	12.177	-10.028
91	PA	271	287.476	2.908	12.153	2.057	10.929	-11.572
91	PA	272	294.411	1.432	12.221	2.047	12.482	-10.317
91	PA	273	300.026	2.752	12.287	2.026	11.235	-11.864
91	PA	274	307.124	1.270	12.352	1.995	12.790	-10.613
	ATOM		M - A	NEUTRON	PROTON	ALPHA	Q BETA -	Q BETA +
92	U	184	210.524	16.767	-6.762	-13.268	-25.556	20.126
92	U	185	204.400	14.491	-6.417	-12.935	-22.936	21.157
92	U	186	196.919	15.848	-6.091	-12.658	-23.439	19.087
92	U	187	191.175	14.112	-5.758	-12.330	-21.368	20.110
92	U	188	184.093	15.449	-5.444	-12.060	-22.364	18.081
92	U	189	178.720	13.741	-5.123	-11.748	-20.333	19.094
92	U	190	172.032	15.055	-4.821	-11.496	-21.319	17.102
92	U	191	167.029	13.370	-4.514	-11.210	-19.323	18.103
92	U	192	160.735	14.661	-4.225	-10.985	-20.299	16.143
92	U	193	156.109	12.994	-3.932	-10.733	-18.334	17.132
92	U	194	150.217	14.259	-3.656	-10.544	-19.298	15.201
92	U	195	145.978	12.606	-3.377	-10.332	-17.362	16.178
92	U	196	140.501	13.845	-3.116	-10.183	-18.314	14.273
92	U	197	136.664	12.204	-2.852	-10.017	-16.403	15.238
92	U	198	131.615	13.417	-2.604	-9.911	-17.344	13.358
92	U	199	128.196	11.786	-2.355	-9.792	-15.457	14.313
92	U	200	123.589	12.975	-2.121	-9.729	-16.389	12.455
92	U	201	120.604	11.352	-1.886	-9.656	-14.524	13.402
92	U	202	116.452	12.520	-1.665	-9.635	-15.449	11.568
92	U	203	113.912	10.907	-1.444	-9.603	-13.606	12.509
92	U	204	110.223	12.057	-1.235	-9.619	-14.527	10.698
92	U	205	108.137	10.453	-1.027	-9.624	-12.707	11.638
92	U	206	104.915	11.590	-.830	-9.669	-13.628	9.850
92	U	207	103.284	9.998	-.634	-9.703	-11.831	10.792
92	U	208	100.525	11.127	-.448	-9.770	-12.755	9.028
92	U	209	99.344	9.548	-.262	-9.824	-10.983	9.976
92	U	210	97.038	10.673	-.085	-9.903	-11.915	8.237
92	U	211	96.295	9.111	.091	-9.967	-10.168	9.195
92	U	212	94.425	10.237	.260	-10.049	-11.111	7.481
92	U	213	94.101	8.691	.428	-10.115	-9.389	8.450
92	U	214	92.645	9.823	.591	-10.191	-10.346	6.761
92	U	215	92.716	8.296	.753	-10.249	-8.649	7.744
92	U	216	91.645	9.438	.911	-10.311	-9.622	6.078
92	U	217	92.083	7.930	1.069	-10.354	-7.950	7.077

TABLE 2

Atomic mass excesses and nuclear binding energies

92	U	218	91.367	9.084	1.224	-10.395	-8.940	5.570
92	U	219	91.805	7.929	1.577	-10.082	-7.625	6.378
92	U	220	91.047	9.126	1.965	-9.733	-8.514	4.462
92	U	221	91.854	7.560	2.315	-9.388	-6.603	5.347
92	U	222	91.430	8.792	2.662	-8.976	-7.493	3.434
92	U	223	92.574	7.223	3.007	-8.643	-5.584	4.322
92	U	224	92.487	8.454	3.350	-8.279	-6.477	2.413
92	U	225	93.970	6.885	3.689	-7.922	-4.572	3.308
92	U	226	94.223	8.114	4.024	-7.571	-5.470	1.405
92	U	227	96.046	6.544	4.356	-7.227	-3.570	2.307
92	U	228	96.639	7.774	4.684	-6.890	-4.475	.413
92	U	229	98.803	6.204	5.008	-6.561	-2.583	1.325
92	U	230	99.735	7.435	5.327	-6.238	-3.496	-.558
92	U	231	102.237	5.866	5.641	-5.923	-1.614	.366
92	U	232	103.505	7.099	5.951	-5.615	-2.539	-1.504
92	U	233	106.339	5.533	6.255	-5.314	-.669	-.566
92	U	234	107.937	6.770	6.553	-5.020	-1.607	-2.420
92	U	235	111.096	5.208	6.846	-4.732	.249	-1.466
92	U	236	113.014	6.449	7.132	-4.452	-.704	-3.303
92	U	237	116.489	4.893	7.413	-4.178	1.134	-2.330
92	U	238	118.717	6.140	7.687	-3.910	.164	-4.148
92	U	239	122.494	4.590	7.955	-3.648	1.984	-3.155
92	U	240	125.018	5.844	8.216	-3.392	.995	-4.951
92	U	241	129.083	4.302	8.470	-3.141	2.795	-3.937
92	U	242	131.887	5.564	8.718	-2.897	1.785	-5.711
92	U	243	136.225	4.030	8.959	-2.657	3.564	-4.674
92	U	244	139.292	5.300	9.192	-2.423	2.533	-6.426
92	U	245	143.883	3.776	9.419	-2.194	4.289	-5.365
92	U	246	147.195	5.055	9.638	-1.971	3.235	-7.093
92	U	247	152.023	3.540	9.850	-1.753	4.969	-6.009
92	U	248	155.562	4.829	10.056	-1.540	3.892	-7.714
92	U	249	160.607	3.322	10.254	-1.332	5.604	-6.607
92	U	250	164.353	4.621	10.445	-1.130	4.504	-8.288
92	U	251	169.598	3.123	10.629	-.934	6.193	-7.158
92	U	252	173.535	4.430	10.806	-.743	5.072	-8.818
92	U	253	178.962	2.941	10.976	-.559	6.739	-7.666
92	U	254	183.074	4.255	11.139	-.381	5.597	-9.305
92	U	255	188.668	2.773	11.296	-.210	7.244	-8.134
92	U	256	192.941	4.095	11.446	-.045	6.082	-9.753
92	U	257	198.689	2.619	11.589	.111	7.710	-8.564
92	U	258	203.111	3.946	11.727	.260	6.531	-10.166
92	U	259	209.003	2.475	11.859	.401	8.143	-8.961
92	U	260	213.564	3.806	11.984	.533	6.947	-10.549
92	U	261	219.593	2.339	12.105	.656	8.544	-9.330
92	U	262	224.288	3.672	12.219	.770	7.335	-10.905
92	U	263	230.449	2.207	12.329	.874	8.921	-9.675
92	U	264	235.275	3.541	12.434	.968	7.701	-11.241
92	U	265	241.567	2.076	12.534	1.052	9.276	-10.003
92	U	266	246.525	3.410	12.630	1.125	8.048	-11.562
92	U	267	252.950	1.943	12.722	1.187	9.617	-10.318
92	U	268	258.043	3.275	12.810	1.239	8.382	-11.872
92	U	269	264.605	1.805	12.894	1.280	9.946	-10.625
92	U	270	269.839	3.133	12.976	1.309	8.708	-12.177
92	U	271	276.546	1.660	13.054	1.328	10.270	-10.929
92	U	272	281.930	2.984	13.131	1.335	9.031	-12.482
92	U	273	288.791	1.506	13.205	1.332	10.592	-11.235
92	U	274	294.334	2.824	13.277	1.319	9.354	-12.790
92	U	275	301.361	1.340	13.347	1.296	10.917	-11.546
	ATOM		M - A	NEUTRON	PROTON	ALPHA	Q BETA -	Q BETA +
93	NP	204	124.750	11.136	-3.253	-10.007	-12.884	14.527

TABLE 2

Atomic mass excesses and nuclear binding energies

93	NP	205	120.844	12.273	-3.036	-10.033	-13.797	12.707
93	NP	206	118.542	10.669	-2.820	-10.049	-11.980	13.628
93	NP	207	115.115	11.795	-2.616	-10.103	-12.892	11.831
93	NP	208	113.280	10.202	-2.411	-10.145	-11.097	12.755
93	NP	209	110.327	11.321	-2.218	-10.218	-12.013	10.983
93	NP	210	108.953	9.742	-2.024	-10.278	-10.241	11.915
93	NP	211	106.462	10.858	-1.840	-10.361	-11.165	10.168
93	NP	212	105.536	9.294	-1.656	-10.430	-9.416	11.111
93	NP	213	103.490	10.413	-1.480	-10.513	-10.351	9.389
93	NP	214	102.991	8.867	-1.305	-10.581	-8.627	10.346
93	NP	215	101.365	9.993	-1.135	-10.656	-9.576	8.649
93	NP	216	101.268	8.465	-.967	-10.714	-7.876	9.622
93	NP	217	100.033	9.602	-.803	-10.773	-8.842	7.950
93	NP	218	100.307	8.093	-.639	-10.814	-7.164	8.940
93	NP	219	99.430	9.244	-.478	-10.849	-8.148	7.625
93	NP	220	99.560	8.237	-.170	-10.383	-6.939	8.514
93	NP	221	98.457	9.470	.174	-9.842	-7.834	6.603
93	NP	222	98.923	7.902	.517	-9.516	-5.929	7.493
93	NP	223	98.158	9.132	.857	-9.122	-6.825	5.584
93	NP	224	98.964	7.561	1.195	-8.770	-4.921	6.477
93	NP	225	98.542	8.790	1.530	-8.425	-5.819	4.572
93	NP	226	99.692	7.217	1.862	-8.087	-3.919	5.470
93	NP	227	99.616	8.443	2.191	-7.755	-4.820	3.570
93	NP	228	101.114	6.870	2.517	-7.431	-2.925	4.475
93	NP	229	101.386	8.096	2.838	-7.114	-3.832	2.583
93	NP	230	103.232	6.522	3.156	-6.805	-1.943	3.496
93	NP	231	103.851	7.748	3.469	-6.503	-2.859	1.614
93	NP	232	106.044	6.175	3.778	-6.209	-.979	2.539
93	NP	233	107.008	7.403	4.082	-5.921	-1.904	.669
93	NP	234	109.543	5.832	4.380	-5.641	-.035	1.607
93	NP	235	110.847	7.063	4.674	-5.367	-.973	-.249
93	NP	236	113.719	5.496	4.962	-5.101	.882	.704
93	NP	237	115.355	6.731	5.244	-4.841	-.070	-1.134
93	NP	238	118.553	5.169	5.521	-4.587	1.770	-.164
93	NP	239	120.510	6.410	5.792	-4.339	.802	-1.984
93	NP	240	124.023	4.854	6.056	-4.096	2.624	-.995
93	NP	241	126.288	6.102	6.314	-3.860	1.637	-2.795
93	NP	242	130.102	4.553	6.566	-3.629	3.441	-1.785
93	NP	243	132.660	5.809	6.812	-3.402	2.435	-3.564
93	NP	244	136.759	4.269	7.050	-3.181	4.218	-2.533
93	NP	245	139.594	5.533	7.282	-2.964	3.191	-4.289
93	NP	246	143.960	4.001	7.508	-2.753	4.953	-3.235
93	NP	247	147.054	5.274	7.726	-2.545	3.904	-4.969
93	NP	248	151.669	3.752	7.938	-2.343	5.644	-3.892
93	NP	249	155.003	5.034	8.144	-2.145	4.573	-5.604
93	NP	250	159.849	3.521	8.342	-1.951	6.292	-4.504
93	NP	251	163.404	4.812	8.534	-1.763	5.199	-6.193
93	NP	252	168.464	3.308	8.719	-1.579	6.896	-5.072
93	NP	253	172.223	4.608	8.897	-1.400	5.782	-6.739
93	NP	254	177.478	3.113	9.069	-1.227	7.458	-5.597
93	NP	255	181.424	4.421	9.235	-1.059	6.323	-7.244
93	NP	256	186.859	2.933	9.394	-.897	7.979	-6.082
93	NP	257	190.979	4.248	9.547	-.741	6.826	-7.710
93	NP	258	196.580	2.766	9.694	-.592	8.464	-6.531
93	NP	259	200.860	4.087	9.835	-.449	7.294	-8.143
93	NP	260	206.617	2.611	9.971	-.314	8.915	-6.947
93	NP	261	211.049	3.936	10.100	-.186	7.729	-8.544
93	NP	262	216.953	2.463	10.225	-.066	9.336	-7.335
93	NP	263	221.528	3.792	10.345	.045	8.137	-8.921
93	NP	264	227.574	2.321	10.459	.148	9.733	-7.701
93	NP	265	232.291	3.651	10.569	.241	8.523	-9.276
93	NP	266	238.477	2.181	10.675	.326	10.108	-8.048

TABLE 2

Atomic mass excesses and nuclear binding energies

93	NP	267	243.333	3.511	10.777	.400	8.890	-9.617
93	NP	268	249.660	2.040	10.874	.465	10.468	-8.382
93	NP	269	254.659	3.369	10.968	.520	9.244	-9.946
93	NP	270	261.131	1.896	11.059	.565	10.818	-8.708
93	NP	271	266.277	3.221	11.147	.600	9.590	-10.270
93	NP	272	272.899	1.745	11.232	.625	11.161	-9.031
93	NP	273	278.199	3.067	11.315	.640	9.931	-10.592
93	NP	274	284.981	1.586	11.396	.645	11.501	-9.354
93	NP	275	290.444	2.903	11.475	.640	10.272	-10.917
93	NP	276	297.394	1.418	11.552	.627	11.844	-9.681
	ATOM		M - A	NEUTRON	PROTON	ALPHA	Q BETA -	Q BETA +
94	PU	207	128.007	10.882	-1.880	-10.486	-13.976	12.892
94	PU	208	124.377	11.997	-1.678	-10.545	-14.870	11.097
94	PU	209	122.340	10.405	-1.475	-10.594	-13.067	12.013
94	PU	210	119.194	11.514	-1.282	-10.670	-13.967	10.241
94	PU	211	117.627	9.934	-1.090	-10.734	-12.186	11.165
94	PU	212	114.952	11.043	-.905	-10.818	-13.095	9.416
94	PU	213	113.841	9.478	-.720	-10.888	-11.338	10.351
94	PU	214	111.617	10.591	-.543	-10.970	-12.259	8.627
94	PU	215	110.941	9.044	-.365	-11.037	-10.527	9.576
94	PU	216	109.143	10.165	-.193	-11.109	-11.465	7.876
94	PU	217	108.874	8.636	-.022	-11.164	-9.757	8.842
94	PU	218	107.471	9.770	.146	-11.217	-10.713	7.164
94	PU	219	107.579	8.260	.313	-11.253	-9.029	8.148
94	PU	220	106.499	9.447	.516	-11.244	-10.080	6.939
94	PU	221	106.291	8.575	.854	-10.598	-9.037	7.834
94	PU	222	104.852	9.807	1.190	-9.876	-9.939	5.929
94	PU	223	104.983	8.236	1.525	-9.568	-8.041	6.825
94	PU	224	103.885	9.465	1.858	-9.229	-8.943	4.921
94	PU	225	104.361	7.892	2.188	-8.897	-7.046	5.819
94	PU	226	103.611	9.117	2.516	-8.572	-7.949	3.919
94	PU	227	104.436	7.542	2.841	-8.253	-6.054	4.820
94	PU	228	104.039	8.765	3.162	-7.943	-6.960	2.925
94	PU	229	105.218	7.188	3.481	-7.639	-5.069	3.832
94	PU	230	105.175	8.410	3.796	-7.343	-5.980	1.943
94	PU	231	106.710	6.833	4.107	-7.055	-4.095	2.859
94	PU	232	107.022	8.055	4.414	-6.774	-5.013	.979
94	PU	233	108.912	6.477	4.716	-6.500	-3.135	1.904
94	PU	234	109.579	7.701	5.014	-6.234	-4.063	.035
94	PU	235	111.820	6.125	5.307	-5.975	-2.195	.973
94	PU	236	112.836	7.352	5.596	-5.722	-3.134	-.882
94	PU	237	115.424	5.779	5.879	-5.476	-1.279	.070
94	PU	238	116.782	7.009	6.157	-5.237	-2.231	-1.770
94	PU	239	119.708	5.442	6.429	-5.003	-.391	-.802
94	PU	240	121.398	6.677	6.696	-4.775	-1.358	-2.624
94	PU	241	124.651	5.115	6.957	-4.552	.466	-1.637
94	PU	242	126.661	6.357	7.212	-4.335	-.519	-3.441
94	PU	243	130.226	4.803	7.461	-4.122	1.288	-2.435
94	PU	244	132.541	6.052	7.704	-3.914	.284	-4.218
94	PU	245	136.403	4.505	7.941	-3.711	2.071	-3.191
94	PU	246	139.008	5.763	8.171	-3.511	1.048	-4.953
94	PU	247	143.150	4.225	8.395	-3.316	2.815	-3.904
94	PU	248	146.025	5.492	8.613	-3.125	1.771	-5.644
94	PU	249	150.430	3.963	8.825	-2.937	3.517	-4.573
94	PU	250	153.558	5.239	9.030	-2.753	2.452	-6.292
94	PU	251	158.206	3.720	9.229	-2.573	4.177	-5.199
94	PU	252	161.568	5.005	9.421	-2.397	3.091	-6.896
94	PU	253	166.441	3.494	9.607	-2.225	4.794	-5.782
94	PU	254	170.020	4.788	9.788	-2.058	3.688	-7.458
94	PU	255	175.101	3.286	9.961	-1.894	5.372	-6.323

TABLE 2

Atomic mass excesses and nuclear binding energies

94	PU	256	178.880	4.589	10.129	-1.735	4.246	-7.979
94	PU	257	184.153	3.094	10.291	-1.581	5.910	-6.826
94	PU	258	188.116	4.404	10.448	-1.433	4.766	-8.464
94	PU	259	193.567	2.917	10.598	-1.289	6.413	-7.294
94	PU	260	197.702	4.232	10.743	-1.152	5.251	-8.915
94	PU	261	203.319	2.750	10.883	-1.021	6.882	-7.729
94	PU	262	207.616	4.071	11.017	-.896	5.706	-9.336
94	PU	263	213.391	2.593	11.147	-.779	7.323	-8.137
94	PU	264	217.842	3.916	11.271	-.668	6.134	-9.733
94	PU	265	223.768	2.441	11.391	-.566	7.739	-8.523
94	PU	266	228.368	3.767	11.507	-.471	6.540	-10.108
94	PU	267	234.443	2.293	11.618	-.385	8.135	-8.890
94	PU	268	239.192	3.619	11.726	-.307	6.927	-10.468
94	PU	269	245.415	2.144	11.830	-.239	8.516	-9.244
94	PU	270	250.313	3.469	11.931	-.179	7.302	-10.818
94	PU	271	256.687	1.993	12.028	-.128	8.885	-9.590
94	PU	272	261.738	3.316	12.123	-.087	7.667	-11.161
94	PU	273	268.268	1.837	12.215	-.054	9.248	-9.921
94	PU	274	273.479	3.157	12.305	-.031	8.028	-11.501
94	PU	275	280.172	1.674	12.393	-.017	9.608	-10.272
94	PU	276	285.550	2.990	12.479	-.011	8.389	-11.844
94	PU	277	292.415	1.503	12.564	-.014	9.969	-10.617
	ATOM		M - A	NEUTRON	PROTON	ALPHA	Q BETA -	Q BETA +
95	AM	210	133.161	10.614	-3.236	-11.009	-12.343	13.967
95	AM	211	129.813	11.715	-3.035	-11.089	-13.234	12.186
95	AM	212	128.047	10.134	-2.835	-11.157	-11.452	13.095
95	AM	213	125.179	11.235	-2.642	-11.243	-12.352	11.338
95	AM	214	123.877	9.670	-2.451	-11.315	-10.592	12.259
95	AM	215	121.468	10.776	-2.266	-11.397	-11.505	10.527
95	AM	216	120.608	9.228	-2.082	-11.463	-9.769	11.465
95	AM	217	118.631	10.344	-1.903	-11.532	-10.698	9.757
95	AM	218	118.185	8.814	-1.725	-11.585	-8.985	10.713
95	AM	219	116.607	9.945	-1.551	-11.633	-9.934	9.029
95	AM	220	116.579	8.396	-1.416	-11.702	-8.167	10.080
95	AM	221	115.328	9.618	-1.245	-11.686	-9.212	9.037
95	AM	222	114.791	8.905	-.915	-10.875	-8.322	9.939
95	AM	223	113.024	10.135	-.587	-9.984	-9.231	8.041
95	AM	224	112.828	8.563	-.261	-9.659	-7.340	8.943
95	AM	225	111.407	9.789	.063	-9.340	-8.249	7.046
95	AM	226	111.560	8.214	.386	-9.028	-6.358	7.949
95	AM	227	110.490	9.437	.705	-8.723	-7.268	6.054
95	AM	228	110.999	7.859	1.023	-8.426	-5.378	6.960
95	AM	229	110.287	9.079	1.337	-8.136	-6.290	5.069
95	AM	230	111.155	7.499	1.648	-7.853	-4.403	5.980
95	AM	231	110.804	8.718	1.955	-7.579	-5.319	4.095
95	AM	232	112.035	7.137	2.259	-7.312	-3.437	5.013
95	AM	233	112.047	8.355	2.560	-7.052	-4.359	3.135
95	AM	234	113.641	6.774	2.856	-6.800	-2.485	4.063
95	AM	235	114.016	7.993	3.147	-6.556	-3.415	2.195
95	AM	236	115.970	6.413	3.435	-6.318	-1.550	3.134
95	AM	237	116.704	7.634	3.718	-6.086	-2.490	1.279
95	AM	238	119.014	6.057	3.996	-5.861	-.636	2.231
95	AM	239	120.099	7.282	4.268	-5.642	-1.589	.391
95	AM	240	122.757	5.710	4.536	-5.429	.252	1.358
95	AM	241	124.185	6.940	4.799	-5.221	-.715	-.466
95	AM	242	127.179	5.372	5.056	-5.018	1.110	.519
95	AM	243	128.938	6.609	5.308	-4.819	.127	-1.288
95	AM	244	132.257	5.049	5.554	-4.625	1.935	-.284
95	AM	245	134.332	6.292	5.794	-4.435	.934	-2.071
95	AM	246	137.960	4.740	6.029	-4.248	2.724	-1.048

TABLE 2

Atomic mass excesses and nuclear binding energies

95	AM	247	140.335	5.992	6.257	-4.066	1.705	-2.815
95	AM	248	144.254	4.448	6.480	-3.886	3.475	-1.771
95	AM	249	146.913	5.709	6.697	-3.710	2.436	-3.517
95	AM	250	151.106	4.174	6.908	-3.536	4.187	-2.452
95	AM	251	154.029	5.444	7.114	-3.366	3.128	-4.177
95	AM	252	158.477	3.919	7.313	-3.199	4.858	-3.091
95	AM	253	161.647	5.198	7.506	-3.035	3.779	-4.794
95	AM	254	166.332	3.682	7.694	-2.873	5.489	-3.688
95	AM	255	169.729	4.970	7.876	-2.716	4.390	-5.372
95	AM	256	174.634	3.463	8.052	-2.561	6.081	-4.246
95	AM	257	178.242	4.759	8.222	-2.410	4.963	-5.910
95	AM	258	183.350	3.259	8.387	-2.263	6.636	-4.766
95	AM	259	187.154	4.564	8.547	-2.121	5.500	-6.413
95	AM	260	192.451	3.071	8.701	-1.982	7.156	-5.251
95	AM	261	196.437	4.381	8.850	-1.849	6.003	-6.882
95	AM	262	201.910	2.894	8.994	-1.721	7.644	-5.706
95	AM	263	206.068	4.210	9.133	-1.598	6.477	-7.323
95	AM	264	211.708	2.727	9.268	-1.481	8.104	-6.134
95	AM	265	216.029	4.047	9.398	-1.371	6.925	-7.739
95	AM	266	221.829	2.567	9.524	-1.267	8.540	-6.540
95	AM	267	226.308	3.889	9.646	-1.170	7.350	-8.135
95	AM	268	232.264	2.411	9.763	-1.081	8.956	-6.927
95	AM	269	236.899	3.733	9.878	-.999	7.759	-8.516
95	AM	270	243.011	2.255	9.988	-.925	9.358	-7.302
95	AM	271	247.802	3.577	10.096	-.859	8.154	-8.885
95	AM	272	254.071	2.098	10.201	-.801	9.748	-7.667
95	AM	273	259.020	3.418	10.303	-.752	8.540	-9.248
95	AM	274	265.451	1.937	10.402	-.711	10.131	-8.028
95	AM	275	270.564	3.254	10.500	-.678	8.921	-9.608
95	AM	276	277.162	1.770	10.595	-.654	10.511	-8.389
95	AM	277	282.446	3.083	10.689	-.637	9.301	-9.969
95	AM	278	289.218	1.595	10.782	-.628	10.891	-8.751
	ATOM		M - A	NEUTRON	PROTON	ALPHA	Q BETA -	Q BETA +
96	CM	213	137.531	10.335	-1.900	-11.582	-13.394	12.352
96	CM	214	134.469	11.429	-1.705	-11.666	-14.281	10.592
96	CM	215	132.974	9.863	-1.512	-11.737	-12.512	11.505
96	CM	216	130.377	10.964	-1.324	-11.816	-13.414	9.769
96	CM	217	129.330	9.415	-1.137	-11.879	-11.669	10.698
96	CM	218	127.170	10.527	-.954	-11.943	-12.588	8.985
96	CM	219	126.541	8.996	-.772	-11.991	-10.867	9.934
96	CM	220	124.747	10.162	-.555	-11.994	-11.882	8.167
96	CM	221	124.540	8.574	-.376	-12.057	-10.108	9.212
96	CM	222	123.113	9.795	-.200	-12.032	-11.145	8.322
96	CM	223	122.255	9.225	.121	-11.067	-10.393	9.231
96	CM	224	120.169	10.454	.440	-10.061	-11.310	7.340
96	CM	225	119.656	8.880	.758	-9.755	-9.427	8.249
96	CM	226	117.918	10.105	1.073	-9.457	-10.343	6.358
96	CM	227	117.758	8.528	1.387	-9.166	-8.459	7.268
96	CM	228	116.377	9.749	1.698	-8.882	-9.375	5.378
96	CM	229	116.576	8.168	2.007	-8.606	-7.492	6.290
96	CM	230	115.558	9.386	2.313	-8.338	-8.409	4.403
96	CM	231	116.123	7.802	2.617	-8.077	-6.528	5.319
96	CM	232	115.472	9.018	2.916	-7.825	-7.449	3.437
96	CM	233	116.407	7.433	3.213	-7.580	-5.572	4.359
96	CM	234	116.126	8.648	3.506	-7.342	-6.498	2.485
96	CM	235	117.431	7.063	3.795	-7.112	-4.628	3.415
96	CM	236	117.520	8.278	4.081	-6.889	-5.561	1.550
96	CM	237	119.193	6.694	4.362	-6.672	-3.699	2.490
96	CM	238	119.650	7.911	4.639	-6.462	-4.641	.636
96	CM	239	121.688	6.330	4.911	-6.258	-2.789	1.589

TABLE 2

Atomic mass excesses and nuclear binding energies

96	CM	240	122.505	7.550	5.179	-6.059	-3.743	-.252
96	CM	241	124.900	5.973	5.442	-5.866	-1.903	.715
96	CM	242	126.069	7.198	5.700	-5.678	-2.870	-1.110
96	CM	243	128.811	5.626	5.953	-5.494	-1.045	-.127
96	CM	244	130.322	6.857	6.201	-5.314	-2.027	-1.935
96	CM	245	133.398	5.292	6.444	-5.138	-.217	-.934
96	CM	246	135.235	6.530	6.682	-4.965	-1.216	-2.724
96	CM	247	138.630	4.972	6.914	-4.795	.577	-1.705
96	CM	248	140.779	6.219	7.141	-4.628	-.440	-3.475
96	CM	249	144.477	4.670	7.362	-4.464	1.334	-2.436
96	CM	250	146.919	5.925	7.579	-4.302	.299	-4.187
96	CM	251	150.901	4.385	7.789	-4.142	2.054	-3.128
96	CM	252	153.619	5.650	7.994	-3.985	1.000	-4.858
96	CM	253	157.868	4.119	8.194	-3.829	2.736	-3.779
96	CM	254	160.843	5.393	8.389	-3.676	1.662	-5.489
96	CM	255	165.339	3.871	8.577	-3.525	3.379	-4.390
96	CM	256	168.553	5.154	8.761	-3.376	2.287	-6.081
96	CM	257	173.280	3.641	8.939	-3.229	3.985	-4.963
96	CM	258	176.715	4.932	9.113	-3.085	2.874	-6.636
96	CM	259	181.654	3.428	9.281	-2.944	4.555	-5.500
96	CM	260	185.295	4.726	9.444	-2.806	3.428	-7.156
96	CM	261	190.434	3.229	9.602	-2.672	5.092	-6.003
96	CM	262	194.266	4.535	9.755	-2.541	3.949	-7.644
96	CM	263	199.591	3.043	9.904	-2.414	5.598	-6.477
96	CM	264	203.604	4.354	10.049	-2.292	4.441	-8.104
96	CM	265	209.104	2.867	10.189	-2.175	6.077	-6.925
96	CM	266	213.289	4.182	10.325	-2.063	4.908	-8.540
96	CM	267	218.957	2.699	10.456	-1.957	6.533	-7.350
96	CM	268	223.308	4.017	10.585	-1.857	5.354	-8.956
96	CM	269	229.140	2.535	10.709	-1.763	6.970	-7.759
96	CM	270	233.653	3.854	10.830	-1.676	5.783	-9.358
96	CM	271	239.648	2.373	10.948	-1.595	7.392	-8.154
96	CM	272	244.323	3.692	11.063	-1.522	6.199	-9.748
96	CM	273	250.480	2.210	11.176	-1.456	7.804	-8.540
96	CM	274	255.320	3.528	11.285	-1.398	6.606	-10.131
96	CM	275	261.643	2.044	11.393	-1.347	8.208	-8.921
96	CM	276	266.650	3.360	11.498	-1.303	7.008	-10.511
96	CM	277	273.144	1.873	11.602	-1.267	8.608	-9.301
96	CM	278	278.326	3.186	11.704	-1.238	7.408	-10.891
96	CM	279	284.997	1.696	11.805	-1.216	9.009	-9.683
	ATOM		M - A	NEUTRON	PROTON	ALPHA	Q BETA -	Q BETA +
97	BK	216	143.791	10.063	-3.232	-12.135	-11.777	13.414
97	BK	217	140.998	11.160	-3.037	-12.210	-12.670	11.669
97	BK	218	139.758	9.608	-2.843	-12.271	-10.919	12.588
97	BK	219	137.408	10.717	-2.653	-12.330	-11.830	10.867
97	BK	220	136.628	9.147	-2.503	-12.411	-10.026	11.882
97	BK	221	134.648	10.347	-2.317	-12.408	-11.033	10.108
97	BK	222	134.258	8.758	-2.133	-12.464	-9.252	11.145
97	BK	223	132.648	9.978	-1.950	-12.431	-10.281	10.393
97	BK	224	131.479	9.536	-1.639	-11.290	-9.651	11.310
97	BK	225	129.082	10.764	-1.329	-10.145	-10.577	9.427
97	BK	226	128.261	9.189	-1.020	-9.861	-8.701	10.343
97	BK	227	126.216	10.412	-.714	-9.583	-9.625	8.459
97	BK	228	125.752	8.832	-.409	-9.314	-7.749	9.375
97	BK	229	124.068	10.051	-.106	-9.052	-8.672	7.492
97	BK	230	123.967	8.468	.194	-8.798	-6.796	8.409
97	BK	231	122.651	9.683	.491	-8.552	-7.720	6.528
97	BK	232	122.922	8.097	.786	-8.314	-5.845	7.449
97	BK	233	121.979	9.310	1.078	-8.083	-6.771	5.572
97	BK	234	122.624	7.722	1.367	-7.860	-4.900	6.498

TABLE 2

Atomic mass excesses and nuclear binding energies

97	BK	235	122.058	8.933	1.652	-7.645	-5.831	4.628
97	BK	236	123.081	7.345	1.935	-7.437	-3.964	5.561
97	BK	237	122.892	8.556	2.213	-7.235	-4.901	3.699
97	BK	238	124.291	6.969	2.487	-7.040	-3.042	4.641
97	BK	239	124.476	8.182	2.758	-6.851	-3.988	2.789
97	BK	240	126.248	6.596	3.025	-6.668	-2.138	3.743
97	BK	241	126.803	7.812	3.287	-6.490	-3.094	1.903
97	BK	242	128.940	6.231	3.545	-6.317	-1.255	2.870
97	BK	243	129.856	7.451	3.798	-6.148	-2.223	1.045
97	BK	244	132.348	5.875	4.047	-5.983	-.398	2.027
97	BK	245	133.615	7.101	4.292	-5.821	-1.380	.217
97	BK	246	136.451	5.531	4.531	-5.662	.431	1.216
97	BK	247	138.054	6.765	4.766	-5.506	-.567	-.577
97	BK	248	141.219	5.202	4.996	-5.353	1.228	.440
97	BK	249	143.142	6.444	5.221	-5.201	.213	-1.334
97	BK	250	146.620	4.890	5.441	-5.051	1.991	-.299
97	BK	251	148.847	6.140	5.656	-4.903	.959	-2.054
97	BK	252	152.619	4.595	5.867	-4.756	2.718	-1.000
97	BK	253	155.132	5.855	6.072	-4.610	1.668	-2.736
97	BK	254	159.181	4.319	6.272	-4.466	3.409	-1.662
97	BK	255	161.960	5.588	6.467	-4.322	2.341	-3.379
97	BK	256	166.266	4.061	6.658	-4.180	4.064	-2.287
97	BK	257	169.294	5.339	6.843	-4.039	2.978	-3.985
97	BK	258	173.840	3.822	7.024	-3.899	4.683	-2.874
97	BK	259	177.099	5.108	7.200	-3.761	3.580	-4.555
97	BK	260	181.868	3.599	7.371	-3.624	5.268	-3.428
97	BK	261	185.342	4.893	7.538	-3.490	4.148	-5.092
97	BK	262	190.318	3.391	7.701	-3.358	5.821	-3.949
97	BK	263	193.992	4.693	7.859	-3.229	4.686	-5.598
97	BK	264	199.163	3.197	8.012	-3.103	6.345	-4.441
97	BK	265	203.027	4.504	8.162	-2.980	5.197	-6.077
97	BK	266	208.381	3.013	8.308	-2.861	6.843	-4.908
97	BK	267	212.424	4.324	8.450	-2.747	5.683	-6.533
97	BK	268	217.954	2.837	8.588	-2.637	7.319	-5.354
97	BK	269	222.170	4.152	8.723	-2.532	6.149	-6.970
97	BK	270	227.870	2.667	8.855	-2.432	7.776	-5.783
97	BK	271	232.255	3.983	8.983	-2.338	6.599	-7.392
97	BK	272	238.124	2.499	9.108	-2.250	8.219	-6.199
97	BK	273	242.677	3.815	9.231	-2.168	7.036	-7.804
97	BK	274	248.713	2.331	9.351	-2.093	8.651	-6.606
97	BK	275	253.435	3.646	9.469	-2.024	7.465	-8.208
97	BK	276	259.642	2.160	9.585	-1.962	9.077	-7.008
97	BK	277	264.536	3.474	9.699	-1.907	7.888	-8.608
97	BK	278	270.918	1.986	9.811	-1.858	9.498	-7.408
97	BK	279	275.989	3.296	9.922	-1.816	8.309	-9.009
97	BK	280	282.551	1.806	10.032	-1.780	9.919	-7.810
	ATOM		M - A	NEUTRON	PROTON	ALPHA	Q BETA -	Q BETA +
98	CF	219	149.237	9.806	-1.895	-12.654	-12.825	11.830
98	CF	220	146.654	10.950	-1.662	-12.668	-13.802	10.026
98	CF	221	145.681	9.340	-1.468	-12.743	-11.990	11.033
98	CF	222	143.509	10.539	-1.276	-12.731	-12.989	9.252
98	CF	223	142.929	8.948	-1.086	-12.779	-11.200	10.281
98	CF	224	141.129	10.167	-.897	-12.774	-12.221	9.651
98	CF	225	139.659	9.838	-.596	-11.509	-11.697	10.577
98	CF	226	136.962	11.064	-.295	-10.240	-12.632	8.701
98	CF	227	135.842	9.488	.004	-9.978	-10.765	9.625
98	CF	228	133.500	10.709	.301	-9.723	-11.697	7.749
98	CF	229	132.740	9.128	.596	-9.475	-9.829	8.672
98	CF	230	130.763	10.344	.890	-9.236	-10.760	6.796
98	CF	231	130.371	8.759	1.181	-9.004	-8.891	7.720

TABLE 2

Atomic mass excesses and nuclear binding energies

98	CF	232	128.767	9.972	1.470	-8.781	-9.822	5.845
98	CF	233	128.750	8.383	1.756	-8.565	-7.953	6.771
98	CF	234	127.524	9.594	2.039	-8.357	-8.886	4.900
98	CF	235	127.889	8.003	2.320	-8.157	-7.020	5.831
98	CF	236	127.045	9.211	2.598	-7.964	-7.956	3.964
98	CF	237	127.793	7.619	2.872	-7.777	-6.095	4.901
98	CF	238	127.333	8.828	3.144	-7.598	-7.037	3.042
98	CF	239	128.464	7.236	3.411	-7.424	-5.182	3.988
98	CF	240	128.386	8.446	3.676	-7.256	-6.130	2.138
98	CF	241	129.896	6.857	3.936	-7.094	-4.284	3.094
98	CF	242	130.195	8.069	4.193	-6.936	-5.242	1.255
98	CF	243	132.079	6.483	4.445	-6.782	-3.405	2.223
98	CF	244	132.746	7.700	4.694	-6.632	-4.375	.398
98	CF	245	134.994	6.119	4.939	-6.486	-2.550	1.380
98	CF	246	136.020	7.342	5.179	-6.342	-3.532	-.431
98	CF	247	138.620	5.767	5.415	-6.200	-1.722	.567
98	CF	248	139.991	6.997	5.647	-6.060	-2.718	-1.228
98	CF	249	142.929	5.430	5.875	-5.922	-.923	-.213
98	CF	250	144.629	6.667	6.098	-5.785	-1.935	-1.991
98	CF	251	147.888	5.108	6.316	-5.649	-.156	-.959
98	CF	252	149.901	6.354	6.531	-5.513	-1.184	-2.718
98	CF	253	153.464	4.805	6.740	-5.378	.578	-1.668
98	CF	254	155.772	6.060	6.945	-5.243	-.468	-3.409
98	CF	255	159.619	4.520	7.146	-5.109	1.278	-2.341
98	CF	256	162.202	5.784	7.343	-4.974	.215	-4.064
98	CF	257	166.317	4.253	7.534	-4.839	1.943	-2.978
98	CF	258	169.157	5.527	7.722	-4.705	.863	-4.683
98	CF	259	173.520	4.005	7.905	-4.571	2.574	-3.580
98	CF	260	176.600	5.287	8.084	-4.438	1.478	-5.268
98	CF	261	181.193	3.774	8.259	-4.305	3.173	-4.148
98	CF	262	184.497	5.064	8.430	-4.173	2.061	-5.821
98	CF	263	189.306	3.558	8.596	-4.042	3.742	-4.686
98	CF	264	192.818	4.855	8.759	-3.914	2.616	-6.345
98	CF	265	197.830	3.356	8.918	-3.787	4.283	-5.197
98	CF	266	201.538	4.659	9.073	-3.662	3.144	-6.843
98	CF	267	206.740	3.165	9.225	-3.541	4.800	-5.683
98	CF	268	210.635	4.473	9.373	-3.422	3.650	-7.319
98	CF	269	216.020	2.982	9.518	-3.307	5.295	-6.149
98	CF	270	220.094	4.293	9.660	-3.196	4.136	-7.776
98	CF	271	225.656	2.806	9.799	-3.090	5.773	-6.599
98	CF	272	229.905	4.119	9.935	-2.988	4.606	-8.219
98	CF	273	235.640	2.632	10.068	-2.891	6.236	-7.036
98	CF	274	240.062	3.946	10.199	-2.799	5.064	-8.651
98	CF	275	245.970	2.459	10.328	-2.713	6.690	-7.465
98	CF	276	250.565	3.772	10.454	-2.633	5.514	-9.077
98	CF	277	256.648	2.285	10.579	-2.559	7.137	-7.888
98	CF	278	261.419	3.596	10.701	-2.490	5.959	-9.498
98	CF	279	267.680	2.107	10.823	-2.428	7.580	-8.309
98	CF	280	272.631	3.416	10.942	-2.372	6.401	-9.919
98	CF	281	279.074	1.924	11.061	-2.321	8.022	-8.730
	ATOM		M - A	NEUTRON	PROTON	ALPHA	Q BETA -	Q BETA +
99	ES	222	156.499	9.540	-3.232	-13.132	-11.160	12.989
99	ES	223	154.128	10.738	-3.034	-13.112	-12.151	11.200
99	ES	224	153.351	9.145	-2.837	-13.113	-10.354	12.221
99	ES	225	151.356	10.362	-2.642	-13.099	-11.367	11.697
99	ES	226	149.594	10.130	-2.350	-11.727	-10.933	12.632
99	ES	227	146.607	11.354	-2.060	-10.350	-11.876	10.765
99	ES	228	145.198	9.777	-1.771	-10.110	-10.018	11.697
99	ES	229	142.569	10.996	-1.484	-9.877	-10.959	9.829
99	ES	230	141.523	9.413	-1.198	-9.653	-9.099	10.760

TABLE 2

Atomic mass excesses and nuclear binding energies

99	ES	231	139.262	10.628	-.914	-9.436	-10.038	8.891
99	ES	232	138.588	9.041	-.632	-9.227	-8.177	9.822
99	ES	233	136.704	10.252	-.353	-9.027	-9.115	7.953
99	ES	234	136.410	8.661	-.075	-8.834	-7.254	8.886
99	ES	235	134.909	9.868	.200	-8.649	-8.194	7.020
99	ES	236	135.002	8.275	.472	-8.471	-6.334	7.956
99	ES	237	133.888	9.481	.742	-8.300	-7.276	6.095
99	ES	238	134.370	7.886	1.008	-8.136	-5.420	7.037
99	ES	239	133.646	9.091	1.272	-7.978	-6.367	5.182
99	ES	240	134.516	7.497	1.533	-7.826	-4.516	6.130
99	ES	241	134.180	8.703	1.790	-7.679	-5.469	4.284
99	ES	242	135.437	7.111	2.045	-7.537	-3.626	5.242
99	ES	243	135.484	8.320	2.295	-7.399	-4.587	3.405
99	ES	244	137.121	6.731	2.543	-7.264	-2.753	4.375
99	ES	245	137.545	7.944	2.786	-7.133	-3.725	2.550
99	ES	246	139.553	6.359	3.026	-7.004	-1.902	3.532
99	ES	247	140.342	7.578	3.263	-6.877	-2.885	1.722
99	ES	248	142.710	6.000	3.496	-6.752	-1.075	2.718
99	ES	249	143.852	7.225	3.724	-6.628	-2.071	.923
99	ES	250	146.565	5.655	3.949	-6.504	-.275	1.935
99	ES	251	148.044	6.888	4.170	-6.381	-1.286	.156
99	ES	252	151.086	5.325	4.387	-6.258	.495	1.184
99	ES	253	152.886	6.567	4.600	-6.134	-.531	-.578
99	ES	254	156.239	5.014	4.810	-6.010	1.235	.468
99	ES	255	158.341	6.265	5.015	-5.885	.192	-1.278
99	ES	256	161.988	4.721	5.216	-5.759	1.941	-.215
99	ES	257	164.374	5.981	5.414	-5.632	.883	-1.943
99	ES	258	168.294	4.447	5.607	-5.504	2.616	-.863
99	ES	259	170.945	5.716	5.797	-5.376	1.541	-2.574
99	ES	260	175.122	4.191	5.982	-5.246	3.259	-1.478
99	ES	261	178.020	5.469	6.165	-5.116	2.169	-3.173
99	ES	262	182.435	3.952	6.343	-4.986	3.871	-2.031
99	ES	263	185.564	5.239	6.518	-4.856	2.767	-3.742
99	ES	264	190.202	3.729	6.689	-4.725	4.455	-2.616
99	ES	265	193.546	5.023	6.856	-4.595	3.337	-4.283
99	ES	266	198.394	3.520	7.021	-4.467	5.013	-3.144
99	ES	267	201.941	4.820	7.182	-4.339	3.882	-4.800
99	ES	268	206.986	3.323	7.340	-4.213	5.547	-3.650
99	ES	269	210.725	4.627	7.495	-4.090	4.406	-5.295
99	ES	270	215.959	3.134	7.646	-3.969	6.061	-4.136
99	ES	271	219.884	4.442	7.796	-3.851	4.912	-5.773
99	ES	272	225.299	2.952	7.942	-3.736	6.559	-4.606
99	ES	273	229.404	4.262	8.086	-3.625	5.403	-6.236
99	ES	274	234.998	2.773	8.227	-3.518	7.044	-5.064
99	ES	275	239.280	4.085	8.367	-3.416	5.882	-6.690
99	ES	276	245.051	2.596	8.504	-3.318	7.519	-5.514
99	ES	277	249.511	3.907	8.639	-3.226	6.353	-7.137
99	ES	278	255.461	2.418	8.772	-3.138	7.987	-5.959
99	ES	279	260.100	3.728	8.904	-3.056	6.820	-7.580
99	ES	280	266.230	2.237	9.034	-2.979	8.452	-6.401
99	ES	281	271.052	3.545	9.164	-2.907	7.284	-8.022
99	ES	282	277.368	2.052	9.291	-2.841	8.915	-6.843
	ATOM		M - A	NEUTRON	PROTON	ALPHA	Q BETA -	Q BETA +
100	FM	226	160.527	10.564	-1.586	-13.408	-13.320	10.933
100	FM	227	158.483	10.411	-1.305	-11.945	-12.958	11.876
100	FM	228	155.216	11.635	-1.024	-10.477	-13.911	10.018
100	FM	229	153.528	10.055	-.746	-10.260	-12.062	10.959
100	FM	230	150.622	11.274	-.468	-10.050	-13.012	9.099
100	FM	231	149.300	9.689	-.193	-9.849	-11.160	10.038
100	FM	232	146.765	10.902	.082	-9.655	-12.108	8.177

TABLE 2

Atomic mass excesses and nuclear binding energies

100	FM	233	145.819	9.313	.354	-9.470	-10.255	9.115
100	FM	234	143.665	10.522	.624	-9.292	-11.201	7.254
100	FM	235	143.103	8.929	.892	-9.123	-9.348	8.194
100	FM	236	141.336	10.134	1.158	-8.960	-10.294	6.334
100	FM	237	141.165	8.539	1.422	-8.805	-8.442	7.276
100	FM	238	139.790	9.742	1.683	-8.656	-9.390	5.420
100	FM	239	140.013	8.145	1.942	-8.514	-7.540	6.367
100	FM	240	139.032	9.348	2.198	-8.378	-8.492	4.516
100	FM	241	139.649	7.750	2.451	-8.247	-6.647	5.469
100	FM	242	139.063	8.954	2.702	-8.120	-7.605	3.626
100	FM	243	140.072	7.359	2.950	-7.998	-5.766	4.587
100	FM	244	139.874	8.565	3.195	-7.879	-6.730	2.753
100	FM	245	141.269	6.972	3.436	-7.764	-4.900	3.725
100	FM	246	141.455	8.182	3.675	-7.651	-5.874	1.902
100	FM	247	143.227	6.595	3.910	-7.539	-4.053	2.885
100	FM	248	143.784	7.810	4.143	-7.429	-5.037	1.075
100	FM	249	145.923	6.229	4.371	-7.319	-3.228	2.071
100	FM	250	146.839	7.451	4.597	-7.210	-4.225	.275
100	FM	251	149.330	5.877	4.819	-7.100	-2.429	1.286
100	FM	252	150.590	7.107	5.038	-6.990	-3.439	-.495
100	FM	253	153.417	5.541	5.254	-6.879	-1.656	.531
100	FM	254	155.005	6.780	5.466	-6.766	-2.681	-1.235
100	FM	255	158.149	5.223	5.675	-6.652	-.913	-.192
100	FM	256	160.046	6.470	5.880	-6.536	-1.953	-1.941
100	FM	257	163.491	4.923	6.082	-6.418	-.200	-.883
100	FM	258	165.678	6.180	6.280	-6.298	-1.255	-2.616
100	FM	259	169.404	4.642	6.475	-6.175	.483	-1.541
100	FM	260	171.863	5.908	6.667	-6.051	-.587	-3.259
100	FM	261	175.851	4.379	6.855	-5.925	1.136	-2.169
100	FM	262	178.564	5.655	7.041	-5.798	.052	-3.871
100	FM	263	182.797	4.134	7.223	-5.669	1.761	-2.767
100	FM	264	185.747	5.418	7.401	-5.538	.663	-4.455
100	FM	265	190.210	3.905	7.577	-5.407	2.359	-3.337
100	FM	266	193.381	5.196	7.750	-5.275	1.249	-5.013
100	FM	267	198.058	3.690	7.920	-5.143	2.932	-3.882
100	FM	268	201.439	4.987	8.087	-5.011	1.811	-5.547
100	FM	269	206.319	3.487	8.251	-4.880	3.484	-4.406
100	FM	270	209.897	4.789	8.413	-4.750	2.353	-6.061
100	FM	271	214.972	3.293	8.572	-4.622	4.017	-4.912
100	FM	272	218.740	4.599	8.728	-4.496	2.877	-6.559
100	FM	273	224.001	3.106	8.883	-4.372	4.534	-5.403
100	FM	274	227.954	4.414	9.034	-4.251	3.388	-7.044
100	FM	275	233.398	2.923	9.184	-4.133	5.040	-5.882
100	FM	276	237.533	4.233	9.332	-4.019	3.889	-7.519
100	FM	277	243.158	2.742	9.478	-3.908	5.536	-6.353
100	FM	278	247.474	4.052	9.622	-3.802	4.382	-7.987
100	FM	279	253.280	2.561	9.765	-3.701	6.026	-6.820
100	FM	280	257.779	3.869	9.906	-3.604	4.870	-8.452
100	FM	281	263.769	2.377	10.046	-3.512	6.513	-7.284
100	FM	282	268.453	3.684	10.185	-3.424	5.355	-8.915
100	FM	283	274.630	2.190	10.322	-3.341	6.998	-7.747
	ATOM		M - A	NEUTRON	PROTON	ALPHA	Q BETA -	Q BETA +
101	MV	229	165.590	11.904	-2.789	-10.625	-13.136	12.062
101	MV	230	163.634	10.324	-2.521	-10.430	-11.297	13.012
101	MV	231	160.460	11.541	-2.254	-10.244	-12.256	11.160
101	MV	232	158.873	9.955	-1.988	-10.066	-10.413	12.108
101	MV	233	156.074	11.166	-1.724	-9.896	-11.370	10.255
101	MV	234	154.866	9.576	-1.462	-9.734	-9.525	11.201
101	MV	235	152.451	10.783	-1.201	-9.580	-10.480	9.348
101	MV	236	151.630	9.188	-.942	-9.433	-8.634	10.294

TABLE 2

Atomic mass excesses and nuclear binding energies

101	MV	237	149.606	10.391	-.686	-9.293	-9.588	8.442
101	MV	238	149.180	8.794	-.431	-9.161	-7.743	9.390
101	MV	239	147.553	9.995	-.178	-9.034	-8.699	7.540
101	MV	240	147.525	8.395	.073	-8.914	-6.855	8.492
101	MV	241	146.296	9.596	.321	-8 799	-7.813	6.647
101	MV	242	146.667	7.996	.567	-8.688	-5.974	7.605
101	MV	243	145.837	9.198	.810	-8.582	-6.936	5.766
101	MV	244	146.605	7.600	1.052	-8.479	-5.102	6.730
101	MV	245	146.169	8.803	1.290	-8.380	-6.071	4.900
101	MV	246	147.328	7.208	1.526	-8.282	-4.244	5.874
101	MV	247	147.280	8.416	1.759	-8.186	-5.221	4.053
101	MV	248	148.822	6.825	1.990	-8.092	-3.403	5.037
101	MV	249	149.151	8.038	2.218	-7.997	-4.390	3.228
101	MV	250	151.064	6.454	2.443	-7.902	-2.582	4.225
101	MV	251	151.758	7.673	2.666	-7.807	-3.580	2.429
101	MV	252	154.029	6.096	2.885	-7.711	-1.784	3.439
101	MV	253	155.073	7.323	3.102	-7.612	-2.794	1.656
101	MV	254	157.686	5.755	3.316	-7.512	-1.011	2.681
101	MV	255	159.063	6.991	3.527	-7.409	-2.035	.913
101	MV	256	161.999	5.431	3.735	-7.304	-.265	1.953
101	MV	257	163.691	6.676	3.940	-7.196	-1.302	.200
101	MV	258	166.933	5.125	4.143	-7.085	.453	1.255
101	MV	259	168.921	6.380	4.342	-6.970	-.598	-.483
101	MV	260	172.450	4.838	4.539	-6.853	1.144	.587
101	MV	261	174.715	6.102	4.733	-6.732	.079	-1.136
101	MV	262	178.512	4.570	4.924	-6.608	1.807	-.052
101	MV	263	181.036	5.843	5.113	-6.482	.728	-1.761
101	MV	264	185.084	4.320	5.298	-6.353	2.443	-.663
101	MV	265	187.851	5.601	5.481	-6.221	1.351	-2.359
101	MV	266	192.132	4.085	5.662	-6.088	3.054	-1.249
101	MV	267	195.126	5.374	5.840	-5.953	1.951	-2.932
101	MV	268	199.628	3.865	6.015	-5.817	3.643	-1.811
101	MV	269	202.835	5.160	6.188	-5.679	2.529	-3.484
101	MV	270	207.545	3.658	6.359	-5.542	4.211	-2.353
101	MV	271	210.955	4.958	6.528	-5.405	3.088	-4.017
101	MV	272	215.863	3.459	6.694	-5.268	4.762	-2.877
101	MV	273	219.467	4.763	6.858	-5.132	3.632	-4.534
101	MV	274	224.566	3.268	7.020	-4.998	5.299	-3.388
101	MV	275	228.358	4.575	7.181	-4.866	4.163	-5.040
101	MV	276	233.644	3.082	7.339	-4.736	5.824	-3.889
101	MV	277	237.622	4.389	7.496	-4.609	4.684	-5.536
101	MV	278	243.092	2.897	7.651	-4.485	6.342	-4.382
101	MV	279	247.254	4.205	7.804	-4.365	5.198	-6.026
101	MV	280	252.909	2.713	7.956	-4.248	6.853	-4.870
101	MV	281	257.256	4.020	8.107	-4.136	5.708	-6.513
101	MV	282	263.097	2.527	8.257	-4.027	7.362	-5.355
101	MV	283	267.632	3.832	8.405	-3.923	6.215	-6.998
101	MV	284	273.662	2.337	8.553	-3.823	7.869	-5.841
	ATOM		M - A	NEUTRON	PROTON	ALPHA	Q BETA -	Q BETA +
102		232	169.286	11.797	-1.241	-10.461	-14.291	10.413
102		233	167.444	10.210	-.986	-10.306	-12.458	11.370
102		234	164.391	11.420	-.732	-10.160	-13.424	9.525
102		235	162.930	9.828	-.480	-10.021	-11.588	10.480
102		236	160.264	11.033	-.229	-9.890	-12.551	8.634
102		237	159.195	9.437	.020	-9.766	-10.714	9.588
102		238	156.923	10.639	.268	-9.649	-11.676	7.743
102		239	156.251	9.039	.514	-9.539	-9.839	8.699
102		240	154.380	10.239	.758	-9.435	-10.801	6.855
102		241	154.110	8.638	1.000	-9.336	-8.965	7.813
102		242	152.641	9.836	1.240	-9.242	-9.930	5.974

TABLE 2

Atomic mass excesses and nuclear binding energies

102	243	152.773	8.235	1.479	-9.152	-8.096	6.936
102	244	151.707	9.434	1.715	-9.065	-9.065	5.102
102	245	152.240	7.834	1.949	-8.982	-7.236	6.071
102	246	151.572	9.035	2.182	-8.900	-8.209	4.244
102	247	152.501	7.438	2.412	-8.820	-6.387	5.221
102	248	152.225	8.644	2.640	-8.741	-7.367	3.403
102	249	153.541	7.051	2.866	-8.662	-5.552	4.390
102	250	153.646	8.262	3.089	-8.583	-6.542	2.582
102	251	155.338	6.675	3.311	-8.502	-4.736	3.580
102	252	155.813	7.892	3.530	-8.420	-5.736	1.784
102	253	157.868	6.313	3.746	-8.336	-3.941	2.794
102	254	158.697	7.538	3.961	-8.248	-4.952	1.011
102	255	161.097	5.967	4.173	-8.158	-3.169	2.035
102	256	162.264	7.200	4.383	-8.065	-4.192	.265
102	257	164.993	5.638	4.591	-7.967	-2.421	1.302
102	258	166.480	6.881	4.796	-7.866	-3.456	-.453
102	259	169.519	5.328	4.999	-7.760	-1.698	.598
102	260	171.306	6.580	5.200	-7.650	-2.747	-1.144
102	261	174.636	5.037	5.398	-7.536	-1.002	-.079
102	262	176.705	6.298	5.594	-7.418	-2.063	-1.807
102	263	180.308	4.764	5.788	-7.295	-.330	-.728
102	264	182.641	6.035	5.980	-7.169	-1.404	-2.443
102	265	186.499	4.509	6.170	-7.039	.316	-1.351
102	266	189.078	5.788	6.357	-6.905	-.769	-3.054
102	267	193.175	4.271	6.542	-6.768	.940	-1.951
102	268	195.985	5.557	6.725	-6.629	-.156	-3.643
102	269	200.306	4.047	6.907	-6.487	1.543	-2.529
102	270	203.334	5.339	7.086	-6.344	.437	-4.211
102	271	207.866	3.835	7.263	-6.199	2.127	-3.088
102	272	211.101	5.133	7.439	-6.053	1.013	-4.762
102	273	215.835	3.633	7.613	-5.906	2.696	-3.632
102	274	219.267	4.935	7.784	-5.760	1.575	-5.299
102	275	224.196	3.439	7.955	-5.615	3.251	-4.163
102	276	227.820	4.743	8.123	-5.470	2.125	-5.824
102	277	232.938	3.249	8.291	-5.328	3.797	-4.684
102	278	236.751	4.555	8.456	-5.187	2.667	-6.342
102	279	242.056	3.062	8.621	-5.049	4.335	-5.198
102	280	246.056	4.368	8.783	-4.913	3.202	-6.853
102	281	251.548	2.874	8.945	-4.781	4.868	-5.708
102	282	255.735	4.180	9.106	-4.652	3.733	-7.362
102	283	261.417	2.686	9.265	-4.527	5.398	-6.215
102	284	265.793	3.991	9.424	-4.406	4.263	-7.869
102	285	271.666	2.495	9.581	-4.288	5.928	-6.723
ATOM		M - A	NEUTRON	PROTON	ALPHA	Q BETA -	Q BETA +
103	235	174.518	11.664	-2.543	-10.449	-12.670	11.588
103	236	172.816	10.070	-2.301	-10.333	-10.844	12.551
103	237	169.909	11.274	-2.060	-10.226	-11.816	10.714
103	238	168.600	9.677	-1.820	-10.125	-9.987	11.676
103	239	166.090	10.877	-1.582	-10.030	-10.958	9.839
103	240	165.181	9.276	-1.345	-9.942	-9.129	10.801
103	241	163.075	10.474	-1.110	-9.859	-10.099	8.965
103	242	162.571	8.871	-.876	-9.781	-8.270	9.930
103	243	160.869	10.068	-.644	-9.709	-9.242	8.096
103	244	160.771	8.466	-.413	-9.637	-7.415	9.065
103	245	159.476	9.663	-.184	-9.570	-8.389	7.236
103	246	159.781	8.062	.043	-9.505	-6.566	8.209
103	247	158.888	9.261	.269	-9.441	-7.545	6.387
103	248	159.592	7.663	.494	-9.378	-5.727	7.367
103	249	159.093	8.866	.716	-9.315	-6.712	5.552
103	250	160.189	7.272	.937	-9.251	-4.901	6.542

TABLE 2

Atomic mass excesses and nuclear binding energies

103	251	160.075	8.481	1.156	-9.186	-5.894	4.736
103	252	161.549	6.893	1.374	-9.119	-4.091	5.736
103	253	161.809	8.108	1.589	-9.049	-5.093	3.941
103	254	163.649	6.527	1.804	-8.975	-3.299	4.952
103	255	164.266	7.750	2.016	-8.898	-4.311	3.169
103	256	166.456	6.178	2.226	-8.817	-2.529	4.192
103	257	167.414	7.409	2.435	-8.731	-3.551	2.421
103	258	169.936	5.846	2.642	-8.641	-1.780	3.456
103	259	171.217	7.086	2.847	-8.545	-2.814	1.698
103	260	174.052	5.532	3.051	-8.444	-1.055	2.747
103	261	175.638	6.782	3.253	-8.338	-2.101	1.002
103	262	178.768	5.237	3.453	-8.226	-.353	2.063
103	263	180.639	6.497	3.651	-8.109	-1.411	.330
103	264	184.045	4.961	3.848	-7.986	.326	1.404
103	265	186.183	6.230	4.043	-7.859	-.743	-.316
103	266	189.847	4.703	4.237	-7.726	.982	.769
103	267	192.235	5.980	4.428	-7.589	-.098	-.940
103	268	196.141	4.461	4.618	-7.448	1.617	.156
103	269	198.763	5.746	4.807	-7.303	.528	-1.543
103	270	202.897	4.234	4.994	-7.155	2.233	-.437
103	271	205.739	5.525	5.180	-7.004	1.135	-2.127
103	272	210.087	4.019	5.364	-6.850	2.833	-1.013
103	273	213.139	5.316	5.546	-6.695	1.727	-2.696
103	274	217.692	3.814	5.727	-6.538	3.418	-1.575
103	275	220.945	5.115	5.907	-6.381	2.306	-3.251
103	276	225.695	3.617	6.086	-6.223	3.992	-2.125
103	277	229.141	4.921	6.263	-6.066	2.875	-3.797
103	278	234.084	3.425	6.439	-5.909	4.557	-2.667
103	279	237.722	4.730	6.614	-5.754	3.437	-4.335
103	280	242.854	3.235	6.787	-5.600	5.115	-3.202
103	281	246.681	4.541	6.960	-5.449	3.993	-4.868
103	282	252.002	3.046	7.131	-5.301	5.669	-3.733
103	283	256.018	4.351	7.302	-5.155	4.546	-5.398
103	284	261.530	2.855	7.471	-5.012	6.222	-4.263
103	285	265.739	4.159	7.640	-4.873	5.097	-5.928
103	286	271.444	2.662	7.807	-4.737	6.773	-4.792
ATOM		M - A	NEUTRON	PROTON	ALPHA	Q BETA -	Q BETA +
104	238	178.587	11.505	-1.093	-10.587	-13.874	9.987
104	239	177.048	9.906	-.864	-10.508	-12.054	10.958
104	240	174.310	11.106	-.635	-10.436	-13.034	9.129
104	241	173.174	9.504	-.408	-10.370	-11.213	10.099
104	242	170.840	10.700	-.181	-10.308	-12.191	8.270
104	243	170.111	9.097	.044	-10.251	-10.370	9.242
104	244	168.186	10.293	.268	-10.197	-11.349	7.415
104	245	167.865	8.688	.491	-10.146	-9.529	8.389
104	246	166.347	9.885	.713	-10.097	-10.510	6.566
104	247	166.433	8.282	.934	-10.050	-8.693	7.545
104	248	165.319	9.481	1.153	-10.003	-9.678	5.727
104	249	165.806	7.881	1.371	-9.956	-7.865	6.712
104	250	165.090	9.083	1.589	-9.908	-8.855	4.901
104	251	165.969	7.488	1.804	-9.859	-7.048	5.894
104	252	165.640	8.696	2.019	-9.807	-8.045	4.091
104	253	166.901	7.106	2.233	-9.751	-6.245	5.093
104	254	166.948	8.321	2.445	-9.693	-7.250	3.299
104	255	168.577	6.738	2.656	-9.630	-5.459	4.311
104	256	168.984	7.960	2.866	-9.562	-6.472	2.529
104	257	170.965	6.386	3.075	-9.488	-4.691	3.551
104	258	171.716	7.617	3.283	-9.410	-5.714	1.780
104	259	174.031	6.052	3.489	-9.325	-3.942	2.814
104	260	175.107	7.292	3.695	-9.234	-4.976	1.055

TABLE 2

Atomic mass excesses and nuclear binding energies

104	261	177.738	5.736	3.899	-9.136	-3.215	2.101
104	262	179.121	6.985	4.102	-9.032	-4.260	.353
104	263	182.049	5.439	4.304	-8.921	-2.509	1.411
104	264	183.719	6.697	4.504	-8.804	-3.564	-.326
104	265	186.926	5.161	4.704	-8.681	-1.825	.743
104	266	188.865	6.428	4.902	-8.551	-2.890	-.982
104	267	192.333	4.900	5.099	-8.415	-1.160	.098
104	268	194.524	6.176	5.296	-8.274	-2.235	-1.617
104	269	198.235	4.656	5.491	-8.127	-.514	-.528
104	270	200.663	5.940	5.685	-7.976	-1.598	-2.233
104	271	204.604	4.427	5.877	-7.820	.114	-1.135
104	272	207.254	5.717	6.069	-7.660	-.977	-2.833
104	273	211.412	4.210	6.260	-7.497	.728	-1.727
104	274	214.274	5.505	6.450	-7.331	-.370	-3.418
104	275	218.638	4.003	6.639	-7.163	1.329	-2.306
104	276	221.703	5.303	6.826	-6.993	.226	-3.992
104	277	226.266	3.804	7.013	-6.822	1.920	-2.875
104	278	229.527	5.106	7.199	-6.651	.813	-4.557
104	279	234.285	3.610	7.384	-6.480	2.504	-3.437
104	280	237.739	4.914	7.568	-6.310	1.394	-5.115
104	281	242.688	3.418	7.751	-6.140	3.082	-3.993
104	282	246.333	4.723	7.933	-5.973	1.970	-5.669
104	283	251.473	3.227	8.114	-5.807	3.658	-4.546
104	284	255.309	4.531	8.294	-5.644	2.544	-6.222
104	285	260.641	3.035	8.474	-5.484	4.231	-5.097
104	286	264.671	4.338	8.653	-5.326	3.118	-6.773
104	287	270.198	2.840	8.831	-5.172	4.804	-5.649
ATOM		M - A	NEUTRON	PROTON	ALPHA	Q BETA -	Q BETA +
105	241	184.386	11.325	-2.492	-10.868	-12.303	11.213
105	242	183.032	9.722	-2.273	-10.823	-10.491	12.191
105	243	180.481	10.918	-2.056	-10.782	-11.478	10.370
105	244	179.535	9.313	-1.839	-10.744	-9.665	11.349
105	245	177.394	10.509	-1.623	-10.710	-10.651	9.529
105	246	176.858	8.904	-1.408	-10.678	-8.839	10.510
105	247	175.126	10.099	-1.193	-10.647	-9.827	8.693
105	248	174.997	8.496	-.980	-10.616	-8.017	9.678
105	249	173.671	9.694	-.767	-10.586	-9.008	7.865
105	250	173.945	8.093	-.554	-10.554	-7.201	8.855
105	251	173.017	9.295	-.343	-10.520	-8.196	7.048
105	252	173.685	7.699	-.132	-10.484	-6.394	8.045
105	253	173.147	8.906	.078	-10.444	-7.395	6.245
105	254	174.198	7.316	.288	-10.400	-5.599	7.250
105	255	174.036	8.530	.497	-10.352	-6.607	5.459
105	256	175.457	6.947	.705	-10.298	-4.818	6.472
105	257	175.656	8.168	.913	-10.238	-5.834	4.691
105	258	177.430	6.594	1.120	-10.172	-4.054	5.714
105	259	177.974	7.823	1.327	-10.099	-5.079	3.942
105	260	180.083	6.258	1.533	-10.018	-3.308	4.976
105	261	180.954	7.497	1.738	-9.931	-4.341	3.215
105	262	183.381	5.941	1.943	-9.836	-2.580	4.260
105	263	184.559	7.189	2.147	-9.733	-3.623	2.509
105	264	187.284	5.642	2.350	-9.622	-1.871	3.564
105	265	188.751	6.900	2.553	-9.504	-2.924	1.825
105	266	191.755	5.363	2.756	-9.378	-1.181	2.890
105	267	193.493	6.630	2.957	-9.245	-2.243	1.160
105	268	196.759	5.101	3.158	-9.105	-.509	2.235
105	269	198.750	6.377	3.359	-8.958	1.580	.514
105	270	202.261	4.856	3.559	-8.805	.146	1.598
105	271	204.490	6.139	3.758	-8.646	-.932	-.114
105	272	208.232	4.625	3.957	-8.481	.786	.977

TABLE 2

Atomic mass excesses and nuclear binding energies

105	273	210.684	5.915	4.155	-8.312	-.299	-.728
105	274	214.644	4.407	4.353	-8.138	1.413	.370
105	275	217.309	5.702	4.550	-7.961	.322	-1.329
105	276	221.477	4.199	4.746	-7.780	2.029	-.226
105	277	224.346	5.498	4.942	-7.598	.934	-1.920
105	278	228.714	3.999	5.137	-7.413	2.637	-.813
105	279	231.781	5.301	5.331	-7.227	1.539	-2.504
105	280	236.345	3.803	5.525	-7.041	3.239	-1.394
105	281	239.605	5.107	5.718	-6.855	2.138	-3.082
105	282	244.362	3.611	5.910	-6.669	3.837	-1.970
105	283	247.815	4.914	6.102	-6.484	2.735	-3.658
105	284	252.764	3.418	6.293	-6.301	4.432	-2.544
105	285	256.410	4.722	6.483	-6.120	3.329	-4.231
105	286	261.553	3.225	6.673	-5.942	5.027	-3.118
105	287	265.394	4.527	6.862	-5.766	3.924	-4.804
105	288	270.733	3.028	7.050	-5.593	5.622	-3.691
ATOM		M - A	NEUTRON	PROTON	ALPHA	Q BETA -	Q BETA +
106	244	189.200	11.127	-1.134	-11.281	-13.559	9.665
106	245	188.045	9.522	-.926	-11.262	-11.754	10.651
106	246	185.696	10.716	-.718	-11.247	-12.749	8.839
106	247	184.953	9.111	-.510	-11.232	-10.944	9.827
106	248	183.014	10.306	-.303	-11.218	-11.940	8.017
106	249	182.678	8.703	-.096	-11.204	-10.136	9.008
106	250	181.145	9.900	.110	-11.189	-11.134	7.201
106	251	181.213	8.300	.316	-11.171	-9.333	8.196
106	252	180.079	9.501	.523	-11.151	-10.334	6.394
106	253	180.542	7.905	.729	-11.127	-8.537	7.395
106	254	179.797	9.112	.935	-11.098	-9.543	5.599
106	255	180.643	7.522	1.140	-11.065	-7.751	6.607
106	256	180.275	8.735	1.346	-11.025	-8.763	4.818
106	257	181.490	7.152	1.551	-10.979	-6.978	5.834
106	258	181.484	8.374	1.757	-10.926	-7.996	4.054
106	259	183.052	6.799	1.962	-10.866	-6.219	5.079
106	260	183.391	8.029	2.167	-10.797	-7.245	3.308
106	261	185.295	6.463	2.373	-10.721	-5.475	4.341
106	262	185.960	7.702	2.578	-10.635	-6.509	2.580
106	263	188.182	6.146	2.783	-10.541	-4.748	3.623
106	264	189.155	7.394	2.989	-10.439	-5.790	1.871
106	265	191.675	5.848	3.194	-10.327	-4.037	2.924
106	266	192.937	7.105	3.399	-10.207	-5.088	1.181
106	267	195.736	5.568	3.604	-10.078	-3.343	2.243
106	268	197.268	6.835	3.809	-9.940	-4.402	.509
106	269	200.330	5.306	4.014	-9.794	-2.665	1.580
106	270	202.115	6.582	4.219	-9.641	-3.732	-.146
106	271	205.422	5.061	4.424	-9.480	-2.002	.932
106	272	207.446	6.344	4.629	-9.312	-3.075	-.796
106	273	210.983	4.830	4.833	-9.138	-1.351	.299
106	274	213.231	6.119	5.038	-8.959	-2.430	-1.413
106	275	216.987	4.612	5.242	-8.773	-.712	-.322
106	276	219.448	5.906	5.446	-8.584	-1.796	-2.029
106	277	223.412	4.403	5.650	-8.391	-.081	-.934
106	278	226.077	5.702	5.853	-8.194	1.169	-2.637
106	279	230.242	4.202	6.057	-7.995	542	1.539
106	280	233.106	5.504	6.260	-7.794	-.548	-3.239
106	281	237.467	4.006	6.462	-7.592	1.161	-2.138
106	282	240.526	5.309	6.665	-7.389	.070	-3.837
106	283	245.081	3.812	6.866	-7.186	1.778	-2.735
106	284	248.332	5.116	7.068	-6.984	.686	-4.432
106	285	253.081	3.619	7.268	-6.784	2.393	-3.329
106	286	256.526	4.922	7.469	-6.584	1.301	-5.027

TABLE 2

Atomic mass excesses and nuclear binding energies

106	287	261.469	3.424	7.668	-6.387	3.009	-3.924
106	288	265.111	4.726	7.867	-6.193	1.917	-5.622
106	289	270.252	3.227	8.066	-6.001	3.625	-4.519
ATOM		M - A	NEUTRON	PROTON	ALPHA	Q BETA -	Q BETA +
107	248	194.953	9.311	-2.416	-11.809	-10.244	11.940
107	249	192.814	10.506	-2.216	-11.811	-11.247	10.136
107	250	192.279	8.903	-2.016	-11.812	-9.451	11.134
107	251	190.546	10.101	-1.816	-11.811	-10.456	9.333
107	252	190.413	8.500	-1.615	-11.807	-8.661	10.334
107	253	189.079	9.702	-1.415	-11.799	-9.668	8.537
107	254	189.340	8.106	-1.214	-11.786	-7.877	9.543
107	255	188.394	9.313	-1.012	-11.768	-8.888	7.751
107	256	189.038	7.724	-.810	-11.743	-7.102	8.763
107	257	188.468	8.937	-.608	-11.712	-8.118	6.978
107	258	189.480	7.355	-.405	-11.673	-6.336	7.996
107	259	189.271	8.577	-.202	-11.626	-7.358	6.219
107	260	190.636	7.003	.001	-11.570	-5.583	7.245
107	261	190.770	8.233	.206	-11.505	-6.611	5.475
107	262	192.470	6.668	.410	-11.431	-4.843	6.509
107	263	192.929	7.907	.616	-11.347	-5.879	4.748
107	264	194.945	6.352	.821	-11.253	-4.118	5.790
107	265	195.712	7.601	1.028	-11.149	-5.160	4.037
107	266	198.025	6.054	1.235	-11.035	-3.407	5.088
107	267	199.079	7.313	1.442	-10.911	-4.457	3.343
107	268	201.671	5.776	1.650	-10.778	-2.710	4.402
107	269	202.995	7.043	1.858	-10.635	-3.767	2.665
107	270	205.847	5.515	2.067	-10.483	-2.027	3.732
107	271	207.424	6.791	2.276	-10.322	-3.090	2.002
107	272	210.521	5.271	2.486	-10.152	-1.356	3.075
107	273	212.334	6.554	2.696	-9.975	-2.425	1.351
107	274	215.661	5.040	2.906	-9.791	-.697	2.430
107	275	217.699	6.330	3.117	-9.600	-1.770	.712
107	276	221.243	4.823	3.328	-9.402	-.046	1.796
107	277	223.493	6.118	3.539	-9.200	-1.123	.081
107	278	227.246	4.615	3.751	-8.993	.598	1.169
107	279	229.700	5.913	3.962	-8.782	-.482	-.542
107	280	233.654	4.414	4.174	-8.567	1.237	.548
107	281	236.306	5.715	4.385	-8.351	.155	-1.161
107	282	240.456	4.217	4.596	-8.132	1.872	-.070
107	283	243.303	5.520	4.808	-7.913	.789	-1.778
107	284	247.647	4.023	5.019	-7.693	2.506	-.686
107	285	250.688	5.327	5.229	-7.473	1.424	-2.393
107	286	255.225	3.830	5.440	-7.254	3.141	-1.301
107	287	258.461	5.132	5.650	-7.036	2.058	-3.009
107	288	263.194	3.634	5.860	-6.821	3.776	-1.917
107	289	266.627	4.935	6.069	-6.607	2.695	-3.625
107	290	271.559	3.435	6.277	-6.397	4.414	-2.533
ATOM		M - A	NEUTRON	PROTON	ALPHA	Q BETA -	Q BETA +
108	251	201.001	9.096	-1.138	-12.439	-11.561	10.456
108	252	199.074	10.294	-.944	-12.451	-12.573	8.661
108	253	198.747	8.695	-.749	-12.460	-10.785	9.668
108	254	197.217	9.897	-.554	-12.463	-11.799	7.877
108	255	197.282	8.302	-.358	-12.460	-10.014	8.888
108	256	196.140	9.510	-.161	-12.451	-11.031	7.102
108	257	196.585	7.921	.037	-12.435	-9.249	8.118
108	258	195.817	9.136	.236	-12.410	-10.270	6.336
108	259	196.629	7.555	.436	-12.377	-8.493	7.358
108	260	196.219	8.778	.637	-12.335	-9.519	5.583

TABLE 2

Atomic mass excesses and nuclear binding energies

108	261	197.381	7.205	.839	-12.282	-7.747	6.611
108	262	197.313	8.436	1.042	-12.220	-8.778	4.843
108	263	198.808	6.872	1.246	-12.147	-7.012	5.879
108	264	199.063	8.113	1.451	-12.063	-8.049	4.118
108	265	200.872	6.558	1.658	-11.968	-6.289	5.160
108	266	201.432	7.808	1.865	-11.862	-7.333	3.407
108	267	203.536	6.263	2.074	-11.745	-5.579	4.457
108	268	204.381	7.522	2.283	-11.617	-6.628	2.710
108	269	206.762	5.986	2.494	-11.478	-4.881	3.767
108	270	207.874	7.255	2.705	-11.329	-5.936	2.027
108	271	210.514	5.728	2.918	-11.169	-4.194	3.090
108	272	211.877	7.004	3.131	-10.999	-5.254	1.356
108	273	214.760	5.485	3.346	-10.821	-3.517	2.425
108	274	216.358	6.769	3.561	-10.633	-4.582	.697
108	275	219.469	5.257	3.777	-10.437	-2.849	1.770
108	276	221.289	6.547	3.994	-10.234	-3.918	.046
108	277	224.616	5.040	4.212	-10.024	-2.188	1.123
108	278	226.648	6.336	4.430	-9.808	-3.260	-.598
108	279	230.182	4.833	4.648	-9.586	-1.532	.482
108	280	232.417	6.133	4.868	-9.360	-2.606	-1.237
108	281	236.151	4.633	5.087	-9.130	-.880	-.155
108	282	238.584	5.935	5.307	-8.897	-1.954	-1.872
108	283	242.513	4.438	5.527	-8.662	-.229	-.789
108	284	245.140	5.741	5.747	-8.425	-1.303	-2.506
108	285	249.264	4.244	5.968	-8.187	.423	-1.424
108	286	252.085	5.547	6.188	-7.950	-.651	-3.141
108	287	256.402	4.050	6.408	-7.712	1.076	-2.058
108	288	259.418	5.352	6.628	-7.477	.003	-3.776
108	289	263.932	3.853	6.847	-7.242	1.731	-2.695
108	290	267.145	5.154	7.066	-7.010	.659	-4.414
108	291	271.859	3.654	7.285	-6.780	2.388	-3.333
ATOM		M - A	NEUTRON	PROTON	ALPHA	Q BETA -	Q BETA +
109	254	209.016	8.883	-2.684	-13.128	-10.104	11.799
109	255	207.296	10.087	-2.494	-13.142	-11.125	10.014
109	256	207.170	8.494	-2.303	-13.148	-9.346	11.031
109	257	205.835	9.703	-2.111	-13.147	-10.369	9.249
109	258	206.087	8.116	-1.916	-13.137	-8.593	10.270
109	259	205.122	9.332	-1.721	-13.119	-9.619	8.493
109	260	205.737	7.752	-1.524	-13.090	-7.847	9.519
109	261	205.128	8.976	-1.325	-13.051	-8.877	7.747
109	262	206.091	7.405	-1.125	-13.001	-7.109	8.778
109	263	205.820	8.638	-.923	-12.940	-8.143	7.012
109	264	207.112	7.075	-.719	-12.867	-6.380	8.049
109	265	207.162	8.318	-.514	-12.782	-7.419	6.289
109	266	208.764	6.765	-.307	-12.685	-5.661	7.333
109	267	209.115	8.017	-.099	-12.576	-6.706	5.579
109	268	211.009	6.473	.112	-12.455	-4.953	6.628
109	269	211.642	7.734	.323	-12.321	-6.002	4.881
109	270	213.810	6.200	.537	-12.176	-4.254	5.936
109	271	214.708	7.470	.751	-12.019	-5.308	4.194
109	272	217.131	5.944	.968	-11.851	-3.564	5.254
109	273	218.277	7.222	1.185	-11.672	-4.623	3.517
109	274	220.940	5.704	1.404	-11.484	-2.883	4.582
109	275	222.318	6.990	1.625	-11.285	-3.945	2.849
109	276	225.207	5.478	1.847	-11.077	-2.208	3.918
109	277	226.805	6.770	2.069	-10.861	-3.272	2.188
109	278	229.908	5.264	2.293	-10.637	-1.538	3.260
109	279	231.715	6.561	2.518	-10.407	-2.604	1.532
109	280	235.023	5.059	2.744	-10.170	-.871	2.606
109	281	237.031	6.359	2.971	-9.929	-1.938	.880

TABLE 2

Atomic mass excesses and nuclear binding energies

109	282	240.538	4.861	3.198	-9.682	-.206	1.954
109	283	242.742	6.163	3.426	-9.433	-1.273	.229
109	284	246.443	4.666	3.655	-9.180	.460	1.303
109	285	248.841	5.969	3.884	-8.926	-.606	-.423
109	286	252.735	4.473	4.113	-8.671	1.128	.651
109	287	255.327	5.776	4.343	-8.415	.063	-1.076
109	288	259.415	4.279	4.572	-8.159	1.798	-.003
109	289	262.201	5.581	4.801	-7.904	.735	-1.731
109	290	266.486	4.083	5.031	-7.652	2.472	-.659
109	291	269.471	5.383	5.259	-7.401	1.410	-2.388
109	292	273.956	3.882	5.488	-7.152	3.149	-1.318
ATOM		M - A	NEUTRON	PROTON	ALPHA	Q BETA -	Q BETA +
110	257	216.204	8.680	-1.449	-13.848	-11.473	10.369
110	258	214.680	9.891	-1.260	-13.853	-12.502	8.593
110	259	214.741	8.306	-1.070	-13.850	-10.733	9.619
110	260	213.584	9.524	-.878	-13.836	-11.764	7.847
110	261	214.005	7.947	-.683	-13.810	-9.997	8.877
110	262	213.200	9.173	-.487	-13.774	-11.032	7.109
110	263	213.963	7.604	-.288	-13.725	-9.268	8.143
110	264	213.492	8.839	-.087	-13.664	-10.306	6.380
110	265	214.581	7.279	.116	-13.590	-8.546	7.419
110	266	214.425	8.523	.321	-13.503	-9.588	5.661
110	267	215.820	6.972	.528	-13.403	-7.832	6.706
110	268	215.962	8.226	.738	-13.290	-8.878	4.953
110	269	217.644	6.685	.950	-13.163	-7.127	6.002
110	270	218.064	7.948	1.163	-13.023	-8.177	4.254
110	271	220.016	6.415	1.379	-12.871	-6.429	5.308
110	272	220.696	7.688	1.597	-12.706	-7.482	3.564
110	273	222.899	6.164	1.817	-12.528	-5.738	4.623
110	274	223.823	7.444	2.039	-12.339	-6.794	2.883
110	275	226.263	5.928	2.262	-12.139	-5.052	3.945
110	276	227.415	7.215	2.488	-11.929	-6.112	2.208
110	277	230.077	5.705	2.715	-11.708	-4.372	3.272
110	278	231.446	6.998	2.943	-11.479	-5.433	1.538
110	279	234.319	5.494	3.174	-11.241	-3.694	2.604
110	280	235.894	6.792	3.405	-10.996	-4.756	.871
110	281	238.969	5.292	3.638	-10.744	-3.017	1.938
110	282	240.743	6.593	3.872	-10.486	-4.079	.206
110	283	244.015	5.096	4.108	-10.223	-2.340	1.273
110	284	245.983	6.399	4.344	-9.957	-3.401	-.460
110	285	249.447	4.903	4.581	-9.687	-1.661	.606
110	286	251.608	6.207	4.818	-9.415	-2.720	-1.128
110	287	255.264	4.711	5.056	-9.141	-.978	-.063
110	288	257.617	6.015	5.294	-8.867	-2.035	-1.798
110	289	261.467	4.518	5.533	-8.594	-.291	-.735
110	290	264.014	5.820	5.772	-8.320	-1.346	-2.472
110	291	268.061	4.321	6.010	-8.049	.401	-1.410
110	292	270.807	5.621	6.249	-7.780	-.652	-3.149
110	293	275.054	4.120	6.487	-7.513	1.097	-2.089
ATOM		M - A	NEUTRON	PROTON	ALPHA	Q BETA -	Q BETA +
111	260	225.348	8.493	-3.022	-14.569	-10.066	11.764
111	261	224.002	9.714	-2.833	-14.558	-11.104	9.997
111	262	224.231	8.138	-2.641	-14.535	-9.342	11.032
111	263	223.231	9.367	-2.447	-14.500	-10.382	9.268
111	264	223.798	7.801	-2.250	-14.452	-8.623	10.306
111	265	223.127	9.038	-2.050	-14.389	-9.665	8.546
111	266	224.013	7.481	-1.848	-14.313	-7.909	9.588
111	267	223.653	8.728	-1.643	-14.223	-8.955	7.832

TABLE 2

Atomic mass excesses and nuclear binding energies

111	268	224.840	7.180	-1.435	-14.119	-7.202	8.878
111	269	224.771	8.437	-1.225	-14.000	-8.250	7.127
111	270	226.241	6.898	-1.011	-13.867	-6.500	8.177
111	271	226.444	8.164	-.796	-13.720	-7.551	6.429
111	272	228.178	6.634	-.577	-13.560	-5.804	7.482
111	273	228.637	7.908	-.356	-13.385	-6.858	5.738
111	274	230.617	6.387	-.133	-13.198	-5.112	6.794
111	275	231.315	7.670	.093	-12.998	-6.168	5.052
111	276	233.527	6.156	.321	-12.786	-4.425	6.112
111	277	234.449	7.445	.551	-12.563	-5.482	4.372
111	278	236.878	5.938	.783	-12.329	-3.740	5.433
111	279	238.013	7.233	1.018	-12.086	-4.798	3.694
111	280	240.649	5.731	1.254	-11.833	-3.055	4.756
111	281	241.986	7.030	1.492	-11.573	-4.113	3.017
111	282	244.822	5.532	1.732	-11.305	-2.370	4.079
111	283	246.355	6.835	1.973	-11.031	-3.426	2.340
111	284	249.384	5.338	2.216	-10.752	-1.682	3.401
111	285	251.108	6.643	2.460	-10.468	-2.737	1.661
111	286	254.327	5.148	2.705	-10.181	-.990	2.720
111	287	256.242	6.453	2.950	-9.891	-2.043	.978
111	288	259.652	4.957	3.197	-9.600	-.293	2.035
111	289	261.758	6.262	3.444	-9.307	-1.343	.291
111	290	265.360	4.765	3.692	-9.015	.409	1.346
111	291	267.660	6.067	3.939	-8.724	-.637	-.401
111	292	271.459	4.569	4.187	-8.434	1.118	.652
111	293	273.957	5.869	4.434	-8.147	.074	-1.097
111	294	277.957	4.367	4.682	-7.862	1.832	-.047
ATOM		M - A	NEUTRON	PROTON	ALPHA	Q BETA -	Q BETA +
112	264	232.421	9.560	-1.605	-15.228	-12.527	8.623
112	265	232.792	7.996	-1.410	-15.178	-10.773	9.665
112	266	231.923	9.237	-1.211	-15.114	-11.820	7.909
112	267	232.607	7.683	-1.009	-15.035	-10.068	8.955
112	268	232.042	8.933	-.804	-14.940	-11.117	7.202
112	269	233.021	7.388	-.596	-14.831	-9.367	8.250
112	270	232.740	8.648	-.385	-14.706	-10.419	6.500
112	271	233.995	7.112	-.170	-14.566	-8.671	7.551
112	272	233.982	8.381	.048	-14.411	-9.724	5.804
112	273	235.494	6.855	.268	-14.241	-7.978	6.858
112	274	235.730	8.132	.492	-14.057	-9.032	5.112
112	275	237.483	6.614	.719	-13.858	-7.287	6.168
112	276	237.952	7.899	.948	-13.647	-8.343	4.425
112	277	239.931	6.388	1.180	-13.422	-6.599	5.482
112	278	240.618	7.680	1.415	-13.186	-7.655	3.740
112	279	242.810	6.175	1.653	-12.939	-5.910	4.798
112	280	243.705	7.473	1.893	-12.681	-6.966	3.055
112	281	246.099	5.973	2.135	-12.413	-5.220	4.113
112	282	247.192	7.275	2.379	-12.137	-6.274	2.370
112	283	249.781	5.778	2.626	-11.853	-4.528	3.426
112	284	251.066	7.083	2.874	-11.563	-5.580	1.682
112	285	253.845	5.588	3.124	-11.266	-3.830	2.737
112	286	255.318	6.894	3.375	-10.965	-4.880	.990
112	287	258.285	5.401	3.628	-10.661	-3.127	2.043
112	288	259.945	6.707	3.881	-10.353	-4.173	.293
112	289	263.101	5.212	4.136	-10.044	-2.418	1.343
112	290	264.951	6.517	4.392	-9.734	-3.460	-.409
112	291	268.297	5.021	4.648	-9.424	-1.700	.637
112	292	270.341	6.324	4.904	-9.114	-2.739	-1.118
112	293	273.883	4.825	5.161	-8.807	-.976	-.074
112	294	276.125	6.125	5.417	-8.502	-2.011	-1.832
112	295	279.869	4.623	5.673	-8.199	-.244	-.792

TABLE 2

Atomic mass excesses and nuclear binding energies

ATOM		M - A	NEUTRON	PROTON	ALPHA	Q BETA -	Q BETA +
113	267	242.675	9.435	-3.168	-15.835	-11.169	10.068
113	268	243.159	7.884	-2.967	-15.752	-9.421	11.117
113	269	242.388	9.138	-2.762	-15.652	-10.475	9.367
113	270	243.159	7.597	-2.553	-15.536	-8.729	10.419
113	271	242.666	8.860	-2.341	-15.404	-9.783	8.671
113	272	243.705	7.328	-2.125	-15.256	-8.038	9.724
113	273	243.472	8.601	-1.906	-15.092	-9.094	7.978
113	274	244.762	7.078	-1.683	-14.912	-7.349	9.032
113	275	244.771	8.359	-1.456	-14.717	-8.405	7.287
113	276	246.295	6.844	-1.226	-14.507	-6.661	8.343
113	277	246.530	8.132	-.993	-14.284	-7.717	6.599
113	278	248.273	6.624	-.757	-14.046	-5.972	7.655
113	279	248.721	7.920	-.518	-13.796	-7.028	5.910
113	280	250.670	6.418	-.275	-13.535	-5.282	6.966
113	281	251.320	7.718	-.030	-13.262	-6.336	5.220
113	282	253.466	6.221	.218	-12.979	-4.588	6.274
113	283	254.309	7.525	.468	-12.687	-5.639	4.528
113	284	256.645	6.031	.720	-12.387	-3.889	5.580
113	285	257.675	7.338	.975	-12.080	-4.937	3.830
113	286	260.198	5.845	1.232	-11.766	-3.184	4.880
113	287	261.412	7.153	1.491	-11.448	-4.228	3.127
113	288	264.119	5.661	1.751	-11.126	-2.471	4.173
113	289	265.518	6.968	2.012	-10.801	-3.511	2 418
113	290	268.411	5.475	2.275	-10.474	-1.749	3.460
113	291	269.997	6.781	2.538	-10.146	-2.785	1.700
113	292	273.080	5.285	2.802	-9.818	-1.019	2.739
113	293	274.858	6.589	3.067	-9.492	-2.050	.976
113	294	278.136	5.090	3.332	-9.166	-.279	2.011
113	295	280.113	6.390	3.597	-8.844	-1.306	.244
113	296	283.592	4.888	3.862	-8.525	469	1.276
ATOM		M - A	NEUTRON	PROTON	ALPHA	Q BETA -	Q BETA +
114	270	251.888	9.343	-1.915	-16.356	-12.626	8.729
114	271	252.449	7.806	-1.706	-16.233	-10.884	9.783
114	272	251.744	9.073	-1.493	-16.093	-11 942	8.038
114	273	252.566	7.545	-1.275	-15.936	-10.201	9.094
114	274	252.111	8.822	-1.054	-15.762	-11.259	7 349
114	275	253.176	7.303	-.829	-15.571	-9.517	8.405
114	276	252.956	8.588	-.600	-15.365	-10.575	6.661
114	277	254.247	7.076	-.367	-15.143	-8.832	7 717
114	278	254.245	8.369	-.131	-14.906	-9.889	5.972
114	279	255.748	6.864	.109	14.656	-8.145	7 028
114	280	255.952	8.163	.353	-14.392	9.200	5.282
114	281	257.655	6.664	.600	-14.115	7.454	6.336
114	282	258.055	7.968	.850	-13.827	-8.506	4.588
114	283	259.948	6.474	1.103	-13.529	-6.757	5.639
114	284	260.535	7 781	1 359	-13.221	-7 806	3.889
114	285	262.613	6.289	1 618	-12.904	-6.053	4.937
114	286	263.381	7 599	1 879	-12.580	-7.098	3.184
114	287	265.640	6.108	2 142	-12.250	-5.341	4.228
114	288	266 590	7.418	2 407	-11 915	-6.381	2 471
114	289	269.029	5.928	2.674	11.575	4 619	3 511
114	290	270.160	7.237	2.943	-11.233	5.654	1 749
114	291	272.783	5 745	3.213	10.889	3 887	2 785
114	292	274.098	7.052	3 484	10 544	4.917	1.019
114	293	276 908	5 557	3.756	10 199	3.144	2 050
114	294	278 414	6.861	4.029	9.854	4.169	.279
114	295	281.419	5.363	4.301	9.513	2.391	1 306
114	296	283 123	6.663	4.575	9.173	3.410	.469

TABLE 2

Atomic mass excesses and nuclear binding energies

114	297	286.330	5.161	4.847	-8.838	-1.627	.554
ATOM		M - A	NEUTRON	PROTON	ALPHA	Q BETA -	Q BETA +
115	274	263.370	7.764	-3.220	-16.602	-9.557	11.259
115	275	262.693	9.045	-2.997	-16.417	-10.618	9.517
115	276	263.530	7.530	-2.770	-16.216	-8.879	10.575
115	277	263.079	8.819	-2.538	-15.997	-9.940	8.832
115	278	264.134	7.312	-2.303	-15.763	-8.199	9.889
115	279	263.893	8.608	-2.063	-15.513	-9.257	8.145
115	280	265.152	7.108	-1.819	-15.248	-7.514	9.200
115	281	265.109	8.411	-1.572	-14.970	-8.570	7.454
115	282	266.560	6.916	-1.320	-14.678	-6.823	8.506
115	283	266.705	8.223	-1.066	-14.375	-7.875	6.757
115	284	268.340	6.732	-.808	-14.061	-6.125	7.806
115	285	268.666	8.042	-.546	-13.737	-7.173	6.053
115	286	270.479	6.554	-.282	-13.404	-5.418	7.098
115	287	270.981	7.866	-.015	-13.063	-6.460	5.341
115	288	272.971	6.378	.254	-12.716	-4.700	6.381
115	289	273.649	7.690	.526	-12.364	-5.737	4.619
115	290	275.814	6.201	.800	-12.008	-3.971	5.654
115	291	276.670	7.512	1.075	-11.648	-5.002	3.887
115	292	279.015	6.022	1.352	-11.287	-3.230	4.917
115	293	280.052	7.330	1.630	-10.925	-4.254	3.144
115	294	282.583	5.837	1.910	-10.563	-2.476	4.169
115	295	283.810	7.141	2.190	-10.203	-3.494	2.391
115	296	286.533	5.644	2.470	-9.845	-1.710	3.410
115	297	287.957	6.944	2.751	-9.490	-2.722	1.627
115	298	290.883	5.441	3.031	-9.138	-.932	2.642
ATOM		M - A	NEUTRON	PROTON	ALPHA	Q BETA -	Q BETA +
116	277	273.018	7.759	-1.903	-16.844	-11.035	9.940
116	278	272.333	9.053	-1.670	-16.613	-12.098	8.199
116	279	273.150	7.550	-1.431	-16.365	-10.360	9.257
116	280	272.666	8.851	-1.189	-16.101	-11.420	7.514
116	281	273.678	7.355	-.941	-15.823	-9.679	8.570
116	282	273.384	8.662	-.690	-15.529	-10.736	6.823
116	283	274.580	7.171	-.435	-15.223	-8.990	7.875
116	284	274.466	8.482	-.176	-14.904	-10.042	6.125
116	285	275.838	6.995	.087	-14.574	-8.291	7.173
116	286	275.897	8.308	.353	-14.234	-9.338	5.418
116	287	277.442	6.823	.623	-13.884	-7.582	6.460
116	288	277.671	8.138	.895	-13.527	-8.623	4.700
116	289	279.386	6.653	1.170	-13.164	-6.860	5.737
116	290	279.786	7.967	1.448	-12.795	-7.894	3.971
116	291	281.672	6.481	1.728	-12.422	-6.125	5.002
116	292	282.245	7.794	2.009	-12.046	-7.152	3.230
116	293	284.307	6.305	2.293	-11.668	-5.376	4.254
116	294	285.059	7.615	2.578	-11.290	-6.396	2.476
116	295	287.304	6.123	2.864	-10.912	-4.612	3.494
116	296	288.243	7.428	3.151	-10.536	-5.625	1.710
116	297	290.680	5.931	3.439	-10.162	-3.835	2.722
116	298	291.816	7.231	3.726	-9.792	-4.841	.932
116	299	294.454	5.729	4.014	-9.426	-3.044	1.940
ATOM		M - A	NEUTRON	PROTON	ALPHA	Q BETA -	Q BETA +
117	280	284.087	7.791	-3.352	-16.947	-9.714	11.420
117	281	283.357	9.097	-3.106	-16.669	-10.777	9.679
117	282	284.119	7.605	-2.856	-16.376	-9.038	10.736
117	283	283.570	8.917	-2.602	-16.068	-10.096	8.990

TABLE 2

Atomic mass excesses and nuclear binding energies

117	284	284.508	7.430	-2.343	-15.746	-8.352	10.042
117	285	284.130	8.745	-2.080	-15.412	-9.405	8.291
117	286	285.236	7.262	-1.812	-15.066	-7.655	9.338
117	287	285.024	8.579	-1.542	-14.710	-8.701	7.582
117	288	286.294	7.097	-1.268	-14.344	-6.944	8.623
117	289	286.246	8.415	-.990	-13.971	-7.984	6.860
117	290	287.680	6.933	-.710	-13.591	-6.220	7.894
117	291	287.797	8.251	-.426	-13.206	-7.252	6.125
117	292	289.397	6.767	-.141	-12.817	-5.480	7.152
117	293	289.683	8.082	.147	-12.425	-6.504	5.376
117	294	291.455	6.595	.437	-12.031	-4.724	6.396
117	295	291.916	7.906	.728	-11.637	-5.740	4.612
117	296	293.868	6.415	1.020	-11.244	-3.952	5.625
117	297	294.514	7.721	1.314	-10.853	-4.960	3.835
117	298	296.657	6.225	1.608	-10.464	-3.165	4.841
117	299	297.499	7.525	1.902	-10.080	-4.165	3.044
117	300	299.843	6.023	2.196	-9.700	-2.363	4.045
ATOM		M - A	NEUTRON	PROTON	ALPHA	Q BETA -	Q BETA +
118	283	293.666	7.858	-1.962	-16.907	-11.189	10.096
118	284	292.859	9.174	-1.705	-16.584	-12.250	8.352
118	285	293.535	7.692	-1.442	-16.247	-10.508	9.405
118	286	292.890	9.012	-1.175	-15.897	-11.562	7.655
118	287	293.725	7.533	-.905	-15.535	-9.813	8.701
118	288	293.238	8.854	-.630	-15.164	-10.860	6.944
118	289	294.230	7.376	-.351	-14.782	-9.103	7.984
118	290	293.900	8.697	-.069	-14.393	-10.142	6.220
118	291	295.048	7.219	.216	-13.998	-8.377	7.252
118	292	294.877	8.539	.504	-13.597	-9.408	5.480
118	293	296.187	7.058	.795	-13.192	-7.634	6.504
118	294	296.179	8.375	1.088	-12.784	-8.656	4.724
118	295	297.656	6.890	1.383	-12.375	-6.873	5.740
118	296	297.821	8.203	1.680	-11.966	-7.886	3.952
118	297	299.475	6.713	1.979	-11.559	-6.094	4.960
118	298	299.821	8.021	2.278	-11.153	-7.098	3.165
118	299	301.664	6.525	2.578	-10.751	-5.298	4.165
118	300	302.205	7.826	2.878	-10.353	-6.294	2.363
118	301	304.249	6.323	3.178	-9.961	-4.485	3.357
ATOM		M - A	NEUTRON	PROTON	ALPHA	Q BETA -	Q BETA +
119	287	303.538	9.282	-3.063	-16.358	-10.912	9.813
119	288	304.098	7.807	-2.788	-15.981	-9.165	10.860
119	289	303.333	9.133	-2.510	-15.594	-10.213	9.103
119	290	304.042	7.658	-2.227	-15.197	-8.457	10.142
119	291	303.425	8.984	-1.941	-14.792	-9.496	8.377
119	292	304.285	7.508	-1.651	-14.381	-7.731	9.408
119	293	303.820	8.832	-1.359	-13.965	-8.761	7.634
119	294	304.835	7.353	-1.063	-13.545	-6.986	8.656
119	295	304.529	8.673	-.765	-13.123	-8.006	6.873
119	296	305.706	7.190	-.465	-12.700	-6.221	7.886
119	297	305.569	8.505	-.163	-12.277	-7.231	6.094
119	298	306.919	7.017	.140	-11.855	-5.437	7.098
119	299	306.962	8.325	.444	-11.436	-6.437	5.298
119	300	308.499	6.830	.750	-11.021	-4.633	6.294
119	301	308.735	8.131	1.055	-10.611	-5.624	4.485
119	302	310.473	6.629	1.361	-10.207	-3.812	5.474
ATOM		M - A	NEUTRON	PROTON	ALPHA	Q BETA -	Q BETA +
120	290	312.498	9.414	-1.581	-15.999	-12.359	8.457

TABLE 2

Atomic mass excesses and nuclear binding energies

120	291	312.921	7.944	-1 295	-15.587	-10.604	9.496
120	292	312.015	9.273	-1.005	15.168	-11.644	7.731
120	293	312.581	7.802	- 712	-14.742	-9.879	8.761
120	294	311.820	9.128	-.415	-14.311	-10.909	6.986
120	295	312.535	7.653	-.115	-13.877	-9.134	8.006
120	296	311.927	8.975	.187	-13.441	-10.153	6.221
120	297	312.800	7.495	.491	-13.004	-8.367	7.231
120	298	312.356	8.811	.798	-12.568	-9.375	5.437
120	299	313.399	7.324	1.105	-12.133	-7.578	6.437
120	300	313.132	8.634	1.414	-11.702	-8.576	4.633
120	301	314.359	7.140	1.724	-11.276	-6.769	5.624
120	302	314.285	8.442	2.035	-10.854	-7.757	3.812
120	303	315.713	6.939	2.345	-10.440	-5.940	4.795
ATOM		M - A	NEUTRON	PROTON	ALPHA	Q BETA -	Q BETA +
121	293	322.460	9.566	-2.860	-15.518	-10.985	9.879
121	294	322.729	8.098	-2.564	-15.078	-9.222	10.909
121	295	321.669	9.428	-2.264	-14.634	-10.252	9.134
121	296	322.080	7.956	-1.961	-14.186	-8.477	10.153
121	297	321.167	9.281	-1.655	-13.737	-9.496	8.367
121	298	321.731	7.803	-1.347	-13.287	-7.709	9.375
121	299	320.977	9.121	-1.036	-12.839	-8.717	7.578
121	300	321.708	7.636	-.725	-12.393	-6.918	8.576
121	301	321.128	8.947	-.412	-11.950	-7.914	6.769
121	302	322.042	7.454	-.098	-11.513	-6.104	7.757
121	303	321.653	8.756	.217	-11.082	-7.089	5.940
121	304	322.766	7.254	.531	-10.658	-5.269	6.919
ATOM		M - A	NEUTRON	PROTON	ALPHA	Q BETA -	Q BETA +
122	297	330.663	8.262	-.998	-14.472	-10.614	9.496
122	298	329.440	9.590	-.689	-14.011	-11.634	7.709
122	299	329.694	8.114	-.378	-13.550	-9.847	8.717
122	300	328.626	9.435	-.064	-13.090	-10.854	6.918
122	301	329.042	7.951	.251	-12.633	-9.055	7.914
122	302	328.146	9.264	.567	-12.181	-10.049	6.104
122	303	328.742	7.771	.884	-11.734	-8.238	7.089
122	304	328.036	9.074	1.202	-11.294	-9.221	5.269
122	305	328.831	7.572	1.520	-10.862	-7.398	6.244
ATOM		M - A	NEUTRON	PROTON	ALPHA	Q BETA -	Q BETA +
123	300	339.480	8.428	-2.202	-13.791	-9.179	10.854
123	301	338.097	9.751	-1.886	-13.321	-10.186	9.055
123	302	338.196	8.269	-1.568	-12.855	-8.387	10.049
123	303	336.980	9.583	-1.249	-12.394	-9.381	8.238
123	304	337.257	8.091	-.929	-11.939	-7.569	9.221
123	305	336.229	9.395	-.609	-11.492	-8.550	7.398
123	306	336.704	7.893	-.288	-11.053	-6.726	8.371

2.J

Nuclear Physics **25** (1961) 136—151; © *North-Holland Publishing Co., Amsterdam*

Not to be reproduced by photoprint or microfilm without written permission from the publisher

THE ANGULAR CORRELATION OF PROMPT NEUTRONS AND FISSION FRAGMENTS IN THERMAL NEUTRON FISSION OF U^{235}

R. RAMANNA, R. CHAUDHRY, S. S. KAPOOR, K. MIKKE †, S. R. S. MURTHY and P. N. RAMA RAO

Atomic Energy Establishment Trombay, Bombay

Received 26 January 1961

Abstract: The angular distributions of the prompt neutrons of specified mean energies emitted in the thermal neutron fission of U^{235} have been measured with respect to the direction of motion of light fragments. A combination of a gridded ionisation chamber and a gas scintillation counter system using Xenon gas was used to measure the energy of the fission fragments as well as their direction of motion relative to the electric field direction of the ionisation chamber. A fast neutron detector was placed along the electric field direction at a distance of one meter to measure the energy of the prompt neutrons by time of flight technique. The distributions obtained are compared with the distributions computed on the assumption of isotropic emission of neutrons with a Maxwellian emission spectrum. It is shown that the laboratory anisotropy $N(0°)/N(90°)$ is an increasing function of the neutron energy in the laboratory system. The laboratory angular distributions are transformed to obtain the centre-of-mass angular distributions for two groups of prompt neutron emission energies. Anisotropy of the form $(a+b\cos^2\theta)$ is indicated for prompt neutrons with emission energies greater than 1 MeV. Anisotropy of emission is discussed in terms of the possibility of the fragments acquiring a large angular momentum at the instant of scission.

1. Introduction

The angular correlation of prompt neutrons and fission fragments is of considerable importance in the study of fission phenomena as it gives valuable information about the mechanism of prompt neutron emission in the fission process. Recent theories [1, 2]) indicate that the neutrons may be emitted from a stage of the fission process prior to the formation of two spherical fragments and this may lead to anisotropic emission of prompt neutrons in the fragment system. The effect of anisotropy of emission on fission neutron spectrum has been investigated by Terrell [3]) and Sher [4]) using the evaporation model. The energy distribution has been found to be insensitive to anisotropy except for an appreciable effect at very low energies. However, assuming anisotropic emission, Terrell [3]) has obtained a closer resemblance to a Maxwellian distribution, thereby suggesting the presence of anisotropy. But in view of the many uncertainties and approximations in the evaporation model, the fission neutron spectrum does not conclusively give any positive information about anisotropy. Several experiments [5–7]) have been performed to determine the actual angular

† On leave of absence from the Institute for Nuclear Research, Polish Academy of Sciences, Poland.

correlations of prompt neutrons and the fission fragments in the laboratory system. For various reasons these have not conclusively detected the presence of anisotropy. Firstly, in these experiments the angular correlations have been obtained for the total neutron spectrum. If the anisotropic component is only due to a portion of the emission spectrum, the presence of anisotropy is likely to be masked by the large background of isotropic emission. Secondly, as suggested by Terrell [3]), it is difficult to distinguish between non-uniform detector response and anisotropic emission, as the efficiency of neutron detectors is a function of the neutron energy and hence the angle of detection.

In the experiment described here the angular distributions of prompt neutrons in the laboratory system with respect to the direction of motion of the light fragments for various prompt neutron energy groups have been obtained. These are transformed to obtain the angular distributions in the centre-of-mass system for specified neutron energy groups. The method described in a previous paper [7]) has been improved to obtain these angular correlations. The prompt neutron energies have been determined by the time of flight technique. This method has the advantage that many angles in the laboratory system can be studied simultaneously for selected prompt neutron energies. Also by comparing the prompt neutron time of flight spectrum with the well established prompt fission neutron spectrum it is possible to obtain the neutron detector efficiencies for various energies.

2. Experimental Arrangement and Method

Fig. 1 shows the experimental arrangement. A gridded ionisation chamber is represented by A. The distance between the collector and the grid and the grid

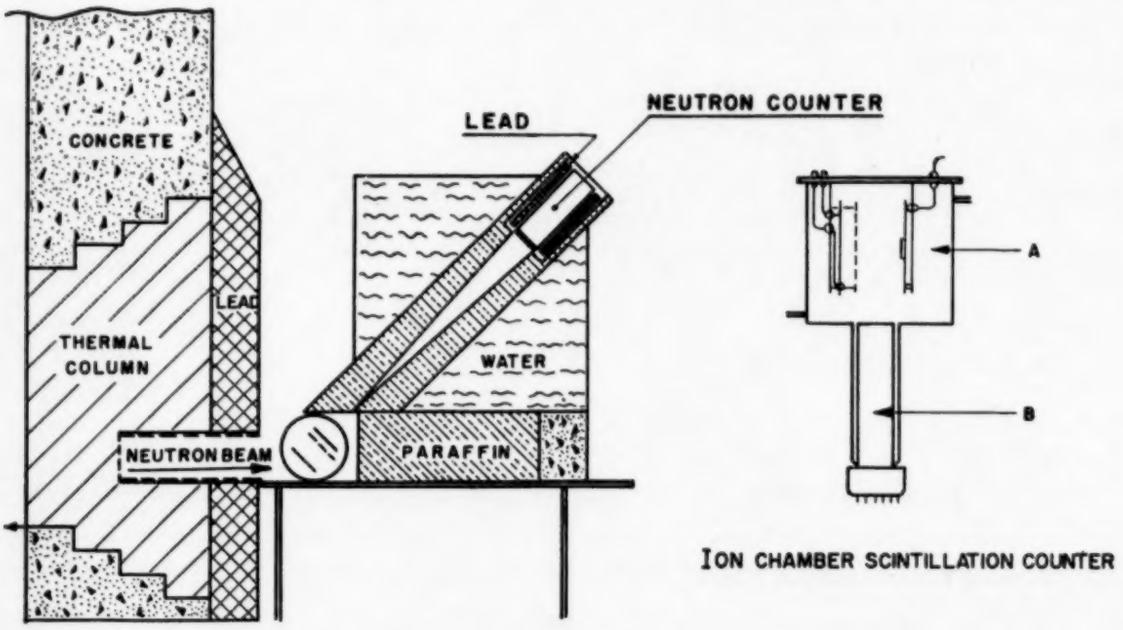

Fig. 1. Schematic diagram of the experimental apparatus.

and the cathode was 0.7 and 2.1 cm, respectively. The cathode of the ion chamber was coated with a layer of U^{235} having thickness 0.5 mg/cm^2. A potential of -1100 V and -638 V was applied to the cathode and grid, respectively, and the collector was kept at the ground potential. In order to avoid electron collection by the grid [8]), the ratio of the fields between the grid collector and grid-cathode regions was kept as 4.14. A photomultiplier B was placed immediately below the electrode system and the whole chamber was filled with Xenon gas at a pressure of 1.3 atm. The photomultiplier was covered with a thin layer of p-quaterphenyl to observe the scintillations produced in the Xenon gas by the passage of fission fragments. Special care was taken to see that the Xenon gas was of the highest purity as the scintillation pulse height is very sensitive to the purity of the gas. The whole system was hermetically sealed to avoid any poisoning of the gas and care was also taken in the choice of materials inside the system so that the gas remained at a high degree of purity for long periods of time. The whole assembly was placed in front of the thermal column of the Apsara reactor where the thermal neutron flux level was of the order of 3×10^6 n/cm^2 sec.

The angle ϕ of the fission fragment track with the field direction, along which the prompt neutrons are detected is determined by the time delay t between the instant of fission (zero time) as given by the fission scintillation pulse observed by the photomultiplier B, and the instant the electrons from the edge of the track cross the grid of the ion chamber. The delay t and angle ϕ are connected by the relation $(\alpha-\beta t) = \cos\phi$, where α and β are constants for a fixed range R'. The range distribution is obtained from the fission fragment energy distribution and only the light fragments of the most probable mode having a small spread in the range R' were studied. The delay distribution $N(t)$ per unit time interval is connected with the angular distribution per unit solid angle $n(\phi)$ by

$$N(t)\,\mathrm{d}t = \text{const.}\; n(\phi)\sin\phi\,\mathrm{d}\phi,$$

which gives

$$n(\phi)\mathrm{d}\phi = \text{const.}\frac{N(t)}{\sin\phi}\frac{\mathrm{d}t}{\mathrm{d}\phi}\mathrm{d}\phi$$

$$= \text{const.}\; N(t)\mathrm{d}\phi$$

for a fixed range R', i.e.

$$n(\phi) = \text{const.}\; N(t).$$

Hence the delay distribution $N(t)$ directly gives the angular distribution $n(\phi)$ of the fission fragments of a fixed range R'. As thermal neutron fission is isotropic, the angular distribution $n(\phi)$ plotted against ϕ, and hence the delay distribution $N(t)$ plotted against t should be rectangular. In the rectangular distribution t_{min} and t_{max} correspond to the angles 0° and 90°, respectively.

Associated with this arrangement was a fast neutron time of flight spectrometer. The fast neutron detector was a plastic scintillator of 10 cm diameter and of 3 cm thickness, kept at a distance of 1 m from the U^{235} foil and along the direction of the electric field of the ionisation chamber. As shown in fig. 1 the neutron counter was well shielded to minimise the effects due to background. A time to pulse height converter [9]) was used to obtain pulse height proportional to the time difference between the fission scintillation pulse which is the "start pulse" and the "neutron counter pulse" which is the "stop pulse". A fast-slow

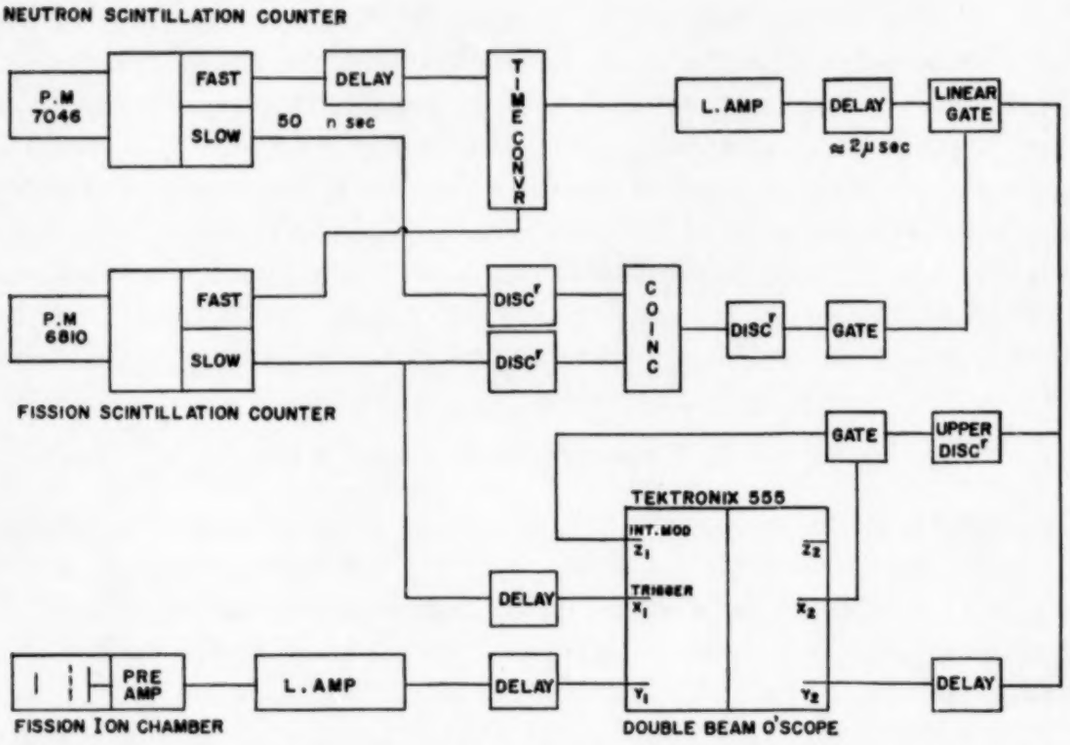

Fig. 2. Block diagram of the electronic set up for recording the events on the Tektronix oscilloscope 555.

coincidence system was used with discriminators in the side channel for pulse height selection. In order to determine the zero time the prompt gamma peak in the time of flight spectrum was used. The delay distribution of the light fragments of the most probable mode which emit the prompt neutrons of the specified energy in the field direction directly gives the angular distribution of prompt neutrons of the fixed energy group with respect to the direction of the light fragments.

The time of flight of the prompt neutron, the fission ionisation pulse associated with the same event, and the delay between the zero time pulse and the start of the fission ionisation pulse were photographed using a double beam Tektronix 555 oscilloscope provided with camera and film moving device. The block diagram of the electronic set up is shown in fig. 2. A typical photograph

of an event giving all the three parameters is shown in fig. 3. About 25 000 event were photographed and analysed, of these the events which corresponded to the most probable mode of the light fragment emission were studied. The chance coincidences due to background were distributed in two different ways over the neutron time of flight spectrum depending upon whether the background pulse follows or preceeds the zero time pulse within the resolution time of the side channel coincidence unit. In the former case the chance coincidences were distributed isotropically over all the time channels. These random coincidences were accurately determined by introducing an inherent delay of 50 n sec in the path of neutron counter pulses. The counts in the channels preceding the prompt gamma peak determine the isotropic background. In the latter case, time-converter gave a large output pulse as there was no "stop pulse" corresponding to the "start pulse". An upper channel discriminator was used to avoid these background pulses triggering the oscilloscope sweep. To obtain the calibration of the time delay in terms of the fragment track angle with the field direction, the upper channel discriminator level was so chosen as to allow a small number of background pulses to trigger the sweep to obtain the isotropic distribution of fission fragments without any reference to the emitted prompt neutrons.

3. Experimental Results

The delay distribution for the light fragment peak without any reference to the emitted neutrons is shown in fig. 4. For the fission fragments of a fixed range R' this should be a rectangular distribution. The departure of the experimental points from the rectangular distribution in the region of small and large delays is due to the following reasons. Firstly, as the U^{235} foil used in the work was not very thin there will be a spread in the ranges of the fragments selected for small energy width at the light fragment peak. Secondly the ionisation pulse for the fission fragment track of fixed range R' which is parallel to the electric field direction has a slow rise. For this reason a slight uncertainty is caused in fixing the point where the fission ionisation pulse just begins to rise. This in effect distributes the delays of the zero degree region over a larger time channel width thereby reducing the counts in each channel. The correction factor in the zero degree region is determined from the departure of the experimental points from rectangular distribution and is used to correct the other delay distribution curves, obtained in coincidence with the neutrons of specified energy groups. The fission fragments emerging at higher angles will lose some energy in the foil and appear with a smaller range. This results in the reduction of counts at the larger delays. An accurate determination of the maximum delay corresponding to the fragment angle of 90° was made by plotting the integral delay spectrum for the total fission fragment spectrum including all the ranges, as the maximum delay is independent of range. The integral delay spectrum is

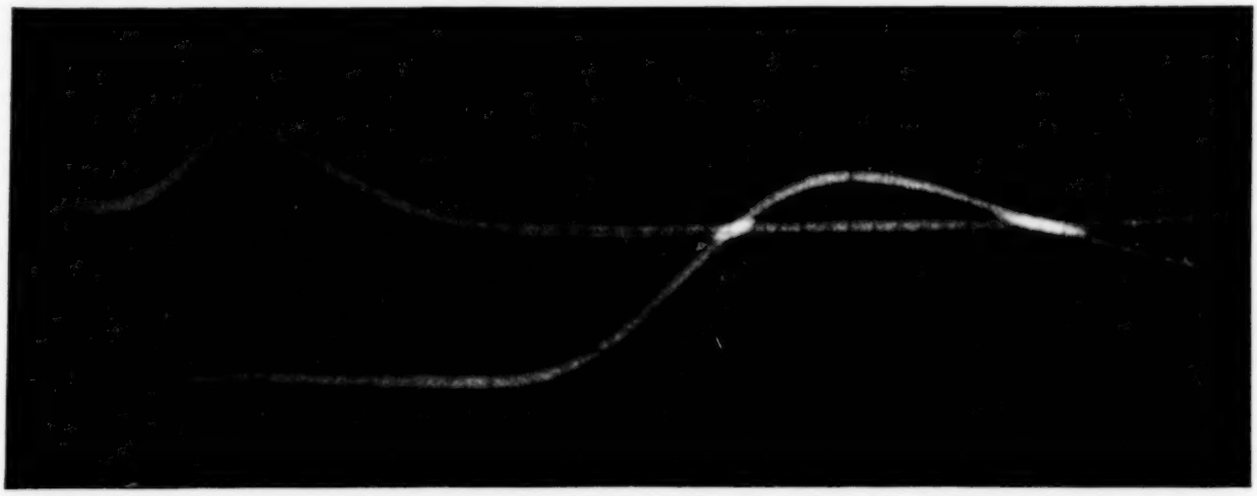

Fig. 3. A photograph of a typical event. The upper pulse is the time converter output giving the neutron time of flight. The lower pulse is the fission ionisation pulse giving the energy of the fission fragment and the track orientation with the field direction. The lower pulse is intensity modulated and intensity is on slightly later than the zero time. Hence the initial portion of the sweep is not photographed. The point of rise of the lower pulse is measured from a reference point corresponding to the start of the upper sweep.

shown in fig. 5. The constants α and β for the light fragment peak were obtained by determining $t_{90°}$ and $t_{60°}$ corresponding to the track angles of 90° and 60°, respectively. The delay $t_{60°}$ can be accurately determined as it divides the isotropic rectangular distribution corrected for foil thickness into two equal areas. The experimental points are considered only up to $t_{60°}$, as higher delays

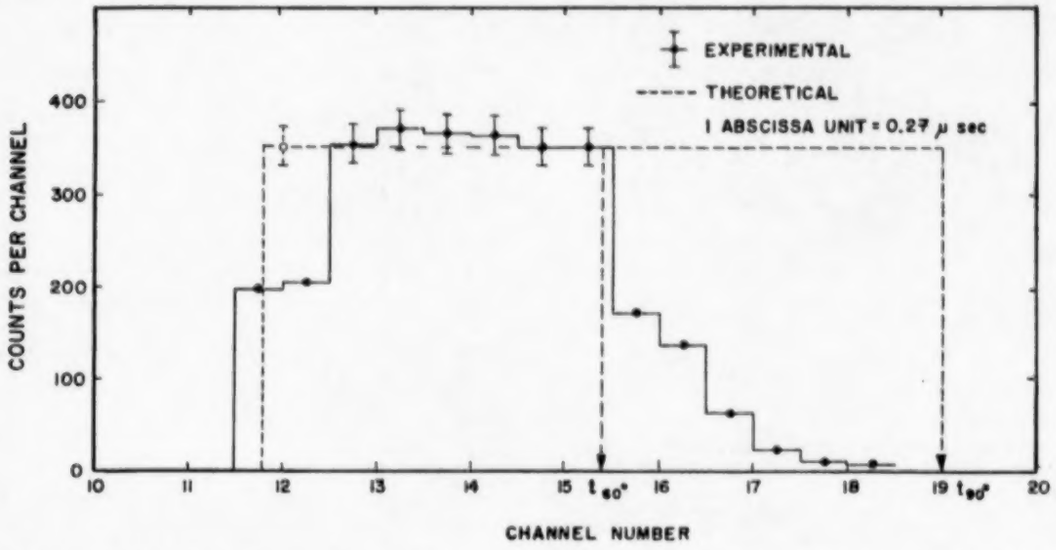

Fig. 4. Isotropic delay distribution of the fragments selected at the light fragment peak having a very small spread in ranges.

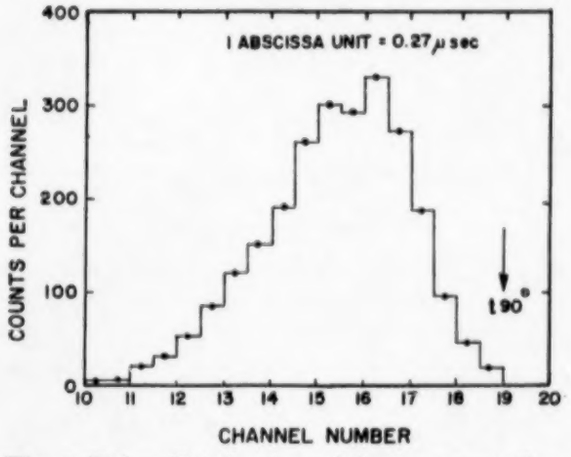

Fig. 5. Delay distribution of the fragments for the total fission ionization spectrum. The maximum delay corresponds to the track angle of 90° with the field direction.

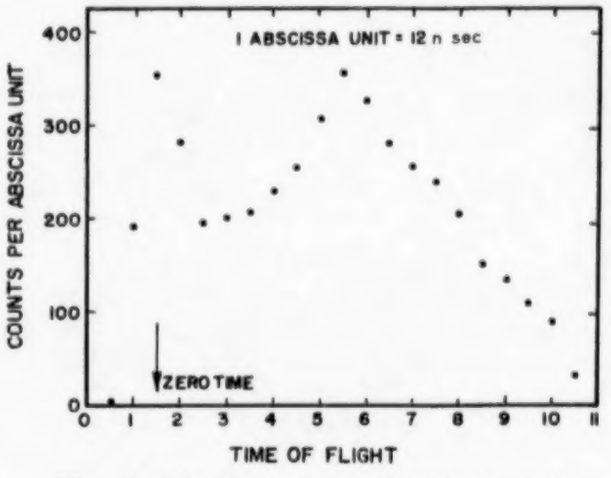

Fig. 6. Observed time of flight spectrum of the prompt neutrons.

are subject to errors due to foil thickness.

The neutron time of flight spectrum after correcting for the chance coincidences is shown in fig. 6. The centre of the gamma peak determines the zero time. The time of flight spectrum was converted to the energy scale and compared with the Watt spectrum to determine the relative efficiency of the neutron

detector, for various neutron energies. The efficiency of the neutron detector was also calculated for different neutron energies on the basis of known (n, p) cross sections and this was found to give reasonably good fit with the experimentally determined response. The prompt neutron energy spectrum was divided into three regions of mean neutron energies of 0.58, 1.49 and 3.00 MeV, respectively. The number of such divisions was restricted by the available statistics.

The chance coincidence pulses of the neutron time of flight spectrum are

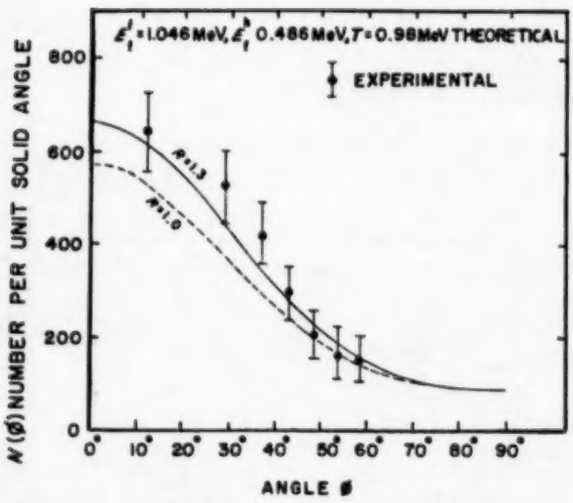

Fig. 7. Comparison of the calculated and experimental angular distributions for the total prompt neutron spectrum. Angle ϕ is measured with the direction of motion of the light fragments.

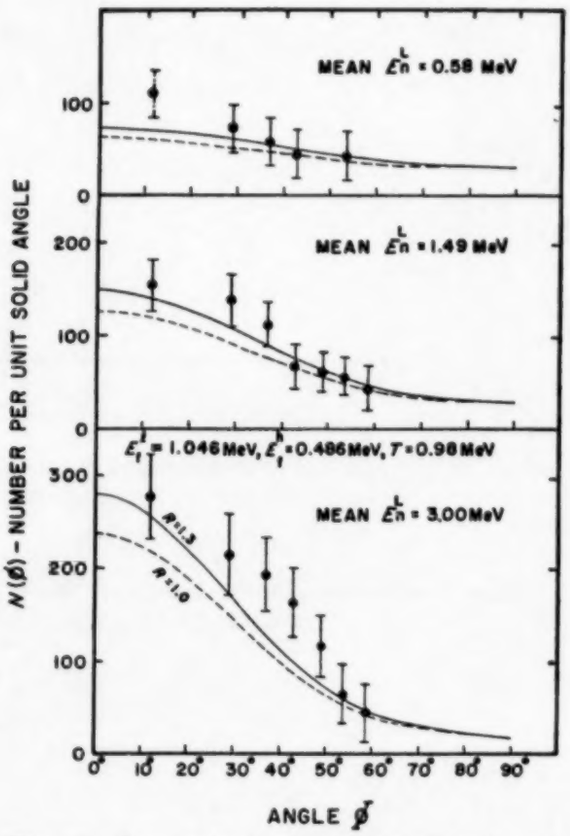

Fig. 8. Comparison of the calculated and experimental angular distributions of prompt neutrons of different mean energies. Angle ϕ measured with the direction of motion of the light fragments.

isotropically distributed over all the delays. The distribution curves were corrected for chance coincidence contribution. These corrected curves directly give the angular distribution of prompt neutrons with respect to the direction of motion of the light fragments. As the neutron detector response is a function of the prompt neutron energy and hence the angle of detection, the experimental points have been corrected for the relative efficiency for various angles of detection. The efficiency correction is discussed in the appendix. The final distribution curves corrected for relative detector efficiencies are shown in figs. 7 and 8.

In the course of the experiments it was noted that when the field in the grid-collector region was reasonably high, two pulses were observed for each event in the fission scintillation counter, the first corresponding to the instant of fission and the subsequent one corresponding to the arrival of the electrons in the grid collector region. It was also noticed that the pulse height of the second pulse increases with the increase of the field in this region and the delay between the two pulses corresponds to the time the electrons take to reach the grid. The occurrence of the second pulse is explained by the fact that when the electrons reach the grid-collector region and if the field in this region is sufficiently high they attain large enough energies between successive collisions to excite the atoms of Xenon gas to a higher state which subsequently de-excites by the emission of photons. The second pulse can be used for directly measuring the angular distributions if the linearity between the pulse height and energy of the fission fragment is established. This point is being investigated. However, in the actual experiment the field in the grid collector region was kept such that it did not give rise to the second pulse.

4. Theory and Discussion

The experimental angular distributions are compared with the theoretical distributions calculated on the following assumptions:

1) All the prompt neutrons are emitted in such a time range that it can be considered that the moving fragment has attained its maximum velocity and at the same time possesses all its kinetic energy. This is true if the neutron time of emission is of the order between 10^{-20} and 10^{-14} sec [3, 6]).

2) The emission spectra of the neutrons are the same for light and heavy fragments.

3) The centre-of-mass spectrum is described by a single Maxwellian distribution per fragment corresponding to a temperature which gives the best fit to the laboratory neutron spectrum.

Feather [10]), using the evaporation model of Weisskopf [11]), has calculated the fission neutron spectrum. This, however, does not seem to be in very good agreement with the experimental data. Fraser [6]) has modified the evaporation spectrum by adding a term given by Feld *et al.* [12]) to account for sufficient internal excitation of the fragment which enables it to emit more than one neutron on the average. This gives satisfactory agreement in both the energy and angular distributions if an additional assumption is made that the light fragments emit 30 % more neutrons than the heavy. Terrell [3]) has shown that the evaporation theory, after making allowance for the changes of nuclear temperatures of fragments resulting from successive emission of neutrons agrees with the experimental neutron energy spectrum. Terrell [3]) concluded that for each fragment the calculated emission spectrum is very nearly equal to the sum of

two normalised Maxwellians. A single Maxwellian emission spectrum leads to the well known Watt spectrum which gives a satisfactory fit with the experimental data. Sher [4]) has shown that the difference between assuming Terrell's emission spectrum approximated by two Maxwellians per fragment and a single Maxwellian per fragment is small in both the energy and angular distributions. Hence for the sake of simplicity we have assumed a single Maxwellian emission spectrum.

If a neutron is emitted from a moving fragment with energy E at an angle ϕ with respect to the direction of the fragment in the laboratory system, the centre-of-mass emission energy η and angle θ are given by

$$\eta = E+E_f-2\sqrt{EE_f}\cos\phi, \tag{1}$$

$$\theta = \tan^{-1}\frac{r\sin\phi}{r\cos\phi-1}, \tag{2}$$

where E_f is the fragment kinetic energy per nucleon, that is the energy $M_n v_f^2/2$ of a neutron moving with the velocity of the fragment v_f and $r = \sqrt{E/E_f}$. The probability $N(E, \phi)$ (per unit solid angle and energy) that a neutron is observed at an angle ϕ with energy E is given by

$$N(E,\phi)\sin\phi\,\mathrm{d}E\,\mathrm{d}\phi = F(\eta,\theta)\sin\theta\frac{\mathrm{d}\eta}{\mathrm{d}E}\frac{\mathrm{d}\theta}{\mathrm{d}\phi}\,\mathrm{d}E\mathrm{d}\phi, \tag{3}$$

where $F(\eta, \theta)$ is the probability per unit solid angle and energy, for a neutron to appear with emission energy η at angle θ in the centre-of-mass system. We assume

$$F(\eta,\theta) = f(\eta)n(\theta).$$

For a Maxwellian distribution, it can be shown that

$$N(E,\phi)\mathrm{d}E\,\mathrm{d}\phi = \text{const.}\; n(\theta)E^{\frac{1}{2}}\exp\left[-\frac{1}{T}(E+E_f-2\sqrt{EE_f}\cos\phi\right]\mathrm{d}E\,\mathrm{d}\phi, \tag{4}$$

where $n(\theta)$ represents the angular distribution per unit solid angle in the centre-of-mass system. Hence we have

$$N(E,\phi)\,\mathrm{d}E\,\mathrm{d}\phi = \text{const.}\; n(\theta)[\text{lab. an. factor}]\,\mathrm{d}E\,\mathrm{d}\phi, \tag{5}$$

the factor in square brackets being the laboratory anisotropy factor.

4.1. ISOTROPIC EMISSION

In case of isotropic emission $n(\theta)$ is constant.

For this case, integration of eq. (4) over all the solid angles leads to the well known Watt spectrum, while integration over all the energies gives the follow-

ing laboratory angular distribution for the total neutron spectrum:

$$N(\phi)\mathrm{d}\phi = \text{const. } \mathrm{e}^{-E_f/T}$$
$$\left[\mathrm{e}^{E_f \cos^2\phi/T}\{1+E_2(\sqrt{E_f/T}\cos\phi)\}\left\{1+\frac{2E_f}{T}\cos^2\phi\right\}+\frac{2}{\sqrt{\pi}}\sqrt{\frac{E_f}{T}}\cos\phi\right]\mathrm{d}\phi, \quad (6)$$

where

$$E_2(x) = \frac{2}{\sqrt{\pi}}\int_0^x \mathrm{e}^{-t^2}\mathrm{d}t.$$

In actual experiments, it is not possible to know whether a neutron counted in coincidence with a light fragment at an angle ϕ appeared at angle ϕ from the light fragment or at angle $\pi-\phi$ from the heavy fragment. If R denotes the ratio of emission probabilities from the light and heavy fragments, the angular distribution of neutrons of laboratory energy E in coincidence with the light fragments is given by

$$N(E,\phi)\mathrm{d}E\,\mathrm{d}\phi = \text{const.}\left[RE^{\frac{1}{2}}\exp\left\{-\frac{1}{T}(E+E_f^{\mathrm{l}}-2\sqrt{EE_f^{\mathrm{l}}}\cos\phi)\right\}\right.$$
$$\left.+E^{\frac{1}{2}}\exp\left\{-\frac{1}{T}(E+E_f^{\mathrm{h}}+2\sqrt{EE_f^{\mathrm{h}}}\cos\phi)\right\}\right]\mathrm{d}E\,\mathrm{d}\phi, \quad (7)$$

where l and h refer to light and heavy fragments respectively.
Similarly, to get the actual angular distribution of the prompt neutrons with respect to the direction of light fragments, for the total neutron spectrum eq. (6) should be written as the sum of two terms representing the contributions from the light and heavy fragments, respectively.

In the course of our discussion, we call the laboratory angular distributions calculated for the case of isotropic emission the "laboratory anisotropy distributions", the energy of a neutron in the laboratory system "neutron energy", and the energy of a neutron in the centre-of-mass system "emission energy".

The theoretical curves for the case of isotropic emission, calculated for $R = 1.0$ and 1.3, are shown in fig. 7, along with the experimental points. The normalization of the theoretical curves with the experiment should have been done at 90°, but as the experimental information beyond 60° is not reliable, the normalization has been done arbitrarily at 60°. Normalization at 60° slightly reduces the effect of anisotropic emission, if any, and brings the experimental data in closer agreement with the curves calculated for isotropic emission. The experimental points are corrected for non-uniform response of the detector at various angles up to a first approximation. It is expected that a more rigorous correction, as discussed in the appendix, will not bring an appreciable change in the experimental curve. The experimental results are in better agreement with the laboratory anisotropy distribution for the case of $R = 1.3$. This is in accordance with Fraser's assumption for the higher emission probability from the

light fragments, which Fraser and Milton [13]) confirmed in a separate experiment. In the vicinity of the forward angles the experimental points are slightly above the theoretical curve even for $R = 1.3$. Other experimenters have found a better fit of their results with the theory based on isotropic emission. It is expected that the angular distribution curve for the total neutron spectrum cannot give much information about anisotropic emission if the anisotropy is only due to a portion of the emission spectrum. The calculated laboratory anisotropy distributions for the cases $R = 1.00$ and $R = 1.3$ for different mean neutron energies are shown in fig. 8 along with the experimental points, corrected for relative angular efficiency, belonging to the group of neutrons

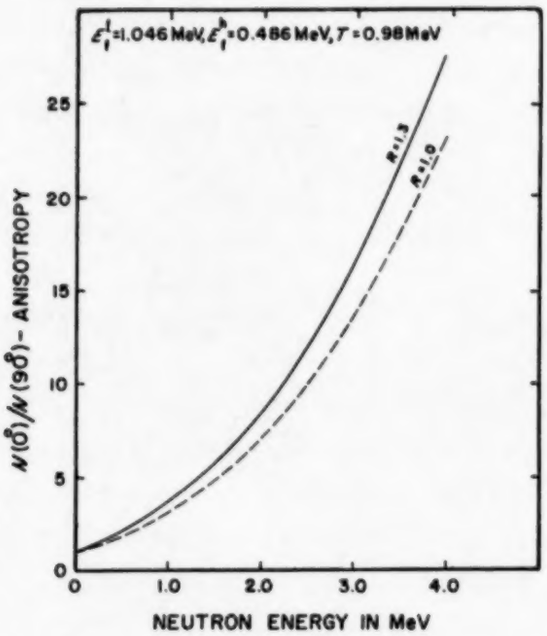

Fig. 9. The dependence of the ratio $N(0°)/N(90°)$ on the neutron energy in the laboratory system, as calculated on the basis of isotropic emission from the moving fragments with the Maxwellian emission spectrum. The angle is measured with the direction of motion of the light fragments.

having the same mean energies as the calculated curves. Here also the experimental results give better fit with the theory for the case $R = 1.3$. Both the experimental results and the theoretical curves show that the laboratory anisotropy increases with the neutron energy. For the case of isotropic emission, the laboratory anisotropy $N(0°)/N(90°)$ is calculated for different neutron energies and the curve is shown in fig. 9. The calculated curve shows that the laboratory anisotropy is an increasing function of the neutron energy.

Leachman [14]), while describing Hoffman's experiment [15]) for determining the angular correlation of prompt gammas and fission fragments, has stated that high energy neutrons, which are likely to be detected along with prompt gammas, are expected to be distributed isotropically. This does not reconcile with the facts discussed above. Hence angular correlation measurements of prompt-

gammas and fission fragments are subject to errors † if either all the prompt neutrons including the fastest are not eliminated by time of flight or the efficiency of the detector is not small for neutrons.

If angular distributions are studied for fixed neutron energies, the neutrons come from different parts of the emission spectrum for various angles of detection. Thus for any individual distribution of fig. 8 corresponding to a fixed neutron energy, the emission energy of the neutrons which contribute to the angular distributions is different for various angles of detection. If the anisotropic emission is a function of emission energy of the neutrons, these distributions cannot give much information about anisotropic emission. However, experimental distributions for different neutron energy groups can be transformed to obtain the angular distributions in the centre-of-mass system of the neutrons belonging to different emission energy groups.

4.2. CENTRE-OF-MASS ANGULAR DISTRIBUTION

The angular distribution of prompt neutrons in the fragment system is obtained in the following manner:

1) The experimental angular distributions are corrected for the contribution of the neutrons coming from heavy fragments at angle $(\pi-\phi)$ for $R = 1.3$. As this contribution is very small for values of ϕ up to 60°, the contribution is calculated on the assumption of isotropic emission.

2) As the energy width and the efficiency of the detector for the three individual groups are not the same, the three curves are normalised with respect to each other.

The total number of events for neutrons having energy between E and $E+\mathrm{d}E$ from 0° to 60° is

$$A(E)\mathrm{d}E = \int_0^{60^\circ} N(E, \phi) \sin\phi \, \mathrm{d}\phi \, \mathrm{d}E$$
$$= \int_{\frac{1}{2}}^{1} N(E, \phi)\mathrm{d}(\cos\phi)\mathrm{d}E.$$

The experimental angular distributions for different energies are plotted against $\cos\phi$ and the area under each curve for a mean neutron energy E is normalised to the calculated $A(E)$. As this is a second order correction, $A(E)$ is calculated assuming $n(\theta) = 1$.

3) The emission energy η and the angle of emission θ are calculated from eqs. (1) and (2). As each experimental curve of fig. 8 is for a small group of neutrons having mean laboratory energy E, the calculated values of η and θ represent the average emission energy and average angle of emission, respectively. From eq. (5), $n(\theta)$ is calculated after correcting for the laboratory anisotropy term.

† However, Hoffman reports that the error due to this effect in the experiment is small, as the efficiency of the detector used in the experiment was very low for neutrons (private communicaiton).

The angular distribution of the prompt neutrons in the fragment system, obtained in the above way, is shown in fig. 10. Fig. 10(a) gives the angular distribution $n(\theta)$ for group of neutrons having mean emission energies less than 1 MeV. The average emission energies contributing to the various angles of emission are also shown. Fig. 10(b) shows the angular distribution $n(\theta)$ for neutrons having mean emission energies more than 1 MeV.

The two distributions of fig. 10(a) and (b) appear different from each other.

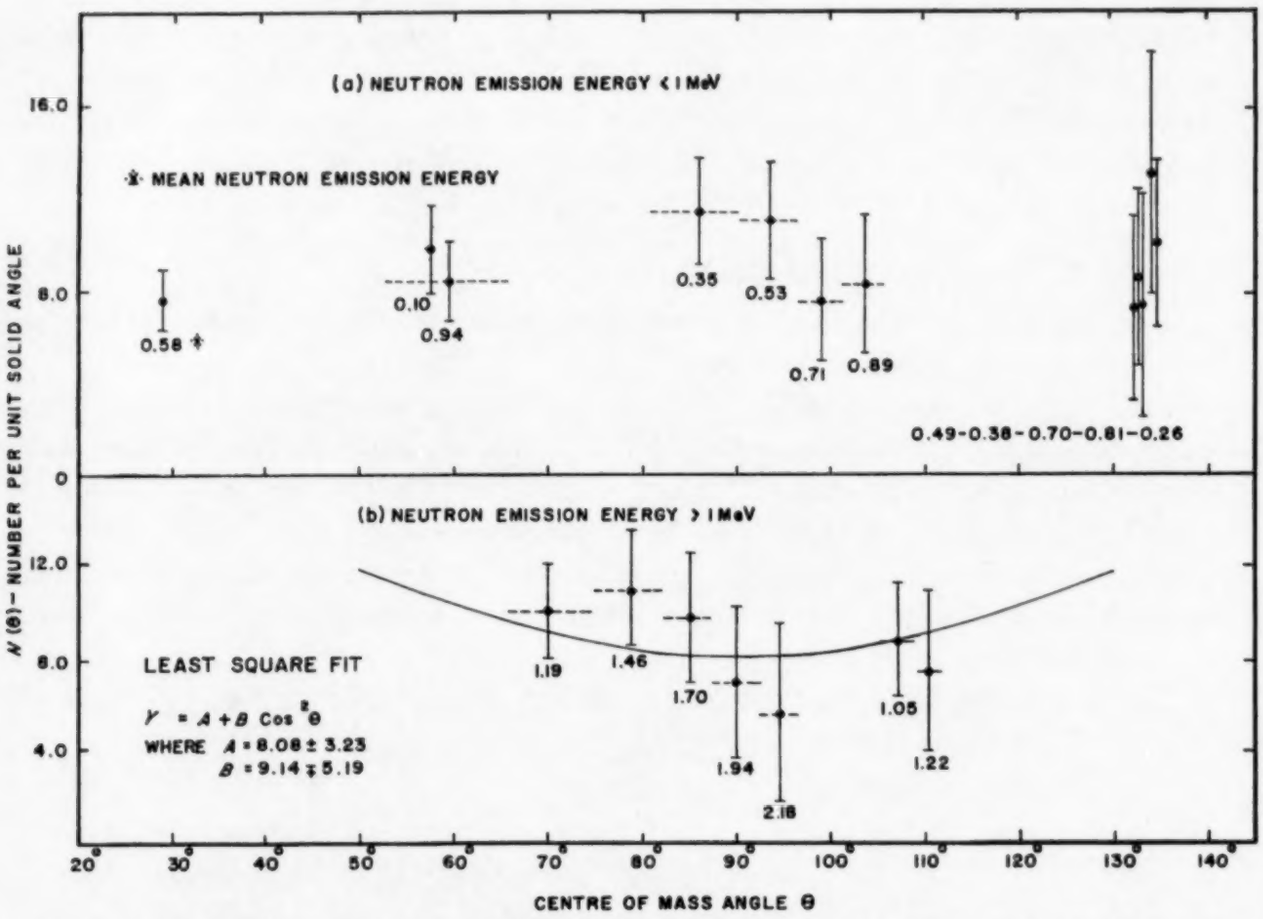

Fig. 10. The transformed angular distribution in the centre-of-mass system (same as fragment system) for two different emission energy groups. The number below each point indicates the mean emission energy in MeV of the neutrons contributing to the c.m. angle.

The experimental points of fig. 10(a) do not show any systematic trend and a straight line with $n(\theta)$ = constant can be made to fit the experimental distribution within experimental errors. On the other hand in fig. 10(b), a dip in the region of 90° is indicated. The experimental curve has been fitted by the least square fit to the form $n(\theta) = (a + b\cos^2\theta)$, where a and b were found to be 8.08 ± 3.23 and 9.14 ∓ 5.19, respectively. This suggests that neutrons with higher emission energy may be more favourably emitted in the centre-of-mass system, along the axis of fission.

With the available statistics it was not possible to obtain experimental points

in the region of 0° in the centre-of-mass distribution shown in fig. 10(b), as this would require us to determine the angular distribution of prompt neutrons having very high mean energies in the laboratory system. The relative number of such high energy neutrons in the prompt neutron energy spectrum is very small.

The experimental results showing anisotropy for higher emission energies of the neutrons can be accounted for in a qualitative way by following the suggestion of Strutinski [16]). Here it is suggested that the presence of a large angular momentum **I** perpendicular to the direction of fragment motion is brought in by the transverse component of Coulomb repulsion between the two stubs of the fission fragments if these are not quite collinear after fission. A rough estimate shows that **I** can be of the value 20, and the small anisotropy of gamma rays as observed by Hoffman [15]) can be accounted for by assuming that the radiation is quadrupole rather than dipole in character.

With the angular momentum **I** associated with each fragment, it is expected that the neutron emission will be hindered with respect to the gamma ray deexcitation, especially in the case of low lying levels [17, 18]). This may explain the fact that the energy observed in the form of prompt gamma rays is much more than expected on the calculation based on the statistical deexcitation of fission fragments.

With the presence of the fragment angular momentum of large magnitude, anisotropy of neutron emission may result as follows. The distribution of states in the residual nucleus is such that the number of available states decreases with the increasing spin of the residual nucleus. This favours the emission of neutrons with orbital angular momentum vector **l** parallel to the direction **I** so as to leave the nucleus in a low spin state. As **l** is perpendicular to the direction of neutron motion, the neutrons will be emitted in an equitorial plane perpendicular to **I**. Taking into account all the orientations of **I** perpendicular to the direction of motion of the fragment, the intersections of the various equitorial planes lead to a distribution symmetrical about 90° and having forward-backward peaking as these directions are contained in all the equitorial planes. Discussing the angular distributions in compound nuclear processes Erikson and Strutinski [19]) have derived the following expression for angular distribution in such cases:

$$n(\theta) \approx 1+\tfrac{1}{2}\alpha_I{}^2\bar{l}^2\bar{I}^2 \cos^2\theta,$$

where $\alpha_I = \hbar^2/2JT$, while J and T are the moment of inertia and the temperature of the emitting nuclei respectively. Furthermore, $\bar{l}^2$ is given by

$$\bar{l}^2 = \tfrac{1}{2}l_{\max}^2 = \frac{\mu_2 E_2 R_2{}^2}{\hbar^2},$$

where μ_2 and E_2 are mass and energy of the emitted particle and R_2 the inter-

action radius. On this picture, more anisotropy is to be expected for higher emission energies and this seems to agree on a qualitative basis with our observations.

Our thanks are due to B. R. Ballal for his assistance in the experimental work. Our thanks are also due to S.L. Raote for the construction of electronic equipment and to R. Rangarajan, C. S. Gopalakrishnan and Ramanan for their help in the analysis of photographs.

Appendix

CORRECTION FOR THE NON-UNIFORM RESPONSE OF THE NEUTRON DETECTOR

The spectrum $N(E, \phi, E_f^1)$ of the prompt neutrons emitted from the light fragments at an angle ϕ, is given by

$$N(E,\phi,E_f^1) = \text{const. } E^{\frac{1}{2}} \exp\left[-\frac{1}{T}(E+E_f^1-2\sqrt{EE_f^1}\cos\phi)\right], \tag{1}$$

and

$$N'(E_f^1, \phi)\mathrm{d}\phi = \left[\int_0^\infty N(E, \phi, E_f^1)\mathrm{d}E\right]\mathrm{d}\phi, \tag{2}$$

assuming $n(\theta) = 1$.

If $\varepsilon(E)$ is the efficiency of the neutron detector for neutrons of energy E, the mean efficiency $\varepsilon(\phi, E_f^1)$ of the detector for neutrons coming at an angle ϕ from the light fragments can be written as

$$\varepsilon(\phi, E_f^1) = \frac{\int_0^\infty \varepsilon(E)N(E, \phi, E_f^1)\mathrm{d}E}{\int_0^\infty N(E, \phi, E_f^1)\mathrm{d}E}. \tag{3}$$

For the case that the efficiency $\epsilon(E)$ varies linearly with the neutron energy, it can be shown that

$$\varepsilon(\phi, E_f^1) = \varepsilon(\bar{E}), \tag{4}$$

where $\bar{E}$ is the mean energy of the distribution $N(E, \phi, E_f^1)$.

If the neutrons are detected at an angle ϕ measured with the direction of motion of the light fragments, there will also be a finite contribution at this angle from neutrons appearing at an angle $\pi-\phi$ from the heavy fragments. If the angle ϕ is measured with the direction of motion of the light fragments the average mean efficiency $\overline{\varepsilon(\phi)}$ of the neutron detector, taking into account mean efficiency $\varepsilon(\pi-\phi, E_f^h)$ for the neutrons coming from the heavy fragments, can be written as

$$\overline{\varepsilon(\phi)} = \frac{\varepsilon(\phi, E_f^1)N'(\phi, E_f^1)+\varepsilon(\pi-\phi, E_f^h)N'(\pi-\phi, E_f^h)}{N'(\phi, E_f^1)+N'(\pi-\phi, E_f^h)}. \tag{5}$$

The angular distribution for the total neutron spectrum shown in fig. 7 has been corrected for relative angular efficiencies of the neutron detector with the approximation given by eq. (4). It is expected that if the curve $\varepsilon(E)$ versus E does not deviate much from a straight line, which is true in the present case, $\varepsilon(\bar{E})$ will not differ appreciably from $\overline{\varepsilon(\phi)}$. Hence the approximation made can be justified.

The angular distributions shown in fig. 8, are obtained for groups of neutrons having specified mean energies. If the groups of neutrons chosen are not sufficiently narrow in energy widths, the efficiency $\varepsilon(E)$ will vary within each group. These distributions have been corrected for relative $\overline{\varepsilon(\phi)}$ in the following way. The higher energy neutrons will be distributed more in the vicinity of forward angles making the neutron detector less efficient for forward angles. A good estimate of average efficiency $\overline{\varepsilon(\phi)}$ has been made by further dividing each group of neutrons into sub-groups, in accordance with the expected number of neutrons at various angles computed from theory. Each sub-group is supposed to be contributing at different angles depending on its mean energy. The energy width of each sub-group is so small that $\varepsilon(E)$ does not vary for neutrons of the same sub-group.

References

1) D. L. Hill and J. A. Wheeler, Phys. Rev. **89** (1953) 1102
2) V. S. Stavinski, JETP (USSR, Soviet Physics) **36** (1959) 629
3) J. Terrell, Phys. Rev. **113** (1959) 527
4) R. Sher, private communication
5) R. R. Wilson, Phys. Rev. **72** (1947) 189
6) J. S. Fraser, Phys. Rev. **88** (1952) 536
7) R. Ramanna and P. N. Rama Rao, Proc. Second Geneva Conference **15** (1958) 361
8) Bunemann, Cranshaw and Harvey, Can. J. Research **27** (1949) 191
9) L. E. Beghian, G. H. R. Ketel and R. P. Scharenberg, Rev. Sci. Inst. **29** (1958) 753
10) Feather, U. S. Atomic Energy Commission Document BR, 335A (1942) unpublished
11) V. F. Weisskopf, Phys. Rev. **52** (1937) 295;
J. M. Blatt and V. F. Weisskopf, Theoretical Nuclear Physics (John Wiley and Sons, New York, 1952) pp. 365–374
12) Feld, Feshbach, Goldberger, Goldstein and Weisskopf, U. S. Atomic Energy Commission, Report, NYO–636 (1951) unpublished
13) J. S. Fraser and J. D. Milton, Phys. Rev. **93** (1954) 818
14) R. B. Leachman, Proc. Second Geneva Conference **15** (1958), 331
15) M. M. Hoffman, Bull. Am. Phys. Soc. **3** (1958) 6
16) V. M. Strutinski, Soviet Physics JETP, **37** (1959) 861
17) G. C. Hanna, Proc. Int. Conf. on Nuclear Structure, Kingston, Canada (North-Holland Publishing Co., Amsterdam, 1960) p. 862
18) R. B. Leachman, Proc. Second Geneva Conference **15** (1958) 229
19) T. Erikson and V. M. Strutinski, Nuclear Physics **8** (1958) 284, **9** (1958/59) 689

9.B

Nuclear Physics **25** (1961) 152—154; © *North-Holland Publishing Co., Amsterdam*

Not to be reproduced by photoprint or microfilm without written permission from the publisher

A NOTE ON ELECTRON PHOTON SHOWERS

A. RAMAKRISHNAN

Department of Theoretical Physics, University of Madras, Madras 25, India

and

S. K. SRINIVASAN

Department of Applied Mathematics, Indian Institute of Technology, Madras 25, India

Received 16 January 1961

Abstract: The mean square deviation of the number of electrons obtained recently by Butcher and Messel is compared with the earlier results based on exact methods of stochastic theory and the degree of validity of Monte Carlo methods for such processes is discussed.

Very recently Butcher and Messel [1]) presented some results of their numerical calculations on the fluctuation problem of electromagnetic cascades based on Monte Carlo methods. To understand their significance and judge the validity of such methods, it is necessary to test whether these results are consistent with those obtained by rigorous analytical methods.

The fundamental problem is to compute the probabilities $\pi^i(n, E, E_0; t)$ that there are n electrons, each of which has an energy above E at thickness t, given that there is an electron ($i = 1$) or a photon ($i = 2$) at $t = 0$ with energy E_0. It is well-known that while exact equations can be written for the π functions, analytical solutions have been obtained only for their moments and numerical results based on these solutions are available only for the first two moments[2–4]). The utility of the Monte Carlo calculation lies in that it is possible to obtain the probabilities π^i for various values of n. However, we wish to emphasize that reliance can be placed on these results only if the mean values and mean square values using such calculated probabilities π^i agree with the analytical solutions. We find that the mean values and mean square values of Butcher and Messel [1]) are, though not in close agreement with those obtained analytically, certainly not inconsistent with the earlier results. This generates the hope that Monte Carlo methods may be used with advantage. It is worthwhile to investigate how near the simulated processes approximate to the physical process.

It has become customary in multiplicative stochastic processes to compare

$$\sigma^2(E, E_0; t) = \varepsilon\{[n(E, E_0; t)]^2\} - [\varepsilon\{n(E, E_0; t)\}]^2$$

with

$$\varepsilon\{n(E, E_0; t)\}$$

and

$$\{\varepsilon[n(E, E_0; t)\}]^2 - \varepsilon\{n(E, E_0; t)\},$$

which we shall denote by σ_P^2 and σ_F^2 respectively, for the obvious reason that they are the values we should expect for the mean square deviation if $n(E, E_0; t)$ were to have a Poisson or a Furry distribution. Ramakrishnan and Mathews [4]) have tabulated σ^2, σ^2/σ_P^2 and σ^2/σ_F^2 and discussed the behaviour of the mean square deviation near the cascade maximum. This was further examined by the authors [5]) and it was shown that there is no reason from a logical and stochastic point of view to expect a Poisson distribution near the cascade maximum. It was also demonstrated that though σ^2/σ_F^2 is small compared to unity, σ^2 may still be many times the Poisson value †. This is now confirmed by the Monte Carlo calculations of Butcher and Messel. The set of their tables 131–138 and 125–130 correspond to the ratios 1000 and 500, respectively, of the energy of the primary election to that of a secondary.

We have tabulated below σ^2/σ_P^2 and σ^2/σ_F^2 near the cascade maximum for the various primary energies (table 1). The results obtained on the basis of stochastic theory are shown in table 2.

TABLE 1

Values of σ^2/σ_P^2 and σ^2/σ_F^2 near the cascade maximum for various primary energies

Primary to secondary ratio	Primary energy in MeV	Air		Aluminium	
		σ^2/σ_P^2	σ^2/σ_F^2	σ^2/σ_P^2	σ^2/σ_F^2
1000	50000	2.7	0.11	6.0	0.16
	20000	2.1	0.14	2.6	0.12
	10000	1.8	0.18	1.9	0.13
	5000	1.5	0.25	1.9	0.19
500	50000	1.9	0.11	2.0	0.10
	10000	1.7	0.20	1.9	0.17
	5000	1.5	0.30	1.5	0.19

TABLE 2

Results obtained on the basis of stochastic theory

Primary to secondary ratio	σ^2/σ_P^2	σ^2/σ_F^2
$e^8 = 2984$	12	0.08
$e^7 = 1097$	6.2	0.10
$e^6 = 403$	3.5	0.15

We have not compared our results corresponding to the ratios less than 500 since the order of magnitude of the mean is a criterion as has been emphasized

† A more detailed discussion based on the analytical results will be found in ref. [6]).

earlier by the authors [5]). It would have been possible to demonstrate more effectively the building up of the ratio of the mean square deviation to the mean if results corresponding to ratios higher than 1000 were available. Nevertheless it is clear from table 1 that near the cascade maximum the mean square deviation is twice and sometimes even six times as large as the mean. It is of interest to note that while $\sigma^2/\sigma_F{}^2$ is as small as 0.1 or 0.2, $\sigma^2/\sigma_P{}^2$ is of the order of 4 or 5.

References

1) J. C. Butcher and H. Messel, Nuclear Physics **20** (1960) 15
2) A. Ramakrishnan, Proc. Camb. Phil. Soc. **46** (1950) 595
3) H. J. Bhabha and A. Ramakrishnan, Proc. Ind. Acad. Sci. **43** (1950) 142
4) A. Ramakrishnan and P. M. Mathews, Prog. Theor. Phys. **11** (1954) 95
5) A. Ramakrishnan and S. K. Srinivasan, Prog. Theor. Phys. **13** (1955) 93
6) A. Ramakrishnan, Theory of Elementary Particles and Cosmic Radiation (Pergamon, London, in press)

1.D.1 *Nuclear Physics* **25** (1961) 155—168; © *North-Holland Publishing Co., Amsterdam*

Not to be reproduced by photoprint or microfilm without written permission from the publisher

SHELL MODEL THEORY OF Pb^{205}

WILLIAM W. TRUE †

Palmer Physical Laboratory, Princeton University ††

Received 9 January 1961

Abstract: The energy eigenvalues and eigenfunctions have been calculated for the lower levels of Pb^{205} for a pure singlet-even two-body force between nucleons and for a singlet-even force plus weak coupling of the particle motion to the quadrupole collective motion of the core. Better agreement with experiment is found when weak coupling of the core is included. More experimental data are needed before a complete decay scheme for Pb^{205} can be determined.

1. Introduction

As pointed out by Pryce, [1]) the nuclei around the double-closed-shell nucleus Pb^{208} should be amenable to explanation by the nuclear shell model. In this paper we will compare the theoretical calculations of the energy levels of Pb^{205} with the experimental data which are available. This paper is an extension of previous work [2]) on Pb^{206}. Pryce [3]) has made a modified zero-range calculation on the energy levels of Pb^{205}. In his calculation, Pryce tried to account for the effects of configuration mixing in a semi-quantitative manner. We compare the results of our calculations with those of Pryce in subsect. 3.3.

In sect. 2 we discuss the experimental data known at present about the lead isotope Pb^{205}. In sect. 3, we discuss the theoretical calculations and compare them with the experimental data. Sect. 4 contains a discussion of transition rates and a consistent decay scheme for Pb^{205}.

2. Experimental Data on Pb^{205}

During the past few years, a large number of gamma transitions in Pb^{205} have been identified [4–19]). The energies of these transitions are given in table 1. Systematic studies of the transitions in Pb^{205} were first made by two groups [4–6]). Fritsch and Hollander [5, 6]) studied the internally converted electrons following the β-decay of Bi^{205}. Independently, and at the same time, Bergström's group [4]) in Sweden studied the gamma rays and the electron-electron and electron-gamma ray coincidences, as well as the internally converted electrons following

† Now at the Physics Department, University of California, Davis, California.

†† This work was supported in part by the U. S. Atomic Energy Commission and the Higgins Scientific Trust Fund.

TABLE 1

Observed transitions in Pb^{205}

Transition energy (keV) [a]	K-line intensity ($K_{703.3} = 100$)	Multipolarity [b]	Ref.
26.22		M2	11, 19)
(31)			5)
(33)			5)
(78)			4)
90		E1	4, 19)
(92)			5)
107.2			19)
(110.3)			4)
112.2			5, 6)
(113.2)			4)
115.2		M1	4, 19)
131.2			5, 6)
(133)			4)
(146)			4)
149			5, 6)
(162)			4)
185.3		(M1, E1)	19)
192.6			5, 6)
(221)			4)
(237)			4)
260.5	110	M1	4, 6, 10, 19)
262.8		M1	15, 19)
282.3	41	M1	4, 6, 10)
284.2	160	M1	4, 6, 10, 19)
(286.6)			4)
310.5		E3	11, 19)
313.1	4.9	(M1, E1)	19)
349.4	28	(E1 or E2 excluded)	4, 6, 10)
383.2	6		4, 6)
493.6	11	(E1 or E2 excluded)	4, 6, 10)
511.7	22	M1	4, 6)
526.0			5, 6)
531.1			5, 6)
550	6.3	E1	4, 6, 10)
571.0	74	M1	4, 6, 10)
573.7			5, 6)
(574.3)			4)
580.0	24	E2	4, 6, 10)
626.5	6.7		4, 6)
688.9	1		4)
703.3	100	E2	4, 6, 10, 19)
(717.5)			4)
745.0	2.1		4, 6)
758.3	3.1		4, 6)
761.0	2.0		4)
910.8	9.8	E2	4, 6, 10)
987.8	27.5	E2	4, 6, 10, 19)
1002.7	2.1		4)
1014.0	4.9	M4	4, 6, 10, 11, 19)

TABLE 1 (Continued)

Transition energy (keV) [a])	K-line intensity ($K_{703.3} = 100$)	Multipolarity [b])	Ref.
1043.7	32.5	M1	[4, 6, 10])
1073.3			[5, 6])
1190.3	7.6		[4, 6])
1337	0.3		[4])
1351.5	1.1		[4])
1502.5	0.4		[4])
1552.0	0.8		[4])
1614.6	3.1		[4])
1766.4	43.6	M1	[4, 10])
1777.4	5.2	(M1)	[4, 10])
1864.4	2.0	E1	[4, 10])
1906.5	0.6	E1	[4, 10])
2567.8	0.029		[10, 19])
2610	0.5		[4])

[a]) The doubtjul transitions are enclosed in parentheses.
[b]) The multipolarity of the transitions are those given in refs. [10, 11, 19]).

the decay of Bi^{205}. Various members connected with the Swedish group [7–11, 16, 18, 19]) have continued their investigations and are continuing to find new experimental data which are helping to unravel the decay scheme of Pb^{205}.

A metastable transition with a half-life of 4.7 ± 1.5 ms was first observed in Pb^{205} by Vegors and Heath [12, 13]). The most recent measurement [18]) of this metastable transition, which is associated with the 987.8 keV gamma-ray transition, has yielded a half-life of 4.1 ± 0.2 ms. Studies [4, 10]) of the internal conversion coefficient of the 987.8 keV transition indicate that it is an E2 transition. It is very hard theoretically to understand why an E2 transition of this energy would have such a long half-life. One then deduces that the 987.8 keV energy level in Pb^{205} is fed by a 4 ms metastable state. This conclusion has now experimental justification.

Work by Stockendal [11, 19]) has now established the existence of a $\frac{13}{2}+$ metastable state at 1014.3 keV in Pb^{205}. This $\frac{13}{2}+$ state decays by a 26.2 keV M2 transition to a level at 987.8 keV, by a 310.5 keV E3 transition to a level at 703.3 keV, and by a 1014.3 keV M4 transition to the ground state of Pb^{205} (see sect. 3 and fig. 4). The 26.2 keV and 310.5 keV transitions have just recently been found by Stockendal and thus have helped to resolve the identity of the metastable state. Alburger [17]) has also independently observed the 26.2 keV transition and has reached the above conclusion.

There are several doubtful or uncertain transitions [4, 5]) in Pb^{205}. These doubtful transitions are enclosed in parentheses in table 1 and are included for completeness. In sect. 3 it will be seen that one of these doubtful transitions can be fitted consistently into a decay scheme.

In table 1 the intensities of the K-conversion lines and the multipolarities of the radiation (when known) have been taken from the work of several people [4, 10, 11, 19]). These K-line intensities and multipolarities are also consistent with the work of Fritsch and Hollander [6]).

Vegors [15]) has found evidence for a 262.5 ± 0.5 transition in Pb^{205} as well as the 260.5 keV transition found by others [4–6]). This 262.5 keV transition is difficult to observe because of the presence of a strong 262.8 keV transition in Pb^{206}. However, Stockendal [19]) recently has also verified that a M1 transition of 262.8 keV does exist in Pb^{205}.

Asaro and Perlman [20]) observed only a 260 ± 5 keV gamma-ray transition following the alpha decay of Po^{209} to Pb^{205}. One concludes that this 260 keV transition is to the $\frac{5}{2}-$ ground state of Pb^{205}. Evidence will be discussed below (subsect. 4.2) to indicate that the 260 ± 5 keV transition found by Asaro and Perlman is to be associated with the 262.8 keV transition and not the 260.5 keV transition.

3. Calculations

It is reasonable to extend the calculations done by True and Ford [2]) on Pb^{206} to the case of Pb^{205}. We are now considering 3 neutron holes in the Pb^{208} core. To within a constant additive energy, which we leave as a free parameter, one knows or can show [21]) that it is possible to treat the calculations for a sum of two-particle forces between 3 holes in a core in exactly the same manner as one treats the shell model calculation of 3 particles outside of a core. This was done [2]) for the 2 neutron holes in Pb^{206}.

Making use of the concept of fractional parentage coefficients and the fact that for antisymmetric wave functions

$$V_{\text{int}} = \langle \Psi_a | \sum_{i>j=1}^{n} V(r_{ij}) | \Psi_a \rangle = \frac{n}{n-2} \langle \Psi_a | \sum_{i>j=1}^{n-1} V(r_{ij}) | \Psi_a \rangle, \qquad (1)$$

we can reduce the matrix element of a sum of two-particle potentials between three-particle wave functions to a sum of terms in which each term consists of a known coefficient times a matrix element of $V(r_{12})$ between two-particle antisymmetric wave functions. This method has been outlined, for example, in sect. III of ref. [22]). In this calculation n in eq. (1) is 3. Expressions for the fractional parentage coefficients for three-particle wave functions have been given in ref. [22]).

3.1. CALCULATIONS WITH SINGLET-EVEN FORCES

The excited energy levels of Pb^{206} were theoretically predicted [2]) by a singlet-even potential with a Gaussian shape for the radial dependence,

$$V(r) = V_0 \exp(-r^2/\beta^2), \qquad (2)$$

where $V_0 = -32.5$ MeV and $\beta = 1.85$ fm. As pointed out in ref. [2]), this potential has a bound state at zero energy and an effective range identical to the effective range determined from the scattering of two free neutrons. For the single-particle wave functions, we use the same harmonic oscillator wave functions as were used in sect. III of ref. [2]).

TABLE 2

Energy eigenvalues in MeV for a pure singlet-even force. The parity of the level is given directly after the eigenvalue

Level spin	$\frac{1}{2}$	$\frac{3}{2}$	$\frac{5}{2}$	$\frac{7}{2}$	$\frac{9}{2}$	$\frac{11}{2}$	$\frac{13}{2}$
Energy eigenvalues in MeV	2.685−	2.581−	2.610−	2.861−	2.630+	2.789+	2.883+
	2.213−	2.213−	2.373−	2.644+	2.368+	2.616+	2.837+
	1.265−	1.893−	1.972−	2.410−	2.288−	2.478−	2.566+
	0.606−	1.771−	1.964−	2.263−	2.088−	2.278+	2.466−
	0.360−	1.625−	1.773−	2.171−	1.978+	2.115+	2.447+
		1.468−	1.436−	1.818−	1.761−	1.768−	2.347+
		1.006−	1.381−	1.519−	1.457−		2.059+
		0.745−	0.961−	0.953−	0.865−		1.394+
		0.082−	0.831−	0.800−			
			0.000−				

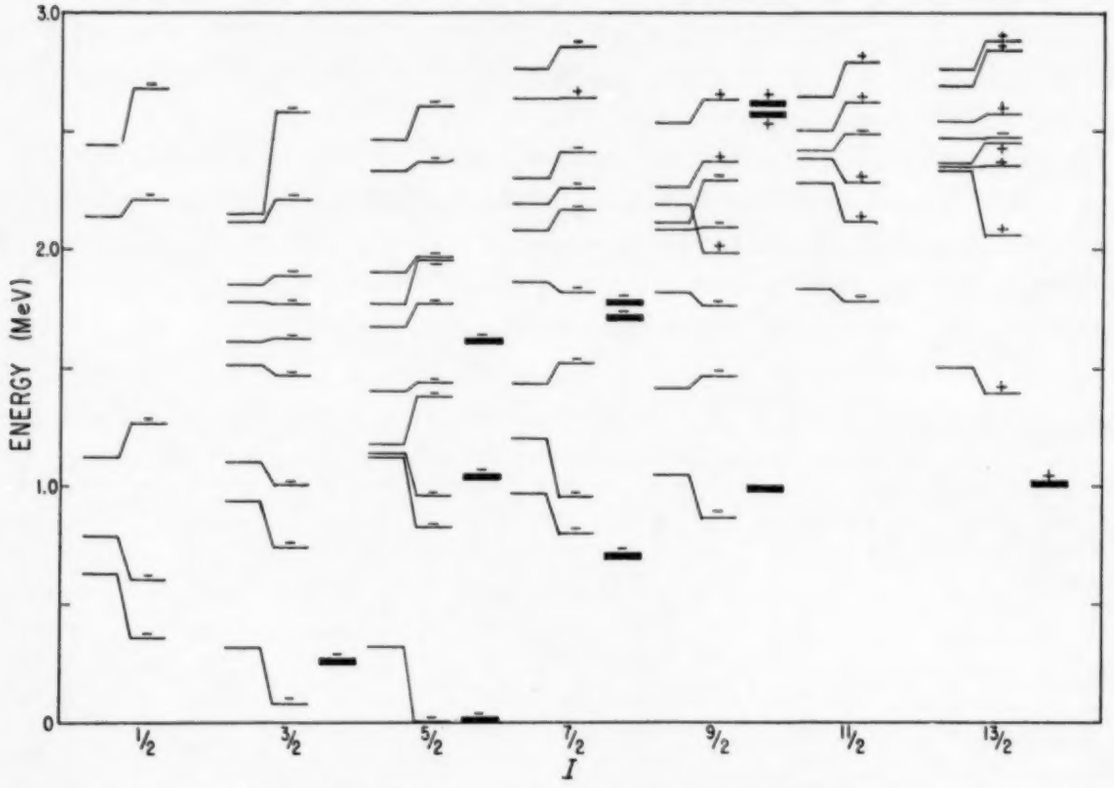

Fig. 1. Energy levels of Pb^{205} for a pure singlet-even force. For each spin, the first column gives the energy levels calculated in lowest order with singlet-even forces. The second column gives the energy levels and parities obtained by exact diagonalization of the energy matrix for the states indicated. The third column gives the experimental levels as listed in table 4.

With the matrix elements between the two-particle wave functions and the fractional parentage coefficients, we can now determine the matrix elements for the potential between three-particle wave functions, i.e. eq. (1). The resulting matrix of the Hamiltonian can then be diagonalized to obtain the energy eigenvalues. The energy eigenvalues for a sum of pure singlet-even two-body forces are given in table 2 and are compared to experiment in fig. 1. How the experimental levels shown in fig. 1 were determined will be discussed below. In fig. 1, the resulting theoretical energy levels have been normalized so that the ground state of Pb^{205} will be at zero energy. The ground state of Pb^{205} is predicted to be $\frac{5}{2}-$ which agrees with the experimental results. Beyond this point, the agreement between theory and experiment is quite poor as is seen in fig. 1. Practically all experimental levels and their corresponding theoretical levels differ by 100 keV or more. From the results obtained in theoretically predicting the energy levels in Pb^{206} we expect better agreement with experiment.

3.2. CALCULATIONS INCLUDING WEAK COUPLING TO THE COLLECTIVE MOTION

As shown in ref. [2]) it was necessary to include weak coupling of the particle motion to the quadrupole collective motion of the core, in order to explain consistently the observed E2 transition rates in Pb^{206} and Pb^{207}. It was also shown [2]) that by taking a singlet-even force $\frac{3}{4}$ as strong as the force in eq. (2) plus an effective force [23]) representing weak coupling of the particle motion to the collective motion, the agreement between theory and experiment for the energy levels in Pb^{206} was slightly improved.

The above calculation (sect. 3.1) was repeated with the singlet-even two-body force replaced by a singlet-even force $\frac{3}{4}$ as strong plus an effective weak coupling force. We shall call this latter force a ($\frac{3}{4}$S.E.+W.C.) force in what follows. The theoretical energy eigenvalues for the ($\frac{3}{4}$S.E.+W.C.) force are listed in table 3 and compared with experiment in fig. 2.

TABLE 3

Energy eigenvalues in MeV for a singlet-even force with weak coupling to the collective motion. The parity of the level is given directly after the eigenvalue

Level spin	$\frac{1}{2}$	$\frac{3}{2}$	$\frac{5}{2}$	$\frac{7}{2}$	$\frac{9}{2}$	$\frac{11}{2}$	$\frac{13}{2}$
Energy eigenvalues in MeV	2.615−	2.693−	2.616−	2.882−	2.557+	2.775+	2.880+
	2.177−	2.193−	2.251−	2.458+	2.340−	2.574+	2.800+
	1.390−	1.952−	2.011−	2.417−	2.292+	2.476−	2.583+
	0.508−	1.876−	1.916−	2.284−	2.121−	2.249+	2.556−
	0.379−	1.726−	1.860−	2.147−	1.808−	1.972+	2.413+
		1.419−	1.497−	1.789−	1.769+	1.778−	2.262+
		1.089−	1.458−	1.706−	1.612−		2.040+
		0.503−	1.043−	0.928−	0.938−		1.051+
		0.158−	0.812−	0.746−			
			0.000−				

It is also reasonable that as one calculates matrix elements for nuclei further and further removed from a closed-shell nucleus, slight changes in the two-body force can cause different effects which will become more pronounced due to additive terms in the matrix elements. That is, while the pure singlet-even force and the ($\frac{3}{4}$S.E.+W.C.) force gave about the same energy eigenvalue results in Pb^{206}, we should be prepared for these two forces to give different results in Pb^{205} (and even more different results in Pb^{204}). Indeed, this is the case for Pb^{205}.

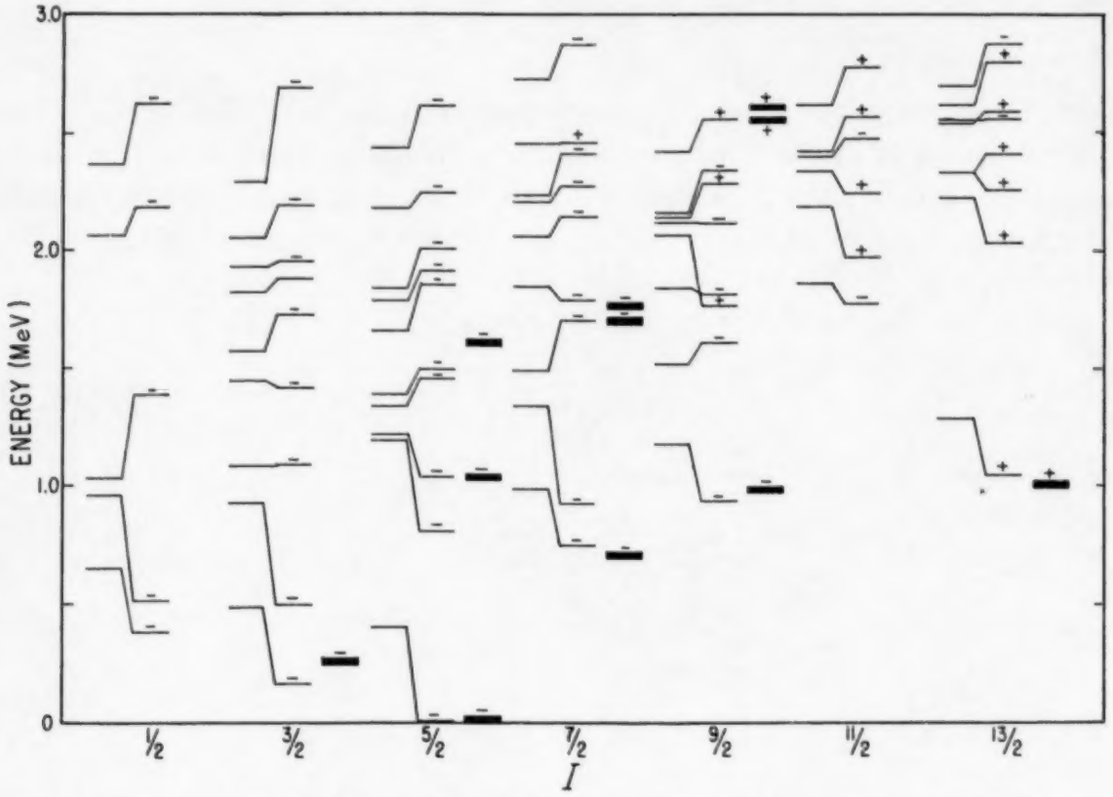

Fig. 2. Energy levels of Pb^{205} for a ($\frac{3}{4}$S.E.+W.C.) force. For each spin, the first column gives the energy levels in lowest order for a ($\frac{3}{4}$S.E.+W.C.) force. The second column gives the energy levels and parities obtained from diagonalization of the energy matrix. The third column gives the experimental levels as listed in table 4.

These calculations are also based on the assumption that the differences in the interaction of a particle in different single-particle energy levels with the "inert" Pb^{208} core are given by the experimental levels in Pb^{207}. As one proceeds to make calculations of this type for nuclei further and further removed from a closed shell, it is questionable how long the above assumption remains valid. In fact, the core will gradually become deformed due to the polarizing effects of several particles outside the core. (In the case of the lead isotopes, one should speak of holes, but the result is the same.) Then, due to this deformation of the core the single particle levels will gradually shift and change their relative positions. As a result, the calculated positions of the energy

levels will be in error even though the correct two-body force is used for the interactions between particles.

It is therefore difficult to estimate whether the disagreement between theory and experiment is due to the incorrect two-body force or to the effects of the deformation of the core. The exceedingly good theoretical results [2]) for Pb^{206} seem to give evidence that the deformation of the core would be the cause of any large discrepancy. In fact, when these calculations were extended to Pb^{204}, the agreement with the experiment energy levels became quite bad even when rather drastic changes in the two-body force were made.

3.3. COMPARISON WITH PRYCE'S RESULTS

For completeness, we shall compare our results for the ($\frac{3}{4}$S.E.+W.C.) force with the results of Pryce [3]) who considered a modified zero-range calculation. Pryce attempted to correct for configuration mixing by modifying the diagonal matrix elements in a semi-quantitative way. Pryce concludes that his resulting energy levels can be in error by as much as 100 keV to 200 keV.

Fig. 3 shows the comparison between our results for a ($\frac{3}{4}$S.E.+W.C.) force

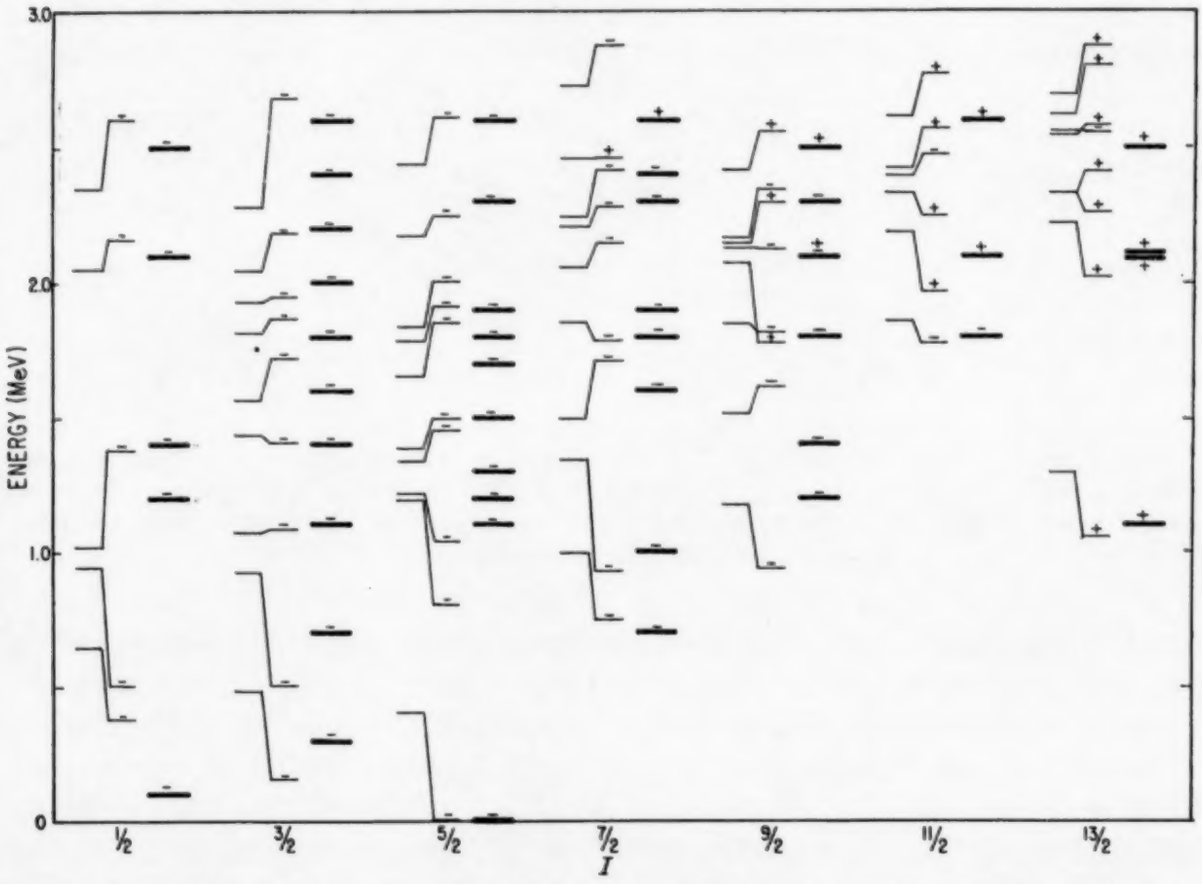

Fig. 3. Comparison of the energy levels of Pb^{205} predicted with a ($\frac{3}{4}$S.E.+W.C.) force and the energy levels predicted by Pryce. For each spin, the first column gives the energy levels in lowest order for a ($\frac{3}{4}$S.E.+W.C.) force. The second column gives the energy levels and parities obtained from diagonalization of the energy matrix. The third column gives the energy levels and parities predicted by Pryce [3]).

and Pryce's results. As seen in fig. 3, there is quite a difference between Pryce's results and our results. One notes that the same number of configurations for a given spin were not always considered in both cases. One expects that this should cause little change for the lower-lying states of each spin.

4. Results

In this section, we shall discuss the comparison between the experimental results and the results for a ($\frac{3}{4}$S.E.+W.C.) force. We do not expect the theoretical energy levels to be too reliable much above 2 MeV. The positions of the levels above about 2 MeV will be affected by the higher configurations which have been neglected in this calculation as well as by "core-excited" states which have also been neglected. We do believe that the positions of the lower-lying levels of each spin should be quite good.

4.1. CONSISTENT DECAY SCHEME

It is possible by using the theoretically predicted levels in fig. 2 and the observed gamma transitions in table 1 to assert at what energy and spin other experimental levels of Pb^{205} could occur. An example is the three transitions, 112.2 keV, 1502.5 keV, and 1614.6 keV. Note that 112.2+1502.5 = 1614.7 keV. In fig. 2, one could put an experimental level at 1502.5 keV with a spin of $\frac{5}{2}-$ to agree with one of the predicted $\frac{5}{2}-$ levels at 1497 keV and 1458 keV with the 112.2 keV transition as the transition between the 1614.6 keV level and the 1502.5 keV level. The 1502.5 keV transition can furthermore represent the cross-over transition of the 745 keV and 758.3 keV transitions (745+758.3 = = 1503.3) with a level either at 745 keV or at 758.3 keV with a spin of $\frac{5}{2}-$. If the above is true, why do we not see the 799 keV transition between the 1502.5 keV $\frac{5}{2}-$ level and the 703.3 keV $\frac{7}{2}-$ level? Also, why are none of the transitions from the 1766.4 keV $\frac{7}{2}-$ or 1705 keV $\frac{7}{2}-$ levels to the 1502.5 keV $\frac{5}{2}-$ or the 745 keV $\frac{5}{2}-$ or the 758 keV $\frac{5}{2}-$ levels seen?

Using energy sums alone, one can in this manner suggest the positions and spins of many experimental levels which will agree in general with the theoretical predictions and experimental data. We have been able to account with a given decay scheme for about 47 of the 63 transitions listed in table 1. (9 of these 16 unaccounted – for transitions are doubtful transitions). To base as complicated a decay scheme as that of Pb^{205} on energy sums alone is a very dangerous procedure. In fact, we have been able to find another quite different decay scheme in addition to the one above which seems to fit the experimental data, and we expect that there are several more decay schemes which fit equally well. In these decay schemes, all levels will have two or more transitions connecting them to other levels.

Stockendal's [19]) latest paper is the most recent survey of the experimental

data concerning Pb^{205}. Stockendal's fig. 8 is a proposed decay scheme for Pb^{205}. In this figure, Stockendal has some uncertain levels which he shows by dotted lines. We have adopted Stockendal's proposed decay scheme by

TABLE 4

Positions and spins of proposed experimental levels

Energy in keV	Spin and parity
0	$\frac{5}{2}-$
262.8 (or 260.5)	$\frac{3}{2}-$
703.3	$\frac{7}{2}-$
987.8	$\frac{9}{2}-$
1014.0	$\frac{13}{2}+$
1043.7	$\frac{5}{2}-(\frac{7}{2}-)$
1614.6	$\frac{5}{2}-$
1705	$\frac{7}{2}-$
1766.4	$\frac{7}{2}-$
2567.8	$\frac{9}{2}+$
2610	$\frac{9}{2}+(\frac{7}{2}+)$

TABLE 5

Transitions between the experimental levels given in table 4

Transition energy (keV)	Transition multipolarity	Initial level		Final level	
		Energy (keV)	Spin, parity	Energy (keV)	Spin, parity
26.2	M2	1014.0	$\frac{13}{2}+$	987.8	$\frac{9}{2}-$
90		1705	$\frac{7}{2}-$	1614.6	$\frac{5}{2}-$
262.8 (or 260.5)	M1	262.8 (or 260.5)	$\frac{3}{2}-$	0	$\frac{5}{2}-$
284.2	M1	987.8	$\frac{9}{2}-$	703.3	$\frac{7}{2}-$
310.5	E3	1014.0	$\frac{13}{2}+$	703.3	$\frac{7}{2}-$
571	M1	1614.6	$\frac{5}{2}-$	1043.7	$\frac{5}{2}-$
626.5		1614.6	$\frac{5}{2}-$	987.8	$\frac{9}{2}-$
703.3	E2	703.3	$\frac{7}{2}-$	0	$\frac{5}{2}-$
717.5		1705	$\frac{7}{2}-$	987.8	$\frac{9}{2}-$
910.8	E2	1614.6	$\frac{5}{2}-$	703.3	$\frac{7}{2}-$
987.8	E2	987.8	$\frac{9}{2}-$	0	$\frac{5}{2}-$
1002.7		1705	$\frac{7}{2}-$	703.3	$\frac{7}{2}-$
1014.0	M4	1014.0	$\frac{13}{2}+$	0	$\frac{5}{2}-$
1043.7	M1	1043.7	$\frac{5}{2}-$	0	$\frac{5}{2}-$
1337		1766.4	$\frac{7}{2}-$	262.8	$\frac{3}{2}-$
1351.5		1614.6	$\frac{5}{2}-$	262.8	$\frac{3}{2}-$
1552.0		2567.8	$\frac{9}{2}+$	1014.0	$\frac{13}{2}+$
1614.6		1614.6	$\frac{5}{2}-$	0	$\frac{5}{2}-$
1766.4	M1	1766.4	$\frac{7}{2}-$	0	$\frac{5}{2}-$
1864.4	E1	2567.8	$\frac{9}{2}+$	703.3	$\frac{7}{2}-$
1906.5	E1	2610	$\frac{9}{2}+$	703.3	$\frac{7}{2}-$
2567.8		2567.8	$\frac{9}{2}+$	0	$\frac{5}{2}-$
2610		2610	$\frac{9}{2}+$	0	$\frac{5}{2}-$

including only one of his uncertain levels, the $\frac{3}{2}-$ level at 262.8 keV see (sect. 4.2). In addition, we have also included a $\frac{7}{2}-$ level at 1705 keV. Table 4 gives the positions and spins of the proposed experimental levels and table 5 lists the various gamma transitions between these proposed levels. Tables 4 and 5 are summarized in fig. 4 which shows the experimental levels and their connecting gamma transitions.

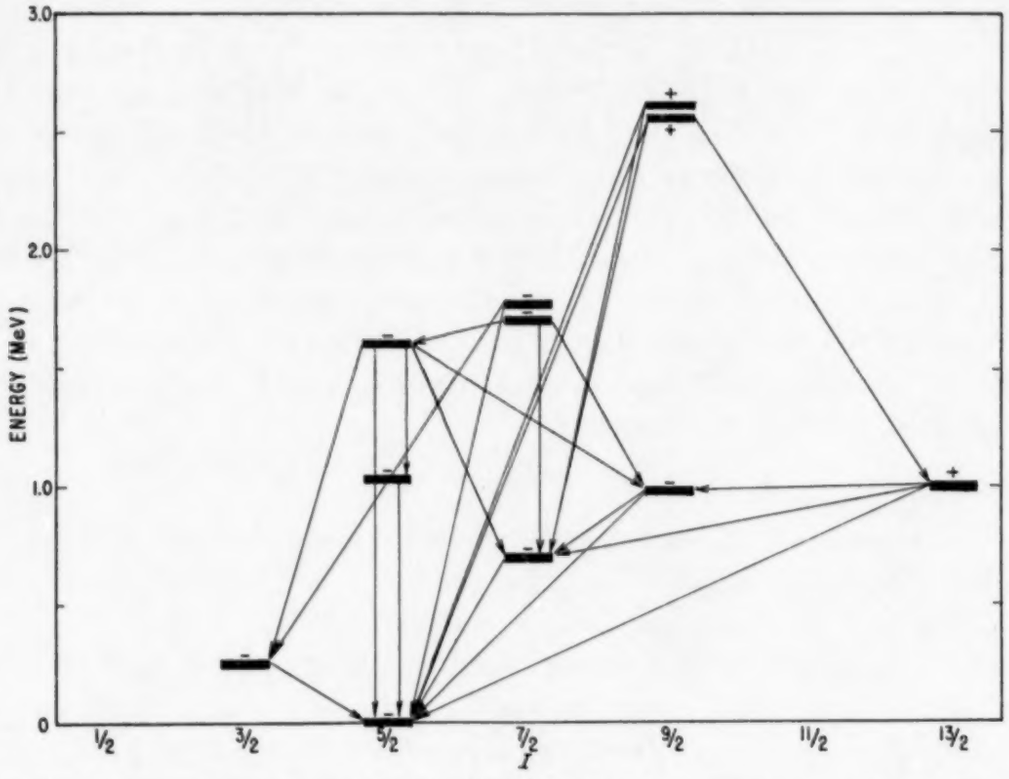

Fig. 4. Proposed experimental energy levels of Pb^{205} and their connecting transitions. The positions and spins of these experimental levels are given in table 4 and the transitions are given in table 5.

TABLE 6

Comparison between the experimental levels and calculated levels for a ($\frac{1}{4}$S.E.+W.C.) force

Experimental energy (keV)	Spin and parity	Corresponding calculated energy (keV)
0	$\frac{5}{2}-$	0
262.8 (or 260.5)	$\frac{3}{2}-$	158
703.3	$\frac{7}{2}-$	746
987.8	$\frac{9}{2}-$	938
1014.0	$\frac{13}{2}+$	1051
1043.7	$\frac{5}{2}-$	1043
1614.6	$\frac{5}{2}-$	1497
1705	$\frac{7}{2}-$	1706
1766.4	$\frac{7}{2}-$	1789
2567.8	$\frac{9}{2}+$	2557
2610	$\frac{9}{2}+$	(core excited level?)

One sees in fig. 2 or table 6, that the agreement between theory and experiment is quite good. It is felt that the ($\frac{3}{4}$S.E.+W.C.) force represents the effective two-body force between particles much better than a pure singlet-even force.

Stockendal assigns a spin of $\frac{5}{2}-$ ($\frac{7}{2}-$) to the 1614.6 keV level. Better agreement between theory and experiment would be obtained if the spin of this level were $\frac{9}{2}-$ as it would then correspond to the calculated $\frac{9}{2}-$ level at 1612 keV. The 1043.7 keV level has been assigned a spin of $\frac{5}{2}-$ even though it could conceivably have a spin of $\frac{7}{2}-$. Likewise, the level at 2610 keV has been given a spin of $\frac{9}{2}+$ even though it could be $\frac{7}{2}+$, $\frac{9}{2}+$, ($\frac{11}{2}+$). Certainly more experimental work must be done to resolve these ambiguities.

Vegors [15]) reports that no gamma transition with an energy greater than 100 keV is in coincidence with the 987.8 keV transition from the lowest $\frac{9}{2}-$ level. Schmorak *et al.* [4]) also observe that no strong transition (not including the 626.5 keV or 717 keV transitions) is in coincidence with the 987.8 keV transition. It is difficult to understand this experimental evidence if the proposed decay scheme in tables 4 and 5 is correct.

4.2. THE LOWEST $\frac{1}{2}$–LEVEL

There is evidence to indicate that the lowest $\frac{3}{2}-$ level is at 262.8 keV and not at 260.5 keV. We have, however, included the 260.5 keV level in parentheses in tables 4, 5 and 6 as the proof is not conclusive.

Theoretical analyses of the energy level spectrum (see figs. 1, 2 and 3) indicate that the only likely spins for a level at about 260 keV would be $\frac{3}{2}-$ or $\frac{1}{2}-$. A spin of $\frac{3}{2}-$ seems more likely as a level of this spin is more easily reached by transitions from the higher $\frac{5}{2}-$ and $\frac{7}{2}-$ levels. We can argue that, when we see the transition feeding a level at about 260 keV, we should also expect to see the cross-over transition as the level(s) feeding the 260 keV level would be expected to have a $\frac{5}{2}-$ or $\frac{7}{2}-$ spin(s) and so should also decay to the ground state of Pb^{205}.

There is no observed transition in Pb^{205} which, when added to 260.5 keV, will form a sum which is equal to another observed transition (the cross-over transition). The above is no longer true when we consider the 262.8 keV transition. There are 5 possible sums, which are

262.8+1351.5 = 1614.3 with 1614.6 in table 1,
262.8+1502.5 = 1765.3 with 1766.4 in table 1,
262.8+ 286.6 = 549.4 with 550 in table 1,
262.8+ 310.5 = 573.3 with 573.7 in table 1,
262.8+1073.3 = 1336.1 with 1337 in table 1.

Note that all these sums need not be meaningful and may just be accidental (in particular, the last three sums). The first two sums do give evidence that a level at 262.8 keV is being fed by levels at 1614.6 keV and 1766.4 keV.

4.3. TRANSITION PROBABILITIES

As pointed out in ref. [2]), whenever a transition can go by M1 radiation or E2 radiation, the M1 transition probability will almost always dominate in Pb^{206}. This dominance of the M1 transition probability also holds for Pb^{205}. For this reason, it is difficult theoretically to understand why the 703.3 keV E2 observed transition from the lowest $\frac{7}{2}-$ level to the $\frac{5}{2}-$ ground state is not an M1 transition. The M1 and E2 probabilities for the 703.3 keV transition have been calculated using the wave functions resulting from the energy eigenvalue calculations. The resulting gamma transition probabilities are

$$T_\gamma(\mathrm{M1})_{703.3} = 126.6\times 10^9\ \mathrm{sec}^{-1}, \tag{3}$$

$$T_\gamma(\mathrm{E2})_{703.3} = 6.043\times 10^9\ \mathrm{sec}^{-1}. \tag{4}$$

Thus the M1 transition probability is about 21 times larger than the E2 transition probability. This result is in direct contradiction to the experimental results as listed in table 1 (refs. [4, 6, 10])).

Note that the E2 transition probability above was calculated with the assumption that the E2 transition is a result of the weak coupling of the particle motion to the collective motion of the core [2]). In order to make the E2 transition probability of this 703.3 keV transition equal to the M1 transition probability, we should have to increase the coupling of the particle motion to the collective core motion by a factor of almost 5. We expect the coupling to the core motion to increase slightly as we go from Pb^{206} to Pb^{205} but not by as large a factor as 5.

Since a complete decay scheme of Pb^{205} is not known, we cannot look at transition probabilities to and from a given level in detail. It is possible, however, to study a few branching ratios from a given level provided the K-line intensities are known experimentally. When the calculated branching ratios are compared with the experimental branching ratios, the agreement is reasonable for all transitions except the transitions from the 1614.6 keV $\frac{5}{2}-$ level. Transition probabilities are quite sensitive to the details of the wave functions and we can therefore only expect semi-quantitative agreement. It is not felt that the wave functions are good enough or that enough K-line intensities are known at the present time to enable one to use the calculated transition probabilities as a tool to unravel the decay scheme of Pb^{205}.

4.4. PAIRING FORCES

Kisslinger and Sorensen [24]) have used pairing forces [25]) to investigate the nuclear properties of several nuclei. Their investigation includes Pb^{205}. Their results are consistent with the results of this paper for a ($\frac{3}{4}$S.E.+W.C.) force. The agreement indicates that a pairing force is a good approximation to the effective force between particles. Calculations with pairing forces are easier to perform for a many-particle system than the type of calculation outlined in

sect. 3. The work of Kisslinger and Sorensen seems to indicate a fruitful approach to calculating various nuclear properties of many particle systems.

5. Conclusions

In order to get agreement between theory and experiment in Pb^{205}, it was necessary to consider, in addition to a singlet-even two-body force, weak coupling of the particle motion to the collective motion of the core. This same conclusion was reached in previous work [2]) on Pb^{206} and Pb^{207}. However, before a more complete decay scheme for Pb^{205} can be determined, more experimental work should be done. This future experimental work should concentrate on coincident measurements and the determination of the multipolarity of the weaker transitions, both of which are difficult tasks.

The author wishes to thank Professor Kenneth Ford for many helpful and pertinent comments. He also wishes to express his gratitude to Professor Seaborg and his group at the University of California Radiation Laboratory for their hospitality during the summer of 1957 when this work was started. The author also wishes to thank Professor M. H. L. Pryce for his interest and helpful comments concerning this paper.

References

1) M. H. L. Pryce, Proc. Phys. Soc. **65** (1952) 773
2) W. W. True and K. W. Ford, Phys. Rev. **109** (1958) 1675
3) M. H. L. Pryce, Nuclear Physics **2** (1956–57) 226
4) M. Schmorak, R. Stockendal, J. A. McDonell, I. Bergström and T. R. Gerholm, Nuclear Physics **2** (1956–57) 193
5) A. R. Fritsch, University of California Radiation Laboratory Report UCRL-3452, June 1956 (unpublished)
6) A. R. Fritsch and J. M. Hollander, J. Inorg. Nuclear Chem. **6** (1958) 165
7) I. Bergström and A. H. Wapstra, Phil. Mag. **46** (1955) 61
8) I. Bergström and G. Andersson, Arkiv. f. Fysik **12** (1957) 415
9) R. Stockendal, J. M. McDonell, M. Schmorak and I. Bergström, Arkiv. f. Fysik, **11** (1956) 165
10) R. Stockendal and S. Hultberg, Arkiv. f. Fysik **15** (1959) 33
11) R. Stockendal, Phys. Rev. **118** (1960) 1074
12) S. H. Vegors, Jr. and R. L. Heath, Bull. Am. Phys. Soc. **3** (1958) 209
13) S. H. Vegors, Jr. and R. L. Heath, Phys. Rev. **118** (1960) 547
14) D. E. Alburger and M. H. L. Pryce, Phys. Rev. **95** (1954) 1482
15) S. H. Vegors, Jr. (private communication)
16) I. Bergström (private communication)
17) D. E. Alburger, Phys. Rev. **118** (1960) 1076
18) I. Bergström, E. C. O. Bonacalza, A. Jech, M. Perez and P. Thieberger, Nuclear Instruments and Methods **8** (1960) 151
19) R. Stockendal, Arkiv. f. Fysik **17** (1960) 553
20) Frank Asaro and I. Perlman (private communication)
21) D. M. Brink and G. R. Satchler, Nuovo Cim. **3** (1956) 549
22) W. W. True, Phys. Rev. **101** (1956) 1342
23) K. W. Ford and C. Levinson, Phys. Rev. **100** (1955) 1
24) L. S. Kisslinger and R. A. Sorensen Mat. Fys. Medd. Dan. Vid. Selsk. **32**, no. 9 (1960)
25) S. T. Belyaev, Mat. Fys. Medd. Dan. Vid. Selsk. **31**, no. 11 (1959)

2.G

Nuclear Physics **25** (1961) 169—174; © *North-Holland Publishing Co., Amsterdam*

Not to be reproduced by photoprint or microfilm without written permission from the publisher

NOTE ON THE TWO-NUCLEON STRIPPING PROCESS

M. L. RUSTGI †

Division of Pure Physics, National Research Council, Ottawa, Canada

Received 22 November 1960

Abstract: An expression is derived for the angular distribution of a process in which a neutron and a proton are captured from an incident He^3 neucleus and the stripped proton imparts an extra unit of angular momentum to the system target nucleus + captured neutron and proton by flipping its spin. No comparison with experiment is made because of the unavailability of experimental data for such a process at present. An expression for the differential cross section of a process, in which two nucleons are captured from an incident He^3 or similar nucleus is derived in the zero-range approximation and compared with the already published theoretical results.

1. Introduction

In the bombardment of nuclei with deuterons, there is now a great deal of evidence that the reactions occurring do not go primarily through the formation of a compound nucleus, but rather that one of its two constituents is stripped off and captured by the target nucleus. The theory of such a process has been given by Butler [1]) and Bhatia *et al.* [2]) and successfully accounts for the forward maximum that is a characteristic feature of the (d, p) and (d, n) stripping reactions. Recent studies [3, 4]) of the angular distribution of the (He^3, p) reactions show clearly that in many cases the reaction does not proceed by the compound nucleus model and that the observed forward peaks in the angular distributions suggest a direct action mechanism.

It was suggested by Wilkinson [5]) that in the (d, p) reaction the stripped proton suffering a close collision with the system of neutron + target nucleus may flip over its spin and thus deliver an extra unit of angular momentum to the system. This idea was successfully used by Bowcock [6]) to explain the anomalous angular distribution in the B^{10}(d, p)B^{11} reaction to the first excited state of the final nucleus. The spin flip stripping may predominate if the ordinary stripping is for some reason inhibited.

It is the purpose of the present note to work out a simple formula for the (He^3, p) stripping process in which the stripped proton may flip over its spin and supply an extra unit of angular momentum to the system (target nucleus) + (captured neutron and proton). Further, an expression for the cross section of the two nucleon stripping process in the zero range approximation is derived.

† National Research Council Postdoctorate Fellow.

2. The (He^3, p) Stripping process

In the centre-of-mass system the cross section for the (He^3, p) stripping process may be written as

$$\sigma(\theta) = \left(\frac{1}{2\pi\hbar^2}\right)^2 \frac{k_1}{k_h} M^*_{1f} M^*_{hi} \frac{1}{2(2j_1+1)} \sum_{m_h, m_1, m_f, \mu_1}$$

$$\left| \int \chi^{m_f *}_{j_f}(\xi, \mathbf{r}_n, \boldsymbol{\sigma}_n, \mathbf{r}_p, \boldsymbol{\sigma}_p) \chi^{\mu_1 *}_{\frac{1}{2}}(\boldsymbol{\sigma}_1) \exp(-i\mathbf{k}_1 \cdot \mathbf{r}'_1) V \right. \tag{1}$$

$$\left. \exp\{\tfrac{1}{3} i\mathbf{k}_h \cdot (\mathbf{r}_1+\mathbf{r}_p+\mathbf{r}_n)\} \varphi_h(r_1, r_p, r_n) \chi^{m_h}_{\frac{1}{2}}(\mu_h) \chi^{m_1}_{j_1}(\xi) d\mathbf{r}_p d\mathbf{r}_n d\mathbf{r}_1 d\xi \right|^2.$$

Here r_1 and r_p denote the coordinates of the protons and r_n of the neutron and r'_1 of the outgoing proton; one has

$$\mathbf{r}'_1 = \mathbf{r}_1 - [(M_n+M_p)/M_f]\mathbf{R}, \tag{2}$$

where $\mathbf{R} = \frac{1}{2}(\mathbf{r}_p+\mathbf{r}_n)$ is the vector displacement of the captured deuteron with respect to the centre of the final nucleus. Furthermore one has

$$\frac{1}{M^*_{1f}} = \frac{1}{M_1} + \frac{1}{M_f}, \qquad \frac{1}{M^*_{hi}} = \frac{1}{M_h} + \frac{1}{M_1},$$

where M_1 and M_f denote the masses of the initial and final nuclei. The wave vectors $\mathbf{k}_1$ and $\mathbf{k}_h$ are associated with the motion of the proton and He^3 respectively. In the above expression the Coulomb effect has been completely neglected although the error will be larger than the corresponding one in the treatment of the (d, p) reaction [2]). The derived formulas should be considered applicable when the energy of the incident particle is well above the Coulomb barrier.

Following Gerjuoy [7]), it can be shown that in the first Born approximation for the (He^3, p) reaction one has

$$V = V_1 + V_{1p} + V_{1n} + V_{pn}. \tag{3}$$

In the conventional stripping theory, one neglects the interaction of the proton 1 with the target nucleus so that it is unable to transfer angular momentum to the other nucleons. However, for the present calculation this will be the only term which will be retained and the other terms V_{1p}, V_{1n} and V_{pn} will be neglected. It will be assumed that V_1 includes only that part of the interaction which is capable of flipping the spin of the outgoing proton and giving up this unit of angular momentum to form the final nucleus.

Assuming that the interaction takes place at the nuclear surface, one can write $V = F(\sigma_1, \xi)\delta(r_1 - R)$, where R is the radius of the target nucleus.

The absolute value $|\mathscr{I}|$ of the integral in eq. (1) is then given by

$$|\mathscr{I}| = \int \Big[\int \chi_{j_t}^{m_t *}(\xi, \mathbf{r}_n, \boldsymbol{\sigma}_n, \mathbf{r}_p, \boldsymbol{\sigma}_p) \chi_{\frac{1}{2}}^{\mu_1 *}(\boldsymbol{\sigma}_1) F(\boldsymbol{\sigma}_1, \xi) \times \chi_{\frac{1}{2}}^{m_h}(\mu_h) \chi_{j_1}^{m_1}(\xi) r_n^2 \mathrm{d}r_n r_p^2 \mathrm{d}r_p \mathrm{d}\xi \Big] \exp(-i\mathbf{k}_1 \cdot \mathbf{r}'_1) \delta(r_1 - R) \times \exp[\tfrac{1}{3} i \mathbf{k}_h \cdot (\mathbf{r}_1 + \mathbf{r}_n + \mathbf{r}_p)] \varphi_h(\mathbf{r}_1, \mathbf{r}_p, \mathbf{r}_n) \mathrm{d}\mathbf{r}_1 \mathrm{d}\Omega_n \mathrm{d}\Omega_p. \quad (4)$$

Expansion of the square bracket in states of given angular momenta of the captured neutron and proton gives

$$|\mathscr{I}| = \sum_{l_n, m_n, l_p, m_p} \Big(\int (\chi_{j_t}^{m_t *}(\xi, \mathbf{r}'_n, \boldsymbol{\sigma}_n, \mathbf{r}'_p, \boldsymbol{\sigma}_p) \chi_{\frac{1}{2}}^{\mu_1 *}(\boldsymbol{\sigma}_1) \times F(\boldsymbol{\sigma}_1, \xi) \chi_{\frac{1}{2}}^{m_h}(\mu_h) \chi_{j_1}^{m_1}(\xi) Y_{l_n}^{m_n}(\Omega'_n) Y_{l_p}^{m_p}(\Omega'_p) \mathrm{d}\mathbf{r}'_p \mathrm{d}\mathbf{r}'_n \mathrm{d}\xi \Big) \times \Big(\exp(-i\mathbf{k}_1 \cdot \mathbf{r}'_1) \delta(r_1 - R) \exp[\tfrac{1}{3} i \mathbf{k}_h (\mathbf{r}_1 + \mathbf{R}_n + \mathbf{R}_p)] \times \varphi_h(\mathbf{r}_1, \mathbf{R}_n, \mathbf{R}_p) Y_{l_n}^{m_n *}(\Omega_n) Y_{l_p}^{m_p *}(\Omega_p) \mathrm{d}\mathbf{r}_n \mathrm{d}\mathbf{r}_p \mathrm{d}\mathbf{r}_1 \Big), \quad (5)$$

where, as in Bhatia *et al.* [2]), R_n and R_p have been substituted for r_n and r_p. The spin of the outgoing proton is now coupled to the spin of the final nucleus and the orbital angular momenta of the captured neutron and proton are coupled to the spin of the target nucleus and He^3. Thus one has

$$\chi_{j_t}^{m_t}(\xi, \mathbf{r}_n, \boldsymbol{\sigma}_n, \mathbf{r}_p, \boldsymbol{\sigma}_p) \chi_{\frac{1}{2}}^{\mu_1 *}(\sigma_1) = \sum_{J, M} \begin{pmatrix} \frac{1}{2} & j_t & J \\ \mu_1 & m_t & M \end{pmatrix} \psi_{\frac{1}{2} j_t J}^{M}, \quad (6)$$

$$\chi_{j_1}^{m_1}(\xi) \chi_{\frac{1}{2}}^{m_h}(\mu_h) Y_{l_n}^{m_n}(\Omega_n) Y_{l_p}^{m_p}(\Omega_p) = \sum_{j, m} \sum_{L, M_L} \sum_{J_1, M_1} \begin{pmatrix} \frac{1}{2} & j_1 & j \\ m_h & m_1 & m \end{pmatrix} \begin{pmatrix} l_n & l_p & L \\ m_n & m_p & M_L \end{pmatrix} \begin{pmatrix} L & j & J_1 \\ M_L & m & M_1 \end{pmatrix} \psi_{l_p l_n j L J_1}^{M_1}. \quad (7)$$

On substituting eqs. (6) and (7) in eq. (5) one obtains

$$|\mathscr{I}| = \sum_{l_n, m_n, l_p, m_p} \sum_{JM, LM_L, jm, J_1 M_1} \begin{pmatrix} \frac{1}{2} & j_t & J \\ \mu_1 & m_t & M \end{pmatrix} \begin{pmatrix} \frac{1}{2} & j_1 & j \\ m_h & m_1 & m \end{pmatrix} \times \begin{pmatrix} l_n & l_p & L \\ m_n & m_p & M_L \end{pmatrix} \begin{pmatrix} L & j & J_1 \\ M_L & m & M_1 \end{pmatrix} \beta(\tfrac{1}{2} j_t J M; j L J_1 M_1; l_n, l_p) \alpha(l_n m_n, l_p m_p), \quad (8)$$

where

$$\beta(\tfrac{1}{2} j_t J M; j L J_1 M_1; l_n l_p) = \Big[\int \psi_{\frac{1}{2} j_t J}^{M} F(\boldsymbol{\sigma}_1, \xi) \psi_{l_p l_n j L J_1}^{M_1} \mathrm{d}\mathbf{r}'_p \mathrm{d}\mathbf{r}'_n \mathrm{d}\xi \Big]_{r'_p = r'_n = R} \quad (9)$$

and

$$\alpha(l_n m_n, l_p m_p) = \int \mathrm{e}^{-i(\mathbf{k}_1 \cdot \mathbf{r}'_1)} \delta(r_1 - R) \mathrm{e}^{\frac{1}{3} i \mathbf{k}_h \cdot (\mathbf{r}_1 + \mathbf{R}_n + \mathbf{R}_p)} \times \varphi_h(\mathbf{r}_1, \mathbf{R}_n, \mathbf{R}_p) Y_{l_n}^{m_n *}(\Omega_n) Y_{l_p}^{m_p *}(\Omega_p) \mathrm{d}\mathbf{r}_1 \mathrm{d}\mathbf{r}_p \mathrm{d}\mathbf{r}_n. \quad (10)$$

Now we have

$$\sum_{m_f,\mu_1,m_h,m_i}|\mathscr{I}|^2=\sum_{jm}\sum_{JM}\sum_{LM_L}\left|\sum_{l_n m_n l_p m_p}\frac{2J+1}{2L+1}\begin{pmatrix}l_n & l_p & L\\ m_n & m_p & M_L\end{pmatrix}\times\beta(\tfrac{1}{2}j_fJM,jLJM,l_n,l_p)\alpha(l_nm_n,l_pm_p)\right|^2, \quad (11)$$

where $F(\sigma_1,\xi)$ is assumed to be a Racah tensor of order zero.

The angular distribution is determined by

$$\left|\sum_{l_n,m_n,l_p,m_p}\frac{2J+1}{2L+1}\begin{pmatrix}l_n & l_p & L\\ m_n & m_p & M_L\end{pmatrix}\beta(\tfrac{1}{2}j_fJM,jLJM,l_n,l_p)\alpha(l_nm_n,l_pm_p)\right|^2,$$

which can be evaluated by expanding the exponentials as sums in spherical harmonics and putting in a suitable He^3 wave function and evaluating the integrals numerically. It should be pointed out that at present there is no way of predicting when the spin-flip stripping may be important and when not. According to D. H. Wilkinson the importance of this irregular stripping may depend on the Q value. It is most likely to be strong when the departing nucleon is brought into strong interaction with the residual nucleus. This happens when the Q value is high since then, particularly when the projectile energy is low, momentum must be picked up through such interaction. If the Q value is low no such interaction is needed and the conditions for spin-flip are not present. Spin-flip stripping may possibly be diagnosed through the polarization of the outgoing proton.

3. Two-Nucleon Stripping in Zero Range Approximation

Let us now neglect the interaction V_1 as is usual in the theories of stripping reactions and expand the wave function of the final nucleus in terms of the wave function of the initial nucleus and that of the captured nucleons,

$$\chi_{j_f}^{m_f}=\sum_{\substack{l_p\,l_n\,Lj_1SJ\\ MM_LM_Sm_1m_pm_n}}B(JLSl_pl_n)\begin{pmatrix}j_1 & J & j_f\\ m_1 & M & m_f\end{pmatrix}\begin{pmatrix}L & S & J\\ M_L & M_S & M\end{pmatrix}\begin{pmatrix}l_p & l_n & L\\ m_p & m_n & M_L\end{pmatrix}\times\chi_{j_1}^{m_1}(\omega_\xi)\chi_S^{M_S}Y_{l_p}^{m_p}(\omega_p)Y_{l_n}^{m_n}(\omega_n)R_{l_n,l_p}(r_n,r_p), \quad (12)$$

where the three bracket symbols denote the Wigner vector-addition coefficients, $R_{l_n,l_p}(r_p,r_n)$ is the product of the radial parts of the wave functions of the captured neutron and proton, ω_ξ, ω_p and ω_n, denote collectively the polar angles defining the directions of the vectors ξ, $\mathbf{r}_p$ and $\mathbf{r}_n$ respectively. The coefficient $B(JLSl_pl_n)$ takes into account such things as fractional parentage coefficients, configuration mixing etc.

In the special case of a zero-range force as represented by El-Nadi's eq. (10)

one has

$$\omega_p = \omega_n = \omega, \tag{13}$$

and one can use the composition theorem for the product of two spherical harmonics of the same argument. One then obtains

$$\chi_{j_f}^{m_f} = \sum_{\substack{l_p l_n L j_1 S J \\ M M_L M_S m_1}} B(JLSl_p l_n) \begin{pmatrix} j_1 & J & j_f \\ m_1 & M & m_f \end{pmatrix} \begin{pmatrix} L & S & J \\ M_L & M_S & M \end{pmatrix} \left[\frac{(2l_p+1)(2l_n+1)}{4\pi(2L+1)}\right]^{\frac{1}{2}} \times \begin{pmatrix} l_n & l_p & L \\ 0 & 0 & 0 \end{pmatrix} \chi_{j_1}^{m_1}(\omega_\xi)\chi_S^{m_S} Y_L^M(\omega) R_{l_n, l_p}(r_n, r_p). \tag{14}$$

The total exponent from eq. (1) may be written as

$$-i\mathbf{k}_1 \cdot \mathbf{r}'_1 + \tfrac{1}{3} i\mathbf{k}_h \cdot (\mathbf{r}_1+\mathbf{r}_p+\mathbf{r}_n) = i\mathbf{Q} \cdot \mathbf{R} + \tfrac{1}{2} i\mathbf{K} \cdot \boldsymbol{\varrho}_p + \tfrac{1}{2} i\mathbf{K} \cdot \boldsymbol{\varrho}_n, \tag{15}$$

where

$$\mathbf{r}_1 = \mathbf{r}_p + \boldsymbol{\varrho}_p = \mathbf{r}_n + \boldsymbol{\varrho}_n = \mathbf{R} + \boldsymbol{\varrho}, \tag{16}$$

$$\mathbf{Q} = \mathbf{k}_h - (M_1/M_f)\mathbf{k}_1, \tag{17}$$

$$\mathbf{K} = \tfrac{1}{3}\mathbf{k}_h - \mathbf{k}_1. \tag{18}$$

Assuming a Gaussian form for the internal wave function of the He^3 nucleus and expressing it in terms of $\boldsymbol{\varrho}_p$ and $\boldsymbol{\varrho}_n$, one has explicitly

$$\exp\left[-\gamma^2 \sum_{i<j}^{3} r_{ij}^2\right] = e^{-2\gamma^2(\rho_p^2 + \rho_n^2 - \rho_n \rho_p \cos\theta)}. \tag{19}$$

The integration over ξ in (1) is straightforward. The integration over ω in (1) can now be easily performed by expanding $\exp(i\mathbf{Q} \cdot \mathbf{R})$ as a sum in spherical harmonics and assuming that the interaction takes place at the nuclear surface. The integration over ρ_p and ρ_n is carried out by assuming a zero-range δ-interaction and using the standard integral

$$\int_0^\infty e^{i\mathbf{b}\cdot\boldsymbol{\rho}} e^{-a^2\rho^2} d\boldsymbol{\varrho} = \frac{\pi^{\frac{3}{2}}}{a^3} e^{-b^2/4a^2}. \tag{20}$$

The complete expression for the differential cross section is obtained by carrying out the summation over the final states and averaging over the initial states and may be written as

$$d\sigma \propto [2\exp(-K^2/32\gamma^2) + \exp(-K^2/8\gamma^2)]^2 R_{l_p, l_n}^2(R_0) \times \sum_{JLS} \frac{1}{(2S+1)} \left| \sum_{l_p l_n} B(JLSl_p l_n) \begin{pmatrix} l_p & l_n & L \\ 0 & 0 & 0 \end{pmatrix} \left[\frac{(2l_p+1)(2l_n+1)}{(2L+1)}\right]^{\frac{1}{2}} j_L(QR_0) \right|^2. \tag{21}$$

The above result automatically contains the selection rule $|\mathbf{l}_p + \mathbf{l}_n + \mathbf{L}| =$ even. After the present work was completed, a paper by Newns on the same subject has appeared. The result obtained above agrees essentially with that of Newns[8]) in two of his approximations and in general has a more compact form. The

result is different from that given by El-Nadi [9]) for (He^3, p) by the factor

$$\left| \begin{pmatrix} l_p & l_n & L \\ 0 & 0 & 0 \end{pmatrix} \left[\frac{(2l_p+1)(2l_n+1)}{(2L+1)} \right]^{\frac{1}{2}} \right|^2,$$

because El-Nadi does not use the fact that $\omega_p = \omega_n$ as implied by his eq. (10). El-Nadi's eqs. (14) and (21) (for the (α, d) reaction) contain a similar inconsistency.

Eq. (21) can also be used for the (α, d) reaction with the following modifications. The form factor in (21) is replaced by

$$[3.07 \exp(-K^2/48\gamma^2)+\exp(-K^2/16\gamma^2)]^2.$$

The following definitions for **Q** and **K** should then be used:

$$\mathbf{Q} = \mathbf{k}_\alpha - (M_1/M_f)K_d, \qquad \mathbf{K} = \tfrac{1}{2}\mathbf{K}_\alpha - \mathbf{K}_d.$$

The author is grateful to Dr. T. Y. Wu for helpful discussions and to Professor M. Moshinsky for checking the calculations and other useful suggestions.

References

1) S. T. Butler, Proc. Roy. Soc. A **208** (1951) 559
2) A. B. Bhatia, K. Huang, R. Hubley and H. C. Newns, Phil. Mag. **43** (1952) 485
3) D. A. Bromley, E. Almqvist, H. E. Gove, A. E. Litherland, E. Paul and A. J. Ferguson, Phys. Rev. **105** (1957) 957
4) Johnston, Homgren, Wolicki and Illsley, Phys. Rev. **109** (1958) 884;
S. Hinds and R. Middleton, Proc. Phys. Soc. **74** (1959) 196;
N. H. Gale *et al.*, Nuclear Physics **20** (1960) 313;
J. R. Priest, D. J. Tendam and E. Bleuler, Phys. Rev. **119** (1960) 1295
5) D. H. Wilkinson, Phys. Rev. **105** (1957) 666
6) J. E. Bowcock, Phys. Rev. **112** (1958) 923
7) E. Gerjuoy, Phys. Rev. **91** (1953) 645
8) H. C. Newns, Proc. Phys. Soc. **76** (1960) 489
9) M. El-Nadi, Phys. Rev. **119** (1960) 242

1.E.1:
4.E

Nuclear Physics **25** (1961) 175—176; © *North-Holland Publishing Co., Amsterdam*
Not to be reproduced by photoprint or microfilm without written permission from the publisher

BETA DECAY OF Tm^{171}

B. L. SHARMA †
Defence Science Laboratory, Delhi

Received 30 January 1961

Abstract: Er_2O_3 enriched in the isotope Er^{170} (87.3 %) was exposed to a thermal neutron flux of 10^{12} cm^{-2} · sec^{-1}. In order to study the beta decay of Tm^{171} (1.9 y), the Er fraction showing strong 7.5 h activity of Er^{171}, obtained by ion exchange column separation of $Er^{170}+n$, was allowed to decay for a considerable time. The well crystal measurements were then made. Apart from Yb K X-rays and their escape peaks, the measurements showed the presence of a highly internally converted photo-peak at 67 keV. The proposed decay scheme of Tm^{171} together with the spin assignments of various states is discussed.

1. Introduction

The beta decay of 1.9 y Tm^{171} was first studied, among others, by Bisi *et al.* [1]). They reported an end point for the beta spectrum of 103 keV. Using scintillation detectors, they found no gamma rays. However, using high purity Er_2O_3 and irradiating it with thermal neutrons, Smith *et al.* [2]) observed two beta groups with end point energies of 96.5 keV and ≈ 30 keV. Because of the discrepancies in the previously reported data, an attempt was made to reinvestigate the beta decay of Tm^{171}.

2. Experimental

In the present investigations Tm^{171} was produced by thermal neutron capture by Er^{170} and a subsequent beta decay of 7.5 hr Er^{171} to Tm^{171}. Some Er_2O_3 enriched in the isotope Er^{170} (87.3 %) was irradiated with a thermal neutron flux of 10^{12} cm^{-2} · sec^{-1}. In order to study the beta decay of Tm^{171}, the Er fraction, obtained by ion exchange column separation of $Er^{170}+n$, was allowed to decay for several weeks. After the decay of 7.5 hr activity, the Tm^{171} samples were made out of this Er fraction.

The well type scintillation detector, consisting of a 7.6 cm × 7.6 cm cylindrical NaI(Tl) crystal with a 0.95 cm hole extending along the longitudinal axis to the centre of the crystal, a DuMont 6394 photomultiplier tube and a preamplifier, were used. The pulses from this detector were fed into a 100-channel pulse height analyzer.

† Work done at the Department of Physics & Astronomy, Ohio State University, Columbus, Ohio.

3. Results and Conclusion

The well crystal measurements of the radiation from Tm^{171} sample were made by placing the sample inside and outside the well. The energy of the most intense photo peak of the Tm^{171} sample was calibrated with the help of known Eu, Tb, Gd and Dy X-rays, and was found to be 52.4 keV. Comparing this value with the recently reported [3]) values of the rare earth X-rays, this peak was found to be due to Yb K_α X-rays. Apart from Yb K_α, Yb K_β X-rays and their escape peaks, the above measurements showed the presence of a highly internally converted photo peak at 67 keV. From the copper absorption measurements, the identity of this highly internally converted photo peak at 67 keV was ascertained. The proposed decay scheme of Tm^{171}, based on the results of the present investigations [4]) together with the previously reported beta spectrum and conversion line measurements is shown in fig. 1.

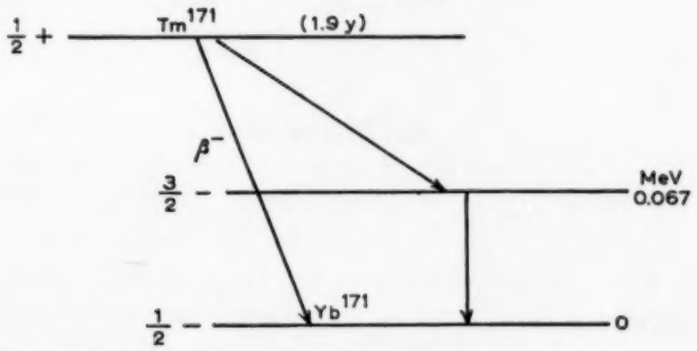

Fig. 1. Proposed decay scheme of Tm^{171}.

The spin assignments of the various states are based on the following considerations. The ground state spin and parity of the Yb^{171} have been determined to be $\frac{1}{2}-$ by Cook *et al.* [5]). Mottelson and Nilsson's [6]) level calculations and the known spin of Tm^{169} suggested that the spin of Tm^{171} is $\frac{1}{2}$. According to Bohr and Mottelson [7]) the spin of the first excited state will be $\frac{3}{2}$ with the same parity as the ground state if the spin of the ground state is $\frac{1}{2}$. Therefore, the spin and parity of the first excited state of Yb^{171} are taken to be $\frac{3}{2}-$.

The author is indebted to Professor M. L. Pool for his interest, suggestions and encouragement throughout this work.

References

1) Bisi, Terrani and Zappa, Nuo. Cim. **2** (1955) 172
2) W. G. Smith, R. L. Robinson, J. H. Hamilton and L. M. Langer, Phys. Rev. **107** (1957) 1314
3) E. L. Chupp, J. W. M. DuMond, F. J. Gordon, R. C. Jopson and Hans Mark, Phys. Rev. **112** (1958) 1183
4) B. L. Sharma, Proc. Ind. Science Congress, Part iii, 80 (1960)
5) A. H. Cook and J. G. Park, Proc. Phys. Soc. **69** (1956) 282
6) B. R. Mottelson and S. G. Nilsson, Phys. Rev. **99** (1955) 1615
7) A. Bohr and B. R. Mottelson, Kgl. Dansk. Vid. Selsk. Mat. Fys. Medd. **27**, No. 16 (1953)

1.E.2 *Nuclear Physics* **25** (1961) 177—215; © *North-Holland Publishing Co., Amsterdam*
Not to be reproduced by photoprint or microfilm without written permission from the publisher

ADJUSTMENT OF RELATIVE NUCLIDIC MASSES (I) $A \leqq 70$

F. EVERLING †, L. A. KÖNIG, J. H. E. MATTAUCH
Max-Planck-Institut für Chemie (Otto-Hahn-Institut) Mainz
and
A. H. WAPSTRA
Instituut voor Kernphysisch Onderzoek, Amsterdam

Received 6 February 1961

Abstract: An outline is given of the general procedure used in the least squares computation of masses from all relevant measurements. The data available for the mass range $1 \leqq A \leqq 70$ are tabulated and discussed.

1. Introduction

Past tables [1–11]) of relative masses of nuclides have been based on a scale in which the unit was $\frac{1}{16}$ of the nuclidic mass of ^{16}O. Recently, the International Union of Physics (IUPAP) has recommended the adoption of a new scale †† in which the unit (1 u) is $\frac{1}{12}$ of the nuclidic mass of ^{12}C. The International Union of Chemistry (IUPAC) is expected to take corresponding action in 1961. In preparation for these recommendations, the present authors prepared a table of nuclidic masses in both scales [12]). The present paper describes the procedures used and the input data accepted in the computation of the part of this table with mass numbers $A \leqq 70$.

In addition to the above organizational reasons, there are also physical reasons why a new computation of nuclidic masses from experimental data is timely. Our last computations [7, 8]) were made using only reaction energies and decay data, since at that time mass-spectroscopical measurements disagreed with them and with one another. New mass-spectroscopical data published since those computations (see sect. 5) agree however much better; their combination with the other data allows us to compute a substantially more accurate mass list.

2. General Remarks (I) The Procedure

The experimental data that can be used in the computation of nuclidic masses are not only extremely numerous, but also very diverse in kind and in

† Now with Nuclear Data Group, National Academy of Sciences, National Research Council, Washington 25, D.C.

†† The old unit, $\frac{1}{16}$ of the nuclidic mass of ^{16}O, will still occur in several places in this paper; it will be indicated by 1MU ($^{16}O = 16$).

precision. This complicates the problem of deriving best values for the nuclidic masses from these data. The ideal situation would be that the data formed a homogeneous group, meaning that they had been obtained in a standard way and that their errors had been assigned according to a unique procedure. Then we could have assigned weights to them in the usual way (inversely proportional to the squares of the standard deviations σ) and applied the conventional method of least squares [13]). As will be shown below, the collection of data about nuclidic masses certainly is not a homogeneous group in this sense.

There is no unique way of treating an inhomogeneous set of data. One may try to obtain a reasonably homogeneous system by scrutinizing, selecting and correcting the data according to some general rules, and this is indeed what we have done; but evidently, this method depends both on the authors' knowledge of the way in which the initial data were obtained and on their experience in treating least squares problems.

Concerning the last point, we shall first make a few pertinent remarks about least squares adjustments of homogeneous groups of N data from which the best values of $n < N$ unknowns are to be computed. If the errors assigned to the input data are so-called standard deviations, the sum χ^2 of the N squared ratios of the residuals to these standard deviations (residual v equals input datum minus its adjusted value) should be equal to $f \pm \sqrt{2f}$, where $f = N-n$ is the number of degrees of freedom; or stated otherwise, the consistency ratio $(R_e/R_1)^2 = \chi^2/f$ is expected to be equal to $1 \pm \sqrt{2/f}$. If this ratio is significantly larger than one, one might try whether this deviation is due to one or a few accidentally deviating data by making adjustments in which one of these data is omitted; if one of these adjustments gives a much better value for R_e/R_1, the values obtained in this adjustment may be better than those obtained in the complete adjustment. If, however, such an analysis of variances does not yield a really considerable improvement, one better supposes that all errors assigned to the initial data have been estimated somewhat optimistically, and, therefore, multiplies all of them with R_e/R_1.

Now, consider the case that the input data can be separated into two independent groups. One can easily prove that solving them in one adjustment yields the same results as solving them in two separate adjustments, and that χ_0^2 in the first case equals the sum of the values $\chi_1^2 + \chi_2^2$ for the separate adjustments; $(R_e/R_1)_0^2$ is, therefore, the weighted average of the separate $(R_e/R_1)^2$ values. If one is convinced that the input data are homogeneous and if a variance analysis does not lead to the detection of very much deviating data, the separate values of R_e/R_1 do not have much significance: in cases in which $(R_e/R_1)_0$ is significantly larger than one, one should multiply errors in *both* groups of data with *this* value.

The situation, however, becomes entirely different in the not homogeneous set of data occurring in the present work. Here, one has to be grateful if the

existence of homogeneous subgroups gives an opportunity to test them separately. It will be seen later that our material indeed contains homogeneous subgroups of data (see sects. 5 and 7). These groups are mostly not independent groups as discussed above. They do not even necessarily present soluble systems; but in most cases a soluble subsystem can be formed by the omission of some of the data. Then, it makes sense to solve the largest soluble subsystem of such a homogeneous subgroup: the value R_e/R_i obtained in this pre-adjustment not only checks whether the errors have been assigned correctly, but it gives also a way of correcting them if necessary, as described above. Even after such an error adjustment, one should be somewhat careful in formulating the final adjustment procedure. Such homogeneous subgroups may contain systematic errors, that do not appear in the pre-adjustment for correcting their errors but that may influence the final adjustment unless it is formulated correctly.

3. General Remarks (II) The Data

In addition to the procedure, the result of the adjustment depends on the selected input data; the method of selecting the input data should therefore be presented with each adjustment. The present data about nuclidic masses can be classified as follows: beta decay energies, energies released in alpha disintegrations and in nuclear reactions, mass-spectroscopical data, and mass ratios obtained from microwave spectroscopy. These classes are not completely independent from one another. Sometimes the data for the ground state decay or reaction energy may be obtained most accurately by combining transitions to excited states with an excitation energy. Thus, the same excitation energy can enter into several input data, which then are not statistically independent. One can of course avoid this difficulty by treating the masses of nuclei in excited states as separate variables. We did not think it necessary to add this complication to our already so much complicated problem since it would cause only minor corrections in the final results. Another, not statistical dependency between our input data is caused by the fact that sometimes decay or reaction energies are assigned to ground state transitions between certain nuclides on the basis of other decay, reaction or mass-spectroscopical results.

There is no unique "best" set of masses that can be derived from the experimental data. It therefore makes no sense to retain data of relatively low weights, especially so where this would introduce danger that incorrect input data would unduly influence the results. When, therefore, a certain measurement yields a result about a certain combination of masses that can be derived with essentially higher accuracy from another measurement or from a simple combination of other data, we have as a rule not accepted this result among the input data.

The data appearing in the present range do not contain alpha decay energies;

microwave measurements are here of essentially lower precision than other available data. Of the remaining data we only accept two large and presumably homogeneous groups of mass doublets; their errors will be checked with pre-adjustments. Part of the nuclear reaction data can also be considered to form a homogeneous group and will be treated as such. The remaining nuclear reaction energies and beta decay energies have been measured rather piecemeal and will therefore be accepted without changes, or rejected on the basis of the above criteria.

4. Arrangement in Sub-Problems

After application of the rules discussed in the two preceding paragraphs one might hope to have arrived at a reasonably homogeneous set of N input data to which the method of least squares can be applied in order to find the best values for the $n < N$ variables (masses). Still, for practical reasons the problem cannot be solved in one step since the numbers N and n are both too large. Also, solving the problem in a few smaller steps instead of one large step yields the possibility for a more detailed check of the data and of the computations The computation was, therefore, simplified in two ways.

4.1. PRIMARY AND SECONDARY DATA

One can divide the data into two groups which we call primary and secondary data. The last ones are those that give useful information about one nuclidic mass only without essentially improving the precision with which other masses can be determined. An obvious example is the decay energy (2560 ± 10) keV for the disintegration $^{49}\mathrm{Cr}(\beta^+)^{49}\mathrm{V}$ which determines only the mass of ^{49}Cr not involved in any other datum. Secondary data were, therefore, not included into the final adjustments.

A somewhat more complex example is ^{49}V itself: it is determined by $^{49}\mathrm{V}(\varepsilon)^{49}\mathrm{Ti} + (620 \pm 10)$ keV and by $^{49}\mathrm{Ti}(\mathrm{p}, \mathrm{n})^{49}\mathrm{V} - (1391 \pm 5)$ keV. Evidently, the inclusion of these two data into the primary ones would not essentially improve the masses of ^{49}Ti, ^{1}H or ^{1}n. Instead, the capture decay energy was combined with the (^{1}n$-^{1}$H) mass difference of 783 keV derived by least squares from the primary data in order to obtain an indirect value $-(1403 \pm 10)$ keV for the last reaction; the average of the two values of the (p, n) reaction was then used as the secondary datum determining the mass of ^{49}V.

For the mass range considered here ($A \leqq 70$) figs. 1 and 2 show clearly the distinction between primary and secondary input data. The primary mass doublets are given in table 1a (p. 194), the primary reaction and decay energies in table 2a (p. 199). In table 1b (p. 198) seven mass doublets are listed which have been treated as secondary input data; they determine respectively the masses of ^{36}S, ^{38}A, ^{46}Ca, ^{48}Ca, ^{50}Ti, ^{50}V and ^{70}Zn, without improving essentially our knowledge of the masses of other nuclides. Table 2b (p. 209) shows the

secondary reaction and decay energies, together with their adjusted values in the cases where a small adjustment has been made as discussed above for ^{49}V. The beta decay energies in the table are sometimes average values from several authors that generally agreed well with one another. Some reaction energies have been treated in the same way as the primary reaction energies, as discussed in sects. 6 and 7.

The fact that secondary data had not been included in the final adjustments does not change in any way the results for the primary masses, and the computation can afterwards be extended easily to obtain the secondary ones.

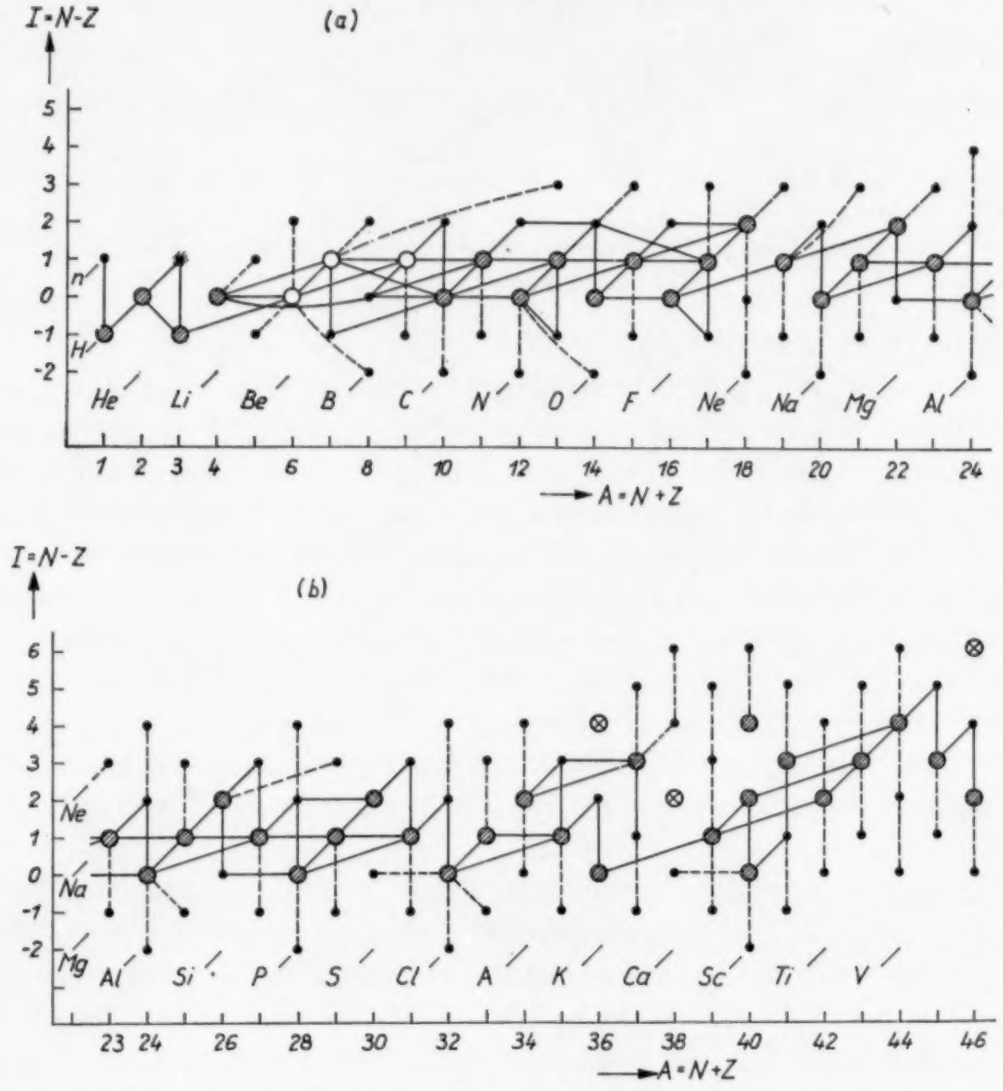

Fig. 1. Survey of the input data of the first adjustment; range $1 \leqq A \leqq 46$.

o Nuclides occurring in nature,

• artificially produced nuclides,

/|/ designation of primary nuclides determined by mass-spectroscopic doublets,

× designation of secondary nuclides determined by mass-spectroscopic doublets,

—— reactions connecting primary nuclides (primary reactions),

- - secondary reactions (at least one of the two nuclides connected thus is a secondary mass).

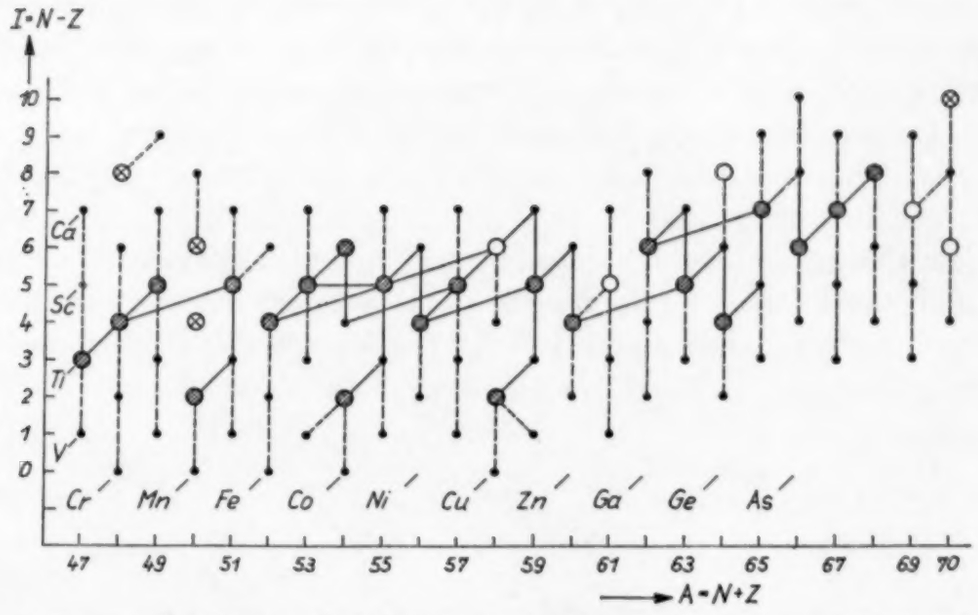

Fig. 2. Survey of the input data of the second adjustment; mass range $47 \leqq A \leqq 70$. Legend as in fig. 1.

4.2. SEPARATION OF ADJUSTMENTS

The remaining set of primary data is still very large. However, it can be divided into a number of subsets between which practically no, or anyhow no important, relations exist. Then correlations between the masses of these subsets should also be (almost) non-existent. The subsets have then been solved by separate least squares adjustments each of wich could be tested by a separate R_e/R_1 check. As has been shown by one of us [14]) such a treatment was practically forced upon us for two reasons: firstly, the saving of computer time is quite considerable, since the time necessary for a least squares adjustment increases approximately as the cube of the number of primary variables; secondly, splitting the entire problem into separate adjustments kept the expenditure necessary to check the correctness of the arithmetical results within reasonable limits.

The range considered in the present paper had been split into two adjustments according to the mass range $1 \leqq A \leqq 46$ and $46 < A \leqq 70$. Some nuclides in the first group occur also in the second one, e.g. ^{1}H, ^{12}C and ^{32}S in the mass doublet ($C\,S\,H_3$—^{47}Ti), or ^{2}D and ^{4}He in the reaction $^{55}Mn(d, \alpha)^{53}Cr$. Their masses are taken from the first adjustment and treated as auxiliary constants in the adjustment of the second group, which is allowed since their accuracy is considerably higher than that of the mass doublet or the reaction energy mentioned. Again, the results are not substantially different from those that would be obtained from one large least squares adjustment, and a more detailed check on the results is possible.

Excepting mass-spectroscopical connections with the nuclides mentioned above, mainly ^{1}H and ^{12}C, the group of nuclides with mass number

$46 < A \leqq 70$ and that with $A > 70$ are only connected through the reaction $^{71}Ga(\gamma, n)^{70}Ga$. The mass of ^{70}Ga is determined with essentially lower precision by the group of nuclides with higher mass combined with the above reaction than by the group of nuclides with lower mass. We therefore separated the two groups and first adjusted the first one; later, the resulting mass of ^{70}Ga together with the reaction mentioned will give an input datum for the next group of higher mass. One might ask why the division has been made between mass numbers 70 and 71 considering that between 68 and 69 no accepted reaction-links exist. This was done since ^{70}Zn belongs to a series of nuclides of lower mass measured mass-spectroscopically with high precision, whereas the data with mass numbers above 70 are of essentially lower precision.

5. Mass Doublets

Only mass doublets measured in Brookhaven [15–16]) and in Minnesota [17–22]) have been accepted in the present work.

Following the advice of the author, only the third and fifth group of doublets measured by Smith [15]) were used excepting the data marked a in table 1 of his paper (which had not been included in his least squares check). The two groups can be considered to be homogeneous in the sense described in sect. 2; their errors should therefore be checked and, if necessary, corrected by separate pre-adjustments. This has already been done by the author himself; data about these pre-adjustments are given in table A. Another group of data measured in

TABLE A

Data about the pre- and final adjustments

		N	n	R_e/R_1	
				found	expected
Pre-adjustments	Smith 3	14	3 [a])	3.58	1 ± 0.21
	Smith 5	39	8	2.35	1 ± 0.13
	Minnesota	36	12	2.65	1 ± 0.14
	Reactions	73	19	0.60	1 ± 0.10
Final adjustments	$1 \leqq A \leqq 46$	358	69	1.105	1 ± 0.042
	$47 \leqq A \leqq 70$	103	38	0.98	1 ± 0.09

[a]) In table III of Smith's paper

Brookhaven [16]) is too small to allow a significant least squares adjustment; as a compromise we applied the average (2.97) of the two above consistency factors to this group.

The mass doublets measured in Minnesota before 1956 are outclassed by the later measurements there and have not been accepted; the more recent work

of Kettner [23]) in the same Laboratory has not been accepted for the same reasons, though it agrees with the later results. The doublets reported in the Minnesota papers [17–22]) quoted above have been combined in a least squares adjustment and thus yielded a consistency factor 2.65. As noticed by the authors themselves [20]) the slight disagreement expressed by the magnitude of this factor is partly caused by the fact that three earlier [17]) values for the CH_4—O mass difference and the doublets containing ^{36}A were found to differ rather much from the later results †; they propose to reject these earlier measurements (see table 1c on p. 198). On the basis of the discussion in sect. 2 this proposal was accepted. Yet we felt that the consistency factor found above should be applied instead of the somewhat lower factor that would be obtained by omitting the five results mentioned, since no convincing reason could be found to explain the difference.

The fact that the above correction factors were applied to the errors reported by the two laboratories mentioned does not imply a criticism. The reported results are averages of a rather large number of repeated measurements of each doublet, and their "errors" are obtained from the spread in the single results. By this averaging procedure, one randomizes some of the actual errors in the single results but probably not all of them. Basically, one can consider the pre-adjustments as a further randomizing of errors; it is therefore to be expected that such a procedure reveals the presence of further errors. The corrected errors represent the truth the better the more data are combined in the pre-adjustment. Since in the above pre-adjustments the number of doublets included is considerable, one may hope that the adjusted errors are rather dependable.

Mass-spectroscopic data published before 1956 have not been accepted for reasons outlined earlier [7, 8]) and also because they are at least an order of magnitude less accurate than the results mentioned above. The same is true for the more recent data of Ewald and collaborators [24, 25]) and even for those of Demirkhanov *et al.* [26]). The only competing value published by the last group is $^2D_2$—^{4}He = (25 600±2)μMU (^{16}O = 16). Another value for this doublet would be very valuable since the Minnesota and Brookhaven data on ^{4}He disagree somewhat (see table 1a). Unfortunately, Demirkhanov's value is much lower than both above results, whereas the value (25 618±6) μMU (^{16}O = 16) computed from nuclear reaction energies alone (the pre-adjustment discussed in sect. 7) is even slightly higher. We thought it therefore advisable to disregard even this new value.

The accepted doublets are given in table 1a, both in the ^{16}O scale in which they were reported, and recomputed in the ^{12}C scale, together with the values obtained in the final adjustments. We did not investigate separately whether

† The same disagreement also affects the ^{15}N doublets, as will be discussed in sect. 9.

the results of Brookhaven and Minnesota agreed; as we will show later, both sets together agree well with the nuclear reaction energies.

Before the mass doublets can be combined with reaction and decay energies, they have to be expressed in energy units. The best known value for the conversion factor X is

$$X = (931\ 145 \pm 10)\ \text{keV/MU}\ (^{16}\text{O} = 16) \tag{1}$$

according to Cohen and DuMond [27]). The error in this factor is not quite negligible: At least a dozen doublets have errors of about 1 part in 30 000 or less. Therefore the conversion factor was treated as an independent variable and eq. (1) as one input datum for the variable X of the final adjustment: otherwise the errors in several of the resulting masses would be slightly too low. In the following the symbol X denotes this variable. The equations representing the mass doublets are then not linear: they have the shape

$$\frac{1}{X}\sum_i \kappa_{Ii} M_i = Q_I \pm \sigma_I \tag{2}$$

where Q_I and σ_I are the mass spectroscopic input values given in μMU ($^{16}\text{O} = 16$). They are linearized in the usual way, using approximations $M_i^{(0)}$ and $X^{(0)}$ for M_i and X. With

$$M_i = M_i^{(0)} + m_i \tag{3}$$

and

$$X = X^{(0)}(1+x), \tag{4}$$

eq. (2) becomes

$$\sum_i \kappa_{Ii} m_i - x\sum_i \kappa_{Ii} M_i^{(0)} = X^{(0)} Q_I - \sum_i \kappa_{Ii} M_i^{(0)} \pm X^{(0)}\sigma_I . \tag{5}$$

6. Nuclear Reaction Energies (I) Recalibration

Most reaction energies have been measured using spectrometers and accelerators calibrated with some energy standard. Almost all of the many measurements (marked M_0 in tables 2) made in the Massachusetts Institute of Technology, for instance, have been calibrated with the ^{210}Po alpha ray line, assuming an energy of 5298 keV for these alpha particles. Thus, in combining these results in a least squares adjustment we introduce a systematic error. Just as in the similar situation at the end of sect. 5 we therefore introduce † a calibration variable Y and write the reaction equations

$$Y\sum_i \kappa_{Ii} M_i = Q_I \pm \sigma_I , \tag{6}$$

† Only in the adjustment for $A \leqq 46$; the reactions for $A > 46$ are less accurate so that this refinement is not necessary there.

where Q_I and σ_I are reaction input values given in keV. We linearize them using eqs. (3), and we put

$$Y = 1+y \tag{7}$$

so that we obtain

$$\sum_i \kappa_{Ii} m_i + y \sum_i \kappa_{Ii} M_i^{(0)} = Q_I - \sum_i \kappa_{Ii} M_i^{(0)} \pm \sigma_I. \tag{8}$$

Still, this does not mean that we even preliminarily adopt the above value 5298 keV for the ^{210}Po alpha rays. As explained more fully elsewhere [28]) recent results indicate a higher value (5304.2$\pm$1.6) keV for this energy. Thus, all reaction energies based on the above mentioned value were increased by 0.096% before we accepted them. As will be understood, the input equation for the calibration variable then becomes

$$y = (0\pm 1.6)/5304.2. \tag{9}$$

The meaning of the value y obtained by the final least squares adjustment will be discussed in sect. 8.

The reaction energies measured in Birmingham (marked B in tables 2) have been calibrated with proton resonance methods. This group measured with the same apparatus a new value for the ^{210}Po alpha ray energy; the ratios of their reaction energy values to the ^{210}Po alpha ray energy are very probably more dependable than their absolute values. Therefore, the calibration variable y was also applied to these results. The reported reaction energies were not changed since their ^{210}Po alpha energy nearly coincides with the value adopted here.

Several measurements (marked C in tables 2) reported by the California Institute of Technology have been calibrated with alpha ray lines from the Thorium active deposit. The ratios of their energies to that of ^{210}Po are known with high accuracy [28]) but the energy values derived from these ratios and our ^{210}Po alpha energy lie about 0.12 % higher than the values adopted by the above group (except a correction for absorption in the source). These reaction energy values were therefore increased by 0.12 % (or even slightly more in cases where the primary particles had been calibrated in another way described below) and the calibration variable was applied to these results.

Other measurements at CIT have been calibrated with the resonances ^{19}F(p, $\alpha\gamma$) and ^{27}Al(p, γ), those in Wisconsin (W in tables 2) with the ^{7}Li(p, n) threshold. The experimental data about these calibration energies did not agree very well within each group at the time that the data for the present mass adjustment were collected, as is shown in table B. In fact, the situation for ^{7}Li(p, n) was worse than commonly realized. We had to increase Sturm and Johnson's value obtained by comparison with the old value for the ^{210}Po alpha energy. On the other hand we agree with Endt and Braams [29]) that the most dependable value for the excitation energy of the first excited state in

^{24}Mg is that of Hedgran and Lind, (1368.7±1.0) keV, so that Jones *et al.*'s comparison with this excitation energy yields only the reported low value for the ^{7}Li(p, n) threshold. As a result, we felt that we could only accept the unweighted average of the four values as an input datum in giving the reaction energy

TABLE B

Energy standards (in keV)

^{7}Li (p, n)	^{19}F (p, $\alpha\gamma$)	^{27}Al (p, γ)
	872.5±1.8 [d])	
	874.5±0.9 [f])	
	871.2±0.4 [g])	990.8±0.2 [g])
1882.9±1.9 [a])	873.5±1.0 [a])	993.3±1.0 [a])
1881.2±1.9 [b])		
1883.8±0.7 [c])		
1879.8±1.4 [e])		

[a]) R. G. Herb, S. C. Snowdon and O. Sala, Phys. Rev. **75** (1949) 246
[b]) W. E. Shoupp, B. Jennings and W. Jones, Phys. Rev. **76** (1949) 502
[c]) W. J. Sturm and V. Johnson, Phys. Rev. **83** (1951) 542
[d]) K. F. Famularo and G. C. Phillips, Phys. Rev. **91** (1953) 1195
[e]) K. W. Jones, R. A. Douglas, M. T. McEllistrem and H. T. Richards, Phys. Rev. **94** (1954) 947
[f]) S. E. Hunt and F. Firth, Phys. Rev. **99** (1955) 786
[g]) F. Bumiller, H. Staub and H. E. Weaver, Helv. phys. Acta **29** (1956) 83

TABLE C

Recalibration of reaction energies

Comparison	Number of comparisons	Average difference	
		before recalibr.	after recalibr.
C − M_0	14	−0.03%	+0.015%
B − M_0	10	+0.08%	−0.016%
W − M_0	8	+0.10%	+0.004%
R − M_0	6	+0.09%	−0.009%

Average differences between reaction energies as given by various groups and those reported by the MIT, before and after the recalibration discussed in sect. 6.

of the ^{7}Li(p, n)^{7}Be reaction †. In most of the primary reactions of importance in the present computation, the exact value of this calibration energy is not important. We therefore did not introduce a systematic correction for reaction energies calibrated in this way.

Table C shows that the values of the different groups discussed above agree much better after the recalibration than they did before. We therefore did not

† As a result, the adjusted value for the ^{7}Li(p, n) threshold will come out rather low: combination of the ^{10}B(p, α)^{7}Be reaction energy with other data in table 2a corresponds to a threshold of only (1875±3) keV. We did not use this datum in the above discussion since the difference may have been caused partly by the accidentally rather high value (1153±4) keV for the ^{10}B(p, α)^{7}Be reaction energy found in the MIT.

see any serious objection against using the calibration variable together with all reactions measured by these groups, and this has been done. (It has not been applied to reaction energies measured in rather different ways: (n, γ), (γ, n), (p, n) and (p, pn) reactions.) Of course, this is only allowed if the final result for the calibration variable Y does not deviate appreciably from 1; sect. 8 will show that this is indeed so.

7. Nuclear Reaction Energies (II) Pre-adjustment

In addition to the discussion in sect. 2, there is another reason to adjust the errors in the rather homogeneous group of data discussed in sect. 6. The errors in these results cannot be determined in as simple a way as those in the mass doublets (sect. 5). They contain parts for the errors in the measurement of the energies of the incoming particles and the reaction products measured at a certain angle, for the way in which the influence of the target thickness is eliminated and for the error in the calibration energy; moreover, several reaction physicists added safety factors to their errors. Before these results are combined with the mass doublets, something should be done to reduce the influence of the safety factor and also (due to the introduction of the calibration variable) that of the error in the calibration energy. This can be done with the help of a pre-adjustment: we may now expect to find a consistency factor R_e/R_i smaller than 1, and multiplication of the errors with this factor will have an effect in the desired direction.

Such error reductions can of course only be applied to groups of data that have really been tested somewhat extensively in the pre-adjustment. The latter was only possible for the five groups mentioned above (M_0, C, B, W, and R) and only in the region $A \leqq 17$. Therefore, only the errors assigned to all the primary reaction energies reported by these groups were reduced by the factor $R_e/R_i = 0.60$ found in this pre-adjustment. This discrimination of course does not imply any criticism on the many data measured at the Nobel Institute of Physics (N), at the Bartol Research Foundation (Ba) or in Chalk River (CR), to mention only those places which contributed most other reaction data. In fact, we discriminated even more. Part of the data reported by MIT were measured with a new, broad range spectrometer; this group M_1 could not be tested in the above pre-adjustment and their errors have therefore not been reduced: the error reduction factor has only been applied to the group M_0 of data measured in the old spectrometer †.

† In fact, there are reasons to be somewhat careful with the errors in the M_1 data. Twelve (d, p) reactions in this group are in the average 13 keV larger than the results computed from mass doublets combined, where necessary, with beta decay energies or (p, n) reaction energies; another 12 (d, p) reaction energies are in the average 13 keV larger than parallel (n, γ) reaction energies indicate. (In the group M_0 these deviations are only +4 keV averaged over 14 cases.) These differences have to be compared with an average reported error of 8 keV in the reaction energies, and somewhat less in the mass-spectroscopical data. An average difference of opposite sign, −9 keV,

The above mentioned pre-adjustment, if considered as an adjustment of nuclear masses, cannot be made with nuclear reactions alone [31]). A system of particle reactions alone determines masses only but for a linear function of mass and charge number $aZ+bA$. One relation between the constants a and b is determined by the requirement that the mass excess should be zero for the standard isotope ^{12}C, another one can be obtained by adding some beta decay energy to the system of equations. For that reason, the very precisely known beta decay energies of ^{3}T and ^{14}C and that of the neutron were added to the pre-adjustment; for the last quantity, a preliminary value (782.42 ± 0.44) keV was derived as an average of separate results obtained by combining (p, n) reactions and beta decay energies regarding the nuclides ^{3}T, ^{14}C, ^{37}A and ^{65}Zn. (Of course, the above average value was not used in the final adjustment).

8. Result of the Final Adjustments

Mathematical details about the adjustments made in the course of this work have been given by one of us [14]). Table A shows the numbers of data and of adjusted masses in the two final adjustments, together with their consistency ratios. The consistency ratio for the second adjustment is entirely satisfactory; that for the most important first adjustment disagrees with the theoretical value 1 ± 0.042, and there is only a chance of 0.61 % that the actual value deviates so much from one. This disagreement, however, means that in the average the errors are only 10 % low; we are therefore inclined to be very satisfied with this result. In fact, the situation is even better since we can point out a source for the greater part of the discrepancy [13]). Of the four input values for the β^+-decay energy of ^{13}N, the two reportedly most accurate ones deviate rather much from the two other ones, and in opposite direction. Other data, combined, give an indirect value (2220.9 ± 1.7) keV for this decay energy, in agreement with the two middle values. On the basis of the considerations in sect. 3, we could therefore have omitted the deviating results; since their average (2222.1 ± 2.4) keV happens to coincide nearly with our output value 2221.2 keV, this would have influenced our mass values and their errors only very slightly and decreased R_e/R_1 to the perfectly reasonable value 1.053. All the other input data deviate less than three times their errors from the adjusted values, and only ten of them yield contributions of more than 5 to χ^2.

The results of the present computation are given elsewhere [12]). Mainly due to the inclusion of the new mass doublets, the new results are much more

is obtained in comparing (p, α) and (d, α) reactions with the other data (-6 keV in group M_0). Unfortunately, no closed cycles of M_1 reactions exist: they should have closure errors of ≈ 17 and ≈ 30 keV for cycles containing a (d, α) and two (d, p) reactions, or a (p, α) and three (d, p) reactions, respectively. Two roughly equivalent cycles containing the ^{58}Fe(p, α) and the ^{65}Cu(p, α) reactions, respectively, have closure errors of (1 ± 18) and (14 ± 25) keV, not in contradiction with the above considerations.

accurate than those in our preceding mass tables [7, 8]), as is shown in table D for a few important nuclides. This table also shows that the new values agree reasonably with the old ones. The largest deviation occurs for the nuclide ^{16}O. (It should be remarked that the last deviation would make the agreement with the earlier results rather worse if the comparison had been made in the ^{16}O scale, thus emphasizing one of the advantages of the ^{12}C scale of nuclidic masses). Also in the mass range 30 to 70 many errors have been improved by at least an order of magnitude, whereas the values agree rather well with the earlier ones [7]).

TABLE D

Comparison with earlier mass values (recomputed to the ^{12}C scale)

	Wapstra [7]) (μu)	Mattauch [8]) (μu)	Present work (μu)
^{1}n	8 666.4± 1.5	8 663.0± 1.7	8 665.44±0.43
^{1}H	7 825.8± 1.5	7 824.1± 1.8	7 825.22±0.08
^{2}D	14 102.0± 2.8	14 097.2± 2.9	14 102.19±0.11
^{4}He	2 605.4± 2.1	2 603.0± 2.1	2 603.61±0.37
^{16}O	− 5 069.1± 7	− 5 074 ± 5	− 5 085.06±0.28
^{20}Ne	− 7 567 ± 9	− 7 578 ±10	− 7 559.6 ±0.53
^{32}S	−27 937 ±26	−27 953 ±20	−27 926.2 ±1.1

The output value of the mass energy conversion factor X defined in sect. 5 differs scarcely from the input value. This is a consequence of the fact that most important reaction equations contain the calibration variable Y (see sect. 6): therefore the above adjustment would essentially only determine the product XY if the input equations (1) and (9) were omitted. Omitting eq. (1) alone would thus only yield a value for X with about the same relative precision as that in the calibration energy; in fact, the result would be

$$X = (931\,200 \pm 200)\ \text{keV/MU}\ (^{16}O = 16),$$

so that the input equation (1) can scarcely be improved by the adjustment. Yet, the above result is a very good check on the validity of Einstein's mass-energy relation.

On the other hand, a relatively much improved value for the calibration energy may be obtained in an adjustment omitting eq. (9) only:

$$E_\alpha(^{210}Po) = (5302.8 \pm 0.5)\ \text{keV}.$$

This result, together with the success of the recalibration procedure demonstrated in table C, strongly indicates that the presently adopted alpha ray energy for ^{210}Po is nearly correct. One has even to ask whether the above result should not be considered as the most precise determination of this alpha ray energy. As discussed elsewhere [28]), one should be somewhat careful with this conclusion

since the above result may very well be spoiled by a systematic error which does not influence the mass adjustment.

The conversion factor between the old and the new scale of nuclidic masses following from the above adjustment is

$$1\text{u} = (1.000\ 317\ 917 \pm 0.000\ 000\ 017)\text{MU}(^{16}\text{O} = 16).$$

The mass energy conversion factor in the new scale is obtained by combining this result with eq. (1):

$$1\text{u} = (931\ 441 \pm 10)\ \text{keV}.$$

The masses and error matrices computed in the present work have been used to derive an extensive list of reaction energies and their adjusted errors; this list will be published elsewhere [32]).

When combining the present mass list [12]) with new data, one is completely free to alter secondary masses but for the fact that changes of some of them may affect one or more others (e.g. in the example of subsect. 4.1, a change of the mass of ^{49}V should be accompanied by a corresponding change of the mass of ^{49}Cr). Alterations of primary data may cause rather complex changes in the system of primary nuclidic masses.

9. Rejected Data

As mentioned in sect. 5, three Minnesota CH_4—O doublets and two ^{36}A doublets have not been used in the final adjustments. The same is true for the CH_3—^{15}N doublet value $(23\ 365.2 \pm 0.9)\mu\text{MU}(^{16}\text{O} = 16)$ (see table 1c). Its sum with the ^{15}NH—O doublet $(13\ 023.4 \pm 0.4)\mu\text{MU}(^{16}\text{O} = 16)$ does not agree with the newer, accepted CH_4—O doublet. Computing both doublets with the help of nuclear reaction energies ^{15}N(p, α)^{12}C, ^{14}N(n, γ)^{15}N, ^{14}N(d, p)^{15}N, ^{17}O(d, α)^{15}N and ^{18}O(p, α)^{15}N all given in table 2a we obtain the values $(23\ 377 \pm 2)$ and $(13\ 020 \pm 2)\mu\text{MU}(^{16}\text{O} = 16)$. We therefore rejected the first doublet and accepted the second one.

Quisenberry *et al.* [19]) themselves rejected their ^{64}Ni doublet, which disagrees with their ^{64}Zn doublet combined with the ^{64}Cu decay energy. Using reaction data published partly after their work, we found two further conspicuous cases. The directly measured value for the C_4H_{10}—^{58}Fe doublet is $(144\ 977 \pm 4)$ $\mu\text{MU}(^{16}\text{O} = 16)$; but values $(145\ 031 \pm 12)$, $(144\ 997 \pm 19)$ and $(145\ 036 \pm 10)$ $\mu\text{MU}(^{16}\text{O} = 16)$ are obtained from their doublets for ^{55}Mn, ^{57}Fe and ^{59}Co combined with the reactions ^{58}Fe(p, α)^{55}Mn, ^{57}Fe(d, p)^{58}Fe, and ^{58}Fe(d, p)^{59}Fe and the decay ^{59}Fe(β^-)^{59}Co. The errors in the first and last value are mainly due to nuclear reactions, that in the middle value is due to the ^{57}Fe doublet (the error of the latter has been increased for the reasons mentioned in sect. 5). The directly measured value for the $C_2H_5O_2$—^{61}Ni doublet is $(97\ 894 \pm 5)\mu\text{MU}$

($^{16}O = 16$); their doublet for ^{60}Ni combined with the $^{60}Ni(d, p)^{61}Ni$ and $^{60}Ni(n, \gamma)^{61}Ni$ reactions yields the value $(97\,948 \pm 15)\mu MU$ ($^{16}O = 16$). The assignment of the two agreeing reaction energy values to ground state transitions is very certain, since other transitions to excited states are reported that agree very well with excitation energies found [33]) in the decay of ^{61}Cu. In view of the above discrepancies, the two doublets mentioned were not included in our final adjustment.

We did not deem it necessary to include a list of reaction energies that have not been used since they are clearly much less accurate than other data, as discussed in sect. 3. Table 2c (p. 215) lists some border cases and some cases with an accuracy comparable to that of accepted data (among them all data measured at the laboratories discussed in sect. 6) that have not been accepted since they disagree with other data. The reasons are mostly clear from comparison with the adjusted values for these reaction energies also given in the table.

All computations in the range $1 \leqq A \leqq 70$ have been carried out on an IBM 705 electronic computer in the Farbwerke Hoechst, kindly put at our disposal by Professor K. Winnacker; we are very thankful to him and to Mr. D. Kobelt who prepared the program for the machine. The work of one of us (A. H. W.) is part of the research program of the „Stichting voor Fundamenteel Onderzoek der Materie (F.O.M.)", which is financially supported by the „Nederlandse Organisatie voor Zuiver Wetenschappelijk Onderzoek (Z.W.O.)".

References

1) M. S. Livingston and H. A. Bethe, Rev. Mod. Phys. **9** (1937) 245;
H. A. Bethe, Elementary Nuclear Theory (Wiley, New York, 1947)
2) O. Hahn, S. Flügge und J. Mattauch, Physikal. Zeitschr. **41** (1940) 1;
S. Flügge und J. Mattauch, Physikal. Zeitschr. **42** (1941) 1; **43** (1942) 1; **44** (1943) 181, 391
(see also J. Mattauch u. S. Flügge, Kernphysikalische Tabellen (Berlin, 1942)
3) A. H. Wapstra, Table of Atomic Nuclei, published in L. Rosenfeld, Nuclear Forces (North-Holland Publishing Co., Amsterdam, 1948)
4) J. Mattauch and A. Flammersfeld, Isotopic Report, Tübingen 1949;
L. Waldmann, Z. Naturforsch. **4a** (1949) 226
5) C. W. Li, W. Whaling, W. A. Fowler and C. C. Lauritsen, Phys. Rev. **83** (1951) 512;
C. W. Li, Phys. Rev. **88** (1952) 1038
6) J. E. Drummond, Phys. Rev. **97** (1955) 1004; **99** (1955) 709
[illegible] Wapstra, Physica **21** (1955) 367, 385;
J. R. Huizenga, Physica **21** (1955) 410;
A. H. Wapstra, Encyclopedia of Physics (Springer, Berlin, 1958) Vol. **38**, 1, p. 1.
8) J. Mattauch, L. Waldmann, R. Bieri and F. Everling, Z. Naturforsch. **11a** (1956) 525;
Ann. Rev. Nucl. Sci. **6** (1956) 179;
J. Mattauch and F. Everling, Progress in Nuclear Physics **6** (1957) 223
9) H. E. Duckworth, Progress in Nuclear Physics **6** (1957) 138; Mass Spectroscopy, Cambridge 1958
10) W. H. Johnson, Jr., K. S. Quisenberry and A. O. Nier, Handbook of Physics (New York, 1958) Vol. **9**—55

11) V. A. Kravtsov, Uspekhi Fiz. Nauk **65** (1958) 451
12) F. Everling, L. A. König, J. H. E. Mattauch and A. H. Wapstra, Nuclear Physics **15** (1960) 342; **18** (1960) 529
13) J. Mattauch, Proc. Hamilton Conf. on Nuclidic Masses (University of Toronto Press, Toronto, 1960) p. 3
14) L. A. König, Proc. Hamilton Conf. on Nuclidic Masses (University of Toronto Press, Toronto, 1960) p. 39
15) L. G. Smith, Phys. Rev. **111** (1958) 1606 (B3, B5)
16) L. Friedman and L. G. Smith, Phys. Rev. **109** (1958) 2214 (B6)
17) K. S. Quisenberry, T. T. Scolman and A. O. Nier, Phys. Rev. **102** (1956) 1071 (M1)
18) T. T. Scolman, K. S. Quisenberry and A. O. Nier, Phys. Rev. **102** (1956) 1076 (M2)
19) K. S. Quisenberry, T. T. Scolman and A. O. Nier, Phys. Rev. **104** (1956) 461 (M3)
20) K. S. Quisenberry, C. F. Giese and J. L. Benson, Phys. Rev. **107** (1957) 1664 (M4)
21) C. F. Giese and J. L. Benson, Phys. Rev. **110** (1958) 712 (M5)
22) J. L. Benson, R. A. Damerov and R. R. Ries, Phys. Rev. **113** (1959) 1105 (M6)
23) M. E. Kettner, Phys. Rev. **102** (1956) 1065
24) H. Liebl and H. Ewald, Z. Naturforsch. **11a** (1956) 406
25) G. v. Schierstedt, H. Ewald, H. Liebl and G. Sauermann, Z. Naturforsch. **11a** (1956) 216
26) R. A. Demirkhanov, T. E. Gutkin, V. V. Dorokhov and A. D. Rudenko, Atomn. Energ. **2** (1956) 21; J. Nucl. Energy **3** (1956) 251
27) E. R. Cohen, J. W. M. DuMond, T. W. Layton and J. S. Rollet, Rev. Mod. Phys. **27** (1955) 363; Phys. Rev. Letters **1** (1958) 291; private communication of E. R. Cohen
28) A. H. Wapstra, Nuclear Physics **18** (1960) 587
29) P. M. Endt and C. M. Braams, Rev. Mod. Phys. **29** (1957) 683
30) J. B. Marion, Technical Report 184, University of Maryland (1960); Rev. Mod. Phys. (to be submitted)
31) J. Mattauch, Z. Naturforsch. **13a** (1958) 572
32) F. Everling, L. A. König, J. H. E. Mattauch and A. H. Wapstra, to be published in 1960 Nuclear Data Tables, U. S. Government Printing Office, Washington 25, D.C.
33) F. H. Nussbaum, A. H. Wapstra, W. A. Bruil, M. J. Sterk, G. J. Nijgh and N. Grobben, Phys. Rev. **101** (1956) 905; and unpublished work

TABLE 1a

Primary mass-spectroscopic doublets (see subsect. 4.1)

Doublet	Measured value (μMU($^{16}O = 16$)		Lab.	Adopted value (μu)		Adjusted value (μu)		$\frac{v}{\sigma}$
$^{1}H_2 - {}^{2}D$	1 547.6	± 0.5	M1	1 547.1	± 1.3	1 548.25	± 0.10	-0.8607
"	1 547.80	0.40	"	1 547.3	1.1			-0.8871
"	1 549.67	0.16	B3	1 549.2	0.6			1.6241
"	1 548.59	0.10	B5	1 548.10	0.24			-0.6371
"	1 549.27	0.18	B6	1 548.8	0.5			0.9936
$^{2}D_6 - {}^{12}C$	84 638.39	0.77	B5	84 611.5	1.8	84 613.2	0.7	-0.9208
$^{2}D_2 - {}^{1}H^{3}T$	4 330.60	0.07	B6	4 329.22	0.21	4 329.76	0.16	-2.5956
$^{1}H^{3}T - {}^{4}He$	21 280.7	0.8	"	21 273.9	2.4	21 271.01	0.41	1.2329
$^{1}H^{2}D - {}^{3}He$	5 899.91	0.07	"	5 898.03	0.21	5 897.48	0.16	2.6890
$^{2}D_2 - {}^{4}He$	25 607.40	0.30	M6	25 599.3	0.8	25 600.78	0.38	-1.9059
"	25 612.27	0.45	B3	25 604.1	1.6			2.0830
"	25 611.6	0.6	B6	25 603.5	1.8			1.5097
$^{10}B^{1}H - {}^{11}B$	11 462.62	0.32	B3	11 459.0	1.1	11 459.1	0.7	-0.0865
$^{10}B^{11}B^{2}D_4 - {}^{12}C_2{}^{1}H_5$	39 541.93	0.66	"	39 529.4	2.4	39 526.7	0.9	1.1259
$^{11}B^{1}H - {}^{12}C$	17 136.35	0.31	"	17 130.9	1.1	17 130.31	0.44	0.5364
"	17 135.53	0.21	"	17 130.1	0.8			-0.2989
$^{11}B^{2}D - {}^{12}C^{1}H$	15 586.95	0.35	"	15 582.0	1.3	15 582.06	0.43	-0.0519
$^{11}B_2{}^{2}D_5 - {}^{16}O_2$	99 324.80	0.78	"	99 293.2	2.8	99 291.3	0.9	0.7068
$^{11}B_4{}^{1}H_4 - {}^{32}S^{16}O$	101 566.6	2.0	"	101 534	7	101 532.5	2.0	0.2493
$^{13}C^{1}H_3 - {}^{16}O$	31 925.3	0.7	M2	31 915.2	1.9	31 915.0	0.7	0.0841
$^{12}C^{1}H_2 - {}^{14}N$	12 580.30	0.40	M1	12 576.3	1.1	12 576.07	0.13	0.2234
"	12 580.4	0.5	"	12 576.4	1.3			0.2542
"	12 579.30	0.30	"	12 575.3	0.8			-0.9608
"	12 579.51	0.15	B3	12 575.5	0.5			-1.0304
"	12 580.43	0.20	B5	12 576.43	0.47			0.7801
"	12 579.88	0.27	"	12 .75.9	0.6			-0.2890
$^{12}C^{2}D - {}^{14}N$	11 033.04	0.42	"	11 029.5	1.0	11 027.82	0.13	1.7390
"	11 031.90	0.23	"	11 028.4	0.5			1.0664
"	11 031.59	0.15	"	11 028.08	0.35			0.7556
"	11 031.69	0.18	"	11 028.18	0.42			0.8661
$^{12}C^{1}H_4 - {}^{2}D^{14}N$	14 129.09	0.20	B5	14 124.60	0.47	14 124.31	0.19	0.6105
$^{14}N^{1}H_2 - {}^{16}O$	23 816.4	0.5	M1	23 808.8	1.3	23 809.87	0.19	-0.7887
"	23 815.9	0.6	"	23 808.3	1.6			-0.9719
$^{14}N^{2}D - {}^{16}O$	22 268.89	0.25	B5	22 261.8	0.6	22 261.63	0.17	0.3155
"	22 268.64	0.35	"	22 261.6	0.8			-0.0786
$^{14}N_2 - {}^{12}C^{16}O$	11 235.5	0.6	M2	11 231.9	1.6	11 233.81	0.24	-1.1837
"	11 236.32	0.28	B3	11 232.7	1.0			-1.0585
"	11 237.81	0.22	B5	11 234.2	0.5			0.8297
"	11 237.88	0.32	"	11 234.3	0.8			0.6635
$^{12}C_3{}^{1}H_8 - {}^{14}N_2{}^{16}O$	61 553.2	2.0	B3	61 534	7	61 538.07	0.41	-0.6193
"	61 557.42	0.67	B5	61 537.9	1.6			-0.1362

TABLE 1a (Continued)

Doublet	Measured value (μMU(^{16}O = 16)		Lab.	Adopted value (μu)		Adjusted value (μu)		$\frac{v}{\sigma}$
$^{12}C_3{}^2D_4 - {}^{14}N_2{}^{16}O$	55 360.83	± 0.43	B5	55 343.2	± 1.0	55 345.08	± 0.37	-1.8264
$^{15}N{}^1H - {}^{16}O$	13 023.40	0.40	M2	13 019.3	1.1	13 018.4	0.9	0.8561
$^{12}C{}^1H_4 - {}^{16}O$	36 396.0	0.5	M4	36 384.4	1.3	36 385.94	0.21	-1.1386
"	36 395.8	1.2	"	36 384.2	3.2			-0.5373
"	36 396.6	0.8	"	36 385.0	2.1			-0.4284
"	36 396.36	0.36	B3	36 384.8	1.3			-0.8905
"	36 397.20	0.43	"	36 385.6	1.5			-0.1999
"	36 395.12	0.48	"	36 383.6	1.7			-1.3895
"	36 397.50	0.35	B5	36 385.9	0.8			-0.0094
"	36 395.48	0.42	"	36 383.9	1.0			-2.0544
"	36 397.50	0.26	"	36 385.9	0.6			-0.0126
"	36 398.13	0.47	"	36 386.6	1.1			0.5634
$^{12}C^2D_2 - {}^{16}O$	33 300.36	0.23	"	33 289.8	0.5	33 289.45	0.17	0.6137
"	33 299.25	0.45	"	33 288.7	1.1			-0.7360
"	33 299.37	0.23	"	33 288.8	0.5			-1.2179
$^{12}C^2D_4 - {}^1H_4{}^{16}O$	30 203.38	0.36	"	30 193.8	0.8	30 192.95	0.31	0.9824
$^{12}C_4 - {}^{16}O_3$	15 262.4	1.6	M4	15 257.5	4.2	15 255.2	0.8	0.5596
$^{16}O{}^1H - {}^{17}O$	3 607.7	0.5	M2	3 606.6	1.3	3 606.7	0.9	-0.1375
$^1H_2{}^{16}O - {}^{18}O$	11 403.3	2.1	"	11 400	6	11 405.55	0.31	-1.0566
$^{12}C^2D_4 - {}^1H_2{}^{18}O$	41 612.00	0.22	B5	41 598.8	0.5	41 598.50	0.25	0.5312
$^2D_2{}^{16}O - {}^1H_2{}^{18}O$	8 310.20	0.40	M1	8 307.6	1.1	8 309.06	0.22	-1.4132
"	8 311.65	0.14	B5	8 309.01	0.33			-0.1431
$^{14}N^2D_3 - {}^1H_2{}^{18}O$	30 581.31	0.27	B5	30 571.6	0.6	30 570.68	0.25	1.4314
$^2D_4{}^{18}O_2 - {}^{12}C{}^{16}O_2$	64 919.24	0.62	B5	64 898.6	1.5	64 898.6	0.7	0.0394
$^{12}C_4{}^1H_4 - {}^{16}O{}^{18}O_2$	38 073.4	1.6	M1	38 061.3	4.2	38 066.3	0.7	-1.1756
$^1H^2D{}^{16}O - {}^{19}F$	18 438.0	1.4	M2	18 432.1	3.7	18 437.8	0.7	-1.5243
$^2D_2{}^{16}O - {}^1H{}^{19}F$	16 894.4	0.5	"	16 889.0	1.3	16 889.5	0.7	-0.3867
$^{10}B^{19}F_2 - {}^{32}S{}^{16}O$	42 773.0	1.7	"	42 759.4	4.5	42 759.4	1.7	0.0075
$^{12}C_4{}^1H_9 - {}^{19}F_3$	75 246.2	2.0	"	75 222	5	75 213.3	2.1	1.6985
$^{12}C_4{}^1H_4{}^{16}O - {}^{11}B{}^{19}F_3$	21 705.2	1.3	"	21 698.3	3.4	21 697.0	2.1	0.3657
$^{12}C^2D_4 - {}^{20}Ne$	63 989.35	0.27	B5	63 969.0	0.6	63 968.35	0.33	1.0475
$^2D_2{}^{16}O - {}^{20}Ne$	30 687.2	0.7	M2	30 677.4	1.9	30 678.90	0.33	-0.7859
"	30 688.57	0.29	B5	30 678.8	0.7			-0.1277
$^{14}N^2D_3 - {}^{20}Ne$	52 957.08	0.27	"	52 940.2	0.6	52 940.53	0.33	-0.4440
$^1H_2{}^{18}O - {}^{20}Ne$	22 377.0	0.6	M2	22 369.9	1.6	22 369.85	0.36	0.0252
"	22 377.11	0.39	B5	22 370.0	0.9			0.1637
$^1H^2D{}^{18}O - {}^{21}Ne$	27 248.2	0.7	M2	27 239.5	1.9	27 238.0	1.6	0.8312
$^2D_2{}^{18}O - {}^{22}Ne$	35 991.20	0.14	B5	35 979.76	0.33	35 979.74	0.31	0.0645
$^{12}C{}^{16}O_2 - {}^{22}Ne_2$	7 061.4	1.2	M2	7 059.2	3.2	7 060.9	0.9	-0.5585
"	7 063.42	0.98	B5	7 061.2	2.3			0.1064
$^{12}C{}^{16}O{}^{18}O - {}^{23}Na_2$	14 518.4	4.0	M2	14 514	11	14 529.6	3.2	-1.4926
$^{12}C_2 - {}^{24}Mg$	14 962.1	1.1	"	14 957.3	2.9	14 955.4	1.9	0.6649

TABLE 1a (Continued)

Doublet	Measured value (μMU($^{16}O = 16$)	Lab.	Adopted value (μu)	Adjusted value (μu)	$\frac{v}{\sigma}$
$^{12}C_2{}^1H - {}^{25}Mg$	21 994.4 ± 1.0	M2	21 987.4 ± 2.6	21 985.5 ± 2.0	0.7296
$^{12}C_2{}^1H_2 - {}^{26}Mg$	33 067.6 1.0	"	33 057.1 2.6	33 059.5 2.4	-0.9117
$^{12}C_2{}^1H_3 - {}^{27}Al$	41 954.8 2.3	"	41 941 6	41 940.8 2.1	0.1136
$^{12}C_6{}^1H_{13} - {}^{28}Si{}^{19}F_3$	129 625.0 4.0	"	129 584 11	129 587.1 3.6	-0.3080
$^{12}C_6{}^1H_{14} - {}^{29}Si{}^{19}F_3$	137 889 7	"	137 845 19	137 848.6 4.0	-0.1833
$^{12}C_4{}^1H_7{}^{16}O_2 - {}^{30}Si{}^{19}F_3$	75 659.0 3.6	"	75 635 10	75 632.0 4.5	0.3088
$^{16}O_2 - {}^{31}P{}^1H$	8 242.3 0.6	M5	8 239.7 1.6	8 241.2 1.5	-0.9785
$^{12}C{}^1H_4{}^{16}O - {}^{32}S$	54 163.0 2.8	B3	54 146 10	54 142.1 1.0	0.3716
$^{16}O_2 - {}^{32}S$	17 759.9 0.9	M1	17 754.3 2.4	17 756.1 1.0	-0.7835
"	17 762.3 1.1	M5	17 756.7 2.9		0.1828
"	17 762.11 0.55	B3	17 756.5 2.0		0.1740
"	17 762.6 2.1	"	17 757 8		0.1107
$^{14}N_2{}^{16}O - {}^{12}C{}^{32}S$	28 998.2 2.5	"	28 989 9	28 989.9 1.0	-0.1060
$^{12}C_4 - {}^{32}S{}^{16}O$	33 026.9 1.3	M1	33 016.4 3.4	33 011.3 1.2	1.4824
$^{12}C_4{}^{16}O - {}^{32}S_2$	50 785.2 1.8	"	50 769.1 4.8	50 767.4 2.0	0.3433
$^{12}C_4{}^1H - {}^{33}S{}^{16}O$	41 460.2 1.5	M5	41 447.0 4.0	41 449.8 3.0	-0.6914
$^{12}C_4{}^1H_2 - {}^{34}S{}^{16}O$	52 889.1 1.5	"	52 872.3 4.0	52 871.0 3.1	0.3176
$^{12}C_5{}^1H_{10} - {}^{35}Cl_2$	140 585.0 3.4	"	140 540 9	140 543 6	-0.3191
$^{12}C_3{}^1H - {}^{37}Cl$	41 934.6 1.2	"	41 921.3 3.2	41 929.3 2.2	-2.5191
"	41 951.89 0.98	B3	41 938.6 3.5		2.6462
$^1H{}^{35}Cl - {}^{36}A$	9 134.6 0.9	M5	9 131.7 2.4	9 131.6 2.2	0.0291
$^{12}C_3{}^1H_4 - {}^{40}A$	68 934.6 1.1	"	68 912.7 2.9	68 917.1 0.7	-1.4996
"	68 934.4 1.3	M1	68 912.5 3.4		-1.3270
"	68 939.45 0.38	B5	68 917.5 0.9		0.5389
$^{12}C_2{}^2D_8 - {}^{40}A$	150 481.76 0.64	"	150 433.9 1.5	150 433.7 0.6	0.1426
$^{14}N_2{}^2D_6 - {}^{40}A$	128 421.06 0.96	"	128 380.2 2.3	128 378.1 0.7	0.9582
$^2D_4{}^{16}O_2 - {}^{40}A$	83 878.0 2.6	M1	83 851 7	83 854.8 0.7	-0.5067
"	83 879.88 0.72	B5	83 853.2 1.7		-0.9509
$^1H_4{}^{18}O_2 - {}^{40}A$	67 258.32 0.48	"	67 236.9 1.1	67 236.7 0.6	0.1997
$^{20}Ne_2 - {}^{40}A$	22 504.86 0.74	"	22 497.7 1.7	22 497.0 0.8	0.3940
$^{12}C_3{}^1H_3 - {}^{39}K$	59 781.9 1.5	M5	59 762.9 4.0	59 761.7 3.0	0.3009
$^{12}C_3{}^1H_4 - {}^{40}K$	67 317.8 2.1	"	67 296 6	67 293.0 3.6	0.6154
$^{12}C_3{}^1H_5 - {}^{41}K$	77 316.7 1.9	"	77 292 5	77 291.0 4.6	0.2287
$^{12}C_3{}^1H_4 - {}^{40}Ca$	68 734.1 1.5	"	68 712.3 4.0	68 711.7 3.7	0.1348
$^{12}C_3{}^1H_6 - {}^{42}Ca$	88 350.0 2.2	"	88 322 6	88 323.7 4.4	-0.2996
$^{12}C_3{}^1H_7 - {}^{43}Ca$	96 018.6 2.6	"	95 988 7	95 996.6 4.8	-1.2328
$^{12}C{}^{16}O_2 - {}^{44}Ca$	34 344.2 2.4	"	34 333 6	34 340.2 4.8	-1.0891
$^{12}C{}^{32}S{}^1H - {}^{45}Sc$	23 987.3 1.8	"	23 979.7 4.8	23 980.1 4.1	-0.0844
$^{12}C{}^{32}S{}^1H_2 - {}^{46}Ti$	35 102.6 1.4	"	35 091.4 3.7	35 090.8 3.5	0.1700
$^{12}C{}^{32}S{}^1H_3 - {}^{47}Ti$	43 803.5 3.0	"	43 790 9	43 791 8	-0.2230
$^{32}S{}^{16}O - {}^{48}Ti$	19 047.6 1.2	"	19 041.5 4.5	19 040.9 3.6	0.1450
$^{12}C_4{}^1H - {}^{49}Ti$	59 978.1 1.5	"	59 959.0 4.0	59 958.6 3.6	0.1177

TABLE 1a (Continued)

Doublet	Measured value (μMU (^{16}O=16))	Lab.	Adopted value (μu)	Adjusted value (μu)	$\frac{v}{\sigma}$
$^{12}C_4{}^1H_3 - {}^{51}V$	79 522.3 ± 1.8	M5	79 497.0 ± 4.8	79 497.8 ± 4.2	-0.1595
$^{12}C_4{}^1H_2 - {}^{50}Cr$	69 621.8 1.8	"	69 599.7 4.8	69 599.7 4.5	-0.0132
$^{12}C_4{}^1H_4 - {}^{52}Cr$	90 816.5 1.7	"	90 787.6 4.6	90 787.1 3.6	0.1099
$^{12}C_4{}^1H_5 - {}^{53}Cr$	98 506.2 2.1	"	98 475 6	98 469.3 3.7	-0.0100
$^{12}C_4{}^1H_6 - {}^{54}Cr$	108 109.9 2.3	"	108 076 6	108 071.9 4.8	0.5775
$^{12}C_4{}^1H_7 - {}^{55}Mn$	116 754.7 2.2	"	116 718 6	116 723.0 4.1	-0.8914
$^{12}C_4{}^1H_6 - {}^{54}Fe$	107 374 4	M3	107 340 11	107 330 6	0.8982
$^{12}C_4{}^1H_8 - {}^{56}Fe$	127 698 4	"	127 657 11	127 670 6	-1.1687
$^{12}C_4{}^1H_9 - {}^{57}Fe$	135 055 7	"	135 012 19	135 033 6	-1.1448
$^{12}C_2{}^1H_3{}^{16}O_2 - {}^{59}Co$	80 146.6 2.3	"	80 121 6	80 116.4 4.6	0.7341
$^{12}C_4{}^1H_{10} - {}^{58}Ni$	142 941 7	"	142 896 19	142 910 6	-0.7825
$^{12}C_2{}^1H_4{}^{16}O_2 - {}^{60}Ni$	90 387 6	"	90 358 16	90 348 6	0.6299
$^{12}C_5{}^1H_2 - {}^{62}Ni$	87 339 6	"	87 311 16	87 305 7	0.3792
$^{12}C_5{}^1H_3 - {}^{63}Cu$	93 909 7	"	93 879 19	93 882 6	-0.1371
$^{12}C_5{}^1H_5 - {}^{65}Cu$	111 377 4	"	111 342 11	111 340 6	0.1616
$^{16}O_4 - {}^{64}Zn$	50 526.6 5.2	"	50 511 14	50 515 5	-0.2872
$^{32}S{}^{16}O_2 - {}^{64}Zn$	32 768.7 3.2	M3,1	32 758 9	32 758 5	-0.0192
$^{12}C_5{}^1H_6 - {}^{66}Zn$	120 935 6	M3	120 897 16	120 903 10	-0.4252
$^{12}C_5{}^1H_7 - {}^{67}Zn$	127 675 7	"	127 634 19	127 627 11	0.3749
$^{12}C_5{}^1H_8 - {}^{68}Zn$	137 781 4	"	137 737 11	137 737 9	0.0515

In the above table the first column denotes the mass-spectroscopic doublet. The second one gives the measured value and its error in μMU(^{16}O = 16). As to the indication of the laboratory in the third column the following abbreviations are used (see sect. 5 and refs. [15–22]):

B3, B5, B6: Brookhaven National Laboratory, Upton, N.Y.
M1—M5: University of Minnesota, Minneapolis, Minn.

The fourth column gives in μu the input datum and its error multiplied with the consistency factor determined by the pre-adjustments (see sects. 2 and 5). In the fifth column the adjusted values of the mass-spectroscopic doublets and their errors are to be found, both again expressed in μu. The last column gives the ratio of the difference v between the two preceding columns divided by the error σ in the adopted input value (fourth column).

TABLE 1b

Secondary mass-spectroscopic doublets (see subsect. 4.1)

Doublet	Measured value (μMU(^{16}O = 16))	Lab.	Adopted value (μu)
$^{12}C_4\,^1H_4 - {}^{36}S\,^{16}O$	69 317.5 ± 3.5	M5	69 295 ± 9
$^1H\,^{37}Cl - {}^{38}A$	11 000.1 1.0	"	10 996.6 2.7
$^{12}C\,^{32}S\,^1H_2 - {}^{46}Ca$	34 046.2 3.9	"	34 035 10
$^{12}C_4 - {}^{48}Ca$	47 496.4 5.5	"	47 481 15
$^{12}C_4\,^1H_2 - {}^{50}Ti$	70 883.9 1.8	"	70 861.4 4.8
$^{12}C_4\,^1H_2 - {}^{50}V$	68 507.6 1.5	"	68 485.8 4.0
$^{12}C_5\,^1H_{10} - {}^{70}Zn$	152 953 6	M3	152 904 16

In the above table the first column denotes the mass-spectroscopic doublet. The second one gives the measured value and its error in μMU(^{16}O = 16). As to the indication of the laboratory in the third column see text below table 1a. The fourth column gives in μu the input datum and its error multiplied with the consistency factor. (See sect. 5).

TABLE 1c

Rejected doublets used in the pre-adjustment (see sect. 9)

Doublet	Measured value (μMU(^{16}O=16))	Lab.	Adopted value (μu)	Adjusted value (μu)	$\frac{v}{\sigma}$
$^{12}C\,^1H_3 - {}^{15}N$	23 365.2 ± 0.9	M2	23 357.8 ± 2.4	23 367.6 ± 0.9	-4.1139
$^{12}C\,^1H_4 - {}^{16}O$	36 393.1 0.9	M1	36 381.5 2.4	36 385.94 0.21	-1.8475
"	36 393.4 0.8	"	36 381.8 2.1		-1.9370
"	36 393.5 0.8	"	36 381.9 2.1		-1.8898
$^{12}C_3 - {}^{36}A$	32 472.9 2.0	"	32 463 5	32 451.9 3.4	2.0145
$^1H_4\,^{16}O_2 - {}^{36}A$	53 587.4 1.2	"	53 570.4 3.2	53 582.7 3.4	-3.8664

In the above table the first column denotes the mass-spectroscopic doublet. The second one gives the measured value and its error in μMU(^{16}O = 16). As to the indication of the laboratory in the third column see text below table 1a. The fourth column gives in μu the input datum and its error multiplied with the consistency factor. (See sect. 5). In the fifth column the adjusted values following from the final adjustment are to be found, both again expressed in μu. The last column gives the ratio of the difference v between the two preceding columns divided by the error σ in the adopted input value (fourth column).

TABLE 2a

Primary reaction and decay energies. (See subsect. 4.1)

Nuclear reaction or decay		Measured value (keV)		Ref.	Lab.	Adjusted value (keV)		$\frac{v}{\sigma}$
$^1n(\beta^-)^1H$		785.0 ±	1.5	a		782.61 ±	0.40	1.5920
$^1H(n,\gamma)^2D$		2 230	5	V_4		2 224.71	0.40	1.0573
$^2D\ (\gamma,n)^1H$		-2 226	3	V_4		-2 224.71	0.40	-0.4289
"		-2 227	3	V_4				-0.7622
$^2D(n,\gamma)^3T$		6 251	8	V_4	CR	6 257.63	0.42	-0.8290
$^2D(d,n)^3He$	*	3 265	9	V_4	C	3 268.44	0.42	-0.7755
"	*	3 271	11	V_7	W			0.2746
$^2D(d,p)^3T$	*	4 034	6	V_4	M_o	4 032.92	0.15	0.0439
"	*	4 036	12	V_4	C			0.2998
$^3T(\beta^-)^3He$		17.9	0.3	b		18.13	0.08	-0.7754
"		18.9	0.5	K_4				1.5348
"		18.3	0.3	K_4				0.5579
"		18.0	0.1	K_4				-1.3262
"		17.6	0.4	K_4				-1.3316
$^3T(p,n)^3He$		- 763.7	1.0	V_4		- 764.48	0.40	0.7794
"		- 764.7	1.0	V_4				-0.2206
$^6Li(p,\alpha)^3He$	*	4 025	6	V_4	M_o	4 021.9	1.0	0.5941
"	*	4 017	12	V_4	C			-0.8142
"	*	4 024	5	V_4	W			0.3795
"	*	4 023	3	V_4	B			0.0769
$^6Li(d,p)^7Li$	*	5 024	7	V_4	M_o	5 027.9	1.2	-1.1994
"	*	5 028	3	V_4	B			-0.5763
$^6Li(d,\alpha)^4He$	*	22 396	12	V_4	B	22 374.4	1.1	2.2882
"	*	22 375	14	V_4	R			-0.5390
$^7Li(p,n)^7Be$		-1 645.4	1.4			-1 643.3	1.1	-1.5045
$^7Li(p,\alpha)^4He$	*	17 357	14	V_4	M_o	17 346.5	1.2	0.7752
"	*	17 359	11	V_4	C			1.2897
"	*	17 352	9	V_4	B			0.2800
"	*	17 344	13	V_4	R			-0.8318
$^8Be\ (\alpha)^4He$	*	93.9	0.8	V_7	C	94.18	0.40	-0.6207
"	*	94.5	1.4	V_4	W			0.3597
$^9Be(\gamma,n)^8Be$		-1 666	2	V_4		-1 665.4	0.7	-0.2872
"		-1 662	3	V_4				1.1419
"		-1 664	4	V_7				0.3564
$^9Be(p,pn)^8Be$	*	-1 666	5	V_7	M_o	-1 665.4	0.7	-0.0644
$^9Be(n,\gamma)^{10}Be$		6 816	6	V_4	CR	6 814.3	2.1	0.2812

The value for the ^{7}Li (p, n)^{7}Be reaction is an average value (see sect. 6).

TABLE 2a (Continued)

Nuclear reaction or decay		Measured value (keV)		Ref.	Lab.	Adjusted value (keV)		$\frac{v}{\sigma}$
$^{9}Be(p,d)^{8}Be$	*	563	± 4	V_4	M_o	559.3	± 0.6	1.4935
"	*	558	3	V_4	C			-0.7866
"	*	560	3	V_4	B			0.3246
"	*	558	2	V_4	W			-1.1799
"	*	558	5	V_4				-0.2831
$^{9}Be(p,\alpha)^{6}Li$	*	2 121	7	V_4	C	2 124.7	0.9	-0.9911
"	*	2 124	4	V_4	W			-0.4844
"	*	2 126	3	V_4	B			0.4654
"	*	2 130	10	V_4				0.4837
$^{9}Be(d,p)^{10}Be$	*	4 590	8	V_4	M_o	4 589.6	2.1	-0.1354
"	*	4 591	9	V_7	M_o			0.0648
"	*	4 591	8	V_4	R			0.0729
$^{9}Be(d,\alpha)^{7}Li$	*	7 157	8	V_4	M_o	7 152.6	1.1	0.5835
"	*	7 160	10	V_4	C			0.9668
"	*	7 159	9	V_4	W			0.8891
"	*	7 153	4	V_4	B			-0.4998
$^{10}Be(\beta^-)^{10}B$		555	5	K_4		555.5	2.1	-0.0959
"		560	5	K_4				0.9041
"		553	15	K_4				-0.1653
"		545	10	c				-1.0479
$^{10}B(n,\alpha)^{7}Li$	*	2 788	4	d	R	2 790.1	1.1	-1.1393
$^{10}B(p,\tau)^{8}Be$	*	- 536	3	V_4	W	- 534.7	0.9	-0.6322
$^{10}B(p,\alpha)^{7}Be$	*	1 153	4	V_4	M_o	1 146.8	1.0	2.4735
"	*	1 148	6	V_4	C			0.2600
"	*	1 147	2.5	V_4	W			-0.0428
$^{10}B(d,p)^{11}B$	*	9 244	11	V_4	M_o	9 231.4	0.7	1.5961
"	*	9 227	6	V_7	B			-1.7965
$^{10}B(d,\alpha)^{8}Be$	*	17 829	10	V_7	B	17 817.7	1.1	1.1997
$^{10}B(\alpha,p)^{13}C$	*	4 068	12	V_7	M_o	4 063.9	1.0	0.4360
$^{10}B(\alpha,d)^{12}C$	*	1 341	2	V_7	W	1 341.6	0.7	-0.7663
$^{11}B(p,\alpha)^{8}Be$	*	8 575	10	V_4	M_o	8 586.4	1.1	-2.2227
"	*	8 585	14	V_4	C			-0.3971
"	*	8 589	5	V_4	B			0.2216
$^{11}B(d,p)^{12}B$	*	1 137	5	V_4	M_o	1 144.9	1.0	-2.7077
"	*	1 140	8	V_4	M_o			-1.0672
$^{11}B(d,\alpha)^{9}Be$	*	8 026	7	V_4	M_o	8 027.1	1.1	-0.6951
"	*	8 023	10	V_7	M_1			-0.5918
"	*	8 029	5	V_7	B			0.0269

TABLE 2a (Continued)

Nuclear reaction or decay		Measured value (keV)		Ref.	Lab.	Adjusted value (keV)		$\frac{v}{\sigma}$
$^{12}C(n,\gamma)^{13}C$		4 949	± 6	V_4	CR	4 947.0	± 0.8	0.3281
$^{12}C(d,n)^{13}N$	*	- 281	3	V_4	R	- 281.4	1.3	0.2841
$^{12}C(d,p)^{13}C$	*	2 719	5	V_4	M_o	2 722.3	0.7	-1.3139
"	*	2 720	3	V_7	B			-1.6342
"	*	2 722	4	V_4	R			-0.3922
"	*	2 732	6	V_4	R			2.5166
"	*	2 722	4	V_4				-0.2353
$^{13}C(p,n)^{13}N$		-3 003	3	V_4		-3 003.8	1.3	0.2549
$^{13}C(d,p)^{14}C$	*	5 948	11	V_7	M_o	5 951.3	0.8	-0.7030
"	*	5 954	8	V_4	M_o			0.2835
"	*	5 948	4	V_4	C			-1.9333
"	*	5 958	10	V_7	N			0.5359
$^{13}C(d,t)^{12}C$	*	1 311	6	V_4	M_o	1 310.6	0.7	0.0276
"	*	1 312	3	V_4	C			0.6108
$^{13}C(d,\alpha)^{11}B$	*	5 165	10	V_4	M_o	5 167.4	0.8	-0.6011
"	*	5 171	6	V_4	C			0.6650
"	*	5 166	5	V_4	R			-0.8688
$^{14}C(\beta^-)^{14}N$		155	2	K_4		156.07	0.35	-0.5333
"		155	1	K_4				-1.0666
"		155	1	K_4				-1.0666
"		157	2	L_7				0.4667
"		155	1	L_7				-1.0666
"		155	1	L_7				-1.0666
"		156	2	L_7				-0.0333
"		158	1	e				1.9334
$^{14}C(p,n)^{14}N$		- 626.4	0.5	V_7	W	- 626.55	0.39	0.2909
$^{14}C(d,\alpha)^{12}B$	*	362	1.5	V_7	W	361.0	0.9	1.0124
$^{14}C(\alpha,n)^{17}O$	*	-1 820	2	V_7	W	-1 819.4	0.9	-0.1488
$^{13}N(\beta^+)^{13}C$		2 220	6	K_4		2 221.2	1.3	-0.1921
"		2 240	4	K_4				4.7118
"		2 224	5	K_4				0.5694
"		2 212	3	f				-3.0509
$^{14}N(n,\gamma)^{15}N$		10 832	8	V_4	CR	10 834.3	0.9	-0.2847
$^{14}N(d,p)^{15}N$	*	8 623	9	V_4	M_o	8 609.6	0.8	2.1232
"	*	8 626	11	V_4	C			2.1918
$^{15}N(p,\alpha)^{12}C$	*	4 965	7	V_4	M_o	4 964.3	0.9	-0.1010
"	*	4 968	6	V_4	C			0.7156
"	*	4 962	4	V_4	B			-1.4268
$^{15}N(d,p)^{16}N$	*	286	12	V_7	C	275	6	1.4792
$^{15}N(d,\alpha)^{13}C$	*	7 688	9	V_4	M_o	7 686.6	1.1	-0.0676

TABLE 2a (Continued)

Nuclear reaction or decay		Measured value (keV)		Ref.	Lab.	Adjusted value (keV)		$\frac{v}{\sigma}$
$^{16}O(d,n)^{17}F$	*	-1 626	± 4	V_7	R	-1 627.0	± 2.2	0.5530
$^{16}O(d,p)^{17}O$	*	1 919	5	V_4	M_o	1 917.4	0.8	0.4003
"	*	1 917	10	V_7	M_o			-0.1332
"	*	1 918	8	V_4	R			0.0418
$^{16}O(d,\alpha)^{14}N$	*	3 115	6	V_4	M_o	3 110.22	0.38	1.1301
"	*	3 113	3.5	V_4	W			0.9849
"	*	3 119	5	V_4	R			2.6896
$^{17}O(d,p)^{18}O$	*	5 827	10	V_7	N	5 822.0	0.9	0.3631
$^{17}O(d,\alpha)^{15}N$	*	9 816	12	V_7	N	9 802.4	1.2	0.9441
$^{18}O(p,\alpha)^{15}N$	*	3 971	9	V_4	N	3 980.4	0.9	-1.1442
$^{18}O(d,\alpha)^{16}N$	*	4 240	9	V_7	N	4 256	6	-1.8496
$^{17}F(\beta^+)^{17}O$		2 770	6	L_7		2 761.7	2.4	1.3829
$^{19}F(n,\gamma)^{20}F$		6 600	11	g	CR	6 598.8	3.7	0.1128
$^{19}F(p,\alpha)^{16}O$	*	8 118	10	V_7	M_1	8 114.0	0.7	0.2141
"	*	8 126	9	V_4	M_o			1.8783
"	*	8 118	10	h	C			0.3570
"	*	8 118	10	h	R			0.3570
$^{19}F(d,p)^{20}F$	*	4 377	7	V_4	M_o	4 374.0	3.7	0.4650
$^{19}F(\alpha,p)^{22}Ne$	*	1 675	11	V_7	M_o	1 675.2	0.8	-0.0848
$^{20}F(\beta^-)^{20}Ne$		7 046	14	K_4		7 027.8	3.8	1.2978
"		7 037	18	K_4				0.5094
$^{20}Ne(d,p)^{21}Ne$	*	4 533	7	V_4	M_o	4 534.4	1.5	-0.5797
"	*	4 531	9	V_4	N			-0.4926
$^{21}Ne(d,p)^{22}Ne$	*	8 150	11	V_4	C	8 142.4	1.5	0.8666
$^{22}Na(\beta^+)^{22}Ne$		2 840	5	K_4		2 841.5	4.6	-0.3098
$^{23}Na(p,\alpha)^{20}Ne$	*	2 372	8	V_7	M_1	2 378.7	1.5	-0.9045
"	*	2 374	8	V_4	M_o			-1.0913
"	*	2 379	3	V_4	W			-0.1320
$^{23}Na(d,p)^{24}Na$	*	4 736	7	V_4	M_o	4 734.2	2.6	0.1666
"	*	4 732	8	V_4	C			-0.6876
$^{23}Na(d,\alpha)^{21}Ne$	*	6 909	10	V_4	M_o	6 913.1	2.0	-0.9454
$^{24}Na(\beta^-)^{24}Mg$		5 512	6	K_4		5 516.3	2.7	-0.7109
"		5 522	15	L_7				0.3823
"		5 516	5	K_4				-0.0531
$^{24}Mg(n,\gamma)^{25}Mg$		7 329	9	g	CR	7 330.7	2.1	-0.1898
"		7 334	7	V_4	CR			0.4703
$^{24}Mg(d,p)^{25}Mg$	*	5 102	7	V_4	M_o	5 106.0	2.1	-1.2295
$^{24}Mg(d,\alpha)^{22}Na$	*	1 955	12	V_7	M_1	1 963.5	4.9	-0.7436
$^{25}Mg(n,\gamma)^{26}Mg$		11 113	12	g	CR	11 097.4	2.7	1.2987
$^{25}Mg\ (d,p)^{26}Mg$	*	8 888	12	V_4	M_o	8 872.7	2.7	1.8427

TABLE 2a (Continued)

Nuclear reaction or decay		Measured value (keV)		Ref.	Lab.	Adjusted value (keV)		$\frac{v}{\sigma}$
$^{25}Mg(d,\alpha)^{23}Na$	*	7 026	± 13	V_4	M_o	7 047.0 ±	2.4	-2.9042
$^{26}Mg(n,\gamma)^{27}Mg$		6 437	7	g	CR	6 437.1	3.1	-0.0082
$^{26}Mg(p,n)^{26}Al$		-4 779	11	i		-4 796.7	4.9	1.6054
$^{26}Mg(d,p)^{27}Mg$	*	4 211	6	V_4	M_o	4 212.3	3.1	-0.6412
$^{27}Mg(\beta^-)^{27}Al$		2 600	10	i		2 617.9	4.0	-1.7935
$^{26}Al(\beta^+)\ ^{26}Mg$		4 010	12	j		4 014.0	4.9	-0.3372
$^{27}Al(n,\gamma)^{28}Al$		7 724	6	V_4	CR	7 723.7	3.4	0.0498
$^{27}Al(p,\alpha)^{24}Mg$	*	1 597	7	V_4	M_o	1 594.5	1.1	0.4993
"	*	1 594	2	V_4	W			-0.7527
"	*	1 597	6	V_7	Ba			0.3494
$^{27}Al(d,p)^{28}Al$	*	5 507	10	V_7	M_1	5 499.0	3.4	0.6752
"	*	5 499	10	V_4	M_o			-0.2078
$^{27}Al(d,\alpha)^{25}Mg$	*	6 700	10	V_4	M_o	6 700.5	2.2	-0.3445
$^{28}Al(\beta^-)^{28}Si$		4 646	10	i		4 639.5	4.2	0.6483
$^{28}Si(n,\gamma)^{29}Si$		8 468	8	V_4	CR	8 477.7	3.4	-1.2151
"		8 482	15	V_7				0.2853
$^{28}Si(d,p)^{29}Si$	*	6 252	10	V_4	M_o	6 253.0	3.4	-0.4065
$^{28}Si\ (d,\alpha)^{26}Al$	*	1 417	8	V_7	M_o	1 420.7	4.2	-0.8351
$^{29}Si(n,\gamma)^{30}Si$		10 601	11	V_4	CR	10 614.3	4.3	-1.2063
$^{29}Si(d,p)^{30}Si$	*	8 396	13	V_4	M_o	8 389.6	4.2	0.5800
$^{29}Si(d,\alpha)^{27}Al$	*	6 000	11	V_4	M_o	6 012.0	3.6	-2.0272
$^{30}Si(d,p)^{31}Si$	*	4 368	7	V_4	M_o	4 367.4	3.7	-0.1014
$^{30}Si(d,\alpha)^{28}Al$	*	3 123	10	V_4	M_o	3 121.4	4.3	0.1420
$^{31}Si(\beta^-)^{31}P$		1 471	8	K_4		1 476.7	4.6	-0.7106
"		1 486	12	K_4				0.7762
$^{31}P(p,\alpha)^{28}Si$	*	1 911	10	V_7	M_1	1 916.8	2.8	-0.6277
"	*	1 911	10	V_4	M_o			-1.0465
"	*	1 913	5	V_7	Ba			-0.8555
$^{31}P(d,p)^{32}P$	*	5 710	8	V_4	M_o	5 712.0	2.4	-0.6994
$^{31}P(d,\alpha)^{29}Si$	*	8 166	11	V_4	M_o	8 169.8	3.3	-0.8663
$^{32}P(\beta^-)^{32}S$		1 712	8	K_4		1 708.4	2.0	0.4491
"		1 718	10	K_4				0.9593
"		1 708	8	K_4				-0.0509
"		1 697	10	K_4				-1.1407
"		1 704	8	K_4				-0.5509
"		1 711	6	L_7				0.4321
"		1 700	5	L_7				-1.6815
"		1 712	8	L_7				0.4491
"		1 712	5	L_7				0.7185
"		1 704	10	L_7				0.4407

TABLE 2a (Continued)

Nuclear reaction or decay		Measured value (keV)		Ref.	Lab.	Adjusted value (keV)		$\frac{v}{\sigma}$
$^{32}S(n,\gamma)^{33}S$		8 640	± 20	V_4	CR	8 642.5	± 2.8	-0.1274
$^{32}S(d,p)^{33}S$	*	6 428	11	V_4	M_o	6 417.8	2.8	1.3177
"	*	6 419	6	k	M_1			-0.0506
$^{34}S(d,p)^{35}S$	*	4 762	10	k	M_1	4 757.1	3.7	0.3782
$^{35}S(\beta^-)^{35}Cl$		167.0	0.5	K_4*		167.34	0.19	-0.6866
"		167.4	0.2	l				0.2836
$^{35}Cl(p,\alpha)^{32}S$	*	1 865	8	V_7	M_1	1 865.1	2.6	-0.0630
"	*	1 862	5	V_7	Ba			-0.7007
$^{35}Cl(d,p)^{36}Cl$	*	6 360	8	V_7	M_1	6 352.0	4.5	0.8155
$^{35}Cl(d,\alpha)^{33}S$	*	8 285	10	V_7	M_1	8 282.9	3.6	0.0192
$^{36}Cl(\beta^-)^{36}A$		714	5	L_7		711.5	4.3	0.5097
$^{37}Cl(p,n)^{37}A$		-1 598	4	V_4	W	-1 598.6	1.5	0.1534
"		-1 598	2	V_4				0.3068
$^{37}Cl(p,\alpha)^{34}S$	*	3 029	8	V_7	M_1	3 030.1	3.1	-0.2187
"	*	3 030	6	V_7	Ba			-0.1250
$^{37}Cl(d,\alpha)^{35}S$	*	7 790	12	V_7	M_1	7 787.2	3.2	0.0860
$^{37}A(\varepsilon)^{37}Cl$		817.2	2.5	m		816.0	1.5	0.4794
$^{39}K(n,\gamma)^{40}K$		7 789	8	V_4	CR	7 797.6	3.3	-1.0693
"		7 795	10	V_7				-0.2555
$^{39}K(p,\alpha)^{36}A$	*	1 287	7	V_7	M_1	1 292.3	3.9	-0.8056
$^{39}K(d,p)^{40}K$	*	5 581	10	V_4	M_o	5 572.8	3.3	1.1473
$^{40}K(\beta^-)^{40}Ca$		1 360	30	K_4		1 321.5	4.5	1.2844
"		1 360	50	K_4				0.7706
"		1 280	30	K_4				-1.3823
"		1 325	15	K_4				0.2354
"		1 320	20	L_7				-0.0734
$^{41}K(p,n)^{41}Ca$		-1 220	20	V_4		-1 196	9	-1.2154
$^{40}Ca(n,\gamma)^{41}Ca$		8 370	30	V_7	CR	8 361	8	0.3132
"		8 350	17	V_7				-0.6238
$^{40}Ca(d,p)^{41}Ca$	*	6 146	10	V_4	M_1	6 136	8	0.8702
$^{42}Ca(p,\alpha)^{39}K$	*	118	7	V_7	M_1	126.0	4.4	-1.1514
$^{42}Ca(d,p)^{43}Ca$	*	5 717	10	V_7	M_1	5 705	5	1.0935
$^{43}Ca(p,\alpha)^{40}K$	*	-14	8	V_7	M_1	-5.9	4.9	-1.0143
$^{43}Ca(d,p)^{44}Ca$	*	8 922	14	V_7	M_1	8 911	6	0.6151
$^{44}Ca(p,\alpha)^{41}K$	*	-1 058	10	V_7	M_1	-1 047	6	-1.0969
$^{44}Ca(d,p)^{45}Ca$	*	5 193	10	V_7	M_1	5 195	6	-0.3037
$^{45}Ca(\beta^-)^{45}Sc$		248	3	K_4		252.0	1.9	-1.3282
"		255	4	K_4				0.7538
"		254	3	K_4				0.6718

TABLE 2a (Continued)

Nuclear reaction or decay	Measured value (keV)		Ref.	Lab.	Adjusted value (keV)		$\frac{v}{\sigma}$
$^{45}Sc(d,p)^{46}Sc$ *	6 540	± 8	n	M_1	6 542	± 5	-0.3947
$^{46}Sc(\beta^-)^{46}Ti$	2 364	5	L_7		2 365.2	4.4	-0.2467
$^{47}Ti(n,\gamma)^{48}Ti$	11 609	20	V_7	CR	11 620	8	-0.5633
$^{48}Ti(n,\gamma)^{49}Ti$	8 141	8	V_7	CR	8 146.9	4.1	-0.7401
"	8 153	10	V_7				0.6067
$^{51}V(p,n)^{51}Cr$	-1 535.5	1.5	V_7		-1 535.3	1.5	-0.1593
$^{51}V(p,\alpha)^{48}Ti$	1 162	10	V_7	M_1	1 165.9	4.8	-0.3861
$^{50}Cr(n,\gamma)^{51}Cr$	9 249	12	V_7	CR	9 249	6	-0.0356
$^{51}Cr(\varepsilon)^{51}V$	750	5	L_7		752.6	1.5	-0.5282
$^{52}Cr(n,\gamma)^{53}Cr$	7 929	8	V_4	CR	7 943.4	3.6	-1.7927
$^{52}Cr(d,p)^{53}Cr$	5 727	6	o	M_1	5 718.6	3.6	1.3922
$^{53}Cr(n,\gamma)^{54}Cr$	9 716	7	V_4	CR	9 721.6	4.8	-0.8055
$^{54}Cr(p,n)^{54}Mn$	-2 162	5	V_7		-2 161.6	4.7	-0.0767
$^{55}Mn(n,\gamma)^{56}Mn$	7 261	6	V_4		7 270.2	3.8	-1.5378
$^{55}Mn(p,n)^{55}Fe$	-1 006	10	V_4		-1 014.4	2.2	0.8355
"	-1 020	5	V_4				-1.1242
"	-1 015	3	V_7				-0.2110
$^{55}Mn(p,\alpha)^{52}Cr$	2 571	8	p	M_1	2 572.1	4.3	-0.1405
$^{55}Mn(d,p)^{56}Mn$	5 052	5	q	M_1	5 045.5	3.8	1.2931
$^{55}Mn(d,\alpha)^{53}Cr$	8 283	8	o	M_1	8 290.8	4.4	-0.9705
$^{56}Mn(\beta^-)^{56}Fe$	3 710	20	r		3 709	7	0.0576
$^{54}Fe(n,\gamma)^{55}Fe$	9 298	7	V_4	CR	9 299.6	4.5	-0.2247
"	9 295	15	V_7				-0.3049
$^{54}Fe(d,p)^{55}Fe$	7 084	8	n	M_1	7 074.9	4.5	1.1422
$^{55}Fe(\varepsilon)^{55}Mn$	233	10	s		231.7	2.2	0.1251
"	232	10	s				0.0251
"	230	10	s				-0.1749
"	220	10	s				-1.1749
$^{56}Fe(n,\gamma)^{57}Fe$	7 639	4	V_4	CR	7 641.2	3.2	-0.5561
"	7 636	10	V_7				-0.5231
$^{56}Fe(d,p)^{57}Fe$	5 426	8	n	M_1	5 416.5	3.2	1.1847
$^{57}Fe(p,\alpha)^{54}Mn$	240	12	n	M_1	238	7	0.1835
$^{57}Fe(d,p)^{58}Fe$	7 815	8	n	M_1	7 823	6	-0.9901
$^{58}Fe(p,\alpha)^{55}Mn$	400	12	n	M_1	410	7	-0.8068
$^{58}Fe(d,p)^{59}Fe$	4 357	8	n	M_1	4 361	6	-0.4524
$^{59}Fe(\beta^-)^{59}Co$	1 561	6	K_4		1 563	5	-0.3393
$^{59}Co(n,\gamma)^{60}Co$	7 486	6	V_4	CR	7 496.8	4.3	-1.7965

TABLE 2a (Continued)

Nuclear reaction or decay	Measured value (keV)		Ref.	Lab.	Adjusted value (keV)		$\frac{v}{\sigma}$
$^{59}Co(p,n)^{59}Ni$	-1 857	± 3	V_4		-1 858.4	± 2.2	0.4791
"	-1 858	4	V_7				0.1119
"	-1 862	5	V_7				-0.7078
$^{59}Co(p,\alpha)^{56}Fe$	3 245	8	t	M_1	3 240	5	0.5729
$^{59}Co(d,p)^{60}Co$	5 288	8	V_7	M_1	5 272.1	4.3	1.9887
$^{60}Co(\beta^-)^{60}Ni$	2 813	8	u		2 816.1	2.1	-0.3851
"	2 823	4	u				1.7298
"	2 811	5	u				-1.0162
"	2 814	3	u				-0.6937
$^{58}Ni(n,\gamma)^{59}Ni$	8 997	5	V_4	CR	9 000.8	3.8	-0.7605
"	8 996	10	V_7				-0.4811
$^{58}Ni(d,p)^{59}Ni$	6 786	8	n	M_1	6 776.1	3.8	1.2373
$^{62}Ni(n,\gamma)^{63}Ni$	6 839	10	r	CR	6 841	5	-0.2449
$^{62}Ni(d,p)^{63}Ni$	4 622	8	n	M_1	4 617	5	0.6578
$^{63}Ni(\beta^-)^{63}Cu$	63	2	w		66.76	0.47	-1.8825
"	67	2	x				0.1175
"	67.0	0.5	y				0.4701
$^{63}Cu(n,\gamma)^{64}Cu$	7 914	6	V_4	CR	7 916.2	4.2	-0.3624
$^{63}Cu(p,\alpha)^{60}Ni$	3 757	8	z	M_1	3 756	6	0.0640
$^{63}Cu(d,p)^{64}Cu$	5 698	8	a1	M_1	5 691.5	4.2	0.8167
$^{64}Cu(\beta^-)^{64}Zn$	578	3	K_4		573.2	1.5	1.6067
"	574	4	T				0.2050
"	571	2	K_4				-1.0900
$^{65}Cu(p,n)^{65}Zn$	-2 137	5	V_7		-2 130.9	0.8	-1.2200
"	-2 136	4	V_7				-1.2736
"	-2 131	5	V_7				-0.0238
"	-2 132.2	1.5	V_7				-0.8502
"	-2 135	3	b1				-1.3612
$^{65}Cu(p,\alpha)^{62}Ni$	4 345	8	z	M_1	4 343	6	0.2573
$^{65}Cu(d,p)^{66}Cu$	4 836	8	a1	M_1	4 836	7	0.0148
$^{66}Cu(\beta^-)^{66}Zn$	2 630	10	L_7		2 630	8	0.0184
$^{64}Zn(n,\gamma)^{65}Zn$	7 990	8	V_7		7 989	6	0.1416
$^{65}Zn(\beta^+)^{65}Cu$	1 347	2	K_4		1 348.3	0.8	-0.6344
"	1 347	2	K_4				-0.6344
"	1 342	4	K_4				-1.5672
"	1 349	3	K_4				0.2438
"	1 347	3	K_4				-0.4229
"	1 347	2	L_7				-0.6344
"	1 346	4	L_7				-0.5672
$^{66}Zn(n,\gamma)^{67}Zn$	7 035	20	V_7		7 046	12	-0.5361
$^{67}Zn(n,\gamma)^{68}Zn$	10 198	12	c1		10 199	10	-0.0618

In the above table the first column denotes the nuclear reaction or decay. Reactions combined with the calibration variable (see sect. 6) are indicated by an asterisk. The second column gives the adopted input datum and its error. The last values have sometimes been changed from the values given in the references of the third column for reasons discussed in sect. 6. Wherever possible, we have referred to the data collections V_4, V_7, K_4, L_7 and T mentioned below. Some averaged β-decay energies have been changed slightly due to taking into account transitions to accurately known (A_5, A_9, E_7, 59—8—43) excited states (as also in the case of the ^{19}F (p, α) reaction; see below). Such data are indicated by an asterisk behind the reference symbol. The symbols of the fourth column refer to the laboratories where the indicated reactions have been measured. They give in some cases a clue to some small calibration corrections and to the application of the consistency factor $R_0/R_1 = 0.60$ to the original errors of the second column as discussed in sects. 6 and 7. Their meaning is explained below. The fifth column gives the adjusted value and its error following from our final adjustment. The sixth column contains the ratio of the difference v between the Q-values in the second and fifth column (including a correction for the influence of the calibration variable) to the error σ in the adopted input value.

Symbols indicating laboratories

B: University of Birmingham, England.
Ba: Bartol Research Foundation, Swarthmore, Penn.
C: California Institute of Technology, Pasadena, Cal.
CR: Atomic Energy of Canada Ltd., Chalk River, Ont.
M_0, M_1: Massachusetts Institute of Technology, Cambridge, Mass.
N: Nobel Institute of Physics, Stockholm, Sweden.
R: Rice Institute, Houston, Tex.
W: University of Wisconsin, Madison, Wisc.

Reference Collections

A_5: F. Ajzenberg and T. Lauritsen, Revs. Mod. Phys. **27** (1955) 77
A_9: F. Ajzenberg-Selove and T. Lauritsen, Nuclear Physics **11** (1959) 1
E_7: P. M. Endt and C. M. Braams, Revs. Mod. Phys. **29** (1957) 683
K_4: R. W. King, Revs. Mod. Phys. **26** (1954) 327
L_7: L. J. Lidofski, Revs. Mod. Phys. **29** (1957) 773
T: K. Way, R. W. King, C. L. McGinnis and R. van Lieshout, Nuclear Level Schemes $A = 40$ to 92, TID-5300 (1955)
V_4: D. M. van Patter and W. Whaling, Revs. Mod. Phys. **26** (1954) 402
V_7: D. M. Van Patter and W. Whaling, Revs. Mod. Phys. **29** (1957) 757
59—8—43: K. Way, G. Andersson, F. Everling, G. H. Fuller, N. B. Gove, R. Levesque, J. B. Marion, C. L. McGinnis, R. Nakasima and M. Yamada, Nuclear Data Sheets, National Academy of Sciences-National Research Council, Washington 25, D.C. (1958—1960); indicated by year, set and page numbers

References

a: this value is computed from $^{65}Zn(\beta^+)^{65}Cu + ^{65}Cu(p, n)^{65}Zn$
b: S. C. Curran, J. Angus and A. L. Cockroft, Phil. Mag. **40** (1949) 53
c: P. R. Bell and J. M. Cassidy, Phys. Rev. **77** (1950) 301
d: H. Bichsel and T. W. Bonner, Phys. Rev. **108** (1957) 1025
e: A. V. Pohm, R. C. Waddell, J. P. Powers and E. N. Jensen, Phys. Rev. **97** (1955) 432
f: H. Daniel and U. Schmidt-Rohr, Z. Naturforsch. **12a** (1957) 750
g: P. J. Campion and G. A. Bartholomew, Can. J. Phys. **35** (1957) 1361
h: From transitions to the (6 135±8) keV and (7 125±8) keV excited states (A_9)
i: P. M. Endt and C. M. Braams, Revs. Mod. Phys. **29** (1957) 683
j: Value by L. J. Lidofsky is 1 022 keV too low. Our value is compounded from a β^+ energy of (1 140±10) keV and values (1 840±10) keV and (1 865±15) keV for the energy of the excited state in the daughter nucleus measured with a gamma ray spectrometer, and in $^{28}Si(d, \alpha)$ reactions respectively (E_7).
k: P. M. Endt and C. H. Paris, Phys. Rev. **110** (1958) 89

l: R. D. Connor and I. L. Fairweather, Proc. Phys. Soc. **70** (1957) 769

m: Adding the K-electron binding energy 2.8 keV to the neutrino energy computed from recoil experiments (L_7)

n: W. W. Buechner, Okt. 1958 (private communication)

o: M. Mazari, W. W. Buechner and A. Sperduto, Phys. Rev. **112** (1958) 1691

p: M. Mazari, W. W. Buechner and A. Sperduto, Phys. Rev. **107** (1957) 1383

q: J. W. Green, A. J. Smith, W. W. Buechner and M. Mazari, Phys. Rev. **108** (1957) 841

r: The best values for the gamma energies in this decay are (845±5) keV, (1 809±9) keV and (2 134±11) keV (59—4—54). Together with the decay branches as reported by various authors (K_4) the value in our table is derived

s: Only the four most modern values (L_7) have been used; three of the four older values (A_5) appear definitely low as compared with the $^{55}Mn(p, n)$ reaction which is anyhow much more precise

t: M. Mazari, A. Sperduto and W. W. Buechner, Phys. Rev. **107** (1957) 365

u: Gamma ray energies of (1 172.8±0.7) keV and (1 332.5±0.3) keV have been used in computing these decay energies, together with β^- energies from K_4 and L_7

v: B. B. Kinsey and G. A. Bartholomew, Phys. Rev. **89** (1953) 375

w: H. W. Wilson and S. C. Curran, Phil. Mag. **40** (1949) 631

x: A. R. Brosi, C. J. Borkowski, E. E. Conn and J. C. Griess, Jr., Phys. Rev. **81** (1951) 391

y: I. L. Preiss, R. W. Fink and B. L. Robinson, J. Inorg, Nuclear Chem. **4** (1957) 233

z: M. Mazari, W. W. Buechner and R. P. de Figueiredo, Phys. Rev. **108** (1957) 373

a1: R. P. de Figueiredo, M. Mazari and W. W. Buechner, Phys. Rev. **112** (1958) 873

b1: E. M. Bernstein and H. W. Lewis, Phys. Rev. **107** (1957) 737; Bull. Am. Phys. Soc. **2**, No. 1, 61 U12. Gives a threshold (2 223±3) keV for the (54±2) keV gamma ray which data combined give the desired threshold

c1: The energy of the capture gamma ray to the first excited level has been increased by a value (1 078±5) keV for the excitation energy of this level found by (p, p) scattering (59−1−19).

TABLE 2b

Secondary reaction and decay energies. (See subsect. 4.1)

Nuclear reaction or decay	Adopted value (keV)		Ref.	Lab.	Adjusted value (keV)	
$^{3}H\ (\tau,p)\ \underline{^{5}He}$	11 180	± 70	V_4		11 138	± 20
	11 130	70	V_4			
$^{4}He\ (d,p)\ ^{5}He$	3 300	100	V_7		3 182	20
$^{5}He\ (n)\ ^{4}He$	900	70	V_4		957	20
	950	70	V_4			
	900	100	V_4			
	1 090	100	V_4			
$^{6}Li\ (\gamma,p)\ ^{5}He$	-4 640	80	A_9		-4 653	20
$^{6}Li\ (n,d)\ ^{5}He$	-2 570	100	V_4		-2 428	20
$^{6}Li\ (d,\tau)\ ^{5}He$	910	90	V_7		840	20
$^{6}Li\ (t,\alpha)\ ^{5}He$	15 150	40	V_7		15 160	20
$^{7}Li\ (d,\alpha)\ ^{5}He$	14 260	90	V_7		14 165	20
	14 110	80	a			
$^{3}He\ (d,\gamma)\ \underline{^{5}Li}$	16 360	200	A_9		16 385	37
$^{3}He\ (\tau,p)\ ^{5}Li$	10 860	150	V_4		10 892	37
$^{5}Li\ (p)\ ^{4}He$	1 900	100	b		1 967	37
$^{6}Li\ (\gamma,n)\ ^{5}Li$	-5 600	100	A_9		-5 663	37
	-5 350	200	V_4			
	-5 730	50	A_9			
$^{6}Li\ (d,p)\ ^{5}Li$	800	150	A_9		595	37
$\underline{^{6}He}\ (\beta^-)\ ^{6}Li$	3 500	20	L_7		3 515	17
$^{7}Li\ (t,\alpha)\ ^{6}He$	9 790	30	V_4		9 828	17
$^{6}Li\ (\tau,n)\ \underline{^{8}B}$	-1 975.5	1.3	c			-
$^{7}Li\ (d,p)\ \underline{^{8}Li}$	- 192	1	V_4	W		-
$^{9}Be\ (p,n)\ \underline{^{9}B}$	-1 852	2	V_4	W	-1 852.8	1.6
	-1 853	3	V_7	R		
	-1 856	6	V_4	W		
$^{10}B\ (p,n)\ \underline{^{10}C}$	-4 350	200	V_4		-4 410	60
	-4 370	50	V_7			
$^{10}C\ (\beta^+)\ ^{10}B$	3 840	100	K_4*		3 620	60
$^{7}Li\ (^{7}Li,p)\ \underline{^{13}B}$	5 970	50	A_9			-
$^{11}B\ (p,n)\ \underline{^{11}C}$	-2 760	10	V_4		-2 765.0	3.0
	-2 762	3	V_4	W		
$^{11}C\ (\beta^+)\ ^{11}B$	1 994	6	L_7		1 982.4	3.0
$^{12}C\ (p,n)\ \underline{^{12}N}$	-18 500	100	V_4		-18 390	90
$^{12}N\ (\beta^+)\ ^{12}C$	17 620	200	K_4*		17 600	90
$^{10}B\ (\tau,n)\ ^{12}N$	1 460	100	V_7		1 310	90

TABLE 2b (Continued)

Nuclear reaction or decay	Adopted value (keV)		Ref.	Lab.	Adjusted value (keV)		
^{12}C (τ,n) ^{14}O	-1 147.0 ±	2.4	V_7		-1 152 ±	5	
	-1 158.5	3.0	V_7				
^{14}O (β^+) ^{14}N	5 150	14	L_7*		5 148		5
^{14}C (d,p) ^{15}C	-1 007	1	V_7	W		-	
^{15}N (p,n) ^{15}O	-3 543.2	1.5	V_7			-	
^{17}N (β^-) ^{17}O	8 800	200	K_4			-	
^{18}O (p,n) ^{18}F	-2 447	10	V_7	M_1	-2 450.0		4.0
	-2 453	4	V_4	W			
^{18}F (β^+) ^{18}O	1 667	8	K_4		1 667.4		4.0
^{18}Ne(β^+) ^{18}F	4 220	200	K_4			-	
^{18}O (d,p) ^{19}O	1 732	6	V_7	C	1 732		4
	1 730	8	V_7	N			
	1 735	8	V_7				
^{19}F (p,n) ^{19}Ne	-4 039	5	V_4		-4 031		5
	-4 028	8	V_7				
	-4 024	5	V_7	R			
^{19}F (t,p) ^{21}F	6 200	25	V_7			-	
^{20}Ne (p,n) ^{20}Na	-16 100	300	V_4			-	
^{21}Na (β^+) ^{21}Ne	3 522	30	K_4			-	
^{22}Ne (d,p) ^{23}Ne	2 967	5	V_4	M_o	2 968		5
	2 971	8	V_7	N			
^{23}Na (p,n) ^{23}Mg	-4 842	10	V_7			-	
^{24}Ne (β^-) ^{24}Na	2 450	40	L_7			-	
^{24}Mg (p,n) ^{24}Al	-14 800	300	V_4			-	
^{24}Mg (p,γ) ^{25}Al	2 287	6	d			-	
^{25}Na (β^-) ^{25}Mg	3 800	200	L_7			-	
^{27}Al (p,n) ^{27}Si	-5 585	10	V_7		-5 598		11
	-5 607	8	V_7				
^{28}Mg (β^-) ^{28}Al	1 837	5	L_7			-	
^{28}P (β^+) ^{28}Si	13 400	400	L_7		13 800		300
^{28}Si (p,n) ^{28}P	-15 100	500	V_4		-14 580		300
	-14 800	500	V_4				
^{26}Mg (α,p) ^{29}Al	-2 900	40	V_7		-2 940		50
^{29}Al (β^-) ^{29}Si	3 950	100	L_7		3 758		50
^{29}P (β^+) ^{29}Si	4 960	10	L_7			-	
^{32}S (d,α) ^{30}P	4 892	10	e	M_1		-	
^{31}P (p,n) ^{31}S	-6 216	20	f		-6 218		17
^{31}S (β^+) ^{31}P	5 440	30	L_7		5 435		17
^{32}Si (β^-) ^{32}P	100	50	K_4			-	

TABLE 2b (Continued)

Nuclear reaction or decay	Adopted value (keV)		Ref.	Lab.	Adjusted value (keV)	
^{32}Cl (β^+) ^{32}S	12 800	± 400	L_7		13 000	± 300
^{32}S (p,n) ^{32}Cl	-13 900	500	V_4		-13 780	300
	-14 100	600	V_4			
^{32}S (p,γ) ^{33}Cl	2 285	12	g			-
^{33}P (β^-) ^{33}S	249	2	L_7			-
^{34}P (β^-) ^{34}S	5 100	200	K_4			-
^{34}Cl (β^+) ^{34}S	5 420†	30	K_4			-
^{35}A (β^+) ^{35}Cl	5 980	40	L_7			-
^{37}S (β^-) ^{37}Cl	4 700	100	L_7		4 790	90
^{40}A (n,α) ^{37}S	-2 500	100	V_7		-2 420	90
^{37}K (β^+) ^{37}A	6 120	100	L_7*			-
^{37}Cl (d,p) ^{38}Cl	3 885	8	V_7	M_o		-
^{38}S (β^-) ^{38}Cl	3 000	150	h			-
^{39}Cl (β^-) ^{39}A	3 430	20	L_7			-
^{39}A (β^-) ^{39}K	565	5	K_4			-
^{39}Ca (β^+) ^{39}K	6 600	40	L_7		6 610	40
^{40}Ca (γ,n) ^{39}Ca	-15 800	100	V_4		-15 729	40
^{40}Ca (d,α) ^{38}K	4 655	10	V_7	M_1		-
^{40}Cl (β^-) ^{40}A	7 500	500	L_7			-
^{40}Sc (β^+) ^{40}Ca	13 800	400	K_4		13 900	400
^{40}Ca (p,n) ^{40}Sc	-15 500	1 000	V_4		-14 680	400
^{41}A (β^-) ^{41}K	2 490	10	L_7			-
^{41}Sc (β^+) ^{41}Ca	5 960	70	K_4		5 950	40
^{40}Ca (d,n) ^{41}Sc	- 600	50	V_7		- 597	41
^{42}K (β^-) ^{42}Ca	3 530	20	L_7*			-
^{42}Sc (β^+) ^{42}Ca	5 820	900	i		5 900	600
^{42}Ca (p,n) ^{42}Sc	-6 800	700	i		-6 700	600
^{43}K (β^-) ^{43}Ca	1 817	10	j			-
^{43}Sc (β^+) ^{43}Ca	2 220	10	L_7			-
^{44}K (β^-) ^{44}Ca	6 100	200	k			-
^{44}Sc (β^+) ^{44}Ca	3 648	5	L_7*			-
^{44}Ti (ε) ^{44}Sc	155	10	l			-
^{45}Sc (p,n) ^{45}Ti	-2 844	4	V_7		-2 841	4
^{45}Ti (β^+) ^{45}Sc	2 040	10	K_4		2 058.4	4.0
^{46}V (β^+) ^{46}Ti	7 300	400	m			-
^{47}Ca (β^-) ^{47}Sc	1 965	20	L_7*			-
^{47}Sc (β^-) ^{47}Ti	600	2	L_7*			-
^{47}V (β^+) ^{47}Ti	2 912	10	T*			-
^{48}Sc (β^-) ^{48}Ti	3 990	9	n			-

TABLE 2b (Continued)

Nuclear reaction or decay	Adopted value (keV)	Ref.	Lab.	Adjusted value (keV)
^{48}V (β^+) ^{48}Ti	4 017 ± 5	n		-
^{48}Cr (ε) ^{48}V	1 400 200	L_7		-
^{48}Ca (d,p) ^{49}Ca	2 919 6	V_7	M_1	-
^{49}Sc (β^-) ^{49}Ti	2 000 50	L_7*		2 070 ± 90
^{49}Ca (β^-) ^{49}Sc	5 080 60	L_7		5 190 90
^{49}Ti (p,n) ^{49}V	-1 391 5	V_4		-1 394 5
^{49}V (ε) ^{49}Ti	620 10	L_7		611 5
^{49}Cr (β^+) ^{49}V	2 560 10	K_4		-
^{50}Sc (β^-) ^{50}Ti	6 300 500	L_7		-
^{50}Mn (β^+) ^{50}Cr	7 700 500	m		-
^{51}Ti (β^-) ^{51}V	2 465 20	L_7*		-
^{51}Mn (β^+) ^{51}V	3 180 50	T		-
^{51}V (n,γ) ^{52}V	7 305 7	V_4	CR	7 304 6
^{51}V (d,p) ^{52}V	5 077 8	V_4	M_o	5 079 6
^{52}Mn (β^+) ^{52}Cr	4 703 8	o		-
^{52}Fe (β^+) ^{52}Mn	2 383 15	p		-
^{53}V (β^-) ^{53}Cr	2 530 50	L_7		-
^{53}Cr (p,n) ^{53}Mn	-1 380 8	V_4		-
^{54}Fe (γ,n) ^{53}Fe	-13 650 50	V_7		-13 620 40
^{53}Fe (β^+) ^{53}Mn	3 700 100	p		3 992 41
^{54}Co (β^+) ^{54}Fe	8 800 500	m		-
^{55}Cr (β^-) ^{55}Mn	2 820 140	L_7		-
^{55}Co (β^+) ^{55}Fe	3 460 10	L_7		-
^{56}Co (β^+) ^{56}Fe	4 600 15	L_7*		-
^{57}Mn (β^-) ^{57}Fe	2 700 300	L_7*		-
^{57}Co (ε) ^{57}Fe	570 30	L_7		-
^{57}Ni (β^+) ^{57}Co	3 235 15	q		-
^{58}Co (β^+) ^{58}Fe	2 312 12	L_7*		-
^{58}Ni (p,n) ^{58}Cu	-9 300 70	f		-
^{58}Ni (p,γ) ^{59}Cu	3 420 20	r		-
^{60}Ni (p,n) ^{60}Cu	-6 913 20	f		-6 930 40
^{60}Cu (β^+) ^{60}Ni	6 240 40	s		6 147 40
^{60}Ni (d,p) ^{61}Ni	5 603 8	t	M_1	5 598 6
^{60}Ni (n,γ) ^{61}Ni	7 817 8	V_7	CR	7 823 6
^{61}Co (β^-) ^{61}Ni	1 290 40	L_7		-
^{61}Cu (β^+) ^{61}Ni	2 231 5	L_7*		-
^{61}Zn (β^+) ^{61}Cu	5 800 300	L_7		-
^{62}Co (β^-) ^{62}Ni	5 220 40	u		-
^{62}Cu (β^+) ^{62}Ni	3 930 10	L_7*		-

TABLE 2b (Continued)

Nuclear reaction or decay	Adopted value (keV)		Ref. Lab.	Adjusted value (keV)		
$\underline{^{62}Zn}$ (β^+) ^{62}Ni	1 690	± 8	v		-	
^{63}Cu (p,n) $\underline{^{63}Zn}$	-4 149	4	V_7		-	
$\underline{^{64}Cu}$ (β^+) ^{64}Ni	1 678	2	K_4		-	
^{64}Zn (p,n) $\underline{^{64}Ga}$	-7 800	150	w		-	
$\underline{^{65}Ni}$ (β^-) ^{65}Cu	2 100	200†	K_4		-	
$\underline{^{65}Ga}$ (β^+) ^{65}Zn	3 259	15	x		-	
$\underline{^{66}Ni}$ (β^-) ^{66}Cu	200	30	L_7		-	
$\underline{^{66}Ga}$ (β^+) ^{66}Zn	5 170	30	K_4		-	
$\underline{^{67}Cu}$ (β^-) ^{67}Zn	572	8	K_4		-	
^{67}Zn (p,n) $\underline{^{67}Ga}$	-1 785	5	V_4	-1 781	± 5	
	-1 777	5	V_7			
$\underline{^{67}Ge}$ (β^+) ^{67}Ga	4 400	100	y		-	
^{68}Zn (p,n) ^{68}Ga	-3 704	5	V_7	-3 700	5	
	-3 694	6	V_7			
$\underline{^{68}Ge}$ (ε) ^{68}Ga	700	600	L_7*		-	
$\underline{^{69}Zn}$ (β^-) ^{69}Ga	905	6	L_7		-	
$\underline{^{69}Ge}$ (β^+) ^{69}Ga	2 237	12	K_4*		-	
$\underline{^{69}As}$ (β^+) ^{69}Ge	3 900	300	L_7		-	
$\underline{^{69}Ga}$ (n,γ) ^{70}Ga	7 730	20	V_7		-	
^{70}Zn (p,n) $\underline{^{70}Ga}$	-1 435	5	z		-	
^{70}Ga (β^-) $\underline{^{70}Ge}$	1 650	10	L_7		-	
$\underline{^{70}As}$ (β^+) ^{70}Ge	6 540	100	L_7		-	

The above data have been arranged in groups used in the determination of the mass of one nuclide each; this nuclide has been underlined in the first datum of each group. The second column gives the adopted results, sometimes corrected as in table 2a, the fifth column gives the adjusted values in the cases where the secondary mass is determined by more than one datum and where therefore a small adjustment has been made. For the meaning of the reference symbols (third column) A_5, A_9, K_4, L_7, T, V_4 and V_7, see table 2a. Again a few averaged beta decay energies are slightly different from the values given in the last three data collections. Such data are marked with an asterisk in the third column. Other references are the following:

a: G. Weber, Phys. Rev. **110** (1958) 529
b: E. W. Titterton, Progr. Nucl. Phys. **4** (1955) 31
c: K. L. Dunning, J. W. Butler and R. O. Bondelid, Phys. Rev. **110** (1958) 1076
d: H. E. Gove, A. E. Litherland, E. Almqvist and D. A. Bromley, Phys. Rev. **111** (1958) 608
e: P. M. Endt and C. H. Paris, Phys. Rev. **110** (1958) 89
f: H. E. Gove, J. A. Kuehner, A. E. Litherland, E. Almqvist, D. A. Bromley, A. J. Ferguson, P. H. Rose, R. P. Bastide, N. Brooks and R. J. Connor, Phys. Rev. Lett. **1** (1958) 251
g: C. Van der Leun and P. M. Endt, Physica **22** (1956) 1234
h: D. R. Nethaway and A. A. Caretto, Jr., Phys. Rev. **109** (1958) 504
i: J. A. R. Cloutier and A. Henrikson, Can. J. Phys. **35** (1957) 1190
j: N. Benczer-Koller, A. Schwarzschild and C. S. Wu, Phys. Rev. **115** (1959) 108
k: Assuming 1160 γ follows 4 900 β (T)
l: J. R. Huizenga and J. Wing, Phys. Rev. **106** (1957) 90

m: see ref. [7]), corrected because of comparison with ^{58}Ni(p, n) ref. f.
n: B. van Nooijen, J. Konijn, A. Heyligers, J. F. van der Brugge and A. H. Wapstra, Physica **23** (1957) 753
o: J. Konijn, Thesis, Delft 1958
p: J. O. Juliano, C. W. Kocher, T. D. Nainan and A. C. G. Mitchell, Phys. Rev. **113** (1959) 602
q: J. Konijn, H. L. Hagedoorn and B. van Nooijen, Physica **24** (1958) 129
r: J. W. Butler and C. R. Gossett, Phys. Rev. **108** (1957) 1473
s: R. H. Nussbaum, R. van Lieshout, A. H. Wapstra, N. F. Verster, F. E. L. Ten Haaf, G. J. Nijgh and L. Th. M. Ornstein, Physica **20** (1954) 555
t: C. H. Paris and W. W. Buechner, Bull. Am. Phys. Soc. **3** (1958) 38 and private communication
u: D. G. Gardner and W. W. Meinke, Phys. Rev. **107** (1957) 1628
v: E. Brun, W. E. Meyerhof, J. J. Kraushaar and D. J. Horen, Phys. Rev. **107** (1957) 1324
w: H. A. Howe, Phys. Rev. **109** (1958) 2083
x: H. Daniel, Z. Naturforsch. **12a** (1957) 363
y: R. A. Ricci and R. van Lieshout, Nuclear Physics **10** (1959) 360

† For the ^{34}Cl(β^+) and ^{65}Ni(β^-) decay energies erroneously the above values 5 420$\pm$30 and 2 100 $\pm$200 were used in the computation instead of the more correct values 5 520$\pm$30 and 2 100$\pm$20.

TABLE 2c

Some rejected reaction and decay energies. (See sect. 9)

Nuclear reaction or decay	Measured value (keV)	Ref.	Lab.	Adjusted value (keV)	$\frac{v}{\sigma}$
$^{2}D\ (d,p)\ ^{3}T$	4 044 ± 5	V_4	W	4 032.92 ± 0.15	2.2160
$^{6}Li\ (p,d)\ ^{5}Li$	-3 000 150	V_4		-3 438 37	2.9200
$^{10}B\ (\alpha,d)\ ^{12}C$	1 390 10	V_4		1 341.6 0.7	4.8400
$^{14}C\ (\beta^-)\ ^{14}N$	158.5 0.5	L_7		156.07 0.35	4.8600
$^{16}O\ (d,\alpha)\ ^{14}N$	3 124 5	V_4	C	3 110.22 0.38	2.7560
$^{19}F\ (d,\alpha)\ ^{17}O$	10 060 10	V_4	M_o	10 031.4 1.1	2.8600
	10 038	V_4	M_o		
$^{20}Ne\ (d,\alpha)\ ^{18}F$	2 813 9	V_7	N	2 784.1 4.0	3.2111
$^{21}Ne\ (d,\alpha)\ ^{19}F$	6 444 10	V_4	C	6 467.2 1.7	-2.3200
$^{20}Ne\ (d,n)\ ^{21}Na$	- 170 50	V_4		230 30	-8.0000
$^{24}Mg\ (\alpha,p)\ ^{27}Al$	-1 613 10	V_4	W	-1 594.5 1.1	-1.8500
$^{27}Al\ (\alpha,p)\ ^{30}Si$	2 380 30	V_4		2 378 10	0.0667
$^{28}Si\ (d,n)\ ^{29}P$	290 40	V_4		510 11	-5.5000
$^{29}Si\ (d,n)\ ^{30}P$	3 270 40	V_4		3 360 11	-2.2500
$^{29}Si\ (n,\gamma)\ ^{30}Si$	10 590 30	V_7		10 614.3 4.3	-0.8100
$^{32}S\ (d,\alpha)\ ^{30}P$	4 831 13	V_7		4 892 10	-4.6923
$^{34}S\ (d,\alpha)\ ^{32}P$	5 040 20	V_7		5 081.1 3.7	-2.0550
$^{35}Cl\ (\gamma,n)\ ^{34}Cl$	-12 350 35	V_7 1)		-12 569 30	6.2571
$^{38}K\ (\beta^+)\ ^{38}A$	5 860 30	K_4		5 929 11	-2.3000
$^{41}K\ (p,\alpha)\ ^{38}A$	4 002 15	V_7		4 035.2 4.8	-2.2133
$^{41}K\ (n,\gamma)\ ^{42}K$	7 340 20	V_4 2)	CR	7 529 21	-9.4500
$^{46}Ti\ (p,\alpha)\ ^{43}Sc$	-3 217 14	59-6-98	M_o	-3 082 11	-9.6429
$^{54}Fe\ (\gamma,n)\ ^{53}Fe$	-11 900 70	V_7		-13 620 70	24.5714
$^{63}Zn\ (\beta^+)\ ^{63}Cu$	3 342 5	L_7 1)		3 366.4 4.0	-4.8800
$^{65}Cu\ (n,\gamma)\ ^{66}Cu$	7 010 20	V_7 2)	CR	7 061 6	-2.5500
$^{68}Zn\ (n,\gamma)\ ^{69}Zn$	6 490 20	V_7 2)	CR	6 406 28	4.2000

1) disagrees with two or more other data

2) target isotope uncertain.

The first column denotes the nuclear reaction or decay, the second one gives in keV the measured value with its error. The third column indicates the data collection, where the measured value is to be found, and the fourth value the laboratory, where this value was measured. As to the abbreviations used in the third and fourth column see the text below table 1a. The fifth column gives the adjusted value following from the final adjustment and the sixth column the ratio of the difference v of the Q-values in the second and fifth column to the standard deviation σ in the second column multiplied by the consistency factor (see sect. 7).

2.J

Nuclear Physics **25** (1961) 216—247; © *North-Holland Publishing Co., Amsterdam*

Not to be reproduced by photoprint or microfilm without written permission from the publisher

RÉACTIONS NUCLÉAIRES DE SPALLATION INDUITES SUR LE THORIUM PAR DES PROTONS DE 150 ET 82 MeV

M. LEFORT, G. N. SIMONOFF et X. TARRAGO

Laboratoire Joliot-Curie de Physique Nucléaire, Orsay, Université de Paris

Reçu le 2 janvier 1961

Abstract: Spallation reactions of thorium by 150 MeV and 82 MeV protons were studied by radiochemical isolation of Pa, Th, Ac and Ra isotopes and measurements of absolute cross sections. Calculations were carried on for comparison, by assuming a model of nuclear reactions by direct interaction and neutron evaporation (Serber-Jackson). Fission-evaporation competition at each step of evaporation was assumed. The agreement is very satisfactory for (p, pxn) reactions. However, experimental values are nearly twice the calculated ones for radium and actinium. Several reasons are discussed in order to explain this discrepancy. Direct interaction occurs also for alpha fragments, deuterons and tritons. Cross sections for alpha particle and triton production were measured at various energies. The formation of tritium is explained in terms of indirect pick up.

1. Introduction sur la spallation

C'est en 1948 que, pour la première fois, O'Connor et Seaborg [1]) ont porté en fonction du nombre de masse les sections efficaces relatives d'un grand nombre d'isotopes formés au cours du bombardement d'uranium naturel par des particules alpha de 380 MeV. Ces auteurs ont observé deux régions sur la courbe ainsi obtenue: l'une correspond aux produits de fission avec une probabilité maximum pour deux fragments symétriques de masse voisine de 115, l'autre représente les produits de réactions nucléaires au cours desquels le noyau très fortement excité ayant reçu le projectile perd un certain nombre de protons, neutrons et fragments légers. Ces derniers phénomènes ont reçu le nom de réactions de spallation.

Dès les premiers travaux sur les noyaux lourds effectués, entre autres, par Bennett [2]), Vinogradov *et al.* [3]) et Mourine *et al.* [4]), il a été remarqué qu'une des caractéristiques de ces réactions est la production d'un grand nombre d'isotopes déficients en neutrons, ce qui dénote une émission préférentielle de ces nucléons par rapport aux particules chargées. Cette particularité a été exploitée pour produire des isotopes légers jusqu'alors inconnus et pour étudier ou préciser leurs propriétés nucléaires. Les isotopes de faible masse de radium, francium, émanation et polonium ont été ainsi découverts en bombardant du thorium par protons de 350 MeV. De même les bismuths de masse 198 à 203 ont été produits

par bombardement de plomb. Une des études les plus complètes sur les réactions de spallation de noyaux lourds est celle de Lindner et Osborne [5]) qui ont bombardé thorium et uranium avec des protons de diverses énergies et plus particulièrement de 350 MeV.

La comparaison de leurs résultats avec ceux de Hunter et Miller [6]) sur le bismuth à 380 MeV met l'accent sur l'importance croissante de la concurrence de la fission lorsque les noyaux ont une valeur de Z^2/A élevée. C'est ainsi que les sections efficaces des réactions (p, xn) sont comprises entre 5.2 et 13.3 mb selon la valeur de x pour le bismuth, entre 1 et 4.2 pour le thorium et de l'ordre de 0.5 à 1.7 pour l'uranium. Si la section efficace globale de spallation est encore 15 fois supérieure à celle de fission pour le bismuth, elle n'est plus que de 30 % à 50 % de la section inélastique pour le thorium et 15 % pour l'uranium. A plus basses énergies, les différences entre noyaux lourds à faible seuil de fission et les autres noyaux sont encore plus marquées. Bell et Skargard [7]) ont trouvé pour la réaction (p, 4n) sur ^{209}Bi à 38.8 MeV une section efficace de 1220 mb, alors que Glass *et al.* [8]) indiquent 0.8 mb pour (α, 4n) sur ^{239}Pu à 40.7 MeV et Sikkeland *et al.* [9]) 1.2$\pm$mb à 40 MeV pour (α, 4n) sur ^{252}Cf.

Une étude approfondie des réactions de spallation par la détermination des probabilités de formation des divers isotopes produits est possible grâce aux séparations radiochimiques. En isolant chaque élément voisin du noyau cible, on est à même de déterminer ensuite les sections efficaces du plus grand nombre possible d'isotopes de chacun de ces éléments. Il est également intéressant d'examiner par d'autres méthodes l'émission des nucléons et de divers fragments projetés; les deux aspects se complètent.

Les sections efficaces des processus qui conduisent à la projection de tritons, hélions et de fragments plus lourds, comme les noyaux de lithium, beryllium, bore et carbone, ne sont pas négligeables surtout aux énergies supérieures à 300 MeV.

Currie, Libby et Wolfgang [10]) ont trouvé que la formation de tritium par des protons de 450 MeV passe de 7.3 mb dans le carbone, à 71 dans le plomb. Kuznetsov *et al.* [11]) ont étudié cette production pour des énergies de protons de 120 à 660 MeV avec diverses cibles allant de l'aluminium au plomb. Pour ce dernier élément à 120 MeV, ils trouvent 17$\pm$5 mb, résultat précisé par Lefort, Simonoff, Tarrago et Bibron [12]) pour le thorium (à 135 MeV, 19.5$\pm$0.5 mb).

On a pu expliquer au moins une partie du tritium formé par l'évaporation à partir des noyaux résiduels disposant d'une énergie d'excitation de plusieurs centaines de MeV. Aux énergies plus basses, un phénomène d'interaction directe décrit sous les termes de „pick up" et „double pick up" rend compte des sections efficaces relativement élevées et de la distribution anisotrope des tritons[13]). Il est à remarquer également que les sections efficaces de formation de tritium sont comparables à une énergie donnée, pour les éléments fissiles et non fissiles, comme l'ont montré Wade *et al.* [14]) pour l'or, le thorium et l'uranium.

1.1. FRAGMENTS PLUS LOURDS

Un certain nombre de travaux ont été effectués [15]) sur la formation de fragments plus lourds en examinant les traces de ces fragments projetés dans des émulsions nucléaires. Par cette méthode, Perfilov et Ostroumov [16]) ont mesuré la section efficace d'émission de particules alpha d'énergie supérieure à 20 MeV pour le bismuth et le tungstène soumis à des protons de 460 MeV; soit 150 à 160 mb. Deutsch [17]) a étudié la distribution angulaire en énergie de ^{3}He, ^{4}He, $^{6\text{à}9}$Li, $^{8\text{à}12}$Be, et $^{10\text{à}14}$C produits par des protons de 332 MeV sur diverses cibles dont l'or et l'uranium. La détermination de la section efficace de formation de fragments ^{6}He a été faite par une technique très différente puisque la période de ce nucléide est inférieure à la seconde. Rowland et Wolfgang [18]) ont mesuré au compteur proportionnel, la radioactivité de l'hélium gazeux recueilli après bombardement de cibles de plomb par des protons de 1 à 3 GeV. Ils ont trouvé une section efficace considérable de 29 mb.

Le problème de la mesure des fragments produits par spallation peut être abordé d'une tout autre façon. La plupart de ces fragments sont émis avec une énergie suffisante pour provoquer à leur tour sur les noyaux cibles des réactions nucléaires, que l'on qualifie de *secondaires*. Les noyaux excités ainsi formés évaporent un nombre de nucléons qui dépend de l'énergie d'excitation, donc de l'énergie du fragment au moment de la réaction.

En mesurant les sections efficaces de plusieurs réactions secondaires correspondant à des nombres définis de neutrons émis, on peut calculer la section efficace de formation et la distribution en énergie des fragments F, moyennant la connaissance ou l'estimation des fonctions d'éxcitation des réactions (F, n), (F, 2n) . . . (F, xn).

Une telle étude a été menée à bien par Metzger et Miller [19]) en bombardant de l'or par des protons de 380 MeV. Ils ont mesuré les sections efficaces de formation de divers isotopes du thallium, du plomb et du bismuth. Ces produits ne peuvent provenir que de réactions d'hélion, de lithium et de béryllium disposant d'une énergie cinétique suffisante pour pénétrer dans les noyaux d'or. La distribution en énergie de ces fragments est déduite par une étude comparative des sections efficaces des divers isotopes. Metzger et Miller ont pu donner ainsi la section efficace globale de production dans l'or, de particules alpha d'énergie supérieure à 20 MeV. Elle est de 300 mb. Kurchatov *et al.* [20]) ont procédé à une étude semblable des hélions produits à partir du bismuth par des protons de 480 MeV. La mesure des sections efficaces apparentes des isotopes 210 et 211 de l'astate les conduit à une section efficace de formation des fragments alpha (700 mb) beaucoup plus élevée que celle des auteurs précédents. Cette étude a été reprise récemment par Kalkhine et ses collaborateurs [21]) et les valeurs trouvées sont en meilleur accord avec celles de Metzger et Miller [19]). Un travail avec des protons d'énergie plus faible (150 MeV) a été réalisé par Lefort, Simonoff et Tarrago [22]) sur les réactions secondaires induites sur le bismuth et

le thallium. En mesurant les sections efficaces des isotopes 206 à 211 de l'astate, ces auteurs trouvent 60 ± 10 mb pour la section efficace des fragments alpha émis dans le bismuth avec une énergie supérieure à 20 MeV. Elle correspond à 5 % de la section inélastique totale des protons sur le bismuth. Les auteurs ont montré qu'il ne peut s'agir seulement d'un processus d'évaporation et que les fragments alpha sont émis vers l'avant. La section efficace des bérylliums est inférieure à 10^{-3} μb et celle des lithiums est d'environ 20 μb. Ces valeurs sont très faibles et la comparaison avec les résultats de Metzger et Miller montre que la baisse d'énergie des protons incidents de 380 à 150 MeV diminue dans des proportions considérables la production de fragments de béryllium.

Les réactions de spallation sont décrites généralement selon un modèle dû à Serber [23]) que nous avons repris comme base de l'interprétation de nos résultats. Rappelons qu'il consiste en une interaction directe du proton incident avec les nucléons du noyau cible, au cours de laquelle des neutrons et protons „immédiats " peuvent être émis hors du noyau. Les noyaux résultant de cette interaction disposent d'une certaine énergie résiduelle qui est alors répartie statistiquement et provoque l'évaporation de nucléons selon la théorie de Blatt et Weisskopf, de la même façon que pour un noyau composé dans la théorie de Bohr et Mottelson des réactions à plus basse énergie.

L'étude de la spallation du thorium par des protons de 155 MeV et de 82 MeV que nous avons entreprise, a consisté à identifier par méthodes radiochimiques les isotopes 232, 230, 229, 228 et 227 du protactinium, les thoriums 231, 229, 228, 227, 226 et 225, les actiniums 228, 227, 226, 225 et 224 et les radiums 227, 225, 224 et 223, à mesurer leurs sections efficaces absolues. Nous avons ensuite tenté d'interpréter ces résultats en comparant avec les sections efficaces calculées des diverses réactions (p, xn) (p, pxn) (p, 2pxn) et (p, 3pxn). Ce calcul a été mené en trois stades:

1) détermination de la distribution des énergies d'excitation résultant de l'interaction directe,

2) évaluation du nombre moyen de neutrons évaporés pour chaque énergie d'éxcitation,

3) intervention du rapport Γ_n/Γ_f entre la probabilité d'émission de neutron et celle de fission au cours de la chaîne d'évaporation.

Les choix des divers paramètres, en particulier de la section efficace géométrique, de la température nucléaire, des énergies de liaison des neutrons et des valeurs de Γ_n/Γ_f pour chaque isotope, ont été discutés.

Une interprétation très semblable a été publiée tout récemment par Lindner et Turkevich [24]) sur les réactions de spallation de l'uranium et du thorium à 340 MeV.

2. Conditions d'Irradiation, Monitorage, Séparations Chimiques, Mesures des Désintégrations

Le thorium métallique de pureté „nucléaire" a été irradié en feuilles de 0.03 à 0.05 mm d'épaisseur selon les cas. La quantité de thorium 228 contenue était mesurée par son rayonnement alpha.

Par activation aux deutérons de 8 MeV et mesure du fluor 18 formé, on a dosé la proportion d'oxyde de thorium. Elle ne dépassait pas 3 %.

Les irradiations ont été effectuées au synchrocyclotron d'Orsay [25]) par des protons d'énergie nominale de 155 et de 85 MeV, soit en faisceau interne, soit en faisceau externe, selon les circonstances et les nécessités de traitement chimique plus ou moins rapide.

Les cibles reçoivent en réalité, en raison des oscillations radiales des orbites, des protons d'énergies variables. Une estimation grossière indique que l'énergie moyenne serait inférieure de quelque 3 à 4 % à l'énergie correspondant au rayon de stabilité. On a pris 150 ± 5 et 82 ± 3 MeV.

Le monitorage du flux de protons est effectuée selon les procédés classiques en juxtaposant à la cible des lames d'aluminium ou de graphite. Des feuilles de garde de 0.02 mm d'épaisseur arrêtent les produits de fission émis par recul. Hicks, Stevenson et Nervick [26]) ont déterminé avec précision les sections efficaces absolues de la réaction ^{27}Al(p, 3pn)^{24}Na en fonction de l'énergie des protons incidents entre 32 et 350 MeV. Les valeurs de 9.1 mb et de 10.2 mb ont été choisies pour 150 et 80 MeV. Nous avons pensé souhaitable de vérifier ce premier type de monitorage par un second moniteur. La section efficace de la réaction ^{12}C(p, pn)^{11}C a été déterminée avec précision par Crandall *et al.* [27]) à diverses énergies. En adoptant la valeur de 9.1 mb pour le sodium 24, on a trouvé 45 mb $\pm$ 1 pour ^{11}C à 150 MeV. Les auteurs précédents indiquent 42 mb, mais des travaux plus récents [28]) proposent également le chiffre de 45 mb.

Le monitorage par des cibles d'aluminium ne permet guère de descendre à des énergies inférieures à 80 MeV, alors que celle au carbone peut être utilisée jusqu'à des énergies d'environ 30 MeV. Par contre, la courte période de 20.5 min rend plus délicat l'emploi du carbone et introduit des erreurs lorsque l'irradiation dure avec un flux variable quelques dizaines de minutes. Nous avons donc cherché sur les cibles de graphite à déterminer les sections efficaces de formation du béryllium 7 — (^{12}C(p, 3p3n)^{7}Be) — à diverses énergies. Ce moniteur peut être utilisé à partir d'une énergie de 40 MeV; la période de 53.6 jours du ^{7}Be et le rayonnement gamma de 479 keV correspondant à 12 % des désintégrations sont particulièrement commodes. La détermination des sections efficaces a été effectuée par rapport au carbone et à l'aluminium et la fonction d'excitation est représentée par la fig. 1.

Des déterminations récentes ont été faites à des énergies supérieures à 200 MeV par Parish [29]). En dessous de 150 MeV, les valeurs admises sont celles de

Dickson et Randle [30]). Nous avons trouvé, à 155 MeV une section efficace de 10 mb$\pm$0.5 en très bon accord avec celles de de Honda et Lal [31]). Par contre, aux énergies plus faibles notre fonction d'excitation prend des valeurs environ 20 % supérieures à celles de Dickson et Randle.

Alors que les désintégrations de ^{24}Na de période 15 h sont comptées par les électrons β^- ou par le rayonnement de 2.754 MeV, la mesure de ^{11}C est obtenue par les rayons gamma d'annihilation des électrons β^+, et la concordance de trois méthodes aussi différentes nous a paru encourageante.

Les protons induisent sur l'aluminium, outre la formation de ^{24}Na, celle de ^{11}C et de ^{18}F dont on a pu identifier les périodes. Enfin, ^{22}Na est également produit. Sa contribution en désintégrations par minute est inférieure au pour cent.

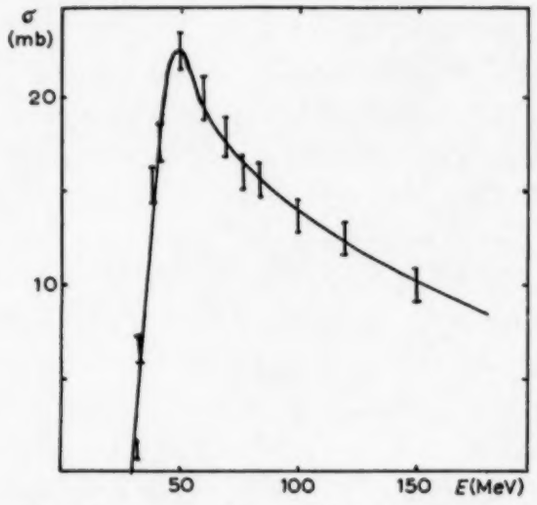

Fig. 1. Fonction d'excitation de la réaction ^{12}C(p, 3p3n)^{7}Be utilisiée pour la monition.

Après irradiation, les cibles étaient attaquées par l'acide nitrique en présence de traces d'acide fluorhydrique et chaque élément était séparé. Les méthodes utilisées pour ces opérations et pour la mesure des rendements chimiques sont décrites par ailleurs [32]) et nous ne rapporterons ici que leurs principes essentiels.

2.1. MESURES DES DÉSINTÉGRATIONS ALPHA

La plupart des isotopes formés par spallation du thorium se désintègrent par émission alpha. Nous avons utilisé pour leur détection et leur mesure plusieurs chambres d'ionisation à collection électronique. Les impulsions sont amplifiées et recueillies sur un sélecteur à multicanaux. Le prototype de ces chambres à boule a été monté initialement par Madame Joliot-Curie et nous ne lui avons apporté que des modifications de détail.

Les conditions de fonctionnement ont été fixées par une étude préalable. Elles correspondent à un remplissage d'argon à 4 kg/cm^2 réduisant le parcours de rayons α de 9 MeV à 23 mm, à des proportions de 3.5 % de CO_2 et une tension négative de 4800 V. Les impulsions délivrées par cette chambre sont comprises

entre 2 et 3 mV et sont amplifiées par un préamplificateur asservi par un bouclage approprié. Une résistance de fuite de 10^8 Ω est utilisée. La valeur limite du taux de comptage est de 3.3×10^5 impulsions par sec. Elle est en pratique réduite surtout par le sélecteur d'amplitude à 100 canaux que nous avons utilisé pour la discrimination des énergies.

Le pouvoir de résolution de l'installation est d'environ 1.4 % pour les sources courantes et préparées rapidement. L'étalonnage en énergie a été effectué avec le polonium 210 et le dépôt actif du thoron (ThC'—ThC).

2.2. MESURES DES DÉSINTÉGRATIONS β^- ET ÉTALONNAGE

Nous avons été amenés à mesurer le nombre de désintégrations par émission β^- de plusieurs isotopes, en particulier pour ^{24}Na formés dans les moniteurs d'aluminium. Le détecteur utilisé était un cristal d'anthracène à fenêtre mince d'aluminium ou un compteur Geiger à fenêtre de 2.4 mg par cm^2.

L'ensemble de comptage comprenait un sélecteur à seuil pour éliminer les impulsions parasites. L'étalonnage de cet ensemble a été effectué avec de grandes précautions avec des sources étalons de ^{24}Na mesurées par comptage absolu avec une chambre à 4π. Un étalonnage de contrôle a été fait avec une source à l'équilibre radioactif de Ra D+Ra E+polonium. Le comptage absolu des désintégrations du polonium était fait au moyen de nos chambres α et le rayonnement β^- d'énergie maximum 1.17 MeV du RaE détecté au scintillateur. Grâce à ce contrôle, les étalonnages *de toutes les mesures et du monitorage* sont ramenés à un seul type d'appareil: la chambre d'ionisation α.

Par ailleurs, nous avons vérifié les mesures par comptage des rayons gamma de 2.754 MeV avec un cristal NaI(Tl.). L'efficacité de ce scintillateur a été mesurée à diverses énergies avec des sources étalons de ^{22}Na, ^{60}Co, ^{137}Cs et de ThC'.

2.3. ÉTALONNAGE POUR LA MESURE DES DÉSINTÉGRATIONS PAR CAPTURE ÉLECTRONIQUE

Le problème de l'étalonnage d'un ensemble de comptage à scintillation dans le but de mesurer le nombre de désintégrations absolues des isotopes du protactinium se désintégrant par capture électronique (e_K) s'est posé au cours de notre travail. Le rayonnement de fluorescence X_K a une énergie de 90 keV. Nous avons cherché une méthode d'étalonnage qui se rattache aux mesures des émissions alpha. Notre choix s'est fixé sur l'astate 211 qui se désintègre avec une période globale de 7.2 h, avec embranchement de 40.9 % en alpha et 59.1 % en capture électronique [33]). Ce mode de désintegration conduit au polonium 211 de 0.52 s de période dont les rayons α ont des énergies de 7.44 MeV (99 %) 6.569 (0.5 %) et 6.895 MeV (0.5 %).

La mesure du nombre absolu de désintégrations était donc faite par le comptage dans 2π des rayons α de ^{211}Po à l'aide de notre chambre à collection électronique et il suffit de comparer au nombre de rayonnements K comptés au scintillateur pour obtenir le facteur d'efficacité de l'ensemble.

Cependant, il faut tenir compte du rendement de fluorescence de 95 % et de la contribution de la capture e_K par rapport aux autres captures.

Les probabilités de capture des électrons des différentes couches dépendent du numéro atomique Z, de l'énergie de la transition $W_0+m_0c^2$ et du degré de d'interdiction de cette transition. Nos mesures correspondent évidemment au réarrangement pour la couche K dans l'atome issu de la désintégration. Pour l'astate 211 l'énergie de la transition est très importante et on peut admettre avec Brysk et Rose [34]) et Hoff et Rasmussen [35]) que 75 % des captures se font sur les électrons de la couche K. Lorsque les énergies de transition sont grandes, on obtient pratiquement le même rapport pour les permises et les interdites d'ordre 1 et même d'ordre supérieur à 1. Nous pensons donc que la proportion (capture e_K)/(capture totale) est de 75 % à 5 % près. Cette incertitude est la plus importante de la méthode et ne pourrait être diminuée par des mesures expérimentales très délicates.

Pour produire l'isotope 211 de l'astate pur, nous avons bombardé des cibles minces de bismuth par des hélions de 30 MeV au cyclotron de Saclay. Dans ces conditions, Kelly et Segré [35]) ont montré que la section efficace de la réaction ^{209}Bi (α, 2n) était maximum et celle conduisant à l'astate 210 pouvait être négligée. Nous avons vérifié qu'il se formait moins de $\frac{1}{100}$ d'astate 210 ou de polonium 210.

Après attaque de la cible de bismuth, on extrayait l'astate par dépôt sur lame d'argent et on suivait la période aussi bien en capture électronique qu'en émission alpha.

Les mesures des photons K ont été faites avec un cristal de INa (Tl) de 2.54 cm de diamètre sur 2.54 cm d'épaisseur, à fenêtre mince d'aluminium. L'installation du scintillateur et du photomultiplicateur était protégée par un château de fer et une gaîne en plexiglass. Les positions de sources étaient repérées par un support monté sur crémaillère. Les spectres étaient analysés sur un sélecteur multicanaux. On a suivi la décroissance pendant plusieurs périodes. Les facteurs d'efficacité trouvés en différentes positions géométriques sont en accord avec les calculs dus à Vegors *et al.* [37]) à 15 % près. Il n'y a pas de variation décelable entre 80 keV et 90 keV, énergies correspondant respectivement aux rayonnements K du polonium et du thorium.

Le facteur d'efficacité a été évalué ainsi à $(1.170\pm0.08)\times10^{-2}$ pour une distance de 50 mm entre la source et la fenêtre du cristal.

Des vérifications ont été obtenues d'une part avec un mélange des deux isotopes 210 et 211 de l'astate produits au synchrocyclotron par spallation du thorium, d'autre part, avec une source étalonnée de mercure 203.

3. Calcul des Sections Efficaces des Divers Isotopes

La section efficace d'un isotope A_Z correspondant à dN_{AZ}/dt désintégrations comptées par unité de temps au moment de la fin de l'irradiation est donnée

par

$$\sigma_{AZ} = \sigma_{Na} \frac{dN_{AZ}}{dN_{Na}} \frac{T_{AZ}}{T_{Na}} \frac{232}{27} \frac{p_{Al}}{p_{Th}}.$$

Il est nécessaire de peser avec précision les cibles de thorium et les moniteurs et de procéder à un alignement rigoureux pour que le flux de protons soit identique.

3.1. PROTACTINIUM

La section efficace absolue de l'isotope 230 a été déterminée par séparation de l'uranium issu de la désintégration β^- de ^{230}Pa selon l'embranchement de 8 % [38]). En effet le rendement d'extraction de l'uranium peut être mesuré avec précision en ajoutant ^{238}U comme entraîneur. La mesure du descendant ^{218}Rn de ^{230}U est la plus commode et précise. L'uranium 232 est obtenu de la même façon (74 ans de période) et donne la σ de ^{232}Pa.

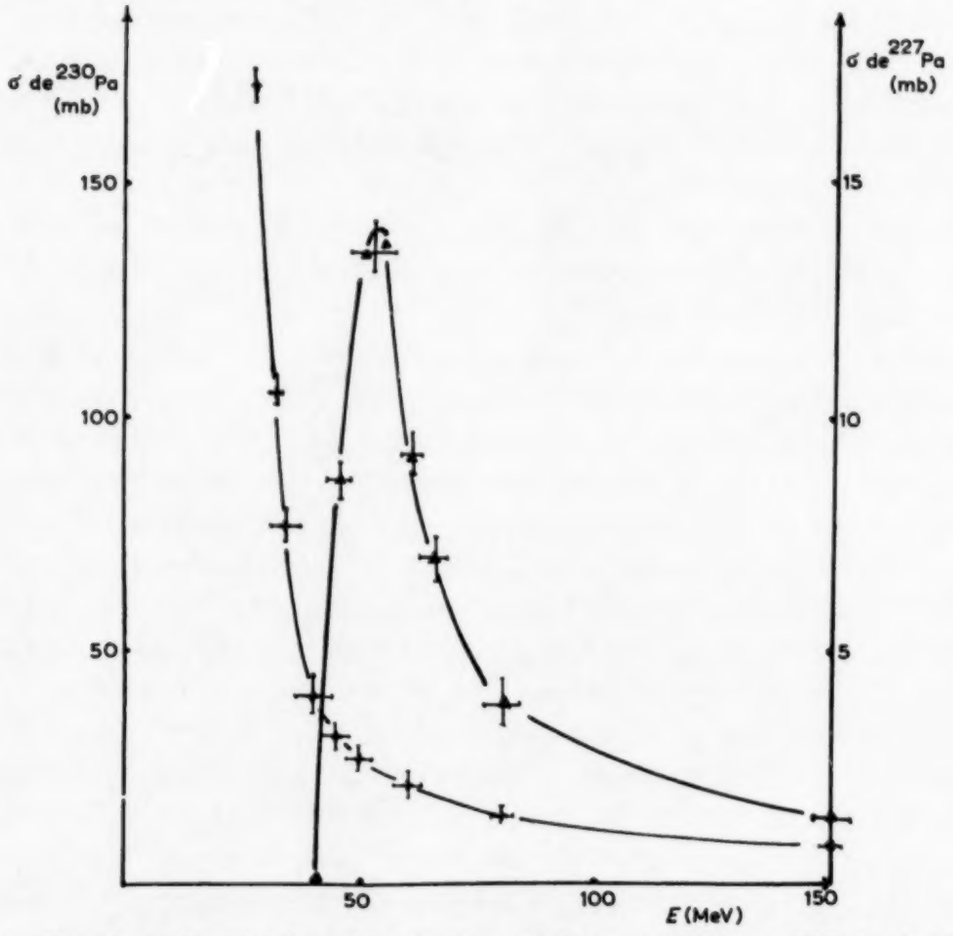

Fig. 2. Fonctions d'excitation des réactions ^{232}Th(p, 3n)^{230}Pa et ^{232}Th(p, 6n)^{227}Pa.

On détermine ensuite les σ relatives de ^{230}Pa et des autres isotopes dans des sources préparées par extraction du protactinium au TTA (thénoyl-trifluorure acétone) sans mesure de rendement.

Le Pa^{227} et ses descendants ^{223}Ac, ^{219}Fr, ^{215}At, ^{211}Bi sont détectés par les pics de 6.46, 6.6, 6.64.

Les trois pics de 6.46 à 6.64 MeV sont comptés ensemble et on a tenu compte de la correction due à l'accumulation de ^{223}Ac et ^{211}Bi et aux embranchements α de 99 % et 99.7 %. L'astate 215 conduit à un pic moins important en raison du temps mort du sélecteur (80 μs à 8 MeV). En effet la période de ^{215}At étant de 10^{-4} s, la particule à α une certaine probabilité d'être émise après celle de ^{219}Fr dans un intervalle de temps inférieur à ce temps mort.

Le ^{228}Pa est compté par le thorium 228 issu de la capture électronique. Le radiothorium est mesuré environ 2 mois après l'irradiation pour que le Rd actinium (227) issu du ^{227}Pa par l'embranchement de 15 % ait entièrement disparu.

Le rapport $^{229}Pa/^{230}Pa$ est mesuré par les désintégrations par capture électronique de l'isotope 229.

Les fonctions d'excitation des réactions (p, 3n) et (p, 6n) qui conduisent à ^{230}Pa et ^{227}Pa ont été étudiées par ailleurs [39]) et nous en avons extrait les valeurs des sections efficaces à 82 MeV dans le but de les comparer aux résultats théoriques. La fig. 2 représente ces deux fonctions d'excitation.

3.2. THORIUM

Le thorium est séparé par extraction par solvant avec le phosphate de tributyle.

La section efficace absolue de l'isotope 226 de 30 min de période est le plus facile à déterminer par les rayons α de 6.33, 6.55, 7.13 et 7.68 MeV.

Le ^{225}Th de période 8 min a un embranchement α de 90 %. Ce sont les rayons α de 6.57 MeV qui permettent la mesure.

Le ^{227}Th (RdAc) est mesuré après décroissance du ^{226}Th sur les rayons α de 5.84 MeV, puis on confirme par l'apparition de l'AcX et ses descendants.

Le ^{228}Th est mesuré plus de 6 mois après l'irradiation par son rayonnement de 5.4 MeV et par celui de 8.78 du ThC'. Il y a lieu de corriger du radiothorium naturel existant dans la cible avant irradiation.

Le ^{228}Th émet des rayons α de 4.9 MeV (7.400 ans). Il est mesuré sur une source de 2 ans d'âge.

Enfin, le ^{231}Th a été mesuré par ses rayonnements β^-. Les conditions d'étalonnage ne sont qu'approximatives et la marge d'incertitude est importante.

3.3. ACTINIUM

Les actiniums sont comptés sur le résidu de la solution d'attaque après prélèvement des Pa, Th, Ra, décroissance des franciums et volatilisation de Po, At et Rn. Il ne subsiste donc aucun émetteur α n'appartenant pas à Ac.

L' ^{226}Ac donne par désintégration β^- (80 %) ^{226}Th. On mesure les rayons α de son descendant ^{218}Rn (7.13 MeV).

L' ^{224}Ac conduit avec une période de 2.9 h au ThX (90 %) et on mesure 5 jours après la séparation le pic de 6.77 MeV (^{216}Po) du descendant du ThX.

L' ^{225}Ac est identifié 15 jours après l'irradiation par le rayonnement α de 5.8 MeV (période de 10 jours).

L' ^{228}Ac par désintégration β^- avec 6.13 h de période conduit au radiothorium que l'on mesure deux mois plus tard.

L' ^{227}Ac décroît avec une période de 22 ans par désintégration β^-. Le Thorium 227 obtenu et ses descendants peuvent être mesurés environ six mois après l'irradiation et on remonte par le calcul au σ Actinium 227.

3.4. RADIUM

Le radium est séparé après addition de baryum comme entraîneur et précipitation du chlorure.

Le ^{227}Ra est suivi par son rayonnement β de spectre voisin de celui du sodium 24.

Le ^{224}Ra (ThX) est suivi selon la période de 3.64 jours sur le pic d'énergie 6.282 MeV du descendant thoron.

Le ^{223}Ra (AcX) est mesuré par le rayonnement de 7.36 MeV dû au descendant Ac A(^{215}Po).

Le ^{225}Ra donne par radioactivité β^- ^{225}Ac identifiable 20 jours après la séparation.

Le ^{228}Ra ($MsTh_1$) décroît avec une période de 6.7 ans et conduit au radiothorium. Sur des sources préparées plus d'un an auparavant, on mesure ce dernier et on calcule la section efficace du Ms Th_1. On trouvera par ailleurs [32]) les détails des séparations chimiques, des mesures, de l'observation des décroissances, des corrections et des calculs pour les différentes filiations.

3.5. VALEURS DES SECTIONS EFFICACES

Les résultats que nous avons obtenus sont rassemblés dans le tableau 1.

Les marges d'erreur indiquées correspondent à l'estimation des incertitudes. Parmi celles-ci, certaines sont systématiques. Elles ne sont pas à considérer dans une étude de comparaison des sections efficaces entre elles. Ce sont les imprécisions du monitorage évaluées à 5 % (erreur de comptage, d'étalonnage et incertitude sur la section efficace absolue du sodium 24).

Les autres incertitudes, par contre, dépendent des conditions précises de détermination d'une section efficace absolue particulière et varient beaucoup selon tel ou tel isotope formé.

Elles comprennent entre autres, d'abord, les conditions de préparation et d'irradiation de la cible. Les pesées, l'alignement des surfaces, l'uniformité des épaisseurs introduisent une erreur comprise entre 3 et 6 %.

Ensuite interviennent les particularités de la séparation chimique dont l'importance est grande pour la détermination avec une plus ou moins bonne

précision du rendement d'extraction. Celui-ci est obtenu, suivant les cas, avec une marge d'erreur comprise entre 5 et 15 %.

TABLEAU 1

Sections efficaces expérimentales

Réactions		Produit		Section efficace (mb)	
		Élément	A	150 MeV	82 MeV
(p, xn)	(p, n)	$_{91}$Pa	232	8.0 ± 1	13 ± 2
	(p, 3n)		230	7.5 ± 1	12 ± 2
	(p, 4n)		229	5.0 ± 1.5	
	(p, 5n)		228	3.25± 0.50	9 ± 1
	(p, 6n)		227	1.5 ± 0.2	3.2± 0.5
(p, pxn)	(p, pn)	$_{90}$Th	231	100 ±20	160 ±30
	(p, p3n)		229	41 ± 8	
	(p, p4n)		228	44 ± 6	54 ± 8
	(p, p5n)		227	34 ± 4	38 ± 6
	(p, p6n)		226	24 ± 3	30 ± 5
	(p, 7n)		225	18 ± 3	< 10
(p, 2pxn)	(p, 2p3n)	$_{89}$Ac	228	15 ±2	
	(p, 2p4n)		227	14 ±2	
	(p, 2p5n)		226	15 ±2	
	(p, 2p6n)		225	14 ±2	
	(p, 2p7n)		224	11 ±1.5	
(p, 3pxn)	(p, 3p2n)	$_{88}$Ra	228	2.1±0.4	
	(p, 3p3n)		227	2.3±0.5	
	(p, 3p5n)		225	2.4±0.5	
	(p, 3p6n)		224	2.5±0.5	
	(p, 3p7n)		223	2.1±0.3	

Enfin, entre en ligne de compte la nature du comptage des désintégrations. Les mesures les plus précises (à 2 % près) sont celles des rayonnements alpha. Le comptage des désintégrations β^- est moins précis à cause de l'étalonnage préalable avec émetteur β^- de même spectre d'énergies ou de spectre d'énergies voisin. La marge d'erreur varie alors entre 5 et 10 %. Dans le cas des mesures de désintégrations par capture électronique, l'imprécision est aggravée par la connaissance souvent approximative des schémas de désintégration, ce qui conduit à une marge d'erreur pouvant atteindre 20 %.

La marge d'erreur totale sur une section efficace est la somme des marges d'erreurs partielles indiquées. Elle varie entre 10 % dans les cas les plus favorables à 45 % dans les conditions les plus mauvaises.

Il est à noter cependant que les marges d'erreurs sont réduites par plusieurs déterminations successives de la section efficace. Nous avons refait plusieurs fois les expériences concernant les isotopes dont la section efficace est mesurée

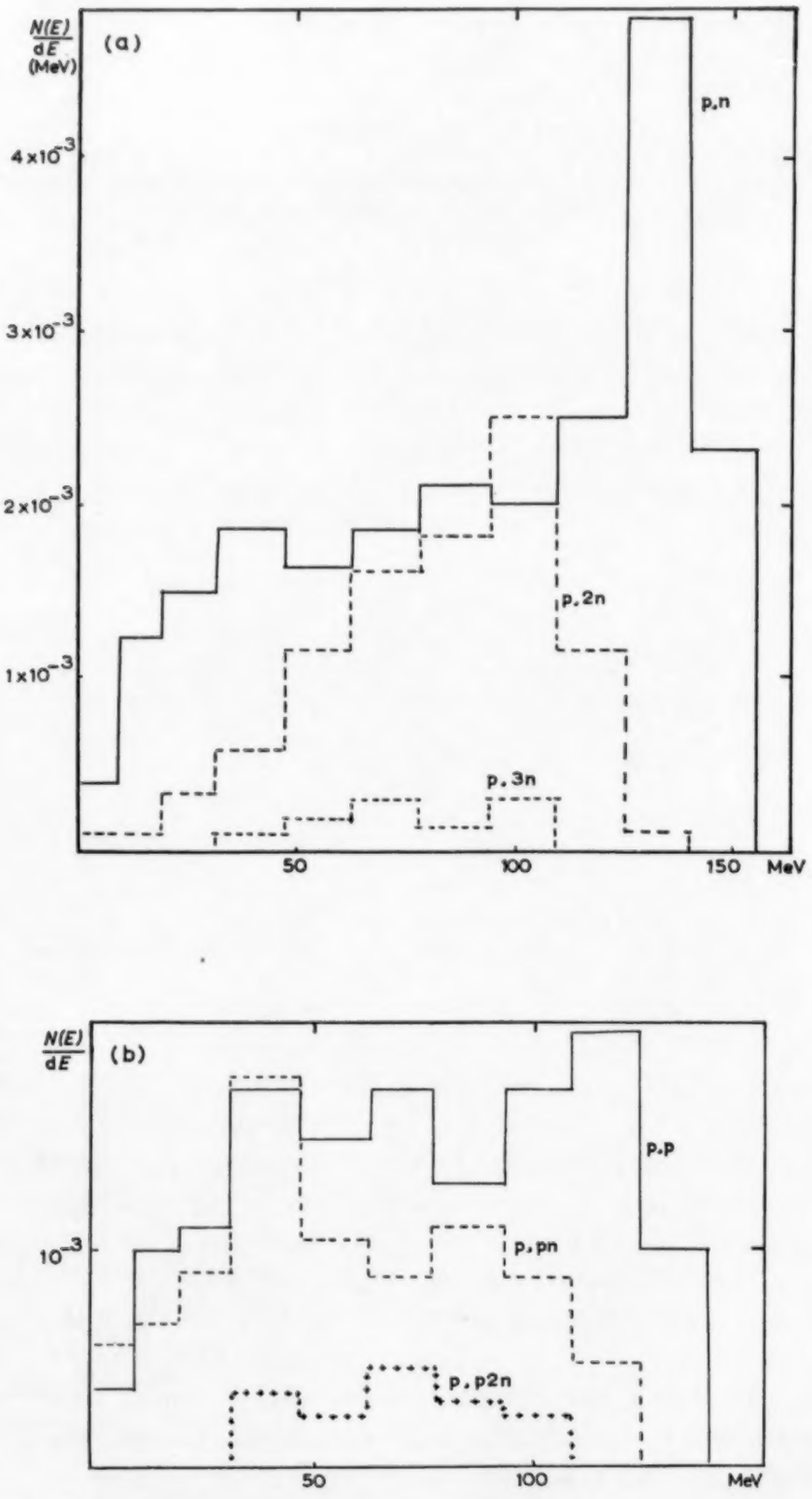

Fig. 3. Fonctions de distribution des énergies d'excitation des noyaux résiduels pour des protons incidents de 150 MeV ($N(E)/\mathrm{d}E$ en millièmes par MeV). (a) Cascades (p, n) (p, 2n) (p, 3n). (b) Cascades (p, p) (p, pn) (p, 2n).

avec une marge d'erreur importante. Celle-ci a pu alors être réduite en appliquant la méthode des moindres carrés.

Dans les premières déterminations [40]) nous avions commis une erreur de monition due à l'insuffisance des feuilles de garde contre le recul des produits de fission. Leur radioactivité β^- avait une période globale voisine des 15 h du sodium 24 servant à la monition, de sorte que le comptage de ce dernier dans les moniteurs d'aluminium était entaché d'une erreur.

4. Interprétation

Les valeurs des sections efficaces de formation des divers isotopes que nous avons mesurées peuvent être comparées aux valeurs calculées des probabilités des réactions nucléaires correspondantes (p, N, xn), (p, P, xn) etc. Nous avons suivi le modèle d'interaction décrit par Serber, en tenant compte de la désexcitation par fission qui entre en compétition avec l'evaporation de neutrons pour des noyaux de rapport Z^2/A élevé. Les principales étapes du calcul sont connues et seront rappelées brièvement.

4.1. INTERACTION DIRECTE

Les protons incidents cèdent leur énergie aux nucléons au cours de chocs individuels. Les transferts de moment sont relativement faibles et les cascades

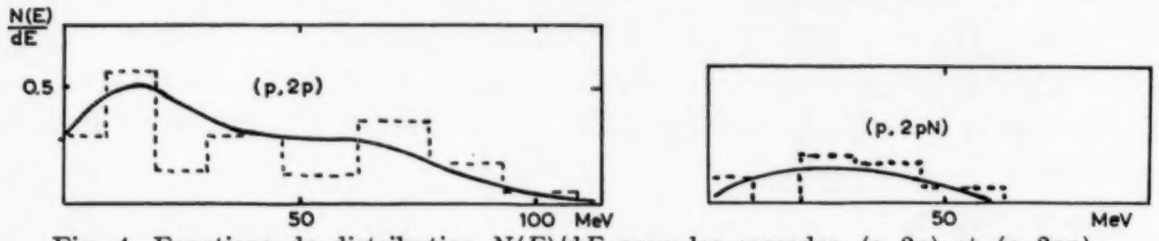

Fig. 4. Fonctions de distribution $N(E)/\mathrm{d}E$ pour les cascades (p, 2p) et (p, 2pn).

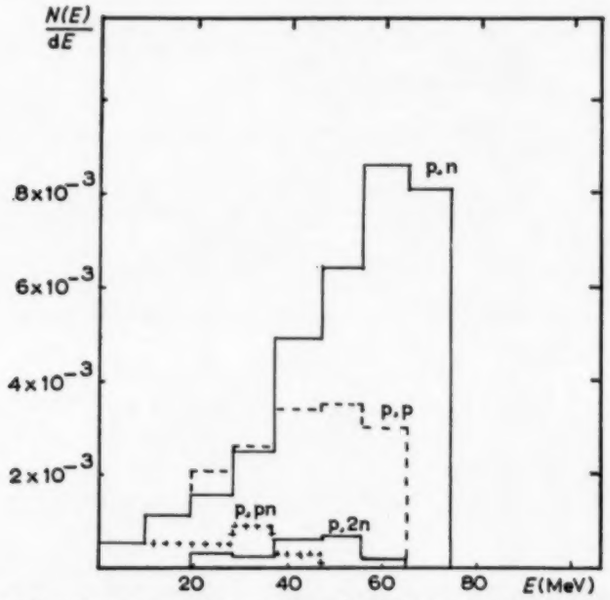

Fig. 5. Fonctions de distribution pour des protons incidents de 82 MeV pour les cascades (p, n), (p, 2n), (p, p) et (p, pn) ($N(E)/\mathrm{d}E$ en millièmes par MeV).

de chocs successifs conduisent à l'émission de neutrons et de protons „immédiats". On sait que par des calculs de hasard dits de „Monte Carle", Metropolis *et al.* [41]) ont déterminé les probabilités d'émission de 1, 2 . . . i protons et de 1, 2 . . . i neutrons par événement. G. Friedlander [42]) nous a communiqué les résultats obtenus pour 1133 événements provoqués par des protons de 150 MeV sur des noyaux d'uranium 238, sur chaque type de cascade (p, N), (p, P), (p, 2N), (p, PN) etc. Nous avons construit les fonctions de distribution des énergies d'excitation résiduelles pour chaque type deréaction immédiate (fig. 3). Cependant, les données relatives aux réactions conduisant à l'actinium (p, 2P et p, 2PN) et au radium (p, 3P) étaient fournies pour un nombre d'événements relativement restreint. Nous avons remplacé les plateaux discontinus des fonctions de distribution par des courbes continues pour compenser dans une certaine mesure les écarts statistiques (fig. 4).

Les fonctions de distribution des énergies d'excitation ont été tracées également pour une énergie de protons incidents de 82 MeV (fig. 5). Les principales caractéristiques utilisées pour ces calculs sont la section géométrique de 2.10 b ($r_0 = 1.3$ fm), l'énergie moyenne de liaison du nucléon le moins lié 6.1 MeV, l'énergie de séparation du proton de 50.9 MeV. Compte tenu de la transparence du noyau, la section inélastique à 150 MeV est de 1.95 b et à 82 MeV de 1.98 b.

4.2. ÉVAPORATION À PARTIR DES NUCLÉIDES D'ÉNERGIE D'EXCITATION E^*

Il est possible de calculer le nombre moyen de neutrons évaporés au cours de la désexcitation d'un noyau disposant d'une énergie E^*. Le spectre d'énergie des neutrons a la forme classique

$$\int_0^{\varepsilon_{max}} C\varepsilon e^{-\varepsilon/T} d\varepsilon = 1,$$

où ε est l'énergie cinétique des neutrons et T la température nucléaire. Jackson [43]) a montré que la probabilité $R(E_j^*, j)$ d'évaporation de j neutrons pour une énergie d'excitation E_j^*, pouvait être obtenue par la formule de récurrence

$$R(E_j^*, j) = I(\Delta_j, 2j-3) - I(\Delta_{j+1}, 2j-1),$$

où $\Delta_j = (E - B_1 - B_2 - \ldots - B_j)/T$, la quantité B_j étant l'énergie de liaison du $j^{ème}$ neutron, et I est une fonction gamma incomplète

$$I(Z, n) = \frac{1}{n!} \int_0^Z y^n e^{-y} dy.$$

On peut en effet montrer que la probabilité d'émission d'au moins j neutrons est égale à

$$P(E, j) = 1 - e^{-\Delta_j} \sum_0^{2j-3} \frac{\Delta_j^a}{a!},$$

et que la probabilité d'émettre exactement j neutrons est égale à la différence entre la probabilité d'évaporation d'au moins j neutrons et celle d'évaporer au moins $j+1$,

$$R(E^*, j) = e^{-\Delta_j} \sum_{0}^{2j-3} \frac{\Delta_j{}^a}{a!} - e^{-\Delta_{j+1}} \sum_{0}^{2j-1} \frac{\Delta_{j+1}^a}{a!},$$

a variant selon le terme de 0 à $2j-3$ ou de 0 à $2j-1$.

Nous avons tracé les courbes de variation de $R(E_j)$ en fonction de l'énergie d'excitation en calculant, à l'aide d'une machine I.B.M. 650, les valeurs R pour toutes les valeurs de Δ_j de MeV en MeV.

Les Δ_j sont obtenues à partir d'une température nucléaire T_j dépendant elle-même de l'énergie d'excitation E^* dont le choix sera indiqué plus loin.

Nous avons également tenu compte de l'énergie de liaison B_n pour chaque noyaa au cours de l'évaporation.

4.2. CHOIX DES ÉNERGIES DE LIAISON ET DE LA TEMPÉRATURE NUCLÉAIRE

Les valeurs des énergies de liaison des neutrons pour les noyaux lourds ont été publiées par Foreman et Seaborg (45). Le choix de T, température nucléaire, est plus délicat. Celle-ci influence notablement les valeurs des Δ_j, c'est-à-dire l'étalement des courbes de probabilité.

La théorie statistique de Blatt et Weisskopf [46]) prévoit que la densité de niveaux a, la température nucléaire T et l'énergie d'excitation E^*, sont liées par une fonction monotone $E^* = aT^\delta$, où δ est égal à 2 dans le cas de l'approximation du gaz de Fermi. Des précisions sur les valeurs de a ont été apportées par diverses études expérimentales, soit sur les spectres de neutrons [47–49]), soit sur les noyaux excités par ions multichargés [50]), soit sur la diffusion inélastique des neutrons [51]), Fong [52]) a calculé pour une série de noyaux les valeurs de a et trouve que l'accord le plus satisfaisant correspond à $a = \frac{1}{20}A$. Cette valeur a été utilisée par Dostrowsky *et al.* [53]) dans leur calcul d'évaporation par la méthode de Monte Carlo.

Nous avons finalement conservé la valeur $a = \frac{1}{19}A$ voisine de la précédente et déduite initialement par Blatt et Weisskopf [46]) de données sur la capture de neutrons lents. Pour le tracé des courbes d'évaporation, la température a été choisie d'après la formule ci-dessus appliquée au noyau de thorium 232, soit $T = 0.28\sqrt{E^*}$. Pour l'émission de j neutrons, nous avons pris une seule valeur de la température T_j correspondant à tout l'intervalle d'énergie au cours duquel la fonction $P(E^*, j)$ varie entre 0 et 1. De même pour $j+1$ neutrons on a pris T_{j+1} de sorte que nous avons introduit une variation discontinue de T en fonction de E^*. Les valeurs de E^* utilisées pour le calcul de chacune des valeurs de T ont été obtenues à l'avance en utilisant l'approximation de Jackson [44]) relative à l'énergie moyenne $\bar{E}_j{}^*$, énergie pour laquelle la probabilité d'émission

de j neutrons est la plus élevée,

$$\bar{E}_j^* = j(B+2T)\frac{B^2-2T^2}{2(B+2T)},$$

avec B constant et T égal à 1.9 MeV. Même si les maxima des fonctions $R(E, j)$ réelles ne sont pas tout à fait égaux à ces valeurs $\bar{E}_j^*$ ainsi obtenues, l'erreur introduite sur $T_j = 0.28\sqrt{\bar{E}_j^*}$ est insignifiante.

4.4. CONDUITE DES CALCULS

Pour connaître la probabilité $P(x, y, j)$ d'une cascade (p, xp yn) suivie de l'évaporation de j neutrons, il faut multiplier la probabilité partielle d'évaporation de j neutrons $R(E^*, j)$ par la probabilité $Q(E^*, xy)$ de formation par interaction directe d'un noyau disposant d'une énergie d'excitation E^*, puis sommer sur tout l'intervalle d'énergie pour lequel la probabilité d'évaporation n'est pas nulle:

$$P_{(j)} = \int Q(E, xy)R(E^*, j)\mathrm{d}E.$$

La même opération doit être faite pour chaque valeur de y puisqu'un isotope peut être obtenu à la fois par une réaction (p, xp yn jn) et par une réaction (p, xp $(y+1)$ n$(j-1)$n).

En pratique, nous disposions d'une part de valeurs $\bar{q}(\Delta E, x, y)$ pour des intervalles d'énergie ΔE de 9 à 15 MeV fournies par Friedlander, d'autre part, des courbes d'évaporation $R(E^*, j)$ construite de MeV en MeV à la machine I.B.M. Nous avons tracé des portions de droite aussi voisines que possibles de ces courbes (écart 1 % au maximum) le long desquelles on peut définir une probabilité moyenne d'évaporation $\bar{r}(\Delta E, j)$. Au lieu de l'intégrale, nous avons effectué la somme des probabilités pour chaque petit intervalle dans lequel q est constante:

$$\sum \bar{q}(\Delta E, x, y)\bar{r}(\Delta E, j).$$

On obtient ainsi, avec une bonne statistique pour q, la probabilité d'émission de $(y+j)$ neutrons en répétant l'opération pour chaque type de cascade avec $y = 1$, $y = 2$ et $y = 3$. En multipliant par la section efficace géométrique $\sigma_g = 2.1$ b, on obtient les résultats indiqués dans le tableau 2.

Il faut remarquer que les valeurs ainsi trouvées ne sont qu'approximatives. En effet, au cours du calcul par la méthode de Monte Carlo, le nombre d'événements considérés n'est pas très grand (environ 1000) et les écarts statistiques sur le nombre n de noyaux résiduels disposant d'une énergie E placée dans un intervalle ΔE (de 9 à 15 MeV), sont importants. En prenant $\sqrt{n}$ comme erreur possible, on a trouvé une imprécision d'environ 20 % pour les réactions (p, xn), 30 % pour les réactions (p, pxn) et 50 % pour les isotopes de l'actinium.

TABLEAU 2

Calcul des sections efficaces d'après le modèle Serber-Jackson

Réaction	Nombre de neutrons	Masse atomique	Section efficace (mb)	
			150 MeV	82 MeV
(p, xn) $_{91}$Pa	1	232	4.5	7
	2	231	19	23
	3	230	27	38
	4	229	46	80
	5	228	50	155
	6	227	70	240
	7	226	90	210
	8	225	120	70
	9	224	130	5
	10	223	160	
	11	222	180	
	12	221	135	
	13	220	100	
	14	219	50	
(p, pxn) $_{90}$Th	0	232	4	7
	1	231	23	25
	2	230	38	60
	3	229	46	70
	4	228	80	110
	5	227	80	80
	6	226	85	35
	7	225	70	3
	8	224	95	
	9	223	85	
	10	222	65	
	11	221	25	
	12	220	7	
	13	219	0.5	
(p, 2pxn) $_{89}$Ac	0	231	4.0	
	1	230	9.0	
	2	229	9.0	
	3	228	8.0	
	4	227	9.0	
	5	226	7.5	
	6	225	8	
	7	224	7.0	
	8	223	3.0	
	9	222	1.0	
	10	221	0.3	
	11	220	0.05	
(p, 3pxn) $_{88}$Ra	2	228	0.61	
	3	227	1.04	
	4	226	1.04	
	5	225	1.04	
	6	224	1.04	
	7	223	0.42	

4.5. COMPÉTITION FISSION-ÉVAPORATION

Pour étendre le mode de calcul de Jackson aux noyaux fissiles, Vandenbosch et Seaborg [54]) ont introduit deux modifications. La première tient compte de ce que le seuil de fission peut être inférieur à l'énergie de liaison des neutrons dans certains noyaux lourds et que, par conséquent, les noyaux résiduels d'énergie d'excitation supérieure à celle du seuil de fission et insuffisante pour l'évaporation se désexciteront par fission. Cette éventualité n'est guère à envisager dans le cas des noyaux de protactinium et de thorium qui font l'objet de notre étude, B_f étant généralement supérieure à B_n de 0.5 à 2 MeV. Par exemple, pour ^{232}Th, on a $B_f = 6.9$ MeV et $B_n = 4.9$ MeV. La deuxième modification essentielle consiste à incorporer la compétition de la fission à chaque stated de l'évaporation, ce qui est justifié par divers travaux dont ceux de Pate [55]), selon lesquels la fission a lieu selon un processus d'égal déplacement des charges. En appelant Γ_n et Γ_f les largeurs d'évaporation et de fission, on peut écrire la probabilité $R'_f(E^*, j)$ d'émission de j neutrons, compte tenu de la fission,

$$R'_f(E^*, j) = R(E^*, j)\left(\frac{\Gamma_{n1}}{\Gamma_{n1}+\Gamma_{f1}}\frac{\Gamma_{n2}}{\Gamma_{n2}+\Gamma_{f2}}\cdots\frac{\Gamma_{n\,j-1}}{\Gamma_{n\,j-1}+\Gamma_{f\,j-1}}\right).$$

Par conséquent, la connaissance des rapports Γ_{nj}/Γ_{fj} tout le long de l'évaporation est nécessaire à la détermination de la section efficace du noyau résiduel désexcité.

Diverses données existent sur les rapports Γ_n/Γ_f à basse énergie. Elles ont été obtenues par des mesures de section efficace de fission, soit par des neutrons [56]) de quelques MeV, doit par des photons [57]).

A plus haute énergie, ce sont surtout Vandenbosch, Seaborg et leurs collaborateurs d'une part [58]), Tarantine *et al.* [59, 60]) de l'autre, qui ont précisé les rapports Γ_n/Γ_f de nombreux nucléides en bombardant par des ions multichargés des hélions ou des deutons des cibles de thorium, uranium et plutonium.

Le principe de la méthode consiste à mesurer les sections efficaces des réactions (α, 4n) (α, 3n) (α, 2n) et (α, n) et à les comparer aux valeurs calculées d'après la théorie de l'évaporation à partir du noyau composé. On obtient un rapport moyen $\overline{\Gamma_n/(\Gamma_n+\Gamma_f)}$ pour un noyau de nombre de masse placé à mi-chemin entre le noyau comparé et le noyau résiduel.

Si la section efficace calculée sans fission est $\sigma_c R(E^*, j)$ et la section efficace mesurée $\sigma(A, j)$, on écrit

$$\sigma(A, j) = \overline{\left(\frac{\Gamma_n}{\Gamma_n+\Gamma_f}\right)^j} R(E^*, j)\sigma_c.$$

Le tableau 3 résume les données qui nous intéressent et qui ont été obtenues, soit par photofission, soit à plus grande énergie.

L'examen de ce tableau et de divers autres résultats montre que les rapports Γ_n/Γ_f ne semblent pas varier considérablement lorsque l'énergie d'excitation des noyaux est augmentée. Par exemple, le rapport $\overline{(\Gamma_n/\Gamma_f)}$ moyen obtenu d'après la réaction (α, 4n) sur le thorium correspond au noyau ^{234,5}U. On trouve 0.92. D'après les sections efficaces de fission par neutrons de 3 MeV sur les isotopes 233 et 234, on peut extrapoler une valeur de 1.0 très voisine de la précédente.

Vandenbosch et Huizenga [61]) ont porté les rapports Γ_n/Γ_f en fonction de A pour divers éléments et ils ont obtenu des droites sensiblement parallèles pour Z

TABLEAU 3

Résumé des réactions de fissions

Noyau cible	Réaction	Noyau fissionnant	$\overline{\Gamma_n/\Gamma_f}$
^{226}Ra	(n, f)	^{227}Ra	10^4
^{226}Ra	(α, 4nf)	^{228,5}Th	4.2
^{230}Th	(γ, f)	^{230}Th	4.9
^{232}Th	(γ, f)	^{232}Th	12
^{232}Th	(n, f)	^{233}Th	24.3
^{232}Th	(p, 3n)	^{232}Pa	2.2
^{231}Pa	(n, f)	^{232}Pa	1.85
^{230}Th	(α, 4n)	^{232,5}U	0.5
^{233}U	(n, f)	^{234}U	0.85
^{234}U	(n, f)	^{235}U	1.17

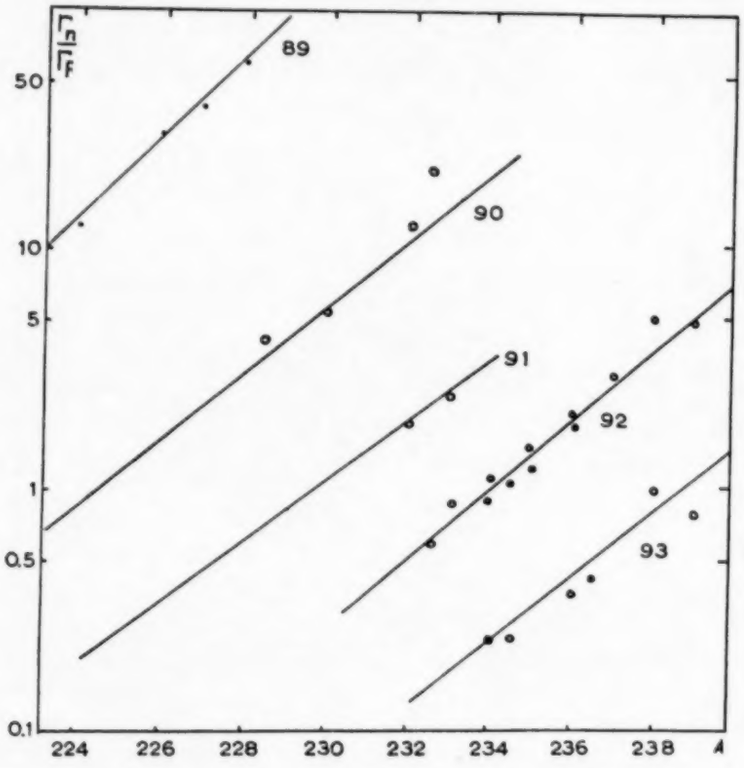

Fig. 6. Rapports Γ_n/Γ_f de largeur d'émission de neutron à largeur de fission.

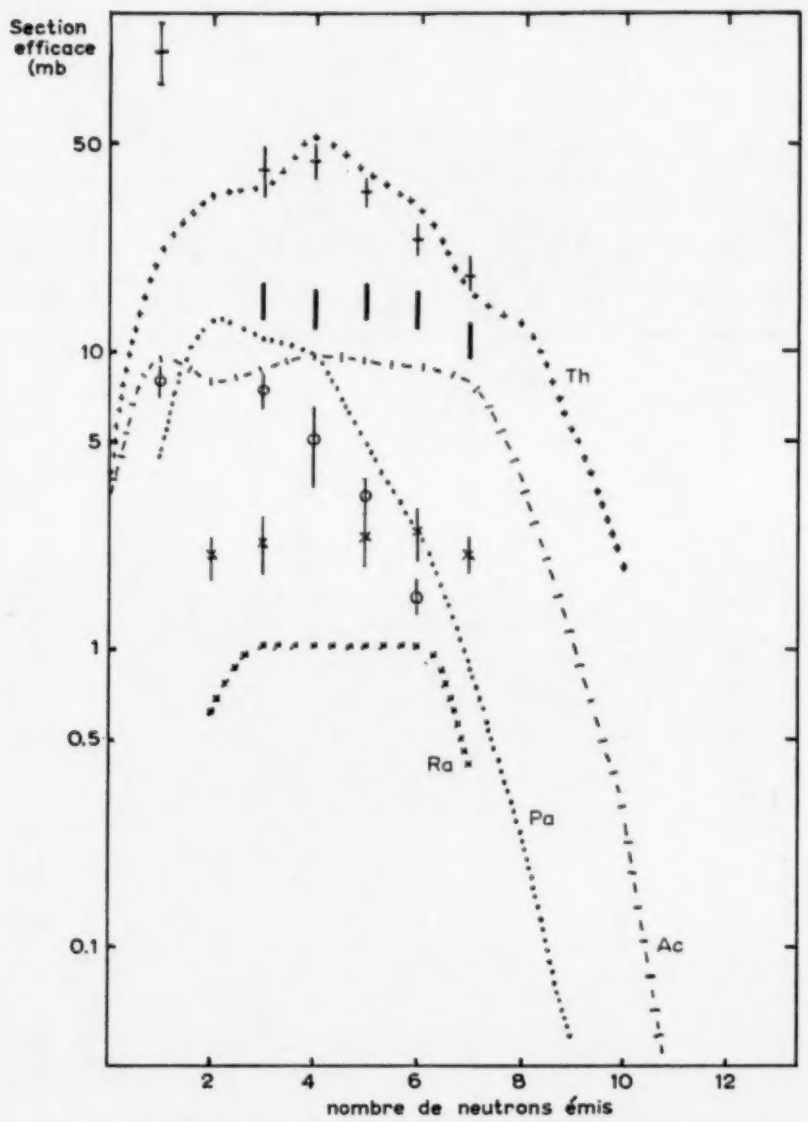

Fig. 7. Sections efficaces des réactions de spallation sur le thorium, en fonction du nombre de neutrons émis x pour des protons incidents 150 MeV.

Réaction	$\sigma_{expérimentale}$	$\sigma_{calculée}$
Pa(p, xn)	⊥○⊥	-·-·-·-·-·-·-·-·-·-
Th(p, pxn)	⊥+⊥	−+−+−+−+−+
Ac(p, 2pxn)	⊥|⊥	|−|−|−|−|−|−|−|
Ra(p, 3pxn)	⊥×⊥	×−×−×−×−×−

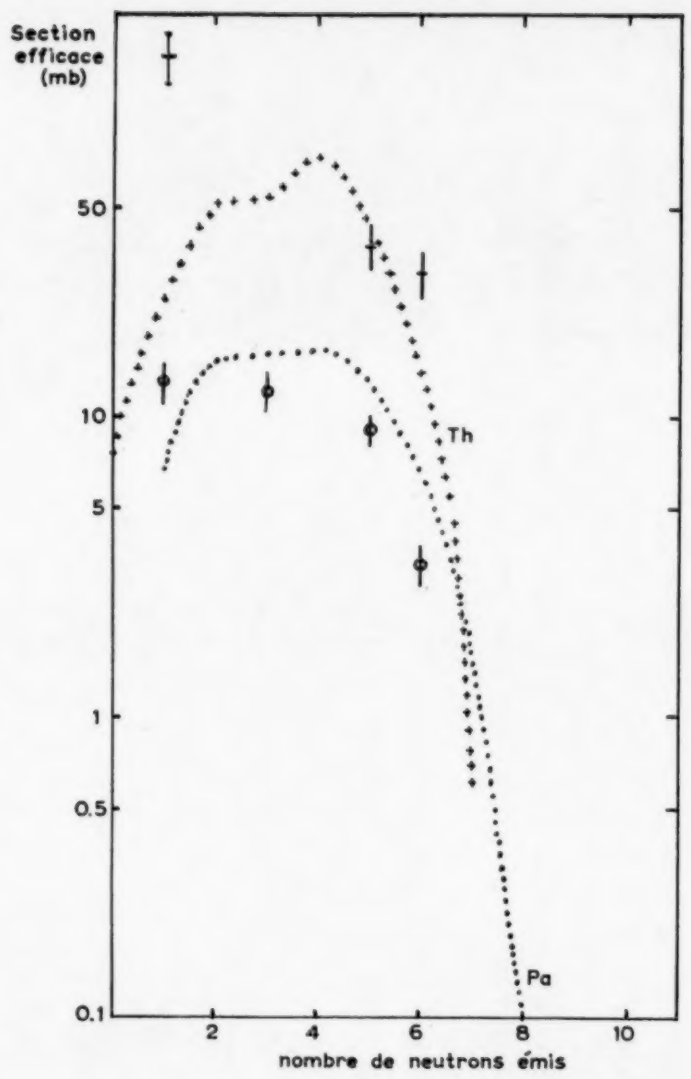

Fig. 8. Sections efficaces en fonction du nombre de neutrons émis pour des protons incidents 82 MeV (Pa et Th).

allant de 90 à 100 et A compris entre 228 et 256. Nous avons calculé les rapports d'après la formule de Fujimoto et Yamaguchi [62])

$$\frac{\Gamma_n}{\Gamma_f} = \tfrac{1}{10} T A^{\frac{2}{3}} \exp \frac{B_f - B_n}{T}$$

et extrapolé les droites vers les faibles A en particulier pour le thorium et l'actinium. Il ne semble pas que des différences importantes apparaissent entre les noyaux pairs et ceux de masse impaire car, comme l'a fait remarquer Huizenga, l'énergie de liaison des neutrons plus grands pour les premiers est compensée par une plus grande tendance à l'évaporation en raison de la densité de niveau plus élevée du descendant de masse impaire.

En portant les valeurs de Γ_n/Γ_f de la fig. 6 à chaque stade des calculs d'évaporation précédemment décrits, on a obtenu les valeurs des sections efficaces représentées par la fig. 7. L'influence de la fission est négligeable pour les actiniums et radiums. Pour les réactions induites par des protons de 82 MeV, nous n'avons des résultats que pour les protactinium et thoriums, comme on peut le voir sur la fig. 8.

Lindner et Turkevich [24]) ont procédé d'une manière analogue pour interpréter les résultats obtenus par Lindner et Osborne [5]) avec des protons de 340 MeV, au cours d'une étude publiée pendant que nous effectuions ce travail.

5. Comparaison avec l'Expérience

L'examen des figures 7 et 8 sur lesquelles sont rassemblés à la fois les résultats expérimentaux et les valeurs calculées appelle quelques remarques.

5.1. LES ISOTOPES DU PROTACTINIUM

Les valeurs calculées pour les isotopes du protactinium (réactions p, xn) sont supérieures de 30 à 40 % aux résultats expérimentaux. Il faut toutefois remarquer qu'il existe quelque incertitude d'une part, comme on l'a déjà indiqué, sur les données calculées, d'autre part, sur les rapports Γ_n/Γ_f. On peut cependant penser que la différence systématique observée a une signification. Une des raisons pourrait être l'évaporation de protons qui diminuerait les sections efficaces des protactiniums. Le spectre d'énergie des protons peut s'écrire d'après Le Couteur [63])

$$P(\varepsilon)\,\mathrm{d}\varepsilon = \frac{1}{T^2}(\varepsilon - V)\mathrm{e}^{-\frac{\varepsilon - V}{T}}\,\mathrm{d}\varepsilon,$$

où V serait la barrière de potentiel pour les protons. Pour un tel spectre, l'énergie médiane est égale à $\varepsilon_m = V + 1.7T$, au lieu de $1.7T$ pour les neutrons. En tenant compte de la pénétrabilité, on peut raisonnablement prendre une valeur de V comprise entre 7 et 8 MeV pour le thorium. Avec une température

nucléaire de 1.9 MeV, on obtient ainsi une énergie médiane de 11 MeV au lieu de 3.20 pour les neutrons. Si l'on suppose que le rapport du nombre de neutrons au nombre de protons évaporés est égal au rapport du nombre de neutrons disposant de l'énergie de 3.2 MeV au nombre de protons de 11 MeV, la distribution des énergies des nucléons d'un gaz de Fermi dégénéré étant

$$P(\varepsilon)\,\mathrm{d}\varepsilon = \frac{\sqrt{\varepsilon}}{T^2}\,\mathrm{e}^{-\varepsilon/T}\,\mathrm{d}\varepsilon,$$

le rapport n/p devient

$$\frac{A-Z}{Z}\,\frac{\sqrt{3}}{\sqrt{11}}\,\frac{\mathrm{e}^{-3/T}}{\mathrm{e}^{-11/T}} = 57.$$

La proportion de protons est, comme on le voit, d'environ 2 %. Cette estimation est assez voisine de celle de Dostrovsky *et al.* [64]), effectuée grâce à des calculs de Monte Carlo sur les noyaux d'or bombardés par des protons de 190 MeV. Les résultats indiquent 12.3 protons d'évaporation pour 980 neutrons. Même si l'on suppose que l'émission d'un proton est suivie de l'évaporation de plusieurs neutrons pour une réaction particulière, la proportion des réactions (p, pxn) d'évaporation ne peut guère dépasser quelques 10 % de celle des réactions (p, (x+1)n).

Metropolis *et al.* [41]) ont suggéré que l'écart entre valeurs théoriques et expérimentales pour ce type de réactions pourrait être dû à l'utilisation du modèle nucléaire compact ne tenant pas compte d'une moindre densité des nucléons à la surface. Diverses raisons favorisant l'émission de protons ont été également examinées par Morrison [65]). Aux grandes énergies d'éxcitation, la barrière coulombienne pouvrait être abaissée par une expansion du noyau. Bagge [66]) a tenté l'estimation semi-empirique de cette diminution. Par ailleurs, lorsque l'évaporation a conduit au départ d'un nombre déjà élevé de neutrons, les énergies de liaisons des neutrons augmentent, ce qui tend à favoriser l'émission de protons. Ceci s'appliquerait surtout aux isotopes légers du protactinium pour lesquels les écarts sont justement les plus importants.

Un autre résultat intéressant relatif au protactinium concerne l'hypothèse de valeurs constantes des rapports $\Gamma_n/(\Gamma_n+\Gamma_f)$ quelle que soit l'énergie d'excitation. En effet, le choix de la même valeur pour des protons incidents de 82 MeV ou de 150 MeV conduit dans les deux cas à un accord relativement bon avec les résultats expérimentaux. Une confirmation en faveur de cette hypothèse est donnée par l'étude des fonctions d'excitation des réactions (p, 3n) et (p, 6n) entre 30 et 60 MeV représentées par la figure 2. En multipliant les sections efficaces expérimentales par le produit des rapports $(\Gamma_n+\Gamma_f)/\Gamma_n$ correspondant à la chaîne d'évaporation, on obtient des courbes voisines de celles calculées à partir de noyaux composés excités. Le tableau 4 montre la comparaision des valeurs obtenues à diverses énergies, soit dans le domaine du noyau composé, soit à 82 et à 150 MeV.

TABLEAU 4

Réactions (p, 3n) et (p, 6n) sur le thorium

Réaction	Énergie incidente (MeV)	σ_{exp} (mb)	$\frac{\Gamma_n}{\Gamma_n/\Gamma_f}$ dernière fission	$\Pi\left(\frac{\Gamma_n}{\Gamma_n/\Gamma_f}\right)$	σ_{exp} × (rapport fission)	σ_{calc} (mb)
^{231}Th(p, 3n)	150	7.5	0.58	2.5	18.5	25
	82	12	0.58	2.6	32	35
	45	33	0.58	3.6	120	130
	40	40	0.58	3.6	144	180
	28	220	0.58	3.6	800	750
^{227}Th(p, 6n)	150	1.5	0.375	30	45	70
	82	3.5	0.375	40	140	240
	56	13.8	0.375	50	690	730

5.2. LES ISOTOPES DU THORIUM

Les résultats sur tous les isotopes du thorium, à l'exception du ^{231}Th, sont en accord très satisfaisant avec les valeurs calculées. On peut donc penser que si l'évaporation des protons doit être prise en considération pour expliquer le déficit des réactions (p, xn), ce déficit dans le cas des réactions (p, pxn) est compensé par l'apport de nucléides issus des protactiniums après l'évaporation d'un proton. Par contre, un écart très important est observé entre la section efficace calculée de la réaction (p, pn) et la mesure expérimentale du thorium 231, et ceci à toutes les énergies d'excitation. Cette observation est d'ailleurs très générale puisque de nombreux auteurs ont constaté des différences de 100 à 200 % entre les valeurs calculées et mesurées radiochimiquement. Rudstam[67]) pour ^{75}As(p, pn), Meadows pour [68]) Cu(p, pn), à 100 MeV, Yule et Turkevich [69]) pour l'or et le cuivre à 83, 156, 235 et 366 MeV, Sergolle [70]) pour l'or entre 40 et 150 MeV ont constaté le phénomène. La fig. 9 représente la fonction d'excitation obtenue pour ^{232}Th(p, pn)^{231}Th entre 30 et 150 MeV. On peut penser que l'actinium 231, isotope inconnu †, est un émetteur β^- de courte période et qu'une fraction de quelques mb de la section efficace de production de ^{231}Th proviendrait de ce parent, mais la correction ne peut dépasser la valeur de 10 mb correspondant aux sections efficaces des isotopes de l'actinium en général.

La première idée qui vient à l'esprit est relative au phénomène de pick up dont on n'a pas tenu compte dans le processus d'interaction directe. L'énergie du proton incident est entièrement communiquée au deutéron, le noyau restant étant ^{231}Th. Un tel mécanisme serait peut-être responsable d'une partie importante de la section efficace pour des énergies de bombardement inférieures à 70 MeV et particulièrement de la région du maximum de la courbe de la fig. 10

† ^{231}Ac a été trouvé récemment [78]). Sa période serai de 15 ± 1 min et son spectre β^- aurait une énergie maximale de 2.1 MeV.

(entre 40 et 60 MeV). Cependant, les sections efficaces de pick up direct décroissent considérablement lorsque l'énergie croît. Heidmann [71]) a calculé une relation en $1/E^6$, et Selove [72]) a observé que la réaction (p, d) correspond à 12 % de la réaction (p, pn) pour des noyaux cibles de carbone à 95 MeV. Et pourtant, un écart de 100 % subsiste encore dans nos expériences à 150 MeV. L'évaporation de deutérons est à écarter, sa contribution ne pouvant être que de quelques mb.

Le phénomène de pick up indirect, sur lequel nous reviendrons un peu plus loin, ne peut expliquer entièrement le désaccord. En effet, il laisse le noyau en moyenne encore fortement excité et il est suivi de l'évaporation de neutrons,

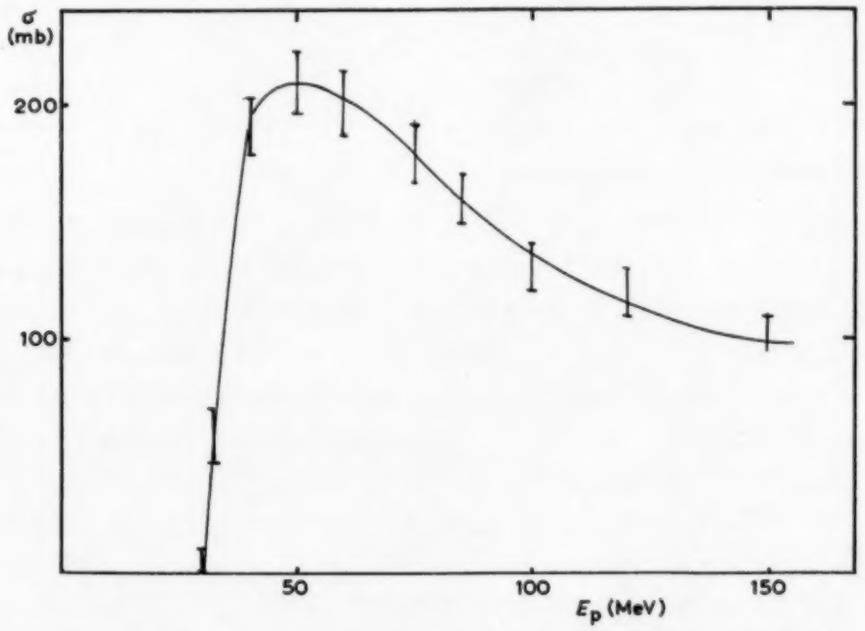

Fig. 9. Fonction d'excitation de la réaction ^{232}Th(p, pn)^{231}Th.

de sorte que son influence devrait s'observer pour les réactions (p, pxn) avec x supérieur à 1. Il faut d'ailleurs remarquer que, sans être décrit explicitement par le modèle de Serber, le pick up indirect est probablement compté dans le calcul de Monte Carle sous forme d'émission de protons et de neutrons „immédiats".

5.3. RÉACTIONS (p, 2p xn) ET ÉMISSION D'HÉLIONS

Pour les isotopes de l'actinium, si la courbe théorique suit bien les valeurs expérimentales, l'écart en valeur absolue est important. Un résultat analogue a été trouvé par Lindner et Turkevich [24]) pour une énergie incidente de 340 MeV. Cet écart nous semble devoir être attribué à l'émission par interaction directe de particules α négligée par le calcul. La formation de fragments lourds tels que hélions, noyaux de lithium et béryllium a été constatée expérimentalement au cours de divers travaux comme ceux de Deutsch [17]) sur des cibles d'or et d'ura-

nium bombardées par protons de 330 MeV. Quelques auteurs [19–21]) ont observé les réactions secondaires induites par ces fragments sur les cibles. De l'étude des produits des réactions secondaires provoquées par les fragments alpha sur le bismuth, nous avons pu, au cours d'un travail fait au laboratoire [22]), déterminer une section efficace d'environ 60 mb pour la production de ces hélions et leur répartition en énergie. En examinant cette répartition, on constate que la quasi-totalité des particules alpha émises au delá du seuil de 20 MeV ont une énergie comprise entre 20 à 50 MeV (voir fig. 10). On peut donc penser que les noyaux restant après cette émission disposent en moyenne de 100 MeV d'énergie d'excitation ou bien même qu'au cours des chocs, l'émission

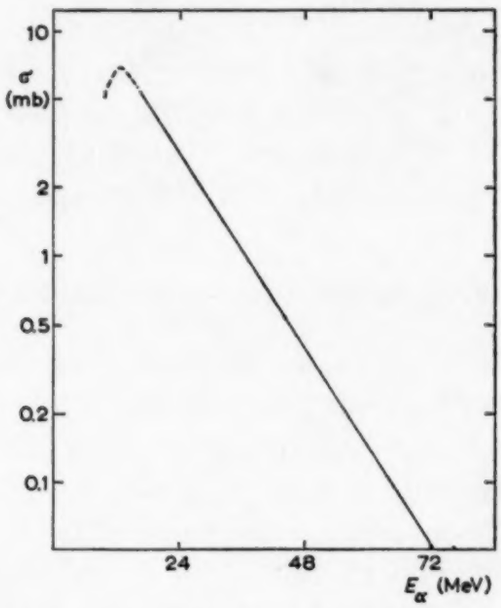

Fig. 10. Répartition en énergie des fragments alpha formés par spallation du bismuth 209 à 150 MeV.

d'une particule alpha et d'un ou plusieurs neutrons ou protons immédiats est encore possible. On obtiendrait ainsi toute une série de noyaux excités correspondant aux éléments 89 ou 88 par un processus s'ajoutant à l'émission de protons immédiats. Ceci suppose en quelque sorte la préexistence de fragments alpha dans le noyau lourd. Si l'on répartit la section efficace de 60 mb sur les isotopes 228 à 223 de l'actinium, cela équivaudrait à environ 10 mb par isotope et on trouverait alors une valeur assez voisine des résultats expérimentaux. Des cascades d'interaction directe du type (p, αp) expliqueraient également les sections efficaces expérimentales des isotopes du radium qui sont environ deux fois plus élevées que celles que l'on peut calculer sur la base de la seule cascade (p, 3p).

Un travail de Tarrago [73]) sur la production de polonium et d'astate à partir de thorium bombardé à diverses énergies de protons, montre que les sections efficaces obtenues s'expliquent correctement par des réactions (p, p) (p, α) et

(p, pα) suivies de filiations d'émissions α à courtes périodes sur des isotopes inconnu. Cet auteur a, par exemple, trouvé que la section efficace de formation de ^{209}At était de 1.4 mb, et celle de l'isotope 207 était seulement de 60 μb. La première pourrait correspondre à une réaction (p, n 11n) donnant ^{221}Pa, suivie de trois filiations α. Mais la compétition de la fission des protactiniums au cours de l'évaporation conduirait à une valeur environ 5 fois trop faible. Une réaction (P, 2P 14n) n'est pratiquement pas possible car l'évaporation de 14 neutrons après l'émission immédiate de deux protons est très peu probable; l'énergie résiduelle maximum laissée est en effet d'environ 110 MeV et correspond à l'évaporation de 10 neutrons. Par contre, l'émission directe d'une particule α emportant une énergie d'une trentaine de MeV, suivie de l'évaporation de 12 neutrons est possible. L' ^{209}At formé serait donc le produit de filiation du noyau ^{217}Ac, lui-même résidu de la spallation (α, 12n). Par contre, le noyau ^{229}Ac ne dispose pas d'assez d'énergie d'excitation pour que 14 neutrons s'évaporent et conduisent à l' ^{215}Ac puis à l' ^{207}At. C'est ce que confirme le calcul, puisqu'il faudrait une énergie résiduelle de 160 MeV pour une telle éventualité.

6. Formation de Fragments Tritons et Double Pick-Up Indirect

L'étude de l'émission de fragments alpha au cours des réactions nucléaires à moyenne énergie montre bien que l'interaction directe ne donne pas lieu seulement au départ de nucléons, mais que des entités plus importantes sont projetées. La formation de tritons se prête à une étude de type radiochimique puisque la mesure du tritium accumulé dans les cibles est possible grâce à sa radioactivité. Au cours d'un travail décrit en détail par ailleurs [12, 74]), nous avons mesuré les sections efficaces de production de tritium dans les empilements de cibles minces de thorium, d'or, de fer, d'aluminium et de carbone, à 150 MeV et dans le cas de l'or, à diverses énergies comprises entre 20 et 150 MeV. Trois caractéristiques principales se dégagent de ces résultats:

1) Les tritons sont projetés en quasi-totalité vers l'avant, dans un angle solide d'environ 1 sr. A 150 MeV, une étude grossière de la distribution en énergie des tritons émis montre que les énergies les plus probables sont situées entre 15 et 20 MeV. La proportion de tritons émis vers l'arrière, ou de façon isotrope, est inférieure à quelque pour cent, au moins pour des énergies de tritons supérieures à 3 MeV.

2) L'influence de l'énergie des protons incidents sur la section efficace absolue est indiquée sur la fig. 11 correspondant au bombardement de cibles d'or. On peut voir que lorsque l'énergie diminue, la section efficace commence par croître légèrement, puis baisse pour des protons incidents d'environ 50 MeV. A basses énergies (40 MeV et moins), la distribution en énergie montre une proportion plus importante qu'à 80 MeV de tritons relativement rapides. D'après leur parcours, on a pu estimer que leur énergie approche 40 MeV.

On peut donc penser que le phénomène observé est alors le double pick-up direct.

La région comprise entre 50 et 60 MeV correspondrait par contre à un domaine de transition entre le pick-up direct et le pick-up indirect.

3) La section efficace de formation de tritium à 150 MeV croît avec le Z de l'élément cible et nous avons trouvé une relation très simple entre ces résultats et les sections efficaces calculées de formation de protons „immédiats". Les calculs de Monte Carle publiés par Metropolis *et al.* [41]) indiquent le nombre moyen de protons émis par choc inélastique pour plusieurs noyaux cibles.

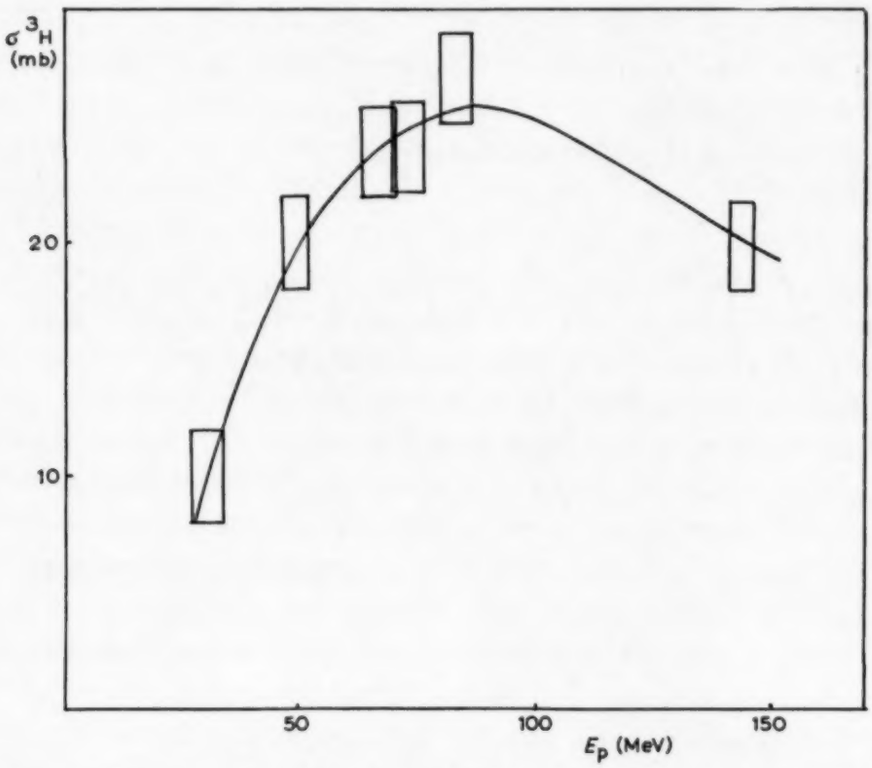

Fig. 11. Fonction d'excitation de la formation de tritium dans des cibles de ^{197}Au bombardés par des protons.

En multipliant par la section géométrique σ_g calculée classiquement on obtient la section efficace moyenne de production de ces protons. Le rapport entre cette valeur et la section efficace mesurée de tritium *est pratiquement constant* quel que soit Z pour une énergie incidente donnée. Ceci correspond par exemple à 1 triton pour 50 protons „immédiats" à 150 MeV et à 1 triton pour 25 protons immédiats à 80 MeV. Cette proportion plus importante à 80 MeV qu'à 150 MeV est liée au fait que la probabilité de formation de tritium augmente lorsque l'énergie moyenne des protons immédiats diminue. Par ailleurs, la contribution du pick-up direct n'est probablement plus négligeable à 80 MeV et au dessous.

Le tableau 5 montre ces résultats à 150 MeV.

TABLEAU 5

Rapport entre la section efficace de formation de tritium et celle de production des protons

Cible	$\sigma/^3H$ mesurée (mb)	σ_g avec $r_0 = 1.35$ fm (b)	N (nombre de protons par choc)	$\sigma_g \times N$ (b)	$\frac{\sigma_g \times N}{\sigma^3H}$
C	6 ± 1.6	0.29	1.2	0.34	57
Al	10 ± 1.5	0.51	1.1	0.56	53
Fe	13 ± 2	0.82	0.8	0.65	50
Au	19 ± 2	1.9	0.5	0.95	48
Th	20 ± 2	2.15	0.45	0.96	48

Il semble donc que le phénomène observé à 150 MeV dépend uniquement du nombre et de l'énergie des protons et des neutrons „immédiats".

Pour les deutérons, ce phénomène a été décrit par Bransden sous le nom de *pick-up indirect* [75]). D'après cet auteur, des deutérons peuvent être formés au cours d'un processus secondaire dans lequel un nucléon de quantité de mouvement relativement faible (lui-même produit par choc de la particule incidente avec un nucléon dans le noyau) capte un second nucléon à la surface du noyau, avant de sortir. Une étude expérimentale de Hess et Moyer [76]) a montré la réalité du phénomène pour une énergie de protons de 300 MeV. Les auteurs ont trouvé que la section efficace de production de deutérons à 40° variait selon l'expression $\sigma_d = kA^{1.2}$ et que celle de production de tritons suivait la loi $\sigma_t = kA^{1.28}$ pour les noyaux de lithium, carbone et aluminium D'après ces mêmes auteurs, le pick-up indirect aurait surtout lieu par des protons immédiats car la proportion de neutrons à la surface des noyaux est plus grande que celle des protons. Cette proportion serait comprise entre 0.564 et 0.652 pour le lithium et entre 0.745 et 0.845 pour l'uranium

Radvanyi et Génin [77]) ont établi les spectres d'énergies à différents angles de deutérons et tritons émis lors du bombardement de noyaux de carbone par des protons de 155 MeV. Leurs résultats sont relatifs aux particules d'énergie supérieure à 40 MeV et montrent qu'outre le pick-up direct caractéristique, on observe des tritons et deutérons d'énergie plus faible. Nos résultats complètent ces spectres vers les basses énergies et montrent que le phénomène quantitativement le plus important pour les tritons est celui du pick-up indirect ou de processus d'interaction de même nature. On peut par exemple penser, que certains tritons sont formés par un processus de stripping des fragments alpha, eux mêmes projetés par les protons incidents. On a vu que l'émission de ces fragments n'était pas négligeable. Lorsqu'ils franchissent la surface du noyau ils pourraient perdre un proton et sortir à l'état de triton.

La production de tritium par évaporation est, en tout état de cause, à écarter puisque les expériences montrent que l'émission n'est pas isotrope. Pourtant,

au cours de calculs de Monte Carle, Dostrowsky *et al.* [64]) ont trouvé que pour des protons incidents de 190 MeV, la section efficace de production de tritons par évaporation de noyaux d'argent pourrait atteindre 6.87 mb · sr^{-1} en prenant $r_0 = 1.7$ fm. Cette valeur conduirait, en répartition isotrope, à 85 mb, résultat très supérieur à tous les résultats expérimentaux. Par contre, avec $r_0 = 1.5$ fm, les auteurs cités obtiennent 1.52 mb · sr^{-1}, valeur très voisine de celle de nos expériences. Cependant, ces expériences ont montré que la proportion de tritons émis vers l'arrière était inférieure à quelques pour cent.

On peut donc conclure que la grande majorité des tritons observés dans les réactions nucléaires à une énergie incidente de 150 MeV sont formés par des processus d'interaction directe comme le pick up indirect ou le stripping secondaire de particules alpha. Ces divers mécanismes contribuent à la production de noyaux résiduels possédant des énergies d'excitations variées.

Ce travail a été effectué au Laboratoire de Physique nucléaire d'Orsay avec l'aide de Mme Brun, technicienne de la Faculté.

Nous voudrions rendre hommage à la mémoire du professeur Joliot-Curie, qui nous a encouragés à entreprendre cette étude. Nous sommes particulièrement reconnaissants au professeur Friedlander qui nous a communiqué les détails des calculs de Monte Carle grâce auxquels il nous a été possible de déterminer les sections efficaces. Nous remercions l'équipe de conduite du synchrocyclotron et le service d'électronique du Laboratoire d'Orsay pour leur collaboration amicale et efficace.

Bibliographie

1) P. R. O'Connor et G. T. Seaborg, Phys. Rev. **74** (1948) 1189
2) W. E. Bennett, Phys. Rev. **94** (1954) 997
3) A. P. Vinogradov, I. P. Alimarine, V. I. Baranov, A. K. Lavroukhina, T. V. Baranova et F. I. Pavlovskay, Sess. Acad. Sci. URSS sur l'Énergie Atomique (1—5 juillet 1955) p. 132
4) A. N. Mourine, B. K. Preobragensky, I. A. Ioutlanov et M. A. Iakimov, Sess. Acad. Sci. URSS sur l'Énergie Atomique (1—5 juillet 1955) p. 160
5) M. Lindner et R. N. Osborne, Phys. Rev. **103** (1956) 378
6) E. T. Hunter et J. M. Miller, Phys. Rev. **115** (1959) 1053
7) R. E. Bell et H. M. Skarsgard, Can. J. Phys. **34** (1956) 745
8) R. A. Glass, R. J. Carr, J. W. Cobble et G. T. Seaborg, Phys. Rev. **104** (1956) 434
9) T. Sikkeland, S. Amiel et S. G. Thompson, J. Inorg. Nucl. Chem. **11** (1959) 261
10) L. A. Currie, W. F. Libby et R. L. Wolfgang, Phys. Rev. **101** (1956) 1557
11) V. V. Kuznetsov et V. N. Mekhedov, JETP **35** (1956) 587
12) M. Lefort, G. Simonoff, X. Tarrago et R. Bibron, J. Phys. et Rad. **20** (1959) 959
13) C. F. Chew et M. L. Goldberger, Phys. Rev. **77** (1950) 430
14) W. H. Wade, J. Gonzalez-Vidal, R. A. Glass et G. T. Seaborg Phys. Rev. **107** (1957) 1311
15) S. Katcoff, Phys. Rev. **114** (1959) 903;
S. C. Wright, Phys. Rev. **79** (1950) 838;
S. O. C. Sorensen, Phil. Mag. **40** (1949) 947;
D. H. Perkins, Proc. Roy. Soc. **203** (1950) 399
16) N. A. Perfilov et V. A. Ostroumov, Dokl. Akad. Nauk. **103** (1955) 227
17) R. W. Deutch, Phys. Rev. **97** (1955) 1110

18) F. S. Rowland et R. L. Wolfgang, Phys. Rev. **110** (1958) 175
19) A. E. Metzger et J. M. Miller, Phys. Rev. **113** (1959) 1125
20) B. V. Kurchatov, V. N. Mekhedov, L. V. Chistiakov, M. Ia. Kuznetsova, N. I. Borissova et V. G. Soloviev, JETP **35** (1958) 56
21) Van Youn Yu, V. V. Kuznetsov, M. Ia. Kuznetsova et V. A. Kalkine, Rap. Inst. Unifié Rech. Nucléaire, Dubna (Fév. 1960);
Van Youn, Yu V. V. Kuznetsov, M. Ia. Kuznetsova, V. I. Mekhedov et V. A. Kalkhine, JETP **39** (1960) 3
22) M. Lefort, G. N. Simonoff et X. Tarrago, Nuclear Physics **19** (1960) 173
23) R. Serber, Phys. Rev. **72** (1947) 1114
24) M. Lindner et A. Turkevich, Phys. Rev. **119** (1960) 1632
25) C. Bergamaschi, J. C. Brun, A. Cabrespine, R. Gayraud, J. Genin, H. Langevin, N. Marty, A. Michalowicz, P. Radvanyi, M. Riou, J. Teillac et C. Victor, J. Phys. **21** (1960) 305
26) H. G. Hicks, P. C. Stevenson et W. E. Nervick, Phys. Rev. **102** (1956) 1390
27) W. E. Crandall, G. P. Millburn, R. V. Pyle et W. Birnbaum, Phys. Rev. **101** (1956) 329
28) I. D. Prokochkine et A. A. Tiapkine, JETP **32** (1957) 177
29) V. Parish, Nuclear Physics **18** (1960) 628
30) J. Dickson et I. Randle, Proc. Phys. Soc. **64** (1951) 902
31) Honda et Lal, Phys. Rev. **118** (1960) 1618
32) G. N. Simonoff, Thèse (1961) Paris
33) H. M. Neumann et I. Perlman, Phys. Rev. **81** (1951) 958
34) Brysk et Rose, ORNL (1955) 1830
35) R. W. Hoff et I. O. Rasmussen, Phys. Rev. **101** (1956) 280
36) E. L. Kelly et E. Segré, Phys. Rev. **75** (1949) 999
37) S. H. Vegors, L. L. Marsden et R. L. Heath, AECE-IDO (1959) 16.370
38) M. H. Studier et E. K. Hyde, Phys. Rev. **74** (1948) 591
39) C. Brun et G. Simonoff, sous presse
40) M. Lefort, G. N. Simonoff et X. Tarrago, J. Phys. **21** (1960) 338
41) N. Metropolis, R. Bivings, M. Storm, A. Turkevich, J. M. Miller et G. Friedlander, Phys. Rev. **110** (1958) 185
42) G. Friedlander, communication personnelle
43) J. D. Jackson, Can. J. Phys. **34** (1956) 767
44) J. D. Jackson, Can. J. Phys. **35** (1957) 21
45) B. M. Foreman et G. T. Seaborg, J. Inorg. Nucl. Chem. **7** (1958) 305
46) J. M. Blatt et V. F. Weisskopf, Theoretical Nuclear Physics, (H. Wiley, New York, 1952) p. 371
47) E. E. Gross, UCRL (1956) 3330
48) J. M. Lang et K. J. LeCouteur, Proc. Phys. Soc. **67** (1954) 585
49) C. D. Goodman et J. L. Need, Phys. Rev. **110** (1958) 676
50) A. Zucker, Nuclear Physics **6** (1958) 420
51) J. S. Levin et E. Cranberg, ORNL 2309 (1958) 84
52) D. Fong, Phys. Rev. **102** (1956) 434
53) I. Dostrowsky, P. Rabinovitz et R. Bivins, Phys. Rev. **111** (1958) 1659
54) R. Vandenbosch et G. T. Seaborg, Phys. Rev. **110** (1958) 507
55) B. D. Pate, Can. J. Chem. **36** (1958) 1707
56) R. L. Henkel, L. A. report (1957) 2122
57) J. R. Huizenga, Phys. Rev. **107** (1958) 484
58) R. Vandenbosch, T. D. Thomas, S. E. Vandenbosch, R. A. Glass, et G. T. Seaborg, Phys. Rev. **111** (1958) 1358
59) N. I. Tarantine, JETP **38** (1960) 250
60) N. I. Tarantine, Guerlit et Gousseva, JETP **34** (1958) 220
61) R. Vandenbosch et J. R. Huizenga, 2e Conf. de l'O.N.U. Genève, P/688 **15** (1958) 284
62) Y. Fujimoto et Y. Yamaguchi, Proc. Theor. Phys. **5** (1960) 76
63) K. J. LeCouteur, Proc. Phys. Soc. A **63** (1950) 259
64) I. Dostrowsky, Z. Fraenkel et L. Winsberg, Phys. Rev. **118** (1960) 781
65) P. Morrison dans Experimental Nuclear Physics, E. Segré, éd. (1953) Vol II, p 156—182

66) E. Bagge, Ann. Phys. **33** (1938) 389
67) G. Rudstam, Thèse, Uppsala (1956)
68) G. W. Meadows, Phys. Rev **98** (1955) 744
69) P. Yule et A Turkevich, Phys. Rev. **118** (1960) 1591
70) H. Sergolle, Diplôme d'étude supérieure, Paris (1960)
71) J. Heidmann, Phys. Rev. **80** (1950) 171
72) W. Selove, Phys. Rev. **101** (1956) 231
73) X. Tarrago, J. Phys., sous presse
74) B. Gatty, M. Lefort, G. Simonoff et X. Tarrago, J. Phys., sous presse (1961)
75) B. H. Bransden, Proc. Phys. Soc. **65** (1952) 738
76) W. N. Hess et B. J. Moyer, Phys. Rev. **101** (1956) 337
77) P. Radvanyi et J. Génin, J. Phys. **21** (1960) 322
78) K. Takahashi et H. Morinaga, Nuclear Physics **19** (1960) 133

2.J

Nuclear Physics **25** (1961) 248—258; © *North-Holland Publishing Co., Amsterdam*

Not to be reproduced by photoprint or microfilm without written permission from the publisher

THE NEUTRON DEFICIENT IRIDIUM ISOTOPES Ir^{182}, Ir^{183} AND Ir^{184}

R. M. DIAMOND, J. M. HOLLANDER, D. J. HOREN and R. A. NAUMANN †

Lawrence Radiation Laboratory, University of California, Berkeley, California ††

Received 23 February 1961

Abstract: The new neutron-deficient iridium isotopes Ir^{182}, Ir^{183} and Ir^{184} have been produced by irradiations with the Berkeley heavy-ion linear accelerator. By means of timed chemical separations, NaI scintillation spectrometers and proportional counters, half lives have been determined as follows: Ir^{182}, 15 ± 1 min; Ir^{183}, 55 ± 7 min; Ir^{184}, 3.2 ± 0.2 h. The gamma-ray spectra of Ir^{182} and Ir^{184} are very complex, each extending above 4 MeV. Positon branches are also seen in both isotopes. Studies of the gamma-ray spectra indicate that the energies of the first and second excited states of Os^{182} are slightly higher than the corresponding states in Os^{184}. These data suggest that there is a maximum in the moment of inertia at Os^{184}.

1. Introduction

The nuclear energy levels of the osmium isotopes are of particular interest in nuclear spectroscopy because these isotopes span the transition region between two broad groups of nuclei whose properties have been characterized in terms of axially symmetric ellipsoidal shapes and of spherical shapes. A knowledge of the level structures of these isotopes can aid the development and testing of nuclear models applicable to this intermediate region, for example, the asymmetric rotor model of Davydov and Filipov. The levels of Os^{188}, Os^{190} and Os^{192} are known primarily from decay-scheme studies of the corresponding iridium and rhenium isotopes [1–6]). In addition some Coulomb excitation work has been reported [6]). Diamond and Hollander have studied the decays of the neutron-deficient isotopes Ir^{185}, Ir^{186} and Ir^{187} [3]). The decay of Ir^{186} has been investigated by Scharff-Goldhaber *et al.* [7]).

In the interval from mass number 186 to 192, two interesting features are noted in the levels of even-mass osmium isotopes: (a) the ratio of energies of the first 4+ to the first 2+ state falls from 3.17 in Os^{186} to 2.94 in Os^{190} and (b) the energy of the second 2+ state decreases sharply from 768 keV in Os^{186} to 489 keV in Os^{192} while the first 2+ state increases from 137 keV in Os^{186} to 206 keV in Os^{192}. The decrease in the ratio $E(4+)/E(2+)$ and the increase in energy of the first excited 2+ state are attributable to a decrease in the equilibrium nuclear deformation between Os^{186} and Os^{192}. The lowering in

† Proctor and Gamble Faculty Fellow on leave from Princeton University, Princeton, N.J.

†† This work was done under the auspices of the U. S. Atomic Energy Commission.

energy of the second 2+ state may be interpreted as indicating that the heavier osmium isotopes become "softer" toward the gamma-type of near-harmonic collective oscillations.

In the interest of extending our knowledge of the level structures of osmium isotopes, we have sought to synthesize and identify iridium isotopes of mass numbers less than 185, by heavy-ion irradiations of suitably chosen targets. In this paper, the syntheses of Ir^{182}, Ir^{183} and Ir^{184} are reported.

2. Experimental Method

Heavy-ion reactions offer a useful method of preparing highly neutron-deficient isotopes relatively free of activities lying nearer to the line of stability. For example, the compound nucleus formed from the irradiation of thulium ($_{69}Tm^{169}$) with oxygen ions is $_{77}Ir^{185}$, already six mass units lighter than the lightest stable isotope Ir^{191}. By this method, Ir^{182} has been produced by the $Tm^{169}(O^{16}, 3n)$ reaction. Production of Ir^{183} and Ir^{184} has been achieved by means of the $Lu^{175}(C^{12}, 4n)$ and $(C^{12}, 3n)$ reactions. Thick metallic targets of thulium and lutetium were irradiated with 160 MeV O^{16} ions or 120 MeV C^{12} ions in the Berkeley heavy-ion linear accelerator (Hilac). Bombardment times varied from 20 min to 6 h, according to the isotope being studied.

After chemical purification of the iridium fractions, their decay was followed by using end-window, flowing-methane, proportional counters. Photon spectra were examined with two scintillation spectrometers. One consisted of a 3.81 cm by 2.54 cm NaI crystal mounted on an RCA 6655A photomultiplier tube, and the other a 7.62 cm by 7.62 cm crystal mounted on a Dumont 6363 tube. Gamma-gamma coincidences were measured with a conventional fast-slow coincidence circuit and with a two-dimensional analyzer [8]). Where possible, half lives and the genetic relationships to known osmium and rhenium isotopes were established by means of timed chemical separations of daughter activities.

3. Chemical Procedures

Iridium was separated from rare-earth metal targets by dissolving the target in 6*N* HNO_3 and boiling the solution almost to dryness in aqua regia to expel OsO_4. The solution was made 6*N* in HCl and passed through a Dowex A–1 column to adsorb iridium (plus rhenium). After thorough washing of the column with 3*N* HCl, the resin was removed and equilibrated with a 10 % hydroxylamine hydrochloride solution at $\approx$ 100° C to reduce iridium to the trivalent state, which is desorbed. A further purification of iridium was effected by precipitation of IrO_2 by standard techniques.

In order to "milk" osmium from irradiated rare-earth targets, the nitric acid solution of the target metal, containing carriers of rhenium, osmium and

iridium, was boiled almost to dryness to expel OsO_4, and then was transferred to a standard "ruthenium" distillation apparatus. For each collection of osmium daughter activity, 5 mg of osmium carrier was added to the still, together with 10 ml of concentrated HNO_3 and 1 ml of concentrated HCl. The OsO_4 was then distilled in a stream of air into 100 ml of 6*N* NaOH solution, which was mounted directly for scintillation analyses.

Rhenium granddaughter activities were isolated essentially by the removal of osmium as osmium sulfide from the 6*N* NaOH solutions of the osmium milked fractions, and the subsequent precipitation of rhenium sulfide from the acidified supernatants.

4. Experimental Results

4.1. IRIDIUM-182

The irradiation of Tm^{169} with 160 MeV O^{16} ions yields isotopes of iridium with mass number lower than 185. It is expected (and found) that the yield of the (O^{16}, n) reaction is very low because of the high excitation of the compound nucleus; hence one does not observe significant amounts of Ir^{184}. Because the number of neutrons that can be evaporated at these energies may be quite large (> 10), many iridium isotopes can be produced. However, in these experiments approximately 45 min was required to perform the initial iridium purifications, so that half lives of $\leqq 10$ min probably would have escaped detection. Thus, the lower limit on observable mass numbers is governed primarily by the speed of chemical separation.

Iridium-182 has been identified both from irradiations of lutetium with carbon ions and of thulium with oxygen ions. The decay curve of the iridium fraction from the Ir(O^{16}, *x*n) reaction is shown in fig. 1. The half life of the shortest component, which we assign to Ir^{182}, is 15 ± 1 min. The curve shown was taken with a $\approx$ 1.5 mm Al absorber interposed between source and detector; the use of an absorber enhanced the counting efficiency of the 15 min component relative to the longer-lived activities.

After an irradiation of lutetium with carbon ions, the genetic relationship of the 15 min Ir^{182} to its descendents Os^{182} and Re^{182}, was established by a series of timed chemical separations (milkings) in which OsO_4 was volatilized out of the iridium fraction every 15 min. In the early milkings, Os^{182} was clearly recognizable by its prominent 510 keV gamma ray [9]) (*not* annihilation radiation), which showed the characteristic 21 h half life of Os^{182} (see fig. 2). The yield of this 510 keV photon in each milking as a function of the time of the milking is shown in fig. 3(A); from this curve a half life of $\approx$ 17 min is obtained for the parent of Os^{182}. As a further check on this assignment, rhenium was separated from the first few osmium fractions 24 h after their isolation. The gamma-ray spectrum of the rhenium fraction contained composite peaks at 1 and 2 MeV similar to those found by Gallagher *et al.* [10]) in 13 h Re^{182}.

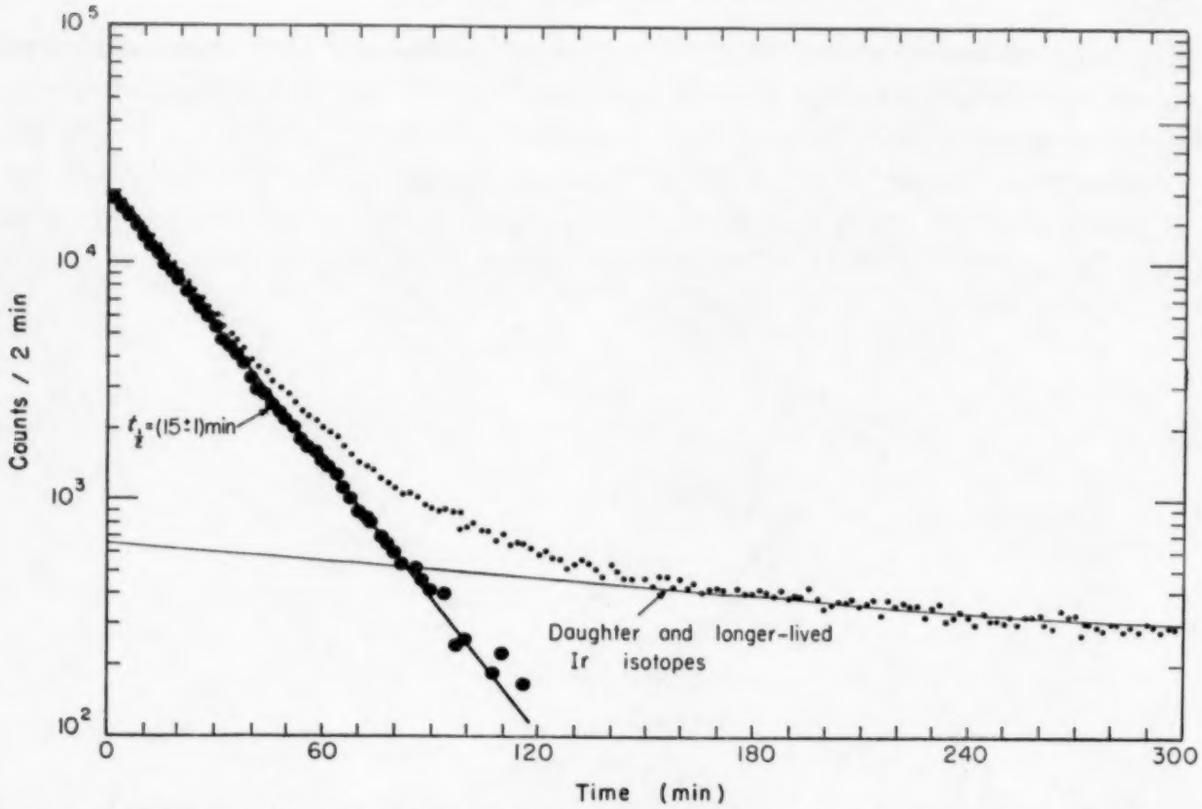

Fig. 1. Decay curve of iridium fraction from Tm(O^{16}, xn)Ir) 1.5 mm aluminium between source and counter).

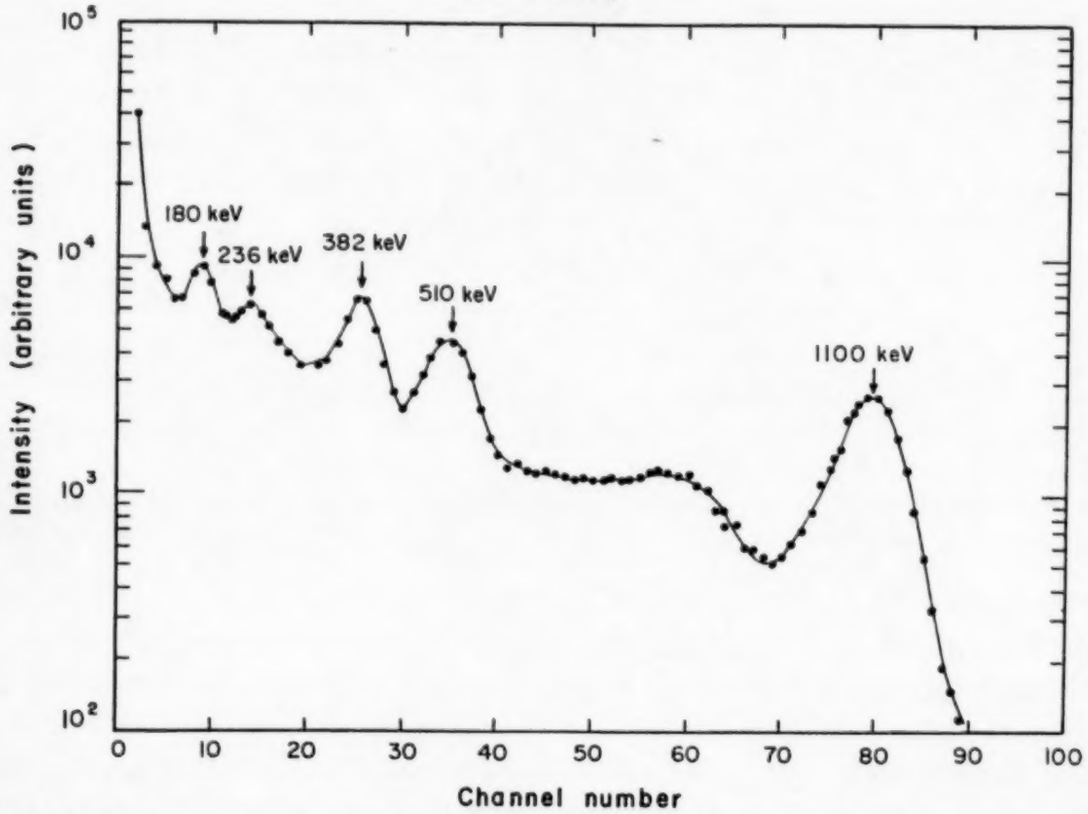

Fig. 2. Gamma-ray spectrum of first Os fraction milked from Lu(C^{12}, xn)Ir. The presence of 12-h Os^{183} is indicated by the prominent photon at 382 keV, 9.9 h Os^{183} by the 1100 keV photon and 21 h Os^{182} by the 510 keV photon [9]).

Fig. 3(B) shows a plot of the 1000 to 1300 keV composite peak versus the time of chemical separation of the osmium parent from the iridium grandparent. From this curve, we obtain $\approx$ 16 min as the half life of Ir^{182}. From the direct decay of the photon peaks in the Ir^{182} gamma spectrum, the measured half life is 15.5 ± 1 min. A consideration of these data leads to the value 15 ± 1 min as the "best value" of the Ir^{182} half life.

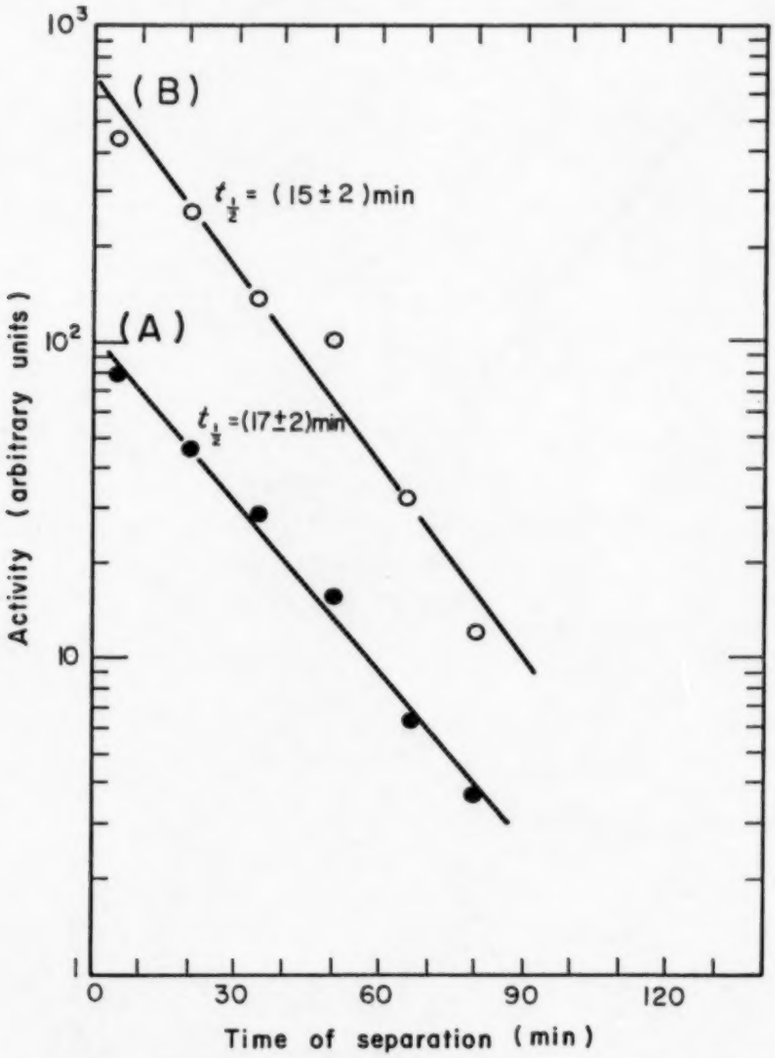

Fig. 3. (A) Yields of 510 keV gamma ray of 21 h Os^{182} as a function of time of separation of Os from parent Ir. (B) Yields of 1 MeV group of 13h Re^{182} in Re fractions separated from Os fractions of (A).

In the $Tm(O^{16}, xn)$ bombardment, a fairly pure gamma-ray spectrum of Ir^{182} could be observed briefly in the iridium fraction without interference from the spectrum of the daughter Os^{182} activity. One of the earliest spectra is shown in fig. 4. Clearly evident are KX-rays and photons of 133 ± 5 keV and 278 ± 5 keV. These photons are interpreted as transitions that de-excite the first and second rotational states of Os^{182}, respectively. The Ir^{182} spectrum above 500 keV is extremely complex and extends higher in energy than 4 MeV.

4.2. IRIDIUM-183

Iridium-183 and -184 were produced from carbon-ion irradiation of lutetium metal by the reactions $Lu^{175}(C^{12}, 4n)$ and $(C^{12}, 3n)$. The proportional-counter decay curve showed the presence of activities of $\approx$ 20 min (Ir^{182}), $\approx$ 1h, $\approx$ 3h and longer half lives.

Iridium 183 was identified principally from several series of milking experiments done at 20 and 40 min intervals for periods of up to 6 h. The milked osmium fractions were examined in liquid form ($\approx$ 100 cm^3) under identical conditions in the scintillation spectrometer. Fig. 2 shows the gamma spectrum of the first osmium milking measured immediately after chemical separation.

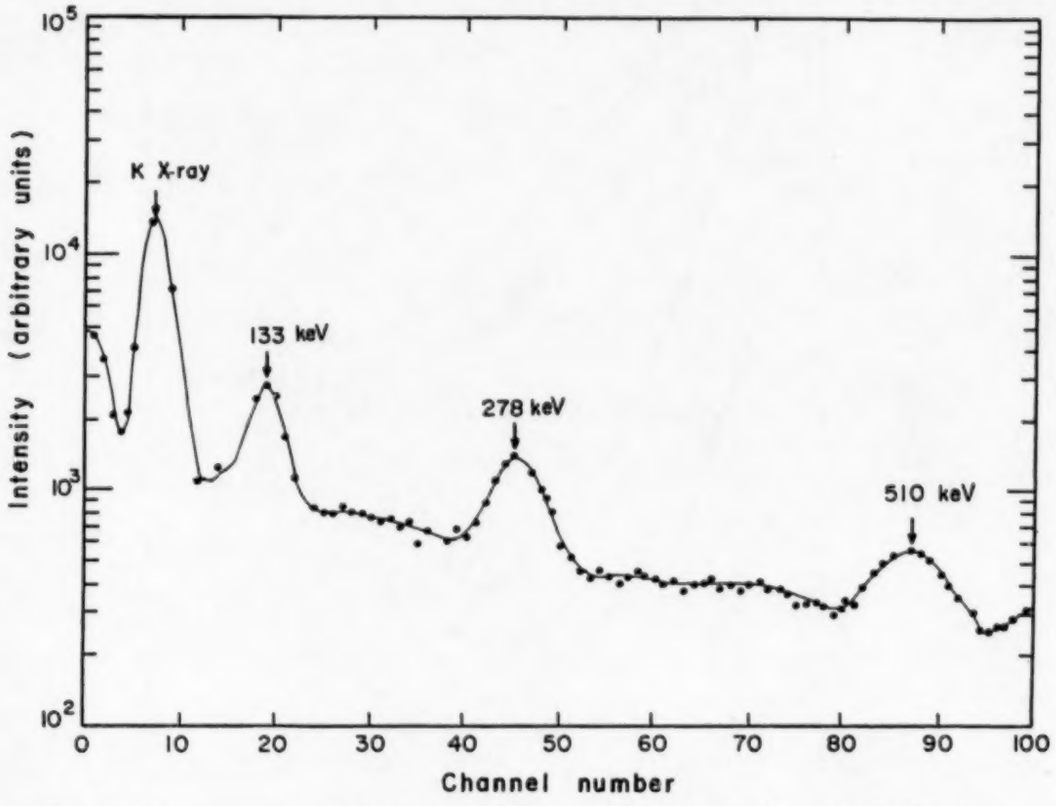

Fig. 4. Low-energy gamma-ray spectrum of 15 min Ir from $Tm(O^{16}, xn)Ir$.

The presence of 12 h Os^{183} is indicated by the prominent photon at 382 keV, while the 1100 keV photon arises from the decay of 9.9 h Os^{183m} as reported by Newton [9]). Since both the 382 and 1100 keV photons (in the osmium milkings) were detected in comparable amounts immediately after the chemical separation, it is evident that the isomeric states of osmium 183 are populated simultaneously in the decay of Ir^{183}. In the first osmium fraction, the presence of Os^{182} which arises from the decay of 15 min Ir^{182} is indicated by the 510 keV photon and by the subsequent growth of Re^{182}. The later osmium fractions showed evidence neither of Os^{182} nor of Re^{182}.

The half life of Ir^{183} was obtained by plotting the relative yield of the

382 keV Os^{183} photon and that of the 1100 keV Os^{183m} photon as a function of the time of separation of osmium from the parent iridium fraction. Fig. 5 shows one such yield curve as well as the yield curves of the 180 and 510 keV photons. The short components of these decays represent the 180 and 510 keV gamma rays in the decay of Os^{182} (which grew from Ir^{182}), while the long components

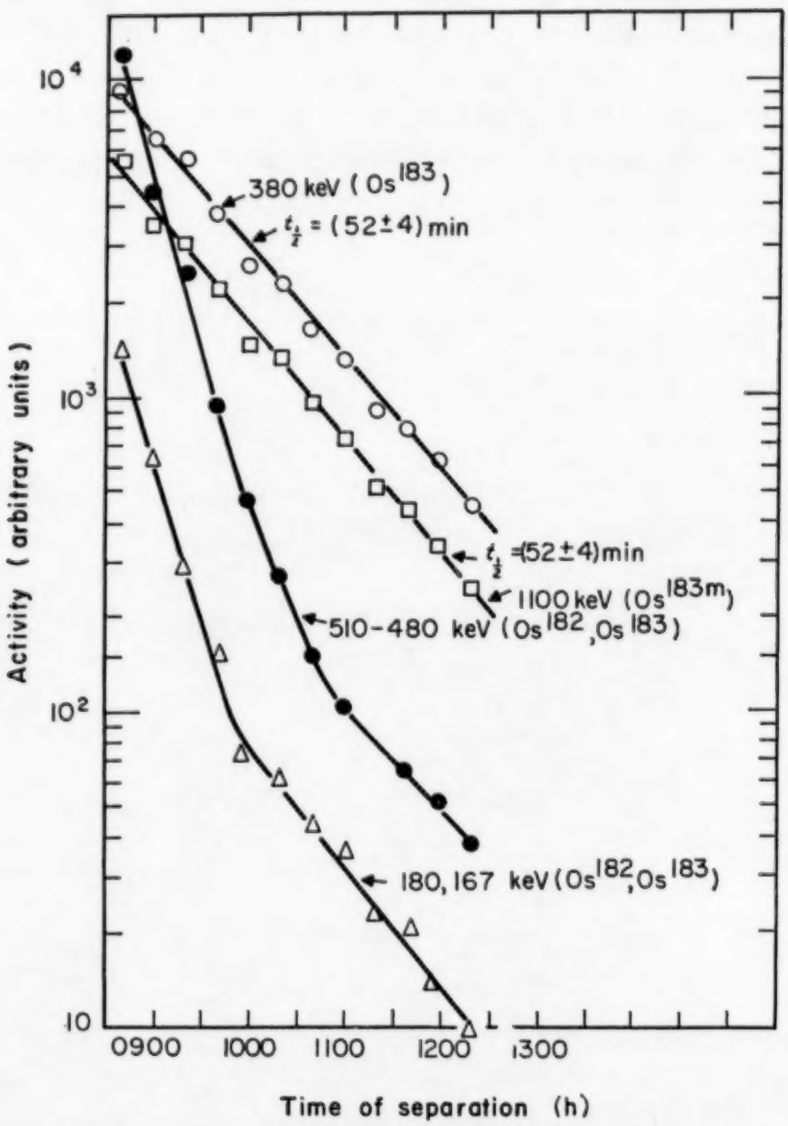

Fig. 5. Yields of gamma rays in Os milked from Ir produced by Lu(C^{12}, xn)Ir.

arise from the 168 and $\approx$ 480 keV gamma rays in the decay of Os^{183}. From several such experiments, the best value of the Ir^{183} half life appears to be 55 ± 7 min. A sample of Ir^{183} sufficiently free of Ir^{182} and Ir^{184} to permit the observation of a distinct Ir^{183} gamma-ray spectrum could not be prepared. However, in the iridium fraction isolated from lutetium bombarded with carbon ions, a photon of energy about 238 keV was observed to decay with a 58 min half life.

It should be noted that the 117, 236 and ≈ 510 keV photon peaks in the osmium milkings showed an initial short-lived decay (about 110 min) as well as the expected longer periods of the Os^{183} isomers. That these gamma rays, with energies similar to those of some Os^{183} gamma rays, show such a short component while the 180 keV photon (known to occur in the decay of Os^{182}) does not might suggest the possibility of a third isomeric state in Os^{183}. It is further observed, however, that the prominent 382-keV gamma ray (of Os^{183}) does *not* show a short-lived component. Therefore, if the 236 and ≈ 510 keV photons seen here really originate from Os^{183} decay, they cannot be identified with the transitions of similar energies in the decay scheme of Os^{183} reported by Newton [9]), since this would require the simultaneous observation of a (short-lived) 380 keV gamma ray.

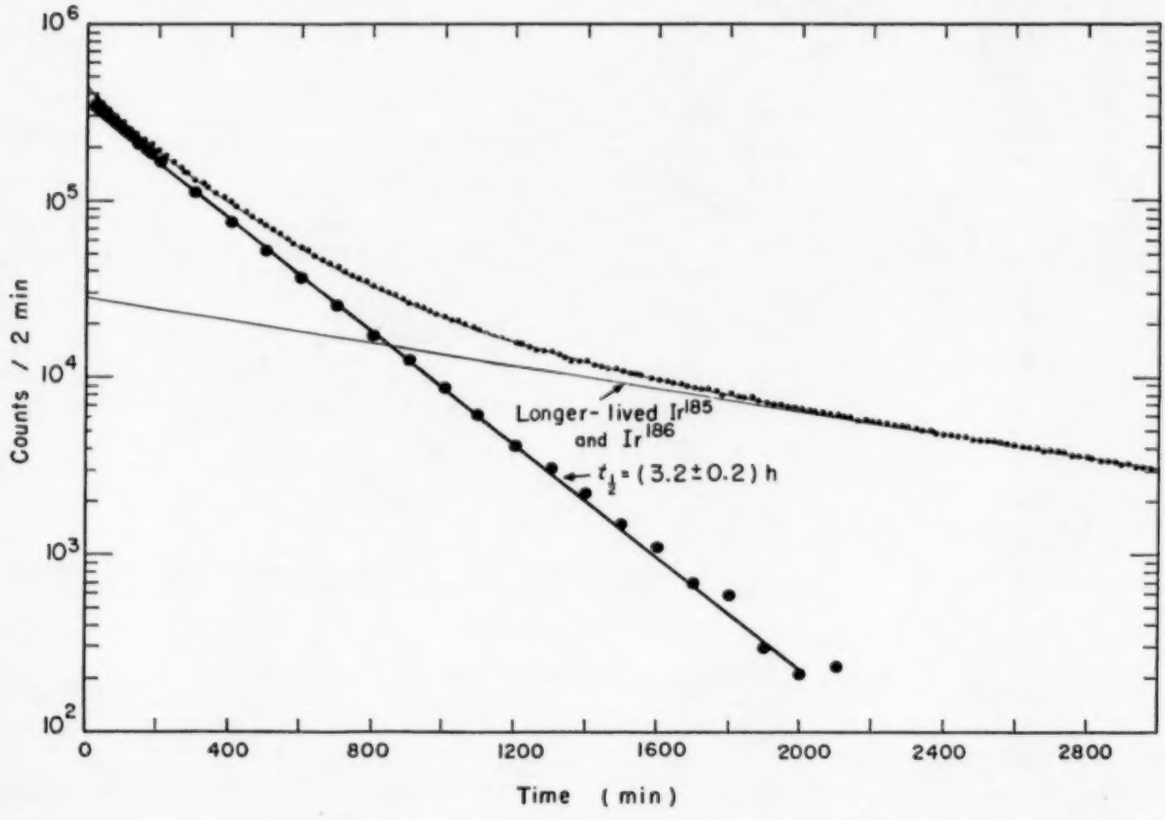

Fig. 6. Decay curve of Ir fraction from Lu(C^{12}, xn)Ir chemically separated 7 h after irradiation.

4.3. IRIDIUM-184

The prominent 3h component of the decay curve from the Lu(C^{12}, xn) bombardments was thought to be associated with Ir^{184}. For a study of this activity, the irradiated target was allowed to stand for about 7h before chemical purification, to permit the shorter-lived iridium isotopes of mass number less than 184 to decay. Fig. 6 shows the decay curve obtained from such a fraction by using a proportional counter. The longer-lived "tail" arises from the presence of Ir^{185} and possibly Ir^{186} (both ≈ 15h) rather than from daughters. This

was shown by a subsequent repurification of the iridium fraction and by the presence in the scintillation spectrum of photons known [3]) to occur in the decays of Ir^{185} and Ir^{186}. The first few points in the resolved 3.2h component are high because of the presence of some 55 min Ir^{183}. Because there was no indication of a 3h iridium parent in the osmium milking experiments and since the gamma-ray spectrum of the 3h activity was similar to that expected for a light even osmium isotope, we conclude that this activity is Ir^{184}, which decays to stable Os^{184}. Our best value for the half life of Ir^{184} is 3.2 ± 0.2h.

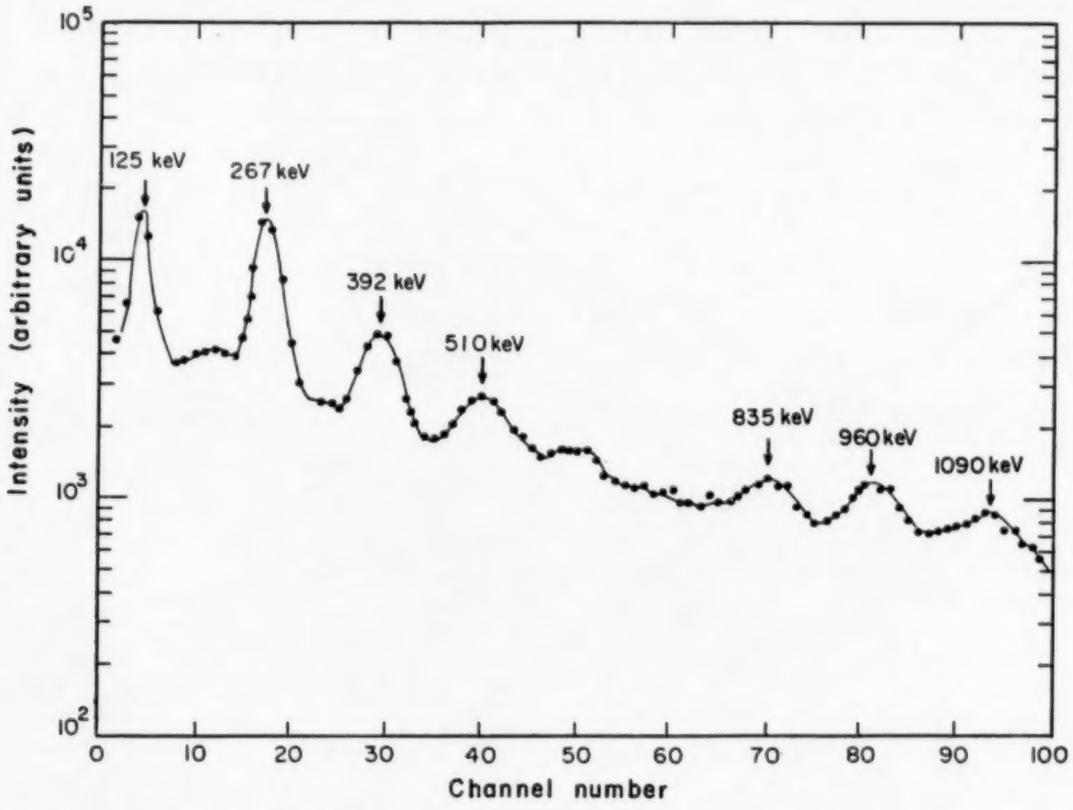

Fig. 7. Low-energy gamma-ray spectrum of Ir^{184}.

The low-energy spectrum of Ir^{184} is shown in fig. 7. Besides the K X-rays (not shown), gamma rays are present with energies of 125 ± 5, 267 ± 5, 392 ± 5 and 511 ± 5 keV (probably annihilation radiation). The relative photon intensities are 100, 203 ± 20, 87 ± 9 and 57 ± 8, respectively. The gamma-ray spectrum above the 511 keV peak is quite complex, but additional gamma rays of about 835, 960 and 1090 keV are evident, as well as others which are not completely resolved. The end point of the gamma-ray spectrum is about 4.3 MeV. Gamma-gamma coincidence experiments show that the 125, 267 and 392 keV gamma rays are in cascade, indicating excited states in Os^{184} at 125, 392 and 784 keV, with possible spins of 2+, 4+ and 6+, respectively. A partial level scheme for Os^{184} is shown in fig. 8.

5. Discussion

In the work reported here, the new neutron-deficient iridium isotopes with mass numbers 182, 183 and 184 have been synthesized and their gross decay properties characterized.

Much remains to be learned about these isotopes. In the case of the mass-183 chain, we see that the two Os^{183} isomers, with widely different spins, are populated to a similar extent in the decay of Ir^{183}. Thus Ir^{183} itself may possess two isomeric states of similar half lives, or the decay of Ir^{183} may lead to high-lying states of Os^{183}, which decay to both isomeric levels. The possibility of triple isomerism in Os^{183} also warrants investigation.

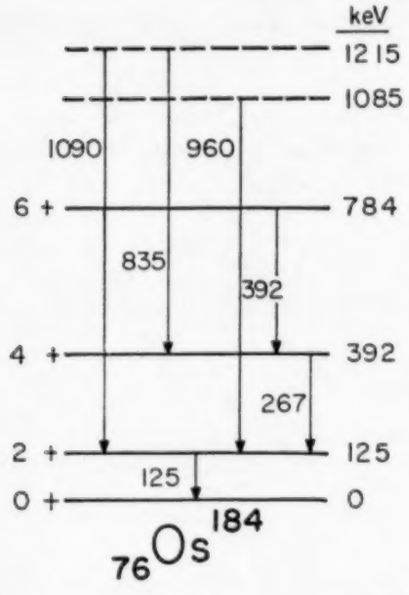

Fig. 8. Partial level scheme of Os^{184}.

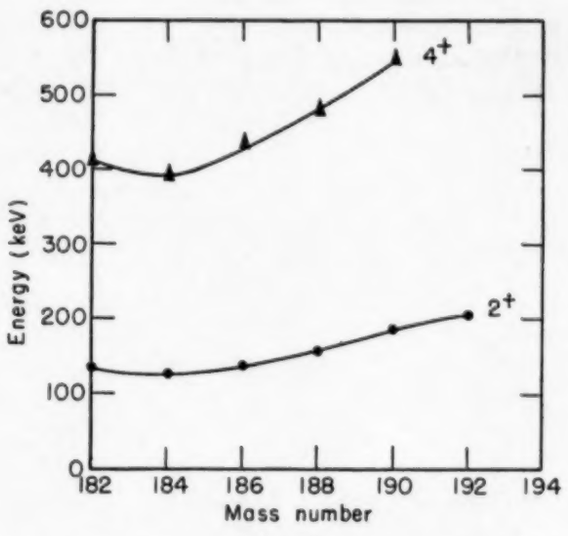

Fig. 9. Energies of first 2+ and 4+ levels in even-mass Os isotopes.

In the even-mass osmium isotopes, it is of interest to correlate the energies of the first 2+ and 4+ excited states. Fig. 9 shows such a correlation diagram in which the energies of Os^{182} and Os^{184} have been included. Note that there is a minimum in the energies of the 2+ and 4+ states at mass number 184. It thus appears that a maximum in the moments of inertia of the osmium isotopes is reached at Os^{184}, which has 108 neutrons. It is interesting to note that Nilsson has calculated theoretically [11]) that the position of this maximum is expected to be at neutron number 106.

Note added in proof: After the writing of this paper, we have read of the recent independent discovery of Ir^{184} by the Leningrad group, V. I. Baranov, K. Ya. Gromov, B. S. Dzhelepov, A. Ch. Bai, T. V. Malisheva, V. A. Morozov, B. A. Khotin, and V. G. Chumin, Izvestia ANCCCR, Ser. Fiz **24** (1960) 1080. Their reported half-live, 3.1 ± 0.3 hours, is in good agreement with our value.

We would like to thank Mr. James Harris for assistance in taking the data. One of us (R. A. N.) wishes to thank Professor I. Perlman for the hospitality accorded him while a guest at the Radiation Laboratory.

References

1) M. W. Johns, C. C. McMullen, I. R. Williams and S. V. Nablo, Can. J. Phys. **34** (1956) 69
2) A. H. W. Aten, Jr., and G. D. DeFeyfer, Physica **21** (1955) 543
3) R. M. Diamond and J. M. Hollander, Nuclear Physics **8** (1958) 143
4) P. S. Fisher and R. A. Naumann, Phys. Rev. **112** (1958) 1717
5) W. R. Kane, G. T. Emery, G. Scharff-Goldhaber and M. McKeown, Phys. Rev. **119**(1960) 1953
6) D. Strominger, J. M. Hollander and G. T. Seaborg, Revs. Mod. Phys. **30** (1958) 585
7) G. Scharff-Goldhaber, Brookhaven National Laboratory, private communication in ref. [6])
8) J. O. Rasmussen and M. Nakamura, University of California, Radiation Laboratory, Report, UCRL-8867, July 1959
9) J. O. Newton, Phys. Rev. **117** (1960) 1510, 1520
10) C. J. Gallagher, Jr., J. O. Newton and V. S. Shirley, Phys. Rev. **113** (1959) 1298
11) S. G. Nilsson, Lawrence Radiation Laboratory, private communication, December 1960

2.E: 2.L

Nuclear Physics **25** (1961) 259—265; © *North-Holland Publishing Co., Amsterdam*

Not to be reproduced by photoprint or microfilm without written permission from the publisher

THE ELASTIC SCATTERING OF 29 MeV ^{3}He-PARTICLES BY Cl, Kr AND Xe

J. AGUILAR, A. GARCÍA,

Department of Physics, University of Valencia, Spain

J. B. A. ENGLAND,

Department of Physics, University of Birmingham, England

P. E. HODGSON

The Clarendon Laboratory, Oxford, England

and

W. T. TONER

Department of Natural Philosophy, University of Glasgow, Scotland

Received 16 February 1961

Abstract: Angular distributions for the scattering of 29 MeV ^{3}He-particles by Cl, Kr and Xe have been measured using a photographic plate method. Absolute differential cross-sections for elastic scattering are given in the centre-of-mass system in the angular range 14° to 80°. The experimental results are analysed in terms of the optical model of the interaction and best fit parameters of this model are obtained.

1. Introduction

In recent papers, Bredin *et al.* [1]), Aguilar *et al.* [2]), Greenlees and Rowe [3]), Greenlees *et al.* [4]) and Wegner and Hall [6]) have reported the experimental angular distributions for the elastic scattering of 29 MeV and 21 MeV ^{3}He-particles by various nuclei from ^{1}H to ^{197}Au. Some of these distributions [2,4,5]) have been analysed in terms of the optical model of the interaction. It has been shown by Hodgson [7]) that the ^{3}He-particle is a particularly suitable projectile for examining the outer diffuse edge of the nucleus, because of its almost completely surface interaction in elastic processes.

In the present work, the elastic angular distributions for the scattering of 29 MeV ^{3}He-particles from naturally occurring Cl, Kr and Xe, are reported. These results lie in the angular range from 14° to 80° in the centre-of-mass system. The distributions have been analysed at Oxford in terms of the optical model.

2. Experimental Method

The experimental procedure, using a nuclear emulsion plate camera, has been described in detail by Gibson *et al.* [8]). The Nuffield Cyclotron of the University

of Birmingham was used as described by Fremlin *et al.* [9]) to produce an external beam of 29 MeV ^{3}He-particles. The collimated beam was passed into a scattering camera filled with the gaseous target and the particles scattered from a well-defined volume of the gas were registered in Ilford C2 and G-special emulsions. The total beam charge passed during the exposure was collected and measured in a Faraday cup. The energy of the beam was determined by measuring the ranges of the elastically scattered particles in emulsion. These ranges were compared with range-energy tables derived from the proton data of Gibson *et al.* [10]), correction being made for loss of energy in the gas filling of the camera as described by England *et al.* [11]). The pressure of the target gas, the total collected beam charge and the beam energy for each exposure are shown in table 1.

TABLE 1

Experimental conditions

Target gas	Pressure (cm of Hg at 15°C)	Collected charge (μC)	Beam energy MeV
CCl_4 (vapour)	11.1	2.91	29.1±0.1
Kr (spectroscopically pure)	6.0	2.39	29.4±0.1
Xe (spectroscopically pure)	5.4	2.41	29.2±0.1

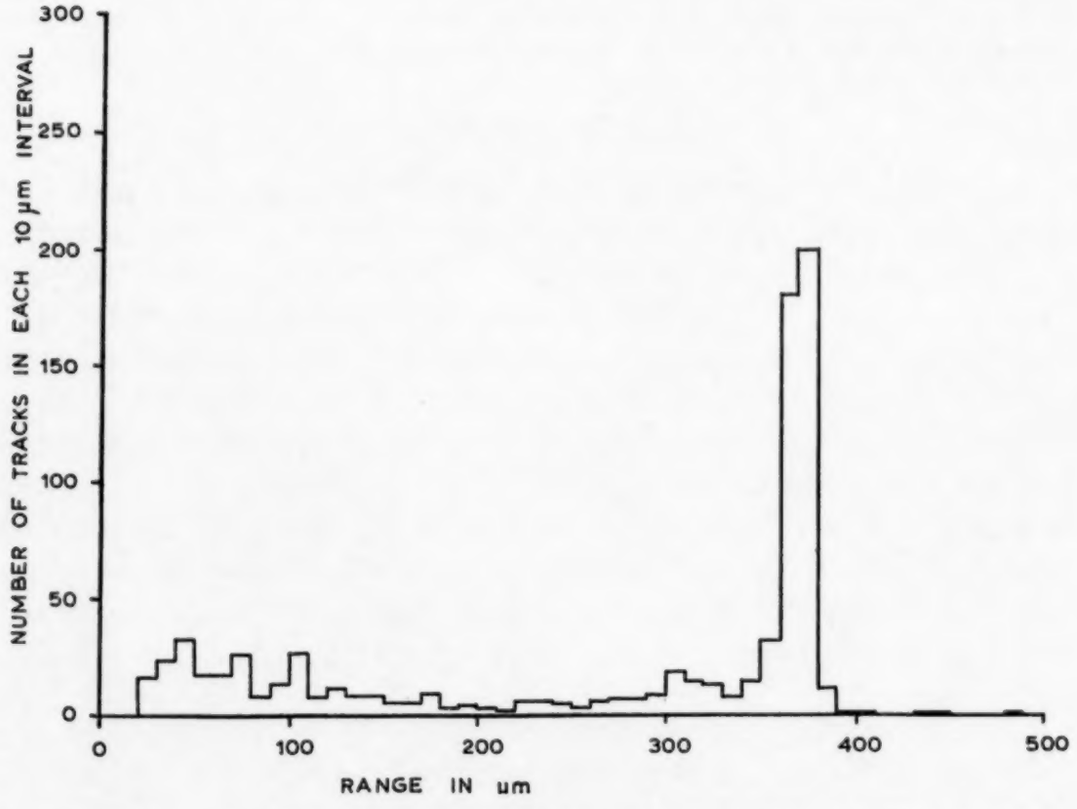

Fig. 1. Range histogram of doubly charged particles scattered by Kr at 36¼° in the laboratory system for an incident 29.4 MeV ^{3}He-particle beam. Ranges are not corrected for dip in the emulsion.

After processing, the plates were scanned for tracks of elastically and inelastically scattered particles as described by Gibson *et al.* [8]). A typical range histogram of the tracks of doubly charged particles scattered by Kr at $36\frac{1}{4}$ degrees in the laboratory system, is shown in fig. 1. The elastic differential cross-sections were calculated from the number of elastically scattered particles, the pressure of the target gas and the total collected beam charge; systematic errors in the absolute values are believed to be less than 5 %.

The plates from the Kr and Xe exposures were scanned in Glasgow and those from the Cl exposure in Valencia.

3. Experimental Results

The experimental elastic differential cross-sections in the centre-of-mass system, plotted as a function of centre-of-mass angle, are shown in figs. 2—4

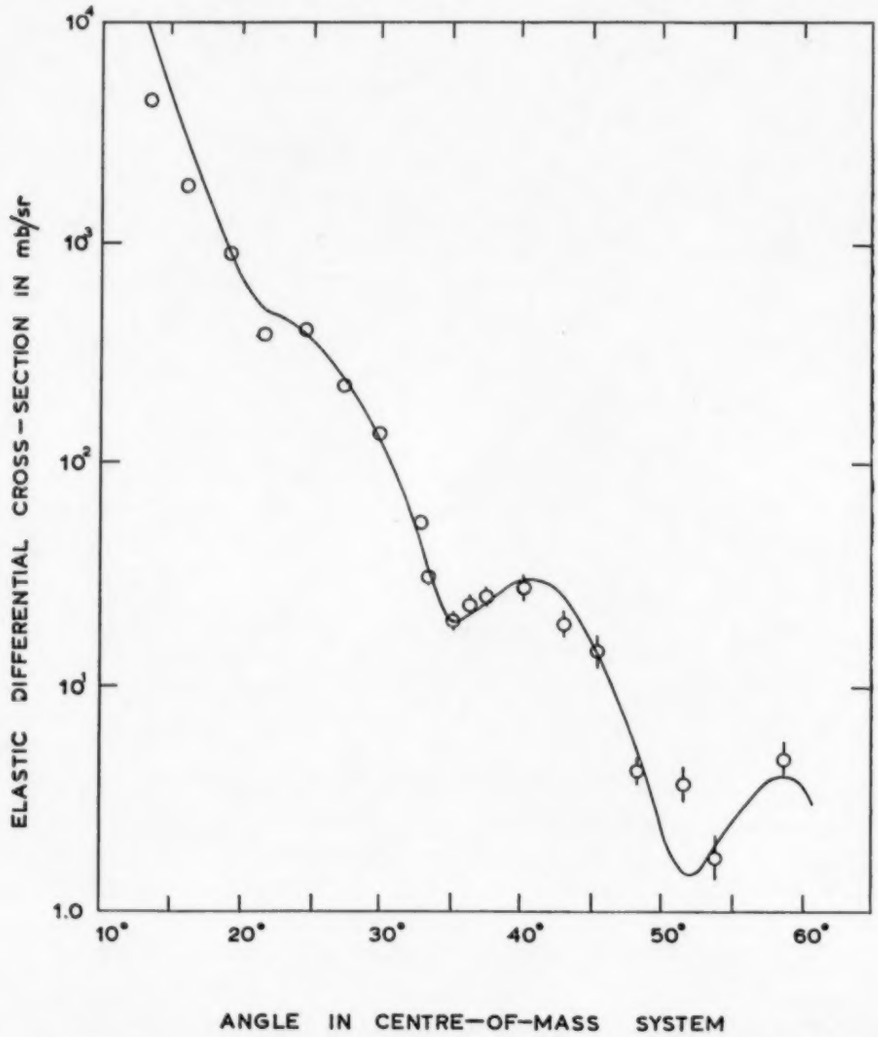

Fig. 2. The experimental elastic differential cross-section in the centre-of-mass system for the scattering of 29.1 MeV ^{3}He-particles from Cl plotted as a function of centre-of-mass angle. The theoretical curve is for the optical model with $U = -30$ MeV, $W = -25$ MeV, $r_0 = 1.60$ fm, $a = 0.65$ fm and $\sigma_R = 1354$ mb.
○ experimental (Aguilar and García), ———— theoretical (Hodgson).

together with the best fit optical model curves. In the results for Kr and Xe, the low lying excitation levels may contribute some inelastic particles which would be included in the elastic results. However, it is unlikely that in the angular ranges covered by the present results that this is greater than 2 %. In the case of the Xe results, a fault in the integrator used to record the beam charge caused the results to be too high. These results were normalized to the Rutherford values at small angles and the normalization factor was found to be 0.87 (ref. [12])).

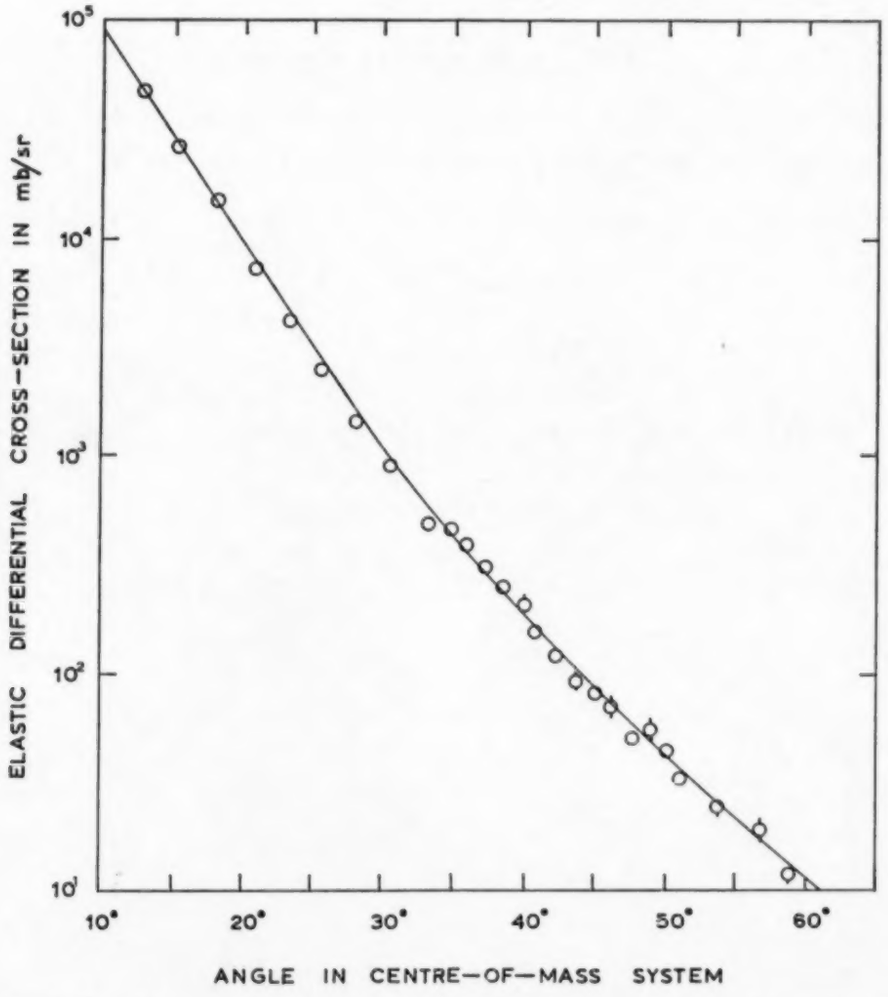

Fig. 3. The experimental elastic differential cross-section in the centre-of-mass system for the scattering of 29.4 MeV ^{3}He-particles from Kr plotted as a function of centre-of-mass angle. The theoretical curve is for the optical model with $U = -6$ MeV, $W = -8$ MeV, $r_0 = 1.52$ fm, $a = 0.58$ fm and $\sigma_R = 1052$ mb.
○ experimental (Toner), ——— theoretical (Hodgson).

The Cl results were obtained by bombarding CCl_4 vapour and subtracting the known carbon cross-sections (Aguilar *et al.* [2])) to obtain the elastic results for Cl. The first two experimental points are too low due to uncertainties in the carbon cross-sections at low angles. Inelastic reactions for this nucleus were masked by the presence of the inelastic ^{3}He reactions in ^{12}C reported by Aguilar *et al.* [2]).

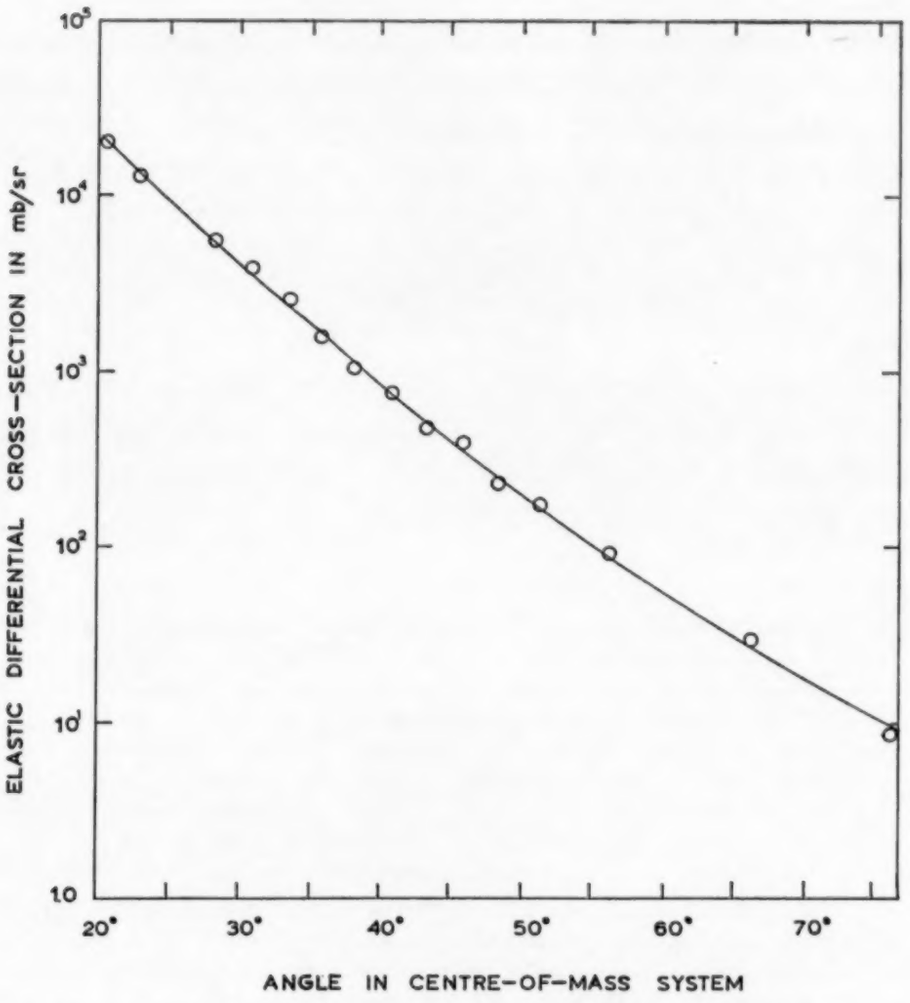

Fig. 4. The experimental elastic differential cross-section in the centre-of-mass system for the scattering of 29.2 MeV ^{3}He-particles from Xe plotted as a function of centre-of-mass angle. The theoretical curve is for the optical model with $U = -10$ MeV, $W = -10$ MeV, $r_0 = 1.54$ fm, $a = 0.62$ fm and $\sigma_R = 1229$ mb.
○ experimental (Toner), ——— theoretical (Hodgson).

4. Optical Model Analysis

The results were analysed by assuming that the interaction between the ^{3}He-particles and the target nuclei can be represented by a potential of the form

$$V(r) = V_C(r) + (U + iW)f(r)$$

where $V_C(r)$ is the Coulomb potential, taken to be that due to a uniformly charged sphere of radius $1.3\,A^{\frac{1}{3}}$ fm, U and W are the refracting and absorbing nuclear potentials and $f(r) = [1+\exp([r-R]/a)]^{-1}$ is the Saxon-Woods radial form factor with nuclear radius $R = r_0 A^{\frac{1}{3}}$ and surface diffuseness a. Spin-orbit forces are not included as their strength is unknown and their effect on the differential cross-section is likely to be small. If suitable numerical values are chosen for the potential parameters the corresponding Schrödinger wave equa-

tion for the interaction may be solved to give the observable quantitites by the methods described by Buck, Maddison and Hodgson [13]). All the calculations were made on the Oxford University Mercury Computer.

In order to find the potential giving the best fit to the data the four parameters U, W, r_0 and a were systematically varied to minimise

$$\Delta_N = \sum_N \left(\frac{(d\sigma/d\Omega)_{exp} - (d\sigma/d\Omega)_{th}}{\delta(d\sigma/d\Omega)_{exp}} \right)^2,$$

where the summation extends over all the experimental points; $\delta(d\sigma/d\Omega)_{exp}$ is the statistical error on the experimental results. The minimisation and normalisation procedures are described elsewhere [12]). The parameters giving the best fit to the data are summarised in table 2.

TABLE 2

Parameters of the best fit potentials, the calculated reaction cross-sections and the values of Δ_N for the N measured points

Nucleus	$-U$ (MeV)	$-W$ (MeV)	r_0(fm)	a(fm)	σ_R(mb)	N	Δ_N	B
Cl	30	25	1.60	0.65	1354	16	70 [a])	1
Kr	6	8	1.52	0.58	1052	26	80	1.05
Xe	10	10	1.54	0.62	1229	15	14	0.87 [b])

B is the normalisation constant by which the experimental distribution was multiplied to agree with the theoretical one. σ_R is the reaction cross-section.

[a]) The first two experimental points were omitted when calculating this number.

[b]) An integrator fault caused this large normalisation factor.

The radial form of the optical model potential chosen for these calculations is not unique; any form with a similar behaviour in the surface region would give an equally good fit to the data. This has been verified by repeating some of the calculations with a surface Gaussian for the radial form of the absorbing potential $W(r)$. This potential is quite different from the Saxon-Woods shape in the nuclear interior, yet is similar in the surface region and gives the same differential and reaction cross-sections. This indicates that the interaction takes place essentially in the surface regions, which is what would be expected on physical grounds. The potentials found in the present work are therefore only meaningful in this region.

An optical model study [5]) of ^{3}He scattering has shown that for incident particles of the same energy the diffraction effects decrease as the charge of the target nucleus increases. This is because the scattering becomes more predominantly Coulomb as the nuclear charge increases so that the ^{3}He-particle only samples the fringe of the nuclear field. When diffraction effects are absent and the energy is not too low, the differential cross-section is particularly sensitive to the surface potential. This is the case for krypton and xenon in the present

work. If measurements were available for incident particles of a range of energies it would be instructive to analyse them to see how the best fit potential changes as the character of the scattering changes from near-Coulomb to bulk diffraction.

We would like to thank Professors W. E. Burcham, F.R.S. and D. H. Wilkinson, F.R.S., for their continuing interest, Dr. P. V. March for helpful discussions, Miss A. Bonet, Miss A. Iscar, Miss M. Thomson and Miss P. A. Lindsay for their help in scanning the photographic plates, the Director of the Oxford University Computing Laboratory for the use of the Mercury Computer, Dr. B. Buck and Mr. R. N. Maddison for their work on the computer programme, Miss N. Reynolds, Mrs. M. Fluendy and the staff of the Computing Laboratory for their assistance and the D.S.I.R. for its support.

References

1) D. J. Bredin, J. B. A. England, D. Evans, J. S. C. McKee, P. V. March, E. M. Mosinger and W. T. Toner, Proc. Roy. Soc. **258** (1960) 202
2) J. Aguilar, W. E. Burcham, J. B. A. England, A. García, P. E. Hodgson, P. V. March, J. S. C. McKee, E. M. Mosinger and W. T. Toner, Proc. Roy. Soc. **257** (1960) 13
3) G. W. Greenlees and P. C. Rowe, Nuclear Physics **15** (1960) 687
4) G. W. Greenlees, J. S. Lilley, P. C. Rowe and P. E. Hodgson, Nuclear Physics **24** (1961) 334
5) P. E. Hodgson, Nuclear Physics **21** (1960) 28
6) H. E. Wegner and W. S. Hall, Bull. Am. Phys. Soc. **3** (1958) 338, private communication (1960)
7) P. E. Hodgson, Nuclear Physics **23** (1961) 499
8) W. M. Gibson, D. J. Prowse and J. Rotblat, Proc. Roy. Soc. **234** (1957) 237
9) J. H. Fremlin, W. Hardy and H. R. Shaylor, J. Sci. Instr. **36** (1959) 390
10) W. M. Gibson, D. J. Prowse and J. Rotblat, Nature **173** (1954) 1180
11) J. B. A. England, R. McKeague and P. E. Hodgson, Nuclear Physics **16** (1960) 52
12) P. E. Hodgson, J. Aguilar, A. García and J. B. A. England, Nuclear Physics **22** (1961) 138
13) B. Buck, R. N. Maddison and P. E. Hodgson, Phil. Mag. **5** (1960) 1181

1.D.3

Nuclear Physics **25** (1961) 266—277; © *North-Holland Publishing Co., Amsterdam*

Not to be reproduced by photoprint or microfilm without written permission from the publisher

ENERGY LEVELS OF EVEN NUCLEI ON THE HYDRODYNAMICAL MODEL WITH VIBRATION-ROTATION INTERACTION

E. D. KLEMA †, C. A. MALLMANN †† and P. DAY

Argonne National Laboratory, Argonne, Illinois ‡

Received 26 January 1961

Abstract: The Davydov and Chaban model for even nuclei, in which the beta-vibration-rotation interaction is taken into account exactly, has been used to calculate the excited states of these nuclei. The calculated energies have been compared with experimental data, special attention being paid to nuclei with known 0^+ excited levels. Where possible, comparison has been made also with the correlation of experimental data by means of the perturbation approach of Mallmann and Kerman and of the Bohr-Mottelson model.

1. Introduction

In a recent paper, Davydov and Chaban [1]) have extended the work of Davydov and Filippov [2]) and Davydov and Rostovsky [3]) to include in an exact manner beta-vibration-rotation interactions of non-axially symmetric even nuclei. This interaction had been taken into account as a perturbation by Mallmann and Kerman [4]).

In the present work, machine calculations have been made of the energies of a large number of excited states according to the model of Davydov and Chaban. The detailed results of the calculations have been made available in an ANL report [5]) to allow others to compare experimental data easily with the model.

The results of the calculations with the model have been compared with presently available data on the measured energies of excited states of even nuclei. Special attention has been paid to those nuclei which have measured 0^+ excited levels, since these levels are the lowest ones arising from the β-vibrational modes.

2. Calculations

The first three roots $\nu_l (l = 1, 2, 3)$ of the transcendental equation derived in ref. [1]) (eq. (2.12)) were obtained numerically by means of a digital computer, and energies were calculated for values of the "non-axiality" parameter γ of

† Permanent address: The Technological Institute, North-western University, Evanston, Illinois.

†† Present address, Comisión Nacional de la Energia Atómica, Av. Lib. Gral. San Martin 8250, Buenos Aires, Argentina.

‡ Based on work performed under the auspices of the U. S. Atomic Energy Commission.

30°, 25°, 20°, 15°, 12°, 10°, 9° and 8° and of the "non-adiabaticity" parameter μ of 1.0, 0.9, 0.8, 0.7, 0.6, 0.5, 0.4, 0.35, 0.3, 0.25, 0.2, 0.15 and 0.1. The energies of the following 36 levels were obtained: $^{1}0$, $^{1}2$, $^{1}4$, $^{1}6$, $^{1}8$, $^{1}10$, $^{1}12$, $^{2}2$, $^{1}3$, $^{2}4$, $^{1}5$ and $^{2}6$ for ν_1, ν_2 and ν_3, where the superscript is the ordering parameter K of Davydov and Filippov [2]) and the main number is the angular momentum J of the level.

In each case the series evaluation of the solution of the transcendental equation was carried out to a sufficient number of terms so that the last term contributed $< 10^{-4}$ to the previous result. The calculations were monitored by printing out in each case the number of terms required to satisfy the above condition. Checks on the present calculations were also obtained by making sure that the results agreed with those given previously by Mallmann and Kerman [4]), which are identical for the case of small μ. The results of the calculations are presented as ratios of the energy of the state in question to that of the first excited state of spin 2 for easy comparison of the energy predictions with experimental results.

3. Comparison with Data

The results of the calculations relevant to the present work are given graphically in figs. 1—8. In each case the first subscript of the R gives the ordering number K of the level of angular momentum given by the number in the parenthesis, and the second subscript l gives the number of the root of the transcendental equation which gives rise to the level. The straight lines represent the perturbation theory results of Mallmann and Kerman [4]), except for the $R_{21}(2)$ lines on figs. 4 and 5. The $R_{21}(2)$ lines have been drawn to allow the data to be compared with the relationship $R_{11}(3) = R_{21}(2)+1$, which is valid for any rotor [4]). The values of the parameters γ and μ are indicated at the ends of the respective curves. As discussed previously [4]), all ratios are plotted as functions of $R_{21}(2)$, the ratio of the energies of the second spin 2 and the first spin 2 states (arising from the root ν_1). The experimental data are given as open circles for the indicated nuclei.

Each experimental point on the graphs corresponds to a value of γ and a value of μ. These values, determined by interpolation on the graphs, are collected in table 1. The uncertainties $\Delta\gamma_e$ and $\Delta\mu_e$ correspond to the uncertainties of the experimentally determined ratios of energies. The uncertainties $\Delta\gamma_i$ and $\Delta\mu_i$ correspond to the uncertainties due to the interpolation procedure for the determination of γ and μ. In each case the identification of the energy level, the ratio of its energy to that of the first spin 2 state, and the corresponding values of γ and μ with their uncertainties are given, with K giving the ordering number of Davydov and Filippov of the level of angular momentum J. The ordering number of the roots is given by the parameter l. Particular care has been taken to include all cases of known spin 0 excited states.

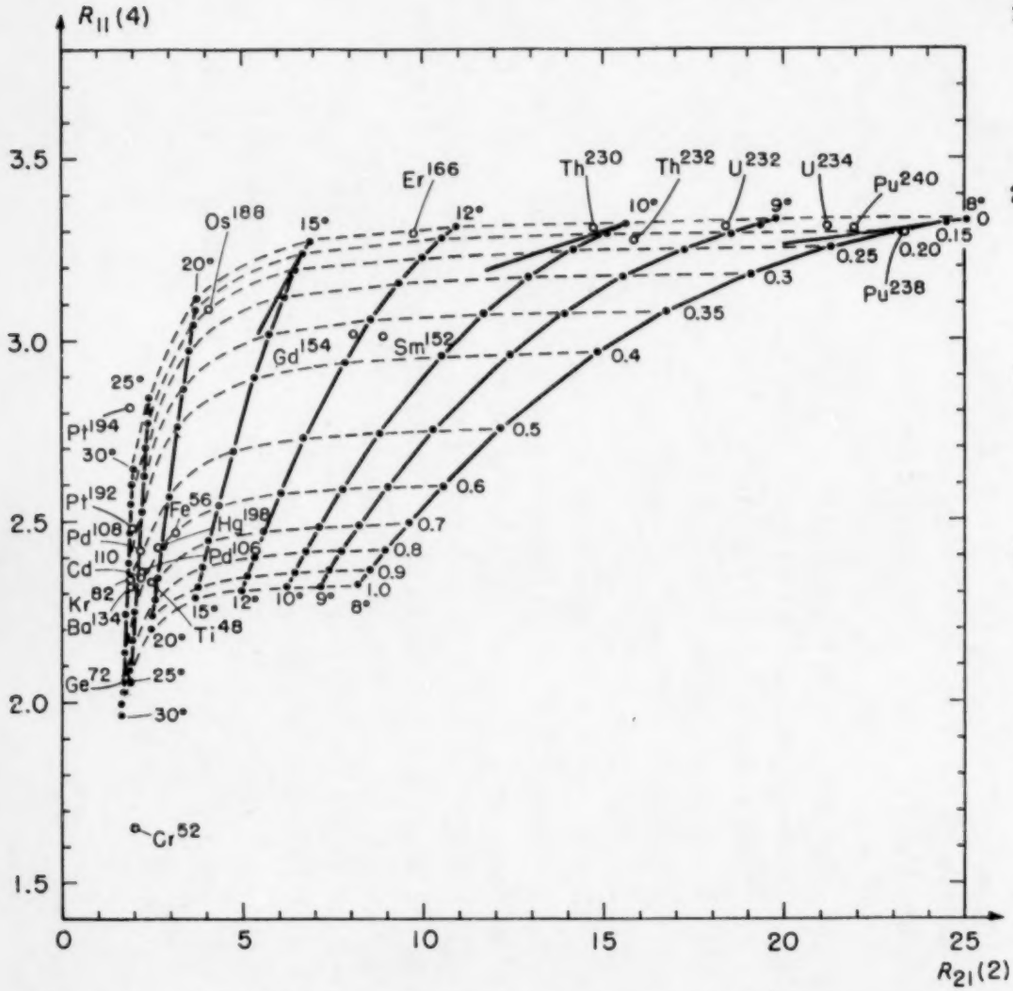

Fig. 1. Values of $R_{KI}(J)$ as a function of $R_{21}(2)$. The open circles represent the experimental data for the indicated nuclei. The solid circles are computed points; the solid lines connect equal values of γ (non-axiality parameter) and the dashed lines connect equal values of μ (non-adiabaticity parameter). The straight solid lines on figs. 1, 3, 4 and 6, except for those marked $R_{21}(2)$ on fig. 4, represent the perturbation theory results of Mallmann and Kerman. The $R_{21}(2)$ lines on figs. 4 and 5 are shown to allow comparison of the data with the relationship $R_{11}(3) = R_{21}(2)+1$, which is valid for any rotor. The curve joining the crosses is for the b value of Mallmann and Kerman corresponding to $\mu = 0.2$.

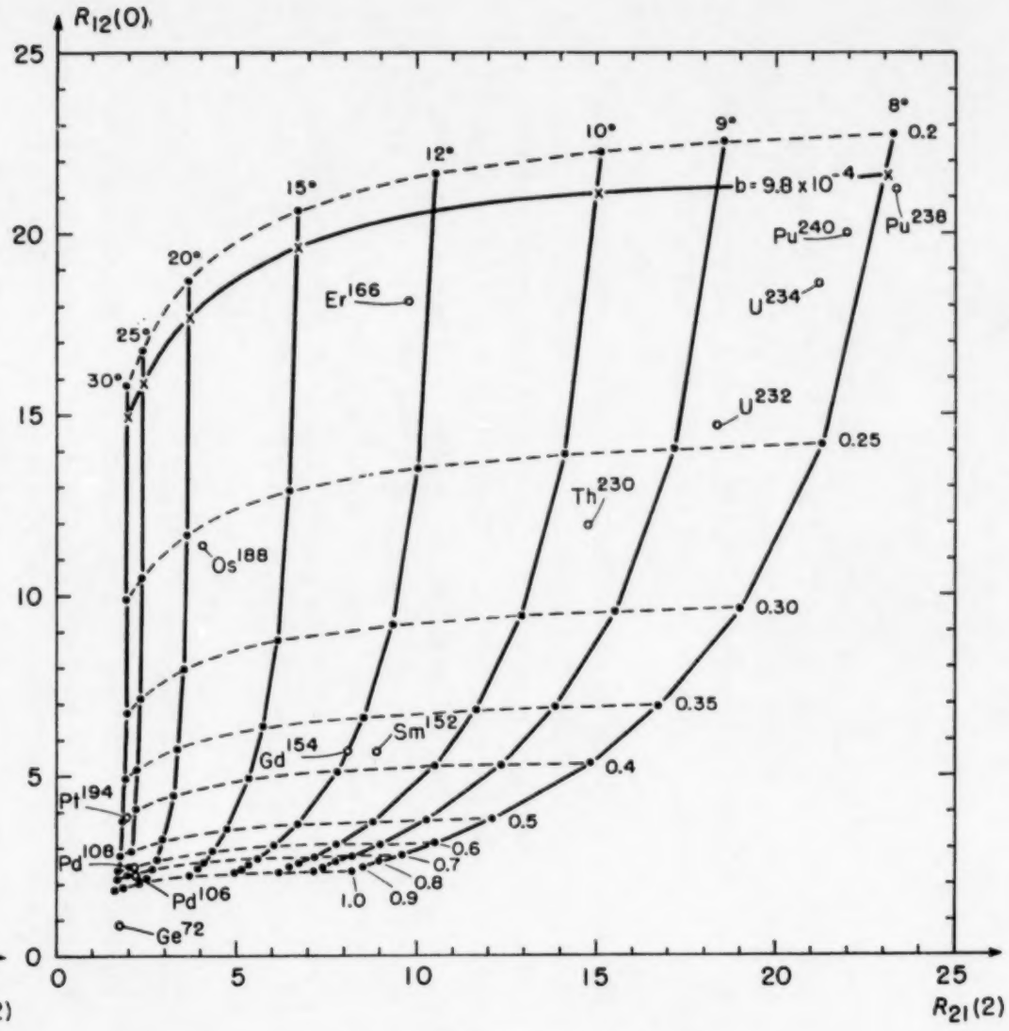

Fig. 2. See caption of fig. 1.

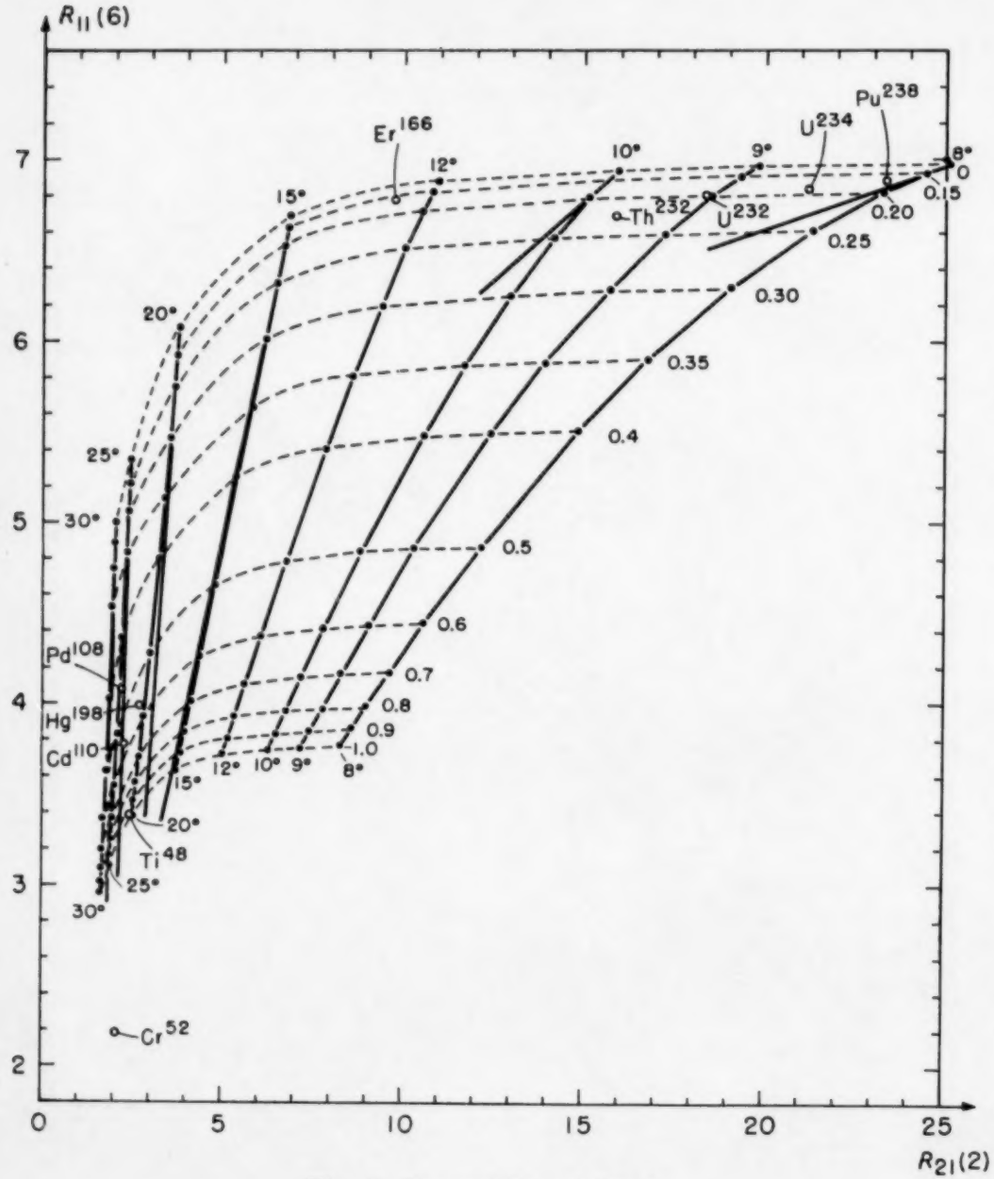

Fig. 3. See caption of fig. 1.

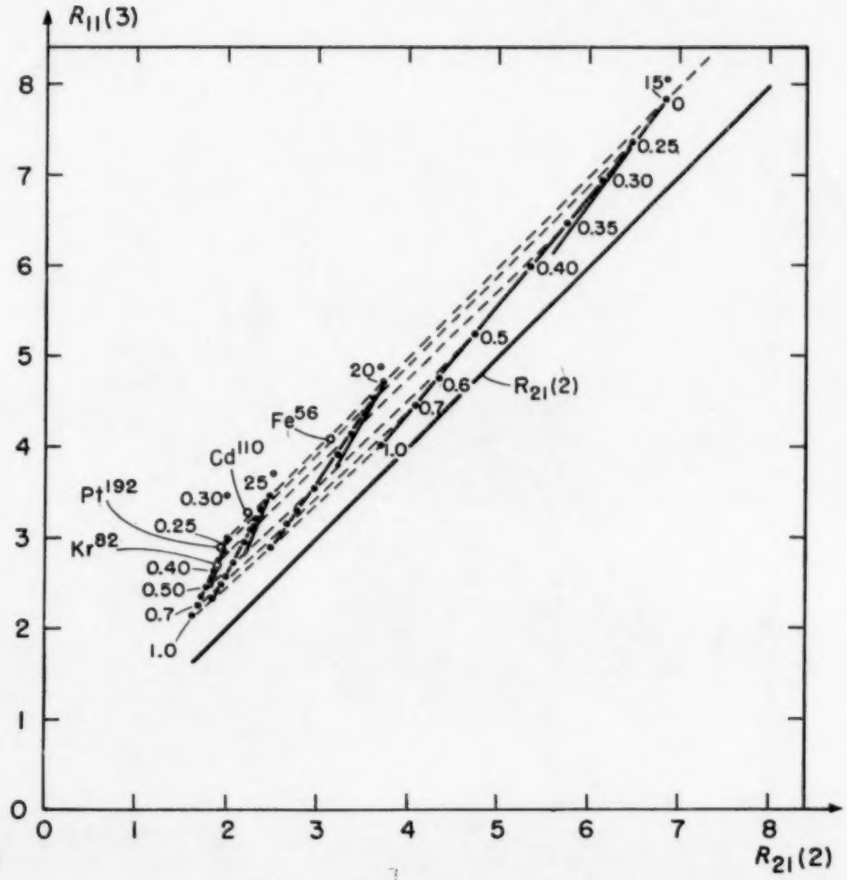

Fig. 4. See caption of fig. 1.

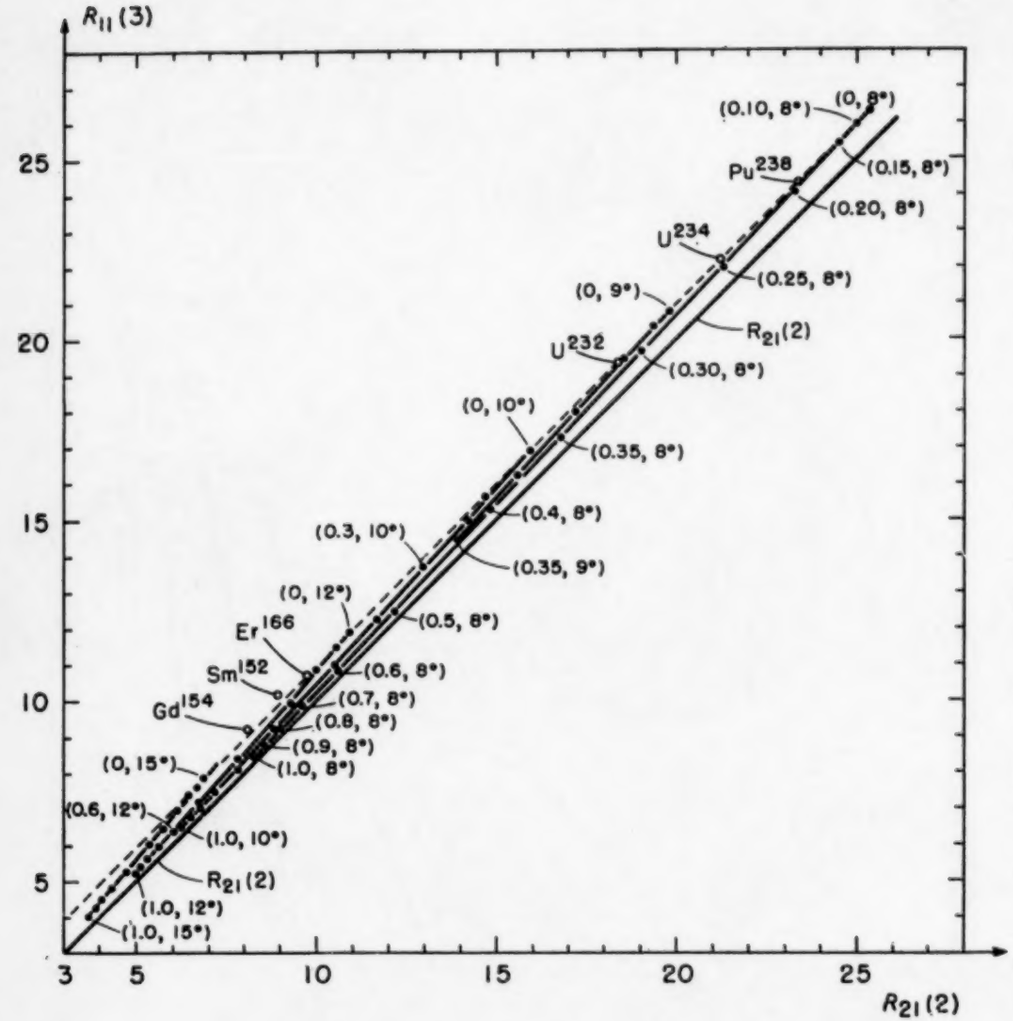

Fig. 5. See caption of fig. 1.

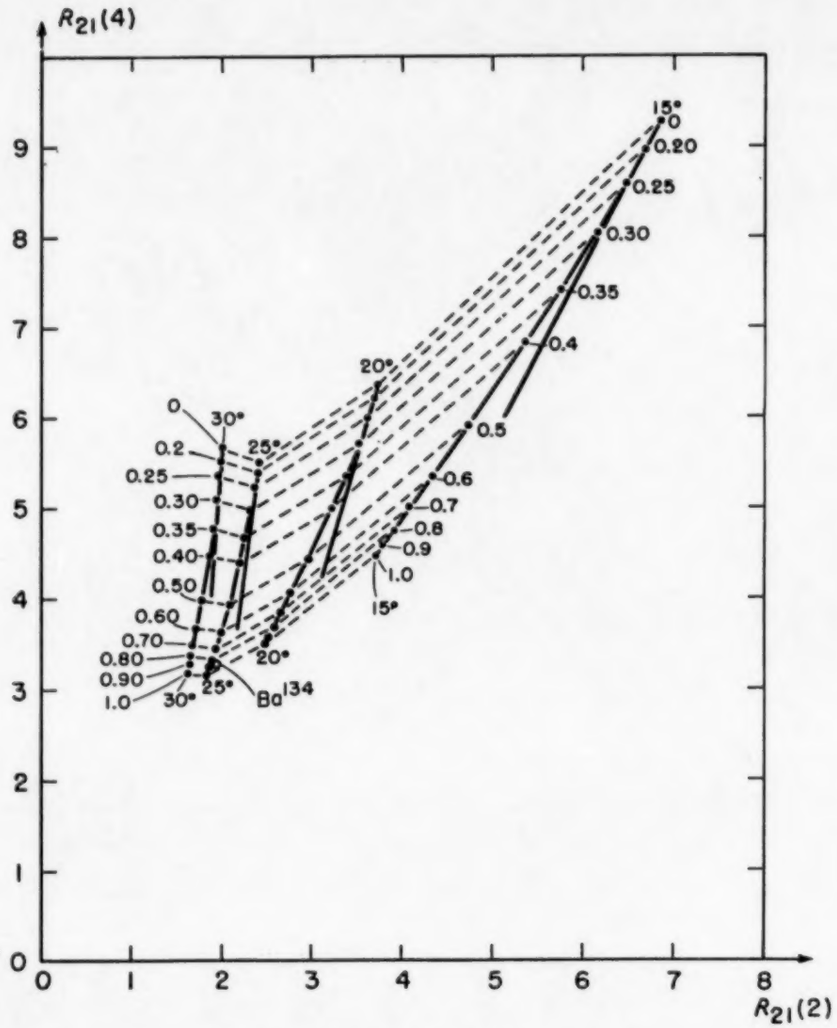

Fig. 6. See caption of fig. 1.

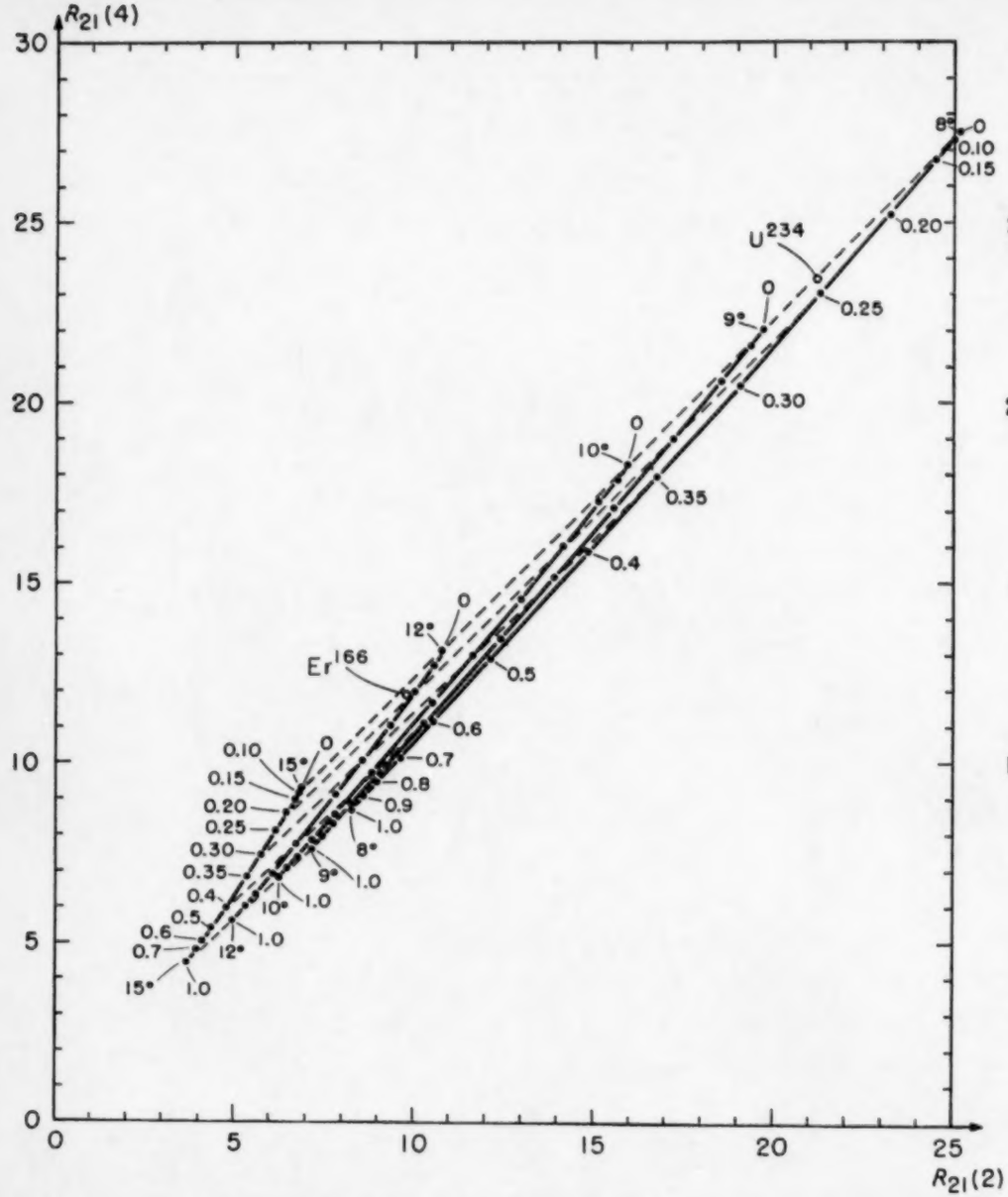

Fig. 7. See caption of fig. 1.

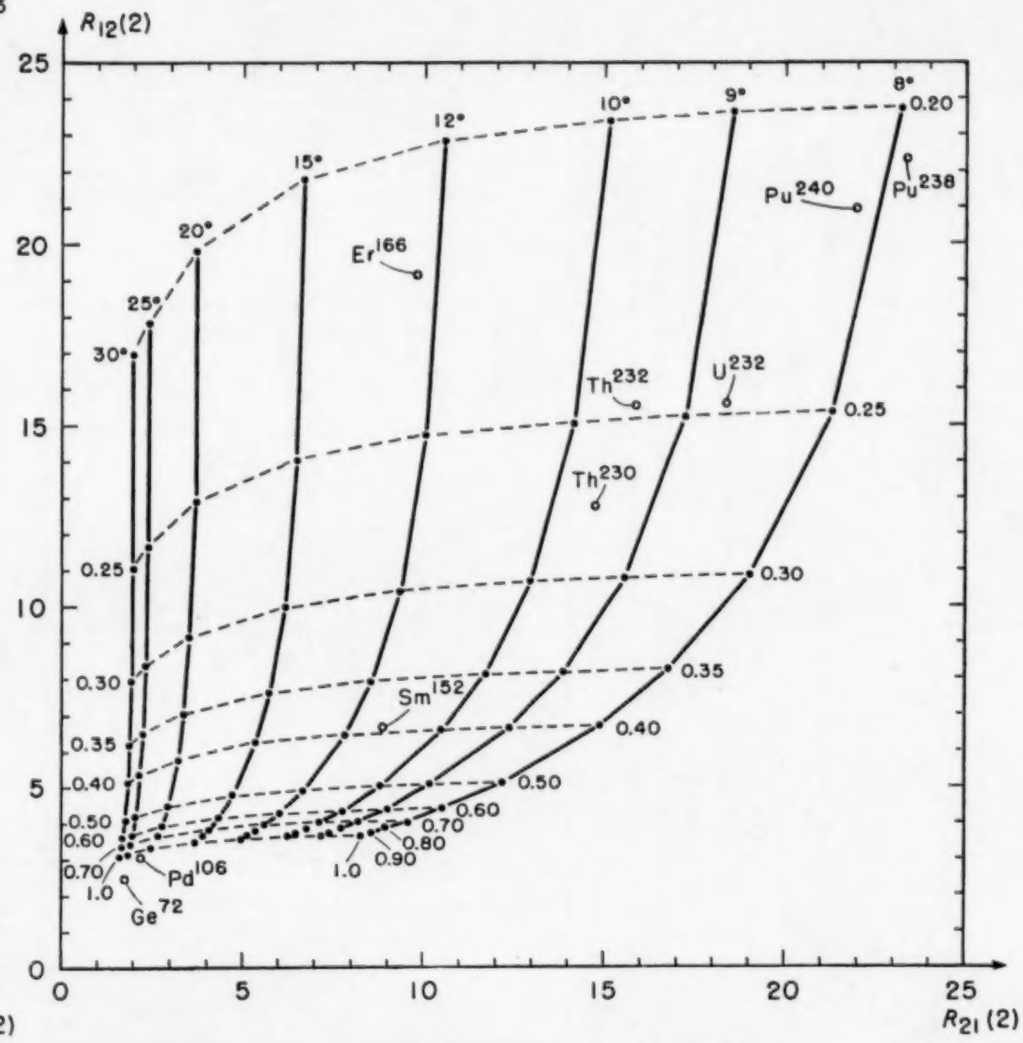

Fig. 8. See caption of fig. 1.

TABLE 1

Values of the "non-axiality" parameter γ and the "non-adiabaticity" parameter μ

The table gives the values of γ and μ as determined from the measured energies of the various excited states of the indicated even nuclei. The measured energies are given as ratios to that of the first spin 2 state in terms of the parameters K and l, defined in the text, and the angular momentum J. The indicated uncertainties $\Delta\gamma_e$ and $\Delta\mu_e$ correspond to the uncertainties of the experimental measurements, and the uncertainties $\Delta\gamma_i$ and $\Delta\mu_i$ correspond to the uncertainties due to the interpolation procedure for the determination of γ and μ. The uncertainties are given as follows: 1.754 20 ≡ 1.754±0.020.

Nucleus	$^{K}J\ \nu_i$	$R_{Kl}(J)$	γ	$\Delta\gamma_i$	$\Delta\gamma_e$	μ	$\Delta\mu_i$	$\Delta\mu_e$	Ref.
Ti^{48}	$^{2}2,\ \nu_1$	2.469 26							a)
	$^{4}4,\ \nu_1$	2.333 13	21.2	2	3	0.66	1	2	
	$^{6}6,\ \nu_1$	3.387 17	20.05	5	30	1.00	1	4	
Cr^{52}	$^{2}2,\ \nu_1$	2.069 13							a)
	$^{4}4,\ \nu_1$	1.654 9	(out of range)						
	$^{6}6,\ \nu_1$	2.178 13	(out of range)						
Fe^{56}	$^{2}2,\ \nu_1$	3.153 35							a)
	$^{4}4,\ \nu_1$	2.467 50	18.4	2	2	0.61	1	6	
	$^{3}3,\ \nu_1$	4.079 65	21.4	2	5	0.25	5	+7 −25	
Ge^{72}	$^{2}2,\ \nu_1$	1.754 20							b)
	$^{4}4,\ \nu_1$	2.071 25	26.9	2	9	0.78	2	10	
	$^{0}0,\ \nu_2$	0.826 11	(out of range)						
	$^{2}2,\ \nu_2$	2.467 33	(out of range)						
Kr^{82}	$^{2}2,\ \nu_1$	1.899 1							b)
	$^{4}4,\ \nu_1$	2.344 1	27.70	20	2	0.450	2	1	
	$^{3}3,\ \nu_1$	2.695 2	29.0	10	1	0.380	20	2	
Pd^{106}	$^{2}2,\ \nu_1$	2.205 37							c)
	$^{4}4,\ \nu_1$	2.364 23	23.6	2	5	0.54	1	4	
	$^{0}0,\ \nu_2$	2.216 42	22.5	2	2	0.75	1	5	
	$^{2}2,\ \nu_2$	3.047 53	(out of range)						
Pd^{108}	$^{2}2,\ \nu_1$	2.170 24							d)
	$^{4}4,\ \nu_1$	2.417 27	24.4	2	4	0.480	10	30	
	$^{6}6,\ \nu_1$	4.083 65	24.8	1	3	0.444	5	20	
	$^{0}0,\ \nu_2$	2.419 35	23.3	2	1	0.627	10	20	
Cd^{110}	$^{2}2,\ \nu_1$	2.245 4							a)
	$^{4}4,\ \nu_1$	2.348 4	23.10	10	5	0.573	10	6	
	$^{6}6,\ \nu_1$	3.776 6	23.20	10	6	0.562	5	6	
	$^{3}3,\ \nu_1$	3.293 5	(out of range)						
Ba^{134}	$^{2}2,\ \nu_1$	1.931 3							a)
	$^{4}4,\ \nu_1$	2.317 1	26.7	10	1	0.489	2	2	
	$^{4}4,\ \nu_1$	3.259 3	24.5	5	1	0.900	30	3	

TABLE I (continued)

Nucleus	$^{K}J\,\nu_i$	$R_{KI}(J)$	γ	$\Delta\gamma_1$	$\Delta\gamma_e$	μ	$\Delta\mu_1$	$\Delta\mu_e$	Ref.
Sm^{152}	$^{2}2,\ \nu_1$	8.914 10							a)
	$^{4}4,\ \nu_1$	3.009 2	11.50	10	1	0.374	3	1	
	$^{3}3,\ \nu_1$	10.136 10	(out of range)						
	$^{0}0,\ \nu_2$	5.624 6	11.28	3	1	0.383	1	1	
	$^{2}2,\ \nu_2$	6.658 20	11.30	20	2	0.390	10	1	
Gd^{154}	$^{2}2,\ \nu_1$	8.090 11							a)
	$^{4}4,\ \nu_1$	3.013 2	12.22	2	1	0.366	3	1	
	$^{3}3,\ \nu_1$	9.162 11	(out of range)						
	$^{0}0,\ \nu_2$	5.681	12.02	3	1	0.379	1		
Er^{166}	$^{2}2,\ \nu_1$	9.770 40							a)
	$^{4}4,\ \nu_1$	3.294 6	12.67	2	5	0.140	30	+ 20 −140	
	$^{6}6,\ \nu_1$	6.774 30	12.58	2	2	0.160	3	30	
	$^{3}3,\ \nu_1$	10.686 60	12.50	15	3	0.200	50	+ 50 −200	
	$^{4}4,\ \nu_1$	11.889 50	12.40	10	10	0.220	10	20	
	$^{0}0,\ \nu_2$	18.12	12.33	10	3	0.217	1		
	$^{2}2,\ \nu_2$	19.13	12.30	10	2	0.220	2		
Os^{188}	$^{2}2,\ \nu_1$	4.085 21							b)
	$^{4}4,\ \nu_1$	3.084 18	18.80	4	10	0.259	2	20	
	$^{0}0,\ \nu_2$	11.37 3	19.20	14	7	0.255	2	1	
Pt^{192}	$^{2}2,\ \nu_1$	1.936 1							b)
	$^{4}4,\ \nu_1$	2.490 4	28.80	20	3	0.346	2	2	
	$^{3}3,\ \nu_1$	2.910 3	(out of range)						
Pt^{194}	$^{2}2,\ \nu_1$	1.897 15							c)
	$^{4}4,\ \nu_1$	2.809 17	(out of range)						
	$^{0}0,\ \nu_2$	3.853 36	29.20	50	20	0.401	1	3	
Hg^{198}	$^{2}2,\ \nu_1$	2.644 3							a)
	$^{4}4,\ \nu_1$	2.44 2	20.80	5	3	0.580	2	20	
	$^{6}6,\ \nu_1$	3.97 3	20.90	10	10	0.561	2	20	
Th^{230}	$^{2}2,\ \nu_1$	14.77							f)
	$^{4}4,\ \nu_1$	3.302	10.20	5		0.175	5		
	$^{0}0,\ \nu_2$	11.96	9.50	10		0.270	5		
	$^{2}2,\ \nu_2$	12.75	9.50	10		0.276	5		
Th^{232}	$^{2}2,\ \nu_1$	15.88 30							a)
	$^{4}4,\ \nu_1$	3.271 60	9.60	5	10	0.225	5	+ 50 −225	
	$^{6}6,\ \nu_1$	6.69 10	9.48	5	10	0.225	5	25	
	$^{2}2,\ \nu_2$	15.54 30	9.45	10	10	0.248	1	2	

TABLE 1 (continued)

Nucleus	$^{K}J, \nu_i$	$R_{KI}(J)$	γ	$\Delta\gamma_1$	$\Delta\gamma_e$	μ	$\Delta\mu_1$	$\Delta\mu_e$	Ref.
	$^{2}2, \nu_1$	18.39 12							
	$^{1}4, \nu_1$	3.311 22	9.20	5	3	0.170	5	+ 40 −170	a)
U^{232}	$^{1}6, \nu_1$	6.801 50	9.02	5	2	0.202	5	10	
	$^{1}3, \nu_1$	19.34 12	9.26	10	5	0.150	80	+130 −150	
	$^{1}0, \nu_2$	14.68	8.75	5	3	0.244	1		
	$^{1}2, \nu_2$	15.57	8.75	5	2	0.248	1		
	$^{2}2, \nu_1$	21.20 9							
	$^{1}4, \nu_1$	3.31 2	8.55	5	2	0.170	5	+ 50 −170	a)
U^{234}	$^{1}6, \nu_1$	6.83 4	8.43	5	2	0.196	5	30	
	$^{1}3, \nu_1$	22.18 9	8.61	10	2	0.100	100	+130 −100	
	$^{2}4, \nu_1$	23.45 11	8.58	5	2	0.145	10	+ 45 −145	
	$^{1}0, \nu_2$	18.6	8.23	5	3	0.219	1		
	$^{2}2, \nu_1$	23.349 70							
	$^{1}4, \nu_1$	3.292 6	7.90	5	2	0.208	5	10	a)
Pu^{238}	$^{1}6, \nu_1$	6.889 14	8.12	5	2	0.170	5	10	
	$^{1}3, \nu_1$	24.302 80	8.19	10	2	0.150	80	+ 80 −150	
	$^{1}0, \nu_2$	21.216 70	7.90	3	2	0.206	1	1	
	$^{1}2, \nu_2$	22.351 70	7.90	5	2	0.208	1	1	
	$^{2}2, \nu_1$	21.96							
Pu^{240}	$^{1}4, \nu_1$	3.305	8.30	5		0.153	5		g)
	$^{1}0, \nu_2$	20.00	8.14	5		0.214	1		
	$^{1}2, \nu_2$	20.98	8.20	10		0.215	1		

a) C. A. Mallmann, Nuclear Physics submitted
b) Nuclear Data Sheets, National Academy of Sciences (National Research Council, Washington D. C.), up to and including the set Number 6 of 1959
c) Robinson, McGowan and Smith, preprint (1960)
d) M. A. Wahlgren and W. W. Meinke, Phys. Rev. **118** (1960) 181; M. E. Bunker and J. W. Starner, Bull. Am. Phys. Soc. **5** (1960) 253
e) Marklund, Van Nooijen and Grabowski, Nuclear Physics **15** (1960) 533
f) E. Arbman and O. B. Nielsen, private communication (1960)
g) Bunker, Dropesky, Knight, Starner and Warren, Phys. Rev. **116** (1959) 143

4. Discussion

The present work was undertaken to provide a detailed comparison between the experimental data and the predictions of the Davydov and Chaban model in view of the work of Mallmann on the correlation of measured energies by means

of the quasi-adiabatic general asymmetric rotor model [7]) and that of Mallmann and Kerman [4]).

Initially considering energy levels arising from the first root ν_1 for those cases [4]) for which $\mu \leqq 0.25$ ($b \leqq 5.3\times 10^{-3}$), there is no distinction to be made between the predictions of the present model and those of the work of Mallmann and Kerman [4]). This point is illustrated in table 2, in which we give the limiting

TABLE 2

Comparison of Davydov-Chaban model with that of Mallmann and Kerman.

The table gives the values of the parameter μ at which the predictions of $R_{KI}(J)$ as a function of $R_{21}(2)$ of the Davydov and Chaban model and the Mallmann and Kerman calculations are in agreement within 1 % for the levels with $({}^K J, \nu_1) = ({}^1 4, \nu_1)$, $({}^1 6, \nu_1)$, $({}^1 3, \nu_1)$, $({}^3 4, \nu_1)$, $({}^1 0, \nu_2)$ and different values of the parameter γ

γ \ ${}^K J, \nu_i$	${}^1 4, \nu_1$	${}^1 6, \nu_1$	${}^1 3, \nu_1$	${}^3 4, \nu_1$	${}^1 0, \nu_2$
8°	0.25	0.23	0.33	0.28	0.09
10°	0.27	0.26	0.35	0.27	0.09
15°	0.31	0.55	0.32	0.28	0.09
20°	0.46	0.31	0.36	0.31	0.09
25°	0.62	0.21	0.36	0.31	0.09
30°	0.70	0.19	0.36	0.31	0.09

values of μ at which the ratios of the energies of the indicated levels to those of the first spin 2 states as given by Mallmann and Kerman agree with those of the present model within 1 %. For smaller values of μ, of course, the agreement is better than 1 %. Thus the comparison of the present model with experimental data is essentially that given in table 2 for $\frac{8}{3} \leqq R({}^1 4) \leqq \frac{10}{3}$ of the paper of Mallmann and Kerman [4]). The quasi-adiabatic general asymmetric rotator model [7]) is in better agreement with these data than the present model. For completeness, the relationship between the parameters of Davydov and Chaban (DC) and those of Mallmann and Kerman (MK) for $\mu \ll 1$ is given by

$$A(\beta_0) = \frac{\hbar^2}{4B\,\beta_0{}^2}\,(1+\tfrac{3}{2}\mu^2), \quad b = \tfrac{1}{2}\mu^4(1+\tfrac{45}{8}\mu^2).$$

From these one obtains

$$(h\omega_0)_{\mathrm{DC}} = (h\omega_0)_{\mathrm{MK}}(1+\tfrac{21}{16}\mu^2).$$

We next consider the cases with $\mu > 0.25$ ($b > 5.3\times 10^{-3}$). For these values of μ the predictions of Davydov and Chaban differ from those of Mallmann and Kerman, which were in disagreement with the experimental results. The predictions of the present model are in agreement within experimental errors with the data for two nuclei, Pd^{108} and Hg^{198}. The data for Cd^{110} are correlated within experimental errors except for the ${}^K J = {}^1 3$ level, and the data for Kr^{82} are in good agreement, although not within experimental errors. The data for

Ti^{48}, Cr^{52}, Fe^{56}, Ba^{134}, Sm^{152}, Gd^{154}, Pt^{192} and Pt^{194} are not in agreement with the present model. Again, the quasi-adiabatic general asymmetric rotor model gives better agreement with the data.

We now consider the levels arising from the root ν_2 and compare their γ and μ values with those arising from the root ν_1. Of these levels the only ones for which there are enough data for comparison with experiment are the ^{10} and ^{12} states. Here it is of interest to compare the present model with the Bohr-Mottelson model also, since the predictions are different enough to make possible a clear-cut distinction. For those nuclei with $\mu \leqq 0.25$ ($b \leqq 5.3\times 10^{-3}$), in the case of the Davydov and Chaban model, the data for Th^{232} agree within experimental errors. The values of γ and μ are in agreement for Er^{166} except for the $^14\ \nu_1$ level and for Pu^{238} except for the $^16\ \nu_1$ level. Good correlation is found, although outside experimental errors in the cases of U^{232} and U^{234}. In the cases of Th^{230} and Pu^{240}, for which no experimental errors are given, good correlation is also found. It is well known [8]) that in the case of the Bohr-Mottelson model the discrepancy between theory and experiment is of the order of a factor 2. The predictions of Mallmann and Kerman are a first approximation to the exact results of Davydov and Chaban, and the two are in agreement only for cases with $\mu \leqq 0.09$ ($b \leqq 3\times 10^{-4}$) (see table 2). There are no nuclei with such small values of b.

Finally, for those nuclei with $\mu > 0.25$ ($b > 5.3\times 10^{-3}$), the data for Os^{188} are correlated by the present model. The data for Sm^{152} and Gd^{154} are in quite good agreement, although outside of experimental errors, with the model if one uses the energies of the first spin 2 and first spin 4 states to determine γ and μ and then calculates the energies of the second spin 0 states; however, the model predicts incorrect energies for the first spin 3 states. The data for the other 4 nuclei, Ge^{72}, Pd^{106}, Pd^{108} and Pt^{194}, are not correlated by the present model.

In summary, the present comparison of the model of Davydov and Chaban with experimental data indicates that it is quite successful for nuclei far away from closed shells ($\mu \lessapprox 0.35$), although the correlation between theory and experiment is not always within experimental error. For nuclei with $\mu \geqq 0.35$, the theory is not in agreement with experimental results; however, if one considers only levels arising from the ν_1 root, fair agreement is found (4 cases out of 10). This fact seems to indicate that taking into account the interaction of the hydrodynamical rotations with the β-vibrations is insufficient to explain the observed spectra, and that it is necessary to take into account additional degrees of freedom, such as γ-vibrations.

It is a pleasure to acknowledge the contributions of Roy A. Kucera and the staff of the IBM 650 computer of the accounting department, who efficiently and speedily processed the calculation described above.

References

1) A. S. Davydov and A. A. Chaban, Nuclear Physics **20** (1960) 499;
Proc. Int. Conf. Nuclear Structure, Kingston (North-Holland Publishing Co., Amsterdam, 1960) p. 801;
A. A. Chaban, JETP **11** (1960) 1174
2) A. S. Davydov and G. F. Filippov, Nuclear Physics **8** (1958) 237
3) A. S. Davydov and V. S. Rostovsky, Nuclear Physics **12** (1959) 58
4) C. A. Mallmann and A. K. Kerman, Nuclear Physics **16** (1960) 105
5) Day, Klema and Mallmann, ANL-6220
6) C. A. Mallmann, Phys. Rev. Lett. **2** (1959) 507
7) C. A. Mallmann, Nuclear Physics (submitted)
8) Raymond K. Sheline, Revs. Mod. Phys. **32** (1960) 1

1.D.2

Nuclear Physics **25** (1961) 278—281; © *North-Holland Publishing Co., Amsterdam*

Not to be reproduced by photoprint or microfilm without written permission from the publisher

THE COMPARISON OF d-SHELL NUCLEI WITH THE NILSSON MODEL

L. L. GREEN, J. C. WILLMOTT and G. KAYE

Nuclear Physics Research Laboratory, University of Liverpool

Received 10 February 1961

Abstract: The effects of the isobaric spin and of the μl^2 term in the harmonic oscillator potential on the energy level spacings of the distorted oscillator potential are discussed.

1. Introduction

In the nuclear d—s shell the energy levels and their dynamic properties have in several cases been discussed in terms of the Nilsson model [1,2,3]). The levels of these nuclei have been identified with eigenfunctions of the distorted oscillator potential, evaluated by Nilsson, and their properties compared with those obtained from these eigenfunctions. The identification of the nuclear states with the distorted oscillator eigenfunctions is often dependent on the magnitude of the decoupling parameter and the rotation-particle coupling parameter, for these parameters strongly affect the energy level spacings. It is the purpose of this note to point out the importance of two factors which are usally ignored in calculating these parameters and other dynamic properties. The factors we discuss are (1) the effect of isobaric spin and (2) the effect of the μl^2 term in the harmonic oscillator potential.

2. Isobaric Spin Factors

The two nuclei F^{19} (ref. [2])) and P^{31} (ref. [3])) have both been discussed in terms of the Nilsson model and the results compared in detail with experimental data. In both these cases we are dealing with three particles outside a core. In describing the energy levels, linear combinations of Nilsson states which result from the rotation-particle coupling are used. The states, constructed in this way, in which either a proton or a neutron is excited to one of the higher Nilsson states do not have isobaric spin as a good quantum number. For the case of P^{31}, for example, with two neutrons and a proton outside a Si^{28} core we need to use correctly antisymmetrized combinations of the three particles and three eigenfunctions. The lowest state available to the nucleons outside the Si^{28} core in the Nilsson scheme is orbit 9. This can accommodate three

nucleons and the fully antisymmetrized wave function can be written

$$\psi = \frac{1}{\sqrt{6}} \begin{vmatrix} |+9n\rangle_1 & |-9n\rangle_1 & |+9p\rangle_1 \\ |+9n\rangle_2 & |-9n\rangle_2 & |+9p\rangle_2 \\ |+9n\rangle_3 & |-9n\rangle_3 & |+9p\rangle_3 \end{vmatrix},$$

where within the ket the sign refers to the spin projection along the symmetry axis, 9 denotes the Nilsson orbit and n or p indicates whether the nucleon is a neutron or proton. The subscript indicates which of the particles occupies the state. The wave function represents a state of isobaric spin $\frac{1}{2}$ and would represent the ground state of P^{31}. The intrinsic excited states in the three-particle configuration have two particles in orbit 9 and one in orbit 8 or 11. Taking the excited particle in orbit 8 the totally antisymmetrized wave function is

$$= A \begin{vmatrix} |+9n\rangle_1 |-9n\rangle_1 |+8p\rangle_1 \\ |+9n\rangle_2 |-9n\rangle_2 |+8p\rangle_2 \\ |+9n\rangle_3 |-9n\rangle_3 |+8p\rangle_3 \end{vmatrix} + B \begin{vmatrix} |+9n\rangle_1 |-9p\rangle_1 |+8n\rangle_1 \\ |+9n\rangle_2 |-9p\rangle_2 |+8n\rangle_2 \\ 9|+n\rangle_3 |-9p\rangle_3 |+8n\rangle_3 \end{vmatrix} + C \begin{vmatrix} |+9p\rangle_1 |-9n\rangle_1 |+8n\rangle_1 \\ |+9p\rangle_2 |-9n\rangle_2 |+8n\rangle_2 \\ |+9p\rangle_3 |-9n\rangle_3 |+8n\rangle_3 \end{vmatrix}.$$

The symmetry properties of the wave function place some restrictions on the constants A, B and C. The condition that the state should be of isobaric spin $\frac{1}{2}$ is that $A+B+C=0$ and of course normalisation gives $A^2+B^2+C^2=1$. Clearly in this state one cannot talk of a proton or a neutron excited to one of the Nilsson orbits. The excited particle can be a neutron or a proton with certain probabilities. This effect will show itself most clearly in the calculation of the magnetic moments and electromagnetic transition probabilities but also affects the rotation particle coupling factors. We illustrate this with three typical examples.

(i) In the state in which orbit 8 with $\Omega = \frac{3}{2}$ is mixed with the ground state, it will readily be verified that the above wave functions give $(A-C)\ C_{SP}$, where C_{SP} is the single particle coupling coefficient. The term involving B does not appear as it differs from the ground state in the wave functions of more than one of the particles and the Kerman coupling operator is a single particle operator. The minus sign associated with the coefficient C arises from permutations required to match the two sets of quantum numbers in the ground state and the excited state.

(ii) In the case in which orbit 11 with $\Omega = \frac{1}{2}$ is mixed with the ground state, we get $(A-B)\ C_{SP}$.

(iii) Mixing of orbit 8 and 11 leads to $(AA'+BB'+CC')\ C_{SP}$, where A, B and C are the set of values corresponding to one state and A', B', C' to the other. If these are similar, we may expect something close to the single particle value. Similar effects occur in calculating radiative transitions to the ground state, and in addition, as the configuration with coefficients B and C correspond to

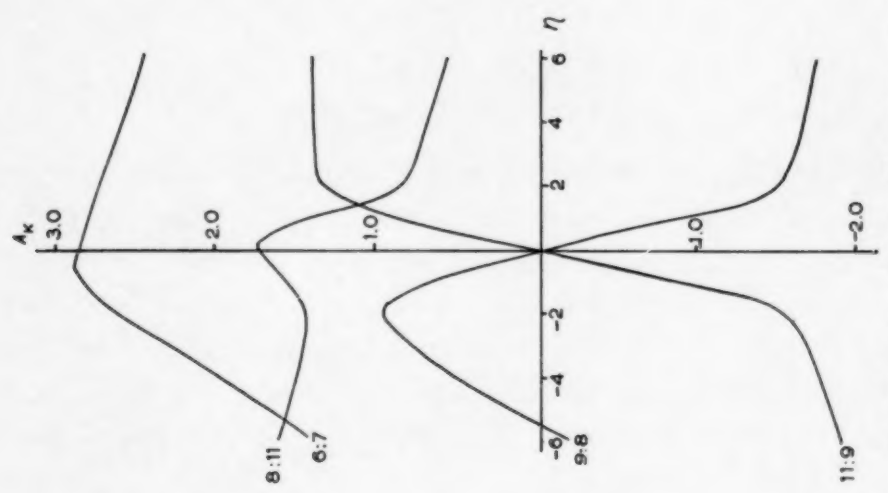

Fig. 3. The Kerman coupling parameter A_K versus the distortion η for $\mu = 0.50$.

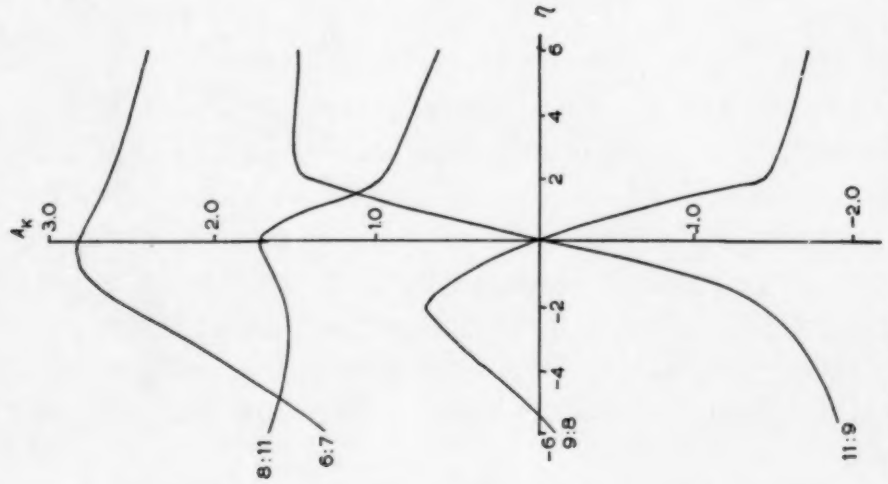

Fig. 2. The Kerman coupling parameter A_K versus the distortion η for $\mu = 0.33$.

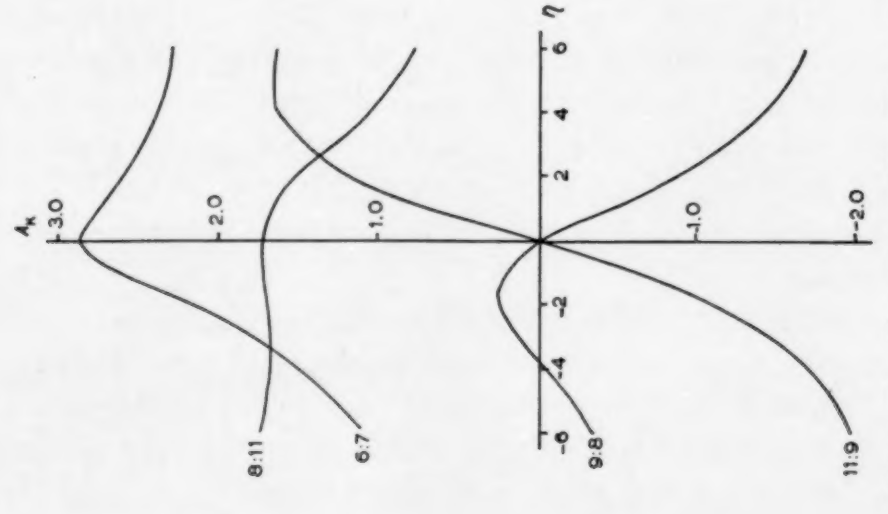

Fig. 1. The Kerman coupling parameter A_K versus the distortion η for $\mu = 0$.

states with an excited neutron, the contributions from these will be different in size from that due to the case when the proton is excited. Clearly then, if isobaric spin is a good quantum number in F^{19} and P^{31}, the values previously obtained from the Nilsson model for coupling constants and for electromagnetic properties may need substantial corrections.

3. Effects of the μl^2 Term in the Nilsson Potential

The eigenfunctions commonly used in the calculation of the de-coupling parameter and the Kerman coupling parameter in the d-shell are those calculated by Nilsson for a distorted harmonic oscillator potential with a spin orbit $\mathbf{l} \cdot \mathbf{s}$ term but no l^2 term. For higher orbits Nilsson included a μl^2 term with values of μ in the range from 0.35 to 0.55. The effect of the μl^2 term on the eigenfunctions used in the s and d shell has been discussed by Bishop [4] †. Bishop has also calculated the effect of this term on the de-coupling parameter and shown that in some orbits in the d-shell the level ordering is quite sensitive to the magnitude of μ.

The Kerman coupling shifts in the nuclei discussed in the d-shell, for example P^{31} and F^{19}, are large. These level shifts depend on the Kerman coupling parameter A_K which would be expected to depend on the μl^2 term. We have used the eigenfunctions obtained by Bishop † to calculate the Kerman coupling parameters relevant to the nuclei F^{19} and P^{31}. Figs. 1, 2 and 3 show the Kerman coupling parameter A_K between bands 6 and 7 and bands 8, 9 and 11 ††. It is apparent from these figures that the Kerman coupling parameter in this region does not depend strongly on the size of the μl^2 term in the potential, but as Bishop has shown the effects of this factor on the de-coupling parameter can be quite large.

It is thus apparent that the level spacing and the electromagnetic properties are quite sensitive to these two effects which have previously been ignored and it is perhaps surprising that such detailed agreement has been obtained in F^{19}.

† There is an error in table 1 of Bishop's paper for $\mu = 0.33$. The last entries for orbits 11 and 9 at $\eta = +2$ should read -0.816 and -2.838 instead of -0.612 and -1.314.

†† The values of A_K for $\mu = 0$ do not agree with those shown in Broude, Green and Willmott [3]. This is because of an error in the phase factor in the calculation of A_K for bands 11 and 9; the result of this will be discussed elsewhere.

References

1) A. E. Litherland, H. McManus, E. B. Paul, D. A. Bromley and H. E. Gove, Can. Jour. Phys. **36** (1958) 378
2) E. B. Paul, Phil. Mag. **2** (1957) 311
3) C. Broude, L. L. Green and J. C. Willmott, Proc. Phys. Soc. **72** (1958) 1122
4) G. R. Bishop, Nuclear Physics **14** (1960) 376

1.E·1:
2.G

Nuclear Physics **25** (1961) 282—291; © *North-Holland Publishing Co., Amsterdam*
Not to be reproduced by photoprint or microfilm without written permission from the publisher

THE $B^{10}(d, n)C^{11}$ REACTION

A. N. JAMES,
Cavendish Laboratory, Cambridge

A. T. G. FERGUSON
A.E.R.E., Harwell

and

C. M. P. JOHNSON †
Cavendish Laboratory, Cambridge

Received 17 February 1961

Abstract: Neutron groups from the reaction $B^{10}(d, n)C^{11}$ were studied at deuteron energies of 1.2, 3 and 4 MeV using time of flight techniques. The results are compared with those for the $B^{10}(d, p)B^{11}$ reaction and with Butler stripping theory for the intermediate coupling shell model.

1. Introduction

In view of the well established experimental energy level scheme [1]) for B^{11} and the difficulty experienced in comparing it with theoretical shell model predictions [2, 3]), an independent study of the mirror nucleus C^{11} is desirable. Experiments [4, 5]) on $B^{10}(p, \gamma)C^{11}$ have provided little information about the C^{11} energy level scheme due to the strong competition from the $B^{10}(p, \alpha_1\gamma)Be^7$ reaction. An alternative method of exciting levels in C^{11} is by the (d, n) reaction ††. Fast neutron time of flight techniques are well suited to study such reactions, particularly as they complement photographic emulsion methods by having better resolution for low energy neutrons.

Several experiments studying the $B^{10}(d, n)C^{11}$ reaction have been reported. The lowest four states [6]), the 6.48 MeV state [7]) and a state [7]) near 8.5 MeV were observed at high bombarding energies. At these energies, the observed neutron angular distributions could be fitted by $l = 1$ deuteron stripping theory. A state near 8.5 MeV was also observed to have an angular distribution fitted by $l = 0$ stripping [8]). At low deuteron energies, the data could not easily be interpreted [9, 10]). Neilson [11]), however, using a time of flight technique for observing n—γ correlations following deuteron bombardment, has observed a strong $l = 1$ stripping pattern at low deuteron energies for the 6.48 MeV level.

† Now at the Clarendon Laboratory, Oxford.

†† With the introduction of new bombarding particles other reactions can also be used (e.g. the $B^{10}(He^3, d)C^{11}$ reaction of ref. [17])).

The pulsed neutron time of flight apparatus of the Cavendish Laboratory 1.4 MV Cockcroft-Walton generator and of the Harwell 5 MV Van de Graaff have recently been improved by the addition of neutron discriminating scintillation counters using Owen's method [12]). In addition to the elimination of the γ-ray peak from the time of flight spectrum (fig. 1), neutron selection reduced the continuous background by a factor of ten. These machines have been used to study the angular distribution of eleven neutron groups observed in the reaction $B^{10}(d, n)C^{11}$, the groups corresponding to the eleven known bound states of C^{11}.

The neutron time of flight was measured using time to pulse-height converters, the best time resolution for the neutron groups being 6 ns at Cambridge

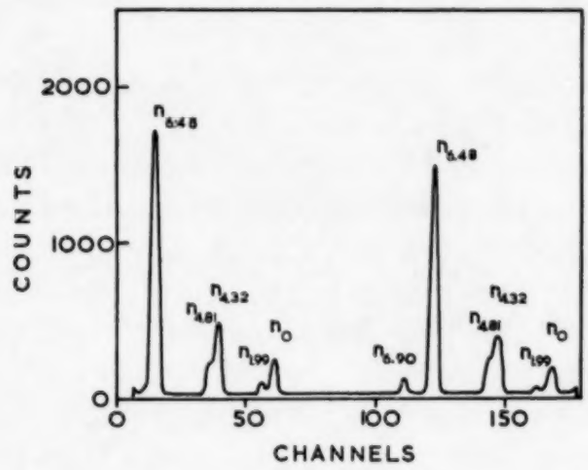

Fig. 1. Time of flight spectrum for $B^{10}(d, n)C^{11}$ at 3 MeV. The flight path was $3\frac{1}{2}$ m, the counter being at 35° relative to the incident deuteron beam. The time spectrum is displayed twice because only one timing pulse was taken from the sweeping oscillator per cycle, two beam pulses reaching the target in this time (250 ns). The γ-ray peak (at channel 100) has been rejected by neutron selection.

and 4 ns at Harwell. The scintillation counter was a 5.08 cm diameter by 5.08 cm long Nuclear Enterprise N.E. 213 liquid phosphor used with an R.C.A. 7264 or E.M.I. 6097 photomultiplier [13]). Counts were recorded in the time of flight spectrum only when they were distinguished by coinciding with a neutron discrimination pulse and a proportional pulse greater than a bias equivalent to E_b MeV recoil proton energy.

The variation of neutron efficiency with energy was determined by comparing the known $T(p, n)He^3$ differential cross section [14]) with that measured, and also, at Cambridge, by comparison with a long counter [15]). Errors in the relative intensities arising from uncertainty in the efficiency correction are less than 10 % within any one angular distribution, and less than 30 % between the different neutron groups. The relative intensities found by Johnson [16]) at 3.4 MeV agree within this limit with the relative intensities observed at 3 and 4 MeV.

The targets of B^{10} were laid down directly on 0.05 cm. Tungsten backings in the Harwell electromagnetic separator. The deposits had masses of 75 $\mu g/cm^2$ and 400 $\mu g/cm^2$. No trace of the B^{11}(d, n)C^{12} neutron time of flight spectrum was found in any of the experiments. (p, γ) investigations indicated that less than 3 % of the boron deposit was B^{11}.

In measuring the angular distributions, the neutron yield from the target was monitored either by a long counter or by a neutron discriminating scintillation counter using a small stilbene crystal. The angular resolution of the neutron counter was negligibly small because the flight path was from 1.5 to 3.5 m long.

2. Experiments at 1.2 MeV Bombarding Energy

The neutron time of flight spectrum at 1.2 MeV deuteron bombarding energy indicated that the excitation energy of the C^{11} state previously reported [6, 16]) as 6.77 MeV was incorrect. The neutron energies of the group forming this level in B^{10}(d, n)C^{11} and the group forming the 4.771 MeV level in B^{10} in the Be^9(d,n)B^{10} reaction are nearly the same. Therefore, a comparison of the time of flight spectra from these two reactions, where all other conditions were identical, yielded an accurate estimate of the Q-value without accurate calibration of either the energy of the incident deuterons or of the neutron flight time. The two targets were of roughly equal thickness (absorbing $\approx$ 25 keV deuteron energy) and errors arising from target thickness considerations were estimated to be less than 0.01 MeV. The Q-value found by this method was -0.44 ± 0.02 MeV corresponding to an excitation of 6.91 MeV in C^{11}. This value was in excellent agreement with the value 6.903 ± 0.010 MeV found by Hinds and Middleton in B^{10}(He^3, d)C^{11} experiments [17]). Their results also give the energy of the third and fourth excited states as 4.32 and 4.81 MeV (table 1).

TABLE 1

The relative yields in C^{11}

Level in C^{11} (MeV)	Q-value (MeV)	Relative yields $\left(\frac{d\sigma}{d\omega}\right)_{90°}$			stripping l-value	Relative stripping reduced widths at 3 and 4 MeV
		1.2 MeV	3 MeV	4 MeV		$(2J+1)\theta^2$
0	6.47	2.0	2.0		1	(4)
1.99	4.48	0.45	0.6			
4.32	2.17	2.4	2.0		1	(2.8)
4.81	1.67	0.86	0.8		1	(0.9)
6.34	0.14	0.75				
6.48	−0.01	7.8	3.5	3.5	1	7.5
6.90	−0.43	1.3	0.9	0.8	(1)	(0.9)
7.50	−1.03			0.3		
8.11	−1.64			0.35		
8.43	−1.96			1.05	1	2.9
8.66	−2.19			3.5	0	10.3

Hinds and Middleton's experiment also revealed the suspected doublet structure of the 6.48 MeV state, a weakly populated state being observed at 6.34 MeV. Previous searches [1, 11]) for such structure using the $B^{10}(d, n)C^{11}$

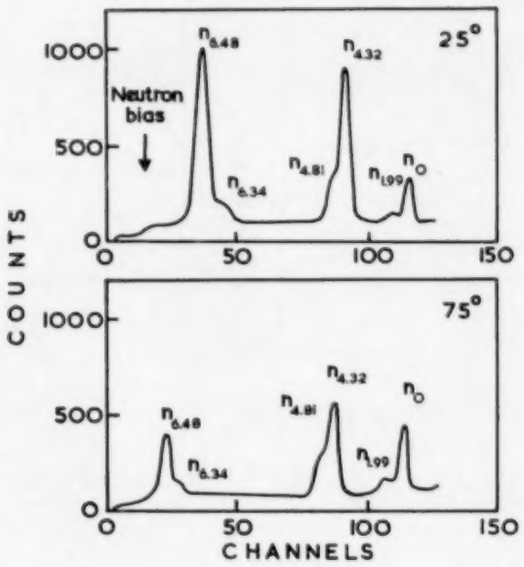

Fig. 2. Time of flight spectrum for $B^{10}(d, n)C^{11}$ at 1.2 MeV deuteron energy. The neutron bias was adjusted so as to accentuate the group $n_{6.34}$ relative to the group $n_{6.48}$.

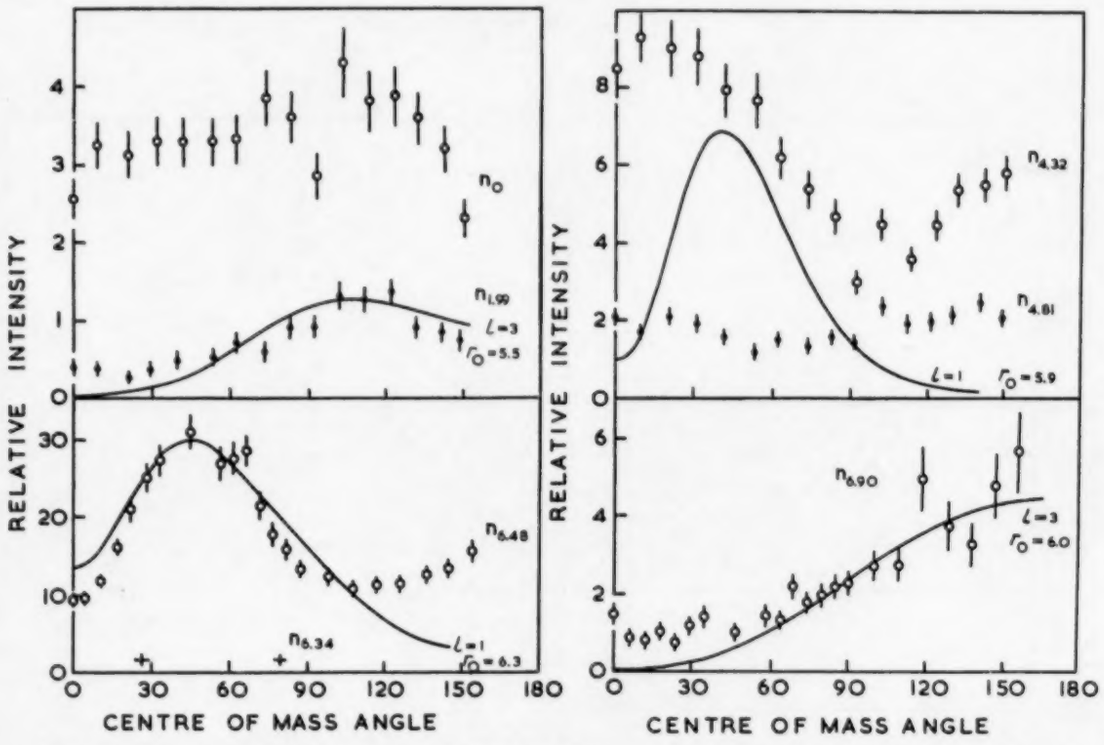

Fig. 3. Angular distributions for $B^{10}(d, n)C^{11}$ at 1.2 MeV deuteron energy.

reaction had been unsuccessful. By adjusting the neutron bias E_b it was possible to reduce considerably the neutron efficiency for the group forming the 6.48 MeV level without seriously affecting the efficiency for a level at 6.34 MeV. Fig. 2

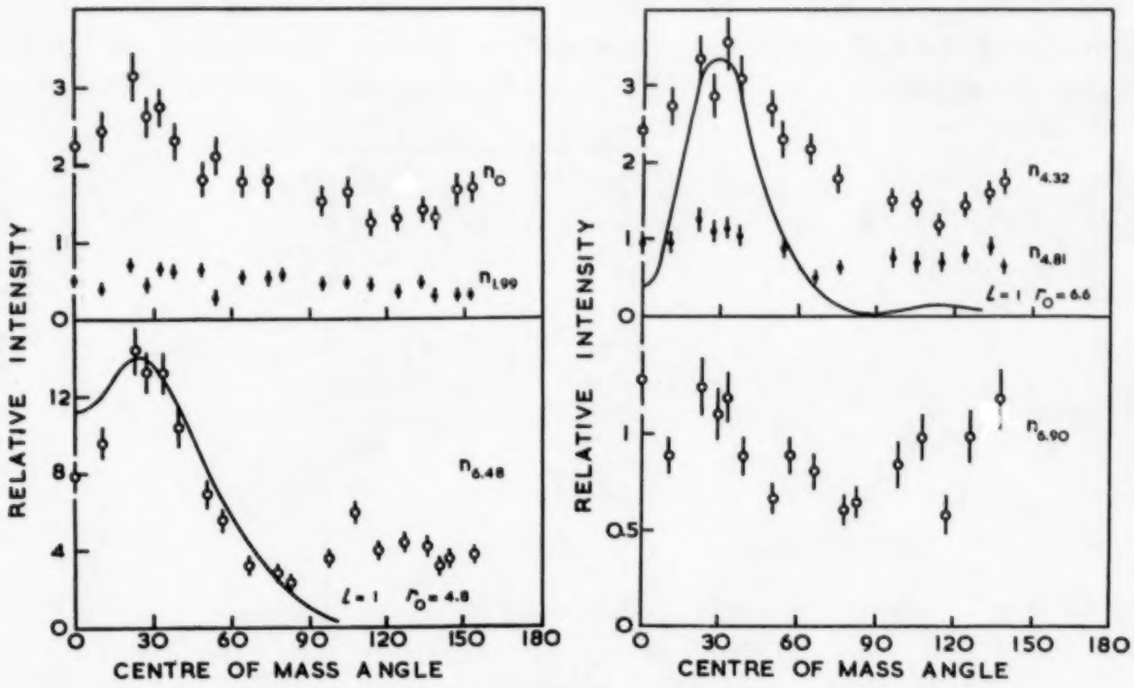

Fig. 4. Angular distributions for $B^{10}(d, n)C^{11}$ at 3 MeV deuteron energy.

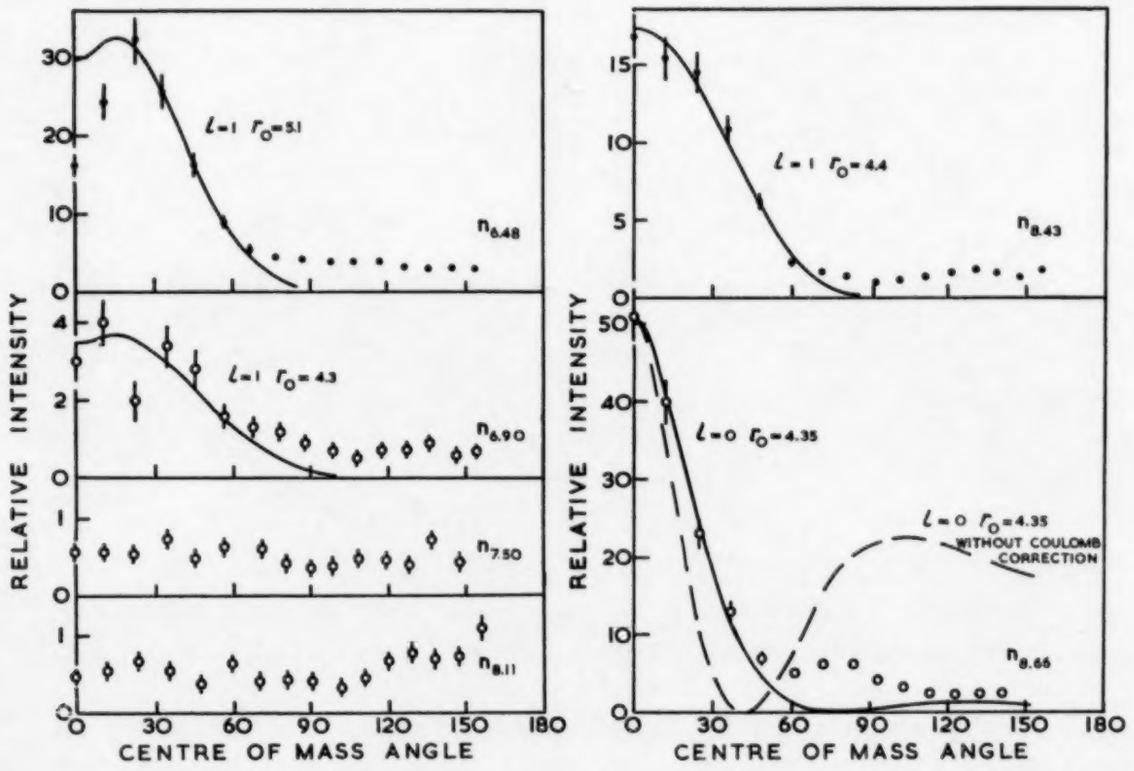

Fig. 5. Angular distributions for $B^{10}(d, n)C^{11}$ at 4 MeV deuteron energy.

shows time of flight spectra for a flight path of $3\frac{1}{2}$ m at 1.2 MeV. The existence of a group forming a level near 6.34 MeV was clear † but an accurate Q-value measurement was impossible. (This group could not have been formed by light element target impurities.) The relative intensity of this group is shown on fig. 3.

Fig. 3 shows angular distributions measured at 1.2 MeV.

3. Experiments at 3 and 4 MeV

The time of flight spectrum of fig. 1 was typical of those obtained at 3 and 4 MeV. The time spectrum was displayed twice because only one timing pulse was taken from the sweeping oscillator per cycle, two beam pulses reaching the target in this time. Angular distributions for the ground, 1.99, 4.32, 4.81, 6.48 and 6.90 MeV levels were measured at 3 MeV (fig. 4), and for the 6.48, 6.90, 7.50, 8.11, 8.43 and 8.66 MeV levels at 4 MeV (fig. 5).

4. Stripping Angular Distributions

Attempts were made to fit the angular distributions by Butler stripping theory. The theoretical angular distributions were calculated from the tables of Lubitz [18]) modified to include a Coulomb correction for the captured proton [19, 20]). This correction has an appreciable effect on the theoretical angular

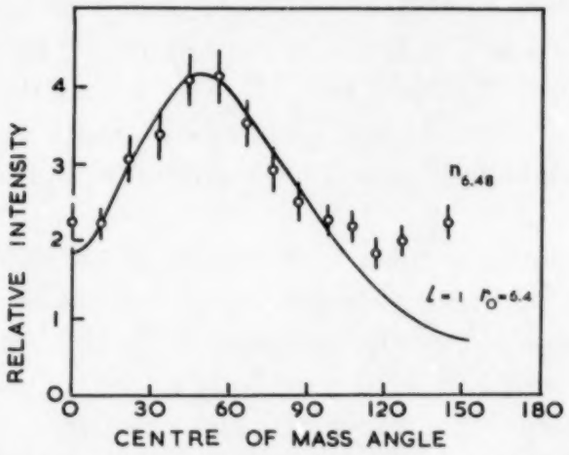

Fig. 6. Angular distribution for $B^{10}(d, n)C^{11}_{6.48}$ at 900 keV deuteron energy.

distribution only for the 8.66 MeV level (fig. 5) where $Q+E_d$ (the binding energy of the deuteron) was very small (0.04 MeV); the reduced width being decreased by a factor of 10. The correction to the reduced width of the 8.43 MeV level is a reduction of 30 %.

The neutron group forming the 6.48 MeV level (Q-value = 0.01 MeV) had an angular distribution which was similar to Butler stripping theory at all energies [21]). Similar distributions were observed by Neilson *et al.* [11]) in their

† Neilson has recently verified the existence of the 6.34 MeV level by $B^{10}(d, n)C^{11}$ experiments (private communication).

n—γ angular correlation experiments. Except at 900 keV (fig. 6), the best fit stripping angular distributions all predicted a value higher than experiment for the differential cross section at angles less than the angle of the stripping peak. Similar behaviour for other (d, n) stripping reactions with $l = 1$ has been noticed by Middleton, El-Bedewi and Tai [22]).

Two other levels had angular distributions which were well fitted by stripping theory. The angular distribution for the 8.66 MeV level was best fitted by $l = 0$; $l = 1$ would have required an abnormally high radius parameter (either with or without the Coulomb correction). The hump in the angular distribution between 60° and 90° could not be accounted for by a partial admixture of $l = 2$ stripping. (Compare the results of Bilaniuk and Hensel [23]), who report such mixtures in B^{10}(d, p)B^{11}).

Attempts to fit the angular distribution of the 8.43 MeV level by $l = 0$ or $l = 2$ stripping led to unlikely values of the radius parameter, the value $r_0 = 4.4$ fm, which gave the best fit for $l = 1$, was consistent with the values found by Holt and Marsham [24]) for the radius parameter in stripping reactions for this mass region. Again it was impossible to fit the experimental distributions by a mixture of even l-values.

Other angular distributions, which had peaks at angles which correspond to $l = 1$ stripping, were those for the ground, 4.32 and 4.81 MeV states at 3 MV, and that for the 6.90 state at 4 MeV. The peak at 0° in the angular distribution for the 4.32 MeV level at 1.2 MeV has been found [11]) to be too broad to fit by $l = 0$. At 3 MeV and 7.5 MeV (ref. [7])), $l = 1$ was the important stripping amplitude. It is possible that the angular distribution of fig. 3 is due to an $l = 1$ stripping peak superimposed on a differential cross section of the form $1 + a \cos^2\theta$.

The backward peaking angular distributions at 1.2 MeV for the 1.99 and 6.90 MeV levels are unlikely to be due to heavy particle stripping in view of the binding energy (8.44 MeV) of the last neutron in B^{10}. An explanation in terms of $l = 3$ stripping (see fig. 3) is also unlikely as the reduced widths corresponding to these distributions are much too high compared with the $l = 1$ width of the 6.48 MeV level to be accounted for by admixture of the p^6f configuration in the wave functions for these states. Both of these levels have angular distributions similar to $l = 1$ stripping at higher deuteron energies. In the case of the 1.99 MeV level, which has spin $\frac{1}{2}$, a stripping mechanism involving spin flip can account for the 'forbidden' $l = 1$ shape [25, 26]).

5. Comparison with B^{10}(d, p)B^{11}

A comparison of the reactions B^{10}(d, p)B^{11} and B^{10}(d, n)C^{11} shows remarkable similarities as expected from the principle of charge symmetry. Fig. 7 shows the energy levels of B^{11} and C^{11}. Correspondence between the levels can

be based firstly on relative yields at 90° (table 1 and refs. [1, 16, 27])) and secondly on the form of the angular distributions. The lengths to which these similarities extend can be judged by comparison with the (d, p) data of Marion and Weber [28]). The 1 MeV and 3 MeV distributions of the groups p_0 and p_1 were in perfect agreement with the (d, n) data, and the 2 MeV p_2 and p_3 distributions were in good qualitative agreement with the (d, n) distributions observed at 1.2 and 3 MeV and with the correlations of Neilson *et al.* [11]).

Evans and Parkinson [29]) and Bilaniuk and Hensel [23]) have observed a large $l = 1$ stripping amplitude for the 6.76 MeV level of B^{11} which corresponded well with the $l = 1$ (d, n) reaction for the 6.48 MeV level of C^{11}. Evans [30]) has

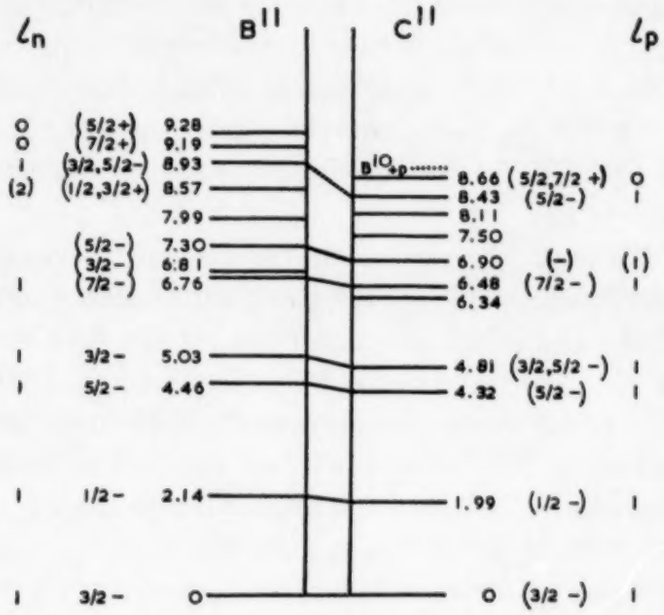

Fig. 7. Energy levels in B^{11} and C^{11} and the l-values observed in deuteron stripping.

also observed a poor $l = 1$ stripping angular distribution at 7.7 MeV for the 7.30 MeV level of B^{11}, which could correspond to the $l = 1$ stripping observed for 6.90 MeV C^{11} level at 4 MeV. This correspondence is further borne out by the recent experiments of Gorodetski *et al.* [31]).

The $l = 1$ stripping observed for the 8.43 MeV level in C^{11} gives its parity as negative. The parity of the 8.93 MeV B^{11} level, the level to which it most probably corresponds, is variously reported. Bilaniuk and Hensel [23]) found a mixture of $l = 0$ and $l = 2$ stripping in the $B^{10}(d, p)B^{11}$ reaction at 7.8 MeV deuteron energy, a result consistent with positive parity. Pullen and Whitehead [32]), studying the same reaction at 3.5 MeV deuteron energy, observed $l = 1$ stripping, which indicates negative parity. Hinds and Middleton [33]) also find negative parity for this state if one assumes that the $Be^9(He^3, p)B^{11}$ reaction proceeds by a double stripping mechanism. Pullen and Whitehead's [32])

results agree with Bilaniuk and Hensel's for the 9.19 and 9.28 MeV B^{11} levels, both levels being formed by $l = 0$ stripping in B^{10}(d, p)B^{11}. The $l = 0$ stripping observed for the 8.66 MeV C^{11} level indicates its correspondence to one of these B^{11} levels.

6. Stripping and the Intermediate Coupling Shell Model

Only three levels of the j—j coupling s^4p^7 configuration of mass 11 nuclei can be formed by $l = 1$ stripping from the ground state of B^{10}. These are Kurath's $(\frac{3}{2}-)_I$, $(\frac{5}{2}-)_{II}$ and $(\frac{7}{2}-)_I$ levels [2, 3]). Calculations of the variations of the stripping reduced widths with the intermediate coupling parameter a/K are reported by Bilaniuk and Hensel [23]). Reduced widths calculated from the data by taking the differential cross section at the angle of the stripping peak as being entirely due to stripping [20]) are given in table 1. These widths are expected to have only an approximate nature for those levels where the angular distribution was not well fitted by stripping theory. Further uncertainty arises from the low deuteron energy.

The reduced width for the ground state is relatively large, in agreement with the accepted [1, 2]) assignment $(\frac{3}{2}-)_I$ for the ground states of C^{11} and B^{11}. The largest reduced width $(2J+1)\theta^2$ was observed for the 6.48 MeV level, which is consistent [23]) with $(\frac{7}{2}-)_I$ for all reasonable values of a/K. If the 8.43 MeV level is $(\frac{5}{2}-)_{II}$, as seems likely from the agreement with stripping theory and its large reduced width, then the ratio of reduced widths for the 6.48 and 8.43 MeV levels gives a value of a/K between 4.5 and 5 in agreement with the value 4.5 found by Ferguson *et al.* [34]) for B^{11}. γ-ray studies in B^{11} indicate that both $\frac{3}{2}-$ and $\frac{5}{2}-$ are reasonable assignments for the corresponding 8.93 MeV level [35]).

The reduced width for the 4.32 MeV level is much larger than expected, the stripping results indicate that the level is most probably $(\frac{5}{2}-)_I$, since the calculated reduced width for this level is an order of magnitude higher than that for $(\frac{3}{2}-)_{II}$ at all values of a/K. This assignment would agree with that for the 4.46 MeV level of B^{11}, which is derived from the γ-ray schemes [34, 35]).

7. Conclusion

The neutron angular distributions in B^{10}(d, n)C^{11} are strikingly similar to the B^{10}(d, p)B^{11} angular distributions. The stripping reduced widths indicate that the spins of the ground state, 4.32, 6.48, 8.43 and 8.66 MeV levels of C^{11} are $\frac{3}{2}-$, $\frac{5}{2}-$, $\frac{7}{2}-$, $\frac{5}{2}-$ and either $\frac{5}{2}+$ or $\frac{7}{2}+$, respectively.

The isotopic boron targets were supplied by A.E.R.E. Harwell. One of us (A. N. J.) is indebted to the Department of Scientific and Industrial Research for the support of a Research Fellowship.

References

1) F. Ajzenberg-Selove and T. Lauritsen, Nuclear Physics **11** (1959) 1
2) D. Kurath, Phys. Rev. **101** (1956) 216
3) D. Kurath, Phys. Rev. **106** (1957) 975
4) S. E. Hunt, R. A. Pope and W. W. Evans, Phys. Rev. **106** (1957) 1012
5) G. B. Chadwick, J. K. Alexander and J. B. Warren, Can. J. Phys. **34** (1956) 381
6) M. Cerineo, Nuclear Physics **2** (1956) 113
7) E. E. Maslin, J. M. Calvert and A. A. Jaffe, Proc. Phys. Soc. **69** (1956) 754
8) A. Graue and B. Trumpy, Phil. Mag. **2** (1957) 138
9) A. Graue, Phil. Mag. **1** (1956) 1027
10) C. H. Paris and P. M. Endt, Physica **20** (1954) 585
11) G. C. Neilson, W. K. Dawson, F. A. Johnson and J. T. Sample, Suffield Technical Paper no. 176 (1959) unpublished
12) R. B. Owen, Nucleonics **17** (1959) 92
13) A. N. James, Nuclear Physics **24** (1961) 132
14) J. L. Fowler and J. E. Brolley, Rev. Mod. Phys. **28** (1956) 103
15) A. N. James, Nuclear Physics **23** (1961) 648
16) V. R. Johnson, Phys. Rev. **86** (1952) 302
17) S. Hinds and R. Middleton, Proc. Phys. Soc. (to be published)
18) C. R. Lubitz, Numerical table of Butler-Born approximation stripping cross sections, University of Michigan (1957), unpublished
19) S. T. Butler and O. M. Hittmair, Nuclear stripping reactions (Horowitz Publications, 1957)
20) M. H. Macfarlane and J. B. French, Rev. Mod. Phys. **32** (1960) 567
21) D. H. Wilkinson, Phil. Mag. **3** (1958) 1185
22) R. Middleton, F. A. El-Bedewi and C. T. Tai, Proc. Phys. Soc. **66** (1953) 95
23) O. M. Bilaniuk and J. C. Hensel, Phys. Rev. **120** (1960) 211
24) J. R. Holt and T. N. Marsham, Proc. Phys. Soc. **66** (1953) 1032
25) D. H. Wilkinson, Phys. Rev. **105** (1957) 666
26) N. T. S. Evans and A. P. French, Phys. Rev. **109** (1958) 1272
27) D. M. Van Patter, S. W. Buechner and A. Sperduto, Phys. Rev. **82** (1951) 248
28) J. B. Marion and G. Weber, Phys. Rev. **103** (1956) 1408
29) N. T. S. Evans and W. C. Parkinson, Proc. Phys. Soc. **67** (1954) 684
30) N. T. S. Evans, Ph. D. Thesis, University of Cambridge (1955)
31) S. Gorodetski, M. Croissiaux, A. Gallmann, P. Fintz, J. Samuel and G. Bassompiere, Nuclear Physics **18** (1960) 286
32) D. H. Wilkinson, Proc. Int. Conf. Nuclear Structure, Kingston, Canada (North Holland Publishing Co., Amsterdam, 1960) Ch. 1
33) S. Hinds and R. Middleton, Proc. Phys. Soc. **75** (1960) 754
34) A. J. Ferguson, H. E. Gove, J. A. Kuehner, A. E. Litherland, E. Almqvist and D. A. Bromley, Phys. Rev. Lett. **1** (1958) 414
35) G. A. Jones, C. M. P. Johnson and D. H. Wilkinson, Phil. Mag. **4** (1959) 796

3B:3C

Nuclear Physics **25** (1961) 292—306; © *North-Holland Publishing Co., Amsterdam*

Not to be reproduced by photoprint or microfilm without written permission from the publisher

ÉTUDE DES TRANSITIONS GAMMA ET DES ÉLECTRONS AUGER DE ^{153}Eu

E. MONNAND et A. MOUSSA †

Institut de Physique Nucléaire, Lyon

Reçu le 2 février 1961

Abstract: A study of the low-energy conversion spectrum of ^{153}Sm $\xrightarrow{\beta}$ ^{153}Eu decay was carried out with an iron-free double focusing spectrometer. The mixing ratios E2/M1 have been determined by analysis of the L conversion lines for the 70, 84 and 103 keV transitions. A 19 keV (E2) transition has been revealed. The Auger K and L electrons have been studied and the K fluorescence yield measured.

1. Introduction

Le noyau de $^{153}_{62}$Sm, de période 47 h, se désintègre par émission complexe β^- pour donner le noyau de $^{153}_{63}$Eu. Un grand nombre de travaux [1–12]) ont porté sur cette désintégration. Tous les auteurs indiquent que le spectre β^- se compose de 3 branches principales d'énergies 820, 720 et 640 keV. Dubey [9]) signale en plus une composante de 130 keV d'intensité très faible.

De même, tous les auteurs indiquent l'existence de rayons γ de 70 et 103 keV, les plus importants du spectre; mais ils donnent des valeurs très différentes pour les coefficients de conversion de ces deux transitions. Nous nous bornons ici à l'étude de la région en dessous de 200 keV. Outre ces 2 rayons γ principaux, Mme Marty [7]) confirme l'existence d'un rayon γ d'intensité très faible à 172 keV. McCutchen [12]) a mis en évidence un rayon γ de 97 keV. Cette dernière transition avait déjà été signalée dans la désintégration par capture K de ^{153}Gd [13, 14]). Enfin, Mme Marty [6, 7]) et Joshi [10]) ont signalé une transition de 84 keV, qui, d'après Mme Marty, proviendrait d'un niveau très faiblement excité dans la désintégration β^- de ^{153}Sm. D'autre part, Temmer et Heydenburg [5, 8]), par excitation coulombienne, sur le noyau de ^{153}Eu, ont mis en évidence des niveaux de rotation à 82 et 187 keV.

Dans le tableau 1, nous donnons les valeurs des rapports des conversions internes K/L, et L/M mesurées par divers auteurs.

Le schéma de désintégration reproduit sur la fig. 1 est celui donné par McCutchen, complété de certaines valeurs fournies par Dubey et par notre présent travail.

† Adresse actuelle: Faculté des Sciences, Grenoble.

TABLEAU 1

Rapports K/L et L/M

	Transition de 70 keV		Transition de 103 keV	
	K/L	L/M	K/L	L/M
Siegbahn [1])			6	
Mihelich [1])	3.5		6.5	
Lee et Katz [2])	$3.8^{+2.5}_{-1.5}$		6.2 ± 1.5	
Graham et Walker [4])	>4.6		>6.1	
Marty [7])	>4.4	3 ± 1	6.2 ± 0.3	4.5 ± 0.5
Joshi [10])	$5\ ^{+1.3}_{-0.9}$		6.2 ± 0.8	

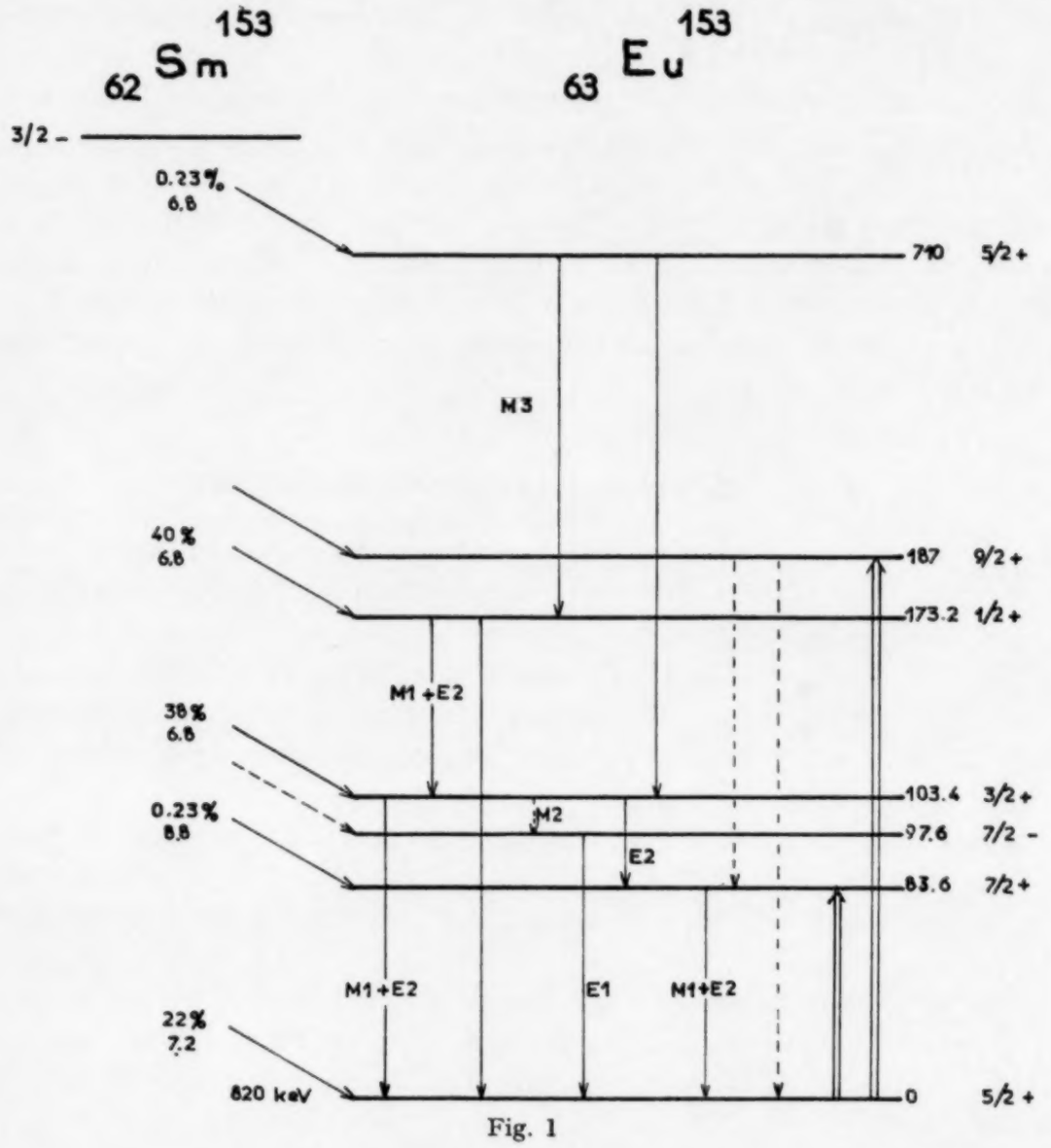

Fig. 1

Dans la première partie de notre travail, nous avons étudié le spectre des électrons de conversion interne de ^{153}Eu. Dans la seconde partie, nous avons fait l'analyse des spectres Auger K et L, qui n'avait jamais été faite jusqu'ici.

2. Appareillage

Nous avons utilisé le spectromètre à double focalisation et à bobines sans fer de l'Institut de Physique Nucléaire de Lyon [15]). Les diaphragmes limitant le faisceau et la fente du spectromètre étaient réglés de manière à assurer le meilleur compromis entre le pouvoir séparateur et le facteur de transmission pour une largeur de source donnée.

Pour l'étude des électrons de conversion et des électrons Auger K, le compteur Geiger-Müller du spectromètre était obturé par une fenêtre de formvar aluminé, de 50 μg/cm^2, sur cadre de néoprène. Le „cut-off" de cette fenêtre se situait vers 3 keV, donc assez bas pour éviter les corrections d'absorption.

Les électrons Auger L ont été étudiés avec une fenêtre de formvar sur lektromesh transparent à 50 %. Son „cut-off" se situait vers 1.5 keV. Compte tenu de la précision des mesures, le facteur de correction d'absorption de la fenêtre est pratiquement égal à 1 au-dessus de 5 keV. Pour étudier le spectre au-dessous de 5 keV, nous avons appliqué aux électrons une post-accélération de 1500 V, ce qui permet d'éviter les corrections d'absorption de la fenêtre entre 5 keV et 3.5 keV, sans pour cela modifier la trajectoire des électrons, ni la forme des raies. Les corrections sont faites entre 3.5 et 2.2 keV. L'étalonnage en énergie a été fait à partir des raies de conversion du thorium B+C, le rapport $B\rho/i$ est égal à 11.7 G · cm/mA.

3. Préparation des Sources

Le ^{153}Sm utilisé pour notre étude a été préparé à partir de la réaction ^{152}Sm (n, γ)^{153}Sm. Pour cela, de l'oxyde de samarium spectroscopiquement pur a été irradié dans les piles EL2 et EL3 à Saclay.

Pour préparer les sources, nous avons transformé l'oxyde de samarium en nitrate, par action d'une solution aqueuse d'acide nitrique concentré. Une partie de cette solution est prélevée et déposée dans une gouttière de tantale destinée à servir d'évaporateur.

Par chauffage très lent à l'air, le nitrate de samarium est desséché, puis sous vide, il est calciné et redonne l'oxyde. L'évaporation de l'oxyde se fait en portant la gouttière de tantale à environ 2300° C, sous une pression de 2×10^{-4} mm de mercure.

L'oxyde de Sm évaporé est recueilli sur du mica dont la masse superficielle varie entre 1 et 2 mg/cm^2. Ces supports de mica sont recouverts d'une couche conductrice de titane évaporé sous vide. L'aluminium ne convient pas car il se

réévapore lors du dépôt de Sm_2O_3, le mica étant assez fortement chauffé. Nous avons ainsi obtenu des épaisseurs de sources variant de 8 à 60 $\mu g/cm^2$.

4. Résultats Obtenus

4.1. ÉLECTRONS DE CONVERSION INTERNE

Dans un article antérieur [17]), nous avons fait figurer le spectre des électrons de conversion obtenu avec une source d'environ 40 $\mu g/cm^2$ d'épaisseur et un pouvoir séparateur de 6×10^{-3}. Les raies de conversion L de la transition de

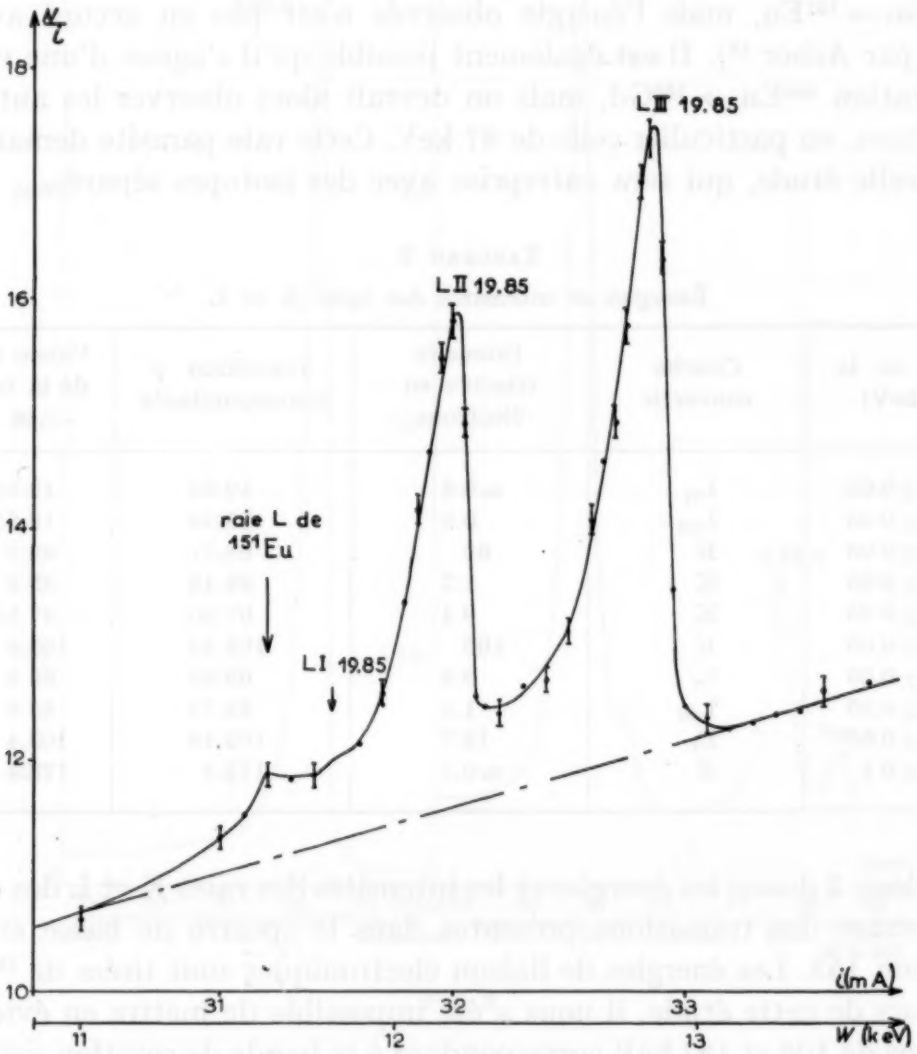

Fig. 2

19.8 keV apparaissent nettement, bien que très faibles, sur le pied de la raie K70. Ces raies ont été de nouveau étudiées avec des sources plus minces ou d'activité spécifique plus élevée.

La fig. 2 reproduit cette région étudiée avec une source de 1 mm de large et de

8 μg/cm^2 d'épaisseur. Le pouvoir séparateur théorique (1.5×10^{-3}) est pratiquement atteint pour les raies d'énergie supérieure à 100 keV, mais il est seulement de 7×10^{-3} pour les raies en question dont l'énergie est de l'ordre de 12 keV (on voit ainsi la nécessité d'employer des sources très minces). On distingue les raies L_{II} et L_{III}, dont les énergies correspondent à une transition γ de 19.85 keV. L'emplacement de la raie L_I est signalé par une flèche, elle est masquée par le pied de la raie L_{II} et surtout par une raie parasite située vers 11.6 keV. Alors que les raies L_{II} et L_{III} décroissent bien avec la période de 47 h du ^{153}Sm, cette raie parasite ne décroît pratiquement pas et finit par subsister seule.

Il pourrait s'agir de la raie L_I de la transition de 20 keV dans la désintégration $^{151}\text{Sm}\rightarrow{}^{151}\text{Eu}$, mais l'énergie observée n'est pas en accord avec celle mesurée par Achor [18]). Il est également possible qu'il s'agisse d'une raie de la désintégration $^{155}\text{Eu}\rightarrow{}^{155}\text{Gd}$, mais on devrait alors observer les autres raies plus intenses, en particulier celle de 87 keV. Cette raie parasite demande donc une nouvelle étude, qui sera entreprise avec des isotopes séparés.

TABLEAU 2

Énergies et intensités des raies K et L

Énergie de la raie (keV)	Couche convertie	Intensité relative en électrons	Transition γ correspondante	Valeur moyenne de la transition en keV
12.23±0.05	L_{II}	≈0.6	19.85	19.85±0.05
12.87±0.05	L_{III}	0.9	19.85	19.85±0.05
21.20±0.05	K	68	69.71	69.8 ±0.1
34.87±0.05	K	1.7	83.48	83.6 ±0.1
49.09±0.05	K	0.4	97.60	97.60±0.1
54.87±0.05	K	100	103.35	103.4 ±0.1
61.82±0.05	L_I	9.4	69.88	69.8 ±0.1
76.74±0.05	L_{III}	1.1	83.72	83.6 ±0.1
95.42±0.05	L_I	13.7	103.48	103.4 ±0.1
124.9 ±0.1	K	≈0.1	173.4	173.4 ±0.1

Le tableau 2 donne les énergies et les intensités des raies K et L des électrons de conversion des transitions présentes dans le spectre de basse énergie de l'Europium 153. Les énergies de liaison électroniques sont tirées de [16]).

Au cours de cette étude, il nous a été impossible de mettre en évidence les transitions de 105 et 187 keV correspondant à la bande de rotation signalée par Temmer et Heydenburg [5, 8]) et dont le premier niveau est celui de 84 keV. L'intensité de la raie K de conversion de ces transitions est certainement inférieure à $\frac{1}{1000}$ de celle de la raie K du rayon γ de 103 keV.

Par contre, nous avons pu mettre en évidence la raie K de conversion de la transition „cross-over" de 173 keV, bien que celle-ci ait une intensité très faible, de l'ordre de $\frac{1}{1000}$ de celle de la raie K de 103 keV.

Signalons enfin que dans la région des raies K 70 et K 103, le spectre continu montre une nette composante d'énergie maximum environ 120 keV. Cette composante avait déjà été signalée par Dubey [9]). Mais n'ayant pu faire les mesures à énergie assez élevée, nous n'avons pu faire une analyse du spectre par décomposition en droites de Kurie.

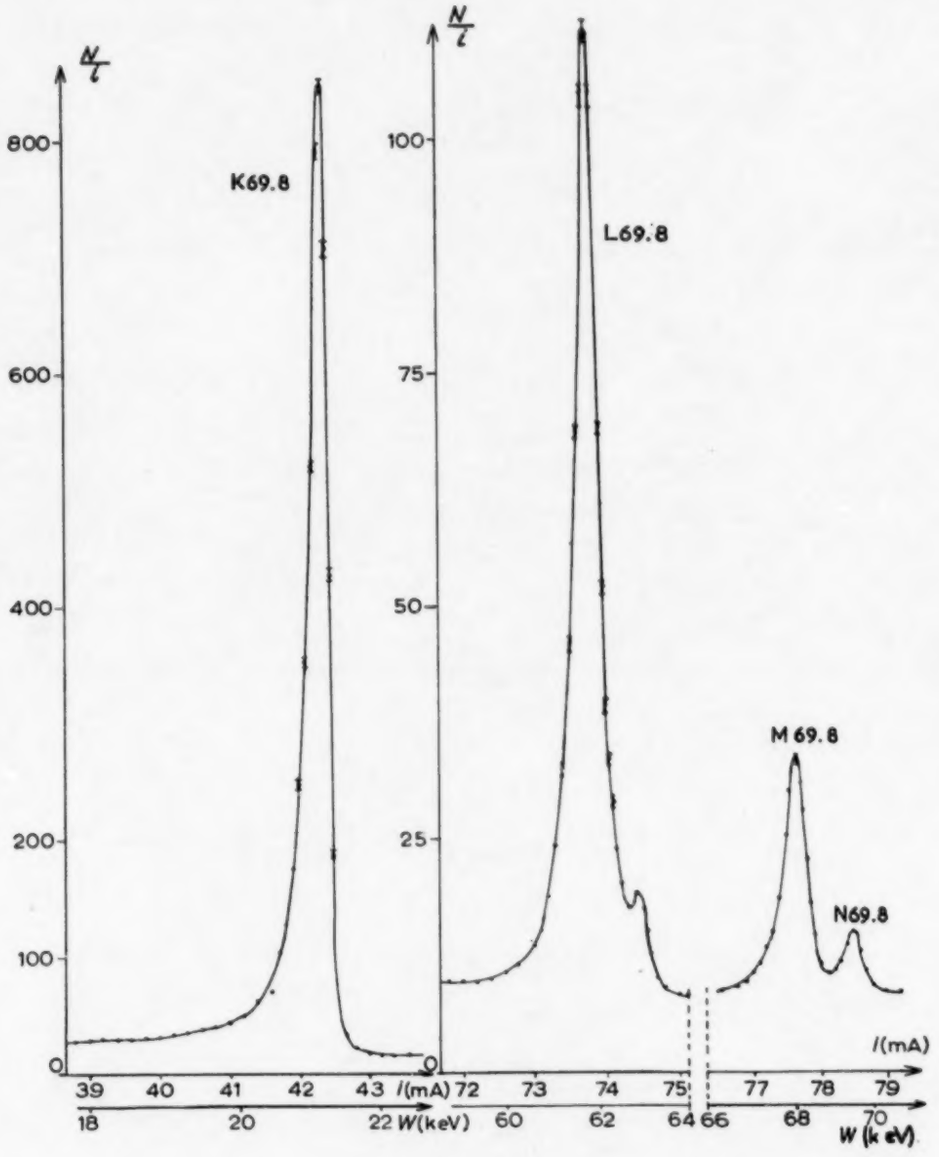

Fig. 3

Pour étudier les rapports de conversion, nous avons utilisé des sources de 1 ou 2 mm de large et de 10 à 40 $\mu g/cm^2$ d'épaisseur. Les rapports K : L : M pour les transitions de 70 et 103 keV sont faciles à obtenir car ces raies sont très bien résolues (figs. 3 et 4). Par contre, pour la transition de 83.6 keV, la raie K est très voisine de la raie d'électrons Auger KL_{III} L_{III} et pour mesurer l'aire de cette raie, nous avons dû faire une décomposition graphique du profil de ces raies

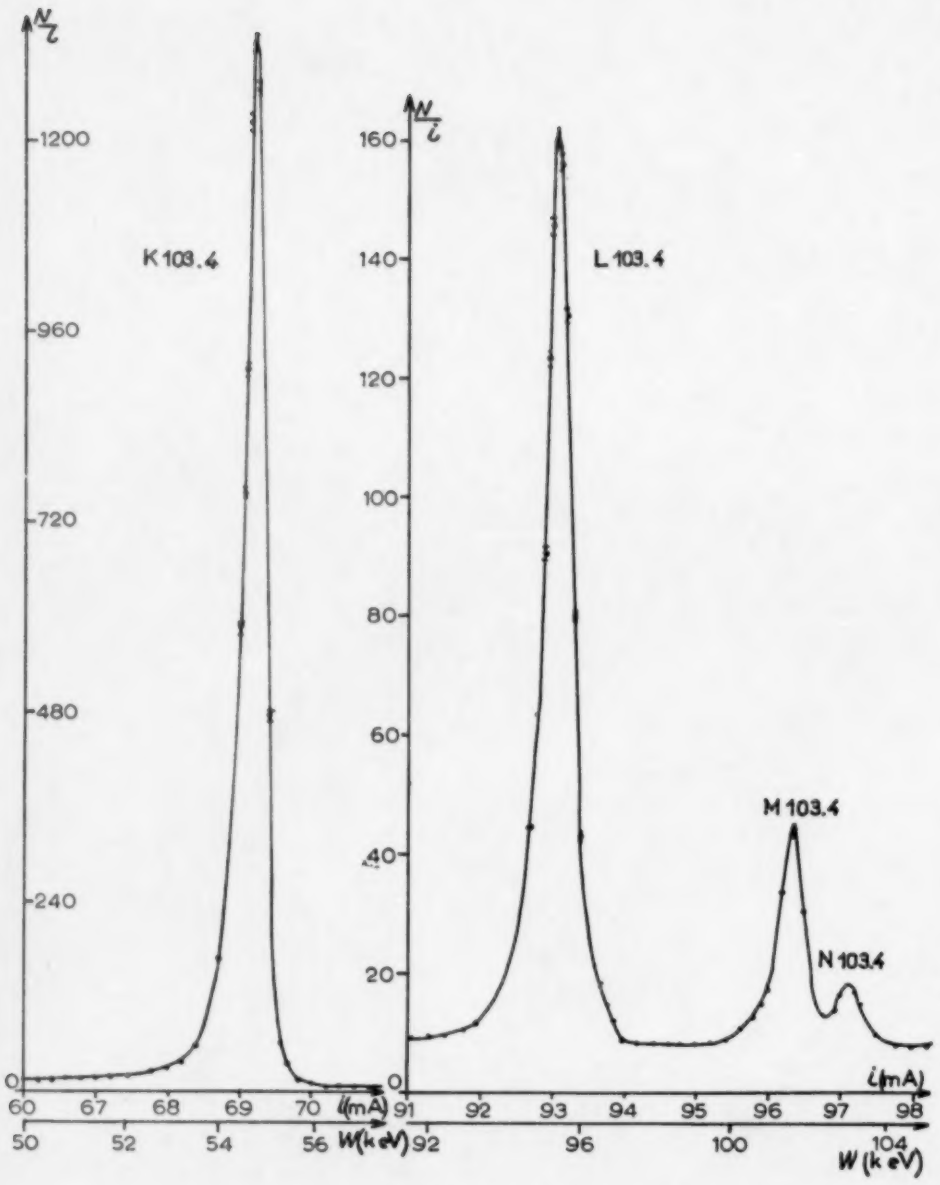
N/i
K 103.4
L 103.4
M 103.4
N 103.4
i(mA)
W(keV)

Fig. 4

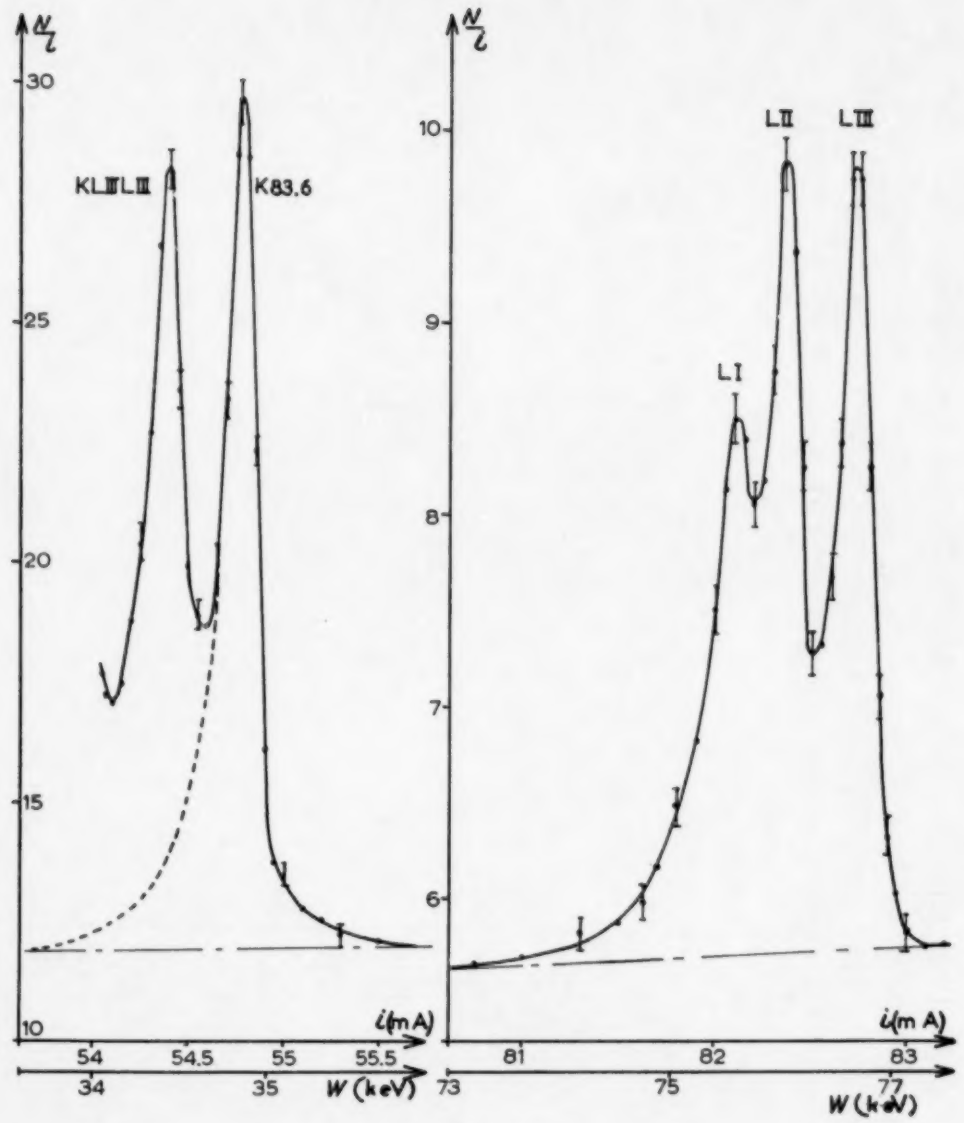
N/i
KLIILII
K83.6
LI
LII
LIII
i(mA)
W (keV)

Fig. 5

(fig. 5). Pour les rapports $L_I : L_{II} : L_{III}$, nous avons effectué une décomposition graphique complète pour les raies L, assez bien résolues, des transitions de 70 et 103 keV (fig. 6), L_{II} étant obtenue comme différence entre le profil réel total et les profils admis pour L_I et L_{III}. Pour les transitions de 19.8 et 84 keV, nous

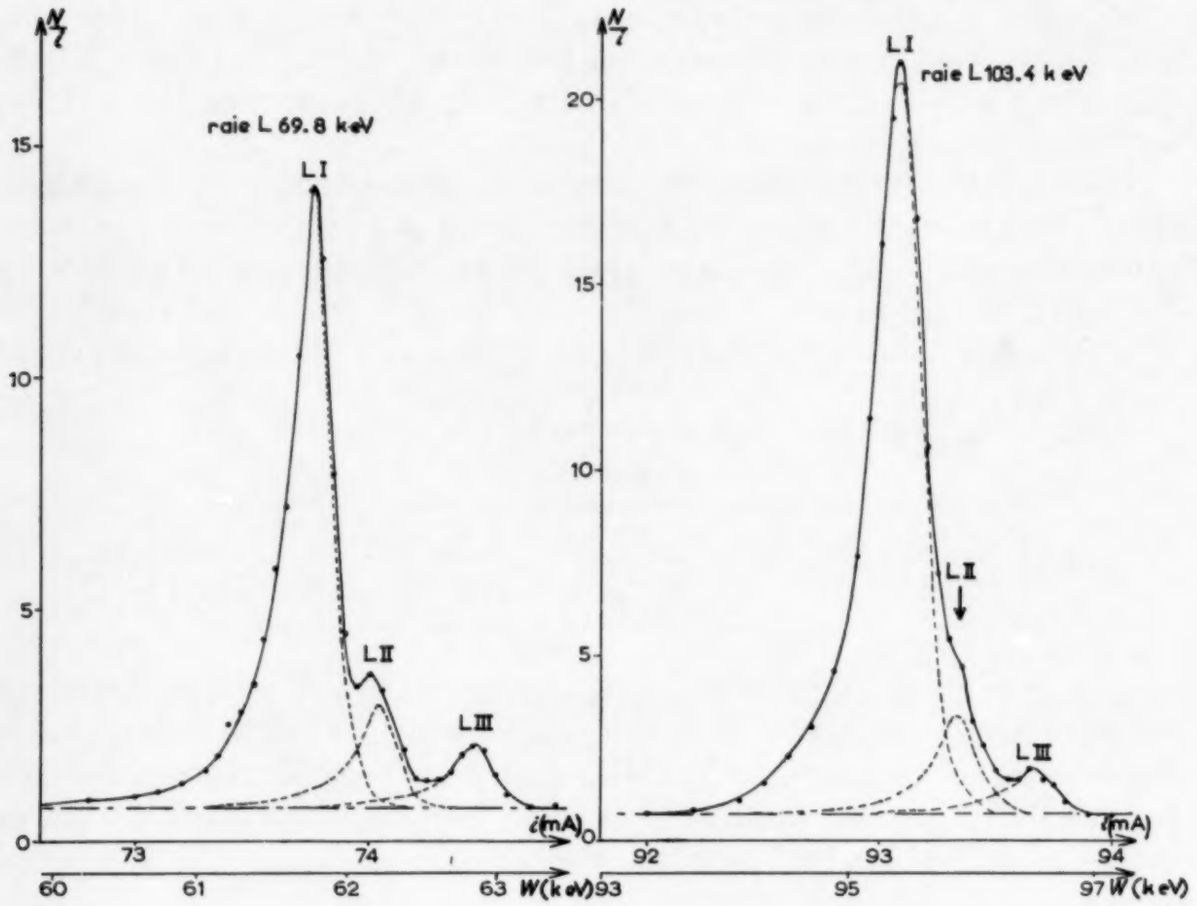

Fig. 6

n'avons déterminé que le rapport $(L_I+L_{II})/L_{III}$, car les raies L_I et L_{II} ne sont pas assez bien séparées pour pouvoir faire une décomposition (figs. 2 et 5).

Les résultats sont donnés dans le tableau 3. En comparent les tableaux 1 et 3,

TABLEAU 3

Rapports K/L et autres

E (keV)	K/L	L_I/L_{II}	L_I/L_{III}	L_{II}/L_{III}	L_I+L_{II}/L_{III}	L/M
19.85					0.70±0.05	2.7±0.5
69.8	7.2 ±0.4	6.0±0.5	9.5±0.5	1.4±0.2	11.2 ±0.2	4.6±0.2
83.6	1.60±0.05				1.37±0.05	2.5±0.5
103.4	7.3 ±0.2	9 ±1	18 ±1	2.0±0.5	20 ±1	4.7±0.3

nous constatons que les valeurs du rapport K/L pour les transitions de 70 et 103 keV ont été nettement sous-estimées par les auteurs précédents, probablement par suite de l'emploi de sources trop épaisses.

4.1.1. *Nature et polarité des transitions*

D'après le spin et la parité des niveaux excités de ^{153}Eu, identiques pour tous les auteurs, nous pouvons admettre que les rayons γ de 70, 84 et 103 keV sont des mélanges de transitions M1 et E2, tandis que le rayon γ de 19.8 keV est une transition E2 pure.

Avec les tables de coefficients de conversion interne de Rose [19]), nous avons obtenu les valeurs théoriques des rapports K/L, L_I/L_{II}, etc. . . . pour des transitions M1 et E2 pures, et nous avons pu ainsi déterminer le rapport de mélange des transitions ci-dessus.

Les résultats obtenus sont indiqués dans le tableau 4. Nous voyons donc que

TABLEAU 4

Rapport E2/M1

E_γ (keV)	69.8	83.6	103.4
E2/M1	$(1.5\pm0.5)\times10^{-2}$	1.25 ± 0.05	$(2.2\pm0.3)\times10^{-2}$

la proportion de E2 dans les transitions de 70 et 103 keV est très faible. Au contraire, pour la transition de 84 keV, les proportions de E2 et de M1 sont du même ordre de grandeur: 55 % de E2 contre 45 % de M1. Cette valeur du rapport M1/E2 pour la transition de 84 keV est en bon accord avec celle donnée par Alder *et al.* [20]): M1/E2 $\approx$ 1, obtenue par excitation coulombienne.

4.1.2. *Étude particulière du niveau de rotation de* 84 keV

La probabilité de transition M1 entre états de rotation est reliée aux rapports gyromagnétiques g_K et g_R des mouvements intrinsèque et collectif du noyau [21]). Nous avons donc pu les calculer d'après notre valeur du rapport M1/E2 pour la transition de 84 keV. En admettant pour la probabilité réduite B(E2), celle fournie par excitation coulombienne, on obtient ainsi

$$g_R = 0.29, \quad g_R = 0.38,$$
$$g_K = 0.44, \quad g_K = 0.23.$$

En l'absence de détermination du signe de $g_K - g_R$, nous ne pouvons conclure. Cependant, la valeur prévue théoriquement pour g_R étant de l'ordre de $Z/A = 0.41$, l'accord est relativement satisfaisant.

D'autre part, en comparent les intensités des transitions de 19.85 keV et de 83.6 keV, nous avons trouvé que le niveau de 83.6 keV est alimenté par une branche β du spectre de ^{153}Sm. L'intensité de cette branche est de 5.10^{-3} par

désintégration. Ceci correspond à une valeur de log $ft = 8.8$, donc à une transition $\Delta I = 2$, oui (transition une fois interdite unique). Il ne semble donc pas que cette branche β soit affectée d'un facteur d'interdiction supplémentaire dû à la transition vers un niveau de rotation.

4.2. ÉTUDE DES ÉLECTRONS AUGER K

Cette étude a été faite avec des sources de 1 mm de large et plus particulièrement avec la source IV de 12 μg/cm^2 d'épaisseur.

4.2.1. *Structure du groupe* KLL

Ce groupe présente 6 pics très bien résolus, sauf le pic correspondant à la raie $KL_{II}L_{II}$ d'intensité très faible (fig. 7).

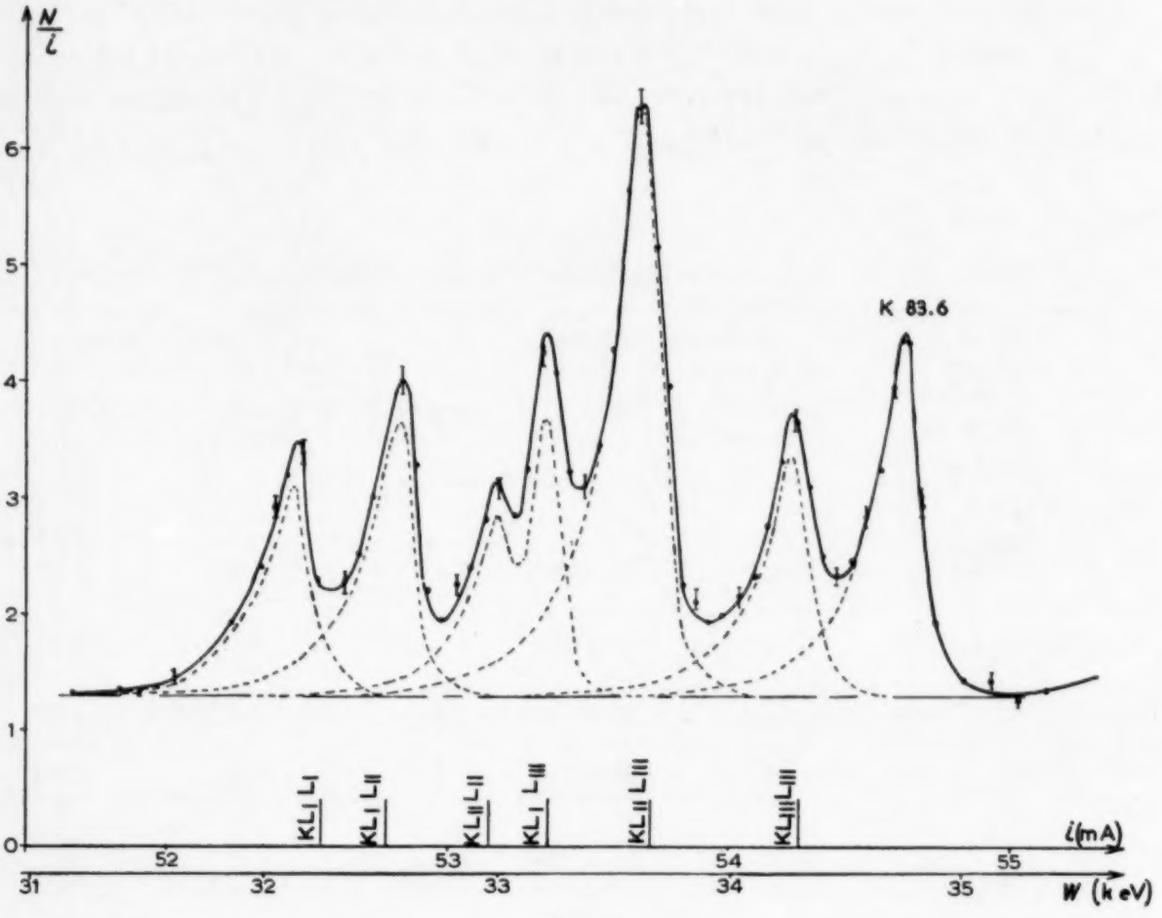

Fig. 7

Les valeurs expérimentales de l'énergie des raies de ce groupe sont portées dans le tableau 5. Ces valeurs sont en bon accord avec les valeurs théoriques calculées à l'aide de la relation:

$$E_{KL_pL_q} = E_K^Z - E_{L_p}^Z - E_{L_q}^{Z+\Delta Z},$$

dans laquelle on a pris $\Delta Z = 0.5$ quand L_q est L_I et $\Delta Z = 1$ quand L_q est L_{II} ou L_{III}.

TABLEAU 5

Énergies du groupe KLL

Raie	Énergie expérim. (keV)	Énergie théor. (keV)
KL_IL_I	32.15±0.10	32.23
KL_IL_{II}	32.59±0.05	32.51
$KL_{II}L_{II}$	32.98±0.05	32.95
KL_IL_{III}	33.22±0.05	33.20
$KL_{II}L_{III}$	33.62±0.05	33.64
$KL_{III}L_{III}$	34.29±0.05	34.28

Après décomposition des raies de ce groupe, nous avons pu mesurer l'intensité de cinq raies ($KL_{II}L_{II}$ et KL_IL_{III} n'ont pas été séparées). Le tableau 6 indique nos valeurs ainsi que celle trouvées par divers auteurs. Nos valeurs s'accordent assez bien avec celles des auteurs précédents.

TABLEAU 6

Intensités relatives du groupe KLL

	Valeurs expériment.				Valeurs théor.	
	Présent travail $Z = 63$	Ewan [22]) $Z = 64$	Ewan [23]) $Z = 62$	Marguin [24]) $Z = 56$	Asaad [25]) $Z = 47$	Asaad [25]) $Z = 80$
KL_IL_I	1	1	1	1	1	1
KL_IL_{II}	1.3±0.1	1.40±0.10	1.39±0.06	1.4±0.1	1.82	1.20
KL_IL_{III} + $KL_{II}L_{II}$	1.5±0.1	1.57±0.06	1.72±0.06	1.8±0.1	1.90	2.42
$KL_{II}L_{III}$	3.0±0.1	3.08±0.18	3.14±0.13	2.9±0.15	4.71	4.32
$KL_{III}L_{III}$	1.2±0.1	1.28±0.09	1.39±0.06	1.5±0.1	1.90	2.40

Les groupes KLX et KXY sont très complexes (fig. 8). On a attribué les 4 pics nettement résolus du groupe KLX aux raies indiquées dans le tableau 7.

Les intensités relatives des 3 groupes d'électrons Auger K, mesurées par les rapports des aires situées au-dessous des courbes donnant N/i en fonction de i (fond continu déduit) sont données dans le tableau 8. Nous indiquons aussi dans ce tableau les valeurs trouvées par divers auteurs. Notre valeur de KXY/KLL est en bon accord avec celles de tous les auteurs, par contre notre valeur de KLX/KLL est nettement plus élevée.

Le rendement Auger K, soit a_K, est mesuré par le rapport des intensités des groupes Auger K et des raies K de conversion de toutes les transitions γ.

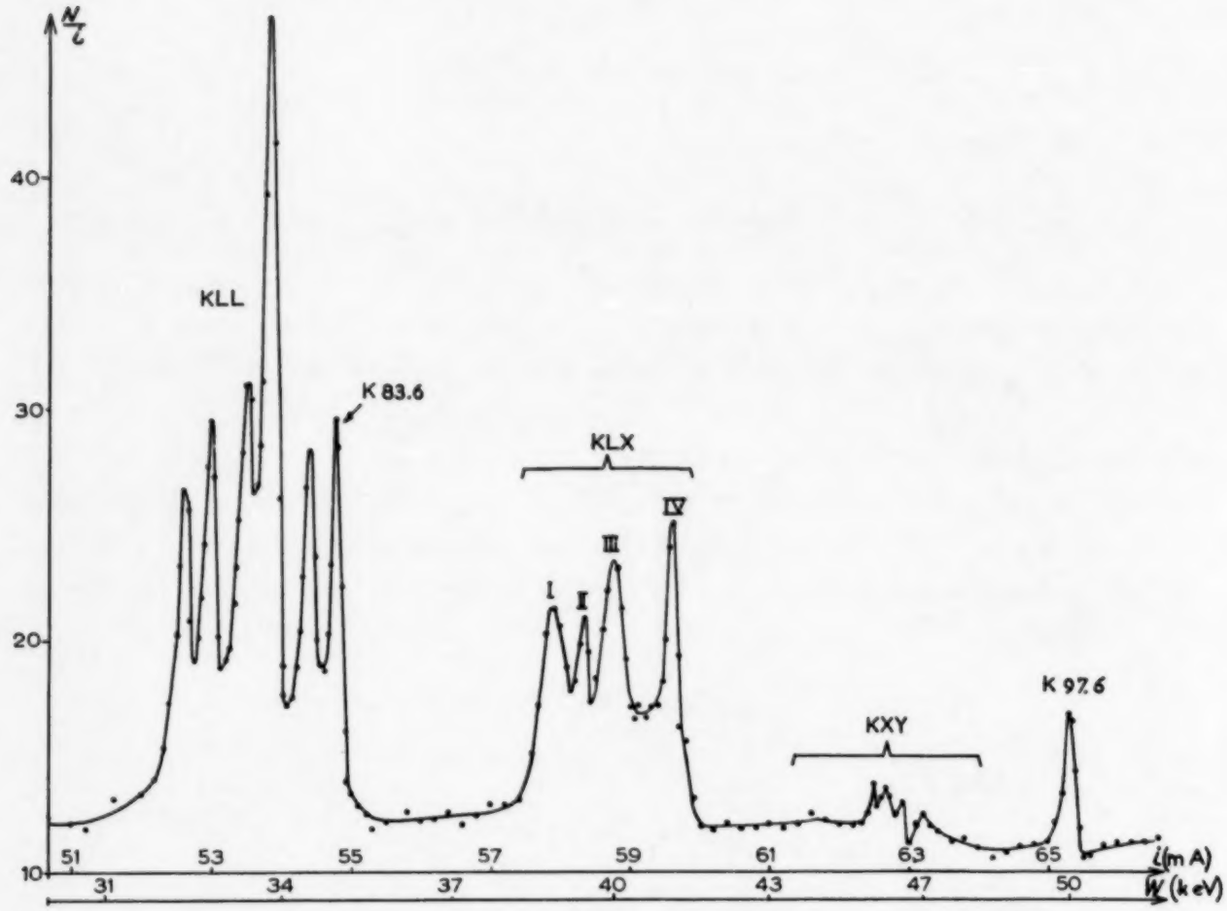

Fig. 8

TABLEAU 7

Pics résolus du groupe KLX

	Pic I	Pic II	Pic III	Pic IV
Énergie (keV)	38.93	39.53	40.05	41.14
Transitions	$KL_I M_{II}$ $KL_I M_{III}$	$KL_{II} M_{III}$	$KL_{III} M_{II}$ $KL_{III} M_{III}$ $KL_I N_I$	$KL_{III} N_I$

TABLEAU 8

Intensités relatives des groupes d'électrons Auger K

	Broyles [26]) $Z = 47$	Marguin [24]) $Z = 47$	Marguin [27]) $Z = 69$	Nall [28]) $Z = 80$	Pincherle [29]) théor.	Présent travail $Z = 63$
KLL	1	1	1	1	1	1
KLX	0.40±0.04	0.42 ±0.02	0.49±0.04	0.496±0.015	0.715	0.60 ±0.03
KXY	0.08±0.02	0.081±0.012		0.094±0.003	0.102	0.086±0.015

Nous avons trouvé

$$a_K = 0.075 \pm 0.005.$$

D'où le rendement de fluorescence K:

$$\overline{\omega}_K = 0.925 \pm 0.005.$$

L'erreur 0.005 englobe l'erreur statistique sur chaque point mesuré et l'erreur due au fait que l'on déduit un peu arbitrairement le fond continu β^-. Cette valeur de $\overline{\omega}_K$ se place très prés de la courbe de Laberrigue et Radvanyi [30]).

4.3. ÉTUDE DES ÉLECTRONS AUGER L

Cette étude a été faite avec la source V de 2 mm de largeur, et d'épaisseur très faible: 8 μg/cm^2. La fig. 9 représente ce spectre corrigé, quand il y a lieu, de l'absorption de la fenêtre. Le spectre présente une queue vers les basses

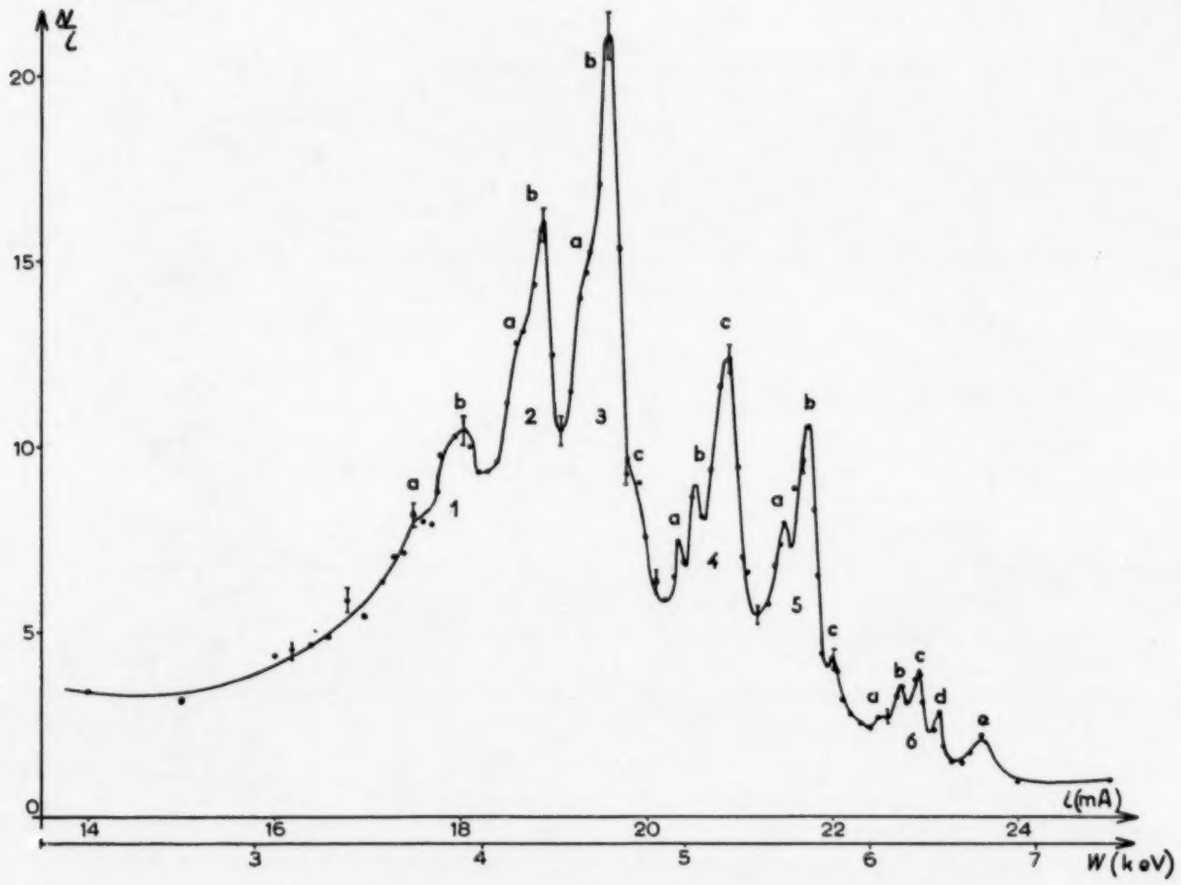

Fig. 9

énergies, due à l'absorption dans l'épaisseur de la source. Le fond continu β^- n'est jamais atteint sur toute l'étendue du spectre, à cause du grand nombre de raies et de l'épaisseur de la source. Ainsi donc, l'étude de ce groupe est trés

complexe. Le tableau 9 donne les énergies des transitions les plus probables, calculées d'après la relation

$$E_{L_p XY} = E^Z_{L_p} - E^Z_X - E^{Z+1}_Y,$$

ainsi que l'identification vraisemblable des pics du spectre, en tenant compte du fait que les vacances les plus nombreuses sont localisées dans les couches L_{II} et L_{III}.

TABLEAU 9

Énergies des transitions Auger L les plus probables

Pics	Énergie expér. (keV)	Identification	Énergie théor. (keV)
1a	3.67	$L_{III}M_{II}M_{II}$	3.669
1b	3.93	$L_{III}M_{III}M_{II,\,III}$	3.812–3.946
2a	4.17	$L_{III}M_{II}M_{IV,\,V}$	4.136–4.171
2b	4.29	$L_{III}M_{III}M_{IV,\,V}$	4.270–4.305
3a	4.46	$L_{II}M_{II}M_{III}$	4.452
3b	4.60	$L_{III}M_{IV}M_{IV,\,V}$	4.589–4.624
3c	4.78	$L_{II}M_{II}M_{IV,\,V}$	4.776–4.811
4a	4.96	$L_{II}M_{III}M_{IV,\,V}$	4.910–4.945
4b	5.03	$L_{I}M_{III}M_{III}$	5.021
4c	5.25	$L_{II}M_{IV}M_{IV,\,V}$	5.229–5.264
5a	5.54	$L_{III}M_{IV}N_{III}$	5.538
5b	5.66	$L_{III}M_{IV}N_{IV}$	5.660–5.666
5c	5.79	$L_{II}M_{III}N_{I,\,II}$	5.748–5.833

Le rendement Auger L moyen a_L, égal au rapport du nombre d'électrons Auger L au nombre de vacances L totales, (primaires et secondaires) peut se calculer à partir de nos mesures, en admettant pour les intensités des raies X, $K\alpha_1$ et $K\alpha_2$ les valeurs données par Nijgh *et al.* [31]). Le calcul donne pour a_L une valeur très voisine de 1, qui est certainement trop élevée, ce qui est dû à la présence d'un excès d'électrons de faible énergie; le même fait avait été signalé par Marguin [27]) pour le ^{170}Yb. D'autre part, la comparaison de la forme du spectre Auger L avec celle des mêmes spectres obtenus par cet auteur pour ^{137}Ba et ^{170}Yb, montre la présence probable d'une raie de conversion (raie 2b) qui pourrait être la raie de conversion M_{III} de la transition de 5.8 keV entre les niveaux de 103.4 et 97.6 keV. (Cette transition doit être de type M2). Une comparaison avec le spectre Auger L d'un autre isotope de l'europium sera nécessaire pour préciser ce point.

Bibliographie

1) D. Strominger, J. M. Hollander et G. T. Seaborg, Rev. Mod. Phys. **30** (1958) 585
2) M. R. Lee et R. Katz, Phys. Rev. **93** (1954) 155
3) F. K. McGowan, Phys. Rev. **93** (1954) 163

4) R. L. Graham et J. Walker, Phys. Rev. **94** (1954) 794
5) G. M. Temmer et N. P. Heydenburg, Phys. Rev. **94** (1954) 1399
6) N. Marty, C. R. Acad. Sc. **238** (1954) 2516
7) N. Marty, J. Phys. Rad. **16** (1955)458
8) N. P. Heydenburg et G. M. Temmer, Phys. Rev. **100** (1955) 150, **104** (1956) 981
9) V. S. Dubey, C. E. Mandeville et M. A. Rothmann, Phys. Rev. **103** (1956) 1430
10) M. C. Joshi, B. N. Subbarao et B. V. Thosar, Proc. Ind. Acad. Sci. **45** (1957) 390
11) J. M. Cork, M. K. Brice, R. G. Helmer et R. M. Woods, Phys. Rev. **110** (1958) 526
12) C. W. McCutchen, Nuclear Physics **5** (1958) 187
13) E. L. Church et M. Goldhaber, Phys. Rev. **95** (1954) 626
14) N. Marty et M. Vergnes, C. R. Acad. Sc. **242** (1956) 1438
15) A. Moussa et J. B. Bellicard, J. Phys. Rad. **15** (1954) 85
16) K. Siegbahn, Beta and gamma spectroscopy (North-Holland Publ. Co., Amsterdam, 1955)
17) A. Moussa et E. Monnand, J. Phys. Rad. **21** (1960) 463
18) W. T. Achor, Thése, Vanderbilt University Nashville, AEC report ORO-207
19) M. E. Rose, Internal conversion coefficients (North-Holland Publ. Co., Amsterdam, 1958)
20) K. Alder, A. Bohr, T. Huus, B. Mottelson et W. A. Winther, Rev. Mod. Phys. **28** (1956) 432
21) A. Bohr et B. Mottelson Mat. Fys. Medd. Dan. Vid. Selsk. **16**, (No. 27 (1953)
22) G. T. Ewan et J. S. Merrit, Can. J. Phys. **38** (1960) 324
23) G. T. Ewan, R. L. Graham et L. Grodzins, Can. J. Phys. **38** (1960) 163
24) P. Marguin et A. Moussa, J. Phys. Rad. **21** (1960) 149
25) W. N. Asaad et E. H. S. Burhop, Proc. Phys. Soc. **71** (1958) 369
26) C. D. Broyles, D. A. Thomas et S. K. Haynes, Phys. Rev. **89** (1953) 715
27) P. Marguin et A. Moussa, J. Phys. Rad. **21** (1960) 17
28) J. C. Nall, Q. L. Baird et S. K. Haynes, Phys. Rev. **118** (1960) 1278
29) L. Pincherle, Nuovo Cim. **12** (1935) 81
30) J. Laberrigue-Frolow et P. Radvanyi, J. Phys. Rad. **17** (1956) 944
31) G. J. Nijgh, A. H. Wapstra et R. van Lieshout, Nuclear spectroscopy tables (North-Holland Publ. Co., Amsterdam, 1959)

1.B

Nuclear Physics **25** (1961) 307—316; © *North-Holland Publishing Co., Amsterdam*

Not to be reproduced by photoprint or microfilm without written permission from the publisher

A SEPARABLE POTENTIAL FOR THE TWO-NUCLEON ($T = 1$) INTERACTION

A. N. MITRA

Department of Physics, University of Delhi, Delhi-6, India

and

J. H. NAQVI

Department of Physics, Muslim University, Aligarh, (U. P.), India

Received 6 February 1961

Abstract: A separable potential in the isobaric state $T = 1$ is proposed on the basis of p—p scattering data up to about 100 MeV. The triplet part of this potential is taken to be purely of the spin-orbit type, with a range about half of that of the singlet potential. Potentials in states $l \geqq 3$ are neglected.

It is found that such a potential can rather satisfactorily explain the angular shape of the unpolarized cross section as well as the magnitude of the polarization in scattering up to 100 MeV.

1. Introduction

In a recent paper [1]) (referred to as MN) an analysis of the low-energy neutron-proton system was carried out, and on this basis a separable potential in the two-nucleon state $T = 0$ proposed as an extension of Yamaguchi's [2]) corresponding potential, so as to include a spin-orbit term. The apparent success of such a potential in predicting the shell model energy levels in some nuclei [3]) encouraged us to extend a similar analysis to the data on p—p scattering (with Coulomb effects) at low and moderate energies, so as to provide a corresponding potential in the state $T = 1$ of a two-nucleon system. Being interested in energies up to about 100 MeV, we have assumed the potential to be operative only in the states $l = 0$, 1 and 2, and neglected the effects of states with $l \geqq 3$.

It may be repeated here that as far as the effects *on the energy shell* are concerned, a separable potential of this type is largely equivalent to a conventional phase shift representation of the scattering data. However, once such a potential (with parameters fixed from scattering data) is obtained, its validity *off the energy shell* automatically becomes a subject of scrutiny — a common problem shared by all potentials, local and non-local. While there is as yet no clear-cut criterion available (on the basis of analysis off the energy shell) for distinguishing one potential shape from another, it is generally recognized that at higher energies, the conventional concept of a local potential breaks down anyway. So one might argue that at lower energies at least, simplicity should be

an important criterion for deciding between various potentials, as long as the observable effects of all of them are essentially the same. We have taken just this attitude here, trying to incorporate in our separable potential as much physical information as is currently available to us.

Sect. 2 summarises the necessary algebraic formulae for the unpolarized differential cross section and polarization in terms of the separable potential parameters. The results of numerical evaluation are analysed in sect. 3. A comparative discussion of our spin-orbit potential vis-a-vis contemporary ones is given in sect. 4.

2. The p—p Cross Section and Polarization

To distinguish the various parameters used in the present case of $T = 1$ from those of $T = 0$ considered in MN it is convenient to identify the relevant quantities (potentials, amplitudes etc.) by a superscript (T). Now for the $T = 1$ interaction we choose a potential to operate on the states ^{1}S, ^{3}P, and ^{1}D, on the lines of MN, and write

$$(\mathbf{p}|V^{(1)}|\mathbf{p}') = (1-\rho)(\mathbf{p}|V_s^{(1)}|\mathbf{p}')+\rho(\mathbf{p}|V_t^{(1)}|\mathbf{p}'), \tag{1}$$

where ρ is the projection operation tor triplet states viz.,

$$\rho = \tfrac{3}{4}+\tfrac{1}{4}\boldsymbol{\sigma}_1 \cdot \boldsymbol{\sigma}_2, \tag{2}$$

and $V_s^{(1)}$ and $V_t^{(1)}$ are respectively the singlet and triplet parts of the potential defined by

$$(\mathbf{p}|V_s^{(1)}|\mathbf{p}') = \sum_{l=0,2} (2l+1)\left(-\frac{\lambda_l^{(1)}}{M}\right) v_l^{(1)}(p)v_l^{(1)}(p')P_l(\hat{p}\cdot\hat{p}') \tag{3}$$

and

$$(\mathbf{p}|V_t^{(1)}|\mathbf{p}') = -\frac{4\pi\lambda_1^{(1)}}{M} v_1^{(1)}(p)v_1^{(1)}(p')\sum_{m=-1}^{1} Y_{1m}^*(\hat{p}')(\mathbf{L}\cdot\mathbf{S})Y_{1m}(\hat{p}'). \tag{4}$$

We have here chosen a pure $\mathbf{L}\cdot\mathbf{S}$ term for the triplet P-interaction. A tensor interaction in the triplet state would have the most general structure of the form

$$\sum_m Y_{1m}^*(\hat{p})[A(S(\hat{p})+S(\hat{p}'))+BS(\hat{p})S(\hat{p}')]Y_{1m}(\hat{p}'), \tag{4a}$$

where $S(\hat{p})$ is the basic tensor operator in the unit vector $\hat{p}$ (see MN). However, such an interaction would necessarily couple the P and F waves. It may be easily seen that the part of (4a) which is operative on $l = 1$ alone, can be expressed algebraically in the form

$$Y_{1m}^*(\hat{p})[a+b(\mathbf{L}\cdot\mathbf{S})+c(\mathbf{L}\cdot\mathbf{S})^2]Y_{1m}(\hat{p}'), \tag{4b}$$

where a, b, c are linear functions of A and B. This form is similar to (4), except

for the a- and c-terms. It will, however, appear from sect. 3 that our choice (4) happens to give a rather good representation of the available data. The question of inclusion of the tensor part is discussed again in sect. 4.

The shapes of the scalar functions $v_l^{(1)}$ in (3) and (4) are left unspecified at this stage, and will be clarified in sect. 3.

It is clear from (1) that the singlet and triplet parts do not interfere, and may be handled separately. In addition, for the singlet part (3) it is easily verified by proceeding as in sect. 4 of MN that in the integral equation for the singlet T-matrix, there is no interference between the ^{1}S and ^{1}D parts of the potential, so that the singlet reaction matrix T_s is simply the sum of the individual ones † for ^{1}S and ^{1}D. As for the triplet part of the T-matrix, it can be worked out in a straightforward way following the procedure outlined in MN. The final form of the T-matrix is then similar to (1) viz.,

$$(\mathbf{p}|T^{(1)}|\mathbf{p}') = (1-\rho)(\mathbf{p}|T_s^{(1)}|\mathbf{p}')+\rho(\mathbf{p}|T_t^{(1)}|\mathbf{p}'), \tag{5}$$

where

$$(\mathbf{p}|T_s^{(1)}|\mathbf{p}') = \sum_{l=0,\,2}\left(-\frac{(2l+1)\lambda_l^{(1)}}{M}\right) A_l^{(1)} v_l^{(1)}(p) v_l^{(1)}(p') P_l(\hat{p}\cdot\hat{p}'), \tag{6}$$

$$(\mathbf{p}|T_t^{(1)}|\mathbf{p}') = -\frac{3\lambda_1^{(1)}}{M} v_1^{(1)}(p) v_1^{(1)}(p')[A_1+B_1(\mathbf{L}\cdot\mathbf{S})+C_1(\mathbf{L}\cdot\mathbf{S})^2]P_1(\hat{p}\cdot\hat{p}'), \tag{7}$$

$$A_l^{(1)} = [1+\mu_l^{(1)}(k)]^{-1}, \tag{8}$$

and

$$\mu_l^{(1)}(k) = (-1)^l\lambda_l^{(1)}\int \mathrm{d}^3\mathbf{p}\,(v_l^{(1)}(p))^2/(k^2-p^2+i\varepsilon) \tag{9}$$

$$\equiv \varepsilon_l^{(1)}(k)+i\tau_l^{(1)}(k). \tag{10}$$

The quantities ε_l and τ_l in (10) are related to the corresponding singlet phase shifts δ_l according to

$$\mathrm{tg}\,\delta_l = -\tau_l^{(1)}(k)/[1+\varepsilon_l^{(1)}(k)]. \tag{11}$$

Finally, the ^{3}P-state coefficients appearing in (7) are defined by

$$A_1 = \frac{2(\mu_1^{(1)})^2\rho}{D_1}, \quad B_1 = \frac{1+2\mu_1^{(1)}}{D_1}, \quad C_1 = \frac{\mu_1^{(1)}}{D_1}, \tag{12}$$

where

$$D_1 = 1+2\mu_1^{(1)}-(\mu_1^{(1)})^2-2(\mu_1^{(1)})^3\rho, \tag{13}$$

and $\mu_1^{(1)}$ is given by (9) and (10) with $l = 1$. The corresponding ^{3}P phase shifts

† More generally, it can be shown that for a more complete singlet $T = 1$ potential, viz. one which includes $l = 0, 2, 4, \ldots$ the total singlet T-matrix is a sum of the individual T-matrices. However, this simplification does not occur for triplet interactions in general, since tensor forces (which are operative only in triplet states) bring about a mixing of T-matrix elements corresponding to different l-values.

$\delta_1^{0,1,2}$ are related to these parameters according to the equations

$$\begin{aligned}\exp(2i\delta_1^0)-1 &= 2i\tau_1^{(1)}(k)(A_1-2B_1+4C_1),\\ \exp(2i\delta_1^1)-1 &= 2i\tau_1^{(1)}(k)(A_1-B_1+C_1),\\ \exp(2i\delta_1^2)-1 &= 2i\tau_1^{(1)}(k)(A_1+B_1+C_1).\end{aligned} \tag{14}$$

To include the Coulomb effect in (6) and (7) we follow the usual approximation of adding the Coulomb amplitude to the nuclear amplitude, which is fairly good except for very small angles [4]). If therefore $f_e(\theta)$ and $f_o(\theta)$ are respectively the even and odd parts of the usual Coulomb amplitude [5]) $f_c(\theta)$, viz.,

$$f_e(\theta),\quad f_o(\theta) = \tfrac{1}{2}[f_c(\theta)\pm f_c(\pi-\theta)], \tag{15}$$

the Coulomb modified T-matrices $T_c^{(1)}$ are given, with due normalizations, by

$$(\mathbf{p}|T_{sc}^{(1)}|\mathbf{p}') = (\mathbf{p}|T_s^{(1)}|\mathbf{p}')+(2M\pi^2)^{-1}f_e(\theta) \tag{16a}$$

and

$$(\mathbf{p}|T_{tc}^{(1)}|\mathbf{p}') = (\mathbf{p}|T_t^{(1)}|\mathbf{p}')+(2M\pi^2)^{-1}f_o(\theta). \tag{16b}$$

The unpolarized p—p differential cross section, including Coulomb effects, is now expressed by the formula

$$\sigma(\theta) = (2\pi^2M)^2\,\mathrm{Tr}[(1-\rho)(\mathbf{p}|T_{sc}^{(1)}|\mathbf{k})(\mathbf{k}|T_{sc}^{(1)}|\mathbf{p})^*+\rho(\mathbf{p}|T_{tc}^{(1)}|\mathbf{k})(\mathbf{k}|T_{tc}^{(1)}|\mathbf{p})^*]_{(p=k)} \tag{17}$$

Substituting for the T-matrices from the earlier equations, eq. (17) may be explicitly written as a sum of nuclear, Coulomb and interference terms, viz.,

$$\sigma(\theta) = \sigma_N(\theta)+\sigma_{Nc}(\theta)+\sigma_c(\theta), \tag{18}$$

where the individual terms have their well-known expressions in terms of phase shifts (see, e.g., ref. [4])).

Finally, the polarization parameter $P(\theta)$ which is given by [6])

$$P(\theta)\sigma(\theta) = (2)^{\frac{1}{2}}(2\pi^2M)^2\,\mathrm{Im}\sum_m T_{0m}(T_{m1}^{\dagger}-T_{m,-1}^{\dagger}), \tag{19}$$

simplifies to

$$\begin{aligned}[P\sigma(\theta)/\sin\theta\cos\theta] &= 2\left(\frac{3\tau_1^{(1)}(k)}{k}\right)^2\mathrm{Im}\,(2B_1^*A_1+3B_1^*C_1-C_1^*A_1)\\ &+\frac{\eta}{2k}\left(\frac{3}{k}\tau_1^{(1)}(k)\right)\sec\theta\,\mathrm{Im}\,(-B_1(X_1+iY_1)+(B_1^*-C_1^*)(X_1-iY_1)),\end{aligned} \tag{20}$$

where the Coulomb interference parameters X_1, Y_1 and η are as defined in ref. [4]).

3. Numerical Results

For a numerical evaluation of the various quantities, the forms of the scalar functions $v_0^{(1)}$ and $v_2^{(1)}$ were chosen as in ref. [2]), viz.,

$$v_0^{(1)}(p) = (\beta_0^2+p^2)^{-1}, \quad v_2^{(1)}(p) = p^2(\beta_2^2+p^2)^{-2}. \tag{21}$$

Such shapes therefore correspond asympotically to $(p|V|p') \approx (pp')^{-2}$ for large p and p'. Now it is easy to see, by taking the Fourier transform of an exponential potential, that in the asymptotic regions the corresponding matrix element † in momentum space for each partial wave also has roughly the above dependence on p and p'. Thus, in a certain sense, our potential (21) should be compared with an exponential potential. A Yukawa-type potential corresponds, in a similar sense, to the shape

$$v_l^{(1)}(p) = p^l(\beta_l^2+p^2)^{-\frac{1}{2}(l+1)}. \tag{22}$$

For algebraic simplicity we prefer the 'exponential' shape (21) for the potential in even states and the 'Yukawa' shape (22) for odd states. A Yukawa form for the L.S. potential should also facilitate a comparison with the famous phenomenological potential of Gammel and Thaler [7]), though not with that of Signell and Marshak [8]), which is more singular. It may be observed here, that the extremely short-ranged L.S. potential of G—T would have looked even shorter-ranged in the exponential shape.

To fix the numerical values of the various parameters we start from the very low-energy end, involving only the singlet s-potential. Now if we were merely interested in fitting the low energy p—p data, we could take about the best estimates available to data, viz. [9]),

$$a \approx -17.7\times10^{-13}\text{ cm}, \quad r_0 \approx 2.7\times10^{-13}\text{ cm}, \tag{23}$$

leading, according to the formulae in ref. [2]), to

$$\beta_0 \approx 5.5\alpha, \quad \lambda_0^{(1)} \approx 13.3\alpha^3, \tag{24}$$

where α^2/M is the binding energy of the deuteron. However, we are more interested in treating our potential in the spirit of charge independence, so that we should make our parameters conform more to singlet n—p scattering than to p—p scattering, since the latter mask the effect of charge independence considerably at low energies. For the n—p case, on the other hand, the singlet scattering length is appreciably larger, and the effective range parameter is not

† These elements for a potential $V(r)$ are

$$(\mathbf{p}|V_l|\mathbf{p}') = \int \mathrm{d}^3\mathbf{r}V(r)\exp(i\mathbf{r}\cdot(\mathbf{p}-\mathbf{p}'))P_l(\hat{p}\cdot\hat{p}')\frac{\mathrm{d}\Omega}{4\pi} = 4\pi\int j_l(pr)j_l(p'r)r^2V(r)\mathrm{d}r,$$

from which the result can be shown to follow.

a well-measured quantity. Thus we have essentially one equation, viz. [2])

$$1.82\alpha \approx -a_s^{-1} = \tfrac{1}{2}\beta_0(\beta_0^3\pi^{-2}\lambda_0^{-1}-1), \tag{25}$$

which we can use to determine λ_0 in terms of β_0. As for β_0, we could, for example like Yamaguchi, [2]) postulate β_0 equal to the corresponding triplet parameter β of MN. In this respect, we have tried to make use of the following indirect information, arising from the effects of such an assumption on the photodisintegration of the deuteron near threshold. Indeed, one of us [10]) has found that the ratio of the M1 to E1 transitions near threshold depends only on β_0, λ_0 and the triplet β defined in MN. A fixed value of this ratio therefore leads, via (26), to a relation between β_0 and β which happens to be such that as β_0 decreases, β increases slowly. In particular, at 2.5 MeV, the experimental ratio of 0.6 ± 0.02 is reproduced for the typical sets $\beta_0 = 5.8\alpha$ and $\beta = 4.1\alpha$ or $\beta_0 = 5\alpha$ and $\beta = 4.3\alpha$. This would seem to suggest that there could be a substantial difference between the triplet and the singlet range parameters of our separable potential. But if we want to maintain approximate equality of these two parameters we should take β_0 nearer 5α than 5.8α. However, a smaller β_0 was found to put a heavy strain on the triplet-P parameter β_1 of eqs. (4) and (22), which had then to increase very sharply, in order to catch up with the polarization and the magnitude of $\sigma(90°)$ at the cost of a disproportionately low value of $\sigma(15°)$. On the other hand, a value of $\beta_0 > 5.8\alpha$, while facilitating a more natural adjustment of both $\sigma(\theta)$ and $P\sigma(\theta)$ would bring about a much wider gap ($\gtrsim 2\alpha$) between β_0 and β. In this respect we have tried to make a compromise by keeping $\beta_0 = 5.8\alpha$ which would of course necessitate some adjustment

TABLE 1

Comparison of experimental and calculated values

	95 MeV		66 MeV		40 MeV	
	Calc.	Expt.	Calc.	Expt.	Calc.	Expt.
$\sigma(90°)$ (mb/sr)	4.66	4.65	6.30	6.6 [a])	11.26	11.2
$\sigma(40°)$ (mg/sr)	5.02	4.93	6.67	6.69 (at 40.7°)	11.01	11.0
$\sigma(\theta_{min})$ (mb/sr)	2.58 (at 13°)	3.40 (at 17°)	4.12 (at 15°)		8.5 (at 20°)	9.6 (at 20°)
a_1 (mb/sr)	1.15	1.0 ± 0.11 [b])	0.694	0.91 ± 0.10 [c])	0.256	
δ_0	32.8°		38.9°		46.7°	
δ_2	3.00°		1.98°		0.95°	
δ_1^0	−8.45°		−6.16°		−3.73°	
δ_1^1	−5.47°		−4.08°		−2.41°	
δ_1^2	+12.9°		+9.74°		+5.90°	

[a]) Extrapolated from ref. [14]).
[b]) From ref. [11]).
[c]) Estimates from ref. [14]).

in the β-parameter of MN if photodisintegration at low energies must also be covered in this scheme. Alternatively, one could ascribe a part of the discrepancy for photodisintegration to electromagnetic effects, like non-additivity of the deuteron magnetic moments, etc., though it is not clear how much these can account for.

Next, the analysis of the scattering at the moderate energies 40, 66 and 95 MeV was carried out on lines similar to those employed by Phillips [11]). The main problem here was to reconcile the magnitude of the polarization with the shape of $\sigma(\theta)$, taking account of the s-state contributions to $\sigma(\theta)$. The polarization is of course measured by the quantity $P\sigma(\theta)/\sin\theta\cos\theta$ which is roughly a constant (called a_1 by Phillips), except for the Coulomb effects (see eq. (20)).

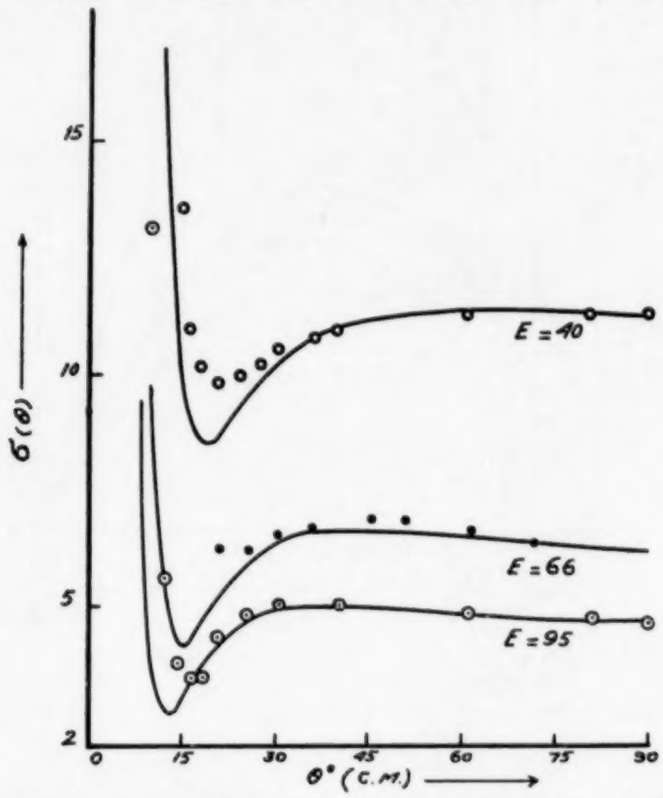

Fig. 1. p—p unpolarized cross sections $\sigma(\theta)$ at 95, 66 and 40 MeV. Open circles with dots are the experimental points of Taylor *et al.* [13]) at 95 MeV, closed circles those of Palmieri *et al.* [14]) at 66 MeV, and open circles those of Johnston and Swennen [15]) at 40 MeV.

The shape of $\sigma(\theta)$ is represented fairly well by the 'reference points' $\sigma(90°)$, $\sigma(40°)$ and $\sigma(\theta_{\min})$ the last being the Coulomb-interference dip in the cross section occurring at an angle $\theta_{\min}$ which is a function of energy. The experimental values of all the relevant quantities are given in table 1, along with the best fits provided by the potential (2) with the following parameters

$$\begin{aligned} \lambda_0^{(1)} &= 18.6\alpha^3, \quad \beta_0 = 5.8\alpha, \\ \lambda_2^{(1)} &= 10.5\alpha^3, \quad \beta_2 = 5.8\alpha, \\ \lambda_1^{(1)} &= 0.288\alpha, \quad \beta_1 = 6\alpha. \end{aligned} \tag{26}$$

The corresponding experimental points and calculated curves for $\sigma(\theta)$ and $P\sigma(\theta)$ are given in figs. 1 and 2 respectively.

It appears that the shape of $\sigma(\theta)$ agrees well with the experimental points down to about 20° which roughly represents the limit of validity of our approximation (16).

The results for polarization appear to be quite good at 95 MeV, but somewhat smaller at 66 MeV. Unfortunately the measurement of this parameter, particularly at lower energies than 100 MeV, still leaves much to be desired †.

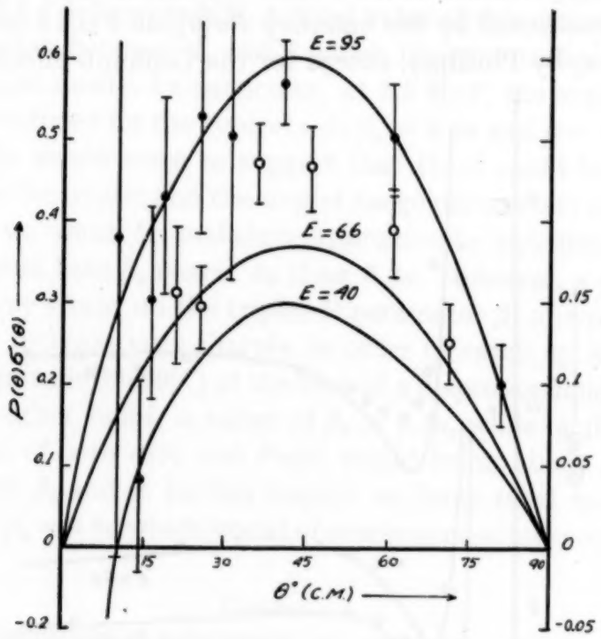

Fig. 2. p—p polarization curves $P\sigma(\theta)$, along with the experimental points of ref. [14]) at 66 MeV (open circles) and of ref. [13]) at 95 MeV (closed circles). The vertical scale on the right is for the 40 MeV polarization curve.

The ^{1}D state parameters in (26) were obtained by choosing β_2 equal to the corresponding ^{1}S-state parameter β_0 viz., $\beta_2 = 5.8\alpha$, and adjusting $\lambda_2^{(1)}$ to produce $\delta_2 = 3°$ at 95 MeV [11]). The effect of slight variation of δ_2 at 95 MeV on the corresponding $\sigma(\theta)$ is shown in fig. 3. It is clear that even a slight increase in δ_2 over 3° brings about a good deal of departure from the observed 'flatness' of the curve beyond about 30°. The values of δ_2 at other (smaller) energies shown in table 1 were calculated from the ^{1}D parameters of (26).

A test of the particular choice (3) and (4) of the potential was carried out through the addition of a small *central* ^{3}P force to (4) with corresponding adjustments of the parameters β_1 and $\lambda_1^{(1)}$. The modification revealed that the polarization was greatly reduced, with no compensating improvement in the

† There are no data at 40 MeV.

unpolarized cross section. This would seem to indicate little or none of central forces in p—p scattering up to moderate energies — a result in conformity with the findings of GT.

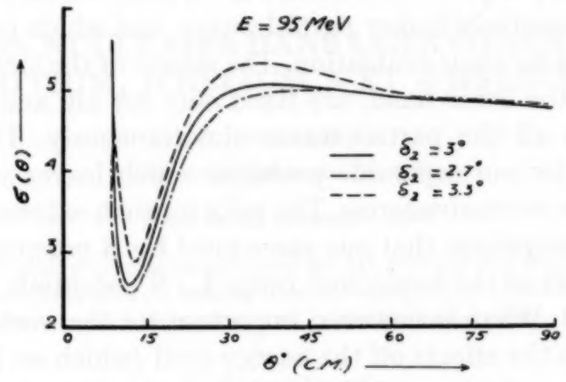

Fig. 3. Effect of the δ_2 phase shift on the shape of $\sigma(\theta)$ at 95 MeV.

4. Discussion

The main factor responsible for bringing about agreement of the theoretical $\sigma(\theta)$ with the experimental magnitudes and flat shapes is the numerical smallness of the ^{3}P phase shifts. An inspection of table 1 shows that this is indeed the case for our potential. In the work of SM the necessary reduction in the magnitude of $\delta(^3P_0)$ was brought about as the result of a large cancellation between the contributions from the tensor and spin-orbit potentials. In the present case, the ^{3}P potential directly leads to small ^{3}P phase shifts, without any cancellations. Of course the results for our ^{3}P phase shifts do indicate the characteristic $\mathbf{L}\cdot\mathbf{S}$ effects, viz., the rough proportionality factors $-1 : -1 : +2$, except for the modifications brought about by the exact evaluation of the reaction matrix. It is interesting to note, however, that there is broad agreement with the work of GT or SM in respect of δ_1^1 and δ_1^2 (magnitude and sign). As for δ_1^0, the disagreement in sign from those of GT or SM is, in our view, not so significant as the requirement that its magnitude be small. In principle, even this disagreement could be removed by the addition of a tensor term to the triplet-odd interaction. However, unlike the case of SM or GT where the tensor and the spin-orbit terms were making large numerical contributions of opposite signs, the addition of an extra tensor term in the present case can only be of the nature of a correction to the interaction (4). In other words, our $\mathbf{L}\cdot\mathbf{S}$ interaction (3) is of an effective nature, already incorporating some tensor contributions (see discussion following eq. (4)).

Finally, there remains the question of ranges of these interactions. Here again, one must at the outset guard against excessive analogies with local potentials. For one thing, the absence of hard cores in this picture already

represents an important contrast with local potentials. As for our spin-orbit potential, it does not share the short-range character of the corresponding $\mathbf{L} \cdot \mathbf{S}$ potentials of GT or SM †. It could be argued, however, that the interaction term (4) is only a part of the entire $\mathbf{L} \cdot \mathbf{S}$ force whose effects should also appear in the successively higher partial waves, and which in turn would need higher energy data for their evaluation. The ranges of the local $\mathbf{L} \cdot \mathbf{S}$ potentials of GT or SM, on the other hand, are fixed once for all, and therefore have a direct bearing on all the partial waves simultaneously. This by no means need be the case for our separable potential which leaves scope for separate adjustments in the successive terms. The price for such extreme phenomenology is of course the recognition that our piece-meal $\mathbf{L} \cdot \mathbf{S}$ potential does not enjoy the physical import of the local short range $\mathbf{L} \cdot \mathbf{S}$ potentials proposed by various authors [7, 8, 12]). What is however, important for the working of this model is that, apart from the effects off the energy shell (which we have no means to estimate), the data at higher energies should not significantly modify the lower partial wave parameters determined here.

† Even so, it may be remarked that the range parameter $\beta_1^{-1} = (6\alpha)^{-1}$ of (26) with a 'Yukawa-type' interaction is effectively much smaller than the $\beta^{-1} = (6\alpha)^{-1}$ of an expotential interaction. For, a calculation made with a corresponding Yukawa-type s-interaction indicated $\beta_0 \approx 3\alpha$ to fit the low energy p—p data.

References

1) A. N. Mitra and V. L. Narasimham, Nuclear Physics **14** (1960) 407 (referred to as MN)
2) Y. Yamaguchi, Phys. Rev. **95** (1954) 1628
3) A. N. Mitra and S. P. Pandya, Nuclear Physics **20** (1960) 455
4) Thaler and Bengston, Phys. Rev. **94** (1954) 674
5) See, e.g., R. G. Sachs, Nuclear theory (Addison Wesley Publishing Co., Reading, Mass., U.S.A., 1953)
6) L. Goldfarb and D. Feldman, Phys. Rev. **88** (1952) 1088
7) J. Gammel and R. Thaler, Phys. Rev. **107** (1957) 291 (referred to as GT)
8) P. Signell and R. Marshak, Phys. Rev. **109** (1958) 1229 (referred to as SM); also P. Signell *et al.*, Phys. Rev. Letters **1** (1958) 416
9) L. Heller, Phys. Rev. **120** (1960) 627
10) J. H. Naqvi, Nuclear Physics (to be published)
11) R. J. N. Phillips, Proc. Phys. Soc. A **70** (1957) 721
12) C. Iddings and P. Platzman, Phys. Rev. **120** (1960) 644
13) A. E. Taylor *et al.*, Nuclear Physics **16** (1960) 320
14) J. N. Palmieri *et al.*, Ann. Phys. **5** (1958) 249
15) L. Johnston and D. Swennen, Phys. Rev. **111** (1958) 212

1.B:3.C

Nuclear Physics **25** (1961) 317—327; © *North-Holland Publishing Co., Amsterdam*

Not to be reproduced by photoprint or microfilm without written permission from the publisher

POLARISATION NUCLÉAIRE DANS LES ATOMES MÉSIQUES DE TRITIUM, D'HÉLIUM 3 ET D'HÉLIUM 4

C. JOACHAIN †

Université Libre de Bruxelles

Reçu le 21 décembre 1960

Abstract: The energy-shift due to polarization of the H^3, He^3 and He^4 nuclei by a bound μ-meson has been evaluated. This effect is smaller than the energy-shift caused by the finite extension of the nucleus. There is no compensation as in the deuteron case.

1. Introduction

La correction d'énergie due à la polarisation nucléaire dans l'atome mésique-μ de deutérium a été évaluée récemment [1]). Les résultats obtenus montrent que, dans ce cas particulièrement favorable, l'effet de polarisation compense à peu près l'effet de volume. Il nous a semblé intéressant d'examiner les mêmes effets dans d'autres atomes mésiques mu légers: c'est ce qui est présenté ici pour le tritium, l'hélium 3 et l'hélium 4. Les effets de volume et de polarisation nucléaire relatifs à ces noyaux sont calculés respectivement aux paragraphes 2 et 3.

Les résultats rassemblés au tableau 1 s'interprètent de la manière suivante: tandis que dans le deutérium mésique, la correction de polarisation nucléaire compense approximativement l'effet de volume [1]), il n'en est plus de même dans les systèmes $H^3-\mu^-$, $He^3-\mu^-$ et $He^4-\mu^-$. Il en résulte que le terme de polarisation du vide [2]) reste partiellement masqué par l'effet de volume dans les atomes mésiques-μ de tritium, d'hélium 3 et d'hélium 4.

Le tableau 1 montre également que lorsqu'on passe du deutéron ($E_0 = -2.23$ MeV) au triton ($E_0 = -8.51$ MeV) l'effet de polarisation nucléaire est divisé par un facteur 5.5. Cette différence doit être attribuée à l'énergie de liaison très faible du deutéron qui permet une polarisation aisée de ce noyau par le méson-μ. Au cours du passage du triton à l'hélium 3 ($E_0 = -7.74$ MeV) la polarisation nucléaire est multipliée environ par 8, ce qui provient en ordre principal du facteur Z^3 fourni par la probabilité de présence du méson à l'origine; la différence des énergies de liaison du triton et de l'hélium 3 est responsable du fait que le facteur multiplicatif vaut 8.8 et est donc supérieur à 8 de 10 %. Enfin, lorsqu'on passe de l'hélium 3 à l'hélium 4 ($E_0 = -28.2$ MeV) l'effet de polarisation nucléaire est divisé par un facteur 4.3 dont l'interprétation est semblable à celle donnée pour le passage du deutéron au triton.

† Aspirant du Fonds National de la Recherche Scientifique.

Notons que dans le tableau 2 qui concerne des déplacements relatifs, le dénominateur E_2-E_1 est proportionnel à Z^2. Dans le cas du passage H^3-He^3, le facteur 8.8 du tableau 1 est donc réduit à un facteur 2.2 dans le tableau 2.

Deux remarques peuvent encore être faites:

1) Il est aisé, par une modification de la masse, de calculer les effets de volume et de polarisation nucléaire pour diverses particules de charge négative qui n'ont avec les noyaux considérés que des interactions électromagnétiques. L'électron étant actuellement, avec le méson μ^-, la seule particule jouissant de telles propriétés, nous avons fait également les évaluations dans ce cas (voir aussi réf. [3])). Les résultats sont rassemblés dans le tableau 3. Le tableau 4 résume et compare les tableaux 1 et 3. Il met en évidence l'influence de la masse de la particule liée.

2) Le noyau He^4 clôture la série des noyaux qui n'ont pas d'autre état lié que le fondamental. La méthode de calcul que nous avons utilisée cesse donc d'être applicable telle quelle si l'on veut calculer la polarisation nucléaire dans les noyaux plus lourds [4,5]).

2. Effet de Volume

2.1. ATOME DE TRITIUM

Le proton, les deux neutrons et le méson étant repérés à partir d'un point fixe O par $\mathbf{r}_p$, $\mathbf{r}_n$, $\mathbf{r}_{n'}$ et $\mathbf{r}_m$ nous utilisons les vecteurs

$$\mathbf{R} = \mathbf{r}_m - \tfrac{1}{3}(\mathbf{r}_p+\mathbf{r}_n+\mathbf{r}_{n'}),$$
$$\boldsymbol{\varrho} = -\mathbf{r}_p+\tfrac{1}{2}(\mathbf{r}_n+\mathbf{r}_{n'}),$$
$$\mathbf{r} = \tfrac{1}{2}\sqrt{3}(\mathbf{r}_n-\mathbf{r}_{n'}),$$

qui sont des coordonnées relatives. Après élimination du mouvement du centre de masse, l'hamiltonien du système triton-méson s'écrit

$$H = -\frac{\hbar^2}{2\mu}\Delta_R - \frac{\hbar^2}{2M'}(\Delta_r+\Delta_\rho)+V_t-\frac{e^2}{|\mathbf{R}-\frac{2}{3}\boldsymbol{\varrho}|},$$

où μ est la masse réduite du méson par rapport au triton, $M'=\frac{2}{3}M$, la quantité M étant la masse d'un nucléon, et V_t est l'énergie potentielle du triton. En ajoutant et en retranchant le potentiel hydrogénoïde $-e^2/r$, on obtient

$$H = H_0+H',$$

avec

$$H_0 = \left[-\frac{\hbar^2}{2\mu}\Delta_R-\frac{e^2}{r}\right]+\left[-\frac{\hbar^2}{2M'}(\Delta_r+\Delta_\rho)+V_t\right],$$

$$H' = \frac{e^2}{r}-\frac{e^2}{|\mathbf{R}-\frac{2}{3}\boldsymbol{\varrho}|}.$$

L'hamitonien H_0, séparable en $H_R(\mathbf{R})$ et $H_{r\rho}(\mathbf{r}, \boldsymbol{\varrho})$, est l'hamiltonien de Schrödinger du système triton-méson μ^- lorsque le triton est considéré comme ponctuel.

Le terme H' est la perturbation qui fournira les effets d'extension finie et de polarisation nucléaire respectivement au premier ordre et au second ordre du calcul des perturbations.

Les fonctions d'onde d'ordre zéro étant définies par

$$\Psi^{(0)}_{mN}(\mathbf{R}, \boldsymbol{\varrho}, \mathbf{r}) = \psi_m(\mathbf{R})\varphi_N(\boldsymbol{\varrho}, \mathbf{r}),$$
$$H_0\Psi^{(0)}_{mN} = E^{(0)}_{mN}\Psi^{(0)}_{mN} = (\varepsilon_m + E_N)\Psi^{(0)}_{mN},$$

l'effet d'extension finie du triton est donné, pour l'état fondamental du système triton-méson μ^-, par

$$E^{(1)}_{1s,0} = \langle 1s0|H'|1s0\rangle.$$

Nous décrivons l'état fondamental du triton par la fonction d'Irving [6])

$$\varphi_0(\rho, r) = N_1^{\frac{1}{2}} e^{-\sqrt{2}\alpha(\rho^2+r^2)^{\frac{1}{2}}}, \tag{1}$$

avec

$$N_1 = \frac{\alpha^6 2^9}{\pi^3 5!}, \quad \frac{1}{\alpha} = 1.462 \times 10^{-13}\,\text{cm}.$$

On a

$$E^{(1)}_{1s,0} = \langle 1s|\bar{V}(R)|1s\rangle,$$

où

$$\bar{V}(R) = -(4\pi e)^2 N_1 (\tfrac{3}{2})^6 R^5 \int_0^{\frac{1}{3}\pi} \mathrm{tg}^2 t \sec^2 t \mathrm{d}t \int_1^\infty u^5 \left(\frac{1}{u} - 1\right) e^{-3\sqrt{2}\alpha R u \sec t}\, \mathrm{d}u$$

est un potentiel moyen central qui n'agit que dans la région occupée par les nucléons. Dès lors, une très bonne approximation est fournie par

$$E^{(1)}_{1s,0} = 4\pi|\psi_{1s}(0)|^2 \int_0^\infty \bar{V}(R) R^2 \mathrm{d}R,$$

ce qui donne

$$E^{(1)}_{1s,0} = \frac{112\ 3^6 e^2 \alpha^6}{a^3 \gamma^8}, \tag{2}$$

où

$$\gamma = 3\sqrt{2}\alpha, \quad a = \frac{\hbar^2}{\mu e^2}.$$

L'évaluation numérique fournit

$$[E^{(1)}_{1s,0}]_{\text{tritium}}/h = 3.1 \times 10^7\ \text{MHz pour un méson } \mu^-,$$
$$[E^{(1)}_{1s,0}]_{\text{tritium}}/h = 3.9\ \text{MHz pour un électron.}$$

La formule (2) peut être généralisée aux états excités du méson ou de l'électron. On trouve

$$E^{(1)}_{m,0} = \begin{cases} \dfrac{1}{n^3} E^{(1)}_{1s,0} & \text{si } m \text{ est un état s,} \\ 0 & \text{si } m \text{ n'est pas un état s.} \end{cases} \tag{3}$$

Les formules (3) sont valables à l'approximation – excellente pour le tritium – où la fonction hydrogénoïde est assimilée à sa valeur à l'origine.

2.2. ATOME D'HÉLIUM 3

Nous n'étudions ici que l'atome mésique d'hélium 3 deux fois ionisé (noyau + un méson μ^-) et son correspondant électronique (noyau He^3 + un électron).

Le système de coordonnées choisi est le même que celui utilisé pour le tritium, à condition de remplacer le neutron n' par le proton p'. L'hamiltonien débarrassé du mouvement du centre de masse s'écrit

$$H = H_0 + H',$$

avec

$$H_0 = \left[-\frac{\hbar^2}{2\mu} \Delta_R - \frac{2e^2}{R} \right] + \left[-\frac{\hbar^2}{2M'} (\Delta_r + \Delta_\rho) + V_{He^3} \right]$$

et

$$H' = \frac{2e^2}{R} - \frac{e^2}{|\mathbf{R} - \frac{2}{3}\boldsymbol{\varrho}|} - \frac{e^2}{\left| \mathbf{R} + \frac{1}{3}\boldsymbol{\varrho} + \frac{1}{\sqrt{3}}\mathbf{r} \right|}.$$

Pour décrire l'état fondamental du noyau He^3 nous utilisons à nouveau la fonction d'Irving (1), qui conduit au résultat

$$[E^{(1)}_{1s,0}]_{He^3} = 16 [E^{(1)}_{1s,0}]_{\text{tritium}}.$$

L'évaluation numérique fournit

$$[E^{(1)}_{1s,0}]_{He^3}/h = 4.9 \times 10^8 \text{ MHz pour un méson } \mu^-,$$
$$[E^{(1)}_{1s,0}]_{He^3}/h = 6.4 \times 10^1 \text{ MHz pour un électron.}$$

Les formules (3) restent valables pour les états excités du méson ou de l'électron.

2.3. ATOME D'HÉLIUM 4

Nous ne traitons que le cas de l'atome mésique d'hélium 4 deux fois ionisé (noyau He^4 + un méson μ^-) ainsi que son correspondant électronique, l'atome d'hélium 4 ordinaire une fois ionisé (noyau He^4 + un électron).

Pour évaluer l'effet d'extension finie, nous avons renoncé à utiliser la méthode du potentiel moyen qui est ici d'application assez malaisée. Nous avons préféré faire usage de la formule de Wilets, Hill et Ford [7])

$$E^{(1)}_{1s,0} = \frac{2Z^4 e^2 r_0^2 A^{\frac{2}{3}}}{5a^3}, \tag{4}$$

dans laquelle le paramètre nucléaire r_0 est choisi conformément aux résultats obtenus par Hofstadter [8]):

$$r_0 = 1.31 \times 10^{-13} \text{ cm}.$$

Les évaluations numériques fournissent

$$[E^{(1)}_{1s,0}]_{He^4}/h = 5.3 \times 10^8 \text{ MHz pour le méson } \mu^-,$$
$$[E^{(1)}_{1s,0}]_{He^4}/h = 6.5 \times 10^1 \text{ MHz pour l'électron.}$$

Les formules (3) subsistent pour les états excités mésiques ou électroniques.

Pour évaluer au paragraphe 3 l'effet de polarisation nucléaire, nous ferons usage du système de coordonnées suivant: les deux protons, les deux neutrons et le méson étant repérés à partir d'un point fixe par $\mathbf{r}_p$, $\mathbf{r}_{p'}$, $\mathbf{r}_n$, $\mathbf{r}_{n'}$, et $\mathbf{r}_m$, nous utilisons les vecteurs

$$\mathbf{R} = \mathbf{r}_m - \tfrac{1}{4}(\mathbf{r}_p + \mathbf{r}_{p'} + \mathbf{r}_n + \mathbf{r}_{n'}),$$
$$\mathbf{u} = \tfrac{1}{2}(\mathbf{r}_p + \mathbf{r}_{p'}) - \tfrac{1}{2}(\mathbf{r}_n + \mathbf{r}_{n'}),$$
$$\mathbf{v} = \frac{1}{\sqrt{2}}(\mathbf{r}_p - \mathbf{r}_{p'}),$$
$$\mathbf{w} = \frac{1}{\sqrt{2}}(\mathbf{r}_n - \mathbf{r}_{n'}).$$

L'hamiltonien débarrassé du mouvement du centre de masse peut s'écrire

$$H = H_0 + H',$$

avec

$$H_0 = \left[-\frac{\hbar^2}{2\mu}\Delta_R - \frac{2e^2}{R}\right] + \left[-\frac{\hbar^2}{2M}(\Delta_u + \Delta_v + \Delta_w) + V_{He^4}\right],$$
$$H' = \frac{2e^2}{R} - \frac{e^2}{|\mathbf{R} - \frac{1}{2}\mathbf{u} - \frac{1}{2}\sqrt{2}\mathbf{v}|} - \frac{e^2}{|\mathbf{R} - \frac{1}{2}\mathbf{u} + \frac{1}{2}\sqrt{2}\mathbf{v}|},$$

où μ est la masse réduite du méson par rapport au noyau He^4.

Nous décrivons l'état fondamental du noyau He^4 par la fonction d'Irving [5])

$$\varphi_0(u, v, w) = N_2^{\frac{1}{2}} e^{-2\alpha(u^2+v^2+w^2)^{\frac{1}{2}}}, \tag{5}$$

avec

$$N_2 = \frac{105 \times 2^{13} \alpha^9}{\pi^4\, 8!}, \quad \frac{1}{\alpha} = 1.087 \times 10^{-13} \text{ cm}.$$

3. Effet de Polarisation Nucléaire

3.1. PRÉLIMINAIRES

a) *État fondamental.* Nous n'évaluons dans la suite que le terme le plus important, à savoir le terme C de la correction dispersive [1]) dont l'expression est donnée par

$$E^{(2)}_{1s,0} \approx C = \sum_{N\neq 0} \sum_{m \text{ continus}} \frac{|\langle 1s0|H'|mN\rangle|^2}{(\varepsilon_{1s}-\varepsilon_m)+(E_0-E_N)}. \tag{6}$$

b) *États excités de la particule négative.* Nous faisons usage des formules

$$\begin{aligned} E^{(2)}_{ns,0} &= \frac{1}{n^3} E^{(2)}_{1s,0} \quad \text{pour un état s,} \\ E^{(2)}_{m,0} &= 0 \qquad\qquad \text{si } m \text{ n'est pas un état s.} \end{aligned} \tag{7}$$

Les formules (7) découlent d'une part du calcul des perturbations dans un cas dégénéré, d'autre part du fait que la fonction d'onde hydrogénoïde a été assimilée à sa valeur à l'origine et que la fonction d'onde nucléaire est à symétrie sphérique.

3.2. ATOME DE TRITIUM

Un raisonnement analogue à celui déjà fait pour l'atome de deutérium [1]) conduit au résultat

$$C_{\text{tritium}} = -8e^4|\psi_{1s}(0)|^2 \int_0^\infty \frac{1}{k} g(k)\mathrm{d}k,$$

où

$$g(k) = \frac{1}{k} \sum_{N\neq 0} \frac{|\langle 0|e^{i\mathbf{k}\cdot\boldsymbol{\rho}}|N\rangle|^2}{\varepsilon(k)+E_N-\varepsilon_{1s}-E_0}.$$

L'étude de la fonction $g(k)$ s'effectue de la même façon que dans l'atome de deutérium. Il suffit de remarquer que le vecteur

$$\mathbf{D} = \tfrac{2}{3}\boldsymbol{\varrho}$$

joue dans le triton un rôle identique à celui du vecteur $\frac{1}{2}\mathbf{R}$ dans le deuton. La distinction entre le cas du méson-μ et celui de l'électron subsiste également et conduit aux formules

$$C_{\text{tritium}} = -8e^4|\psi_{1s}(0)|^2 \frac{D_0^2}{3\hbar c}\left[\log\frac{u_1+k_0+(u_1^2+2k_0u_1)^{\frac{1}{2}}}{u_0+k_0+(u_0^2+2k_0u_0)^{\frac{1}{2}}} - \frac{(u_1^2+2k_0u_1)^{\frac{1}{2}}}{u_1} + \frac{(u_0^2+2k_0u_0)^{\frac{1}{2}}}{u_0}\right]$$

pour le méson μ^-, et

$$C_{\text{tritium}} = -8e^4|\psi_{1s}(0)|^2 \frac{D_0^2}{3\hbar c} \log \frac{\hbar c}{D_0 E_0}$$

pour l'électron. Dans ces formules, on a

$$u_1 = (D_0^{-2}+k_0^2)^{\frac{1}{2}}-k_0, \quad u_0 = (E_0^2/\hbar^2c^2+k_0^2)^{\frac{1}{2}}-k_0,$$

$$D_0^2 = \langle 0|(\tfrac{2}{3}\rho)^2|0\rangle, \qquad k_0 = \frac{\mu c}{\hbar}.$$

L'évaluation numérique fournit

$$[E^{(2)}_{1s,0}]_{\text{tritium}}/h \approx C_{\text{tritium}}/h = \begin{cases} -6.6\times 10^6 \text{ MHz pour le méson } \mu^-, \\ -9.8\times 10^{-2} \text{ MHz pour l'électron.} \end{cases}$$

3.3. ATOME D'HÉLIUM 3

Le fait nouveau est la présence de deux protons dans le noyau. On obtient cette fois

$$C_{\text{He}^3} = -8e^4|\psi_{1s}(0)|^2 \int_0^\infty \frac{1}{k} g(k)\mathrm{d}k,$$

où

$$g(k) = \frac{1}{k} \sum_{N\neq 0} \frac{|\langle 0|e^{i\mathbf{k}\cdot\mathbf{D}}+e^{i\mathbf{k}\cdot\mathbf{D}'}|N\rangle|^2}{\varepsilon(k)+E_N-\varepsilon_{1s}-E_0},$$

avec

$$\mathbf{D} = \tfrac{2}{3}\boldsymbol{\varrho}, \quad \mathbf{D}' = -\tfrac{1}{3}\boldsymbol{\varrho} - \frac{1}{\sqrt{3}}\mathbf{r}.$$

La fonction $g(k)$ ne prend ses valeurs significatives que dans la région

$$\frac{E_0}{\hbar c} \ll k \ll \frac{1}{D_0},$$

où E_0 est l'énergie de liaison du noyau d'hélium 3, et où D_0 a été défini en sous-paragraphe 3.2.

Remarquant que

$$\langle 0|D'^2\cos^2\theta'|0\rangle = \langle 0|D^2\cos^2\theta|0\rangle,$$

$$\langle 0|2DD'\cos\theta\cos\theta'|0\rangle = -\langle 0|D^2\cos^2\theta|0\rangle,$$

$$\langle 0|D\cos\theta|0\rangle = \langle 0|D'\cos\theta'|0\rangle = 0,$$

où θ et θ' sont les angles formés par les vecteurs $\mathbf{D}$ et $\mathbf{D}'$ avec le vecteur $\mathbf{k}$ pris

comme axe polaire, on a

$$C_{\mathrm{He}^3} = -8e^4|\psi_{1s}(0)|^2\frac{D_0^2}{3\hbar c}\left[\log\frac{u_1+k_0+(u_1^2+2k_0u_1)^{\frac{1}{2}}}{u_0+k_0+(u_0^2+2k_0u_0)^{\frac{1}{2}}}\right.$$
$$\left.-\frac{(u_1^2+2k_0u_1)^{\frac{1}{2}}}{u_1}+\frac{(u_0^2+2k_0u_0)^{\frac{1}{2}}}{u_0}\right]$$

pour le méson μ^-, et

$$C_{\mathrm{He}^3} = -8e^4|\psi_{1s}(0)|^2\frac{D_0^2}{3\hbar c}\log\frac{\hbar c}{D_0E_0}$$

pour l'électron, avec

$$u_1 = (D_0^{-2}+k_0^2)^{\frac{1}{2}}-k_0, \quad u_0 = (E_0^2/\hbar^2c^2+k_0^2)^{\frac{1}{2}}-k_0.$$

L'évaluation numérique fournit

$$[E^{(2)}_{1s,0}]_{\mathrm{He}^3}/h = C_{\mathrm{He}^3}/h = \begin{cases}-5.8\times10^7\ \text{MHz pour le méson } \mu^-,\\ -8.1\times10^{-1}\ \text{MHz pour l'électron.}\end{cases}$$

3.4. ATOME D'HÉLIUM 4

Nous avons

$$C_{\mathrm{He}^4} = -8e^4|\psi_{1s}(0)|^2\int_0^\infty\frac{1}{k}\,g(k)\mathrm{d}k,$$

où

$$g(k) = \frac{1}{k}\sum_{N\neq0}\frac{|\langle0|e^{i\mathbf{k}\cdot\mathbf{F}}+e^{i\mathbf{k}\cdot\mathbf{F}'}|N\rangle|^2}{\varepsilon(k)+E_N-\varepsilon_{1s}-E_0},$$

avec

$$\mathbf{F} = \tfrac{1}{2}\mathbf{u}+\tfrac{1}{2}\sqrt{2}\mathbf{v}, \quad \mathbf{F}' = \tfrac{1}{2}\mathbf{u}-\tfrac{1}{2}\sqrt{2}\mathbf{v}.$$

La contribution la plus importante de g se fait dans le domaine

$$\frac{E_0}{\hbar c}\ll k\ll\frac{1}{F_0},$$

où E_0 est l'énergie de liaison de la particule alpha et

$$F_0^2 = \langle0|F^2|0\rangle.$$

On démontre facilement que

$$\langle0|F'^2\cos^2\theta'|0\rangle = \langle0|F^2\cos^2\theta|0\rangle,$$
$$\langle0|2FF'\cos\theta\cos\theta'|0\rangle = -\tfrac{2}{3}\langle0|F^2\cos^2\theta|0\rangle,$$
$$\langle0|F\cos\theta|0\rangle = \langle0|F'\cos\theta'|0\rangle = 0,$$

où θ et θ' sont les angles formés par les vecteurs $\mathbf{F}$ et $\mathbf{F}'$ avec le vecteur $\mathbf{k}$ pris comme axe polaire. Il en résulte que

$$C_{\mathrm{He}^4} = -8e^4|\psi_{1s}(0)|^2\tfrac{4}{9}\frac{F_0^2}{\hbar c}\left[\log\frac{u_1+k_0+(u_1^2+2k_0u_1)^{\frac{1}{2}}}{u_0+k_0+(u_0^2+2k_0u_0)^{\frac{1}{2}}}\right.$$
$$\left.-\frac{(u_1^2+2k_0u_1)^{\frac{1}{2}}}{u_1}+\frac{(u_0^2+2k_0u_0)^{\frac{1}{2}}}{u_0}\right]$$

pour le méson μ^-, et

$$C_{\mathrm{He}^4} = -8e^4|\psi_{1s}(0)|^2\tfrac{4}{9}\frac{F_0^2}{\hbar c}\log\frac{\hbar c}{F_0E_0}$$

pour l'électron, avec

$$u_1 = (F_0^{-2}+k_0^2)^{\frac{1}{2}}-k_0, \quad u_0 = (E_0^2/\hbar^2c^2+k_0^2)^{\frac{1}{2}}-k_0.$$

L'évaluation numérique fournit

$$[E^{(2)}_{1s,0}]_{\mathrm{He}^4}/h = C_{\mathrm{He}^4}/h = \begin{cases}-1.4\times10^7 \text{ MHz pour le méson } \mu^-,\\ -4.4\times10^{-1} \text{ MHz pour l'électron.}\end{cases}$$

4. Résultats

Les tableaux 1 à 4 résument nos résultats. Ceux relatifs au méson-μ sont présentés dans le tableau 2 sous une forme analogue à celle de Foldy et Eriksen [2]). Dans chaque tableau nous avons comparé les résultats obtenus aux paragraphes 2 et 3 avec ceux que Demeur et Joachain [1]) ont calculés pour le deutérium.

TABLEAU 1

Déplacements des niveaux dus à l'effet de volume et à la polarisation nucléaire (en MHz) pour un méson μ^-.

Noyau	Effet de volume		Effet de polarisation	
	1s	2s	1s	2s
Deutéron	4.3×10^7	5.4×10^6	-3.6×10^7	-4.5×10^6
Triton	3.1×10^7	3.8×10^6	-6.6×10^6	-8.3×10^5
He^3	4.9×10^8	6.1×10^7	-5.8×10^7	-7.3×10^6
He^4	5.3×10^8	6.6×10^7	-1.4×10^7	-1.7×10^6

TABLEAU 2

Déplacements des raies dans les atomes mésiques d'hydrogène, de deutérium, de tritium, et dans les systèmes $He^3-\mu^-$ et $He^4-\mu^-$

	Atome mésique	H^1	H^2	H^3	He^3	He^4
$\frac{\Delta E_{2p\frac{1}{2}}-\Delta E_{1s\frac{1}{2}}}{E_2-E_1}\times 10^3$	Polarisation du vide	1.00	1.00	1.00	2.22	2.22
	Relativité	0.02	0.02	0.02	0.07	0.07
	Effet de volume		-0.08_8	-0.06_2	-0.24_2	-0.26_3
	Effet de polarisation		0.07_4	0.01_3	0.02_9	0.00_7
$\frac{\Delta E_{2p\frac{1}{2}}-\Delta E_{1s\frac{1}{2}}}{E_2-E_1}\times 10^3$	Polarisation du vide	1.00	1.00	1.00	2.22	2.22
	Relativité	0.01	0.01	0.01	0.05	0.05
	Effet de volume		-0.08_8	-0.06_2	-0.24_2	-0.26_3
	Effet de polarisation		0.07_4	0.01_3	0.02_9	0.00_7
$\frac{\Delta E_{2s\frac{1}{2}}-\Delta E_{1s\frac{1}{2}}}{E_2-E_1}\times 10^3$	Polarisation du vide	0.89	0.89	0.89	2.02	2.02
	Relativité	0.01	0.01	0.01	0.05	0.05
	Effet de volume		-0.07_8	-0.05_4	-0.21_5	-0.23_4
	Effet de polarisation		0.06_6	0.01_2	0.02_6	0.00_6

TABLEAU 3

Déplacements des niveaux dus à l'effet de volume et à la polarisation nucléaire (en MHz) pour un électron

Noyau	Effet de volume		Effet de polarisation	
	1s	2s	1s	2s
Deutéron	5.1	0.7	-2.1×10^{-1}	-2.6×10^{-2}
Triton	3.9	0.5	-9.8×10^{-2}	-1.2×10^{-2}
He^3	6.4×10^{1}	8.0	-8.1×10^{-1}	-1.0×10^{-1}
He^4	6.5×10^{1}	8.2	-4.4×10^{-1}	-5.5×10^{-2}

Le tableau 4 donne, pour le méson μ^- et l'électron, le rapport de l'effet de volume à l'effet de polarisation dans les systèmes étudiés.

TABLEAU 4

Rapport de l'effet de volume à l'effet de polarisation

Noyau	Méson μ^-	Électron
Deutéron	— 1.2	— 27
Triton	— 4.5	— 40
He^3	— 8.4	— 76
He^4	—39	—150

Je tiens à exprimer ma gratitude à Monsieur le professeur M. Demeur pour les conseils qu'il m'a donnés au cours de nombreuses discussions.

Bibliographie

1) M. Demeur et C. Joachain, Nuclear Physics **17** (1960) 329
2) L. L. Foldy et E. Eriksen, Phys. Rev. **95** (1954) 1048
3) N. A. Krall et E. E. Salpeter, Phys. Rev. **115** (1959) 457
4) L. N. Cooper et E. Henley, Phys. Rev. **92** (1953) 801
5) W. Lakin et W. Kohn, Phys. Rev. **94** (1954) 787
6) J. Irving, Phil. Mag. **42** (1951) 338
7) L. Wilets, D. L. Hill et K. W. Ford, Phys. Rev. **91** (1953) 1488
8) R. Hofstadter, Ann. Rev. of Nucl. Science **7** (1957) 231

4.B

Nuclear Physics **25** (1961) 328—332; © *North-Holland Publishing Co., Amsterdam*

Not to be reproduced by photoprint or microfilm without written permission from the publisher

INTERNAL BREMSSTRAHLUNG IN $0^- \rightarrow 0^+$ BETA-TRANSITIONS

FRANTIŠEK JANOUCH

Nuclear Research Institute of Czechoslovak Academy of Sciences, Prague

Received 24 January 1961

Abstract: Internal bremsstrahlung accompanying a $0^- \rightarrow 0^+$ β-transition is considered. It is shown that experimental investigations of the energy dependence of the degree of circular polarization of the internal bremsstrahlung quanta would allow the determination of the possible role of pseudo-scalar interaction in nuclear β-decay.

1. Introduction

The V—A interaction hypothesis in weak interactions may now be regarded as experimentally verified. On the other hand, the question of the possible role of small admixtures of scalar, tensor and pseudoscalar interactions in nuclear β-decay has not yet been completely solved. Although theoretical calculations and arguments show that the role of the pseudoscalar interaction in nuclear β-decay cannot be large [1]), this has not yet been verified experimentally.

In this note we indicate a possible method for determining the type of interaction responsible for the so-called $0^- \rightarrow 0^+$ β-transitions and thus solving the question of the role of pseudoscalar interaction in nuclear β-decay.

It is well known that the selection rules for parity and angular momentum show that the $0^- \rightarrow 0^+$ β-transition can be induced either by pseudoscalar interaction (matrix element $M(\gamma_4\gamma_5)$) or by the first forbidden axial vector interaction (matrix elements $M(\gamma_5)$ and $M(\boldsymbol{\sigma} \cdot \mathbf{r})$). All other first forbidden axial interaction matrix elements and all first forbidden vector interaction matrix elements vanish for these transitions.

2. Circular Polarization of Bremsstrahlung

Let us now consider the internal bremsstrahlung which accompanies the studied $0^- \rightarrow 0^+$ transition. It is well known that the internal bremsstrahlung of β-electrons will be circularly polarized because of parity non-conservation [2]). It is also known that the degree of circular polarization of the internal bremsstrahlung depends on the type of interaction responsible for the corresponding β-transition. The latest experimental papers show that both the dependence of the internal bremsstrahlung cross-section on the energy of the gamma-quantum k, on the angle θ between the direction of emission of quantum and the β-electron and also the dependence of the degree of circular polarization of the

internal bremsstrahlung quanta on their energy, can be successfully investigated experimentally [3, 4]). Thus we can expect that a comparison of the experimental results for the degree of circular polarization of the internal bremsstrahlung with theoretical formulae can help to solve the question of the interactions responsible for the $0^- \to 0^+$ β-transition.

The theoretical calculations (see ref. [5]), where general formulae are given for the degree of circular polarization P of internal bremsstrahlung quanta in first forbidden transitions) show that for $0^- \to 0^+$ transitions we can write

$$P_s = \frac{x^2(1-\eta^2)b_1+b_2+2x(b_{12}+\eta b'_{12})}{x^2(1+\eta^2)a_1+a_2+2x(x\eta a_{12}+a'_{12}+\eta a''_{12})}. \tag{1}$$

Here η is the ratio of the pseudoscalar and axial vector interaction constants, $\eta = C_P/C_A$, and x the ratio of the reduced nuclear matrix elements: $x = M(\gamma_5)/M(\boldsymbol{\sigma}\cdot\mathbf{r})$ (we assume that $M(\gamma_4\gamma_5) \approx M(\gamma_5)$). The coefficients a_1, a_2, a_{12}, a'_{12}, a''_{12}, b_1, b_2, b_{12} and b'_{12} are listed in table 1. In deriving formula

TABLE 1

The coefficients a and b

a_1	$\Lambda(\varepsilon_s p^2\sin^2\theta - k^2p')$
a_2	$3^{-2}\Lambda[(p^2+q^2+k^2+2kp\cos\theta)(\varepsilon_s p^2\sin^2\theta - k^2p')$ $+2pk\{(p+k\cos\theta)p^2\sin^2\theta - k^2p'\cos\theta\}+2qk\{(k+p\cos\theta)p^2\sin^2\theta - k^2p'\}]$
a_{12}	$\Lambda p^2\sin^2\theta$
a'_{12}	$3^{-1}\Lambda[-(p+k\cos\theta)p^2\sin^2\theta+(p\cos\theta+k)k^2p'-(k+p\cos\theta)kp^2\sin^2\theta - qp^2\sin^2\theta]$
a''_{12}	$3^{-1}\Lambda qp^2\sin^2\theta$
b_1	$-\Lambda(kp^2\sin^2\theta - k^2p')$
b_2	$-3^{-2}\Lambda[(p^2+q^2+k^2+2kp\cos\theta)(kp^2\sin^2\theta - k^2p')$ $+2qp(k\varepsilon p\sin^2\theta - k^2p'\cos\theta)+2kp(kp^2\sin^2\theta - k^2p')]$
b_{12}	$-3^{-1}\Lambda[-\varepsilon_s kp^2\sin^2\theta+(k+p\cos\theta)k^2p']$
b'_{12}	$3^{-1}\Lambda kp^2\sin^2\theta$

The quantities ε, p are the energy and the absolute value of the momentum of the β-electron after emission of the internal bremsstrahlung quantum, $q = \Delta-\varepsilon-k$ is the energy of the neutrino, Δ the energy of the β-transition, k the energy of the internal bremsstrahlung quantum, θ the angle between the directions of emission of internal bremsstrahlung quantum and the β-electron. Furthermore, we have $\varepsilon_s = \varepsilon+k$, $p' = -\varepsilon+p\cos\theta$ and $\Lambda = (\sqrt{\varepsilon^2-1}/kp'^2)(\Delta-\varepsilon-k)^2\sin\theta$.

(1) we integrated over the directions of the neutrino emission. If now only axial interaction figures in the studied transition, i.e. $\eta = 0$, eq. (1) reduces to

$$P_A = \frac{x^2b_1+b_2+2xb_{12}}{x^2a_1+a_2+2xa'_{12}}. \tag{2}$$

On the other hand, if only pseudoscalar interaction figures in this transition, then

$$P_{\mathrm{P}} = -\frac{b_1}{a_1}. \tag{3}$$

Note that for $\theta = 0$ (or $\theta = \pi$) the degree of polarization P does not depend on the energy of the quanta or on the nuclear matrix elements; for pure axial interaction it equals

$$P_{\mathrm{A}}(\theta = 0 \quad \text{or} \quad \pi) = -1. \tag{4}$$

For pure pseudoscalar interaction the sign is opposite, i.e.

$$P_{\mathrm{P}}(\theta = 0 \quad \text{or} \quad \pi) = +1. \tag{5}$$

Although the cross-section of the internal bremsstrahlung was measured for certain values of θ, difficulties may be met with when experimentally measuring the quantities (4) and (5). Usually one measures the degree of circular polarization averaged over the angle θ and integrated over the energies of the electron. The results of such an averaging and integrating of the formula (1) are too complicated to be published in analytical form in this paper (they are listed in ref. [5])).

3. Example of Pr^{144} Transition

We now illustrate the results stated above on the concrete example of the well known $0^- \to 0^+$ transition of Pr^{144} with a transition energy † $\Delta = 6.2$.

If the studied $0^- \to 0^+$ β-transition is due to pseudoscalar interaction the rate P will depend only on the energy of the quanta (see fig. 1). If it is due to axial interaction only, the degree of circular polarization will depend not only on the energy of the internal bremsstrahlung quanta, but also on the ratio $x = M(\gamma_5)/M(\boldsymbol{\sigma} \cdot \mathbf{r})$ of the nuclear matrix elements. As is shown in ref. [6]), this ratio is $x = 5 \pm 2$. In order to study the influence of changes of x on P_{A}, we also plotted in fig. 1 the dependence of P_{A} on the energy of the internal bremsstrahlung quanta for three different values of the parameter $x = 10$, 5 and 1. It is obvious from fig. 1 that the dependence of P_{A} on x is not substantial so that even if x is not known exactly, it cannot seriously affect further considerations.

In the general case, when the studied transition is induced by a mixture of the pseudoscalar and axial interactions, the degree of circular polarization P depends not only on the energy of the internal bremsstrahlung quanta, but also on the parameters x and η. If the Goldberger-Treiman [1]) theoretical estimations are valid for nuclear β-decay, then $\eta \approx 2 \times 10^{-2}$ and the dependence of the circular polarization on the energy is practically the same as in fig. 2. If the

† The energies are given in mc^2 units and $\hbar = c = 1$.

pseudoscalar interaction plays a more important role in nuclear β-decay, i.e. if the constant of pseudoscalar interaction C_P is greater than given in ref. [1]), one can expect that the dependence of P on the energy will alter quite consider-

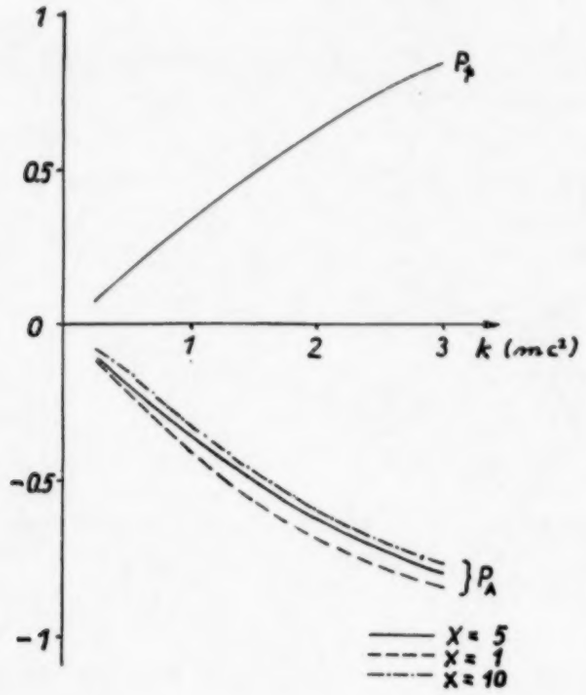

Fig. 1. The degree of circular polarization for pseudoscalar interaction only (P_P) and for axial-vector interaction only (P_A) as functions of the energy k.

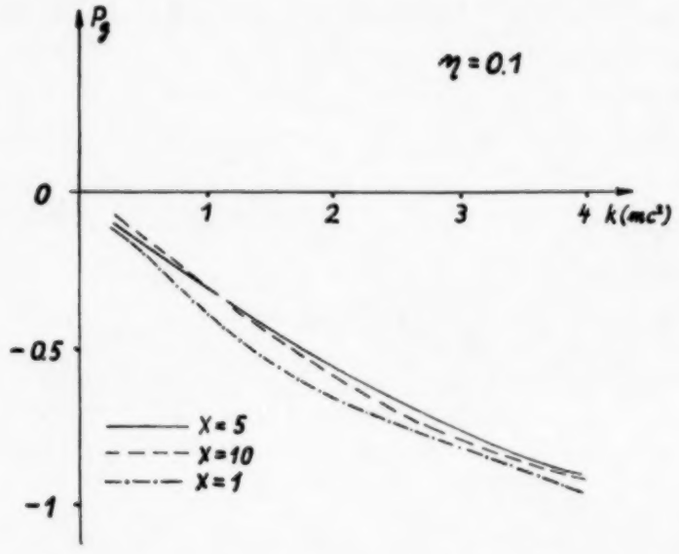

Fig. 2. The degree of circular polarization for a mixture of pseudoscalar and axial-vector interaction ($\eta = 0.1$).

ably. In figs. 2 and 3 for instance, this dependence (for the same values of x as in fig. 1) is given for $\eta = 10^{-1}$ and $\eta = 1$. The obtained results show that

the degree of circular polarization of the internal bremsstrahlung is quite sensitive to the magnitude of the pseudoscalar interaction constant. It may

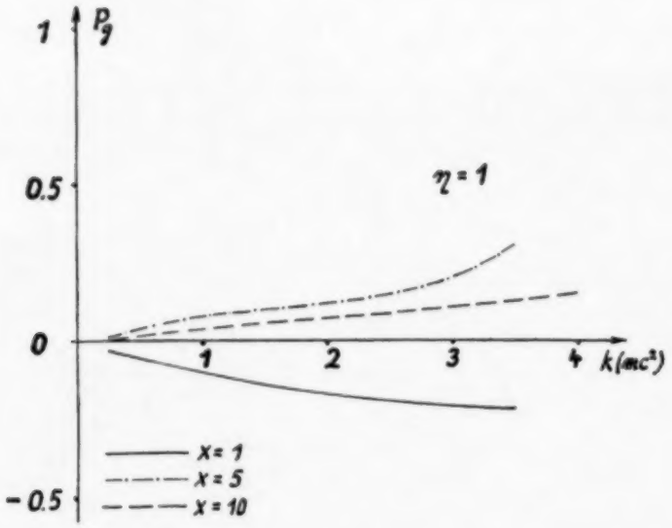

Fig. 3. The degree of circular polarization for a mixture of pseudoscalar and axial-vector interaction ($\eta = 1$).

be expected that the observation of the rate of circular polarization is more convenient and accurate in a number of cases (due to considerations forced by experimental methods) than the other experimental methods used up to now. Therefore we may expect that the experimental measurement of this quantity and its comparison with corresponding theoretical results will make it possible to obtain more detailed and accurate information about the role of pseudoscalar interaction in nuclear β-decay.

In conclusion the author would like to express his gratitude to professor G. Alaga for interesting discussions on this problem. The author also would like to thank Mrs. Frančíková for help in carrying out the numerical calculations.

References

1) M. L. Goldberger and S. B. Treiman, Phys. Rev. **111** (1958) 354
2) T. D. Lee and C. N. Yang, Phys. Rev. **104** (1956) 254
3) E. Thun, B. G. Petterson and K. Siegbahn, Nuclear Physics **18** (1960) 131
4) H. Schopper, Phys. Rev. Lett. **4** (1960) 296
5) F. Janouch, Czechosl. J. Phys. (to be published)
6) F. T. Porter and P. O. Day, Phys. Rev. **114** (1959) 1286

1.D.2:
1.E.6

Nuclear Physics **25** (1961) 333—347; © *North-Holland Publishing Co., Amsterdam*
Not to be reproduced by photoprint or microfilm without written permission from the publisher

ON THE THEORY OF COLLECTIVE ROTATIONS

SHINZO NAKAI and MUNEO SASAKI

Department of Physics, Tokyo Metropolitan University, Tokyo, Japan

Received 19 December 1960

Abstract: An analysis is made of descriptions of collective rotations of many-particle systems, in which the emphasis is laid upon the analysis of the flow pattern function generated when the system is set rotating. Some results of recent investigations devoted to the problem of the moment of inertia are also discussed from the present viewpoint. The essential point of the present approach consists in calculating the flow pattern function subject to a constraint. This constraint equation, in simple cases, coincides with that of Tomonaga which was employed to define the canonical momentum describing incompressible deformation. The comparison is made with the work based upon Tomonaga's theory of collective motion. The outcome of the present work will throw light on the method of evaluating the moment of inertia and, in particular, on the question why interactions of the type leading to superfluidity could appreciably change the rigid moment.

1. Introduction

In the past few years, various theoretical investigations have been carried out to account for the observed magnitude of the moment of inertia of nuclei. One of the available approaches is Inglis' "cranking" model, in which the nucleus is supposed to be rotated externally with fixed angular momentum and its rotational energy is then determined [1]). From his computations it was conjectured that any independent-particle system should have the rigid moment of inertia independently of the potential form. The rigid value is, however, too large for the observed nuclear moments of inertia, and attempts have been made to investigate the effect of particle-particle interactions on the rigid moment [2]). It was found that the moment of inertia of a Fermi gas with periodic boundary conditions has the classical or rigid value both when one neglects particle-particle interactions and when one takes them into account by perturbation in first order. It was further shown [3]) that the moment of inertia is not affected to the approximation in which one admits Coulomb-type interactions between the particles and treats their ground state in the high density approximation [4]).

There is an alternative approach based upon the theory of quantal collective motion [5]). We know that dynamical systems consisting of many particles have the common feature that the constituent particles can perform collective motion. The indistinguishability of the nuclear particles would tend to suppress the rotation in states with small rotational quantum number, and would give

rise to large rotational excitation energies and small effective moments of inertia [6]). This is also the view of Bohr and Mottelson [7]). On this view one can formulate the theory of collective rotations of nuclei and arrive at the irrotational flow value $I = \beta^2 I_{\text{rig}}$ for the moment of inertia. This prediction, however, gives much too small moments of inertia, suggesting that the picture of irrotational flow is again unsatisfactory in its present form. To overcome the difficulty, the possibility was considered of adding to the moment of inertia a contribution from the individual motions of the particles. These attempts, however, did not reach the stage of giving any quantitative results, because of the scanty knowledge about the collective states.

None of these investigations had been successful, until it was shown [8, 9]) that an interaction of the type leading to superfluidity at low temperatures can appreciably affect the rigid moment in better agreement with experiment, even if calculated on the cranking model. The question now arises why the interaction of the type leading to the superfluid behaviour could appreciably change the rigid moment. To this question, Wentzel [10]) answered that the results so far obtained could be anticipated on the basis of a series of papers by Blatt, Butler and Schafroth [11]), employing the analogy between a rotating nuclear system and a magnetic one. It seems, however, that the exact correspondence between these two systems is somewhat obscure, and a direct proof will be desirable. We want to investigate this problem on the basis of the flow pattern analysis, first put forward by Gross [12]). The present analysis reveals under what approximations one gets the rigid value, and shows that the moment of inertia is rather sensitive to the effect of the pairing correlations.

2. Description of the Collective Rotation

The cranking model of Inglis is often used to calculate the moments of inertia of many-particle systems. The validity of this model is, however, sometimes questioned, since the rotation of the nucleus in this model is the forced rotation imposed by "cranking" the external potential, while the collective rotation in the actual nucleus is the free rotation which results from the interaction of the nucleons. We shall find in the following a different interpretation of the cranking formula. The view given in this section has been put forward by Gross [12]). However, we formulate and extend it with some modifications, and thus some of his results will be derived again for completeness.

For simplicity we treat rotations around the z-axis. Let H stand for the total Hamiltonian which describes a system with a fixed number N of particles. We note that the Lagrange multiplier approach is appropriate to the determination of collective properties, and consider the effective Hamiltonian

$$\mathcal{H} = H - \lambda J_z \tag{2.1}$$

instead of H, where J_z is the total angular momentum operator of all the

particles around the z-axis. A Lagrange multiplier λ is fixed by the condition

$$\langle \Psi | J_z | \Psi \rangle = \hbar K, \tag{2.2}$$

where K is an integer and Ψ the solution of the Schroedinger equation

$$\mathscr{H}\Psi = E\Psi. \tag{2.3}$$

The determination of λ gives the average value of J_z, and the solution which corresponds to the Hamiltonian (2.1) will therefore describe only average properties of the system.

We observe in (2.1) that $\mathscr{H}$ represents the transformed Hamiltonian when a canonical transformation is performed from the rest system to the rotating coordinate system with angular velocity λ. To remove the extra term $-\lambda J_z$, we carry out the transformation

$$\Psi = \exp(iS/\hbar)\psi. \tag{2.4}$$

Using the relations

$$\begin{aligned} e^{-iS/\hbar} H e^{iS/\hbar} &= H-(i/\hbar)[S, H]_-+(-i)^2/2\hbar^2[S, [S, H]_-]_-+\ldots, \\ [A, B]_- &\equiv AB-BA, \end{aligned} \tag{2.5}$$

we fix the transformation function S so that

$$\{(i/\hbar)[S, H]_-+\lambda J_z\}\psi = 0 \tag{2.6}$$

may hold. With the above choice of S, eq. (2.1) is transformed into

$$\exp(-iS/\hbar)\mathscr{H}\exp(iS/\hbar) = H+O(\lambda^2). \tag{2.7}$$

This shows that ψ should depend on λ^2 only, and for low values of the angular momentum we may neglect this correction. It is therefore permitted to take as the wave function ψ in (2.6) any eigenfunction ψ_n which obeys the Schroedinger equation

$$H\psi_n = \varepsilon_n\psi_n, \tag{2.8}$$

where ε_n is an eigenvalue of the total Hamiltonian H under the appropriate boundary conditions. Substitution of ψ_n for ψ in the equation (2.6) gives

$$S\psi_n = i\hbar\lambda\frac{1}{\varepsilon_n-H}J_z\psi_n. \tag{2.6}'$$

This form of S with the choice of the ground-state eigenfunction ψ_0 for ψ_n leads to the result

$$\begin{aligned} \langle \Psi | J_z | \Psi \rangle &= \langle \psi_0 | J_z | \psi_0 \rangle - (i/\hbar)\langle \psi_0 | SJ_z - J_z S | \psi_0 \rangle \\ &= -2\lambda\langle \psi_0 | J_z \frac{1}{\varepsilon_0-H} J_z | \psi_0 \rangle. \end{aligned} \tag{2.9}$$

Here, ε_0 is the lowest eigenvalue of H.

By equating the last expression (2.9) to $\hbar K$, we determine the value of λ. With this value of λ, we may compute the energy of the system

$$\langle \Psi|\mathscr{H}|\Psi\rangle = \langle \psi_0|H|\psi_0\rangle - (\hbar K)^2/2I, \tag{2.10}$$

$$I = 2\langle \psi_0|J_z \frac{1}{H-\varepsilon_0} J_z|\psi_0\rangle. \tag{2.11}$$

Eq. (2.10) suggests that I corresponds to the moment of inertia. Inserting the complete system of ψ_n's between two J_z operators in (2.9), we have

$$I = 2\sum_{n\neq 0} \frac{|\langle \psi_n|J_z|\psi_0\rangle|^2}{\varepsilon_n-\varepsilon_0}, \tag{2.12}$$

which is just the expression of Inglis [1]). The expression (2.11) can be rewritten as

$$I = \frac{i}{\hbar\lambda}\langle \psi_0|J_z S - SJ_z|\psi_0\rangle, \tag{2.12}'$$

if we also take into account (2.9). This form will be employed in the following.

Next we consider the simpler case when S depends on the particle coordinates $\mathbf{x}_i$ only and not on the momenta $\mathbf{p}_i$. Assuming the explicit form of the Hamiltonian

$$H = \frac{1}{2M}\sum_{j=1}^{N} \mathbf{p}_j{}^2 + \tfrac{1}{2}\sum_{i\neq j} V(\mathbf{x}_i-\mathbf{x}_j), \tag{2.13}$$

we find that (2.6) becomes

$$\left\{\frac{1}{M}\sum_j \nabla_j S(\mathbf{x})\cdot\mathbf{p}_j - \lambda J_z\right\}\psi = 0,$$

or if we introduce the function ϕ by

$$S(\mathbf{x}) = M\lambda\phi(\mathbf{x}), \tag{2.14}$$

the equation defining $\phi(\mathbf{x})$ for the given state ψ becomes

$$\{\sum_j \nabla_j\phi(\mathbf{x})\cdot\mathbf{p}_j - J_z\}\psi(\mathbf{x}) = 0 \tag{2.15}$$

and the expression (2.12)′ can be transformed into

$$I = M\int \psi_0{}^*(\mathbf{x})(\sum_j \nabla_j\phi\cdot\nabla_j\phi)\psi_0(\mathbf{x})\mathrm{d}\tau_1\ldots\mathrm{d}\tau_N. \tag{2.12}''$$

The procedure hitherto followed is that of Gross [12]), except for some modifications. We note that the quantity $\sum_j(\nabla_j\phi\cdot\mathbf{p}_j)$ has the same form as the canonical momentum operator used by Tomonaga, which describes the deformation in an incompressible fluid [13]). The function $\phi(\mathbf{x})$ satisfies the equation

$\Delta\phi(\mathbf{x}) = 0$ and is considered to be the displacement potential of a particle in an incompressible fluid.

We note that this way of approach will be better understood in terms of quantum hydrodynamics. The formulation of quantum hydrodynamics was performed by several authors [14]). According to them, the scalar fields ρ and χ, representing the density and the velocity potential, satisfy the commutation relation

$$[\chi(\mathbf{r}), \rho(\mathbf{r}')]_- = i\hbar\delta(\mathbf{r}-\mathbf{r}'), \tag{2.16}$$

if the motion of the fluid is irrotational. The Hamiltonian is written in the form

$$H = \tfrac{1}{2}\int \{\nabla\chi \cdot \rho\nabla\chi + \rho W(\rho)\}\mathrm{d}\tau; \tag{2.17}$$

the function

$$W(\rho) = \int_{\rho_0}^{\rho} \frac{p-p_0}{\rho^2}\mathrm{d}\rho, \tag{2.18}$$

where p denotes the pressure, represents the compressional energy per unit mass of fluid and, in the case of an incompressible fluid, is simply given by p/ρ. The effective Hamiltonian (2.1) is

$$\mathscr{H} = H + \lambda\int \rho(\mathbf{r}\times\nabla\chi)_z \mathrm{d}\tau, \tag{2.19}$$

where we have replaced the velocity vector $\mathbf{u}$ by

$$-\nabla\chi = \mathbf{u}. \tag{2.20}$$

We must now remark that the second term in (2.19) should be correctly written as

$$\tfrac{1}{2}\lambda\int \{\rho(\mathbf{r}\times\nabla\chi)_z + (\mathbf{r}\times\nabla\chi)_z\rho\}\mathrm{d}\tau, \tag{2.21}$$

since ρ and χ do not commute. Hereafter, however, we utilize the simplified form, as in (2.19), instead of the exact expression (2.21), since no confusion will be expected. If the canonical transformation

$$\Psi = \left\{\exp(i\lambda/\hbar)\int \rho\phi\mathrm{d}\tau\right\}\psi$$

is carried out, the equation defining ϕ becomes

$$\left\{\int \nabla\phi\cdot\rho\nabla\chi\mathrm{d}\tau - \int \rho(\mathbf{r}\times\nabla\chi)_z\mathrm{d}\tau\right\}\psi = 0, \tag{2.22}$$

which is to be compared with (2.15). The moment of inertia is given by

$$I = \langle\psi_0|\int \nabla\phi\cdot\rho\nabla\phi\mathrm{d}\tau|\psi_0\rangle, \tag{2.23}$$

where ψ_0 is the ground state of the Hamiltonian (2.17).

At this stage, it is of considerable interest to investigate the work by Hayakawa and Marumori [15]), based upon Tomonaga's theory of collective motion. We employ their notations and put

$$\phi = \langle \beta^2 \tau \rangle \theta, \quad \theta = \tfrac{1}{2} \tan^{-1}(\xi_2/\xi_1), \tag{2.24}$$

$$\xi_1 = \sum_{j=1}^{n} \tfrac{1}{2}(x_j^2 - y_j^2), \quad \xi_2 = \sum_j x_j y_j, \tag{2.25}$$

$$\beta = \frac{2}{\tau}\sqrt{\xi_1^2+\xi_2^2}, \quad \tau = \sum_j (x_j^2+y_j^2), \tag{2.26}$$

where the braces stand for the expectation value which is to be taken in the eigenstate ψ. The equation (2.15) becomes

$$\{N_z - J_z\}\psi = 0, \quad N_z = \langle \beta^2 \tau \rangle (\sum_i \nabla_i \theta \cdot \mathbf{p}_i). \tag{2.27}$$

Using the relation

$$\nabla_i \theta = \{(\xi_1 y_i - \xi_2 x_i)\mathbf{i} + (\xi_1 x_i + \xi_2 y_i)\mathbf{j}\}/2(\xi_1^2+\xi_2^2)$$

and the approximation $\langle \beta^2 \tau \rangle \approx \beta^2 \tau$, we have

$$\left(\left\{\frac{2(\xi_1 y_i - \xi_2 x_i)}{\tau} + y_i\right\}\frac{\partial}{\partial x_i} + \left\{\frac{2(\xi_1 x_i + \xi_2 y_i)}{\tau} - x_i\right\}\frac{\partial}{\partial y_i}\right)\psi = 0.$$

This equation shows that the wave function ψ should have the form $\psi(\sum x_i^2, \sum y_i^2, \sum x_i y_i)$. The subsidiary condition

$$(\sum_i x_i y_i)\,\psi = 0 \tag{2.28}$$

given by them further restricts the wave function to the form $\psi(\sum x_i^2, \sum y_i^2)$ $\delta(\sum x_i y_i)$. With the value of ϕ we may compute

$$\langle \Psi | J_z | \Psi \rangle = \lambda M \langle \beta^2 \tau \rangle, \tag{2.29}$$

$$\langle \Psi | H | \Psi \rangle = \langle \psi | H | \psi \rangle + \tfrac{1}{2}\lambda^2 M \langle \beta^2 \tau \rangle, \tag{2.30}$$

where $[J_z, \theta]_- = -i\hbar$. These results with the subsidiary condition (2.28) lead to the value of the moment of inertia

$$I = M \int \psi^* \frac{(\sum (x_i^2 - y_i^2))^2}{\sum (x_i^2+y_i^2)} \psi \mathrm{d}\tau, \tag{2.31}$$

which is the irrotational flow value found by Bohr [7]).

It is also possible to improve the approximation: e.g., we remove the condition that the wave-function ψ is a function of only the variables, $\sum x_i^2$, $\sum y_i^2$ and $\sum x_i y_i$, while preserving the subsidiary condition (2.28). Putting

$$S = M\lambda \langle \beta^2 \tau \rangle \theta + S', \tag{2.32}$$

$$J_z^{\text{in}} = J_z - N_z, \tag{2.33}$$

we get

$$\{(i/\hbar)[S', H]_- + \lambda J_z^{\text{in}}\}\psi = 0$$

in place of (2.15): now, J_z^{in} is considered as the "internal" angular momentum. Simple calculation gives

$$I = M\langle\beta^2\tau\rangle + 2\sum_{n\neq 0}\frac{|\langle\psi_n|J_z^{\text{in}}|\psi_0\rangle|^2}{\varepsilon_n - \varepsilon_0} \tag{2.34}$$

for the moment of inertia. These are the main steps in Hayakawa and Marumori's treatment. The effective moment of inertia given by (2.34) suggests how the moments of inertia deduced from the rotational spectra may deviate from the hydrodynamical values.

A quantitative study of this problem is, however, difficult without more knowledge of the collective excited states. It seems that the quantum-hydrodynamical approach is more appropriate to the problem. We understand (2.24) and (2.25) as

$$\xi_1 = \tfrac{1}{2}\int\rho(x^2-y^2)\mathrm{d}\tau, \quad \xi_2 = \int\rho xy\mathrm{d}\tau. \tag{2.35}$$

The operator N_z is read as

$$N_z = -\langle\beta^2\tau\rangle\int\rho\nabla\theta\cdot\nabla\chi\mathrm{d}\tau.$$

If we pass over to the representation in which ρ is diagonal, the equation (2.27) will take the form

$$\left(\left\{\frac{2(\xi_1 y-\xi_2 x)}{\tau}+y\right\}\frac{\partial}{\partial x}+\left\{\frac{2(\xi_1 x+\xi_2 y)}{\tau}-x\right\}\frac{\partial}{\partial y}\right)\frac{\delta\psi}{\delta\rho}=0.$$

This equation requires that the wave-function should have the form

$$\psi\left(\int\rho x^2\mathrm{d}\tau, \int\rho y^2\mathrm{d}\tau, \int\rho xy\mathrm{d}\tau\right). \tag{2.36}$$

As was shown by Tomonaga [13]), the variables

$$\int\rho x^2\mathrm{d}\tau, \quad \int\rho y^2\mathrm{d}\tau, \int\rho xy\mathrm{d}\tau$$

can actually be regarded as coordinates specifying the surface deformation.

We should like here to remark on the choice of the function $\phi = \sum_i \eta x_i y_i$ given by Gross [12]), which leads to the value

$$I = M\left\{\int\psi^*\sum_j(x_j^2-y_j^2)\psi\mathrm{d}\tau\right\}^2 \Big/ \sum_i\int\psi^*(x_i^2+y_i^2)\psi\mathrm{d}\tau.$$

In this case we have to assume that ψ is a function of $\sum_i(ax_i^2+by_i^2)$ alone and to take the value $\eta = (b-a)/(a+b)$ in order to satisfy the equation (2.15).

This simpler choice of the flow pattern function comes from the more restricted functional form of the ground state wave-function. We thus observe that the determination of the function ϕ is sensitively affected by the functional form of the ground state wave-function, and accordingly by the strength of the correlation between particles in the ground state.

3. Evaluation of the Moment of Inertia

We consider a box of volume V filled with N identical particles, each of mass M. When this box is set rotating, there will be generated in the box a flow of the particles, which is associated with the state before rotation. According to the properties of the fluid and the magnitude of the angular velocity, various kinds of flow may appear. Among them we shall limit our considerations to the irrotational flow with small angular velocity; we shall determine the flow pattern function ϕ for given ground-state wavefunctions and investigate the corresponding values of the moment of inertia of the system.

For illustration, we shall begin with the evaluation of the moment of inertia of a system of non-interacting fermions. A single-particle plane-wave state in the box, with the momentum (k_x, k_y, k_z), is taken as

$$\begin{aligned} &|k_x, k_y, k_z\rangle = (1/V)^{\frac{1}{2}} \exp i(k_x x+k_y y+k_z z), \\ &k_x = 2\pi l/L, \quad k_y = 2\pi m/L, \quad k_z = 2\pi n/L, \end{aligned} \tag{3.1}$$

where (l, m, n) are positive or negative integers. We write down the ground-state wave-function, disregarding the exclusion principle, as

$$\psi_0 \equiv |\mathbf{k}_1, \mathbf{k}_2, \ldots \mathbf{k}_N\rangle = (1/V^N)^{\frac{1}{2}} \exp i(\mathbf{k}_1\mathbf{x}_1+\mathbf{k}_2\mathbf{x}_2+ \ldots +\mathbf{k}_N\mathbf{x}_N). \tag{3.2}$$

Insertion of the expression (3.2) into (2.15) gives

$$\sum_{j=1}^{N} \left\{ \frac{\partial\phi}{\partial x_j} k_x{}^j + \frac{\partial\phi}{\partial y_j} k_y{}^j - (x_j k_y{}^j - y_j k_x{}^j) \right\} |\mathbf{k}_1 \ldots \mathbf{k}_N\rangle = 0. \tag{3.3}$$

We determine the explicit form of $\phi(\mathbf{x})$, or $S(\mathbf{x})$. It does not appear possible to get the function ϕ from eq. (2.15) as it is. In fact, the flow pattern in a rotating system is, as the cranking formula shows, considered to depend upon the excited states of the non-rotating system. The appearance of the excited states can, however, be avoided. Under the assumption of the functional form of the ground-state wave-function in the form (3.2), momentum operators may be replaced by their respective eigenvalues, and in view of the fact that the motions of the individual particle are entirely independent, each term under the symbol of summation may be put equal to zero separately. Hence, by taking

$$\phi(\mathbf{x}) = \sum_{i=1}^{N} \{a_i x_i y_i + \tfrac{1}{2} b_i (x_i{}^2 - y_i{}^2)\}, \tag{3.4}$$

we fix the coefficients a_i and b_i. They are easily computed and expressed in terms of $\mathbf{k}_i$ as

$$a_i = -\frac{(k_x^i)^2-(k_y^i)^2}{(k_x^i)^2+(k_y^i)^2}, \quad b_i = \frac{2k_x^i k_y^i}{(k_x^i)^2+(k_y^i)^2}. \tag{3.5}$$

It is to be noted that the two functions occurring in (3.4), $F_1 = xy$ and $F_2 = x^2-y^2$, obey the Laplace equation $\Delta F = 0$, which is a condition required for the commutability of $\mathbf{p}_i$ and $\nabla_i\phi$ in (2.15). The result is in agreement with the statement that an irrotational displacement of a particle in an incompressible fluid can be described with the help of a displacement potential F which satisfies $\Delta F = 0$. The direction of infinitesimal displacement of a particle at any point (x, y) is given by the gradient of F. The functions F_1 and F_2 are the simplest non-trivial forms for the potential F and, as is easily seen, $\nabla F_1 \cdot \nabla F_2 = 0$: the two directions of motion determined by F_1 and F_2 are orthogonal to each other. We thus see that the two terms in (3.4) give orthogonal flow patterns in a two-dimensional irrotational flow, and their coefficients determined by the ground-state wave-function fix the intensities of these two flows.

The function $\phi(\mathbf{x})$, with the coefficients (3.5), yields for the moment of inertia, from eq. (2.12)'', the following value:

$$I = M\int \psi_0^* \sum_j (x_j^2+y_j^2)\psi_0 \, d\tau_1 \ldots d\tau_N. \tag{3.6}$$

This formula directly leads to the classical value $\frac{1}{6}NML^2$ which is just what Amado and Brueckner obtained. The calculation shows that the independence of the motion of the particles is responsible for the rigid value of the moment of inertia.

It is desirable to take the exclusion principle into account. For this purpose, it is convenient to employ the method of second quantization. Using the momentum space, we can write the ground-state wave-function, instead of (3.2), as

$$|\mathbf{k}_1, \mathbf{k}_2, \ldots \mathbf{k}_N\rangle = a_{k_N}^* a_{k_{N-1}}^* \ldots a_{k_1}^* |0\rangle, \tag{3.7}$$

where $|0\rangle$ denotes the vacuum state; a_k^* and a_k stand for the creation and annihilation operators of a particle with momentum $\mathbf{k}$, and satisfy the commutation relations

$$[a_k, a_{k'}^*]_+ \equiv a_k a_{k'}^* + a_{k'}^* a_k = \delta_{kk'}.$$

The equation (2.15) takes the form

$$\sum_{k,\,k'} \{\langle \mathbf{k}'|\nabla\phi \cdot \mathbf{p}|\mathbf{k}\rangle - \langle \mathbf{k}'|J_z|\mathbf{k}\rangle\} a_{k'}^* a_k |\mathbf{k}_1 \ldots \mathbf{k}_N\rangle = 0, \tag{3.8}$$

where $\langle \mathbf{k}'| \ldots |\mathbf{k}\rangle$ denotes the matrix element between the one-particle states

(3.1) and J_i is now read as $(x\partial/\partial y - y\partial/\partial x)(\hbar/i)$. With the notation

$$\bar{k}_x = \tfrac{1}{2}(k_x + k'_x), \quad \bar{k}_y = \tfrac{1}{2}(k_y + k'_y),$$

we have therefore

$$\hbar^{-1}\langle \mathbf{k}'|J_z|\mathbf{k}\rangle = \bar{k}_y\langle \mathbf{k}'|x|\mathbf{k}\rangle - \bar{k}_x\langle \mathbf{k}'|y|\mathbf{k}\rangle,$$

and we can readily verify that we may take the flow function as

$$\langle \mathbf{k}'|\phi|\mathbf{k}\rangle = -\frac{\bar{k}_x^2 - \bar{k}_y^2}{\bar{k}_x^2 + \bar{k}_y^2}\langle \mathbf{k}'|xy|\mathbf{k}\rangle + \frac{\bar{k}_x\bar{k}_y}{\bar{k}_x^2 + \bar{k}_y^2}\langle \mathbf{k}'|x^2 - y^2|\mathbf{k}\rangle; \tag{3.9}$$

in fact, with this expression, we find

$$\begin{aligned}
&\hbar^{-1}\langle \mathbf{k}'|\nabla\phi\cdot\mathbf{p}|\mathbf{k}\rangle \\
&\quad = -\frac{\bar{k}_x^2 - \bar{k}_y^2}{\bar{k}_x^2 + \bar{k}_y^2}\{\langle \mathbf{k}'|y|\mathbf{k}\rangle\bar{k}_y + \langle \mathbf{k}'|x|\mathbf{k}\rangle\bar{k}_x\} + \frac{2\bar{k}_x\bar{k}_y}{\bar{k}_x^2 + \bar{k}_y^2}\{\langle \mathbf{k}'|x|\mathbf{k}\rangle\bar{k}_x - \langle \mathbf{k}'|y|\mathbf{k}\rangle\bar{k}_y\} \\
&\quad = \bar{k}_y\langle \mathbf{k}'|x|\mathbf{k}\rangle - \bar{k}_x\langle \mathbf{k}'|y|\mathbf{k}\rangle.
\end{aligned}$$

We then get for the moment of inertia

$$\begin{aligned}
I &= M\langle \mathbf{k}_1 \ldots \mathbf{k}_N|\sum_{k,k'}\langle \mathbf{k}|\nabla\phi|\mathbf{k}'\rangle\langle \mathbf{k}'|\nabla\phi|\mathbf{k}\rangle a_k^* a_k|\mathbf{k}_1 \ldots \mathbf{k}_N\rangle \\
&= M\langle \mathbf{k}_1 \ldots \mathbf{k}_N|\sum_{k}\langle \mathbf{k}|x^2 + y^2|\mathbf{k}\rangle a_k^* a_k|\mathbf{k}_1 \ldots \mathbf{k}_N\rangle,
\end{aligned} \tag{3.10}$$

which is the same expression as (3.6).

The next step is to investigate how the rigid moment of inertia obtained above is modified by particle interaction. The flow pattern in a rotating system is expected to depend on the detailed interactions between particles and to require information about the excited states. It is known that the effect of pairing correlation is dominant in some nuclear phenomena, and in particular in the collective nuclear excitations in which we are interested. We should therefore like to consider primarily the effects of pairing interactions. It is also worth noting that we can make use of the fact that the major contribution to the moment of inertia comes from states near the Fermi surface because of the exclusion principle. We thus try to approximate the particle-particle interaction through the interaction between particle-hole pairs. Accordingly, we deal, as our second example, with a degenerate electron gas in the high-density limit [3]), and explore the effects of particle interaction on the moment of inertia.

We start with the diagonalization of the Hamiltonian. The Hamiltonian (2.13) is rewritten as

$$\begin{aligned}
H = &\sum_k \varepsilon_k(a_{k+}^* a_{k+} + a_{k-}^* a_{k-}) \\
&- \tfrac{1}{2}\sum_{(k,\sigma)}\langle \mathbf{k}_1\sigma_1, \mathbf{k}_2\sigma_2|V|\mathbf{k}'_2\sigma'_2, \mathbf{k}'_1\sigma'_1\rangle a^\dagger_{k,\sigma_1} a^\dagger_{k_2\sigma_2} a_{k'_2\sigma'_2} a_{k'_1\sigma'_1},
\end{aligned} \tag{3.11}$$

where the indices (+), (−) stand for the sign of the projection of the spin angular momentum along the z-axis. We make the usual replacement of the fermion pair operators $a_k^* a_{k+q}$, $a_{k+q}^* a_k$ by the boson operators $C_q(\mathbf{k})$, $C_q^*(\mathbf{k})$, ignoring spin indices for the sake of simplicity. Following Wentzel [16], one obtains

$$\begin{aligned} H &= H_0+H', \quad H_0 = \sum_{k,\,q} \{\varepsilon(\mathbf{k}+\mathbf{q})-\varepsilon(\mathbf{k})\} C_q^*(\mathbf{k}) C_q(\mathbf{k}), \\ H' &= -\sum_{\substack{(k,\,k',\,q) \\ k\neq k'}} C_q^*(\mathbf{k}) C_q(\mathbf{k}') A_q(\mathbf{k},\mathbf{k}') \\ &\quad -\tfrac{1}{2} \sum_{\substack{(k,\,k',\,q) \\ k\neq k'}} B_q(\mathbf{k},\mathbf{k}') \{C_q^*(\mathbf{k}) C_{-q}^*(\mathbf{k}) + C_{-q}(\mathbf{k}') C_q(\mathbf{k})\}, \end{aligned} \tag{3.12}$$

where the c-number coefficients A and B are expressed in terms of the matrix elements $\langle \ldots |V| \ldots \rangle$:

$$\begin{aligned} A_q(\mathbf{k},\mathbf{k}') &= \langle \mathbf{k}+\mathbf{q}, \mathbf{k}'|V|\mathbf{k}, \mathbf{k}'+\mathbf{q}\rangle + \langle \mathbf{k}+\mathbf{q}, \mathbf{k}'|V|\mathbf{k}'+\mathbf{q}, \mathbf{k}\rangle, \\ B_q(\mathbf{k},\mathbf{k}') &= \langle \mathbf{k}+\mathbf{q}, \mathbf{k}'-\mathbf{q}|V|\mathbf{k}, \mathbf{k}'\rangle + \langle \mathbf{k}+\mathbf{q}, \mathbf{k}'-\mathbf{q}|V|\mathbf{k}', \mathbf{k}\rangle. \end{aligned}$$

In these formulas, we ignore the second term compared with the first. Diagonallization of the Hamiltonian is carried out by introducing operators

$$U_q = \sum_k \left(C_q(\mathbf{k}) \varphi_q(\mathbf{k}) - C_{-q}^*(\mathbf{k}) \chi_q(\mathbf{k})\right). \tag{3.13}$$

Here, the c-number functions $\varphi_q(\mathbf{k})$ and $\chi_q(\mathbf{k})$ are the solutions of the simultaneous equations

$$\begin{aligned} \{\varepsilon(\mathbf{k}+\mathbf{q})-\varepsilon(\mathbf{k})-E\}\varphi_q(\mathbf{k}) &= \sum_{k'} A_q(\mathbf{k},\mathbf{k}')\varphi_q(\mathbf{k}') + \sum_{k'} B_q(\mathbf{k},\mathbf{k}')\chi_q(\mathbf{k}'), \\ \{\varepsilon(\mathbf{k}-\mathbf{q})-\varepsilon(\mathbf{k})+E\}\chi_q(\mathbf{k}) &= \sum_{k'} B_{-q}(\mathbf{k},\mathbf{k}')\varphi_q(\mathbf{k}') + \sum_{k} A_{-q}(\mathbf{k},\mathbf{k}')\chi_q(\mathbf{k}'), \end{aligned} \tag{3.14}$$

along with the normalization condition

$$\sum_k \left(\varphi_q^2(\mathbf{k}) - \chi_q^2(\mathbf{k})\right) = 1. \tag{3.15}$$

The secular equation which determines the eigenvalue E is that of the plasma oscillation. The ground state wave-function is defined by

$$U_q \psi_0 = 0 \tag{3.16}$$

and the eigenfunction of a plasma excitation is given by

$$\psi_{\mathrm{pl}} = U_q^+ \psi_0 = \sum_k \{\varphi_q(\mathbf{k}) C_q^*(\mathbf{k}) - \chi_q(\mathbf{k}) C_{-q}(\mathbf{k})\}. \tag{3.17}$$

Now our problem is well-defined. Using the expression

$$H = \sum_q E_q U_q^* U_q \tag{3.18}$$

and the operators

$$\phi(\mathbf{x}) \to \sum_q \{\sum_k \langle \mathbf{k}|\phi|\mathbf{k}+\mathbf{q}\rangle C_q(\mathbf{k}) + \sum_k \langle \mathbf{k}+\mathbf{q}|\phi|\mathbf{k}\rangle C_q^*(\mathbf{k})\},$$
$$J_z(\mathbf{x}) \to \sum_q i\{\sum_k \langle \mathbf{k}|J_z|\mathbf{k}+\mathbf{q}\rangle C_q(\mathbf{k}) - \sum_k \langle \mathbf{k}+\mathbf{q}|J_z|\mathbf{k}\rangle C_q^*(\mathbf{k})\},$$

and substituting, for $S = M\lambda\phi(\mathbf{x})$ and $J_z(\mathbf{x})$, the expressions

$$M\lambda \sum_{k,q} \{\langle \mathbf{k}+\mathbf{q}|\phi|\mathbf{k}\rangle U_q^*(\varphi_q(\mathbf{k})+\chi_q(\mathbf{k}+\mathbf{q})) + \langle \mathbf{k}|\phi|\mathbf{k}+\mathbf{q}\rangle U_q(\chi_q(\mathbf{k}+\mathbf{q})+\varphi_q(\mathbf{k}))\}, \quad (3.19)$$

$$i\sum_{k,q} \{\langle \mathbf{k}+\mathbf{q}|J_z|\mathbf{k}\rangle U_q^*(\varphi_q(\mathbf{k})-\chi_q(\mathbf{k}+\mathbf{q})) - \langle \mathbf{k}|J_z|\mathbf{k}+\mathbf{q}\rangle U_q(\chi_q(\mathbf{k}+\mathbf{q})-\varphi_q(\mathbf{k}))\} \quad (3.20)$$

in (2.6), we have an equation defining ϕ, which gives

$$\langle \mathbf{k}+\mathbf{q}|\phi|\mathbf{k}\rangle = \frac{\hbar}{M} \frac{\langle \mathbf{k}+\mathbf{q}|J_z|\mathbf{k}\rangle}{\varepsilon(\mathbf{k}+\mathbf{q})-\varepsilon(\mathbf{k})}. \quad (3.21)$$

Eq. (3.21) results from the relation

$$E_q(\varphi_q(\mathbf{k})+\chi_q(\mathbf{k}+\mathbf{q})) = (\varepsilon(\mathbf{k}+\mathbf{q})-\varepsilon(\mathbf{k}))(\varphi_q(\mathbf{k})-\chi_q(\mathbf{k}+\mathbf{q})), \quad (3.22)$$

which is derived from (3.14) with the aid of explicit forms of A_q and B_q. We obtain from (2.12)′ for the moment of inertia

$$I = 2\sum_{k,q} \frac{|\langle \mathbf{k}+\mathbf{q}|J_z|\mathbf{k}\rangle|^2}{\varepsilon(\mathbf{k}+\mathbf{q})-\varepsilon(\mathbf{k})}, \quad (3.23)$$

which is the rigid value in the form given by Rockmore [3]). We see that the flow generated by rotation is the same as in the noninteracting system (3.9), and it gives the rigid value for the moment of inertia. This result shows that the particle correlations have no effect upon the flow in the case of plasma excitation, and this fact can be attributed to the relation (3.22). In this connection we should like to point out that the flow pattern leading to superfluidity is quite different from that treated above.

We shall first study the Bardeen-Cooper-Schieffer-Bogoliubov model of a superconductor, introducing the energy gap in the spectrum of excitations. Here our notations and conventions closely follow those of Belyaev [8]). The ground state of the superconducting state is represented by the vacuum state with respect to the Bogoliubov fermions α_k and β_k. The operators α_k and β_k are derived by the transformation

$$\alpha_k = u_k a_{k+} - v_k a_{k-}^*,$$
$$\beta_k = u_k a_{k-} - v_k a_{k+}^*,$$

where u_k and v_k are given by

$$u_k^2 = \tfrac{1}{2}\{1+\varepsilon_k/\sqrt{\varepsilon_k^2+\Delta^2}\}, \quad v_k^2 = \tfrac{1}{2}\{1-\varepsilon_k/\sqrt{\varepsilon_k^2+\Delta^2}\}. \tag{3.24}$$

Here, Δ is the quantity corresponding to half the energy gap. The Hamiltonian (3.11) is now approximated by

$$H = \sum_k E_k(\alpha_k^*\alpha_k+\beta_k^*\beta_k), \quad E_k = \sqrt{\varepsilon_k^2+\Delta^2}. \tag{3.25}$$

The component of the angular momentum operator becomes

$$\sum_{k,q} i\langle \mathbf{k}|J_z|\mathbf{k}+\mathbf{q}\rangle\{(u_k u_{k+q}-v_k v_{k+q})(\alpha_k^*\alpha_{k+q}-\beta_{k+q}^*\beta_k) + (u_k v_{k+q}-v_k u_{k+q})(\alpha_k^*\beta_{k+q}^*-\beta_k\alpha_{k+q})\}+\text{herm. conj.} \tag{3.26}$$

Putting the flow function as

$$\sum_{k,q}\langle \mathbf{k}|\phi|\mathbf{k}+\mathbf{q}\rangle(\alpha_k^*\beta_{k+q}^*-\beta_k\alpha_{k+q})+\text{herm. conj.}, \tag{3.27}$$

we obtain from (2.6),

$$\langle \mathbf{k}|\phi|\mathbf{k}+\mathbf{q}\rangle = \frac{\hbar}{M}\frac{\langle \mathbf{k}|J_z|\mathbf{k}+\mathbf{q}\rangle}{E_k+E_{k+q}}(u_k v_{k+q}-v_k u_{k+q}). \tag{3.28}$$

From (2.12)′ this directly leads to the value of moment of inertia derived by Migdal and Balayev [8]),

$$I = 2\sum_{k,q}\frac{|\langle \mathbf{k}|J_z|\mathbf{k}+\mathbf{q}\rangle|^2}{E_k+E_{k+q}}(u_k v_{k+q}-v_k u_{k+q})^2. \tag{3.29}$$

Our aim is to discuss the difference between the two flow patterns (3.21) and (3.28). To this end, we consider a flow function of the type $\sum_{i\neq j}\tau(\mathbf{x}_i-\mathbf{x}_j)$. As is seen from (3.4) and (3.5), the additive form $\sum_j\sigma(\mathbf{x}_j)$ does not include correlations in the flow of particles, whereas the flow function $\sum_{i\neq j}\tau(\mathbf{x}_i-\mathbf{x}_j)$ will depend on the correlation function for the ground state. For simplicity we assume that the particle number N is even and ignore the exclusion principle. To illustrate our way of reasoning without any inessential complication, we consider a ground state wave function of the following type:

$$\psi_0 \propto f_1(\mathbf{x}_1\pm\mathbf{x}_2)f_2(\mathbf{x}_3\pm\mathbf{x}_4)\ldots f_{\frac{1}{2}N}(\mathbf{x}_{N-1}\pm\mathbf{x}_N). \tag{3.30}$$

Eq. (2.15) then becomes, for example,

$$\{\nabla_1\phi^{(1)}\mathbf{p}_1+\nabla_2\phi^{(2)}\mathbf{p}_2-(J_z^{(1)}+J_z^{(2)})\}\psi_0(\mathbf{x}) = 0,$$

where we have put $\phi(\mathbf{x}) = \sum_{i=1}^{\frac{1}{2}N}\phi^{(i)}(\mathbf{x}_{2i-1}, \mathbf{x}_{2i})$. If we take $f_i \propto \exp i\mathbf{k}^i\cdot(\mathbf{x}_{2i-1}\pm\mathbf{x}_{2i})$, it follows from (3.4) and (3.5), after the separation of the relative coordinates

and those of the centre-of-mass,

$$\phi^{(1)} = -\frac{(k_x{}^1)^2-(k_y{}^1)^2}{(k_x{}^1)^2+(k_y{}^1)^2}\frac{(x_1\pm x_2)(y_1\pm y_2)}{2} + \frac{k_x{}^1 k_y{}^1}{(k_x{}^1)^2+(k_y{}^1)^2}\left\{\frac{(x_1\pm x_2)^2-(y_1\pm y_2)^2}{2}\right\}. \quad (3.31)$$

With the aid of (3.31), we obtain for the moment of inertia for the two choices of signs,

$$\begin{aligned} I &= \tfrac{1}{2}M\sum_{i=1}^{\frac{1}{2}N}\langle\{(x_{2i-1}+x_{2i})^2+(y_{2i-1}+y_{2i})^2\}\rangle, \\ I &= \tfrac{1}{2}M\sum_{i=1}^{\frac{1}{2}N}\langle\{(x_{2i-1}-x_{2i})^2+(y_{2i-1}-y_{2i})^2\}\rangle, \end{aligned} \quad (3.32)$$

where the braces stand for the expectation value taken in the ground state. The sum of the two expressions (3.32), of course, gives the rigid value. As is seen from (3.6), (3.10) and (3.23), we observe that the independence of the motion of each particle assures the rigid value of the moment of inertia. On the other hand, considering the boundary condition that the system is enclosed in a finite box, we see from (3.32) that the moment of inertia will be changed provided that the freedom of the motion may be suppressed by such correlations as are expressed in (3.30). Actually, in superconductors, pairs of particles with momenta of the same magnitude but opposite direction and opposite spin angular momenta are considered to form a bound pair, and the other freedom of this pair is suppressed because of the large excitation energies, which leads, with the exclusion principle, to the value (3.29). Indeed, if the pairing interaction is absent, we have u_k, $v_k = 1$, 0 and (3.29) leads to the rigid value. On the contrary, if the pairing interaction is strong, and freezes all freedom, we see from (3.24) that (3.29) becomes vanishingly small; this results in extreme superfluidity.

4. Discussion

In our treatment the emphasis is laid on the analysis of the flow pattern function generated when the system is set rotating. In the case of rotation around the z-axis, we findt wo flow patterns which are independent and orthogonal to each other. In some cases, we can attribute these flow patterns to the independent motion of individual particles in a box: then, we get the rigid value for the moment of inertia. In other cases, the liquid drop model or the superconducting case, some of the $2N$ degrees of freedom in the flow pattern are restricted by large excitation energies, resulting in a smaller value of the moment of inertia. We therefore conclude that such correlations of particles as those which diminish or restrict the degree of freedom in the flow pattern can

appreciably change the rigid value of moment of inertia. This assertion is quite similar to that of Teller and Wheeler [6]), that the prevention of rotation in states with small rotational quantum number leads to large rotational excitation energies and hence to small moments of inertia.

According to Blatt, Butler and Schafroth [11]), in real fluids, there exitst a maximum distance Λ beyond which all correlations can be ignored. For $R \gg \Lambda$, where R is the dimension of the container, they have proved that the moment of inertia approaches the rigid value I_0; i.e.,

$$I = I_0(1+0(\Lambda/R)).$$

We think that such interactions as restrict some of the existent degree of freedom lead to the value $\Lambda \approx R$.

Finally, it must be remarked that our considerations hold only for low values of the angular momentum, i.e. for small values of λ.

References

1) D. R. Inglis, Phys. Rev. **96** (1954) 1059; **103** (1956) 1786
2) R. D. Amado and K. A. Brueckner, Phys. Rev. **115** (1959) 778
3) R. M. Rockmore, Phys. Rev. **116** (1959) 469
4) M. Gell-Mann and K. A. Brueckner, Phys. Rev. **106** (1957) 374;
   K. Sawada, Phys. Rev. **106** (1957) 372;
   K. Sawada, K. A. Brueckner, N. Fukuda and R. Brout, Phys. Rev. **108** (1957) 507
5) F. Villars, Ann. Rev. of Nuclear Science **7** (1957) 185 (references to other work are given)
6) E. Teller and J. A. Wheeler, Phys. Rev. **53** (1958) 778
7) A. Bohr and B. R. Mottelson, Mat. Fys. Medd. Dan. Vid. Selsk. **27**, No. **16** (1954)
8) S. T. Belyaev, Mat. Fys. Medd. Dan. Vid. Selsk. **31**, No. 11 (1959);
   A. B. Migdal, JETP **37** (1960) 249
9) R. M. Rockmore, Phys. Rev. **118** (1960) 1645
10) G. Wentzel, Phys. Rev. Lett. **4** (1960) 349
11) J. M. Blatt, S. T. Butler and M. R. Schafroth, Phys. Rev. **100** (1955) 481, 476, 1221
12) E. P. Gross, Nuclear Physics **14** (1960) 389
13) S. Tomonaga, Prog. Theor. Phys. **13** (1955) 467
14) R. Kronig and A. Thellung, Physica **18** (1952) 749;
   A. Thellung, Physica **19** (1953) 217;
   J. M. Ziman, Proc. Roy. Soc. **219** (1953) 257
15) S. Hayakawa and T. Marumori, Prog. Theor. Phys. **18** (1957) 396
16) G. Wentzel, Phys. Rev. **108** (1957) 1593

7.C

Nuclear Physics **25** (1961) 348—352; © *North-Holland Publishing Co., Amsterdam*

Not to be reproduced by photoprint or microfilm without written permission from the publisher

ANTINUCLEON-NUCLEON ANNIHILATION TO TWO MESONS

R. J. N. PHILLIPS

A.E.R.E., Harwell, England

Received 23 January 1961

Abstract: A partial wave description is given for two-meson annihilation in flight. Angular distributions and polarization effects are illustrated; they are sensitive to the range of the annihilation region.

1. Introduction

The annihilations in flight $\overline{\mathrm{N}}+\mathrm{N} \to \pi+\pi$ or $\overline{\mathrm{K}}+\mathrm{K}$ are very infrequent †. However, being two-particle processes they are particularly simple to describe and understand, and information about them would be valuable. While these processes are interesting in their own right, they may also illuminate some general features of the $\overline{\mathrm{N}}\mathrm{N}$ interaction, such as the range of the annihilation region.

At fairly low incident energies, where few angular momentum states may be expected to take part, a partial wave description has advantages. This note gives such a description and illustrates its use.

The illustration takes only the partial waves indicated by the Ball-Chew model [2]). The short range of annihilation in this model leads to very simple angular distributions and polarization effects.

2. The Reaction Amplitude

It is reasonable to treat the $\overline{\mathrm{N}}+\mathrm{N}$ spin non-relativistically at the energies of interest. Then the c.m. reaction amplitude $M(\theta, \phi)$ is a row matrix in the 4×4 spin space, which contracts with the column matrix representing the incident spin state. In general we have to consider a statistical mixture of initial spin states, described by a density matrix ρ. The corresponding cross section is

$$\sigma(\theta, \phi) = \frac{k'}{k} M\rho M^*/\mathrm{tr}\,\rho, \tag{1}$$

where M^* is the Hermitian conjugate. In particular, $\rho = 1$ gives the unpolarized cross section. Eq. (1) fixes our normalization convention for M.

† The annihilations $\bar{\mathrm{p}}+\mathrm{p} \to \pi^-+\pi^+$ or $\mathrm{K}^-+\mathrm{K}^+$ are less than $\frac{1}{400}$ or $\frac{1}{1000}$, respectively, of those seen at 1.6 GeV/c [1]).

The angles θ and ϕ are the polar angles of the meson relative momentum $\mathbf{k}'$. We choose the 3-axis ($\theta = 0$) to be along the incident relative momentum $\mathbf{k}$, and take a spin representation in which the $\bar{\mathrm{N}}$+N singlet and three triplet states are basic, labelling the latter by s and 1, 0, −1, (according to S_3). Thus $M = (M_s, M_1, M_0, M_{-1})$.

Let χ be some column matrix for initial spin. Then $M\chi$ is the corresponding S-matrix element for annihilation (within a trivial factor) and has the form $M\chi = v^* Q u$, where u is the N 2-spinor and v is a "negative-energy" spinor related to the $\bar{\mathrm{N}}$ spinor u' by $u' = -i\sigma_2 (v^*)^{\mathrm{T}}$. From parity conservation †, Q is restricted to the form $Q = F\boldsymbol{\sigma}\cdot\mathbf{k} + G\boldsymbol{\sigma}\cdot\mathbf{k}'$, in terms of the Pauli matrices $\boldsymbol{\sigma}$, where F and G are complex functions of the energy and $\cos\theta$. Hence the components of M have the general forms

$$\begin{aligned} -\mathrm{e}^{-i\phi} M_1 = \mathrm{e}^{i\phi} M_{-1} &= Gk' \sin\theta, \\ M_0 &= \sqrt{2}(Fk + Gk'\cos\theta), \\ M_s &= 0. \end{aligned} \tag{2}$$

(Ref. [3]) contains a similar result for inverse reactions $\pi+\pi \to \bar{\mathrm{N}}+\mathrm{N}$.)

The charge independence hypothesis relates reaction amplitudes for different assignments of $\bar{\mathrm{N}}$, N and meson charge, as noted by various authors (e.g. ref. [4])). For convenience we give the rules †† in full, denoting the π and K amplitudes for total isobaric spin T by $M_\pi(T)$ and $M_{\mathrm{K}}(T)$,

$$M(\bar{\mathrm{p}}+\mathrm{p} \to \pi^- + \pi^+) = \frac{1}{\sqrt{6}} M_\pi(0) + \tfrac{1}{2} M_\pi(1), \tag{3}$$

$$M(\bar{\mathrm{p}}+\mathrm{p} \to \pi^0 + \pi^0) = -\frac{1}{\sqrt{6}} M_\pi(0), \tag{4}$$

$$M(\bar{\mathrm{p}}+\mathrm{n} \to \pi^- + \pi^0) = M(\bar{\mathrm{n}}+\mathrm{p} \to \pi^+ + \pi^0) = \frac{1}{\sqrt{2}} M_\pi(1), \tag{5}$$

$$M(\bar{\mathrm{p}}+\mathrm{p} \to \mathrm{K}^- + \mathrm{K}^+) = \tfrac{1}{2} M_{\mathrm{K}}(0) + \tfrac{1}{2} M_{\mathrm{K}}(1), \tag{6}$$

$$M(\bar{\mathrm{p}}+\mathrm{p} \to \bar{\mathrm{K}}^0 + \mathrm{K}^0) = \tfrac{1}{2} M_{\mathrm{K}}(0) - \tfrac{1}{2} M_{\mathrm{K}}(1), \tag{7}$$

$$M(\bar{\mathrm{p}}+\mathrm{n} \to \mathrm{K}^- + \mathrm{K}^0) = M(\bar{\mathrm{n}}+\mathrm{p} \to \bar{\mathrm{K}}^0 + \mathrm{K}^+) = M_{\mathrm{K}}(1). \tag{8}$$

If $\bar{\mathrm{p}}+\mathrm{p}$ is replaced by $\bar{\mathrm{n}}+\mathrm{n}$ anywhere above, the coefficient of the $T = 1$ amplitude changes sign. We suppose the reaction angle θ is defined in each case

† The $\bar{\mathrm{N}}\mathrm{N}$ parity is odd; the $\pi\pi$ parity is even. We assume charged and neutral K-mesons have the same parity, as is necessary if they are to form an isobaric multiplet; however, the other possibility is briefly considered at the end of sect. 4.

†† The nucleons N and $\bar{\mathrm{N}}$ are represented by $\binom{\mathrm{p}}{\mathrm{n}}$ and $\binom{\bar{\mathrm{n}}}{-\bar{\mathrm{p}}}$, so that the same isobaric spin operators serve for both [4, 5]); similarly for K and $\bar{\mathrm{K}}$.

between the first meson and the antinucleon, e.g. between π^- and $\bar{\mathrm{p}}$ in eq. (3); if two pions are interchanged, the $T = 1$ coefficient changes sign.

Electromagnetic effects violate charge independence and are ignored in eqs. (3)—(8). A way to allow for them approximately is given in sect. 3.

3. Partial Wave Decomposition

Analyzing in terms of angular momentum, we find

$$M_{SS_3} = \sum_{J,L,S} \frac{1}{\sqrt{kk'}} (i)^{L-J-1} \sqrt{(2L+1)\pi} (LSJS_3|LS0S_3) R_{LSJ} Y_{JS_3}(\theta, \phi), \quad (9)$$

where S and S_3 denote the $\bar{\mathrm{N}}+\mathrm{N}$ spin and 3-component, R_{LSJ} is the S-matrix element for annihilation from a state of total angular momentum J, orbital angular momentum L and spin S, restricted by unitarity to $|R_{LSJ}| \leqq 1$, Y_{JS_3} is a spherical harmonic and $(LSJS_3|LS0S_3)$ is a Clebsch-Gordan coefficient. The element M_{SS_3} is one previously written M_s, M_1, M_0, M_{-1}.

Parity conservation requires that we sum only over $J = L \pm 1$; it may then be verified that eqs. (2) and (9) agree. For pions, Bose statistics further require that $M_\pi(0)$ and $M_\pi(1)$ have summations only over J even and J odd, respectively. For K-mesons there is no such restriction. Other invariance considerations [4–8]) add no more selection rules.

We can now include electromagnetic corrections to charge independence, if we assume they appear mainly through long-range Coulomb forces and have negligible effect on the wave function in the region of nuclear interaction †. Then the only correction is the appearance of Coulomb phase shifts in the partial wave amplitude, which is related to the "pure nuclear" amplitude ($e^2 = 0$) as follows:

$$R_{LSJ}(e^2 \neq 0) = R_{LSJ}(e^2 = 0) e^{i(\sigma_L + \sigma_J)}. \quad (10)$$

The Coulomb phase shifts for the ingoing and outgoing channels are denoted by σ_L and σ_J, to be put zero where appropriate. This treatment of Coulomb corrections is similar to that used in N—N scattering (see e.g. ref. [9])).

Small mass differences, presumably electromagnetic, will affect cross sections at a given total c.m. energy through the factor k'/k, for initial and final phase space, in eq. (1); corrections are at most a few percent. The effect on transition matrix elements is unknown and must be neglected.

4. Illustration: The Ball-Chew Model

According to the model of Ball and Chew [2]), $\bar{\mathrm{N}}\mathrm{N}$ annihilation up to moderate energy (< 260 MeV) is significant in only a few partial waves. Those which

† This will not be true for $\bar{\mathrm{p}}+\mathrm{p}$ at very low energy.

can contribute to the pion modes are $^3P_0$ and $^3P_2$ for $T = 0$ and $^3S_1$ for $T = 1$; $^3S_1$—$^3D_1$ and $^3P_2$—$^3F_2$ mixing are supposed unimportant. For brevity, let us denote the corresponding amplitudes by R_0, R_2 and R_1, respectively (according to the label J, suppressing L, S and T).

Consider first $\bar{p}+p \to \pi^-+\pi^+$, the easiest mode to detect. From eqs. (1), (3) and (9) we find the unpolarized cross section

$$\begin{aligned}\sigma_0(\theta) &= \frac{k'}{4k}(|M_1|^2+|M_0|^2+|M_{-1}|^2)\\ &= \frac{1}{64k^2}\{3|R_1|^2+\tfrac{1}{3}|\sqrt{2}R_0-\sqrt{5}R_2|^2+2\cos\theta\,\mathrm{Re}\,R_1^*(\sqrt{2}R_0+2\sqrt{5}R_2)\\ &\qquad +\cos^2\theta(5|R_2|^2+2\sqrt{10}\,\mathrm{Re}\,R_0^*R_2)\}.\end{aligned} \tag{11}$$

Suppose now the incident $\bar{p}$ has polarization $\mathbf{P}$. Then the density matrix is $\rho = 1+\mathbf{P}\cdot\boldsymbol{\sigma}^{(1)}$, where $\boldsymbol{\sigma}^{(1)}$ is the $\bar{p}$ spin operator. The cross section becomes

$$\sigma(\theta,\phi) = \sigma_0(\theta)(1+A(\theta)\mathbf{P}\cdot\mathbf{N}), \tag{12}$$

where $\mathbf{N}$ is a unit vector along $\mathbf{k}\times\mathbf{k}'$. The term $A(\theta)$ describes an azimuthal asymmetry and is at $\phi = 0$ given by

$$\begin{aligned}\sigma_0(\theta)A(\theta) &= \frac{k'}{\sqrt{2}k}\,\mathrm{Im}\,(M_1M_0^*)|_{\phi=0}\\ &= \frac{1}{32k^2}\sin\theta\,\mathrm{Im}\{R_1^*(\sqrt{2}R_0-\sqrt{5}R_2)-\sqrt{10}R_0^*R_2\cos\theta\}.\end{aligned} \tag{13}$$

The same results (12) and (13) follow if $\mathbf{P}$ refers to polarization of the target proton instead. The term $A(\theta)$ is essentially the analyzing power of the reaction for $\bar{p}$ or p polarization. Note that if π^- and π^+ were hard to distinguish in a particular experiment, their summed cross sections $\sigma(\theta,\phi)+\sigma(\pi-\theta,\pi+\phi)$ would still have an asymmetry in general, from the $\sin\theta\cos\theta$ term in eq. (13).

Similarly, we could discuss more remote possibilities, with both $\bar{p}$ and p polarized. However, in the present example $\sigma_0(\theta)$ and $A(\theta)$ are enough to determine M within a phase (though perhaps not uniquely), for the five coefficients in their angular distributions are independent functions of the moduli and relative phases of the three R_J.

Consider now $\bar{n}+p \to \pi^+ + \pi^0$ and $\bar{p}+n \to \pi^- + \pi^0$. Though harder to observe, these cases are much simpler theoretically, since only R_1 can contribute (compare eqs. (3) and (5)). Putting $R_0 = R_2 = 0$ and replacing $\frac{1}{2}R_1$ by $R_1/\sqrt{2}$ in eqs. (11) and (13), we see that $\sigma_0(\theta)$ is isotropic and $A(\theta) = 0$. Similarly, we can modify eqs. (11) and (13) to describe other pion modes, interpreting the R_J by eq. (10) in each case.

The K-meson modes are not restricted by Bose statistics and more partial waves contribute. For instance, with the Ball-Chew model, both $^3S_1$ and $^3P_2$

can contribute to the $T = 1$ process $\bar{p}+n \to K^-+K^0$ (the angular distributions can again be deduced from eqs. (11) and (13)), which is therefore less simple than the $\pi^-+\pi^0$ case above. Similarly, up to four partial waves contribute in $T = 0$ states, compared with two for pions.

Finally, we mention the possibility that charged and neutral K-mesons have opposite parities [10]). If so, eq. (2) is false for annihilation to one of each kind (we have $Q = D+E\boldsymbol{\sigma}\cdot\mathbf{k}\times\mathbf{k}'$ instead) and eq. (9) has summation only over $J = L$. Also charge independence is violated. If we still take the charge-independent Ball-Chew model as qualitatively true, $\bar{p}+n$ and $\bar{n}+p$ annihilation to K-mesons proceeds from $^1S_0$, $^1P_1$ and $^3P_1$ states. The unpolarized cross section and dependence on $\bar{p}$ polarization are qualitatively similar to the equal-parity case, but the asymmetries for $\bar{p}$ and n polarizations now have opposite signs. In principle the K^-K^0 parity could be determined from such annihilation processes, but this seems highly impractical.

If the Ball-Chew model were wrong in postulating a short-range annihilation region [11]), we should expect higher partial waves to contribute to M and higher terms to appear in the angular distributions. Conversely, if such higher terms appeared in experiment, they would suggest longer-range annihilation, assuming the two-meson modes were not exceptional.

References

1) F. Solmitz, Report 1960 Rochester Conf. on high energy physics
2) J. S. Ball and G. F. Chew, Phys. Rev. **109** (1958) 1385;
J. S. Ball ond J. R. Fulco, Phys. Rev. **113** (1959) 647
3) W. R. Frazer and J. R. Fulco, Phys. Rev. **117** (1960) 1603
4) H. A. Bethe and J. Hamilton, Nuovo Cim. **4** (1956) 1
5) T. D. Lee and C. N. Yang, Nuovo Cim. **3** (1956) 749
6) D. Amati and B. Vitale, Nuovo Cim. **2** (1955) 719
7) R. Gatto, Nuovo Cim. **4** (1956) 526
8) C. Goebel, Phys. Rev. **103** (1956) 258
9) R. J. N. Phillips, Rep. Prog. Phys. **22** (1959) 562
10) A. Pais, Phys. Rev. **112** (1958) 624
11) M. Lévy, Phys. Rev. Letters **5** (1960) 380

7.A

Nuclear Physics **25** (1961) 353—367; © *North-Holland Publishing Co., Amsterdam*

Not to be reproduced by photoprint or microfilm without written permission from the publisher

ON A SYMMETRICAL SCHEME OF INTEGRAL EQUATIONS FOR SPECTRAL FUNCTIONS

K. TER-MARTIROSYAN

Theoretical and Experimental Physics Institute of the Academy of Sciences of the USSR, Moscow, USSR

Received 16 September 1960

Abstract: A self-contained set of integral equations for the spectral functions of the scattering amplitudes has been obtained in two-particle approximation. The equations are perfectly symmetrical with respect to the three channels of the "four-tail" vertex; if the Mandelstam spectral representations is written with allowances for the subtraction, there arises a coupled set of equations connecting the spectral functions of two types: depending on two variables and on one variable.

The iteration of the equations over the coupling constants yields the contribution of a class of renormalized Feynman graphs consisting in each part of two parts connected by two lines (only a portion of the contribution of these graphs is adequately taken into account, viz. that which has singularities at the two-particle production threshold). If the spectral functions depending on two variables are neglected, there remain the equations of the type obtained by Chew and Mandelstam and by Cini and Fubini.

1. Introduction

A very stimulating scheme of the quantum field theory based directly on the unitarity and the analyticity properties of the amplitudes has begun to be evolved of late. Mandelstam [1–3]) has proposed a double spectral representation for the amplitudes of the transition of two particles into two particles ("four-tails", fig. 1) and showed that from the unitarity condition one can derive a set of integral relations for the spectral functions of this representation.

Fig. 1. "Four-tails": the amplitude of the processes
$a+b \rightleftarrows c+d$, $a+d \rightleftarrows b+c$ and $a+c \rightleftarrows b+d$.

Below it will be shown that these relations can be written in the form of a closed set of integral equations perfectly symmetrical with respect to three channels of the "four-tail" amplitude. With the subtraction taken into account, there arises a set of coupled equations for the spectral functions of two types: depending on two variables and on one variable.

If the terms containing spectral functions depending on two variables are

neglected, the resulting set of equations becomes similar to those obtained by Chew and Mandelstam [4]) for the particular case of the π–π interaction amplitude.

2. Equations for Spectral Functions

Consider the amplitude A, the "four-tails" of fig. 1, which determines (in three channels) the transitions between four arbitrary particles a, b, c and d.

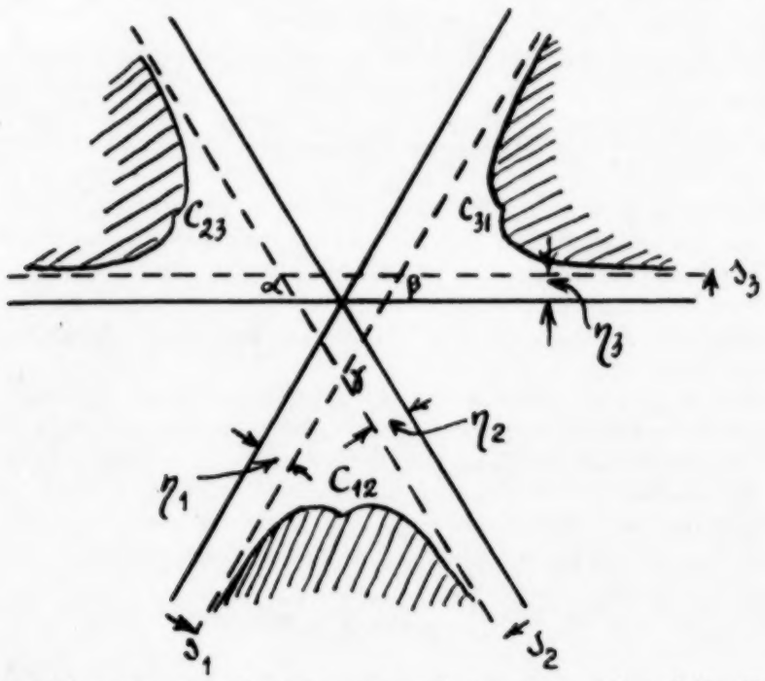

Fig. 2. A system of triangular coordinates s_1, s_2, $s_3 (s_1+s_2+s_3 = \gamma)$ and the lines of the nearest singularities of the amplitude A; through η_1, η_2 and η_3 are designated the nearest thresholds of the production of two particles in each of the three channels. The spectral functions A_{ij} differ from zero in cross-hatched non-physical regions.

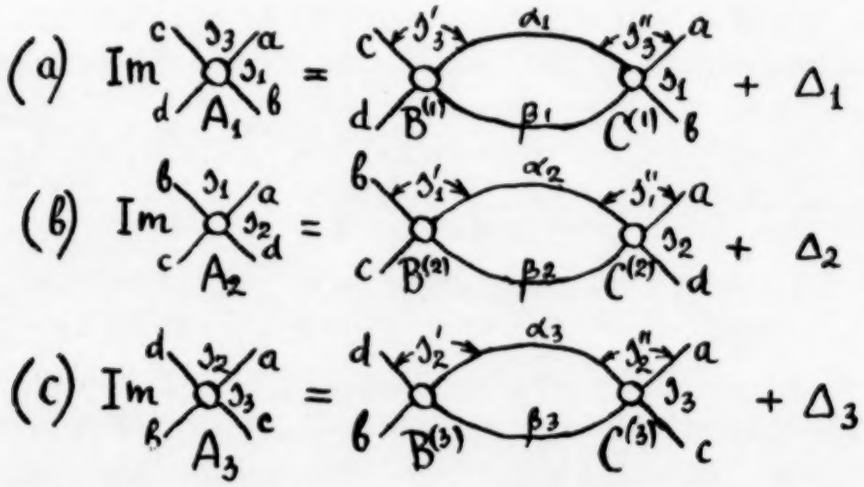

Fig. 3. The unitarity conditions for three channels. By Im on the left-hand side are designated the absorptive parts of amplitudes. Arrows indicate the square of the sum of which momenta corresponds to each of the invariants s'_j and s''_j on which the amplitudes $B^{(i)}$ and $C^{(i)}$ depend. The numbering of the channels of these amplitudes corresponds to the notations indicated.

It depends on three invariants $s_1 = (p_a+p_b)^2$, $s_2 = (p_a+p_d)^2$ and $s_3 = (p_a+p_c)^2$, which are the squares of the energy of the particles (in the centre-of-mass system) in the first, second and third channels. The sum $s_1+s_2+s_3 = \gamma$ is a constant equal to the sum of the squares of the masses of the particles ($\gamma = m_a^2+m_b^2+m_c^2+m_d^2$) and therefore it is convenient to consider the amplitude A in the triangular coordinates of fig. 2 as a function of the position of the point $\xi = (s_1, s_2, s_3)$ on the plane of fig. 2.

According to fig. 3, the unitarity conditions written for each of the three channels of the amplitude are of the form

$$A_1(s_1, s_2, s_3) = \zeta_1(s_1)\int B^{(1)*}(s_1, s'_2, s'_3)C^{(1)}(s_1, s''_2, s''_3)\frac{d\mathbf{n}_1}{4\pi}+\Delta_1(s_1, s_2, s_3),$$

$$A_2(s_1, s_2, s_3) = \zeta_2(s_2)\int B^{(2)*}(s'_1, s_2, s'_3)C^{(2)}(s''_2, s_2, s''_3)\frac{d\mathbf{n}_2}{4\pi}+\Delta_2(s_1, s_2, s_3), \quad (1)$$

$$A_3(s_1, s_2, s_3) = \zeta_3(s_3)\int B^{(3)*}(s''_1, s''_2, s_3)C^{(3)}(s''_1, s''_2, s_3)\frac{d\mathbf{n}_3}{4\pi}+\Delta_3(s_1, s_2, s_3).$$

Let us first explain the notations in the first of these three equations. The left-hand side of it contains the quantity $A_1(s_1, s_2, s_3) = [A(s_1+i\tau, s_2, s_3)-A(s_1-i\tau, s_2, s_3)]/2i$ (where $\tau \to 0$, $\tau > 0$), which is the absorptive part of the amplitude in the first channel; the first term in the right-hand side denotes the contribution from the states with two particles and the term Δ_1 is the contribution from the states with more than two particles. The quantity Δ_1 vanishes if s_1 is below the production threshold of three particles (or four particles, if the production of three particles in the first channel is forbidden by the conservation laws). By $C^{(1)}$ is designated (according to fig. 3a) the amplitude of the transition $a+b \to \alpha_1+\beta_1$ and by $B^{(1)}$ that of the transition $c+d \to \alpha_1+\beta_1$, where α_1 and β_1 is any pair of particles into which the particles a, b (or c, d) can be converted in the interaction. It is assumed that the quantity $B^{(1)*}C^{(1)}$ in (1) is summed over all possible types of pairs of particles α_1 and β_1; for the sake of brevity (here and further on) this summation is not indicated †.

Integration in the first term on the right-hand side of the first equation of (1) is performed over the directions $\mathbf{n}_1$ of the momentum $\mathbf{q}_{\alpha_1\beta_1}$ of the particle α_1 in the c.m. system. It is on this direction that the invariants

$$s'_2 = (p_{\alpha_1}+p_d)^2, \quad s'_3 = (p_{\alpha_1}+p_c)^2, \quad s''_2 = (p_a-p_{\alpha_1}), \quad s''_3 = (p_b-p_{\alpha_1})^2$$

depend. The factor $\zeta_1(s_1)$ determines the statistical weight of the states of the particles α_1 and β_1 and depends on the normalization of the amplitudes. If, for example, all amplitudes are normalized so that the cross sections $d\sigma_1/d\Omega_1$ (of

† In particular, if the particles α_1 and β_1 have non-zero spins the quantity $B^{(1)*}C^{(1)}$ in (1) has to be summed over all spin states. In the following we shall assume that all particles are zero-spin bosons. Taking account of the spin does not lead to any difficulties, but essentially complicates all equations.

the transition a+b → c+d) in the first channel are connected with the amplitudes through the relations of the type $(d\sigma_1/d\Omega_1) = s_1^{-1}|A|^2$, then

$$\zeta_1(s_1) = (\kappa_1 s_1^{\frac{1}{2}})^{-1} q_{\alpha_1\beta_1},$$

where $q_{\alpha_1\beta_1} = |\mathbf{q}_{\alpha_1\beta_1}|$, and $\kappa_1 = 2$ if α_1 and β_1 are identical particles and $\kappa_1 = 1$ if they are different.

In the two last equations (1) all notations are perfectly similar; in particular, each of the quantities Δ_2 and Δ_3 turns into zero if the energy (s_2 or s_3) of the particles in the corresponding channels is below the threshold of the production of three (or four) particles. The amplitudes $B^{(2)}$, $C^{(2)}$ and $B^{(3)}$, $C^{(3)}$ are determined, according to figs. 3b and 3c similarly to $B^{(1)}$ and $C^{(1)}$ (the values of the invariants on which they depend being indicated in the caption of fig. 3 and in the figure itself). In (1) as elsewhere below all relations are perfectly symmetrical with respect to three channels of the amplitude A: all relations for the second and third channels can be obtained from similar relations for the first channel by cyclically permuting all subscripts once ($1 \to 2$, $2 \to 3$, $3 \to 1$) and twice ($1 \to 3$, $2 \to 1$, $3 \to 2$).

It is convenient to write the three variables s_1, s_2 and s_3 (the coordinates of a point of the plane of fig. 2 on the position of which the amplitudes and their absorption parts depend), always in the sequence s_1, s_2, s_3, even after the above-mentioned permutations.

Below we shall confine ourselves to the "normal" relation [5]) of the mass of the particles when double integral Mandelstam representation holds for all "four-tail" amplitudes. With the help of this representation it is possible to represent (see ref. [2]), p. 1643, eqs. (2.8)–(2.10)) the left-hand side of eqs. (1) in the form of analytic functions of the square of the momentum transfer (e.g., in the form of analytic functions of the invariants s_3 and $s_2 = \gamma - s_1 - s_3$, for the case of the first of the relations (1)),

$$\begin{aligned}
A_1 &= \frac{1}{\pi}\int_0^\infty \frac{A_{31}(\sigma, s_1)}{\sigma - s_3}\,d\sigma + \frac{1}{\pi}\int_0^\infty \frac{A_{12}(s_1, \sigma)}{\sigma - s_2}\,d\sigma,\\
A_2 &= \frac{1}{\pi}\int_0^\infty \frac{A_{12}(\sigma, s_2)}{\sigma - s_1}\,d\sigma + \frac{1}{\pi}\int_0^\infty \frac{A_{23}(s_2, \sigma)}{\sigma - s_3}\,d\sigma, \qquad (2)\\
A_3 &= \frac{1}{\pi}\int_0^\infty \frac{A_{23}(\sigma, s_3)}{\sigma - s_2}\,d\sigma + \frac{1}{\pi}\int_0^\infty \frac{A_{31}(s_3, \sigma)}{\sigma - s_1}\,d\sigma
\end{aligned}$$

(everywhere the integration actually begins not from zero but from a certain value of the variable σ at which the spectral functions begin to differ from zero).

Mandelstam [1]) showed that the first term on the right-hand side of the first, second and third equations in (1) respectively can be reduced to exactly the

same form as in (2),

$$\begin{aligned}
&\frac{1}{\pi}\int_0^\infty \frac{Q_1(\sigma, s_1)}{\sigma - s_3}\,\mathrm{d}\sigma + \frac{1}{\pi}\int_0^\infty \frac{P_1(s_1, \sigma)}{\sigma - s_2}\,\mathrm{d}\sigma,\\
&\frac{1}{\pi}\int_0^\infty \frac{Q_2(\sigma, s_2)}{\sigma - s_1}\,\mathrm{d}\sigma + \frac{1}{\pi}\int_0^\infty \frac{P_2(s_2, \sigma)}{\sigma - s_3}\,\mathrm{d}\sigma,\\
&\frac{1}{\pi}\int_0^\infty \frac{Q_3(\sigma, s_3)}{\sigma - s_2}\,\mathrm{d}\sigma + \frac{1}{\pi}\int_0^\infty \frac{P_3(s_3, \sigma)}{\sigma - s_1}\,\mathrm{d}\sigma,
\end{aligned} \tag{3}$$

where

$$\begin{aligned}
Q_1(s_3, s_1) &= \frac{1}{\pi^2}\iint_0^\infty \Gamma_1(m', m''; s_3, s_1)[B_2^{(1)*} C_2^{(2)} + B_3^{(1)*} C_3^{(1)}]\mathrm{d}m'^2 \mathrm{d}m''^2,\\
P_1(s_1, s_2) &= \frac{1}{\pi^2}\iint_0^\infty \Gamma'_1(m', m''; s_2, s_1)[B_2^{1(*)} C_3^{(1)} + B_3^{(1)*} C_2^{(1)}]\mathrm{d}m'^2 \mathrm{d}m''^2,
\end{aligned} \tag{4}$$

and the values Q_2, P_2 and Q_3, P_3 follow hence after the cyclic permutation of all subscripts.

Let us explain the notations in (4). By $B_2^{(1)}$ the absorption part of the amplitude $B^{(1)}$ in the second channel is designated:

$$B_2^{(1)} = B_2^{(1)}(s_1, m'^2, \gamma'_1 - s_1 - m'^2)$$

(the variable s_2 is here replaced by m'^2, and s_3 by $\gamma'_1 - s_1 - m'^2$, where γ'_1 is the sum of the squares of the masses of the particles α_1, β_1, c, d). Similarly

$$B_3^{(1)} = B_3^{(1)}(s_1, \gamma'_1 - m'^2 - s_1, m'^2), \quad C_2^{(1)} = C_2^{(1)}(s_1, m''^2, \gamma''_1 - m''^2 - s_1),$$
$$C_3^{(1)} = C_3^{(1)}(s_1, \gamma''_1 - m''^2 - s_1, m''^2), \quad \gamma''_1 = m_a^2 + m_6^2 + m_{\alpha_1}^2 + m_{\beta_1}^2.$$

By $\Gamma_1(m', m''; s_3, s_1)$ is designated the spectral function (of the type A_{31}) of the Feynman graph † of fig. 4a and by $\Gamma''_1(m', m''; s_2, s_1)$ the spectral function

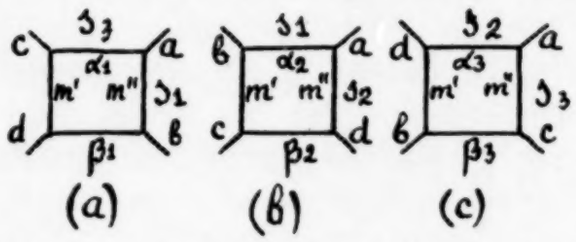

Fig. 4. Feynman's graphs the spectral functions of which are the quantities Γ_1, Γ_2 and Γ_3. The quantities Γ'_1, Γ'_2 and Γ'_3 correspond to the same graphs with the particles transmuted in the left-hand side of each of them (for example, the particles c and d in the graph for Γ_1).

of the same graph, but with the transposed particles c and d. Similar quantities Γ_2, Γ_3 and Γ'_2, Γ'_3 arise in (4) after the cyclic permuation of all subscripts;

† With the above-mentioned normalization $\Gamma_1 = -2\pi\kappa_1^{-1} A_{13}^{(0)}$, where $A_{13}^{(0)}$ is a quantity determined by eq. (3.25) of ref. [2]).

figs. 4b and 4c indicate the graphs whose spectral functions (of the type of A_{12} and A_{23}) are equal to the quantities Γ_2 and Γ_3 (the same graphs, but with transposed particles b, c and d, b on the left-hand side, correspond to the quantities Γ''_2 and Γ''_3).

The function $\Gamma_1(m', m''; s_3, s_1)$ does not vanish only in the region beyond the curve C'_1 in fig. 5; in particular it is certainly equal to zero if $s_3 < (m'+m'')^2$. Consequently, also the quantity $Q(s_3, s_1)$ does not vanish only in a certain part of the plane of fig. 6 of the variables s_3, s_1.

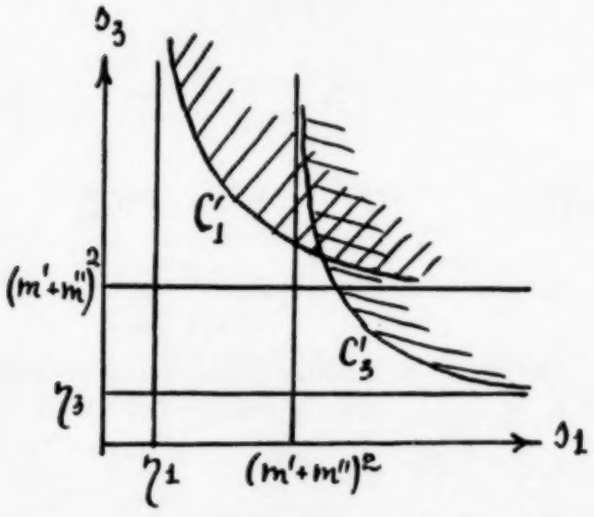

Fig. 5. The curves of the singularities of the graphs in fig. 4a (C'_1) and fig. 4c in which the particles d and b are permuted (C'_3). The quantities Γ_1 and Γ'_3 differ from zero in the cross-hatched region beyond these curves.

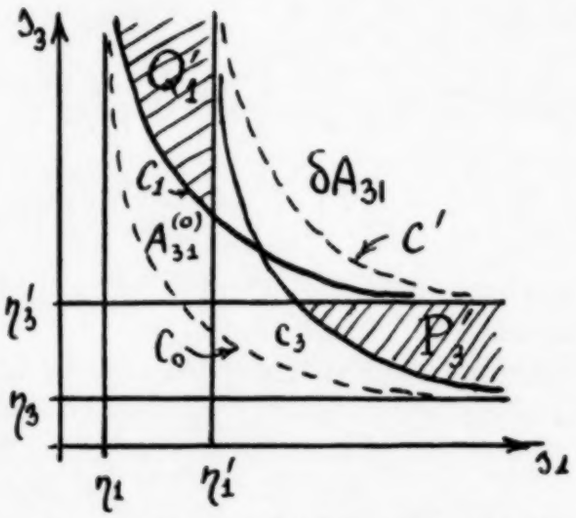

Fig. 6. Regions in which the quantities $A_{31}^{(0)}$ (beyond the curve C_0), $P'_3(s_3, s_1)$ (beyond the curve C_3) Q'_1 (beyond C_1) and δA_{31} (beyond C') differ from zero. Through η'_1 and η'_3 are designated the thresholds of the production of three (four) particles. Cross-hatched is the region in which the spectral function A_{31} is determined correctly (accurately within minor corrections) from eqs. (9) or (9′).

If the amplitudes $B^{(1)}$ and $C^{(1)}$ have pole terms, their absorptive parts ($B_2^{(1)}$, $B_3^{(1)}$, or $C_2^{(1)}$, $C_3^{(1)}$) can contain terms of the type $\pi g'^2\delta(m'^2-\mu_{\beta_3}^2)$, or $\pi g''^2\delta(m''^2-\mu_{\alpha_3}^2)$, where μ_{β_3} and μ_{α_3} are the masses of the bound states and g' and g'' are the coupling constants. A part of the integral (4) for Q_1, which contains the product of these δ functions and which is proportional to $\Gamma_1(\mu_{\beta_3}, \mu_{\alpha_3}; s_3, s_1)$, is the spectral function $A_{31}^{(0)}(s_3, s_1)$ of the graph of fig. 4a in which $m' = \mu_{\beta_3}$, $m'' = \mu_{\alpha_3}$. This part does not vanish in the region beyond the dotted curve C_0 in fig. 6. It will be noted that the same quantity $A_{31}^{(0)}$ is contained in the integral for $P_3(s_3, s_1)$ (its explicit form follows from (4) after the cyclic permutation of all subscripts),

$$P_3(s_3, s_1) = \frac{1}{\pi^2}\int\!\!\int_0^\infty \Gamma'_3(m', m''; s_1, s_3)[B_2^{(3)} * C_1^{(3)} + B_1^{(3)} * C_2^{(3)}]\mathrm{d}m'^2\mathrm{d}m''^2. \quad (4')$$

Here Γ'_3 is the spectral function of the little square of fig. 4c in which the particles b and d are transposed. It can readily be noticed that with the pole values $m' = \mu_{\beta_1}$ and $m'' = \mu_{\alpha_1}$ this graph exactly coincides with that of fig. 4a (in which $m' = \mu_{\beta_3}$, $m'' = \mu_{\alpha_3}$), i.e., $\Gamma'_3(\mu_{\beta_1}, \mu_{\alpha_1}; s_1, s_3) \equiv \Gamma_1(\mu_{\beta_3}, \mu_{\alpha_3}; s_3, s_1)$. Therefore the "pole" part of the integral (4') just as for the integral (4) for Q_1 is equal to the function $A^{(0)}_{31}$.

Separating the "pole" part we shall write Q_1 and P_3 in the form

$$\begin{aligned} Q_1(s_3, s_1) &= A^{(0)}_{31}(s_3, s_1) + Q'_1(s_3, s_1), \\ P_3(s_3, s_1) &= A^{(0)}_{31}(s_3, s_1) + P'_3(s_3, s_1), \end{aligned} \tag{5}$$

where Q'_1 and P'_3 are the parts of the integrals (4) and (4') in which at least one of the variables m'^2 or m''^2 is larger than the two-particle production threshold η. These parts of the integrals (4)–(4') will be denoted below by $(1/\pi^2)\iint_\eta^\infty \mathrm{d}m'^2\,\mathrm{d}m''^2$, e.g., $Q'_1 = (1/\pi^2)\iint_\eta^\infty$ [integrand of (4)] $\mathrm{d}m'^2\mathrm{d}m''^2$. It is obvious that in such integrals for Q'_1 and P'_3 the sum $(m'+m'')^2$ is never less than the production threshold of at least three particles η' †.

Fig. 5 represents the regions in which Γ_1 and Γ'_3 are different from zero; the functions Q'_1 and P'_3 do not vanish only in the regions beyond the curves C_1 and C_3 in fig. 6. In particular, the quantity $Q'_1(s_3, s_1)$ certainly equals zero if s_3 is below the production threshold of three particles and $P'_3(s_3, s_1)$ if s_1 is below it.

If the amplitudes $B^{(1)}$, $C^{(1)}$ and $B^{(3)}$, $C^{(3)}$ have no pole terms, the term $A^{(0)}_{31}$ is lacking in (5) and the curves C_1 and C_3 in fig. 6 approaches asymptotically (over one of the variables) the production threshold not of three but four particles. This takes place, for example, in the case of π–π or π–K scattering.

The quantities Δ_1, Δ_2 and Δ_3 which are equal, according to (1), to the difference between (2) and (3) can evidently also be written in a form quite similar to (2),

$$\begin{aligned} \Delta_1 &= \frac{1}{\pi}\int_0^\infty \frac{u_1(\sigma, s_1)}{\sigma - s_3}\,\mathrm{d}\sigma + \frac{1}{\pi}\int_0^\infty \frac{v_1(s_1, \sigma)}{\sigma - s_2}\,\mathrm{d}\sigma, \\ \Delta_2 &= \frac{1}{\pi}\int_0^\infty \frac{u_2(\sigma, s_2)}{\sigma - s_1}\,\mathrm{d}\sigma + \frac{1}{\pi}\int_0^\infty \frac{v_2(s_2, \sigma)}{\sigma - s_3}\,\mathrm{d}\sigma, \\ \Delta_3 &= \frac{1}{\pi}\int_0^\infty \frac{u_3(\sigma, s_3)}{\sigma - s_2}\,\mathrm{d}\sigma + \frac{1}{\pi}\int_0^\infty \frac{v_3(s_3, \sigma)}{\sigma - s_1}\,\mathrm{d}\sigma, \end{aligned} \tag{6}$$

where $u_i(\sigma, s_i)$ and $v_i(s_i, \sigma)$ (similarly to A_{ij}, or Q_i, P_i) are real functions non-vanishing only in the region of values s_i ($i = 1, 2, 3$) above the threshold of the production of three particles.

From (1), (2), (3) and (6) obviously follow six equations for three spectral

† The sum $(m'+m'')^2$ is equal to this threshold η' if one of the variables, m'^2, for example, has a pole value and the other is equal to the two-particle production threshold η.

functions: two equations for each function. Let us write these equations for the function $A_{31}(s_3, s_1)$:

$$\begin{aligned} A_{31}(s_3, s_1) &= Q_1(s_3, s_1)+u_1(s_3, s_1), \\ A_{31}(s_3, s_1) &= P_3(s_3, s_1)+v_3(s_3, s_1). \end{aligned} \tag{7}$$

They follow from the unitarity conditions (1) for the first and third channels. Similar equations for A_{12} and A_{23} can hence be obtained by cyclical permutation of all subscripts. If the amplitudes $B^{(i)}$ and $C^{(i)}$ $(i = 1, 2, 3)$ have pole terms, it is convenient to isolate the quantity $A_{31}^{(0)}$ subtracting it from both parts of eq. (7). As a result we have

$$\begin{aligned} A'_{31}(s_3, s_1) &= Q'_1(s_3, s_1)+u_1(s_3, s_1), \\ A'_{31}(s_3, s_1) &= P'_3(s_3, s_1)+v_3(s_3, s_1), \end{aligned} \tag{7'}$$

where

$$A'_{31} = A_{31}-A_{31}^{(0)}. \tag{5'}$$

The quantities Q'_1 and P'_3 in (7') shall be regarded as known: the two equations of (7') having the following general solution for three unknowns A'_{31}, u_1 and v_3:

$$\begin{aligned} A'_{31} &= (P'_3+Q'_1)+\delta A_{31}, \\ u_1 &= P'_3+\delta A_{31}, \quad v_3 = Q'_1+\delta A_{31}, \end{aligned} \tag{8}$$

where δA_{31} is a certain function whose form cannot be found from (7). It is essential that δA_{31} vanishes if at least one of the two variables s_3 or s_1 is below the threshold of the production of three particles. Indeed, if s_1 is below this threshold, then $u_1 \equiv P'_3 \equiv 0$ and if s_3 is, then $v_3 \equiv Q'_1 \equiv 0$. In both cases, δA_{31}, according to (8), is equal to zero. The region in which the function δA_{31} does not vanish is limited in fig. 6 by the dotted curve C'. Therefore in two-particle approximation the term δA_{31} in (8) should not be taken into account at all (the quantity δA_{31} can be found if all terms corresponding to the production of three and more particles are fully taken into account in the unitarity conditions).

Omitting the term δA_{31} we obtain for A_{31} from (8), (5) and (5') a value which contains no unknowns at all. Together with analogous values of the functions A_{12} and A_{23} (which follow from the formula for A_{31}, after a cyclic permutation of subscripts) we obtain the following set of equations:

$$A_{31} = -A_{31}^{(0)}+P_3+Q_1, \quad A_{12} = -A_{12}^{(0)}+P_1+Q_2, \quad A_{23} = -A_{23}^{(0)}+P_2+Q_3. \tag{9}$$

Let us write this set in detail by substituting the values of the type (4) and (4') of the quantities P_i and Q_i:

$$A_{31} = -A_{31}^{(0)} + \frac{1}{\pi^2}\iint_0^\infty \{\Gamma'_3(B_1^{(3)*}C_2^{(3)}+B_2^{(3)*}C_1^{(3)}) + \Gamma_1(B_2^{(1)*}C_2^{(1)}+B_3^{(1)*}C^{(1)})\}\mathrm{d}m'^2\mathrm{d}m''^2,$$

$$A_{12} = -A_{12}^{(0)} + \frac{1}{\pi^2}\iint_0^\infty \{\Gamma'_1(B_2^{(1)*}C_3^{(1)}+B_3^{(1)*}C_2^{(1)}) + \Gamma_2(B_3^{(2)*}C_3^{(2)}+B_1^{(2)*}C_1^{(2)})\}\mathrm{d}m'^2\mathrm{d}m''^2, \qquad (9')$$

$$A_{23} = -A_{23}^{(0)} + \frac{1}{\pi^2}\iint_0^\infty \{\Gamma'_2(B_3^{(3)*}C_1^{(2)}+B_1^{(2)*}C_3^{(2)}) + \Gamma_3(B_1^{(2)*}C_1^{(3)}+B_2^{(3)*}C_2^{(3)})\}\mathrm{d}m'^2\mathrm{d}m''^2.$$

Dependent on the variables m'^2 and m''^2 are all absorptive parts of the amplitudes $B^{(i)}$ and $C^{(i)}$ (see above) as well as the spectral functions $\Gamma_i(m', m''; s_j, s_i)$ and $\Gamma''_i(m', m''; s_j, s_i)$ of the graphs of figs. 4a, b and c and the same graphs, but with the particles transposed in the left-hand part of each graphs.

Eqs. (9') can be regarded as a complete set of equations if they are complemented with analogous relations for the spectral functions of all amplitudes $B^{(i)}$ and $C^{(i)}$ (where $i = 1, 2, 3$) and if use is made of formulas of the type (2) connecting the absorptive parts of the amplitudes with the spectral functions.

The region of fig. 4 in which the spectral functions are determined correctly (with the accuracy of small corrections) by the set of equations (9') is cross-hatched.

3. Equations for Spectral Functions with Allowances for Subtraction

With the subtraction taken into account, instead of the first of the equations (2) we obtain the relation (see ref. [2]), eqs. (2.8a), (2.10a))

$$A_1 = a_1(s_1) + \frac{1}{\pi}\int_0^\infty [\varphi(\sigma, s_3)A_{31}(\sigma, s_1)+\varphi(\sigma, s_2)A_{12}(s_1, \sigma)]\mathrm{d}\sigma, \qquad (10)$$

where

$$\varphi(\sigma, s_3) = \frac{1}{\sigma - s_3} - \frac{1}{\sigma - s_{30}} = \frac{s_3 - s_{30}}{(\sigma - s_3)(s - s_{30})},$$

$\varphi(\sigma, s_1)$ having a similar value. Here $a_1(s_1)$ is a real spectral function depending on one variable. By s_{10}, s_{20}, and s_{30} ($s_{10}+s_{20}+s_{30} = \gamma$) are designated the values of the invariants at the point in which the subtraction is performed.

Similarly, instead of the first of the equations (6) with the subtraction taken into account, we obtain the following relation:

$$\Delta_1 = \delta a_1(s_1) + \frac{1}{\pi}\int_0^\infty [\varphi(\sigma, s_3)u_1(\sigma, s_1)+\varphi(\sigma, s_2)v_1(s_1, \sigma)]\mathrm{d}\sigma. \qquad (11)$$

Here $\delta a_1(s_1)$ is a real (as can be shown) function non-vanishing only in the region of values s_1 above the threshold of the production of three (four) particles.

Representations similar to (10) and (11) for A_2, A_3 and Δ_2, Δ_3 obviously follow from (10) and (11) after a cyclic permutation of all subscripts.

A single spectral representation of the amplitude taking account of the subtraction is also of a form similar to (10),

$$A = F_1(s_1) + \frac{1}{\pi}\int_0^\infty [\varphi(\sigma, s_3)A_3(s_1, \gamma - s_1 - \sigma, \sigma) + \varphi(\sigma, s_2)A_2(s_1, \sigma, \gamma - s_1 - \sigma)]\mathrm{d}\sigma, \quad (12)$$

where

$$F_1(s_1) = a_0 + \frac{1}{\pi}\int_0^\infty \varphi(\sigma, s_1)a_1(\sigma)\mathrm{d}\sigma + \frac{1}{\pi^2}\int\int_0^\infty \frac{(s_1 - s_{10})A_{23}(\sigma, \sigma')\mathrm{d}\sigma\mathrm{d}\sigma'}{(\gamma - s_1 - \sigma - \sigma')(\sigma - s_{20})(\sigma' - \sigma_{30})}. \quad (12a)$$

Two other similar representations can hence be obtained by a cyclic permutation of all subscripts. By a_0 is here designated the value of A at the point $\xi_0 = (s_{10}, s_{20}, s_{30})$, ($a_0$ being real if the point ξ_0 in fig. 2 is chosen within the triangle $\alpha\beta\gamma$). It can be directly checked that the substitution of the representations (10) (written for A_2 and A_3) into (12) leads to the double Mandelstam spectral representation of well-known form (see ref. [2]), eq. (2.13)).

A simple analysis will show [6]) that taking account of the subtraction does not change the form of eq. (9'). The change reduces itself to the absorptive parts of the amplitudes $B^{(i)}$ and $C^{(i)}$ on the right-hand side of (9') being connected, when the subtraction is taken into account, with their spectral functions through relations of the form (10). For the set of equations to be complete (i.e., to contain as many equations as there are unknown functions) it is necessary to have equations also for the functions a_1, a_2 and a_3 apart from (9).

These equations can be obtained by averaging the eq. (1) of unitarity over the directions of the momenta of the particles in the final state (in the c.m.s.) in each of the three channels.

Let us designate by $z_i = \cos\vartheta_i$ the cosine of the angle between the directions of the momenta of particles (in the c.m.s.) in the initial and final states in channel i.

Let us first consider the first channel. Here we have

$$\cos\vartheta_1 = \mathbf{q}_{ab}\mathbf{q}_{cd}/q_{ab}q_{cd},$$

where $\mathbf{q}_{ab}$ is the momentum of the particle a and $\mathbf{q}_{cd}$ is the momentum of the particle c (all momenta are in the c.m.s.). Let us designate the average value over $z_1 = \cos\vartheta_1$ of the quantity A, A_1, $B^{(1)}$, $C^{(1)}$ and Δ_1 respectively through $\langle A(s_1)\rangle_1$, $\langle A_1(s_1)\rangle_1$, $\langle B^{(1)}(s_1)\rangle$, $\langle C^{(1)}(s_1)\rangle_1$ and $\langle \Delta_1(s_1)\rangle_1$. All these quantities depend on the energy s_1 of particles in the first channel.

From the representation (12), (10) and (11) with averaging over z_1, it obviously follows †

$$\langle A(s)\rangle_1 = F_1(s) + \frac{1}{\pi}\int_0^\infty [l_3(\sigma, s)A_3(s, \gamma-s-\sigma, \sigma)+l_2(\sigma, s)A_2(s, \sigma, \gamma-s-\sigma)]\mathrm{d}\sigma, \tag{13}$$

$$\langle A_1(s)\rangle_1 = a_1(s) + \frac{1}{\pi}\int_0^\infty [l_3(\sigma, s)A_{31}(\sigma, s)+l_2(\sigma, s)A_{12}(\sigma, s)]\mathrm{d}\sigma, \tag{14}$$

$$\langle A_1(s)\rangle_1 = \delta a_1(s) + \frac{1}{\pi}\int_0^\infty [l_3(\sigma, s)u_1(\sigma, s_1)+l_2(\sigma, s)v_1(s, \sigma)]\mathrm{d}\sigma. \tag{15}$$

Here $l_3(\sigma, s_1)$ is the average over $z_1 = \cos\vartheta_1$ of the function $\varphi(\sigma, s_3)$,

$$l_3(\sigma, s_1) = (4q_{ab}q_{cd})^{-1}\ln\frac{\sigma-s_3^{\mathrm{I}}}{\sigma-s_3^{\mathrm{II}}} - \frac{1}{\sigma-s_{30}}$$

and

$$s_3^{\mathrm{I,II}} = (\sqrt{\mu_a^2+q_{ab}^2} - \sqrt{\mu_a^2+q_{cd}^2})^2-(q_{ab}\pm q_{cd})^2.$$

The plus sign refers to the subscript I and the minus sign to the subscript II. The function $l_2(\sigma, s_1) = \langle\varphi(\sigma, s_2)\rangle_1$ has a similar value.

Averaging the first of the unitarity equations (1) over z_1 we obtain

$$\langle A_1(s)\rangle_1 = \zeta_1(s)\langle B^{(1)}(s)\rangle_1{}^*\langle C^{(1)}(s)\rangle+\langle \Delta_1(s)\rangle_1.$$

With the help of (14) and (15) and the relations of the form (7) this equation can easily be reduced to the form

$$a_1(s)+\frac{1}{\pi}\int_0^\infty [l_3(\sigma, s)Q_1(\sigma, s)+l_2(\sigma, s)P_1(s, \sigma)]\mathrm{d}\sigma = \zeta_1(s)\langle B^{(1)}(s)\rangle_1{}^*\langle C^{(1)}(s)\rangle_1+\delta a_1(s).$$

All terms on both sides of this equation with the exception of the quantity $\delta a_1(s)$ are in general different from zero in the region of values s above the threshold of production of two particles. The quantity δa_1 becomes different from zero only in a region above the production threshold of three (or four) particles. In two-particle approximation this quantity cannot be found and should not be taken into account, just as the quantity δA_{31} in eq. (8). Discarding the term δa_1 we obtain for $a_1(s)$ an equation without unknown quantities.

Let us write this equation for a_1 together with two others for a_2 and a_3,

† For the sake of brevity the subscript i of the variable s_i will sometimes be dropped; for example, in (13)–(15) s is written instead of s_1.

which follow from the first one after a cyclic permutation of all subscripts:

$$a_1(s)+\frac{1}{\pi}\int_0^\infty [l_3(\sigma,s)Q_1(\sigma,s)+l_2(\sigma,s)P_1(s,\sigma)]\mathrm{d}\sigma=\zeta_1(s)\langle B^{(1)}(s)\rangle_1{}^*\langle C^{(1)}(s)\rangle_1,$$

$$a_2(s)+\frac{1}{\pi}\int_0^\infty [l_1(\sigma,s)Q_2(\sigma,s)+l_3(\sigma,s)P_2(s,\sigma)]\mathrm{d}\sigma=\zeta_2(s)\langle B^{(2)}(s)\rangle_2{}^*\langle C^{(2)}(s)\rangle_2, \quad (16)$$

$$a_3(s)+\frac{1}{\pi}\int_0^\infty [l_2(\sigma,s)Q_3(\sigma,s)+l_3(\sigma,s)P_3(s,6)]\mathrm{d}\sigma=\zeta_3(s)\langle B^{(3)}(s)\rangle_3{}^*\langle C(s)\rangle_3.$$

The set of integral equations (9′) and (16) determine all spectral functions of the "four-tail" amplitudes connected with each other through the relations of unitarity of the form of fig. 3. Obviously it is assumed that the equations of the form (16) are written not only for the amplitude A but also for all amplitudes $B^{(i)}$, $C^{(i)}$, while the averages $\langle B^{(i)}(s)\rangle_i$ and $\langle C^{(i)}(s)\rangle_i$ are determined by formulas of the form (13) (if N "four-tails" are connected in (1), there will be $6N$ equations of the form (9′) and (16) for $6N$ unknown functions).

4. Iteration Solution and Equations of the Chew-Mandelstam and Cini-Fubini Type

The solution of eqs. (9′) and (16) can easily be found in the form of series in powers of coupling constants. For the sake of simplicity let us consider the case when there are no pole terms in any amplitudes (the case when there are pole terms do not differ in principle). The coupling constants will be the values a_0, $b_0{}^{(i)}$ and $c_0{}^{(i)}$ of the amplitudes A, $B^{(i)}$ and $C^{(i)}$ at the point in which the subtraction is performed. From (16) and (9′) it follows that the spctral functions a_i will be quantities of the second order with respect to these constants, and A_{ij} of the fourth order.

In the first approximation † from (16) we obtain

$$a_i(s)=\zeta_i(s)b_0{}^{(i)*}c_0{}^{(i)}. \quad (17)$$

The simplest graphs of fig. 7a correspond to this value. From (10) it follows that in the same approximation the absorptive parts of all amplitudes (A as well as $B^{(i)}$ and $C^{(i)}$), are equal to the spectral functions of the type $a_i(s_i)$ and have a value of the form (17). Substituting these values of the absorptive parts into the right-hand side of the equations of the form (13) (written for the amplitudes $B^{(i)}$ and $C^{(i)}$), we obtain from (16) quantities corresponding to the graphs of fig. 7b of the third and fourth orders. The substitution of the same values of the absorptive parts into (9′) yield the values A_{ij} corresponding to the graphs of

† The second term on the left-hand side of (16) being neglected, and substituting $B^{(i)}\approx b_0{}^{(i)}$, $C^{(i)}\approx c_0{}^{(i)}$ on the right-hand side.

fig. 8a, the "barrels" (the contribution of which depending on two variables). In this process the numbers of all graphs are the same as in the conventional perturbation theory. It is not clear to the author, however, whether account is fully taken of the contribution from the graphs of the type of fig. 7c or 7d which

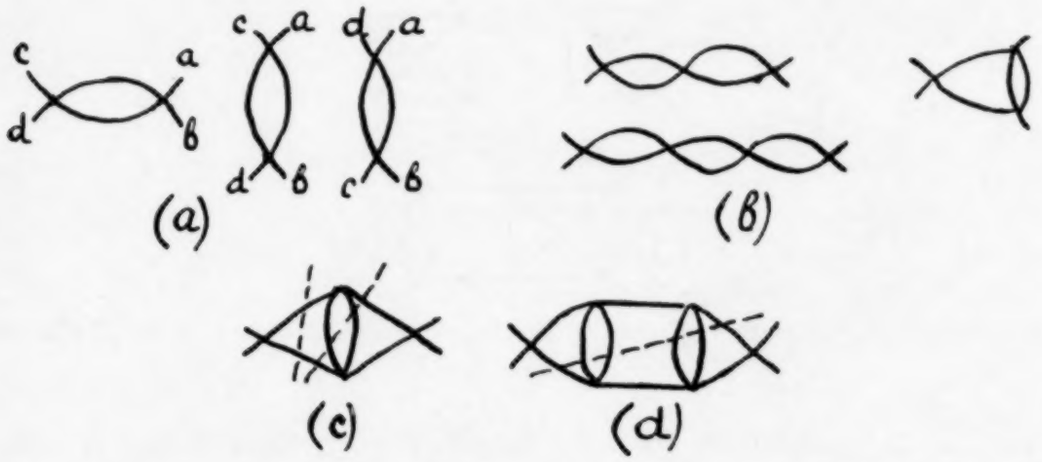

Fig. 7. The simplest graphs of the "parquet type" the contribution of which depends on one variable (the latter occurs always if two external lines reach one point or if a graph consists of two parts connected by only one common point).

can be divided into two parts with crossing of lines of two particles, four particles, or even six particles, as in the case of fig. 7d. The two-particle part is taken into account in (9′) and (16) undoubtedly correctly; it appears that four-, six-particle parts, etc., of the contribution from these graphs are not taken into account correctly.

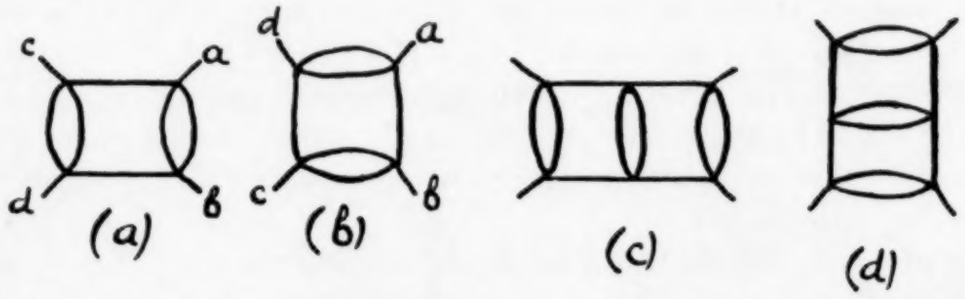

Fig. 8. The simplest graphs the contribution of which depends on two variables.

In the subsequent approximations the contributions of more complex graphs are restored, for example, the chains of "barrels" of fig. 8c and 8d. The graphs of the type of fig. 9a which do not divide into two parts with crossing of only two lines in any direction (as well as more complex graphs of the type of fig. 9b including these in some of their parts) are not taken into account by the set (9′) and (16) in any iteration approximation.

Another approach to the solution of the set of eqs. (9) and (16) will be mentioned. Let us neglect the terms containing the spectral functions A_{ij} in (16), assuming that the influence of these terms on the values of $a_i(s_i)$ is small (since the singularities of the amplitudes corresponding to the functions A_{ij} are situated

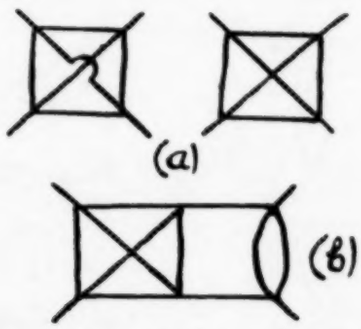

Fig. 9. Graphs the contribution of which are definitely not taken into account by the set of eqs. (9)–(16).

in the plane of fig. 2 further than the singularities connected with the functions $a_i(s_i)$). We obtain thereby the following equations for the functions $a_i(s_i)$:

$$a_1(s) = \zeta_1(s)\langle B^{(1)}(s)\rangle_1{}^*\langle C^{(1)}(s)\rangle_1, \tag{18}$$

where, according to (12a) and (13),

$$\langle B^{(1)}(s)\rangle_1 = b_0{}^{(1)} + \frac{1}{\pi}\int_0^\infty [\varphi(\sigma,s)b_1{}^{(1)}(\sigma) + l_2(\sigma,s)b_2{}^{(1)}(\sigma) + l_3(\sigma,s)b_3{}^{(1)}(\sigma)]\mathrm{d}\sigma \tag{19}$$

and $\langle C^{(1)}(s)\rangle_1$ has a similar form. The equations for a_2 and a_3 can be hence obtained by a cyclic permutation of subscripts.

The quantities A_{ij} can be determined in the first approximation by substituting, according to (14), the solution of eq. (18) into (9'), $B_j{}^{(i)} \approx b_j{}^{(i)}(m'^2)$ and $C_j{}^{(i)} \approx C_j{}^{(i)}(m''^2)$. The values of A_{ij} thus obtained can again be substituted into (14), (13) and (12) and corrections be found to the solution of eq. (18). The possibility of this interation procedure with respect to the functions A_{ij} can actually be checked.

In the particular case of the iteraction of neutral mesons (when there is only one amplitude A, i.e. all $B^{(i)} = A$ and $C^{(i)} = A$), eq. (17) coincides with the equation of the Chew-Mandelstam theory [4]). In the form (18) they can easily be written for any system of interacting particles.

5. Conclusion

The kernels in the integral equations (9') are the spectral functions of the simplest graphs of fig. 4. Therefore the equations in the above-mentioned two-particle approximation have a "graphic structure". Their iteration over the

coupling constants gives rise to a set of the Feynman graphs of the type of figs. 7 and 8 consisting (in each part) of two parts connected by the lines of only two particles.

At present it is not yet clear whether the equations will keep a similar "graphic" structure in subsequent approximation, i.e., for example, if account is taken of three- or four-particle states. Nor is it clear whether this sequence of approximations gives a series converging rapidly to the correct values.

References

1) S. Mandelstam, Phys. Rev. **112** (1958) 1344
2) S. Mandelstam, Phys. Rev. **115** (1959) 1741
3) S. Mandelstam, Phys. Rev. **115** (1959) 1752
4) G. Chew and Mandelstam, Phys. Rev. **119** (1960) 467
5) R. Karplus, C. M. Sommerfield and E. H. Wichman, Phys. Rev. **114** (1959) 376
6) K. Ter-Martirosyan, JETP **39** (1960) 827

7.A

Nuclear Physics **25** (1961) 368—384; © *North-Holland Publishing Co., Amsterdam*

Not to be reproduced by photoprint or microfilm without written permission from the publisher

EQUATIONS FOR SPECTRAL FUNCTIONS IN THE SIMPLEST CASES

K. TER-MARTIROSYAN

Theoretical and Experimental Physics Institute of the USSR Academy of Sciences, Moscow, USSR

Received 16 September 1960

Abstract: The integral equations for the spectral functions of "four-tail" amplitudes are written in detail for the case when two of the four particles are identical.

The equations obtained are applicable to the cases of the π–π, π–K, and K–K interactions, the spins and isospins of all particles being assumed equal to zero.

1. Introduction

In the preceding paper [1]) the equations of the symmetrized Mandelstam scheme (two-particle approximation) were written in the general form.

Below, these equations are considered in greater detail for some of the simplest cases: for the interaction of neutral mesons, for the scattering of a meson of mass μ on a particle of mass m, when $\mu/m < 1$, and for the scattering of particles of mass m on each other (due to the exchange of mesons of mass μ with $\mu/m < 1$).

The equations for the spectral functions depending on one variable are reduced to a form in which their solution can be obtained in a semi-analytical form by the method considered by Simonov and the present author [2]).

2. Two Identical Particles

Let us first consider a very important case: two of the four particles in fig. 1 (the particles a and c, for example), are identical. We assume that all particles a, b, c and d in fig. 1 are bosons. With the reciprocal change of the momenta p_a and p_c of identical particles, the amplitude $A(s_1, s_2, s_3)$ corresponding to fig. 1 does not change. Yet the invariants $s_1 = (p_a+p_b)^2$ and $s_2 = (p_c+p_b)^2$

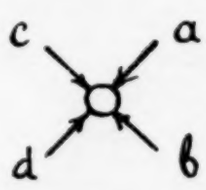

Fig. 1. "Four-tail"-amplitude of the processes a+b ↔ c+d, a+d ↔ b+c and a+c ↔ b+d.

exchange, while $s_3 = (p_a+p_c)^2 \to s_3$. Therefore the amplitude A must be a symmetrical function of s_1 and s_2 : $A(s_1, s_2, s_3) = A(s_2, s_1, s_3)$. Hence it follows that $A_3(s_1, s_2, s_3) = A_3(s_2, s_1, s_3)$ and $A_1(s_1, s_2, s_3) = A_2(s_2, s_1, s_3)$. From the integral representations for the absorptive parts of the amplitude (see ref. [3]), eqs. (2.8a) and (2.10a) or ref. [1]), eqs. of the type (10)) it follows that in the case under consideration the spectral functions of the amplitude have the following properties:

$$A_{31}(s_3, s_1) = A_{23}(s_1, s_3), \tag{1}$$

$$A_{12}(s_1, s_2) = A_{12}(s_2, s_1) \tag{2}$$

and

$$a_1(s_1) = a_2(s_2). \tag{3}$$

It is convenient to introduce the notations $A_{31}(s_3, s_1) = A_{23}(s_1, s_3) = \rho\ (s_3, s_1)$, $A_{12}(s_1, s_2) = \rho_c(s_1, s_2)$, $a_1(s) = a_2(s) = \alpha(s)$, $a_3(s) = \beta(s)$, the double Mandelstam representation and the representations for the absorptive parts of the amplitude clearly expressing the necessary properties of its symmetry:

$$A = a_0 + \frac{1}{\pi}\int_0^\infty \{[\varphi(\sigma, s_1)+\varphi(\sigma, s_2)]\alpha(\sigma)+\varphi(\sigma, s_3)\beta(\sigma)\}\mathrm{d}\sigma$$
$$+\frac{1}{\pi^2}\iint_0^\infty \{\varphi(\sigma, s_1)\varphi(\sigma', s_2)\rho_c(\sigma, \sigma')+[\varphi(\sigma', s_1)+\varphi(\sigma', s_2)]\varphi(\sigma, s_3)\rho(\sigma, \sigma')\}\mathrm{d}\sigma\mathrm{d}\sigma', \tag{4}$$

$$A_1 = \alpha(s_1)+\frac{1}{\pi}\int_0^\infty [\varphi(\sigma, s_2)\rho_c(\sigma, s_1)+\varphi(\sigma, s_3)\rho(\sigma, s_1)]\mathrm{d}\sigma,$$

$$A_2 = \alpha(s_2)+\frac{1}{\pi}\int_0^\infty [\varphi(\sigma, s_1)\rho_c(\sigma, s_2)+\varphi(\sigma, s_3)\rho(\sigma, s_2)]\mathrm{d}\sigma, \tag{5}$$

$$A_3 = \beta(s_3)+\frac{1}{\pi}\int_0^\infty [\varphi(\sigma, s_1)+\varphi(\sigma, s_2)]\rho(s_3, \sigma)\mathrm{d}\sigma.$$

Here is

$$\varphi(\sigma, s_i) = \frac{1}{\sigma - s_i} - \frac{1}{\sigma - s_{i0}}, \qquad i = 1, 2, 3.$$

Thus, in the case under consideration the amplitude is determined by four real spectral functions: $\alpha(\sigma)$, $\beta(\sigma)$, $\rho(\sigma, \sigma')$, $\rho_c(\sigma, \sigma')$.

Let us show that the general equations (9′) and (15) of ref. [1]) yield the relations (1)–(3) as well as the equations for the spectral functions α, β, ρ, and ρ_c.

Analysing figs. 3a and 3b of ref. [1]) it can readily be appreciated that in the case when the particles a and c are identical the unitarity conditions for the first two channels coincide identically; they differ only in that the particles at the entry and the exit of the reactions are inverted. In particular, the pair of particles α_1 and β_1 in fig. 3a and α_2 and β_2 in fig. 3b of ref. [1]) are therefore the

same and the amplitudes $B^{(2)*}$ and $C^{(2)}$ are those of the same transitions as $C^{(1)}$ and $B^{(1)*}$ respectively. Namely:

$$B^{(1)*}(s_2, s_3, s_1) \equiv C^{(2)}(s_1, s_2, s_3), \qquad C^{(1)}(s_2, s_1, s_3) \equiv B^{(2)*}(s_1, s_2, s_3). \quad (6)$$

Apart from this, it is clear that the amplitude $C^{(3)}$ (see ref. [1]), fig. 3c) just as A must be a symmetrical function of the invariants s_1 and s_2:

$$C^{(3)}(s_1, s_2, s_3) \equiv C^{(3)}(s_2, s_1, s_3). \quad (7)$$

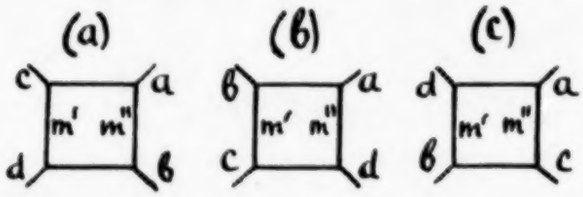

Fig. 2. Graphs corresponding to the quantities Γ_1, Γ_2 and Γ_3.

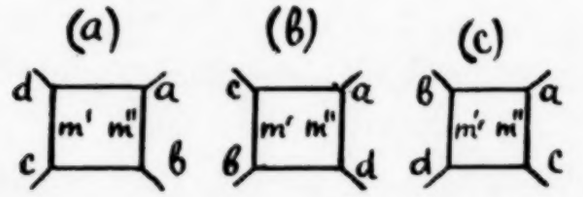

Fig. 3. Graphs corresponding to the quantities Γ'_1, Γ'_2 and Γ'_3.

Comparing the graphs of figs. 2a, b and c and figs. 3a, b and c we likewise conclude that

$$\begin{aligned}
\Gamma_1(m', m''; s_3, s_1) &\equiv \Gamma'_2(m'', m'; s_3, s_1), \\
\Gamma_2(m', m''; s_1, s_2) &\equiv \Gamma'_1(m'', m'; s_1, s_2), \\
\Gamma_3(m', m''; s_2, s_3) &\equiv \Gamma'_3(m', m''; s_2, s_3).
\end{aligned} \quad (8)$$

Substituting the relations † (6), (7) and (8) into eqs. (4)–(4′) of ref. [1]) the following equations can be obtained:

$$Q_1(s_3, s_1) \equiv P_2(s_1, s_3), \quad Q_2(s_1, s_2) \equiv P_1(s_2, s_1), \quad Q_3(s_2, s_3) \equiv P_3(s_3, s_2). \quad (9)$$

Therefore the functions P_i can be excluded altogether and the functions Q_i be introduced instead everywhere. By substituting eq. (9) (together with the relations of the type (1) and (2) for the quantities $A_{ij}^{(0)}$ which are obvious for them) into eqs. (9) of ref. [1]) we obtain the relations (1) and (2), with the follow-

† Eqs. (6) lead in particular to the following relations between the absorption parts of the amplitudes: $C_1^{(2)}(s_1, s_2, s_3) = B_3^{(1)*}(s_2, s_3, s_1)$, $C_3^{(2)}(s_1, s_2, s_3) = B_2^{(1)*}(s_2, s_3, s_1)$, $B_1^{(2)*}(s_1, s_2, s_3) = C_2^{(1)}(s_2, s_1, s_3)$, $B_3^{(2)*}(s_1, s_2, s_3) = C_3^{(1)}(s_2, s_1, s_3)$.

ing values for the spectral functions $\rho = A_{31}$ and $\rho_c = A_{12}$:

$$\begin{aligned} \rho(s_3, s_1) &= -\rho^{(0)}(s_3, s_1)+Q_1(s_3, s_1)+Q_3(s_1, s_3), \\ \rho_c(s_1, s_2) &= -\rho_c{}^{(0)}(s_1, s_2)+Q_2(s_1, s_2)+Q_2(s_2, s_1). \end{aligned} \tag{10}$$

Here $\rho^{(0)}(s_3, s_1)$ is the spectral function of the simplest graph of fig. 2a, $\rho_c{}^{(0)}(s_1, s_3)$ that of fig. 2b and Q_1, Q_2 and Q_3, according to eqs. (14) of ref. [1]), have the values

$$\begin{aligned} Q_1(s_3, s_1) &= \frac{1}{\pi^2}\iint_0^\infty \Gamma_1(m', m''; s_3, s_1)[B_2{}^* C_2+B_3{}^* C_3]\mathrm{d}m'^2\mathrm{d}m''^2, \\ Q_2(s_1, s_2) &= \frac{1}{\pi^2}\iint_0^\infty \Gamma_2(m', m''; s_1, s_2)[B_2{}^* C_3+B_3{}^* C_2]\mathrm{d}m'^2\mathrm{d}m''^2, \\ Q_3(s_1, s_3) &= \frac{1}{\pi^2}\iint_0^\infty \Gamma_3(m', m''; s_1, s_3)[B_1{}^{(3)}+B_2{}^{(3)}]^* C_1{}^{(3)}\mathrm{d}m'^2\mathrm{d}m''^2. \end{aligned} \tag{11}$$

The amplitudes $B^{(2)}$ and $C^{(2)}$ are eliminated from (11) with the aid of the relations (6) (see the footnote above) and B_j and C_j are written for the sake of brevity instead of $B_j{}^{(1)}$ and $C_j{}^{(1)}$ $(j = 2, 3)$.

The equations for the spectral functions $\alpha(\sigma)$ and $\beta(\sigma)$ can be obtained from eqs. (16) of ref. [1]). The only point to be noted is that in the case when the particles a and c are identical the function $l_2(\sigma, s_1)$, with the substitutions of $s_1 \to s_2$, coincides with the function $l_1(\sigma, s_2)$; the common value of these functions will be designated by $l(\sigma, s_2)$. Besides, in the last of eqs. (16) of ref. [1]) the functions $l_2(\sigma, s_3)$ and $l_1(\sigma, s_3)$ coincide and accordingly we shall designate them by $L(\sigma, s_3)$. According to (6): $\langle B^{(1)}(s)\rangle_1{}^* = \langle C^{(2)}(s)\rangle_2$ and $\langle B^{(2)}(s)\rangle_2{}^* = \langle C^{(1)}(s)\rangle_2$; hence and from (9) it follows that the first two equations of (16) of ref. [1]) coincide; therefore $a_1(s) = a_2(s) = \alpha(s)$ and for the functions $\alpha(s)$ and $\beta(s)$ the following equations hold:

$$\begin{aligned} \alpha(s)+\frac{1}{\pi}\int_0^\infty [l_3(\sigma, s)Q_1(\sigma, s)+l(\sigma, s)Q_2(\sigma, s)]\mathrm{d}\sigma &= \zeta(s)\langle B(s)\rangle_1{}^*\langle C(s)\rangle_1, \\ \beta(s)+\frac{2}{\pi}\int_0^\infty L(\sigma, s)Q_3(\sigma, s)\mathrm{d}\sigma &= \zeta_3(s)\langle B^{(3)}(s)\rangle_3{}^*\langle C^{(3)}(s)\rangle_3. \end{aligned} \tag{12}$$

Here (just as in (11)) B and C are written instead of $B^{(1)}$ and $C^{(1)}$ and the common value of the functions $\zeta_1(s) = \zeta_2(s)$ is designated by $\zeta(s)$.

Eqs. (10) and (12) (together with (4), (5) and (11)) are a complete set of equations for the four spectral fuctions α, β and ρ, ρ_c.

The case considered above when the amplitude A is the function of the form (4) symmetrical with respect to two variables (s_1 and s_2) holds practically always. A certain modification which arises when the isobaric spin is taken into account consists in that apart from the amplitude symmetrical with

respect to s_1 and s_2 of the form (4) there also arises an amplitude anti-symmetrical with respect to s_1 and s_2. Taking account of the spin of the particles leads to some other purely technical complications.

3. Interaction of Neutral Scalar Mesons

Let us consider the simplest case when all four particles a, b, c and d in fig. 1 as well as all particles α_i and β_i, $(i = 1, 2, 3)$ in fig. 3 of ref. [1]) are the same. In unitarity conditions (fig. 3, ref. [1])) all amplitudes $B^{(i)}$ and $C^{(i)}$ $(i = 1, 2, 3)$ coincide with the elastic scattering amplitudes A, while in (4)

$$\alpha(\sigma) = \beta(\sigma), \quad \rho(\sigma, \sigma') = \rho_c(\sigma, \sigma'),$$

i.e.

$$A = -\lambda_0 + \frac{1}{\pi}\int_0^\infty [\varphi(\sigma, s_1)+\varphi(\sigma, s_2)+\varphi(\sigma, s_3)]\alpha(\sigma)\mathrm{d}\sigma$$
$$+\frac{1}{\pi^2}\iint_0^\infty [\varphi(\sigma, s_1)\varphi(\sigma', s_2)+\varphi(\sigma, s_2)\varphi(\sigma', s_3)+\varphi(\sigma, s_3)\varphi(\sigma', s_1)]\rho_c(\sigma, \sigma')\mathrm{d}\sigma\mathrm{d}\sigma'. \tag{13}$$

By $(-\lambda_0)$ is here designated the value of $A(s_1, s_2, s_3)$ at the point $s_1 = s_2 = s_3 = \frac{1}{3}\gamma_0 = s_0$ in which the subtraction is performed ($\gamma_0 = 4\mu^2$, where μ is the mass of particles). Thus the amplitude A is determined by two real spectral functions $\alpha(s)$ and $\rho_c(s, s') \equiv \rho_c(s', s)$. According to (10) and (12), these functions satisfy the equations

$$\rho_c(s, s') = Q(s, s')+Q(s', s), \tag{14}$$

$$\alpha(s)+\frac{2}{\pi}\int_0^\infty l(\sigma, s)Q(\sigma, s)\mathrm{d}\sigma = \zeta(s)|\langle A(s)\rangle_1|^2. \tag{15}$$

Here we have

$$Q(s, s')=\frac{2}{\pi^2}\iint_0^\infty \Gamma_1(m', m''; s', s)$$
$$\times A_1^*(m'^2, \gamma_0-m'^2-s, s)A_1(m''^2, \gamma_0-m''^2-s, s)\mathrm{d}m'^2\mathrm{d}m''^2, \tag{16}$$

and (see eqs. (13) and (12a) of ref. [1]))

$$\langle A(s)\rangle_1 = -\lambda_0+\frac{1}{\pi}\int_0^\infty [\varphi(\sigma, s)\alpha(\sigma)+2l(\sigma, s)A_1(\sigma, \gamma_0-\sigma-s, s)]\mathrm{d}\sigma$$
$$+\frac{1}{\pi^2}\iint_0^\infty \frac{(s-s_0)\rho_c(\sigma, \sigma')\mathrm{d}\sigma\mathrm{d}\sigma'}{(\gamma_0-s-\sigma-\sigma')(\sigma-s_0)(\sigma'-s_0)}, \tag{17}$$

while, according to (5),

$$A_1(\sigma, \gamma_0-\sigma-s, s) = \alpha(\sigma)+\frac{1}{\pi}\int_0^\infty [\varphi(\sigma', \gamma_0-\sigma-s)+\varphi(\sigma, s)]\rho_c(\sigma, \sigma')\mathrm{d}\sigma'. \tag{18}$$

The functions $\zeta(s)$, $l(\sigma, s)$ and Γ_1 have the following explicit values †:

$$\zeta(s) = \sqrt{\frac{s-4\mu^2}{s}},$$

$$l(\sigma, s) = (s-4\mu^2)^{-1} \ln\left(1+\frac{s-4\mu^2}{\sigma}\right) - \frac{1}{\sigma-s_0}$$

and

$$\Gamma_1 = \frac{2\pi}{s}\{(s-4\mu^2)s'^2+2[(s-4\mu^2)(m'^2+m''^2)+2m'^2m''^2]s' - (s-4\mu^2)(m'^2-m''^2)^2\}^{-\frac{1}{2}}\Theta(s'-s'_c),$$

while

$$s_c = m'^2+m''^2+\frac{2m'^2m''^2}{s-4\mu^2}+\sqrt{\left((m'^2+m''^2+\frac{2m'^2m''^2}{s-4\mu^2}\right)^2-(m'^2-m''^2)^2}.$$

The function Θ is equal to zero if $s' < s_c$ and is equal to unity when $s' > s_c$.

If in (15) we neglect the second term of the left-hand side and in (17) and (18) the terms containing the spectral function $\rho_c(\sigma, \sigma')$, then (15), (17) and (18) will yield the equations of Chew and Mandelstam [4])

$$\alpha(\sigma) = \sqrt{\frac{\sigma-4\mu^2}{\sigma}}|\langle A(\sigma)\rangle_1|^2, \tag{19}$$

$$\langle A(s)\rangle_1 = -\lambda_0+\frac{1}{\pi}\int_0^\infty [\varphi(\sigma, s)+2l(\sigma, s)]\alpha(\sigma)\mathrm{d}\sigma. \tag{20}$$

To obtain the Chew-Mandelstam equation in the conventional form, the last term in (20) should be transformed by partial integration. Introducing the convenient variables $\nu = (s-4\mu^2)/4\mu^2$ and $\nu' = (\sigma-4\mu^2)/4\mu^2$, eq. (20) can easily be transformed to the form

$$\langle A(\nu)\rangle_1 = -\lambda_0+\frac{1}{\pi}\int_0^\infty\left(\frac{1}{\nu'-\nu}-\frac{1}{\nu'-\nu_0}\right)\alpha(\nu')\mathrm{d}\nu'+\frac{1}{\pi}\int_{-\infty}^{-1}\left(\frac{1}{\nu'-\nu}-\frac{1}{\nu'-\nu_0}\right)b(\nu')\mathrm{d}\nu', \tag{21}$$

where

$$b(\nu) = \frac{2}{\nu}\int_0^{-1-\nu}\alpha(\nu')\mathrm{d}\nu'. \tag{22}$$

The value $\nu = \nu_0$ corresponds to $s = s_0$ (at $s_0 = \frac{4}{3}\mu^2$, $\nu_0 = -\frac{2}{3}$). The substitution of (19) into (21) and (22) yields the Chew-Mandelstam equation in the conventional form. To obtain the solution it is convenient to transform this equation

† This value of $\zeta(s)$ corresponds to the normalisation used by Chew and Mandelstam [4]) according to which $\mathrm{d}\sigma_1/\mathrm{d}\Omega_1 = 16s^{-1}|A|^2$. The value Γ_1 was given in a footnote to ref. [1]).

as in ref. [4]) by introducing the inverse function instead of $\langle A(\nu)\rangle_1$,

$$h(x) = -\langle A(\nu)\rangle_1^{-1}, \tag{23}$$

and introducing the variable $x = \nu/(\nu+1) = (s-4\mu^2)/s$. We shall confine ourselves to the consideration of only those solutions $\langle A(\nu)\rangle_1$ of eqs. (21)–(22) which have no zeros at any value of ν, i.e., only those functions $h(x)$ which have no poles at any values of the variable x. For this class of functions eqs. (19) and (21) are equivalent to the relation

$$h(x) = g + \frac{x}{\pi}\int_0^1 \frac{dy}{y^{\frac{1}{2}}(y-x)} + \frac{2}{\pi}\int_0^1 \frac{y^{\frac{1}{2}}v(y)dy}{y-1/x}, \tag{24}$$

where $g = h(0)$, while from (22) and (19) it follows that

$$v(y) = \frac{1-y}{y^{\frac{1}{2}}}|h(1/y)|^2\int_0^y \frac{\sqrt{\eta}\,d\eta}{(1-\eta)^2|h(\eta)|^2}. \tag{25}$$

According to (23) one has $h(x_0) = -\lambda_0^{-1}$, where $x_0 = (s_0-4\mu^2)/s_0$ ($x_0 = -2$ corresponds to the value $s_0 = \frac{4}{3}\mu^2$); therefore λ_0 and g are connected through an equation of the form

$$\lambda_0^{-1} = g + \frac{x_0}{\pi}\int_0^1 \frac{dy}{y^{\frac{1}{2}}(y-x_0)} + \frac{2}{\pi}\int_0^1 \frac{y^{\frac{1}{2}}v(y)dy}{y-1/x_0}. \tag{26}$$

The Chew-Mandelstam equation written in the form (24)–(25) can easily be solved semi-analytically if one takes into account that the function $v(y)$ in (24) can be expanded into a power series of y : $v(y) = \alpha_0+\alpha_1 y+\alpha_2 y^2+\ldots$. For a large region of the values of the coupling constant λ the radius of the convergence of the series seems to be larger than unity so that only the first terms of the series can be taken into account in the substitution into (24), the latter yielding a solution in the form of a sum of simple analytical functions with numerical coefficients α_j the values of which can be found with the aid of (25). This method of constructing the solution of eqs. (24)–(25) was considered in detail in ref. [2]).

Given the solution $\alpha(s) = \sqrt{\{(s-4\mu^2)/s\}}|h(x)|^{-2}$, where $x = (s-4\mu^2)/s$, of eqs. (24)–(25) the spectral function (14) $\rho_c(s', s)$ can be constructed [under the assumption in the first approximation in (16) that $A_1(m'^2, \gamma_0-m'^2-s, s)\approx \alpha(m'^2)$]; the possibility of neglecting this function in the general equations (14) and (15) in the transition to the Chew and Mandelstam equations can be checked. No such estimation has been carried out so far.

4. Interaction of Neutral Particles with Masses μ and m at $\mu/m = \varepsilon < 1$

The case of scattering of particles with mass μ on particles with mass m is somewhat more complex. We assume that the quantity $\varepsilon = \mu/m < 1$ and below

we shall consider in particular the limiting case $\varepsilon \to 0$. The unitarity conditions (fig. 4) include the scattering amplitude of particles with mass μ on each other considered in the foregoing sections, apart from the amplitude A of the scattering of particles with mass μ on particles with mass m. The former amplitude will be designated here by $\lambda(s_1, s_2, s_3)$, where $s_1+s_2+s_3 = \gamma_0$, $\gamma_0 = 4\mu^2$.

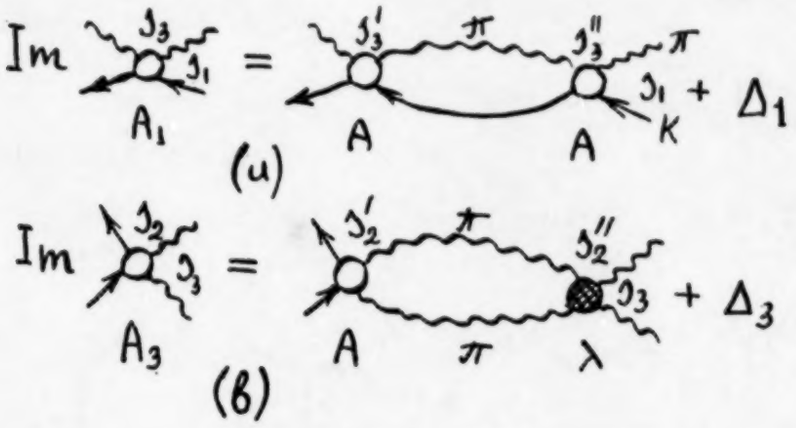

Fig. 4. Unitarity conditions in case of π–K-scattering.

For the sake of simplicity we shall consider the case when the amplitude A has no pole terms. This will occur, for example, when the interaction is such that there are no triple vertices and the contribution from the pole graphs of

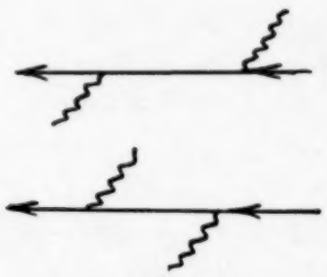

Fig. 5. Pole graphs.

the type of fig. 5 should not be taken into account (as in π—K interaction). Then the amplitude can be represented in the form (4), an equation of the form (10) being obtained for the functions ρ and ρ_c (without the terms $\rho^{(0)}$ and $\rho_c{}^{(0)}$, lacking due to the absence of the pole terms in the amplitudes A and λ):

$$\begin{aligned} \rho(s', s) &= Q_1(s', s)+Q_3(s, s'), \\ \rho_c(s, s') &= Q_2(s, s')+Q_2(s', s). \end{aligned} \tag{27}$$

Here, according to (11)

$$Q_1(s', s) = \frac{1}{\pi^2}\int\int_0^\infty \Gamma_1(m', m''; s', s)A_3^*(s, \gamma-s-m'^2, m'^2) \times A_3(s, \gamma-s-m''^2, m''^2)\mathrm{d}m'^2\mathrm{d}m''^2,$$

$$Q_2(s', s) = \frac{1}{\pi^2}\int\int_0^\infty \Gamma_2(m', m''; s', s)A_1^*(m'^2, s, \gamma-m'^2-s) \times A_3(\gamma-m''^2-s, s, m''^2)\mathrm{d}m'^2\mathrm{d}m''^2, \quad (28)$$

$$Q_3(s, s') = \frac{1}{\pi^2}\int\int_0^\infty \Gamma_3(m', m''; s, s')A_1^*(m'^2, \gamma-m'^2-s', s') \times \lambda_1(m''^2, \gamma_0-m''^2-s', s')\mathrm{d}m'^2\mathrm{d}m''^2,$$

Γ_1, Γ_2, and Γ_3 being the spectral functions † of the graphs of fig. 6 (in which the vertical boldface lines correspond to the Green's functions of bosons with masses

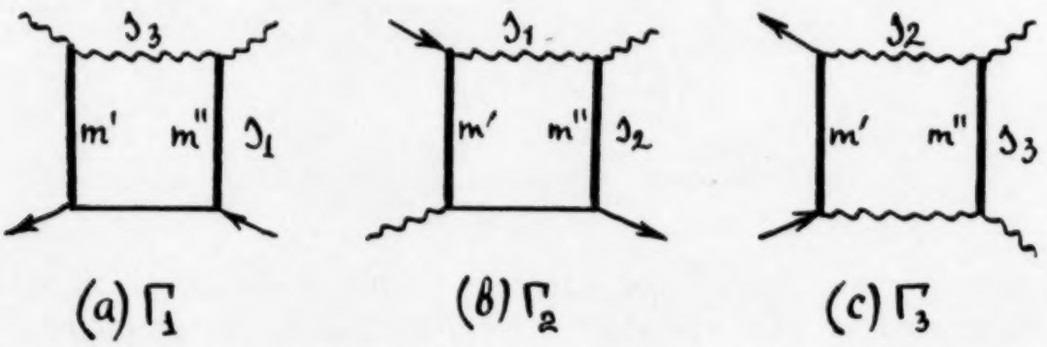

Fig. 6. Graphs corresponding to the quantities Γ_1, Γ_2 and Γ_3 in case of π–K-scattering.

m' and m''). In obtaining these expressions from (11), it was taken into account that, according to fig. 4, $B \equiv C \equiv A$, $B^{(3)} = A$, $C^{(3)} = \lambda$. In eq. (11) for Q_1 the contribution from the term $B^{(2)*}C^{(2)}$ was not taken into account since this contribution (unlike that from the term $B^{(3)*}C^{(3)}$) do not vanish only in a region of very large values s_3 (at s_3 larger than $4m^2$) definitely exceeding the production threshold of a large number of particles with mass μ. Besides, it was taken into account that in analogous formulas for Q_2 and Q_3 the contribution from each of the two terms in the square brackets in (11) are equal. The equations for the

† Their explicit value can easily be obtained from the formula deduced in a footnote of ref. [1]): the functions $\Gamma_1(m', m''; s', s)$ and $\Gamma_2(m', m''; s's)$ are determined formally by the same expression

$$\Gamma_1(m', m''; s', s) = (\pi/4q^2)\xi(s)[z^2+z_0'^2+z_0''^2-2zz'_0z''_0-1]^{-\frac{1}{2}},$$

in which z, z'_0 and z''_0 are connected through simple formulas with s', m'^2, and m''^2 respectively; actually however Γ_1 and Γ_2 are different functions of the variables s' and s'' (at the given values m' and m''), since the connection between z'_0 and m'^2 for the case of the functions Γ_1 and Γ_2 are different (see figs. 4a and 4b). Similarly (fig. 4c),

$$\Gamma_3(m', m''; s', s) = (\pi/4pk^3)\xi_3(s)[1+2z_3z'_{30}-z_3^2-z_{30}'^2-z_{30}''^2]^{-\frac{1}{2}},$$

where $2k = \sqrt{s-4\mu^2}$ and $2p = \sqrt{4m^2-s}$. The functions $\zeta(z)$ and $\zeta_3(s)$ are determined in the text; the quantities z_3, z'_{30} and z''_{30} are connected through the conventional formulas [1]) with s', m'^2 and m''^2.

spectral functions $\alpha(s)$ and $\beta(s)$ follow from (12) (at $B \equiv C \equiv B^{(3)} \equiv A$):

$$\begin{aligned}\alpha(s)+\frac{1}{\pi}\int_0^\infty [l_3(\sigma, s)Q_1(\sigma, s)+l(\sigma, s)Q_2(\sigma, s)]\mathrm{d}\sigma &= \zeta(s)|\langle A(s)\rangle_1|^2,\\ \beta(s)+\frac{2}{\pi}\int_0^\infty \mathscr{L}(\sigma, s)Q_3(\sigma, s)\mathrm{d}\sigma &= \zeta_3(s)\langle A(s)\rangle_3\langle\lambda(s)\rangle_3^*.\end{aligned} \tag{29}$$

Here,

$$\zeta_3(s)\langle\lambda(s)\rangle_3^* = \mathrm{e}^{-i\delta_0(s)}\sin\delta_0(s),$$

where $\delta_0(s)$ is the phase shift of scattering of particles with mass μ on each other in the S-state ($\zeta_3(s) = \sqrt{\{(s-4\mu^2/s)\}}$), and $\langle A(s)\rangle_1$, $\langle A(s)\rangle_3$ can be written (see eqs. (13) and (12a) of ref. [1])) in the form

$$\begin{aligned}\langle A(s)\rangle_1 &= a_0+\frac{1}{\pi}\int_0^\infty [\varphi(\sigma, s)\alpha(\sigma)+l(\sigma, s)A_1(\sigma, s, \gamma-\sigma-s)\\ &\quad +l_3(\sigma, s)A_3(s, \gamma-\sigma-s, \sigma)]\mathrm{d}\sigma+\frac{1}{\pi^2}\iint_0^\infty \frac{(s-s_{10})\rho(\sigma', \sigma)\mathrm{d}\sigma'\,\mathrm{d}\sigma}{(\gamma-s-\sigma-\sigma')(\sigma-s_{20})(\sigma'-s_{30})},\\ \langle A(s)\rangle_3 &= a_0+\frac{1}{\pi}\int_0^\infty [\varphi(\sigma, s)\beta(\sigma)+2L(\sigma, s)A_1(\sigma, \gamma-\sigma-s, s)]\mathrm{d}\sigma\\ &\quad +\frac{1}{\pi^2}\int_0^\infty \frac{(s-s_{30})\rho_c(\sigma, \sigma')\mathrm{d}\sigma\mathrm{d}\sigma'}{(\gamma-s-\sigma-\sigma')(\sigma-s_{10})(\sigma'-s_{20})}.\end{aligned} \tag{30}$$

The absorption parts A_1 and A_3 should be substituted into (30) in the form (5), the functions l, l_3 and L having the following values:

$$\begin{aligned}l(\sigma, s) &= (4q^2)^{-1}\ln\left(1+\frac{4q^2}{\sigma-(m^2-\mu^2)^2s^{-1}}\right),\\ l_3(\sigma, s) &= (4q^2)^{-1}\ln\left(1+\frac{4q^2}{\sigma}\right),\\ L(\sigma, s) &= (2pk)^{-1}\operatorname{arc\,tg}\frac{2pk}{\sigma+m^2+\mu^2-\frac{1}{2}s},\end{aligned}$$

while $4q^2 = s-2(m^2+\mu^2)+(m^2-\mu^2)^2s^{-1}$, and $2pk = \frac{1}{2}\sqrt{\{(s-4\mu^2)(4m^2-s)\}}$. If the normalisation is such that

$$\mathrm{d}\sigma_1/\mathrm{d}\Omega_1 = (m^2/\mu^2 s)|A|^2,$$

then

$$\zeta(s) = \frac{m}{\sqrt{s_1}}\,\frac{q}{\mu}.$$

Eqs. (29) and (30) can be substantially simplified if all terms containing the functions Q_1, Q_2 and Q_3 are neglected in them (i.e., the spectral functions (27) ρ and ρ_c are neglected).

According to (30) and (5), we have

$$\langle A(s)\rangle_1 = a_0+\frac{1}{\pi}\int_0^\infty \{[\varphi(\sigma,s)+l(\sigma,s)]\alpha(\sigma)+l_3(\sigma,s)\beta(\sigma)\}\mathrm{d}\sigma,$$
$$\langle A(s)\rangle_3 = a_0+\frac{1}{\pi}\int_0^\infty [\varphi(\sigma,s)\beta(\sigma)+2L(\sigma,s)\alpha(\sigma)]\mathrm{d}\sigma, \tag{31}$$

where $\alpha(\sigma)$ and $\beta(\sigma)$ have, according to (29), the following values:

$$\alpha(s) = \frac{m}{\sqrt{s}}\sqrt{\frac{[s-(m+\mu)^2][s-(m-\mu)^2]}{4\mu^2}}\,|\langle A(s_1)\rangle_1|^2,$$
$$\beta(s) = \langle A(s)\rangle_3 e^{-i\delta_0(s)}\sin\delta_0(s). \tag{32}$$

It will be noted that eqs. (31)–(32) of the Chew andMandelstam type or of the type considered by Cini and Fubini [6]) naturally follow directly from the Mandelstam representation (4) for the amplitude A if from the outset we neglect the terms containing the spectral functions ρ and ρ_c, i.e., represent A in the form

$$A = a_0+\frac{1}{\pi}\int_0^\infty \{[\varphi(\sigma,s_1)+\varphi(\sigma,s_2)]\alpha(\sigma)+\varphi(\sigma,s_3)\beta(\sigma)\}\mathrm{d}\sigma. \tag{33}$$

In averaging (33) over the directions of the emission of particles in the first and third channels we directly obtain (31); eqs. (32) are evidently the unitarity conditions in these channels for the amplitudes (31) of the transition in S-states.

In the limiting casse when $\varepsilon = \mu/m \to 0$ eqs. (31) and (32) are substantially simplified. This case can be investigated in the simplest way if we proceed directly from the representation (33). We shall write this representation replacing the variables s_1, s_2, and s_3 by the c.m. momentum of particles and the cosinus of the scattering angle in the first and third channels respectively; we get

$$A = a_0+\frac{1}{\pi}\int_0^\infty \left\{\frac{1-\frac{1}{2}\varepsilon\nu(1-z)(1+\nu')^{-\frac{1}{2}}}{[\sqrt{1+\nu'}-\frac{1}{2}\varepsilon\nu(1-z)]^2-[\sqrt{1+\varepsilon^2\nu}\sqrt{1+\nu}+\frac{1}{2}\varepsilon\nu(1+z)]^2}\right.$$
$$\left.-\frac{1+\varepsilon(1+\nu')^{-\frac{1}{2}}}{(\sqrt{1+\nu'}+\varepsilon)^2}\right\}\alpha(\nu')\mathrm{d}\nu'+\frac{1}{\pi}\int_0^\infty\left\{\frac{1}{\nu'+1+\frac{1}{2}\nu(1-z)}-\frac{1}{\nu'}\right\}\beta(\nu')\mathrm{d}\nu', \tag{34}$$

$$A = a_0+\frac{1}{\pi}\int_0^\infty \left\{\frac{1+\varepsilon(1+\nu_3)(1+\nu')^{-\frac{1}{2}}}{[\sqrt{1+\nu'}+\varepsilon(1+\nu_3)]^2-z_3^2\nu_3[1-\varepsilon^2(1+\nu_3)]}\right.$$
$$\left.-\frac{1+\varepsilon(1+\nu')^{-\frac{1}{2}}}{(\sqrt{1+\nu'}+\varepsilon)^2}\right\}\alpha(\nu')\mathrm{d}\nu'+\frac{1}{\pi}\int_0^\infty\left(\frac{1}{\nu'-\nu_3}-\frac{1}{\nu'}\right)\beta(\nu')\mathrm{d}\nu'. \tag{35}$$

By $\alpha(\nu')$ is designated here the quantity $\alpha(\sigma)$ at $\sigma = m^2+\mu^2+2m\mu\sqrt{1+\nu'}$ and

by $\beta(\nu')$ the quantity $\beta(\sigma)$ at $\sigma = 4\mu^2(1+\nu')$; in eqs. (34) ν and z are connected with the invariants s_i through the relations

$$s_1 = m^2+\mu^2+2\mu^2\nu+2m\mu\sqrt{1+\varepsilon^2\nu}\,\sqrt{1+\nu},$$
$$s_2 = m^2+\mu^2-2\mu^2\nu z-2m\mu\sqrt{1+\varepsilon^2\nu}\,\sqrt{1+\nu},$$
$$s_3 = -2\mu^2\nu(1-z).$$

Here, $\nu = q^2/\mu^2$, $z = \cos\vartheta_1$ (q being the c.m. meson momentum); similarly, (35) is obtained from (33) with the following substitution of variables

$$s_1 = m^2+\mu^2-2\mu^2(1+\nu_3)+2m\mu\sqrt{1-\varepsilon^2(1+\nu_3)}\,\sqrt{-\nu_3}\,z_3,$$
$$s_2 = m^2+\mu^2-2\mu^2(1+\nu_3)-2m\mu\sqrt{1-\varepsilon^2(1+\nu_3)}\,\sqrt{-\nu_3}\,z_3,$$
$$s_3 = 4\mu^2(1+\nu_3).$$

Here, $\nu_3 = k^2/\mu^2$, $z_3 = \cos\vartheta_3$ (k being the meson momentum in the third channel; the ratio μ/m is designated by ε everywhere). The subtraction in (34) and (35) is performed at the point $s_{10} = s_{20} = m^2-\mu^2$, $s_{30} = 4\mu^2$, i.e., at $\nu = z = -1$ in (34) and at $\nu_3 = 0$ in (35). At $\varepsilon \to 0$ the representations (34), (35) are simplified

$$A = a_0+\frac{1}{\pi}\int_0^\infty\left(\frac{1}{\nu'-\nu}-\frac{1}{\nu'+1}\right)\alpha(\nu')\mathrm{d}\nu'+\frac{1}{\pi}\int_0^\infty\left(\frac{1}{\nu'+1+\frac{1}{2}\nu(1-z)}-\frac{1}{\nu'}\right)\beta(\nu')\mathrm{d}\nu', \tag{34'}$$

$$A = a_0+\frac{1}{\pi}\int_0^\infty\left(\frac{1}{\nu'+1+\nu_3 z_3{}^2}-\frac{1}{\nu'+1}\right)\alpha(\nu')\mathrm{d}\nu'+\frac{1}{\pi}\int_0^\infty\left(\frac{1}{\nu'-\nu}-\frac{1}{\nu'}\right)\beta(\nu')\mathrm{d}'\nu. \tag{35'}$$

The averages over z of (34') and over z_3 of (35') are equal to the first and second of the quantities (31) respectively,

$$\langle A(\nu)\rangle_1 = a_0+\frac{1}{\pi}\int_0^\infty\left(\frac{1}{\nu'-\nu}-\frac{1}{\nu'+1}\right)\alpha(\nu')\mathrm{d}\nu' + \frac{1}{\pi}\int_0^\infty\left[\nu^{-1}\ln\left(1+\frac{\nu}{\nu'+1}\right)-\frac{1}{\nu'}\right]\beta(\nu')\mathrm{d}\nu',$$
$$\langle A(\nu)\rangle_3 = a_0+\frac{1}{\pi}\int_0^\infty\left[\frac{\operatorname{arctg}(\nu/\nu'+1)^{\frac{1}{2}}}{\sqrt{\nu(\nu'+1)}}-\frac{1}{\nu'+1}\right]\alpha(\nu')\mathrm{d}\nu'+\frac{1}{\pi}\int_0^\infty\left(\frac{1}{\nu'-\nu}-\frac{1}{\nu'}\right)\beta(\nu')\mathrm{d}\nu' \tag{36}$$

(in the second relation ν is written instead of ν_3 for the sake of brevity). The relations (36) can also be obtained directly from (31) by the substitution of variables and the transition to the limit $\varepsilon \to 0$.

Performing the relevant substitution of variables in (32) too, we obviously obtain ($\varepsilon \to 0$)

$$\alpha(\nu) = \sqrt{\nu}|\langle A(\nu)\rangle_1|^2, \qquad \beta(\nu) = e^{-i\delta_0(\nu)} \sin\delta_0(\nu)\langle A(\nu)\rangle_3. \tag{37}$$

Here, $\delta_0(\nu)$ designates the quantity $\delta_0(s)$ at $s = 4\mu^2(1+\nu)$.

Eqs. (36)–(37) can be easily reduced to a form perfectly analogous to (24)–(25). For this purpose the first of eq. (36) should be written exactly in the form of (21)

$$\langle A(\nu)\rangle_1 = -\eta^{-1} + \frac{1}{\pi}\int_0^\infty \left(\frac{1}{\nu'-\nu} - \frac{1}{\nu'-\nu_0}\right)\alpha(\nu')d\nu' + \frac{1}{\pi}\int_0^\infty \left(\frac{1}{\nu'-\nu} - \frac{1}{\nu'-\nu_0}\right)\beta(\nu')d\nu', \tag{21'}$$

where $\nu_0 = -1$, and further

$$b(\nu) = \frac{1}{\nu}\int_0^{-1-\nu} \beta(\nu')d\nu', \tag{22'}$$

$$-\eta^{-1} = a_0 - \frac{1}{\pi}\int_0^\infty \left[\frac{1}{\nu'} - \ln\left(1+\frac{1}{\nu'}\right)\right]\beta(\nu')d\nu'. \tag{26'}$$

Similarly to the case of four identical particles the function

$$h(x) = -\langle A(\nu)\rangle_1^{-1}$$

should be introduced, where $x = \nu/(\nu+1)$.

Then, confining ourselves to the consideration of only those solutions $\langle A(\nu)\rangle_1$ which have no zeros at any value of ν we obtain for $h(x)$ the representation, perfectly equivalent to (24),

$$h(x) = \eta + \frac{1}{\pi}\int_0^1 \sqrt{\frac{y}{1-y}}\,\frac{dy}{y-x} + \frac{1}{\pi x}\int_0^1 \frac{y^{\frac{1}{2}}v(y)}{y-1/x}\,dy, \tag{38}$$

where, according to (22'),

$$v(y) = \frac{1-y}{y^{\frac{3}{2}}}|h(1/y)|^2\int_0^\nu \frac{\beta(y')dy'}{(1-y'0)^2}. \tag{39}$$

The function $\beta(x)$ in turn can be expressed through a set of two equations: the second equation in (36) and the second one in (37) (solving them by the well-known methods [7,8]) through the functions $\alpha(\nu) = \sqrt{\nu}|h(x)|^{-2}$, i.e., through $|h(x)|^2$]; we get

$$\beta(x) = \left[\alpha_0 + \frac{1}{2\pi}\int_0^1 \frac{\sqrt{1-y}\,e^{-U(1/y)}}{1/x-y}\,dy\int_0^\nu \frac{\sqrt{\eta}d\eta}{(1-\eta)^2|h(\eta)|^2}\right] e^{U(x)}\sin\delta_0(x), \tag{40}$$

where

$$U(x) = \frac{x}{\pi} \mathrm{P} \int_0^1 \frac{\delta_0(y)\mathrm{d}y}{y(y-x)}.$$

In the form of (38), (39) and (40) the equations obtained are analogous to those of (24) and (25) of the preceding sections. They can be solved by expanding the function (39) into the power series in y and finding the expansion coefficients from (38)–(40).

5. Scattering of Particles of Mass m on Each Other

Let us designate the amplitude of the scattering of particles of mass m on each other through $\mathscr{A}$; we assume that the number of these particles is conserved (i.e., if a line of a particle reaches some vertex in the Feynman graph, the same line leaves this vertex). If the directions of the lines of particles are such as indicated in fig. 7, the first and second channels correspond to the processes of

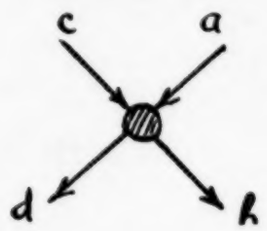

Fig. 7. Four-tail vertices corresponding to K–K-scattering.

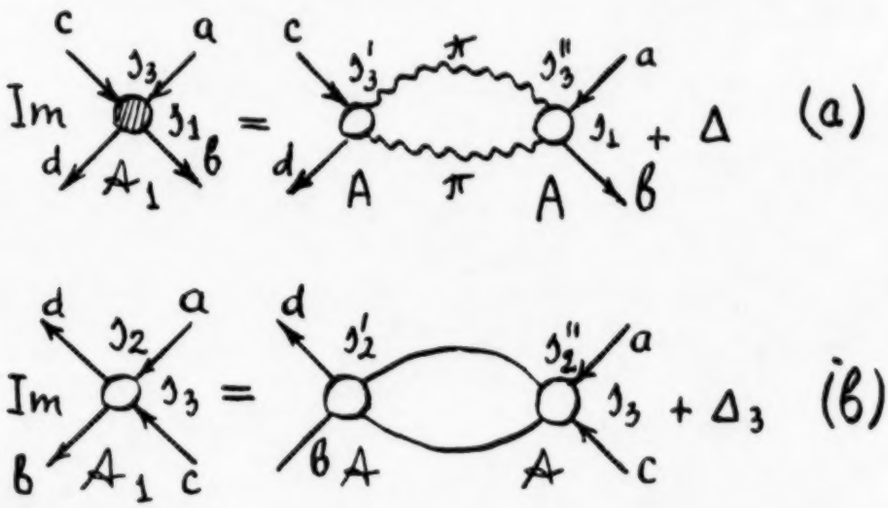

Fig. 8. Unitarity conditions in case of K–K-scattering.

scattering of anti-particles on particle and the third to the scattering of particles on each other. The unitarity conditions for $\mathscr{A}$ are indicated graphically in fig. 8; the graphs of fig. 9 for the quantities Γ_1, Γ_2 and Γ_3 correspond to

these conditions. From comparing the graphs of fig. 9a and those of fig. 9b it follows that $\Gamma_1(m', m''; s', s) \equiv \Gamma_2(m', m''; s', s)$. From the unitarity condition of fig. 8a it follows that in (11) the amplitudes B and C coincide with the

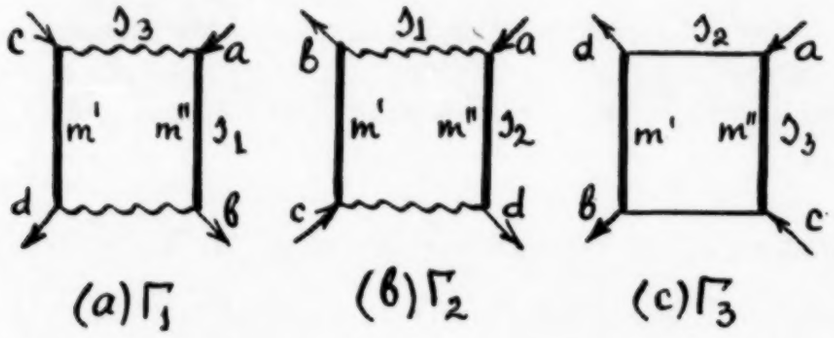

Fig. 9. Quantities Γ_1, Γ_2 and Γ_3 in case of K–K-scattering.

amplitude of the scattering particles with mass μ on particles with mass m, while $B^{(3)} = C^{(3)} = \mathscr{A}$. Therefore $Q_1(s', s) \equiv Q_2(s', s)$; designating the common value of these functions through $Q(s', s)$ we obtain from (11)

$$Q(s', s) = \frac{2}{\pi^2}\int\int_0^\infty \Gamma_1(m', m''; s', s) A_1^*(m'^2, \gamma - m'^2 - s, s) \\ A_1(m''^2, \gamma - m''^2 - s, s)\mathrm{d}m'^2\mathrm{d}m''^2, \quad (41)$$

$$Q_3(s', s) = \frac{2}{\pi^2}\int\int_0^\infty \Gamma_3(m', m''; s', s)\mathscr{A}_1^*(m'^2, \gamma_1 - m'^2 - s, s) \\ \mathscr{A}_1(m''^2, \gamma_1 - m'' - s, s)\mathrm{d}m'^2\mathrm{d}m''^2.$$

Here we have (fig. 9a),

$$\Gamma_1(m', m''; s', s) = \frac{\pi\zeta_1(s)}{4k^2(-p^2)}\,[z^2 + z_0'^2 + z_0''^2 - 2zz'_0z''_0 - 1]^{-\frac{1}{2}},$$

$$\zeta_1(s) = \sqrt{\frac{s-4\mu^2}{s}} = \frac{2k}{\sqrt{s}}, \quad 2k = \sqrt{s-4\mu^2}, \quad 2p = \sqrt{4m^2-s}, \quad s' = -2p^2(1-z),$$

$$m'^2 = m^2 + \mu^2 - \tfrac{1}{2}s + 2kpiz'_0, \qquad m''^2 = m^2 + \mu^2 - \tfrac{1}{2}s + 2kpiz_0''^2.$$

Similarly (fig. 9b),

$$\Gamma_2(m', m''; s', s) = \frac{\pi\zeta_3(s)}{4q^4}\,[z^2 + z_0'^2 + z_0''^2 - 2zz'_0z''_0 - 1]^{-\frac{1}{2}},$$

where

$$2q = \sqrt{s-4m^2}, \quad s' = 2q^2(1-xz), \quad m'^2 = 2q^2(1-z'_0), \quad m''^2 = 2q^2(1-z''_0)$$

and

$$\zeta_3(s) = \frac{2m}{\sqrt{s}}\,(q/\mu)$$

if the normalization is such that the scattering cross section has the following value:

$$\frac{d\sigma_3}{d\Omega_3} = \frac{1}{\mu^2}\left[\frac{m^2}{4\mu\sqrt{s}}\right]^2 |\mathscr{A}|^2.$$

The amplitude $\mathscr{A}$ is determined by a representation of the form (4) in which according to (10)

$$\begin{aligned} \rho(s', s) &= Q(s', s)+Q_3(s, s'), \\ \rho_c(s', s) &= Q(s', s)+Q(s, s') \end{aligned} \tag{42}$$

(the terms $\rho^{(0)}$ and $\rho_c^{(0)}$ are lacking in (10) if the amplitudes A and $\mathscr{A}$ have no pole terms). According to (12) and fig. 8 the spectral functions $\alpha(s)$ and $\beta(s)$ satisfy the equations

$$\begin{aligned} \alpha(s)+\frac{2}{\pi}\int_0^\infty l(\sigma, s)Q(\sigma, s)d\sigma &= \zeta(s)|\langle A(s)\rangle_3|^2, \\ \beta(s)+\frac{2}{\pi}\int_0^\infty l(\sigma, s)Q_3(\sigma, s)d\sigma &= \zeta_3(s)|\langle \mathscr{A}(s)\rangle_1|^2, \end{aligned} \tag{43}$$

where †

$$l(\sigma, s) = (s-4m^2)^{-1}\ln\left(1+\frac{s-4m^2}{\sigma}\right)-(\sigma-\tfrac{4}{3}m^2)^{-1},$$

$$\begin{aligned} \langle \mathscr{A}(s)\rangle_1 = a_0+\frac{1}{\pi}\int_0^\infty \{\varphi(\sigma, s)\alpha(\sigma)+l(\sigma,s)[A_1(\sigma,s,\gamma-\sigma-s)+A_3(s,\gamma-\sigma-s,\sigma)]\}d\sigma \\ +\frac{1}{\pi^2}\iint_0^\infty \frac{(s-\frac{4}{3}m^2)\rho(\sigma', \sigma)d\sigma d\sigma'}{(4m^2-s-\sigma-\sigma')(\sigma-\frac{4}{3}m^2)(\sigma'-\frac{4}{3}m^2)}, \end{aligned} \tag{44}$$

while $\langle A(s)\rangle_3$ is determined (through the spectral functions of the amplitude) in (30).

If in (43)–(44) quantities proportional to the functions Q, Q_3 are neglected (i.e., the contribution from the spectral functions ρ and ρ is neglected) from (44) and (43) follow equations of the type obtained by Cini and Fubini. The solution of these equations determines the function $\beta(s)$ (the function $\alpha(s)$ according to (43) is known in the same approximation if the amplitude A was known beforehand). If the right-hand sides of eq. (41) the terms proportional to the spectral functions ρ and ρ_c are neglected, the quantities Q and Q_3 are determined in the form of integrals containing only the function $\alpha(s)$ .We hope to treat the set of equations (41)–(44) in greater detail in the future.

† It is assumed that in the representation of the form (4) of the amplitude $\mathscr{A}$ the subtraction is performed at the point $s_{10} = s_{20} = s_{30} = \frac{4}{3}m^2$.

References

1) K. Ter-Martirosyan, Nuclear Physics **25** (1961) 353
2) Yu. Simonov and K. Ter-Martirosyan, JETP **39** (1960) 1442
3) S. Mandelstam, Phys. Rev. **115** (1959) 1741
4) G. Chew and S. Mandelstam, Phys. Rev. **119** (1960) 647
5) L. Castellejo, R. Dalitz and F. J. Dyson, Phys. Rev. **101** (1956) 453
6) M. Cini and S. Fubini, Ann. of Phys.
7) N. I. Muskhelishvili, Singular Integral Equations (GITTL); R. Omnes, Nuovo Cim. **8** (1958) 316
8) W. R. Frazer and H. R. Fulco, Phys. Rev. **117** (1960) 1603

1.D.2:
1.E.3

Nuclear Physics **25** (1961) 385—403; © *North-Holland Publishing Co., Amsterdam*
Not to be reproduced by photoprint or microfilm without written permission from the publisher

THE GYROMAGNETIC RATIO OF THE 155 keV-ROTATIONAL LEVEL IN Os^{188}

E. KARLSSON, C.-A. LERJEFORS and E. MATTHIAS
Institute of Physics, University of Uppsala, Uppsala

Received 13 February 1961

Abstract: Using a 4-channel coincidence apparatus we have investigated the influence of an external magnetic field on the angular correlation of the 931—155 keV cascade in Os^{188}. The strength of the magnetic interaction was found to be $|\omega_L \tau_N| = 0.0423 \pm 0.0034$ rad for a magnetic field of ± 29200 G. Averaging the results of all lifetime determinations we got $T_{\frac{1}{2}} = (5.8 \pm 0.5) 10^{-10}$ s, which gives $g_R = +0.36 \pm 0.04$ for the gyromagnetic ratio of the 155-keV rotational state. This result was derived under the assumption that no other perturbations were present in the liquid source used. This assumption is supported by our own measurements as well as earlier determinations of the angular correlation coefficients of the 0—2—0-cascade. The result is in agreement with recent calculations based on the superconductor theory of the nucleus.

1. Introduction

Recently, it was shown by E. M. Bernstein and J. de Boer [1]) that for odd-mass nuclei in the region $153 \leqq A \leqq 187$, the gyromagnetic ratio of the rotational motion g_R is dependent upon the mass number A. These authors calculated g_R from the experimental values of the magnetic dipole transition probability $B(M1)$ and the ground-state magnetic moment μ_0. Theoretical calculations of S. T. Belyaev [2]) demonstrate that the effect of pairing correlations between nucleons will, for strongly deformed nuclei, generally reduce the rotational g-factor to below Z/A, the value predicted by the hydrodynamical conception of the earlier rotational model [3]). Therefore for even nuclei one expects g_R to show a dependence on A in the region $150 \leqq A \leqq 190$ similar to that shown in ref. [1]). However, there are only a few experimental values of g_R in this region and at present, the knowledge of g_R is far from being systematical. The reason for this is experimental difficulties; the only known method to determine the rotational g-factor of an even nucleus is to measure the rotation or attenuation of a γ-γ angular correlation or the angular distribution of γ-rays following Coulomb exitation in an external magnetic field [3, 4]). In this way one gets the g_R-value directly if the intermediate level of the γ-γ cascade belongs to the ground state rotational band ($K = 0$). On the other hand, the half-lives of these levels which decay by pure E2-transitions are rather short, i.e. the available magnetic fields will produce only a small perturbation of the

angular correlation. Fig. 1 shows the values of g_R known at present as measured by the method mentioned above.

Another difficulty is the paramagnetism of the rare earth elements in the mass number region where the unified model is valid. In g_R-factor measurements, correction must be made for the resulting enlargement of the effective magnetic field at the position of the nucleus. The accuracy of the corrections calculated earlier was estimated [10]) to about 5 %. This uncertainty arises mainly from the calculation of $\langle r^{-3} \rangle$, which was thought to be computed with

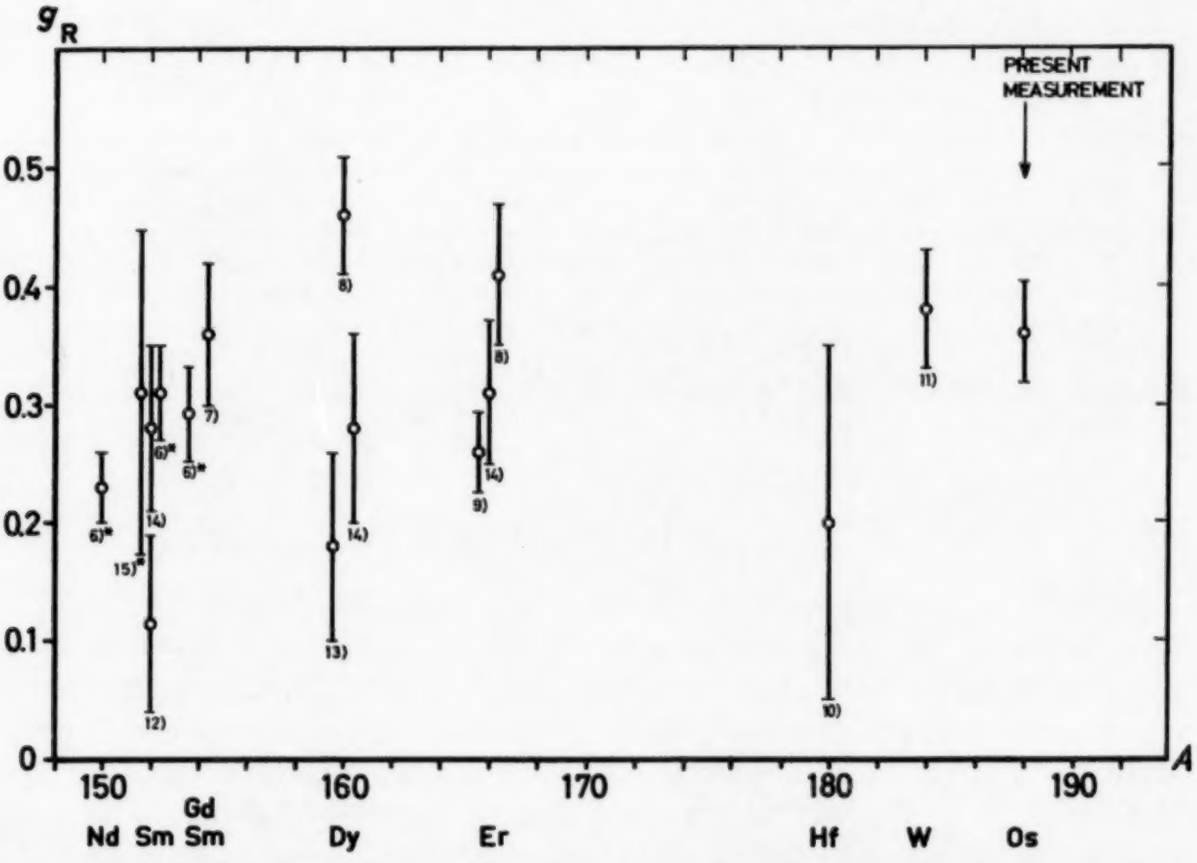

Fig. 1. Summary of available experimental data on rotational g-factors of even nuclei in the region $150 < A < 190$. The values marked with asterisks were corrected for the paramagnetic influence by the authors. The new values for $\langle r^{-3} \rangle$ given in ref. [5]) have not been taken into account.

5 % error. Recently, however, Judd and Lindgren [5]) made new calculations using modified hydrogenic wave functions and arrived at values 25 % higher than the earlier ones. It seems therefore that an upward correction must be applied to all g-factors measured in this region. However, it can be noticed that there are still some even nuclei showing well-defined rotational states in the region $72 \leq Z \leq 76$ where it should be possible to measure the rotational g-factor without the necessity of a paramagnetic correction. One of these cases is Os^{188}, resulting from the β^--decay of Re^{188}, where the 155 keV-level is the first excited state of the ground state rotational band. The half-life of this

level was determined to $T_{\frac{1}{2}} = (6.5 \pm 1.5) \times 10^{-10}$s by the method of delayed coincidences [16]). Coulomb excitation measurements made by several groups gave the results $T_{\frac{1}{2}} = (5.0 \pm 1.5) \times 10^{-10}$ s (see ref. [17])), $T_{\frac{1}{2}} = (6.2 \pm 0.7) \times 10^{-10}$ s (see ref. [18])) and $T_{\frac{1}{2}} = (5.0 \pm 1.0) \times 10^{-10}$ s (see ref. [19])). Angular correlation measurements have been performed by I. Marklund *et al.* [20]) and R. G. Arns *et al.* [21]); these, among others, confirmed the existence of a 0—2—0 γ-γ cascade with an intensity not too small for an angular correlation measurement. Using this γ-γ cascade for the determination of the nuclear g_R-factor provides a great advantage, because the angular correlation for this spin sequence shows a very large anisotropy and allows the measurement of even a small rotation of the angular correlation pattern in an external magnetic field of about 30000 G, which was at our disposal.

2. The Experimental Set-Up

The angular correlation measurements were performed with a four detector system with the electronic equipment arranged according to the block diagram in fig. 2. The principle of a fixed detector arrangement discussed by

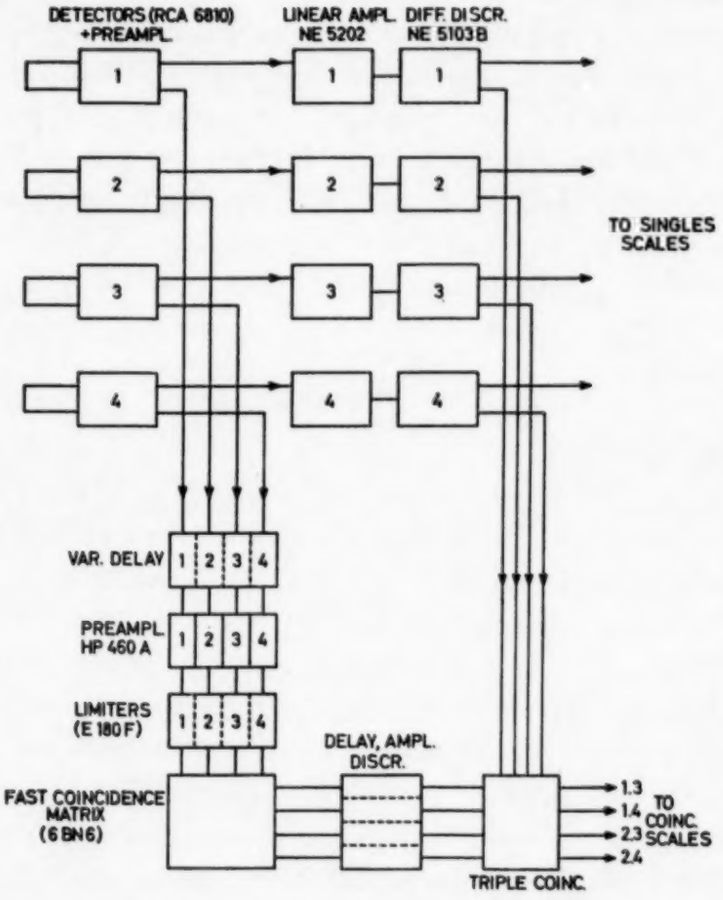

Fig. 2. Block diagram of the electronics.

T. R. Gerholm *et al.* [22]) and T. Lindqvist and E. Karlsson [23]) has been employed. The electronic coupling and equipment, however, are not as described in ref. [22]) but have been re-arranged.

Instead of measuring the coincidence counting rate as a function of the angle between two detectors, the four detectors in our arrangement are placed at fixed positions during the whole run. The coincidences between the different detector combinations will be used to give the angular correlation ratios $W(\Theta_1)/W(\Theta_2)$. In principle, the coincidences C_{ij} of all the six combinations of four detectors can be measured, i.e. C_{12}, C_{13}, C_{14}, C_{23}, C_{24} and C_{34}, where the numbers stand for the different detectors. However, our equipment is not yet complete and therefore we could only use coincidences of the four combinations (1,3), (1,4), (2,3) and (2,4). This implies that each detector will accept only one energy of the γ-γ cascade and suitable absorbers can be used.

As shown in fig. 2 each detector combination consists of an ordinary fast-slow coincidence circuit. In order to get the desired coincidence combinations, it is necessary to apply a fast coincidence matrix coupling where each matrix element (i, j) is represented by a 6BN6-circuit according to J. Fisher and J. Marshall [24]). For a γ-energy of 511 keV, the lower limits of the resolving time of the fast coincidence circuits are about 7 ns without a noticeable loss of true coincidences.

An electromagnet with about 25000 A-turns was used to generate a magnetic field perpendicular to the plane of the detectors. With an air gap of 6 mm over a circular area of 57 mm^2 the field strength was about 30000 G. The detectors consisted of 3.81 cm $\times$ 5.08 cm NaI(Tl) crystals mounted onto RCA 6810 photomultipliers. Lightguides of 18.5 cm length were used in order to remove the multiplier tubes from the strong magnetic field. Furthermore, two Mu-metal cylinders of 2 mm and one iron cylinder of 10 mm thickness served as magnetic shielding.

3. The Decay of Re^{188}

3.1. SOURCE PREPARATION

To produce the activity, we irradiated 98.8 % enriched Re^{187} at a flux of about 10^{12} neutrons/cm^2 · sec in the R1 reactor in Stockholm. For angular correlation measurements and especially for the determination of the g-factor, the choice of a suitable chemical environment for the rhenium nuclei is very important. In the case of Re^{188}, it was shown by the angular correlation measurement of R. G. Arns *et al.* [21]) that a dilute solution of metallic rhenium powder in nitric acid gave the unperturbed correlation for the pure E2-E2 cascade of 931 keV—155 keV. We dissolved the metallic powder in 13N HNO_3 and sent this solution in a sealed quartz tube to the reactor. The irradiated liquid was diluted with distilled water before it was used as the source for the measurements.

3.2. DECAY SCHEME AND SINGLE CHANNEL SETTINGS

The decay of 18h Re^{188} to excited states in Os^{188} has been studied by several investigators [25–27]). These results together with some angular correlation measurements [20, 21, 28–30]) lead to the decay scheme shown in fig. 3. Most of the β^--decay goes to the ground state (80.0 %) and to the first excited state (16.7 %); the upper levels are only weakly populated. It is well established that the first excited state at 155 keV belongs to the ground state rotational band [3]). Among the cascades involving the 155 keV level, the one starting

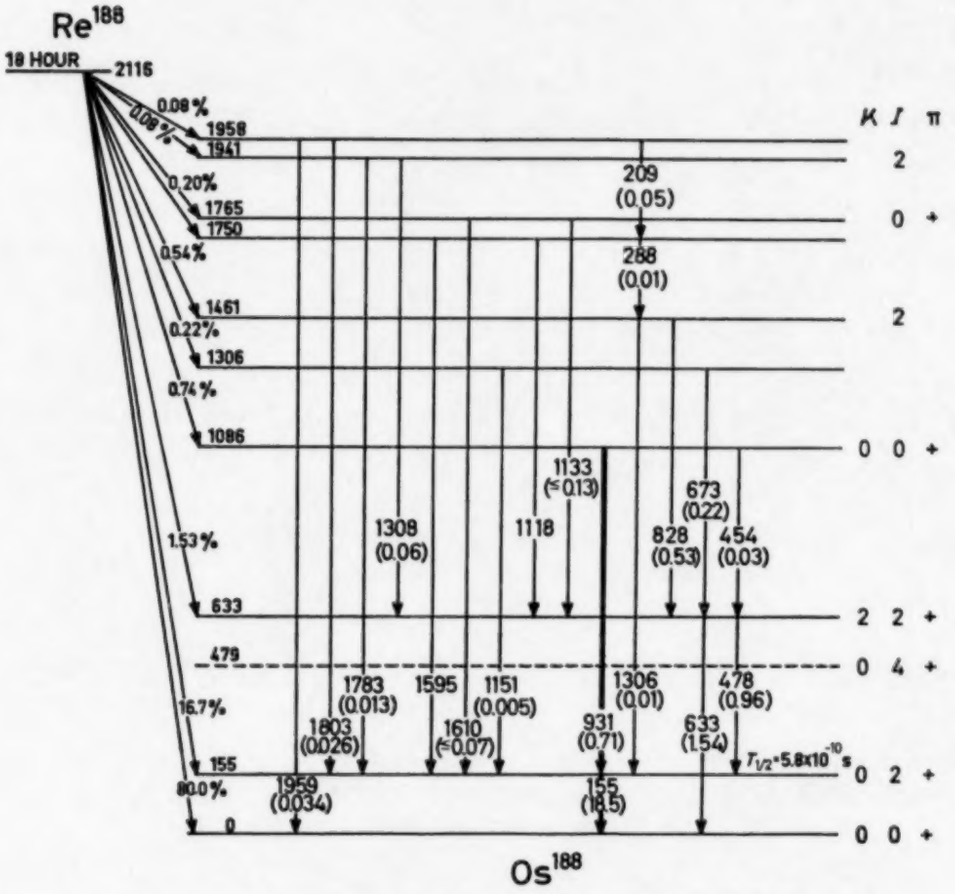

Fig. 3. Decay scheme of Re^{188} (taken from ref. [21])).

from the 0^+ state at 1086 keV was supposed to be the most useful for our purposes as it shows the very anisotropic correlation of a 0—2—0 cascade. Due to the complexity of the decay, however, one can not expect to measure this cascade without interference from others.

The low and high energy parts of the single spectrum, as taken with a 3.81 cm × 5.08 cm NaI(Tl) crystal, are shown in fig. 4. A 0.25 mm thick tin-absorber has been used in order to reduce the very intense K-X-ray peak of about 62 keV. For this special absorber thickness the 155 keV intensity will not decrease more than 10 %. The crystals of the two detectors that accepted the high energy part of the spectrum were provided with 1.8 mm lead absorbers to

suppress the intense low energy peaks. The channel settings are indicated in fig. 4. In order to avoid admixtures from the K-X-ray peak, which cause undesired coincidences, the width of the two low energy channels was chosen to be rather small. The high energy channels accepted mainly the 931 keV peak but also parts of the 828 keV peak since these could not be well resolved. In addition, Compton distributions from higher energy γ-rays were present in the channels. As long as all coincidences arise from cascades that involve the 155 keV level, it is not necessary to select out one cascade, for the determina-

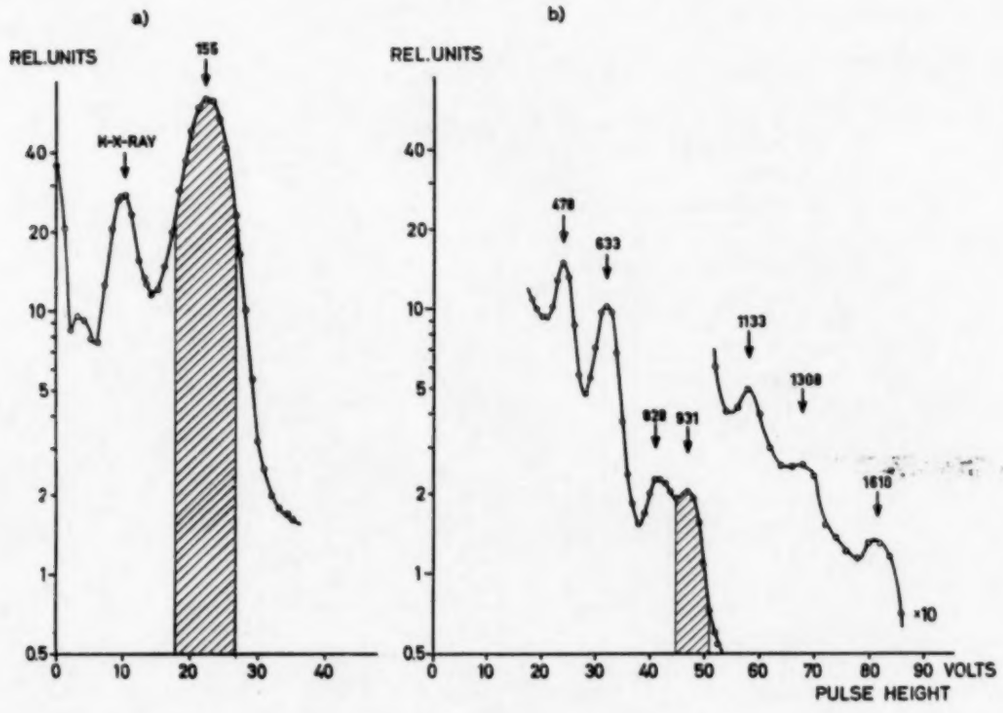

Fig. 4. Single spectra of Re^{188} taken with 3.81 cm × 5.08 cm NaI(Tl) crystals and lightguides of 18.5 cm length. Channel settings are indicated. a) Low energy part (absorber: 0.25 mm tin). b) High energy part (absorber: 1.8 mm lead).

tion of the g-factor, by correcting for the contribution from the others. It can be seen from fig. 3, however, that there are some coincidences coming from cascades that do not pass through the 155 keV level. From the intensities and branching ratios given in the decay scheme shown in fig. 3, and the Compton cross-sections of our NaI(Tl) crystals for the different energies, we have estimated the relative contributions from "wanted" and "not wanted" coincidences with the actual channel settings. The result is given in table 1. It is obvious from table 1 that an upper limit of 3.8 % can be set for the contribution of those coincidences which are not influenced by the magnetic field. As it is hardly possible to correct for this, it will be considered as an additional 3.8 % uncertainty in the final result. However, as the mean correlation of the unwanted cascades probably is considerable less than that of the

931 keV—155 keV cascade, the relative uncertainty in the result is expected to be much less than the 3.8 % mentioned.

Because of the fact that the intensity of the 931 keV γ-rays is only 0.71 % of the whole decay [21]), the coincidence counting rate was very low even though

TABLE 1

Relative intensities from "wanted" and "not wanted" coincidences

Cascades involving the 155-keV level	Rel. int.	Other cascades	Rel. int.
828—155	60	828—478	10
931—155	1000	1133—478	$\leqq$2
1133—155	$\leqq$10	1308—478	4
1308—155	21	828—633	17
1610—155	$\leqq$60	1133—633	$\leqq$3
1790—155	23	1308—633	6
1104 $\leqq$ total int. $\leqq$ 1174		37 $\leqq$ total int. $\leqq$ 42	
Ratio of "not wanted" to "wanted" coincidences: $<$ 0.038			

almost the entire 931 keV peak was accepted. Thus for statistical reasons angular correlation measurements are very tedious and require a high stability of the electronic system. The measurement of the influence of an external magnetic field, a second order effect, will be remarkably facilitated by the high counting efficiency of the multichannel-system described above.

4. Treatment of Data

The primary data in the measurements are the numbers of true coincidences C_{ij} obtained by the different detector combinations (i, j). In order to calculate the angular correlation, the C_{ij} values must be normalized so that detector efficiencies, channel settings etc. cancel. It is possible to find a formula of high symmetry which gives the normalized ratio of the angular correlation for two angles [22]). For this purpose we write the coincidence counting rate C_{ij} in the form

$$C_{ij} = N_0(t)\omega_i\omega_j\varepsilon_i(E_{\gamma_\nu})\varepsilon_j(E_{\gamma_\mu})p_i(E_{\gamma_\nu})p_j(E_{\gamma_\mu})\varepsilon_{ij}^{c}W(\theta_{ij}). \quad (1)$$

Here, $N_0(t)$ is the total activity of the source, ω_i and ω_j are the solid angles of the detectors i and j, $\varepsilon_i(E_{\gamma_\nu})$ and $\varepsilon_j(E_{\gamma_\mu})$ the total efficiency of the detectors for γ_ν and γ_μ, respectively, $p_i(E_{\gamma_\nu})$ and $p_j(E_{\gamma_\mu})$ the fractions of the pulse-height spectrum of γ_ν and γ_μ, respectively, given by the actual channel settings, ε_{ij}^{c} is the coincidence efficiency of the fast-slow system for the coincidence combination (i, j) and $W(\theta_{ij})$ the angular correlation function for the angle

θ_{ij} between the counters i and j. If it is arranged that $\varepsilon_{ij}^{c} = 1$ for all (i, j), it is possible to combine the C_{ij} into a formula of the type [23])

$$\sqrt{\frac{C_{13}\,C_{24}}{C_{14}\,C_{23}}} = \frac{W(\theta_1)}{W(\theta_2)}, \tag{2}$$

which gives the ratio of the correlation function $W(\theta)$ at two angles provided that the geometrical arrangement is such that C_{13}, C_{24} and C_{14}, C_{23} measure the same or corresponding angles. The formula (2) eliminates the need for a source decay correction and, to a first approximation, also provides cancelation of errors in the single-channel settings due to electronic drifts. In this case the

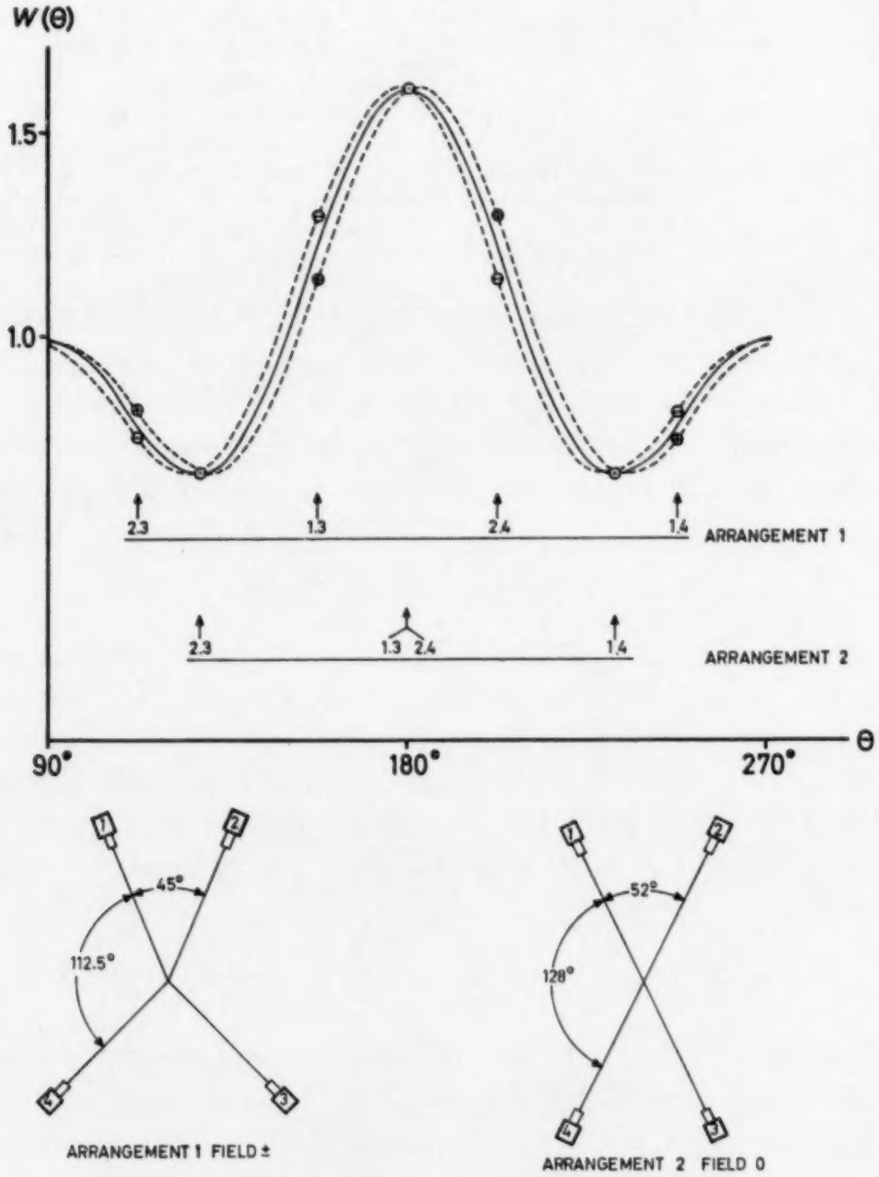

Fig. 5. Uncorrected angular correlation drawn for $\alpha_2 = 0.317$, $\alpha_4 = 0.301$. The shift due to a magnetic field of ± 29200 G is indicated. Lower part of the figure shows the geometric arrangements used.

integral correlation was measured. To fulfil the condition $\varepsilon_{ij}^{c} = 1$, the resolving time of the fast-slow coincidence system was chosen so that $2\,\tau_0 \gg \tau_N$. For $\tau_N \approx 1$ ns this does not lead to inconveniently long resolving times. In the case of Re^{188}, it was found that a resolving time of $2\,\tau_0 = 60$ ns was sufficient to keep the ratio of true to accidental coincidences greater than 10 with the source-strengths used.

When measuring changes in the correlation function $W(\theta)$, at a certain angle θ, induced by the application of a magnetic field $\pm B$ each ratio $C_{ij}(+B)/C_{ij}(-B)$ would be a directly useful quantity, but we have preferred to combine also the set of "field data" in such a way that source decay is corrected for and influences from drifts are minimized. The choice of angle settings of the detectors depends on the shape of $W(\theta)$ in the particular problem. With a rough knowledge of $W(\theta)$, sensitive angular arrangements can be chosen for a careful determination of $W(\theta)$ itself and for shifts in $W(\theta)$.

It is seen from fig. 5 that $W(\theta)$ for the actual $0-2-0$ γ-γ cascade has a minimum between 90° and 180° and therefore has two intervals which are very sensitive to angular shifts. These intervals are in the vicinity of $\frac{5}{8}\pi$ and $\frac{7}{8}\pi$, which were the angles chosen for the field measurements.

If the unperturbed correlation is described by [4])

$$W(\theta) = 1+\alpha_2 \cos 2\theta+\alpha_4 \cos 4\theta; \qquad \alpha_k = \frac{b_k}{b_0}, \tag{3}$$

the angle settings $\frac{5}{8}\pi$ and $\frac{7}{8}\pi$ lead to $\cos 4\theta = 0$. Starting from the general expression of an angular correlation perturbed by an external magnetic field [4])

$$W'(\theta, B) = \sum_k \frac{b_k}{1+(k\omega_L\tau_N)^2}\,(\cos k\theta+k\omega_L\tau_N \sin k\theta), \tag{4}$$

one gets a simple expression for the correlation influenced by a magnetic field $\pm B$,

$$W(\tfrac{5}{8}\pi; \pm B) = 1-\frac{1/\sqrt{2}\,(1\pm 2\omega_L\tau_N)}{1+(2\omega_L\tau_N)^2}\,\alpha_2 \pm \frac{4\omega_L\tau_N}{1+(4\omega_L\tau_N)^2}\,\alpha_4 \tag{5a}$$

$$W(\tfrac{7}{8}\pi; \pm B) = 1+\frac{1/\sqrt{2}(1\mp 2\omega_L\tau_N)}{1+(2\omega_L\tau_N)^2}\,\alpha_2 \mp \frac{4\omega_L\tau_N}{1+(4\omega_L\tau_N)^2}\,\alpha_4, \tag{5b}$$

where τ_N is the mean life of the intermediate level and $\omega_L = gB\,\mu_N/\hbar$, the Larmor frequency.

In principle it would be sufficient to measure only the ratios

$$\frac{W(\frac{7}{8}\pi;+B)}{W(\frac{3}{8}\pi;+B)} = \frac{W(\frac{7}{8}\pi;+B)}{W(\frac{5}{8}\pi;-B)} = \frac{W(\frac{9}{8}\pi;-B)}{W(\frac{5}{8}\pi;-B)}, \tag{6a}$$

$$\frac{W(\frac{7}{8}\pi;-B)}{W(\frac{3}{8}\pi;-B)}=\frac{W(\frac{7}{8}\pi;-B)}{W(\frac{5}{8}\pi;+B)}=\frac{W(\frac{9}{8}\pi;+B)}{W(\frac{5}{8}\pi;+B)}, \tag{6b}$$

$$\frac{W(\frac{7}{8}\pi;0)}{W(\frac{3}{8}\pi;0)}=\frac{W(\frac{7}{8}\pi;0)}{W(\frac{5}{8}\pi;0)}=\frac{W(\frac{9}{8}\pi;0)}{W(\frac{5}{8}\pi;0)} \tag{6c}$$

to obtain the quantities α_2, α_4 and $\omega_L\tau_N$. However, the small angular shifts which are expected in the case of Re^{188} with this particular shape of $W(\theta)$, render this method quite inaccurate, and we therefore preferred to measure the coefficients α_2 and α_4 separately by two different angular arrangements (arrangements 1 and 2, fig. 5). From eqs. (3) and (6c) it follows immediately that α_2 is unambigously given by the ratio

$$\frac{W(\frac{7}{8}\pi;0)}{W(\frac{5}{8}\pi;0)}=\frac{\sqrt{2}+\alpha_2}{\sqrt{2}-\alpha_2}, \tag{7}$$

which is obtained in a zero-field measurement with the detectors arranged as in arrangement 1, fig. 5. Actually we determined α_2^{att} from the measurements with the magnetic field in both directions (indicated by + and −) which gives the ratio

$$b=\sqrt{\frac{C_{13}^{+}C_{24}^{+}}{C_{14}^{+}C_{23}^{+}}}=\sqrt{\frac{C_{13}^{-}C_{24}^{-}}{C_{14}^{-}C_{23}^{-}}}=\sqrt{\frac{W(\frac{7}{8}\pi;+B)W(\frac{7}{8}\pi;-B)}{W(\frac{5}{8}\pi;+B)W(\frac{5}{8}\pi;-B)}}. \tag{8}$$

By putting in eqs. (5a) and (5b), this ratio will get the form

$$b=\sqrt{\frac{\left(1+\frac{1}{\sqrt{2}}\,\frac{\alpha_2}{1+(2\omega_L\tau_N)^2}\right)^2-\left(\frac{\sqrt{2}\,\omega_L\tau_N}{1+(2\omega_L\tau_N)^2}\,\alpha_2+\frac{4\omega_L\tau_N}{1+(4\omega_L\tau_N)^2}\,\alpha_4\right)^2}{\left(1-\frac{1}{\sqrt{2}}\,\frac{\alpha_2}{1+(2\omega_L\tau_N)^2}\right)^2-\left(\frac{\sqrt{2}\,\omega_L\tau_N}{1+(2\omega_L\tau_N)^2}\,\alpha_2-\frac{4\omega_L\tau_N}{1+(4\omega_L\tau_N)^2}\,\alpha_4\right)^2}}. \tag{9}$$

If we define the attenuated coefficients by $\alpha_k^{att}=\alpha_k/1+(k\omega_L\tau_N)^2$, the ratio b can be written

$$b=\sqrt{\frac{\left(1+\frac{1}{\sqrt{2}}\,\alpha_2^{att}\right)^2-(\sqrt{2}\,\omega_L\tau_N\alpha_2^{att}+4\omega_L\tau_N\alpha_4^{att})^2}{\left(1-\frac{1}{\sqrt{2}}\,\alpha_2^{att}\right)^2-(\sqrt{2}\,\omega_L\tau_N\alpha_2^{att}-4\omega_L\tau_N\alpha_4^{att})^2}}. \tag{10}$$

Now, taking the experimental values of both α_2^{att} and α_4 as about 0.3 and the expected value of $\omega_L\tau_N\approx 0.05$ it can be shown that the ratio b is for this actual case, within an error of $1^0/_{00}$.

$$b=\frac{\sqrt{2}+\alpha_2^{att}}{\sqrt{2}-\alpha_2^{att}}. \tag{11}$$

This was expected because the unperturbed angular correlation for the angles $\frac{5}{8}\pi$ and $\frac{7}{8}\pi$ is only determined by α_2. Therefore for small shifts of the correlation pattern the influence of the magnetic field can be treated in the first approximation as an attenuation of the α_2—coefficient.

The validity of eq. (8) was checked in a stability test (fig. 6) where the ratio b is plotted for + and − fields alternatingly. With α_2^{att} known, a sensitive measurement of α_4 was obtained by a detector arrangement according to

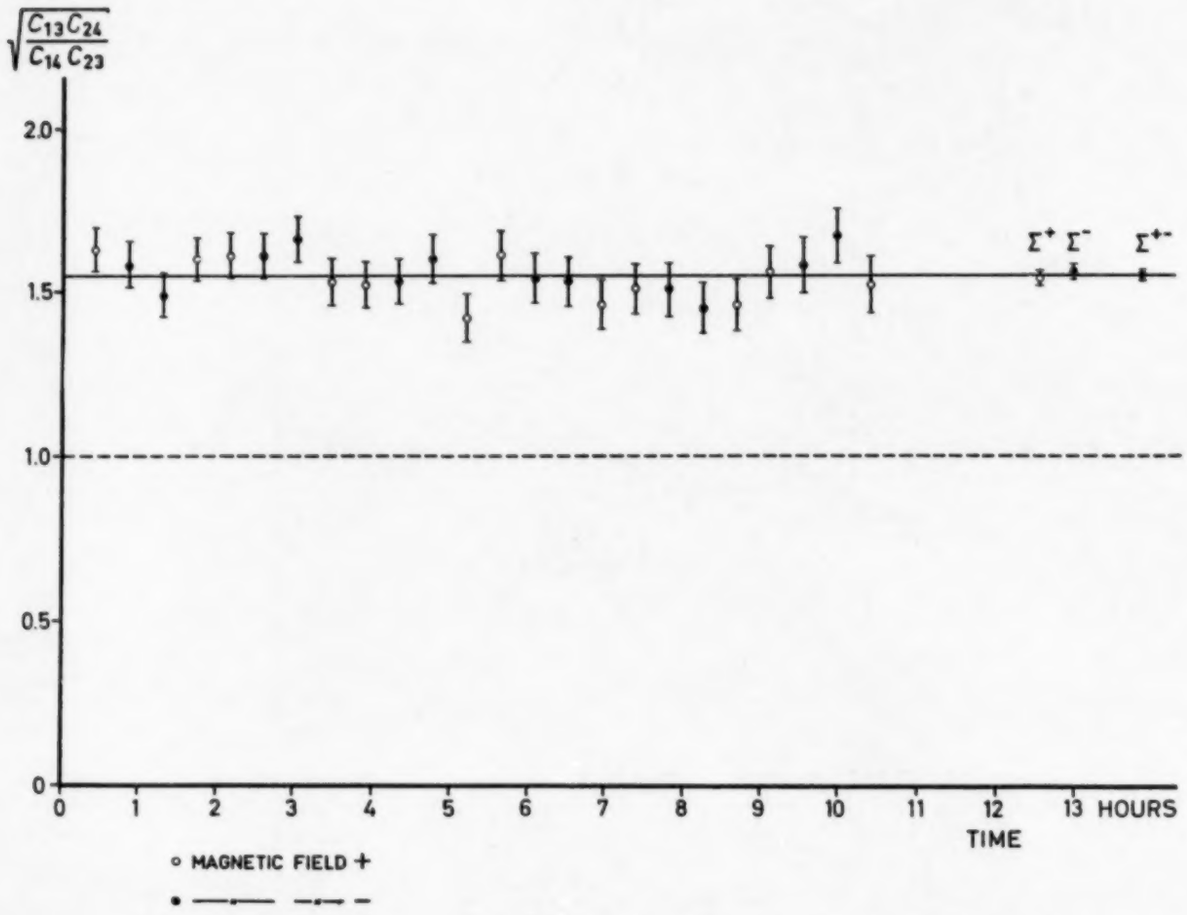

Fig. 6. Stability test and verification of eq. (8) during one of the runs.

arrangement 2 in fig. 5. The special angle setting $\theta_{13} = \theta_{24} = 180°$ and $\theta_{14} = \theta_{23} = 128°$ was chosen because the theoretical correlation function $W(\theta)$ has a minimum value at about $\theta = 128°$ for a 0—2—0 cascade for which the ratio of A_2/A_4 is equal to + 0.312. The ratio $W(180°)/W(128°)$ for zero magnetic field was measured separately and alternatingly with the series of field measurements. This ratio, combined with the value of α_2, gives α_4. As, however, only α_2^{att}, which contains $\omega_L \tau_N$, has been determined, we used the method of successive approximation to calculate α_4, presuming $(\omega_L \tau_N)^2 \ll 1$.

The shift data were taken with the field changed alternatingly, in a series of 30 min intervals, $+--++--\ldots--++-$ in order to eliminate drifts as

much as possible. Smaller time intervals were not favourable because of the low coincidence counting rate. From each consecutive pair of data set C_{ij}^{+} and C_{ij}^{-} the quantity

$$P_i = \frac{C_{13}^{-}C_{14}^{-}C_{23}^{+}C_{24}^{+}}{C_{23}^{-}C_{24}^{-}C_{13}^{+}C_{14}^{+}} = \left\{\frac{W(\frac{7}{8}\pi;\,-\mathrm{B})}{W(\frac{7}{8}\pi;\,+\mathrm{B})}\,\frac{W(\frac{5}{8}\pi;\,+\mathrm{B})}{W(\frac{5}{8}\pi;\,-\mathrm{B})}\right\}^2 \tag{12}$$

was calculated. A weighted mean $\bar{P}$ of the P_i for the whole series was combined

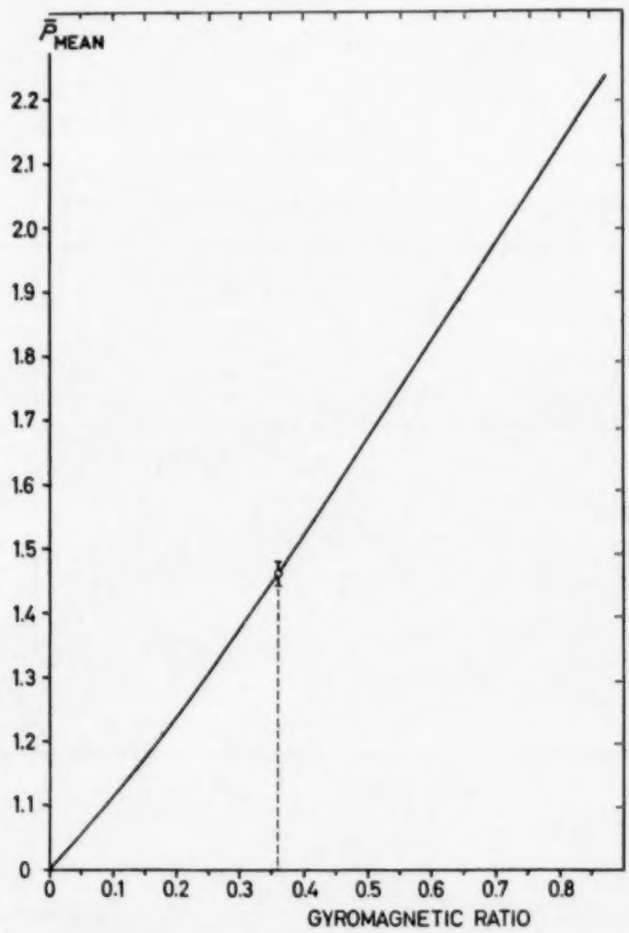

Fig. 7. Graphical solution of eq. (13).

with α_2 and α_4 into the formula

$$\bar{P} = \frac{\left(1+\dfrac{4\omega_L\tau_N}{1+(4\omega_L\tau_N)^2}\,\alpha_4\right)^2 - \left(\dfrac{1}{\sqrt{2}}\,(1+2\omega_L\tau_N)\,\alpha_2^{att}\right)^2}{\left(1-\dfrac{4\omega_L\tau_N}{1+(4\omega_L\tau_N)^2}\,\alpha_4\right)^2 - \left(\dfrac{1}{\sqrt{2}}\,(1-2\omega_L\tau_N)\,\alpha_2^{att}\right)^2}, \tag{13}$$

which is derived by inserting (5a) and (5b) into (12). Eq. (13) is solved graphically by plotting the right hand side as a function of $\omega_L\tau_N$ or g. This is illustrated in fig. 7. A separate calculation for each source was carried out and the values

TABLE 2

Values of several parameters for each source

Measurement number	α_2^{att}	α_2	α_4	P	$\lvert\omega_L\tau_N\rvert$	$\frac{\Delta\omega_L\tau_N}{\omega_L\tau_N}$ (%)
1	+0.313	+0.316	+0.282	1.477	0.0459	16
2	+0.274	+0.275	+0.332	1.422	0.0340	15
3	+0.296	+0.298	+0.289	1.464	0.0438	13
4	+0.332	+0.336	+0.289	1.527	0.0496	17
5	+0.309	+0.310	+0.303	1.306	0.0288	16
6	+0.330	+0.334	+0.265	1.451	0.0506	9
7	+0.306	+0.308	+0.344	1.432	0.0342	16
8	+0.306	+0.307	+0.338	1.450	0.0359	9
9	+0.325	+0.331	+0.248	1.571	0.0649	14
10	+0.325	+0.329	+0.299	1.588	0.0525	15
11	+0.330	+0.333	+0.291	1.522	0.0491	12
12				1.448		
13				1.501		
14				1.470		
Weighted mean	+0.314±0.018	+0.317±0.018	+0.301±0.030	1.462±0.018	0.0423±0.0034	

obtained for α_2^{att}, α_2, α_4, $\bar{P}$ and $\omega_L\tau_N$ for different sources are given in table 2.

The weighted mean value for $\omega_L\tau_N$ is

$$\omega_L\tau_N = 0.0423 \pm 0.0034 \text{ rad.}$$

With a magnetic field of $|B| = 29200$ G and a mean life $\tau_N = (8.4 \pm 0.7) \times 10^{-10}$ s, the gyromagnetic ratio is

$$g_R = +0.36 \pm 0.04.$$

The mean life τ_N used for the calculation of g_R is the weighted mean value of the four results [16–19]) mentioned above. The error in g_R, due to the uncertainty in τ_N, is about 9 %. It is therefore desirable that a more accurate measurement of the mean life of the 155 keV-state is performed.

5. Discussion of the Results

5.1. POSSIBLE INTERNAL PERTURBATIONS

As mentioned above, the choice of a suitable chemical environment for the nuclei is very important. The angular correlation in the absence of an external magnetic field should be unperturbed, or, if there are internal perturbations of electric or magnetic character, corresponding corrections must be applied to the *g*-factor value. In the foregoing calculations we have assumed that no such perturbations exist in our case. This presumption is based on the following arguments: Several angular correlation measurements have been performed earlier on different cascades in Os^{188} involving the 155 keV level (table 3). Recently, extensive measurements were made by Arns *et al.* [21]), who investigated, among others, two cascades passing through the 155 keV level. Because of the spin sequence 0—2—0 of the 931 keV-155 keV cascade, a deviation from the theoretical coefficients can be interpreted as a real attenuation due to internal fields. Using a dilute solution of metallic Re-powder in nitric acid, Arns *et al.* [21]) found the experimental coefficients to be in good agreement with the theoretical ones. They confirmed this result by a measurement of the 478 keV—155 keV cascade with the spin sequence 2—2—0, where they got the theoretical coefficients assuming that the 478 keV transition is nearly pure E2, which is supported by other investigations [27]). For this reason no attenuation for this special kind of source is expected. Similar measurements with a source prepared in the same way were carried out by Marklund *et al.* [20]), who obtained the attenuation factors $G_2 = 0.79 \pm 0.03$ and $G_4 = 0.81 \pm 0.03$. If there exists a real time-dependent perturbation, the attenuation factors should, according to Abragam and Pound's theory [4]), obey the relation

$$\frac{\lambda_2}{\lambda_4} = \frac{1-G_2}{1-G_4}\frac{G_4}{G_2} = 1.70 \qquad (14)$$

TABLE 3

Comparative measurements on different cascades in Os^{188}

Authors	$\gamma-\gamma$-cascade	coefficients		Form of the source	attenuation factors	
		A_2	A_4		G_2	G_4
R. G. Arns *et al.* [21])	931—155 keV	0.35 ±0.05	1.06 ±0.17	Dilute solution of Re in HNO_3	1	1
	478—155 keV	−0.079±0.054	0.402±0.083	Dilute solution of Re in HNO_3	1	1
I. Marklund *et al.* [20])	931—155 keV	0.276±0.012	0.930±0.025	Dilute solution of Re in HNO_3	0.79±0.03	0.81±0.03
W. J. King and M. W. Johns [30])	931—155keV	0.313±0.060	0.640±0.080	Polycrystalline metallic powder	0.87±0.16	0.56±0.06
	478—155 keV	−0.048±0.010	0.162±0.015	Re dissolved in H_2O_2 liquid+solid source-measurements averaged	0.87±0.16	0.56±0.06
V. R. Potnis *et al.*[29])	478—155 keV	−0.040	0.353	Solid metallic Re	1	1
T. Wiedling [28])	478—155 keV	−0.04 ±0.01	0.29 ±0.01	Re dissolved in HNO_3	1	0.90±0.03
		−0.05 ±0.01	0.27 ±0.03	Metallic Re	1	0.83±0.10
		−0.024±0.021	0.21 ±0.02	Crystalline powder $ReNO_3$	0.48	0.65

for a spin $I = 2$. The attenuation factors obtained by Marklund *et al.* give the ratio $\lambda_2/\lambda_4 = 1.13 \pm 0.28$, and therefore it seems rather unlikely that they describe a real time-dependent quadrupole interaction. Because of the complexity of the spectrum it may be possible that the deviation from $G_k = 1$ results from an insufficient correction for admixtures. The result of King and Johns[30]) is hard to interpret, because they found the same coefficients for polycrystalline and liquid sources. This indicates an undisturbed correlation, but they still did not get the theoretical coefficients, for either the 0—2—0 or the 2—2—0 cascade. The authors removed this inconsistency by introducing attenuation factors as listed in table 3. Because they apply also to liquid sources, these factors should satisfy eq. (14). Actually they give $\lambda_2/\lambda_4 = 0.19 \pm 0.27$. Besides, King and John's results for liquid sources are not directly comparable with ours because these authors used a liquid source of Re dissolved in H_2O_2. The same is true for the results of Potnis *et al.* [29]), who measured the 478 keV-155 keV cascade with a solid source of metallic Re. Without the need of attenuation factors they found coefficients which indicate that the first transition is nearly pure E2, in agreement with the results of Arns *et al.* [21]) measured with a liquid source. Finally, Wiedling [28]) measured the 478 keV-155 keV cascade under different source conditions. He found agreement between the results for a metallic source and a liquid source prepared by dissolving metallic Re in nitric acid, which indicates that the angular correlation is unperturbed in both cases. Wiedling's being obliged to introduce an attenuation factor G_4, in order to get a consistent value of the mixing ratio δ, may also be caused by the complexity of the spectrum.

Thus, summing up all existing information, it seems plausible that no perturbation is present if dilute solutions of Re-powder in HNO_3 are used as sources. Therefore, our own measurements were performed with such liquid sources, the dilution of which ranged from pure 63 % nitric acid ($\rho = 1.38$ g/cm^3) to 63 % nitric acid diluted by 400 parts distilled water. No difference in the measured coefficients could be observed. After correction for the finite solid angle and the admixtures listed in table 1 we got the coefficients $A_2 = 0.28 \pm 0.06$ and $A_4 = 0.99 \pm 0.09$ for the 931 keV—155 keV cascade. These values should be compared with the theoretical coefficients $A_2 = 0.357$ and $A_4 = 1.143$ for a 0—2—0 cascade. Comparison between the theoretical and experimental values leads to attenuation factors $G_2 = 0.78$ and $G_4 = 0.87$. However, this should not be taken as evidence for a time dependent perturbation because the attenuations are probably caused by the following facts:

a) The correction for overlapping cascades according to table 1 is somewhat uncertain.

b) The scattering from the pole shoes of the magnet cannot be avoided entirely by the lead shields.

c) For the low energy gamma ray the scattering in the source is not negligible.

d) There is no exact way to correct for the finite dimension of a radially extended source.

The last two effects are believed to be the largest ones because the source diameter was made fairly large (4 mm) in order to increase the source strength and still allow sufficient dilution of the acid. With these facts in mind, our values seem to be compatible with an undisturbed correlation in accordance with the results of Arns *et al.* [21]). Therefore, no correction for internal perturbations was applied to the calculated g-factor.

5.2. SOME THEORETICAL REMARKS

Recently, calculations based on the superfluidity model [2]) of the nucleus have been published by Griffin and Rich [31]) and by Migdal [32]), who investigated theoretically the moments of inertia of deformed nuclei. Starting from Belyaev's theory [2]), Griffin and Rich got good agreement with the experimental values by introducing an effective energy gap parameter Δ, which approximately represented the weighted average over the experimental values given by the nucleon separation energies. Furthermore, they assumed that Δ is the same for both protons and neutrons. Migdal [32]) studied the superfluidity of finite size systems and used the results to calculate the moments of inertia for the oscillator and the rectangular potential. Comparison with the experimental values showed that the correct potential lies between these two limiting cases but considerably nearer the oscillator potential. However, Migdal, in contradiction to Griffin and Rich, used a ratio $\Delta_p/\Delta_n = 1.5$ for the energy gap parameters of proton and neutron.

According to Migdal it is possible to separate a nucleus with $Z-20 \gg 1$ into a proton and a neutron fluid and therefore the moments of inertia can be represented in the form [32])

$$\frac{J}{J_0} = \frac{N}{A}\phi(X_n) + \frac{Z}{A}\phi(X_p), \tag{15}$$

where $J_o = J_{\text{rigid}}$ in the case of strong deformations ($\beta \gtrsim A^{-\frac{1}{3}}$). The $\phi(X_n)$ and $\phi(X_p)$ are rather complicated functions of the deformation β, and the energy gap parameters and can be considered as weight factors describing to what extent the moments of inertia J_p and J_n of the proton and neutron fluid, respectively, contribute to the total amount of J,

$$\frac{\phi(X_n)}{\phi(X_p)} = \frac{Z}{N}\frac{J_n}{J_p}. \tag{16}$$

This ratio can be evaluated directly, using the experimental value of the nuclear rotational g-factor, by the equation [32])

$$\frac{\phi(X_n)}{\phi(X_p)} = \frac{Z}{N}\frac{(1-g_R)}{g_R}. \tag{17}$$

Evidently, for uniformly charged nuclear matter, $\phi(X_n)/\phi(X_p) = 1$. The appearance of pairing correlations between nucleons in conjugate states changes this ratio, and it turns out that the neutron fluid is more effective than the proton fluid in producing the total moment of inertia. This ratio will increase with increasing deformation.

Introducing the result of the present measurement in relation (17), we find for Os [188]

$$\frac{\phi(X_n)}{\phi(X_p)} = 1.20 \pm 0.22.$$

A comparison, with the theoretical values $\phi(X)_{osc}$ and $\phi(X)_{rect}$, calculated by Migdal, can be made if one computes $\phi(X_n)$ and $\phi(X_p)$ separately with the aid of the experimental ratio [3]) J/J_{rigid}. As a result we obtain

$$\phi(X_n) = 0.26 \pm 0.02, \qquad \phi(X_p) = 0.21 \pm 0.03.$$

It should be noticed that no attention was paid to the errors of J/J_{rigid}. These values should be compared with the theoretical ϕ-functions [32])

$$\phi_{osc}(X_n) = 0.27, \qquad \phi_{osc}(X_p) = 0.10$$
$$\phi_{rect}(X_n) = 0.10, \qquad \phi_{rect}(X_p) = 0.04.$$

The X_n-values were obtained by using an energy gap parameter Δ_n given by the nucleon separation energies which was measured by Johnson and Bhanot [33]). Moreover, the X_p-values were computed under the assumption that the ratio of the energy gap parameters of the proton and neutron fluid is $\Delta_p/\Delta_n = 1.5$. It is evident from the results that this assumption no longer holds for Os^{188} probably because of the fact that the deformation is already rather small. Obviously, the oscillator potential fits the experimental result quite well for the ϕ-function of the neutron fluid; this must also be valid for the proton fluid. Therefore it is possible to deduce Δ_p from the experimental value of $\phi(X_p)$. As a result we got for the ratio of the energy gap parameters of proton and neutron

$$\frac{\Delta_p}{\Delta_n} = 1.06 \pm 0.10.$$

It follows from the calculation that for this region of A, i.e. for the moderately deformed nuclei, the assumption of Griffin and Rich [31]) that $\Delta_n \approx \Delta_p$ is more justified than the ratio $\Delta_p/\Delta_n = 1.5$ accepted by Migdal [32]). Also, for the $Sm^{152, 154}$ and Nd^{150} nuclei mentioned in Migdal's work, lower values of the ratio are obtained if the g-values used are properly altered to correct for the paramagnetic influences on the measurements [5, 10]). In the cases of $Sm^{152, 154}$, the corrected g_R-factors lead to the ratio $\Delta_p/\Delta_n = 1.3$.

It is a pleasure to express our gratitude to the director of this institute, Professor Kai Siegbahn, for his continuous interest in this work and for his generous support in constructing the apparatus. Our thanks are due to Mr. K. Sevier for correcting the English.

References

1) E. M. Bernstein and J. de Boer, Nuclear Physics **18** (1960) 40
2) S. T. Belyaev, Mat. Fys. Medd. Dan. Vid. Selsk. **31**, No. 11 (1959)
3) K. Alder, A. Bohr, T. Huus, B. Mottelson and A. Winther, Rev. Mod. Phys. **28** (1956) 432
4) R. M. Steffen, Phil. Mag. Sup. **4** (1955) 293
5) B. R. Judd and I. P. K. Lindgren, UCRL-9188, May 1960, Phys. Rev. (to be published)
6) G. Goldring and R. P. Scharenberg, Phys. Rev. **110** (1958) 701
7) R. Stiening and M. Deutsch, in press
8) W. Kündig, in press
9) E. Bodenstedt, H. J. Körner, C. Günther and J. Radeloff, Nuclear Physics **22** (1961) 145
10) E. Bodenstedt, Die magnetischen Momente angeregter Atomkerne, Habilitationsschrift (Hamburg, 1960)
11) E. Bodenstedt, E. Matthias, H. J. Körner, E. Gerdau, F. Frisius and D. Hovestadt, Nuclear Physics **15** (1960) 239
12) P. Debrunner and W. Kündig, Helv. Phys. Acta **33** (1960) 395
13) P. Debrunner, W. Kündig and P. Scherrer, Helv. Phys. Acta **31** (1958) 326
14) G. Manning and J. Rogers, Nuclear Physics **19** (1960) 675
15) K. Sugimoto, J. Phys. Soc. Japan **13** (1958) 240
16) A. W. Sunyar, Phys. Rev. **98** (1955) 653
17) R. Barloutaud, P. Lehmann and A. Lévêque, Compt. rend. **245** (1957) 523
18) F. K. McGowan and P. H. Stelson, Phys. Rev. **109** (1958) 901
19) F. E. Durham, D. H. Rester and C. M. Class, Bull. Am. Phys. Soc. **4** (1959) 98, oral report
20) I. Marklund, B. van Nooijen and Z. Grabowski, Nuclear Physics **15** (1960) 533
21) R. G. Arns, R. D. Riggs and M. L. Wiedenbeck, Nuclear Physics **15** (1960) 125
22) T. R. Gerholm, T. Lindqvist and H. de Waard, Nuclear Instruments **1** (1957) 107
23) T. Lindqvist and E. Karlsson, Ark. f. Fys. **12** (1957) 519
24) J. Fisher and J. Marshall, Rev. Sci. Instr. **23** (1952) 417
25) M. W. Johns, C. C. McMullen, I. R. Williams and S. V. Nablo, Can. J. Phys. **34** (1956) 69
26) V. R. Potnis, Phys. Rev. **104** (1956) 722
27) K. O. Nielsen and O. B. Nielsen, Nuclear Physics **5** (1958) 319
28) T. Wiedling, Thesis, University of Stockholm (1956)
29) V. R. Potnis, V. S. Dubey and C. F. Mandeville, Phys. Rev. **102** (1956) 459
30) W. J. King and M. W. Johns, Can. J. Phys. **37** (1959) 755
31) J. J. Griffin and M. Rich, Phys. Rev. **118** (1960) 850
32) A. B. Migdal, Nuclear Physics **13** (1959) 655
33) W. H. Johnson and V. B. Bhanot, Phys. Rev **107** (1957) 1669

1.E.3 *Nuclear Physics* **25** (1961) 404—408; © *North-Holland Publishing Co., Amsterdam*
Not to be reproduced by photoprint or microfilm without written permission from the publisher

THE GYROMAGNETIC RATIO OF THE 137 keV ROTATIONAL LEVEL IN Os^{186}

C.-A. LERJEFORS, E. MATTHIAS and E. KARLSSON
Institute of Physics, University of Uppsala, Uppsala

Received 23 February 1961

Abstract: Using a 4-channel coincidence apparatus we have investigated the influence of an external magnetic field on the angular correlation of the 631—137 keV cascade in Os^{186}. The strength of the magnetic interaction was found to be

$$|\omega_L \tau_N| = 0.043 \pm 0.010 \text{ rad}$$

for a magnetic field of ± 29200 G. Averaging the result of all lifetime determinations, we get $T_{\frac{1}{2}} = (7.0 \pm 0.9) \times 10^{-10}$ s. This gives

$$g_R = +0.30 \pm 0.08$$

for the gyromagnetic ratio of the 137 keV rotational state. There is no evidence for the existence of internal perturbations in the liquid source used.

1. Introduction

In a previous paper [1]), the authors reported the measurement of the gyromagnetic ratio of the first excited state in Os^{188}. This nucleus is one of the last in the deformed region that shows rotational properties. In trying to systematize the variation of the rotational g-factor for deformed even nuclei, we have now undertaken the measurement of the nearby isotope Os^{186}. The effect of the larger deformation of this nucleus [2]), compared to Os^{188}, is expected to appear in the results of the g-factor measurements. Neither of these cases require a paramagnetic correction.

From the isotopes measured so far [1]), it is evident that the picture of uniformly charged nuclear matter, giving $g_R = Z/A$, does not describe the situation properly. Effectively all results show a value considerably below Z/A. A more refined theory of nuclear structure, the superfluidity model [3]), may however be able to explain some details of the nuclear structure and imply relationships between nuclear properties, e.g. the dependence of the g-factor on the mass number A. A bulk of experimental data is required, however, to make such trends apparent. Although, for intensity reasons, it is difficult to determine the g-factor in Os^{186} accurately, the result should still be valuable from a systematical point of view.

The method used is based on the observation of the shift $\omega_L \tau_N$ in the angular correlation pattern that results from the application of an external magnetic

field. The measurements were performed with the 4-channel coincidence apparatus described earlier [1]). Because of its gain in statistical accuracy this instrument is of great advantage for low intensity cascades.

2. Experimental

The decay of 90 h Re^{186} goes partly [4]) to W^{186} (4 %) partly to Os^{186} (96 %). Only one excited state in W^{186} is populated and therefore no coincidences from this branch interfere with our measurements. Only 0.07 % of the total decay feeds the 768 keV level, while 23.1 % and 73.0 % go to the first excited state and the ground state, repectively (fig. 1). For this reason the 631—137 keV

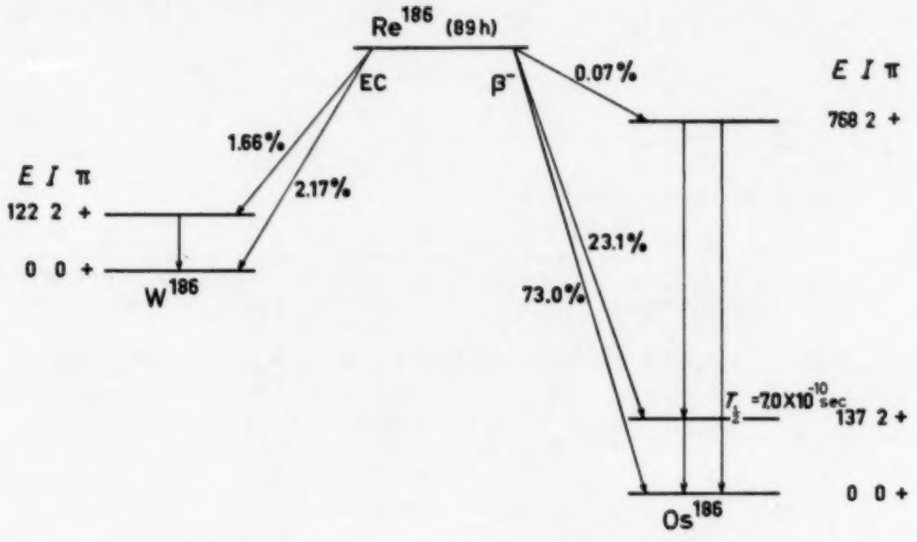

Fig. 1. Decay scheme of Re^{186}

cascade is extremely weak. The high population of the 137 keV level causes a large amount of accidental coincidences which makes it necessary to use rather weak sources. The time resolution of the fast coincidence matrix was 30 ns.

Earlier γ—γ angular correlation measurements are summarized in table 1. The results obtained with a metallic Re source obviously show a strong perturbation due to electric quadrupole interactions. For the liquid source the perturbation should be time-dependent and the ratio $\lambda_2/\lambda_4 = 1.70$ is expected for spin 2 of the intermediate level [7]). The attenuation factors given by King and Johns for Re dissolved in hydrogen peroxide leads to $\lambda_2/\lambda_4 = 0.3$. For this reason, it is not probable that these attenuation factors are due to a real internal perturbation. In fact, it is expected that the effect of the source conditions should be nearly the same for both Os^{186} and Os^{188} as the life-time of the corresponding states and the quadrupole moments of these nuclei are almost equal. As pointed out before [1]), a liquid source of Re metal dissolved in nitric acid and diluted does not seem to show any appreciable attenuation effects. Therefore, all our measurements were performed with such sources.

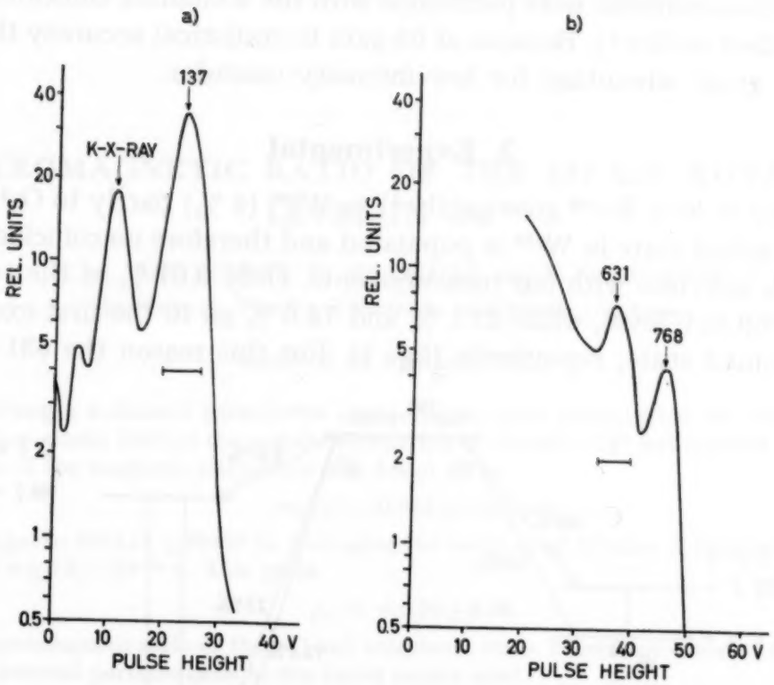

Fig. 2. Single spectrum of Re^{186} taken with 3.81 cm by 5.04 cm NaI(Tl) crystals and light guides of 18.5 cm lengths. a) Low energy part with 0.25 mm tin absorber. b) High energy part with 1.8 mm lead absorber.

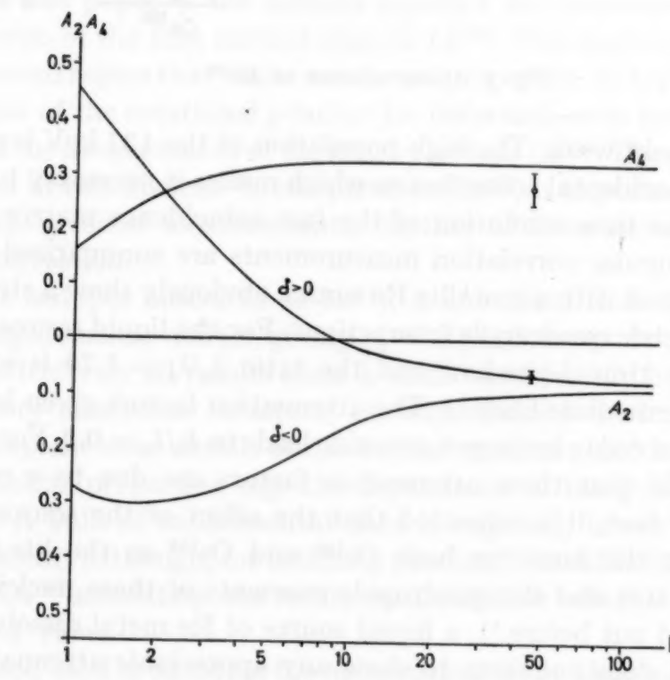

Fig. 3. Mixing ratio for the first transition of the 2−2−0 cascade in Os^{186}.

A typical single spectrum taken with a 3.81 cm by 5.08 cm crystal is shown in fig. 2. The detectors accepting the high energy γ-rays were equipped with 1.8 mm lead absorbers in order to avoid pile up effects in the channels. Tin absorbers, 0.25 mm thick, were used in front of the low energy detectors to suppress the intense K-X-ray peak. Scattering between the detectors was prevented by heavy lead shields. Four combinations of the 4-detector system [1]) were used in obtaining the coincidence data. The angular correlation was such that the shifts were obtained most exactly at the angles 112.5° and 157.5°. In addition, for the determination of the coefficients the ratio $W(180°)/W(132°)$, which showed the maximum anisotropy, was measured. After correction for the solid angles of the detectors, we obtained the angular correlation coefficients

$$A_2 = -0.06 \pm 0.01, \quad A_4 = +0.28 \pm 0.03.$$

The A_2-term indicates a lower limit $\delta > 20$ for the mixing ratio of the 631 keV transition (fig. 3). A possible attenuation in A_2 would displace the limit for δ still higher. The condition $\delta > 20$ requires, however, that A_4 should have the value +0.327. This discrepancy is probably caused by an attenuation due to uncontrollable factors such as scattering in the magnet iron and in the source as well as geometrical uncertainties for the source of 4 mm diameter. From the measured A_4-coefficients, we obtained an attenuation factor $G_4^{\text{eff}} = 0.86 \pm 0.09$. It should be noticed that in the corresponding measurements of Os^{188} performed with the same experimental set up [1]), we found $G_4^{\text{eff}} = 0.87$. This was probably caused by the same effects. For the above reasons, we have in the following calculations assumed that no internal perturbations were present.

TABLE 1

Previous γ—γ angular correlation measurements

Authors	T. Lindqvist and I. Marklund [5])	W. J. King and M. W. Johns [6])	
Source conditions	metallic powder	metallic powder	Re powder dissolved in H_2O_2
A_2	-0.02 ± 0.01	-0.026 ± 0.003	-0.056 ± 0.003
A_4	$+0.18 \pm 0.03$	$+0.061 \pm 0.003$	$+0.123 \pm 0.004$
G_2		0.44	0.69
G_4		0.19	0.38
δ	10 ± 2	10	10

3. Results

The measurements and the treatment of data were performed in exactly the same manner as described earlier [1]). The result obtained for the magnetic interaction was

$$|\omega_L \tau_N| = 0.043 \pm 0.010 \text{ rad}$$

for a magnetic field of $\pm 29\,200$ G.

The evaluation of the g-factor requires a knowledge of the life-time of the excited state in question. Three measurements of the life-time have been reported:

$$T_{\frac{1}{2}} = (8.0 \pm 1.0) \times 10^{-10} \text{ sec } (\text{ref. } ^{8}),$$
$$T_{\frac{1}{2}} = (6.0 \pm 2.0) \times 10^{-10} \text{ sec } (\text{ref. } ^{9}),$$
$$T_{\frac{1}{2}} = (5.1 \pm 1.5) \times 10^{-10} \text{ sec } (\text{ref. } ^{10}).$$

The first two values were obtained by the delayed coincidence method; the third was calculated from Coulomb excitation data. Since we cannot estimate the reliability of the different measurements, we preferred to use the weighted mean

$$\tau = (1.01 \pm 0.13) \times 10^{-9} \text{ sec.}$$

The final result of the gyromagnetic ratio is

$$g = +0.30 \pm 0.08.$$

If the attenuations mentioned above should actually prove to be due to internal time-dependent interactions, which is very improbable, this value would be increased by at most 14 %. Our result thus seems to fit well into the general trend of data [1, 11]) for gyromagnetic ratios of rotational states in the deformed region, showing $g_R < Z/A$.

The authors are indebted to Professor K. Siegbahn for excellent working conditions and his stimulating interest in this work. Our thanks are due to Mr. K. Sevier for correcting the English.

References

1) E. Karlsson, C. A. Lerjefors and E. Matthias, Nuclear Physics **24** (1961) 385
2) K. Alder, A. Bohr, T. Huus, B. Mottelson and A. Winther, Rev. Mod. Phys. **28** (1956) 432
3) A. B. Migdal, Nuclear Physics **13** (1959) 655
4) F. T. Porter, M. S. Freedman, T. B. Novey and F. Wagner Jr., Phys. Rev. **103** (1956) 921
5) T. Lindqvist and I. Marklund, Nuclear Physics **4** (1957) 189
6) W. J. King and M. W. Johns, Can. J. Phys. **37** (1959) 755
7) A. Abragam and R. V. Pound, Phys. Rev. **92** (1953) 943
8) F. K. McGowan, Phys. Rev. **81** (1951) 1066
9) E. E. Berlovich, JETP (Soviet Physics) **6** (1958) 1176
10) F. E. Durham, D. H. Rester and C. M. Class, Bull. Am. Phys. Soc. **4** (1959) 98
11) E. M. Bernstein and J. de Boer, Nuclear Physics **18** (1960) 40

1.D.2:
1.E.1:2.C

Nuclear Physics **25** (1961) 409—420; © *North-Holland Publishing Co., Amsterdam*
Not to be reproduced by photoprint or microfilm without written permission from the publisher

THE REACTION $^{28}Si(p, \gamma)^{29}P$

K. J. VAN OOSTRUM †, N. HAZEWINDUS, A. H. WAPSTRA,
Laboratorium voor Technische Natuurkunde, Technische Hogeschool, Delft, Nederland
J. W. OLNESS and J. L. PARKER
Aeronautical Research Laboratory, Wright-Patterson Air Force Base, Ohio, USA

Received 10 February 1961

Abstract: The level structure of ^{29}P has been investigated with the reaction $^{28}Si(p, \gamma)^{29}P$ for proton energies between 0.3 MeV and 2.3 MeV. Levels of ^{29}P at 3.09 MeV, 4.34 MeV and 4.76 MeV were excited with (p, γ) resonances at proton energies of 0.371 MeV, 1.65 MeV and 2.09 MeV, respectively. The strength γ of a resonance expected for excitation of a 3.49 MeV level in ^{29}P has been derived to be less than 5×10^{-4} eV. This low value is attributed to K-forbiddenness of the gamma ray decay of this level. Gamma rays from the 0.371 MeV resonance lead to levels at 1.95 MeV and 1.37 MeV; those from the 1.65 MeV resonance lead to the ground state and, rather weakly, to the 1.37 MeV state; gamma rays from the 2.09 MeV resonance lead to the ground state only. Angular distributions are in agreement with the following spin assignments for the levels of ^{29}P: 1.37 MeV ($\frac{3}{2}$), 1.95 MeV ($\frac{5}{2}$), 3.09 MeV ($\frac{5}{2}$), 4.34 MeV ($\frac{3}{2}$) and 4.76 MeV ($\frac{1}{2}$). The excited states found in these experiments are assigned to rotational bands based on Nilsson orbits 8, 9, 10, 11 and 16.

1. Introduction

The rotational collective model has been succesfully applied to the description of low-lying levels of ^{29}Si by Bromley and co-workers [1]). As a test of the collective model, however, their work was necessarily restricted to the extent that an experimental description of this nucleus had been obtained. Since the mirror nucleus ^{29}P differs from ^{29}Si only in the last added nucleon, having in common a relatively stable ^{28}Si core, it is expected that the low-lying levels of ^{29}P should exhibit essentially the same collective properties as those of ^{29}Si. An investigation of the level structure of ^{29}P should thus permit further conclusions with respect to the collective behaviour of these nuclei. The $^{28}Si(d, n)^{29}P$ measurements of Macefield and Towle [2]) and the ^{28}Si (p, p)^{28}Si measurements of Vorona *et al.* [3]) have resulted in the level ordering presented in fig. 1.

The experiments described in the present paper were undertaken to provide a more complete description of the lower-lying levels of ^{29}P through investigation of the reaction $^{28}Si(p, \gamma)^{29}$ P for proton energies between 0.3 and 2.3 MeV. The measurements reported here were carried out simultaneously at the two laboratories listed in the title of this paper [4, 5]). The agreement between the

† Present address: Instituut voor Kernphysisch Onderzoek, Amsterdam, Nederland.

experimental determinations of resonance energies and gamma ray energies lies well within the experimental errors, and hence average values have been quoted throughout the following sections. Because of the essential similarities of the experimental apparatus only that of the Delft group is described in detail.

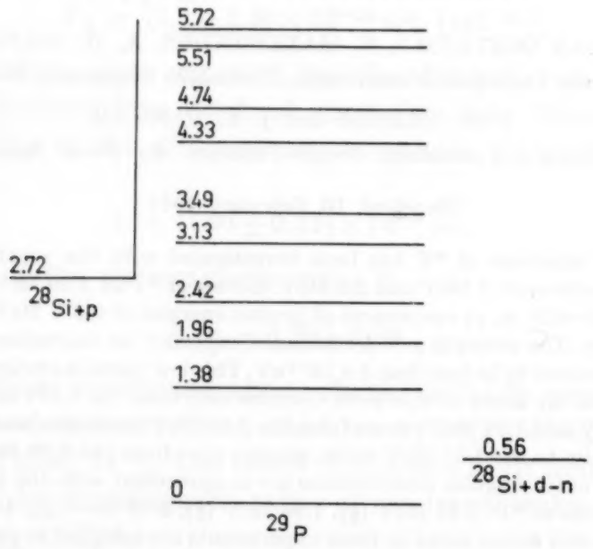

Fig. 1. Excitation energies of levels of ^{29}P determined from the reactions ^{28}Si(d, n)^{29}P (ref. [2])) and ^{28}Si(p, p)^{28}Si (ref. [3])).

After this paper had been sent to the editor, an article by Newton [6]) appeared describing measurements on the resonances at 1.65 MeV and 2.09 MeV. Since most of his results agree with ours, the original text was abridged at these points.

2. Experimental Apparatus and Procedure

Protons from the Delft 2.5 MeV Van de Graaff accelerator were analyzed by a 90° analyzing magnet with a radius of curvature of 80 cm. The energy spread of the emergent proton beam, as defined to first order by a set of tantalum exit slits, was measured to have a minimum value of 1 keV at 1 MeV proton energy [4]).

The target apparatus and counter assembly are shown in fig. 2. The electrically isolated target, located at an angle of 35° with respect to the beam direction, consisted of a tantalum disc 2.5 cm in diameter and 0.2 mm thick onto which the target material had been evaporated in vacuo. Natural silicon targets were prepared by evaporating silicon dioxide; targets enriched in ^{28}Si were obtained from A.E.R.E., Harwell. An oil cooling system (not shown in the diagram) was used to absorb heat generated in the exit slit and target

holder. The beam current was measured with a simple current integrator [7]). A repeller ring, maintained at a potential of −300 V, was located between the beam-defining diaphragm and target to improve the accuracy of this measurement. In order to prevent the possible evaporation of the target material it was necessary to limit the intensity of the incident beam to values corresponding to a power dissipation in the target of 10 W or less.

The gamma radiations produced under bombardment were measured with two 7.6 cm × 7.6 cm Harshaw NaI(Tl) scintillation crystals, one coupled to an EMI 9531 photomultiplier (window diameter 7.6 cm) and the other to a Dumont 6364 photomultiplier (window diameter 10.4 cm). The crystals were

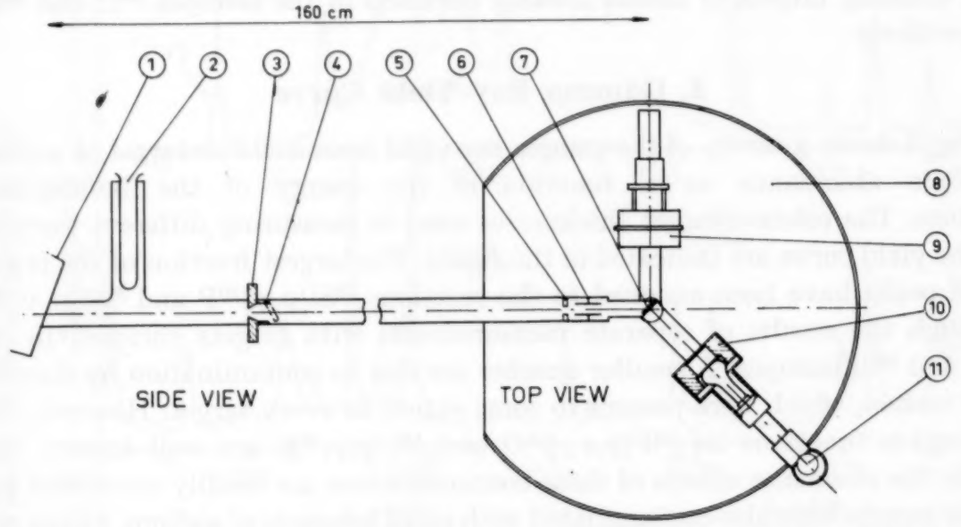

Fig. 2. Schematic drawing of the experimental setup. 1: Analysing magnet. 2: Liquid air trap. 3: Tantalum exit slit. 4: Vacuum valve. 5: Circular tantalum diaphragm. 6: Cylindrical repeller. 7: Electrically isolated target. 8: Angular distribution arrangement. 9: Scintillation counter. 10: Lead shielding. 11: Servomotor.

shielded with 4.5 cm of lead, and could be placed directly against the target holder, where some additional shielding was also provided. The efficiency of this geometry was measured by means of a new semi-empirical method [8]).

The scintillation detectors were fixed to apparatus suitable for angular distribution measurements, as shown in fig. 2. One counter could be rotated in a horizontal plane about an axis through the target spot by means of a small servomotor which acted on a bicycle chain around the side of the table. The second counter was located in a fixed position with respect to the beam direction.

Spectra were recorded with a 256-channel pulse-height analyzer, R.C.L. model 20611. For coincidence measurements a Franklin model-348 linear amplifier with discriminator was used to open the coincidence gate of the analyzer.

The arrangement at the A.R.L. was essentially similar, the principal differences being the use of an air-water spray for target cooling and the selection of 30° for the target angle. Targets of zone-refined metalic silicon (of natural isotopic composition) and also of silicon dioxide enriched in ^{28}Si were prepared by evaporation onto a tantalum disc. A single 7.6 cm × 7.6 cm NaI(Tl) crystal shielded by 8 cm of lead was used for measurements of yield curves and angular distributions; a second 7.6 cm × 7.6 cm counter was employed as a monitor in the angular distribution measurements. Pulse height spectra were analyzed with a 256-channel R.I.D.L. analyzer and amplifier. The A.R.L. work also included the measurement of yield curves for ^{29}Si(p, γ)^{30}P and ^{30}Si(p, γ)^{31}P, utilizing targets of silicon dioxide enriched in the isotopes ^{29}Si and ^{30}Si, respectively.

3. Gamma Ray Yield Curve

Fig. 3 shows a survey of the gamma ray yield from a silicon target of natural isotopic abundance as a function of the energy of the bombarding protons. The relative target thicknesses used in measuring different portions of the yield curve are indicated in the figure. The largest fraction of the resonance peaks have been assigned to the reactions ^{29}Si(p, γ)^{30}P and ^{30}Si(p, γ)^{31}P through the results of separate measurements with targets enriched in the ^{29}Si and ^{30}Si isotopes. A smaller number are due to contamination by fluorine and carbon, which were present to some extent in every target. However, the excitation functions for ^{19}F(p,$\alpha\gamma$)^{16}O and ^{12}C(p,γ)^{13}N are well known, and hence the resonance effects of these contaminations are readily accounted for. Some targets were also contaminated with small amounts of sodium, giving rise to resonance peaks from ^{23}Na(p, γ)^{24} Mg and ^{23}Na(p, $\alpha\gamma$)^{20}Ne. Again, the excitation functions for these reactions are known well enough to account for the effects of this contamination on the resonance curve of fig. 3.

Having first eliminated from consideration those resonances due to the contaminations listed above, two additional criteria were applied to determine whether or not the remaining resonances were indeed due to resonances in ^{28}Si(p, γ)^{29}P, as follows†:

a) The excitation energies in ^{29}P calculated from the energies of the gamma rays involved in the decay of the level must agree with the value calculated from the resonance proton energy and the Q-value for ^{28}Si(p, γ)^{29}P, given by Everling *et al.* [9]) as 2.735±0.011 MeV.

b) The resonance must also appear in the yield curve measured with targets enriched in the isotope ^{28}Si.

† The silicon targets used in the yield curve measurements of fig. 3 were prepared from a crystal-ingot of zone-refined silicon, which had as principal contaminants only trace amounts of ^{19}F and ^{12}C. In this respect, these targets were far superior to those prepared from $^{28}SiO_2$, which exhibited rather severe contaminations of the above elements and also of sodium. The sequence of considerations given above was therefore chosen as being superior to possible alternative sequences.

As a conclusion of these considerations, the resonance peaks at 0.37, 1.65 and 2.09 MeV have been assigned to resonances in $^{28}Si(p, \gamma)^{29}P$ (see table 1). No evidence was found for a resonance in ^{28}Si $(p, \gamma)^{29}P$ expected to excite the 3.49 MeV level of ^{29}P. The position of this level is given from recent (d,n) measurements [2]) as 3.49 ± 0.03 MeV. This portion of the yield curve of fig. 3, in the region

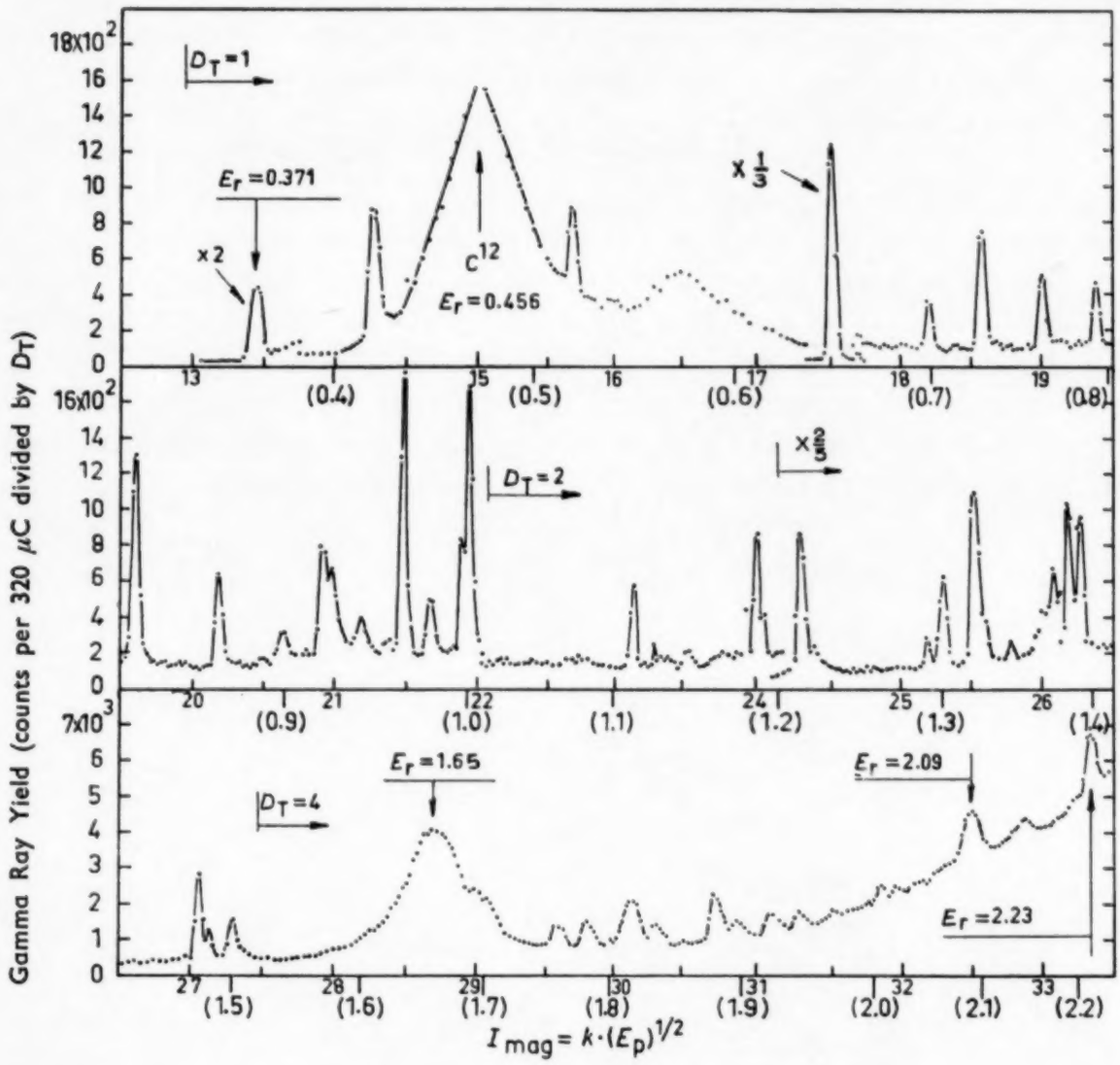

Fig. 3. Gamma ray yield from proton bombardment of natural silicon. The relative yield of gamma rays of energy greater than 1.2 MeV is plotted versus the current I_{mag} through the beam analysing magnet. Proton energies as calculated from a subsequent calibration of the analyzer are also shown. The relative thickness of the targets used for different portions of the run are given as D_T. Values of I_{mag} and D_T are given in arbitrary units.

of $E_p = 0.78$ MeV, exhibits only resonance peaks due to ^{29}Si and ^{30}Si; these peaks do not appear in the yield curve measured with a $^{28}SiO_2$ target. An upper limit for the resonance strength of this undetected level is given in sect. 5.

Special attention was centered on the 2.23 MeV peak shown in fig. 3, since the gamma ray spectrum obtained at this peak shows a single strong line at

4.88 MeV, which corresponds very closely to the energy expected for a ground state transition in ^{29}P. However, additional measurements have shown that the peak does not appear in the yield curves obtained with the $^{28}SiO_2$ targets, and hence does not arise as a resonance in ^{28}Si (p, γ)^{29}P. It should also be pointed out that no evidence was found for such a level in the (p, p) scattering data of Vorona [3]). The 2.30 MeV resonance in ^{28}Si (p, p' γ) ^{28}Si reported by Newton is evidently not identical with the 2.23 MeV resonance discussed above, since the first shows a 1.78 MeV gamma ray not present in the other.

4. Gamma Ray Spectra

Gamma ray spectra were measured at the three resonance energies with the crystal axis at an angle of 55° with respect to the proton beam in order to measure intensity values averaged for angular distributions (if no terms of higher order than $\cos^2 \vartheta$ occurred in the angular distribution function). The resonance spectra are shown in figs. 4, 5, 6. The "background" spectra, measured at proton energies slightly below the resonance energies, are shown by the dashed curves. The proposed decay scheme of each resonance level is shown as an insert in these figures.

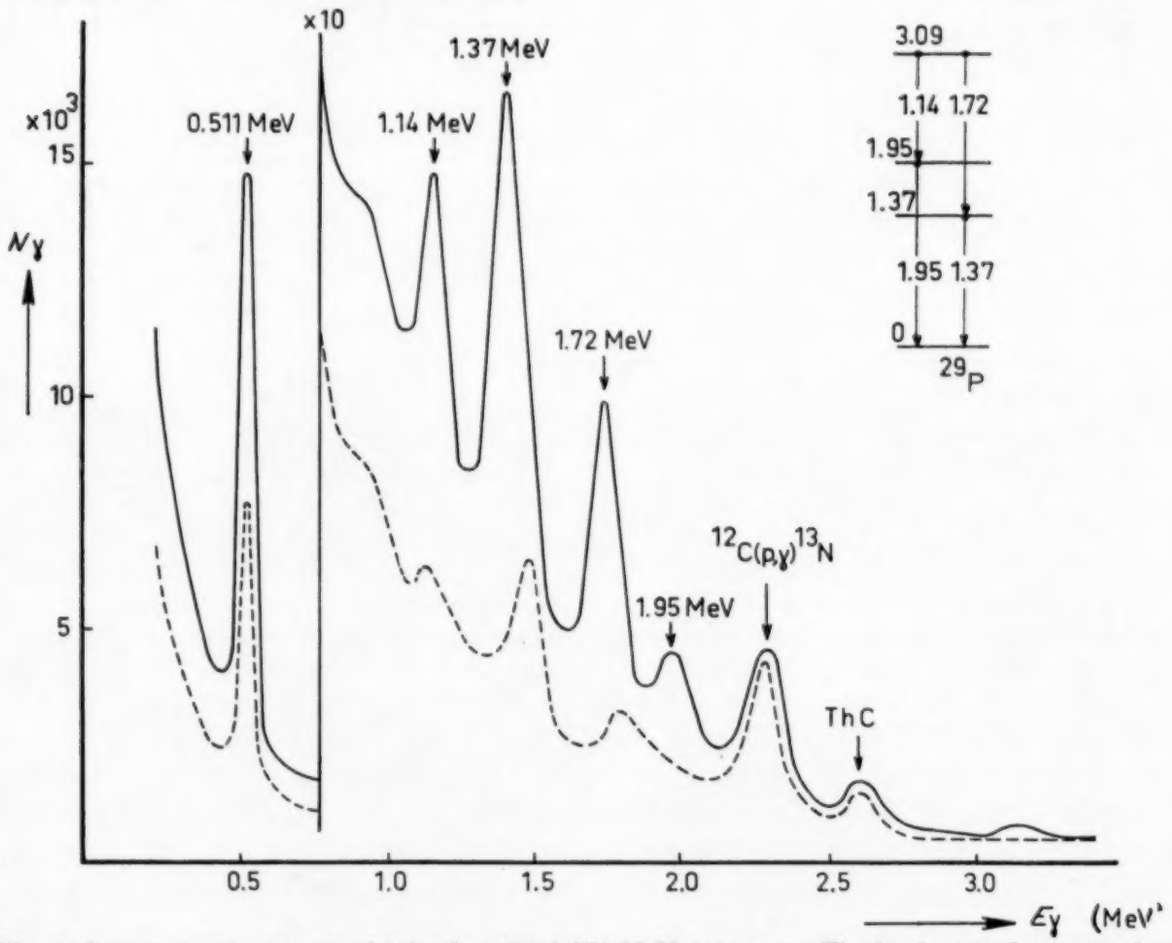

Fig. 4. Gamma ray spectrum obtained at the 0.371 MeV resonance. The background measured at 0.365 MeV is shown as a dashed curve. The insert shows the decay scheme.

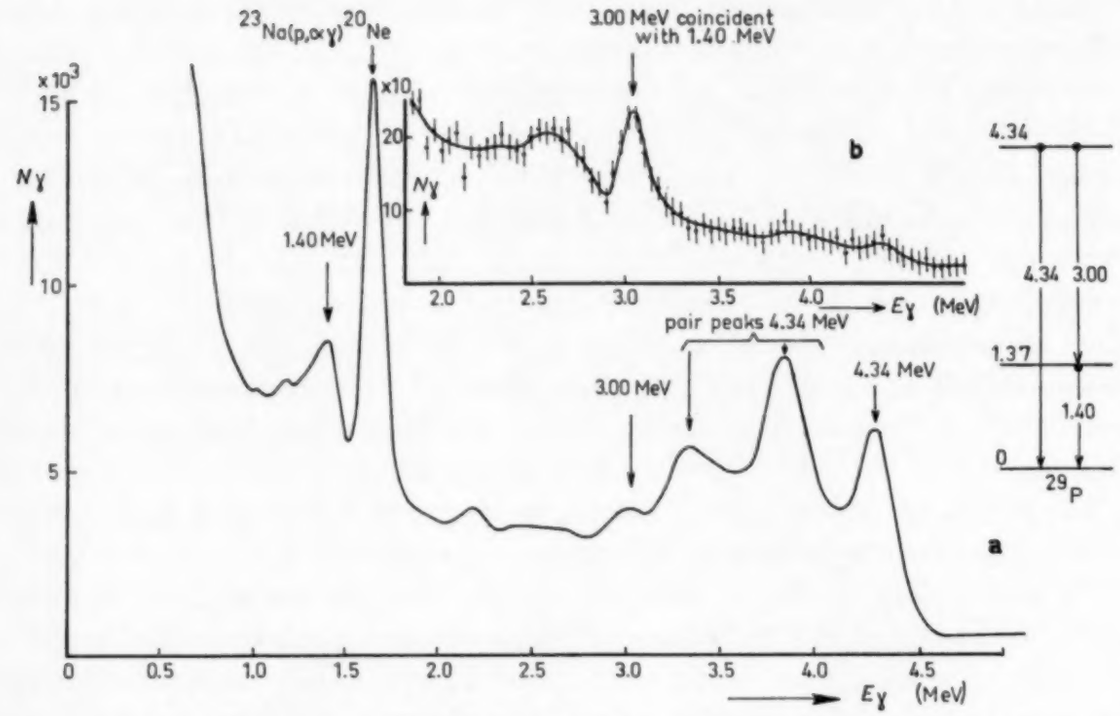

Fig. 5. Gamma ray spectra obtained at the 1.65 MeV resonance. a) Spectrum obtained with a single crystal. b) Spectrum obtained in coincidence with the 1.40 MeV gamma ray as seen by a second crystal. The insert shows the decay scheme.

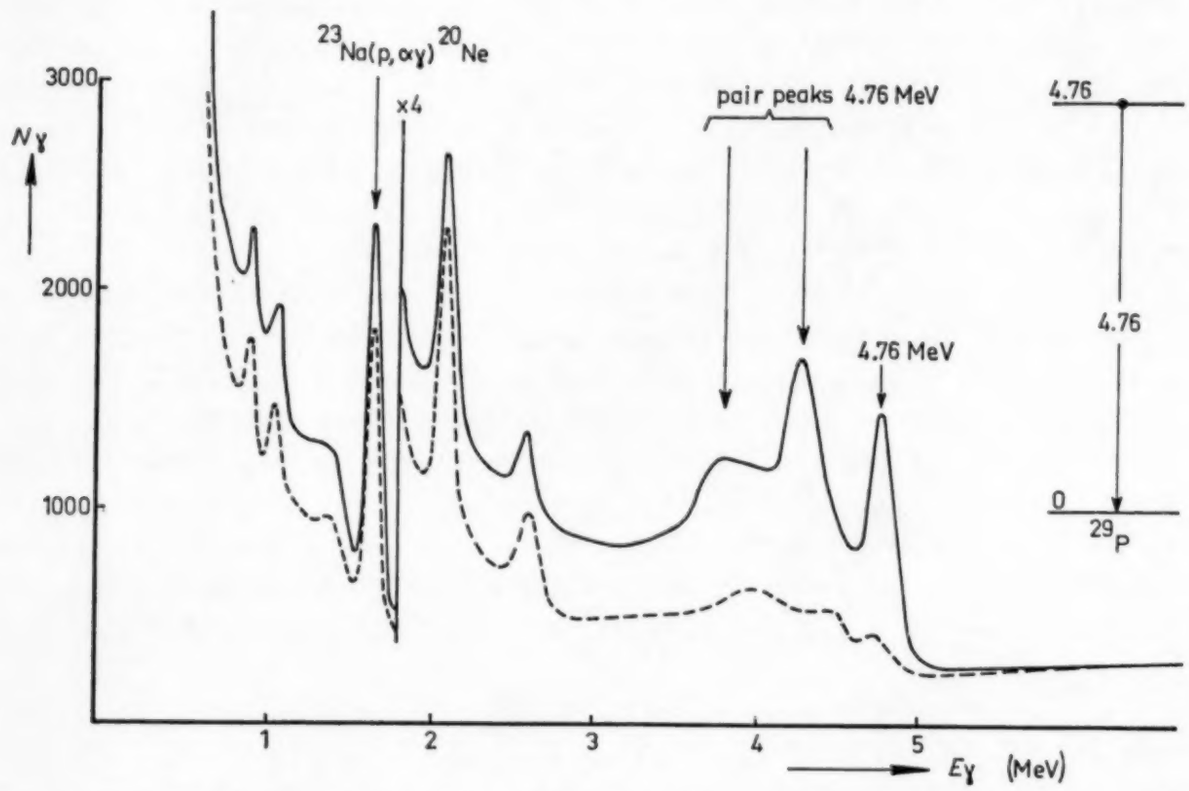

Fig. 6. Gamma ray spectrum obtained at the 2.09 MeV resonance. The background measured at 2.07 MeV proton energy is shown by the dashed curve. The insert shows the decay scheme.

The spectrum obtained at 0.371 MeV proton energy shows five peaks in addition to those present in the background spectrum. (The prominent background lines are labelled as follows: 1.12 MeV from ^{65}Zn; 1.46 MeV from ^{40}K; 2.3 MeV from the broad ^{12}C (p, γ)^{13}N resonance at 0.450 MeV proton energy; and 2.6 MeV from Th C.) The energies and intensities of the 1.14 MeV, 1.37 MeV, 1.72 MeV and 1.95 MeV resonance lines are fitted by the two cascade decays shown in the proposed decay scheme. The fifth peak at 3.1 MeV can be entirely explained as the sum peak of these cascade transitions. No coincidence measurements have been carried out because of the weakness of this resonance, but the assignment of these lines to cascade transitions in ^{29}P is quite certain from a full examination of the above considerations. The intensity ratios (see table 1) confirm the tentative decay scheme based on a densitogram of this spectrum given in a previous paper [10]). The energies and intensity ratios agree with the results of Tabata and co-workers [11]).

The gamma ray spectrum obtained at 1.65 MeV proton energy is shown in fig. 5. No background spectrum was measured here; since the half-width of this resonance is very large, the background spectrum taken below the peak would probably not be representative. The strongest background line at 1.6 MeV can be attributed to ^{23}Na (p, $\alpha\,\gamma$)^{20}Ne. The energies of the 1.40 and 3.00 MeV lines sum up to the energy of the highest peak at this resonance, 4.34 MeV, within the experimental errors. A coincidence measurement with the full-absorption peak of the 1.40 MeV radiation gave the spectrum shown in fig. 5b, indicating coincidence between the 1.40 and 3.00 MeV lines. The cascade has not been found by Newton [6]) who placed only an upper limit of 20 % on its intensity, which does not disagree with our results. The energies of other small peaks in the gamma ray spectrum could not be fitted into the level scheme of ^{29}P, and are probably due to unidentified contamination. A coincidence measurement did not give information about these lines.

Figure 6 shows the resonance spectrum obtained at $E_p = 2.09$ MeV. The dashed curve shows a background spectrum measured at 2.07 MeV. Only the 4.76 MeV gamma ray could be unambiguously attributed to the resonance considered.

The information on level energies and modes of decay obtained from these spectra are summarized in table 1. The excitation energies given for the ^{29}P levels have been calculated from the gamma ray energies. For each resonance the Q-value has been calculated from the proton energy and the excitation energy. The most accurate value, as obtained for the 0.371 MeV resonance, does not quite agree with the value (2.760 ± 0.013 MeV) given by Okano and co-workers [12]).

Gamma ray spectra were measured at several angles ϑ with respect to the incident proton beam direction for each of the 3 resonances thus studied. Our results were in agreement with those of Okano *et al.* [12]) and Newton [6]), as already described elsewhere [4]).

TABLE 1

Resonances in $^{28}Si(p, \gamma)^{29}P$

proton energy (MeV)		0.371±0.001				not found	1.65±0.01		2.09 ±0.01
excitation energy (MeV) resonance level		3.091±0.008				3.49 ±0.03 [a]	4.34±0.02		4.76 ±0.02
Q-value (MeV)		2.735±0.008					2.75±0.02		2.74 ±0.02
gamma ray energy (MeV)		1.373 ±0.008	1.947 ±0.008	1.719 ±0.008	1.143 ±0.008		1.40 ±0.03	4.34 ±0.02	3.00 ±0.03	4.76 ±0.02
excitation energy (MeV)	initial level	1.373 ±0.008	1.947 ±0.008	3.091 ±0.008	3.091 ±0.008	3.49 ±0.03	1.373 ±0.008	4.34 ±0.02	4.34 ±0.02	4.76 ±0.02
	final level	0	0	1.373 ±0.008	1.947 ±0.008	1.947 ±0.008 [b]	0	0	1.373 ±0.008	0
gamma quanta per proton		$(4.9\pm0.5)\times10^{-13}$	$(2.4\pm0.2)\times10^{-13}$	$(5.5\pm0.5)\times10^{-13}$	$(1.8\pm0.3)\times10^{-13}$			$(5.9\pm0.5)\times10^{-10}$	$(0.8\pm0.2)\times10^{-10}$	$(6.9\pm0.7)\times10^{-11}$
branching ratio (%)		100	100	71	29		100	88	12	100
resonance strength γ(eV)		$(0.8\pm0.1)\times10^{-3}$				$<0.5\times10^{-3}$	1.85±0.40			0.43 ±0.08
gamma ray width Γ_γ(eV)		$>0.8\times10^{-3}$				$<0.5\times10^{-3}$	1.85±0.40			0.43 ±0.08
proton width Γ_p(eV)		$<10^3$, $>0.8\times10^{-3}$					$(44\pm4)\times10^3$			$(15\pm3)\times10^3$
reduced proton width θ_p		$>1.2\times10^{-3}$					0.34			2.3×10^{-2}

[a]) According to results obtained by Macefield and Towle [2]) with the reaction $^{28}Si(d, n)^{29}P$.

[b]) If the resonance level decays in the same way as its mirror level [14]) in ^{29}Si.

5. Resonance Strengths

The resonance strengths γ of four of the resonance levels in ^{29}P were calculated from the experimental determinations of N_1, the number of resonance levels produced per proton striking a "thick" target. The graphs given by Gove [13]) for target stopping powers were used in these calculations. The results given in table 1 are in agreement with those given by Okano [12]) and Newton [6]) for the three detected resonance levels.

The upper limit on γ for the 3.49 MeV level, which was not detected, was obtained from the measured gamma ray yield curve in the region $0.75 < E_p < 0.81$ MeV. It was assumed in this calculation that the level should decay to the ground state via cascade through the 1.95 MeV level, in analogy to the 3.62 MeV level [14]) of the mirror nucleus ^{29}Si.

The calculated values of γ were used to obtain lower limits for proton widths Γ_p and gamma ray widths Γ_γ. For either of the two extremes $\Gamma_p \gg \Gamma_\gamma$ or $\Gamma_\gamma \gg \Gamma_p$ the resonance strength is approximately equal to the smaller of the two widths. Thus for the 3.49 MeV level it has been shown that (probably) $\Gamma_p > \Gamma_\gamma$ for the alternative assumption $\Gamma_\gamma > \Gamma_p$ leads to a value for the reduced proton width of $\vartheta_p < 10^{-4}$, which is considerably less than the lower limit set by van der Leun [15]) of $\vartheta_p > 7 \times 10^{-4}$. (Proton reduced widths are given here as fraction of the Wigner single-particle limit.)

6. Discussion

A summary of the information presently available on the excited levels of nuclei having a 15th nucleon as odd particle (^{29}P, ^{29}Si and ^{31}P) is presented schematically in fig. 7. The application of the rotational collective model to ^{29}Si and ^{31}P is reported in the literature: the work of Broude *et al.* [16]) on ^{31}P resulted in the assignment of the ground state and six excited levels to rotational bands based on Nilsson orbits [17]) 8, 9 and 11, Bromley *et al.* [1]) assigned the low-lying levels of ^{29}Si to bands based on orbits 8, 9 and 10. (Bands 8 and 9 give rise to the same level order in these nuclei, while different orders are obtained for bands of higher orbit number.) Both of the above groups deduced an oblate shape for the deformation of these nuclei.

In view of the obvious correspondence between the level structure of the mirror nuclei ^{29}P and ^{29}Si, especially for the low-lying levels, we have assumed in the following that the collective model assignments of ^{29}Si are equally valid for ^{29}P. In this respect the assignment of the 3.07 MeV level in ^{29}Si as the $J = \frac{5}{2}$ member of the $\Lambda = \frac{3}{2}$ band based on orbit 8 obtains support from the spin value $J = \frac{5}{2}$ of the 3.09 MeV mirror level in ^{29}P. The modes of decay of these two mirror levels are found to be quite similar; somewhat less similarity is observed to exist between these levels and the 3.29 MeV level in ^{31}P.

The 3.62 MeV level in ^{29}Si has been shown to have a spin of either $\frac{5}{2}$ or $\frac{7}{2}$ and negative parity. The assignment of this level to the $K = \frac{7}{2}$ band based on orbit 10 provided one of the arguments used by Bromley *et al.* [1]) in deducing a negative distortion parameter for ^{29}Si. From the experiments described in the present paper it has been found that the 3.49 MeV mirror level in ^{29}P has a gamma ray width of les than 5×10^{-4} eV. The Weisskopf-estimate for this width, assuming an E1 transition to the 1.95 MeV level (in analogy to

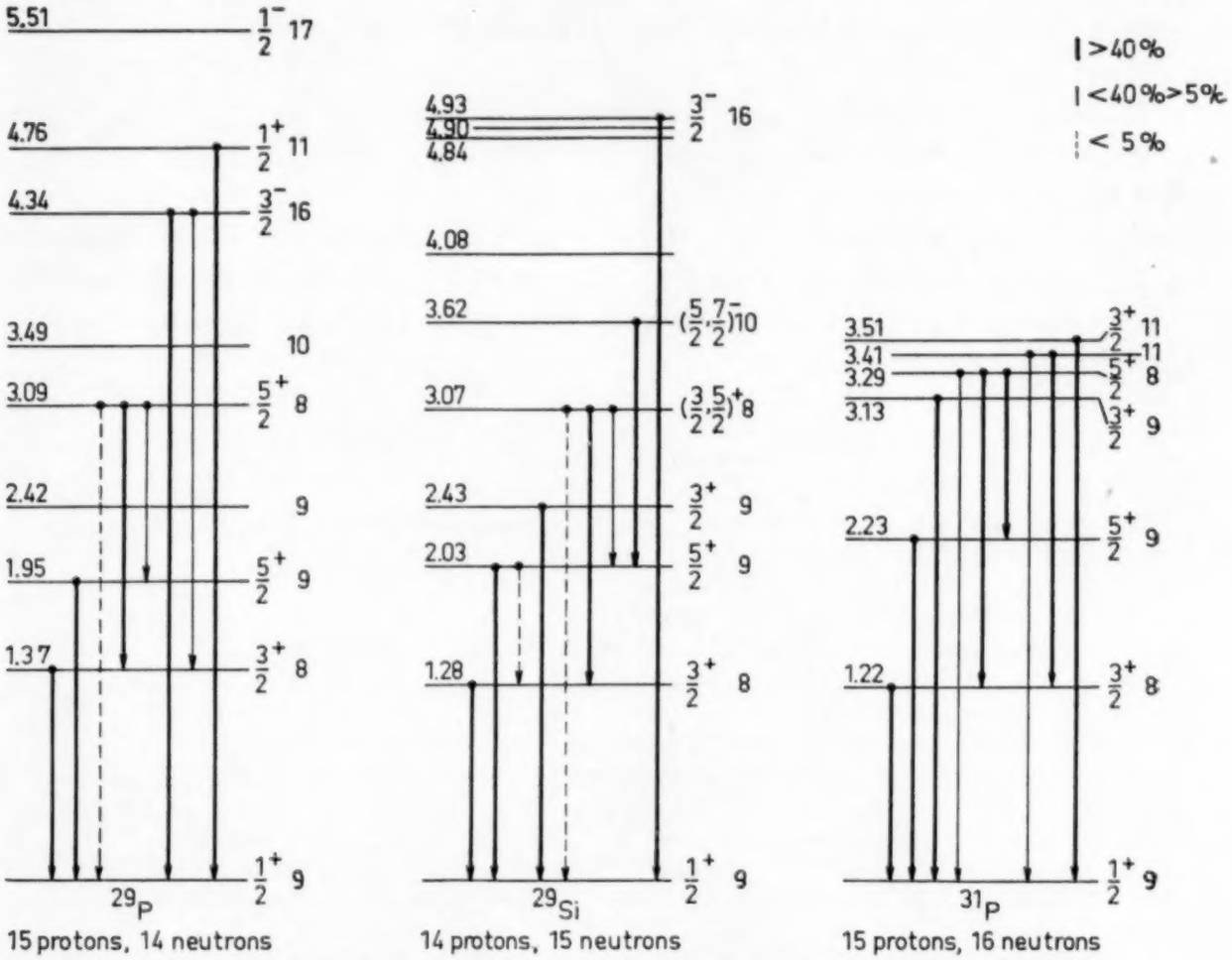

Fig. 7. Level schemes of three nuclei with the odd particle in Nilsson orbit 9($s_{\frac{1}{2}}$) in the ground state. For each level the excitation energy is given on the left side of the figure. The spin, parity and the Nilsson orbit-number are given on the right side. The relative intensities of the gamma transitions are indicated by the various line thicknesses.

the decay of the 3.62 MeV level in ^{29}Si as reported by Litherland [14]) is 2.6 ev, so that an inhibition factor of at least 5×10^{3} must exist for this transition. This large factor can be explained as due to the operation of K-forbiddeness for transitions between $K = \frac{7}{2}$ and $K = \frac{3}{2}$ bands, and is taken as additional evidence for the assignment of this level, and also the mirror level in ^{29}Si, to orbit 10.

A band based on orbit 11 has been assigned in ^{31}P but not in ^{29}Si. The spin

and parity of the 4.76 MeV level in ^{29}P have been established as $\frac{1}{2}^+$. Within this region of excitation energy such a level can arise only as an excitation of orbit 11. We have concluded that this level is the lowest member of the band based on orbit 11.

Manning and Bartholomew [18]) have assigned the 4.93 and 6.38 MeV levels in ^{29}Si as p-levels due to orbits 16 and 17. The 4.34 and 5.51 MeV levels in ^{29}P have very large proton reduced widths and were also assigned as p-levels by Vorona *et al.* [3]). It is therefore suggested that these two pairs of levels arise as conjugate excitations of orbits 16 and 17.

The Delft group expresses their thanks to Prof. Dr. Ir. F. A. Heyn for permission to use the Van de Graaff accelerator and to Ir. J. H. Makkink and his collaborators for operating this machine.

Appreciation is expressed by the A.R.L. members to Mr. D. V. Breitenbecher and to Capt. J. W. Daughtry for help in the operation of the A.R.L. accelerator and in the computation of correlation functions required for the angular distribution analysis.

References

1) D. A. Bromley, H. E. Gove, A. E. Litherland, Can. J. Phys. **35** (1957) 1057
2) B. E. F. Macefield and J. H. Towle, Proc. Phys. Soc. **76** (1960) 56
3) J. Vorona, J. W. Olness, W. Haeberli and H. W. Lewis, Phys. Rev. **116** (1959) 1563
4) K. J. van Oostrum, thesis, Delft (1960)
5) J. W. Olness and J. L. Parker, Bull. Am. Phys. Soc. **5** (1960) 56
6) J. O. Newton, Nuclear Physics **21** (1960) 529
7) W. C. Elmore and M. Sands, "Electronics" (McGraw-Hill Book Co., New York, 1949)
8) K. J. van Oostrum and A. C. Meijer, Nuclear Instruments **10** (1961) 31
9) F. Everling, L. A. König, J. H. E. Mattauch and A.H. Wapstra, Nuclear Physics **15** (1960) 342
10) K. J. van Oostrum, J. Alster, N. Hazewindus and A. H. Wapstra, Physica **24** (1958) 1051
11) T. Tabata, K. Fukuda and K. Okano, J. Phys. Soc. Japan **15** (1960) 364
12) K. Okano, T. Tabata, K. Fukuda and J. Muto, J. Phys. Soc. Japan **15** (1960) 1556
13) H. E. Gove, Nuclear Reactions, ed. by P. M. Endt and M. Demeur (North-Holland Publishing Co., Amsterdam, 1959)
14) A. E. Litherland and G. J. Mac Callum, Can. J. Phys. **38** (1960) 927
15) C. van der Leun, thesis, Utrecht (1958)
16) C. Broude, L. L. Green and J. C. Willmott, Proc. Phys. Soc. **72** (1958) 1122
17) S. G. Nilsson, Mat. Fys. Medd. Dan. Vid. Selsk., **29**, No. 16 (1955)
18) G. Manning and G. A. Bartholomew, Phys. Rev. **115** (1959) 401

7.C

Nuclear Physics **25** (1961) 421—430; © *North-Holland Publishing Co., Amsterdam*

Not to be reproduced by photoprint or microfilm without written permission from the publisher

PHOTOPRODUCTION OF NEUTRAL MESONS IN HELIUM

J. L. COOK

Department of Applied Mathematics and Theoretical Physics, University of Cambridge

Received 13 February 1961

Abstract: For photon energies above 280 MeV, it is found that the experiments for elastic photoproduction of π^0 mesons can be explained in the impulse approximation. At lower energies, multiple scattering is large and is estimated using the method of Chappelear. The r.m.s. radius of He_4 is determined, from the experiments at 290 MeV by Palit and Bellamy, and is found to be 1.5 ± 1 fm, for eight different wave functions.

1. Introduction

The differential cross section for elastic photoproduction of neutral mesons in helium in the process

$$\gamma + He_4 \rightarrow \pi^0 + He_4 \tag{1}$$

has been investigated experimentally by Goldwasser, Koester and Mills [1]), Goldwasser and Koester [2]) de Saussier and Osborne [3]) and Palit and Bellamy [4]). De Saussier *et al.* compared their results with a theoretical calculation based on the impulse approximation of Chew and Lewis [5]), using a non-structural Gaussian wave function of the type employed by Hofstadter [6]) for the He_4 ground state. They were unable to explain their results satisfactorily, although rough qualitative agreement was achieved. Yamaguchi [7]) presented a theoretical calculation also based on the impulse approximation, which utilized a ground state wave function of the Irving [8, 9]) variety. Palit and Bellamy claimed that evaluation of this work agreed with other experiments but not their own. They maintain that the other experiments contain large contributions from inelastic processes around the energy of 300 MeV for the gamma photons, and their own cross sections are much smaller. This poses the question as to why Yamaguchi's former calculations over-estimated the elastic differential cross section.

Previous theoretical work in the literature has been based upon the formulae of Chew and Saltzman [10]), for the amplitudes of the processes

$$\gamma + p \rightarrow p + \pi^0, \tag{2}$$

$$\gamma + n \rightarrow n + \pi^0. \tag{3}$$

In this work, the simple phenomenological theory of Feld [11]), together with a number of different ground state wave functions, are used to analyse the results found by Palit and Bellamy.

2. Theory

2.1. THE IMPULSE APPROXIMATION

It is assumed that the nuclear recoil velocities are small compared with the velocity of light, but the outgoing meson is treated relativistically. We take $\hbar = c = 1$, and further ν_0 is the initial photon energy, $\boldsymbol{\nu}$ the initial photon momentum, μ_0 the total energy of the emitted meson and $\boldsymbol{\mu}$ the momentum of the emitted meson, all these quantities being measured in the laboratory system of the nucleus. The momentum of the recoiling nuclear system is $\mathbf{k}$, and the final energy binding the nucleus is ε_f. The initial energy of the entire system is $\nu_0+2M_p+2M_n+\varepsilon_i$, where ε_i is the binding energy of the initial nucleus. The final energy is $\mu_0+(4(M_p+M_n)^2+\mathbf{k}^2)^{\frac{1}{2}}+\varepsilon_f$. Following Chew and Lewis, one finds that the cross section for meson emission into the momentum interval $\mathrm{d}\boldsymbol{\mu}$ and nuclear recoil into the interval $\mathrm{d}\mathbf{k}$, with internal state f, may be expressed as

$$\frac{\mathrm{d}\sigma_f}{\mathrm{d}\boldsymbol{\mu}\mathrm{d}\mathbf{k}} = \frac{1}{4\pi^2}\,|Q_f|^2\delta(\mu_0+4(M_p+M_n)^2+\mathbf{k}^2)^{\frac{1}{2}}+\varepsilon_f-2(M_p+M_n)-\varepsilon_i-\nu_0), \quad (4)$$

where Q_f is the matrix element for the process. In the impulse approximation, the conjecture is made that the production matrix T can be represented by $T = \sum_j T_j$, where T_j is the matrix element for photoproduction from free nucleons, (cf. Hamilton [12]). In general

$$T_j = (\boldsymbol{\sigma}_j \cdot \mathbf{K}_j + L_j)\, \mathrm{e}^{i(\boldsymbol{\nu}-\boldsymbol{\mu})\cdot\mathbf{r}_j}\, \tau_j^+, \quad (5)$$

where $\mathbf{K}$ is explicitly dependent upon photon polarization, $\boldsymbol{\sigma}_j$ is the spin of the j-th nucleon, $\mathbf{r}_j$ its spacial co-ordinate and τ_j^+ the third component of its isospin. The first term in (5) is the spin-dependent part of the interaction, while L_j is independent of spin.

The quantity $|Q_f|^2$ is to be summed over final states and averaged over initial states of spin and isospin. This must yield a weight factor of unity in the process (1), since He_4 occurs predominantly in the $^1S_0$ ground state configuration before and after the collision, giving zero components of spin and isospin in each case. In support of this assumption, Irving [9]) and Foldy [13]) have shown that contributions from possible D states have an insignificant effect upon the calculated binding energy and root-mean-square radius.

The wave function describing the initial motion is $|\mathrm{i}> = U_1(\mathbf{r}_{ij})$, where $\mathbf{r}_{ij} = \mathbf{r}_i - \mathbf{r}_j$. The linear transformations of Flowers and Mandl [14]) are used to fix the relative orientation of the nucleons. They are

$$\begin{aligned} 3\mathbf{t}_1 &= \mathbf{r}_1+\mathbf{r}_2+\mathbf{r}_3-3\mathbf{r}_4, \qquad 2\mathbf{t}_2 = \mathbf{r}_1+\mathbf{r}_2-2\mathbf{r}_3, \\ \mathbf{t}_3 &= \tfrac{1}{2}\sqrt{3}(\mathbf{r}_1-\mathbf{r}_4) \quad \text{together with the centre-of-mass co-ordinate,} \\ \mathbf{R} &= \tfrac{1}{4}\,(\mathbf{r}_1+\mathbf{r}_2+\mathbf{r}_3+\mathbf{r}_4). \end{aligned} \quad (6)$$

The contribution of the j-th nucleon to the matrix element is

$$\begin{aligned}(Q_f) &= \langle U_f(\mathbf{t}_1,\mathbf{t}_2,\mathbf{t}_3)\chi_f e^{-i\mathbf{k}\cdot\mathbf{R}}|T_j|U_1(\mathbf{t}_1,\mathbf{t}_2,\mathbf{t}_3)\chi_1\rangle \\ &= \langle\chi_f|\boldsymbol{\sigma}_j\cdot\mathbf{K}_j+L_j|\chi_1\rangle\iiiint U_f^*U_1 e^{i(\boldsymbol{\nu}-\boldsymbol{\mu})\cdot\mathbf{r}_j-i\mathbf{k}\cdot\mathbf{R}}d\mathbf{R}d\mathbf{t}_1d\mathbf{t}_2d\mathbf{t}_3.\end{aligned} \tag{7}$$

Here, $U_f e^{i\mathbf{k}\cdot\mathbf{R}}$ is the wave function of the final state configuration, including the centre-of-mass motion and χ_1 and χ_f are the initial and final spin states. Suppose a production event occurs in the vicinity of the 4th nucleon. In this case we put

$$\mathbf{R} = \mathbf{r}_4-\tfrac{3}{4}\mathbf{t}_1, \tag{8}$$

so that the integration over $\mathbf{R}$ in (7) leads to the momentum conservation delta function $\delta(\boldsymbol{\nu}-\boldsymbol{\mu}-\mathbf{k})$. Neglect of this factor in (7) gives

$$(Q_f)_4 = (2\pi)^3\langle\chi_f|\boldsymbol{\sigma}_4\cdot\mathbf{K}_4+L_4|\chi_1\rangle\iiint U_f^*U_1 e^{-\frac{3}{4}i\mathbf{k}\cdot\mathbf{t}_1}d\mathbf{t}_1d\mathbf{t}_2d\mathbf{t}_3. \tag{9}$$

2.2. THE MATRIX ELEMENT

We now consider the matrix elements for production from each nucleon. Let S_{fi} be the transition amplitude for each spin state of the individual nucleons; i and f refer to the initial and final states of polarization of a nucleon in the direction of the incident beam, while the $\pm$ symbol designates the states of circular polarization of the photon. Feld showed that for the processes (2) and (3), these amplitudes are represented by

$$\begin{aligned}
S^-_{\frac{1}{2}\frac{1}{2}} &= Y\sin\theta\, e^{-i\phi}, & S^+_{\frac{1}{2}\frac{1}{2}} &= -Y\sin\theta\, e^{i\phi} \\
S^-_{-\frac{1}{2}-\frac{1}{2}} &= X\sin\theta\, e^{-i\phi}, & S^+_{-\frac{1}{2}-\frac{1}{2}} &= -X\sin\theta\, e^{i\phi}, \\
S^-_{-\frac{1}{2}\frac{1}{2}} &= S^+_{\frac{1}{2}-\frac{1}{2}} = -E_1+K\cos\theta, & & \\
S^-_{\frac{1}{2}-\frac{1}{2}} &= E'_1\sin^2\theta\, e^{-2i\phi} \text{ (vii)} & S^+_{-\frac{1}{2}\frac{1}{2}} &= E'_1\sin^2\theta\, e^{2i\phi}.
\end{aligned} \tag{10}$$

Furthermore, we have

$$X = 2M_3-\tfrac{1}{2}(M_3-E_3)+\tfrac{1}{2}E\beta, \qquad Y = M_1+\tfrac{1}{2}(M_3-E_3)-\tfrac{1}{2}E\beta,$$
$$K = -M_1+M_3-E_3,$$

where these amplitudes signify the multipole transitions M1($P_{\frac{1}{2}}$), E3($P_{\frac{3}{2}}$), M3($P_{\frac{3}{2}}$) and E1 ($S_{\frac{1}{2}}$). Also $p = v/c$, where v is the pion velocity, M and E are the usual symbols for magnetic and electric multipole amplitudes, while $E'_1 = E_1\beta^2/2(1-\beta\cos\theta)$ is the "retardation term". θ is the angle between the emitted pion and incident photon in the plane of the scattering and ϕ is the azimuthal angle of the pion.

No spin-flip can occur in the process (1), as this would imply the subsequent disintegration of the α-particle; therefore, we clearly have $S^+_{-\frac{1}{2}\frac{1}{2}} = S^+_{\frac{1}{2}-\frac{1}{2}} = S^-_{-\frac{1}{2}\frac{1}{2}} = S^-_{\frac{1}{2}-\frac{1}{2}} = 0$. Since each of the initial spin states is equally probable

within the nucleus, we sum over the production matrix elements for each state of circular polarization:

$$S^{-}_{\frac{1}{2}\frac{1}{2}}+S^{-}_{-\frac{1}{2}-\frac{1}{2}} = (X+Y)\sin\theta\, e^{-i\phi}, \qquad S^{+}_{\frac{1}{2}\frac{1}{2}}+S^{+}_{-\frac{1}{2}-\frac{1}{2}} = -(X+Y)\sin\theta\, e^{i\phi}. \quad (11)$$

Application of eqs. (10) and (11) shows that

$$(X+Y) = 2M_3+M_1. \quad (12)$$

This illustrates how the magnetic dipole moment is responsible for all the photoproduction in the impulse approximation. Note that even the retardation correction cancels together with all electric absorption terms, as a consequence of the paired nucleon spins. The differential cross section for a beam of unpolarized photons is

$$\frac{d\sigma}{d\Omega} = \tfrac{1}{2}\textstyle\sum_{if}|S^{\pm}_{fi}|^2 = 4|X+Y|^2\sin^2\theta, \quad (13)$$

from eq. (11). Feld put $M_1 = 0$ in the energy region of the (3,3) resonance, so that

$$\frac{d\sigma}{d\Omega} = 16m_{33}^2\sin^2\theta, \quad (14)$$

where $M_3=m_{33}e^{i\alpha 33}$ and α_{33} is the phase shift for (3,3) transitions from nucleons. The magnitude of m_{33}^2 can be obtained from the work of Chew *et al.* [15]), Chew [16]) or Jackson [17]) as

$$m_{33}^2 = \tfrac{4}{9}\frac{e^2}{f^2}\left(\frac{\mu_p-\mu_n}{4M}\right)^2\frac{\nu_0\sin^2\alpha_{33}}{\mu^3}, \quad (15)$$

where f^2 is the pion-nucleon coupling constant, e^2 is the fine-structure constant, μ_p and μ_n are the magnetic moments of the proton and neutron, and M is the nucleon mass. With $\mu_p = 2.79e/2M$, $\mu_n = -1.91e/2M$, $e^2 = \frac{1}{137}$, $M = 6.72$ and Woolcock's value [18]) of $f^2 = 0.082$, the matrix element in (15) becomes

$$m_{33}^2 = 24\nu_0\sin^2\alpha_{33}/\mu^3 \ \ \mu\text{b}. \quad (16)$$

This result is compared with the experimental total cross sections for process (2) compiled by Bernadini [28]) in fig. 1. This cross section is given by $\sigma_t(p\pi^0) = 8\pi m_{33}^2$ and the differential cross section is

$$\frac{d\sigma}{d\Omega} = \tfrac{1}{2}m_{33}^2(2+3\sin^2\theta)$$

for pure magnetic dipole production. Now, of course, these cross sections are functions of energy in the barycentric $(p\pi^0)$ system, and must be evaluated independently for the $(He_4\pi^0)$ barycentric system. The phase shift α_{33} can be calculated as a function of the photon energy from the effective range approxi-

mation of Chew and Low [19]). We have

$$\mathrm{tg}\alpha'_{33} = \tfrac{4}{3} f^2 \frac{\mu'^3/\omega'}{1-\omega'/\omega'_r}, \tag{17}$$

where ω' is the total energy in the barycentric system, not including the nuclear rest mass. The primes denote quantities to be calculated in the ($He_4\pi^0$) barycentric system and ω'_r is the energy at exact resonance.

The sum over the matrix elements $(Q_t)_j$, given by eq. (9), is substituted into eq. (4), to give

$$\frac{\mathrm{d}\sigma}{\mathrm{d}\Omega} = 2.16|L|^2|F(\mathbf{k}')|^2, \tag{18}$$

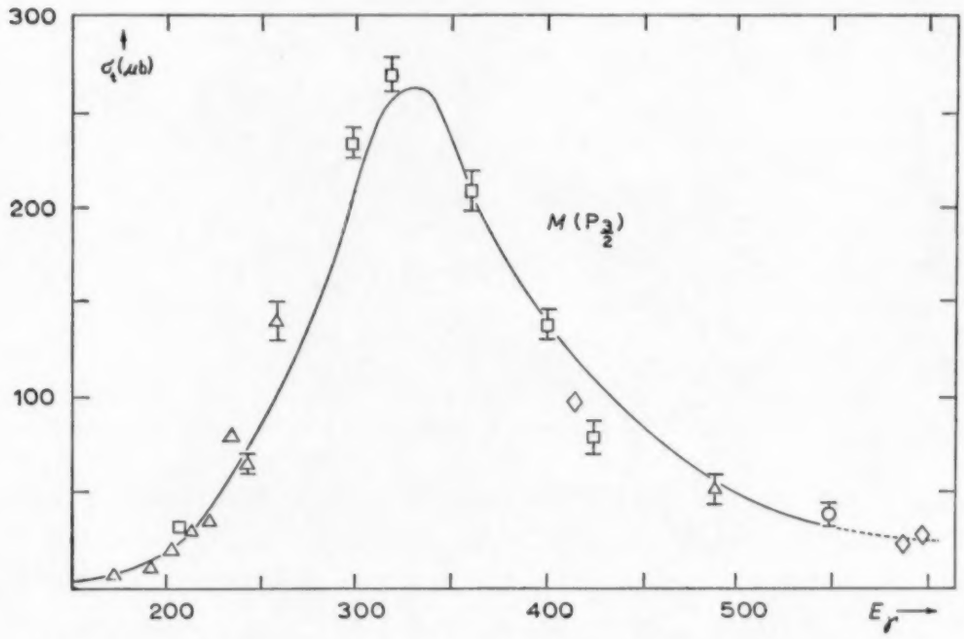

Fig. 1. Total cross section for the reaction (1) as a function of photon laboratory energy. The experimental points are taken from Bernadini [28]). The theoretical curve is calculated for magnetic dipole only.

where

$$F(\mathbf{k}') = \int\int U_t U_1 \mathrm{e}^{-\mathrm{i}\mathbf{k}'\cdot\mathbf{t}_1}\,\mathrm{d}\mathbf{t}_1\,\mathrm{d}\mathbf{t}_2\,\mathrm{d}\mathbf{t}_3 \tag{19}$$

is known as the "nuclear form factor". It purportedly takes account of the spatial distribution of scattering centres. Eq. (18) may be taken over to the barycentric system without modification in its functional form, except that k becomes the momentum transfer $\mathbf{k}' = \boldsymbol{\nu}' - \boldsymbol{\mu}'$ and not the nuclear recoil. A comparison of eq. (18) and (14) makes it obvious that the latter must be modified for consistency to give the final equation

$$\frac{\mathrm{d}\sigma}{\mathrm{d}\Omega} = 16 m_{33}^2\, \nu'_0 \sin^2\theta\, |F(\mathbf{k}')|^2 = 385\, \nu'_0 \sin^2\alpha'_{33} \sin^2\theta\, |F(\mathbf{k}')|^2/\mu^3 \ \mu\mathrm{b}. \tag{20}$$

2.3. NUCLEAR FORM FACTORS

Table 1 exhibits an array of form factors computed for both structural and non-structural wave functions. Entry 2 is that used by Yamaguchi, and entry 8 is that which Hofstadter found to be the best fit to the experiments. Entry 5 gives the same result as the latter. It will be noted that all wave functions

TABLE 1

Form factors for He_4 (using $a = \frac{1}{8}\sqrt{3}\, r_0 k$ and $b = \frac{1}{8}\sqrt{6}\, r_0 k$)

Wave function		No.	n	Form factor	R.m.s. radius
A. Structural					
Irving	$[\Sigma(\mathbf{r}_i-\mathbf{r}_j)^2]^n \times e^{-[\Sigma(\mathbf{r}_i-\mathbf{r}_j)^2]^{\frac{1}{2}}/r_0}$	1	$-\frac{1}{2}$	$1/(1+a^2)^4$	$\frac{36}{32}\, r_0$
		2	0	$1/(1+a^2)^5$	$\frac{45}{32}\, r_0$
		3	$\frac{1}{2}$	$(1-\frac{1}{9}a^2)/(1+a^2)^6$	$\frac{55}{32}\, r_0$
		4	1	$(1-\frac{1}{3}a^2)/(1+a^2)^7$	$\frac{66}{32}\, r_0$
Gaussian	$[\Sigma(\mathbf{r}_i-\mathbf{r}_j)^2]^n \times e^{-\Sigma(\mathbf{r}_i-\mathbf{r}_j)^2/r_0^2}$	5	0	$e^{-\frac{1}{4}b^2}$	$\frac{3}{8}\, r_0$
		6	1	$(1-\frac{1}{18}b^2)e^{-\frac{1}{4}b^2}$	$\frac{11}{8}\, r_0$
		7	2	$(1-\frac{1}{3}b^2+\frac{1}{396}b^4)e^{-\frac{1}{4}b^2}$	$\frac{13}{8}\, r_0$
B. Non structural					
e^{-r^2/r_0^2}		8		$\frac{1}{8}e^{-r_1^2K^2}$	r_1

which possess a shell-like spatial configuration have form factors displaying at least one diffraction minimum and maximum. Such features have been observed in other light nuclei, particularly in the striking experiments of Fregeau [20]), who investigated the scattering of electrons from the carbon-12 nucleus. The effect has not been noticed in He_4, as perhaps sufficiently large momentum transfers have not been realised. For the purposes of this analysis, only the values of the form factors near the pion threshold are required. Table 2 shows

TABLE 2

Form factors at 90° cm system as a function of photon energy in the laboratory system

Photon energy (MeV)	No. of wave function in table 1 for $\bar{r} = 1.61$ fm						
	1	2	3	4	5	6	7
170	0.490	0.483	0.486	0.484	0.475	0.472	0.474
230	0.220	0.214	0.210	0.207	0.180	0.178	0.179
290	0.091	0.082	0.078	0.076	0.059	0.052	0.056
350	0.038	0.027	0.031	0.027	0.030	0.028	0.029

that all of those tabulated in table 1 differ to a negligible degree, for a given

r.m.s. radius, in this energy range. This fact was anticipated, as the asymptotic behaviour of the wave function should dominate the cross sectional behaviour for low nuclear momentum transfers. It is only for photon energies above 700 MeV in the laboratory system, that the inner spatial regions of the nucleus begin to contribute to the elastic production. For instance, the wave function (4) has a diffraction minimum at $E = 980$ MeV and $\theta = 180°$, which moves across the angular distribution as the energy increases, and reaches the forward scattering region at about 2.8 GeV. The relative magnitudes of the cross sections calculated from wave functions (1)—(4) at about 1 GeV are $1 : 10^{-2} : 10^{-4} : 0$, at 180°, with a value of 10^{-38} cm²/sr in the first case. Such cross sections are probably not worth investigating by present-day methods.

3. Results

In fig. 2, the differential cross section at a photon energy of 290 MeV is plotted as a function of the centre-of-mass angle for the emitted π^0. The fit

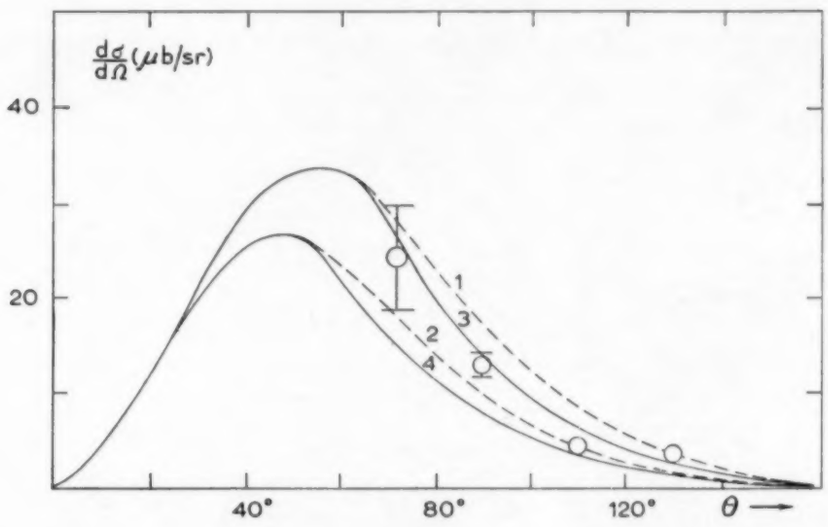

Fig. 2. Differential cross sections at 290 MeV as a function of the barycentric scattering angle. (1) Irving, $\bar{r} = 1.40$ fm. (2) Irving, $\bar{r} = 1.61$ fm. (3) Gaussian, $\bar{r} = 1.40$ fm. (4) Gaussian, $\bar{r} = 1.61$ fm.

with both the Irving and Gaussian wave functions is reasonably good, giving an r.m.s. radius of 1.5 ± 1 fm for the He_4 nucleus. Foldy's[13]) sum rule determination, the work of Bransden, Douglas and Robertson [21]) and similar research by Dalitz and Ravenhall [22]), provide evidence that the Irving wave functions yield underestimates of the r.m.s. radius when compared with experiment. Gorbunov and Spiridonov [23]), as well as Bransden *et al.* conclude that the Gaussian wave functions do not fit the low energy data as well as those of Irving, but both appear to be inadequate. The former find an experimental value of 1.57 ± 0.06 fm, in satisfactory agreement with Hofstadter's value of

1.61 ± 0.08 fm. However, as discussed above, our results are insensitive to the choice of wave function, and this is reflected in the good agreement we obtain with these values.

In fig. 3, it is apparent that the energy-dependence of the differential cross section at 90° is not so well reproduced. Although the errors in the experimental

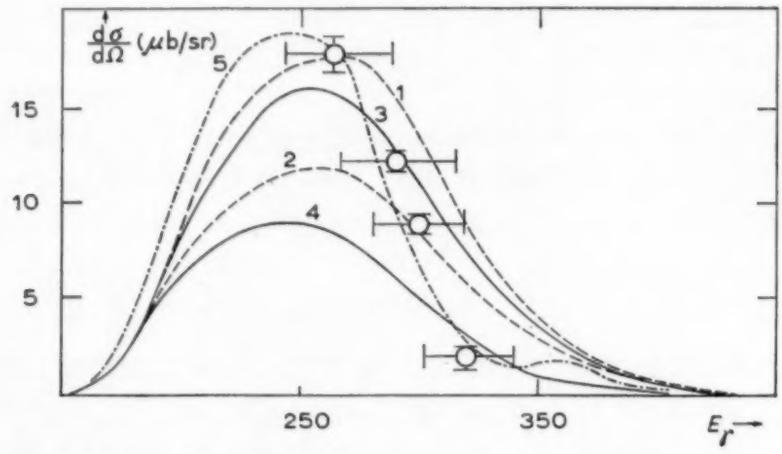

Fig. 3. Differential cross section at 90° c.m.s. as a function of photon laboratory energy. (1) Irving, $\bar{r} = 1.40$ fm. (2) Irving, $\bar{r} = 1.61$ fm. Gaussian, (3) $\bar{r} = 1.40$ fm. (4) Gaussian, $\bar{r} = 1.61$ fm.

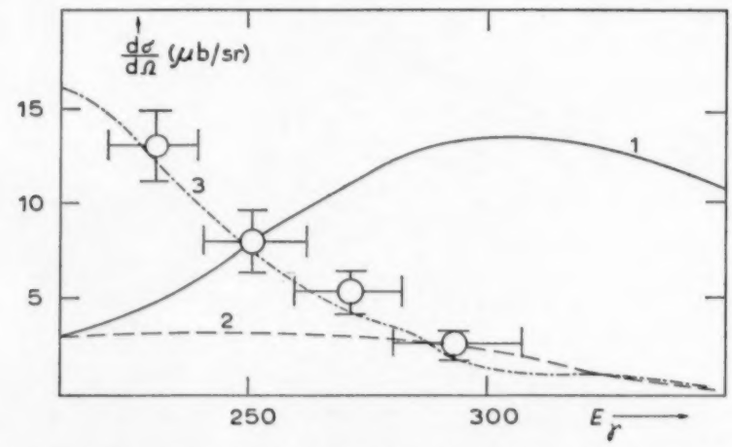

Fig. 4. Differential cross section at 135° c.m.s. as a function of photon laboratory energy. (1) Inelastic scattering. (2) Elastic scattering. (3) Elastic + multiple scattering.

points bring them just inside the range of theoretical error, the experimental curve is falling much more quickly with increasing energy than the theory can predict. This can be taken as a strong indication that multiple scattering processes hold sway in the region from threshold to about 280 MeV. We have estimated this correction using the method of Chappelear [24]), but retained only the first-order correction to the amplitude. This amounts to including only double scattering events between pairs of nucleons. Even though charge exchange scattering was included, the resulting cross section is seen to differ little from the similar computations reported by Palit and Bellamy as performed by Stoodley [25]).

As in fig. 4, the discrepancy at 135° appears to be even worse between the impulse approximation without multiple scattering and experiment. However, there is one mitigating feature. The points at a given energy differ from the theory at all angles by the same fraction, to a close approximation. In the barycentric system, this is precisely the behaviour one anticipates from multiple scattering contributions. Also shown in fig. 3 is the expected order of magnitude of inelastic scattering contributions, calculated from Yamaguchi's closure approximation, and which is almost co-incident with the incoherent superposition of the amplitudes from the individual nucleons. Thus, inelastic production, occurring as contamination in the experiment, could not produce the observed behaviour. On the other hand, the first correction of the multiple scattering does give roughly the right behaviour. All these corrections were evaluated using wave function 8 of table 1 and an r.m.s. radius of 1.61 fm.

We regard this close agreement as very misleading, especially in the light of recent work summarised by MacDonald [26]), who maintains that Brueckner's [27]) neglect of scattering "off the energy shell", is probably not justifiable. If this is so, Chappelear's work, and also our corrections are equally invalid. Nevertheless, the experiments show that multiple scattering is negligible at 290 MeV, in all probability, by the good agreement achieved at this energy. Since our determination of the r.m.s. radius was carried out at this energy, we expect the result to be reliable. Finally, it is obvious that more powerful methods of analysis are required, such as the application of disperson theory to Chappelear's work, in order to clear up the problem of calculating the higher-order corrections in a convincing fashion.

In a recent paper by Odian *et al.* [29]), corrections were made to the He_4 differential cross section by including the pion-nucleon phase shifts α_{11}, α_{13} and α_{31} in our eq. (13). The constant A in the differential cross section, which they determine on p. 1476 as 5.2 ± 0.02 μb, is in agreement with our theoretical value of 5.40, provided we use their value of $f^2 = 0.088$ for the pion-nucleon coupling constant. However, these authors examine only the threshold behaviour, and neglect multiple scattering entirely, as they are concerned chiefly in determining the mass of the π^0 meson. Apart from these minor differences, our results are in agreement in the region where they overlap.

4. Conclusion

It has been found that in the energy ranges above 280 MeV, the differential cross section for the elastic photoproduction of π^0 mesons is given reasonably well by the impulse approximation without multiple scattering. Below this energy, there is clear evidence of strong enhancement of the cross section by multiple scattering, which can be estimated to first order by the method of Chappelear, although recent work has shown that this estimation is not to be

trusted. Using the angular distribution at 290 MeV obtained by Palit and Bellamy, we arrived at a value of 1.50 ± 1 fm for the He_4 r.m.s. radius, in good agreement with other determinations.

The author thanks Professor J. Hamilton for much enlightenment and continual encouragement.

References

1) E. L. Goldwasser, L. J. Koester and F. E. Mills, Phys. Rev. **95** (1954) 1692
2) E. L. Goldwasser and L. J. Koester, Nuovo Cim. **4** (1956) 950
3) G. de Saussiere and L. S. Osborne, Phys. Rev. **99** (1955) 843
4) P. Palit and E. Bellamy, Proc. Phys. Soc. **72** (1958) 880
5) G. F. Chew and H. W. Lewis, Phys. Rev. **84** (1951) 779
6) R. Hofstadter, Rev. Mod. Phys. **28** (1956) 214
7) Y. Yamaguchi, Prog. Theor. Phys. **13** (1955) 459
8) J. Gunn and F. Irving, Phil. Mag. **42** (1951) 1353
9) M. L. Rustgi and J. S. Levinger, Phys. Rev. **106** (1957) 530
10) G. F. Chew, Phys. Rev. **95** (1954) 1669;
F. F. Saltzman, Phys. Rev. **95** (1954) 286
11) B. T. Feld, Cornell University lectures (1958)
12) J. Hamilton, Theory of elementary particles (Oxford University Press, 1959) p. 230
13) L. L. Foldy, Phys. Rev. **107** (1957) 1303
14) B. H. Flowers and F. Mandl, Proc. Roy. Soc. **206** (1951) 131
15) Chew ,Goldberger, Low and Nambu, Phys. Rev. **106** (1957) 1337
16) G. F. Chew, Handbuch der Physik **43** (1958)
17) J. D. Jackson, The physics of elementary particles (Princeton University Press, Princeton 1958)
18) W. Woolcock, private communication
19) G. F. Chew and F. E. Low, Phys. Rev. **101** (1956) 1570
20) J. H. Fregeau, Phys. Rev. **104** (1956) 225
21) B. H. Bransden, A. C. Douglas and H. H. Robertson, Phil. Mag. **2** (1953) 1211
22) R. H. Dalitz and D. G. Ravenhall, Stanford University preprint (1956)
23) A. N. Gorbunov and V. M. Spiridonov, JETP **7** (1958) 596
24) J. Chappelear, Phys. Rev. **99** (1955) 254
25) K. D. C. Stoodley, Ph. D. thesis, Glasgow University (1957)
26) N. MacDonald, Nuovo Cim. **15** (1959) 301
27) K. A. Brueckner, Phys. Rev. **89** (1953) 834
28) G. Bernadini, Proc. CERN Conf. on High Energy Physics, 7366/Sc/kw CERN Preprint Geneva (1958)
29) O. Odian, G. Stoppini and T. Yamagata, Phys. Rev. **120** (1960) 1468

7.B

Nuclear Physics **25** (1961) 431—434; © *North-Holland Publishing Co., Amsterdam*

Not to be reproduced by photoprint or microfilm without written permission from the publisher

CURRENT-CHARGE DENSITY COMMUTATION RELATIONS

KENNETH JOHNSON

Physics Department, Massachusetts Institute of Technology, Cambridge, Mass. †

Received 6 March 1961

Abstract: It is shown that the non-vanishing of the current-charge density commutator at equal times is required by and is compatible with the continuity equation.

A troublesome point in quantum electrodynamics has been the equal time commutator

$$[j^0(x), j^k(y)]_{x^0=y^0}. \tag{1}$$

If it does not vanish one finds an apparent contradiction to the conservation of the current operator calculated when an external field is present. To lowest order in the external field, the usual formula for the vacuum polarization current is

$$\langle \text{out}|j^\mu(x)|\text{in}\rangle = i\int \langle 0|T(j^\mu(x)j^\nu(y))|0\rangle A_\nu^{\text{ext}}(y)(\mathrm{d}y). \tag{2}$$

But if we calculate the divergence of the expression (2),

$$\partial_\mu\langle \text{out}|j^\mu(x)|\text{in}\rangle = i\int \langle 0|[j^0(x), j^\nu(y)]|0\rangle_{x^0=y^0} A_\nu^{\text{ext}}(y)(\mathrm{d}^3y), \tag{3}$$

we find that, unless

$$[j^0(x), j^\nu(y)]_{x^0=y^0} = 0, \tag{4}$$

apparently the induced current is not conserved. Yet if (4) holds we also have a contradiction to well founded principles [1]). For, from (3) and the equation of continuity we get

$$0 = [j^0(x), \partial_k j^k(y)] = [j^0(x), -\partial_0 j^0(y)]. \tag{5}$$

Thus, if H is the field Hamiltonian, we have

$$[j^0(x), [H, j^0(y)]] = 0. \tag{6}$$

If we take the vacuum matrix element of (6), we find

$$\langle 0|j^0(x)Hj^0(y)|0\rangle = 0 \tag{7}$$

† This work was supported in part through the A.E.C. contract AT(30—1) 2098 by funds provided by the U. S. Atomic Energy Commission, The office of Naval Research and the Air Force Office of Scientific Research.

and in a space of positive metric this gives

$$\langle 0|j^0(x) = 0$$

or by covariance

$$\langle 0|j^\mu(x) = 0.$$

Hence, from locality, covariance and positive definiteness [2]),

$$j^\mu(x) = 0, \tag{8}$$

which is even more unsatisfactory than (3).

We can resolve these difficulties by making a simple observation. Certainly, eq. (4) cannot hold. In fact, let us calculate the vacuum matrix element of the commutator (4). We have

$$i\langle 0|j^\mu(x)j^\nu(y)|0\rangle = (-\Box^2 g^{\mu\nu} + \partial^\mu \partial^\nu)F^{(+)}(x-y), \tag{9}$$

where $F^{(+)}$ is an invariant function of $(x-y)^2$, with only positive frequencies. Let $F^{(-)}$ be the analogous function with only negative frequencies. Then we have

$$i\langle 0|[j^0(x), j^k(y)]|0\rangle = -\partial^k \left[\frac{\partial F^{(+)}}{\partial x^0} - \frac{\partial F^{(-)}}{\partial x^0}\right]_{x^0 \to y^0 + 0} \tag{10}$$

Now we note that with a positive-definite structure and the usually assumed mass spectrum, the Lehmann-Kallén representation for $F^{(+)}$ has the form

$$F^{(+)} = i\int \frac{\mathrm{d}q}{(2\pi)^3} \mathrm{e}^{iq(x-y)}\theta(q)\int_0^\infty \mathrm{d}m\rho(m)m^2\delta(q^2+m^2), \tag{11}$$

Therefore,

$$\left[\frac{\partial F^{(+)}}{\partial x^0} - \frac{\partial F^{(-)}}{\partial x^0}\right]_{x^0 \to y^0 + 0} = \int_0^\infty \mathrm{d}m\, m^2\rho(m)\delta^{(3)}(x-y).$$

Thus we see the absurdity of the vanishing of (10) since $\rho(m) > 0$.

But this also means that $i\langle 0|T(j^\mu j^\nu)|0\rangle$ is not a covariant function. An elementary calculation gives

$$i\langle 0|T(j^\mu(x)j^\nu(y))|0\rangle = (-\Box^2 g^{\mu\nu} + \partial^\mu \partial^\nu)F(x-y) + \delta^{\mu k}\delta^{k\nu}\delta(x-y)\int_0^\infty \mathrm{d}m m^2\rho(m), \tag{12}$$

where

$$F(x-y) = \int \frac{\mathrm{d}q}{(2\pi)^4} \mathrm{e}^{iq(x-y)} \int \mathrm{d}m \frac{\rho(m)m^2}{q^2+m^2-i\varepsilon}, \quad \varepsilon \to +0 \tag{13}$$

and

$$T(j^\mu(x)j^\nu(y)) \equiv \theta(x^0-y^0)j^\mu j^\nu + \theta(y^0-x^0)j^\nu j^\mu. \tag{14}$$

But now we must also realize that if $[j^0(x), j^k(y)] \neq 0$, eq. (2) is an incorrect formula and this will resolve the initial paradox.

The law of current conservation is valid because the field equations are invariant under the group

$$\delta\psi(x) = -i\alpha\psi(x) \tag{15}$$

which is generated by the total charge operator

$$\delta\psi(x) = \frac{1}{i}[\psi(x), Q\alpha], \qquad Q = \int \mathrm{d}^3x j^0(x). \tag{16}$$

In particular, the current operator is invariant under (15), i.e.

$$[j^k(x), Q] = 0. \tag{17}$$

However, this does not mean that $j^k(x)$ is invariant under the group generated by $j^0(y)$, i.e., that

$$[j^k(x), j^0(y)] = 0.$$

In fact, the operator $\int j^0(x)\alpha(x)\mathrm{d}^3x$ generates the local version of (15),

$$\delta\psi(x) = -i\alpha(x)\psi(x), \tag{18}$$

but the field equations are *not* invariant under (18). In fact, however, they *are* invariant under (18) followed by

$$\delta A_\mu^{\mathrm{ext}}(x) = -\partial_\mu\alpha(x). \tag{19}$$

Hence $j^k(x)$ *must be* invariant under (18) followed by (19). In fact, we should define [3]) the current so that it is automatically invariant under (18) and (19), in terms of a limit applied to the operator

$$\tfrac{1}{2}\Big[\bar\psi(x+\varepsilon)\gamma^\mu\psi(x)\mathrm{e}^{i\int_x^{x+\varepsilon}\mathrm{d}\xi^\mu A_\mu^{\mathrm{ext}}(\xi)} - \psi(x)\bar\psi(x-\varepsilon)\gamma^\mu\mathrm{e}^{-i\int_{x-\varepsilon}^{x}\mathrm{d}\xi^\mu A_\mu^{\mathrm{ext}}(\xi)}\Big].$$

Since the first factor has singular matrix elements as $\varepsilon \to 0$ the second factor gives important contributions. Only a current defined in terms of a limit applied to such a non-local but gauge invariant expression is guaranteed to be conserved in the local limit in the presence of an external field.

Now, under (18) we have

$$\begin{aligned}\delta j^k(x) &= -i\Big[j^k(x), \int j^0(y)\alpha(y)\mathrm{d}^3y\Big] \\ &= -i\int \mathrm{d}^3y\alpha(y)[j^k(x), j^0(y)],\end{aligned}$$

and hence under (19) alone

$$\tilde\delta j^k(x) = +i\int \mathrm{d}^3y\alpha(y)[j^k(x), j^0(y)].$$

Therefore, we have, in particular,

$$\langle 0|\tilde{\delta}j^k(x)|0\rangle = i\int \mathrm{d}^3y\alpha(y)\langle 0|[j^k(x), j^0(y)]|0\rangle$$
$$= +\partial^k\alpha(x)\int_0^\infty \mathrm{d}m\, m^2\rho(m)$$

or

$$\langle 0|\tilde{\delta}j^k(x)|0\rangle = -\delta A_k^{\mathrm{ext}}(x)\int_0^\infty \mathrm{d}m\, m^2\rho(m), \tag{20}$$

where in (20), $\delta A^{\mathrm{ext}}(x)$ stands for a general variation of the external potential. Eq. (20) holds since $j^k(x)$ must be a local function of the external potential. Hence, in calculating the current in the vacuum induced by a perturbation in the external field, we must take into account the fact that the *definition* of the Heisenberg current operator explicitly depends on the external field according to (20). Thus, we find instead of (2)

$$\langle \mathrm{out}|j^\mu(x)|\mathrm{in}\rangle$$
$$= \int \left[i\langle 0|T(j^\mu(x)j^\nu(y))|0\rangle - \delta^{\mu k}\delta^{k\nu}\int_0^\infty \mathrm{d}m\, m^2\rho(m)\delta(x-y)\right] A_\nu^{\mathrm{ext}}(\mathrm{d}y). \tag{21}$$

By (13), this is equal to

$$\int (-\Box^2 g^{\mu\nu} + \partial^\mu\partial^\nu)F(x-y)A_\nu^{\mathrm{ext}}(y)\mathrm{d}y, \tag{22}$$

which is both covariant and manifestly gauge invariant. It is also the usual result obtained by less straightforward reasoning. We also remark that these considerations have no obvious relation to the question of whether or not the physical mass of the photon vanishes, i.e., as to whether or not $\rho(m)$ contains a delta-function term at some finite mass. (This point is discussed in the following note [4]).

We should finally remark that these formal considerations are founded on the assumption that $\int \mathrm{d}m\, m^2\rho(m) < \infty$ although the validity of the final expression (22) only requires $\int \mathrm{d}m\rho(m) < \infty$.

This problem also finds a nice illustration in the two-dimensional field theory model of Thirring [5]) and will be discussed elsewhere in that context.

References

1) J. Schwinger, Phys. Rev. Letters **3** (1959) 296
2) P. Federbush and K. Johnson, Phys. Rev. **120** (1960) 1926
3) J. Schwinger, Phys. Rev. **82** (1951) 664
4) K. Johnson, Nuclear Physics **25** (1961) 435
5) W. Thirring, Annals of Physics **3** (1959) 91

7.B

Nuclear Physics **25** (1961) 435—437; © *North-Holland Publishing Co., Amsterdam*

Not to be reproduced by photoprint or microfilm without written permission from the publisher

RELATION BETWEEN THE BARE AND PHYSICAL MASSES OF VECTOR MESONS

KENNETH JOHNSON †

Imperial College of Science and Technology, London

Received 20 February 1961

Abstract: Assuming the usual canonical commutation relations to hold, a relation is found between the bare and the physical masses of vector mesons, which implies that the physical mass of the photon is zero.

The vector meson field coupled to a conserved source satisfies the equations

$$\partial_\mu G^{\mu\nu} = -j^\nu + m_0{}^2\phi^\nu, \tag{1}$$

$$G^{\mu\nu} = \partial^\mu\phi^\nu - \partial^\nu\phi^\mu, \tag{2}$$

where m_0 is the so-called "bare" mass of the meson. The canonical commutation rules are

$$[\phi^k(x), G^{l0}(y)] = i\delta^{kl}\delta^{(3)}(x-y). \tag{3}$$

The field component ϕ^0 is given by (1) as an explicit function of the kinematically independent fields

$$\phi^0 = \frac{1}{m_0{}^2}[j^0 + \partial_k G^{k0}]. \tag{4}$$

Hence, $\dot{\phi}^k$ is given, by rewriting (2), as

$$\dot{\phi}^k = G^{k0} - \partial^k\phi^0 = G^{k0} - \frac{1}{m_0{}^2}\partial^k[j^0 + \partial_l G^{l0}]. \tag{5}$$

If we suppose that

$$[j^\mu, \phi^l] = 0, \tag{6}$$

the commutation rules

$$[\phi^k, \dot{\phi}^l] = i\left(\delta^{kl} - \frac{1}{m_0{}^2}\partial^k\partial^l\right)\delta^{(3)}(x-y), \tag{7}$$

$$[\phi^0, \phi_k] = -\frac{i}{m_0{}^2}\partial^k\delta^{(3)}(x-y) \tag{8}$$

are obeyed by ϕ^μ.

† Permanent address: Massachusetts Institute of Technology, Cambridge, Massachusetts

Now ϕ^μ obeys the divergence condition

$$\partial_\mu \phi^\mu = 0, \tag{9}$$

so that we may write on invariance grounds

$$i\langle 0|\phi^\mu(x)\phi^\nu(y)|0\rangle = (\Box^2 g^{\mu\nu} - \partial^\mu \partial^\nu) \int \mathrm{d}K \, \frac{\sigma(K)}{K^2} \, \Delta^{(+)}(x-y; K) \tag{10}$$

where $\Delta^{(+)}(x-y; K)$ is the solution of the equation $(-\Box^2+K^2)\Delta^{(+)} = 0$ with only positive frequencies. It then follows from the commutation relations given, that

$$\int \mathrm{d}K \, \frac{\sigma(K)}{K^2} = \frac{1}{m_0{}^2}, \tag{11}$$

$$\int \mathrm{d}K \sigma(K) = 1. \tag{12}$$

Eqs. (11) and (12) may be written more explicitly if we assume that there is a physical vector particle with mass m. In this case $\sigma(K) = Z_3\delta(K-m)+\rho(K)$, where $\rho(K)$ is non-vanishing only for $K \geqq 3m$, and eqs. (11) and (12) take the form

$$\frac{1}{m_0{}^2} = \frac{Z_3}{m^2} + \int_{3m}^{\infty} \mathrm{d}K \, \frac{\rho(K)}{K^2}, \tag{11}'$$

$$1 = Z_3 + \int_{3m}^{\infty} \mathrm{d}K \rho(K), \tag{12}'$$

where Z_3 is also the charge renormalization constant.

From the field equation for ϕ^μ,

$$(-\Box^2+m_0{}^2)\phi^\mu = j^\mu,$$

we find

$$i\langle 0|j^\mu(x)\phi^\nu(y)|0\rangle = (\Box^2 g^{\mu\nu} - \partial^\mu \partial^\nu) \int \mathrm{d}K \, \frac{\sigma(K)}{K^2} \, (-K^2+m_0{}^2)\Delta^{(+)}, \tag{13}$$

and therefore, the relation

$$[j^\mu, \phi^k] = 0$$

is consistent with (13) in virtue of (11), (12). However, we see that

$$\langle 0|[j^k, \dot{\phi}^l]|0\rangle$$

cannot vanish. Indeed, we have

$$\begin{aligned} i\langle 0|[j^k, \dot{\phi}^l]|0\rangle &= -\int (K^2\delta^{kl} - \partial^k \partial^l) \frac{\sigma(K)}{K^2} \, (K^2-m_0{}^2)\mathrm{d}K \cdot \delta^{(3)}(x-y) \\ &= -\delta^{kl}\delta^{(3)}(x-y) \int \sigma(K)(K^2-m_0{}^2)\mathrm{d}K. \end{aligned} \tag{14}$$

Now, if we were to require that $\int \sigma(K)(K^2-m_0^2)\mathrm{d}K = 0$ we would come into contradiction with the charge-current commutation relations. In fact, if we make use of the continuity equation we find

$$\begin{aligned}\partial_k\langle 0|[j^k, \dot{\phi}^i]|0\rangle &= -\langle 0|[\partial_0 j^0, \dot{\phi}^i]|0\rangle = \langle 0|[j^0, \ddot{\phi}^i]|0\rangle \\ &= \langle 0|[j^0, (-\Box^2+m_0^2)\phi^i]|0\rangle = \langle 0|[j^0, j^i]|0\rangle,\end{aligned} \tag{15}$$

and as discussed elsewhere [1, 2] $[j^0, j^i]$ cannot vanish without the current density itself vanishing. Hence, for vector mesons, the formula which replaces [3]

$$\int \sigma(K)(K^2-m_0^2)\mathrm{d}K = 0 \tag{16}$$

(which perhaps can be maintained for scalar particles), is

$$\int \sigma(K)\left(\frac{1}{K^2} - \frac{1}{m_0^2}\right)\mathrm{d}K = 0, \tag{11}$$

or

$$\frac{1}{m_0^2} = \frac{Z_3}{m^2} + \int_{3m}^{\infty} \frac{\mathrm{d}K}{K^2}\,\rho(K). \tag{11'}$$

We also see that in the limit $m_0^2 \to 0$ this relation is only consistent with $m^2 \to 0$, i.e. a vanishing *physical* mass for the vector particles. Hence, we have a direct proof that a vanishing bare mass implies a vanishing physical mass for vector mesons (photons).

References

1) J. Schwinger, Phys. Rev. Letters **3** (1959) 296
2) K. Johnson, Nuclear Physics **25** (1961) 431
3) H. Lehmann, Nuovo Cim. **11** (1954) 343

1.E.1:
2.G

Nuclear Physics **25** (1961) 438—442; © *North-Holland Publishing Co., Amsterdam*
Not to be reproduced by photoprint or microfilm without written permission from the publisher

NUCLEAR ENERGY LEVELS OF N^{16}

M. G. SILBERT, NELSON JARMIE and DARRYL B. SMITH

Los Alamos Scientific Laboratory, University of California, Los Alamos, New Mexico †

Received 15 February 1961

Abstract: Thirteen energy levels of N^{16} have been determined in the range of excitation from 0 to 5.6 MeV by a high resolution study of the proton spectrum from the N^{14}(t, p)N^{16} reaction. Levels above the well-known ground state quartet are found at 3.340, 3.506, 3.956, 4.318, 4.392, 4.773, 5.059, 5.141, 5.230 and 5.526 MeV. These energies have been assigned standard deviations of from 10 to 25 keV. Level widths and reaction cross sections are also reported. The results of this experiment are compared with previous experiments.

1. Introduction

The first few levels of many light nuclei are now well determined, but there is often little agreement concerning the nuclear level structure above a few MeV. The nucleide N^{16} is no exception to this observation. The ground state of N^{16} is part of a quartet of levels whose characteristics are now well established theoretically and experimentally [1]). Above 1 MeV of excitation, however, there is very little consistency in experimental results. In the region of concern, 1 to 6 MeV excitation, there are several experimental reports. Warburton and McGruer [2]) studied proton spectra from the N^{15}(d, p)N^{16} reaction; Sikkema and van Wageningen [3]) and also Schellenberg, Baumgartner, Huber and Seiler [4]) have analyzed excitation functions of N^{15}(n, n)N^{15} elastic scattering; and Bonner, Davis, Din and Kuan [5]) have looked at alphas from the F^{19}(n, α)N^{16} reaction.

Because of the importance of the structure of light nuclei, particularly to the shell model in intermediate coupling [6]), we have attempted to clarify the energy level scheme of N^{16} by studying the spectra of protons from the reaction N^{14}(t, p)N^{16}.

2. Experimental Apparatus and Procedure

The outline of the experiment is as follows: a 2.2 to 2.7 MeV triton beam from an electrostatic accelerator bombarded a natural nitrogen gas target. The reaction protons emerging at a laboratory angle of 30° were analyzed with high resolution in a 40.6 cm double-focussing magnetic spectrometer and detected by a CsI scintillation counter. The experiment is almost identical with previous studies [7]) of the energy levels of light nuclei; and details of the apparatus,

† Work performed under the auspices of the U. S. Atomic Energy Commission.

particle identification tests, effects of possible contaminants, background runs, etc., are not repeated here. A mass-spectrometric analysis of the target gas showed that the N^{14} concentration was always greater than 99 atom-percent and significant contaminants such as carbon and oxygen were always less than 0.1 atom-percent.

3. Results

A typical proton spectrum with a bombarding triton energy of 2.2 MeV is seen in fig. 1. Spectra taken at 2.4 and 2.6 MeV were similar. It was determined

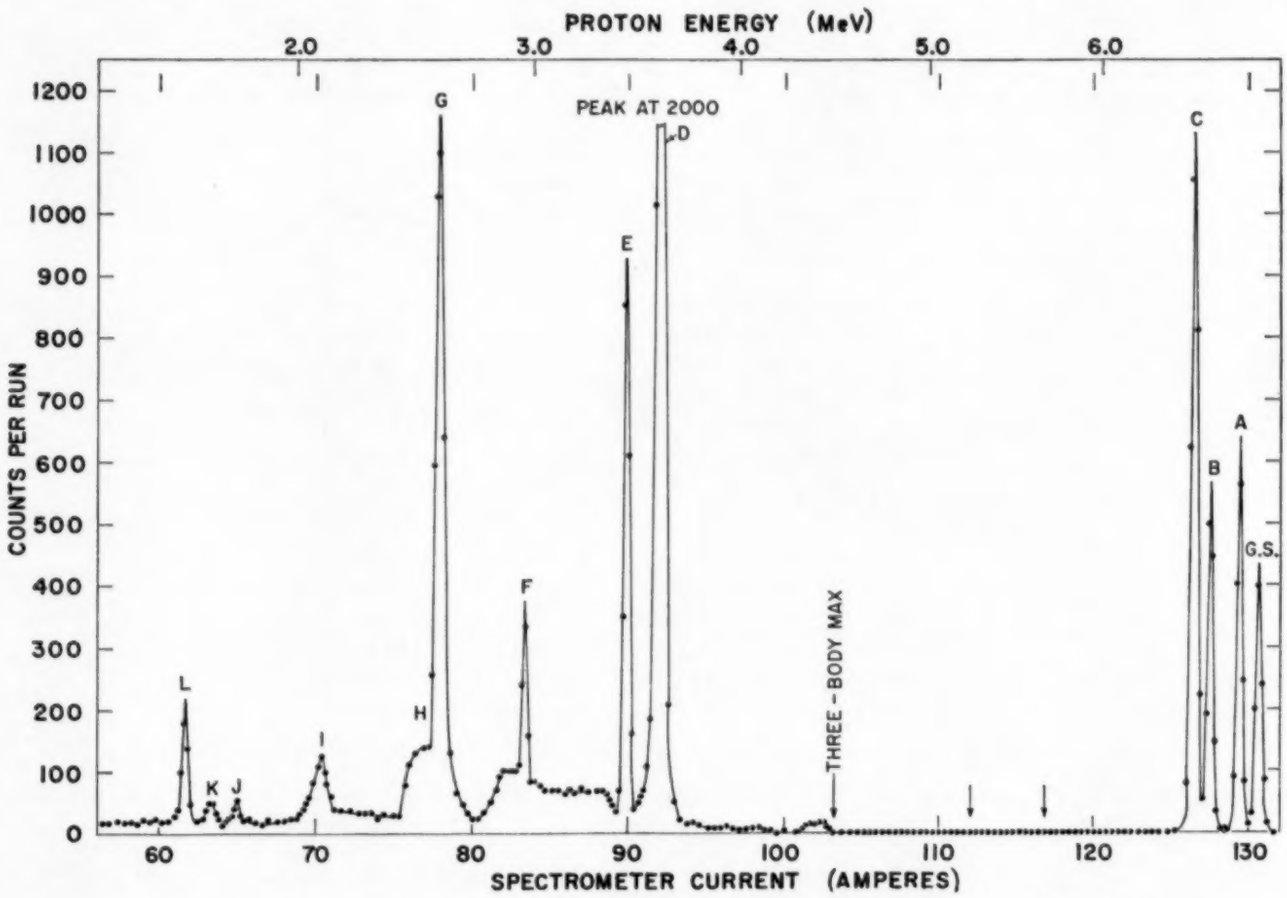

Fig. 1. Typical proton spectrum from nitrogen bombarded by 2.2-MeV tritons. The lettered peaks correspond to energy levels of N^{16} from the N^{14}(t, p)N^{16} reaction. Spectra at the other bombarding energies are similar and show peak "M" not shown here. An estimate of the statistical error can be gained by noting that the ordinates are actually the number of counts per run for a typical case. See the text for additional information on this spectrum.

that all the structure shown was due to protons from N^{14} bombarded by tritons. Of note is the ground state quartet at high proton energies followed (going down in proton energy) by the expected gap before more peaks appear. The small lump at a magnet current of 102 A and the structure (underlying peak F) between 82 and 89 A were shown to be from the two-stage N^{14}(t, n)O^{16*}(p)N^{15} reaction, and are discussed in the following paper [8]).

"Three-body Max" in fig. 1 indicates the calculated maximum energy of protons coming from the N^{14}(t, p)n, N^{15} reaction. This three-body breakup partly accounts for the low continuous spectrum seen below this energy. This low background and the lumps from the N^{14}(t, n)O^{16*}(p)N^{15} process limit our ability to detect levels in N^{16} above an excitation of about 2.60 MeV which correspond to small, or low broad proton peaks. Below 2.35-MeV excitation, the background is almost negligible and we estimate an upper limit for the cross section of a missed level at about 1 % of a typical observed group. Between 2.35 and 2.60 MeV, the upper limit is about 2 %.

TABLE 1

Energy levels and level widths of N^{16}, and some differential cross sections for the N^{14}(t, p)N^{16} reaction for 30° (lab) and 2.60 MeV tritons. Absolute standard deviations of the cross sections are ±25 %

Group	Excitation energy (MeV)	Width (keV)	σ(30°) (mb/sr)
G.S.	0		
A	0.121±0.010		
B	0.297±0.010		0.55
C	0.396±0.010		0.80
D	3.340±0.025	≦25±17	2.73
E	3.506±0.025	≦25± 8	1.18
F	3.956±0.025	≦25± 8	0.79
G	4.318±0.025	≦25± 8	2.95
H	4.392±0.025	110±31	1.00
I	4.773±0.025	66± 7	0.58
J	5.059±0.025	≦25± 8	0.35
K	5.141±0.025	38±12	0.23
L	5.230±0.025	≦20± 8	0.77
M	5.526±0.025	≦20± 8	0.11

Table 1 displays the main results of this experiment. Shown are the energy levels of N^{16} found in this experiment up to an excitation of 5.63 MeV, the widths of these levels and estimates of the cross sections of the reaction leading to some of the levels. All of these N^{16} levels were deduced from prominent and definite peaks.

The estimates of error on the energies are standard deviations and are conservative. The widths have had the experimental resolution of about 30 keV unfolded from them. The cross sections are for a lab angle of 30° and a triton energy of 2.6 MeV, and have an absolute standard deviation of ±25 %.

4. Comparison with Other Experiments

Fig. 2 shows a graphical summary of the experimental work up to 6 MeV of excitation in N^{16}. The only work not shown is that of Schellenberg *et al.* [4]), who found a level similar to the level at 5.30 MeV found by Sikkema [3]) except that Schellenberg *et al.* assigned a width of 140 keV instead of 270 keV. The

range of investigation in each experiment is indicated by the vertical dashed line. The width (in keV) is written in the level only when it is greater than 40 keV.

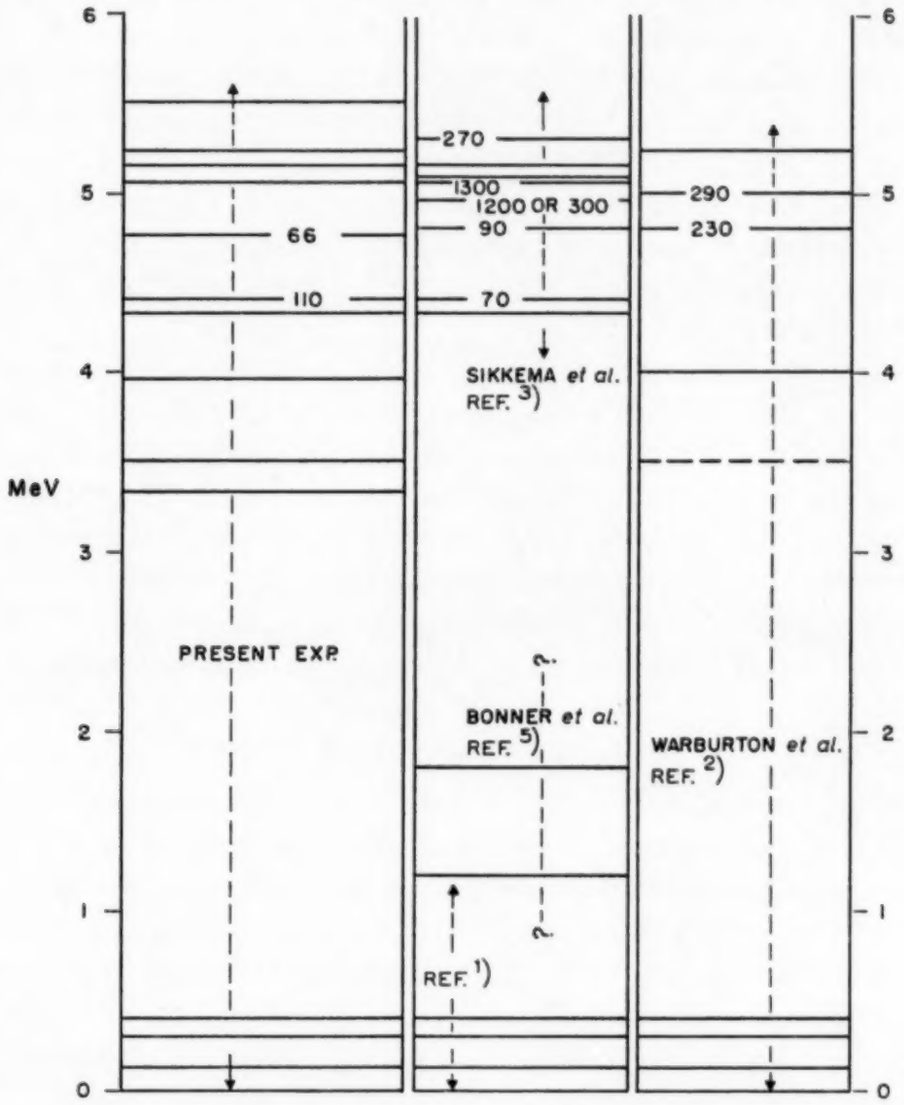

Fig. 2. Summary of experimental energy levels of N^{16}. The range of investigation in each experiment is indicated by the vertical dashed line. The width (in keV) is written in the level only when it is greater than 40 keV.

Our values for the ground state quartet agree well with published values and need no further comment. We do not see any evidence for the levels measured by Bonner *et al.* [5]) at 1.21 and 1.79 MeV and can put an upper limit of 1 % (about 10 μb/sr) of a typical peak for the production of groups corresponding to these levels at our various bombarding energies. The unmarked arrows in fig. 1 between 110 and 120 A show where we should have observed these levels. It is not clear why there should be such a severe selection aginst the N^{14}(t, p)N^{16} reaction going to these levels if they exist. Warburton and McGruer [2]) also see no evidence for these levels but might have missed a small level because of background and contaminant reactions.

We feel that the data of Warburton and McGruer [2]) are in essential agreement with the present data even though they do not report several levels and several of the widths that they report are much larger. The basis for this conclusion lies mostly in a background to their experiment, which was not discussed in their report. This is the three-body breakup N^{15}(d, p)n, N^{15}, which should become noticeable in their spectrum at proton energies below about 12.3 MeV. The effect of these three-body protons and the various contaminant-reaction protons could have been the cause of the missed levels and the difficulty in estimating widths of the levels near 5 MeV excitation in N^{16}.

The agreement with Sikkema and van Wageningen [3]) is less clear. Two areas of disagreement stand out:

(1) We do not observe the two very broad levels reported at an excitation of 4.95 and 5.05 MeV. This is unfortunate as Sikkema and van Wageningen had suggested that these might be the important 1^- and 2^- single particle states formed by the neutron moving into the $1d_{\frac{3}{2}}$ shell [the $(1p_{\frac{1}{2}})^{-1}(1d_{\frac{3}{2}})$ configurations]. It is possible that we may have missed a weak broad level. (See sect. 3.)

(2) Our two sharp levels at 5.23 and 5.53 MeV do not agree with the 270 keV broad level observed by Sikkema and van Wageningen at 5.30 MeV.

Five other levels in the common region are in reasonable agreement.

5. Comparison with Theory

It is difficult to make a detailed comparison of our results with theory such as the calculations of Elliott and Flowers [6]) for the negative parity states. Their prediction of a close quartet at the ground state followed by a large energy gap free of levels is again substantiated, but the size of the gap and the nature of the levels above the gap must await experiments detailing the spins, parities and reduced widths of the levels. It would also be helpful to have calculations on the positive parity states, which would presumably involve configurations with hole states in the $1p_{\frac{3}{2}}$ shell.

References

1) F. Ajzenberg-Selove and T. Lauritsen, Nuclear Physics **11** (1959) 1;
Landolt-Börnstein tables, Supplementary volume on nuclear physics (Springer-Verlag, Berlin, 1961) 6th Ed.
2) E. K. Warburton and J. N. McGruer, Phys. Rev. **105** (1957) 639
3) C. P. Sikkema and R. van Wageningen, in Proc. Int. Conf. Nuclear Structure, ed. by D. A. Bromley and E. W. Vogt (North-Holland Publishing Co., Amsterdam, 1960) p. 513;
C. P. Sikkema, Physica **26** (1960) 379
4) Schellenberg, Baumgartner, Huber and Seiler, Helv. Phys. Acta **32** (1959) 357
5) Bonner, Davis, Din and Kuan, Proc. Int. Conf. Nuclear structure, ed. by D. A. Bromley and E. W. Vogt (North-Holland Publishing Co., Amsterdam, 1960) p. 470
6) J. P. Elliott and B. H. Flowers, Proc. Roy. Soc. **242** (1957) 57
7) N. Jarmie and M. G. Silbert, Phys. Rev. **120** (1960) 914;
M. G. Silbert and N. Jarmie, Phys. Rev., to be published
8) N. Jarmie, M. G. Silbert and D. B. Smith, Nuclear Physics **25** (1961) 443

2.J

Nuclear Physics **25** (1961) 443—446; © *North-Holland Publishing Co., Amsterdam*

Not to be reproduced by photoprint or microfilm without written permission from the publisher

THE TWO-STAGE NUCLEAR REACTION $N^{14}(t, n)O^{16*}(p)N^{15}$

NELSON JARMIE, M. G. SILBERT and DARRYL B. SMITH

Los Alamos Scientific Laboratory, University of California, Los Alamos, New Mexico †

Received 15 February 1961

Abstract: A remarkably clear example of a two-stage nuclear reaction has been observed. Broad, steep-sided proton groups, observed during the bombardment of nitrogen by tritons, have been ascribed to the process $N^{14}(t, n)O^{16*}(p)N^{15}$. It is notable that this reaction appears to proceed by way of particular sharp states in O^{16} at an excitation of about 15 MeV.

1. Introduction

The last year or two has seen a sharp rise in interest in the interpretation of nuclear reactions of a three-body nature [1–4]) such as $p+d \rightarrow p+p+n$, $t+t \rightarrow \alpha+n+n$, $Li^6+d \rightarrow t+p+\alpha$ and $a+b \rightarrow c+Be^8+n$. Such interpretations seem amenable to discussion in terms of interactions in the final state of the reaction [1, 5, 6]), in terms of the effects of the thresholds of other channels and in terms of a cluster model [6]) of the nucleus. A phenomenon that is both predicted and observed is that such a three-body breakup should often proceed in a two-stage series of two-body reactions. Most experimental examples of this sort of event have been somewhat obscure because of poor experimental resolution or because the first-stage products have disintegrated in the second stage so rapidly that the energetics have been complicated by the broad states involved.

We have observed a remarkably clear example of a two-stage process. The first stage is the reaction $N^{14}(t, n)O^{16*}$. The highly excited oxygen nucleus has two energetically possible channels, $O^{16*}(p)N^{15}$ or $O^{16*}(\alpha)C^{12}$. The alpha channel did not produce results clear enough to interpret, but the proton channel gave very distinctive experimental results; this case is discussed in this paper. Part of the simplicity in the proton case lies in the fact that only the ground state of N^{15} may be produced, the first excited state being too high in energy (5.28 MeV).

2. Results and Discussion

During an investigation [7]) of the proton energy spectra [at 30° (lab) with 2.6-MeV tritons ††)] from the $N^{14}(t, p)N^{16}$ reaction, several anomalous "lumps"

† Work performed under the auspices of the U. S. Atomic Energy Commission.

†† See ref. [8]) for experimental details.

were observed (see fig. 1, arrows A and B). We have ascribed these broad, steep-sided groups to protons from the two-stage process $N^{14}(t, n)O^{16*}(p)N^{15}$. This identification is guided by several considerations. First it was noted that as the triton beam energy was changed, the lumps did not shift in energy at all like the proton peaks corresponding to N^{16} states. Then it was found that the experimental lump energy position and energy width could be predicted almost exactly by assuming the O^{16} excited nucleus to be in a sharp state and finding the energy limits by straightforward energy-momentum considerations. The width of the lump arises primarily from the fact that the O^{16*} nucleus comes from the first reaction with a distribution of recoil energies and directions.

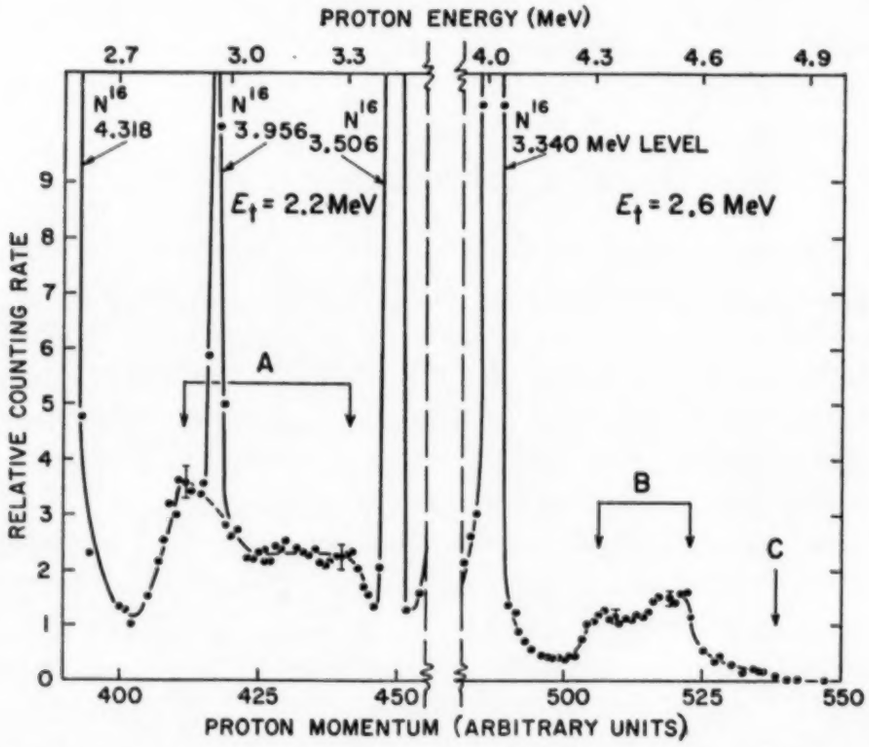

Fig. 1. Energy spectrum of protons at 30° (lab) from the bombardment of N^{14} by 2.2 and 2.6 MeV tritons. Peaks from the reaction $N^{14}(t, p)N^{16}$ corresponding to excited states in N^{16} are seen together with protons (A and B) from the $N^{14}(t, n)O^{16*}(p)N^{15}$ two-stage reaction. A low proton continuum from the $N^{14}(t, p)n$, N^{15} breakup underlies the above spectra. The error bars shown are examples of the statistical counting error. Arrow C indicates the energetic maximum for the three-body breakup.

It appears that two previously known levels in O^{16} form the intermediate steps for the two lumps shown in fig. 1. In fact, using the known energies of these levels results in the width predictions shown by the connected arrows A and B in fig. 1. The high-energy group (B) apparently is associated with the 16.22-MeV ($J = 1^+$, $\Gamma = 23$ keV) state in O^{16} observed in the $N^{15}(p, n)O^{15}$ reaction [9]) while the lower energy group (A) goes by way of the 14.94-MeV ($J = 4^+$, $\Gamma = 43$ keV) state observed in the $N^{15}(p, \alpha\gamma)C^{12}$ reaction [9]). There are four states between these two, and it is not at all clear why the two-stage reaction

does not also proceed by way of these states. The $O^{16*}(p)N^{15}$ breakup must use an $l = 1$ mode from the 1^+ state and must use an $l = 3$ or 5 mode from the 4^+ state. The detailed shape of the lumps should reflect these angular momenta as well as the angular distribution of the primary (first stage) process. Note that the high-energy lump is peaked at high proton energies while the low-energy lump is peaked at low proton energies.

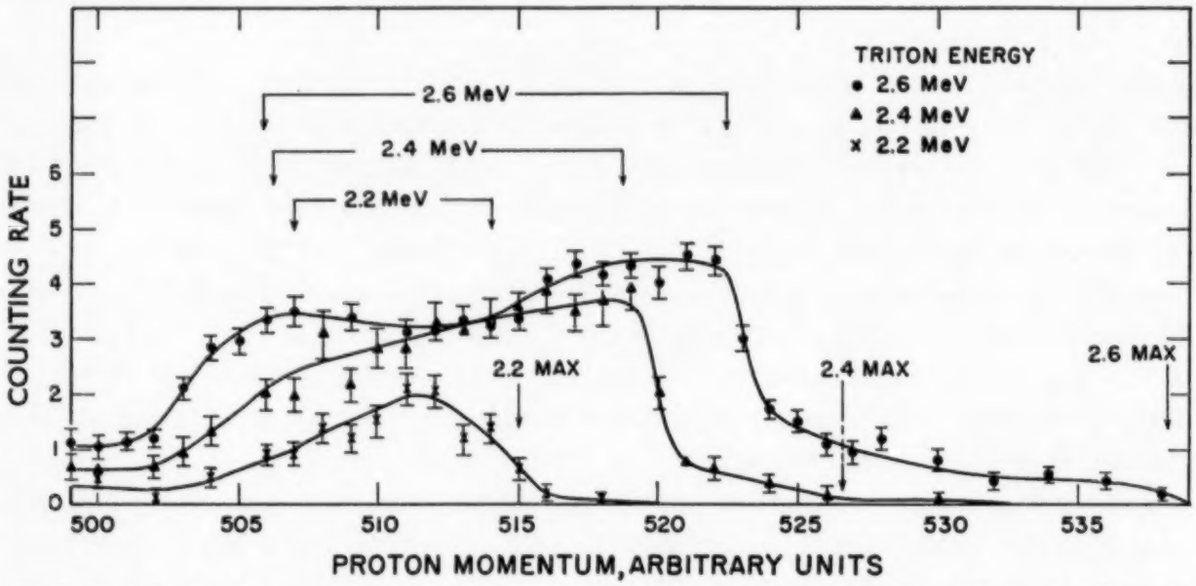

Fig. 2. Detail of the shape of the "high-energy" $N^{14}(t, n)O^{16*}(p)N^{15}$ lump (B) for three bombarding triton energies, 2.2, 2.4 and 2.6 MeV. The single arrows labeled 2.2 Max etc. indicate the calculated maximum proton energy for the three-body breakup. The connected arrows labeled with the energy indicate the calculated energetic range of each lump assuming the reaction goes through the 16.22-MeV state in O^{16} (see text). The errors shown are statistical counting errors.

TABLE 1

Approximate differential cross sections for processes resulting from the bombardment of N^{14} by tritons (lab angle 30°). Absolute standard deviations are ±25 %.

Process	Triton energy (MeV)	Cross section (mb/sr)
High-energy two-stage lump (B)	2.2	0.055
High-energy two-stage lump (B)	2.4	0.21
High-energy two-stage lump (B)	2.6	0.31
Low-energy two-stage lump (A)	all	1.2
Three-body breakup spectrum	2.6	4.4
Typical N^{16} proton peak	all	1

The energetic maximum for protons from the one-stage three-body breakup, $N^{14}+t \rightarrow p+n+N^{15}$, is also indicated by an arrow C in fig. 1 and a low continuous spectrum of protons is seen below this point. It should be noted that this maximum is quite close to the high-energy lump. This means that the primary process is proceeding with a very low available energy and the neutron is emitted with a low energy.

Experimental runs were made measuring the shape of these lumps in detail for triton energies of 2.2, 2.4 and 2.6 MeV. The shape and cross section for the low-energy lump did not change significantly with triton energy. However, the high-energy lump shape did change, and these spectra are shown in fig. 2. Some of this change is probably the effect of the three-body breakup energy maximum (which is also the maximum for the two-stage process) moving down into the lump. Approximate cross sections for the various processes are shown in table 1.

Probably it is wise to view these processes from the general point of view of the three-body breakup $N^{14}+t \rightarrow n+p+N^{15}$. Correlations of the outgoing neutron and proton lead to distortions in the continuous proton spectra or to a bound deuteron. Correlations of the neutron and N^{15} give broad or sharp proton peaks corresponding to states in N^{16}. Correlations of the proton and N^{15} give the two-stage effects in the proton spectrum that are being discussed. Those interactions, which last a long time and give sharp states, are probably independent of the other correlations, but fast breakups with broad states should interfere with the other possible modes and the interpretation of the proton spectra is then not clear.

It is interesting to speculate how often these two-stage groups have been mistaken for broad peaks in the spectra of a one-stage reaction in an experiment † with relatively poor resolution.

It is a pleasure to acknowledge helpful discussions with A. W. Schardt on several aspects of this subject.

† See for example the various strangely shaped groups in the neutron spectra described in ref. [10]).

References

1) V. V. Komarov and A. M. Popova, Nuclear Physics **18** (1960) 296
2) N. Jarmie and R. C. Allen, Phys. Rev. **111** (1958) 1121
3) R. T. Frost and S. S. Hanna, Phys. Rev. **110** (1958) 939
4) D. Miller, Phys. Rev. **109** (1958) 1669
5) A. B. Migdal, JETP (USSR) **28** (1955) 3 [JETP (Soviet Physics) **1** (1955) 2]
6) G. C. Phillips, T. A. Griffy and L. C. Biedenharn, in Proc. Int. Conf. Nuclear Structure, ed. by D. A. Bromley and E. W. Vogt (North-Holland Publishing Co., Amsterdam, 1960); Nuclear Physics **21** (1960) 310
7) M. G. Silbert, N. Jarmie and D. B. Smith, Nuclear Physics **25** (1961) 438
8) N. Jarmie and M. G. Silbert, Phys. Rev. **120** (1960) 914;
Nelson Jarmie and R. C. Allen, Phys. Rev. **111** (1958) 1121
9) F. Ajzenberg-Selove and T. Lauritsen, Nuclear Physics **11** (1958) 1
10) F. Ajzenberg-Selove, C. F. Osgood and C. P. Baker, Phys. Rev. **116** (1959) 1521

2.D

Nuclear Physics **25** (1961) 447—458; © *North-Holland Publishing Co., Amsterdam*

Not to be reproduced by photoprint or microfilm without written permission from the publisher

SUR LA LOI LIMITE DE L'ESPACEMENT DES VALEURS PROPRES D'UNE MATRICE ALÉATOIRE

MICHEL GAUDIN

Centre d'Études Nucléaires de Saclay, Gif-sur-Yvette (S. et O.), France

Reçu le 16 Janvier 1961

Abstract: The distribution function of the level spacings for a random matrix in the limit of large dimensions is expressed by means of a rapidly converging infinite product which has been used for a numerical calculation. Comparison with Wigner's hypothesis gives a very good agreement.

1. Introduction

Cet article fait suite à un travail de M. L. Mehta [1]), où la fonction de distribution de l'espacement des valeurs propres d'une matrice symétrique d'ordre n, à coefficients aléatoires, est donnée explicitement. Adoptant les hypothèses de Mehta, dont nous désignerons l'article par (M), nous nous proposons ici de donner la forme limite de cette distribution lorsque n augmente indéfiniment. L'expression obtenue dérive d'un produit infini rapidement convergent, ce qui nous a permis de présenter une table de valeurs numériques dans tout l'intervalle utile. La comparaison avec la fonction de Wigner [2]) $p_W(S)$ pour la densité de probabilité d'un espacement S, montre que celle-ci diffère de moins de 5 % de la fonction exacte pour $S/D < 2$, et constitue donc une excellente approximation dans la région où cette fonction n'est pas très petite.

2. Formules de Base

Nous reprenons les notations de (M). La fonction $P(\theta_1, \theta_2)$ (voir (M), § 5) est la densité de probabilité d'observer tel niveau en θ_1 et tel autre en θ_2, sans aucun niveau dans l'intervalle θ_1, θ_2. Dans la région où la densité de niveaux est constante et égale à $D^{-1} = 2\sqrt{n}/\pi$, il est plausible que $P(\theta_1, \theta_2)$ ne dépende que de l'espacement $S = \theta_2 - \theta_1$. Il a donc suffi de considérer $P(-\theta, \theta)$, que la formule (M.48) donne sous la forme suivante:

$$P(-\theta, \theta) = \frac{(2m-2)!}{\mu_0} \frac{\mathrm{d}}{\mathrm{d}\theta} \left(\mathrm{e}^{-2\theta^2} R_1(\theta)\right), \tag{1}$$

avec

$$R_1(\theta) = \frac{2^{m-1}}{(m-1)!} \int_\theta^\infty \mathrm{d}y_1 \ldots \int_\theta^\infty \mathrm{d}y_{m-1} \mathrm{e}^{-2(y_1^2+\ldots+y_{m-1}^2)} \prod_i (y_i^2-\theta^2)^2 \prod_{i<j} (y_i^2-y_j^2)^2, \tag{2}$$

et $n = 2m$. Si nous définissons $\phi_m(\theta)$ par l'égalité

$$\phi_m(\theta) = \int_\theta^\infty \mathrm{d}y_1 \ldots \int_\theta^\infty \mathrm{d}y_m \mathrm{e}^{-2(y_1^2+\ldots+y_m^2)} \prod_{i<j}^{m} (y_i^2 - y_j^2)^2, \tag{3}$$

nous pourrons combiner (1) et (2) sous la forme

$$2m(2m-1)\,P(-\theta, \theta) = \frac{2m!2^{m-1}}{m!\mu_0} \frac{\mathrm{d}^2}{\mathrm{d}\theta^2} \phi_m(\theta). \tag{4}$$

Par la suite nous ne nous soucierons pas de la normalisation de $P(-\theta, \theta)$ telle qu'elle est donnée par (3) et (4). La formule (M.47) s'écrit en effet

$$\int_0^\infty 2m(2m-1)DP(-\theta, \theta)\mathrm{d}(2\theta) = 1. \tag{5}$$

La densité de probabilité $p(S)$ de l'espacement S est donc égale à $2m(2m-1)$ $DP(-\theta, \theta)$, et la normalisation est déterminée par les équations

$$\int_0^\infty p(S)\mathrm{d}\left(\frac{S}{D}\right) = 1, \int_0^\infty Sp(S)\mathrm{d}\left(\frac{S}{D}\right) = D. \tag{6}$$

Par commodité, nous rapporterons $\phi_m(\theta)$ à sa valeur à l'origine et poserons $\Psi_m(\theta) = \phi_m(\theta)/\phi_m(0)$. Notre but est maintenant de chercher la forme limite de la fonction $\Psi_m(\theta)$ lorsque m augmente indéfiniment et que la variable θ reste de l'ordre de l'espacement moyen des niveaux, c'est-à-dire lorsque $\theta/D = 2\theta\sqrt{2m}/\pi$ tend vers une limite finie. Nous poserons $2\theta\sqrt{2m} = t$, de sorte que l'on a

$$\frac{S}{D} = \frac{2\theta}{D} = \frac{2t}{\pi}.$$

Soit $\Psi(t)$ la limite de $\Psi_m(\theta)$ dans ces conditions; d'après (4) la fonction $p(S)$ est proportionnelle à $\mathrm{d}^2\Psi/\mathrm{d}t^2$ et les égalités (6) s'écrivent

$$\int_0^\infty \frac{\mathrm{d}^2\Psi}{\mathrm{d}t^2} \frac{2}{\pi} \mathrm{d}t \propto 1, \qquad \int_0^\infty t \frac{\mathrm{d}^2\Psi}{\mathrm{d}t^2} \frac{4D}{\pi^2} \mathrm{d}t \propto D,$$

d'où l'on déduit

$$\left(\frac{\mathrm{d}\Psi}{\mathrm{d}t}\right)_{t=0} = -\frac{2}{\pi}, \text{ puisque l'on a } \Psi(0) = 1.$$

La fonction $p(S)$ s'écrit donc

$$p(S) = \tfrac{1}{4}\pi^2 \frac{\mathrm{d}^2\Psi}{\mathrm{d}t^2}, \tag{7}$$

et la fonction de distribution $F(S)$, probabilité d'un espacement inférieur à S est égale à

$$F(S) = \int_0^S p(S')\mathrm{d}\left(\frac{S'}{D}\right) = 1 + \tfrac{1}{2}\pi \frac{\mathrm{d}\Psi}{\mathrm{d}t}. \tag{8}$$

3. La Fonction $\Psi_m(\theta)$

Dans l'intégrale (3) qui nous donne $\phi_m(\theta)$, effectuons le changement de variables

$$\sqrt{2}\, y_i = z_i, \quad i = 1, 2, \ldots, m,$$
$$\sqrt{2}\, \theta = \tau.$$

Nous obtenons pour $\phi_m(\theta)$, à un facteur constant près,

$$\phi_m(\theta) = \phi_m\left(\frac{\tau}{\sqrt{2}}\right) \propto \int_\tau^\infty dz_1 \ldots \int_\tau^\infty dz_m e^{-(z_1^2+\ldots+z_m^2)} \Delta^2(z_1, z_2, \ldots, z_m),$$

où $\Delta(z_1, z_2, \ldots, z_m)$ est le déterminant

$$\begin{vmatrix} 1 & z_1^2 & z_1^4 \ldots z_1^{2m-2} \\ 1 & z_2^2 & z_2^4 \ldots z_2^{2m-2} \\ \ldots\ldots\ldots\ldots\ldots\ldots \\ \ldots\ldots\ldots\ldots\ldots\ldots \\ 1 & z_m^2 & z_m^4 \ldots z_m^{2m-2} \end{vmatrix}.$$

Par une méthode déjà utilisée dans un précédent travail [3]), nous exprimons Δ en fonction des polynômes d'Hermite; chaque monôme z_i^{2p} qui figure dans Δ est en effet une forme linéaire de polynômes pairs de degré inférieur ou égal à $2p$. Nous avons donc

$$\Delta(z_1, z_2, \ldots, z_m) \propto \begin{vmatrix} H_0(z_1) & H_2(z_1) \ldots H_{2m-2}(z_1) \\ H_0(z_2) & H_2(z_2) \ldots H_{2m-2}(z_2) \\ \ldots\ldots\ldots\ldots\ldots\ldots\ldots \\ \ldots\ldots\ldots\ldots\ldots\ldots\ldots \\ H_0(z_m) & H_2(z_m) \ldots H_{2m-2}(z_m) \end{vmatrix}.$$

Ceci nous permet d'exprimer $\phi_m(\tau/\sqrt{2})$ au moyen des fonctions normalisées de l'oscillateur harmonique $u_{2p}(z)$

$$\phi_m\left(\frac{\tau}{\sqrt{2}}\right) \propto \int_\tau^\infty dz_1 \ldots \int_\tau^\infty dz_m \begin{vmatrix} u_0(z_1) & u_2(z_1) \ldots u_{2m-2}(z_1) \\ u_0(z_2) & u_2(z_2) \ldots u_{2m-2}(z_2) \\ \ldots\ldots\ldots\ldots\ldots\ldots\ldots \\ \ldots\ldots\ldots\ldots\ldots\ldots\ldots \\ u_0(z_m) & u_2(z_m) \ldots u_{2m-2}(z_m) \end{vmatrix}^2.$$

Les u_{2p} vérifient donc les relations

$$\int_{-\infty}^{+\infty} u_{2i}(z) u_{2j}(z) dz = \delta_{ij}.$$

Le théorème de Gram appliqué à (10) nous conduit à l'expression suivante:

$$\phi_m\left(\frac{\tau}{\sqrt{2}}\right) \propto \begin{vmatrix} \int_\tau^\infty u_0^2(z)\mathrm{d}z & \int_\tau^\infty u_0(z)u_2(z)\mathrm{d}z & \cdots\cdots\int_\tau^\infty u_0(z)u_{2m-2}(z)\mathrm{d}z \\ \int_\tau^\infty u_2(z)u_0(z)\mathrm{d}z & \int_\tau^\infty u_2^2(z)\mathrm{d}z & \cdots\cdots\int_\tau^\infty u_2(z)u_{2m-2}(z)\mathrm{d}z \\ \cdots\cdots & \cdots\cdots & \cdots\cdots \\ \cdots\cdots & \cdots\cdots & \cdots\cdots \\ \int_\tau^\infty u_{2m-2}(z)u_0(z)\mathrm{d}z & \int_\tau^\infty u_{2m-2}(z)u_2(z)\mathrm{d}z\cdots\cdots & \int_\tau^\infty u_{2m-2}^2(z)\mathrm{d}z \end{vmatrix}; \qquad (11)$$

ϕ_m est donc un déterminant d'ordre m, d'éléments $\int_\tau^\infty u_{2i}(z)u_{2j}(z)\mathrm{d}z = \frac{1}{2}(\delta_{ij}-\int_{-\tau}^{+\tau} u_{2i}u_{2j}\mathrm{d}z)$. Sa valeur à l'origine $\tau = 0$ se calcule simplement: les éléments non diagonaux sont nuls et les éléments diagonaux égaux à $\frac{1}{2}$, d'où la valeur de la fonction $\Psi_m(\tau/\sqrt{2}) = \phi_m(\tau/\sqrt{2})/\phi_m(0)$:

$$\Psi_m\left(\frac{\tau}{\sqrt{2}}\right) = \text{dét}\left|\delta_{ij}-\int_{-\tau}^{+\tau} u_{2i}(z)u_{2j}(z)\mathrm{d}z\right|. \qquad (12)$$

Ψ_m prend la valeur 1 pour $\tau = 0$ par définition, et la valeur 0 pour $\tau = \infty$, et reste toujours compris entre ces deux valeurs puisque, d'après (9), elle est décroissante.

4. La Fonction Ψ_m Comme Déterminant de Fredholm

La fonction Ψ_m, définie par (12), est le déterminant de Fredholm, pour la valeur $\lambda = 1$, relatif au noyau symétrique, continu, borné

$$K_m(x, y) = \sum_{k=0}^{m-1} u_{2k}(x)u_{2k}(y), \quad |x| \leqq \tau, \quad |y| \leqq \tau. \qquad (13)$$

L'équation homogène de Fredholm s'écrit en effet

$$\lambda f(x) = \int_{-\tau}^{+\tau} K_m(x, y)f(y)\mathrm{d}y, \qquad (14)$$

où $f(x)$ est une fonction propre et λ la valeur propre correspondante.

A l'aide de la définition (13), l'équation (14) s'écrit

$$\lambda f(x) = \sum_{k=0}^{m-1} u_{2k}(x)\int_{-\tau}^{+\tau} u_{2k}(y)f(y)\mathrm{d}y.$$

Posant $c_k = \int_{-\tau}^{+\tau} u_{2k}(y)f(y)\mathrm{d}y$, nous obtenons le système linéaire

$$\lambda c_q = \sum_{k=0}^{m-1} c_k \int_{-\tau}^{+\tau} u_{2k}(x)u_{2q}(x)\mathrm{d}x, \qquad q = 0, 1, \ldots, m-1,$$

qui possède une solution, si dét $|\lambda\delta_{kq}-\int_{-\tau}^{+\tau} u_{2k}u_{2q}\mathrm{d}x| = 0$. Cette équation caractéristique possède m racines réelles $\lambda_1, \lambda_2, \ldots, \lambda_m$. Nous avons donc

$$\text{dét}\,|\delta_{ij}-\int_{-\tau}^{+\tau} u_{2i}u_{2j}\mathrm{d}z| = (1-\lambda_1)(1-\lambda_2)\ldots(1-\lambda_m),$$

qui est bien le déterminant de Fredholm de l'équation inhomogène correspondant à (14) pour $\lambda = 1$.

La formule de Christoffel [4]) donne une expression plus concise du noyau $K_m(x, y)$,

$$K_m(x, y) = \sum_{k=0}^{m-1} u_{2k}(x)u_{2k}(y)$$

$$= \frac{1}{\sqrt{\pi}} e^{-\frac{1}{2}(x^2+y^2)} \sum_{k=0}^{m-1} \frac{1}{2^{2k}\,2k!} H_{2k}(x)H_{2k}(y)$$

$$= \text{partie paire en } x \text{ de } \frac{1}{\sqrt{\pi}} e^{-\frac{1}{2}(x^2+y^2)} \sum_{k=0}^{2m-1} \frac{1}{2^k k!} H_k(x)H_k(y) \tag{15}$$

$$= \text{partie paire en } x \text{ de } \frac{1}{\sqrt{\pi}} e^{-\frac{1}{2}(x^2+y^2)} \frac{1}{2^{2m}(2m-1)!} \frac{H_{2m}(x)H_{2m-1}(y) - H_{2m}(y)H_{2m-1}(x)}{x-y}$$

$$= \text{partie paire en } x \text{ de } \sqrt{m}\, \frac{u_{2m}(x)u_{2m-1}(y) - u_{2m}(y)u_{2m-1}(x)}{x-y}.$$

5. Forme Limite de l'Équation (14) pour m Infini

Nous effectuons d'abord le changement de variables qui fait passer de $\tau = \theta\sqrt{2}$ à $t = 2\theta\sqrt{2m}$, en posant

$$\xi = 2x\sqrt{m}, \qquad \eta = 2y\sqrt{m}.$$

L'équation homogène (14) s'écrit alors

$$\lambda f\left(\frac{\xi}{2\sqrt{m}}\right) = \int_{-t}^{+t} \frac{1}{2\sqrt{m}} K_m\left(\frac{\xi}{2\sqrt{m}}, \frac{\eta}{2\sqrt{m}}\right) f\left(\frac{\eta}{2\sqrt{m}}\right) d\eta. \tag{16}$$

Dans le domaine $|\xi| \leqq t$, $|\eta| \leqq t$, le noyau devient donc

$$Q_m(\xi, \eta) = \frac{1}{2\sqrt{m}} K_m\left(\frac{\xi}{2\sqrt{m}}, \frac{\eta}{2\sqrt{m}}\right)$$

$$= \text{Partie paire en } \xi \text{ de } \sqrt{m}\, \frac{u_{2m}\left(\frac{\xi}{2\sqrt{m}}\right)u_{2m-1}\left(\frac{\eta}{2\sqrt{m}}\right) - u_{2m}\left(\frac{\eta}{2\sqrt{m}}\right)u_{2m-1}\left(\frac{\xi}{2\sqrt{m}}\right)}{\xi-\eta}. \tag{17}$$

Notons que le déterminant de Fredholm relatif à l'équation (14) est identique à celui de l'équation (16) écrite sous la forme

$$\lambda f_1(\xi) = \int_{-t}^{+t} Q_m(\xi, \eta) f_1(\eta) d\eta \tag{18}$$

où

$$f_1(\xi) = f\left(\frac{\xi}{2\sqrt{m}}\right).$$

Il est maintenant facile d'obtenir la limite de $Q_m(\xi, \eta)$ lorsque m tend vers l'infini, ξ, η, t restant fixes. Uniformément par rapport à ξ sur tout intervalle fini $|\xi| \leqq t$, nous avons †.

$$\lim_{m\to\infty} \frac{(-)^m\sqrt{m}}{2^{2m}m!} H_{2m}\left(\frac{\xi}{2\sqrt{m}}\right) = \frac{1}{\sqrt{\pi}} \cos \xi,$$

$$\lim_{m\to\infty} \frac{(-)^m}{2^{2m}m!} H_{2m+1}\left(\frac{\xi}{2\sqrt{m}}\right) = \frac{1}{\sqrt{\pi}} \sin \xi,$$

c'est-à-dire

$$\lim_{m\to\infty} m^{\frac{1}{4}}(-)^m u_{2m}\left(\frac{\xi}{2\sqrt{m}}\right) = \frac{1}{\sqrt{\pi}} \cos \xi,$$

$$\lim_{m\to\infty} m^{\frac{1}{4}}(-)^m u_{2m-1}\left(\frac{\xi}{2\sqrt{m}}\right) = \frac{-1}{\sqrt{\pi}} \sin \xi.$$

Par conséquent, uniformément par rapport à ξ, η,

$$Q(\xi, \eta) = \lim_{m\to\infty} Q_m(\xi, \eta) = \text{Paire en } \xi \text{ de} \frac{-1}{\pi} \frac{\cos \xi \sin \eta - \cos \eta \sin \xi}{\xi - \eta}$$

$$= \text{Partie paire en } \xi \text{ de} \frac{1}{\pi} \frac{\sin(\xi - \eta)}{\xi - \eta}.$$

Alors, on a

$$Q(\xi, \eta) = \frac{1}{2\pi}\left\{\frac{\sin(\xi - \eta)}{\xi - \eta} + \frac{\sin(\xi + \eta)}{\xi + \eta}\right\}, \quad |\xi| < t, |\eta| < t.$$

Ce noyau est symétrique, continu, borné. La forme limite de l'équation homogène (14) ou plutôt (18) est donc

$$\lambda g(\xi) = \int_{-t}^{+t} Q(\xi, \eta) g(\eta) d\eta. \tag{19}$$

6. Les Fonctions Sphéroïdales Solutions de l'Équation (19)

Les solutions $g(\xi)$ sont nécessairement paires. L'équation intégrale (19) est alors équivalente à la suivante [5])

$$\lambda g(\xi) = \frac{1}{\pi} \int_{-t}^{+t} \frac{\sin(\xi \pm \eta)}{\xi \pm \eta} g(\eta) d\eta, \tag{20}$$

à condition de se restreindre au sous-espace des fonctions paires, ce que nous ferons dans tout le paragraphe.

† Voir réf. [4]), Vol. II, ch. X, §§ 10, 13, formules (24), (25).

Le noyau $\sin(\xi+\eta)/\pi(\xi+\eta)$ est le carré du noyau $\exp(i\xi\eta/t)/\sqrt{2\pi t}$, équivalent lui-même à $\cos(\xi\eta/t)/\sqrt{2\pi t}$, symétrique, réel, dont les valeurs propres sont donc réelles. Si nous obtenons un système complet de fonctions $L^2(-t, +t)$, paires, solutions de l'équation

$$\mu g(\xi) = \frac{1}{\sqrt{2\pi t}} \int_{-t}^{+t} e^{i\xi\eta/t} g(\eta) d\eta, \tag{21}$$

nous aurons par là même les solutions de (20) et (19) avec la correspondance $\lambda = \mu^2$. Par le changement d'échelle $\xi = xt$, $\eta = yt$, qui ramène les limites d'intégration aux valeurs ± 1, l'équation (21) prend la forme

$$\gamma f(x) = \int_{-1}^{+1} e^{itxy} f(y) dy, \tag{22}$$

avec $f(x) = g(tx)$ et $\gamma = \mu\sqrt{2\pi/t}$, c'est-à-dire

$$\lambda = \frac{t}{2\pi}\gamma^2. \tag{23}$$

Les solutions de l'équation (22) sont les fonctions dites sphéroïdales [5, 6]) dépendant du paramètre t. Celles-ci sont définies comme les solutions régulières aux points ± 1 de l'équation différentielle

$$(L-l)f(x) = 0, \tag{24}$$

avec

$$L \equiv (x^2-1)d^2/dx^2 + 2xd/dx + t^2x^2.$$

Cet opérateur self-adjoint commute avec le noyau e^{itxy} défini sur l'intervalle -1, $+1$. Supposons en effet que $\varphi(x)$ soit une solution particulière de (24)

$$(L-l)\varphi(x) = 0.$$

Posons $\chi(x) = \int_{-1}^{+1} e^{itxy}\varphi(y)dy$. Il est facile de vérifier que $(L-l)\chi = 0$, sous les conditions suivantes

$$\left.\begin{aligned}(1-x^2)\varphi\ (x) &= 0\\ (1-x^2)\varphi'(x) &= 0\end{aligned}\right\} \quad \text{pour} \quad |x| = 1. \tag{25}$$

Or les conditions (25) imposent la régularité de $\varphi(x)$ en $x = \pm 1$ et déterminent les valeurs de l. La fonction χ nécessairement régulière en ± 1, est donc proportionnelle à $\varphi(x)$, d'où

$$\chi(x) = \gamma\varphi(x).$$

Les fonctions sphéroïdales $f_2, f_4, \ldots, f_{2q}, \ldots$ forment un système complet de fonctions paires $L^2(-1, +1)$. Elles constituent donc le système des fonctions propres du noyau $\exp(itxy)$, de son carré $\sin t(x+y)/(x+y)$ et du noyau original

Q, après le changement d'échelle $\xi = tx$. Les valeurs propres γ s'obtiennent par exemple en posant $x = 0$ dans l'équation (22), c'est-à-dire

$$\gamma_{2q} = \int_{-1}^{+1} f_{2q}(x)\mathrm{d}x / f_{2q}(0), \tag{26}$$

et

$$\lambda_q = \frac{t}{2\pi}\gamma_{2q}^2.$$

7. La Fonction $\Psi(t)$

Le noyau $Q(\xi, \eta)$ admet pour valeurs propres toutes positives les nombres $\lambda_q = (t/2\pi)\gamma_{2q}^2$, où les γ_{2q} sont définis par (26). C'est donc un noyau positif [7]). Cette propriété nous permet d'écrire le déterminant de Fredholm relatif à l'équation (19), sous la forme du produit infini suivant:

$$D(\lambda) = \prod_{q=0}^{\infty}\left(1 - \frac{1}{\lambda}\frac{t}{2\pi}\gamma_{2q}^2\right), \tag{27}$$

qui est une fonction entière de $1/\lambda$.

Considérons maintenant, pour t fixé, la suite des noyaux $Q_m(\xi, \eta)$; nous avons montré (§§ 4 et 5) que $\Psi_m(\tau/\sqrt{2})$ est le déterminant de Fredholm relatif à l'équation

$$f(\xi) - \int_{-t}^{+t} Q_m(\xi, \eta) f(\eta)\mathrm{d}\eta = \text{second membre},$$

or $Q_m(\xi, \eta)$ converge uniformément vers $Q(\xi, \eta)$ (§ 5) on en déduit [7]) que Ψ_m converge vers le déterminant de Fredholm du noyau Q, avec $\lambda = 1$, c'est-à-dire

$$\Psi(t) = \lim_{m\to\infty} \Psi_m\left(\frac{t}{2\sqrt{2m}}\right) = D(1), \tag{28}$$

soit

$$\Psi(t) = \prod_{q=0}^{\infty}\left(1 - \frac{t}{2\pi}\gamma_{2q}^2\right).$$

8. Propriétés de $\Psi(t)$ et Calcul Numérique

La fonction $\Psi(t)$, limite de quantités positives, est positive. Elle décroît de 1 à 0, lorsque t augmente de 0 à $+\infty$. Pour les petites valeurs de t, les fonctions sphéroïdales sont voisines des fonctions de Legendre et l'on peut calculer les coefficients du développement des premières fonctions sur les secondes par une méthode de perturbation. Les tables des fonctions sphéroïdales de Stratton [6]) donnent la valeur de ces coefficients jusqu'à $t = 10$

(page 203 et suivantes). Les fonctions $f_{2q}(x)$ sont alors définies par les séries

$$f_{2q}(x) = \sum_p d_{2p}(t|2q) P_{2p}(x). \tag{29}$$

Par exemple, à l'ordre 0, nous obtenons d'après (26)

$$\gamma_{2q} = \int_{-1}^{+1} P_{2q}(x)\mathrm{d}x / P_{2q}(0) = 0, \quad \text{si} \quad q \neq 0,$$

$$\gamma_0 = 2,$$

c'est-à-dire

$$\Psi(t) = 1 - \frac{2t}{\pi} + \ldots,$$

d'où

$$\left(\frac{\mathrm{d}\Psi}{\mathrm{d}t}\right)_{t=0} = -\frac{2}{\pi}$$

De cette façon, nous avons jusqu'au 5ème ordre en t

$$\Psi(t) = 1 - \frac{2t}{\pi} + \frac{2t^3}{9\pi^2} - \frac{2t^5}{75\pi} + \text{termes en } t^6 + \ldots$$

ou encore pour la fonction $F(S)$

$$F = 1 + \tfrac{1}{2}\pi \frac{\mathrm{d}\Psi}{\mathrm{d}t} = \tfrac{1}{3}t^2 - \tfrac{1}{15}t^4 + \ldots, \quad \frac{S}{D} = \frac{2t}{\pi}.$$

M. L. Mehta avait obtenu par un calcul direct (voir (M.63) et suivante)

$$\{1-F(S)\}\mathrm{e}^{\left(\frac{\pi S}{4D}\right)^2} = 1 - \tfrac{1}{3}(2m\theta^2) + \tfrac{7}{30}(2m\theta^2)^2 + \ldots,$$

qui coïncide bien avec le développement limité de

$$\begin{aligned}\{1-F\}\mathrm{e}^{\frac{1}{4}t^2} &= (1 - \tfrac{1}{3}t^2 + \tfrac{1}{15}t^4 + \ldots)(1 + \tfrac{1}{4}t^2 + \tfrac{1}{2}\tfrac{1}{16}t^4 + \ldots) \\ &= 1 - \tfrac{1}{3}\tfrac{1}{4}t^2 + \tfrac{7}{30}(\tfrac{1}{4}t^2)^2 + \ldots, \quad \tfrac{1}{4}t^2 = 2m\theta^2.\end{aligned}$$

Pour les grandes valeurs de t, les fonctions sphéroïdales tendent vers celles de l'oscillateur harmonique, tous les λ_q tendent vers l'unité et $\lim_{t\to\infty} \Psi(t) = 0$. Cependant nous n'avons rien pu dire sur le comportement asymptotique de $\Psi(t)$.

Nous avons effectué le calcul numérique des premières valeurs de γ_{2q} dans l'intervalle $0 \leqq t \leqq 5$, afin d'éprouver l'utilité du produit infini (28). Il se trouve que le calcul est simple et la convergence rapide. Grâce aux tables [6]) des coefficients $d_{2p}(t|2q)$, nous exprimons les γ_{2q} sous la forme suivante:

$$\gamma_{2q} = \frac{\int_{-1}^{+1} f_{2q}(x)\mathrm{d}x}{f_{2q}(0)} = \frac{2d_0(t|2q)}{\sum_p (-)^p \dfrac{1.3.5.\ldots.(2p-1)}{2.4.6.\ldots.2p} d_{2p}(t|2q)}.$$

Il est facile de voir que les γ_{2q} sont de l'ordre de grandeur des $d_0(2q)$ et décroissent vite avec q. Dans l'intervalle exploré $0 \leqq t \leqq 5$, il a suffi des 4 premiers facteurs de Ψ pour obtenir cinq chiffres exacts. Les valeurs numériques de $\Psi(t)$, de $F(S) = 1+\frac{1}{2}\pi \mathrm{d}\Psi/\mathrm{d}t$ et de $p(S) = \frac{1}{4}\pi^2 \mathrm{d}^2\Psi/\mathrm{d}t^2$ sont présentées dans la table 1, ainsi que les valeurs des fonctions $F_{\mathrm{W}}(S)$ et $p_{\mathrm{W}}(S)$, définies par les égalités

$$F_{\mathrm{W}}(S) = 1-\exp\left[-\tfrac{1}{4}\pi\left(\frac{S}{D}\right)^2\right] = 1-\mathrm{e}^{-t^2/\pi}, \quad p_{\mathrm{W}}(S) = \tfrac{1}{2}\pi\frac{S}{D}\exp\left[-\tfrac{1}{4}\pi\left(\frac{S}{D}\right)^2\right].$$

Les dérivations successives de $\Psi(t)$ laissent respectivement 4 chiffres et 3 chiffres exacts aux fonctions F et p.

TABLE 1

Les fonctions Ψ, F et p

t	S/D	Ψ	F	F_{W}	p	p_{W}
0	0	1	0	0	0	0
0.1	0.064	0.936408	0.00330	0.00317	0.104	0.0996
0.2	0.127	0.873239	0.01321	0.01265	0.207	0.1974
0.3	0.191	0.810904	0.02947	0.02824	0.303	0.2915
0.4	0.255	0.749796	0.05168	0.04965	0.395	0.3801
0.5	0.318	0.690283	0.07947	0.07649	0.477	0.4617
0.6	0.382	0.632698	0.11219	0.10827	0.549	0.5350
0.7	0.446	0.577337	0.14920	0.14441	0.6117	0.5989
0.8	0.509	0.524450	0.18982	0.18430	0.6630	0.6525
0.9	0.573	0.474248	0.23338	0.22727	0.7032	0.6954
1	0.637	0.426889	0.27908	0.27262	0.7308	0.7273
1.2	0.764	0.341117	0.37410	0.36768	0.7547	0.7587
1.4	0.891	0.267527	0.46962	0.46414	0.7396	0.7502
1.6	1.018	0.205888	0.56114	0.55730	0.6933	0.7083
1.8	1.146	0.155459	0.64529	0.64346	0.6255	0.6417
2	1.273	0.115153	0.71986	0.72007	0.5445	0.5598
2.2	1.400	0.083669	0.78376	0.78575	0.4587	0.4713
2.4	1.528	0.059626	0.83681	0.84014	0.3750	0.3836
2.6	1.655	0.041674	0.87956	0.88372	0.2978	0.3023
2.8	1.782	0.028563	0.91307	0.91749	0.2301	0.2308
3	1.910	0.019199	0.93863	0.94300	0.1730	0.1709
3.2	2.037	0.012654	0.95760	0.96159	0.1267	0.1229
3.4	2.164	0.008177	0.97133	0.97476	0.0906	0.0857
3.6	2.292	0.005182	0.98104	0.98384	0.0631	0.0581
3.8	2.419	0.003219	0.98772	0.98991	0.0429	0.0383
4	2.546	0.001961	0.99223	0.99386	0.0286	0.0245
4.2	2.674	0.001171	0.99518	0.99635	0.0185	0.0153
4.4	2.801	0.0006858	0.99708	0.99789	0.0117	0.0092
4.6	2.928	0.0003937	0.9983	0.99881	0.0062	0.0054
4.8	3.055	0.0002216	0.9990	0.99934	0.0030	0.0031
5	3.183	0.0001222	0.9994	0.99965	0.002	0.0017

Sur la fig. 1, on a représenté F et F_{W}, peu distinguables à l'échelle adoptée, encadrées par les bornes inférieure F_0, et supérieure F_1, données par Mehta

(M.60),

$$F_0 = 1-\exp(-\tfrac{1}{4}t^2), \quad F_1 = 1-(1-\tfrac{1}{12}t^2)\exp(-\tfrac{1}{4}t^2).$$

F et F_W diffèrent de moins de 1 % pour $S < 1.4D$ et la différence absolue est inférieure à 0.0066 dans la région $S < 3D$. La fig. 2 représente les fonctions p et p_W dont la différence relative est inférieure à 5 % pour $S < 2D$, et l'écart moindre que 0.0162.

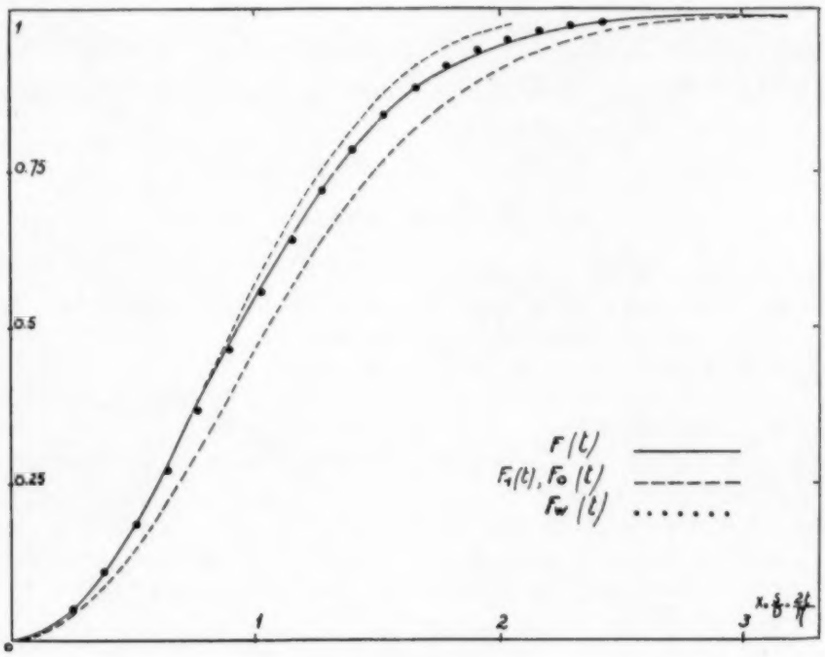

Fig. 1. La distribution de Wigner $F_W(S)$ et la fonction exacte $F(S)$ comprise entre F_0 et F_1.

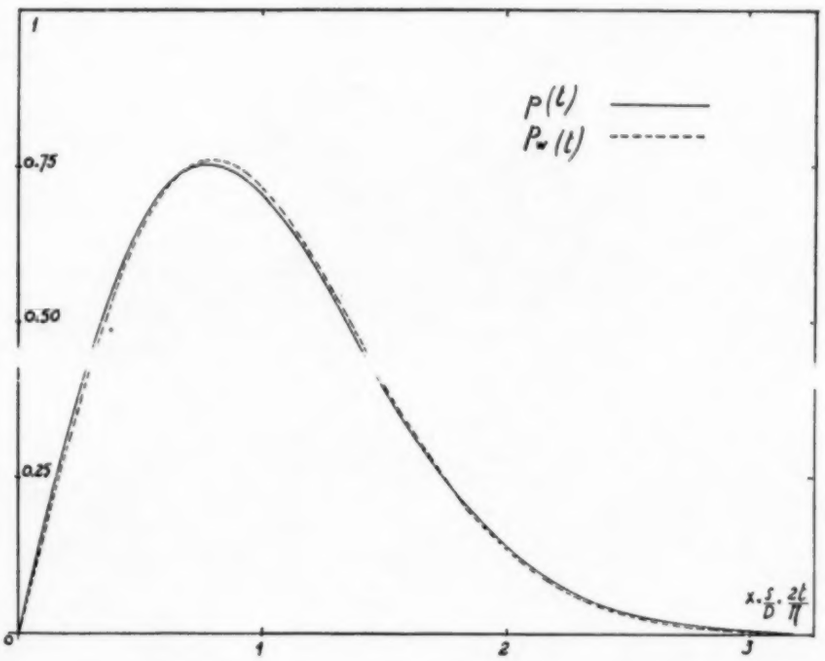

Fig. 2. Les densités de probabilité $p(S)$ et $p_W(S)$.

M. L. Mehta a mis au point une méthode de calcul de la fonction $I_m(\theta)$, donnée sous forme de déterminant (M.54) à l'aide de laquelle s'exprime F. La convergence est rapide et pour $m = 8$, la courbe de F se superpose à celle qui est donnée fig. 1.

Il propose de représenter la fonction F dans la région $S < 2D$ par la forme $(1+at^2)^{-\alpha} \exp(-\frac{1}{4}t^2)$, qui réalise une meilleure approximation que F_W, si l'on prend $\alpha = 1.003$ et $a = 0.078$.

Je remercie le Professeur C. Bloch et Monsieur M. L. Mehta de l'intérêt qu'ils ont pris à ce travail, ainsi que Mademoiselle N. Castille du Bureau de Calcul de Saclay pour les résultats numériques.

Bibliographie

1) M. L. Mehta, Nuclear Physics **18** (1960) 420
2) Wigner et Gatlinberg, Conf. on Neutron Physics by time of flight, Oak-Ridge, National Laboratory Report ORNL 2309 (1957) p. 59
3) M. L. Mehta et M. Gaudin, Nuclear Physics **18** (1960) 420
4) Bateman, dans Manuscript Project, édité par A. Erdélyi (New-York, Toronto, London) Vol. II, ch. X, §§ 10, 13, formule (11)
5) L. Robin, Fonctions sphériques de Legendre et fonctions sphéroïdales (Gauthiers-Villars, 1959) Tome III, p. 250, formule (255)
6) J. A. Stratton, P. M. Morse, L. J. Chu, J. D. C. Little and F. J. Corbato, Spheroïdal wave functions (The Technology Press of M.I.T.-Wiley)
7) E. Goursat, Cours d'Analyse Mathématique (Gauthiers-Villars, Paris, 1956) Tome III, p. 454 § 592, p. 389 § 572

1.D.2:
2.H

Nuclear Physics **25** (1961) 459—471; © *North-Holland Publishing Co., Amsterdam*
Not to be reproduced by photoprint or microfilm without written permission from the publisher

MULTIPLE COULOMB EXCITATIONS OF VIBRATIONAL NUCLEI

D. W. ROBINSON

Institut für Theoretische Physik, E.T.H., Zürich

Received 13 February 1961

Abstract: An analysis is made of the multiple Coulomb excitation of vibrational nuclei taking into account both one-phonon and two-phonon processes. Some of the results of Alder and Winther concerning the one-phonon transitions are re-derived together with some new results concerning the excitation of the triplet of substates forming the second excited state. It is shown that the weak two-phonon processes can affect the excitation probabilities through interference with the strong one-phonon processes. The interference is destructive at energies for which a particular state is being primarily excited and constructive at higher energies for which the state is being de-excited in favour of higher states.

1. Introduction

The characteristic energy spectrum of a vibrational nucleus is a series of equally spaced levels, each containing a set of substates which may be classified by their total angular momentum. The most important vibrational nuclei are those in which the oscillations are of a quadrupole nature. The "quasi-particle" picture describes these nuclei with the help of phonons carrying one quantum of energy and two quanta of angular momentum. The ground state of the nucleus is the zero-phonon state and the n-th excited state contains n phonons, which may combine together into substates of total angular momentum less than or equal to $2n$ quanta. Quadrupole Coulomb excitation of the nucleus may occur through processes involving one, two, or even more, phonons. The most important of the processes is that involving only one phonon. Multiple excitation of the nucleus may occur through a series of one-phonon transitions, a mixture of one-phonon and two-phonon transitions, or by other higher order processes.

Recently, K. Alder and A. Winther [1]) have calculated the cross-sections for multiple Coulomb excitation of vibrational nuclei assuming that the excitation occurs through one-phonon transitions only. In this paper the effect of including two-phonon transitions in the calculation, to first order, is examined. A detailed calculation is also made of the relative excitation probabilities of the triplet of substates forming the second excited state and the results of Alder and Winther are corrected.

Sect. 2 gives a short summary of the general theory necessary for the ensuing calculations, whilst sect. 3 contains the general methods of solution. Sect. 4 contains the explicit solution for the time development matrix of the nuclear states, assuming only one-phonon processes, and some results identical to those of Alder and Winther are given. The excitation of the substates of the second excited state is also considered in sect 4. Sect. 5 deals with the effect of introducing two-phonon transitions.

2. General Theory

The simplest form of the vibrational model of nuclei is assumed, in which the vibrations are harmonic. Therefore the Hamiltonian describing the oscillations has the form

$$H = \sum_{\mu} \left[\frac{1}{2B} \dot{p}_{\mu} \dot{p}_{\mu}^{+} + \tfrac{1}{2} C x_{\mu} x_{\mu}^{+} \right], \tag{1}$$

where the x_{μ} are parameters of the nuclear quadrupole deformation and the $\dot{p}_{\mu}$ are their conjugate momenta. The set of uncoupled harmonic oscillators described by the above Hamiltonian have a spectrum of equally spaced energy levels, spacing $\hbar\omega = \sqrt{C/B}$. We next introduce phonon annihilation and creation operators by the definitions

$$\begin{aligned} \alpha_{\mu} &= \frac{1}{\sqrt{2\omega}} \left[\sqrt{C} x_{\mu}^{+} + i \frac{\dot{p}_{\mu}}{\sqrt{B}} \right], \\ \alpha_{\mu}^{+} &= \frac{1}{\sqrt{2\omega}} \left[\sqrt{C} x_{\mu} - i \frac{\dot{p}_{\mu}^{+}}{\sqrt{B}} \right]. \end{aligned} \tag{2}$$

The operator α_{μ}^{+} creates a phonon with two units of angular momentum with z-component equal to μ, while the operator α_{μ} destroys such a phonon. The nuclear states may be classified by the numbers n_{μ} of phonons of each type in the state, and the three lowest energy states of the nucleus may be completely classified by the three quantum numbers (N, L, M), where N is the total number of phonons in the state, L is the total angular momentum of the state and M is the z-component of angular momentum.

In particular the wave function of the second excited state may be written

$$|2LM\rangle = \sqrt{\frac{2L+1}{2}} \sum_{\mu\nu} \begin{pmatrix} 2 & 2 & L \\ \mu & \nu & M \end{pmatrix} \alpha_{\mu}^{+} \alpha_{\nu}^{+} |0\rangle, \tag{3}$$

where $|0\rangle$ represents the nuclear ground state.

Now the Hamiltonian describing the electric quadrupole Coulomb excitation of the nucleus due to its interaction with a charged projectile is given by

ref. [2]) as

$$H_{\mathrm{E}}(t) = \frac{4\pi}{5} Z_1 e \sum_{\mu} \frac{Y_{2\mu}(\theta_{\mathrm{p}}, \varphi_{\mathrm{p}})}{r_{\mathrm{p}}^3} M^*(\mathrm{E2}, \mu). \tag{4}$$

The notation used here and in the following is that of ref. [2]), in which the standard parameters, functions and methods of Coulomb excitation calculations are defined and discussed. The time dependence of the excitation Hamiltonian enters through the coordinates of the projectile $(r_{\mathrm{p}}, \theta_{\mathrm{p}}, \varphi_{\mathrm{p}})$ and for convenience we introduce functions

$$f_\mu(t) = \frac{Y_{2\mu}(\theta_{\mathrm{p}}, \varphi_{\mathrm{p}})}{r_{\mathrm{p}}^3} = (-1)^\mu f^*_{-\mu}(t). \tag{5}$$

The electric quadrupole moment of the nucleus $M(\mathrm{E2}, \mu)$ can be expressed in terms of phonon annihilation and creation operators if some assumption is made about the charge density of the nucleus. Assuming the charge density is uniform a straightforward calculation yields

$$M(\mathrm{E2}, \mu) = M_\mu{}^1 + M_\mu{}^2 + \ldots, \tag{6}$$

where

$$M_\mu{}^1 = \frac{3}{4\pi\sqrt{5}} Z_2 e R_0{}^2 \beta [\alpha_\mu + (-1)^\mu \alpha^+_{-\mu}], \tag{7}$$

$$M_\mu{}^2 = -\frac{3}{4\pi}\sqrt{\frac{2}{7\pi}} Z_2 e R_0{}^2 \beta^2 k \sum_{\lambda\nu} \begin{pmatrix} 2 & 2 & 2 \\ \lambda & \mu & \nu \end{pmatrix} [\alpha_\lambda{}^+ + (-1)^\lambda \alpha_{-\lambda}][\alpha_\nu{}^+ + (-1)^\nu \alpha_{-\nu}]. \tag{8}$$

The first term in the expression for the quadrupole moment is the one responsible for one-phonon transitions, the second term leads to two-phonon transitions and the omitted terms correspond to higher order interactions. The root mean square deformation of the nuclear surface β has been introduced and this is defined by

$$\beta^2 = \sum_{\mu} |\langle 0 | x_\mu x_\mu{}^+ | 0 \rangle|^2 = \tfrac{5}{2} \frac{1}{\sqrt{BC}}. \tag{9}$$

The factor k in the expression for $M_\mu{}^2$ needs some explanation. The nuclear model that is being considered here is a very simplified version of the real state of affairs. In general, nuclear vibrations are not purely harmonic, this is shown for instance by the non-degeneracy of the angular momentum substates of each principal state, and in assuming the Hamiltonian (1) we are really neglecting all but first order terms in the Hamiltonian. Hence for consistency the interaction Hamiltonian should be taken only to lowest order. However, the harmonic vibration model predicts higher order terms in the interaction, the second order term being $M_\mu{}^2$ with $k = 1$. Therefore, in nuclei which are nearly harmonic, we keep the Hamiltonian (1) but modify the interaction Hamil-

tonian (4), by the introduction of the enhancement factor k in (8). The lowest observable transition in which the second order term (8) may occur is the so-called cross-over transition from the ground state of the nucleus to the second state, and it is found from this transition [2]) that k is usually larger than 1. Nevertheless, if k is not much different from 1 this method should be meaningful. It is interesting to include a term of the type (8) for besides transitions of the nature of the cross-over transition in which two phonons are created this form of interaction may induce transitions in which one phonon is created whilst a second is annihilated. In the first type of transition two quanta of energy are created and in the second the total change of energy is zero, for this reason the second type of transition is preferred. However, this type of transition is also unobservable directly and may only be investigated indirectly.

3. The Wave Equation

The wave equation determining the nuclear excitation is

$$\frac{i\partial\psi}{\partial t} = [H+H_{\mathrm{E}}(t)]\psi,$$

where H and $H_{\mathrm{E}}(t)$ are given by (1) and (4), respectively, and units are chosen such that $\hbar = 1$. Simultaneously changing to the interaction representation and introducing the time development operator $U(t, t_0)$ by the transformation

$$\psi(t) = \mathrm{e}^{-iHt}\, U(t, t_0)\mathrm{e}^{iHt_0}\psi(t_0),$$

we find

$$\frac{i\partial U(t, t_0)}{\partial t} = \mathrm{e}^{iHt}H_{\mathrm{E}}(t)\mathrm{e}^{-iHt}U(t, t_0). \tag{10}$$

This may be simplified by using the identity

$$\mathrm{e}^{iHt}\alpha_\mu\mathrm{e}^{-iHt} = \alpha_\mu\mathrm{e}^{-i\omega t} \equiv \alpha_\mu(t).$$

The derivation of this identity is dependent upon the commutation properties of the phonon operators and the Taylor's series expansion of the left hand side.

From this identity it follows that

$$\mathrm{e}^{iHt}H_{\mathrm{E}}(\alpha_\mu, t)\mathrm{e}^{-iHt} = H_{\mathrm{E}}(\alpha_\mu(t), t) = \tilde{H}_{\mathrm{E}}(t). \tag{11}$$

This function $\tilde{H}_{\mathrm{E}}(t)$ is now resolved into two terms corresponding to the decomposition of the quadrupole moment operator $M(\mathrm{E2}, \mu)$ into $M_\mu{}^1$ and $M_\mu{}^2$. The splitting is designated by

$$\tilde{H}_{\mathrm{E}}(t) = \tilde{H}_{\mathrm{E}}{}^1(t)+\tilde{H}_{\mathrm{E}}{}^2(t),$$

and it follows that $\tilde{H}_{\mathrm{E}}{}^1(t)$ is linear in the phonon operators, whilst $\tilde{H}_{\mathrm{E}}{}^2(t)$ is

quadratic in these operators. Therefore, if we have

$$[\tilde{H}_E{}^1(t'), \tilde{H}_E{}^1(t'')] = ig(t', t''),$$

the commutation rules of the phonon operators give us the important property that $g(t', t'')$ is a real c-number function of the time variables.

It is shown in the Appendix that this condition is sufficient for the equation

$$\frac{i\partial V(t, t_0)}{\partial t} = \tilde{H}_E{}^1(t)\, V(t, t_0) \tag{12}$$

to have the exact solution

$$V(t, t_0) = \exp\left\{-i\int_{t_0}^{t} \tilde{H}_E{}^1(t')\mathrm{d}t'\right\} \exp\left\{-\tfrac{1}{2}i\int_{t_0}^{t}\int_{t_0}^{t'} g(t', t'')\mathrm{d}t'\,\mathrm{d}t''\right\}. \tag{13}$$

The second factor in this expression is a phase factor only, and the phase has been normalised so that $V(t_0, t_0) = 1$. The solution of (12) may now be utilised to solve eq. (10) to all orders in $\tilde{H}_E{}^1(t)$ and to arbitrary order in $\tilde{H}_E{}^2(t)$. We put

$$U(t, t_0) = V(t, t_0)\, W(t, t_0)$$

and substitute this in (10). It is found that $W(t, t_0)$ satisfies

$$\frac{i\partial W(t, t_0)}{\partial t} = V^+(t, t_0)\tilde{H}_E{}^2(t)V(t, t_0)W(t, t_0).$$

The solution of this equation to first order in $\tilde{H}_E{}^2(t)$ is obtained by iteration, and then we have

$$U(t, t_0) = V(t, t_0)\left[1 - i\int_{t_0}^{t} V^+(t', t_0)\tilde{H}_E{}^2(t')V(t', t_0)\mathrm{d}t'\right]. \tag{14}$$

This expression may be rearranged, using the properties

$$V(t_1, t_2) = V(t_1, t)V(t, t_2) = V^+(t_2, t_1).$$

Then in the limit $t \to \infty$, $t_0 \to -\infty$, eq. (14) becomes

$$U(\infty, -\infty) = \left[1 - i\int_{-\infty}^{\infty} V(\infty, t)\tilde{H}_E{}^2(t)V^+(\infty, t)\mathrm{d}t\right] V(\infty, -\infty). \tag{15}$$

It can be immediately seen from (15) that the phase factor in (13) contributes an overall phase factor to $U(\infty, -\infty)$. As an overall phase factor is of no importance in the calculation of transition probabilities we ignore it in the following and take the solution for $V(t, t_0)$ as

$$V(t, t_0) = \exp\left\{-i\int_{t_0}^{t} \tilde{H}_E{}^1(t')\mathrm{d}t'\right\}. \tag{16}$$

This expression is the time development matrix for the nuclear states assuming one-phonon processes only.

4. One-Phonon Processes

In order to calculate the matrix elements of the operator (16) it is desirable to express it as a normal ordered product of the phonon operators. The first step in this direction is made by using (4), (7) and (11) to write

$$\tilde{H}_{\mathrm{E}}{}^{1}(t) = \frac{3}{5\sqrt{5}} Z_1 Z_2 e^2 R_0{}^2 \beta \sum_{\mu} f_{\mu}(t)[\alpha_{\mu}{}^{+} e^{i\omega t} + (-1)^{\mu} \alpha_{-\mu} e^{-i\omega t}]. \tag{17}$$

The integral over the time variable in (17) introduces the classical orbital integrals $S_{\mathrm{E2},\,\mu}$, μ defined in ref. [2]), p. 436. To simplify the subsequent algebra, new definitions are taken:

$$\begin{aligned} S_{\mathrm{E2},\,\mu} &= \int_{-\infty}^{\infty} f_{\mu}(t) e^{i\omega t} dt = \frac{1}{a^2 \eta} J_{\mu}(\theta, \xi), \\ q &= \frac{3}{5\sqrt{5}} \eta \frac{R_0{}^2}{a^2} \beta. \end{aligned} \tag{18}$$

The parameters θ, ξ, η and a are defined in ref [2]), and the functions $J_{\mu}(\theta, \xi)$ are relared to the functions $I_{2\mu}(\theta, \xi)$, tabulated on p. 478 of this paper, by the formulae

$$J_{\mu}(\theta, \xi) = Y_{2\mu}(\tfrac{1}{2}\pi, 0) I_{2\mu}(\theta, \xi). \tag{19}$$

Combining (16), (17) and (18), it is found that

$$V(\infty, -\infty) = \exp\{-iq \sum_{\mu} [J_{\mu}(\theta, \xi)\alpha_{\mu}{}^{+} + \text{h.c.}]\}. \tag{20}$$

Finally, the normal ordering of (20) follows, with the aid of the ordering theorem [3]) quoted in the Appendix, and explicitly

$$V(\infty, -\infty) = \prod_{\mu} \exp\{-iq J_{\mu} \alpha_{\mu}{}^{+}\} \exp\{-iq J_{\mu}{}^{+} \alpha_{\mu}\} \exp\{-\tfrac{1}{2} q^2 J_{\mu} J_{\mu}{}^{+}\}, \tag{21}$$

where the arguments of $J_{\mu}(\theta, \xi)$ have been omitted.

The probability of exciting the nucleus from its ground state to the state with N phonons can now be calculated using (21). This probability is given by

$$P_N = \sum_{\{n_{\mu}\}} |\langle \{n_{\mu}\} | V(\infty, -\infty) | 0 \rangle|^2, \tag{22}$$

where $\{n_{\mu}\}$ signifies the possible partitions of the phonon occupation numbers n_{μ}, such that the total number of phonons in the state is N. Substituting (21) into (22), we have

$$P_N = \sum_{\{n_{\mu}\}} q^{2N} \prod_{\mu} \frac{[J_{\mu} J_{\mu}{}^{+}]^{n_{\mu}}}{n_{\mu}!} \exp\{-q^2 J_{\mu} J_{\mu}{}^{+}\},$$

and using the multinomial theorem we get

$$P_N = q^{2N} \frac{[X(\theta, \xi)]^N}{N!} \exp\{-q^2 X(\theta, \xi)\}, \tag{23}$$

where

$$X(\theta, \xi) = \sum_{\mu} J_\mu(\theta, \xi) J_\mu{}^+(\theta, \xi).$$

This result is in agreement with that of Alder and Winther [1]), and demonstrates that, under the assumption that nuclear excitation takes place through one-phonon processes only, the states of the excited nucleus are populated in a Poisson distribution.

It is also possible, using (21), to calculate the probability of exciting the nucleus into a particular angular momentum substate of any principal state, in particular the probability of exciting the substate of angular momentum L contained in the second excited state is given by

$$P_L = \sum_{M} |\langle 2LM|V(\infty, -\infty)|0\rangle|^2.$$

Substituting (3) and (21) into this expression, we find

$$P_L = \frac{q^4}{2} (2L+1) A_L \exp\{-q^2 X\},$$

where

$$A_L = \sum_{\substack{\mu\nu \\ \mu'\nu' M}} \begin{pmatrix} 2 & 2 & L \\ \mu & \nu & M \end{pmatrix} \begin{pmatrix} 2 & 2 & L \\ \mu' & \nu' & M \end{pmatrix} J_\mu J_\nu J^+_{\mu'} J^+_{\nu'}. \tag{24}$$

These formulae may be evaluated directly, using the tabulated values of $I_{2\mu}(\theta, \xi)$, or, more easily, the derived equations

$$\sqrt{\frac{5P_0}{P}} = 1 - \frac{(J_2 - J_{-2})^2}{X},$$

$$7P_2 - 10P_0 = 8 \frac{J_0{}^2 (J_2 - J_{-2})^2}{X^2} P, \tag{25}$$

$$4P_4 - 3P_2 - 6P_0 = 4 \frac{(J_2{}^2 - J^2_{-2})^2}{X^2} P,$$

(where $P = P_0 + P_2 + P_4$) may be solved for the relative probabilities.

Eqs. (25) immediately demonstrate the general features of the ratios $P_4 : P_2 : P_0$. The functions $J_\mu(\theta, \xi)$ have the property that

$$J_2(\theta, \xi) = J_{-2}(\theta, \xi) \tag{26}$$

for all values of ξ when $\theta = \pi$, i.e. the scattering is in the backward direction.

It immediately follows from (25) that in this case

$$P_4 : P_2 : P_0 = 18 : 10 : 7. \tag{27}$$

If $\xi = 0$, relation (26) is valid for all angles of scattering and the ratios (27) are preserved. However, if $\xi \neq 0$ the difference

$$J_{-2}(\theta, \xi) - J_2(\theta, \xi)$$

increases with decreasing angle of scattering and the ratios P_4/P_2 and P_4/P_0 consequently decrease. An explicit example has been calculated for $\theta = \frac{1}{2}\pi$, $\xi = 0.3$ and it is found that

$$P_4 : P_2 : P_0 \approx 18 : 6 : 2.6.$$

5. One- and Two-Phonon Processes

In this section we consider the matrix elements of the operator defined by (15). Again it is most convenient if the operator may be put into normal ordered form. This may be achieved using (21), and a similar expression for $V(\infty, t)$. The expression $V(\infty, t)$ differs from $V(\infty, -\infty)$ only in so far as the integral over time (18), which defines $J_\mu(\theta, \xi)$, has a different lower limit. In the following, the arguments θ, ξ of $J_\mu(\theta, \xi)$ are replaced by the limits of the appropriate defining integral of the type (18).

Considering the integrand of the second term of (15) and denoting it by $\hat{H}_E{}^2(t)$, we find

$$\hat{H}_E{}^2(t) = \prod_{\mu,\nu} e^{-iqJ_\mu(\infty,t)\alpha_\mu{}^+} e^{-iqJ_\mu{}^+(\infty,t)\alpha_\mu} \tilde{H}_E{}^2(t) e^{iqJ_\nu{}^+(\infty,t)\alpha_\nu} e^{iqJ_\nu(\infty,t)\alpha_\nu{}^+}, \tag{28}$$

where the ordering theorem has been again used. Now from the commutation properties of the phonon operators it is easily proved that

$$e^{-iqJ_\mu{}^+(\infty,t)\alpha_\mu}\alpha_\mu{}^+ e^{iqJ_\mu{}^+(\infty,t)\alpha_\mu} = \alpha_\mu{}^+ - iqJ_\mu{}^+(\infty, t).$$

Using this and similar identities, it is seen that $\hat{H}_E{}^2(t)$ is derived from $\tilde{H}_E{}^2(t)$ simply by the transformation

$$\alpha_\mu \to \alpha_\mu + iqJ_\mu(\infty, t), \qquad \alpha_\mu{}^+ \to \alpha_\mu{}^+ - iqJ_\mu{}^+(\infty, t).$$

Extending this method a little further, we find eventually

$$U(\infty, -\infty) = \prod_\mu e^{-iqJ_\mu\alpha_\mu{}^+} \left[1 - i\int_{-\infty}^{\infty} \bar{H}_E{}^2(t)\mathrm{d}t\right] e^{-iqJ_\mu{}^+\alpha_\mu} e^{-\frac{1}{2}q^2 J_\mu J_\mu{}^+}, \tag{29}$$

where $\bar{H}_E{}^2(t)$ is derived from $\tilde{H}_E{}^2(t)$ by the transformation

$$\alpha_\mu \to \alpha_\mu - iqJ_\mu(t, -\infty), \qquad \alpha_\mu{}^+ \to \alpha_\mu{}^+ - iqJ_\mu{}^+(\infty, t). \tag{30}$$

To complete the normal ordering of $U(\infty, -\infty)$ it is only necessary to put $\bar{H}_E{}^2(t)$ in ordered form. Although this is straightforward, the general formalism becomes too unwieldly at this point to make the full investigation worthwhile, hence we consider a special case only.

When the projectile causing the nuclear excitation is scattered backwards, a great simplification occurs. In this case it is possible to choose a coordinate system for the projectile orbit which results in all the classical orbital integrals vanishing except that with $\mu = 0$. This coordinate system has been used extensively in connection with the sudden approximation [1, 4]). The classical orbital integrals in this new coordinate system $K_\mu(\theta, \xi)$ are connected with the functions used so far in this paper by the formulae

$$K_\mu(\theta, \xi) = \sum_\nu \mathscr{D}^2_{\mu\nu}(0, \tfrac{1}{2}\pi, 0) J_\nu(\theta, \xi), \tag{31}$$

where $\mathscr{D}^2_{\mu\nu}$ is the rotation matrix [5]). In the rest of this section we use this coordinate scheme and restrict our considerations to backward scattering ($\theta = \pi$). Thus, eq. (29) becomes

$$U(\infty, -\infty) = \mathrm{e}^{-iqK\alpha^+} \left[1 - i \int_{-\infty}^{\infty} \bar{H}_E{}^2(t)\mathrm{d}t\right] \mathrm{e}^{-iqK^+\alpha} \mathrm{e}^{-\frac{1}{2}q^2KK^+}, \tag{32}$$

where the arguments of $K_0(\pi, \xi)$ have again been omitted and the zero suffices on this function and the phonon operators have also been dropped.

Now from (4), (8) and (30), we have

$$\bar{H}_E{}^2(t) = \frac{6}{35\sqrt{5\pi}} Z_1 Z_2 e^2 R_0{}^2 \beta^2 k f(t) [\alpha^+ \mathrm{e}^{i\omega t} + \alpha \mathrm{e}^{-i\omega t} - iqF(t)]^2, \tag{33}$$

where

$$F(t) = K^+(\infty, t)\mathrm{e}^{i\omega t} + K(t, -\infty)\mathrm{e}^{-i\omega t}.$$

To complete the normal ordering of $U(\infty, -\infty)$, we next write

$$-i \int_{-\infty}^{\infty} \bar{H}_E{}^2(t)\mathrm{d}t = A - iB\alpha^+ + iC\alpha^+\alpha^+ + \text{ terms with } \alpha. \tag{34}$$

A, B and C are functions which are more closely examined in the Appendix; they have the properties that A and B are complex whilst C is real. Using (32) and (34), it is now straightforward to calculate the probability of exciting the nuclear state containing N phonons from the ground state. This is given by

$$\begin{aligned} P_N &= |\langle N|U(\infty, -\infty)|0\rangle|^2 \\ &= \left[\frac{q^{2N}K^{2N}}{N!}(1 + A + A^+) + \frac{q^{2N-1}K^{2N-1}}{(N-1)!}(B + B^+)\right] \mathrm{e}^{-q^2K^2} \end{aligned}$$

to the first order in A, B and C. The property that K is real has been used. This expression is dependent upon the real parts of both A and B and from

the Appendix we have the relations

$$A+A^+ = -q^3\beta k K(\xi)P(\xi), \qquad B+B^+ = q^3\beta k P(\xi), \tag{35}$$

where $P(\xi)$ is defined in the Appendix. Therefore

$$P_N = \left[\frac{q^{2N}K^{2N}}{N!} + \frac{q^{2N+1}K^{2N-1}}{N!}\beta k P(\xi)\{N-q^2K^2\}\right] e^{-q^2K^2}. \tag{36}$$

The first term in this probability is that calculated in the previous section and given by (23), the second term is the result of interference between one- and two-phonon processes. The function $P(\xi)$ is negative for all positive ξ (see Appendix) so that the interference is destructive at low energies and constructive at high energies, the change taking place when

$$q^2K^2(\xi) = N.$$

This is also the condition for the first term in (36) to have a maximum so that the probabilities (36) now form a modified Poisson distribution. The modification to the curves forming the distribution consists of a depression before their maxima and an elevation after it.

To have an idea of the order of magnitude of these interferences terms a particular example has been calculated for $\xi = 0.3$. It is found that $P(0.3) \approx -0.03$ and $K(0.3) \approx 0.3$. The maximum correction to P_N occurs for $q^2K^2 = \frac{1}{3}N$ and assuming $\beta k \approx 0.5$, the percentage contribution of the interference terms to (36) is given approximately by C_N, where

$$C_N = 6N^{\frac{1}{2}}\ \%,$$

so that $C_1 = 6\ \%$, $C_2 = 17\ \%$, $C_3 = 30\ \%$ etc. In deriving (36) terms of higher order than the first in the two-phonon operator have been ignored, and the magnitude of the correction C_N indicates that this is not a good approximation when states higher than the third are being strongly excited.

Eq. (36) is only strictly valid for backward scattering but it is also a good approximation for nearly backward scattering [1]). The general features of the interference term, discussed above, remain valid in the case of general scattering. The specialization to backward scattering ensures that no new results can be calculated for the relative excitations of angular momentum substates because, if only one type of phonon can be created the calculation of relative excitations is simplified to a calculation of the probability of coupling the angular momentum carried by the phonons to give the required final angular momentum, and is independent of the detailed structure of the interaction.

Most of the work contained in this paper was carried out whilst the author was a member of the Clarendon Laboratory, Oxford. During this period financial support was provided by D.S.I.R. and many helpful discussions were

held with Dr. D. Brink and Dr. B. Buck. The work was completed in Zürich, with the support of N.A.T.O. The author would like to thank Prof. Dr. R. Jost and his colleagues for their hospitality.

Appendix

A.1. CONDITION FOR SOLUBILITY

Consider the wave equation

$$\frac{i\partial U(t, t_0)}{\partial t} = V(t)\, U(t, t_0). \tag{A.1}$$

A sufficient condition for solubility is that

$$[V(t), V(t')] = ig(t, t'),$$

where $g(t, t')$ is a c-number function.

To prove this we write the wave equation in the form

$$\lim_{t_1 \to t_2} \frac{U(t_1, t_0)U^{-1}(t_2, t_0) - 1}{t_1 - t_2} = -i\, V(t_1) \tag{A.2}$$

and we substitute

$$U(t, t_0) = \exp\left\{-i \int_{t_0}^{t} V(t')\mathrm{d}t' - if(t)\right\}, \tag{A.3}$$

where $f(t)$ is an undetermined c-number function. To rearrange the product occurring on the left hand side of (A.2), use is made of the ordering theorem [3]), which states that if we have

$$[X, Y] = Z,$$

where Z is a c-number, we can write

$$\mathrm{e}^{X}\mathrm{e}^{Y} = \mathrm{e}^{X+Y}\mathrm{e}^{\frac{1}{2}Z}.$$

Eq. (A.2) is then satisfied if

$$\frac{\mathrm{d}f(t)}{\mathrm{d}t} = \tfrac{1}{2}\int_{t_0}^{t} g(t, t')\mathrm{d}t'.$$

We choose

$$f(t) = \tfrac{1}{2}\int_{t_0}^{t}\int_{t_0}^{t_1} g(t_1, t_2)\mathrm{d}t,\, \mathrm{d}t_2. \tag{A.4}$$

The hermiticity of $V(t)$ ensures the reality of $g(t, t')$.

A.2. CALCULATION OF THE FUNCTIONS A AND B

From (33) and (34), using the commutation properties of the phonon operators,

we find

$$A = i\frac{6}{35\sqrt{5\pi}} Z_1 Z_2 e^2 R_0^2 k\beta^2 \int_{-\infty}^{\infty} f(t)\{q^2 F(t)F(t) - 2\}\mathrm{d}t, \tag{A.5}$$

$$B = -i\frac{12}{35\sqrt{5\pi}} qZ_1 Z_2 e^2 R_0^2 k\beta^2 \int_{-\infty}^{\infty} f(t)F(t)\mathrm{e}^{i\omega t}\mathrm{d}t. \tag{A.6}$$

A property of the coordinate system is that $f(t)$ is a real even function of t. To find the real part of B we consider the integral

$$\int_{-\infty}^{\infty} f(t)F(t)\mathrm{e}^{i\omega t}\,\mathrm{d}t = \int_{-\infty}^{\infty} \{K^+(\infty, t)\mathrm{e}^{2i\omega t} + K(t, -\infty)\}f(t)\mathrm{d}t. \tag{A.7}$$

This may be brought into a more convenient form by completing the range of integration of the integrals defining $K^+(\infty, t)$ and $K(t, -\infty)$ by introduction of the step function

$$\varepsilon(t'-t) = \lim_{\delta\to 0+} \frac{i}{2\pi}\int_{-\infty}^{\infty} \frac{\mathrm{e}^{iz(t'-t)}}{z+i\delta}\,\mathrm{d}z = \begin{cases} 1 \text{ for } t > t', \\ 0 \text{ for } t < t'. \end{cases} \tag{A.8}$$

Thus, we have

$$K^+(\infty, t) = \frac{1}{a^2 v}\int_t^{\infty} f(t')\mathrm{e}^{-i\omega t'}\mathrm{d}t' = \frac{i}{2\pi a^2 v}\int_{-\infty}^{\infty} \frac{\mathrm{d}z}{z+i\delta} K(\xi+z)\mathrm{e}^{izt},$$

where the limit on δ is understood and the argument of K is in the θ, ξ notation and $\theta = \pi$ is also understood. Using this, (A.7) becomes

$$\frac{i}{2\pi a^2 v}\int_{-\infty}^{\infty} \frac{\mathrm{d}z}{z+i\delta} K(\xi+z)\{K(2\xi+z)+K(z)\}. \tag{A.9}$$

The function K is real so that the imaginary part of (A.9) is

$$\frac{1}{2\pi a^2 v} P\int_{-\infty}^{\infty} \frac{\mathrm{d}z}{z} K(\xi+z)[K(2\xi+z)+K(z)].$$

Thus the real part of B is given by

$$B + B^+ = q^2\beta k P(\xi),$$

where

$$P(\xi) = \frac{4}{7\pi^{\frac{3}{2}}} P\int_{-\infty}^{\infty} \frac{\mathrm{d}z}{z} K(\xi+z)[K(2\xi+z)+K(z)]. \tag{A.10}$$

A similar calculation for A shows that

$$A + A^+ = -q^3\beta k K(\xi)P(\xi).$$

From the tabulated values of the classical orbital integrals it is seen that $K(\xi)$ is an even function of ξ rapidly decreasing from a maximum at the origin.

Examination of (A.10) then shows that $P(\xi)$ is an odd function vanishing at the origin and at infinity, which, for positive ξ, rapidly decreases, passes through a minimum and then slowly increases toward zero.

References

1) K. Alder and A. Winther, Mat. Fys. Medd. Dan. Vid. Selsk. **32**, No. 8 (1960)
2) K. Alder *et al.*, Rev. Mod. Phys. **28** (1956) 432
3) S. Gartenhaus and C. Schwartz, Phys. Rev. **108** (1957) 482
4) D. W. Robinson, thesis, Oxford (unpublished)
5) A. R. Edmonds, Angular momentum in quantum mechanics (Princeton University Press, Princeton, 1957)

7.C

Nuclear Physics **25** (1961) 472—482; © *North-Holland Publishing Co., Amsterdam*

Not to be reproduced by photoprint or microfilm without written permission from the publisher

COLLECTIVE CORRELATION BETWEEN VACUUM NUCLEONS IN PS—PS MESON THEORY

OSAMU HARA †

School of Physics, University of Minnesota, Minneapolis, Minnesota, USA

Received 16 January 1961

Abstract: The effect of the collective correlation between vacuum nucleons is calculated using an approximation in which the kinetic energy of the nucleons is neglected as compared with their rest energy. The point is that there can exist a strong collective correlation between vacuum nucleons just as between electrons in metal, since interactions between vacuum nucleons due to pions is dominantly attractive. It is shown that this effect can play in fact an important role, if this attractive interaction is sufficiently strong, and that the low energy behaviour of the phase shift δ_3 of the S-wave pion-nucleon scattering and the position of the (33) resonance are rather sensitive to this effect.

As an example, the phase shift δ_3 is calculated using a Tamm-Dancoff approximation including up to two pions and one nucleon-antinucleon pair. It is shown that the result agrees reasonably well with experiment if parameters specifying the strength and the range of the attractive potential are chosen suitably.

1. Introduction

Recently investigations into interacting systems of many particles have made great advances, and for Fermi systems, it has been found that if the interaction is dominantly attractive, a strong collective correlation arises, and the system exhibits properties very different from the free one. It seems possible that this effect can play an important role in pion physics also, since the internucleon force between vacuum nucleons due to pions is dominantly attractive. Thus, it is expected that the structure of the vacuum would be drastically changed by introducing this effect, and that processes in which the properties of the vacuum appear explicitly, such as the formation or the annihilation of nucleon-antinucleon pairs, would be greatly modified.

To treat this effect, a direct application of B. C. S.'s or Bogoliubov's methods does not seem adequate [1]), since they resort to an approximation which violates the conservation law of nucleon number. In this paper we adopt an approximation in which the kinetic energy of the nucleon is neglected as compared with its rest energy. In this approximation, an exact solution can be found easily, and the problem can be formulated in a rather unambiguous way. As a result, it is shown that this effect can play in fact an important role, if the attractive potential between vacuum nucleons is stronger than some critical

† On leave of absence from Nihon University, Tokyo, Japan.

value which is determined by the bare nucleon mass. It is not certain whether the actual nuclear potential satisfies this condition. If we assume, however, that this is the case, it can be shown that the low energy behaviour of the phase shift δ_3 of the S-wave pion-nucleon scattering and the position of the (33) resonance are very sensitive to this effect.

As an example, we calculate δ_3 using a Tamm-Dancoff approximation which include up to two pions and one nucleon-antinucleon pair, and it is shown that the result agrees reasonably well with experiment if the parameters specifying the strength and the range of the attractive potential between vacuum nucleons are chosen suitably.

2. Vacuum and One-Nucleon States

Let us start from the Hamiltonian

$$H = H_0 + H', \tag{2.1}$$

where H_0 is the free Hamiltonian, and H' is the usual ps–ps interaction term. This can be written as

$$H = H_0+H_2+(H'-H_2), \tag{2.2}$$

where H_2 is the term describing the nuclear potential. It can be shown that the eigenvalue problem for (H_0+H_2) can be solved exactly after some simplifications for (H_0+H_2). Thus we shall use these eigenfunctions as an unperturbed system, regarding $(H'-H_2)$ as the interaction term. This approximation is certaintly better than the usual ones since it includes the effect of H_2 in a non-perturbative way.

Thus, we shall begin with the discussion of vacuum and one particle states described by (H_0+H_2). If we assume that the nuclear potential is expressed by a simple Yukawa potential $-g^2 e^{-\mu r}/r$, the Hamiltonian H_0+H_2 is given by †, ††

$$\begin{aligned} H_0+H_2 = &\sum_{\mathbf{k},\sigma} \omega_k n^{(+)}_{\mathbf{k},\sigma} - \frac{1}{2V}\sum v(\mathbf{k}_2-\mathbf{k}'_2)\, a^{(+)*}_{\mathbf{k}'_2,\sigma_2} a^{(+)}_{\mathbf{k}_2,\sigma_2} a^{(+)*}_{\mathbf{k}'_1,\sigma_1} a^{(+)}_{\mathbf{k}_1,\sigma_1} \\ &-\sum_{\mathbf{k},\sigma} \omega_k n^{(-)}_{\mathbf{k},\sigma} - \frac{1}{2V}\sum v(\mathbf{k}_2-\mathbf{k}'_2) a^{(-)*}_{\mathbf{k}'_2,\sigma_2} a^{(-)}_{\mathbf{k}_2,\sigma_2} a^{(-)*}_{\mathbf{k}'_1,\sigma_1} a^{(-)}_{\mathbf{k}_1,\sigma_1}, \end{aligned} \tag{2.3}$$

where the second and the fourth summations extend over $\mathbf{k}_1$, $\mathbf{k}'_1$, $\mathbf{k}_2$, $\mathbf{k}'_2$ (with $\mathbf{k}_1+\mathbf{k}_2 = \mathbf{k}'_1+\mathbf{k}'_2$), σ_1 and σ_2 and where ω_k is the energy of the nucleon including its rest energy. The symbols $a^{(\pm)*}_{\mathbf{k},\sigma}$ and $a^{(\pm)}_{\mathbf{k},\sigma}$ denote creation and destruction operators for nucleons in positive and negative energy states, and

† For simplicity, we omit the pion term in H_0, which is irrelevant in the following discussions.

†† In this paper, we neglect the potentials between pairs of nucleons one of which is in positive energy state. It can be chown that, at least in purturbation, the effect of these potentials is negligible.

$n^{(\pm)}_{\mathbf{k},\sigma}$ are their number operators. The function $v(\mathbf{k}_2-\mathbf{k}'_2)$ is given by

$$v(\mathbf{k}_2-\mathbf{k}'_2)=\frac{4\pi g^2}{\mu^2+(\mathbf{k}_2-\mathbf{k}'_2)^2}\,, \tag{2.4}$$

where μ is the reciprocal of the Compton wave length of the pion, and V is the normalization volume.

Rewriting H_2 as

$$\begin{aligned} H_2=-\frac{1}{2V}\sum_{\substack{\mathbf{k},\mathbf{k}',\mathbf{p}\\ \sigma_1,\sigma_2}} v(\mathbf{k}-\mathbf{k}')a^{(+)*}_{\mathbf{k}',\sigma_1}a^{(+)*}_{-\mathbf{k}'+\mathbf{p},\sigma_2}a^{(+)}_{-\mathbf{k}+\mathbf{p},\sigma_2}a^{(+)}_{\mathbf{k},\sigma_1} \\ +(\text{the same expression for } a^{(-)}_{\mathbf{k},\sigma}), \end{aligned} \tag{2.5}$$

we shall take, following B. C. S. [2]) only terms with $\mathbf{p}=0$ and $\sigma_1=-\sigma_2$. Then, eq. (2.5) becomes

$$H_2=-\frac{1}{V}\sum_{\mathbf{k},\mathbf{k}'}v(\mathbf{k}-\mathbf{k}')a^{(+)*}_{\mathbf{k}}a^{(+)}_{\mathbf{k}'}+(\text{the same expression for } a^{(-)}_{\mathbf{k}}), \tag{2.6}$$

where $a^{(\pm)}_{\mathbf{k}}=a^{(\pm)}_{-\mathbf{k}\downarrow}a^{(\pm)}_{\mathbf{k}\uparrow}$ and $a^{(\pm)*}_{\mathbf{k}}=a^{(\pm)*}_{\mathbf{k}\uparrow}a^{(\pm)*}_{-\mathbf{k}\downarrow}$ are creation and annihilation operators for nucleon pairs with opposite spin and momentum. As seen from (2.4), $v(\mathbf{k}-\mathbf{k}')$ vanishes for large momentum transfer. Therefore, we shall restrict the sum over $\mathbf{k}$ and $\mathbf{k}'$ within $|\mathbf{k}|, |\mathbf{k}'|<\bar{k}$ in (2.6), where $\bar{k}$ is supposed to be of order μ. Thus replacing $v(\mathbf{k}-\mathbf{k}')/V$ by its average value v, we get † as the simplification of (2.3),

$$\begin{aligned} H_0+H_2=2\sum_{\mathbf{k}}\omega_k n^{(+)}_{\mathbf{k}}-v\sum_{\substack{\mathbf{k},\mathbf{k}'\\ \mathbf{k}\neq\mathbf{k}'}}^{|\mathbf{k}|,|\mathbf{k}'|<\bar{k}} a^{(+)*}_{\mathbf{k}}a^{(+)}_{\mathbf{k}'} \\ -2\sum_{\mathbf{k}}\omega_k n^{(-)}_{\mathbf{k}}-v\sum_{\substack{\mathbf{k},\mathbf{k}'\\ \mathbf{k}\neq\mathbf{k}'}}^{|\mathbf{k}|,|\mathbf{k}'|<\bar{k}} a^{(-)*}_{\mathbf{k}}a^{(-)}_{\mathbf{k}'}\,, \end{aligned} \tag{2.7}$$

where $n^{(\pm)}_{\mathbf{k}}$ is the number operator for the pair specified by the momentum $\mathbf{k}$ in positive or negative energy states. This is the standard B. C. S. Hamiltonian. Although it includes only a part of the original Hamiltonian, it has been shown in the theory of superconductivity that it is the most important part to determine the behaviour of the system.

It is clear that no change occurs in levels with $|\mathbf{k}|\geqq\bar{k}$. Therefore, we shall omit these terms, and limit the summation to $|\mathbf{k}|<\bar{k}$ in the first and the third sums also. Then, eq. (2.7) can be simplified if we assume that ω_k is independent of k, which means that we neglect kinetic energy as compared with the rest energy. Using the spin matrix device found by Wada *et al.* and by Anderson [3]),

† In (2.7), we exclude terms with $\mathbf{k}\neq\mathbf{k}'$ to make clear the invariance under charge conjugation. Obviously, this makes no difference in the limit $V\to\infty$. (Strictly speaking, the above discussion is not sufficient to exclude high momentum parts in $v(\mathbf{k}-\mathbf{k}')$. For a further discussion, see sect. 4).

$a_{\mathbf{k}}^{(\pm)}$ and $a_{\mathbf{k}}^{(\pm)*}$ can be expressed as

$$\begin{aligned} a_{\mathbf{k}}^{(\pm)} &= \tfrac{1}{2}(\sigma_{x\mathbf{k}}^{(\pm)}+i\sigma_{y\mathbf{k}}^{(\pm)}) = m_{x\mathbf{k}}^{(\pm)}+im_{y\mathbf{k}}^{(\pm)}, \\ a_{\mathbf{k}}^{(\pm)*} &= \tfrac{1}{2}(\sigma_{x\mathbf{k}}^{(\pm)}-i\sigma_{y\mathbf{k}}^{(\pm)}) = m_{x\mathbf{k}}^{(\pm)}-im_{y\mathbf{k}}^{(\pm)}. \end{aligned} \tag{2.8}$$

Therefore, we can write the Hamiltonian as follows:

$$\begin{aligned} H_0+H_2 = &-2\omega(M_z^{(+)}-M_z^{(-)})-v(\mathbf{M}^{(+)2}-M_z^{(+)2}) \\ &-v(\mathbf{M}^{(-)2}-M_z^{(-)2})+2vM, \end{aligned} \tag{2.9}$$

where $M_x = \sum_{\mathbf{k}} m_{x\mathbf{k}}$, etc., and M is one half of the total number of levels in positive or negative energy states.

Eigenvalues and eigenfunctions of the system described by (2.9) can be obtained easily. They are

$$\begin{aligned} E = &-vJ^{(+)}(J^{(+)}+1)-vJ^{(-)}(J^{(-)}+1) \\ &+v(K^{(+)}-\omega/v)^2+v(K^{(-)}+\omega/v)^2-2\omega^2/v+2vM, \end{aligned} \tag{2.10}$$

and

$$\begin{aligned} \psi(J^{(+)},K^{(+)};J^{(-)},K^{(-)}) = &\frac{1}{2M!}\sqrt{\frac{(M+K^{(+)})!}{(M-K^{(+)})!}\frac{(M+K^{(-)})!}{(M-K^{(-)})!}} \\ &\times(\sum_{\mathbf{k}} a_{\mathbf{k}}^{(+)*})^{M-K^{(+)}}(\sum_{\mathbf{k}} a_{\mathbf{k}}^{(-)*})^{M-K^{(-)}}|0\rangle, \end{aligned} \tag{2.11}$$

where for $\psi\,(J^{(+)},K^{(+)};J^{(-)},K^{(-)})$ we only write down the case corresponding to $J^{(+)}=J^{(-)}=M$ for simplicity; $|0\rangle$ represents the state where no particle exists. In the spin matrix representation, this corresponds to the state in which all spins point in the same direction. (Note that in this formalism the numbers of nucleon pairs in positive or negative energy states are given by $N^{(\pm)}=M-K^{(\pm)}$). The quantities $J^{(\pm)}(J^{(\pm)}+1)$ and $K^{(\pm)}$ are eigenvalues for $\mathbf{M}^{(\pm)2}$ and $M_3{}^{(\pm)}$, respectively. They take the following values †:

$$J^{(\pm)} = 0,\ 1,\ 2,\ \ldots,\ M-1,\ M; \tag{2.12}$$

$$K^{(\pm)} = -J^{(\pm)},\ -J^{(\pm)}+1,\ \ldots,\ J^{(\pm)}-1,\ J^{(\pm)}. \tag{2.13}$$

Among these eigenstates, the vacuum corresponds to the one with the lowest energy eigenvalue. In order that E should be lowest, it is clear from (2.12) that $J^{(\pm)}$ must have the largest possible value. Thus we have

$$J^{(+)} = J^{(-)} = M. \tag{2.14}$$

To find $K^{(\pm)}$ corresponding to the lowest energy, it is convenient to consider the two cases (using $r \equiv \omega/v$)

$$r/M > 1 \tag{2.15}$$

and

$$r/M \leqq 1 \tag{2.16}$$

† For definiteness, we assume that M is an integer.

separately, since $K^{(\pm)}$ cannot exceed $J^{(\pm)}$. In the first case, the smallest eigenvalue of the Hamiltonian corresponds to

$$K^{(+)} = -K^{(-)} = M.$$

Therefore, in this case, the eigenfunction (2.11) reduces to the usual free vacuum one, and nothing appears which is essentially new. In contrast to this, in the latter case, the smallest eigenvalue of the Hamiltonian corresponds † to

$$K^{(+)} = -K^{(-)} = r, \tag{2.17}$$

with the eigenvalue

$$E_0 = -2vM^2 - 2\omega^2/v, \tag{2.18}$$

and the eigenfunction

$$\psi_0 = \frac{1}{2M!}\left(\sum_{\mathbf{k}} a_{\mathbf{k}}^{(+)*}\right)^{M-r}\left(\sum_{\mathbf{k}} a_{\mathbf{k}}^{(-)*}\right)^{M+r}|0\rangle. \tag{2.19}$$

Eq. (2.19) reduces to the usual free vacuum in the weak coupling limit ($r \to M$) as in the former case, but goes over to an entirely different one in the strong coupling limit ($r \to 0$) in which all levels in positive and negative energy states are occupied with equal probability. The physical implication of this result is as follows. By moving a nucleon in a negative energy state to a positive energy state, the energy of this single nucleon is increased by 2ω, but the potential energy of the total system is decreased by doing so, since the attractive potential, which had no effect when all levels were filled due to the Pauli principle, becomes effective. Therefore, the total energy of the system can be decreased by moving some of the nucleons in negative energy states to positive energy states, and can take a minimum value for a distribution different from the usual free vacuum ††.

Of course, in order that such a situation occurs, the attractive potential must be so strong that the decrease of the total potential energy can exceed the increase of the energy of the single nucleon. This condition is expressed by (2.16). Therefore, it is a very important condition which determines whether the effect of collective correlation can be really important or not †††. It is not certain whether the inequality (2.16) is satisfied by the actual nuclear potential. In the following, however, we shall assume that this is the case. Thus, if we want to define the vacuum as the eigenstate of the total Hamiltonian with the lowest energy eigenvalue, we must take the eigenfunction (2.19) as the true vacuum of our system. It is satisfying that it satisfies the conservation law of nucleon number and is invariant under charge conjugation (under charge conjugation, $J^{(\pm)} \to J^{(\mp)}$ and $K^{(\pm)} \to -K^{(\mp)}$.)

† For definiteness, we assume that r is an integer.

†† This is entirely the same situation which makes the superconducting state energetically more stable than the normal state.

††† Such a condition does not appear in the case of electrons in metal, since in this case there is no gap corresponding to 2ω.

Eigenfunctions and eigenvalues of the states in which one of the nucleon pairs is replaced by an unpaired nucleon are given by

$$\psi_{\mathbf{k}}^{(+)} = \frac{1}{2M!}\sqrt{\frac{2M}{M+r}}\,(\sum_{\mathbf{k}'}{}' a_{\mathbf{k}'}^{(+)*})^{M-r}(\sum_{\mathbf{k}} a_{\mathbf{k}}^{(-)*})^{M+r} a_{\mathbf{k}\uparrow(\downarrow)}^{(+)}|0\rangle, \tag{2.20}$$

when an unpaired nucleon is added in a positive energy state, and by

$$\psi_{\mathbf{k}}^{(-)} = \frac{1}{(2M-1)!}\sqrt{\frac{M+r}{2M}}\,(\sum_{\mathbf{k}} a_{\mathbf{k}}^{(+)*})^{M-r}(\sum_{\mathbf{k}'}{}' a_{\mathbf{k}'}^{(-)*})^{M+r-1} a_{\mathbf{k}\uparrow(\downarrow)}^{(-)*}|0\rangle, \tag{2.21}$$

when one nucleon pair in a negative energy state is replaced by an unpaired nucleon †. Here we used the method given by Wada and Fukuda [3]; $\sum'_{\mathbf{k}'}$ means the sum omitting $\mathbf{k}$, and $a_{\mathbf{k}\uparrow(\downarrow)}^{(\pm)*}$ denotes the creation operator for a nucleon in a positive or negative energy state with momentum $\mathbf{k}$ and spin up (down). Their energies relative to that of the vacuum are both equal to

$$\omega' = vM. \tag{2.22}$$

They represent respectively the states in which a nucleon with momentum $\mathbf{k}$ and spin up (down) or an antinucleon with momentum-$\mathbf{k}$ and spin up (down) exists.

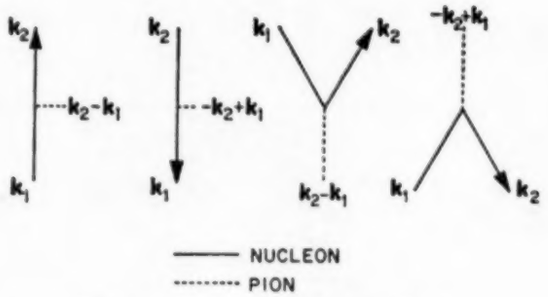

Fig. 1. Pion-nucleon vertices.

Thus, the introduction of collective correlations causes two effects. One is the alteration of the rest energy from ω to ω', and the other is the modification of matrix elements. We shall assume that the former is absorbed into the mass renormalization ††. For the latter, we can show easily that the effect of the correlations is to multiply every vertex shown in fig. 1 by the factor

$$\left(\frac{M+r}{2M}\right)^{\varepsilon(\mathbf{k}_1)+\varepsilon(\mathbf{k}_2)} \tag{2.23}$$

† We shall not consider states in which an unpaired nucleon is added in a negative energy state, or in which one nucleon pair in a positive energy state is replaced by an unpaired nucleon, assuming that all of the states which reduce to free ones in the weak coupling limit form a complete set.

†† Strictly speaking, this mass renormalization is not consistent, since levels with $|\mathbf{k}| \geqq \tilde{\kappa}$ remain unchanged. As to its approximate consistency, see discussion in sect. 4.

neglecting terms of order $1/M$, where $\mathbf{k}_1$ and $\mathbf{k}_2$ are the momenta of the nucleon before and after the transition, and $\varepsilon(\mathbf{k})$ is defined by

$$\varepsilon(\mathbf{k}) = \begin{cases} \frac{1}{2} & \text{if} \quad |\mathbf{k}| < \bar{k}, \\ 0 & \text{if} \quad |\mathbf{k}| \geqq \bar{k}. \end{cases} \tag{2.24}$$

Hereafter we shall assume that this is the only modification brought about in our model †.

3. S-Wave Pion-Nucleon Scattering

As an example of the effect expressed by (2.23), let us consider the scattering of an S-wave pion by a nucleon. In the Tamm-Dancoff approximation in which up to one nucleon-antinucleon pair and two pions are included, the scattering amplitude is given by ††

$$f(p) = f_{\mathrm{B}}(p) + P\int_0^K \frac{s^2}{\omega_0 - \omega} K(p, s) f(s) \mathrm{d}s, \tag{3.1}$$

if we disregard nucleon recoil; here K is the cut off momentum, $f_{\mathrm{B}}(p)$ is the Born term

$$f_{\mathrm{B}}(p) = \frac{1}{7}\frac{G^2}{4\pi^2} k \left[\frac{\omega(k)}{\omega(p)}\right]^{\frac{1}{2}} v(p, k), \tag{3.2}$$

and $K(p, s)$ is given by

$$K(p, s) = \frac{1}{7}\frac{G^2}{4\pi^2} \frac{1}{[\omega(p)\omega(s)]^{\frac{1}{2}}} v(p, s), \tag{3.3}$$

where $v(p, s)$ is the factor expressing the effect of collective correlation:

$$v(p, s) = \left(\frac{M + \gamma}{2M}\right)^{\varepsilon(p)+\varepsilon(s)+2\varepsilon(\sqrt{p^2+s^2})} \tag{3.4}$$

In eqs. (3.2) and (3.3), the factor G is the pseudo-scalar coupling constant, ω is the energy of the pion, ω_0 is its initial value ††† with momentum k, and μ is used as unit of momentum and energy. Here we shall calculate only δ_3, since there is an ambiguity related to renormalization in the calculation of δ_1. The equation (3.1) reduces in the static approximation to the result of Dyson *et al.* [4]) in the limit $\gamma \to M$, as it should.

An approximate solution to eq. (3.1) can be obtained by Chew's variational method [5]). According to this method, $f(k)$ is given by

$$f(k) = \frac{f_{\mathrm{B}}(k)}{1 + \Delta(k)}, \tag{3.5}$$

† In this model, nucleons can take two states corresponding to $\pm\omega'$ in addition to the freedoms of spin and isospin. In this sense, it may be regarded as a natural extension of Chew's static model.

†† For the details of the derivation of the Tamm-Dancoff equation, see refs. [1, 4]).

††† In sect. 3 the symbol ω is used in a sense different from that it has the other sections.

where

$$\Delta(k) = \frac{1}{K(k,k)} \mathrm{P}\int_0^K \frac{K^2(p,k)p^2}{\omega(p)-\omega(k)}\,\mathrm{d}p. \tag{3.6}$$

We can show that the main contribution to the integral (3.6) comes from the region with large p. Therefore, in the approximation neglecting terms of order $1/K$, the quantity (3.6) is expressed as

$$\Delta(k) \approx v(k,k)^{-1}\left(\frac{M+r}{2M}\right)^{2\varepsilon(k)}\Delta^{(0)}(k), \tag{3.7}$$

where $\Delta^{(0)}(k)$ is obtained by putting $v(p,k) = 1$ in eq. (3.6). Obviously, $\Delta^{(0)}(k)$ is the value of $\Delta(k)$ in which the effect of the collective correlation is neglected. (We shall hereafter use the suffix 0 to denote quantities in this approximation.) In our case, $\Delta^{(0)}(k)$ is large, of order 10 for $G^2/4\pi \approx 15$ and $K \approx 5$. Therefore the quantity (3.5) can be expressed as

$$f(k) = \frac{v(k,k)f_{\mathrm{B}}^{(0)}(k)}{1+v(k,k)^{-1}\left(\frac{M+r}{2M}\right)^{2\varepsilon(k)}\Delta^{(0)}(k)} \tag{3.8}$$

$$\approx \left(\frac{M+r}{2M}\right)^{2\varepsilon(k)+4\varepsilon(\sqrt{2}k)} f^{(0)}(k), \tag{3.9}$$

neglecting terms of order $1/K$, where $f^{(0)}(k)$ is the amplitude which does not include the effect of collective correlation. Neglecting terms of order $1/K^2$, it is given by

$$f^{(0)}(k) = \frac{\frac{1}{7}\frac{G^2}{4\pi^2}k}{1+\frac{1}{7}\frac{G^2}{4\pi^2}\left\{K+\sqrt{1+k^2}\log 2K - k\log(k+\sqrt{1+k^2}) - \frac{k^2}{K}\right\}}. \tag{3.10}$$

The phase shift is calculated using the formula $\tan\delta_3 = -\pi f(k)$.

Calculated from $f^{(0)}(k)$, δ_3 is almost linear. The introduction of $v(p,k)$ reduces its slope by the factor $((M+r)/2M)^3$ at low energy. The slope then changes at $k = \bar{k}/\sqrt{2}$ and at $k = \bar{k}$. Thus, agreement with experiment is greatly improved, and almost complete agreement with experiment is obtained by taking $r/M \approx 0.3$ and $\bar{k} \approx 2$ for reasonable values of the other parameters †. (See fig. 2).

For P-wave scattering, the situation †† is very different between δ_{13} or δ_{31} and δ_{33}. In the former case, $\Delta^{(0)}(k)$ is positive and small, of order 0.5 for the

† For the consistency of the choice of these parameters, see discussion in sect. 4.

†† We do not calculate δ_{11} for the same reason as δ_1.

energies considered here. Therefore, the term containing $\Delta^{(0)}(k)$ can be neglected in (3.8). Thus δ_{13} and δ_{31} are not so sensitive as δ_3 to the effect of correlation. However, in the latter case, $\Delta^{(0)}(k)$ is negative and approaches -1 at energies near 200 MeV, where it causes resonance. The introduction of $v(k, k)$ shifts this

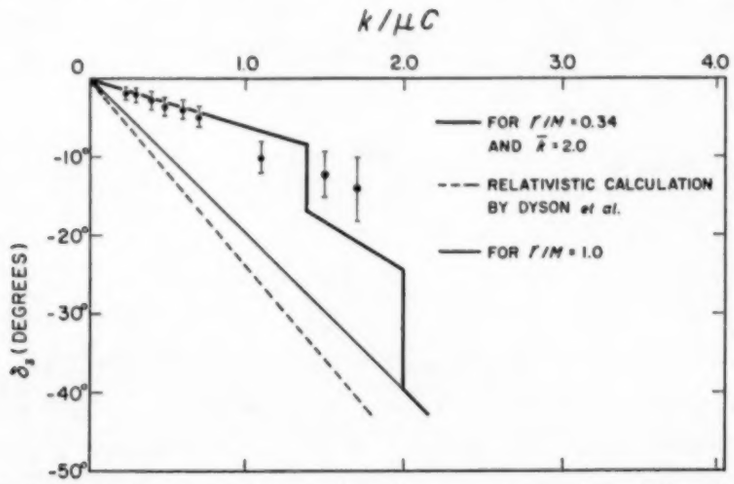

Fig. 2. Phase shift δ_3 plotted versus the centre-of-mass momentum. Experimental points were taken from ref. [8]). Discontinuities at $k/\mu c = 1.4$ and 2.0 are of course due to the crudeness of our model.

resonance to a lower energy. Thus, the position of the (33) resonance is very sensitive to theeffect of correlation. A detailed discussion of P-wave scattering will be given elsewhere together with the discussion of other problems.

4. Discussion

We have seen that if the attractive potential is sufficiently strong, the effect of the collective correlation between vacuum nucleons modifies in fact the behaviour of the system appreciably, and that by taking into account this effect, the agreement between the theory and the experiment on the low energy behaviour of δ_3 can be greatly improved.

Of course it is premature to say that the discrepancy between the existing theories and the experiment is due to this effect, because it is not certain whether the condition (2.16) is satisfied or not. It must be emphasized, however, that the effect must exist if this condition is satisfied, and it is of interest that the low energy behaviour of δ_3 and the position of the (33) resonance are rather sensitive to it, since these (especially the behaviour of δ_3) are problems for which no satisfactory solution has been given so far †.

We shall finally check the consistency of the choice of our parameters and also the procedure of mass renormalization. Integrating $v(\mathbf{k}-\mathbf{k}')$ over $\mathbf{k}'$

† Recently, it has been shown that $(\delta_1-\delta_3)$ can be given correctly if we include the effect of pion-pion interaction [6]). It is, however, still an open question whether δ_1 and δ_3 are separately given correctly. According to Sugawara [7]), it seems that pion-pion interaction does not explain all the discrepancy between existing theories and experiment.

within a sphere with radius K we get †

$$\frac{1}{V}\int v(\mathbf{k}-\mathbf{k}')\mathrm{d}\mathbf{k} \approx g^2 K. \tag{4.1}$$

Therefore, v is given by

$$v \approx g^2 K/M, \tag{4.2}$$

where

$$M = \tfrac{1}{2}\frac{4\pi V}{(2\pi)^3}\int_0^{\bar{k}} k^2 \mathrm{d}k. \tag{4.3}$$

From this we get

$$r/M = \frac{\omega}{vM} \approx \frac{1}{g^2}\frac{\omega}{K}. \tag{4.4}$$

The relations (2.16) and (2.22) suggest that the large mass of the nucleon is mainly a renormalization effect, and the bare mass ω is rather a small part of it. Therefore, let us take, for example, $\omega \approx \mu$. Then from (4.4) we get

$$r/M \approx \frac{1}{g^2}\frac{\mu}{K}, \tag{4.5}$$

where $1/g^2$ would be of order 10. Therefore, we may expect that (2.16) is satisfied if $K \gtrsim \kappa$, where κ^{-1} is the Compton wave length of the nucleon.

In the region $|\mathbf{k}| \geqq \bar{k}$, the quantity ω cannot be taken to be small, it must rather be of order K. So, in this region, the inequality (2.16) can never be satisfied, and it may be admissible to treat nucleons in this region as free at least in the first approximation.

The assumption $\omega \approx \mu$ also justifies our mass renormalization procedure. The relation $E = \sqrt{k^2+m^2}$ gives $\delta E \approx m/\sqrt{k^2+m^2}\,\delta m$. From this, we see that the variation of the energy due to the variation of the rest mass in the region $|\mathbf{k}| \geqq \bar{k}$ is much smaller, of order μ/K, than that in the region $|\mathbf{k}| < \bar{k}$. Therefore, this variation can be neglected in the first approximation, and our procedure of mass renormalization is consistent in this approximation.

To be more quantitative, it is necessary to assume further

$$vM \approx g^2 K \approx \kappa, \tag{4.6}$$

since according to eq. (2.22), vM is equal to the renormalized nucleon mass. At first sight, it seems difficult to satisfy eq. (4.6). It should be noted, however, that v given by eq. (4.2) is underestimated. In eq. (2.5), we neglected all terms with $\mathbf{p} \neq 0$. To include them it would not be unreasonable to assume that v is

† Strictly speaking, the upper limit of the integration should be $\bar{k}$. As seen from (2.4), however, integration in the region with $|k'| > \bar{k}$ gives a non-negligible contribution. To take this contribution into account, we extend the integral up to K.

larger than the value (4.2) by an order of magnitude. In addition, there could be contributions from particles other than pions, for example, K-mesons. Also, it should be noted that the magnitude of K is largely undetermined. Considering all these circumstances, it would not be unreasonable to expect that there is a chance that eq. (4.6) is satisfied. If this is the case, $r/M \approx 0.3$ is obtained by taking $\omega \approx 2\mu$.

Thus, we see that our whole scheme can be consistent at least in the first approximation in μ/κ if the bare nucleon mass is assumed to be small. This assumption is tempting, since in this scheme, a large mass of the nucleon is understood in connection with its strong interaction with pions †.

In conclusion, the author wishes to express his sincere gratitude to the members of Theoretical Division of School of Physics for valuable discussions and criticism.

† A similar attempt was recently made by Nambu and Jona-Lasinio [9]).

References

1) O. Hara, Progr. Theor. Phys. **24** (1960) 495
2) J. Bardeen, L. N. Cooper and J. R. Schriefer, Phys. Rev. **108** (1957) 1175
3) Y. Wada, F. Takano and N. Fukuda, Progr. Theor. Phys. **19** (1958) 597;
Y. Wada and N. Fukuda, Progr. Theor. Phys. **22** (1959) 775;
P. W. Anderson, Phys. Rev. **112** (1958) 1900
4) F. J. Dyson, M. Ross, E. E. Salpeter, S. S. Schweber, M. K. Sundaresan, W. M. Visscher and H. A. Bethe, Phys. Rev. **95** (1954) 1644
5) G. F. Chew, Phys. Rev. **93** (1954) 341
6) J. Bowcock, W. N. Cottingham and D. Lurié, Nuovo Cim. **16** (1960) 918;
J. Bowcock, W. N. Cottingham and D. Lurié, Phys. Rev. Letters **5** (1960) 386;
M. Cini, Report at the Tenth Annual International Conference on High Energy Nuclear Physics
7) M. Sugawara and A. Kanazawa, Phys. Rev. **115** (1959) 1310
8) J. Hamilton and W. S. Woolcock, Phys. Rev. **118** (1960) 291
9) Y. Nambu and G. Jona-Lasinio, Phys. Rev. **122** (1961) 345

4.A:8.A

Nuclear Physics **25** (1961) 483—501; © *North-Holland Publishing Co., Amsterdam*

Not to be reproduced by photoprint or microfilm without written permission from the publisher

THE ELECTRON-NEUTRINO ANGULAR CORRELATION IN BETA DECAY OF HELIUM 6

B. W. RIDLEY

Atomic Energy Research Establishment, Harwell, England

Received 23 January 1961

Abstract: The electron-neutrino angular correlation in decay of He^6 has been determined by measuring the distribution of electron energies and recoil velocities without selection of angle. The correlation parameter α was found to be $-0.353^{+0.033}_{-0.053}$, confirming current belief that the Gamow-Teller interaction is of axial vector type. The maximum admixture of a tensor interaction is given by $|C_T|^2/|C_A|^2 < 0.08$.

1. Introduction

The elucidation of the β decay interaction has remained one of the most important problems in β decay work for many years. As the techniques of β spectrometry improved, it became evident by 1948 that the spectral distributions were inconsistent with any simple interaction involving derivatives of the particle field operators [1, 2]). The choice of interactions consistent with relativistic invariance was thereby restricted to a linear combination of five independent types, each quadrilinear in the particle operators, representing a generalization of Fermi's original formulation of β decay theory [3]). These were the scalar (S), vector (V), tensor (T), axial vector (A) and pseudoscalar (P) invariants, and the interaction was thought to be completely determined by their respective coupling constants C_S, C_V, C_T, C_A and C_P. The physical significance of these interactions appears in the angular correlation of the emitted leptons and in the possibility of a spin flip of the transforming nucleon. Thus for the Fermi group of interactions, characterized by absence of spin flip, the S interaction implies that leptons are emitted preferentially in opposite directions while V is associated with emission in predominantly the same direction. For Gamow-Teller interactions, with which spin flip does occur, T implies enhanced emission in the same direction and A in opposite directions. The pseudoscalar interaction can play no significant role in allowed transitions and no evidence is known for its occurrence in β decay.

Although spectral distributions placed some restrictions on the possible combination of these invariants, only the measurement of electron-neutrino angular correlations could provide an unambiguous determination. Unfortunately technical difficulties in the latter experiments obscured the issue for a

considerable period and it is only within the last three years that the general features of the interaction have become clear. This has largely been due to the work of Allen *et al.* [4]) who have shown in experiments on He^6, Ne^{19}, Ne^{23} and A^{35} that the correct combination is essentially (V, A) and that the maximum admixture of S and T interactions is 10 %. Concurrently Pleasonton *et al.* [5]) using a technique similar in principle to Allen's confirmed that the Gamow-Teller interaction in decay of He^6 was predominantly A. Lauterjung *et al.* [6]) and Barnes *et al.* [7]) found that this was also true in decay of Li^8.

The discovery in 1957 of parity violation in β decay showed that the above picture, though valid so far as it went, was incomplete and that the helicities of the emitted leptons must also be specified in a full description of the process. The formal problem was correspondingly broadened by the resolution of each invariant into parity conserving and violating parts and five new unknowns C_S', C_V', C_T', C_A' and C_P' had to be introduced to describe the degrees of parity mixing. Nevertheless the greater experimental opportunities more than offset the increased complexity of the problem and the combination of results from specifically "parity" experiments provided an independent determination of the basic invariants. Thus by combining separate measurements of positon and neutrino helicities [8–10]) with the known absence of Fierz interference terms in allowed transitions [11]), independent proof was obtained that the Gamow-Teller interaction is predominantly A. No measurement has yet been made of the neutrino helicity in a Fermi transition but the observation of maximal values for interference terms of the kind (V, A) in experiments measuring the directional asymmetries from decay of polarized nuclei [12, 13]) implies that this is largely V. Moreover the asymmetries of electrons and recoil protons emitted in decay of polarized neutrons indicate that the relative sign of the V and A coupling constants is negative [13]).

Despite this new approach, measurements of electron neutrino angular correlations still provide the most direct clarification of those aspects of β decay which are independent of parity mixing, and so form an important link in establishing the mutual compatibility of evidence about the interaction. On the other hand angular correlation experiments have proved prone to systematic errors arising from an imcomplete understanding of auxiliary effects in apparatus. This has made it especially desirable to establish consistency of results from a variety of techniques. The work described below forms part of this programme by using a recoil time of flight technique to determine the electron-neutrino angular correlation in decay of He^6.

2. Theoretical Expressions for the Electron-Neutrino Angular Correlation

Expressions for the electron-neutrino angular correlation have been derived both on the basis of the old β decay theory [14]) and the current parity violating

version [15]). These both show that, in an allowed transition, the probability that an electron will be emitted with energy E in a direction at angle θ with that of the neutrino is of the form

$$P(E,\theta)\mathrm{d}E\mathrm{d}\theta = AF(Z,E)E(E_0-E)^2(E^2-1)^{\frac{1}{2}}\left[1+\alpha\frac{v}{c}\cos\theta+\frac{b}{E}\right]\mathrm{d}E\ \mathrm{d}\theta. \quad (1)$$

The units are such that $\hbar = c = m = 1$. The quantity E is the total relativistic energy of the electron, A a proportionality constant, $F(Z, E)$ the well known Fermi Coulomb factor, E_0 the maximum energy of the β spectrum and v the electron velocity. The Fierz term b contains interference products of the kind (S, V) and (T, A). This is known to be zero within a few per cent [11]) and the upper limit is negligible within the context of the present work. The angular correlation coefficient α has the following form:

$$\alpha = \frac{[-|C_S|^2+|C_V|^2]|M_F|^2+\frac{1}{3}[|C_T|^2-|C_A|^2]|M_{GT}|^2}{[|C_S|^2+|C_V|^2]|M_F|^2+[|C_T|^2+|C_A|^2]|M_{GT}|^2}. \quad (2)$$

No distinction is made here between contributions from the parity conserving and violating parts of each interaction since their intensities are additive. $|M_F|^2$ and $|M_{GT}|^2$ represent the nuclear matrix elements for the Fermi and Gamow-Teller parts of the interaction, respectively.

The transition $He^6 \rightarrow Li^6$ involves a nuclear spin change $\Delta I = 1$, so $|M_F|^2$ must in this case be zero. The expression for α then reduces to a form involving Gamow-Teller interactions alone,

$$\alpha = \frac{1}{3}\frac{|C_T|^2-|C_A|^2}{|C_T|^2+|C_A|^2}. \quad (3)$$

If the interaction is not invariant under time reversal a small Coulomb correction to α may be necessary. While present evidence is insufficient to confirm with certainty that T invariance is valid, all experiments designed to test this principle have proved compatible with its validity [16, 17]). In any case the Coulomb correction in He^6 decay cannot exceed 0.003 for the range of β-particle energies detected in the present experiment.

3. Discussion of Experimental Technique

Since the neutrino itself is so difficult to detect, the electron-neutrino angular correlation is generally inferred from measurements involving detection of the β particle and recoil nucleus. The simplest of these in concept requires detection of the recoil nuclei alone and measured the recoil energy spectrum by electrostatic or magnetic analysis of a recoil beam (Allen *et al.* [4]) and Pleasonton *et al.* [5])). Most of the other methods used have required the detection of both β and recoil particles in coincidence. These include the β-recoil angular correla-

tion (He^6, Rustad and Ruby [18])), the momentum distribution of either β or recoil particles within a limited angular range (Ne^{19}, Alford and Hamilton [19])), (n^0, Robson [20])) and the energy distributions of both β and recoil particles without angular discrimination (Ne^{23}, Ridley [21])). When the β particle is followed by γ-emission, the condition for resonant scattering of the latter can be used to determine the recoil momentum without direct detection of the recoil nucleus and Booth *et al.* [22]) have applied this technique to the study of Ne^{23}.

The large collision cross-sections of recoil particles (10^{-14} to 10^{-16} cm^2) dictate the use of gaseous sources at low pressure to avoid distortion of their spectra by scattering. Diffusion of the source throughout the apparatus has always made it difficult to distinguish clearly the genuine effect from background. The background may in principle be eliminated in coincidence experiments at the extreme limit of low counting rates, but in practice accidental coincidences usually prevent full use being made of available source strengths. For this reason Allen *et al.* [4]) chose to detect recoil nuclei alone and to measure their energies with an electrostatic spectrometer. Their ratio of genuine effect to background was determined only by their geometry and the effectiveness of the differential pumping system and was of the order of 1 : 10. Accurate spectrum determination in the presence of so large a background necessitated high counting numbers and these were met by the use of very strong sources. In addition to the usual problem of recoil detector sensitivity, two further difficulties occur with this technique. One of these arises from the high background, small fluctuations in which inevitably arise from variations in efficiency of the pumps even when the activity in the source volume is constant. These could be significant relative to the effect sought and counting statistics are not necessarily a reliable guide to accuracy. Secondly, electrostatic (or magnetic) analysis of the recoil beam, demanded by this approach, is complicated by the presence of multiply charged recoils. As Allen points out, doubly charged recoils are transmitted at a spectrometer setting corresponding to half the energy of singly charged particles, so the lower half of the energy spectrum cannot be interpreted unless the charge spectrum is known. An additional uncertainty arises from the possibility that the charge spectrum is a function of recoil energy, although theoretical arguments suggest that such a dependence is rather weak. These difficulties can be fully met only by combining energy and charge analysis in a system of combined electrostatic and magnetic spectrometers [5]).

As we have remarked, the background problem is substantially reduced by using coincidence techniques, provided one accepts a sufficiently low counting rate. If recoil velocities are determined by time of flight (T.O.F.), the reduced counting rate is partially offset by the simultaneous measurement of the whole spectrum. This also has advantages in simplifying the problem of normalization

and in providing a continuous monitor of background, accidental coincidences due to which appear at flight times inaccessible to genuine events. Moreover neither T.O.F. nor β-recoil angular correlation measurements distinguish between single and multiply charged recoils apart from minor effects related to recoil detector transit times and sensitivity. The detection and measurement of β particle energy also provides a welcome source of additional information of value in testing the internal consistency of the data. On the debit side, apart from smaller counting rates, coincidence experiments are generally more critically sensitive to the distribution of activity within and near the source volume on account of changing solid angle efficiencies. Uncertainty in the source distribution has in the past led to serious errors in both β-recoil angular correlations [18, 23]) and in recoil T.O.F. distributions [21, 24]).

The experiment described below is similar in principle to the author's previous work on Ne^{23} (see ref. [21])), in which the distribution of β energy and flight time of the associated recoil nucleus was measured without selection of angle. It contains some improvements in technique and a more exhaustive examination of possible sources of error. These, incidentally, revealed a substantial systematic error in the earlier Ne^{23} result, of which more will be said later. A novel feature of the experiment was the use of a magnetic tape recorder for data collection, enabling the pulse amplitudes from both the β and recoil detectors to be recorded in addition to the time of flight.

4. The Apparatus

4.1. THE DETECTOR SYSTEM

The arrangement of detectors is illustrated in fig. 1. The geometry was essentially that of a cylindrical source 12 mm in length by 2 mm diameter aligned along the axis of the recoil flight path. β particles were detected in a plastic scintillator that almost completely surrounded the source. The recoil detector, of aperture 4 cm diameter, was situated 25 cm from the source. The minimum flight time of Li^6 recoils from He^6 decay in this arrangement was about 1.25 μsec corresponding to a maximum energy of 1405 eV. The source volume was partially defined by the geometry as that volume visible to both the β and recoil detectors. Shielding around the β detector prevented its viewing external activity except through the aperture for emerging recoils. The differential gas pumping system ensured a relatively low concentration of activity outside the source volume and around the recoil detector. A more precise definition of the source volume was provided by a repelling field that could be applied to recoils within the β detector, enabling the contribution from all activity outside the source volume to be determined separately.

The β detector is shown in greater detail in the plan view of fig. 2. The source volume was contained in a 2 mm hole drilled along one radius of a cylindrical

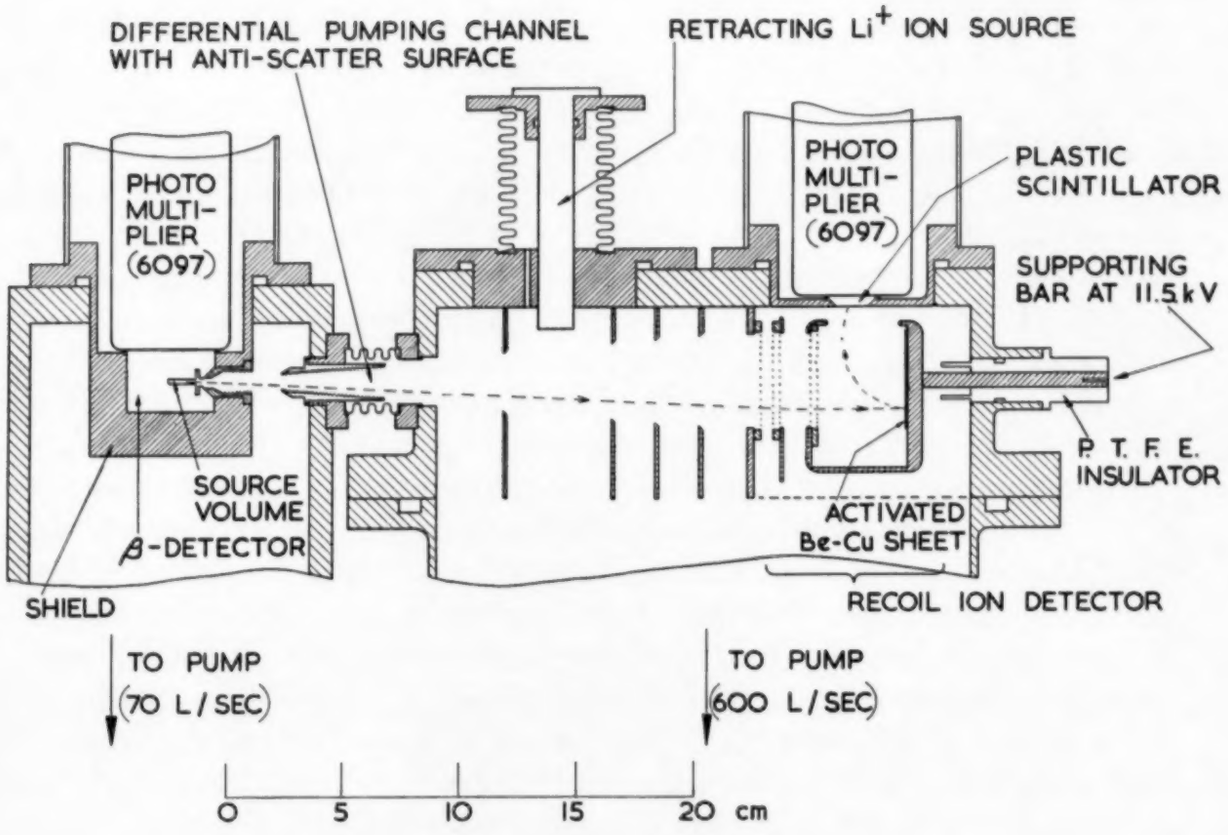

Fig. 1. General arrangement of detectors.

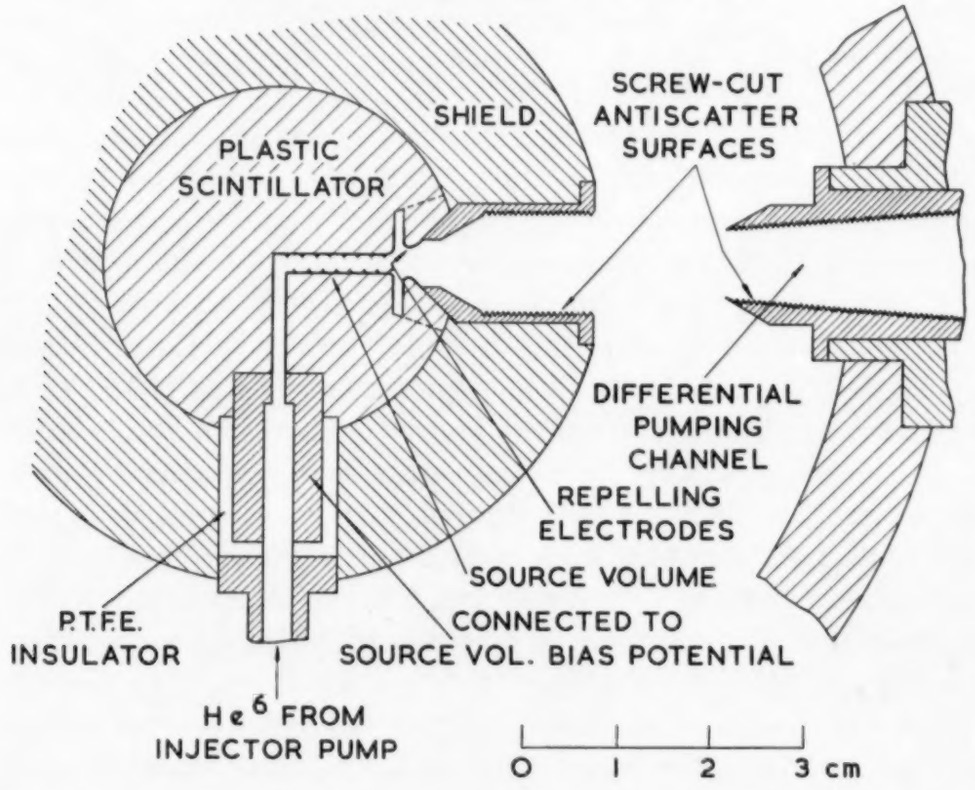

Fig. 2. The β particle detector and source volume as seen from above.

block of NE 102 plastic scintillator. The inner end was fed with He^6 gas pumped into a 1 mm hole drilled into it at 90°. The gas then diffused out through the aperture for emerging recoils giving an approximately linearly decreasing distribution of activity in the source volume. The feed tube and source volume were lined with 7 mg/cm² aluminium foil, the latter containing a helical rib impressed in its surface as an antiscatter collimator. This was normally maintained at earth potential but, for background determination, the source potential was dropped to −1500 V and a repelling field sufficient to prevent emission of recoils developed between evaporated aluminium microelectrodes situated at its mouth. The electrodes were separated by 0.7 mm and were situated sufficiently far inside the phosphor to enable β particles emitted at near forward angles from the source volume, whose energies range to only 1.5 MeV, to be completely stopped in the phosphor. With the full potential of −1500 V applied, no trace of discharge or field emission was discernable in the counter output.

In order to define the source volume precisely, one must ensure that relatively little activity is present in the region of the repelling field when the background measurement is made. For this reason the diameter of the pumping channel was increased outside the source volume, though at the expense of incomplete shielding in this direction. The fraction of the total source volume activity present in the repelling field was calculated to be less than 0.6 %.

The gas pressure at the inner end of the source volume during runs varied between 1.8 and 2.5×10^{-4} mm Hg. Mass spectroscopic analysis revealed this to consist almost entirely of hydrogen. Since the pressure over the greater part of the flight path was less than 2×10^{-7} mm Hg, scattering effects which might result in spectrum distortion were limited principally to the source volume. Published investigations on the passage of alkali ions through hydrogen have shown that at energies greater than 50 eV the sum of momentum exchange and charge exchange scattering cross sections does not exceed 5×10^{-16} cm² (see refs. [25, 26]). On this basis the mean probability for gas scattering of recoils within the source volume was calculated to be less than 0.1 %. The scattering of ions by the ribbed aluminium lining to the source volume was investigated in a separate experiment with Li^+ ions from an ion source. From this an upper limit of 0.1 % was placed on the total probability for detection of surface scattered recoils.

The uniformity of counter reponse to β particles from different regions of the source volume was checked with a source of Cs^{137} mounted on a thin probe. This showed a maximum variation of 3 % in pulse amplitude throughout the length of the source volume. The energy resolution of the detector, expressed as the width at half height of the 626 keV Cs^{137} internal conversion peak, was 13%. No effect on the counter response to γ-rays was observed when the source volume potential was changed to −1500 V.

The construction and performance of the recoil ion detector are described in detail in a separate paper [27]). Briefly, this consisted of a single stage box and grid type of electron multiplier using surface oxidized Be-Cu alloy as the secondary emitter. Ions incident upon the earthed grids in front of the detector were accelerated through 11.5 kV into the box. The resulting secondary electrons from the sensitive surface lining the back of the box were accelerated back to earth through a hole in its roof and focused onto a small scintillation counter. The pulse height distribution from the detector due to Li^+ from an ion source is shown by the solid curve in fig. 3. This was substantially independent of the energy of incident ions in the range 50 to 1500 eV, and the detection

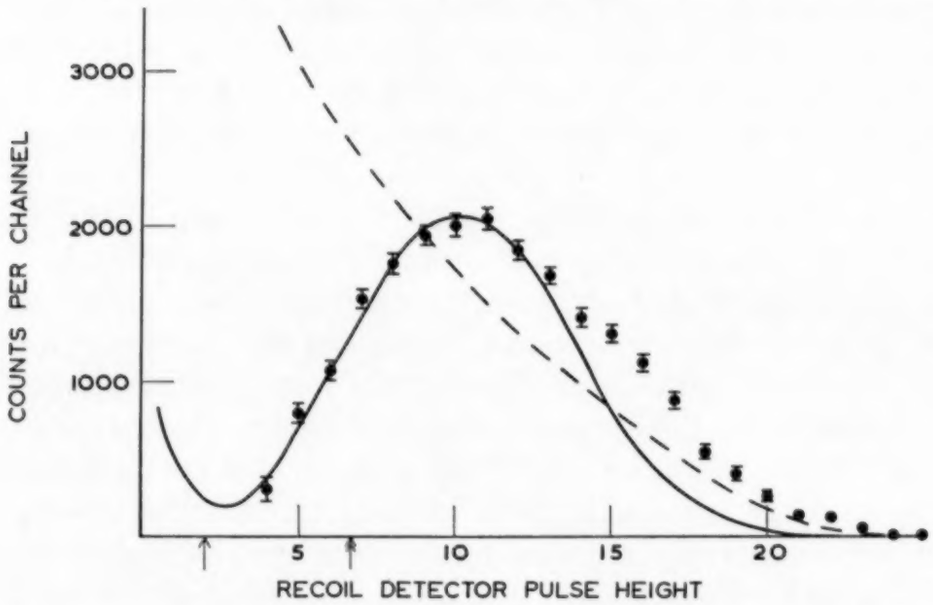

Fig. 3. Pulse height distributions from the recoil ion detector. The solid curve shows the distribution obtained with Li^+ from an ion source while the experimental points show that due to recoil ions from He^6 decay. The form of the background distribution is given by the dashed curve. The single headed arrow indicates the lower limit of recorded pulse height and the double headed arrow the bias condition on playback.

efficiency inferred from the distribution was greater than 99 % at a noise level of 0.3 counts per sec. However, when the counting rate was measured as a function of ion energy for constant ion current, an unexpected variation of 4 % was observed over the same energy range. A rough calculation suggested that this may be due to a change in transparency of the earthed grids before the ion detector, which should vary from 100 % for zero energy ions to the geometrical shadow factor of 95 % at 3 keV. In view of its importance as a correction to the recoil spectrum, the transmission function was therefore remeasured to an accuracy of 0.5 %, attention being paid to design of an ion source in which a similar transmission effect occurred below 50 eV. When the detector aperture was scanned with a narrow Li^+ beam, the detector efficiency was found to be uniformly maintained over the entire aperture.

Under normal running conditions the recoil detector counting rate, at a pulse height acceptance level of 99 %, was about 10 % of that in the β detector. Since the solid angle subtended at the source volume was only $\frac{1}{625}$ of a sphere, this rate must have arisen primarily from diffused activity. The associated pulse amplitude spectrum, illustrated by the dashed curve in fig. 3, showed a large excess of small pulses relative to the ion source Li^+ spectrum. However, the "true" recoil pulse spectrum in coincidence with β particles, obtained as the difference between tape recorded spectra taken with the source volume at 0 and -1500 V, respectively, closely resembled the Li^+ spectrum except near its upper limit. Here, an excess of large amplitude pulses was interpreted as due to the presence of 13 ± 4 % of Li^{2+} ions, which would have received 23 keV of energy on acceleration into the detector. The small pulses in the background distribution are believed to have arisen from disintegrations occurring inside the box and from fast β particles, since these persisted when genuine recoils were prevented from entering the detector by a repelling field applied between the screening grids in front of it.

4.2. SOURCE PRODUCTION AND TRANSPORT

The He^6 was made by irradiating Be metal powder with neutrons in the BEPO reactor at Harwell. The activity was carried to the counting equipment by methanol vapour circulating in a semi closed loop under a differential pressure of 8 cm Hg maintained by a column of liquid methanol between a solid CO_2 cooled condenser and an electrically heated evaporator beneath it. The He^6 was drawn off from the condenser and passed through a liquid nitrogen trap to freeze out the remaining traces of methanol vapour. It was then passed through an oven containing calcium at 550° C to remove possible N^{16} contamination before being pumped into the source volume. Some N^{16} was expected from neutron bombardment of oxygen in the methanol. Its removal was particularly important since, of all possible gaseous impurities, this was the only one whose recoil velocity spectrum overlapped with the region of interest of that from He^6.

The radiochemical purity of the He^6 was tested by lifetime and β-particle energy measurements. More than 99 % of the activity decayed with a half life of 0.82 ± 0.05 sec. That this was He^6 was confirmed by the maximum β energy (3.5 MeV) and the minimum recoil flight time (1.25 μsec). No evidence was found from lifetime measurements for the presence of N^{16} and a search for high energy electrons from the 10 MeV decay of this isotope gave an upper limit of 0.1 % contamination.

Methanol was chosen as the carrier on account of its convenient thermodynamic properties. Radiation decomposition gave rise primarily to hydrogen with about 14 % admixture of hydrocarbons, aldehydes and organic acids.

The effect of the hydrogen on the recoil spectrum has already been discussed. The majority of the more complex products were held in the traps.

5. Data Recording and Analysis

5.1. DATA RECORDING: EQUIPMENT AND PROCEDURE

As the minimum flight time of recoils from He^6 decay in the apparatus was about 1.25 μsec, a 90 % coverage of the recoil energy spectrum required measurement of flight times up to 4 μsec. The detection of a β particle followed within 4 μsec by that of a recoil ion was therefore treated as an "event". When this occurred the pulse amplitudes from both detectors and the time interval between them were recorded by a 3 channel magnetic tape recorder. The time interval was recorded as the pulse amplitude output from a time to amplitude converter operated by fast signals from the detectors. The effective time resolution of the converter was 0.03 μsec and its stability was better than 0.5 % throughout the experiment.

The recorder was of the kind developed by Cavanagh and Boyce [28]), in which the amplitudes of rectangular pulses of suitable length, mixed with an appropriate r.f. bias, were written directly onto magnetic tape. During recording the tape was run at a speed of 0.76 cm per sec ($\frac{1}{50}$ of the replay speed) in order to achieve a reasonable balance between economic data packing and dead time losses during writing. At this speed the writing time for each event was 10 msec and 1 % of events were lost due to dead time. The amplitude resolution of the recorder, using instrumentation tape, was typically 2.2 % with minor variations from tape to tape.

The experimental data were taken by recording total and background spectra alternately by switching the recoil repelling bias on the source volume between zero and −1500 V, respectively. Each run was taken for the same number of accumulated counts in the β detector. The counting rate in the β detector was maintained as near as possible to a nominal rate of 1500 per sec by regulation of the methanol pressure in the carrier system. This was important since the ratio of accidental to genuine coincidences varies in proportion to the input activity. Under these conditions the mean coincidence rate was 1 per sec and the ratio of peak genuine effect to background better than 1 : 1. Acceptance conditions on pulse amplitudes from the detectors were such that β particles of energy greater than 200 keV were recorded and the recoil detector efficiency was 99 %.

Calibration pulses were written on the tape before and after each run at a given source potential. These were obtained by substituting for the detectors a double pulse generator whose output signal waveforms closely simulated those from the detectors. The pulse interval time scale of the generator was calibrated against a 1 MHz crystal controlled pulser. The simulated β pulse amplitude

was calibrated in terms of equivalent β particle energy by reference to the cut-off edges of Compton spectra obtained by irradiating the β detector with γ rays from Cs^{137} (0.662 MeV) and Na^{24} (1.37 and 2.75 MeV).

5.2. DATA ANALYSIS: EQUIPMENT AND PROCEDURE

Although the recoil T.O.F. spectrum alone is sufficient in principle to determine the electron-neutrino angular correlation, the measurement of recoil subspectra in coincidence with selected ranges of β energy provides a useful redundancy of data that can be used to test their internal consistency. In addition, the performance of the spectrometer under true experimental conditions may be tested with the nearly monokinetic recoils associated with β particles of near maximum energy. Since analysis of the recorded data essentially involved the repetition of the experiment many times under different pulse selection conditions, a considerable saving in time was effected by increasing the tape speed on replay by a factor of 50.

The recorded data were basically analysed into T.O.F. spectra associated with bands of β energy 1 mc^2 wide. This was achieved by feeding the amplified tape replay pulses from the T.O.F. channel through a gate into a 100-channel pulse-height analyser. The gate admitted pulses to the analyser only when the associated β particle pulse fell in the energy range selected by a single channel analyser and at the same time the recoil pulse amplitude exceeded a given discriminator level. The multichannel analyser was set up with a T.O.F. channel width of 0.05 μsec by referring to calibration pulses at 0.5 μsec T.O.F. intervals recorded on the tape. The single channel analyser window limits were adjusted to select the desired range of β energy by reference to calibration pulses on the corresponding tape track. In choosing the lower limit to acceptance of recoil pulse amplitudes a compromise was made between eliminating the large background of accidental coincidences due to low amplitude pulses and retention of the greater part of the genuine recoil spectrum. This limit is indicated by the double arrow in fig. 3. The elimination of genuine recoils whose pulse amplitudes fell below the limit made it essential to determine whether the recoil detector spectrum was a function of recoil energy. Although the spectrum due to Li^+ ions from an ion source had previously been found to be insensitive to energy, such an effect might have arisen from an energy dependent charge spectrum. Analysis of the recorded recoil pulse spectra in coincidence with different selected ranges of recoil T.O.F. showed however that the net detection efficiency with respect to pulse amplitude under these conditions was constant within 0.5 %.

6. Experimental Results

6.1. THE RECOIL TIME OF FLIGHT SPECTRA

The true recoil T.O.F. spectra were assumed to be given by the difference between distributions obtained with and without bias on the source volume.

The recoil subspectra so obtained in coincidence with selected ranges of β particle energy are shown in fig. 4. The recoil spectrum obtained by integrating over all β particle energies $\geqq 2\ mc^2$ is shown in fig. 5. The curves show the corre-

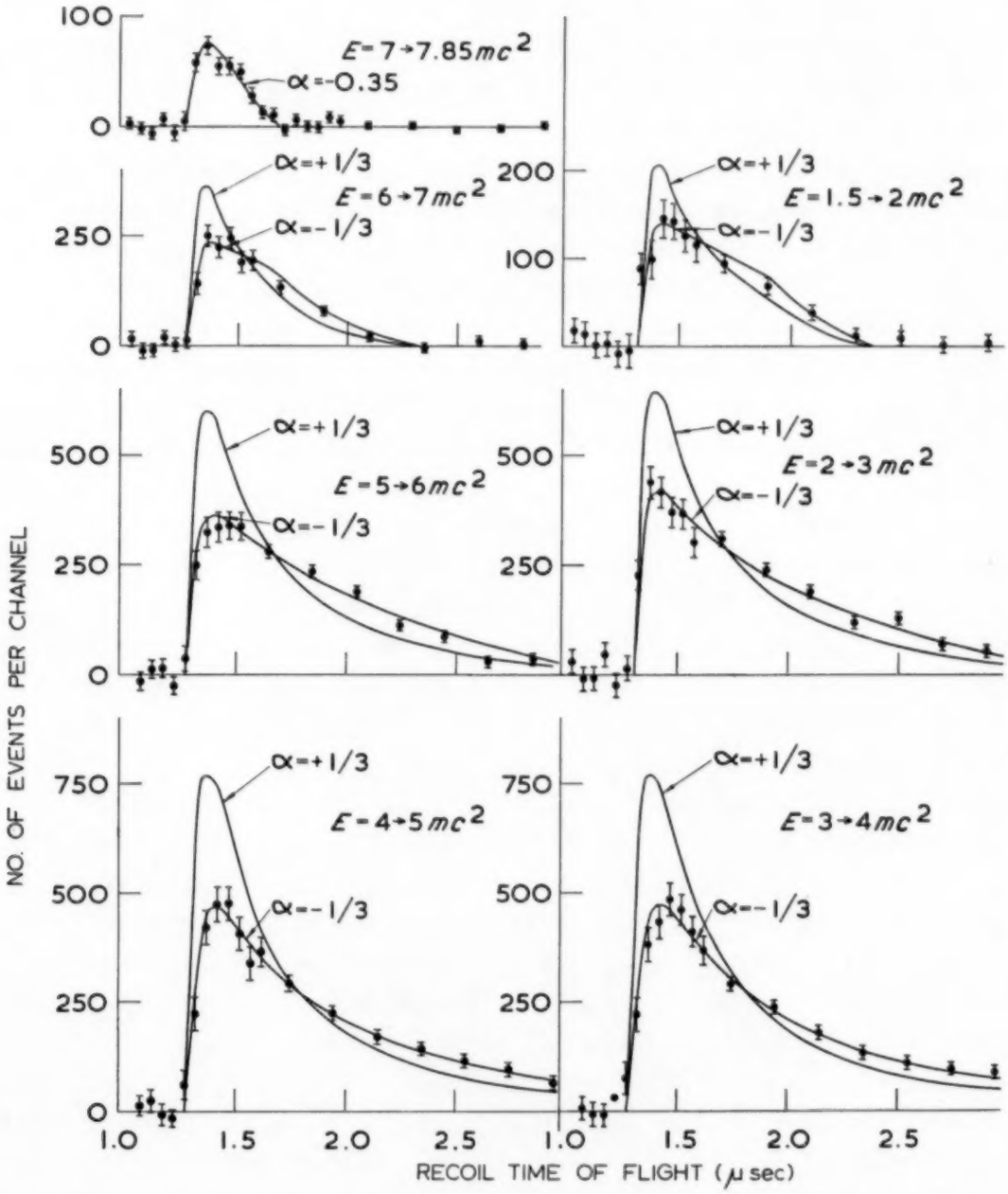

Fig. 4. Recoil time of flight spectra in coincidence with selected ranges of β particle energy E. Where the distribution is slowly varying the number of events is averaged over groups of 4 channels. The smooth curves represent the normalized theoretical distributions calculated for pure $T(\alpha = +\frac{1}{3})$ and pure $A(\alpha = -\frac{1}{3})$ interactions.

sponding theoretical spectra calculated on the basis of pure $T(\alpha = +\frac{1}{3})$ and pure A $(\alpha = -\frac{1}{3})$ interactions as described in section 7.

The maximum and minimum observed times of flight shown in fig. 4 are in all cases in excellent agreement with the cut-off values required by momentum

conservation. In addition, the small velocity spread of recoils associated with β particles of near maximum energy should provide a limited test of the spectrometer characteristics throughout the experiment. For this reason, the recoil T.O.F. spectrum in coincidence with β particles in the energy range $E = 7 \rightarrow 7.85$ mc^2 has been compared in fig. 4 with the theoretical distribution calculated for $\alpha = -0.35$, the best value obtained from combining all other data. A further

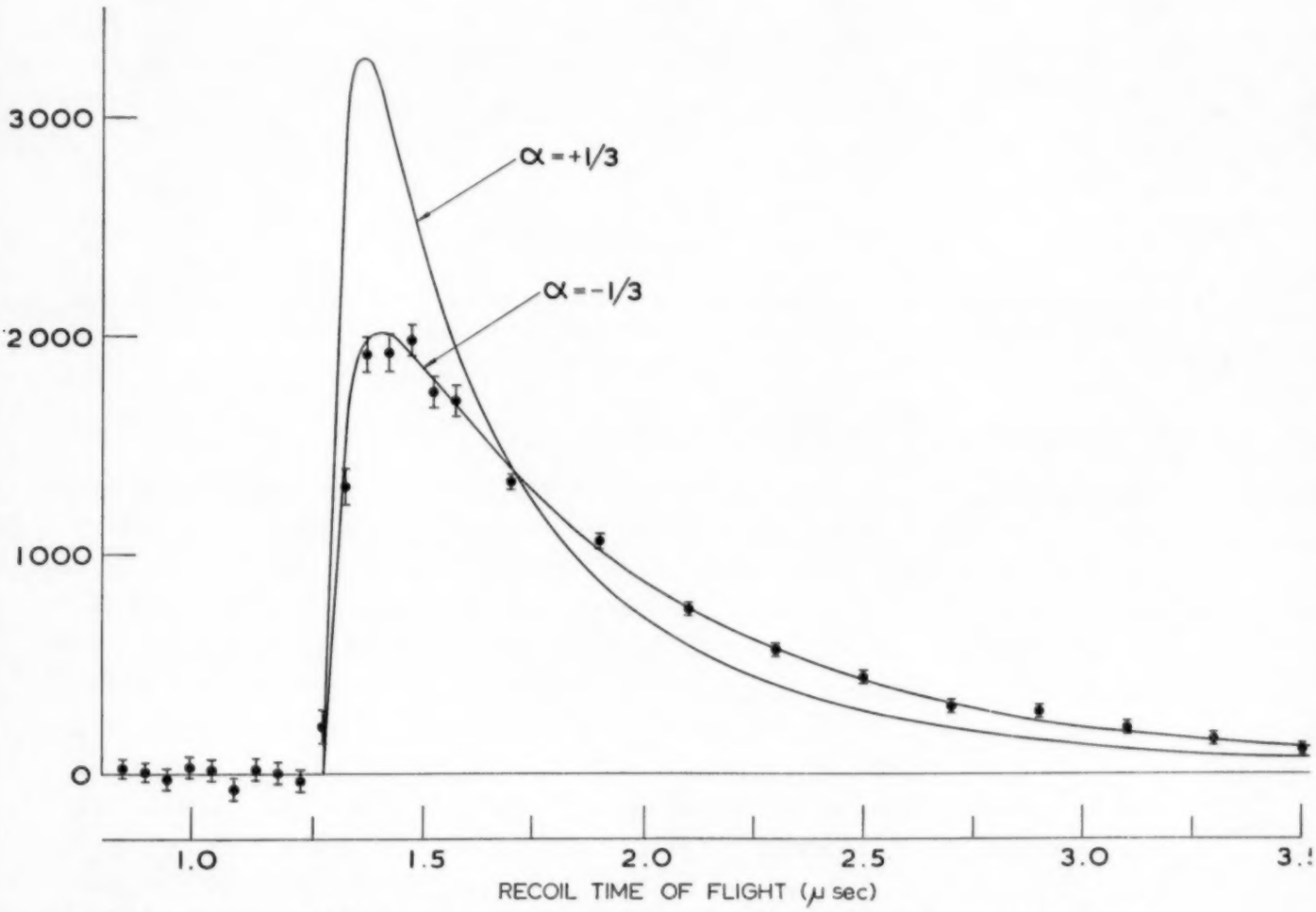

Fig. 5. Recoil time of flight spectrum in coincidence with all β particles of energy $E \gg 2\,mc^2$. The smooth curves represent the normalized theoretical distributions calculated for pure $T(\alpha = +\frac{1}{3})$ and pure $A(\alpha = -\frac{1}{3})$ interactions.

test of the mutual consistency of the subspectra is that the normal β energy spectrum should be reproduced by integration over all flight times within each range of E. Unfortunately those T.O.F. spectra associated with β particles of around half maximum energy extend beyond the observed time scale and the integral over the observed range will depend upon their forms. However, one can choose a limited range of time extending each side of the cross-over point for the theoretical distributions for which the integral is independent of shape (see section 7). The modified experimental β energy spectrum thus obtained is

shown in fig. 6 and is evidently consistent with the corresponding theoretical spectrum.

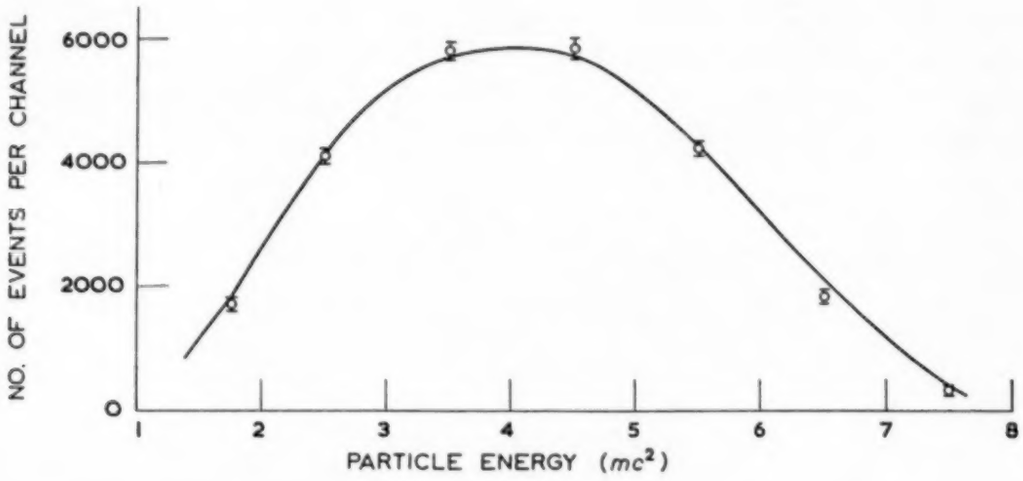

Fig. 6. Experimental and theoretical β particle energy spectra obtained by integrating recoil subspectra over a range of flight times such that these are independent of the electron-neutrino angular correlation.

6.2. DISCUSSION OF THE BACKGROUND

An understanding of the origin of the background in recoil experiments is of some importance since this may in certain circumstances lead to significant systematic errors. The data concerning the background are collected in fig. 7. The recorded T.O.F. distributions associated with all β energies $\geqq 2\ mc^2$ obtained with source volume potentials of zero and -1500 V are shown in curves (a) and (b), respectively. The difference between them represents the true recoil T.O.F. spectrum as shown in fig. 4. The form of the background distribution (b) suggests that it contains two components: a random distribution arising from accidental coincidences, superimposed upon which is a broad peak due to genuine coincidences from events occurring outside the source volume. These ideas were substantiated by a variety of auxiliary experiments, and the background peak, extending to times shorter than are permissible for events occurring inside the source volume, was identified as due to activity between the β detector and the interior of the differential pumping channel. The different origins of the two components of the background distribution were illustrated by the associated recoil detector pulse spectra, that associated specifically with the peak being characteristic of genuine Li^+ recoils whereas that associated with the random T.O.F. distribution resembled the detector background pulse height spectrum. The peak was reproduced as shown in curve (c) of fig. 7 when He^6 activity was introduced into the vacuum chamber containing the β detector by an alternative route to the source volume, and was unaffected by application of bias to the source volume. The peak disappeared and the random background alone remained when 1500 V repelling bias was applied between screening grids

in front of the ion detector. The magnitude of the background peak relative to the number of genuine events was in rough agreement with prediction based upon the calculated distribution of activity.

The apparent suppression of long flight times in the background peak relative to the genuine spectrum may be ascribed to the preferential detection of β particles emitted in the opposite direction to recoil nuclei. In other words this instrumental effect would simulate the presence of a T component in the

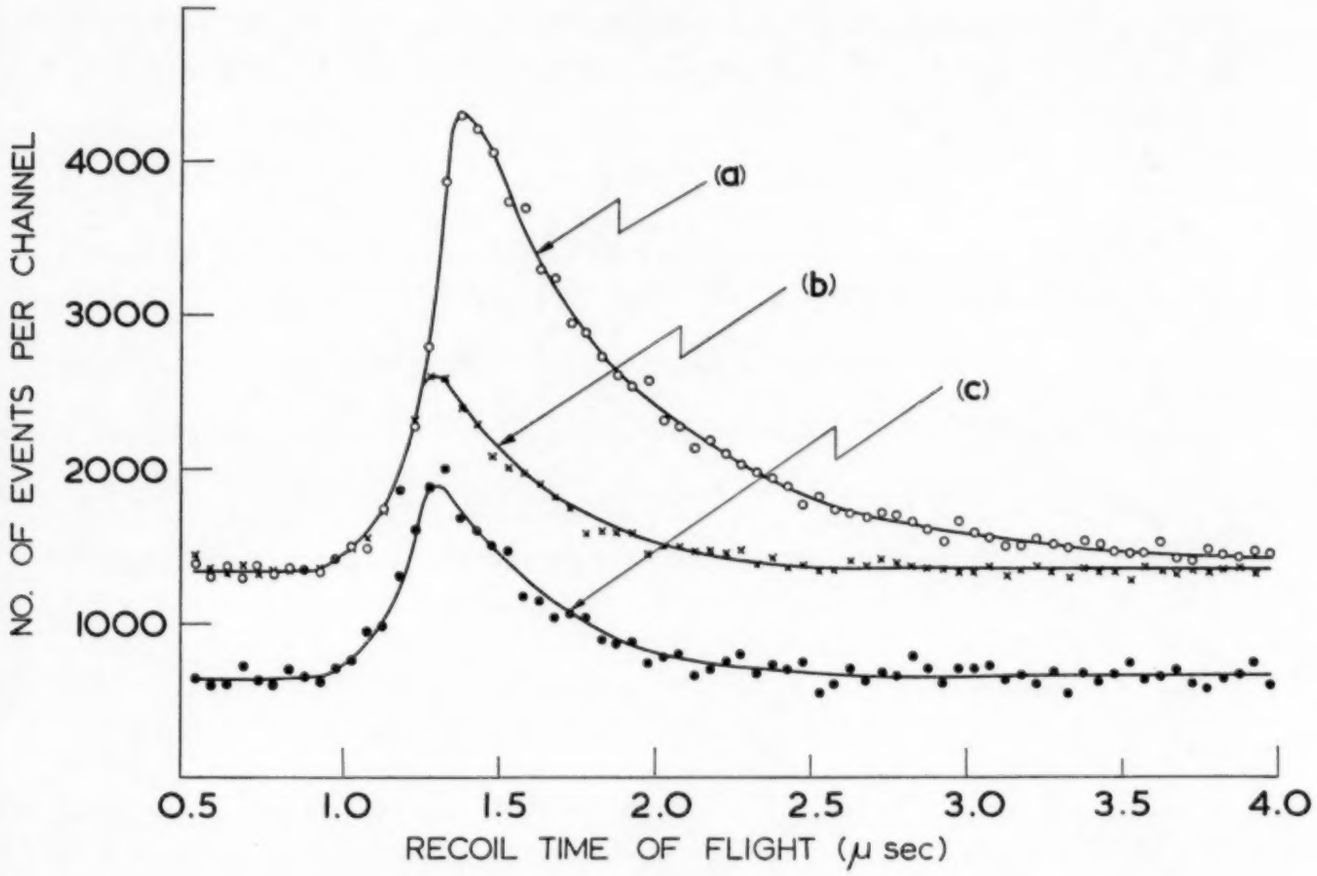

Fig. 7. Recoil time of flight distributions (a) with zero bias on source volume, (b) with -1500 V bias on source volume and (c) with He^6 pumped into the vacuum chamber surrounding the β detector but not into the source volume. The curves are intended only to guide the eye and have no theoretical significance.

interaction. This is of particular interest in connection with the interpretation of the author's earlier recoil experiment with Ne^{23} (see ref. [21])). Using a T.O.F. technique, but without provision for direct background determination, a value of $\alpha = -0.05 \pm 0.10$ was obtained, implying a strong admixture of T with A interactions and in disagreement with the result $\alpha = -0.37 \pm 0.04$ subsequently obtained by Allen *et al.* [4]). The recoil velocity resolution in the apparatus used for Ne^{23} was insufficient to distinguish disintegrations occurring just outside the source volume from those occurring inside and a correction was made only for the calculated accidental background. A rough calculation of the additional

correction suggests that it would be of the same sign and order of magnitude as the discrepancy, but no reliable quantitative estimate could be made.

7. Evaluation of the Angular Correlation Coefficient

The angular correlation coefficient α was determined by comparison of the observed distributions with theoretically predicted T.O.F. spectra to which corrections for instrumental affects had been made. A convenient starting point for the computation was provided by the distribution $P(E, r)$ of β energy E, and recoil momentum r, obtained by transforming the angular correlation function $P(E, \theta)$ given in eq. (1),

$$P(E, r)\mathrm{d}E\mathrm{d}r = KF(Z, E)\{E(E_0-E)r+\tfrac{1}{2}\alpha r[r^2-E^2+1-(E_0-E)^2]\}\mathrm{d}E\mathrm{d}r. \quad (4)$$

The Fierz term b in eq. (1) is here assumed to be zero; E and r are in units of mc^2 and mc, respectively. Eq. (2) may be rewritten

$$P(E,r)\mathrm{d}E\ \mathrm{d}r = [P_1(E, r)+\alpha P_2(E, r)]\mathrm{d}E\mathrm{d}r, \quad (5)$$

where $P_1(E, r)$ and $P_2(E, r)$ are each independent of the correlation coefficient α.

The distributions $P_1(E, r)$ and $P_2(E, r)$ were separately integrated over E in bands of width 1 mc^2 taking into account conservation of linear momentum which limits the range of E for each value of r. The maximum energy E_0 was taken to be 7.85 mc^2 (3.50 MeV kinetic energy).

In the transformation to the corresponding recoil T.O.F. distributions, $P_1(E, t)$ and $P_2(E, t)$, the following instrumental effects were folded in. (1) distribution of activity in the source volume, (2) the resolution characteristics of the time to amplitude converter and of the tape recorder, (3) recoil transit times in the ion detector, separate corrections being made for Li^+ and Li^{2+}, and (4) the transmission function of the screening grids in front of the ion detector. Finally the distributions were integrated over the experimental T.O.F. channel widths to give numerical distributions that could be compared directly with observation.

Overall normalization of the theoretical spectra to the total number of observed events was not possible because the fraction of the latter which are lost beyond the 4 μsec time limit depends upon the value of α. The normalization was performed over a limited range of recoil T.O.F. for which the integral of $P_2(E, t)$ was zero and which was therefore independent of the value of α. The normalized theoretical distributions were of the form

$$N(E_i, t_j) = N_1(E_i, t_j)+\alpha N_2(E_i, t_j). \quad (6)$$

These are illustrated for the cases $\alpha = +\frac{1}{3}$ (T interaction) and $\alpha = -\frac{1}{3}$

(A interaction) in figs. 4 and 5 by smooth curves drawn through the midpoints of the corresponding theoretical histograms.

Separate analyses were made of the recoil T.O.F. spectrum associated with all $E \geqq 2mc^2$ and of the subspectra associated with selected ranges of E. In each case a least squares procedure was adopted to determine the value of α giving the best fit. The experimental points were weighted according to their statistical accuracy and sensitivity to the value of α.

The value deduced from the overall T.O.F. spectrum of fig. 5 was

$$\alpha = -0.353 \pm 0.022.$$

The value of χ^2 indicated a 60 % probability level for the observed spectrum with respect to the theoretical distribution for this value of α. No evidence was found for systematic variation of α with T.O.F. through the spectrum.

The results from analysing the T.O.F. subspectra are collected in table 1.

TABLE 1

Values of α from analysis of recoil T.O.F. subspectra associated with selected ranges of β-particle energy E

E	α
1.5→2	-0.20 ± 0.15
2 →3	-0.30 ± 0.06
3 →4	-0.34 ± 0.05
4 →5	-0.37 ± 0.05
5 →6	-0.38 ± 0.06
6 →7	-0.25 ± 0.10

The T.O.F. spectrum associated with all $E > 2\,mc^2$ has the best statistical accuracy and the good fit to theory throughout the observed range of t suggests that systematic distortion of the spectrum is unlikely to have occurred unless it accidentally simulates the presence of more or less of the theoretical function $N_2(E, t)$.

The errors quoted above and in table 1 are of purely statistical origin. In addition to these, systematic errors for which no reliable correction can be

TABLE 2

Limits to systematic errors in α resulting from uncorrected instrumental effects

Source of error	Limits to error in α	
Presence of activity in repelling field at mouth of source volume	+0	−0.010
Scattering of recoils by surfaces and residual gas molecules	+0.003	−0
Calibration errors in recoil detector sensitivity	+0.008	−0.008
Emission of β particles through holes drilled in phosphor	+0	−0.003
Total limits to systematic error in α	+0.011	−0.021

calculated, may arise from several of the instrumental effects described in previous sections. These are listed in table 2 together with limiting values to the errors.

The final result may therefore be quoted as

$$\alpha = -0.353 \pm 0.022 \text{ (statistical error)}^{+0.011}_{-0.021}\text{(systematic error)}.$$

8. Summary and Conclusion

The electron-neutrino angular correlation in decay of He^6 has been determined by measuring the distribution of electron energy and recoil time of flight over a known field-free path without selection of angle. It is believed that the major auxiliary effects in the apparatus have been understood and a variety of subsidiary measurements have been made to evaluate the appropriate corrections. A substantial redundancy in the data taken has enabled a variety of tests to be made of their internal consistency and these have proved satisfactory within statistical limits.

The electron-neutrino angular correlation coefficient evaluated from the data was

$$\alpha = -0.353 \begin{cases} \pm 0.022 & \text{(statistical standard deviation),} \\ {}^{+0.011}_{-0.021} & \text{(maximum systematic error).} \end{cases}$$

From this it is concluded that the Gamow-Teller interaction is predominantly axial vector. The maximum admixture of a tensor interaction is given with 90 % confidence by

$$\frac{|C_T|^2}{|C_A|^2} < 0.08.$$

This result confirms those of Allen *et al.* [4]) and Pleasonton *et al.* [5]) on the electron-neutrino angular correlation in He^6 decay and is in accord with current theoretical ideas on a universal weak interaction, requiring a (V, A) combination [29, 30]).

I should like to express my gratitude to Dr. E. Bretscher and Dr. P. E. Cavanagh for their faith in supporting this work over an extended period of time and to Dr. Cavanagh and other members of his group for many useful discussions. Much of the apparatus was constructed by Mr. M. E. Young whose skill and enthusiasm contributed substantially to the experiment. My thanks are due to Mr. R. Panter for providing facilities in the BEPO reactor and Mr. R. G. Collins and his colleagues for their co-operation in installing the apparatus. Finally I am greatly indebted to my wife for her help in computing the results.

References

1) E. J. Konopinski and G. E. Uhlenbeck, Phys. Rev. **48** (1935) 7
2) R. D. Albert and C. S. Wu, Phys. Rev. **74** (1948) 847
3) E. Fermi, Z. Physik **88** (1934) 161
4) J. S. Allen, R. L. Burman, W. B. Herrmannsfeld, P. Stähelin and T. H. Braid, Phys. Rev. **116** (1959) 134
5) F. Pleasonton, C. H. Johnson and A. H. Snell, Bull. Am. Phys. Soc. **4** (1959) 78
6) K. H. Lauterjung, B. Schimmer and H. Maier-Leibnitz, Z. Physik **150** (1958) 657
7) C. A. Barnes, W. A. Fowler, H. B. Greenstein, C. C. Lauritsen and M. E. Nordberg, Phys. Rev. Letters **1** (1958) 328
8) M. Deutsch, B. Gittelman, R. W. Bauer, L. Grodzins and A. W. Sunyar, Phys. Rev. **107** (1957) 1733
9) F. Boehm, T. B. Novey, C. A. Barnes and B. Stech, Phys. Rev. **108** (1957) 1497
10) M. Goldhaber, L. Grodzins and A. W. Sunyar, Phys. Rev. **106** (1957) 826
11) A. V. Pohm, R. C. Waddell and E. N. Jensen, Phys. Rev. **101** (1956) 1315
12) F. Boehm and A. H. Wapstra, Phys. Rev. **109** (1958) 456;
H. Schopper and W. Jungst, Z. Naturforsch. **13** (1958) 505
13) M. T. Burgy, V. E. Krohn, T. B. Novey, G. R. Ringo and V. L. Telegdi, Phys. Rev. **110** (1958) 1214
14) S. R. De Groot and H. A. Tolhoek, Physica **16** (1950) 456
15) J. D. Jackson, S. B. Trieman and H. W. Wyld, Nuclear Physics **4** (1957) 206
16) M. T. Burgy, V. E. Krohn, T. B. Novey, G. R. Ringo and V. L. Telegdi, Phys. Rev. Letters **1** (1958) 324;
M. A. Clark, J. M. Robson and R. Nathans, Phys. Rev. Letters **1** (1958) 100
17) J. F. Turner and T. W. P. Brogden, private communication
18) B. M. Rustad and S. L. Ruby, Phys. Rev. **97** (1955) 991
19) W. P. Alford and D. R. Hamilton, Phys. Rev. **105** (1957) 673
20) J. M. Robson, Can. J. Phys. **36** (1958) 1450
21) B. W. Ridley, Nuclear Physics **6** (1958) 34
22) N. E. Booth, G. W. Hutchinson, A. M. Segar, G. G. Shute and D. H. White, Nuclear Physics **11** (1959) 341
23) B. M. Rustad and S. L. Ruby, post-deadline paper New York meeting Am. Phys. Soc. (1958)
24) J. S. Allen, The Neutrino (Princeton Univ. Press, 1958) p. 111
25) F. M. Durbin, Phys. Rev. **30** (1927) 844
26) K. H. Bracewell, Phys. Rev. **54** (1938) 639
27) B. W. Ridley, to be submitted
28) P. E. Cavanagh and D. A. Boyce, Rev. Sci. Instr. **27** (1956) 1028
29) E. C. G. Sudarshan and R. E. Marshak, Phys. Rev. **109** (1958) 1860
30) R. P. Feynman and M. Gell-Mann, Phys. Rev. **109** (1958) 193

6.A:8.A

Nuclear Physics **25** (1961) 502—510; © *North-Holland Publishing Co., Amsterdam*

Not to be reproduced by photoprint or microfilm without written permission from the publisher

SEPARATION OF HIGH ENERGY PARTICLES BY MEANS OF STRONG INTERACTIONS

G. GOLDHABER †, S. GOLDHABER ††

CERN, Geneva, Switzerland

and

B. PETERS

Institute for Theoretical Physics, University of Copenhagen, Denmark

Received 7 February 1961

Abstract: A method is discussed by which nucleons and pions emitted from an accelerator target can be eliminated preferentially so that one obtains beams which consist mainly of antinucleons and K-mesons. The method which is applicable to relativistic particles is not confined to the range of energies which are available in the laboratory at present. At the CERN Proton Synchrotron secondary particle production is sufficiently high to make such separated beams of antinucleons and K-mesons useful for bubble chamber work up to particle momenta well above 8 GeV/c.

1. Introduction

During the last few years, knowledge of strong interaction processes has increased to the point, where it appears possible to use them for physically separating different particles. This becomes important in an energy region where mass separation by electromagnetic methods is no longer possible or becomes cumbersome and expensive. Apart from being useful for separating high-energy charged particles, separation by strong interactions possesses the advantage of being applicable to neutral particles as well.

Nuclear properties have been applied before, to effect physical separation of particles; one often makes use of the difference in the total absorption cross-sections of two types of particles by using filters, in which the more strongly interacting component is absorbed preferentially. In this manner one obtains for instance pure μ-meson beams of arbitrarily high energy by filtering out π-mesons, K-mesons and nucleons. It appears possible, however, to apply nuclear forces also to the physical separation of high-energy π-mesons, K-mesons, baryons and antibaryons from each other, by making use of more subtle differences in the behaviour of the various types of particles: kinematics, partial cross-sections, angular distributions etc.

† Ford Foundation Fellow at CERN, on sabbatical leave from the Physics Department, University of California, Berkeley, California.

†† Ford Foundation Fellow at CERN on leave from the Lawrence Radiation Laboratory, University of California, Berkeley, California. In part supported by U.S.A.E.C.

The study of strongly interacting particles in the GeV region has produced some experimental results of a general nature which seem fairly well established, and can be extrapolated to 10 GeV (and probably even to much higher energies as discussed in the last section).

These results are:

1) In high-energy nuclear reactions of π-mesons, K-mesons, baryons and antibaryons the cross-section for charge exchange with small transfer of momentum, remains an appreciable fraction of the total cross-section; therefore, there are many interactions in which a particle, belonging to the same isobaric multiplet and carrying the same baryon number as the incident particle, emerges within a narrow cone around the forward direction and with a large share of the available energy [1–4]).

2) In collisions between high-energy π-mesons (presumably also K-mesons) with nucleons, a baryon is emitted in the backward hemisphere in the centre-of-mass system. This has been shown to be the case in π—p collisions at 7 and 8 GeV, where the baryon may be emitted as nucleon, hyperon or as cascade particle [5, 6]) and for protons from π—n collisions in the same energy interval [7]). It has also been shown that it holds for Λ and Σ production in π—p collisions at 16 GeV [8]).

Sects. 2, 3 and 4 of this paper contain a discussion of the application of these two experimental results to the problem of obtaining enriched antineutron, antiproton and K-meson beams in the energy range accessible to present day particle accelerators. In the last section we consider the extension of the method to particles of higher energy which may become available in the future.

2. Separator for High-Energy Neutral Particles

The two experimentally established properties of high-energy collisions mentioned above can be used to eliminate, for instance, most of the neutrons in a neutral beam and make it possible to obtain a fairly well focused high-energy beam of antineutrons and K_2^0-mesons. The intensity of such a beam

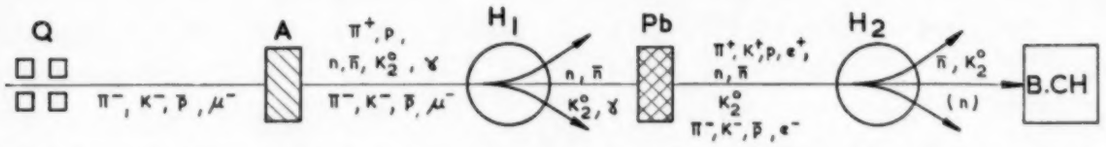

Fig. 1. Schematic diagram showing a possible experimental arrangement for obtaining an enriched anti-neutron-K_2^0 beam.

should be more than adequate for bubble chamber work. Fig. 1 illustrates a possible arrangement.

A momentum analysed beam of negative particles is focused by the quadrupole magnets Q onto the bubble chamber B. Ch. An absorber A converts some of the negative particles into other charged and neutral particles.

The charged component is removed from the beam by the sweeping magnet H_1 while the neutral particles proceed.

The neutral particles consist of:

a) antineutrons which are produced mainly in charge exchange reactions and therefore are strongly collimated in the forward direction;

b) neutral K-mesons which are produced partly by K^--mesons in quasi-elastic charge exchange reactions, partly in collisions of π^--mesons with protons; the former presumably will be strongly collimated, but the latter only slightly, since the angular distribution of K^0-mesons in the centre-of-mass system of π—N collisions is known to be nearly isotropic [5, 8]);

c) neutrons which are produced primarily in interactions of pions with the nucleons in the target; they move backward in the centre-of-mass system of the collision and therefore have a wide angular distribution and comparatively low energies in the laboratory system.

The three types of particles listed here, as well as γ-rays from decay processes, fall onto the lead sheet Pb, which absorbs most of the γ-rays or degenerates them into low-energy quanta emerging at large angles. All other neutral particles, including the K_1^0-component of the neutral K-mesons, do not reach the lead but decay within or shortly behind the converter A.

The lead sheet Pb is followed by a second magnet H_2, which removes electron pairs as well as other charged particles emerging from the lead. Thus the particles proceeding towards the detector consist of high-energy antineutrons and K_2^0-mesons in a fairly narrow and focused beam, and some K_2^0-mesons which are less well collimated and have probably lower energy. The beam is still contaminated by some neutrons and γ-rays with comparatively low energy and a large angular spread.

Apart from the unwanted background due to neutrons and γ-rays, all interactions occurring in the bubble chamber represent either the transformation or the annihilation of an antibaryon or else the production of at least one strange particle. The relative frequency of such events per picture will therefore be considerably higher than can be obtained in unseparated secondary beams.

A rough estimate of the expected intensities in a particular momentum interval can be made as follows: At the CERN Proton Synchrotron, in a pulse of 2×10^{11} protons with an energy of 25 GeV, about 50 % of the particles interact in the target and give rise to a negative secondary beam which in the forward direction, at $\approx$ 8 GeV/c, has an intensity of $\approx 2\times10^{10}$ particles per sr per GeV/c. In addition to negative pions such a beam contains near the target about $\approx$ 4 % K^--mesons and $\approx$ 0.8 % antiprotons [9]).

One may select a fairly wide momentum band of 8 ± 0.2 GeV/c and then focus the beam on a bubble chamber. With an aperture of 10^{-4} sr for the focusing magnet, the beam will then contain about 8×10^5 particles per pulse of which 6400 are antiprotons. If one now inserts a low Z converter, for

instance lithium hydride, paraffin or liquid hydrogen into the beam, some antiprotons will annihilate or be removed from the beam by inelastic collisions; others will suffer a charge exchange reaction and proceed as antineutrons with high energy and with only a small change in the direction of motion. Since diffraction scattered particles in our geometry remain part of the beam, the optimum production of antineutrons occurs for a thickness of absorber equal to one absorption mean free path for antinucleons; the fraction of antiprotons suffering charge exchange will then be

$$\frac{\sigma_{\text{charge exchange}}}{\sigma_{\text{absorption}}} e^{-1}.$$

In the momentum range from 0.5 to 3 GeV/c, the charge exchange cross-section for antinucleons remains reasonably constant and approaches 10 % of the total cross-section [10]) at 3 GeV/c. In the following estimates we have assumed that the charge exchange cross section remains equal to $\approx$ 10 % of the total cross section up to momenta of 8—10 GeV/c; this seems justified provided not only completely elastic but also quasi-elastic charge exchange processes are included †. In that case $\approx$ 3 % of the antiprotons incident on the converter A will undergo charge exchange. In this process the antinucleons suffer a deflection whose angle is of the order of magnitude $\mu_\pi/P_{\bar{p}}$, where μ_π is the pionmass and $P_{\bar{p}}$ the antinucleon momentum.

If one interprets this characteristic angle as representing the half-angle of the cone which contains 50 % of the antineutrons, one finds that 8 antineutrons per pulse will traverse the bubble chamber. (We assume that the chamber subtends a solid angle of 10^{-4} sr at the converter A.)

If, on the other hand, one bases one's estimate on the available experimental data [1]) at the comparatively low momentum of 1.65 GeV/c, one obtains a half-angle of 2.6 $\mu_\pi/P_{\bar{p}}$. This leads to 1 antineutron per pulse, an estimate which is perhaps somewhat conservative.

The K_2^0-mesons traversing the bubble chamber consist of two groups. Of those produced in charge exchange reactions by the K^--component, there will be 4 per pulse or 0.5 per pulse, depending on which of the two methods is used for estimating the angular distribution characteristic of the charge exchange reaction. The second component consists of K_2^0-mesons which arise from neutral K-mesons produced in πp collisions. Their distribution in the centre-of-mass system is nearly isotropic at high energies [5, 8]) and contributes about one or two K_2^0-meson per pulse ††. On the average, their energy will be much lower than that of the charge exchange K-mesons. (The K-flux has been calculat-

† This assumption may be interpreted geometrically, i.e. that beyond a certain radius there exists a zone around the target nucleon, where an incident baryon has a reasonable chance of producing or exchanging a small number of mesons and altering its charge without at the same time losing a large fraction of its energy.

†† Beams of K_2^0-mesons have been obtained at 1.1 GeV/c by this reaction. See ref. [11]).

ed on the assumption that the distance from machine target to converter is 80 m and from the converter to the bubble chamber, 15 m.)

Finally, one can estimate the intensity of the background neutrons. Practically all of them must be due to the interaction of π^--mesons with the nuclei of the converter. The reaction $\pi^- + N \rightarrow p + x\pi$ at 7—8 GeV/c, leads to protons which in the *centre of-mass* system are emitted into the backward hemisphere with an average momentum [5, 7]) of 0.9 GeV/c and an average transverse momentum of 0.37 GeV/c. Thus the characteristic solid angle in the *laboratory* system is of the order of 0.7 sr. Assuming a similar distribution for neutrons produced in π^-N collisions, the fraction falling into a solid angle interval of 10^{-4} sr is 0.35×10^{-4}. On the basis of these estimates, the expected beam will contain 1—2 neutrons.

The estimates together with the expected number of interactions † in an 80 cm bubble chamber are summarized in table 1.

TABLE 1

Yield of neutral particles from an incident beam of 8×10^5 negative particles with a momentum of 8 GeV/c

Particles	Estimated yield per pulse	Mean free path in liquid H_2 (in m) [a])	Estimated number of interactions in a 80 cm H_2 bubble chamber per 100 pictures
$\bar{n}$	1—8	5.0	15—120
K_2^0	2—5	12.0	12—30
n	1—2	6.5	12—125

[a]) From cross section measurements quoted in refs. [9, 12]).

The neutral beam which one obtains in one stage of charge exchange reactions from a momentum analysed and focused negative beam is still a mixture of three types of particles, so that the interpretation of nuclear reactions observable in the chamber will often be ambiguous. There are, however, certain reactions in the class of associated production of hyperon-antihyperon pairs, which can be attributed uniquely to antineutrons. Such reactions are,

$$\bar{n} + p \rightarrow \bar{\Sigma}^{\pm} + \Sigma^{\pm} + \pi^+ + x\pi,$$
$$\bar{n} + p \rightarrow \bar{\Xi}^- + \Xi^- + \pi^+ + x\pi,$$
$$\bar{n} + p \rightarrow \bar{\Xi}^- + \Xi^0 + x\pi.$$

The reactions

$$\bar{n} + p \rightarrow \bar{\Lambda} + \Lambda + x\pi,$$
$$\bar{n} + p \rightarrow \bar{\Xi}^0 + \Xi^- + 2\pi^+ + x\pi$$

† It is important to note that by using neutral instead of charged particles for studying the behaviour of fast antinucleons and of strange particles, the bubble chamber can handle a very large number of incident particles per picture. Certain types of data can therefore be accumulated much faster than it could be done if the incident particles were electrically charged.

can be identified uniquely in a heavy liquid bubble chamber and also in a hydrogen chamber, provided the antibaryon decays in the charged mode. Other combinations involving Σ^0, and baryon-antibaryon pairs of unequal mass, for instance $(\bar{\Lambda}\Sigma)$ or $(\bar{\Sigma}\Lambda)$, will occur. They all lead to baryon pairs whose mean life is short enough so that a considerable fraction will decay in the chamber. In addition to the above mentioned processes we also expect associated production of hyperon-K meson pairs ($\bar{\mathrm{Y}}\bar{\mathrm{K}}\mathrm{N}$ and $\mathrm{YK}\bar{\mathrm{N}}$) corresponding to similar reactions in nucleon-nucleon collisions (YKN). It might be expected that all the above mentioned processes leading to strangeness $S = +1$ anti-hyperons will have comparable cross sections.

There are also a number of reactions involving K-mesons and hyperons which in favourable cases can be attributed unambiguously to the K^0-component of the beam. An example is the reaction

$$\mathrm{K}^0 + \mathrm{p} \rightarrow \mathrm{K}^+ + \Xi^0 + x\pi.$$

Finally it should be noted that the ratio of antiprotons to K^--mesons in the negative beam can be varied somewhat before conversion by changing the distance between the machine target and the converter A (see fig. 1); this will produce a corresponding change in the ratio of antineutrons to K_2^0-mesons in the converted beam.

3. A Separator for High-Energy Negative Particles

The method discussed above is also applicable for obtaining a negative beam enriched in K^--mesons and antiprotons. The arrangement could be that shown in fig. 2. Here an unanalysed but collimated beam of neutral particles is permitted to fall on the converter A. The emerging charged particles are focused by quadrupole magnets Q on to the bubble chamber.

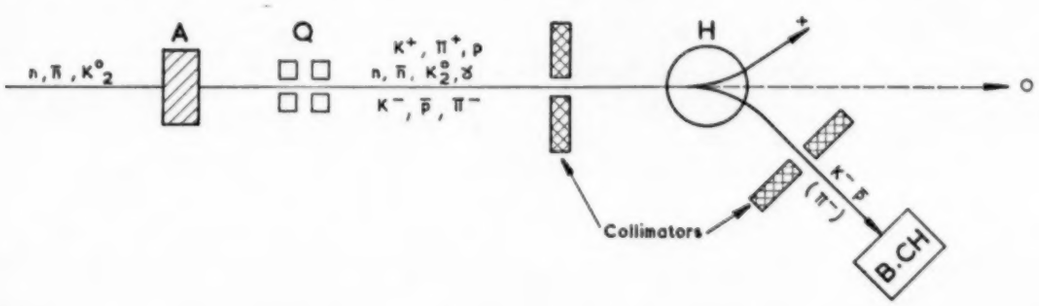

Fig. 2. Schematic diagram showing a possible experimental arrangement for obtaining an enriched antiproton-K^- beam.

One selects again only particles within a narrow cone of order 1° in the forward direction and then makes a charge and momentum analysis in the

field H. The negative beam is directed towards the bubble chamber. Since antiprotons and K^--mesons produced in charge exchange reactions are strongly collimated in the forward direction, the beam contained in this narrow cone will be highly enriched in these two components.

The contamination consists of π^--mesons, most of which are produced in n—n and n—p collisions at angles distributed over a fairly wide cone in the laboratory system. It is difficult, however, to calculate the composition of such a beam since this involves detailed knowledge of the composition and energy spectrum of the neutral beam, before conversion.

The enrichment may well be lower than in the first case which we discussed. Furthermore, the useful flux is limited here, not by the output of the machine but by the permissible number of incident particle tracks in each bubble chamber picture.

4. A Two-Stage Separator for High-Energy Charged Particles

Given a negative secondary beam which after rough momentum analysis and focusing contains $\approx 10^7$ particles or more, it is possible to operate the two separators (figs. 1 and 2) in series; one then obtains comparatively weak but pure and still useful separated beams †. The output of the second stage in a momentum interval close to the incident momentum consists now of a positive beam of K^+-mesons and a negative beam containing a mixture of antiprotons and K^--mesons. These are the only energetic charged particles which can be present, since they can be produced by charge exchange of high energy antineutrons and K_2^0-mesons which in turn have been produced in charge exchange reactions. None of the other particles of the intermediate neutral beam possess sufficient energy to produce charged particles in the same momentum range. Most protons and π-mesons remaining as background in the separated beam are therefore eliminated in the second momentum analysis.

In estimating the flux obtainable in the two-stage charge exchange separator, one should take into account that it is possible to transport the K-mesons over appreciable distances in the long-lived K_2^0-state.

5. Separation of Particles at Very High Energies

The method of particle separation described here makes use of two asymmetries in the family of elementary particles:

a) the absence of negative nucleons in ordinary terrestrial matter;

b) the absence of neutral pions with a lifetime comparable to that of the charged pion component.

† At the completion of this paper an internal report by F. J. M. Farley (CERN 1958, unpublished) was pointed out to us in which he suggests a method of double-charge exchange to obtain enriched antiproton beams in the 0.5—2 GeV region.

These asymmetries make it possible to eliminate most nucleons in a strongly collimated beam by passing through a negative beam stage and most pions by passing through a neutral beam stage.

We have given numerical estimates for the particular case of particles with momenta in the range of 8 GeV/c where relevant experimental data on pion-nucleon and proton-nucleon collisions exist. One can show, however, that the method remains applicable and that the obtainable separation factor actually increases as one goes to still higher energy. In order to make this plausible it is necessary to establish the following points:

(1) The cross-section for charge exchange collisions of nucleons (and therefore presumably of antinucleons) in which the incident baryon loses a comparatively small fraction of its energy, remains an appreciable part of the geometric cross-section;

(2) the laboratory angle characteristic of such charge exchange interactions decreases at least as fast or faster with increasing energy as the angle characteristic of the production of nucleons in pion-nucleon collisions and of pions in nucleon-nucleon collisions.

Evidence for point (1) can be found in the studies of nuclear interactions at cosmic-ray energies †. It has been established that nucleons in the energy range of 10^{11}—10^{14} eV lose on the average less than 25 % of their energy in pion producing collisions in air. The average energy loss per collision in hydrogen is certainly smaller and lies perhaps within 15—20 %. Since these collisions are accompanied by the production of several charged particles, the emerging nucleon, which in half the cases carries more than 80 % of the available energy, has a nearly equal chance of being charged or neutral. The cross-section for such "quasi-elastic charge exchange" processes in which no more than 20 % of the incident energy is lost in particle production represents, therefore, about 25 % of the geometric cross-section. (One could interpret these collisions as being associated with impact parameters greater than some fixed value, independent of energy.) These experiments show that the probability of such quasi-elastic charge exchange processes does not decrease and may possibly increase somewhat as one approaches ultra-relativistic energies. We expect a similar behaviour in antinucleon-nucleon collisions. At these energies the annihilation process will probably be confined to small impact parameters corresponding to antinucleon-nucleon core collisions and should not compete significantly with the quasi-elastic charge exchange process.

Regarding point (2), the particle emerging close to the forward direction in the centre-of-mass system retains a large fraction of its original momentum. Therefore the characteristic angle in the laboratory system for quasi-elastic charge exchange processes decreases as $1/P$, where P is the momentum in the laboratory system. In pion-nucleon collisions on the other hand, the nucleon is

† See ref. [13]) and other papers quoted there.

emitted backwards in the centre-of-mass system; the characteristic angle varies then as $1/\sqrt{P}$ for completely inelastic collisions and tends to a large and constant value if the collision is quasi-elastic. It varies, therefore, less rapidly with primary momentum than the angle associated with the charge exchange process.

The angle characteristic of the production of pions in nucleon-nucleon collisions has been studied actively over a very wide range of energies during the last few years. All investigators agree that it has a value of $\alpha\mu_\pi/P_\pi$, where α lies between 2 and 3. Since the pion multiplicity increases somewhat, if only slowly, with the primary energy, the momentum of the meson P_π increases less rapidly than the primary momentum P.

From these considerations it follows that the fraction of background nucleons and pions which fall into the solid angle characteristic of quasi-elastic charge exchange reactions tends to decrease with energy. The method for separating particles by strong interactions which we have discussed here is therefore not limited to the energies available in the laboratory at present. Separation of particles by strong interactions should also be possible in beams of the larger accelerators which are being planned for the future.

We thank our colleagues at Copenhagen and Geneva for many helpful discussions concerning details of the ideas expressed here. Two of the authors (G. G. and S. G.) would like to express their appreciation for the hospitality offered them at CERN.

References

Most references are to the Proceedings of the 1960 Annual Int. Conf. on High-Energy Physics at Rochester, (Interscience, New York-London, 1960). These will be referred to as "Proc.".

1) Hinriches, Parker, Moyer and Poirier, as quoted by Wenzel, Proc. p. 154
2) Goldhaber, Goldhaber, Powell and Silberberg, Phys. Rev. **121** (1961) 1525
3) Cook, Cork, Hoang, Keefe, Kerth, Wenzel and Zipf, Proc. p. 456
4) S. D. Drell, Proc. p. 177;
   G. Salzman, Proc. p. 348
5) M. I. Soloviev, Proc. p. 388
6) Maenchen, Fowler, Powell and Wright, Phys. Rev. **108** (1957) 850
7) V. Petrzilka, Proc. p. 82
8) Bartke, Bock, Budde, Cooper, Filthuth, Goldschmidt-Clermont, Grard, MacLeod, Minguzzi-Ranzi, Montanet, Moorhead, Morrison, Peyrou, Powell, Trembley, Wiskott Bertanza, Franzinetti, Mannelli, Silvestrini, Brautti, Ceschia, and Chersovani, Proc. p. 402
9) G. Cocconi, Proc. p. 799
10) W. A. Wenzel, Proc. p. 151
11) Muller, Birge, Fowler, Good, Hirsch, Matsen, Oswald, Powell and White and Piccioni, Proc. p. 597;
    Adair, Bull. Am. Phys. Soc. **5** (1960) 516
12) Von Dardel, Frisch, Mermod, Milburn, Piroué, Vivargent, Weber, and Winter, Proc. pp. 148, 484
13) N. A. Dobrotin and S. A. Slavatinsky, Proc. p. 819;
    D. Perkins, in Progress of elementary particle and cosmic-ray physics, ed. by Wilson and Wouthuysen (North Holland Publishing Company, 1960, Amsterdam) p. 257

2.D

Nuclear Physics **25** (1961) 511—521; © *North-Holland Publishing Co., Amsterdam*

Not to be reproduced by photoprint or microfilm without written permission from the publisher

MONTE CARLO CALCULATION OF NEUTRON EVAPORATION; EXCITATION ENERGY DEPENDENCE OF NUCLEAR LEVEL DENSITY

R. VANDENBOSCH, J. R. HUIZENGA, W. F. MILLER and E. M. KEBERLE †

Argonne National Laboratory, Argonne, Illinois ††

Received 17 February 1961

Abstract: Experimental excitation function data in the heavy element region have been analyzed by a Monte Carlo technique to investigate the dependence of the nuclear level density on excitation energy. The analysis supports the prediction of the completely degenerate Fermi gas model that the nuclear temperature varies as the square root of the excitation energy. The value of the level density parameter a deduced from the experimental data is changed significantly when shell and pairing effects are taken into account by displacement of the characteristic energy surface from which the excitation energy is measured.

1. Introduction

Evaporation theory for emission of particles from the compound nucleus predicts the energy spectrum $I(\varepsilon)$ to be of the form

$$I(\varepsilon)\mathrm{d}\varepsilon = \text{const}\ \varepsilon\sigma_c(\varepsilon)\rho(E_x - B - \varepsilon)\mathrm{d}\varepsilon. \tag{1}$$

In eq. (1), $\sigma_c(\varepsilon)$ is the cross section for the inverse process, that is, the cross section for particle with kinetic energy ε reacting with a nucleus of excitation energy $E_x - B - \varepsilon$ to form a compound nucleus with excitation energy E_x. The binding energy of the particle to the compound nucleus is designated by B and $\rho(E_x - B - \varepsilon)$ is the level density of the residual nucleus corresponding to the value ε of the kinetic energy of the emitted particle.

Different physical assumptions lead one to various forms for the level density $\rho(E)$. For a nuclear temperature T which is constant (independent of excitation energy), $\rho(E)$ takes the form

$$\rho(E) = C \exp \frac{E}{T}, \tag{2}$$

where C is a numerical constant. Another formulation which is often used is that based on a completely degenerate Fermi gas,

$$\rho(E) = C \exp 2\sqrt{aE}, \tag{3}$$

† Now at Institute of Mathematical Science, New York University.

†† Based on work performed under the auspices of the U. S. Atomic Energy Commission.

where the excitation energy dependence of C is usually neglected. This expression for the energy dependence of the nuclear level density leads to a nuclear temperature which varies as the square root of the excitation energy. The simplified theory predicts that the level density parameter a is proportional to the mass number A. Because of nucleon pairing effects, it is thought that even nuclei, for example, have a smaller level density at a given excitation energy (at least for low excitation energies) than odd-neutron, odd-proton or odd nuclei. For even nuclei, only those levels arising from collective effects are expected at an excitation energy less than that required to break a nucleon pair, resulting in a paucity of levels for these excitation energies in even nuclei. It has been suggested that effects of this type be compensated for by letting C depend on nuclear type[1]). Alternatively, it has been suggested that one correct for this effect by letting the excitation energy be measured from a characteristic energy surface which may be different from the ground state mass surface [2]). This can be done by use of a correction factor Δ so that eqs. (2) and (3) become

$$\rho(E) = C \exp \frac{E-\Delta}{T} \tag{4}$$

and

$$\rho(E) = C \exp 2\sqrt{a(E-\Delta)}. \tag{5}$$

There is some experimental evidence [3, 4]), which supports the constant nuclear temperature form (2) of the level density, and other evidence [5, 6]) that favours the form of eq. (3). It has been suggested [3, 7]) that the level density expression of eq. (3) is a limiting form valid only at high excitation energies, and that at low excitation energies the nuclear temperature is approximately constant. The type of experimental data often analyzed to investigate this problem is the kinetic energy distribution of particles emitted in nuclear reactions. Because of experimental difficulties encountered in measuring neutron kinetic energy distributions, usually energy distributions of charged particles only are measured. This leads to considerable difficulty because the analysis depends strongly on the inverse cross sections for particles with energies close to the Coulomb barrier. Small changes in the assumed inverse cross section can in some cases lead to support of either eq. (2) or eq. (3) by the same set of experimental data [8]). A simplification results if one considers emission of neutrons, as the inverse cross section for neutrons is not very energy dependent.

The purpose of this report is to examine excitation functions for multiple neutron emission in the light of eqs. (2) and (3) in order to see which description is supported by these data. Since this work was initiated, Dostrovsky *et al.* [9]) have reported Monte Carlo calculations of the evaporation process for nuclei with mass numbers A between 50 and 74. These workers assumed a level density equation of the form of eq. (5) and did not explore the use of eq. (4). Their emphasis was on the determination of the characteristic level parameters Δ.

As these workers have pointed out, competition between reactions leading to the emission of different particles, for example neutrons and protons, is very sensitive to Δ but not to the constant a, whereas the competition between reactions leading to the emission of various numbers of the same particle is more sensitive to the value of a.

The calculations reported in this work have been limited to cases in which proton emission is negligible compared to neutron emission, as is the case for the heavier elements. In particular, many of the calculations were made for reactions induced in Pb and Bi, where it has been possible to measure the excitation functions very accurately because the product nuclei are alpha emitters. It has also been assumed in these calculations that the inverse cross section $\sigma_c(\varepsilon)$ is a constant independent of ε, which is a fairly good assumption for neutrons reacting with heavy elements. The calculations for the constant temperature law, eqs. (2) or (4), have been performed using the model of Jackson [10]) and are not described in detail here. The use of eqs. (3) or (5) for the level density in eq. (1) results in an expression which cannot be integrated in closed form for multiple neutron emission. A Monte Carlo approach has been used and is described briefly in the following section.

2. Monte Carlo Approach

Use of eq. (5) together with eq. (1) gives rise to an expression for the neutron kinetic energy spectrum which can be put in the form

$$I(\varepsilon_i) \propto \varepsilon_i \exp 2\sqrt{a(E_i - B_i - \Delta_i - \varepsilon_i)}. \tag{6}$$

A typical spectrum is illustrated in fig. 1. The objective of the Monte Carlo technique is to sample uniformly the area under the curve defined by this distribution function, so that for a large sample size the number of points falling in the region between ε and $\varepsilon + d\varepsilon$ is proportional to the area enclosed by these boundaries. Since in practice it is relatively simple to generate random numbers uniformly over a constant interval, the rejection technique [11]) is well suited for this problem. In applying the rejection technique, the curve representing the energy spectrum up to some suitable cut-off is enclosed by a rectangle. Points are selected uniformly over the area of this rectangle by sampling uniformly along each side of the rectangle; then, by rejecting those points which lie above the curve, the remaining points are distributed uniformly over the area under the spectral curve. The smallest rectangle which encloses this curve is bounded by $I(\hat{\varepsilon}_i)$, the value of $I(\varepsilon_i)$ for the most probable kinetic energy $\hat{\varepsilon}_i$ and $\varepsilon_{i,\max}$, the maximum kinetic energy available to the emitted neutron. This process can become rather inefficient when the ratio of the area above the curve to the area below the curve becomes large, as is the case for the distribution function of interest here. In order to reduce the rejection rate and thus the

computer time required, it was decided to divide the spectrum into three regions R_1, R_2 and R_3, as indicated in fig. 1. Examination of spectra for a wide range of E_i and a enabled a choice of three regions defined in terms of $\hat{\varepsilon}_i$ such that $I(\varepsilon_i)$ in these regions would always be less than $I(\hat{\varepsilon}_i)$, α_2 and α_1. The bounds α_2 and α_1 were determined empirically. The sampling now requires three random numbers. The first random number determines which of the three regions is being sampled. The second and third random numbers are chosen uniformly along the abscissa and ordinate of the region being sampled. If the

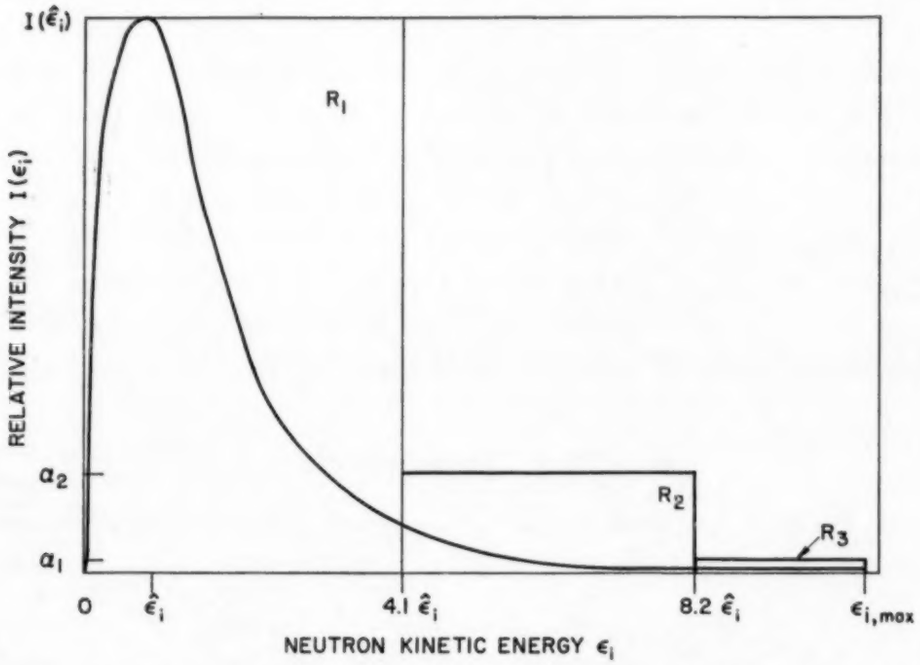

Fig. 1. Schematic drawing of neutron energy spectrum showing division into three regions. $\hat{\varepsilon}_i$ is the most probable neutron kinetic energy. α_1 and α_2 are determined empirically.

point chosen is found to lie above the curve, the sample is rejected. If the sample is not rejected, a new spectrum characterized by $E_2 = E_1 - \varepsilon_1 - B_1$ is sampled. The process continues until $E_{i+1} \leqq B_{i+1}$, the condition that no more neutrons may evaporate, and the history for this particular neutron emission cascade is terminated. The calculations were performed on the Argonne digital computer GEORGE. The time required for a typical cascade was a little less than 1 sec.

3. Results

Most of the calculations were performed for $\Delta = 0$. Exploratory runs were made at several energies to determine the best value of the parameter a for fitting the experimental data. After a choice of a had been made, calculations were made at 1 or 2 MeV intervals, taking 1000—5000 cascades at each energy to obtain statistical accuracy. These evaporation calculations give only the

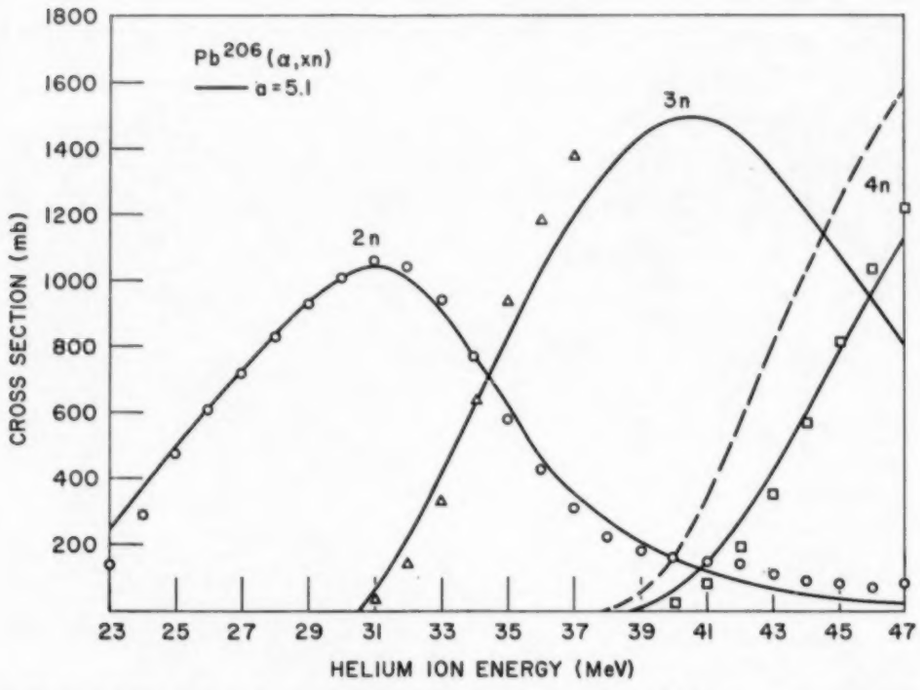

Fig. 2. Experimental [14]) and calculated excitation functions for $Pb^{206}(\alpha, xn)$ reactions. The solid line curves were calculated with a level density depending on the square root of the excitation energy. The dashed curve is the constant temperature prediction for the (α, 4n) reaction when the nuclear temperature is chosen to fit the (α, 2n) reaction.

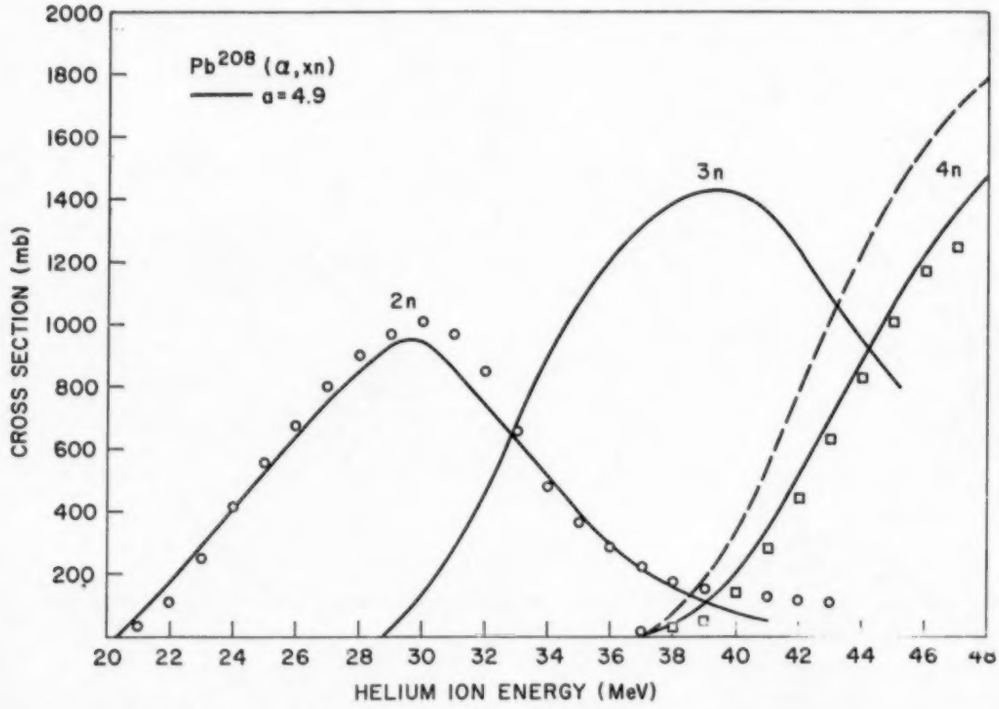

Fig. 3. Experimental [14]) and calculated excitation functions for $Pb^{208}(\alpha, xn)$ reactions. The solid line curves were calculated with a level density depending on the square root of the excitation energy. The dashed curve is the constant temperature prediction for the (α, 4n) reaction when the nuclear temperature is chosen to fit the (α, 2n) reaction.

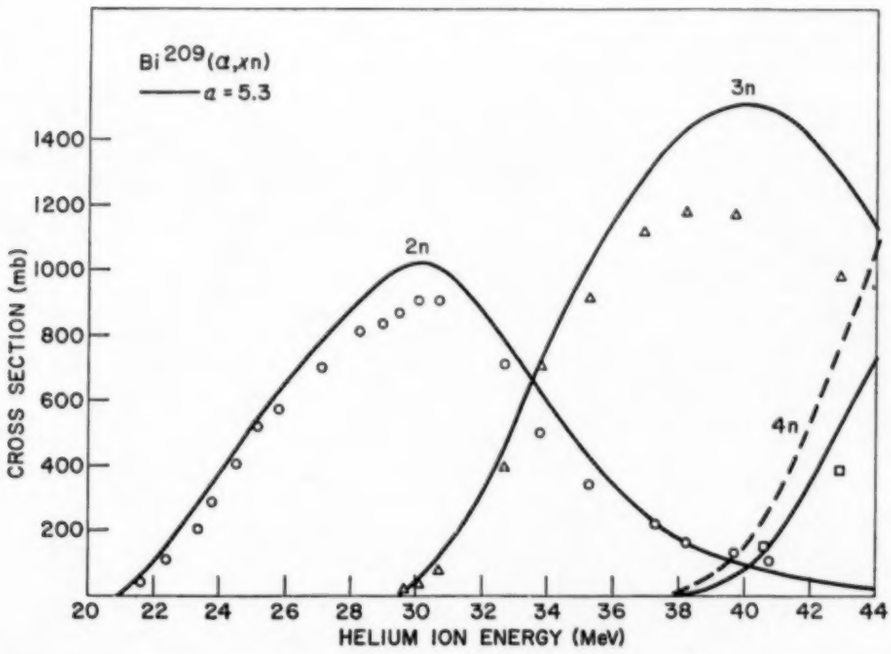

Fig. 4. Experimental [15]) and calculated excitation functions for $Bi^{209}(\alpha, xn)$ reactions. The solid line curves were calculated with a level density depending on the square root of the excitation energy. The dashed curve is the constant temperature prediction for the (α, 4n) reaction when the nuclear temperature is chosen to fit the (α, 2n) reaction.

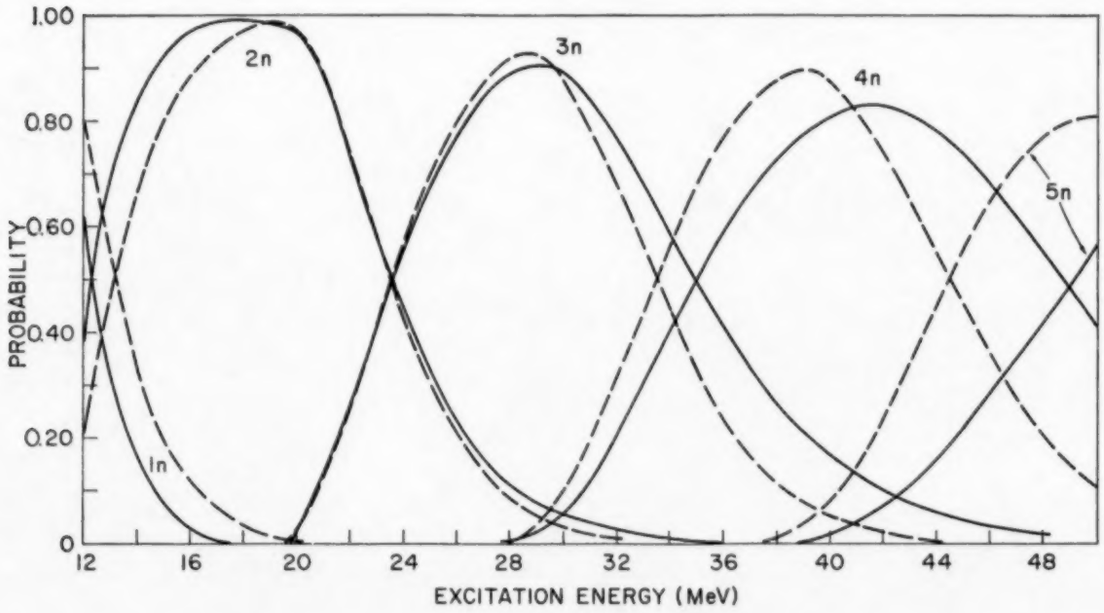

Fig. 5. Theoretical emission probabilities comparing the prediction of the two level density laws. The solid line curves are the prediction of the degenerate Fermi gas level density law with $a = 5.3$. The dashed-line curves are the predictions of the constant temperature model where the temperature was chosen to match the degenerate Fermi gas law prediction in the region between two and three neutrons emitted ($T = 1.35$ MeV).

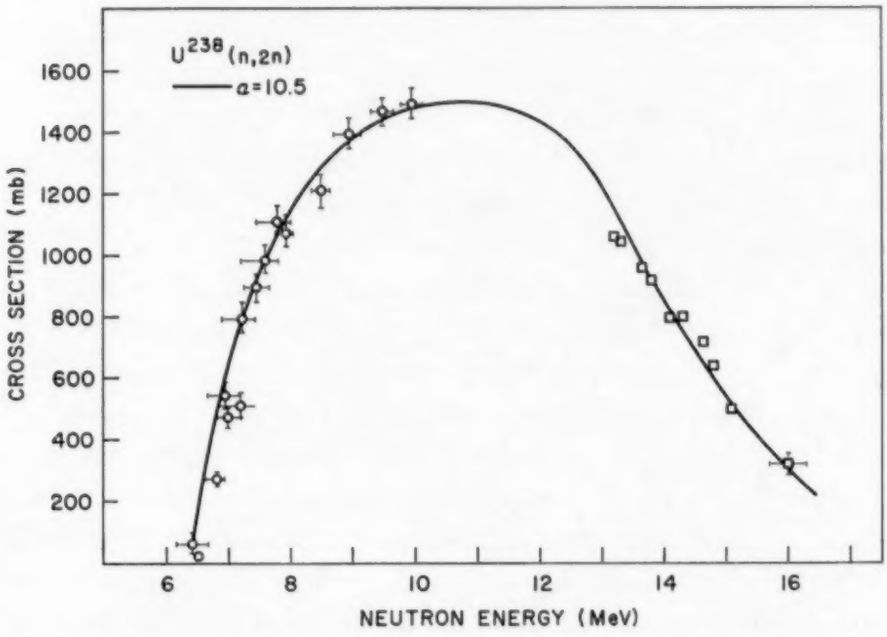

Fig. 6. Experimental [16, 17]) and calculated excitation functions for the U^{238}(n, 2n) reaction. The solid curve is that given by the Fermi gas law with $a = 10.5$.

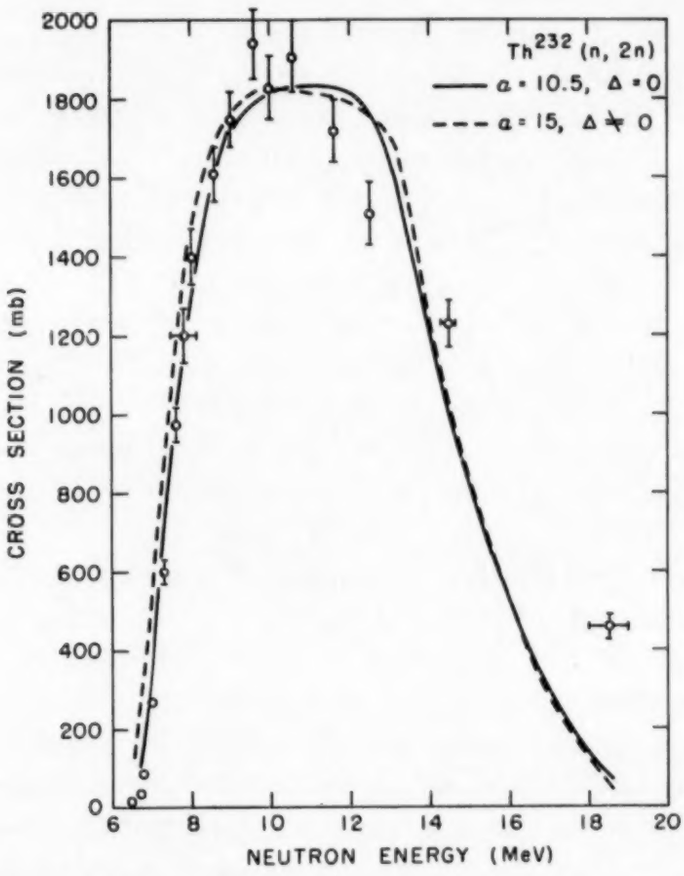

Fig. 7. Experimental [18]) and calculated excitation functions for the Th^{232}(n, 2n) reaction. The solid curve is for a level density given by eq. (3) with $a = 10.5$. The dashed line is for a level density given by eq. (5) with $a = 15$ and $\Delta = 0.57$ MeV for Th^{232} and Th^{230} and $\Delta = 0$ for Th^{231}.

relative probabilities for emitting various numbers of neutrons, so that unless one restricts oneself to examining cross section ratios, one must know the total reaction cross section. We have used the optical model reaction cross sections of Igo [12]) for alpha particles and of Beyster *et al.* [13]) for neutrons. Figs. 2 and 3 show a comparison of the Monte Carlo calculations with the experimental data of John [14]) for helium ion induced reactions in Pb^{206} and Pb^{208}. The solid lines were calculated using values of the level density parameter a (eq. (3)) of 5.1 and 4.9, respectively. A similar comparison for the excitation function data of Ramler *et al.* [15]) for Bi^{209} is shown in fig. 4, where a level density parameter a of 5.3 was used. The discrepancies between the experimental data and the calculations arise from the failure of the total reaction cross sections to match the observed total (neutron emission) cross sections rather than failure of the evaporation theory. If one takes the constant temperature level density law (eq. (2)) rather than eq. (3), and chooses a nuclear temperature which matches the (α, 2n) Monte Carlo calculations, one predicts (α, 4n) cross sections indicated by the dashed curves in figs. 2—4. In all cases the experimental data seem to favour a nuclear temperature dependent on the square root of the excitation energy rather than the constant temperature law. The predicted shifts in the peaks of the curve become more pronounced as the excitation energy is increased, as can be seen in fig. 5.

The only other data available in the heavy element region of comparable accuracy are a U^{238}(n, 2n) excitation function [16, 17]) and a Th^{232} (n, 2n) excitation function [18]). The fit to these data, with a level density parameter a of 10.5 (solid line) is shown in figs. 6 and 7. Because of fission competition which reduces the absolute value of the observed cross section, the calculations have been normalized to the experimental data, assuming the competition between neutron emission and fission to be independent of excitation energy. Fig. 8 shows the predicted U^{238}(α, 4n) excitation function for the same values of a (solid line) and T (dashed line) which fit the U^{238}(n, 2n) excitation function. Although the experimental data [19, 20]) are not extensive for the U^{238}(α, 4n) excitation function, the degenerate Fermi gas model prediction seems to be supported again.

The values of the level density parameter a determined in this work are listed in the second column of table 1. The values of a determined for targets in the closed shell region are much less than one would expect from the theoretically predicted proportionality to the mass number A.

A few investigations of variations resulting from taking pairing and shell corrections (Δ in eq. (5)) into account were performed. The reference surface from which one measures Δ is somewhat arbitrary, but the usual procedure is to use a reference surface which results in positive Δ for even and closed shell nuclei. Thus a positive Δ in eq. (5) is equivalent to saying there are no nuclear levels which can be populated until the energy Δ above the true ground state.

(Of course this is not strictly true in nature—there is at least always the ground state).

Since Th^{232} and U^{238} are far away from closed shells, Δ values for this region

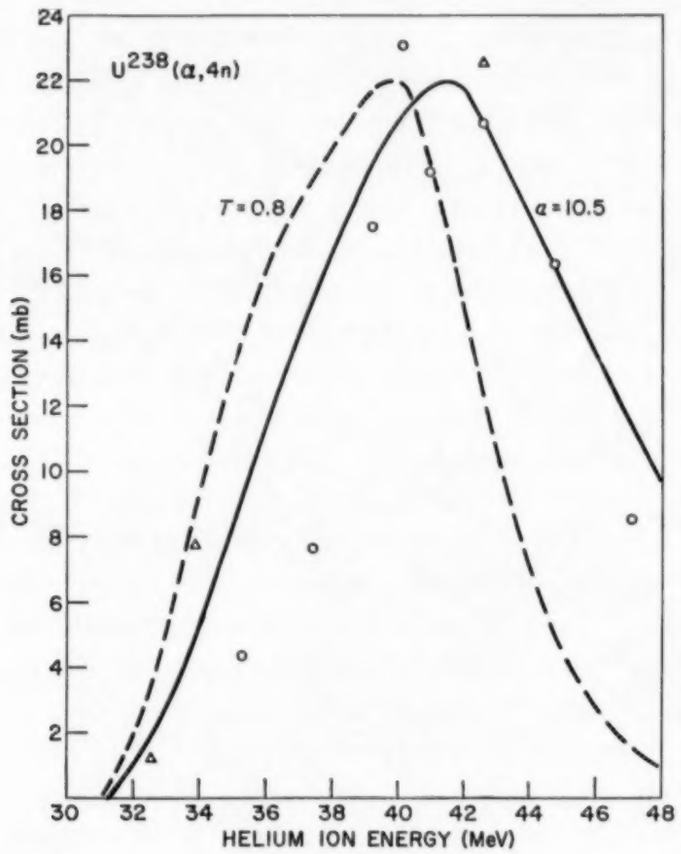

Fig. 8. Experimental points of Wing *et al.* [19]) (triangles) and Coleman [20]) (circles) and calculated excitation functions for the $U^{238}(\alpha, 4n)$ reaction. The solid curve is the prediction of the Fermi gas law using the value of the parameter a which gave the best fit to the $U^{238}(n, 2n)$ excitation function. The dashed curve is the prediction of the constant temperature model using a temperature of 0.8 MeV which gave the best fit to the $U^{238}(n, 2n)$ excitation function.

TABLE 1

Values of the level density parameter a (eq. (3)) determined by fitting experimental excitation function data

Target nucleus	a (MeV^{-1})	
	$\Delta = 0$	$\Delta \neq 0$
Pb^{206}	5.1±0.5	
Pb^{208}	4.9±0.5	
Bi^{209}	5.3±0.5	(see text)
Th^{232}	10 ±2	14±3
U^{238}	10.5±1	14±3

The errors listed refer only to the range of a values which would produce a satisfactory fit to the data, and do not include uncertainties arising from assumptions made in the model.

were deduced from the average difference between the even and odd-neutron mass surface [21]), yielding $\Delta = 0$ for odd-neutron nuclei and $\Delta = 0.57$ MeV for even nuclei. It was found that one could now fit the excitation functions in the region away from closed shells by values of the level density parameter a which are approximately 30 % larger than for the case when $\Delta = 0$ The values of a deduced are shown in the third column of table 1, and in fig. 7 a calculated excitation function is illustrated. In the lead-bismuth region of the periodic table, shell effects are very important and it becomes more difficult to define the reference surface. Ideally one might take as a reference the surface which would be expected for odd-neutron nuclei with no shell effects. Shell effects would then give positive Δ values for even, odd-proton and perhaps also odd nuclei. To investigate the interaction of Δ and a values in the closed shell region, we chose a to be 12, similar to the values obtained away from closed shells, and searched for Δ values which would reproduce the $Bi^{209}(\alpha, xn)$ excitation function about as well as $a = 5.3$ and $\Delta = 0$. The Δ values obtained are: At^{212}, $\Delta = 1.6$; At^{211}, $\Delta = 2.3$; At^{210}, $\Delta = 1.9$; At^{209}, $\Delta = 1.8$. This choice of Δ values with $a = 12$ is not unique, demonstrating that deduction of level density parameters from excitation functions for nuclei near closed shells is difficult. However, if charged particle emission is probable and their excitation functions are known, one is in a better position to find a unique fit.

It is interesting to note that a few calculations were performed with negative Δ values, that is, the reference surface was lowered to that of even nuclei so that the level density of odd-mass nuclei starts at a higher value than that of even nuclei. In this case there is no longer a gap where no levels are assumed to be present, so that the effect on a is much less. Due to a more subtle effect arising from a change in the ratio of the level density at different excitation energies, the use of negative values still leads to a slight increase in the parameter a.

The authors are indebted to Gerald Duffy for programming this problem for the computer.

References

1) V. F. Weisskopf, Lecture series in nuclear physics, MDDC **1175** (U. S. Government Printing Office, Washington D.C., 1947)
2) H. Hurwitz, Jr., and H. A. Bethe, Phys. Rev. **81** (1951) 898
3) D. L. Livesey, Can. J. Phys. **33** (1955) 391
4) Fulbright, Lassen and Poulson, Mat. Fys. Medd. Dan. Vid. Selsk. **31**, No. 10 (1959)
5) Eisberg, Igo and Wegner, Phys. Rev. **100** (1955) 309
6) A. Zucker, Nuclear Physics **6** (1958) 420
7) T. Ericson, Nuclear Physics **11** (1959) 489
8) F. Paul Brady and R. Sherr, Bull. Am. Phys. Soc. **5** (1960) 249
9) I. Dostrovsky, Z. Fraenkel and G. Friedlander, Phys. Rev. **116** (1959) 683
10) J. D. Jackson, Can. J. Phys. **34** (1955) 391

11) H. Kahn, AECU-3259 April 19 (1954) p. 10ff
12) G. Igo, Phys. Rev. **115** (1959) 1665
13) R. G. Schrandt, J. R. Beyster, M. Walt and E. W. Salmi, LA-2099 (1957) unpublished
14) W. John, Jr., Phys. Rev. **103** (1956) 704
15) W. J. Ramler, J. Wing, D. J. Henderson and J. R. Huizenga, Phys. Rev. **114** (1959) 154
16) J. D. Knight, R. K. Smith and B. Warren, Phys. Rev. **112** (1958) 259
17) Graves, Connor, Ford and Warren, unpublished data quoted in ref. [16])
18) J. P. Butler and D. C. Santry, Can. J. Chem. (in press)
19) J. Wing, W. J. Ramler, A. L. Harkness and J. R. Huizenga, Phys. Rev. **114** (1959)163
20) J. A. Coleman, UCRL-8186 (1958), unpublished
21) B. M. Foreman, Jr. and G. T. Seaborg, J. Inorg. Nucl. Chem. **7** (1958) 305

1.C

Nuclear Physics **25** (1961) 522—528; © *North-Holland Publishing Co., Amsterdam*

Not to be reproduced by photoprint or microfilm without written permission from the publisher

ON THE DEGENERACY OF THE SUPERCONDUCTIVE STATE

P. MITTELSTAEDT

Max-Planck-Institut für Physik und Astrophysik, München

Received 16 January 1961

Abstract: The ground state of the BCS theory is investigated in the limit of infinite volume. Using a theorem of Bogoljubov it is shown that the energy density of the ground state can be obtained exactly using either states degenerate with respect to the gauge transformation or a state with a fixed number of particles.

1. General Formalism

To describe a Fermion many-body system we use the second quantization formalism. The creation and annihilation operators of a Fermi particle with momentum $\mathbf{k}$ and spin up ($\uparrow$), and with momentum $-\mathbf{k}$ and spin down, ($\downarrow$) respectively, are designated by

$$a_{\mathbf{k}}^{\dagger} = a_{\mathbf{k}\uparrow}^{\dagger}, \quad a_{\mathbf{k}} = a_{\mathbf{k}\uparrow}, \quad b_{\mathbf{k}}^{\dagger} = a_{-\mathbf{k}\downarrow}^{\dagger}, \quad b_{\mathbf{k}} = a_{-\mathbf{k}\downarrow}.$$

The commutation relations are

$$[a_{\mathbf{k}}, a_{\mathbf{k}'}]_+ = [a_{\mathbf{k}}^{\dagger}, a_{\mathbf{k}'}^{\dagger}]_+ = 0, \quad [a_{\mathbf{k}}^{\dagger}, a_{\mathbf{k}'}] = \delta_{\mathbf{k}\mathbf{k}'},$$
$$[b_{\mathbf{k}}, b_{\mathbf{k}'}]_+ = [b_{\mathbf{k}}^{\dagger}, b_{\mathbf{k}'}^{\dagger}]_+ = 0, \quad [b_{\mathbf{k}}^{\dagger}, b_{\mathbf{k}'}] = \delta_{\mathbf{k}\mathbf{k}'}.$$

The operator of the number of particles is

$$N = \sum_{\mathbf{k}} (a_{\mathbf{k}}^{\dagger} a_{\mathbf{k}} + b_{\mathbf{k}}^{\dagger} b_{\mathbf{k}}) = \sum_{\mathbf{k}} N_{\mathbf{k}}.$$

The bare vacuum state $|\,\rangle$ is defined by

$$a_{\mathbf{k}}|\rangle = b_{\mathbf{k}}|\rangle = 0.$$

We are discussing here the BCS Hamiltonian [1, 2])

$$H_{\mathrm{BCS}} = \sum_{\mathbf{k}} E(\mathbf{k})(a_{\mathbf{k}}^{\dagger} a_{\mathbf{k}} + b_{\mathbf{k}}^{\dagger} b_{\mathbf{k}}) + \frac{1}{2\Omega} \sum_{\mathbf{k}\mathbf{k}'} I(\mathbf{k}, \mathbf{k}') a_{\mathbf{k}'}^{\dagger} b_{\mathbf{k}'}^{\dagger} a_{\mathbf{k}} b_{\mathbf{k}},$$

where Ω is the volume, $I(\mathbf{k}, \mathbf{k}')$ the interaction and $E(\mathbf{k})$ the kinetic energy of a particle with momentum $\mathbf{k}$.

For the discussion of this Hamiltonian it has been found to be useful not to introduce the particle-conserving subsidiary condition

$$\sum_{\mathbf{k}} (a_{\mathbf{k}}^{\dagger} a_{\mathbf{k}} + b_{\mathbf{k}}^{\dagger} b_{\mathbf{k}}) = N_0,$$

where N_0 is the total number of particles, but to replace H_{BCS} by

$$H = H_{\mathrm{BCS}} - \lambda N,$$

where λ is a Lagrangian multiplier determined by the condition that the expectation value $\bar{N}$ of N is

$$\bar{N} = N_0.$$

Using $\varepsilon(\mathbf{k}) = E(\mathbf{k}) - \lambda$, we get

$$H = \sum_{\mathbf{k}} \varepsilon(\mathbf{k})(a_{\mathbf{k}}^{\dagger} a_{\mathbf{k}} + b_{\mathbf{k}}^{\dagger} b_{\mathbf{k}}) + \frac{1}{2\Omega} \sum_{\mathbf{k}\mathbf{k}'} I(\mathbf{k}, \mathbf{k}') a_{\mathbf{k}'}^{\dagger} b_{\mathbf{k}'}^{\dagger} a_{\mathbf{k}} b_{\mathbf{k}}.$$

The ground state of this Hamiltonian and its energy are designated by $|0\rangle$ and E, respectively, so that

$$H|0\rangle = E|0\rangle.$$

We now introduce new creation and annihilation operators $\alpha_{\mathbf{k}}^{+}$, $\beta_{\mathbf{k}}^{+}$ and $\alpha_{\mathbf{k}}$, $\beta_{\mathbf{k}}$ by the canonical transformation [2, 3]),

$$\alpha_{\mathbf{k}} = u_{\mathbf{k}} a_{\mathbf{k}} - v_{\mathbf{k}} b_{\mathbf{k}}^{\dagger}, \quad a_{\mathbf{k}} = u_{\mathbf{k}} \alpha_{\mathbf{k}} + v_{\mathbf{k}} \beta_{\mathbf{k}}^{\dagger},$$
$$\beta_{\mathbf{k}} = v_{\mathbf{k}} a_{\mathbf{k}}^{\dagger} + u_{\mathbf{k}} b_{\mathbf{k}}, \quad b_{\mathbf{k}} = u_{\mathbf{k}} \beta_{\mathbf{k}} - v_{\mathbf{k}} a_{\mathbf{k}}^{\dagger},$$

where $u_{\mathbf{k}}$ and $v_{\mathbf{k}}$ are real numbers which satisfy the condition

$$u_{\mathbf{k}}^2 + v_{\mathbf{k}}^2 = 1.$$

The generator of this transformation is

$$T(u, v) = \mathrm{e}^{iS}, \quad S = -i \sum_{\mathbf{k}} \theta_{\mathbf{k}} (a_{\mathbf{k}}^{\dagger} b_{\mathbf{k}}^{\dagger} - b_{\mathbf{k}} a_{\mathbf{k}}),$$

where

$$\cos \theta_{\mathbf{k}} = u_{\mathbf{k}}, \quad \sin \theta_{\mathbf{k}} = v_{\mathbf{k}}.$$

The new particles are usually called quasi-particles. The operator of the number of quasi-particles is

$$n = \sum_{\mathbf{k}} n_{\mathbf{k}} = \sum_{\mathbf{k}} (\alpha_{\mathbf{k}}^{\dagger} \alpha_{\mathbf{k}} + \beta_{\mathbf{k}}^{\dagger} \beta_{\mathbf{k}}).$$

The vacuum state of the quasi-particles, the quasivacuum $|q\rangle$.

$$|q\rangle = \mathrm{e}^{iS}|\,\rangle = \prod_{\mathbf{k}} (u_{\mathbf{k}} + v_{\mathbf{k}} a_{\mathbf{k}}^{\dagger} k_{\mathbf{k}}^{\dagger})|\,\rangle,$$

where

$$a_{\mathbf{k}}|q\rangle = \beta_{\mathbf{k}}|q\rangle = 0.$$

If we use also for the quasivacuum state the condition

$$\langle q|N|q\rangle = 2 \sum_{\mathbf{k}} v_{\mathbf{k}}^2 = N_0,$$

the standard deviation of real particles in this state is

$$\langle q|N|q\rangle^2 - \langle q|N^2|q\rangle = cN_0,$$

where c is the number

$$c = \frac{4}{\rho(2\pi)^3}\int \mathrm{d}\mathbf{k} v^4(\mathbf{k})$$

and $\rho = N_0/\Omega$ is the density of particles.

To transform the Hamiltonian H we use the normal product of a bilinear operator R with respect to the state $|q\rangle$,

$$R = :R: + \langle q|R|q\rangle.$$

Then we write $H = H_0 + H_1$, where

$$H_1 = \frac{1}{2\Omega}\sum_{\mathbf{k}\mathbf{k}'} I(\mathbf{k},\mathbf{k}') :a_{\mathbf{k}}^\dagger b_{\mathbf{k}'}^\dagger: :a_{\mathbf{k}} b_{\mathbf{k}}:$$

and H_0 is a quadratic form in the Fermion operators. Therefore the coefficients $u_{\mathbf{k}}$, $v_{\mathbf{k}}$ can be chosen such that H_0 is diagonal, i.e.

$$H_0 = E_0 + \sum_{\mathbf{k}} \eta_{\mathbf{k}}(\alpha_{\mathbf{k}}^\dagger \alpha_{\mathbf{k}} + \beta_{\mathbf{k}}^\dagger \beta_{\mathbf{k}}).$$

The quasivacuum state is then the ground state of H_0 and

$$H|q\rangle = E_0|q\rangle.$$

For the following investigations we introduce the gauge transformation

$$a_{\mathbf{k}} \to a_{\mathbf{k}} \mathrm{e}^{-i\varphi}, \qquad b_{\mathbf{k}} \to b_{\mathbf{k}} \mathrm{e}^{-i\varphi},$$
$$a_{\mathbf{k}}^\dagger \to a_{\mathbf{k}}^\dagger \mathrm{e}^{+i\varphi}, \qquad b_{\mathbf{k}}^\dagger \to b_{\mathbf{k}}^\dagger \mathrm{e}^{+i\varphi},$$

with the generator

$$G(\varphi) = \mathrm{e}^{iN\varphi}.$$

This gauge transformation does not commute with the canonical transformation $T(u, v)$ discussed above. The product of these transformations,

$$T(u, v; \varphi) = G(\varphi)T(u, v)G^{-1}(\varphi),$$

is again a canonical transfromation $T(u, v)$, where the real $v(\mathbf{k})$ is replaced by the complex variable $v(\mathbf{k})\mathrm{e}^{2i\varphi}$, and the subsidiary condition is replaced by

$$u_{\mathbf{k}}^2 + |v_{\mathbf{k}}|^2 = 1.$$

The parameter φ is not determined by the diagonalization of H_0 and is therefore a free parameter in H_0 and in the state $|q\rangle$. The total Hamiltonian is invariant under this gauge transformation

$$[H, G] = 0,$$

but it is not necessary that the ground state $|0\rangle$ be an eigenstate of G.

The decomposition of H into H_0+H_1 is not gauge invariant, for

$$[H_0, G] \neq 0, \quad [H_1, G] \neq 0,$$

and the quasivacuum state is not an eigenstate of G. This can be seen from the explicit formula

$$|q_\varphi\rangle = G(\varphi)|q\rangle = \prod_{\mathbf{k}} (u_{\mathbf{k}} + v_{\mathbf{k}} e^{2i\varphi} a_{\mathbf{k}}^\dagger b_{\mathbf{k}}^\dagger)|\,\rangle.$$

Using the canonical transformation T we obtain

$$|q_\varphi\rangle = G(\varphi)T(u, v)|\,\rangle.$$

2. The Limit of infinite Volume

The limit of infinite volume is of particular interest, for the following theorem has been proved recently by Bogoljubov [4]):

$$\lim_{\Omega\to\infty} \{\langle q|H|q\rangle - \langle 0|H|0\rangle\} = l, \tag{1}$$

where l is a finite positive number independent of Ω. On the other hand, it is easily seen that

$$\langle q|H_1|q\rangle = -d^2, \quad \langle q|H_1{}^2|q\rangle = +c^2,$$

where d^2 and c^2 are numbers independent of Ω. Therefore it follows that the difference

$$H|q\rangle - E|q\rangle = (E_0 - E + H_1)|q\rangle,$$

has a finite norm in the limit of infinite volume:

$$\lim_{\Omega\to\infty} |H|q\rangle - E|q\rangle|^2 = l^2 + c^2 - 2ld^2. \tag{2}$$

If we consider the finite quantities H/Ω and E/Ω instead of H and E, we see that

$$\lim_{\Omega\to\infty} \left| \frac{H}{\Omega}|q\rangle - \frac{E}{\Omega}|q\rangle \right|^2 = 0. \tag{3}$$

This means that the Schrödinger equation for the ground state energy E is satisfied asymptotically even by the quasivacuum state $|q\rangle$. Furthermore it follows, since the gauge transformation operator $G(\varphi)$ is unitary, that the same relation holds for any state

$$|q_\varphi\rangle = G(\varphi)|q\rangle,$$

i.e.

$$\lim_{\Omega\to\infty} \left| \frac{H}{\Omega}|q_\varphi\rangle - \frac{E}{\Omega}|q_\varphi\rangle \right|^2 = 0. \tag{4}$$

Therefore it seems that the ground state of H is asymptotically degenerate with respect to the operator $G(\varphi)$. The states $|q_\varphi\rangle$ are not eigenstates of the particle number N but satisfy the subsidiary condition $\langle q_\varphi|N|q_\varphi\rangle = N_0$. Furthermore, we shall show that the important relation (3) is also valid for a state having a well-defined number of particles and which is an element of the closed linear manifold $\{q_\varphi\}$, formed by the states $|q_\varphi\rangle$.

For this purpose, we decompose the quasivacuum state

$$|q\rangle = \prod_{\mathbf{k}} u_{\mathbf{k}} \prod_{\mathbf{k}} (1+\varepsilon_{\mathbf{k}}),$$

where $\varepsilon_{\mathbf{k}} = (v_{\mathbf{k}}/u_{\mathbf{k}}) a_{\mathbf{k}}^\dagger b_{\mathbf{k}}^\dagger$ into a sum of states with a fixed number of particles. This gives

$$\begin{aligned} |q\rangle &= \prod_{\mathbf{k}} u_{\mathbf{k}} (1 + \sum_i \varepsilon_i + \sum_{i<\mathbf{k}} \varepsilon_i \varepsilon_{\mathbf{k}} + \ldots)|\rangle \\ &= |q_0\rangle + |q_2\rangle + |q_4\rangle + \ldots . \end{aligned}$$

The states $|q_0\rangle$, $|q_2\rangle$, $|q_4\rangle$ are eigenstates of N with the eigenvalues 0, 2, 4, respectively. On account of the relation $\varepsilon_{\mathbf{k}}^2 = 0$ we can write the states $|q_{2N}\rangle$ in a more compact form,

$$|q_{2N}\rangle = \prod_{\mathbf{k}} u_{\mathbf{k}} \frac{1}{N!} (\sum_{\mathbf{k}} \varepsilon_{\mathbf{k}})^N |\,\rangle .$$

The norm of these states is

$$\langle q_{2N}|q_{2N}\rangle = \prod_{\mathbf{k}} u_{\mathbf{k}}^2 \sum_{\mathbf{k}_1 \langle \mathbf{k}_2 \langle \ldots \langle \mathbf{k}_N} \frac{v^2(\mathbf{k}_1) v^2(\mathbf{k}_2) \ldots v^2(\mathbf{k}_N)}{u^2(\mathbf{k}_1) u^2(\mathbf{k}_2) \ldots u^2(\mathbf{k}_N)} .$$

If we introduce the projection operator

$$P_{N'} = \frac{1}{2\pi} \int_0^{2\pi} \mathrm{e}^{i(N-N')\varphi} \, \mathrm{d}\varphi ,$$

which projects onto the state with the particle number N', we obtain

$$P_N|q\rangle = |q_N\rangle = \frac{1}{2\pi} \int_0^{2\pi} \mathrm{e}^{-iN\varphi} |q_\varphi\rangle \mathrm{d}\varphi$$

and

$$\langle q_N|q_N\rangle = \langle q P_N q\rangle .$$

Instead of the state $|q_N\rangle$, we use here the normalized states

$$|N\rangle = \frac{1}{C_N} P_N|q\rangle$$

with $\langle N|N\rangle = 1$ and $C_N^2 = \langle q P_N q\rangle$. The state $|N\rangle$ is a normalized eigenstate of N, and is an element of the closed linear manifold $\{q_\varphi\}$.

Using the definition

$$(H-E)|q\rangle = |\delta\rangle,$$

we obtain

$$H|N\rangle - E|N\rangle = \frac{1}{C_N} P_N|\delta\rangle$$

and

$$|H|N\rangle - E|N\rangle|^2 = \frac{\langle\delta|P_N|\delta\rangle}{\langle q|P_N|q\rangle}. \tag{5}$$

To prove the relation (3) for the states $|N\rangle$ we must discuss the right-hand side of (5) in the limit of infinite volume. We shall see, that in this limit relation (3) is valid not only for the special state $|N_0\rangle$ but for any state $|N\rangle$ with a particle number N which is not too far from the average value N_0.

1) N is a finite number. If $N_0 = \langle q|N|q\rangle$ is the mean value of particles in the state $|q\rangle$, and the density $\rho = N_0/\Omega$ is a Ω-independent number, we obtain the asymptotic formulas for large Ω,

$$\langle q|P_{2N}|q\rangle \sim \alpha\Omega^N e^{-\gamma\Omega}, \quad \langle\delta|P_{2N}|\delta\rangle \sim \beta\Omega^{N+2}e^{-\gamma\Omega},$$

where α, β, γ are Ω independent numbers. Therefore the right-hand side of (5) is asymptotically proportional to Ω^2 and relation (3) cannot be proved for the state $|N\rangle$.

2) The distribution of particles in the state $|q\rangle$ is such that the standard deviation is proportional to $\sqrt{N_0}$. Therefore the coefficients $C_N{}^2 = \langle q|P_N|q\rangle$, for values of N, which are not too far from the average value N_0, are of the order of magnitude $N_0{}^{-\frac{1}{2}}$. If we use states $|N\rangle$ which have this property, we obtain asymptotically

$$|H|N\rangle - E|N\rangle|^2 \sim \text{const.}\,\langle\delta|P_N|\delta\rangle\sqrt{\Omega}.$$

The value of $\langle\delta|P_N|\delta\rangle$ is bounded for large Ω because

$$\langle\delta|P_N|\delta\rangle \leqq \langle\delta|\delta\rangle,$$

and because $\langle\delta|\delta\rangle$ is bounded for large Ω according to (2). Therefore we obtain

$$\lim_{\Omega\to\infty}\left|\frac{H}{\Omega}|N\rangle - \frac{E}{\Omega}|N\rangle\right|^2 = 0.$$

In the limit of infinite volume the mean value N_0 becomes infinite, and because of its definition the eigenvalue N of the state $|N\rangle$ also becomes infinite; relation (6) shows that the only relevant result which can be derived in the limit of infinite volume, i.e. relation (3), may be obtained either with the states $|q_\varphi\rangle$, with an indeterminate number of particles, or with a state $|N\rangle$, which is an eigenstate of N and $G(\varphi)$.

The author is greately indebted to Professor Garsiorowicz, Professor Lüders, Professor Heisenberg, Dr. Mitter and Dr. Yamazaki for many stimulating discussions.

References

1) J. Bardeen, L. N. Cooper and J. R. Schrieffer, Phys. Rev. **108** (1957) 1175
2) J. G. Valatin, Nuovo Cim. **7** (1958) 843
3) N. N. Bogoljubov, V. V. Tolmochov and D. V. Schirkov, A new method in the theory of superconductivity (New York, 1960)
4) N. N. Bogoljubov, Report at the Utrecht Conference on the many-body problem (June 1960), private communication by K. Yamazaki

1.C

Nuclear Physics **25** (1961) 529—567; © *North-Holland Publishing Co., Amsterdam*

Not to be reproduced by photoprint or microfilm without written permission from the publisher

FORMULATION DE LA MÉCANIQUE STATISTIQUE EN TERMES DE NOMBRES D'OCCUPATION (I)

ROGER BALIAN, CLAUDE BLOCH et CYRANO DE DOMINICIS

Centre d'Études Nucléaires de Saclay, Gif-sur-Yvette (S. et O.)

Reçu le 16 Janvier 1961

Abstract: The perturbation expansions of the Gibbs potential and the propagators at finite temperature are put into a new form by means of an algebraic theorem on creation and annihilation operators. The new diagrams are made of subdiagrams having exactly the same structure as the ground state diagrams (the "anomalous" diagrams having disappeared). These subdiagrams play a part analogous to the self-energy insertions in field theory, and their explicit summation can be carried out in a time-dependent formulation. It leads to the replacement in the expansions of the unperturbed statistical factors f_m^- by new factors $\mathscr{F}_m^-$ which can be interpreted as the true occupation numbers. A general argument based on the topological structure of the diagrams shows that the expansion thus obtained for the Gibbs potential is stationary with respect to variations of the $\mathscr{F}_m$. The formulation presented here leads to an elimination of the activity e^{α}. It appears therefore as a generalization of the classical virial expansion.

1. Introduction et Résumé

Les développements dans la théorie des perturbations des grandeurs thermodynamiques pour un système de particules en interaction ne prennent une forme simple que lorsque l'on considère un système grand canonique, ce qui conduit à exprimer par exemple l'équation d'état sous forme paramétrique en fonction de l'activité e^{α}. Cette quantité n'apparaît, dans la contribution de chacun des diagrammes représentant les développements, que dans les facteurs statistiques associés aux lignes de ces diagrammes. Le facteur f_m^- associé à une ligne descendante relative à l'état m s'interprète comme le nombre d'occupation de l'état m dans le système grand canonique non perturbé. De la même façon que dans l'établissement du développement du viriel pour un système classique inhomogène [1]), nous allons remplacer grâce à une sommation partielle [2,3]) chaque facteur statistique f_m^-, qui contient la dépendance par rapport à α, par le nombre d'occupation vrai $\bar{n}_m$, qui jouera ici le même rôle que la densité locale dans le développement du viriel. Le nombre total de particules, qui dans la formulation primitive était donné par une somme de termes associés à une infinité de diagrammes, s'exprime alors simplement comme la somme des nombres d'occupation vrais.

Parallèlement, bien que le développement du potentiel de Gibbs [4]) présente dans le cas des fermions de grandes analogies avec le développement de l'énergie

de l'état fondamental [5, 6]), il contient les contributions de toute une série de diagrammes, dits „anormaux", qui n'ont pas d'équivalent dans le développement de l'énergie de l'état fondamental, et qui jouent un rôle important dans le passage à la limite de la température nulle [3, 7, 8]). Les seuls termes de l'expression initiale du nombre de particules du système qui contiennent explicitement l'interaction sont en fait associés à des diagrammes anormaux, et l'élimination de ceux-ci sera un trait essentiel à la fois du problème de la limite de la température nulle et de celui de l'élimination de α. Ces diagrammes sont caractérisés par le fait qu'ils comprennent des lignes de trous ayant identiquement même impulsion (et même spin) que des lignes de particules, en vertu de la conservation de l'impulsion (et du spin) pour un système infini. Ces diagrammes contiennent donc des parties de self-énergie et il est naturel de considérer, comme en théorie des champs, que tout diagramme résulte de l'insertion de parties de self-énergie dans un diagramme squelette. Luttinger et Ward [9]) ont appliqué cette méthode à la représentation du développement du potentiel de Gibbs en termes de propagateurs non perturbés, analogue à la représentation énergie-impulsion en théorie des champs. Le potentiel de Gibbs prend alors la forme d'un développement ne faisant intervenir que des diagrammes squelettes sans partie de self-énergie, le facteur associé à chaque ligne étant maintenant le propagateur complet. L'expression ainsi obtenue est stationnaire par rapport aux variations des facteurs associés aux lignes.

Ce développement est bien adapté à l'étude de la limite de la température nulle. Cependant, pour les problèmes de mécanique statistique à température non nulle, il est préférable, dans l'application de la méthode des diagrammes squelettes, d'utiliser une représentation faisant intervenir des grandeurs plus simples à interpréter que les propagateurs, et d'éviter ainsi la sommation sur les variables d'énergie des propagateurs complets. C'est ainsi que Lee et Yang [10]) ont effectué la sommation des insertions dans les diagrammes représentant le développement du potentiel de Gibbs en puissances de l'activité e^{α}. Le potentiel de Gibbs prend alors la forme d'un développement ne faisant intervenir que des diagrammes squelettes, le facteur associé à chaque ligne étant cette fois directement relié au nombre d'occupation $\bar{n}_m$ de l'état correspondant. Ce facteur est en effet $e^{\alpha}(1+\bar{n}_m)$ pour des bosons ou $e^{\alpha}(1-\bar{n}_m)$ pour des fermions. Ici encore, l'expression du potentiel de Gibbs est stationnaire.

Dans notre formulation, c'est le nombre d'occupation $\bar{n}_m$ lui-même qui sera le facteur associé à chaque ligne [2, 3]). Le potentiel de Gibbs, et plus généralement toutes les fonctions intervenant en mécanique statistique, telles que le propagateur, s'exprimeront comme des développements représentés simplement par des diagrammes „normaux" et faisant intervenir seulement les nombres d'occupation vrais $\bar{n}_m$ et les éléments de matrice de l'interaction. La méthode employée est encore une méthode de sommation d'insertions dans des diagrammes squelettes, effectuée sur une nouvelle représentation en diagrammes

des développements en puissances de l'interaction. Cette représentation est d'abord établie, par une méthode purement algébrique qui remplace les diagrammes „anormaux" par des diagrammes composés de plusieurs parties dont chacune est un diagramme „normal" (§ 2). Ensuite, la sommation des insertions de ces diagrammes, effectuée dans une représentation dépendant du temps, remplace les nombres d'occupation non perturbés f_m^-, qui sont les facteurs associés aux lignes descendantes, par les nombres d'occupation vrais $\bar{n}_m$ (§ 3). L'expression obtenue pour le potentiel de Gibbs est ici encore stationnaire, et nous montrerons que cette propriété variationnelle générale a son origine dans la structure des diagrammes contenant des insertions et sur lesquels la sommation partielle est effectuée (§ 4).

Il faut souligner que les diagrammes anormaux sont ici éliminés à toute température et non pas seulement à la limite de la température nulle. Ce passage à la limite n'est cependant pas simple dans la formulation présentée ici pour des raisons qui seront indiquées au § 4.4.

L'expression de l'énergie libre en fonction des nombres d'occupation ne dépend pas explicitement du potentiel chimique α/β. Notre développement du potentiel de Gibbs en termes de nombres d'occupation peut donc être considéré comme une généralisation quantique du développement du viriel en mécanique statistique classique [1, 11]), vers lequel il tend d'ailleurs à la limite classique (§ 6).

Enfin, pour comprendre la signification physique des principes variationnels, il est intéressant de chercher l'interprétation des développements en fonction des nombres d'occupation $\bar{n}_m$, lorsqu'on y remplace chaque $\bar{n}_m$ par une variable arbitraire. Nous montrerons que la répartition statistique des nombres d'occupation à la température considérée s'exprime directement en fonction de ces développements, dont on peut par conséquent déduire tous les moments et corrélations des nombres d'occupation (§ 5).

Pour ne pas compliquer, nous nous restreindrons au cas d'un système dont l'interaction a des propriétés de conservation telles que l'état relatif à une ligne qui entre dans une partie de self-énergie soit le même que celui de la ligne qui en sort. Pour un tel système, le propagateur est diagonal, et la valeur moyenne du produit d'un opérateur de création par un opérateur d'annihilation est nulle s'ils ne sont pas relatifs au même état, et égale au nombre d'occupation s'ils le sont. Notre formulation est donc particulièrement adaptée au cas d'un système de volume infini.

Au § 2, nous exposons la méthode générale qui conduit à une nouvelle représentation en diagrammes pour les développements obtenus en théorie des perturbations.

Le calcul de l'insertion d'une ou de plusieurs parties de self-énergie (ou bulles) est compliqué par le fait que les facteurs f^+ ou f^- introduits par l'insertion dépendent de la position relative (dans le temps) de ces bulles les unes par rapport aux autres et par rapport au reste du diagramme. Pour trouver des

résultats simples, il est nécessaire de considérer les contributions des familles de diagrammes obtenus en croisant les lignes des insertions de toutes les façons possibles (§ 2.3.1). Le résultat le plus simple est alors obtenu dans le cas de bulles non enchevêtrées dans le temps qui est traité au § 2.3.2.

L'extension au cas de bulles quelconques est effectuée aux paragraphes 2.3.3 et 2.3.4 et dans l'appendice A, grâce à un théorème algébrique permettant le désenchevêtrement des bulles, c'est-à-dire le remplacement des bulles enchevêtrées dans le temps par de nouvelles entités, ou ,,bulles composées'', désenchevêtrées. Ces bulles composées peuvent contenir des parties de self-énergie, mais ne sont jamais de type anormal: les lignes identiquement relatives au même état y sont obligatoirement toutes montantes ou toutes descendantes.

On aboutit ainsi à la nouvelle représentation en diagrammes ,,désenchevêtrés'' ou diagrammes D, pour les développements du potentiel de Gibbs (§ 2.4) et du propagateur (§ 2.5).

Le paragraphe 3 est consacré à la sommation des insertions dans ces diagrammes, en considérant comme une insertion le fait d'adjoindre une bulle composée à un diagramme D.

On montre d'abord (§ 3.1) que la sommation de toutes les insertions possibles dans un diagramme squelette conduit à remplacer les facteurs statistiques $f_m^{\pm}$ associés aux lignes par de nouveaux facteurs $\mathscr{F}_m^{\pm}$. On démontre ensuite (§ 3.2) que le facteur $\mathscr{F}_m^{-}$ associé aux lignes descendantes es tle nombre d'occupation vrai $\bar{n}_m$.

La sommation des insertions est effectuée au § 3.3 pour le potentiel de Gibbs. Il apparaît ici une complication qui n'existe pas dans le cas des diagrammes ayant des lignes ouvertes: on ne peut en effet distinguer sans ambiguïté un squelette et des insertions dans un diagramme vide-vide. Cette difficulté est résolue grâce à une propriété très simple liée à la structure en arbre des diagrammes vide-vide contenant des insertions. Cette même propriété est à l'origine des propriétés variationnelles exposées au § 4.

On vérifie au § 4.1 que l'expression du potentiel de Gibbs est stationnaire par rapport aux variations des nombres d'occupation. L'expression de la fonction de corrélation calculée dans l'appendice C montre que cette valeur stationnaire est un minimum.

La généralité de l'argument employé au § 4.2 pour démontrer cette propriété de stationnarité explique pourquoi on la retrouve dans toutes les formulations, en fait complètement différentes, basées sur une sommation d'insertions dans des diagrammes squelettes vide-vide [1, 2, 8, 9, 10, 12]).

On exprime au § 4.3 l'énergie libre en fonction des nombres d'occupation, et on montre que dans la formulation variationnelle correspondante, le potentiel chimique α/β est éliminé.

Finalement, le § 5 et le § 6, qui feront l'objet d'un article ultérieur, seront respectivement consacrés le premier à l'étude de la répartition statistique des

nombres d'occupation, ce qui permet d'interpréter les résultats précédents, et le second au calcul de la limite classique, qui redonne le développement du viriel.

2. Nouvelle Forme des Développements en Puissances de l'Interaction du Potentiel de Gibbs et des Propagateurs

2.1. RAPPEL DU DÉVELOPPEMENT DU POTENTIEL DE GIBBS

Nous considérons un système de particules identiques dont nous écrivons l'hamiltonien sous la forme

$$H = H_0 + V,$$

avec

$$H_0 = \sum_m \varepsilon_m a_m^\dagger a_m, \tag{1}$$

$$V = \tfrac{1}{2} \sum_{rsmn} \langle rs|v|mn\rangle a_r^\dagger a_s^\dagger a_n a_m. \tag{2}$$

Les opérateurs de création et d'annihilation $a_m^\dagger$ et a_m satisfont aux relations de commutation

$$a_m a_n - \varepsilon a_n a_m = 0, \quad a_m a_n^\dagger - \varepsilon a_n^\dagger a_m = \delta_{mn},$$

où $\varepsilon = 1$ dans le cas des bosons et $\varepsilon = -1$ dans le cas des fermions.

Le développement, dans la théorie des perturbations dépendante du temps, du potentiel de Gibbs

$$A(\alpha, \beta) = -\frac{1}{\beta} \log \operatorname{Tr} e^{\alpha N - \beta H} \tag{3}$$

est donné [4]) par

$$A = A_0 - \frac{1}{\beta} \sum_{p=1}^{\infty} (-)^p \int_{\beta > u_1 > \ldots > u_p > 0} du_1 \ldots du_p \langle V(u_1) \ldots V(u_p)\rangle_c, \tag{4}$$

où

$$V(u) = e^{uH_0} V e^{uH_0},$$

et où A_0 est le potentiel de Gibbs du système de particules sans interaction décrit par H_0,

$$A_0 = -\frac{\varepsilon}{\beta} \sum_m \log f_m^+. \tag{5}$$

La contribution au développement (4) associée à chaque diagramme vide-vide connexe s'obtient en formant le produit des facteurs suivants:

(a) à chaque interaction est associé le facteur

$$\tfrac{1}{2} \langle rs|v|mn\rangle e^{u(\varepsilon_r + \varepsilon_s - \varepsilon_m - \varepsilon_n)}, \tag{6}$$

où u est l'instant auquel se produit l'interaction;

(b) à chaque ligne est associé un facteur f_m^- ou f_m^-, suivant qu'il s'agit d'une ligne de particule ou de trou, donné par

$$f_m^- = a_m^\dagger a_m = \frac{1}{e^{\beta\varepsilon_m - \alpha} - \varepsilon},$$
$$f_m^+ = a_m a_m^\dagger = \frac{1}{1 - \varepsilon e^{\alpha - \beta\varepsilon_m}} = 1 + \varepsilon f_m^- , \tag{7}$$

(rappelons qu'une ligne de longueur nulle doit être considérée comme une ligne de trou);

(c) chaque terme est affecté, en plus du signe $(-)^p$ figurant déjà dans (4), du signe ε^{h+l}, où h est le nombre de lignes de trous et l le nombre de boucles fermées.

Enfin, on effectue l'intégration sur les instants d'interaction ordonnés de 0 à β, et la sommation sur tous les états pour chacune des lignes.

Pour éviter toute difficulté de comptage, nous avons admis ici (d'où le facteur $\frac{1}{2}$ dans (6)) qu'on considérait comme distincts deux diagrammes qui ne diffèrent que par l'échange de r, m avec s, n dans une interaction $\langle rs|v|mn\rangle$, c'est-à-dire tels que l'operateur contracté avec $a_r^\dagger$ dans un diagramme soit contracté avec $a_s^\dagger$ dans l'autre et inversement, et que l'opérateur contracté avec a_m dans un diagramme soit contracté avec a_n dans l'autre et inversement.

Remarquons enfin que les règles indiquées ici sont loin d'être les seules possibles. En particulier, on peut associer les exponentielles dépendant du temps figurant dans (6) aux lignes, au lieu de les affecter aux interactions, de façon à faire apparaître un propagateur non perturbé $G_m^{(0)}(u)$ pour chaque ligne m de longueur u. On peut aussi utiliser l'invariance cyclique pour modifier la contribution de chaque diagramme, sans changer la contribution totale d'une famille de diagrammes équivalents [4]). Citons simplement l'un des divers développements de $A(\alpha, \beta)$ en puissances de l'interaction ainsi obtenus:

$$A = A_0 - \sum_{p=1}^{\infty} \frac{(-)^p}{p} \int_{\beta > u_1 > \ldots u_{p-1} > 0} \mathrm{d}u_1 \ldots \mathrm{d}u_{p-1} \langle V(u_1) \ldots V(u_{p-1}) V(0) \rangle_c . \tag{8}$$

La formulation (4) choisie plus haut est cependant celle qui est la mieux adaptée aux transformations que nous avons en vue.

2.2 STRUCTURE DES DIAGRAMMES COMPRENANT DES PARTIES DE SELF-ÉNERGIE

Dans le cas des systèmes infiniment grands qui nous intéresse plus particulièrement, les fonctions de base les plus naturelles sont les ondes planes. Chaque interaction introduit alors une relation de conservation de l'impulsion (et éventuellement du spin) entre les quatre lignes qui y aboutissent. Ceci entraîne l'existence de lignes à impulsions identiquement égales dans tout diagramme contenant des parties de self-énergie, au sens habituel de la théorie des champs.

Plus généralement, nous raisonnerons sur un système dont l'interaction a des *propriétés de conservation telles que l'état de la ligne entrant dans une partie de self-énergie soit identiquement le même que celui de la ligne en sortant.*

Imaginons maintenant qu'on mette en évidence sur un diagramme contenant des parties de self-énergie tous les ensembles de lignes dont les états soient identiquement égaux. Il est facile de voir que la structure topologique obtenue est celle d'un *arbre de colliers de bulles* (fig. 1). Par *bulle*, il faut entendre ici une

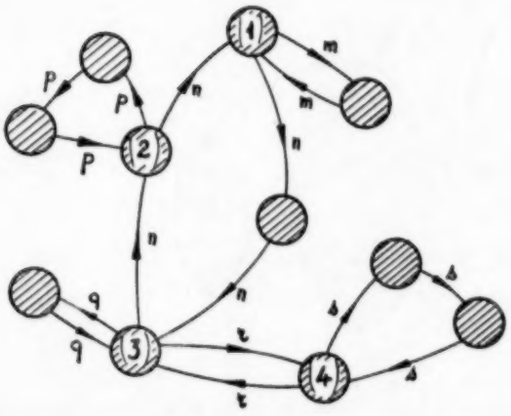

Fig. 1. Structure d'un diagramme contenant des lignes identiquement relatives au même état. Les cercles hachurés schématisent les interactions et les lignes intérieures des bulles. Pour chacun des états m, n, p, q, r, s les bulles sont reliées en colliers. Ces colliers sont reliés en arbres par l'intermédiaire de leurs bulles communes (1), (2), (3), (4).

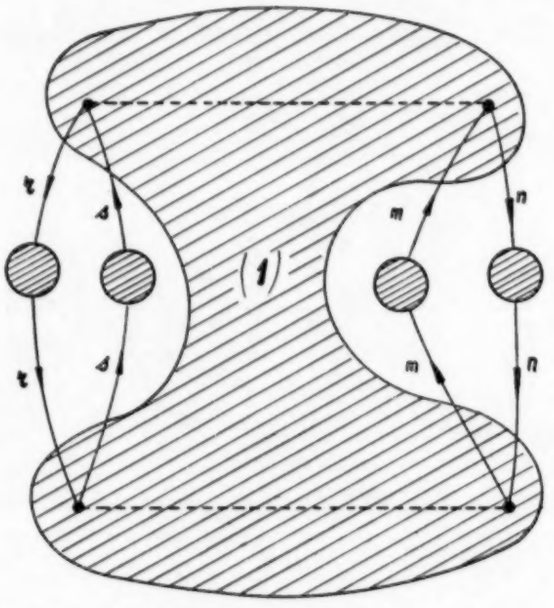

Fig. 2. Une bulle non connexe: la bulle (1), commune aux colliers m, n, r, s et constituée simplement de deux interactions, ne devient connexe que lorsqu'on referme les lignes qui se correspondent, sur chaque collier.

partie de diagramme ouverte, dont aucune des lignes intérieures ne soit identiquement relative au même état qu'aucune autre ligne du diagramme. En d'autres termes, *si on referme les lignes extérieures d'une bulle qui se correspondent* (c'est-à-dire qui sont identiquement relatives au même état), *on obtient un diagramme vide-vide connexe ne contenant aucune partie de self-énergie.*

Chaque ensemble de lignes d'états identiquement égaux relie un certain nombre de bulles de façon à former un *collier*. Les différents colliers du diagramme sont reliés les uns aux autres par l'intermédiaire de bulles communes (ayant par conséquent au moins deux paires de lignes extérieures) de façon à former un *arbre connexe*, c'est-à-dire une structure connexe qui cesse de l'être si on supprime n'importe laquelle des bulles communes à plusieurs colliers.

On notera qu'il peut arriver qu'une bulle ne devienne connexe que si on referme les lignes qui se correspondent. C'est le cas par exemple, de la bulle centrale sur la fig. 2.

2.3. CONTRIBUTION TOTALE DES FAMILLES DE COLLIERS

2.3.1. *Définition des familles*

Etant donné un diagramme du type décrit au paragraphe précédent, il est intéressant de considérer la famille des diagrammes obtenus en *formant chacun des colliers de toutes les manières possibles à l'aide de lignes reliant les bulles correspondantes*. Tous ces diagrammes sont constitués des mêmes bulles, ont la même structure en arbre; les états de chacune des lignes et les instants d'interaction sont fixés. Par exemple, trois bulles peuvent être reliées de façon à former un collier de deux manières différentes, indiquées par la fig. 3.

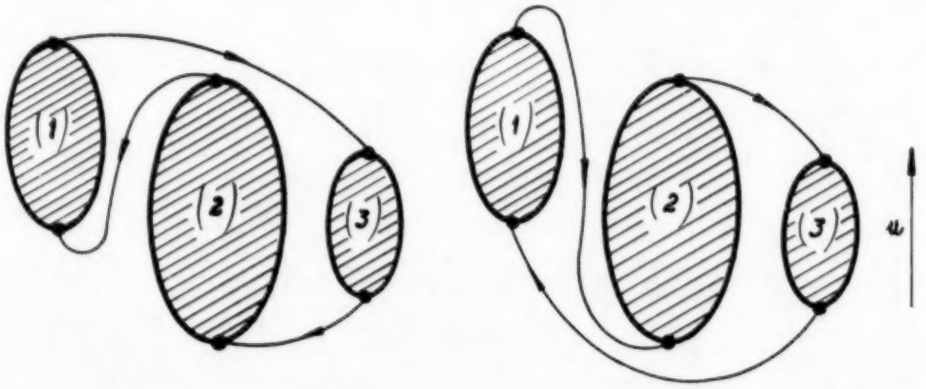

Fig. 3. La famille des diagrammes obtenus en croisant, de toutes les manières possibles, les lignes d'un collier de 3 bulles (1), (2), (3).

Les contributions de diagrammes d'une même famille, déduits l'un de l'autre en changeant le mode de formation des colliers, ne diffèrent que par les facteurs f_m^- ou f_m^- des lignes joignant les bulles, ainsi que par le signe correspondant au nombre des lignes de trous se trouvant parmi ces lignes. Nous allons montrer que la somme des contributions des diagrammes de chacune des familles peut être mise sous une forme générale simple. Pour le voir, il suffit naturellement de raisonner sur chacun des colliers séparément, même lorsque l'état relatif à un collier est *accidentellement* (dans la sommation sur les états) égal à l'état d'une autre ligne du diagramme. Nous pourrons donc nous contenter de *faire tous nos raisonnements sur un seul collier*, et nous pourrons omettre dans le § 2.3 l'indice m spécifiant l'état relatif à ce collier. Nous écrirons donc f^+, f^-, a, $a^\dagger$, ε pour f_m^+, f_m^-, a_m, $a_m^\dagger$, ε_m.

La somme, pour tous les colliers d'une famille, des produits des facteurs f^+ et f^- est, par définition, la valeur probable connexe du produit des opérateurs a et $a^\dagger$ correspondant aux lignes extérieures des bulles. Par exemple, la contribution de la famille des colliers (fig. 3) formés à partir des bulles de la fig. 4 est

$$\langle a_{(1)}^\dagger a_{(2)}^\dagger a_{(3)} a_{(1)} a_{(3)}^\dagger a_{(2)} \rangle_c , \tag{9}$$

où les indices (1), (2), (3) indiquent la bulle à laquelle est rattaché chaque opérateur (rappelons que tous ces opérateurs se rapportent au même état de

particule indépendante, qui n'est pas spécifié explicitement). En appliquant le théorème de Wick généralisé [4, 13, 14]) à (9), on voit en effet immédiatement que cette expression est égale à une somme de termes représentés par la fig. 3

$$a^{\dagger\cdot}_{(1)}\, a^{\dagger\cdots}_{(2)}\, a^{\cdot}_{(3)}\, a^{\cdot\cdot}_{(1)}\, a^{\dagger\cdots\cdot}_{(3)}\, a^{\cdots}_{(2)}\,, \tag{9a}$$

$$a^{\dagger\cdot}_{(1)}\, a^{\dagger\cdots}_{(2)}\, a^{\cdot\cdot}_{(3)}\, a^{\cdots\cdot}_{(1)}\, a^{\dagger\cdots\cdot}_{(3)}\, a^{\cdot}_{(2)}\,, \tag{9b}$$

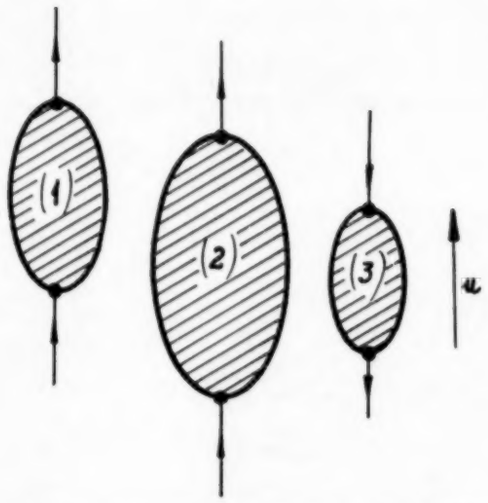

Fig. 4. Les trois bulles enchevêtrées de la fig. 3.

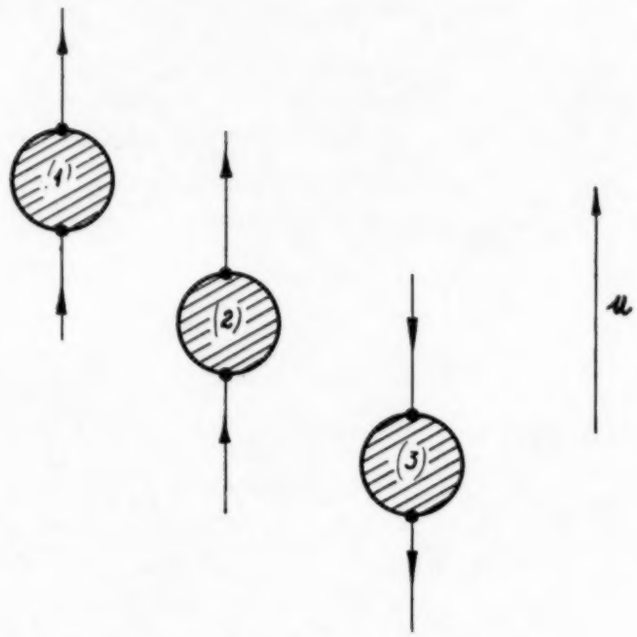

Fig. 5. Trois bulles non enchevêtrées.

égaux respectivement (au signe près) au produit des facteurs $f^{\pm}$, associé à chacun des colliers qu'on peut former avec les bulles considérées. Les indices (1), (2), (3) jouent un rôle important: on n'a en effet à considérer, dans le calcul de (9), que les systèmes connexes de contractions. Les opérateurs relatifs à l'entrée et à la sortie d'une même bulle sont connectés par les lignes intérieures de cette bulle, tous les colliers autres que le collier m étant supposés ici refermés.

Nous procéderons en deux étapes, en commençant par considérer le cas d'un collier formé à l'aide de *bulles non-enchevêtrées* (fig. 5), c'est-à-dire telles que, pour chaque bulle, les interactions d'entrée et de sortie (auxquelles aboutissent les lignes du collier) ne soient jamais, dans l'ordre chronologique, séparées par une interaction d'entrée ou de sortie d'une autre bulle du même collier. Nous généraliserons ensuite le résultat obtenu au cas des *bulles enchevêtrées* (fig. 4).

2.3.2. *Cas des bulles non-enchevêtrées*

Lorsque les bulles ne sont pas enchevêtrées, les opérateurs dans (9) sont placés dans un ordre tel que les opérateurs a et $a^{\dagger}$ relatifs à la même bulle soient toujours l'un à côté de l'autre. L'expression à calculer s'écrit donc

$$\langle a^{\dagger}_{(1)}\, a_{(1)}\, a^{\dagger}_{(2)}\, a_{(2)} \ldots a^{\dagger}_{(p)}\, a_{(p)} \rangle_{\mathrm{c}}\,. \tag{10}$$

Nous avons ici numéroté les p bulles qui constituent le collier relatif à l'état m en partant du haut du diagramme. Il faut remarquer qu'on pourrait avoir aussi des couples de la forme $a_{(i)}\,a^{\dagger}_{(i)}$, correspondant à des bulles „descendantes", c'est-à-dire dont la sortie se trouve sur la diagramme au-dessous de l'entrée (bulle (3) de la fig. 5). Toutefois ceci se traduirait, puisque $p > 1$, au plus par un changement de signe (dans le cas des fermions), car on peut considérer, dans (10), que $a_{(i)}$ et $a^{\dagger}_{(i)}$ commutent (ou anticommutent) exactement. En effet, dans tout système complet *connexe* de contractions, ces opérateurs ne peuvent être contractés ensemble.

Pour calculer (10), que nous écrirons sous la forme condensée $\langle (a^{\dagger}a)^p \rangle_c$, il suffit de considérer un problème fictif, où il n'y aurait qu'un état de particule indépendante (l'état associé au collier considéré), et dont l'hamiltonien s'écrirait

$$H = H_0 + V,$$

avec

$$H_0 = \varepsilon a^{\dagger}a, \quad V = v a^{\dagger}a. \tag{11}$$

Le développement (4) s'écrit dans ce cas

$$A = -\frac{\varepsilon}{\beta}\log f^+ - \frac{1}{\beta}\sum_{p=1}^{\infty}(-)^p \int_{\beta > u_1 > \ldots u_p > 0} \mathrm{d}u_1 \ldots \mathrm{d}u_p v^p \langle (a^{\dagger}a)^p \rangle_c$$

$$= -\frac{\varepsilon}{\beta}\log f^+ + \sum_{p=1}^{\infty}(-\beta)^{p-1}\frac{v^p}{p!}\langle (a^{\dagger}a)^p \rangle_c. \tag{12}$$

Mais d'autre part, A est évidemment égal à l'expression (5) (voir aussi (7)) de A_0 où ε est simplement remplacé par $\varepsilon + v$,

$$A = -\frac{\varepsilon}{\beta}\log f^+(\varepsilon + v) = -\frac{\varepsilon}{\beta}\sum_{p=0}^{\infty}\frac{v^p}{p!}\left(\frac{\partial}{\partial\varepsilon}\right)^p \log f^+(\varepsilon). \tag{13}$$

Étant donné que

$$-\frac{\varepsilon}{\beta}\frac{\partial(\log f^+)}{\partial\varepsilon} = f^-, \tag{14}$$

on peut encore écrire cette série de Taylor sous la forme

$$A = -\frac{\varepsilon}{\beta}\log f^+ + \sum_{p=1}^{\infty}\frac{v^p}{p!}\left(\frac{\partial}{\partial\varepsilon}\right)^{p-1} f^-,$$

et en comparant avec (12), on voit que

$$\langle a^{\dagger}_{(1)}\,a_{(1)} \ldots a^{\dagger}_{(p)}\,a_{(p)} \rangle_c \equiv \langle (a^{\dagger}a)^p \rangle_c = \left(-\frac{1}{\beta}\frac{\partial}{\partial\varepsilon}\right)^{p-1} f^- = \left(\frac{\partial}{\partial\alpha}\right)^{p-1} f^-. \tag{15}$$

Le résultat (15) s'applique à un nombre de bulles $p > 1$, avec cependant un changement de signe dans le cas des fermions s'il y a un nombre impair de

bulles ,,descendantes''. Par exemple, les deux colliers qui peuvent être formés à partir des 3 bulles non enchevêtrées de la fig. 3 donnent la contribution

$$\varepsilon[(f^+)^2 f^- + \varepsilon (f^-)^2 f^+] = \varepsilon f^+ f^- (f^+ + \varepsilon f^-) = \varepsilon \frac{\partial^2 f^-}{\partial x^2}.$$

Pour $p = 1$, c'est-à-dire pour une bulle unique, on n'a plus vraiment affaire à un collier, mais nous aurons cependant besoin du résultat correspondant dans ce qui suit. Suivant que la bulle est ,,montante'' ou ,,descendante'', la contribution est simplement

$$\langle a^\dagger a \rangle_c = f^-, \qquad \text{ou} \qquad \langle a a^\dagger \rangle_c = f^+. \tag{16}$$

2.3.3. *Cas des bulles enchevêtrées*

Dans le cas général, les bulles sont enchevêtrées et les $2p$ opérateurs (relatifs au même état m) $a^\dagger_{(1)} a^\dagger_{(2)} \ldots a^\dagger_{(p)} a_{(1)} a_{(2)} \ldots a_{(p)}$ sont placés dans un ordre quelconque. Nous allons nous ramener au cas particulier précédent: *nous ramènerons côte à côte*, en utilisant les relations de commutation des a et $a^\dagger$, *les opérateurs de chaque paire*; il nous restera alors à calculer une somme de termes, dont chacun correspondra à une famille de colliers à bulles non enchevêtrées.

Raisonnons sur l'exemple simple de la figure 4 dont la contribution est donnée par (9). Dégageons, vers la gauche dans le produit d'opérateurs, la première bulle rencontrée, c'est-à-dire la bulle (1); pour cela, nous commutons successivement dans (9) $a_{(1)}$ avec $a_{(3)}$ et $a^\dagger_{(2)}$ pour le ramener à côté de l'opérateur $a^\dagger_{(1)}$ *le plus à gauche*, ce qui donne (fig. 6(a), (b))

$$a^\dagger_{(1)} a^\dagger_{(2)} a_{(3)} a_{(1)} a^\dagger_{(3)} a_{(2)} \tag{17}$$

$$= a^\dagger_{(1)} \overbrace{a^\dagger_{(2)} a_{(3)}} a_{(1)} a^\dagger_{(3)} a_{(2)} \tag{18a}$$

$$+ a^\dagger_{(1)} a_{(1)} a^\dagger_{(2)} a_{(3)} a^\dagger_{(3)} a_{(2)}. \tag{18b}$$

Pour effectuer cette opération, nous avons dû introduire, dans (18a), le commutateur (ou l'anticommutateur) de $a^\dagger_{(2)}$ avec $a_{(1)}$. Nous emploierons la notation

$$\begin{aligned} \overbrace{a^\dagger a} &\equiv a^\dagger a - \varepsilon a a^\dagger = -\varepsilon, \\ \overbrace{a a^\dagger} &\equiv a a^\dagger - \varepsilon a^\dagger a = 1. \end{aligned} \tag{19}$$

Cette quantité peut être considérée comme une contraction d'un type nouveau que nous appellerons *contraction de désenchevêtrement, ou contraction* D, par opposition aux contractions usuelles (7). Un *produit d'opérateurs partiellement contracté* D, tel que (18a), s'obtiendra par définition en remplaçant les opérateurs contractés D par la valeur des contractions, et en introduisant, pour des

fermions, un signe moins si la permutation amenant côte à côte les opérateurs contractés D est impaire. Nous représenterons une contraction D par une ligne pointillée, ou *ligne* D, orientée du point correspondant à l'opérateur de création vers le point correspondant à l'opérateur d'annihilation (fig. 6(a)).

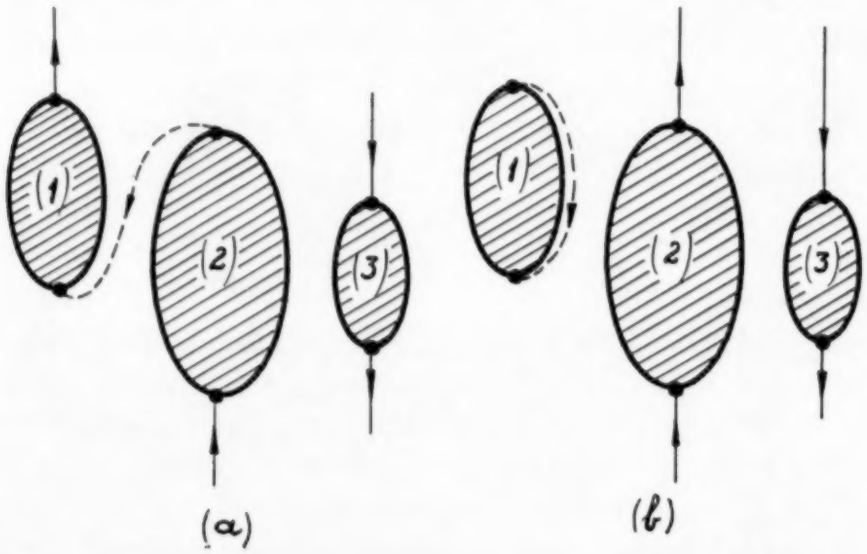

Fig. 6. Première étape du désenchevêtrement des bulles de la fig. 4. Dans (a), les bulles (1) et (2) sont reliées en une chaîne par une ligne D. Dans (b), la bulle (1) est désenchevêtrée, ce qui se représente par une ligne D de fermeture.

Pour représenter le terme (18b), dans lequel la bulle (1) a été désenchevêtrée, nous ramènerons l'entrée $a_{(1)}$ de la bulle (1) à côté de sa sortie $a^\dagger_{(1)}$ au moyen d'une *ligne* D *de fermeture*, qu'on peut sans inconvénient tracer en pointillés comme une ligne D, puisque le facteur numérique associé à une ligne D est ± 1 (fig. 6(b)).

Reprenons le terme (18a), représenté par la fig. 6(a). La somme des colliers connexes correspondants s'obtient en considérant que nous avons maintenant deux paires, d'une part $a^\dagger_{(1)}$ et $a_{(2)}$ connectés par l'intérieur des bulles (1) et (2) et par la ligne D représentant $\overbrace{a^\dagger_{(2)} a_{(1)}}$, et d'autre part $a_{(3)}$ et $a^\dagger_{(3)}$. Nous avons ainsi formé une *chaîne* avec les bulles (1) et (2), et c'est cette chaîne que nous allons désenchevêtrer du côté des temps croissants en ramenant $a_{(2)}$ à côté de $a^\dagger_{(1)}$. L'expression (18a) devient donc (fig. 7(a), (b))

$$a^\dagger_{(1)} \overbrace{a^\dagger_{(2)} a_{(3)} a_{(1)}} a^\dagger_{(3)} a_{(2)} \tag{18a}$$

$$= a^\dagger_{(1)} \overbrace{a^\dagger_{(2)} a_{(3)} a_{(1)}} \overbrace{a^\dagger_{(3)} a_{(2)}} \tag{20a}$$

$$+ a^\dagger_{(1)} a_{(2)} \overbrace{a^\dagger_{(2)} a_{(3)} a_{(1)}} a^\dagger_{(3)}. \tag{20b}$$

La valeur moyenne connexe de (20a) est

$$a^\dagger_{(1)} \overbrace{a^\dagger_{(2)} a_{(3)} a_{(1)}} \overbrace{a^\dagger_{(3)} a_{(2)}} = \varepsilon f^-, \tag{21a}$$

qu'on peut représenter par le diagramme de la fig. 7(a), dans lequel la chaîne formée par les bulles (1), (2) et (3) est *refermée par une ligne ordinaire* représentant la contraction $a^{\dagger}_{(1)} a_{(3)}$. Nous appellerons *chaîne complète* une chaîne de ce type, où *toutes les bulles relatives à l'impulsion m sont reliées entre elles* par des lignes D. C'est le seul cas où, après désenchevêtrement des opérateurs, il ne reste plus que deux opérateurs non contractés D; la valeur moyenne connexe, donnée par (16), est (au signe près) f^{+} ou f^{-}.

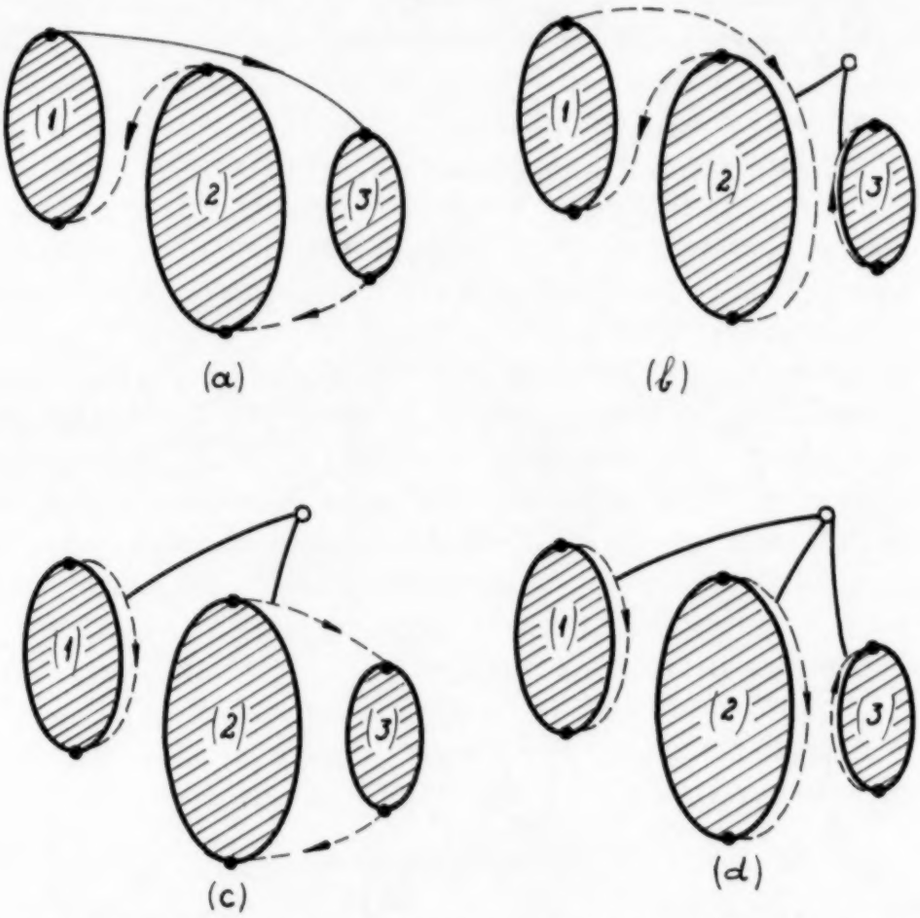

Fig. 7. Les diagrammes résultant du désenchevêtrement des bulles de la fig. 4. La fig. 7(a) se réduit à une chaîne complète descendante; les autres se composent de chaînes incomplètes rattachées par des nœuds (représentés par des lignes épaisses partant d'un cercle).

Le terme (20b) (fig. 7(b)) contient deux paires d'opérateurs désenchevêtrés: $a^{\dagger}_{(1)}$ et $a_{(2)}$ d'une part (extrémités de la chaîne (1), (2)), $a_{(3)}$ et $a^{\dagger}_{(3)}$ d'autre part (qu'on peut ramener côte à côte). La valeur moyenne connexe de leur produit a été calculée au § 2.3.2 (formule (15)). Nous obtenons donc la contribution

$$\varepsilon \langle a^{\dagger}_{(1)} a_{(2)} a^{\dagger}_{(2)} a_{(3)} a^{\dagger}_{(3)} a_{(1)} \rangle_{c} = (-\varepsilon) \frac{\partial f^{-}}{\partial \alpha}, \tag{21b}$$

qui est représentée par le diagramme de la fig. 7(b). Les deux *chaînes incomplètes* constituées par les bulles (1), (2) d'une part, la bulle (3) d'autre part, sont *refer-*

mées par des lignes D *de fermeture* représentant le fait que les extrémités de chaque chaîne sont désenchevêtrées. Le facteur $\partial f^-/\partial\alpha$, correspondant à la valeur moyenne connexe de deux paires désenchevêtrées, est représenté par un *nœud* reliant entre elles les deux chaînes.

On remarquera (fig. 7) que toutes les lignes (D ou de fermeture) d'une même chaîne sont de même sens. Cette propriété caractérise les chaînes, et résulte du processus de désenchevêtrement: *les lignes* (D *ou de fermeture*) *d'une chaîne sont toutes descendantes ou toutes montantes suivant que l'opérateur le plus à gauche de la chaîne est un opérateur de création ou d'annihilation*. Soit en effet $a^\dagger_{(1)}$ l'opérateur le plus à gauche de la chaîne; l'opérateur $a_{(1)}$ qui lui est associé et qu'on ramène par des commutations à côté de $a^\dagger_{(1)}$ est un opérateur d'annihilation; il ne peut être contracté D qu'avec un opérateur de création $a^\dagger_{(2)}$ situé entre $a^\dagger_{(1)}$ et $a_{(1)}$, c'est-à-dire à sa gauche. La ligne D ainsi introduite est donc descendante. L'opérateur $a_{(2)}$, qui termine maintenant la chaîne, doit être ramené à côté de $a^\dagger_{(1)}$, et se trouve à droite de celui-ci; il ne peut donc être contracté D qu'avec un opérateur de création situé à sa gauche, ce qui introduit encore une ligne D descendante; et ainsi de suite. Enfin, la ligne de fermeture [ligne ordinaire dans le cas d'une chaîne complète (fig. 7(a)), ligne D pointillée dans le cas d'une chaîne incomplète (fig. 7(b))] va de $a^\dagger_{(1)}$ au dernier opérateur de la chaîne; c'est donc également une ligne descendante. Inversement, si l'opérateur le plus à gauche avait été un opérateur d'annihilation (chaîne (3) de la figure 7(b)), les lignes de la chaîne auraient été toutes montantes.

Reprenons maintenant le terme (18b) représenté par la figure 6(b). Une première chaîne constituée simplement par la bulle (1) a été désenchevêtrée, mais les bulles (2) et (3) sont encore enchevêtrées. Nous répétons donc le même processus de désenchevêtrement en formant des chaînes à partir de la première bulle encore enchevêtrée, c'est-à-dire de (2). Ce qui donne (fig. 7(c), (d))

$$a^\dagger_{(1)}\,a_{(1)}\,a^\dagger_{(2)}\,a_{(3)}\,a^\dagger_{(3)}\,a_{(2)} \tag{18b}$$

$$= a^\dagger_{(1)}\,a_{(1)}\,a^\dagger_{(2)}\,a_{(3)}\,\overbrace{a^\dagger_{(3)}\,a_{(2)}} \tag{20c}$$

$$+ a^\dagger_{(1)}\,a_{(1)}\,a^\dagger_{(2)}\,a_{(2)}\,a_{(3)}\,a^\dagger_{(3)}\,. \tag{20d}$$

Les opérateurs subsistant dans ces termes sont complètement désenchevêtrés. Le calcul d'après (15) de leurs valeurs moyennes connexes conduit aux contributions

$$\langle a^\dagger_{(1)}\,a_{(1)}\,a^\dagger_{(2)}\,a_{(3)}\,\overbrace{a^\dagger_{(3)}\,a_{(2)}}\rangle_c = (-\varepsilon)\,\frac{\partial f^-}{\partial\alpha}\,, \tag{21c}$$

$$\langle a^\dagger_{(1)}\,a_{(1)}\,a^\dagger_{(2)}\,a_{(2)}\,a_{(3)}\,a^\dagger_{(3)}\rangle_c = \varepsilon\,\frac{\partial^2 f^-}{\partial\alpha^2}\,, \tag{21d}$$

qui sont représentées par les diagrammes des figs. 7(c) et 7(d), constitués

respectivement de deux et trois chaînes incomplètes reliées par un nœud.

En définitive, nous avons, par le processus de désenchevêtrement, remplacé la somme (9a, b) des contributions des deux colliers de la fig. 3 par la somme (21a, b, c, d) des contributions des diagrammes de la fig. 7. Pour chacun de ces diagrammes, le facteur statistique relatif au collier m se réduit à *un seul facteur*, f^+, f^-, $\partial f^-/\partial\alpha$ ou $\partial^2 f^-/\partial\alpha^2$, suivant la nature de la chaîne complète ou le nombre des chaînes incomplètes reliées par le nœud.

Nous donnons, dans l'appendice A, la démonstration formelle d'un *théorème de désenchevêtrement* qui généralise le résultat établi ici sur l'exemple de la fig. 4. On aboutit ainsi aux nouvelles règles de calcul du développement du potentiel de Gibbs énoncées au § 2.4.

2.3.4. *Le problème de la connexité*

Remarquons cependant que le raisonnement fait plus haut est encore incomplet. Nous avions en effet à calculer non pas le produit (17), mais sa valeur moyenne connexe (9), somme des systèmes complets *connexes* de contractions (9a, b). Examinons donc la relation (18) du point de vue de la connexité. Soit d'abord un système complet connexe de contractions de (17), dans lequel $a^{\dagger}_{(1)}$ et $a_{(1)}$ ne sont pas contractés ensemble (système (9b)); il lui correspond un système complet connexe de contractions de (18b) ayant la même propriété, et réciproquement; ces systèmes de contractions donnent la même contribution. Soit ensuite un système complet connexe de contractions de (17), dans lequel $a^{\dagger}_{(2)}$ et $a_{(1)}$ sont contractés ensemble (système (9a)); il lui correspond un système complet connexe de contractions de (18b) ayant la même propriété et un système complet de contractions (ordinaires ou D) de (18a); la contribution provenant de (9a) est égale à la somme de ces contributions provenant de (18a) et (18b), en vertu de la relation

$$a^{\dagger\cdot}_{(2)}\, a^{\cdot}_{(1)} = \overbrace{a^{\dagger}_{(2)}\, a_{(1)}} + \varepsilon a^{\cdot}_{(1)}\, a^{\dagger\cdot}_{(2)}\,.$$

On doit donc considérer que *les lignes* D *jouent, du point de vue de la connexité, le même rôle que les lignes ordinaires*: la somme des contributions des colliers connexes (constitués de lignes ordinaires) formés avec (17) est égale à la somme des contributions des colliers connexes (constitués de lignes ordinaires ou de lignes D) formés avec (18a) et (18b).

De manière générale, *toute égalité entre produits de paires d'opérateurs partiellement contractés* D *entraîne l'égalité correspondante entre valeurs moyennes connexes*, la connexité étant assurée par les lignes ordinaires, les lignes D, et l'intérieur des bulles. Cette propriété traduit le fait qu'on peut, dans un système complet de contractions, permuter les opérateurs qui ne sont pas contractés ensemble sans en changer la valeur, et que, pour des opérateurs contractés

ensemble, on a les relations

$$a^{\dagger\cdot} a^{\cdot} = \varepsilon a^{\cdot} a^{\dagger\cdot} + \overbrace{a^{\dagger} a}$$

et (22)

$$a^{\cdot} a^{\dagger\cdot} = \varepsilon a^{\dagger\cdot} a^{\cdot} + \overbrace{a\, a^{\dagger}},$$

qui correspondent à $f^{-} = \varepsilon f^{+} - \varepsilon$ et $f^{+} = \varepsilon f^{-} + 1$.

2.4. NOUVELLE FORME DU DÉVELOPPEMENT DU POTENTIEL DE GIBBS

En appliquant les résultats du § 2.3 simultanément à tous les colliers des diagrammes représentant le développement (4), on voit qu'on peut mettre celui-ci sous la forme d'une somme de contributions associées à chacun des *diagrammes* D construits de la manière suivante.

Un diagramme D (fig. 8) est constitué de (une ou plusieurs) bulles composées reliées entre elles par des nœuds de façon à former un arbre connexe.

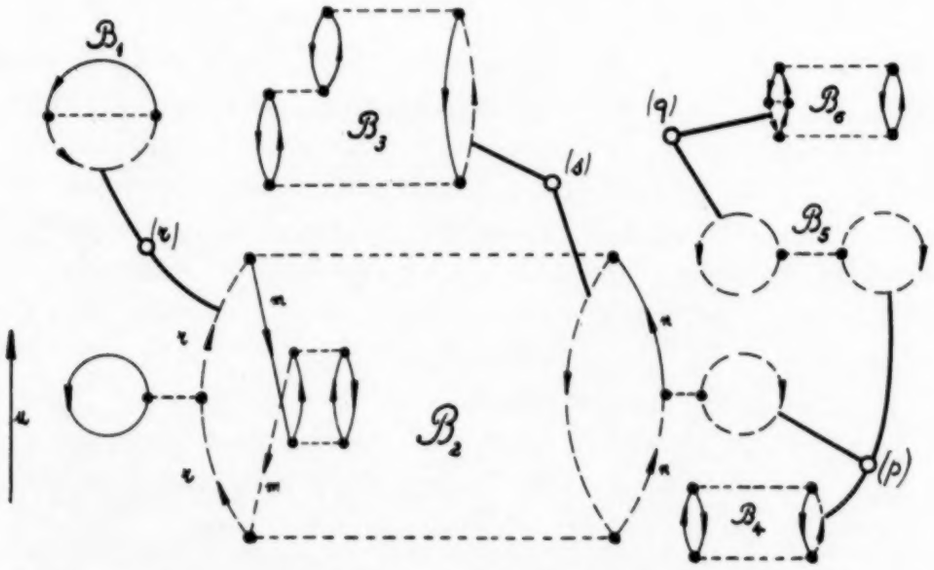

Fig. 8. Exemple de diagramme D. Les bulles composées sont désignées par $\mathcal{B}_1$, $\mathcal{B}_2$ . . . Les lignes m d'une part, n d'autre part constituent des chaînes complètes, ainsi que chacune des autres lignes pleines du diagramme. Les lignes r constituent une chaîne incomplète, ainsi que chacune des lignes pointillées sans indice. Les chaînes incomplètes sont reliées les unes aux autres par des nœuds, désignés par les états (r), (s), (p), (q) qui leur correspondent. Par rapport aux bulles composées et aux nœuds, le diagramme a une structure d'arbre.

Chaque *bulle composée* est représentée par un diagramme vide-vide du type habituel, pouvant contenir des parties de self-énergie, *à condition que les lignes dont les états sont identiquement égaux soient de même nature* (toutes montantes ou toutes descendantes).

A l'intérieur d'une bulle composée, nous appelons *chaîne* chaque ensemble de (une ou plusieurs) lignes identiquement relatives au même état.

Les *nœuds* relient entre elles deux ou plusieurs chaînes (que nous appelons

chaînes incomplètes) appartenant à des bulles composées différentes, de façon à former une *structure d'arbre connexe*. Chaque chaîne ne peut être reliée à plus d'un nœud. Le fait qu'un nœud relie plusieurs chaînes impose à celles-ci d'être relatives au même état.

La contribution à (4) associée à un diagramme D comprend tout d'abord les mêmes éléments de matrice (6) de $V(u)$ que précédemment. *A chaque nœud reliant* q ($q \geqq 2$) *chaînes* (*relatives à l'état* m) *est associé le facteur*

$$\left(\frac{\partial}{\partial\alpha}\right)^{q-1} f_m^- . \tag{23}$$

A chaque chaîne qui n'est reliée à aucun nœud (et que nous appelons *chaîne complète*) *est associé le facteur* f_m^+ *ou* f_m^-, suivant qu'il s'agit d'une chaîne de lignes montantes ou descendantes.

On effectue ensuite l'intégration sur les temps d'interaction ordonnés de 0 à β, et la sommation sur tous les états de particule indépendante, pour chaque chaîne complète et chaque nœud.

Enfin, chaque contribution est affectée, en plus du facteur $(-)^p$ figurant dans (4), du signe

$$\begin{aligned} &(-)^{n_-+h} \quad \text{dans le cas des bosons,} \\ &(-)^{h+l+n'_+} \quad \text{dans le cas des fermions,} \end{aligned} \tag{24}$$

où n_- est le nombre de chaînes descendantes (complètes ou incomplètes), h le nombre de lignes descendantes, l le nombre de boucles fermées, et n'_+ le nombre de chaînes incomplètes montantes (voir appendice B).

On notera (fig. 8) qu'une bulle composée présente la même structure que les diagrammes vide-vide qui interviennent dans le développement de l'énergie de l'état fondamental d'un système de fermions [5, 6]). En effet, dans ce développement, toutes les lignes relatives à un même état m sont de même sens, montantes ou descendantes suivant que $|m|$ est supérieur ou inférieur à l'impulsion de Fermi. Ici, la même règle apparaît, *pour une raison purement algébrique*, pour les lignes identiquement égales d'une chaîne; mais le sens des lignes peut être *différent d'une chaîne à l'autre*, soit que ces chaînes soient accidentellement relatives au même état, soit que, faisant partie de bulles composées différentes reliées par un nœud, elles soient identiquement relatives au même état.

Remarque 1

On pourrait établir, de la même façon, une représentation en diagrammes D pour chacun des développements du potentiel de Gibbs ayant une représentation en diagrammes vide-vide, par exemple pour le développement (8), ou encore dans une représentation indépendante du temps [3, 8]). La représentation en diagrammes D traduit en effet une simple manipulation algébrique sur les facteurs statistiques $f^{\pm}$. Bien que leurs résultats soient égaux à un ordre donné,

ces diverses formes du développement de A ne sont pas équivalentes. En particulier, la forme indépendante du temps [3, 8]) conduit après sommation partielle à des développements utiles à basse température, alors que la forme présentée ici est mieux adaptée à la limite classique.

Remarque 2

Le développement de Brout et Englert [15]) présente une grande analogie avec la représentation en diagrammes D du développement (8). Les facteurs f_m^-, nombres d'occupation de chaque état dans le système grand canonique non perturbé y sont simplement remplacés par les nombres d'occupation dans le système petit canonique non perturbé. L'utilisation d'un système grand canonique évite cependant de se restreindre au cas du volume infini.

2.5. NOUVELLE FORME DU DÉVELOPPEMENT DU PROPAGATEUR

Nous avons souligné, dans la remarque 1 du § 2.4, la généralité de la méthode précédente. Nous allons maintenant l'appliquer au propagateur relatif à l'état m, défini par

$$G_m(u-u') = \frac{\mathrm{Tr}\,[\mathrm{e}^{\alpha N-\beta H}\,\mathrm{T}(\mathrm{e}^{uH}\,a_m\,\mathrm{e}^{-uH})\,(\mathrm{e}^{u'H}\,a_m^\dagger\,\mathrm{e}^{-u'H})]}{\mathrm{Tr}\,\mathrm{e}^{\alpha N-\beta H}}, \tag{25}$$

où T désigne le T-produit pour les „temps" u et u' compris entre 0 et β.

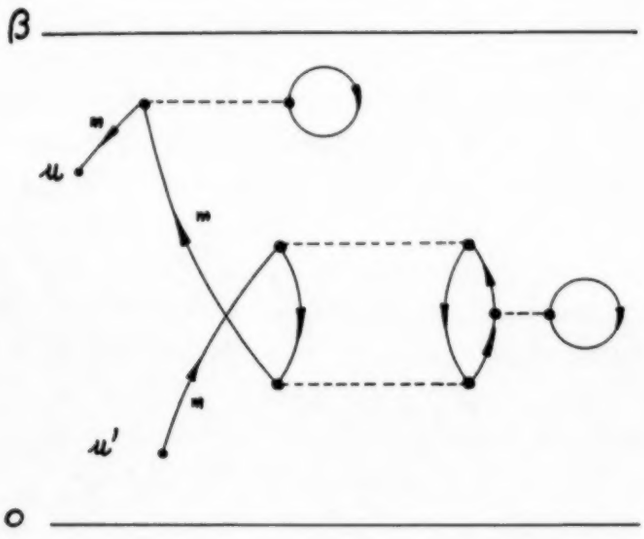

Fig. 9. Un diagramme contribuant au propagateur $G_m(u-u')$.

Les propriétés de conservation de l'interaction entraînent que le propagateur est diagonal: les opérateurs de création et d'annihilation doivent être relatifs au même état.

Dans la formulation dépendante du temps, on établit pour $G_m(u-u')$ un développement en puissances de l'interaction de la même façon que pour A.

Ce développement est représenté par l'ensemble des diagrammes connexes distincts, ayant une ligne ouverte (correspondant à l'état m fixé), partant de u' et arrivant en u (fig. 9). Leurs contributions sont calculées par les règles du paragraphe 2.1, avec un facteur supplémentaire $e^{-\epsilon_m(u-u')}$ provenant de la dépendance dans le temps des opérateurs a_m et $a_m^\dagger$ en représentation interaction.

Du point de vue des lignes identiquement égales, la structure des diagrammes contribuant à $G_m(u-u')$ est la même que celle des diagrammes vide-vide. Le collier relatif à l'état m fixé présente cependant une particularité: il contient une bulle d'un genre différent, formée de l'entrée $a_m^\dagger$ et de la sortie a_m du diagramme; on peut en effet considérer ces points respectivement comme la sortie et l'entrée d'une bulle fictive, faisant partie du collier m, qui se trouve ainsi refermé.

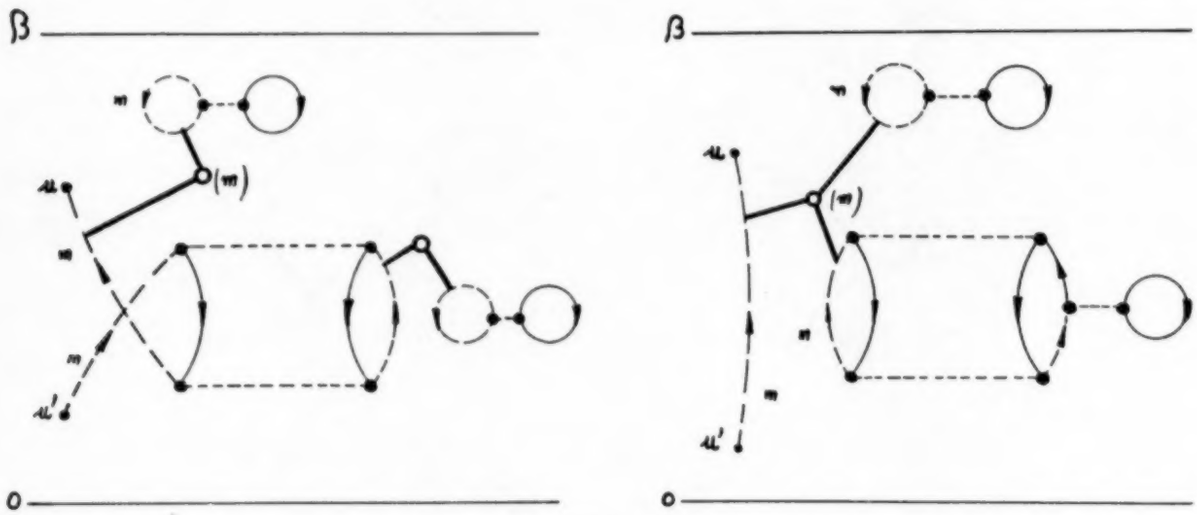

Fig. 10. Deux diagrammes D contribuant au propagateur $G_m(u-u')$.

Appliquons les résultats du § 2.3 au calcul de la contribution totale de la famille des diagrammes ayant les mêmes bulles et la même structure en arbre. Nous obtenons pour le développement de $G_m(u-u')$ en puissances de l'interaction une représentation en diagrammes D, analogue à celle du § 2.4 (fig. 10). Ici, l'une des bulles composées, celle qui contient la paire $a_m^\dagger a_m$, est ouverte et contient une chaîne relative à l'état m fixé. Les règles de calcul des contributions sont celles du § 2.4, un facteur supplémentaire $e^{-\epsilon_m(u-u')}$ étant associé aux extrémités $a_m^\dagger a_m$.

3. La Sommation des Insertions dans les Diagrammes Squelettes

3.1. SOMMATION DES INSERTIONS DANS UNE CHAÎNE

Considérons dans un diagramme D donné, considéré comme *squelette*, une chaîne complète relative à l'état m (fig. 11(a)). Nous dirons qu'on a fait une

insertion dans cette chaîne lorsqu'on a adjoint à celle-ci, par un nœud, une ou plusieurs bulles composées (fig. 11(b)(c)). Calculons la somme des contributions de toutes les insertions qui peuvent être faites dans une chaîne donnée.

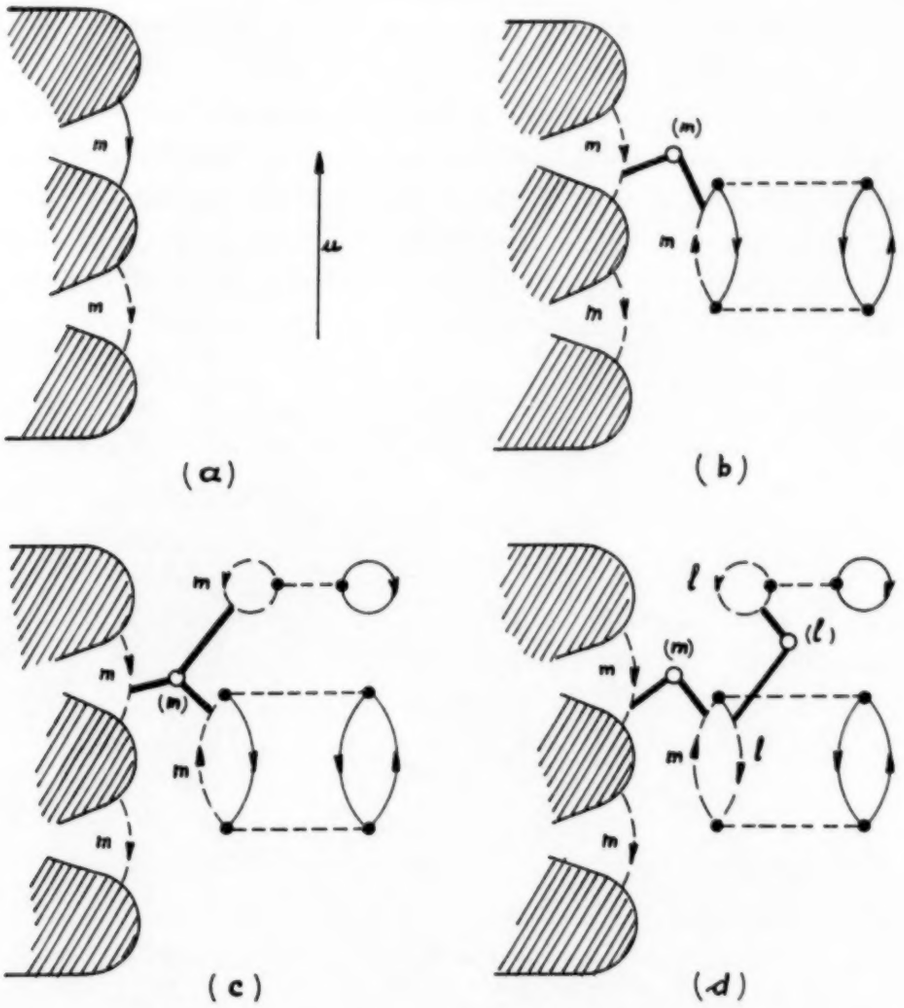

Fig. 11. Insertions dans une chaîne. Les parties hachurées schématisent dans (a) le diagramme D dont m est une chaîne complète. En (b) et (c), on a effectué dans cette chaîne respectivement une et deux insertions. En (d), on a effectué une insertion sur la chaîne l de la bulle composée insérée dans m.

Pour une chaîne complète descendante m, la contribution est (abstraction faite des facteurs provenant du squelette) égale à f_m^-. Effectuons une insertion quelconque et considérons la somme des contributions des diagrammes D déduits les uns des autres en déplaçant, de toutes les façons possibles, les bulles composées de l'insertion les unes par rapport aux autres et par rapport au squelette. D'après les règles du § 2.4, la contribution totale de cette famille (avant la sommation sur les états) se calcule en effectuant les intégrations sur les temps indépendamment pour chaque bulle composée entre 0 et β.

Considérons alors la contribution à A d'un diagramme Γ, formé d'une seule

bulle composée (dont toutes les chaînes sont donc complètes). Remplaçons le facteur statistique f_i^+ attaché à chaque chaîne montante par $1+\varepsilon f_i^-$. Cette contribution peut être considérée comme une fonction $\mathscr{D}_\Gamma\{f^-;\beta\}$ de l'ensemble des variables f_i^- et de β (par l'intermédiaire des bornes d'intégration et du facteur $-1/\beta$ explicité dans (4)). Considérons maintenant les bulles composées déduites de Γ en remplaçant successivement chacune des chaînes complètes par une chaîne incomplète relative à l'état m. La somme de leurs contributions, intégrée librement entre 0 et β, pour une valeur fixée de m et compte non tenu du facteur $-1/\beta$ figurant explicitement dans (4) et dans $\mathscr{D}_\Gamma\{f^-;\beta\}$, est la dérivée partielle $-\beta\partial\mathscr{D}_\Gamma\{f^-;\beta\}/\partial f_m^-$. La dérivation par rapport à f_m^- remplace en effet, pour chaque chaîne relative à l'état l, f_l^- par δ_{lm} ou $f_l^+ = 1+\varepsilon f_l^-$ par $\varepsilon\delta_{lm}$.

Appelons $\mathscr{D}\{f^-;\beta\}$ la contribution à A, calculée d'après les règles du paragraphe 2.4, *de l'ensemble des diagrammes* D *formés d'une seule bulle composée. Nous considérons $\mathscr{D}\{f^-;\beta\}$ comme une fonction des variables f_l^-* (après remplacement du facteur f_l^+ associé à chaque chaîne montante par $1+\varepsilon f_l^-$). La somme des contributions, intégrées librement entre 0 et β, de toutes les bulles composées à une seule chaîne incomplète m est égale à $-\beta\partial\mathscr{D}\{f^-;\beta\}/\partial f_m^-$.

Reprenons le problème des insertions dans une chaîne descendante m (fig. 11(a)). L'insertion d'une bulle composée quelconque (fig. 11(b)) a pour effet de remplacer f_m^- par

$$\left(\frac{\partial f_m^-}{\partial\alpha}\right)\left(-\beta\,\frac{\partial\mathscr{D}\{f^-;\beta\}}{\partial f_m^-}\right)=\frac{\partial f_m^-}{\partial\varepsilon_m}\,\frac{\partial\mathscr{D}\{f^-;\beta\}}{\partial f_m^-}.$$

L'insertion dedeux bulles composées quelconques dans le nœud m (fig. 11(c)) donne la contribution

$$\frac{1}{2}\left(\frac{\partial^2 f_m^-}{\partial\alpha^2}\right)\left(-\beta\,\frac{\partial\mathscr{D}}{\partial f_m^-}\right)^2=\frac{1}{2!}\,\frac{\partial^2 f_m^-}{\partial{\varepsilon_m}^2}\left(\frac{\partial\mathscr{D}}{\partial f_m^-}\right)^2.$$

Le facteur 1/2! doit être introduit pour tenir compte du fait que chaque diagramme apparaît 2! fois lorsqu'on déplace de toutes les façons possibles l'une par rapport à l'autre les deux bulles de l'insertion. De même, pour p bulles composées insérées dans le même nœud m, on obtient

$$\frac{1}{p!}\,\frac{\partial^p f_m^-}{\partial{\varepsilon_m}^p}\left(\frac{\partial\mathscr{D}}{\partial f_m^-}\right)^p. \tag{26}$$

En définitive, la sommation des insertions effectuées dans la chaîne complète descendante m à l'aide *d'un seul* nœud (relatif à l'état m) a pour effet de remplacer simplement dans l'expression (7) du facteur f_m^- associé à la chaîne l'énergie non perturbée ε_m par

$$\varepsilon_m+\frac{\partial\mathscr{D}\{f^-;\beta\}}{\partial f_m^-}. \tag{27}$$

Effectuons le même type d'insertions dans une chaîne montante. Le développement est dans ce cas

$$f_m^+ + \varepsilon \frac{\partial f_m^-}{\partial \varepsilon_m} \frac{\partial \mathscr{D}}{\partial f_m^-} + \frac{\varepsilon}{2!} \frac{\partial^2 f_m^-}{\partial \varepsilon_m{}^2} \left(\frac{\partial \mathscr{D}}{\partial f_m^-}\right)^2 + \dots$$

$$= f_m^+ + \frac{\partial f_m^+}{\partial \varepsilon_m} \frac{\partial \mathscr{D}}{\partial f_m^-} + \frac{1}{2!} \frac{\partial^2 f_m^-}{\partial \varepsilon_m{}^2} \left(\frac{\partial \mathscr{D}}{\partial f_m^-}\right)^2 + \dots . \quad (28)$$

Le signe ε provient du remplacement de la chaîne complète montante qui sert de squelette par une chaîne incomplète. Comme dans le cas précédent, ces insertions ont pour effet de remplacer ε_m par $\varepsilon_m + \partial \mathscr{D}\{f^-; \beta\}/\partial f_m^-$ dans f_m^+.

Si maintenant *nous effectuons toutes les insertions possibles* dans une chaîne m, puis dans les chaînes l des bulles composées insérées dans m, et ainsi de suite (fig. 11(d)), *les facteurs statistiques* $f_m^\pm$ *seront remplacés par les* $\mathscr{F}_m^\pm$ *déterminés par les équations couplées*

$$\mathscr{F}_m^+ = 1 + \varepsilon \mathscr{F}_m^- = \frac{1}{1 - \varepsilon e^{\alpha - \beta(\varepsilon_m + w_m)}}, \quad (29)$$

$$w_m = \frac{\partial \mathscr{D}\{\mathscr{F}^-; \beta\}}{\partial \mathscr{F}_m^-}. \quad (30)$$

La fonction $\mathscr{D}\{\mathscr{F}^-; \beta\}$ *est réelle pour toutes les valeurs réelles des variables* $\mathscr{F}_m^-$. Il suffit pour le voir de grouper par deux les contributions des diagrammes déduits l'un de l'autre par un changement de sens des flèches et un retournement haut-bas. La résolution des éqs. (29) (30) donne donc en général des valeurs réelles pour $\mathscr{F}_m^-$, même si on prend pour $\mathscr{D}$ une expression approchée se limitant aux diagrammes d'un ordre donné.

3.2. INTERPRÉTATION DU NOUVEAU FACTEUR STATISTIQUE

Appliquons le résultat du § 3.1 au développement en diagrammes D de $G_m(u-u')$, en considérant comme *squelette la bulle composée partant de* u' *et arrivant en* u. Le résultat de la sommation de toutes les insertions faites dans ce squelette (fig. 10) est simplement le remplacement des facteurs statistiques $f^\pm$ par $\mathscr{F}^\pm$. *Le propagateur peut donc être mis sous la forme*

$$G_m(u-u') = \mathscr{F}_m^+ g_m^+(u, u') + \mathscr{F}_m^- g_m^-(u, u'), \quad (31)$$

où les deux termes sont les contributions, après remplacement des $f^\pm$ *par les* $\mathscr{F}^\pm$, *des bulles squelettes dont la chaîne m est montante ou descendante respectivement.* Alors que $G_m(u-u')$ se déduit de l'opérateur de masse $\Sigma_m(u)$ par itération à l'aide du propagateur non perturbé $G_m{}^{(0)}(u)$, qui est représenté par une ligne montante ou descendante, $g_m^+(u, u')$ (ou $g_m^-(u, u')$) se déduit d'une manière semblable de $\Sigma_m(u)$, mais en ne faisant intervenir dans l'itération que des lignes

toutes montantes (ou toutes descendantes), auxquelles on attache simplement un facteur $e^{-\epsilon_m u}$. Dans tous les cas, les diagrammes représentant cette itération partent de u' et arrivent en u, les instants des interactions intermédiaires devant être intégrés dans tout l'intervalle 0, β.

En particulier, si nous posons dans (31) $u = 0$, $u' \to +0$, le diagramme squelette ne peut être composé que d'une ligne descendante de longueur nulle, de sorte que

$$g_m^+(0, +0) = 0, \qquad g_m^-(0, +0) = \varepsilon,$$

et par suite

$$\bar{n}_m \equiv \frac{\operatorname{Tr} e^{\alpha N - \beta H} a_m^\dagger a_m}{\operatorname{Tr} e^{\alpha N - \beta H}} = \varepsilon G_m(-0) = \mathscr{F}_m^-. \tag{32}$$

Le facteur statistique modifié $\mathscr{F}_m^-$, déterminé par les éqs. (29), (30) *est donc le nombre d'occupation vrai $\bar{n}_m$ de l'état m,* alors que f_m^- est le nombre d'occupation non perturbé.

Indiquons encore quelques propriétés des fonctions $g_m^\pm$. En utilisant la propriété

$$G_m(u) = \varepsilon e^{\alpha} G_m(u+\beta), \tag{33}$$

et en prenant dans (31) des valeurs particulières pour u et u', on peut exprimer le nombre d'occupation en fonction de g_m^+ ou g_m^-, soit

$$e^{-\beta(\epsilon_m + w_m)} = g_m^+(\beta, 0) = \frac{\varepsilon}{g_m^-(0, \beta)}. \tag{34}$$

On peut également exprimer g_m^+ et g_m^- en fonction l'un de l'autre, en utilisant les relations

$$g_m^+(u, u') + \varepsilon g_m^-(u, u') = \frac{G_m(u) G_m(-u')}{G_m(+0) G_m(-0)} = \frac{g_m^+(u, 0) g_m^+(\beta, u')}{g_m^+(\beta, 0)} = \varepsilon \frac{g_m^-(0, u') g_m^-(u, \beta)}{g_m^-(0, \beta)}, \tag{35}$$

déduites des équations intégrales satisfaites par g_m^+ et g_m^-.

3.3. EXPRESSION DU POTENTIEL DE GIBBS EN FONCTION DU NOMBRE D'OCCUPATION

La sommation des insertions dans les diagrammes contribuant au potentiel de Gibbs A est compliquée par le fait que *la bulle composée squelette servant de point de départ aux insertions n'est pas bien définie dans le cas d'un diagramme vide-vide.*

Il est naturel de considérer l'expression

$$\mathscr{D}\{\mathscr{F}^-; \beta\}, \tag{36}$$

et, pour la comparer au développement de A, de la développer en puissances

de l'interaction suivant une marche inverse de celle du paragraphe précédent, en utilisant simultanément les relations (29), (30). Cette expression est alors représentée par les *mêmes diagrammes* D *que le potentiel de Gibbs, sauf que l'une des bulles composées est distinguée.* Cette bulle composée (jouant le rôle de squelette) provient de $\mathscr{D}$, et les autres (jouant le rôle d'insertions) proviennent du redéveloppement des facteurs $\mathscr{F}^{\pm}$. Chaque bulle composée d'un diagramme D peut successivement être considérée comme le squelette; au lieu de figurer une fois comme dans le développement de A, *chaque diagramme* D *figure donc dans le développement de* $\mathscr{D}\{\mathscr{F}^{-}; \beta\}$ *un nombre* $\mathscr{N}_{\mathrm{B}}$ *de fois,* où $\mathscr{N}_{\mathrm{B}}$ est le nombre de ses bulles composées.

Pour calculer A, *nous utiliserons la relation suivante, valable pour tout diagramme* D *et résultant de sa structure en arbre*:

$$\mathscr{N}_{\mathrm{N}} - \mathscr{N}_{\mathrm{C}} + \mathscr{N}_{\mathrm{B}} = 1, \tag{37}$$

où $\mathscr{N}_{\mathrm{N}}$ est le nombre des *nœuds,* $\mathscr{N}_{\mathrm{C}}$ le nombre des *chaînes incomplètes,* et $\mathscr{N}_{\mathrm{B}}$ le nombre de *bulles composées* du diagramme. *Nous construirons des expressions, représentées par les mêmes diagrammes que* A, *mais où les contributions sont affectées des poids* $\mathscr{N}_{\mathrm{C}}$, $\mathscr{N}_{\mathrm{N}}$, *de même que* $\mathscr{D}\{\mathscr{F}^{-}; \beta\}$ *est affecté du poids* $\mathscr{N}_{\mathrm{B}}$, *et nous les combinerons de la manière suggérée par la relation* (37).

La relation (37) est évidente s'il y a un seul nœud. Tout diagramme D pouvant, par suite de sa structure en arbre, être obtenu par une succession d'adjonctions d'un nœud, il suffit de vérifier qu'une telle opération ne modifie pas la quantité $\mathscr{N}_{\mathrm{N}} - \mathscr{N}_{\mathrm{C}} + \mathscr{N}_{\mathrm{B}}$. Effectivement, lorsqu'on ajoute un nœud ($\mathscr{N}_{\mathrm{N}} \to \mathscr{N}_{\mathrm{N}}+1$), le nombre de chaînes incomplètes qu'on introduit est égal au nombre p des bulles composées introduites plus un, puisque la chaîne complète sur laquelle se fait l'insertion devient incomplète ($\mathscr{N}_{\mathrm{B}} \to \mathscr{N}_{\mathrm{B}}+p$, $\mathscr{N}_{\mathrm{C}} \to \mathscr{N}_{\mathrm{C}}+p+1$).

Considérons maintenant l'expression

$$-\frac{1}{\beta}\sum_m \left[\frac{(-\beta w_m)^2}{2!}\left(-\frac{1}{\beta}\frac{\partial f_m^-}{\partial \varepsilon_m}\right) + \ldots + \frac{(-\beta w_m)^{p+1}}{(p+1)!}\left(-\frac{1}{\beta}\frac{\partial}{\partial \varepsilon_m}\right)^p f_m^- + \ldots\right] \tag{38}$$

$$= -\frac{\varepsilon}{\beta}\sum_m (\log \mathscr{F}_m^+ - \log f_m^-) - \sum_m f_m^- w_m, \tag{39}$$

dont la sommation a été effectuée en utilisant la relation (14). En la redéveloppant en puissances de l'interaction de la même façon que (36), on peut la représenter par les mêmes diagrammes D vide-vide connexes que ceux qui figurent dans le développement de A, *sauf que l'un des nœuds est distingué.* Tous les nœuds d'un diagramme D peuvent ainsi être considérés successivement comme le squelette sur lequel sont effectuées les insertions; *chaque diagramme* D *figure donc* $\mathscr{N}_{\mathrm{N}}$ *fois dans le développement de* (39). On remarquera que le facteur $1/(p+1)!$ doit être introduit dans (38) pour tenir compte du fait

que les $p+1$ bulles composées (avec insertions sur les chaînes autres que m) sont identiques et sont intégrées librement entre 0 et β.

Enfin l'expression

$$\sum_m w_m \frac{(-\beta w_m)}{1!}\left(-\frac{1}{\beta}\frac{\partial f_m^-}{\partial \varepsilon_m}\right)+\ldots+\frac{(-\beta w_m)^p}{p!}\left(-\frac{1}{\beta}\frac{\partial}{\partial \varepsilon_m}\right)^p f_m^-+\ldots \quad (40)$$

$$=\sum_m w_m(\mathscr{F}_m^- - f_m^-) \quad (41)$$

se déduit de (38) en multipliant chaque terme par le nombre $p+1$ des chaînes incomplètes d'impulsion m. Dans le développement de (41) en puissances de l'interaction, *chaque diagramme* D *figure* $\mathscr{N}_C$ *fois, puisque chaque chaîne incomplète peut successivement être distinguée.* En effet chaque chaîne incomplète peut ici être considérée comme le squelette, point de départ des insertions, qui sont effectuées soit sur les autres chaînes de la bulle composée à laquelle cette chaîne appartient, soit à partir du nœud rattaché à cette chaîne.

En ajoutant à A_0 les expressions (36), (39) et (41), on obtient immédiatement en tenant compte de (37) l'expression

$$A=-\frac{\varepsilon}{\beta}\sum_m \log \mathscr{F}_m^+ - \sum_m w_m \mathscr{F}_m^- + \mathscr{D}\{\mathscr{F}^-;\beta\} \quad (42)$$

du potentiel de Gibbs en fonction des nombres d'occupation $\bar{n}_m = \mathscr{F}_m^-$. Rappelons que $\mathscr{D}\{\mathscr{F}^-;\beta\}$ se calcule à partir des diagrammes D à une seule bulle composée par les règles du § 2.4 en associant à chaque chaîne montante (ou descendante) le facteur $\mathscr{F}_m^+$ (ou $\mathscr{F}_m^-$), et que les valeurs des $\mathscr{F}_m^-$ et w_m sont déterminées par les éqs. (29), (30).

La méthode employée ci-dessus est très générale. *Elle peut s'appliquer à toutes les sommations partielles de diagrammes vide-vide connexes ayant une structure en arbre.* Elle explique la similarité formelle entre l'expression du potentiel de Gibbs trouvée ici et celles des réfs. [8–10, 12]). Nous l'appliquons au § 6 pour retrouver le développement du viriel pour un système classique inhomogène [1]).

3.3.1. *Remarque* **1.** *Déduction directe de l'éq.* (42)

Il aurait été possible de déduire directement l'expression (42) des éqs. (29), (30) et (32), en intégrant par rapport à α l'équation

$$\frac{\partial A(\alpha,\beta)}{\partial \alpha}=-\frac{1}{\beta}\bar{N}=-\frac{1}{\beta}\sum_m \bar{n}_m,$$

comme il est fait dans les réfs. [10, 12]). Mais la méthode que nous avons employée montre que la possibilité d'effectuer explicitement cette intégration est liée à la structure en arbre des diagrammes D.

3.3.2. *Remarque* 2. *Interprétation de w_m comme un potentiel self-consistant*

On aurait également pu effectuer les sommations partielles conduisant à (31) et (42) en ajoutant un *potentiel self-consistant* $\sum_m w_m a_m^\dagger a_m$ à l'hamiltonien non perturbé et en le retranchant de l'interaction, puis en choisissant w_m de manière à éliminer tous les diagrammes D comprenant plus d'une bulle composée [3, 8]). Les trois termes de (42) s'interprétent alors le premier comme le terme non perturbé, le second comme la contribution du diagramme D ne contenant que l'interaction $-w_m$, et le dernier comme la contribution de tous les autres diagrammes (formés d'une seule bulle composée). Dans ces derniers diagrammes, w_m intervient comme interaction, mais figure aussi dans les facteurs exponentiels dépendant du temps attachés à chaque interaction (et naturellement dans les facteurs statistiques $\mathscr{F}^\pm$, donnés par (29)). Ces deux dépendances, toutefois, se compensent exactement. On voit de la même façon que la condition de self-consistance, qui détermine w_m, équivaut à (30).

On a montré sur un modèle particulier [16]) que l'introduction à température non nulle d'un potentiel de Hartree-Fock [17]) facilitait l'élimination de α, simplifiait l'expression des grandeurs thermodynamiques en fonction des facteurs statistiques ainsi modifiés (en éliminant les contributions de certains diagrammes anormaux), et améliorait la convergence. Le potentiel self-consistant w est donc une généralisation de ce potentiel de Hartree-Fock à tous les ordres, qui permet la sommation des diagrammes anormaux, et, comme nous le verrons plus loin, l'élimination de α.

3.3.3. *Remarque* 3. *Le passage aux variables continues*

Pour les calculs pratiques relatifs à un système de volume Ω infini, on doit remplacer les états discrets m de particule indépendante, correspondant à des conditions aux limites périodiques, par un continuum. Si pour simplifier l'écriture on considère des particules sans spin, chaque état de particule indépendante est caractérisé par son impulsion $\mathbf{p}$. Les expressions précédentes et celles qui seront établies dans la suite restent valables, à condition d'y remplacer $\sum_m$ par $(\Omega/h^3)\int \mathrm{d}^3\mathbf{p}$ et $\delta_{mm'}$ par $(h^3/\Omega)\delta^3(\mathbf{p}-\mathbf{p}')$. La fonction $\mathscr{D}\{\mathscr{F}^-;\beta\}$ des variables $\mathscr{F}_m^-$ devient une fonctionnelle de la fonction $\mathscr{F}_\mathbf{p}^-$, proportionnelle au volume par l'intermédiaire d'un facteur Ω/h^3, et la dérivation partielle $\partial/\partial\mathscr{F}_m^-$ doit être remplacée par la dérivation fonctionnelle $(h^3/\Omega)\delta/\delta\mathscr{F}_\mathbf{p}^-$. On notera en particulier sur l'expression (30) que $w_\mathbf{p}$ est indépendant du volume.

4. Propriétés Variationnelles et Applications

4.1. STATIONNARITÉ DE A

Remplaçons, dans (42), w_m par sa valeur exprimée en fonction de $\mathscr{F}_m^-$ à l'aide de (29),

$$w_m = \frac{1}{\beta}\log\frac{\mathscr{F}_m^+}{\mathscr{F}_m^-} + \frac{\alpha}{\beta} - \varepsilon_m. \tag{43}$$

Nous obtenons ainsi la fonction suivante des variables $\mathscr{F}^-$:

$$\hat{A}\{\mathscr{F}^-;\alpha,\beta\}=\frac{1}{\beta}\sum_m \mathscr{F}_m^-\log\mathscr{F}_m^- - \frac{\varepsilon}{\beta}\sum_m \mathscr{F}_m^-\log\mathscr{F}_m^+ - \frac{\alpha}{\beta}\sum_m \mathscr{F}_m^- + \sum_m \varepsilon_m\mathscr{F}_m^- + \mathscr{D}\{\mathscr{F}^-;\beta\}, \quad (44)$$

où nous considérons *les $\mathscr{F}_m^-$ comme des variables indépendantes*, avec $\mathscr{F}_m^+ = 1 + \varepsilon\mathscr{F}_m^-$. La notation $\bar{n}_m$ sera réservée aux nombres d'occupation moyens (32), solutions des éqs. (29), (30).

Le potentiel de Gibbs $A(\alpha,\beta)$ est alors égal à la valeur prise par cette fonction $\hat{A}\{\mathscr{F}^-;\alpha,\beta\}$ lorsqu'on y remplace chaque variable $\mathscr{F}_m^-$ par le nombre d'occupation vrai $\bar{n}_m$ correspondant aux valeurs fixées de α et β,

$$A(\alpha,\beta)=\hat{A}\{\bar{n};\alpha,\beta\}. \quad (45)$$

Les dérivées partielles de $\hat{A}$ par rapport aux variables $\mathscr{F}^-$ s'écrivent

$$\frac{\partial\hat{A}\{\mathscr{F}^-;\alpha,\beta\}}{\partial\mathscr{F}_l^-}=\frac{1}{\beta}\log\frac{\mathscr{F}_l^+}{\mathscr{F}_l^-}-\frac{\alpha}{\beta}+\varepsilon_l+\frac{\partial\mathscr{D}\{\mathscr{F}^-;\beta\}}{\partial\mathscr{F}_l^-}. \quad (46)$$

Ces dérivées partielles sont nulles lorsque les variables $\mathscr{F}_m^-$ sont égales à $\bar{n}_m$, en vertu de l'expression (43) (30) de $\bar{n}_m$. Inversement, écrire que les expressions (46) sont nulles entraîne que les $\mathscr{F}_m^-$ satisfont aux éqs. (29), (30), qui équivalent donc à

$$\frac{\partial\hat{A}\{\bar{n};\alpha,\beta\}}{\partial\mathscr{F}_l^-}=0. \quad (47)$$

Au lieu de résoudre les éqs. (29), (30), *on peut donc déterminer les nombres d'occupation $\mathscr{F}_m^-=\bar{n}_m$ en rendant l'expression $\hat{A}\{\mathscr{F}^-;\alpha,\beta\}$ stationnaire* par rapport aux variations des $\mathscr{F}^-$, pour α et β fixés.

Considérons enfin les dérivées partielles secondes

$$\frac{\partial^2\hat{A}\{\mathscr{F}^-;\alpha,\beta\}}{\partial\mathscr{F}_l^-\partial\mathscr{F}_m^-}=\frac{\delta_{lm}}{\beta\mathscr{F}_m^+\mathscr{F}_m^-}+\frac{\partial^2\mathscr{D}\{\mathscr{F}^-;\beta\}}{\partial\mathscr{F}_l^-\partial\mathscr{F}_m^-} \quad (48)$$

comme les éléments d'une matrice (symétrique réelle), dont l et m sont les indices. Nous montrons dans l'appendice C que cette matrice est, pour $\mathscr{F}_m^-=\bar{n}_m$, l'inverse de la matrice $\beta\mathscr{C}_{lm}$, où $\mathscr{C}_{lm}$, définie par

$$\mathscr{C}_{lm}=\frac{\mathrm{Tr}\,[e^{\alpha N-\beta H}(a_l^\dagger a_l-\bar{n}_l)(a_m^\dagger a_m-\bar{n}_m)]}{\mathrm{Tr}\,e^{\alpha N-\beta H}}, \quad (49)$$

est la *fonction de corrélation* (considérée également comme un élément de matrice dont les indices sont l et m), soit

$$\frac{\beta\partial^2\hat{A}\{\bar{n};\alpha,\beta\}}{\partial\mathscr{F}_l^-\partial\mathscr{F}_m^-}=(\mathscr{C}^{-1})_{lm}, \quad (50)$$

de même que dans la réf. [10]). Nous établissons pour cela, de la même manière que pour le propagateur, le développement de $\mathscr{C}_{lm}$ en fonction des nombres d'occupation, par une représentation en diagrammes D. (Nous donnerons au § 5 une autre démonstration de (50). Celle de l'appendice C montre le lien entre cette propriété et la structure des diagrammes). La matrice symétrique réelle $\mathscr{C}_{lm}$ est définie positive. Il suffit pour le voir d'effectuer, sur l'expression (49) qui la définit, la transformation unitaire qui la diagonalise. La matrice (50) est donc également définie positive. *Le potentiel de Gibbs* $A(\alpha, \beta)$ *est par conséquent le minimum de l'expression* $\hat{A}\{\mathscr{F}^-; \alpha, \beta\}$ *pour* α *et* β *fixés.*

4.2. LIEN DE LA STATIONNARITÉ AVEC LA STRUCTURE DES DIAGRAMMES

La propriété de stationnarité de $\hat{A}\{\mathscr{F}^-; \alpha, \beta\}$ est une propriété très générale, tenant à la structure en arbre des diagrammes D. Ceci explique pourquoi on la trouve également dans les formalismes des références [1, 8, 9, 10, 12]) par exemple. La démonstration est analogue à celle du § 3.3.

Partons en effet de l'expression

$$\tilde{A}\{w; \alpha, \beta\} = A_0 + \left[\sum_m \sum_{p=1}^{\infty} \frac{(w_m)^{p+1}}{(p+1)!} \frac{\partial^p f_m^-}{\partial \varepsilon_m{}^p}\right] - \left[\sum_m w_m \sum_{p=1}^{\infty} \frac{(w_m)^p}{p!} \frac{\partial^p f_m^-}{\partial \varepsilon_m{}^p}\right] + \mathscr{D}\left\{\sum_{n=0}^{\infty} \frac{(w)^p}{p!} \frac{\partial^p f^-}{\partial \varepsilon^p}; \beta\right\}, \quad (51)$$

considérée comme une fonction des variables w_m, et déduite de (44) en exprimant $\mathscr{F}_m^{\pm}$ en fonction de w_m à l'aide de l'équation (29). Les trois termes de cette expression proviennent respectivement de (38), (40) et (36). Les dérivées partielles de chacun de ces termes par rapport à w_m peuvent être représentées,

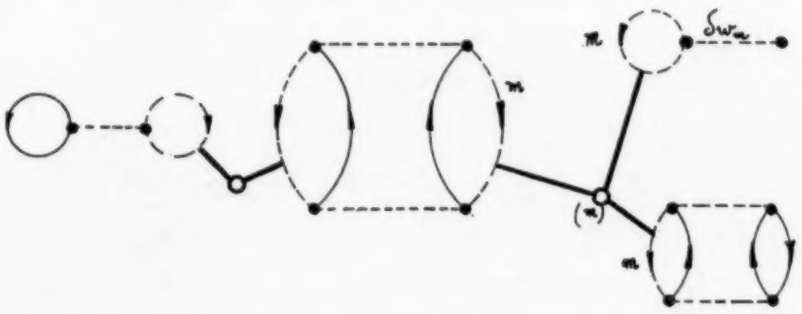

Fig. 12. Un diagramme contribuant à chacun des trois termes de $\partial \tilde{A}/\partial w_m$.

après redéveloppement en puissances de l'interaction, par l'ensemble des diagrammes D vide-vide connexes, ayant une *bulle composée fictive* δw_m (fig. 12). Cette bulle δw_m est placée en bout d'arbre, elle est rattachée à un nœud (d'impulsion m fixée) par l'intermédiaire d'une chaîne incomplète d'impulsion m, et sa contribution est égale à 1. Pour le premier terme, chaque diagramme

apparaît autant de fois qu'il y a de nœuds d'impulsion m, soit $\mathcal{N}_{N_m} = 1$ fois; pour le deuxième terme, chaque diagramme apparaît autant de fois qu'il y a de chaînes incomplètes d'impulsion m, soit $\mathcal{N}_{C_m}$ fois; pour le troisième terme, chaque diagramme apparaît autant de fois qu'il y a de bulles composées (autres que δw_m) rattachées au nœud m, soit $\mathcal{N}_{B_m} - 1$ fois. La stationnarité de $\tilde{A}$ par rapport aux variations des w_m, et par suite *la stationnarité de* $\hat{A}$ *par rapport aux variations des* $\mathscr{F}^-$ *résulte alors de l'égalité*

$$\mathcal{N}_{N_m} - \mathcal{N}_{C_m} + (\mathcal{N}_{B_m} - 1) = 0, \tag{52}$$

valable pour tout diagramme.

4.3. ÉNERGIE LIBRE ET ÉLIMINATION DE α

Le potentiel thermodynamique associé aux variables $\bar{N}$ et β, qui s'introduit lorsqu'on élimine α par l'équation

$$\bar{N} = -\beta \frac{\partial A(\alpha, \beta)}{\partial \alpha}, \tag{53}$$

est l'énergie libre

$$F(\bar{N}, \beta) = A(\alpha, \beta) + \frac{\alpha}{\beta} \bar{N}. \tag{54}$$

Nous allons montrer qu'en reformulant le problème variationnel précédent en termes de l'énergie libre, α s'élimine explicitement.

Introduisons pour cela la fonction

$$\hat{F}\{\mathscr{F}^-; \beta\} = \frac{1}{\beta} \sum_m \mathscr{F}_m^- \log \mathscr{F}_m^- - \frac{\varepsilon}{\beta} \sum_m \mathscr{F}_m^+ \log \mathscr{F}_m^+ + \sum_m \varepsilon_m \mathscr{F}_m^- + \mathscr{D}\{\mathscr{F}^-; \beta\} \tag{55}$$

des variables indépendantes $\mathscr{F}_m^-$ et β. L'équation (44), qui s'écrit encore

$$\hat{A}\{\mathscr{F}^-; \alpha, \beta\} = \hat{F}\{\mathscr{F}^-; \beta\} - \frac{\alpha}{\beta} \sum_m \mathscr{F}_m^-, \tag{56}$$

et l'équation (47) peuvent être considérées comme donnant la solution, par la méthode du multiplicateur de Lagrange $-\alpha/\beta$, du problème variationnel suivant: chercher, pour β fixé, à rendre $\hat{F}\{\mathscr{F}^-; \beta\}$ stationnaire en faisant varier les $\mathscr{F}^-$, non plus librement comme pour $\hat{A}$, mais avec la restriction

$$\sum_m \mathscr{F}_m^- = \bar{N}, \tag{57}$$

où $\bar{N}$ est une constante. *Les nombres d'occupation moyens* $\bar{n}_m$ *sont donc, pour* $\bar{N}$ *et* β *fixés, les valeurs des* $\mathscr{F}_m^-$ *qui rendent* (55) *stationnaire compte tenu de la restriction* (57), et nous pouvons assimiler la constante $\bar{N}$ au nombre moyen de

particules du système. *L'énergie libre*

$$F(\bar{N}, \beta) = \hat{F}\{\bar{n}; \beta\} \tag{58}$$

est alors la valeur stationnaire de $\hat{F}\{\mathcal{F}^-; \beta\}$ *qui est un minimum,* puisque

$$\frac{\partial^2 \hat{F}\{\mathcal{F}^-; \beta\}}{\partial \mathcal{F}_l^- \partial \mathcal{F}_m^-} = \frac{\partial^2 \hat{A}\{\mathcal{F}^-; \alpha, \beta\}}{\partial \mathcal{F}_l^- \partial \mathcal{F}_m^-} = \frac{1}{\beta} (\mathscr{C}^{-1})_{lm}. \tag{59}$$

Cette nouvelle manière de poser le problème, en déduisant de $\hat{F}\{\mathcal{F}^-; \beta\}$ (dont nous connaissons explicitement le développement) toutes les propriétés à l'équilibre thermodynamique *élimine complètement* α. On peut d'ailleurs inverser l'équation (53) en déduisant le potentiel chimique de l'énergie libre par

$$\frac{\alpha}{\beta} = \frac{\partial F(\bar{N}, \beta)}{\partial \bar{N}}, \tag{60}$$

soit

$$\frac{\alpha}{\beta} = \frac{\partial \hat{F}\{\bar{n}; \beta\}}{\partial \mathcal{F}_m^-} = -\frac{1}{\beta} \log \frac{1+\varepsilon \bar{n}_m}{\bar{n}_m} + \varepsilon_m + \frac{\partial \mathscr{D}\{\bar{n}; \beta\}}{\partial \mathcal{F}_m^-}, \tag{61}$$

équation qui équivaut au principe variationnel pour $\hat{F}$. Nous montrerons au § 6 comment nos résultats généralisent à la mécanique quantique le développement du viriel, qui s'obtient également, en mécanique classique, par élimination de α.

4.4. APPLICATION À L'EXPRESSION DES GRANDEURS THERMODYNAMIQUES

Les propriétés de stationnarité de $\hat{A}$, ou de $\hat{F}$, sont utiles pour calculer les dérivées des potentiels thermodynamiques. Pour le nombre moyen de particules du système, on retrouve ainsi

$$\bar{N} = -\beta \frac{\partial A(\alpha, \beta)}{\partial \alpha} = -\beta \frac{\partial \hat{A}\{\bar{n}; \alpha, \beta\}}{\partial \alpha} - \beta \sum_m \frac{\partial \hat{A}\{\bar{n}; \alpha, \beta\}}{\partial \mathcal{F}_m^-} \frac{\partial \bar{n}_m}{\partial \alpha},$$

d'où en utilisant (47)

$$\bar{N} = -\beta \frac{\partial \hat{A}\{\bar{n}; \alpha, \beta\}}{\partial \alpha} = \sum_m \bar{n}_m.$$

De même, pour l'énergie moyenne, on a

$$\bar{E} = \frac{\partial [\beta A(\alpha, \beta)]}{\partial \beta} = \frac{\partial [\beta \hat{A}\{\bar{n}; \alpha, \beta\}]}{\partial \beta} + \beta \sum_m \frac{\partial \hat{A}\{\bar{n}; \alpha, \beta\}}{\partial \mathcal{F}_m^-} \frac{\partial \bar{n}_m}{\partial \beta},$$

soit

$$\bar{E} = \frac{\partial [\beta \hat{A}\{\bar{n}; \alpha, \beta\}]}{\partial \beta} = \frac{\partial [\beta \hat{F}\{\bar{n}; \beta\}]}{\partial \beta}, \tag{62}$$

qui s'écrit

$$\bar{E} = \sum_m \varepsilon_m \bar{n}_m + \frac{\partial[\beta \mathscr{D}\{\bar{n}; \beta\}]}{\partial \beta}. \tag{63}$$

Le dernier terme de cette expression est représenté par les mêmes diagrammes que ceux de $\mathscr{D}$, mais ici le temps d'interaction le plus bas est fixé à 0.

Plus généralement, partons de l'équation

$$\bar{E} = \varepsilon \sum_m \varepsilon_m G_m(-0) - \tfrac{1}{2}\varepsilon \sum_m \int_0^\beta \mathrm{d}u' \, G_m(u'-u-0)\Sigma_m(u-u'), \tag{64}$$

qu'il est facile d'établir et qui donne l'énergie moyenne pour toute valeur fixée de u. Si on remplace G_m par l'expression (31), et Σ_m par une expression analogue, obtenue en effectuant sur sa représentation en diagrammes D la sommation partielle qui remplace f_m^- par $\bar{n}_m$, on trouve

$$\bar{E} = \sum_m \varepsilon_m \bar{n}_m + \mathscr{D}u\{\bar{n}; \beta\}. \tag{65}$$

La fonction $\mathscr{D}_u\{\bar{n}; \beta\}$ se déduit de $\mathscr{D}\{\bar{n}; \beta\}$ en fixant successivement chacun des temps d'interaction à l'instant u arbitraire, au lieu de les intégrer librement entre 0 et β, et en multipliant par β. De même que (64), l'expression (65) est indépendante de u; cette propriété est une conséquence de l'invariance cyclique de la trace [4]), comme on le vérifie sur la représentation en diagrammes ordinaires du développement de (64) en puissances de l'interaction. On trouve encore une expression équivalente pour $\bar{E}$ en intégrant (65) par rapport à u entre 0 et β,

$$\bar{E} = \sum_m \varepsilon_m \bar{n}_m + \mathscr{D}'\{\bar{n}; \beta\}. \tag{66}$$

La contribution de chaque diagramme à $\mathscr{D}'\{\bar{n}; \beta\}$ se déduit simplement de celle de $\mathscr{D}\{\bar{n}; \beta\}$ en la multipliant par le nombre d'interactions du diagramme.

On déduit de (63) l'entropie S du système par

$$\frac{S}{k} = -\beta A + \beta \bar{E} - \alpha \bar{N} = \beta \frac{\partial \hat{F}\{\mathscr{F}^-; \beta\}}{\partial \beta} = \varepsilon \sum_m \mathscr{F}_m^- \log \mathscr{F}_m^- - \sum_m \mathscr{F}_m^- \log \mathscr{F}_m^- + \beta^2 \frac{\partial \mathscr{D}\{\mathscr{F}^-; \beta\}}{\partial \beta}, \tag{67}$$

où k est la constante de Boltzmann, pour $\mathscr{F}_m^- = \bar{n}_m$. La dépendance de S par rapport aux interactions est entièrement contenue dans le dernier terme.

4.4.1. *Remarque* 1. *Variation des énergies non perturbées*

Considérons le potentiel de Gibbs

$$A = -\frac{1}{\beta} \log \mathrm{Tr}\, \mathrm{e}^{\alpha N - \beta \sum_m \varepsilon_m a_m^\dagger a_m - \beta V}$$

comme une fonction des variables ε_m caractérisant l'hamiltonien non perturbé. Le nombre d'occupation de l'état m peut alors s'écrire

$$\bar{n}_m = \frac{\partial A(\alpha, \beta)}{\partial \varepsilon_m}, \tag{68}$$

soit, en utilisant (47) puis (44),

$$\bar{n}_m = \frac{\partial \hat{A}\{\bar{n}; \alpha, \beta\}}{\partial \varepsilon_m} + \sum_i \frac{\partial \hat{A}\{\bar{n}; \alpha, \beta\}}{\partial \mathscr{F}_i^-} \frac{\partial \bar{n}_i}{\partial \varepsilon_m} = \frac{\partial \hat{A}\{\bar{n}; \alpha, \beta\}}{\partial \varepsilon_m} = \bar{n}_m + \frac{\partial \mathscr{D}\{\bar{n}; \beta\}}{\partial \varepsilon_m}.$$

Par suite,

$$\frac{\partial \mathscr{D}\{\bar{n}; \beta\}}{\partial \varepsilon_m} = 0. \tag{69}$$

La fonction $\mathscr{D}\{\mathscr{F}^-; \beta\}$ est donc stationnaire par rapport aux variations des ε_m, pour $\mathscr{F}_m^- = \bar{n}_m$.

Retrouvons directement cette propriété de $\mathscr{D}$. Puisque $\mathscr{D}$ ne dépend explicitement des ε_m que par l'intermédiaire des facteurs $e^{-\varepsilon_m(u_1-u_2)}$ attachés à chaque ligne (allant de u_2 à u_1), la dérivation par rapport à ε_m revient à introduire successivement sur chaque ligne un point dont l'instant u variera entre u_2 et u_1, et à maintenir fixe l'état correspondant à cette ligne. On a donc, pour $\mathscr{F}_m^- = \bar{n}_m$, en séparant les contributions d'après le sens de cette ligne,

$$\frac{\partial \mathscr{D}\{\mathscr{F}^-; \beta\}}{\partial \varepsilon_m} = \frac{\varepsilon}{\beta} \int_0^\beta \mathscr{F}_m^+ g_m^+(u-0, u) + \frac{\varepsilon}{\beta} \int_0^\beta \mathscr{F}_m^- g_m^-(u+0, u)$$

$$= \frac{\varepsilon}{\beta} \int_0^\beta [G_m(+0) - \mathscr{F}_m^+] = 0.$$

4.4.2. *Remarque 2. Comparaison avec le développement de Lee et Yang*

On notera l'analogie de ces résultats avec ceux de Lee et Yang [10]). De même que dans leur formulation, nous séparons, bien que de façon moins complète, la dynamique du système de sa statistique, et nous obtenons les nombres d'occuptation vrais $\bar{n}_m$ par minimisation de functions A ou F. Mais il existe des différences essentielles entre les deux formulations. D'une part, $\hat{A}$ et $\hat{F}$ sont ici des fonctions du nombre d'occupation $\mathscr{F}_m^-$ de l'état m au lieu d'être des fonctions de $M(m) = e^{\alpha}(1+\varepsilon \mathscr{F}_m^-)$. D'autre part, la fonction $\hat{F}[\mathscr{F}^-; \beta]$ ne dépend pas de $\bar{N}$ et sa forme explicite est donnée par (55); au contraire, chez Lee et Yang, la fonction correspondante dépend explicitement de $\bar{N}$, et elle ne peut être calculée qu'après avoir exprimé α comme fonction de $M(m)$, de $\bar{N}$ et β à l'aide de l'équation

$$\bar{N} = \frac{\partial \mathscr{P}\{M; \alpha, \beta\}}{\partial \alpha},$$

où la fonction $\mathscr{P}\{M; \alpha, \beta\}$ (dont le maximum représente $-\beta A$) est connue par

son développement. Notre formulation en termes du nombre d'occupation permet donc pour toutes ces raisons l'élimination complète et explicite de α, comme dans le développement du viriel en mécanique classique.

4.4.3. *Remarque* 3. *Comparaison avec les développements relatifs à l'état fondamental*

L'analogie entre les expressions que nous avons obtenues et celles qui se rapportent à l'état fondamental est remarquable: les expressions données plus haut pour A, F et $\bar{E}$ ont la même représentation en diagrammes que l'énergie de l'état fondamental [5, 6]); les diagrammes anormaux sont également éliminés dans l'expression (31) du propagateur; les diagrammes représentant respectivement les expressions (30) et (34) de w_m sont les mêmes que ceux qui représentent les développements de l'énergie de Fermi, et des énergies des états excités à une particule ou un trou établis par Hugenholtz et Van Hove ($\partial\mathscr{D}\{\mathscr{F}^-;\beta\}/\partial\mathscr{F}_m^-$ est analogue à l'expression $\bar{B}_k$ de la réf. [18]), $g_m^+(\beta, 0)$ ou $g_m^-(0, \beta)$ sont analogues aux expressions $\bar{D}_k$ ou $\bar{D}_m$ de la réf. [6])). Mais cette analogie n'est que formelle, et les développements présentent des différences essentielles. D'une part, les contributions des diagrammes doivent ici être calculées dans une *représentation dépendant du temps*, entre 0 et β, avec des dénominateurs d'énergie de signes quelconques, de sorte qu'on ne peut passer immédiatement à la limite $\beta \to \infty$. D'autre part, les facteurs de pondération $\mathscr{F}_m^+$ ou $\mathscr{F}_m^-$, associés à l'impulsion d'une chaîne montante ou descendante, ne peuvent être considérés comme les analogues à température non nulle des facteurs $\Gamma(\varepsilon_m - \varepsilon_F)$ ou $\Gamma(\varepsilon_F - \varepsilon_m)$ (où $\Gamma(x) = 1$ si $x > 0$, $\Gamma(x) = 0$ si $x < 0$, et où ε_F est l'énergie de Fermi non perturbée), associés aux chaînes montantes ou descendantes des diagrammes représentant l'énergie de l'état fondamental ou l'énergie de Fermi. En effet, à la limite de la température nulle, $\mathscr{F}_m^- = \bar{n}_m$, nombre d'occupation *vrai*, ne peut tendre vers le nombre d'occupation *non perturbé* $\Gamma(\varepsilon_F - \varepsilon_m)$. Ce sont en fait les expressions des réfs. [3, 8]) qui généralisent le plus naturellement les développements relatifs à l'état fondamental.

Appendice A

THÉORÈME DE DÉSENCHEVÊTREMENT D'UN PRODUIT DE PAIRES D'OPÉRATEURS DE CRÉATION ET D'ANNIHILATION

Nous allons mettre un produit d'opérateurs de création et d'annihilation associés par paires, mais placés dans un ordre quelconque, sous la forme d'une somme de produits dans lesquels les opérateurs associés se trouveront l'un à côté de l'autre. Nous établirons pour cela un théorème algébrique par une méthode analogue à celle de Wick [13]).

La notion de contraction D dans un produit d'opérateurs ayant été définie comme au début du § 2.3.3 (pour alléger, nous écrirons partout dans cet appendice contraction au lieu de contraction D), nous appellerons *produit de désen-*

chevêtrement ou *produit* D d'un produit $\mathscr{P}$ d'opérateurs associés par paires, tout produit partiellement contracté et ordonné des opérateurs de $\mathscr{P}$ formé d'après les lois suivantes:

(a) Les contractions doivent être placées de manière à former des chaînes dont chacune est de la forme

$$\alpha\,\overline{\alpha'\,\beta}\;\;\overline{\beta'\gamma}\;\;\overline{\gamma'\ldots\omega}\,\omega', \tag{A.1}$$

où $\alpha\alpha'$; $\beta\beta'$; etc.... désignent des paires d'opérateurs associés, l'ordre des opérateurs dans le produit $\mathscr{P}$ n'étant pas forcément celui qui est indiqué dans (A.1). Nous dirons par extension qu'une paire non contractée constitue une chaîne.

(b) L'opérateur α commençant une chaîne doit être situé dans le produit $\mathscr{P}$ à gauche de tous les autres opérateurs de la chaîne. En ce qui concerne les contractions, l'opérateur β doit être dans $\mathscr{P}$ à gauche de α', γ à gauche de β', etc....

(c) Pour chaque chaîne, on ramène le dernier opérateur ω' immédiatement à droite du premier opérateur α.

(d) On affecte le produit du signe ε^P, où P est la parité de la permutation nécessaire pour amener l'un à côté de l'autre les opérateurs contractés ensemble et les opérateurs terminaux de chaque chaîne.

Etant donné un produit $\mathscr{P}$ d'opérateurs associés par paires, on peut construire l'ensemble de ses produits D de la manière suivante. Soit α l'opérateur situé le plus à gauche dans $\mathscr{P}$, et α' son associé. Ou bien on ne contracte pas α', et alors $\alpha\alpha'$ constituent une première chaîne; ou bien on contracte α' avec n'importe lequel des opérateurs situés entre α et α' (s'il y en a) que nous appellerons β. Ensuite, ou bien on ne contracte pas β', et alors $\alpha\overline{\alpha'\,\beta}\beta'$ constituent une première chaîne; ou bien on contracte β' avec n'importe lequel des opérateurs non encore contractés situés entre α et β'; et ainsi de suite. Chaque fois qu'une chaîne est terminée, on recommence les mêmes opérations en utilisant les opérateurs de $\mathscr{P}$ non encore incorporés dans une chaîne, jusqu'à épuisement du produit.

Par exemple, partant du produit $\mathscr{P} = \alpha\beta\gamma\gamma'\delta\delta'\alpha'\beta'$, on peut construire les produits D suivants (où les différentes chaînes sont mises entre crochets):

$$\mathrm{D}(\alpha\beta\gamma\gamma'\delta\delta'\alpha'\beta') = \varepsilon[\alpha\alpha'][\beta\beta'][\gamma\gamma'][\delta\delta'],$$

$$\mathrm{D}(\alpha\overline{\beta\gamma\gamma'\delta}\,\overline{\delta'\alpha'\beta'}) = [\alpha\alpha'][\beta\gamma'\overline{\delta'\beta'}\,\overline{\gamma\delta}],$$

$$\mathrm{D}(\overline{\alpha\beta\gamma\gamma'\delta}\,\overline{\delta'\alpha'\beta'}) = \varepsilon[\alpha\gamma'\overline{\delta'\alpha'}\,\overline{\beta\delta}\,\overline{\gamma\beta'}],$$

etc....

On notera que, contrairement à ce qui se passe pour les produits normaux con-

tractés de la théorie de Wick, dans lesquels les contractions peuvent être placées arbitrairement, il n'existe pas de produits D tels que $D(\alpha\beta\gamma\gamma'\delta\delta'\alpha'\beta')$ ou $D(\alpha\beta\gamma\gamma'\delta\delta'\alpha'\beta')$, qui violent la loi (a), $D(\alpha\beta\gamma\gamma'\delta\delta'\alpha'\beta')$ ou $D(\alpha\beta\gamma\gamma'\delta\delta'\alpha'\beta')$, qui violent la loi (b).

Théorème de désenchevêtrement:

Un produit d'opérateurs associés par paires et placés dans un ordre quelconque est égal à la somme de tous les produits D *qu'on peut construire à partir de ce produit.*

Procédant par récurrence, supposons le théorème vrai pour tous les produits de $n-1$ paires. Considérons un produit $\mathscr{P}_n$ de n paires. α étant le premier opérateur de ce produit, amenons son associé α' à côté de α en le commutant successivement avec chacun des k opérateurs situés entre α et α'. Le produit $\mathscr{P}_n$ s'exprime ainsi comme une somme de $k+1$ termes.

(1) Le premier d'entre eux est le produit de $\varepsilon^k \alpha\alpha'$ par le produit $\mathscr{P}_{n-1}$ des $n-1$ autres paires. Si on applique le théorème à $\mathscr{P}_{n-1}$, $\varepsilon^k \alpha\alpha' \mathscr{P}_{n-1}$ s'interprète immédiatement comme la somme de tous les produits D qu'on peut construire à partir de $\mathscr{P}_n$ et dont la première chaîne est constituée par la paire non contractée $\alpha\alpha'$.

(2) Chacun des k autres termes est de la forme $\varepsilon^{k'} \beta\alpha' \mathscr{P}'_{n-1}$, et s'obtient en contractant α' avec chacun des k opérateurs situés dans $\mathscr{P}_n$ entre α et α'. Ici $k'(0 \leqq k' \leqq k-1)$ est le nombre d'opérateurs situés entre β et α' dans $\mathscr{P}_n$. Dans le produit $\mathscr{P}'_{n-1}$ des opérateurs de $\mathscr{P}_n$ autres que β et α', tous les opérateurs sont associés par paires, sauf α (le premier) et β'. Considérons alors α et β' comme formant une paire. Si on applique le théorème à $\mathscr{P}'_{n-1}$, le produit $\varepsilon^{k'} \beta\alpha' \mathscr{P}'_{n-1}$ s'interprète comme la somme de tous les produits D qu'on peut construire à partir de $\mathscr{P}_n$ et dans lesquels α' est contracté avec β.

La somme de ces k termes s'interprète donc comme la somme de tous les produits D qu'on peut construire à partir de $\mathscr{P}_n$ et dont la première chaîne commence par $\alpha\alpha'\beta \ldots$.

Le théorème étant vrai pour $n = 1$ (le seul produit D est alors le produit lui-même), est donc démontré pour n quelconque.

Le résultat établi sur l'exemple du § 2.3.3 se généralise en appliquant le théorème de désenchevêtrement au produit des opérateurs, tous relatifs au même état, correspondant à l'entrée et à la sortie des bulles d'un collier donné, puis en prenant la valeur moyenne connexe de chacun des produits D ainsi obtenus (cette opération est justifiée au § 2.3.4). Comme les opérateurs de chaque paire sont de nature opposée, la loi (b) de définition des produits D montre que, dans la représentation en diagrammes de chaque chaîne, les lignes (D ou de fermeture) doivent être toutes de même sens.

Appendice B

SIGNE ASSOCIÉ À UN DIAGRAMME D

Bosons

Le signe provient simplement des valeurs numériques (19) des contractions D. Un signe moins apparaît donc pour chaque ligne D descendante, à l'exclusion des lignes de fermeture. On peut donc associer un signe moins à chaque ligne descendante et un signe moins à chaque chaîne descendante.

Fermions

Le signe associé à un diagramme D est celui de la parité de la permutation qui, d'une part, ramène côte à côte les opérateurs contractés ensemble (soit par des contractions D, soit par les contractions ordinaires de fermeture (16) des chaînes complètes), et qui, d'autre part, replace les opérateurs formant les extrémités de chaque chaîne incomplète dans l'ordre $a^\dagger a$ (ordre auquel correspond la valeur (15) ou (23) du facteur associé à chaque nœud).

Ramenons d'abord côte à côte d'une part les opérateurs contractés ensemble, d'autre part les opérateurs formant les extrémités de chaque chaîne incomplète (sans changer leur ordre). Le signe correspondant à cette permutation est le même que celui du système complet de contractions, représenté par l'ensemble des lignes (ordinaires, D, ou de fermeture) des bulles composées du diagramme D. Ce signe est donc $(-)^{h+l}$, où h est le nombre de lignes descendantes et l le nombre de boucles fermées du diagramme.

Il nous reste alors à commuter chacune des paires d'opérateurs formant les extrémités des chaînes incomplètes qui sont de la forme $aa^\dagger$ (les opérateurs de chaque paire ont été ramenés côte à côte par la précédente permutation), ce qui introduit un signe moins pour chaque paire $aa^\dagger$, c'est-à-dire pour chaque chaîne incomplète montante.

Le signe de la permutation cherchée est donc $(-)^{l+h+n'_+}$, où n'_+ est le nombre de chaînes incomplètes montantes.

Appendice C

EXPRESSION DE LA FONCTION DE CORRÉLATION

Nous allons établir, de la même façon qu'aux § 2.5 et § 3.2 pour le propagateur, un développement de la fonction de corrélation

$$\mathscr{C}_{lm} = \frac{\operatorname{Tr} e^{\alpha N - \beta H} a_l^\dagger a_l a_m^\dagger a_m}{\operatorname{Tr} e^{\alpha N - \beta H}} - \bar{n}_l \bar{n}_m \qquad \text{(C.1)}$$

en fonction des nombres d'occupation $\bar{n}_m$.

La méthode des perturbations fournit pour $\mathscr{C}_{lm}$, de même que pour A ou G_m, une représentation en diagrammes compris entre 0 et β, avec les mêmes règles

de calcul (fig. 13). Ces diagrammes ont deux points d'entrée $a_l^\dagger$ et $a_m^\dagger$ et deux points de sortie a_l et a_m, tous placés à l'instant 0. Par convention, on les mettra de gauche à droite dans l'ordre $a_l^\dagger a_l a_m^\dagger a_m$, et tout se passera, en ce qui concerne le sens des lignes qui peuvent éventuellement les joindre, comme s'ils étaient de haut en bas dans le même ordre. Le dénominateur élimine toutes les parties vide-vide des diagrammes, de sorte que $\mathrm{Tr}\, e^{\alpha N-\beta H} a_l^\dagger a_l a_m^\dagger a_m / \mathrm{Tr}\, e^{\alpha N-\beta H}$ est représenté par la somme des diagrammes liés, c'est-à-dire sans partie vide-vide; le terme $-\bar{n}_l \bar{n}_m$ dans (C.1) élimine alors tous les diagrammes liés composés de deux parties disconnectées dont l'une va de $a_l^\dagger$ à a_l et l'autre de $a_m^\dagger$ à a_m.

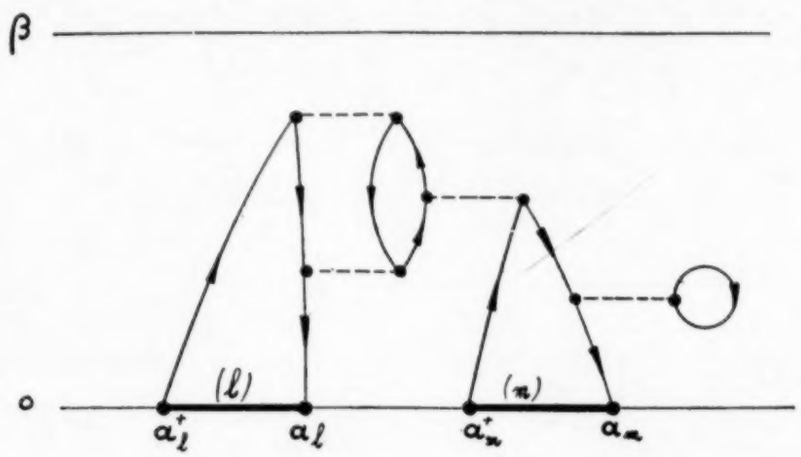

Fig. 13. Un diagramme contribuant à $\mathscr{C}_{lm}$.

Pour nous ramener au problème déjà traité, groupons les opérateurs $a_l^\dagger$ et a_l d'une part, $a_m^\dagger$ et a_m d'autre part par paires, en les considérant comme points de sortie et d'entrée de deux bulles montantes fictives, placées à l'instant 0 et ne se chevauchant pas. Les diagrammes qui contribuent à $\mathscr{C}_{lm}$ sont alors tous les diagrammes connexes contenant ces deux bulles (l) et (m), et ceci même lorsque l'état l est le même que l'état m (fig. 13).

Ces diagrammes ayant même structure que les diagrammes vide-vide, l'application du théorème de désenchevêtrement conduit, de la même façon que pour A, à une représentation en diagrammes D. Les deux bulles particulières (l) et (m), étant désenchevêtrées, doivent être refermées sur elles-mêmes par une chaîne incomplète descendante, et forment à elles seules deux bulles composées. Ce résultat est valable même lorsque $l = m$, auquel cas les deux bulles (l) et (m) peuvent être rattachées au même nœud.

Grâce à la structure en arbre des diagrammes D contribuant à $\mathscr{C}_{lm}$, il existe un chemin unique pour aller en suivant les nœuds et les bulles composées, de la bulle (l) à la bulle (m), ce qui permet de définir un squelette (fig. 14). Lorsque $l \neq m$, tout diagramme D peut donc être obtenu en effectuant des insertions dans les diagrammes D des figures 14(b), (c) . . . de deux manières différentes:

(1) sur les chaînes complètes (autres que l, l_1, l_2, . . ., m) appartenant aux

bulles composées $\mathscr{B}_1$, $\mathscr{B}_2$, ... Avant ces insertions, la contribution de la bulle composée $\mathscr{B}_1$, par exemple, est (après intégration par rapport aux temps d'interaction)

$$-\beta \frac{\partial^2 \mathscr{D}\{f^-; \beta\}}{\partial f_l^- \partial f_{l_1}^-}. \tag{C.2}$$

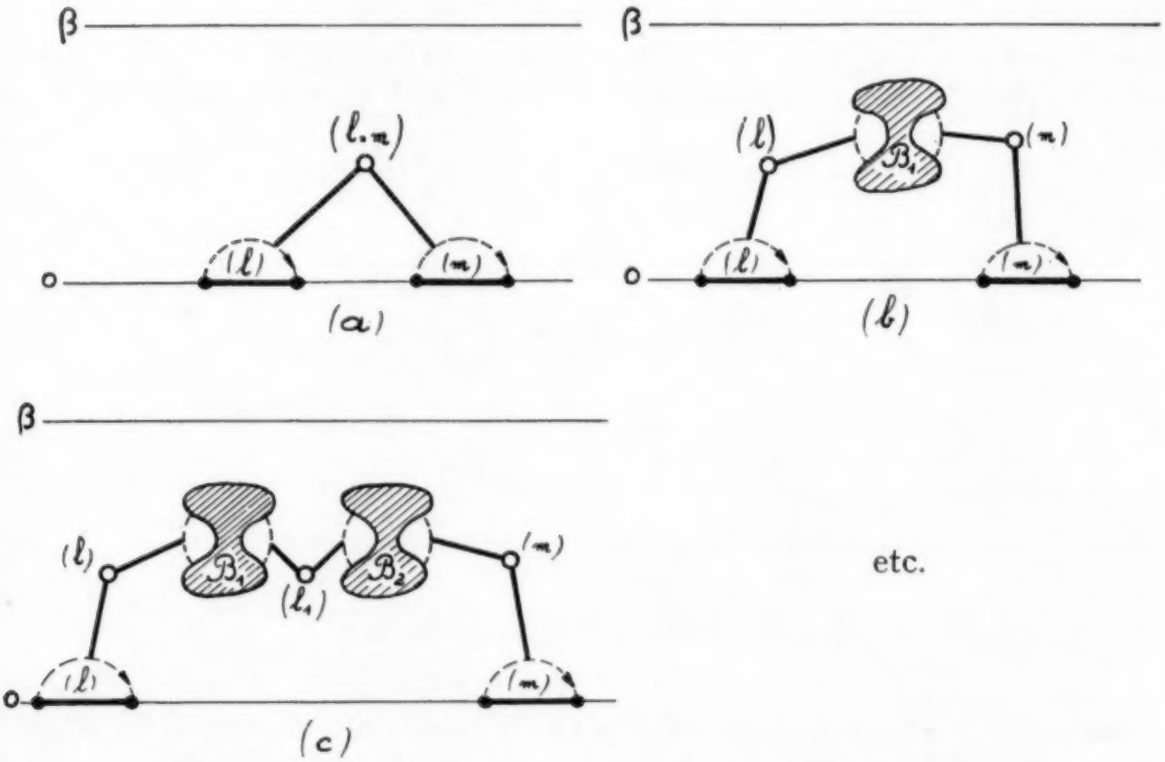

etc.

Fig. 14. Les squelettes de la représentation en diagrammes D de $\mathscr{C}_{lm}$. Les parties hachurées $\mathscr{B}_1 \mathscr{B}_2 \ldots$ représentent des bulles composées à deux chaînes incomplètes, schématisées par des lignes pointillées. Le diagramme (a) n'existe que pour $l = m$. Dans les diagrammes (c) et suivants, il faut sommer sur les états l_1, etc.

La double dérivation fonctionnelle remplace en effet de toutes les manières possibles deux chaînes complètes de la bulle composée par des chaînes incomplètes relatives aux états l et l_1. L'ensemble de ces insertions a pour effet de remplacer dans (C.2) les facteurs $f^{\pm}$ attachés aux chaînes par les $\mathscr{F}^{\pm}$ (déterminés par les équations (29), (30)). Chaque bulle composée donne donc une contribution de la forme

$$-\beta \frac{\partial^2 \mathscr{D}\{\mathscr{F}^-; \beta\}}{\partial \mathscr{F}_l^- \partial \mathscr{F}_{l_1}^-}; \tag{C.3}$$

(2) sur les nœuds (l), (l_1), (l_2), ... (m). L'ensemble des insertions effectuées sur le nœud (l) par exemple a pour effet de remplacer le facteur

$$-\frac{1}{\beta} \frac{\partial f_l^-}{\partial \varepsilon_l} = f_l^+ f_l^-$$

associé à ce nœud, par

$$\left(-\frac{1}{\beta}\frac{\partial}{\partial\varepsilon_l}\right)f_l^- + (-\beta w_l)\left(-\frac{1}{\beta}\frac{\partial}{\partial\varepsilon_l}\right)^2 f_l^- + \frac{(-\beta w_l)^2}{2!}\left(-\frac{1}{\beta}\frac{\partial}{\partial\varepsilon_l}\right)^3 f_l^- + \ldots$$

$$= -\frac{1}{\beta}\frac{\partial\mathscr{F}_l^-}{\partial\varepsilon_l} = \mathscr{F}_l^+\mathscr{F}_l^-. \quad \text{(C.4)}$$

Ces résultats restent valables en cas d'égalité accidentelle des états l, l_1, $l_2 \ldots, m$, sauf lorsque $l = m$. Dans ce cas en effet, en plus des diagrammes D précédents, on doit considérer les diagrammes D où les bulles (l) et (m) sont rattachées au même nœud. Ces diagrammes se déduisent de celui de la fig. 14(a) en effectuant sur le nœud (l) toutes les insertions possibles, de même que dans (C.4).

En définitive, la sommation partielle des diagrammes D conduit donc à

$$\mathscr{C}_{lm} = \delta_{lm}\mathscr{F}_l^+\mathscr{F}_l^- + \mathscr{F}_l^+\mathscr{F}_l^-\left(-\beta\frac{\partial^2\mathscr{D}\{\mathscr{F}^-;\beta\}}{\partial\mathscr{F}_l^-\partial\mathscr{F}_m^-}\right)\mathscr{F}_m^+\mathscr{F}_m^-$$

$$+\sum_{l_1}\mathscr{F}_l^+\mathscr{F}_l^-\left(-\beta\frac{\partial^2\mathscr{D}\{\mathscr{F}^-;\beta\}}{\partial\mathscr{F}_l^-\partial\mathscr{F}_{l_1}^-}\right)\mathscr{F}_{l_1}^+\mathscr{F}_{l_1}^-\left(-\beta\frac{\partial^2\mathscr{D}\{\mathscr{F}^-;\beta\}}{\partial\mathscr{F}_{l_1}^-\partial\mathscr{F}_m^-}\right)\mathscr{F}_m^+\mathscr{F}_m^+ + \ldots, \quad \text{(C.5)}$$

qui est l'inverse de la matrice

$$\beta\frac{\partial^2\hat{A}\{\mathscr{F}^-;\alpha,\beta\}}{\partial\mathscr{F}_l^-\partial\mathscr{F}_m^-} = \frac{\delta_{lm}}{\mathscr{F}_m^+\mathscr{F}_m^-} + \beta\frac{\partial^2\mathscr{D}\{\mathscr{F}^-;\beta\}}{\partial\mathscr{F}_l^-\partial\mathscr{F}_m^-}. \quad \text{(C.6)}$$

Bibliographie

1) J. Yvon, Actual. Sc. et Indust. **203** (1935)
2) R. Balian, C. Bloch et C. De Dominicis, Compt. Rend. **250** (1960) 2850;
   C. Bloch, Int. Conf. on the Many-Body Problem, Utrecht (1960)
3) R. Balian, C. Bloch et C. de Dominicis, Int. Spring School, Naples (1960)
4) C. Bloch et C. De Dominicis, Nuclear Physics **7** (1958) 459
5) J. Goldstone, Proc. Roy. Soc. **A 239** (1957) 267;
   C. Bloch, Nuclear Physics **7** (1958) 451
6) N. M. Hugenholtz, Physica **23** (1957) 481
7) W. Kohn et J. M. Luttinger, Phys. Rev. **118** (1960) 41
8) R. Balian et C. De Dominicis, Compt. Rend. **250** (1960) 3285 et 4111;
   C. De Dominicis, Int. Conf. on the Many-Body Problem, Utrecht (1960)
9) J. M. Luttinger et J. C. Ward, Phys. Rev. **118** (1960) 1417
10) T. D. Lee, et C. N. Yang Phys. Rev. **117** (1960) 22
11) H. D. Ursell, Proc. Camb. Phil. Soc. **23** (1927) 685;
   J. E. Mayer, J. Chem. Phys. **5** (1937) 67
12) R. Balian et C. De Dominicis, Nuclear Physics **16** (1960) 502
13) G. Wick, Phys. Rev. **80** (1950) 268
14) T. Matsubara, Progr. Theor. Phys. **14** (1955) 351;
   T. Thouless, Phys. Rev. **107** (1957) 1162;
   M. Gaudin, Nuclear Physics **15** (1960) 89
15) R. Brout et F. Englert, Phys. Rev. **120** (1960) 1519
16) R. Balian, Nuclear Physics **13** (1959) 594
17) K. Husimi, Proc. Phys. Math. Soc. Japan **22** (1940) 264;
   C. Bloch et C. De Dominicis, Nuclear Physics **10** (1959) 181
18) N. M. Hugenholtz et L. Van Hove, Physica **24** (1958) 363

7.A

Nuclear Physics **25** (1961) 568—603; © *North-Holland Publishing Co., Amsterdam*

Not to be reproduced by photoprint or microfilm without written permission from the publisher

THE ANALYTICITY DOMAIN OF THE FOUR POINT FUNCTION

GUNNAR KÄLLÉN

Department of Theoretical Physics, University of Lund, Lund, Sweden †

Received 10 February 1961

Abstract: A characterization of the boundary curves determining the analyticity domain of the four point function is given. In this paper, we investigate only the analyticity domain that follows when local commutativity of the field operators is not invoked. The domain turns out to be bounded by obvious generalizations of the surfaces one has for the three point function and by an entirely new surface which is not an analytic hypersurface. The equation of the new surface is investigated in some detail and its properties are illustrated with numerical plots.

1. Introduction

During the last few years considerable effort has been devoted to the investigation of the mathematical properties of vacuum expectation values of field operators. These questions are of interest because such vacuum expectation values or, rather, linear combinations of them enter directly into physically observable quantities like scattering amplitudes and other S-matrix elements. Moreover, these vacuum expectation values are of fundamental importance for the more fundamental aspects of the theory as they can conveniently be used to discuss the result of measurements of space time averages of the fields. Finally, it has been known for some time that the high energy behaviour of the Fourier transforms of these objects determine directly the convergence properties of the theory like the magnitude of the renormalization constants etc. The simplest case of such an expectation value is the expectation value of a product of two field operators. The general properties of such a quantity have been known for several years. The first investigation of this kind was made by Umezawa and Kamefuchi in 1951 [1]). Later, similar arguments were presented by several authors [2]). Today, we know that this vacuum expectation value can be understood as the boundary value of an analytic function depending on the Lorentz square of a complex four vector. The real part of this four vector is equal to the difference of the two points appearing in the expectation value, and the imaginary part lies inside the backward light cone. As the analytic function mentioned above depends only on the square of this

† Part of this work was done while the author was a guest at the Institut des Hautes Études Scientifiques in Paris. The hospitality of this institute and of its director, Prof. L. Motchane, is gratefully acknowledged.

vector it follows that one can also use every vector that can be obtained from the given one with the aid of a complex Lorentz transformation. The analytic function is regular in the whole complex plane of the square of the vector except on the positive real axis. We refer to this domain as the "cut plane". But, when one investigates the product of three field operators, the situation is considerably more complicated. In analogy with the situation for the product of two operators (the two point function) one might expect that the product of three operators (the three point function) should be regular in the topological product of the three cut planes for the complex variables which can be obtained from the squares of the three differences entering in the functions. But this is not the case. If one does not assume that the field operators commute for space like separations but only that they are Lorentz-covariant quantities and that the "mass spectrum" of the theory has a reasonable shape †, one finds that the three point function is also the boundary value of an analytic function regular in a certain domain. This domain is bounded by two of the cuts mentioned above but also by pieces of more complicated surfaces [3]). If one further imposes the condition that the fields are local, i.e. that they commute for space-like separations, one finds that the analyticity domain is considerably enlarged and can be described as the union of the original domain and two other domains. It further appears that this union is not a natural domain of analyticity and, therefore, that the three point function is regular in the holomorphy envelope of this union [3]). In this paper, we want to indicate the first steps in a similar approach to the four point function. This function is of special importance as it enters directly into two particle scattering problems. As can perhaps be expected, the algebraic complications increase considerably when one goes from the three point function to the four point function just as they increase when one goes from the two point function to the three point function. We therefore think that even a small part of this program justifies a separate publication. Consequently, we are here going to limit ourselves to a discussion of the domain that follows from the general properties mentioned in KW but without use of local commutativity. The domain we are going to find turns out to be bounded not only by the cuts and by obvious generalizations of the boundaries of the three point function but also by an entirely new surface of a much more complicated character than those found before. The discussion of the further properties appearing when local commutativity is invoked is postponed to a later publication.

† The details of these concepts are explained e.g. in a paper by G. Källén and A. Wightman [3]). This paper, which is referred to as KW below, also contains more complete references to earlier work.

2. Definitions and Preliminary Results

Consider four scalar fields $A_1(x_1)$, $A_2(x_2)$, $A_3(x_3)$ and $A_4(x_4)$ and define a function $F^{A_1A_2A_3A_4}(x_1-x_2, x_2-x_3, x_3-x_4)$ by

$$F^{A_1A_2A_3A_4}(x_1-x_2, x_2-x_3, x_3-x_4) = \langle 0|A_1(x_1)\, A_2(x_2)\, A_3(x_3)\, A_4(x_4)|0\rangle. \quad (1)$$

From the general properties mentioned above and described in more detail, e.g. in KW, one finds that this function F is the boundary value of a certain analytic function depending on the complex variables z_{jk} defined by

$$F^{A_1A_2A_3A_4}(x_1-x_2, x_2-x_3, x_3-x_4) = \text{B.V. } F^{A_1A_2A_3A_4}(z_{11}, z_{22}, z_{33}, z_{12}, z_{13}, z_{23}), \quad (2)$$

$$z_{jk} = -(\xi_j - i\eta_j)(\xi_k - i\eta_k), \quad (2a)$$

$$\xi_j = x_j - x_{j+1}. \quad (2b)$$

The function $F^{A_1\cdots A_4}(z_{11}, \ldots, z_{23})$ or, for shortness, $F(z_{jk})$, is regular when the vectors η above are all real vectors lying in the forward light cone †. Using standard techniques we can immediately write a representation of the function $F(z_{jk})$ with the aid of a function $\Delta_4^{(+)}$ in the following way [4])

$$F(z_{jk}) = \int \ldots \int \prod \mathrm{d}a_{jk}\, G(a_{jk}) \Delta_4^{(+)}(z_{jk}, a_{jk}), \quad (3)$$

$$\Delta_4^{(+)}(z_{jk}, a_{jk}) = \frac{1}{(2\pi)^{12}} \int \ldots \int \mathrm{d}p_1\, \mathrm{d}p_2\, \mathrm{d}p_3\, \mathrm{e}^{i\Sigma\zeta_k p_k} \prod_{j\leqq k} \delta(p_j p_k + a_{jk}) \prod \theta(p_j). \quad (3a)$$

The domain of integration over the "mass variables" a_{jk} in eq. (3) is defined by

$$a_{jk} \geqq 0 \text{ for all } j \text{ and } k, \quad (4a)$$

$$a_{jk}^2 - a_{jj}a_{kk} \geqq 0 \text{ for } j \neq k, \quad (4b)$$

$$\mathrm{Det}|a_{jk}| \geqq 0. \quad (4c)$$

The vectors ζ_k are the above mentioned complex vectors whose scalar products (with a minus sign) give the complex numbers z_{jk} (we use the metric $x^2 = \bar{x}^2 - x_0^2$). The function $G(a_{jk})$ in eq. (3) is determined by the Fouriertransform of the original function F

$$F^{A_1A_2A_3A_4}(\xi_1, \xi_2, \xi_3) = \frac{1}{(2\pi)^{12}} \int \ldots \int \mathrm{d}p_1 \ldots \mathrm{d}p_3\, \mathrm{e}^{i\Sigma p_k \xi_k} G(-p_j p_k) \prod \theta(p_j). \quad (5)$$

The function $\Delta_4^{(+)}$ in eq. (3) can be explicitly computed. Here we are only interested in its regularity properties. One finds that this function is regular analytic and exponentially damped for every point z_{jk} except for those z_{jk} which fulfil the equation [4])

$$(t^2-Q)^2 - R - t\sqrt{S} = 0, \quad (6a)$$

† Cf. in particular the last paper mentioned in ref. [2]).

$$Q = \mathrm{Tr}[M] = \sigma_1+\sigma_2+\sigma_3, \tag{6b}$$

$$R = 4(\sigma_1\sigma_2+\sigma_2\sigma_3+\sigma_3\sigma_1) = 2[(\mathrm{Tr}[M])^2-\mathrm{Tr}[M^2]], \tag{6c}$$

$$S = 64\sigma_1\sigma_2\sigma_3 = 64\ \mathrm{Det}\ |M|, \tag{6d}$$

$$M = Za. \tag{6e}$$

The last equation defines the matrix M as the 3×3 matrix which is obtained when the two 3×3 matrices $Z = ||z_{jk}||$ and $a = ||a_{jk}||$ are multiplied together. The quantities Q, R and S can be expressed in terms of the eigenvalues σ_j of M or in terms of traces of various powers of M. The numerical factors in Q, R and S are chosen in such a way that one has no extra numerical coefficients in eq. (6a). The quantity t in this equation is an arbitrary real number and the masses a_{jk} have any values in the domain described by eqs. (4). Eq. (6a) expresses the condition that some linear combination of $\pm\sqrt{\sigma_j}$ is a real number or

$$\pm\sqrt{\sigma_1}\pm\sqrt{\sigma_2}\pm\sqrt{\sigma_3} = t. \tag{7}$$

We thus have two alternative ways to characterize the analyticity domain of the function $F(z_{jk})$. We can either say that F is regular analytic in every point z_{jk} which can be obtained with the aid of scalar products from complex four vectors with the imaginary parts in the backward light cone or that every point z_{jk} which fulfils eq. (6a) for some value of the masses a_{jk} in the domain described by eqs. (4) and some real number t lies outside the regularity domain. These two descriptions are entirely equivalent, and it is a question of convenience which one is preferred. In particular, we notice that the boundary of our domain can be described as the set of points which fulfil eq. (6a) and at the same time can be obtained as limiting points from the complex vectors. Actually, this characterization of the boundary turns out to be convenient for the discussion below.

We first remark that, if we put e.g. $a_{33} = a_{13} = a_{23} = 0$ and consider masses $a_{12} \geqq \sqrt{a_{11}a_{22}}$; $a_{11} \geqq 0$; $a_{22} \geqq 0$, we are certainly inside the domain of integration in eq. (4). For this particular choice of the masses one finds that

$$S = 0, \tag{8a}$$

$$R = 4(a_{12}^2-a_{11}a_{22})(z_{12}^2-z_{11}z_{22}), \tag{8b}$$

$$Q = a_{11}z_{11}+a_{22}z_{22}+2a_{12}z_{12}. \tag{8c}$$

For this case eq. (6a) reduces to exactly the equation which was investigated in App. I of KW and which led to a description of the three point function regularity domain †. We therefore conclude that every point z_{jk} which is such

† Cf. eq. (A4) in KW. Note that the relation between the notation used here and the notation in KW is given by $z_1 = z_{11}$, $z_2 = z_{22}$, $z_3 = z_{11}+z_{22}+2z_{12}$, $a = a_{11}$, $b = a_{22}$, $c = a_{12}$. A somewhat modified version of the discussion in App. 1 in KW with the aid of techniques developed here is given in App. 2 of the present paper.

that the points z_{11}, z_{22} and z_{12} lie outside the regularity domain for the corresponding three point function is certainly outside the regularity domain for the four point function. By obvious permutations one finds a similar result also for points z_{jk} such that z_{11}, z_{33} and z_{13} in one case and z_{22}, z_{33} and z_{23} in the other case lie outside the corresponding three point function regularity domains. We therefore conclude that the following analytic hypersurfaces [3] †:

$$z_{jj}\text{-cut:} \qquad z_{jj} = r, \qquad r > 0, \tag{9a}$$

$$F_{jk}: \qquad 2z_{jk} = \frac{z_{jj}z_{kk}}{r} + r, \qquad r > 0; \tag{9b}$$

$$S_{ij} \qquad 2z_{ij} = k\, z_{ii} + \frac{1}{k} z_{jj}, \qquad k < 0, \tag{9c}$$

are either outside the regularity domain of the four point function or possibly parts of its boundary. The curves F_{jk} can be relevant when the imaginary parts of z_{jj} and z_{kk} have the same signs, and the curves S_{jk} when they have opposite signs.

However, these surfaces are not the only surfaces making up the boundary. To see this we make the following construction. Consider three light like vectors v_k with negative time components and such that $v_k v_l = -1$ for $k \neq l$. Complex vectors of the form

$$\zeta_k = d_k \sum_l A_{kl} v_l, \tag{10}$$

where the d_k are positive real numbers and where the A_{kl} form a symmetric matrix with real non-diagonal elements and positive imaginary parts of the diagonal elements, are clearly limiting cases of vectors of the kind described in eq. (2). Therefore, the corresponding point z_{jk} lies inside the regularity domain or, possibly, on the boundary of this domain. The corresponding matrix Z can be written

$$Z = DANAD, \tag{11}$$

where D is the diagonal matrix whose elements are given by the numbers d_k, A is the matrix $||A_{jk}||$ and N is the matrix formed by the negative of the scalar products of the vectors v_k. It has zeros for its diagonal elements and one for its non-diagonal elements. Next, consider a mass matrix a of the form $a = D^{-1}ND^{-1}$. These masses obviously lie inside the domain of integration described in eq. (4). From this mass matrix and the matrix Z above we can

† The reader who is unfamiliar with the terminology customary in the theory of analytic functions depending on several complex variables is referred e.g. to H. Behnke and P. Thullen [5]) or S. Bochner and W. T. Martin [6]). A useful summary is given in the lecture notes by A. Wightman [7]).

form the matrix M of eq. (6e) and obtain

$$M = D(AN)^2D^{-1}. \tag{12}$$

The matrix M has the same eigenvalues σ_k as the matrix $(AN)^2$. Therefore, the σ_k are the squares of the eigenvalues of the matrix AN. Les us denote the latter eigenvalues by τ_k. We obtain

$$\mathrm{Tr}[AN] = \sum \tau_k = \sum_{j \neq k} A_{jk} = \text{(real number)} = t, \tag{13}$$

$$\tau_k^2 = \sigma_k. \tag{13a}$$

Consequently, the matrix M fulfils eq. (6a) with $t = \mathrm{Tr}[AN]$ and we conclude that every point z_{jk} of the form (11) lies either outside the analyticity domain or on its boundary. Combining these two results we conclude that the manifold (11) consists of points on the boundary †.

The argument presented so far shows that the manifold (11) is certainly part of the four point function boundary and that the manifolds (9) are possibly parts of the same boundary. However, it does not show that these manifolds make up the whole boundary. The next section is devoted to a discussion of this question.

3. Four point function Boundary

In this section we are going to exploit eq. (6) to show that the manifolds (9) and (11) above are the only eleven dimensional manifolds which enter into the boundary of our regularity domain. For this purpose, we consider eq. (6a) as a relation which determines, e.g., the complex number z_{23} as a function of the masses a_{jk} and the parameter t when all the other z_{jk} are given. The masses vary over the domain described by eq. (4) and the parameter t goes from $-\infty$ to $+\infty$. As we have all in all seven real parameters in the numbers z_{23} this means that the manifold we obtain in this way is twelve dimensional. It corresponds to the region where our analytic function might have singularities. (Whether or not such a singularity really appears depends on the properties of the weight $G(a_{jk})$ in eq. (3).) The boundary of this region is also the boundary of the domain in which our function F is guaranteed to be analytic as a consequence of the assumptions invoked here. The boundary can be obtained either when the masses a_{jk} fulfil some of the limiting conditions in eqs. (4) or as envelopes when the masses a_{jk} and the number t vary inside their domain. Even when one of the conditions (4) is fulfilled, the number z_{23} depends on the other complex numbers z and several real parameters. This means that on one of the "boundary surfaces" of the domain described by eqs. (4) we also have, in

† This parametrization of the boundary was first obtained by R. Jost [8]).

general, to compute envelopes to obtain the boundary of our regularity domain for the function F. This appears to be quite a complicated task but the procedure can be systematized and made rather compact.

In App. 1 we have indicated a general technique to compute envelopes of the kind wanted here. Eq. (6) reads

$$\phi = (t^2-Q)^2-R-t\sqrt{S} = 0. \tag{14}$$

The condition that we have an envelope can be written as

$$\frac{\partial\phi}{\partial t} - = \jmath, \tag{14a}$$

$$\frac{\partial\phi}{\partial a_{jk}} = \tfrac{1}{2}\jmath\alpha_{jk}, \tag{14b}$$

where $\jmath$ is some complex number and α_{jk} are real numbers. (The factor $\frac{1}{2}$ is introduced to simplify later formulae.) Eqs. (14), (14a) and (14b) are expected to define an eleven dimensional surface in the space of our complex z. More explicitly, eq. (14b) reads

$$2(t^2-Q)Z+4QZ-4ZaZ+\tfrac{1}{2}t\sqrt{S}a^{-1} = \tfrac{1}{2}[-\sqrt{S}+4t(t^2-Q)]\alpha. \tag{15}$$

The number $\jmath$ in (14a) is given by $-\sqrt{S} + 4t(t^2-Q)$ and we have computed the differentials of the quantities Q, R and S from

$$\mathrm{d}Q = \mathrm{d}(\mathrm{Tr}[Za]) = \mathrm{Tr}[Z\mathrm{d}a], \tag{16a}$$

$$\mathrm{d}R = 2\mathrm{d}((\mathrm{Tr}[Za])^2-\mathrm{Tr}[ZaZa]) = 4Q\,\mathrm{Tr}[Z\mathrm{d}a]-4\mathrm{Tr}[ZaZ\,\mathrm{d}a], \tag{16b}$$

$$\mathrm{d}S = S\mathrm{Tr}[a^{-1}\mathrm{d}a]. \tag{16c}$$

All these formulae have been written in terms of a convenient matrix notation. The matrix formed by the differentials $\mathrm{d}a_{jk}$ is written as $\mathrm{d}a$ while $\alpha = \alpha^{\mathrm{T}}$ is the matrix formed by the real numbers α_{jk} in eq. (14b).

To solve eq. (15) for the matrix Z we first multiply it by the mass matrix a and express everything in terms of the matrix M,

$$4M^2-2(t^2+Q)M-\tfrac{1}{2}t\sqrt{S} = \tfrac{1}{2}[\sqrt{S}-4t(t^2-Q)]\alpha a. \tag{17}$$

The matrix M is a 3×3 matrix and has to fulfil the equation

$$M^3-QM^2+\tfrac{1}{4}RM-\tfrac{1}{64}S = 0. \tag{18}$$

We can now, in principle, combine eqs. (17) and (18) to solve for M as a linear combination of the two first powers of the matrix αa and a term proportional to the unit matrix. For this purpose, we have to square eq. (17) as it stands and eliminate the powers M^3 and M^4 from the left hand side with the aid of eq. (18). The result expresses $(\alpha a)^2$ as a linear combination of terms with M^2, M

and the unit matrix. Afterwards, we can eliminate M^2 between the resulting equation and the original eq. (17) and get the desired result. For the particular case we have here the result turns out to be remarkably simple, and one finds immediately after having computed the square of eq. (17) and eliminated the high powers of the matrix M the relation

$$M = (\alpha a)^2. \tag{19}$$

This means that the matrix Z can be written as

$$Z = \alpha a \alpha, \tag{20}$$

at least when the matrix a is non-singular.

Let us next consider the case when we are on the boundary surface $\mathrm{Det}|a| = 0$ for the domain defined in eqs. (4). In that case, the formula for ϕ in eq. (14) simplifies because the last term vanishes. On the other hand we have the complication that all the masses cannot be considered as independent variables, but that they are restricted by eq. (4c). Let us suppose that, in some way or other, we have computed an envelope for z_{23} on this surface (4c). Next, let us assume that we change the masses a_{jk} to values $a_{jk}+\delta a_{jk}$ in such a way that $\mathrm{Det}|a| = 0(\delta a_{jk})$ for the new masses. The complex number z_{23} changes from the value $z_{23}^{(0)}$ which it has on the envelope to another value given by

$$z_{23} = z_{23}^{(0)} + \left[-t\sqrt{S}+\sum \frac{\partial \phi}{\partial a_{jk}}\,\delta a_{jk}\right]\left(\frac{\partial \phi}{\partial z_{23}}\right)^{-1} = z_{23}^{(0)} - t\sqrt{S}\left(\frac{\partial \phi}{\partial z_{23}}\right)^{-1}. \tag{21}$$

The term with $t\sqrt{S}$ has to be disregarded in the computation of the derivative of ϕ with respect to a_{jk} inside the square bracket in eq. (21). The last version of the right hand side of eq. (21) is obtained if one observes that the first term inside the square bracket is much larger than the second one under the assumptions which we have made. As eq. (14) with $S = 0$ depends only on t^2, we have two real numbers t, equal in magnitude but opposite in signs, for every point $z_{23}^{(0)}$ on the envelope. This means that the change in the number z_{23} from the envelope when the masses are moving into the domain (4) is given by

$$z_{23} = \pm|t|\sqrt{S}\left(\frac{\partial \phi}{\partial z_{23}}\right)^{-1}. \tag{22}$$

Unless the number t or the number S (or both) is equal to zero or if the number $\sqrt{S}\,(\partial\phi/\partial z_{23})^{-1}$ happens to lie along the tangent of the envelope, we find that, for some masses inside our domain (4), we can obtain points z_{23} on both sides of the envelope corresponding to $z_{23}^{(0)}$. We remark, in passing, that this is true not only for the envelope but also for any other curve obtained from the manifold $\mathrm{Det}|a| = 0$. In particular, it is also true if the masses a_{jk} fulfil some of the boundary conditions in eqs. (4b). Consequently, any curve obtained for

$\mathrm{Det}|a| = 0$ usually lies somewhere inside a domain where we can obtain singularities and is therefore not a relevant part of our boundary. The only exception to this happens for the cases

(i) $\mathrm{Det}|Z| = 0$,

(ii) $\mathrm{Im}(\mathrm{Det}|Z|/\jmath^2) = 0$,

(iii) $t = 0$,

(iv) when it is impossible to change the masses a_{jk} corresponding to the point $z_{23}^{(0)}$ by infinitesimal amounts in such a way that $\mathrm{Det}|a|$ is of the same order as the changes in the masses.

Case (i) can immediately be disregarded as the manifold $\mathrm{Det}|Z| = 0$ is itself only of ten dimensions. Therefore, the corresponding part of the boundary can at most be ten dimensional.

In case (ii) we find that every change of the masses a_{jk} produces a change of z_{23} along a line, the direction of which is given by $\zeta\,(\partial\phi/\partial z_{23})^{-1}$. Consequently, we are not only on the envelope obtained when the masses vary subject to the restriction $\mathrm{Det}|a| = 0$ but also on the envelope obtained when the masses vary freely inside the domain (4). It follows that we get nothing new for this case but obtain at most a limiting case of the envelope described by eqs. (14).

Summarizing our discussion so far, we can say that we can disregard the boundary surface in eq. (4c) except in the two special cases denoted by (iii) and (iv) above.

A similar discussion can be carried through when the masses fulfil also one or more of the restrictions (4b). For definiteness, we assume that we have $a_{12} = \sqrt{a_{11}a_{22}}$. Straight-forward computations show that we now have $\mathrm{Det}|a| = -(\sqrt{a_{11}}a_{23} - \sqrt{a_{22}}a_{13})^2$. The inequality (4c) tells us that we cannot be on one of the boundary surfaces in eq. (4b) without at the same time being on the boundary surface of eq. (4c). Therefore, the discussion above is relevant also for this case, and we find that the envelope obtained when the masses vary subject to one or more of the restrictions in eqs. (4b) can be disregarded except, possibly, in the special case indicated by (iii) and (iv) above.

After these preliminary considerations we are now ready to turn to a more systematic discussion of our envelopes. Let us start by considering the case when all the masses a_{jk} are varying freely inside the domain described by eq. (4). Our envelope is then given by eq. (20) with real matrices a and α. Consequently, the imaginary parts of all the z_{jk} vanish, and we have at most a six dimensional manifold. This is of too low a dimension to be an interesting part of our boundary.

When we move to the boundary surface of the domain in eq. (4) where $\mathrm{Det}|a| = 0$, we can apply the discussion given above in connection with eq. (21) and find that we get no new interesting part of our boundary except possibly in the cases denoted by (iii) and (iv). If we start with the last case, we

find that it is always possible to change one of the non-diagonal masses a_{jk} in such a way that we move out of the surface in eq. (4c) as long as the matrix a has rank two. This is trivial when none of the conditions in eqs. (4b) is fulfilled. If we have, e.g., $a_{12} = \sqrt{a_{11}a_{22}}$ and when both a_{11} and a_{22} are different from zero, we find that $a_{13} = a_{23}\sqrt{a_{11}/a_{22}}$. The matrix a' adjoint to the matrix a is given by

$$a' = \frac{a_{23}^2 - a_{22}a_{33}}{a_{22}} \begin{Vmatrix} -a_{22} & \sqrt{a_{11}a_{22}} & 0 \\ \sqrt{a_{11}a_{22}} & -a_{11} & 0 \\ 0 & 0 & 0 \end{Vmatrix}. \tag{23}$$

The change in $\mathrm{Det}|a|$ when the masses a_{jk} are changed by amounts δa_{jk} is given by $\delta(\mathrm{Det}|a|) = \mathrm{Tr}[a'\,\delta a]$ and we see that by changing a_{12} by a small amount we can move into a domain where the inequality (4c) is fulfilled. When two of the conditions in eqs. (4b) are fulfilled, we find that also the third one must hold. From $a_{12} = \sqrt{a_{11}a_{22}}$ and $a_{13} = \sqrt{a_{11}a_{33}}$ we get $\mathrm{Det}|a| = -a_{11}(a_{23} - \sqrt{a_{22}a_{33}})^2$, and, when $a_{11} \neq 0$, we conclude $a_{23} = \sqrt{a_{22}a_{33}}$. Consequently, the matrix a has rank one. The adjoint a' vanishes in this case, and the change in $\mathrm{Det}|a|$ is zero in first order. Summarizing, we have found that when all three diagonal masses are different from zero we get no interesting part of our boundary except possibly when the mass matrix a has rank one or when $t = 0$. We return to these two cases below.

When one of the diagonal masses vanishes, the situation is slightly more complicated. If we first assume that all the other masses a_{jk} are moving inside the domain described in (4), we can compute an envelope and the result is still given by eq. (20). However, the matrix α is not completely real for this case because one of its diagonal elements is a complex number. (Cf. App. 1.) For definiteness, let us put $a_{11} = 0$ and $\mathrm{Im}\alpha_{11} \neq 0$. Eq. (20) then tells us that the imaginary parts of z_{22}, z_{33} and z_{23} are all zero. The corresponding manifold has at most nine dimensions and can be disregarded.

When we move to the boundary surface of the domain (4) where $\mathrm{Det}|a| = 0$ and have $a_{11} = 0$, $t \neq 0$, we find that the adjoint a' is given by

$$a' = \begin{Vmatrix} a_{22}a_{33} - a_{23}^2 & a_{13}a_{23} - a_{12}a_{33} & a_{12}a_{23} - a_{13}a_{22} \\ a_{13}a_{23} - a_{12}a_{33} & -a_{13}^2 & a_{12}a_{13} \\ a_{12}a_{23} - a_{13}a_{22} & a_{12}a_{13} & -a_{12}^2 \end{Vmatrix}. \tag{24}$$

As long as both a_{12} and a_{13} are different from zero, i.e. as long as we are away from the boundary surfaces in eq. (4b), we can change a_{23} by an infinitesimal amount and have the determinant of the matrix a changed by an amount of the same order of magnitude. This is still true also in the limiting case $a_{23} = \sqrt{a_{22}a_{33}}$

when the matrix a' simplifies to

$$a' = \frac{a_{13}^2}{a_{33}} \begin{Vmatrix} 0 & 0 & 0 \\ 0 & -a_{33} & \sqrt{a_{22}a_{33}} \\ 0 & \sqrt{a_{22}a_{33}} & -a_{22} \end{Vmatrix}. \tag{24a}$$

When one of the masses a_{12} or a_{13} vanishes, it follows from the inequality (4c) that the other quantity is also zero. The matrix a' vanishes for this case, and it is possible that we get some interesting part of the boundary from here. However, it is unnecessary to carry through a detailed discussion of this case as eq. (14) now reduces to exactly the same equation we have for the three point function. Consequently, we know that this situation could at most yield the boundary surfaces F_{23}, S_{23}, the z_{22}-cut and the z_{33}-cut. (Cf. App. I in KW or App. 2 in this paper.) However, as we have explicitly assumed that both a_{22}, a_{33} and t are different from zero, we get none of these boundaries here.

When two of the diagonal masses vanish but when there is no other restriction on the remaining masses a_{jk}, we can compute an envelope as above, and the result is still given by eq. (20) but with two of the diagonal elements of α given by complex numbers. For definiteness, let us assume $a_{11} = a_{22} = 0$ and $\mathrm{Im}\alpha_{11} \neq 0$, $\mathrm{Im}\alpha_{22} \neq 0$. Eq. (20) then tells us that z_{33} is a real number. If we should not be on the z_{33}-cut, which is anyhow known to be part of the boundary, z_{33} must be negative. Intuitively, it is clear that this can hardly be part of the boundary as a negative and real z_{33} can be obtained from a complex vector which is purely imaginary. In App. 3 we shall show that eq. (20) for this case defines only a ten dimensional manifold which can be disregarded.

For $\mathrm{Det}|a| = 0$, $a_{11} = a_{22} = 0$, $a_{33} \neq 0$, $t \neq 0$ we can still use eq. (24) to compute the adjoint a'. As long as a_{12} and a_{13} are both different from zero, it is possible to change a_{23} by an infinitesimal amount and get a change of $\mathrm{Det}|a|$ of the same order of magnitude. When $a_{12} = 0$, the determinant of the matrix a vanishes identically but a' is still given by eq. (24) and the matrix element a'_{12} is different from zero. A small change of a_{12} is then sufficient to change the determinant of a by an amount of the same order of magnitude. When a_{13} or a_{23} is equal to zero, we have $\mathrm{Det}|a| = -a_{12}^2 a_{33}$ and conclude that a_{12} also has to vanish. As earlier, this corresponds to a three point function case but this time with only one diagonal mass different from zero. Consequently, we get the z_{33}-cut as part of our boundary when both a_{23} and a_{13} vanish.

When all three diagonal masses are equal to zero, we have $\mathrm{Det}|a| = 2a_{12}a_{13}a_{23}$. The envelope for this case is still given by eq. (20), but all three diagonal α are now complex numbers. Further, the imaginary parts of all α_{jj} must have the same sign (cf. App. 1) We introduce a diagonal matrix D with positive elements d_k and write

$$a = D^{-1}ND^{-1}, \tag{25}$$

where the matrix N is defined below eq. (11). Denoting the matrix $D^{-1}\alpha D^{-1}$ by A we can write eq. (20) as

$$Z = DANAD. \tag{26}$$

This is the manifold given in eq. (11) and discussed in section 2. We already know that this manifold is part of the relevant boundary for the four point function domain.

When the determinant of the matrix a is zero, one of the non-diagonal masses vanishes. Let us first assume that $a_{12} = 0$ and that both the other a_{jk} are different from zero. Clearly, it is now possible to change a_{12} by an infinitesimal amount and have a change of the same order of magnitude in $\mathrm{Det}|a|$. Therefore, the corresponding envelope is not an interesting part of our boundary since it is at most a limiting case of the surface $DANAD$ in eq. (26). When two of the non-diagonal a_{jk} are zero, we get immediately a three point function boundary F_{jk} without any computation of envelopes.

The discussion above has proved that there is no relevant part of the boundary except the manifolds in eqs. (9) and (11) as long as the number $t \neq 0$ and as long as the rank of the mass matrix a is not equal to one. We proceed by considering the case $t = 0$. Since the function ϕ in eq. (14) depends not only on t^2 but also on t itself, this is, in general, not an interesting case. A small change in the value of t from zero has as a consequence a change in the number z_{23} given by

$$z_{23} = +t\sqrt{S}\left(\frac{\partial\phi}{\partial z_{23}}\right)^{-1}. \tag{27}$$

As t can have either sign, we find that we can obtain points z_{23} on both sides of a possible envelope corresponding to the surface $t = 0$ unless either $S = 0$ or when $\sqrt{S}$ happens to be parallel to the number $\jmath$ for our envelope. In the last case we have at most a limiting case of what has been obtained earlier. Therefore, we are only interested in the intersection of the boundary surfaces $t = 0$ and $\mathrm{Det}|a| = 0$ in our domain (4). Eq. (6a) now reduces to $Q^2 = R$. This is a quadratic relation between the numbers z_{jk}. It can be solved for anyone of them, e.g. for z_{23}. After some algebraic manipulations one finds that the whole expression $Q^2 - R$ can be written as a product of two factors each of which is linear in z_{jk}. Both factors are of the form

$$X = 2z_{23} + \kappa_{23}\, z_{22} + \frac{1}{\kappa_{23}}\, z_{33} + 2\kappa_{13} z_{12} + 2\kappa_{12} z_{13} + \kappa_{12}\kappa_{13} z_{11}, \tag{28}$$

$$\kappa_{23} = \frac{a_{23} \pm \sqrt{a_{23}^2 - a_{22}a_{33}}}{a_{33}} > 0, \tag{28a}$$

$$\kappa_{13} = \frac{a_{13} \mp \sqrt{a_{13}^2 - a_{11}a_{33}}}{a_{33}} > 0, \tag{28b}$$

$$\kappa_{12} = \frac{a_{12} \pm \sqrt{a_{12}^2 - a_{11}a_{22}}}{a_{22}} > 0, \tag{28c}$$

$$\kappa_{12}\kappa_{23} = \kappa_{13}, \tag{28d}$$

where the upper signs in eqs. (28a), (28b) and (28c) belong together. It must be emphasized that to obtain the factors X as well as the relation (28d) between the various κ_{ij} it is essential to use the vanishing of $\mathrm{Det}|a|$. By putting $X = 0$ in (28) we obtain z_{23} expressed in terms of the other z and, effectively, two real numbers κ_{ij}. Before we try to compute the envelope from this relation we remark that each equation $X = 0$ can also be written $\mathrm{Tr}[Za] = 0$ with $a_{jk} = b_j b_k$ for some positive real numbers b_j. This can be considered as a special case of our previous formalism where the mass matrix a has rank one, and we conclude that it is sufficient to investigate the case $t = 0$ when the rank of a is one.

We now handle this situation together with the case which was previously left open, viz. when the rank of the mass matrix is one and t is varying. We put $a_{jk} = b_j b_k$ and write down the envelope conditions

$$\phi = t^2 - Q = t^2 - \sum b_j b_k z_{jk} = 0, \tag{29}$$

$$\jmath = \frac{\partial \phi}{\partial t} = 2t, \tag{29a}$$

$$\sum z_{jk} b_k = \jmath \alpha_j. \tag{29b}$$

The number $\jmath$ is real when t is varying but could be complex for $t = 0$ since eq. (29a) has to be dropped for that case. The numbers α_j are always real. If we change the masses a_{jk} to $a_{jk} = b_j b_k + \varepsilon/b_l$ with ε a small positive number and the indices j, k and l all different (the diagonal masses are unchanged), the quantity R changes to

$$R = 8\varepsilon \left[\jmath^2 \left(\frac{\alpha_1 \alpha_2}{b_3} + \frac{\alpha_1 \alpha_3}{b_2} + \frac{\alpha_2 \alpha_3}{b_1} \right) - 2\jmath (z_{12}\alpha_3 + z_{13}\alpha_2 + z_{23}\alpha_1) \right.$$
$$\left. + 2(z_{12}z_{13}b_1 + z_{13}z_{23}b_3 + z_{12}z_{23}b_2) \right]. \tag{30}$$

The corresponding change in the number z_{23} is given by

$$z_{23} = \pm \frac{1}{b_2 b_3} \sqrt{R} + O(\varepsilon). \tag{31}$$

In these computations we have assumed that the numbers b_j are all different

from zero. As earlier, we find that eq. (31) yields points on both sides of our envelope except when the square bracket in eq. (30) is either zero or parallel to the number $\mathfrak{z}^2$. When t is varying, this means that the bracket has to be a real number. This implies one extra relation between the imaginary parts of z_{jk} and the numbers α_j and b_j. Therefore, this is at most a ten dimensional part of our boundary. This situation does not change in an appreciable way when $t = 0$ and $\mathfrak{z}$ is a complex number. The actual algebraic relation becomes somewhat more involved for this case but still yields a non-trivial condition between the z and the real parameters α and b. The envelope is at most part of the boundary on a ten dimensional manifold, and we can say that there is no eleven dimensional generalization of the S-manifold for the four point function case similar to the way in which F_{12} is generalized to the four point function boundary $DANAD$. As an illustration of this we refer to fig. 9 below.

It remains to discuss what happens when one or more of the numbers b_j is zero. For definiteness, let us suppose that we have $b_1 = 0$. It follows $a_{11} = a_{12} = a_{13} = 0$ and eq. (28) yields the manifold S_{23} without further computations. We know that this is part of the boundary.

We have now proved that there are no other eleven dimensional surfaces entering into the boundary of our analyticity domain except the generalized three point function boundaries in eqs. (9) and the new surface $DANAD$ in eq. (11). The three point function boundaries are already well-known [3]) and we devote the next section to a discussion of some properties of the new surface (11).

4. Some Properties of the Surface (11)

The three point function boundaries in eqs. (9) are analytic hypersurfaces. This is a fact which was extremely helpful in the discussion of the analyticity domain for the three point function and in the computation of the corresponding holomorphy envelope (cf. KW). One interesting question which immediately arises is whether or not the $DANAD$-surface (11) has the same property. This is not easily decided, for one should first eliminate all the parameters entering into eq. (11) and afterwards test whether or not a certain differential form of the second order is positive semi definite [7]). Only a few initial steps of such an elimination are easily done, but one very fast runs into considerable algebraic complications. We therefore prefer not to do the corresponding elimination completely but only to eliminate the diagonal elements of the matrix A in eq. (11). It is more convenient to eliminate the diagonal elements and leave the non-diagonal elements as they stand because the former are complex quantities. If we eliminate real numbers by formal algebraic manipulations from our equations, it is necessary first to split every relation into its real and imaginary parts. For an elimination of complex numbers this is not necessary.

In this way we find that we can write the *DANAD*-surface in the following form which has a certain similarity to the three point function boundaries:

$$2z_{jk} = \lambda_{jk} S_{jk} + (1-\lambda_{jk}) F_{jk}, \qquad j \neq k, \tag{32a}$$

$$S_{jk} = k_{jk} z_{jj} + k_{kj} z_{kk}, \tag{32b}$$

$$F_{jk} = \frac{z_{jj} z_{kk}}{r_{jk}} + r_{jk}, \tag{32c}$$

$$\lambda_{jk} = \frac{A_{jl} A_{kl}}{(A_{jk}+A_{jl})(A_{jk}+A_{kl})}, \tag{32d}$$

$$k_{jk} = \frac{d_k}{d_j} \frac{A_{kl}}{A_{jl}} = \frac{1}{k_{kj}}, \tag{32e}$$

$$r_{jk} = 2 d_j d_k A_{jk} (A_{12}+A_{13}+A_{23}). \tag{32f}$$

Note that the real numbers λ_{jk}, k_{jk} and r_{jk} are not independent quantities but are related to each other through eqs. (32d)—(32f) †.

Eqs. (32) determine, in principle, a curve e.g. in the z_{23}-plane when all the other z_{jk} are given fixed complex values. This curve can be parametrized with the aid of any of the real numbers appearing above. We choose to use r_{12} as independent parameter. One can then, e.g., solve the equation for z_{12} in (32a) for the real quantity λ_{12}. The condition that the imaginary part of λ_{12} is zero gives one real relation between the numbers k_{12} and r_{12}. As r_{12} is given, we can solve for k_{12}. In practice, this turns out to be an equation of the second degree which has either two real solutions or no real solution at all. When this equation has no real solution, the corresponding value of r_{12} does not appear in the boundary. When k_{12} is real, one can compute the real number λ_{12} from the given relation. In this way, one obtains k_{12} and λ_{12} as (double-valued) functions of r_{12}. To determine r_{13}, k_{13} and λ_{13} as functions of r_{12} one notes that eqs. (32e) and (32f) imply that the two ratios r_{12}/k_{12} and r_{13}/k_{13} are equal. If we solve eq. (32a) with $j = 1$ and $k = 3$ for λ_{13}, we get an expression the imaginary part of which has to be zero. As before, this relation involves only k_{13} and r_{13}. The ratio between those two numbers is given and we can rewrite everything as one equation for r_{13}. A computation of this kind gives the result

$$r_{13}^4 + 2r_{13}^3 \left[\frac{x_{11}y_{13}-y_{11}x_{13}}{y_{11}} - \frac{y_{13}}{y_{11}} b\right] + r_{13}^2 \frac{y_{33}}{y_{11}} (b^2 - |z_{11}|^2) \tag{33}$$
$$+ 2r_{13} \frac{b^2}{y_{11}} \left[x_{33}y_{13} - y_{33}x_{13} + \frac{x_{13}(x_{11}y_{33}+x_{33}y_{11}) - y_{13}(x_{11}x_{33}-y_{11}y_{33})}{b}\right] - b^2 |z_{33}|^2 = 0,$$

$$b = \frac{r_{12}}{k_{12}} = \frac{r_{13}}{k_{13}}. \tag{33a}$$

† Explicit formulae of this kind were first obtained by D. Kleitman (unpublished).

The quartic equation (33) has at least two real solutions as the last term is negative. For special values of the parameters it might have four real solutions. For each real solution to this equation we compute the numbers k_{13} and λ_{13}. They are then given as functions of r_{12}. In the most unfavourable case one has eight pairs of values of r_{13} and k_{13} for each value of r_{12}. We now turn to eq. (32a) with $j = 2$ and $k = 3$. The real number λ_{23} can be computed from λ_{12} and λ_{13}. Eqs. (32d) imply the relation

$$(1-\lambda_{12}-\lambda_{13}-\lambda_{23})^2 = 4\lambda_{12}\lambda_{13}\lambda_{23}. \tag{34}$$

As this is a second degree equation for λ_{23}, we have in the most unfavourable case sixteen different values of λ_{23} for each value of r_{12}. We further remark that r_{23} and k_{23} can be computed from the relations $k_{23} = k_{13}/k_{12}$, $r_{23} = k_{13}r_{12}$. When these parameters are all known, we obtain a complex number for z_{23} directly from the remaining equation (32a). In the most unfavourable case we get sixteen values of z_{23} for each value of r_{12}. However, all of these values do not really belong to the manifold described by the equation $Z = DANAD$ with the restriction we have on the matrices A and D, viz. that the imaginary parts of the diagonal elements in A all have the same sign and that the diagonal elements of the matrix D all have the same sign. One finds that the condition on the diagonal elements of A can be formulated as

$$E_1 = (1+v)\,(v+w)y_{11}y_{22} > 0, \tag{35a}$$

$$E_2 = (1+w)\,(v+w)y_{11}y_{33} > 0, \tag{35b}$$

$$v = \frac{1}{\lambda_{12}-\lambda_{13}}\left[1-\lambda_{12}-\lambda_{13}+\frac{\lambda_{12}+\lambda_{13}+\lambda_{23}-1}{2\lambda_{12}}\right], \tag{35c}$$

$$w = \frac{1}{\lambda_{13}-\lambda_{12}}\left[1-\lambda_{12}-\lambda_{13}+\frac{\lambda_{12}+\lambda_{13}+\lambda_{23}-1}{2\lambda_{13}}\right]. \tag{35d}$$

Further, one finds that the conditions on the diagonal elements of D can be formulated as

$$E_3 = r_{12}v(1+v+w) > 0, \tag{35e}$$

$$E_4 = r_{13}w(1+v+w) > 0, \tag{35f}$$

$$E_5 = r_{23}(1+v+w) > 0. \tag{35g}$$

Only those combinations of the parameters r_{jk} and λ_{jk} which fulfil the inequalities (35) are accepted. This scheme allows us to plot the $DANAD$-curve in the z_{23}-plane but the actual plotting requires rather long numerical computations. It is convenient to have an electronic computer for the routine work. Before discussing the result of these numerical plots we want to mention a few general properties that can be proved from the computation scheme above.

We first want to prove that the *DANAD* surface is not an analytic hypersurface. For this purpose we remark that, if the *DANAD* were an analytic hypersurface, it would still remain an analytic hypersurface in the space of the variables z_{12}, z_{13} and z_{23} if we consider the particular case when all the diagonal z_{jj} are equal and equal to i. We can then specialize further and put z_{13} equal to z_{23} and investigate the resulting manifold in the four dimensional space of the two complex variables z_{12} and z_{13}. If the *DANAD* were an analytic hypersurface, this specialization of it would still remain so †. For this special case one can pick a particular solution of the computational scheme above with $r_{13} = r_{23}$, $k_{13} = k_{23}$ and $\lambda_{13} = \lambda_{23}$. It is then comparatively easy to carry through the above elimination completely and write the whole *DANAD* surface as one real relation between x_{12}, y_{12}, x_{13} and y_{13}. One finds

$$f = 4x_{13}^2(1-\sqrt{y_{12}})^2-4y_{13}^2(1+\sqrt{y_{12}})^2-8x_{12}x_{13}y_{13}+x_{12}^2+(1-y_{12})^2=0. \quad (36)$$

Alternatively, we can express f in terms of z_{12}, $\bar{z}_{12}$, z_{13} and $\bar{z}_{13}$. This gives

$$f = (1-iz_{12}+2z_{13}^2)\,(1+i\bar{z}_{12}+2\bar{z}_{13}^2)-4\left[z_{13}\bar{z}_{13}+\sqrt{\frac{z_{12}-\bar{z}_{12}}{2i}}\right]^2 = 0. \quad (36a)$$

There exists a very convenient test for a surface of this kind to be an analytic hypersurface, viz. the so called Levi determinant condition [7]). A surface in a space of two complex variables is an analytic hypersurface if and only if

$$L(f) = -\begin{vmatrix} 0 & \dfrac{\partial f}{\partial z_1} & \dfrac{\partial f}{\partial z_2} \\ \dfrac{\partial f}{\partial \bar{z}_1} & \dfrac{\partial^2 f}{\partial z_1 \partial \bar{z}_1} & \dfrac{\partial^2 f}{\partial z_2 \partial \bar{z}_1} \\ \dfrac{\partial f}{\partial \bar{z}_2} & \dfrac{\partial^2 f}{\partial z_1 \partial \bar{z}_2} & \dfrac{\partial^2 f}{\partial z_2 \partial \bar{z}_2} \end{vmatrix} = 0. \quad (37)$$

Computing the determinant (37) for the surface (36a) with $z_1 = z_{12}$ and $z_2 = z_{13}$ we find

$$L(f) = 2(Ax_{13}+By_{13})^2\,(A^2+B^2)^2\,(y_{12})^{-\frac{3}{2}}, \quad (38)$$

$$A = \sqrt{4y_{13}^2-(1-\sqrt{y_{12}})^2}, \quad (38a)$$

$$B = \sqrt{4x_{13}^2+(1+\sqrt{y_{12}})^2}. \quad (38b)$$

Obviously, the expression (38) is not zero in general, which proves that this particular case of *DANAD* is not an analytic hypersurface. To be pedantic, we

† This argument as well as some of the material in the previous section were constructed in collaboration with J. Toll [9]). Cf. also G. Källén [10]). We want to thank Prof. Toll for his kind permission to include this material here.

should also prove that some point on the manifold described by eq. (36a) is able to pass the tests in eqs. (35). One easily finds that, if y_{12} lies in the range $0 < y_{12} < 1$ and if $2y_{13} > 1-\sqrt{y_{12}}$, the inequalities (35) are fulfilled. Therefore, the *DANAD* curve is not an analytic hypersurface.

The argument in the previous paragraph does not exclude that some other special case of a submanifold of the *DANAD* could be an analytic hypersurface. An amusing situation where this happens is the case when all diagonal z are real, negative and equal. For definiteness, let us put them equal to -1†. At the first moment one might expect that there should be no finite part at all of *DANAD* for this case. If the diagonal z are real, the right hand sides of eqs. (32a) all appear to be real, and we should be tempted to conclude that the non-diagonal z also must be real on *DANAD*. However, this conclusion is not right. If we understand this case as the limit when ε goes to zero of a situation with $z_{11} = z_{22} = z_{33} = -1+i\varepsilon$, we can see that there is a solution of the *DANAD* equations where the real parameters λ_{12} and λ_{13} are both of the order of magnitude ε^{-1} while λ_{23} is of the order of magnitude ε^{-2}. In this limit one gets $r_{12}-r_{13} = O(\varepsilon)$, $k_{12}-k_{13} = O(\varepsilon)$, $k_{12}r_{12}+1 = O(\varepsilon)$ and $k_{23}-1 = O(\varepsilon)$. It further appears that one can also carry through for this case the elimination of all parameters above and express z_{23} explicitly as function of r_{12}. The result is the analytic hypersurface

$$z_{23} = 2\frac{(\rho-z_{12})(\rho-z_{13})}{\rho^2-1} - 1, \tag{39}$$

$$\rho = \frac{1}{2}\left(r_{12}+\frac{1}{r_{12}}\right). \tag{39a}$$

The inequalities $E_i > 0$ in eq. (35) imply that r_{12} has to be positive for this case which means that the real parameter ρ in (39) is bigger than one. Further, they imply that y_{12} and y_{13} have to have the same sign if this curve is going to be relevant.

The fact that the *DANAD* surface is not an analytic hypersurface raises the question of whether or not it can be the boundary of a natural domain of holomorphy. The condition for this to be true is that the surface has to be pseudoconvex from the right side in the twelve dimensional space of our six complex variables [7]). To show this by explicit computations is rather involved. With the aid of the discussion above we can, however, answer the question in the affirmative as we have explicit examples of functions which have singularities on arbitrary points of the *DANAD* surface. Functions with this property are the $\Delta_4^{(+)}$—functions in eq. (3a). An integral with a suitable weight over the masses a_{jk} gives a function with singularities all over the *DANAD*

† We are indebted to N. Burgoyne and A. Wightman for drawing our attention to this particular case.

surface but regular on one side of it. Therefore, *DANAD* is the boundary of a natural domain of holomorphy in spite of the fact that it is not an analytic hypersurface.

The computational scheme indicated above is rather involved. In particular, the tests $E_i > 0$ in eqs. (35) are nor very transparent, and there exists a possibility that for certain combinations of z_{11}, z_{22}, z_{33}, z_{12} and z_{13} there is no solution to our equations at all. This would imply that the z_{23}-plane in such a case does not intersect the *DANAD* surface. However, this possibility does not happen, a fact we now want to prove. For this proof we divide the discussion into several parts. Let us first consider the case when the imaginary parts of all the diagonal z have the same sign. The particular value of r_{12} given by

$$r_{12} = \frac{1}{y_{11}}\left[x_{12}y_{11} - y_{12}x_{11} + \frac{y_{11}}{|y_{11}|}\sqrt{(x_{12}y_{11} - y_{12}x_{11})^2 + y_{11}y_{22}|z_{11}|^2}\right] > 0 \quad (40)$$

corresponds to a point on the *DANAD* surface. Clearly, this value of r_{12} is adjusted in such a way that one of the corresponding values of k_{12} is infinite and, consequently, λ_{12} vanishes in such a way that $k_{12}\lambda_{12} = \rho_{12}$ with

$$2z_{12} = \rho_{12}z_{11} + \frac{z_{11}z_{22}}{r_{12}} + r_{12}. \quad (41)$$

Because of eq. (33a) this point corresponds to a situation where k_{13} is also infinite and λ_{13} also vanishes. Introducing the product $k_{13}\lambda_{13} = \rho_{13}$ we obtain from eq. (33) with b very large

$$r_{13} = \frac{1}{y_{11}}\left[x_{13}y_{11} - y_{13}x_{11} + \frac{y_{11}}{|y_{11}|}\sqrt{(x_{13}y_{11} - y_{13}x_{11})^2 + y_{11}y_{33}|z_{11}|^2}\right] > 0, \quad (42)$$

and

$$2z_{13} = \rho_{13}z_{11} + \frac{z_{11}z_{33}}{r_{13}} + r_{13}. \quad (43)$$

With the assumption we have made about the signs of y_{jj} the two numbers r_{12} and r_{13} are both positive. For the points z_{12} and z_{13} to lie inside the corresponding three point function domains it is therefore necessary that ρ_{12} and ρ_{13} are positive real numbers. Eq. (34) implies for this case that λ_{23} is equal to one. Further, r_{23} becomes infinite but in such a way that

$$(1-\lambda_{23})r_{23} = (\sqrt{r_{13}\rho_{12}} + \sqrt{r_{12}\rho_{13}})^2, \quad (44)$$

and, consequently, we get

$$z_{23} = \frac{1}{2}\left[\frac{r_{13}}{r_{12}}z_{22} + \frac{r_{12}}{r_{13}}z_{33} + (\sqrt{r_{13}\rho_{12}} + \sqrt{r_{12}\rho_{13}})^2\right]. \quad (45)$$

Further, one finds that the two numbers v and w become very large in this

limit and that their ratio is given by $v/w = \sqrt{r_{12}\rho_{13}/r_{13}\rho_{12}}$. Therefore, all the tests E_1, E_2, E_3 and E_4 are trivially fulfilled. The actual behaviour of v and w is illustrated by the relation $v\lambda_{12} = v\rho_{12}/k_{12} = \sqrt{r_{13}\rho_{12}}[\sqrt{r_{12}\rho_{13}}+\sqrt{r_{13}\rho_{12}}]^{-1}$. It follows that v and r_{23} and, consequently, $1+v+w$ all have the same signs, and the test E_5 is also fulfilled. We conclude that the point (45) is a relevant point on the *DANAD* surface. Further, this point does not lie on the F_{23} curve in eq. (9b), which is the relevant three point function boundary for this case. From this follows that there is at least some part of the *DANAD* surface in the neighbourhood of the point (45) which is relevant for the boundary. The corresponding range of the parameter r_{12} lies in the neighbourhood of the number (40).

It is of some interest to compute the non-diagonal masses a_{jk} corresponding to the ten dimensional manifold indicated above. One finds $a_{23} = 0$ and some non-zero values for a_{13} and a_{12}. To be more precise, we can write the last two numbers as $a_{12} = \frac{1}{2}t^2\sqrt{\rho_{13}/r_{12}}\,(\sqrt{r_{12}\rho_{13}}+\sqrt{r_{13}\rho_{12}})^{-1}$ and $a_{13} = \frac{1}{2}t^2\sqrt{\rho_{12}/r_{13}}\,(\sqrt{r_{12}\rho_{13}}+\sqrt{r_{13}\rho_{12}})^{-1}$. It follows that the ten dimensional manifold in eq. (45) is not only on the *DANAD* surface but also on the "two mass envelope" obtained in the case $\mathrm{Det}|a| = 0$. We here have exactly the situation when the number $\sqrt{S}$ in eq. (22) is parallel to the number y in eq. (14a) for the *DANAD* curve. This means that the tangent in the z_{23}-plane is proportional to $\sqrt{\mathrm{Det}|Z|}/z_{11}$. (Cf. fig. 1 below.)

The cases when the imaginary parts of the diagonal z do not all have the same signs can be handled in a similar way. As we have chosen to plot the *DANAD* curve in the z_{23}-plane the indices 2 and 3 appear in a completely symmetrical way in our formalism while the index 1 is somewhat distinguished. Therefore, we have to treat two separate cases depending on whether or not y_{11} has the same sign as one of the other diagonal y (e.g. $y_{11}y_{22} > 0$, $y_{11}y_{33} < 0$ in one case and $y_{11}y_{22} < 0$, $y_{22}y_{33} > 0$ in the other case). In the first case we pick the following value for r_{12}:

$$r_{12} = \frac{1}{y_{22}}\left[x_{12}y_{22}-y_{12}x_{22}+\frac{y_{11}}{|y_{11}|}\sqrt{A}\right] > 0, \tag{46}$$

$$A = (x_{12}y_{22}-y_{12}x_{22})^2+y_{11}y_{22}|z_{22}|^2 > 0. \tag{46a}$$

This corresponds to a situation where k_{12} and λ_{12} vanish in such a way that their ratio has a finite value which we denote by ρ_{12}. We get

$$2z_{12} = \rho_{12}z_{22}+\frac{z_{11}z_{22}}{r_{12}}+r_{12}. \tag{47}$$

For z_{12} to lie inside the three point function regularity domain it is necessary that ρ_{12} is positive. The corresponding value of the parameter k_{13} can be com-

puted just as was the case before. We obtain

$$k_{13} = \frac{1}{y_{11}}\left[y_{13} - \frac{y_{11}}{|y_{11}|}\sqrt{y_{13}^2 - y_{11}y_{33}}\right] < 0. \tag{48}$$

The value of r_{13} belonging to this case is infinite while the parameter λ_{13} is equal to one. The product $(1-\lambda_{13})r_{13}$ is finite and we denote it by $-\sigma_{13}$. We get

$$2z_{13} = k_{13}z_{11} + \frac{1}{k_{13}}z_{33} - \sigma_{13}. \tag{49}$$

The parameter σ_{13} has to be positive if the point z_{13} lies inside its three point function domain. From this it is now a straight-forward matter to compute the parameters r_{23}, k_{23} and λ_{23}. The point z_{23} becomes

$$z_{23} = \frac{1}{2}\left[-z_{22}\left(\sqrt{\frac{\sigma_{13}}{r_{12}}} + \sqrt{-k_{13}\rho_{12}}\right)^2 + \frac{z_{22}z_{33}}{k_{13}r_{12}} + k_{13}r_{12}\right]. \tag{50}$$

The numbers v and w can also be computed and one finds

$$v = -[1+\sqrt{-\sigma_{13}/\rho_{12}k_{13}r_{12}}], \tag{50a}$$

$$w = -[1+\sqrt{-\rho_{12}k_{13}r_{12}/\sigma_{13}}]\,\frac{\sigma_{13}}{r_{13}} \to 0. \tag{50b}$$

From here, it is easy to verify that all the tests $E_1, \ldots, E_5$ are fulfilled. This proves that in this case we also have a non trivial part of the *DANAD* surface in our four point function boundary.

The numbers a_{jk} are given by

$$a_{12} = \tfrac{1}{2}(t^2/r_{12})[1+\sqrt{-\rho_{12}k_{13}r_{12}/\sigma_{13}}], \tag{50c}$$

$$a_{13} = 0, \tag{50d}$$

$$a_{23} = \tfrac{1}{2}(-t^2/k_{13}r_{12})\sqrt{-\sigma_{13}/\rho_{12}k_{13}r_{12}}. \tag{50e}$$

The manifold (50) lies on the intersection of the *DANAD* surface and an envelope obtained from $\mathrm{Det}|a| = 0$. We had $a_{23} = 0$ for the manifold (45) but here we have $a_{13} = 0$.

The remaining case $y_{11}y_{22} < 0$, $y_{22}y_{33} > 0$ can be handled in exactly the same way. The result can be written

$$2z_{1i} = k_{1i}z_{11} + \frac{1}{k_{1i}}z_{ii} - \sigma_{1i} \qquad (i = 2,3), \tag{51a}$$

$$k_{1i} = \frac{1}{y_{11}}\left[y_{1i} - \frac{y_{11}}{|y_{11}|}\sqrt{y_{1i}^2 - y_{11}y_{ii}}\right] < 0, \tag{51b}$$

$$z_{23} = \frac{1}{2}\left[\frac{k_{13}}{k_{12}}z_{22} + \frac{k_{12}}{k_{13}}z_{33} + (\sqrt{-k_{13}\sigma_{12}} + \sqrt{-k_{12}\sigma_{13}})^2\right]. \tag{51c}$$

The numbers v and w turn out to be given by

$$v/\sqrt{-\sigma_{12}k_{13}} = w/\sqrt{-\sigma_{13}k_{12}} = -[\sqrt{-\sigma_{12}k_{13}}+\sqrt{-\sigma_{13}k_{12}}]^{-1}. \quad (51d)$$

It follows that we have $t = \mathrm{Tr}[\alpha a] \propto 2(1+v+w) = 0$. This can either be so understood that we have a finite value of the parameter t and infinite values of all the masses a_{jk}, or, alternatively that the masses are finite but $t = 0$. In either case only the ratios of the masses are well defined and given by $a_{12}/a_{23} = vk_{13}$; $a_{13}/a_{23} = wk_{12}$. This suggests that the manifold (51) is on the common intersection of the *DANAD* surface and the envelope obtained from eq. (28). Actually, this conjecture is correct and one can verify that (51) corresponds to the following values of the parameters κ_{12} and κ_{13} in (28):

$$\kappa_{12} = -k_{12}+\sqrt{k_{12}k_{13}\,\sigma_{12}/\sigma_{13}}, \qquad \kappa_{13} = -k_{13}+\sqrt{k_{12}k_{13}\,\sigma_{13}/\sigma_{12}}. \quad (51e)$$

(Cf. also fig. 9.) Further, all the inequalities $E_1, \ldots, E_5$ are fulfilled for (51).

This proves that we always have at least one relevant branch of the *DANAD* surface in the z_{23}-plane for all values of the numbers z_{11}, z_{22}, z_{33}, z_{12} and z_{13} as long as they are consistent with the three point function boundary conditions. We next want to prove that the *DANAD* surface, when plotted in the z_{23}-plane as indicated above, is normally a finite curve. We hereby assume that all the other z are given fixed finite values. Every point on the *DANAD* curve is finite unless z_{23} becomes infinite for some value (or values) of the parameter r_{12}. For this to happen, we must either have λ_{23} infinite or r_{23} or k_{23} either zero or infinity. We discuss these cases separately.

If λ_{23} becomes infinite for some value of r_{12}, eq. (34) implies that at least one of the numbers λ_{12} and λ_{13} is infinite for the same value of r_{12}. For definiteness, let us assume that λ_{12} is infinite. As z_{12} has been assumed to be a finite number, the difference $S_{12}-F_{12}$ must be zero for this value of r_{12}. However, it is easily proved that the manifolds F_{12} and S_{12} never intersect unless at least one of the two numbers z_{11} and z_{22} is real. (Cf. footnote 21 on p. 40 in KW.) Except, possibly, for the special case that at least one diagonal z is real and negative, we conclude that λ_{23} never becomes infinite. (The fact that z_{23} really can become infinite in the exceptional case is illustrated in fig. 6 below.)

When r_{23} goes to zero, z_{23} becomes infinite unless λ_{23} happens to be equal to one at the same time. Eqs. (32) imply $r_{23} = k_{13}r_{12} = k_{12}r_{13}$. For $r_{23} = 0$ we must on one hand have at least one of the numbers k_{13} and r_{12} and, on the other hand, at least one of the numbers k_{12} and r_{13} equal to zero. If z_{12} is a finite number, r_{12} can only be equal to zero if λ_{12} is simultaneously equal to one, and k_{12} can only be equal to zero if λ_{12} is simultaneously equal to zero. As λ_{12} cannot be both zero and one, we cannot have k_{12} and r_{12} equal to zero at the same time. Therefore, we are left with two possibilities, viz.

(α) $r_{12} = k_{13} = 0$. If z_{12} and z_{13} are both finite numbers, we must have $\lambda_{12} = 1$; $\lambda_{13} = 0$. Eq. (34) now yields $\lambda_{23} = 1$ and z_{23} is a finite number.

(β) $r_{13} = k_{12} = 0$. We now get $\lambda_{13} = 1$; $\lambda_{12} = 0$; $\lambda_{23} = 1$ and z_{23} is finite.

When r_{23} goes to infinity, we find from the relation above that some of the numbers r_{12}, r_{13}, k_{12} and k_{13} must also be infinite. As before, r_{12} and k_{12} cannot be infinite simultaneously and we have two cases, viz.

(α) $k_{13} = k_{12} = \infty$. We here get $\lambda_{12} = \lambda_{13} = 0$ and, consequently, $\lambda_{23} = 1$. As before, z_{23} stays finite in this case and the *DANAD* curve is finite.

(β) $r_{12} = r_{13} = \infty$. We get $\lambda_{12} = \lambda_{13} = 1$ and, consequently, $\lambda_{23} = 1$, and z_{23} remains a finite number.

When k_{23} vanishes, we conclude from the relation $k_{23} = k_{13}/k_{12} = r_{13}/r_{12}$ and the remark that r_{12} and k_{12} cannot simultaneously have the values zero or infinity that we have to discuss the following two cases:

(α) $k_{13} = 0$, $r_{12} = \infty$. We get $\lambda_{12} = 1$ and $\lambda_{13} = 0$ which implies $\lambda_{23} = 0$ with the aid of eq. (34). As k_{23} was equal to zero for this case, $\lambda_{23} = 0$ is exactly what is needed to yield a finite limit for z_{23}, and the *DANAD* remains a finite curve.

(β) $k_{12} = \infty$, $r_{13} = 0$. Here, we have $\lambda_{13} = 1$; $\lambda_{12} = \lambda_{23} = 0$ and z_{23} remains a finite number.

Finally, we have the case when k_{23} becomes infinite. As above, we have two possibilities:

(α) $k_{12} = 0$, $r_{13} = \infty$. The same argument as before yields $\lambda_{13} = 1$ and $\lambda_{12} = \lambda_{23} = 0$ and z_{23} is finite.

(β) $k_{13} = \infty$; $r_{12} = 0$. This yields $\lambda_{12} = 1$, $\lambda_{13} = \lambda_{23} = 0$ and z_{23} remains finite.

Summarizing, we have proved that, unless at least one of the imaginary parts of the diagonal z is zero, every point z_{23} obtained on the *DANAD* curve is a finite complex number.

5. Numerical plots of the Four Point Function Boundary Surface

The discussion in the previous sections has given us some insight into the general structure of the *DANAD* surface. We now want to illustrate these features with the aid of numerical plots. As a first case we consider a situation when z_{11}, z_{22} and z_{33} all lie in the upper half plane. The three point function boundaries are then given by F_{12}, F_{13} and F_{23}. Picking values z_{12} and z_{13} on that side of these curves which corresponds to the analyticity domain of the three point function, we plot the *DANAD* surface as well as the F_{23}-curve in the z_{23}-plane. A typical example is shown in fig. 1. This graph is based on the numerical values of the parameters shown in the upper left corner. For this particular case we see that the *DANAD* surface is a closed curve which intersects the F_{23}-curve in two points. That point on *DANAD* which corresponds to eq.

(45) is denoted by P in the diagram. Further, the regularity domain is the domain inside the *DANAD* curve and above the F_{23}-curve. The shading in the plot shows the domain where the function can have singularities. This plot

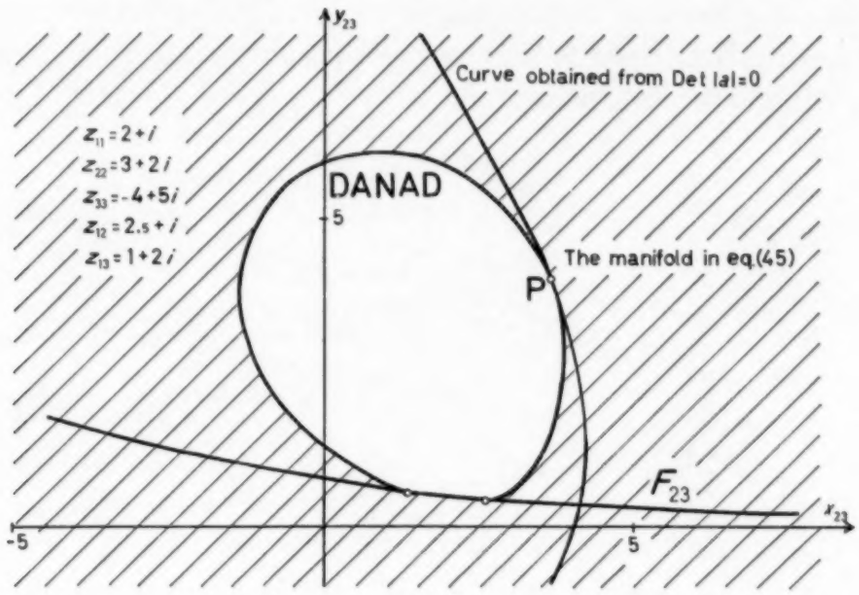

Fig. 1.

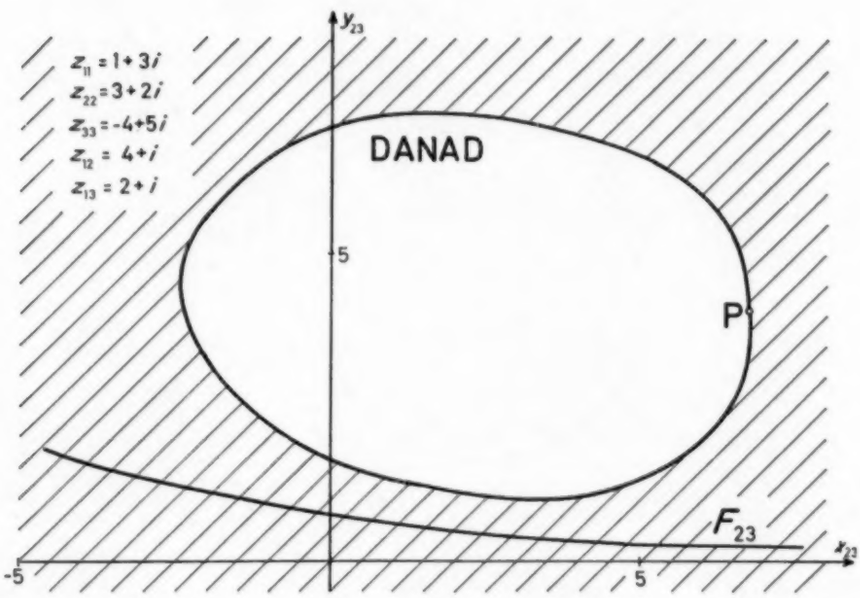

Fig. 2.

raises the question whether or not *DANAD* always intersects the three point function boundary. That this is not always the case can be most easily illustrated with another numerical example which is shown in fig. 2. The complex parameters have slightly different values as compared to fig. 1. The new values are shown in the plot.

Another interesting question is what happens to *DANAD* in the z_{23}-plane if

one of the points z_{12} or z_{13} approaches its three point function boundary. If we take the case illustrated in fig. 2 and let, say, z_{13} approach F_{13} by changing the imaginary part y_{13}, we find that the limiting value is given by $y_{13} = -\frac{7}{38}(\sqrt{23}-2)$. For this case one finds the limiting form of *DANAD* shown in fig. 3. It is worth noting that the *DANAD* curve does not shrink down to a point but remains a finite curve also in the limit.

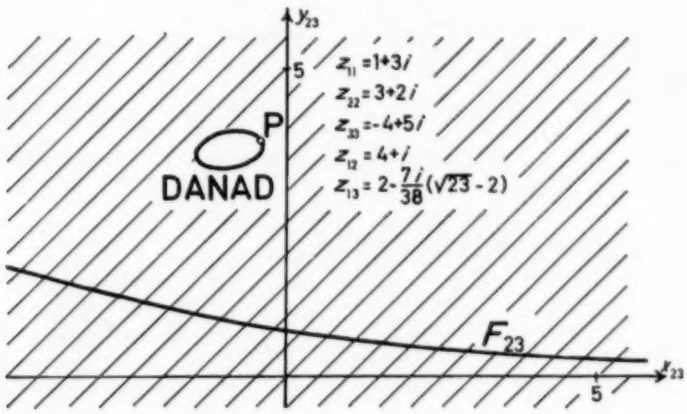

Fig. 3.

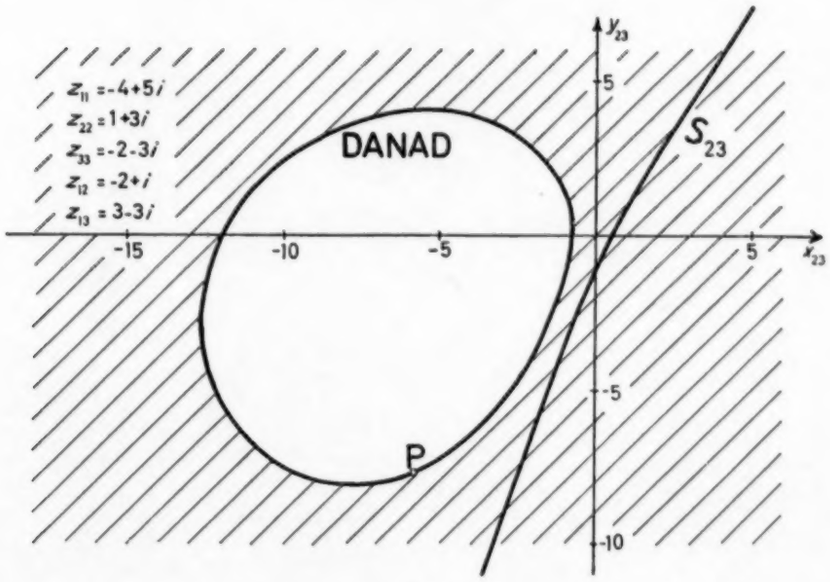

Fig. 4.

When the imaginary parts of the diagonal y do not all have the same signs, we sometimes get S-curves as three point function boundaries but otherwise no important change of a qualitative nature in our diagrams. A few special cases are illustrated in figs. 4 and 5. The corresponding values of the parameters are given in plots.

It is of some interest to look at the limiting forms of *DANAD* given in eq. (39). An example is illustrated in fig. 6. One of the curves shown here corresponds exactly to eq. (39) while the equation for the other curve is obtained from (39)

by a permutation of the indices 1 and 3. In this case, the curve corresponding exactly to (39) goes to infinity. This is not in contradiction with our previous

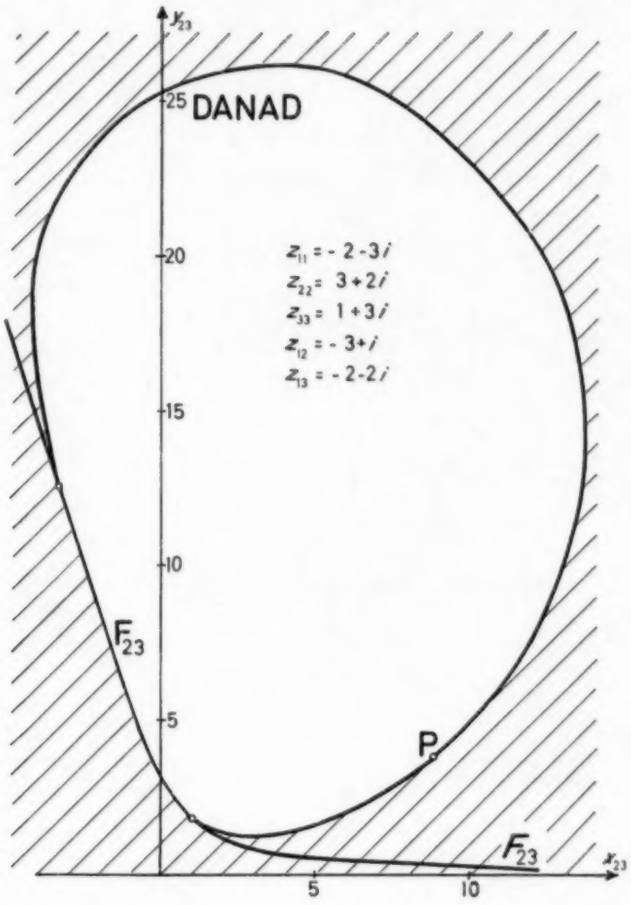

Fig. 5.

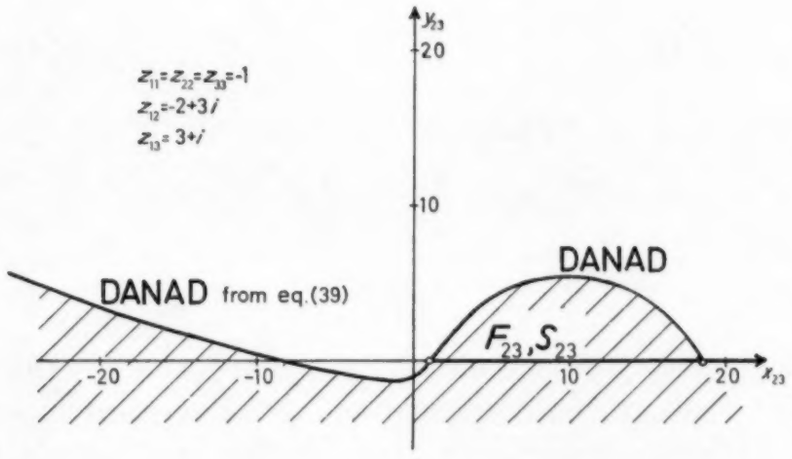

Fig. 6.

argument as we here have a degenerate case where the imaginary parts of the diagonal z are all equal to zero. The asymptote in our case is obtained when ρ

approaches one and has an equation given by

$$z_{23} = \frac{1}{\rho - 1}(1-z_{12})(1-z_{13}) + 1 - z_{12} - z_{13}. \tag{52}$$

This curve is relevant for all values of ρ as y_{12} and y_{13} have the same signs here. The other curve, however, is relevant only when y_{23} and y_{13} have the same signs, i.e. as long as it lies in the upper half plane. The F_{23} and S_{23} in this plot

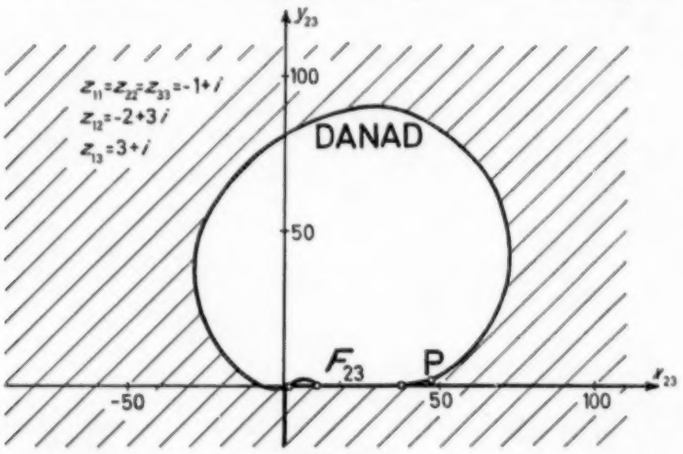

Fig. 7.

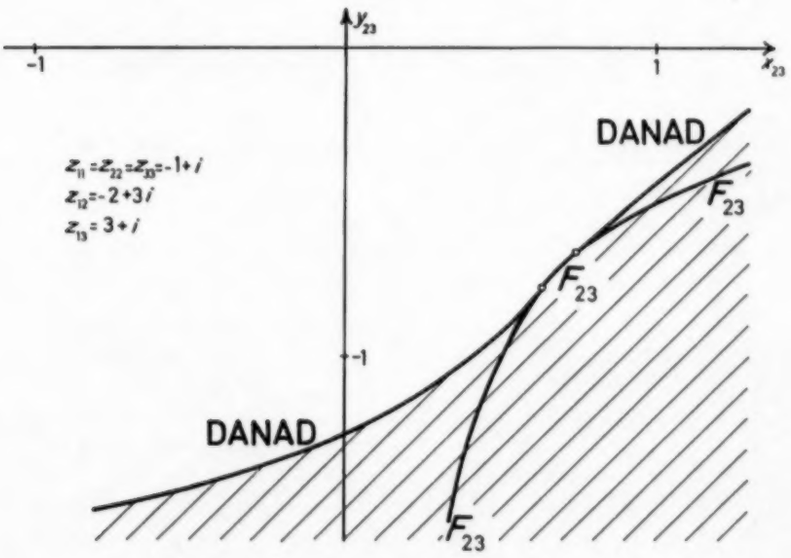

Fig. 8.

coincide with the positive real axis with $x_{23} \geqq 1$. As before, the shaded region in fig. 6 corresponds to the domain where the four point function can have singularities. It is illuminating to compare this plot with a corresponding situation when the diagonal z are not exactly negative and real but also have an imaginary part. This is done in fig. 7. We have here put $z_{jj} = -1+i$. This imaginary part is not particularly small, but the numerical plot is still similar enough to the previous picture to be of interest. We note that *DANAD*

in this case is a closed finite curve, as it must be, and that one part of it corresponds to rather large absolute values of z_{23}. In the limit when the imaginary parts of the diagonal z become zero this part of $DANAD$ disappears out at infinity.

Another rather interesting feature in this situation is that $DANAD$ for this case consists of two separate parts corresponding to the two different curves obtained in the limit in fig. 6. Fig. 8 shows the intersection between $DANAD$ and F_{23} in the fourth quadrant, plotted in a different scale so as to exhibit the two disconnected parts of $DANAD$ in an obvious way.

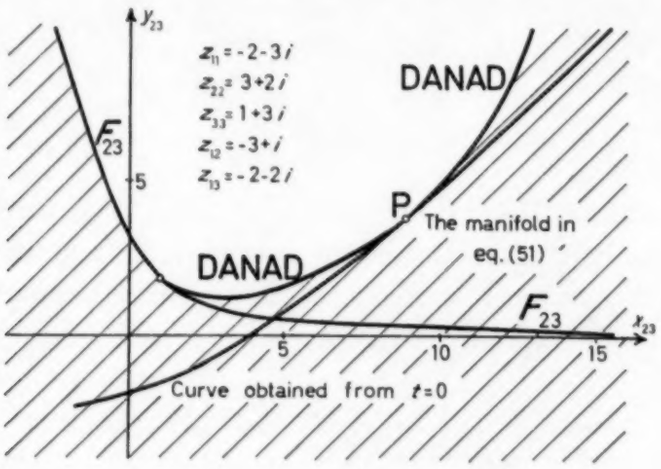

Fig. 9.

Finally, fig. 9 illustrates the statement made before that the obvious generalization of the S-manifold does not form any new eleven dimensional part of the boundary. We have here plotted the same case as in fig. 4 but on a different scale. The new curve in fig. 9 is the envelope obtained for $t = 0$. The figure shows how this curve always lies outside the analyticity domain except at one point where it touches the $DANAD$ surface. This point corresponds to the case when all the parameters a_{jk} in the $DANAD$ surface are infinite. As $DANAD$ effectively only depends on the ratios a_{jk}/t^2, this is equivalent to the statement that $t = 0$.

It is a pleasure to thank Prof. C. E. Fröberg and his staff for valuable aid with the numerical computations done on the electronic computer, SMIL, at Lund University. We further want to thank Profs: J. Toll and A. Wightman as well as Dr. D. Kleitman for helpful discussions and comments.

Appendix 1

A SPECIAL TECHNIQUE FOR COMPUTING ENVELOPES

From the elementary theory of envelopes it is well-known that a necessary condition to obtain the envelope of a family of curves $F(x, y, a_i) = 0$ in the

(x,y)-plane is given by the simultaneous equations

$$F(x,y,\,a_i) = 0, \tag{A.1a}$$

$$\frac{\partial F(x,\,y,\,a_i)}{\partial a_i} = 0. \tag{A.1b}$$

When the family of curves is given in parametric form $x = x(a_i)$, $y = y(a_i)$, one finds by straight forward computations that one can replace eq. (A.1b) by the determinant conditions

$$\begin{vmatrix} \dfrac{\partial x}{\partial a_i} & \dfrac{\partial y}{\partial a_i} \\ \dfrac{\partial x}{\partial a_j} & \dfrac{\partial y}{\partial a_j} \end{vmatrix} = 0, \tag{A.2}$$

for all combinations of the indices i and j. This is a formulation which is particularly well adapted for our complex notation. A family of curves in the plane of a complex variable $z = x+iy$ can be expressed compactly as $z = z(a_i)$. The envelope conditions in eq. (A.2) can now be written as

$$\mathrm{Im}\left[\frac{\partial z}{\partial a_i} \Big/ \frac{\partial z}{\partial a_j}\right] = 0 \quad \text{for} \quad \text{all } i \text{ and } j. \tag{A.3}$$

Eq. (A.3) can be interpreted to mean that all derivatives of the complex number z with respect to the parameters a_i are proportional to the same complex number $\jmath$, or

$$\frac{\partial z}{\partial a_i} = \alpha_i \jmath, \tag{A.4}$$

where the α_i are real numbers and $\jmath$ is a complex number. When the relation between z and the parameters a_i is given implicitly as $F(z,\,a_i) = 0$, it is not necessary to solve for the number z, but one can write the envelope equations as

$$F(z,\,a_i) = 0, \tag{A.5a}$$

$$\frac{\partial F(z,\,a_i)}{\partial a_i} = \jmath\alpha_i. \tag{A.5b}$$

This is the technique which was used in the text. It can be mentioned that the complex number $\jmath$ has a certain geometrical significance. If we consider one point z on the envelope and its variation with a_i, we find

$$\mathrm{d}z = \frac{-1}{\dfrac{\partial F}{\partial z}} \sum_i \frac{\partial F}{\partial a_i}\,\mathrm{d}a_i = \frac{-\jmath}{\dfrac{\partial F}{\partial z}} \sum_i \alpha_i \mathrm{d}a_i. \tag{A.6}$$

Consequently, the complex number $\jmath\ (\partial F/\partial z)^{-1}$ lies along the tangent of the envelope in the z-plane. This interpretation is of some interest in connection with the discussion in the main text. Consider the case when two or more of the diagonal masses a_{ii} are equal to zero and the corresponding envelope conditions

$$\frac{\partial \phi}{\partial a_{jk}} = \jmath \alpha_{jk}. \tag{A.7}$$

The tangent of the envelope in the z_{23}-plane is given by $\jmath(\partial\phi/\partial z_{23})^{-1}$. Eqs. (A.7) should be written down for all combinations of the indices j and k where the corresponding mass is different from zero. This means that (A.7) holds for all non-diagonal elements of the matrix α and for some of the diagonal ones. Alternatively, this can be so expressed that the matrix α is real except for some of its diagonal elements. The change of the number z_{23} for arbitrary variations of the masses can now be written

$$\mathrm{d}z_{23} = \left(\frac{\partial \phi}{\partial z_{23}}\right)^{-1} \jmath[\sum{}' \alpha_{jk}\mathrm{d}a_{jk} + \alpha_{11}\mathrm{d}a_{11} + \alpha_{22}\mathrm{d}a_{22} + \ldots]. \tag{A.8}$$

The prime after the summation sign in eq. (A.8) indicates that only the real α_{jk} appear in this sum. The complex α_{jj} are written out explicitly in the formula. If we should not obtain points z_{23} on both sides of our envelope, the imaginary part of the square bracket in eq. (A.8) must have a definite sign. As the masses a_{11}, a_{22} etc. vary from their extreme value zero to positive values, the imaginary parts of those diagonal α which are complex numbers must all have the same sign. This condition was used in the text in connection with eqs. (25) and (26).

For completeness, we want to mention without proofs that, when the parameters a_i in eq. (A.5) are not varying independently but restricted by one or more relations of the form $f_j(a_i) = 0$, we can use a similar formalism but have to replace eqs. (A.5) by

$$F(z, a_k) + i\jmath \sum_j \lambda_j f_j(a_k) = 0, \tag{A. 9a}$$

$$\frac{\partial F}{\partial a_k} + i\jmath \sum_j \lambda_j \frac{\partial f_j}{\partial a_k} = \jmath \alpha_k, \tag{A.9b}$$

$$f_j(a_k) = 0. \tag{A.9c}$$

As before, $\jmath$ is a complex number with a direction which is intimately related to the slope of the envelope. The α_k are real numbers and the λ_j are real Lagrangian multipliers. However, it is not necessary to use this refinement in the main text as we are able to dispose of the envelopes corresponding to the surface $\mathrm{Det}|a| = 0$ without explicit computations.

Appendix 2

THE THREE POINT FUNCTION BOUNDARY

As an application of the formalism in the previous appendix we use this technique to compute the boundary of the analyticity domain for the three point function without local commutativity. This discussion is equivalent to the corresponding argument in App. I in KW.

The function ϕ for the three point function can be written as

$$\phi = (t^2-Q)^2-R = 0. \tag{A.10}$$

The quantities Q and R are given by the same equations as for the four point function, viz. eqs. (6b) and (6c) except that the matrices Z and a and, consequently, also the matrix M are 2×2 matrices. Note the condition $R = 4\ \mathrm{Det}|M| = 4\ \mathrm{Det}|Z|\ \mathrm{Det}|a|$. The masses a_{jk} are all positive and fulfil the inequality

$$a_{12} \geqq \sqrt{a_{11}a_{22}}. \tag{A.11}$$

This equation corresponds to eqs. (4) in the main text. The envelope condition when all masses and t are varying can be written as

$$2(t^2-Q)Z+Ra^{-1} = 2t(t^2-Q)\alpha. \tag{A.12}$$

We multiply (A.12) by the matrix a from the right and find with the aid of (A.10)

$$2M+t^2-Q = 2t\,\alpha a. \tag{A.13}$$

As in the main text we can square this equation and eliminate M^2 from the left hand side with the aid of the relation

$$M^2-QM+\tfrac{1}{4}R = 0. \tag{A.14}$$

Eq. (A.14) corresponds to eq. (18) in the main text. A computation as indicated above gives $M = (\alpha a)^2$ or

$$Z = \alpha a \alpha, \tag{A.15}$$

at least when the matrix a is non-singular. When all the masses are varying, α and a are completely real matrices, and the manifold (A.15) is at most three dimensional and not an interesting part of our boundary.

When the masses fulfil the limiting condition (A.11), we have $R = 0$, and eq. (A.10) reduces to

$$\phi = t^2-Q = 0. \tag{A.16}$$

Let us suppose that we have computed an envelope from this relation and consider one point $z_{12}^{(0)}$ on this envelope. If both the masses a_{11} and a_{22} are different from zero, we can change a_{12} to the value $a_{12} = \sqrt{a_{11}a_{22}}+\varepsilon$ and get

$$\sqrt{R} = \sqrt{-8\varepsilon \,\mathrm{Det}|Z|\,\sqrt{a_{11}a_{22}}}.$$

This changes the value of z_{12} to

$$z_{12} = z_{12}^{(0)} \pm 2\sqrt{-2\mathrm{Det}|Z|\sqrt{a_{11}a_{22}}}\sqrt{\varepsilon} + 0(\varepsilon). \tag{A.17}$$

Arguing as below eq. (21) we conclude that the point $z_{12}^{(0)}$ does not lie on the relevant boundary unless $\mathrm{Det}|Z|$ is either zero or parallel to the tangent of the envelope. In the first case we have at most a four dimensional manifold, and in the second case we have at most a limiting case of what has been considered above.

When one of the diagonal masses is equal to zero, we can first compute an envelope and find the result (A.15) with a complex value for one of the diagonal α. For definiteness, let us assume $a_{11} = 0$ and α_{11} complex. Eq. (A.15) tells us that z_{22} is a real number on this envelope. However, for this case we have one further restriction between our complex numbers. By straight forward computations one finds that the formulae above also imply the relation $\mathrm{Im}z_{12} = \pm\mathrm{Im}\sqrt{\mathrm{Det}|Z|}$. (Note that this corresponds to the F_{12} manifold.) Consequently, this case only yields the intersection of the z_{22}-axis and some other five dimensional manifold. Therefore, it is a manifold of only four dimensions and not an interesting part of our boundary.

We next put both a_{11} and a_{12} equal to zero. This implies $R = 0$ and $Q = a_{22}z_{22}$, and eq. (A.10) reduces to $z_{22} = t^2/a_{22}$. This is the z_{22}-cut which is part of the boundary.

When two diagonal masses are zero but a_{12} does not vanish, we have $Q = 2a_{12}z_{12}$ and $R = 4a_{12}^2(z_{12}^2 - z_{11}z_{22})$. Eq. (A.10) now gives

$$\left(\frac{t^2}{a_{12}} - 2z_{12}\right)^2 = 4(z_{12}^2 - z_{11}z_{22}), \tag{A.18}$$

or

$$2z_{12} = \frac{z_{11}z_{22}}{r} + r, \tag{A.18a}$$

with

$$r = \frac{t^2}{2a_{12}}. \tag{A.18b}$$

This is the analytic hypersurface F_{12}, which is part of our boundary.

Finally, we consider what happens when $t^2 = 0$. We note, that the parameter t enters only as t^2 in ϕ. Therefore, the effective range of this parameter is from zero to infinity, and we have to investigate the case $t = 0$. Here we get

$$\phi = Q^2 - R = 0. \tag{A.19}$$

Inspection shows that this equation can be rearranged to read

$$\left(2z_{12}+k_1z_{11}+\frac{1}{k_1}z_{22}\right)\left(2z_{12}+k_2z_{11}+\frac{1}{k_2}z_{22}\right)=0, \tag{A.20}$$

$$k_{1,\,2}=\frac{1}{a_{11}}(a_{12}\pm\sqrt{a_{12}^2-a_{11}a_{22}}). \tag{A.21}$$

This is also an analytic hypersurface and identical with the S-manifold which is part of our boundary. We notice the great similarity between the algebraic rearrangement leading from eq. (A.19) to (A.20) on one hand and from eq. (6a) to eq. (28) in the main text on the other hand.

In this way we see that all the four analytic hypersurfaces which make up the boundary of the three point function regularity domain appear very naturally in this successive computation of envelopes. (The z_{11}-cut comes quite analogously to the z_{22}-cut from the case when a_{22} and a_{12} are both equal to zero). It can also be remarked that this organization of the computation of the three point function regularity domain is such that it very naturally generalizes to the treatment of the four point function domain given in the main text. Similarly, it should not be too difficult to generalize the argument of this paper to the n-point function domain.

Appendix 3

DISCUSSION OF EQ. (20) WHEN TWO OF THE DIAGONAL MASSES ARE ZERO

There was one case which was not completely discussed in the main text, viz. when two of the diagonal masses are zero and the corresponding α are complex numbers. Eq. (20) then defines a manifold on which the imaginary part of one diagonal z is zero. It was stated in the text that the negative real axis of a diagonal z is very improbable as a relevant part of the boundary, but no definite proof of this was given. In this appendix we want to demonstrate that the manifold defined by eq. (20) is really only ten dimensional in this case and further that it is only a degenerate case of the $DANAD$ manifold in eq. (26). We prove this by explicit but somewhat lengthy computations.

For definiteness, assume $a_{11}=a_{22}=0$, $a_{33}\neq 0$, α_{11} and α_{22} complex numbers and α_{33} a real number. Eq. (20) becomes, in a somewhat explicit notation,

$$z_{ij}=a_{12}(\alpha_{i1}\alpha_{j2}+\alpha_{i2}\alpha_{j1})+a_{13}(\alpha_{i1}\alpha_{j3}+\alpha_{i3}\alpha_{j1})+a_{23}(\alpha_{i2}\alpha_{j3}+\alpha_{i3}\alpha_{j2})+a_{33}\alpha_{i3}\alpha_{j3}. \tag{A.22}$$

If we specialize eq. (A.22) to the two cases $i=j=1$ and $i=j=2$ and solve for α_{11} and α_{22}, we get the results

$$\alpha_{11}=\frac{z_{11}-2a_{23}\alpha_{12}\alpha_{13}-a_{33}\alpha_{13}^2}{2(a_{12}\alpha_{12}+a_{13}\alpha_{13})}, \tag{A.23}$$

$$\alpha_{22} = \frac{z_{22} - 2a_{13}\alpha_{12}\alpha_{23} - a_{33}\alpha_{23}^2}{2(a_{12}\alpha_{12} + a_{23}\alpha_{23})}. \tag{A.24}$$

As both α_{11} and α_{22} are complex numbers, it is convenient to eliminate them completely in the numbers z_{ij}. In particular, we obtain with the aid of eq. (A.22) and (A.23) a result for z_{12} which closely resembles eq. (32) in the main text

$$2z_{12} = \lambda_{12}\left(z_{11}k_{12} + z_{22}\frac{1}{k_{12}}\right) + (1-\lambda_{12})\left(\frac{z_{11}z_{22}}{r_{12}} + r_{12}\right), \tag{A.25}$$

$$k_{12} = \frac{\alpha_{23}}{\alpha_{13}}, \tag{A.26}$$

$$r_{12} = 2\alpha_{12}(a_{12}\alpha_{12} + a_{13}\alpha_{13} + a_{23}\alpha_{23}) + a_{33}\alpha_{13}\alpha_{23}, \tag{A.27}$$

$$\lambda_{12} = \frac{a_{13}a_{23}\alpha_{13}\alpha_{23} - \frac{1}{2}a_{33}a_{12}\alpha_{13}\alpha_{23}}{(a_{12}\alpha_{12} + a_{13}\alpha_{13})(a_{12}\alpha_{12} + a_{23}\alpha_{23})}. \tag{A.28}$$

We note that these formulae become identical with eqs. (32) in the main text when we put a_{33} equal to zero and note the relation (25) and $A = D^{-1}\,\alpha\,D^{-1}$ between the matrices A and D on one hand and α and a on the other hand.

As the number α_{33} is real and, furthermore, appears quadratically on the right hand side of eq. (A.22) for $i = j = 3$, the elimination of α_{33} is not quite so straight forward as the elimination of α_{11} and α_{22}. To be systematic, we first eliminate α_{11} from the right hand side of eq. (A.22) for $i = 1$, $j = 3$. We get

$$\begin{aligned} 2z_{13} = {} & \frac{z_{11} - 2a_{23}\alpha_{12}\alpha_{13} - a_{33}\alpha_{13}^2}{a_{12}\alpha_{12} + a_{13}\alpha_{13}}(a_{12}\alpha_{23} + a_{13}\alpha_{33}) \\ & + 2\alpha_{13}(a_{12}\alpha_{12} + a_{13}\alpha_{13} + a_{23}\alpha_{23}) + 2a_{23}\alpha_{12}\alpha_{33} + 2a_{33}\alpha_{13}\alpha_{33}. \end{aligned} \tag{A.29}$$

If we really are on the manifold $DANAD$, the right hand side of eq. (A.29) must be expressable in the form shown in eq. (32a) in the main text, with z_{33} a real number. Comparing the real and imaginary parts of (32a) and (A.29) or, alternatively, comparing the coefficients of different powers of z_{11} we find

$$\lambda_{13}k_{13} + \frac{1-\lambda_{13}}{r_{13}}z_{33} = \frac{a_{12}\alpha_{23} + a_{13}\alpha_{33}}{a_{12}\alpha_{12} + a_{13}\alpha_{13}}, \tag{A.30}$$

$$\begin{aligned} \lambda_{13}\frac{z_{33}}{k_{13}} + (1-\lambda_{13})r_{13} = {} & \frac{a_{12}\alpha_{23} + a_{13}\alpha_{33}}{a_{12}\alpha_{12} + a_{13}\alpha_{13}}(-2a_{23}\alpha_{12}\alpha_{13} - a_{33}\alpha_{13}^2) \\ & + 2\alpha_{13}(a_{12}\alpha_{12} + a_{13}\alpha_{13} + a_{23}\alpha_{23}) + 2a_{23}\alpha_{12}\alpha_{33} + 2a_{33}\alpha_{13}\alpha_{33}, \end{aligned} \tag{A.31}$$

$$\frac{r_{13}}{k_{13}} = \frac{r_{12}}{k_{12}} = 2\frac{\alpha_{13}\alpha_{12}}{\alpha_{23}}(a_{12}\alpha_{12} + a_{13}\alpha_{13} + a_{23}\alpha_{23}) + a_{33}\alpha_{13}^2. \tag{A.32}$$

These three equations determine the three real numbers k_{13}, r_{13} and λ_{13}. The equations appear to be quite complicated, but some remarkable simplifications occur when one tries to solve them. The result can be written

$$k_{13} = \frac{\alpha_{23}}{\alpha_{12}} X, \tag{A.33}$$

$$r_{13} = \alpha_{13}\, \rho X, \tag{A.34}$$

$$\rho = 2(a_{12}\alpha_{12}+a_{13}\alpha_{13}+a_{23}\alpha_{23})+a_{33}\frac{\alpha_{13}\alpha_{23}}{\alpha_{12}}, \tag{A.35}$$

$$\rho(X-1) = \frac{\alpha_{12}\alpha_{33}-\alpha_{13}\alpha_{23}}{\alpha_{23}\alpha_{13}}\left[a_{13}\alpha_{13}+a_{23}\alpha_{23}+a_{33}\frac{\alpha_{13}\alpha_{23}}{\alpha_{12}}-\sqrt{R}\right], \tag{A.36}$$

$$R = (a_{13}\alpha_{13}+a_{23}\alpha_{23})^2-2a_{33}a_{12}\alpha_{13}\alpha_{23}, \tag{A.37}$$

$$\lambda_{13} = \tfrac{1}{2}\left[1-\frac{a_{13}\alpha_{13}(a_{12}\alpha_{12}+a_{13}\alpha_{13}+a_{23}\alpha_{23})-a_{12}\alpha_{23}(a_{23}\alpha_{12}+a_{33}\alpha_{13})}{\sqrt{R}(a_{12}\alpha_{12}+a_{13}\alpha_{13})}\right]. \tag{A.38}$$

The square root in eq. (A.36) has to be defined in such a way that X reduces to 1 for $a_{33} = 0$. We note that eqs. (A.33) to (A.38) become analogous to eq. (A.28) in the limit when $a_{33} = 0$. In exactly the same way we can obtain formulae for r_{23}, k_{23} and λ_{13}. They are obtained from eqs. (A.33) to (A.38) if we permute the indices 1 and 2 everywhere. To prove that we actually are on *DANAD* we have to verify that the relations $k_{23}\, k_{12} = k_{13}$ and $r_{23} = k_{13} r_{12}$ as well as eq. (34) in the main text are fulfilled by this results. This is a straight forward task which can be done with the aid of the explicit formulae given here, and we do not insist on giving all the details.

To be sure that we are on *DANAD* we have to verify that all the parameters r_{ij}, k_{ij} and λ_{ij} are real numbers. A necessary and sufficient condition for this is $R > 0$. This is not necessarily true if a_{33} is big enough and if the signs of α_{13} and α_{23} are the same. However, in that case one finds that the number z_{33} from eq. (A.22) becomes positive and real, and we are on the z_{33}-cut. This manifold is known to be part of the relevant boundary.

The discussion in this appendix proves that eq. (20) with the two diagonal masses a_{11} and a_{22} equal to zero either corresponds to the z_{33}-cut or to the intersection between the negative z_{33}-axis and the *DANAD* manifold.

References

1) H. Umezawa and S. Kamefuchi, Prog. Theor. Phys. **6** (1951) 543
2) G. Källén, Helv. Phys. Act. **25** (1952) 417;
H. Lehmann, Nuovo Cim. **11** (1954) 342;
M. Gell-Mann and F. E. Low, Phys. Rev. **95** (1954) 1300;
A. Wightman, Phys. Rev. **101** (1956) 860

3) G. Källén and A. Wightman, Mat. Fys. Skr. Dan. Vid. Selsk. **1**, No. 6 (1958)
4. G. Källén and H. Wilhelmsson, Mat. Fys. Skr. Dan. Vid. Selsk. **1**, No. 9 (1959) and earlier work referred to in this paper
5) H. Behnke and P. Thullen, Ergebn. d. Math. **3** (1934)
6) S. Bochner and W. T. Martin, Several complex variables (Princeton, 1948)
7) A. Wightman, École d'Été de Physique Théorique, Les Houches (Hermann et Cie, Paris, 1960)
8) R. Jost, Proc. Naples Conf. spring 1959 (to be published)
9) J. Toll, Proc. Naples Conf. spring 1959 (to be published)
10) G. Källén, École d'Été de Physique Théorique, Les Houches (Hermann et Cie, Paris, 1960)

2.B: 2.L

Nuclear Physics **25** (1961) 604—610; © *North-Holland Publishing Co., Amsterdam*

Not to be reproduced by photoprint or microfilm without written permission from the publisher

POLARIZATION OF 0.3 TO 1.4 MeV NEUTRONS SCATTERED BY COPPER, ZINC, MOLYBDENUM AND CADMIUM

D. BROWN †, A. T. G. FERGUSON and R. E. WHITE

A.E.R.E., Harwell, Didcot, Berks., England

Received 17 February 1961

Abstract: Measurements have been made of the polarization of 0.5 to 1.5 MeV neutrons elastically scattered by Cu, Zn, Mo and Cd at 55° and Cu and Mo at 90°. Marked departures are found between the results obtained and the predictions of optical model calculations including a real spin-orbit potential.

1. Introduction

The polarization of neutrons of energy less than 2 MeV scattered from medium and heavy nuclei has been studied by a number of workers [1–4]). These measurements have been restricted to two energies, 380 keV and 980 keV, and three scattering angles, 55°, 90° and 130°. The variation of polarization with respect to the parameter A, the atomic weight, has been rather extensively explored. The most comprehensive set of results in this field is that of Clement *et al.* [5]) at neutron energies of 380 keV and 980 keV. They found that an optical model with spin-orbit coupling gave a general description of their results giving the change in sign indicative of the p-wave resonance.

Bjorklund, using a refined optical model with spin-orbit coupling, reported attempts [6]) to fit the data in more detail. He found that the calculated polarizations were in general too large, and the parameters required to fit the data fluctuated considerably from element to element.

The present series of measurements were undertaken to explore the variation with energy in more detail. For four elements, measurements have been made at 50 keV intervals from 350 keV up to 1600 keV. These measurements were made at 55° and 90° scattering angles, these angles being chosen for comparison with the results of earlier workers.

2. Experimental Procedure

The experimental arrangement used is shown in fig. 1. Details of the experimental arrangement have already been given [7]) and it is only described briefly here. Neutrons from the $Li^7(p, n)$ reaction, emitted at 50° to the proton beam

† On leave from Department of Physics, University of Auckland, New Zealand.

of the Harwell 5.5 MeV Van de Graaff generator, were collimated and allowed to scatter from rectangular samples 1.9 cm × 3.2 cm × 7.5 cm. The neutron energy spread was about 40 keV. Scattered neutrons were detected in 4 cm × 2.5 cm stilbene scintillators, gamma ray pulses being largely excluded by pulse shape discrimination. To prevent inelastic events being recorded, the neutron pulses were also required to exceed a bias level set, on a linear output, about 400 keV below the elastic neutron level and only coincidences between the

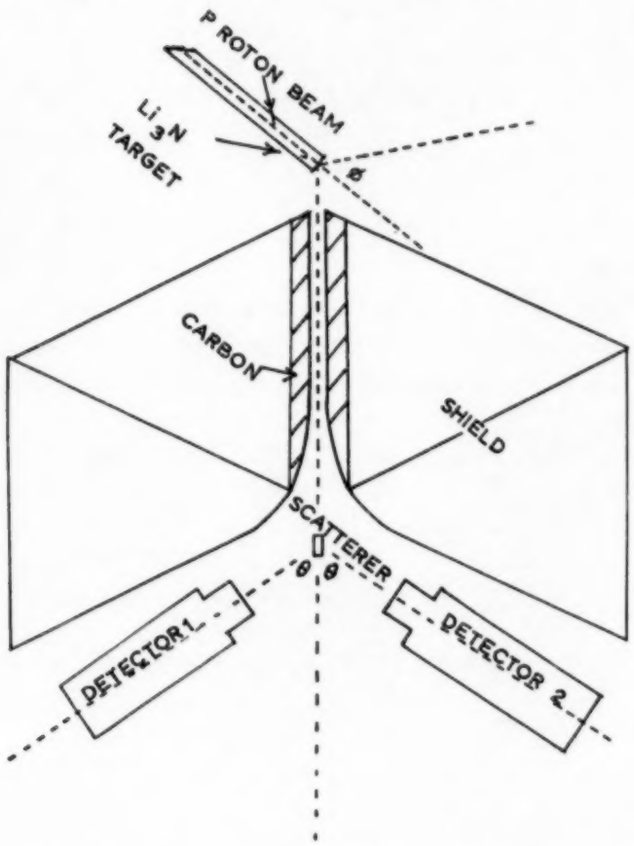

Fig. 1. General arrangement of the apparatus. The shield material was paraffin, the Li^3N target to scatterer distance being 50 cm.

pulse shape output and the linear output were recorded. Background was measured by taking a "scatterer out" run.

The experiment was carried out by measuring the true counts N_1 and N_2, i.e. total counts minus background, in each of the counters 1 and 2 with the assembly in a position corresponding to $\phi = +50°$ (see fig. 1). The measurement was then repeated with $\phi = -50°$ giving N'_1 and N'_2. Clearly, if the incident polarization in the first case is P_1, then in the second it is $-P_1$. Then if the true asymmetry is calculated as

$$\sqrt{\frac{N_1 N'_2}{N_2 N'_1}},$$

spurious effects arising from differences in counting efficiencies are avoided.

At a later stage in the experiment a simpler method was used. Here ϕ was kept constant. The positions of detectors 1 and 2 were adjusted so that their geometrical efficiencies were identical. Instead, then, of moving to $-\phi$ counters, 1 and 2 are interchanged. The method of analysis is very similar to that described above.

For the sign of the polarization, we use in this paper the Basle convention †. This is opposite to the convention adopted by Clement *et al.* [5]).

The polarisation of neutrons scattered from carbon for neutrons of energies less than 1 MeV should be zero as there are no strong p-wave or higher resonances in this region. This material was used as a check that we had eliminated artificial asymmetries. This topic is discussed in some detail elsewhere [7]).

Asymmetries were measured at 55° for copper, zinc, molybdenum and cadmium, and at 90° for copper and molybdenum. In view of the somewhat surprising nature of the results, considerable care was taken to ensure their consistency and reliability. Measurements were made using both methods described above and within the errors there appeared to be good agreement. Carbon checks were made during the course of these measurements.

3. Results

The asymmetries found at 55° and 90° have already been reported [7]). Recent results for the $Li^7(p, n)$ neutron polarization are shown in fig. 2. The

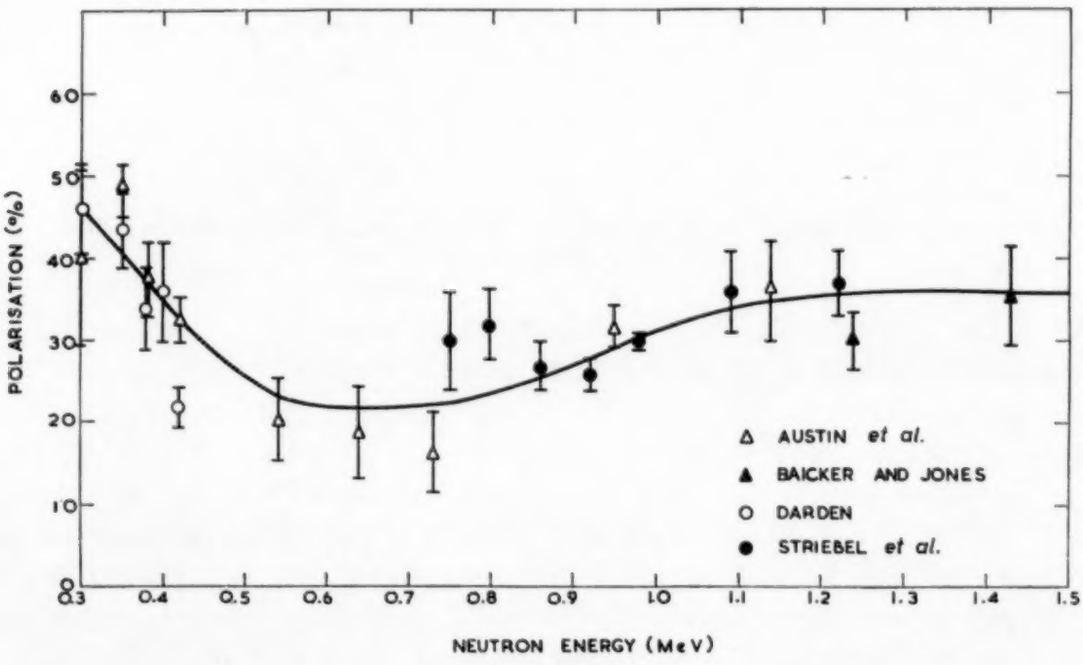

Fig. 2. Polarization of neutrons emitted in the $Li^7(p, n)Be^7$ reaction at 50° (lab.) to the proton beam as measured by Austin *et al.* [8]), Baicker and Jones [9]), Darden [10]) and Striebel *et al.* [11]).

† The convention is stated, e.g., in this journal **21** (1960) 696.

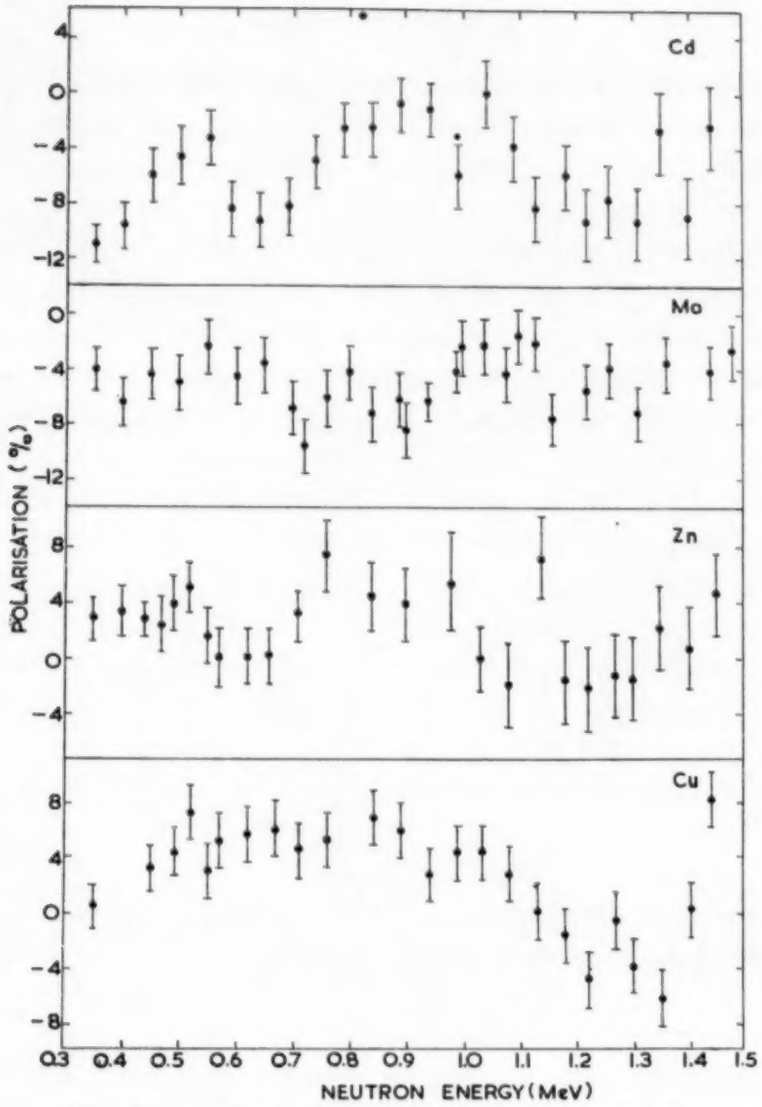

Fig. 3. Polarizations observed for 55° scattering.

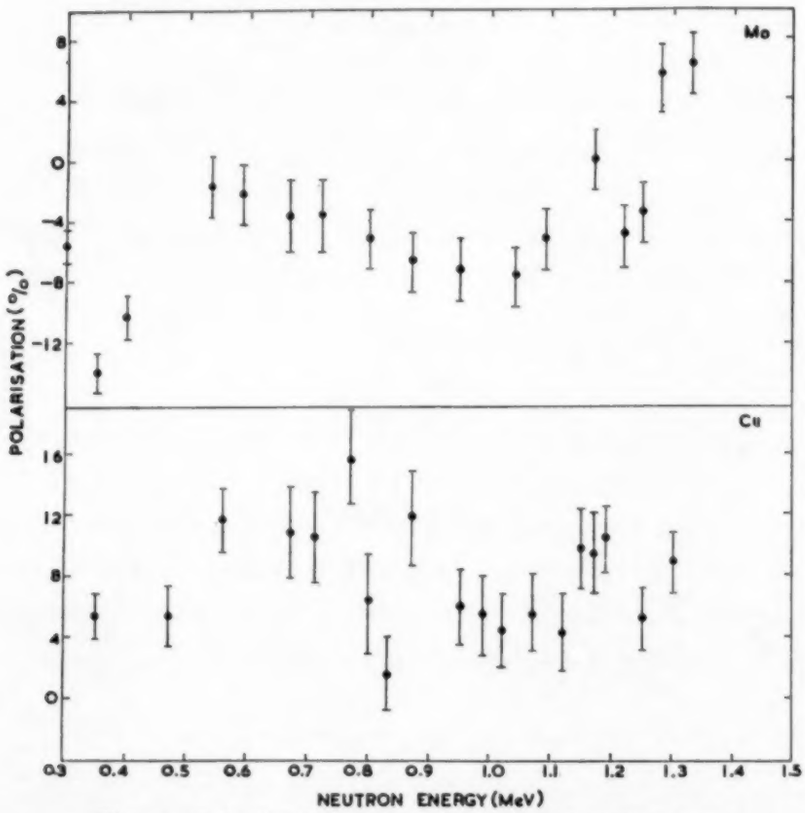

Fig. 4. Polarizations observed for 90° scattering.

polarizations corresponding to our observed asymmetries have been calculated and are given in figs. 3 and 4 for 55° and 90°, respectively, using values taken from the full line in fig. 2 for the Li(p, n) polarization.

We have examined the question of the effects of multiple scattering on our results by calculating the fraction of the observed scattered neutron intensity which arises from doubly scattered neutrons. Using the method of Blok and Jonker [12]), and assuming that the scattered neutrons have an isotropic distribution in the laboratory, we find for the case of copper that the doubly scattered neutrons constitute 30 % of the total intensity measured at 55° or 90°. The maximum effect of correcting for such a contribution would be to increase the observed asymmetries by the order of the statistical errors. However, in view of the approximate nature of the calculation and of other uncertainties present, especially in the incident neutron polarization data, it does not seem reasonable to modify our results at this stage. Finally, since the scattering cross-sections for the elements studied vary only slowly and monotonically in this energy region, this correction would not modify the main features of our results.

4. Discussion

Calculations were made using the version of the optical model with spin orbit coupling proposed by Bjorklund and Fernbach. Here the potential has the form

$$
\begin{aligned}
V &= V_C + V_S, \\
V_C(r, E) &= V_{CR}(E)\rho(r) + iV_{CI}(E)\exp\left[-(r-R_0)^2/b^2\right], \\
V_S(r, E) &= \left[V_{SR}(E) + iV_{SI}(E)\right]\left(\frac{\hbar}{\mu c}\right)^2 \frac{1}{r}\frac{d\rho(r)}{dr}\,\boldsymbol{\sigma}\cdot\mathbf{l}, \\
\rho(r) &= \left[1+\exp\left[(r-R_0)/a\right]\right]^{-1}, \\
R_0 &= 1.25\,A^{\frac{1}{3}}\ \text{fm},
\end{aligned}
$$

where V_C and V_S are a central and a spin-orbit potential, respectively, both being complex. Values of the parameters were taken from the summary of best values given at the Florida Conference in 1959 [6]). They were $V_{CR} = 56$ MeV, $V_{CI} = 2$ MeV, $V_{SR} = 10$ MeV, $V_{SI} = 0$, $a = 0.65$ or 0.4 and $b = 1.0$. The comparison of these calculations with the data is shown in figs. 5 and 6. It is clear that this optical model cannot reproduce the detailed features observed. Although no serious exploration of the parameter space could be undertaken through lack of computer time, it appeared that with some quite reasonable variation of the parameters each point could be fitted. Using the above parameters the calculated angular distributions of scattered neutrons at 1 MeV fitted the work of Walt and Barschall [13]) fairly well.

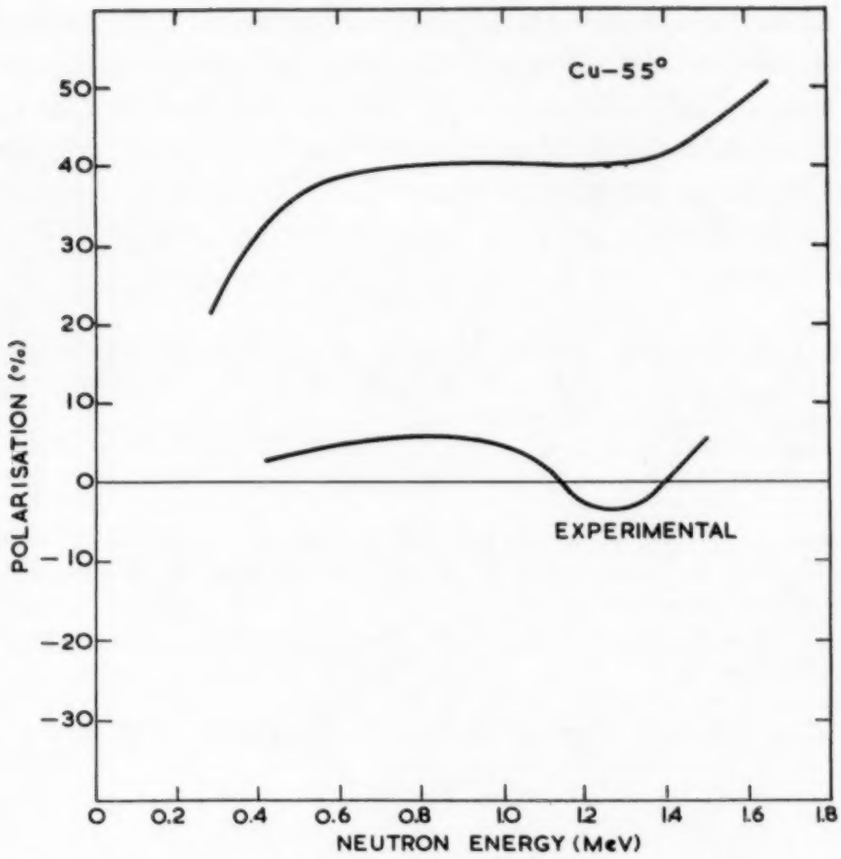

Fig. 5. Comparison of observed polarization in scattering from copper at 55° with the predictions of an optical model (upper curve; $a = 0.65$).

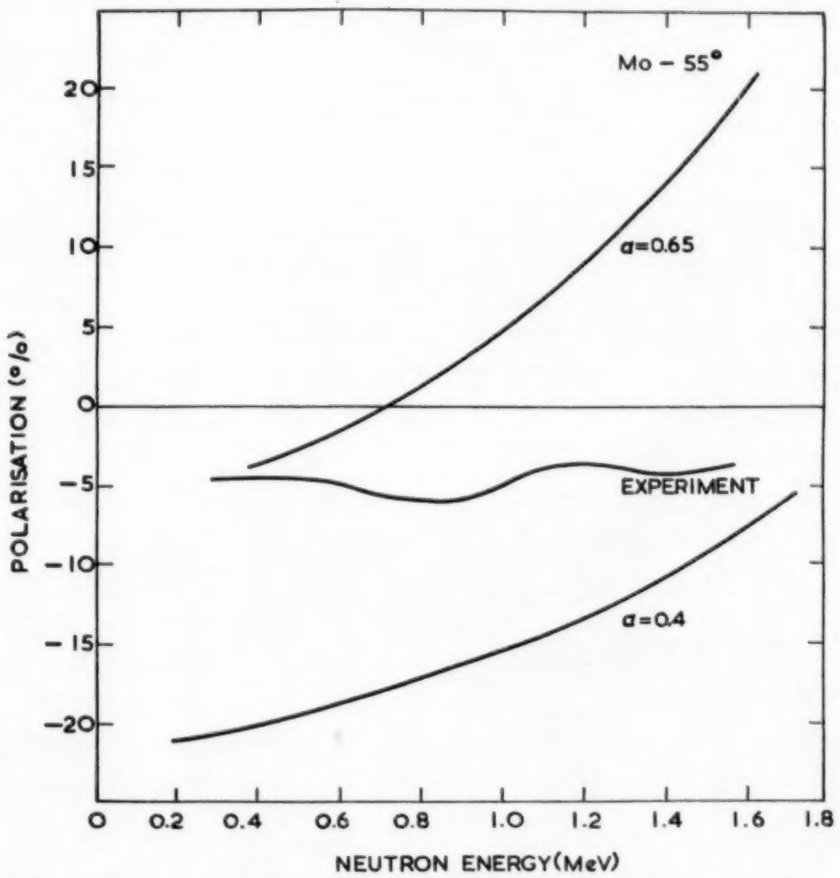

Fig. 6. Comparison of observed polarization in scattering from molybdenum at 55° with the predictions of an optical model.

Note added in proof: Several of the measurements reported above have now been further checked for spurious effects by using a magnetic field transverse to the initial neutron path to invert the incident neutron polarisation and comparing field on to field off asymetries. The results obtained are quite consistent with those presented here.

References

1) R. K. Adair, S. E. Darden and R. E. Fields, Phys. Rev. **96** (1954) 503
2) H. B. Willard, J. K. Bair and J. D. Kington, Phys. Rev. **98** (1955) 669
3) A. Okazaki, Phys. Rev. **99** (1955) 55
4) B. M. McCormac, M. F. Steuer, C. D. Bond and F. L. Hereford, Phys. Rev. **104** (1958) 718
5) J. D. Clement, F. Boreli, S. E. Darden, W. Haberli and H. R. Striebel, Nuclear Physics **6** (1958) 179
6) F. Bjorklund, Proc. Int. Conf. Nuclear Optical model, Florida State University, 1959
7) D. Brown, A. T. G. Ferguson and R. E. White, Proc. Basel Conf. July 1960, Helv. Phys. Acta Suppl., to be published
8) S. M. Austin, Proc. Basel Conf. July 1960, Helv. Phys. Acta Suppl., to be published
9) J. A. Baicker and K. W. Jones, Nuclear Physics **17** (1960) 424
10) S. E. Darden, private communication
11) H. R. Striebel, S. E. Darden and W. Haberli, Nuclear Physics **6** (1958) 188
12) J. Blok and C. C. Jonker, Physica **18** (1952) 809
13) M. Walt and H. H. Barschall, Phys. Rev. **93** (1954) 1062

1.D.1:
1.E.3

Nuclear Physics **25** (1961) 611—623; © *North-Holland Publishing Co., Amsterdam*
Not to be reproduced by photoprint or microfilm without written permission from the publisher

MAGNETIC DIPOLE MOMENTS OF ODD-MASS NUCLEI IN THE SPHERICAL REGION

N. FREED and L. S. KISSLINGER

Department of Physics, Western Reserve University, Cleveland 6, Ohio †

Received 19 January, 1961

Abstract: The magnetic dipole moments of odd-mass nuclei are calculated and compared to the experimental data for nuclei with particles in the 28–126 shells, except for the deformed region of $150 \leqq A \leqq 190$. The wave functions upon which the calculation is based are admixtures of seniority-one wave functions produced by a pairing interaction and obtained by projecting eigenfunctions of the number operator out of Bardeen-type wave functions. Perturbation theory is used to compute the seniority-three admixtures produced by a delta-function residual interaction.

1. Introduction

The shell model of the nucleus with the coupling scheme of Mayer and Jensen predicts [1]) that the magnetic dipole moment of an odd-mass nucleus is the same as that of the odd particle moving in an effective single-particle potential. If the magnetic properties of a shell model particle are the same as those of a nucleon, the magnetic dipole moment of the nucleus is thereby given as the single-particle (Schmidt) value [2]), and depends only upon the type (i.e. proton or neutron), the orbital angular momentum, and the spin direction of the odd particle.

Although the observed values of the magnetic dipole moments do not agree quantitatively with this extreme single-particle model, there are several striking systematic features which have been found by comparing the Schmidt prediction with the experimental data [3]). For instance, one finds that the observed values for each j for the magnetic moments usually lie between the Schmidt values for spin parallel and antiparallel for the same j and are close to the Schmidt value for $P_{\frac{1}{2}}$ nuclei and for light nuclei with one particle outside of a double closed shell. In the spherical region, many of these features have been accounted for qualitatively in perturbation theory calculations. Starting with pure configurations, Blin-Stoyle [4]) and Arima and Horie [5]) have demonstrated that small admixtures of certain configurations can result in large changes in the calculated values for the magnetic moments, and in systematic

† Work supported in part by the Air Force Office of Scientific Research and by the National Science Foundation.

studies the latter authors have shown that the trends of the observed moments away from the Schmidt values are consistent with such calculations.

However, it is now believed that even in the spherical region the states are not represented very well as pure configurations of shell model particles. The residual interactions, which give rise to the even-odd-A mass difference and lead to the gap in the intrinsic spectra of even-mass nuclei as well as other effects, seem to give rise to much more complex wave functions. These effects are too strong to be calculated in perturbation theory. On the other hand, one expects that the ground and low excited states of odd-mass nuclei might often be well approximated by admixtures of configurations of pure seniority one. We shall refer to such states hereafter as seniority one states.

Until recently, the calculation of the wave functions for shell model particles interacting with a two-body force has been prohibitively complicated, except for special simple cases. But now one can calculate approximate wave functions for a particular two-body interaction, the pairing interaction, which has non-zero elements in two-particle states only when they are of zero angular momentum. It has been shown that this force can reproduce certain features characteristic of a short-range force [6]). The solutions, obtained by methods developed in the theory of superconductivity [7]), have been studied by Belyaev [8]) for the nuclear problem.

More recently, these methods have been applied to the calculation of the low energy properties of nuclei with one closed shell, i.e. either neutrons or protons, but not both, moving in single-particle levels whose energy and spin are taken from experiment [9]). For odd-mass nuclei, the solutions lowest in energy are seniority one states, with one such state for each of the single-particle levels used in the calculation. The theory seemed to be able to account semi-quantitatively for the spins and positions of the low-lying levels, as well as other properties.

Among the properties considered in ref. [9]) were the magnetic dipole moments of the odd-mass nuclei. Starting with the seniority one states, which have the single-particle values for the magnetic dipole moment, a perturbation theory calculation was carried out to find the contribution to the magnetic moment from the seniority three states. Although the results were promising, there are so few data for single closed shell nuclei that it was difficult to see if these seniority one wave functions were within perturbation theory of predicting the correct moments, for with these methods one only tries to do calculations which are approximately correct and it is important to carry out a systematic study of nuclear properties to find if the method is successful.

In the present work, the calculation of the magnetic dipole moments by these methods is extended to nuclei in which both neutrons and protons are in the levels outside of the closed shells. A large number of accurate measurements have been made so that one can obtain a better test of the validity of the

calculation. Both the long-range force and the pairing force between neutrons and protons are neglected, and only the simplest calculation is made to try to see to what extent pairing correlations might provide the essential mixture of pure seniority one configurations which are needed to predict the magnetic moments. The methods of ref. [9]) are briefly reviewed and the magnetic moments of the ground states are compared to the observed values for nuclei in which the extra core particles are in shells from 28 to 126 particles, except for the deformed region and for cases in which the ground state spin cannot be associated with one of the seniority one states.

2. Pairing Correlations

If we denote by $|jm\rangle$ the state of a single shell model particle outside of the closed shell, with angular momentum j and z-component m, a pure configuration of shell model particles is represented as

$$|j_1^{n_1}(J_1)j_2^{n_2}(J_2)\ldots jm\rangle,$$

which is the same notation as in ref. [5]). This is a configuration, with total angular momentum j, composed of n_1 particles in the j_1-level coupled to angular momentum J_1, etc. In the brief outline of the pairing force calculation which follows, we shall always be referring to odd-mass isotopes.

The Hamiltonian for shell model particles interacting with a pairing force is [using the number operator n_{jm}, which is 1 (0) if the (jm) particle is present (absent)]

$$H = \sum_{jm} \varepsilon_j n_{jm} - \tfrac{1}{2} \sum_{ns} G_{ns}, \tag{1}$$

where the ε_j are the single-particle energy levels and the second sum is over pairs of particles, and the two-particle matrix element of the pairing interaction G_{12} in the jm representation is

$$\langle j'_1 m'_1 j'_2 m'_2 | G | j_1 m_1 j_2 m_2 \rangle = \begin{cases} G(\delta_{j_1 j_2}\delta_{j'_1 j'_2}\delta_{m_1,-m_2}\delta_{m'_1,-m'_2} \\ 0 \end{cases}. \tag{2}$$

In (2) the top line applies to the case that both particles 1 and 2 are protons or neutrons, while the lower line applies to the neutron-proton case. This approximation is used because the protons and neutrons are filling different orbits beyond the 28 shell and thus the effect of the short-range force between them is diminished compared to the interaction between identical particles.

The single-particle levels which are used in the present work are the same which were used in ref. [9]), and the strength G of the pairing force parameter has been chosen to be $23/A$ for both the protons and the neutrons. No attempt has been made to try to find more nearly correct single-particle energy levels or to adjust the strength of the pairing force for a best fit of the data.

The wave functions which are approximate eigenfunctions of the Hamilto-

nian (1) are obtained by the method described in refs. [6, 8, 9]). Since the neutron-proton pairing force has not been included, and the other components of the residual force have been neglected, the neutron and proton parts of the wave function can be obtained independently, one with an even number and the other with an odd number of particles. For a state of angular momentum j, one may write $\Psi_j = \Psi^{(e)}\Psi_j^{(o)}$, and the wave function of the even group is given by

$$\Psi^{(e)} = \mathscr{A}\prod_{j'm'}(U_{j'}\phi_0 + V_{j'}\phi(j', m', j', -m')) \tag{3}$$

where $\mathscr{A}$ is the antisymmetrization operator, and that of the odd group is given by

$$\Psi_j^{(o)} = \mathscr{A}\prod_{j'm'\neq jm}(U_{j'}\phi_0 + V_{j'}\phi(j', m'; j', -m'))|jm\rangle. \tag{4}$$

In eqs. (3) and (4), ϕ_0 is the state with no particles, $\phi(j', m'; j', -m')$ is the state with two particles in the j'-level with z-components m' and $-m'$ and the U and V coefficients are obtained from a variational calculation or its equivalent and have the physical interpretation that $V_j^2(U_j^2)$ is the probability of a j-level being occupied (unoccupied). These quantities are determined from the equations

$$V_j^2 = \tfrac{1}{2}\left[1 - \frac{\varepsilon_j - \lambda}{\sqrt{(\varepsilon_j-\lambda)^2 + \Delta^2}}\right], \quad U_j^2 = 1 - V_j^2, \tag{5}$$

in which the quantity λ has the physical interpretation of the Fermi energy for the particles spread over the levels being filled and Δ is approximately one-half the gap in the intrinsic states of even-mass nuclei or the even-odd-A mass difference.

One can see that the wave functions $\Psi^{(e)}$ and $\Psi_j^{(o)}$ are extremely complicated linear combinations of pure shell model configurations. Since the number of particles is not conserved, configurations from isotopes other than the correct one are present. However, the average number of particles is the correct value for the even group and is approximately correct for the low-lying states in the odd group. These solutions seem to be quite accurate in explaining the energy systematics of the even and odd groups separately[9]); and, in the same way, one expects from the fact that the magnetic moments as well as other nuclear properties seem to change gradually from isotope to isotope that this spread in the number of particles might not be a serious one.

In the present calculation we do not use these wave-functions, but the wave-functions which are obtained from them by projecting out the correct number of particles. In this way we use wave functions which are eigenstates of the number of particles. The pairing correlations are thus included by taking the same mixture of pure shell model configurations as is given by this approximate

solution with pairing forces included for the proper mean number of particles. The wave functions which we obtain by this procedure, $\Phi_j = \Phi^{(e)}\Phi_j^{(o)}$, are of the form

$$\Phi_j^{(e)} = \sum_{n_1+n_2+\ldots=n_e} a^{(e)}_{n_1 n_2\ldots}|j_1^{n_1}(0)j_2^{n_2}(0)\ldots\rangle \tag{6}$$

for the even group, and for the odd group

$$\Phi^{(o)} = \sum_{n_1+n_2+\ldots+p=n_o} a^{(o)}_{n_1 n_2\ldots p}|j_1^{n_1}(0)j_2^{n_2}(0)\ldots j^p(j)jm\rangle, \tag{7}$$

in which n_e and n_o stand for the total number of particles in the even and odd group, respectively. One can easily see that for a properly normalized wave function the coefficients are given by

$$|a^{(e)}_{\ldots n_i\ldots}|^2 = \frac{1}{\sum_l |a_l^{(e)}|^2}\prod_i U_i^{2j_i+1-n_i}V_i^{n_i}(j_i+\tfrac{1}{2})^{\frac{1}{2}n_i}/[(\tfrac{1}{2}n_i)!]^2, \tag{8}$$

and

$$|a^{(o)}_{\ldots n_i\ldots p}|^2 = \frac{1}{\sum|a_l^{(o)}|^2}\Big[\prod_{>i} U_i^{2j_i+1-n_i}V_i^{n_i}(j_i+\tfrac{1}{2})^{\frac{1}{2}n_i}/[(\tfrac{1}{2}n_i)!]^2 \times U_j^{2j-p}V_j^{p-1}(j+\tfrac{1}{2})^{\frac{1}{2}(p-1)}/[(\tfrac{1}{2}(p-1))!]^2, \tag{9}$$

in which the index i runs over all the levels which contain an even number of particles and l runs over all the levels.

3. Perturbation Theory for the Magnetic Dipole Moments

Since each of the component configurations of the wave functions Φ_j with the form of eqs. (6) and (7) give the single-particle value for the magnetic moment, the magnetic dipole moments for these states are just the single-particle values

$$\mu_{s.p.} = j\left[g_l \pm \frac{1}{2l+1}(g_s - g_l)\right], \quad j = l \pm \tfrac{1}{2}, \tag{10}$$

with $g_l = 1(0)$ and $g_s = 5.585\ (-3.826)$ for protons (neutrons). The reason for this result is that the wave functions which result from the pairing force used in this work only contain configurations of seniority one, i.e. all the particles are coupled two by two to angular momentum zero except one odd particle which must be in the j-level and thus each configuration gives the same [single-particle] value for this moment.

This particular two-body interaction has been used because of the feasibility of finding approximate eigenfunctions, and because it seems to represent many important characteristics of what is believed to be the actual residual interaction. However, one expects that a more realistic interaction will differ from this

pairing force to some extent, and in particular will not completely exclude the mixing of the higher seniorities in the ground and low excited states. For instance, a force which has the spatial dependence of a delta function can admix states of seniority three to the seniority one ground state when the particles are in several different j-levels, although this is not true for a single j-level. These admixtures are generally small, so that one might hope to calculate them in perturbation theory.

In principle, this means that one uses the wave functions with the pairing correlations included by admixtures of seniority one configurations as a basis, and finds the admixture of seniority three states by perturbation theory, using the difference between the pairing force and a more realistic interaction as the perturbation. In practice, if the form of eqs. (6) and (7) is used for the wave function and a delta force is used to approximate the residual two-body interaction, the determination of the magnetic dipole moments becomes simply the summing of the contributions of the different configurations as determined by the methods of refs. [4]) and [5]) weighted by the coefficients which are obtained from the pairing force calculation †. Although somewhat tedious, the calculation is straight-forward.

The contributions to the magnetic moments from the individual configurations have been derived by Arima and Horie [5]). We use, with them, a two-body interaction.

$$v_{ij} = \tfrac{1}{8}(11 + \boldsymbol{\sigma}_i \cdot \boldsymbol{\sigma}_j) V_s \delta(\mathbf{r}_{ij}),$$

where V_s is the singlet force strength. The only seniority three admixtures which contribute are those which involve transfer of particles between two levels of a spin-orbit doublet. First let us consider the even group.

Each j-level is a member of a spin-orbit doublet characterized by the orbital angular momentum l_i. Calling $l_i \pm \frac{1}{2} = j_i^{\pm}$, the contribution to the magnetic moment of the state of angular momentum j (and orbital angular momentum l) due to the even group is

$$\mu^{(e)} = \sum_c |a_c^{(e)}|^2 \delta\mu_c^{(e)}, \tag{11}$$

in which the index c runs over all contributing configurations and

$$\delta\mu_c^{(e)} = -\left[1 + (-1)^{l+\frac{1}{2}-j}\left(\tfrac{1}{2}(2j+1)\right)\right] \frac{(g_s - g_l)_e}{2j+2} \times \sum_i n_i^{+} \left(\frac{2l_i - n_i^{-}}{2l_i}\right) \frac{l_i}{2l_i+1} \frac{V_s I(n_i l_i^2 nl^2)}{4\Delta E_i} \tag{12}$$

† In a private communication to the authors, Dr. B. Mottelson has pointed out that this procedure is not quite the simple perturbation procedure that it seems to be. The particles which are excited by the perturbation-force in turn act on the unexcited particles; and, because of the exchange nature of the force, this enhancement appears to be a large effect. The result, however, is essentially just a renormalization of the effective strength of the perturbation by something like a factor of two.

is the contribution to the magnetic moment from a configuration of the even group. In eq. (12), n_i^+ and n_i^- stand for the number of particles in the levels j_i^+ and j_i^-, respectively, and $(g_s-g_l)_e$ indicates that the g-factors take the value corresponding to the type of particle in the even group. The radial integral is

$$I(n_i l_i^2 nl^2) = \tfrac{1}{2}\int R_{n_i l_i}^2 R_{nl}^2 r^2 \mathrm{d}r,$$

and ΔE_i is the energy needed to excite a particle from the j_i^+ to the j_i^- level.

The contribution from the odd group is

$$\mu^{(o)} = \mu_{s.p.} + \sum_c |a_c^{(o)}|^2 \delta\mu_c^{(o)}, \tag{13}$$

with

$$\begin{aligned}\delta\mu_c^{(o)} = &-[1+(-1)^{l+\frac{1}{2}-j}(\tfrac{1}{2}(2j+1))]\,\frac{(g_s-g_l)_o}{2j+2} \\ &\times \sum_i \frac{n_i^a(2j_i^b+1-n_i^b)}{(2j_i^a+1)(2j_i^b+1)}\,\frac{2l_i(l_i+1)}{2l_i+1}\left(-\frac{V_s I(n_i l_i^2 nl^2)}{\Delta E_i}\right).\end{aligned} \tag{14}$$

The notation in eq. (14) is the same as eq. (12), except for the quantities with the superscripts a and b. For $l_i \neq l$, $n^a = n^+$, $n^b = n^-$, $j^a = j^+$ and $j^b = j^-$, the case when the excitation occurs in a doublet with an even number of particles. For $l_i = l$ (i.e. in the case that the excitation occurs in the doublet which contains the level j with its odd number of particles p), if the odd particle is in the level $j = l-\frac{1}{2}$ the quantities in eq. (14) are to be taken as $n^a = n^+$, $j^a = j^+ = l+\frac{1}{2}$, $n^b = p-1$, and $j^b = j-1$; and if the odd particle is in the level $j = l+\frac{1}{2}$ these quantities are $n^a = p-1$, $n^b = n^-$, $j^a = j-1$, and $j^b = j^- = l-\frac{1}{2}$.

The quantity $V_s I$ is closely related to the strength of the pairing force, except for the renormalization (see footnote above) and is expected to be roughly inversely proportional to A, although there will be shell effects. The energy denominators are composed of two parts, the single-particle spin-orbit splitting plus the energy needed to break one pair of particles coupled to spin zero. Although the latter quantity depends to some extent upon the particular states in which the excitation is taking place, it is approximately the gap in the even-mass intrinsic spectra. In most cases, neglecting the dependence of this energy upon the states is an error of the same magnitude as neglecting the dependence of Δ on j which is done in this calculation. In this work we use a semi-empirical fit for the spin-orbit splitting and take for the energy denominators

$$\Delta E_i = 7(2l_i+1)A^{-\frac{2}{3}} + E_p, \tag{15}$$

where E_p, the energy to break a pair, is taken from ref. [9]) for each isotope.

In this work the radial matrix elements $I(n_i l_i^2 nl^2)$ have been chosen to have a smooth dependence on A. Calculations have been carried out with both harmonic oscillator and square-well wave functions to estimate how large an error

this introduces. We conclude that to the accuracy of our approximations one cannot obtain clear systematic improvements, and that there are more important corrections which must be carried out first.

Finally, when one of the levels of a doublet which contributes to the magnetic dipole moment lies in the major shell above or below the one which is being filled, the number of particles in that level is taken as empty or filled, respectively.

4. Results and Conclusions

The magnetic moment of the ground states of the odd-mass nuclei, calculated by the method described in the previous section for the quantity $V_s I$, the product of the singlet force strength and the radial integral, inversely proportional to A, are given in figs. 1 and 2. Many of the qualitative conclusions about the effect of individual particle conviguration mixing which have been reached on the basis of the study of pure configurations remain unchanged [10]). In the first place, if $j = l - \frac{1}{2}$ and the odd group is composed of protons, or if $j = l + \frac{1}{2}$ and the odd group consists of neutrons, the situations in which $\mu_{s.p.}$ is the smaller of the Schmidt values, each contribution in eqs. (12) and (13) is positive; and, conversely, for odd protons and $j = l + \frac{1}{2}$ or odd neutrons and $j = l - \frac{1}{2}$, each seniority three contribution is negative. Thus the magnetic moment always lies between the Schmidt values for these types of admixtures. Also, for a $p_{\frac{1}{2}}$ state the seniority three contributions are all zero, which is consistent with the experimental indication that in the spherical regions the magnetic dipole moments of the $p_{\frac{1}{2}}$ nuclei are approximately the single-particle values.

From figs. 1 and 2, it is obvious that for the quantity $V_s I = \text{const}/A$, the choice of the constant which enables one to fit the data on the average for the ligher nuclei leads to deviations from the single-particle value which are too large for heavier nuclei. Thus a somewhat stronger variation of this quantity than $1/A$ seems to be indicated. For instance, figs. 1 and 2 show that for both the protons and neutrons a choice of $V_s I \propto A^{-\frac{4}{3}}$ gives a better systematic fit to the data than $V_s I \propto A^{-1}$. Such a result has not been obtained for the calculations with a pairing force, where a $1/A$ dependence is not inconsistent with the various data [9]). Even if this conclusion is unchanged by more accurate calculations, it does not necessarily mean that the force strength actually has this A dependence, but could reflect the difference in the spin polarization for the heavy elements compared to the light ones (see footnote above). With respect to this, one might note that the magnitude of the interaction needed, $V_s I \approx 60/A$, is something like twice the value which has been used for the strength of the pairing force.

In this work there has been no attempt to choose the single-particle energy levels or the strength of the pairing force to try to obtain the best fits for the

Fig. 1. Magnetic dipole moments of odd-neutron nuclei in the spherical region. The theoretical results are obtained for the pairing force strength G of $23/A$ MeV, using the single-particle levels of ref. [9]). The dashed curve is the theoretical result for $-V_s I$ (see text) $= 60A^{-1}$ MeV, while the solid curve gives the results for $-V_s I = 275A^{-\frac{5}{3}}$ MeV. The isotopes Os^{187} and Os^{189}, which are at the end of the $150 \leqq A \leqq 190$ deformed region, have been included for comparison. All results are in nuclear magnetons, and the single-particle values are given for each isotope with the (l_j) labels to the right.

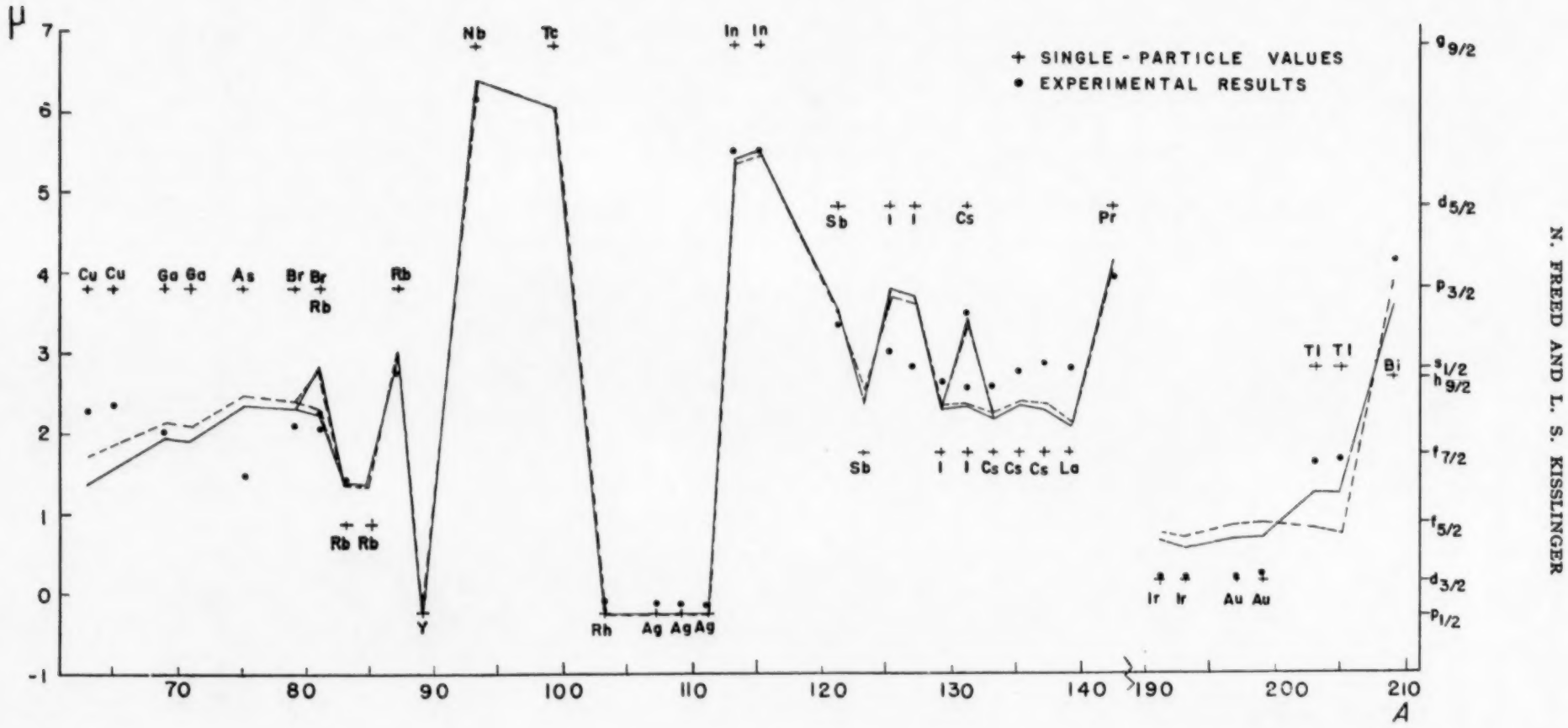

Fig. 2. Magnetic dipole moments of odd-proton nuclei in the spherical region. The notation is the same as in fig. 1. In the two cases of isobars which occur, Br^{81}–Rb^{81} and Cs^{131}–I^{131}, the larger experimental and theoretical values are for Br^{81} and Cs^{131}, respectively.

magnetic dipole moments or for any other nuclear data, except that the results are not inconsistent with the single closed shell information. In spite of this, it is interesting to note that in some regions the theoretical results follow the trends of the deviations of the observed moments away from the single-particle values quite well. The most striking systematic example of this is the degree to which this trend is fit for Pd^{105}, Cd^{111}, Cd^{113}, Sn^{115}, Sn^{117}, Sn^{119}, Te^{123}, Te^{125}, Nd^{143}, Nd^{145}, Sm^{147} and Sm^{149}, and to a lesser extent the other odd-neutron nuclei with $j = +\frac{1}{2}$ for $83 \leqq A \leqq 150$, nuclei which all display large deviations from the single-particle value.

The isotope Bi^{209} is an especially interesting case. Since the shell model prediction for this isotope is a single $h_{\frac{9}{2}}$ proton outside of the closed shell, the effect of both the pairing force and the long range force are small, and the only obvious source of the deviation from the Schmidt value is the seniority three contribution. The zero-th order wave function is essentially a single $h_{\frac{9}{2}}$ proton plus filled $h_{\frac{11}{2}}$ level in the closed proton shells and a closed $i_{\frac{13}{2}}$ level with an empty $i_{\frac{11}{2}}$ level for the neutrons, all the other spin-orbit doublets being either both filled or both empty, so that they give no contribution. The calculation thus reduces to the previous one [5, 10]) with the same result that a large deviation from the single-particle value, of the order of the observed one, is clearly predicted.

It is of particular interest to notice the situations in which the observations seem to be in disagreement with the theory. For the odd-neutron nuclei, the three isotopes Xe^{131}, Ba^{135} and Ba^{137} are found to have the opposite trend in the theoretical result compared to the observed values, a circumstance which precludes fitting all three by simply changing the strength of the perturbation. Of course, the difference between these three experimental values is so small that the theoretical moments in all three cases are still in reasonable agreement, and a better choice of single particle-levels and a better treatment of the energy denominators might change the relative magnitudes sufficiently to alter the trend. In general, these methods do not tend to give large differences in the moments of successive isotopes of the same element, so that such a rapid change, say as in Ga^{69} and Ga^{71}, suggests the influence of effects other than those considered in this work.

The Os^{187} result is especially interesting in that this isotope, with spin $\frac{1}{2}$ and odd parity, displays a large deviation from the $P_{\frac{1}{2}}$ single-particle value of 0.64, a result which can never be obtained by the methods used in this work, as has been discussed above. This discrepancy and that of Os^{189} correspond to the entry into the deformed region and apparently reflect the effects of collective motions, which have been completely disregarded in this work.

In the odd-proton nuclei, there seems to be a discrepancy for the I and Cs isotopes, in which cases there do not result sufficiently large contributions from the seniority three admixtures, although a more nearly accurate calculation

might show that the discrepancy does not escit. The nearby even isotopes do show rather low vibrational levels, so that collective surface contributions to the magnetic dipole moments could be playing an important role.

The large difference in the experimental value of As^{75} when compared to the other $p_{\frac{3}{2}}$ nuclei, a result which seems hard to explain by the methods used in this work, suggests once more the possibility of collective effects. The fact that there are quite low-lying vibrational levels in the Ge and Se even-mass isotopes, and that a $\frac{7}{2}^+$ level is found to be low-lying and even the ground state in isotopes in this region, when no such single-particle level is being filled, also suggests the influence of the collective motions. That is, other components of the residual interaction, in addition to the short range ones, seem to be important.

It should be noted that although the results quoted in this work have been limited to the magnetic dipole moments of ground states, the methods used are also applicable to excited states; and one would expect that the calculated values of the moments of the low excited states of odd-mass nuclei would, in most cases, be as accurate as those of the ground states. While at the present time there are few data on the moments of excited states, many such measurements might be performed in the near future. As an example, using parameters which give the correct value for the $S_{\frac{1}{2}}$ ground state, our calculations for the 279 keV $d_{\frac{3}{2}}$ state in Tl^{203}, the magnetic moment of which is presently being measured [11]), yield $\mu = 0.47$ n.m.

In conclusion, the changes in the magnetic dipole moments which result from the seniority three admixtures, calculated in perturbation theory using wave functions which contain pairing correlations, seem to account for the major systematic deviations from the single-particle values in the spherical region. In some regions, the influence of collective motions is suggested.

The authors would like to acknowledge helpful discussions with Drs. A. Arima and B. Mottelson. They would also like to acknowledge the computing assistance of Mrs. M. Ratner and the cooperation of the Case Institute of Technology Computing Center for making time available on their computers.

References

1) M. G. Mayer, Phys. Rev. **75** (1949) 1969; **78** (1950) 16;
Haxel, Jensen and Suess, Phys. Rev. **75** (1949) 1766;
Haxel, Jensen and Suess, Z. Phys. **128** (1950) 295
2) T. Schmidt, Z. Phys. **106** (1937) 358;
A. Schüler, Z. Phys. **107** (1937) 12
3) R. J. Blin-Stoyle, Rev. Mod. Phys. **28** (1956) 75
4) R. J. Blin-Stoyle, Proc. Phys. Soc. **66** (1953) 1158;
R. J. Blin-Stoyle and M. A. Perks, Proc. Phys. Soc. **67** (1954) 885
5) A. Arima and H. Horie, Prog. Theor. Phys. **11** (1954) 509

6) B. R. Mottelson, Notes from Cours de l'École d'Été de Physique Théorique des Houches (Dunod, Paris, 1958) p. 283;
A. Bohr and B. R. Mottelson (to be published)
7) Bardeen, Cooper and Schrieffer, Phys. Rev. **108** (1957) 1175;
N. N. Bogolubov, JETP (USSR) **34** (1958) 58, **73**; Nuovo Cim. **7** (1958) 794;
J. G. Valatin, Nuovo Cim. **7** (1958) 843
8) S. T. Belyaev, Mat. Fys. Medd. Dan. Vid. Selsk. **31**, No. 11 (1959)
9) L. S. Kisslinger and R. A. Sorensen, Mat. Fys. Medd. Dan. Vid. Selsk. **32**, No. 9 (1960)
10) H. Noya, A. Arima and H. Horie, Prog. Theor. Phys. Supp. **8** (1958) 33
11) B. Deutch (private communication)

1.D.2

Nuclear Physics **25** (1961) 624—633; © *North-Holland Publishing Co., Amsterdam*

Not to be reproduced by photoprint or microfilm without written permission from the publisher

ON THE PREPONDERANCE OF PROLATE DEFORMATIONS IN NUCLEI

RICHARD H. LEMMER and VICTOR F. WEISSKOPF

Department of Physics and Laboratory for Nuclear Science, Massachusetts Institute of Technology, Cambridge, Massachusetts †

Received 30 January 1961

Abstract: An attempt is made to understand the preponderance of prolate nuclear deformations in terms of a simple Nilsson-type model for the deformed nucleus.

1. Introduction

The origin of the giant nuclear quadrupole moments many times the single particle value can be qualitatively explained in terms of the spheroidally deformed core model proposed by Rainwater [1]), which takes into account the the polarization of the nuclear "core", formed by the inner nucleons, due to the interaction of the more loosely bound nucleons with it. The charge distribution of the protons embedded in the core is consequently deformed and the core itself acquires an induced quadrupole moment. For large deformations the contribution of the core to the nuclear quadrupole moment can easily exceed the single proton contribution because of the large amount of charge involved. The large quadrupole moments turn out to be almost always positive, indicating that an elongated or cigar-shaped core is energetically preferred for a whole range of nuclei [2]).

The idea of Rainwater was later pursued in much greater detail by Nilsson [3]). He did not distinguish between the outer nucleons as the cause of the deformation and the core as the deformed sphere, but treated the entire nucleus as an assembly of independent particles moving in a deformed potential well. He then calculated the energy states which would be filled in this well and, by minimizing the total energy, he was able to obtain the deformation and other characteristic properties of the nucleus. He used as potential an anisotropic harmonic oscillator with a correction term to simulate a plausible one particle potential as seen by a single nucleon in a deformed nucleus. The Nilsson potential has been remarkably successful in describing a variety of ground

† This work is supported in part through AEC Contract AT(30—1)—2098, by funds provided by the U. S. Atomic Energy Commission, the Office of Naval Research and the Air Force Office of Scientific Research.

state properties of strongly deformed nuclei [4,5]). When the level scheme of this potential is used to calculate the total energy as a function of deformation, the predicted equilibrium deformations can be found as a function of mass number and are in excellent agreement with experiment both in magnitude and shape, i.e. the preponderance of prolate nuclear shapes is produced. One would like to understand more clearly why a simple Nilsson-type model is successful in this respect and what aspect of the potential makes the prolate deformations more stable.

2. Simple Oscillator Model

Let us first reconsider the simple model of A identical nucleons moving independently in an anisotropic oscillator potential with frequency parameters $\omega_x = \omega_y$, ω_z along the three axes. The total energy may be simply expressed [6]) † as

$$E(A, \delta) = \tfrac{3}{4}\sum_i \{(N^i + \tfrac{3}{2}) - \tfrac{1}{3}\delta(2n_3{}^i - n^i) + \tfrac{1}{9}\delta^2(N^i + \tfrac{3}{2})\}\hbar\omega_0. \tag{1}$$

Here the sum is taken over all particles, N^i is the total number of oscillation quanta of the particle i, $n_3{}^i$ and $n^i = N^i - n_3{}^i$ are the numbers of oscillation quanta along the z-axis and in the x-y plane of the i-th particle, and δ is the deformation parameter introduced by Nilsson [3]). One has the approximate relation $(\omega_x - \omega_z) \approx \delta\omega_0$ in terms of the average frequency ω_0.

The minimum value of $E(A, \delta)$ as a function of δ for a fixed number of particles defines the ground state of the deformed nucleus. From eq. (1) one finds a minimum energy at the deformation

$$\bar{\delta} = \tfrac{3}{2}\frac{\sum_i (2n_3{}^i - n^i)}{\sum_i (N^i + \frac{3}{2})}, \tag{2}$$

which is lower than the energy at zero deformation by the amount

$$E(A, 0) - E(A, \bar{\delta}) = \tfrac{1}{9}\bar{\delta}^2 E(A, 0). \tag{3}$$

The expression for $\bar{\delta}$ shows that only particles in unfilled shells can polarize the nuclear shape, since the sum $\sum_i (2n_3{}^i - n^i)$ is just the average of the quadrupole operator $q = (2z^2 - x^2 - y^2)$ which vanishes for a filled shell.

We now consider how the minimum value of the total energy of the deformed nucleus varies with A as the oscillator well is filled. Since the middle term in eq. (1) changes sign when the deformation goes from prolate to oblate, the order of levels in the deformed potential inverts and we get two expressions for

† Ref. [6]) is a comprehensive recent review.

$E(A, \delta)$ depending on the nuclear shape. We denote the corresponding values of the equilibrium deformation by $\bar{\delta}_p$ and $\bar{\delta}_o$ for the prolate and oblate shapes, respectively. Then according to eq. (3), the larger of the two possible values of $\bar{\delta}$ will give the ground state. Clearly, any change in level order is of no consequence to particles in filled shells.

Let us follow in some detail how the total energy behaves as the $N = 4$ shell fills. The significant quantity here is the difference between the energy minima of the two competing shapes,

$$D(A) = E(A, \bar{\delta}_o) - E(A, \bar{\delta}_p) = \tfrac{1}{9}(\bar{\delta}_p^2 - \bar{\delta}_o^2)E(A, 0). \quad (4)$$

The solid curve in fig. 1 shows how this difference varies with the number of particles in the shell. For comparison the equilibrium deformations for both

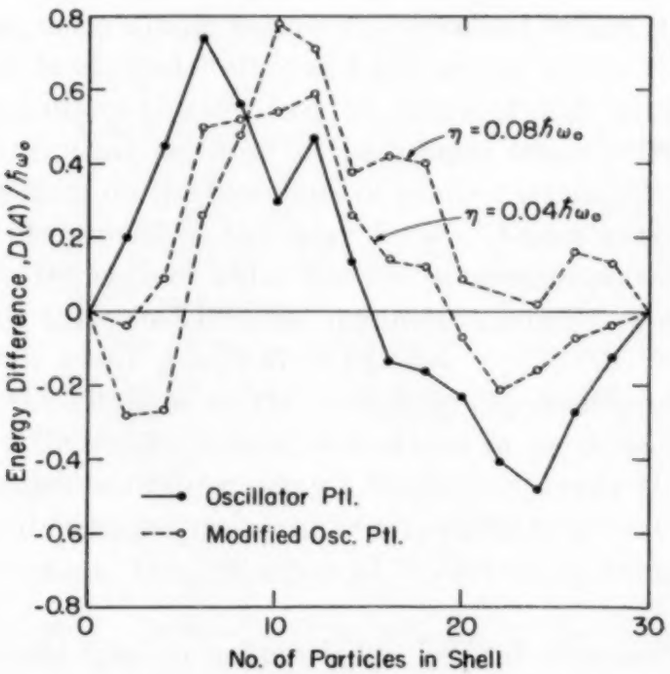

Fig. 1. Difference in minimum energy for prolate and oblate deformations as a function of the number of particles in the $N = 4$ shell. The solid curve is for the oscillator potential while the broken curves show the effect of steepening the oscillator walls.

shapes are listed in table 1. We have the usual result; prolate shapes ($\bar{\delta} > 0$) are favoured in the first half of the shell, oblate ones ($\bar{\delta} < 0$) in the second half [6]).

This sequence of preferred shapes may be understood by noting from eq. (3) that the particle configuration producing the largest deformation is always the stable one. Since $\bar{\delta}$ is proportional to the quadrupole moment of the particles in the unfilled shell, one gets the larger deformation for a prolate shape as the shell begins to fill because the quadrupole operator q weights the z-axis more than the x- or y-axes and is thus larger for particles in orbits with a

prolate-like ($n_3 > n$) density distribution. Likewise, removing particles in prolate-like orbits from a closed shell configuration will also produce the larger deformation, which means an oblate preferred shape just before shell closure.

Although one finds an equal number of stable prolate and oblate shapes for the simple oscillator model, this symmetry does not carry over to the values of the deformation. A glance at table 1 shows that particles in the first half of the shell produce a larger deformation of the nucleus than the same number of missing particles ("holes") in the second half, in spite of the fact that the quadrupole moments of the particles and holes are equal in magnitude.

TABLE 1

Values of the equilibrium deformations $\bar{\delta}_p$ or $\bar{\delta}_o$ for prolate or oblate deformations when the levels in $N = 4$ are filled consecutively with two particles per available space state.

Number of particles	$\bar{\delta}_p$	$\bar{\delta}_o$
0	0	0
2	0.14	−0.07
4	0.23	−0.14
6	0.29	−0.20
8	0.31	−0.25
10	0.32	−0.29
12	0.33	−0.29
14	0.30	−0.29
16	0.28	−0.29
18	0.25	−0.29
20	0.23	−0.25
22	0.18	−0.22
24	0.13	−0.19
26	0.10	−0.13
28	0.04	−0.08
30	0	0

This difference stems from the last term $\propto \delta^2$ in eq. (1) for the total energy, which is repulsive and tends to restore the system to a spherical shape. Since this restoring effect increases with mass number (the coefficient $\sum_i (N^i + \frac{3}{2})$ increases about as $A^{\frac{4}{3}}$), a nucleus with a few holes in the last shell becomes harder to deform than one with the same number of particles in the last shell. In turn, this means that the minimum energies for the competing prolate and oblate shapes lie closer for the holes than for the particles, and the relative stability of the oblate shapes in the second shell half is reduced accordingly. A representative case is illustrated in fig. 2 for 6 particles and 6 holes in $N = 4$. In this example, the energy difference favouring a prolate shape for the nucleus is nearly twice the difference which favours an oblate shape. One can then imagine the entirely possible situation that some perturbation of

the oscillator walls which opposes the formation of the normal stable shape of the oscillator could cause a cross-over of the oblate and prolate energy minima in the second half of a shell, but leave the more stable prolate shapes in the first half unchanged. This possibility suggests a means of understanding the greater stability of prolate deformations in non-spherical nuclei and is discussed in the following section with the aid of a specific example.

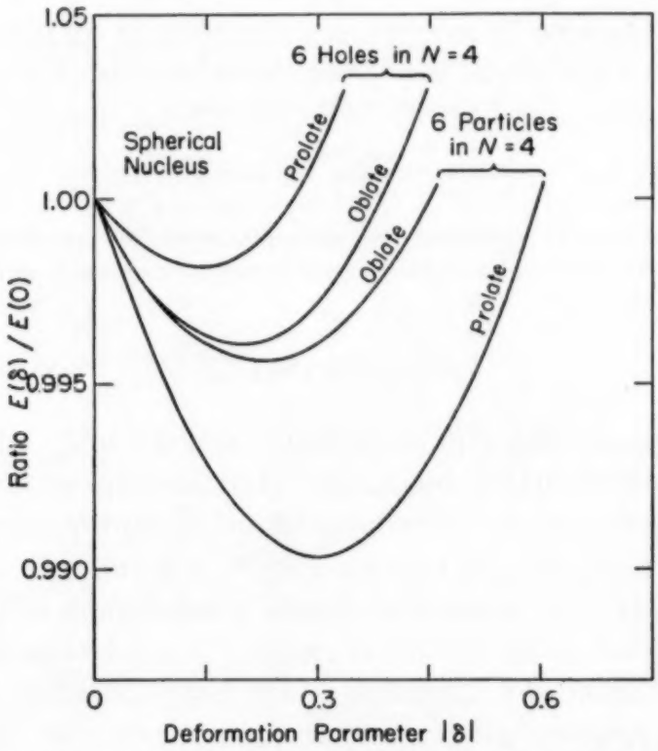

Fig. 2. Comparison of the total energy as a function of deformation for six particles and six holes in $N = 4$. The nuclear shape is indicated in each case.

3. Modified Oscillator Model

We turn next to the question of what happens when the extreme assumption of a pure oscillator potential is modified to simulate more nearly the actual situation in a deformed nucleus. This problem has been investigated in detail by Nilsson [3]), using a deformed oscillator potential with an additional interaction term $D\mathbf{l}^2 + C(\mathbf{l} \cdot \mathbf{s})$ depending on the particle's spin and orbital momenta to approximate the nuclear field. The constants C and D are then fixed by comparison with experiment. Both constants turn out to be negative, which means that the higher angular momentum states experience a stronger binding in the modified well and the resulting level order begins to resemble that of a square well potential.

Unfortunately, the Nilsson potential exhibits two features which make its interpretation difficult in terms of the line of reasoning we wish to take. First

s states are not affected contrary to what would happen if the oscillator walls were steepened to take on a more realistic shape approaching that of a square well potential since these states have the largest oscillation amplitude in the oscillator well and would thus respond strongly to changes in shape at the well surface. Secondly, when the potential itself is allowed to assume a strongly deformed shape, the angular momentum is no longer conserved and the meaning of a $\mathbf{l}^2$ interaction becomes obscured.

With these remarks in mind let us consider what happens when we steepen the walls of the oscillator potential by adding a term $H' = \eta r^4$ isotropically. Here $\mathbf{r}$ (measured in units of $a_0 \propto \omega_0^{-\frac{1}{2}}$) is the particle position vector and η some constant.

To see the effect of H', let us consider the perturbation of the isotropic oscillator levels first. Then the zero-order wave function separates in spherical coordinates with the usual quantum numbers (N, l, m) and the energy shift in first order is given by

$$\langle H' \rangle = \tfrac{1}{2}\eta\,[(N+\tfrac{3}{2})^2+\tfrac{3}{4}]-\tfrac{1}{2}\eta l\,(l+1). \tag{5}$$

Thus, the perturbation has the greatest effect when $l = 0$. This is because the s-state wave function has a large spatial extension and thus picks up the strong effect that r^4 has at large distances. As l increases the wave function contracts (classically, this means that the eccentricity of the particle orbit is decreasing) and the contribution from r^4 gets smaller. The "circular" orbit with $l = l_{\max} = N$ is thus shifted least in energy. Taking $\eta > 0$ we get a level sequence with low angular momentum states pushed up, i.e. the same *order* of levels as in the Nilsson potential where, by contrast, the high angular momenta are pushed down instead.

As the deformation is turned on in the oscillator part of the potential, the zero-order wave function goes over into a linear combination of angular momentum states and H' forms part of a non-diagonal energy matrix which must be diagonalized by numerical methods. However, in the limit of strong deformations a simple treatment ot the H' perturbation again becomes possible, if one works with the exact solutions of the anisotropic oscillator potential in cylindrical coordinates. Then the asymptotic quantum numbers (n_3, n, m) are appropriate, where n_3 and n have been defined previously, and m is the angular momentum component of the particle along the z-axis. For given n, the quantum number m can take on the values $-n, -(n-2), \ldots, (n-2), n$. In this scheme, the first-order energy shift due to H' is given by

$$\Delta E = \tfrac{1}{2}\eta[3(n+1)^2+3(n_3+\tfrac{1}{2})^2+4(n+1)(n_3+\tfrac{1}{2})+\tfrac{7}{4}]-\tfrac{1}{2}\eta m^2, \tag{6}$$

if one neglects a small additional contribution due to the difference in length unit in the z- and x- or y-dependence of the asymptotic wave functions. Eq. (6) is a rather good approximation as long as the energy separation of the

deformed oscillator levels is larger than the matrix elements of H' that couple these levels. Since H' has the selection rules $\Delta n_3 = \pm 2, \Delta n = \mp 2, \Delta m = 0$ in terms of the asymptotic quantum numbers, only levels differing by at least $2\hbar(\omega_x - \omega_z)$ are coupled by this perturbation. Taking $H'_c \approx \frac{1}{2}\eta n n_3$ as an order of magnitude estimate of these matrix elements, the coupling is unimportant when the ratio

$$\rho = \left| \frac{H'_c}{2\hbar(\omega_x - \omega_z)} \right| \approx \frac{n n_3}{4\delta} \frac{\eta}{\hbar\omega_0} \lesssim \frac{N^2}{16\delta} \frac{\eta}{\hbar\omega_0} \tag{7}$$

is small. If we assume $\eta \approx 2|D|$ and take Nilsson's value $D = -0.035\hbar\omega_0$, this will always be small at large deformations and not too large N. For example, levels in $N = 4$ have a coupling parameter $\rho = 0.35$ for deformations around $\delta = 0.2$.

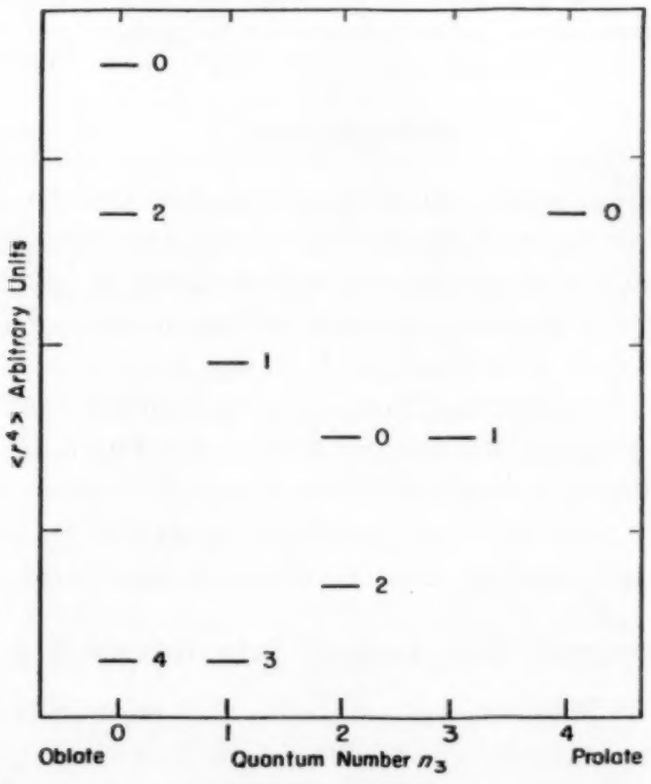

Fig. 3. Values of $\langle r^4 \rangle$ in the $N = 4$ oscillator shell displayed as a function of the quantum number n_3. The value of m is indicated next to each state.

The displacement ΔE shows an angular momentum dependence similar to eq. (5). States with $m = 0$ are again displaced more than states of higher m, because of the difference in spatial extension in their wave functions. In addition, for two states having the same value of m but with the values of n and n_3 interchanged, the oblate-like level with $n > n_3$ is displaced more. This effect is due to the extra boundary condition occurring at the origin for the part of the motion in the x-y plane, which introduces an additional node at

zero so that the particle density for the $n > n_3$ state is pushed further away from the centre of the potential. In particular the oblate state $n_3 = 0$, $n = N$ will experience both the smallest ($m = N$) and largest ($m = 0$) energy shift. Fig. 3 shows the range of values of $\langle r^4 \rangle$ in the $N = 4$ shell †.

To study the additive effect that the energy shift coming from H' has on the total energy of our system, we first "freeze" the nucleus at either of the equilibrium deformations given by the simple oscillator model and then turn on the perturbation. Proceeding in this manner the changes in equilibrium energy can be calculated and compared as before. We see from fig. 3 that as a shell begins to fill, a repulsive r^4-interaction will try to force the added particles into states with large m in order to keep their additional energy as small as possible. Hence, the first particle after a full shell will preferentially go into the oblate state $n_3 = 0$, $n = m = N$ rather than the alternative $n_3 = N$, $n = m = 0$, which is a linear oscillation along z producing a prolate shape. If on the other hand, we remove particles from a filled shell the first two levels involved are the zero angular momentum states $n_3 = N$, $n = m = 0$ and $n_3 = 0$, $n = N$, $m = 0$. Then fig. 3 shows that to have the largest reduction in r^4 we must also remove a particle from the oblate state $n_3 = 0$, $n = N$, $m = 0$. A hole in this state will cause the nucleus to assume a prolate shape. Thus, the additional perturbation favours an oblate shape at the beginning of a shell and a prolate shape as the shell closes in contrast with the oscillator part of the single particle potential. Denoting the additional energy difference coming from H' by

$$d(A) = \sum(\Delta E_{\text{oblate}}) - \sum(\Delta E_{\text{prolate}}), \tag{8}$$

the difference in total energies of the two competing shapes at equilibrium now becomes

$$D(A) = D_{\text{osc}}(A) + \tfrac{1}{2} d(A), \tag{9}$$

where $D_{\text{osc}}(A)$ is the energy difference for the unperturbed oscillator. The factor $\frac{1}{2}$ is included to get the correct contribution from ΔE which is supposed to be made up of two-body interactions only. Since the r^4 term is usually in competition with the oscillator potential as regards the preferred deformed shape, we get the broken curves shown in fig. 1 for the difference given by eq. (9). The extent to which the last term in eq. (9) modifies the energy difference curve of the simple oscillator depends of course on the value of the constant η. For small η, the energy difference $d(A)$ stays smaller than the energy difference $D_{\text{osc}}(A)$ for the pure oscillator and the preference for as many

† One realizes this effect best by comparing the states $m = 0$, $n_3 = N$, and $m = 0$, $n = N$. Both are states of highest ellipticity. The first one is stretched along the z-axis, the second one is stretched along some undetermined direction in the x–y plane. The latter state has the larger $\langle r^4 \rangle$ term. The reason can be expressed in the following form: The fact that the direction of motion is not as well determined in the second state, allows the fluctuations of the total angular momentum around the average value zero to be smaller; hence the motion is more linear and therefore reaches larger values of r.

prolate as oblate shapes is not affected. On the other hand for large η the difference $d(A)$ can dominate in eq. (9). Then oblate shapes will be preferred first, followed by prolate shapes in the latter half of the shell. However, the smaller relative stability of the oblate shapes of the pure oscillator in the second shell half makes it possible to switch over these minima in favour of a prolate shape with a value of η, which at the same time is not large enough to destroy the stability of the prolate shapes in the first half of the shell. From fig. 1, we see that a value $\eta \approx 0.08\hbar\omega_0$ would be sufficient to make a prolate shape preferred throughout most of $N = 4$. This is of the same order of magnitude as the change in potential found necessary in Nilsson's calculations to produce an acceptable level scheme [3]).

We have the result then that steepening the walls of the oscillator potential can "override" the normal tendency of the oscillator potential to deform into an oblate shape in the second half of a shell. If the extent of such an effect is proportional to the steepness $\partial V/\partial r$ of the potential walls, one would expect a maximum effect in the extreme case of a square well potential. Detailed calculations support this point. A study of particle motion in a spheroidally deformed infinite square well indicates that prolate deformations are usually more stable for this type of well [7]).

Finally, we mention additional refinements to the model like the Coulomb energy and spin-orbit interaction which have been ignored entirely in our crude estimate of the total energy. The suggestion has been made [8]) that the nuclear Coulomb energy may be partially responsible for the predominance of prolate shaped nuclei. However, this effect has been shown to be unimportant within the framework of a simple oscillator model for the nucleus [9]).

The need for some type of spin-orbit interaction in the shell model for spherical nuclei is well-known [10]). This means that for small deformations at any rate, the spin-orbit interaction will be the more important part of the single particle potential. For strong deformations, on the other hand, the rough estimate $\langle \mathbf{l} \cdot \mathbf{s} \rangle \approx l_z s_z = \frac{1}{2} m$ indicates that deformation and spin-orbit effects are about equally important in determining the deformed level scheme. However since an $\mathbf{l} \cdot \mathbf{s}$ type spin-orbit interaction splits each energy level symmetrically, the average spin-orbit energy contribution in the total energy is zero. Therefore one expects the qualitative trends indicated by a spinless model to remain unchanged although there can be differences in detail. For instance, changes in level order brought about by a spin-orbit interaction can in certain instances have a substantial effect on the magnitude of nuclear deformations. The sudden increase in deformation as one passes from neutron number $N = 88$ to $N = 90$ is attributed to an effect of this type [4]).

Finally, one notes that a restoring term $\propto \delta^2$ will be a common feature of any deformed potential well, so that the effect of the restoring force pointed out in this discussion is not restricted to the oscillator potential alone, but

should play a similarly important part in determining the equilibrium shape irrespective of the details of the assumed potential well.

References

1) J. Rainwater, Phys. Rev. **79** (1950) 432
2) C. H. Townes, H. M. Foley and W. Low, Phys. Rev. **76** (1949) 1415
3) S. G. Nilsson, Mat. Fys. Medd. Dan. Vid. Selsk. **29**, No. 16 (1955)
4) B. R. Mottelson and S. G. Nilsson, Mat. Fys. Skr. Dan. Vid. Selsk. **1**, No. 8 (1959)
5) B. R. Mottelson and S. G. Nilsson, Phys. Rev. **99** (1955) 1615
6) S. A. Moskowski, Handbuch der Physik (Springer-Verlag, Berlin, 1957) vol. XXXIX
7) S. A. Moskowski, Phys. Rev. **99** (1955) 803
8) S. A. Moskowski and C. H. Townes, Phys. Rev. **93** (1954) 306
9) K. Gottfried, Phys. Rev. **103** (1956) 1017
10) M. Goeppert-Mayer and J. H. D. Jensen, Elementary theory of nuclear shell Structure (John Wiley and Sons, New York, 1955)

1.D.2:
1.E.4:2.H

Nuclear Physics **25** (1961) 634—641; © *North-Holland Publishing Co., Amsterdam*
Not to be reproduced by photoprint or microfilm without written permission from the publisher

INELASTIC SCATTERING FROM HAFNIUM AND WOLFRAM ISOTOPES

O. HANSEN, M. C. OLESEN, O. SKILBREID and B. ELBEK
Institute for Theoretical Physics, University of Copenhagen, Denmark

Received 16 February 1961

Abstract: The reduced electric quadrupole transition probabilities and the excitation energies of the accessible low lying states in the stable isotopes of Hf and W (except the rare isotope W^{180}) have been measured by Coulomb excitation. The measurements were performed on inelastically scattered protons and deuterons recorded in a heavy particle spectrograph. The results are discussed in terms of the rotational model. The measured transition probabilities are compared with those derived from lifetime measurements.

1. Introduction

The work reported here is a continuation of earlier investigations into the Coulomb excitation cross sections for rotational levels in deformed nuclei [1–5]). The isotopes of Hf and W are located in a region of the periodic table where the deformation of the nuclear shape has started to decrease from the large values attained among the rare earth nuclei. It is interesting to follow the behaviour of the deformation and the nuclear moment of inertia for these nuclei in order to see whether the regularities observed in the rare earth region are still present [5]). Special attention is given to the nucleus of W^{183} where a Coriolis coupling between the rotational band built on the ground state and that built on the first intrinsic state gives rise to relatively strong transitions to higher states [6]).

2. Experimental Method and Targets

The experimental method and procedure are identical to those used in our earlier work. Targets were prepared in the isotope separator of this institute by means of a sputtering technique [5]). Some W^{183} targets were also made in the isotope separator by the de-acceleration method [3]) and by vacuum evaporation of WO_3 enriched to 86.2 % in W^{183}. The target thickness varied from 25 $\mu g/cm^2$ to 40 $\mu g/cm^2$. In all cases thin carbon foils were used as backings. When the de-acceleration method was used, the carbon foil was first covered by a 30 $\mu g/cm^2$ layer of evaporated aluminium to suppress heavy sputtering from the carbon.

3. Results

The values of the reduced electric quadrupole transition probability $B(E2)$

and the excitation energies of the nuclear levels are collected in table 1. The table also gives the more accurate excitation energies obtained by DuMond *et al.* [7, 8, 9]) with a bent crystal spectrometer. The deviations in the energy values are in all cases inside our experimental error. In the evaluations of the data we have used the more accurate energies, when available.

TABLE 1

Measured excitation energies and reduced electric quadrupole transition probabilities in the isotopes of Hafnium and Wolfram

Nucleus	E (keV)	E (keV)	$B(E2)/e^2$ (10^{-48} cm^4)	Q_0 (10^{-24} cm^2)	β	$\mathcal{I}/\mathcal{I}_{rig}$
Hf^{176}	89	88.35	5.27±0.25	7.29	0.282	0.410
Hf^{177}	112	112.91	1.92±0.10	6.74	0.261	0.484
	249		0.50±0.05			
Hf^{178}	94	93.14	4.66±0.25	6.85	0.265	0.383
Hf^{179}	123	122.66	1.76±0.10	6.85	0.263	0.528
	269		0.41±0.05			
Hf^{180}	92	93.29	4.35±0.20	6.61	0.254	0.377
W^{182}	100	100.07	4.00±0.20	6.34	0.236	0.347
W^{183}	46	46.48	1.52±0.07	6.37	0.236	0.440
	98	99.07	2.04±0.08			
	211	208.81	0.08±0.02			
	293	291.71	0.30±0.05			
W^{184}	112	111.13	3.62±0.20	6.04	0.224	0.308
W^{186}	124	122.48	3.57±0.25	5.99	0.220	0.275

Column 2 gives the energies determined in the present experiment. Column 3 shows the more accurate energies of the same states [7–9]). The $B(E2)$ values are determined in the present experiment and the errors are standard errors of the mean. The intrinsic quadrupole moments Q_0 and the deformation parameters β are derived from the transition probabilities to the first excited state by the formulae of the rotational theory as in refs. [4, 5]), whereas for W^{183} we have used the formulae of ref. [6]). The ratio $\mathcal{I}/\mathcal{I}_{rig}$ is obtained from the excitation energies of the first excited states.

The reduced transition probabilities are derived from the inelastic scattering cross sections, using the semi-classical theory of the Coulomb excitation process [10]). Under the present experimental conditions, the error [11]) introduced by using the semi-classical theory instead of the quantum theory is less than 1 %. The inelastic scattering cross sections were in the usual way obtained from the ratio of inelastic to elastic scattering by assuming the elastic scattering cross section to be given by the Rutherford cross section. A small correction from the transition from laboratory coordinates to centre-of-mass coordinates has been taken into account.

4. Discussion

In table 1 the values of the intrinsic quadrupole moment Q_0 as calculated from the reduced transition probability to the first excited state are given. Also the nuclear deformation parameter β obtained from the intrinsic quadru-

pole moment, and the nuclear moment of inertia $\mathscr{I}$ obtained from the excitation energies, are shown. The moment of inertia is given in units of the moment of inertia of a rigid spheroid with deformation β. The details of the evaluation of these parameters are as described earlier [4, 5]).

For the even nuclei, the discussion is quite similar to that given for the even nuclei in the region of the rare earths [5]). In fig. 1, which is an extended version of fig. 3 of ref. [5]), we have plotted the intrinsic quadrupole moment Q_0 against mass number. It is seen that the Q_0 for the even isotopes of Hf and W is a

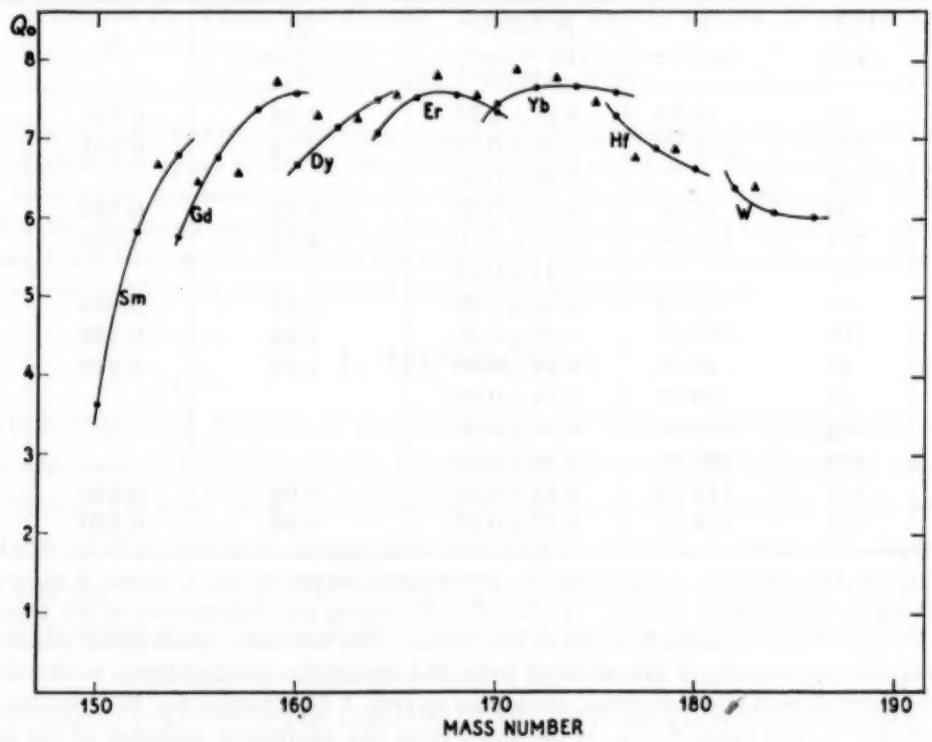

Fig. 1. Intrinsic quadrupole moments as a function of the mass number. The points marked with triangles correspond to odd isotopes, while the even isotopes are marked with dots.

smoothly decreasing function of the mass number reflecting a corresponding decrease in deformation. Unfortunately we have not yet been able to obtain a target of the rare isotope W^{180} (0.14 %), which would have given an overlap in mass number for the isotopes of Hf and W. The transition from 70 protons in Yb to 72 protons in Hf appears to give a decrease in deformation. This is in agreement with the behaviour of the Nilsson energy levels, which from the 71st proton are strongly increasing functions of the deformation, thus favouring smaller deformations [12]). The intrinsic quadrupole moments of the odd isotopes, also shown in fig. 1, fit fairly well in among those of the even isotopes.

The correlation between the moment of inertia and the nuclear deformation for the even nuclei is shown in fig. 2 which is an extended version of fig. 6 of ref. [5]). The new points lie approximately on the empirical straight line found to represent the results for the rare earth nuclei, although there is a tendency for

the points to move against smaller deformations. If a similar plot is made for the very heavy elements of mass numbers around 230, it is very clearly seen that these points follow a separate curve [5, 13]). Although there is no a priori reason for the relation between the moment of inertia and the deformation to be a unique one, independent of the nuclear structure and the mass number, it is worth remembering that the assumption of the nucleus being a homogeneously charged

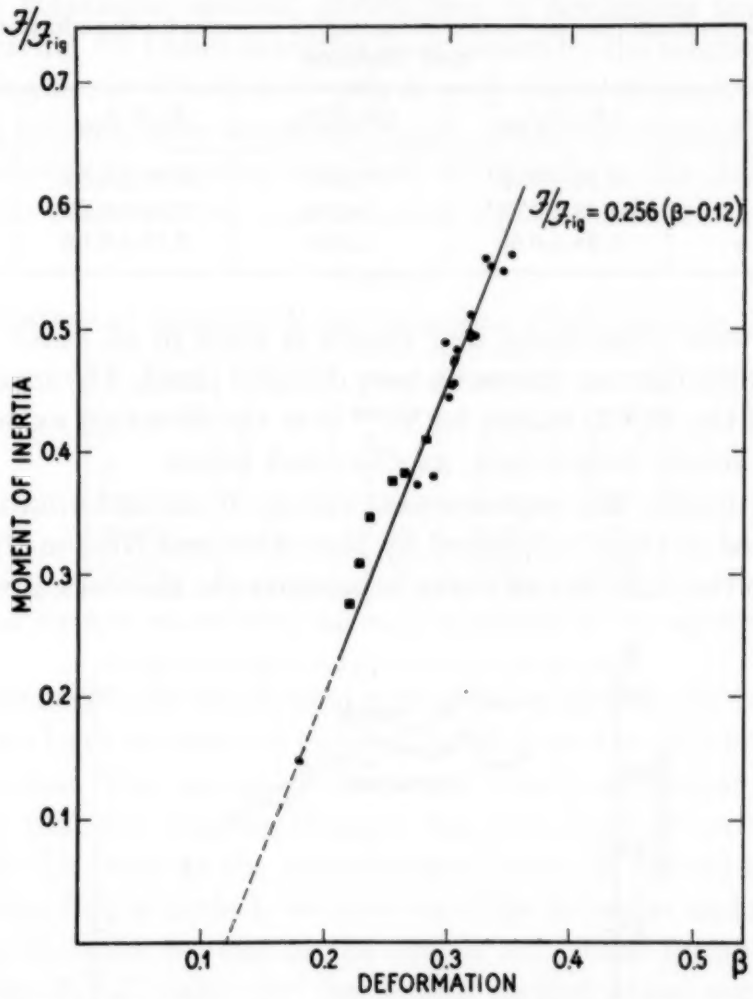

Fig. 2. Correlation between the moment of inertia and the nuclear deformation. The points for the isotopes of Hf and W are marked by squares.

spheroid, which underlies the evaluation of the deformation parameter β, is more or less arbitrary. A more exact evaluation of the deformation from the intrinsic quadrupole moment based on the particle structure of the nucleus has been attempted [14]). This calculation gives deformations which essentially bring the points for the lighter and the heavier nuclei together on a common curve [15]) when plotted as on fig. 1. However, another calculation of similar type but using somewhat different parameters yields deformations in close agreement with the uniform charge model [16]).

In the odd nuclei the two first members of the rotational band are populated.

According to the rotational theory, the ratio of the reduced E2-transition probabilities from the ground state to these two states should depend only on the ground state spin if the description in terms of a common intrinsic quadrupole moment is justified. Also the ratios of the excitation energies are given by the spin. The experimental and theoretical ratios are collected in table 2. The

TABLE 2

Ratios of transition probabilities and ratios of excitation energies for the odd isotopes of Hafnium and Wolfram

Nucleus	I_0	$(B_2/B_1)_{exp}$	$(B_2/B_1)_{th}$	$(E_2/E_1)_{exp}$	$E_2/E_1)_{th}$
Hf^{177}	$\frac{7}{2}$	0.26 ± 0.03	0.257	2.22 ± 0.05	2.22
Hf^{179}	$\frac{9}{2}$	0.23 ± 0.03	0.204	2.19 ± 0.05	2.18
W^{183}	$\frac{1}{2}$	1.34 ± 0.08	1.500	2.13 ± 0.06	

agreement between experiment and theory is good in all cases, although the experimental uncertainties prevent a very detailed check. The small discrepancy for the ratio of the B(E2) values for W^{183} is in the direction expected from the effect of the Coriolis interaction, as discussed below.

For the odd nuclei, the experimental values of the deformation parameter can be compared to those calculated by Mottelson and Nilsson [12]). This is done in fig. 3, where the fully drawn curve represents the theoretical values and the

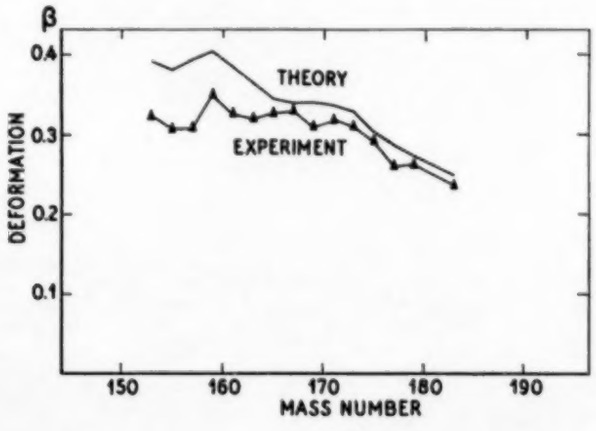

Fig. 3. Deformation parameter β for ellipsoidal shapes obtained from the measured Q_0-values. The solid line shows the β-values calculated by Mottelson and Nilsson.

triangles are the experimental results. In converting the values of the deformation parameter δ used by Mottelson and Nilsson to the parameter β used here, we have employed the relation

$$\delta+0.5\delta^2 = 0.946(1+0.16\beta),$$

which is correct to second order. The over-all agreement is reasonable, but it seems as if the theory somewhat over-estimated the deformation, especially for

the lighter nuclei. Application of the more refined methods [14]) mentioned above to the evaluation of the experimental deformations makes the agreement for the lighter nuclei even worse.

W^{183} is known to have a somewhat irregular rotational spectrum [6]). This is due partly to the fact that the ground state has the K-quantum number of the rotational theory equal to $\frac{1}{2}$, in which case there is a partial decoupling of the nucleon spin from the rotational motion, giving rise to deviations from the simple rotational spectrum [10]). Other deviations are caused by the rotational band built on the intrinsic state at 208.81 keV with $K = \frac{3}{2}$, which through a Coriolis force couples to the ground state rotational band. Under the present experimental conditions, the Coriolis coupling manifests itself only in the $B(E2)$ values. In table 3 we have collected the experimental $B(E2)$ values for the four states

TABLE 3

Comparison of experimental and theoretical $B(E2)$ values in W^{183}

E (keV)	46.5	99.1	208.8	291.7
I	$\frac{3}{2}$	$\frac{5}{2}$	$\frac{3}{2}$	$\frac{5}{2}$
K	$\frac{1}{2}$	$\frac{1}{2}$	$\frac{3}{2}$	$\frac{3}{2}$
$B(E2)_{th}$	1.52 [a])	2.14	0.09	0.30
$B(E2)_{exp}$	1.52	2.04	0.08	0.30
error		0.12	0.02	0.05

[a]) The $B(E2)_{th}$ for the first excited state has been normalized to the experimental value.

observed together with the theoretical estimates by Kerman [6]). In the theoretical estimates, we have normalised the $B(E2)$ value for the 46.5 keV state to the experimental value. The agreement between theory and experiment is very good. It is seen that the coupling changes the ratio B_2/B_1 from 1.50 to 1.41 in agreement with the trend of the experimental value. It should be noted that, in the evaluation of Q_0 in table 1, we have used the formulae and mixing amplitudes given by Kerman instead of the simple rotational formulae. With the exception of the $B(E2)$ value for the second excited state, our values agree within errors with those of Stelson and McGowan [17]). It should be stressed that, without the Coriolis coupling between the bands, the transition probabilities to the states in the higher band would have been smaller by one order of magnitude.

5. Comparison with Lifetimes

For several of the even nuclei in table 1, the lifetime of the first excited state has been determined by delayed coincidence techniques [18, 19, 20]) or by Coulomb excitation with pulsed proton beams [21]). From the measured lifetimes we have calculated the $B(E2)$ values, using the K- and L-conversion coefficients of Rose [22]). The total (M+N+ . . .)-conversion coefficient was taken as $\frac{1}{3}$ of the

total L-conversion coefficient. The $B(E2)$ values obtained in this manner are collected in table 4 together with our results for the same nuclei. In those cases in

TABLE 4

Transition probabilities derived from measured half-lives for E2 transitions in the even isotopes of Hf and W compared with transition probabilities for the same transitions determined from inelastic scattering cross sections

Nucleus	$\tau_{\frac{1}{2}}$	α	$B(E2)$	$B(E2)_{\text{i.sc.}}$	Refs. for $\tau_{\frac{1}{2}}$
Hf^{176}	1.35	5.80	5.70	5.27	[18])
Hf^{178}	1.87	4.66	3.80	4.66	[20, 21])
Hf^{180}	1.51	4.66	4.67	4.35	[19–21])
W^{182}	1.41	3.90	4.07	4.00	[19, 21])
W^{184}	1.33	2.63	3.43	3.62	[21])

$\tau_{\frac{1}{2}}$ is a simple average of the measurements of the half-lives in units of 10^{-9} sec. α is the total internal conversion coefficient from the tables of Rose [22]). The reduced transition probability from the lifetime and from the inelastic scattering measurements is in units of 10^{-48} cm$^4 \times e^2$.

which several measurements of the same lifetime have been made, a simple arithmetical mean has been used in the comparison. On the average, the transition probabilities obtainable from the lifetimes are only about 1 % lower than those from the inelastic scattering experiments, but this result may be unduly affected by the measured half-life of the first excited state in Hf^{178}, which appears somewhat high. It might be noted that the lifetime of the first excited state in Hf^{180}, which is based on three independent measurements and has a standard deviation of only 4 %, deviates a little from our value. Although the discrepancy is not outside the limits of error, it is interesting to observe that it goes in a direction consistent with a slight increase in the total conversion coefficient, as indicated by a direct measurement of the K- and L-conversion coefficients for this transition [23]).

In the odd nuclei, the first rotational state will decay to the ground state by mixed M1 and E2 radiation, and the lifetime will be shorter than in the even nuclei. Nevertheless, the lifetime of the first excited state in Hf^{179} has recently been determined [24]) to $(5.4 \pm 0.4) \times 10^{-11}$ sec. This measurement determines the combined M1+E2 transition rate, whereas our measurement gives the E2 transition probability alone. By using the theoretical M1 and E2 conversion coefficients, it is thus possible to obtain the mixing ratio δ^2, which gives the ratio of the number of E2 gammas to M1 gammas in the decay. The numerical value of δ^2 for the decay to the ground state of the first excited state in Hf^{179}, calculated from the above-mentioned lifetime and the value of $B(E2)$ from table 1, is 0.095 ± 0.010. This is somewhat lower than one would expect from the measured value of δ^2 for the cascade transition from the second excited state to the first excited state [25]) and the rotational theory, but not definitely outside the experimental errors. For Hf^{177}, only a lower limit $\tau_{\frac{1}{2}} \leqq 60 \times 10^{-11}$ sec is available [24]), which gives a mixing ratio $\delta^2 \leqq 3$.

We wish to thank Professor Niels Bohr for the excellent working conditions at his institute. We are grateful to Miss Jette Taulø, Miss Jette Laursen and Miss Jette Ewerløf for scanning the photographic plates. One of us (O. H.) is indebted to "Fru Lørups Mindelegat" for a grant.

References

1) B. Elbek, K. O. Nielsen and M. C. Olesen, Phys. Rev. **108** (1957) 406
2) V. Ramšak, M. C. Olesen and B. Elbek, Nuclear Physics **6** (1958) 451
3) B. Elbek, M. C. Olesen and O. Skilbreid, Nuclear Physics **10** (1959) 294
4) M. C. Olesen and B. Elbek, Nuclear Physics **15** (1960) 134
5) B. Elbek, M. C. Olesen and O. Skilbreid, Nuclear Physics **19** (1960) 523
6) A. K. Kerman, Mat. Fys. Medd. Dan. Vid. Selsk. **30**, No. 15 (1956)
7) E. L. Chupp, J. W. M. DuMond, F. J. Gordon, R. C. Jobson and Hans Mark, Phys. Rev. **112** (1958) 518
8) J. J. Murray, F. Boehm, P. Marmier and J. W. M. DuMond, Phys. Rev. **97** (1955) 1007
9) E. L. Chupp, A. F. Clark, J. W. M. DuMond, F. J. Gordon and Hans Mark, Phys. Rev. **107** (1957) 745
10) K. Alder, A. Bohr, T. Huus, B. R. Mottelson and A. Winther, Revs. Mod. Phys. **28** (1956) 432
11) J. Bang, Mat. Fys. Medd. Dan. Vid. Selsk. **32**, No. 5 (1960)
12) B. R. Mottelson and S. G. Nilsson, Mat. Fys. Skr. Dan. Vid. Selsk. **1** No. 8 (1959)
13) R. E. Bell, S. Bjørnholm and J. C. Severiens, Mat. Fys. Medd. Dan. Vid. Selsk. **32**, No. 12 (1960)
14) N. K. Glendenning and J. Sawicki, Nuclear Physics **18** (1960) 596
15) B. Elbek, Proc. Kingston Conf. (North-Holland Publishing Co., Amsterdam, 1960) 601
16) D. Bès and Z. L. Szymansky, private communication
17) P. H. Stelson and F. K. McGowan, Phys. Rev. **109** (1958) 901
18) F. K. McGowan, Phys. Rev. **87** (1952) 542
19) A. W. Sunyar, Phys. Rev. **98** (1955) 653
20) M. Deutsch, private communication
21) M. Birk, G. Goldring and Y. Wolfson, Phys. Rev. **116** (1959) 730
22) M. E. Rose, Internal conversion coefficients (North Holland Publishing Company, Amsterdam, 1958)
23) W. Farrel Edwards and F. Boehm, Proc. Kingston Conf. (North-Holland Publishing Co., Amsterdam, 1960) 598
24) A. E. Blaugrund, Y. Dar and G. Goldring, Proc. Kingston Conf. (North-Holland Publishing Co., Amsterdam, 1960) 590, and private communication
25) E. M. Bernstein and J. de Boer, Nuclear Physics **18** (1960) 40

2.E:2.L

Nuclear Physics **25** (1961) 642—655; © *North-Holland Publishing Co., Amsterdam*

Not to be reproduced by photoprint or microfilm without written permission from the publisher

PROTON SCATTERING FROM LIGHT ELEMENTS AT 142 MeV

A. E. TAYLOR and E. WOOD

Atomic Energy Research Establishment, Harwell, Berks.

Received 17 February 1961

Abstract: Measurements have been made of the elastic scattering and total cross-section of Be, C, N, O and Al for 142 MeV protons and the results have been compared with neutron measurements at about the same energy. A simple modification of the original optical model of Fernbach, Serber and Taylor [7]) has been found sufficient to explain the proton scattering results, especially in the region of the Coulomb-nuclear interference where the results are sensitive to the choice of the real part of the potential. The addition of spin dependent scattering amplitudes improves the fits to the cross-section data as well as giving fits to polarization measurements.

1. Introduction

Considerable success has been obtained in explaining high energy neutron cross sections by means of an optical model which regards the scattering of the neutron waves as taking place at a sphere of complex refractive index (Fernbach, Serber and Taylor [7]). With a simple choice of parameters, T. B. Taylor [14]) has been able to fit experimental neutron total cross sections in the range 50 to 400 MeV, absorption cross sections at 95 and 270 MeV and forward elastic scattering cross sections at 84 MeV.

It is of interest to compare the scattering of protons with that of neutrons and also to find to what extent the optical model can be used to fit the proton experimental results. Richardson, Ball, Leith and Moyer [13]) have measured the proton elastic scattering distribution at 340 MeV, and proton total cross sections have been measured at 208 and 315 MeV (de Carvalho [3])), 408 MeV (Marshall, Marshall and Nedzel [10])) and at 860 MeV (Chen, Leavitt and Shapiro [5])). Absorption cross section measurements have been made at 134 MeV by Cassels and Lawson [4]), 185, 240 and 305 MeV by Hecks and Kirshbaum [8]) and at 290 MeV by Millburn, Birnbaum, Crandall and Schector [11]). This paper reports measurements of the total cross section and elastic scattering distributions of 142 MeV protons scattered by Be, C, N, O and Al.

There are certain advantages in using protons since they are easier to detect, the incident beam is usually mono-energetic and inelastically scattered particles are more easily excluded. However, there is the complication of Coulomb scattering, which distorts the diffraction pattern at small angles where interference between the Coulomb and nuclear scattering is to be expected. For this reason

the measurements reported here have been restricted to light elements. For the same reason, proton total cross sections have to be measured in 'poor' geometry and extrapolated to 'good' geometry. Comparison with neutron total cross sections can be made only if the extent and magnitude of the Coulomb nuclear interference is known. This information was obtained by comparing the measured angular distribution of the elastically scattered protons with the predictions of the optical model, reasonably modified to take account of the Coulomb interaction.

Any difference between the nuclear parameters required to fit the proton angular distribution results and the parameters used in fitting the neutron cross sections provides a comparison of the scattering of neutrons with that of protons. In addition there is the direct comparison of the total cross sections.

The angular distribution measurements are described first as these results are needed to interpret the total cross-section measurements.

2. The Angular Distribution of Elastically Scattered Protons

2.1. EXPERIMENTAL METHOD

The unpolarized external proton beam of the Harwell synchrocyclotron was collimated to 1 cm diameter, at a point 9m from the target in the cyclotron, and the scatterers were set up a further 4m away behind a 2m thick concrete shielding wall (fig. 1). The trajectory of the beam was investigated with a small probe counter and the scattering table and counter telescope were aligned to better than $\frac{1}{10}°$. The beam was monitored by a carefully calibrated ionization

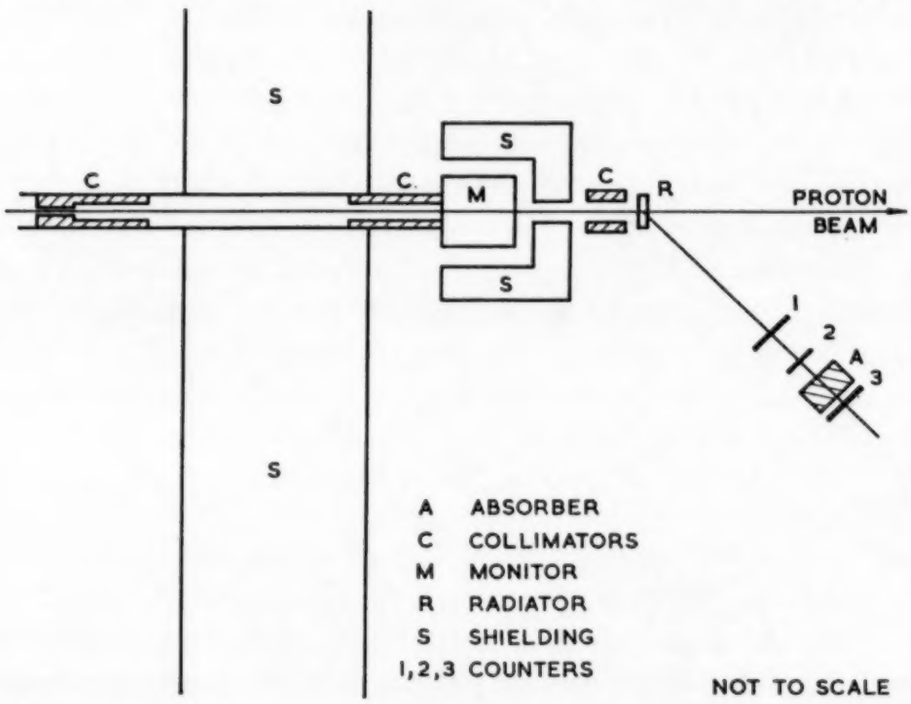

Fig. 1. Schematic diagram of angular distribution experimental layout.

chamber. Extra shielding around the monitor was provided to prevent protons scattered at the collimators and monitor from entering the counter telescope. Thin scatterers were placed above the pivot of the scattering table and the scattered protons were detected by a triple coincidence scintillation counter telescope, the second phosphor of which acted as the defining aperture.

The energy of the incident beam was 149 MeV with a full width at half-height of approximately 2 MeV. Aluminium absorbers were placed between the second and third counters so that the only protons recorded were those arising from collisions of incident protons within 6 MeV of the maximum energy. The same amount of absorber was kept in the telescope for all angles since, over the range of angles covered there was only a small variation of the energy of the elastically scattered proton.

The detection efficiency of the telescope was measured by placing the counters in the direct beam, which was greatly reduced in intensity, with the scatterer in front of the collimators. This ensured that the energy of the incident beam was approximately the same as that of the scattered protons. With no absorber in the telescope, the ratio of triple to double coincidence was 0.985, the difference from unity being accounted for by nuclear and Coulomb scattering in the counters and air and by counting losses. The efficiency was therefore taken as the ratio of triple to double coincidences with the absorber in position, which was about 0.60, and small corrections were made for counting losses. The large reduction in efficiency was due to nuclear absorption and Coulomb scattering in the absorber.

The background counting rate at each angle was determined by removing the scatterer and placing it in the telescope so as to maintain the same total amount of absorber. For the runs with liquid scatterers a dummy target, which had been part of the absorber in the telescope, was interchanged with the liquid scatterer at the pivot. The background was appreciable only at the smallest angles where it was about 10 % of the counting rate with the scatterer in position.

The angular resolution of the telescope was determined by the geometry of the detecting system and the multiple Coulomb scattering in the target and the air; the angular divergence of the incident beam was negligible. The effect of multiple scattering was to put a tail on the angular resolution, which became important at the smallest scattering angles. For the different scatterers the angular resolution varied slightly but was always about 1°.

2.2. RESULTS

The angular distribution for Be, C, N, O and Al are given in table 1 in laboratory co-ordinates but plotted in centre-of-mass co-ordinates (figs. 2 to 5 and 9). The error on the absolute scale depends upon the calibration of the monitor, the true area of the defining counter and the accuracy of the various small corrections which have been applied. This error is thought to be not more than 3 %.

No results are presented for scattering angles greater than 20 ° because a significant number of inelastic protons might have been counted and also the validity of the optical model with which comparison is made may be in doubt beyond this angle.

TABLE 1

Laboratory values of the differential cross section in mb/sr

θ_L	Be	C	N	O	Al
4	463±30	600±20		1854±89	
4½	342±10			904±54	
5	270± 8	460±10	845±52	677±27	1650±20
5½	270±11			603±18	1520±20
6	273± 8	355±11	540±14	572±18	1390±20
6½					1320±40
7	287± 6	365±11	493± 9	553±18	1270±20
7½					1280±50
8	264± 8	390±11	500± 9	546±14	1180±20
8½					1150±40
9	252± 8	362±11	453±12	519±15	1070±20
10	228± 7	330±10	420± 7	470±11	890±20
11	193± 6	297±10	377± 9	423±15	730±20
12	168± 6	258± 9	335±10	325±14	580±10
13	134± 7	209± 8	256±10	297±16	400±20
15	92± 6	155± 7	179± 8	158±11	188±20
17½	61± 6	83± 5	80± 5	80±10	97±15
20	35± 4	46± 4	37± 4	44±10	43±15

2.3. COMPARISON WITH THE OPTICAL MODEL

It was assumed that to determine the proton angular distribution it was reasonable at this energy to obtain the scattering amplitude by the addition of the nuclear amplitude to the Coulomb amplitude calculated in Born approximation up to the nuclear surface. The parameters of the optical model were the same as those used for neutrons (Taylor [14])) except that the real part of the nuclear potential was reduced by the Coulomb barrier height. The phase of the Coulomb scattering amplitude has been added to the Born approximation calculation.

The solid curve shown in figs. 2 to 5 and 9 is this calculated distribution modified to take account of the experimental angular resolution. The tail on this angular resolution is such that the deep minimum in the calculated distribution is not observed and also such that the cross sections at angles smaller than the minimum are greatly increased. Agreement of the experimental results with this simple model is seen to be good especially at small angles and for the lightest elements.

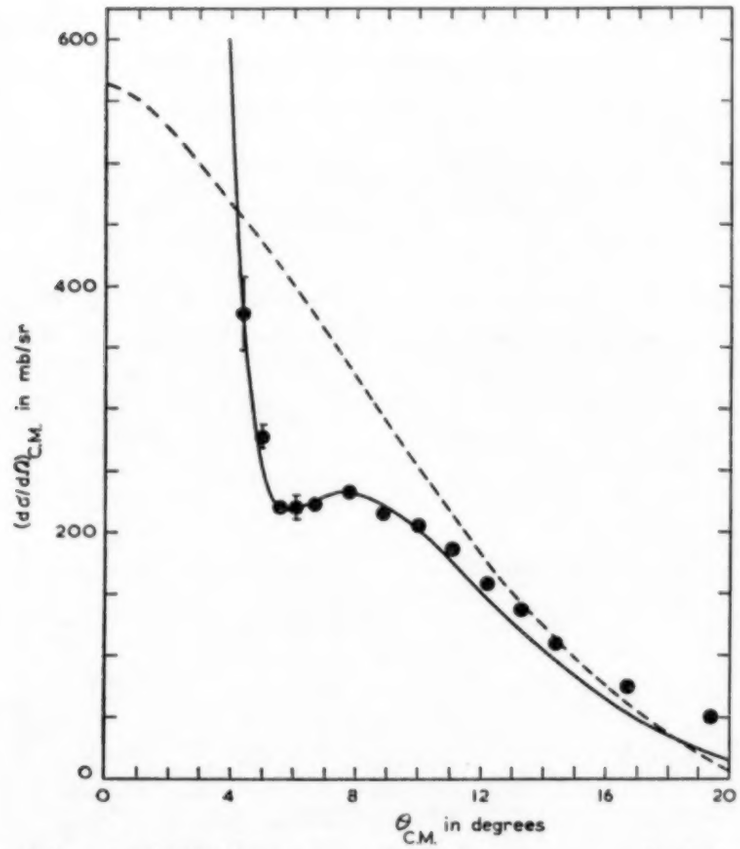

Fig. 2. Elastic scattering of 142 MeV protons on beryllium. ——— Optical model for protons. – – – – Optical model for neutrons.

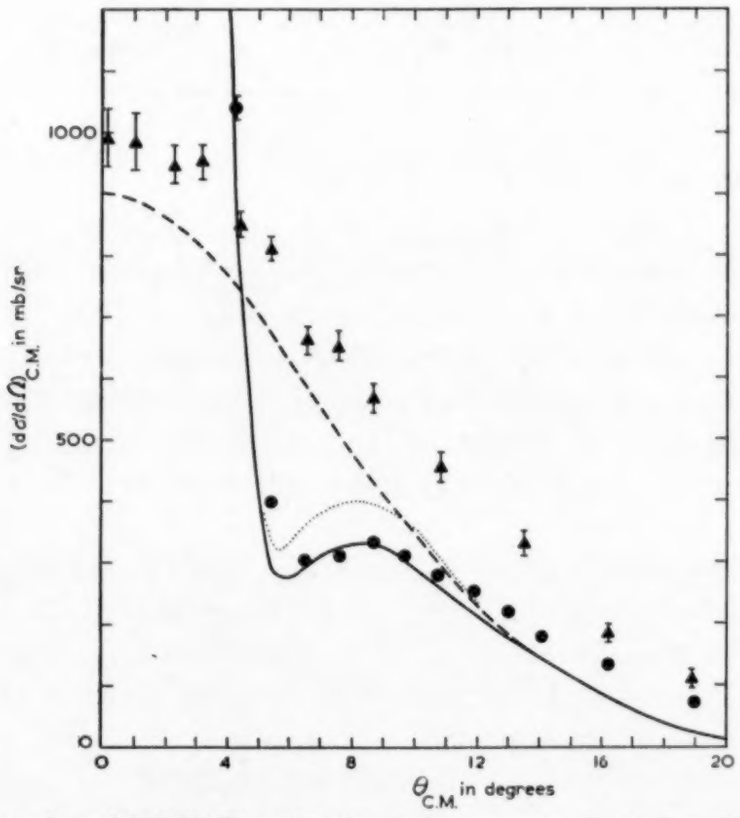

Fig. 3. Elastic scattering of 142 MeV protons on carbon. ····· Optical model for protons V = 13.6 MeV. ——— Optical model for protons V = 10.8 MeV. – – – – Optical model for neutrons V = 13.6 MeV. • Exp. point for protons. ▲ Exp. point for neutrons at 13.6 MeV (ref. [15])).

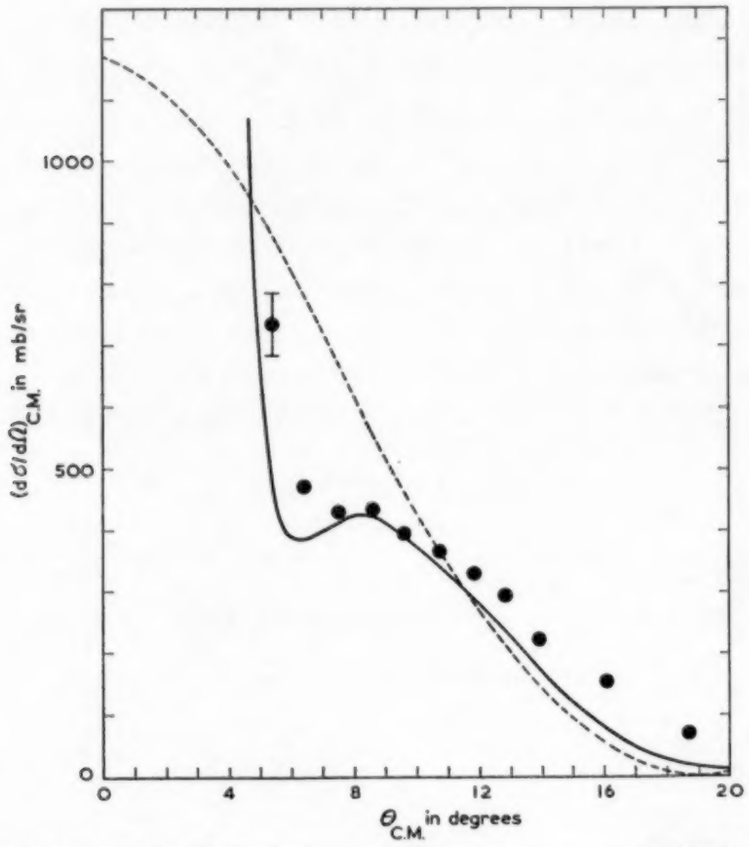

Fig. 4. Elastic scattering of 142 MeV protons on nitrogen. ——— Optical model for protons. - - - - Optical model for neutrons.

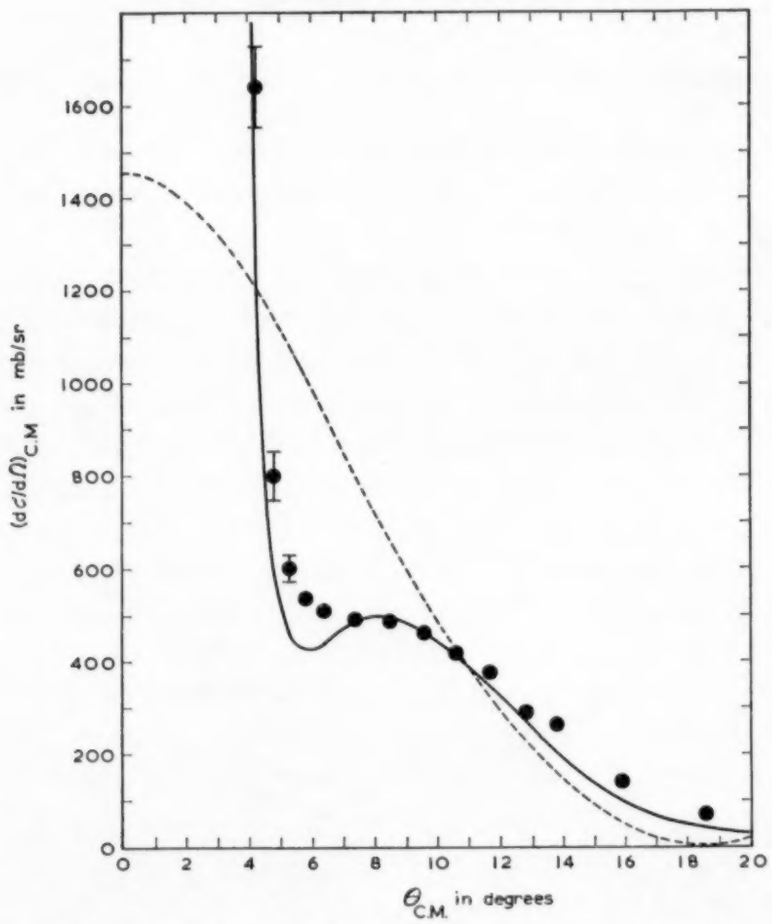

Fig. 5. Elastic scattering of 142 MeV protons on oxygen. ——— Optical model for protons. - - - - Optical model for neutrons.

3. Total Cross-Section Measurements

3.1. EXPERIMENTAL METHOD

Total cross section measurements have been made for the four elements, Be, C, N and O. The experimental layout used is that shown in fig. 6. The first two scintillation counters, operated in double coincidence, defined and monitored the beam, and the attenuators were placed immediately behind them. By varying the distance of the large area scintillation counter, which was operated in triple coincidence with the beam defining counters, measurements of attenuation were made for various values of θ, where θ is the half angle subtended by this counter. The detection efficiency of this large area counter was carefully

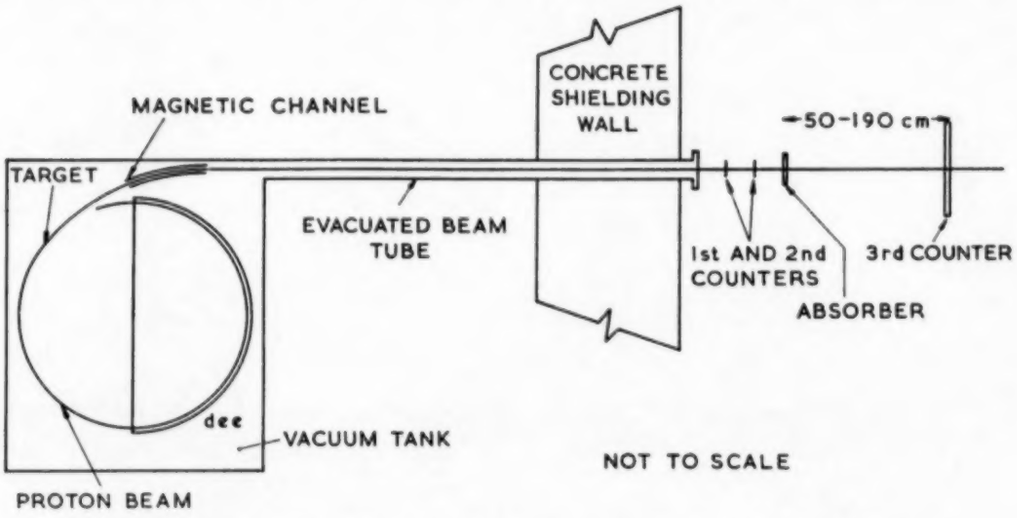

Fig. 6. Schematic diagram of total cross-section experimental layout.

checked and found to be constant over the surface. The difference between the triple and double coincidence counts is related to the cross section for scattering through angles greater than θ.

Only thin attenuators, producing about 5 % nuclear attenuation, could be used because only a small energy loss could be tolerated and because multiple Coulomb scattering effects must be kept small. Hence, the difference between the triple and double coincidence counting rates was small and particularly attention had to be paid to counting losses and the stability of the apparatus. The coincidence unit was the same as that used for the angular distribution measurements and had a resolution time of 10^{-8} sec. The beam was reduced in intensity so that the mean double coincidence rate was kept at about 6 counts per sec, at which rate counting losses had a negligible effect on the cross section.

The short resolution time of the coincidence circuit together with the long flight path used gave some energy selection of the particles detected such that no errors could be introduced by charged secondaries or beam contamination of energy less than about 40 MeV at the largest angles and about 100 MeV at the smallest angles.

Without an attenuator in the beam the triple coincidence counting rate was about 98.5 % of the double counting rate, and varied slightly with the position of the third counter. The greater part of the difference from 100 % could be accounted for by nuclear and Coulomb scattering in the counters and air path, and by counting losses. The efficiency of detection, which was taken as the ratio of the triple to double counting rates was not the same with and without the attenuator in position because the losses were slightly different at the different energies. A small correction, which amounted to about 1 % of the nuclear attenuation produced, was applied to take account of this.

3.2. RESULTS

At each angle, repeated measurements were made with and without an attenuator in position and the weighted mean of the ratio was corrected for the change in efficiency of detection with angle θ. The cross section obtained was for nuclear and Coulomb scattering and involved the interference between them.

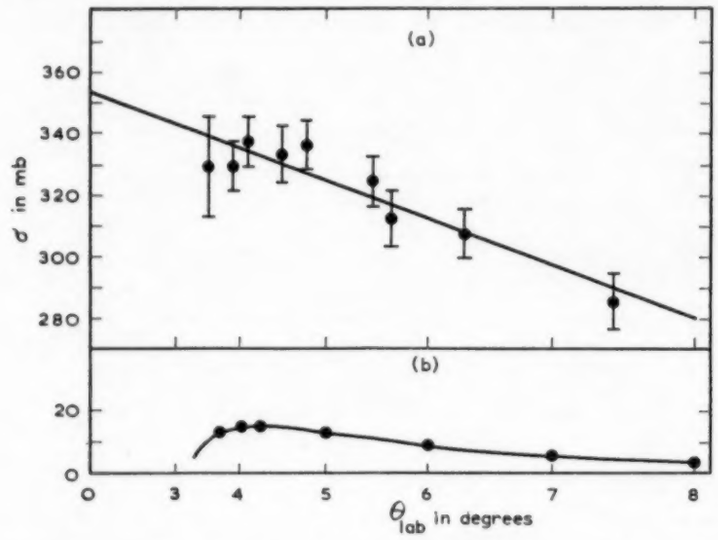

Fig. 7. Proton total cross section of carbon at 137 MeV. (a) $\sigma_t^c = 353+7$ mb. (b) Interference.

In order to extract the extent and magnitude of this interference, it is necessary to know the angular distribution of the scattered protons in the absence of the Coulomb interaction. In view of the agreement of the experimental angular distributions with the predictions of the modified optical model, this proton angular distribution was calculated in the same way as for a neutron angular distribution given by the optical model. That the optical model gives a good representation of the angular distribution for neutrons is shown (fig. 3) where the prediction for C is compared with the results of van Zyl, Voss and Wilson [15]). The total cross sections were then corrected by the difference between the theoretical neutron and proton angular distributions. The magnitude of this correction for carbon is shown (fig. 7) together with a plot of the carbon cross section against solid angle. It will be seen that the correction is a small

fraction of the total cross section and since the error in estimating the correction is thought to be small, the errors on the total cross section have not been increased.

Since in the angular range of the total cross-section measurements, the sum of the integrated elastic cross section and the effective inelastic cross section have a linear dependence on the solid angle, the corrected results were plotted against solid angle and the intercept at $\theta = 0°$ was taken as the total cross section. The error on the intercept determined from a least squares analysis was consistent with the errors on the points themselves.

As an alternative method of obtaining the total cross section, the results were corrected for the elastically scattered protons and a horizontal straight line fitted to the points. No significantly different value of the total cross section was obtained in the two methods, confirming that inelastic events contribute little to the variation of the total cross section with solid angle and that little error is introduced in the extrapolation.

Similar results were obtained for Be, N and O, which together with the C result are given in table 2.

TABLE 2

Experimental total cross sections

Element	Energy (MeV)	Proton 'total cross section' (mb)	Neutron total cross section (mb)
Be	134	304± 5	286
C	137	353± 7	355
N	138	411±15	404
O	138	493±10	490

4. Discussion

The proton total cross sections are compared in table 2 with the corresponding neutron values, which are taken from a smooth curve through published values. Where there were few published values, the shape of the curve was guided by the predictions of the optical model. The agreement is good except for Be where a difference might be expected since the nucleus does not contain the same number of protons and neutrons. Indeed the optical model would predict about a 4 % higher Be total cross section for protons. This assumes that the n—n cross section is equal to the p—p cross section, which is suggested by the agreement between the neutron and proton total cross sections for the other three elements which do contain the same number of neutrons as protons.

This agreement, together with the good fit obtained to the angular distributions, suggests that it is possible to modify the optical model in a simple way to account for proton-nuclear scattering in light elements. Indeed, the region of

the Coulomb-nuclear interference is seen to be very sensitive to the value of the real potential as is illustrated by fig. 3. Here the experimental angular distribution of elastically scattered protons from C is plotted together with the theoretical distributions obtained for two values of the real part of the potential. One value is that used by T. B. Taylor [14]) for neutrons, namely, 13 MeV, and the other is this value reduced by the Coulomb barrier height, that is, to 10.8 MeV. The difference between the two theoretical distributions is well outside the statistical errors on the experimental determination, and these are such as to enable the real part of the potential to be fixed within 0.5 MeV.

However, the agreement between experimental results and theoretical prediction of this simple model is worse at large angles. This may arise from the neglect of a spin-orbit interaction which will tend to increase the cross section at large angles. Calculations for carbon using a Saxon-Woods shape indicate that at large angles the scattering amplitudes are larger than those calculated with the square well shape of Fernbach, Serber and Taylor [7]). This would again increase the cross sections at larger angles. These considerations are followed up in the appendix.

More exact treatments of the scattering may yield better agreement for larger angles and elements of higher atomic weight, but the treatment presented here seems adequate for the measurements which have been made and suggests that there is equality of proton and neutron scattering from light elements at 142 MeV.

The authors wish to thank many colleagues and in particular Dr. T. H. R. Skyrme for useful discussions and assistance.

Appendix

In this brief note, consideration is given to those modifications of the simple optical model mentioned in section 4. Only scattering from carbon and aluminium will be considered. Since the original calculations, measurements at about the same energy have been made of the polarization in proton scattering (Dickson & Salter [6]) and Alphonce, Johansson and Tibell [1]) and more recently of the triple scattering parameter R (Bird, Edwards, Rose, Taylor and Wood [2])). Also it is of interest to see to what extent the same model can fit the neutron polarization results (Harding [9])). As a starting point, the scattering amplitudes calculated previously for the central potentials have been taken without modification together with the spin orbit scattering amplitudes derived from the data.

Putting the scattering amplitudes for the spin independent and spin dependent parts of the interaction as g and h, respectively, and their relative phase as

α, the experimental results can be expressed as follows:

$$\text{Differential cross section: } \sigma(\theta) = |g|^2+|h|^2,$$

$$\text{Polarization: } P(\theta)\sigma(\theta) = 2|g||h| \cos \alpha,$$

$$\text{Rotation parameter: } R(\theta) = (1-P^2(\theta))^{\frac{1}{2}} \cos (\beta-\theta),$$

where

$$(1-P^2(\theta))^{\frac{1}{2}}\sigma(\theta) \sin \beta = -2\,|g||h| \sin \alpha.$$

There is an ambiguity in the sign of β and the negative values have been preferred in this analysis. Further, g and h can be distinguished by the following argument. If the spin dependent interaction is represented mainly by a real potential, the scattering amplitude is mainly imaginary. Comparison can then be made of its angular variation with what would be expected in a simple calculation. This would put

$$h = K \sin \theta F(\theta),$$

where K is a constant and $F(\theta)$ is a form factor, whereas g has no $\sin \theta$ dependence.

The values of $F(\theta)$ obtained in the previous calculation for neutron scattering for both the square well and Saxon-Woods shape have been compared with $h/\sin \theta$. Almost exact proportionality is obtained for the Saxon-Woods shape. The same angular variation has therefore been assumed for the smaller real part of the spin dependent scattering amplitude. This has been chosen as $\frac{1}{7}$ of the imaginary part, which is in rough accord with the ratio of potentials given by Ohnuma [12]). With such a small contribution from this term, the results in fact are not very sensitive to the exact ratio of real and imaginary parts. Since the object of the calculation is to fit the experimental results and there is no preconceived idea of the value of h, it is legitimate to choose the constant of proportionality K from the data as it is not governed by the choice of g.

It then remains to see to what extent the combination of these scattering amplitudes with the spin independent amplitudes calculated previously can fit the experimental data. The magnitude of the spin dependent amplitude for aluminium has been increased over that for carbon in the ratio of the cube of the radii of aluminium to carbon. In figs. 8 and 9, the differential cross section is shown and it is immediately seen by comparison with the previous figures that some improvement is obtained at large angles by the inclusion of the spin dependent terms. Better agreement would be obtained if the spin independent amplitude, in particular the imaginary part, did not decrease so rapidly at large angles. This is also the situation for the polarization which is shown in figs. 10 and 11. Since calculations with a Saxon-Woods shape indicated that the imaginary part of the scattering amplitude at large angles departs strongly from that for a square well shape, an empirical modification has been made to fit the

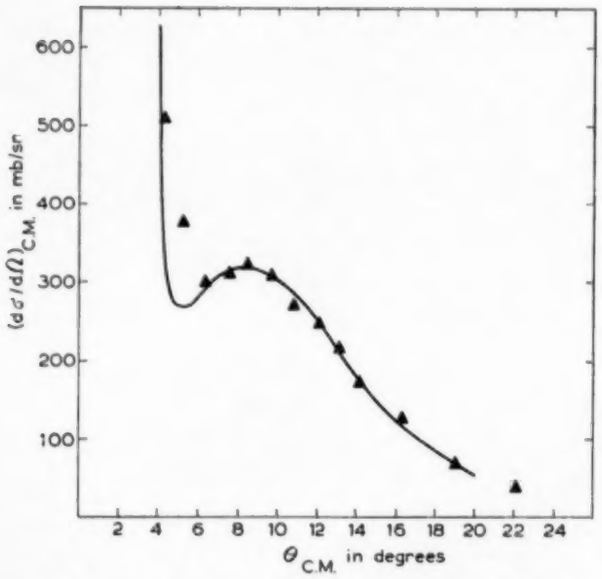

Fig. 8. Scattering of protons on carbon at 142 MeV. ——— Calculation for a modified square well with spin orbit coupling. ▲ Experimental points.

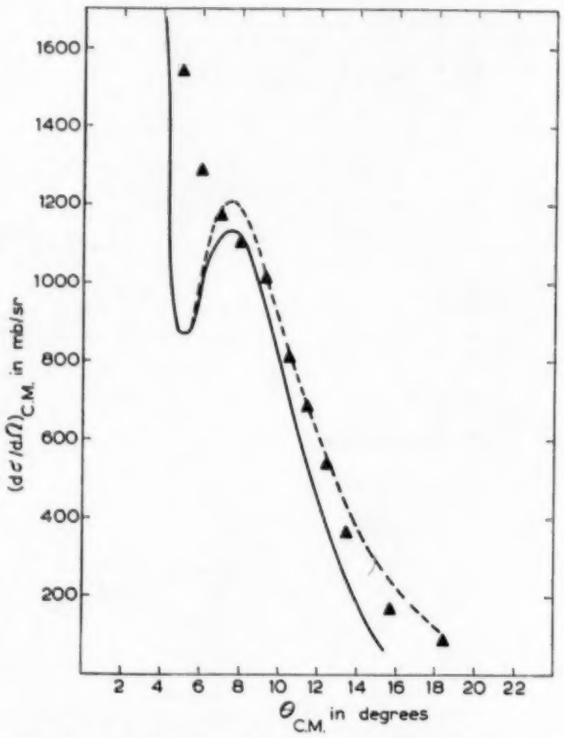

Fig. 9. Scattering of protons on aluminium at 142 MeV. ——— Optical model for protons. – – – – Calculation for a modified square well with spin orbit coupling. ▲ Experimental points.

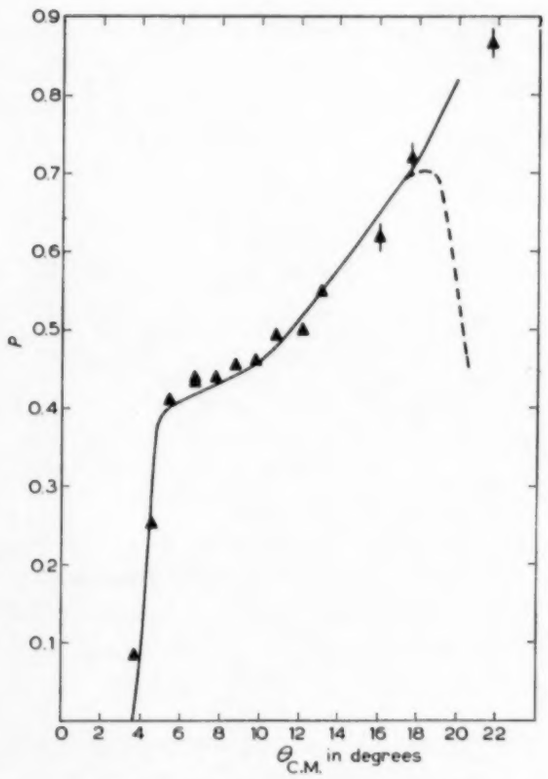

Fig. 10. Scattering of protons on carbon at 142 MeV. – – – – Calculation for an unmodified square well. ——— Calculation for a modified square well. ▲ Experimental points.

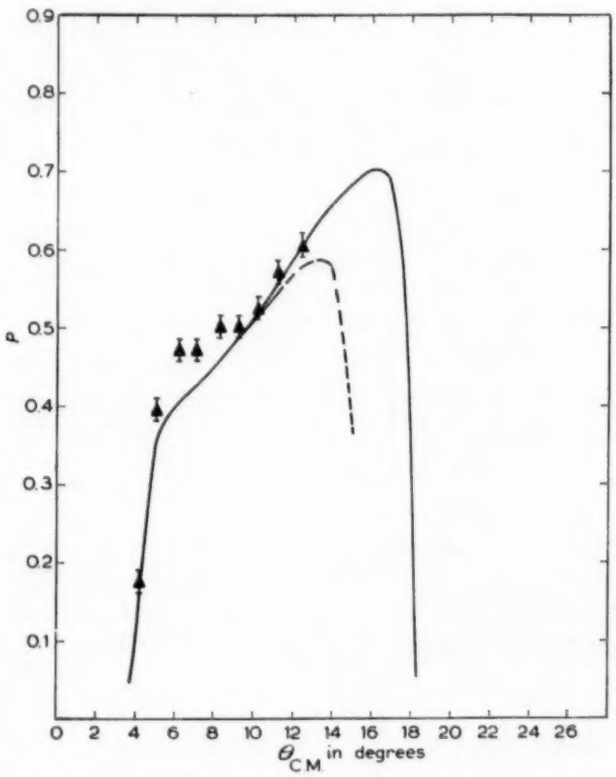

Fig. 11. Scattering of protons on aluminium at 142 MeV. – – – – Calculation for an unmodified square well. ——— Calculation for a modified square well. ▲ Experimental points.

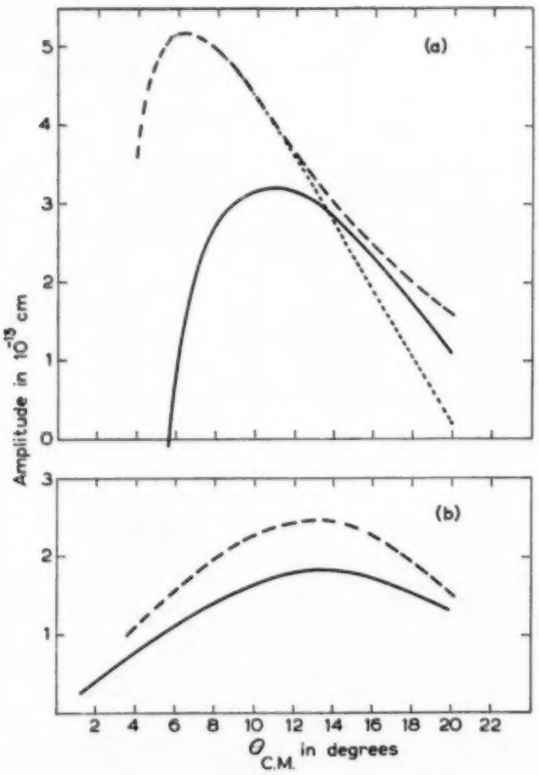

Fig. 12. Scattering amplitudes for protons on carbon at 142 MeV. (a) ——— Re g, – – – – Im g for modified square well, - - - - Im g for unmodified square well. (b) ——— Im h, – – – – Re $h \times 10$.

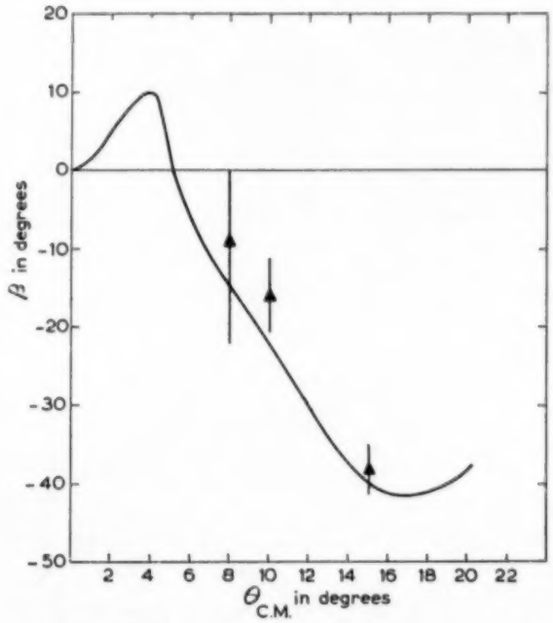

Fig. 13. Phase angle in P-nucleon scattering at 142 MeV. ——— Triple scattering rotation parameter $R = (1-P^2)^{\frac{1}{2}} \cos(\beta-\theta)$.

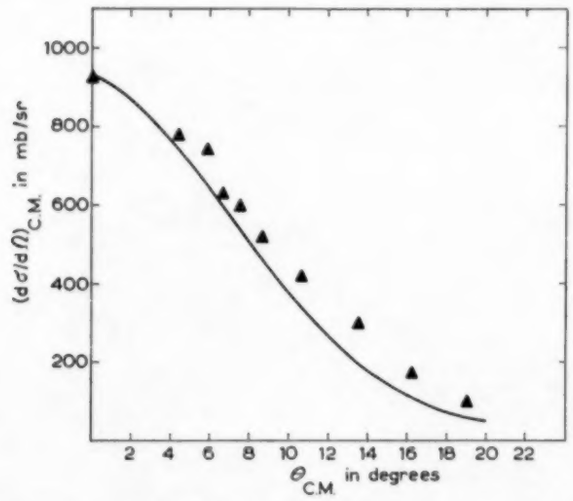

Fig. 14. Scattering of neutrons on carbon at 142 MeV. ——— Calculation for neutrons using same parameters as for protons at 142 MeV. ▲ Experimental points (ref. [15])) at 136 MeV reduced by 0.85.

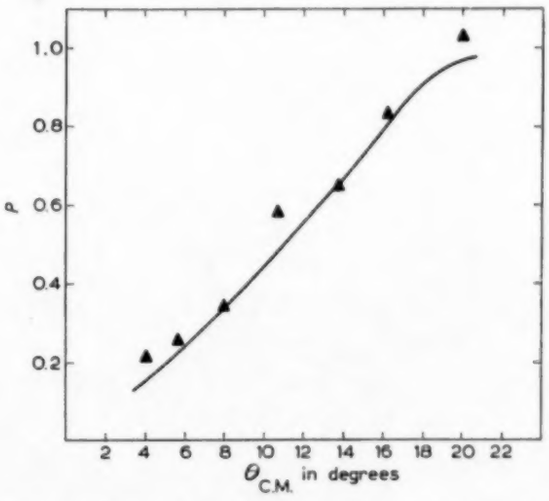

Fig. 15. Scattering of neutrons on carbon at 142 MeV. ——— Calculation for neutrons using same parameters as for protons at 142 MeV. ▲ Experimental points (ref. [9])) at 155 MeV.

data beyond 15° scattering angle. The extend of this modification is shown (fig. 12) together with the other scattering amplitudes used in these fits. A similar modification was made for aluminium. With this modification better

fits are obtained to both the differential cross section and polarization as shown on figs. 8—11). The agreement with the triple scattering experiment is also seen to be good (fig. 13).

The same spin dependent scattering amplitudes have been used when making comparison with the neutron data. Also the previously calculated values of the spin independent scattering amplitudes for neutron scattering from a square well have been used but with the modification to the imaginary part for scattering angles greater than 15°. The results for carbon are shown on figs. 14 and 15. However, in order to obtain a fit to the differential cross section, it has been necessary to decrease the experimental values by twice the absolute scale error. Some of this difference may be accounted for by the difference in energy.

Had the positive values of β been chosen, such a good fit to the data would not have been obtained. Further, with the values of g used in this analysis, the positive values of β would have implied that h was almost wholly real. This in its turn implies that the spin orbit potential was mainly imaginary which is contrary to what is normally assumed. The ambiguity in the sign of β would be removed by the measurement of the A parameter which is given by $A = = (1-P^2)^{\frac{1}{2}} \sin(\beta-\theta)$.

It is therefore seen that it is possible to fit the available data by the addition to the previous calculations of a spin dependent scattering amplitude which has a reasonable angular variation and which can be derived independently from the data. The slight modification of the imaginary part of the spin independent scattering amplitude for large angles is perhaps an indication of the unreality of a square well.

References

1) Alphonce, Johansson and Tibell, Nuclear Physics **4** (1957) 672
2) Bird, Edwards, Rose, Taylor and Wood, J. de Phys. et Rad. **21** (1960) 329
3) H. G. de Carvalho, Phys. Rev. **96** (1954) 398
4) Cassels and Lawson, Proc. Phys. Soc. **67** (1954) 125
5) Chen, Leavitt and Shapiro, Phys. Rev. **99** (1955) 857
6) Dickson and Salter, Nuovo Cim. **6** (1957) 235
7) Fernbach, Serber and Taylor, Phys. Rev. **75** (1949) 1352
8) Hecks and Kirschbaum, Livermore Report MTA-28 (1952)
9) R. S. Harding, Phys. Rev. **111** (1958) 1164
10) Marshall, Marshall and Nedzel, Phys. Rev. **91** (1953) 767
11) Millburn, Birnbaum, Crandall and Schecter, Phys. Rev. **95** (1954) 1268
12) S. Ohnuma, Phys. Rev. **111** (1958) 1173
13) Richardson, Ball, Leith and Moyer, Phys. Rev. **86** (1952) 29
14) T. B. Taylor, Phys. Rev. **92** (1953) 831
15) Van Zyl, Voss and Wilson, Phil. Mag. **1** (1956) 1003

8.B

Nuclear Physics **25** (1961) 656—660; © *North-Holland Publishing Co., Amsterdam*

Not to be reproduced by photoprint or microfilm without written permission from the publisher

ABOUT THE PION-HYPERON RESONANCE

P. G. O. FREUND, A. M. LONGONI † and E. PREDAZZI ††

Institute for Theoretical Physics, University of Vienna

Received 17 February 1961

Abstract: The spectral function of the Σ-hyperon propagator calculated with the aid of a method proposed by Redmond under the assumptions of odd Σ—Λ relative parity and strong $(\Sigma\Lambda)\pi$ interaction is used for a theoretical derivation of the position and width of the Λ—π resonance recently discovered by Alvarez *et al.* The computed figures are in good agreement with experimental data. The same method is applied also for a discussion of the possibility of a high energy (1,1) π—N resonance and for the computation of the low energy (1,1) cross-section in π—N scattering.

1. Introduction

Recently Alvarez *et al.* [1]) found experimental evidence for a $\pi-\Lambda$ resonance corresponding to a mass of 1385 MeV with a width $\leqq 20$ MeV in an $I = 1$ state. Some possible applications of the existence of this resonance have been discussed by Meyer, Prentki and Yamaguchi [2]).

It is natural that this resonance should show up in the spectral function of the Σ-hyperon propagator (but of course not in the Λ-hyperon propagator because of the wrong isobaric spin). We prove in this paper that in a certain approximation this is the case if one assumes a strong $(\Sigma\Lambda)\pi$ interaction and odd $\Sigma-\Lambda$ relative parity. It is a well-known fact that propagators obtained by the iteration of perturbative graphs contain ghost poles. Redmond [3]) showed that if one moreover requires the existence of the correct spectral representation (i.e. correct analytic behaviour) for the propagator, one can avoid this difficulty. Redmond's prescription for a fermion propagator can be formulated as follows. If $\rho(l)$ is the spectral function corresponding to the graphs which one iterates, the spectral function $\chi(l)$ leading to the correct spectral representation is

$$\chi(l) = \frac{\rho(l)}{[1-R(l)]^2+\pi^2(l-M)^2\rho^2(l)}, \tag{1}$$

where

$$R(l) = (l-M)\mathrm{P}\int_{-\infty}^{+\infty} \mathrm{d}c\, \frac{\rho(c)}{l-c} \tag{2}$$

and M is the mass of the fermion.

† Now at Istituto di Fisica dell'Universita di Torino, Italy.

†† On leave of absence from Istituto di Fisica dell'Universita di Torino, Italy and at Istituto di Fisica dell'Universita di Padova, Italy.

Looking at formula (1), one sees that the denominator has a resonant character. Using the first perturbative approximation for ρ we show that one can obtain out of this feature of $\chi(l)$ the correct position and width of the above-mentioned $\Lambda-\pi$ resonance. Finally we compute the (1,1) cross-section in $\pi-$N scattering for low energies using the correctly iterated propagator for the nucleon and discuss the possibility of a high energy (1,1) $\pi-$N resonance.

2. Position of the $\Lambda-\pi$ Resonance

If in the Σ-hyperon propagator one iterates the graph represented in fig. 1 (which is the lowest order graph), assuming odd $\Sigma-\Lambda$ relative parity (which

Fig. 1. The lowest order self-energy graph for the Σ-hyperon.

because of the pseudoscalarity of the pion means a scalar $(\Sigma\Lambda)\,\pi$ interaction), one finds by standard methods [4])

$$\rho(l) = \frac{g^2}{32\pi^2}\,\frac{\sqrt{(l^2-m^2-\mu^2)^2-4m^2\mu^2}}{(l-M)^2|l|^3}\,[(l+m)^2-\mu^2]\,\theta(l^2-(m+\mu)^2), \qquad (3)$$

where $g/\sqrt{(4\pi)}$ is the renormalized scalar $(\Sigma\Lambda)\pi$ coupling constant and M, m and μ are respectively the Σ, Λ and π masses. Inserting (3) in (2) and neglecting higher order terms in μ/m, one obtains after long but straightforward calculations

$$\begin{aligned} R(l) = \frac{g^2}{32\pi^2}\,\frac{1}{l+M}\Bigg\{ & \frac{l^2-m^2}{l^2-M^2}\left[\alpha+\frac{\beta}{l^2}+\frac{\gamma}{l^4}\right]\ln\frac{l^2-(m+\mu)^2}{(m+\mu)^2} \\ & + \frac{1}{l^2-M^2}\left[\alpha(m^2-l^2)+\beta\left(\frac{m^2(2M^2-l^2)}{M^4}-1\right)\right. \\ & \left. + \frac{\gamma}{M^2}\left(\frac{m^2+l^2}{M^2}-\frac{2m^2(l^2-M^2)}{M^4}-2\right)\ln\frac{(m+\mu)^2-M^2}{(m+\mu)^2}\right. \qquad (4a) \\ & \left. + \frac{M^2-m^2}{(m+\mu)^2-M^2}\left[\alpha+\frac{\beta}{M^2}+\frac{\gamma}{M^4}\right]-\frac{\gamma m^2(l^2-M^2)}{M^4 l^2(m+\mu)^2}\right\}, \end{aligned}$$

where

$$\alpha = l+2(M+m), \quad \beta = l(M^2+m^2+4mM)+2mM(m+M), \quad \gamma = lm^2M^2. \qquad (4b)$$

According to eq. (1) the position l_0 of the resonance is given by the equation

$$R(l_0)-1 = 0. \qquad (5)$$

Inserting eqs. (4a, b) in eq. (5), one finds $l_0 = 1390$ MeV for g^2 [illegible] for a strong $(\Sigma\Lambda)\pi$ vertex, one can localize the resonance in [illegible] value. It should be mentioned that the assumption of o[illegible] parity is essential for this result (see sect. 5).

3. Width of the Resonance

The denominator in (1) vanishes for $l = l_0 - \frac{1}{2}i\Gamma$, where Γ [illegible] resonance. If we assume $\Gamma \ll l_0$ (which will turn out to be [illegible] the condition

$$[1-R(l_0-\tfrac{1}{2}i\Gamma)]^2+\pi^2(l_0-\tfrac{1}{2}i\Gamma-M)^2\rho^2(l_0-\tfrac{1}{2}i[illegible]$$

one finds

$$\tfrac{1}{2}\Gamma = \frac{\pi(l_0-M)\rho(l_0)}{|R'(l_0)|}.$$

Using (3), (4) and (7) and inserting the numerical values f[illegible] obtain $\frac{1}{2}\Gamma = 9.7$ MeV. This is in good agreement with the [illegible] ($\frac{1}{2}\Gamma_{\text{exp}} \leqq 10$ MeV).

4. The (1,1) Cross-Section in π—N Scat[illegible]

The (1,1) cross-section in π—N scattering, iterating gra[illegible] been computed a long time ago [5]) without avoiding ghosts.

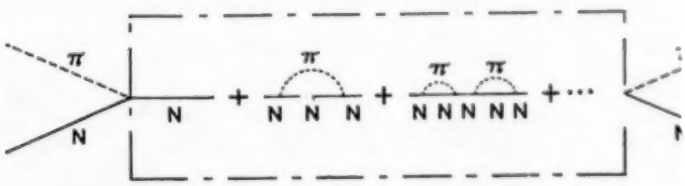

Fig. 2. Iteration of graphs for π—N scattering

these we simply have to correct in the sense of ref. [3]) the iter[illegible] gator that appears in fig. 2. Since now the interaction is [illegible]

$$\rho_{\pi N}(l) = \frac{g^2}{32\pi^2}\,\frac{(l^2-m^2-\mu^2)^2-4m^2\mu^2}{|l|^3}\,\theta(l^2-(m-[illegible])$$

where m, μ are the nucleon and meson [illegible]asses, respectiv[illegible] the renormalized *ps* π—N coupling constant.

† This is a reasonable value since in accordance with our assumptio[illegible] constant.

Inserting eqs. (4a, b) in eq. (5), one finds $l_0 = 1390$ MeV for $g^2/4\pi = 1.66$ †. Thus for a strong $(\Sigma\Lambda)\pi$ vertex, one can localize the resonance in the experimental value. It should be mentioned that the assumption of odd $\Sigma-\Lambda$ relative parity is essential for this result (see sect. 5).

3. Width of the Resonance

The denominator in (1) vanishes for $l = l_0 - \frac{1}{2}i\Gamma$, where Γ is the width of the resonance. If we assume $\Gamma \ll l_0$ (which will turn out to be correct), then from the condition

$$[1-R(l_0-\tfrac{1}{2}i\Gamma)]^2+\pi^2(l_0-\tfrac{1}{2}i\Gamma-M)^2\rho^2(l_0-\tfrac{1}{2}i\Gamma) = 0 \tag{6}$$

one finds

$$\tfrac{1}{2}\Gamma = \frac{\pi(l_0-M)\rho(l_0)}{|R'(l_0)|}. \tag{7}$$

Using (3), (4) and (7) and inserting the numerical values found in sect. 2, we obtain $\frac{1}{2}\Gamma = 9.7$ MeV. This is in good agreement with the experimental result ($\frac{1}{2}\Gamma_{\text{exp}} \leqq 10$ MeV).

4. The (1,1) Cross-Section in π—N Scattering

The (1,1) cross-section in π—N scattering, iterating graphs as in fig. 2, has been computed a long time ago [5]) without avoiding ghosts. If we want to avoid

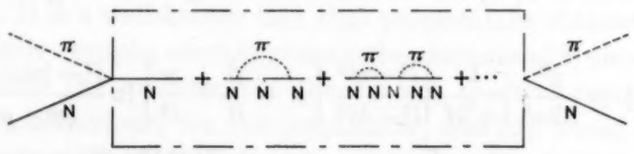

Fig. 2. Iteration of graphs for π—N scattering.

these we simply have to correct in the sense of ref. [3]) the iterated nucleon propagator that appears in fig. 2. Since now the interaction is ps, we get

$$\rho_{\pi N}(l) = \frac{g^2}{32\pi^2}\frac{(l^2-m^2-\mu^2)^2-4m^2\mu^2}{|l|^3}\,\theta(l^2-(m+\mu)^2), \tag{8}$$

where m, μ are the nucleon and meson masses, respectively and $g/\sqrt{(4\pi)}$ is the renormalized *ps* π—N coupling constant.

† This is a reasonable value since in accordance with our assumptions g is a scalar coupling constant.

This yields (neglecting higher order terms in μ/m)

$$\frac{\dfrac{g^2}{32\pi^2}\dfrac{\sqrt{(l^2-m^2-\mu^2)^2-4m^2\mu^2}}{|l|^3}\,\theta(l^2-(m+\mu)^2)}{\left[1-\dfrac{l-m}{l}\dfrac{g^2}{32\pi^2}\left\{\ln\left|\dfrac{l^2-(m+\mu)^2}{(m+\mu)^2}\right|\left(1-\dfrac{m^2}{l^2}\right)-\dfrac{m^2}{l^2}\dfrac{l^2-(m+\mu)^2}{(m+\mu)^2}\right\}\right]^2+\pi^2(l-m)^2\dfrac{g^2}{32\pi^2}\dfrac{(l^2-m^2)^2}{l^6}}. \tag{9}$$

Hence, the corrected propagator reads

$$G(p) = \frac{1}{m-\gamma p}+\int_{-\infty}^{+\infty}\frac{\chi_{\pi N}(l)\,dl}{l-\gamma p}. \tag{10}$$

The integral appearing in eq. (10) is rather involved. Numerical evaluation at vanishing π-momentum shows that it improves the too large Born approximation for the cross-section by a factor 0.58. Moreover, from formula (9) one is justified to expect the existence of a wide (1,1) π—N resonance at some 4000 MeV.

5. Concluding Remarks

The nice agreement with experimental evidence we found in sects. 2 and 3 supports the validity of the assumptions we have made, there namely, a) the existence of a strong $(\Sigma\Lambda)\pi$ interaction and b) odd $\Sigma-\Lambda$ relative parity (one can see from sect. 4, since the hyperon-nucleon mass differences are small, that even Σ—A relative parity, i.e. pseudoscalar $(\Sigma\Lambda)$ π interaction, would shift the resonance towards higher energies). Assumption b) could be tested experimentally according to the suggestions of ref. [2]) †.

An essential condition for the applicability of the method used in this paper to other problems is the convergence of the principal-value integral in eq. (2). This is a rather restrictive condition since in many interesting cases (e.g. a three-fermion intermediate state) it is violated.

Finally we wish to express our deep gratitude to Prof. W. Thirring for his constant advice and many valuable discussions, and two of us (A. M. L., E. P.) also for the kind hospitality extended to them at the Institute for Theoretical Physics of the University of Vienna. Our thanks are due also to Dr. J. Prentki for an important remark.

† Recent experimental work [6]) seems to indicate that actually the $\Sigma-\Lambda$ relative parity is odd and the $\pi-\Lambda$ resonance occurs in a $J = \frac{1}{2}$ state, as one should expect from our model.

References

1) M. Alston, L. W. Alvarez, P. Eberhard, M. L. Good, W. Graziano, H. K. Ticho and S. Wojcicki, Phys. Rev. Lett. **5** (1960) 520;
H. J. Martin, L. B. Leipuner, W. Chinowsky, F. T. Shively and R. K. Adair, Phys. Rev. Lett. **6** (1961) 283
2) Ph. Meyer, J. Prentki and Y. Yamaguchi, Phys. Rev. Lett. **5** (1960) 442
3) P. J. Redmond, Phys. Rev. **112** (1958) 1404;
N. N. Bogoliubov, A. A. Logunov and D. V. Shirkov, JETP **37** (1959) 805
4) W. E. Thirring, Principles of quantum electrodynamics (Academic Press Inc., New York, 1958) pp. 175, 215
5) R. Karplus, M. Kivelson and P. C. Martin, Phys. Rev. **90** (1953) 1072
6) M. Cini, private communication

1.D.1 *Nuclear Physics* **25** (1961) 661—673; © *North-Holland Publishing Co., Amsterdam*
Not to be reproduced by photoprint or microfilm without written permission from the publisher

PAIRINGS IN THE SHELL MODEL (II)

MINORU UMEZAWA

Institut de Recherches Nucléaires, Université de Strasbourg

Received 13 December 1960

Abstract: Coupling schemes are explained for a system of nucleons interacting with each other through a singlet-paring force in addition to a strong spin-orbit force.

Results are applied in particular to ground states of nuclei with $n = 4j_+ + 1$, that is, B^{11} and Al^{27}. Assuming a strong spin-orbit force, it is found that the effect of the pairing force in mixing the spin-orbit partners in a j–j coupling scheme is comparatively large near closure of the j–j subshells. The ratio V_{01}/V^0 of the depths of the pairing force and spin-orbit force is chosen for each nucleus so that the deviation of the nuclear magnetic moment from the j–j limit would be explained by the competition of the two forces. It is found that such a ratio becomes relatively larger as the nucleus becomes heavier irrespective of the parity of the orbital state of the individual nucleon.

1. Introduction

It has recently been pointed out that the interaction energies between pairs of identical nucleons become additive when the members of the pairs are oriented oppositely to each other in space and in intrinsic spin space. This lowers the ground state considerably. For deformed nuclei, this result has been applied to explain the reduction of the rotational moment of inertia [1]). In spherical nuclei, this pairing energy is reduced to the interaction between a pair of two identical nucleons which couple to form a scalar function. However, in light nuclei it is necessary to take into account the pairing correlation between pairs of protons and neutrons.

On the other hand it has been pointed out by Mayer from the outset of present shell model that it is necessary to introduce the pairing energy between identical nucleons, in order to explain various features of the ground states of nuclei [1a]).

Later it was shown that the model in which, for odd mass nuclei, each pair of nucleons couples to form an isobaric-triplet S state, leaving the one odd nucleon uncoupled, can explain magnetic moments. Numerical estimates of the magnetic moment were made in the extreme j–j and L–S limits, and it was found that most of the magnetic moments of light nuclei can be explained well by either the j–j or L–S limit, except in certain cases, in particular those of nuclei near the closure of a j–j subshell (in particular when $n = 2\ (2j+1)-1$).

Thus, corresponding to the pairing force defined for heavy nuclei, it is natural to define, for light nuclei, a pairing force which acts in an isobaric-triplet S state of a pair of nucleons. Among several kinds of such a pairing force, we

deal, in this paper, with the simplest case, a spin-singlet pairing force. More general pairing forces will be dealt with in a future paper.

The introduction of such a pairing force in addition to the spin-orbit force gives rise to an intermediate case of pairing coupling scheme (intermediate pairing scheme †).

In sects. 2 and 3, possible quantum numbers in the above coupling scheme are recapitulated from (I). In section 4, the matrix elements of the pairing force are derived for j–j and L–S representations. In section 5 matrix elements related to two configurations $(j_+)^n$ and $(j_+)^{n-2}(j_-)^2$ are calculated ††. As a result it will be shown that the mixing of these two configurations becomes important near closure of j–j subshells. In section 5 this result is applied to B^{11}, Al^{27} and V^{51}.

2. Quantum Numbers in the Intermediate Pairing Scheme

For the sake of simplicity we assume the spin-singlet pairing force given in (I) in addition to the one-body spin-orbit force †††

$$\begin{aligned} V^0 q_{ij} &= V^0 q'_{ij}(\tfrac{1}{2} - 2\boldsymbol{\sigma}_i \cdot \boldsymbol{\sigma}_j), \\ (l^2 LM|q'_{ij}|l^2 LM) &= \delta_{L0}(2l+1). \end{aligned} \tag{1}$$

Since we assume here a charge independent interaction, total isobaric spin is a good quantum number. It follows from this that the symmetry characters $[\lambda_\tau]$, $[\lambda_{ls}]$ of the isobaric functions and the space-spin functions of nuclear wave functions are preserved and $[\lambda_{ls}]^\dagger = [\tau_\tau]$.

As pointed out in (I), the pairing force (1) preserves the seniority quantum number in the combined space of orbital and intrinsic spins.

These quantum numbers together with total isobaric spin J, are obtained in the following scheme:

$$U^n_{2\times 2\times(2l+1)} \to U^n_{\underset{[\lambda_{ls}]}{2\times(2l+1)}} \times U_2{}^n_{\underset{T}{}}, \tag{3}$$

$$U^n_{2\times(2l+1)} \to Sp^n_{\underset{\langle\lambda_{ls}\rangle}{2(2l+1)}} \to R_3{}^n \times_{\underset{J}{}} U^n{}_2. \tag{4}$$

The symbols $[\lambda_{ls}]$ and $\langle\lambda_{ls}\rangle$, which are labelled beneath the two space symbols U^n and Sp^n, characterize irreducible representations in each space. However, it is not necessary to preserve $\langle\lambda_{ls}\rangle$ in this case, since certain states in $Sp^n_{2\times(2l+1)}$ are degenerate in the pairing force (1). Therefore, in the following we only quote the seniority quantum number to designate each state.

† See ref. [2]), which will be referred to as (I).
†† The notations j_+ and j_- are defined in ref. [5]).
††† The notation used in this section is that of (I).

3. Pairing Energy in j–j and L–S Representation

3.1. SYSTEMS OF ONE KIND OF PARTICLE

For systems of one kind of nucleon, the pairing energy of the Racah operator $Q = \sum_{i<j} q_{ij}$ in L–S representation, where

$$(l^2 LSM_L M_S | q_{ij} | l^2 LSM_L M_S) = 2(2l+1)\delta_{L0}\delta_{S0}, \tag{5}$$

has been obtained by Racah [4]), and is given by

$$(l^n \mathscr{S} LS | Q | l^n \mathscr{S} LS) = Q(l^n \mathscr{S}) = \tfrac{1}{2}(n-\mathscr{S})\{2(2l+1)+2-n-\mathscr{S}\}. \tag{6}$$

For the j–j representation, the pairing energy for two particles is given in ref. [5]) and

$$(j^2 JJ_z | q_{ij} | j^2 JJ_z) = (2j+1)\delta_{J0}. \tag{7}$$

From this, pairing energies for systems of more than two particles in the pure j–j coupling scheme can be obtained by the same method as that used by Racah in the L–S representation. The result is

$$(j^n \mathscr{S} | Q | j^n \mathscr{S}) = Q(j^n \mathscr{S}) = \tfrac{1}{2}(n-\mathscr{S})(2j+3-n-\mathscr{S}). \tag{8}$$

3.2. SYSTEMS OF PROTONS AND NEUTRONS

For systems of protons and neutrons, the above method is not sufficient to calculate the pairing energy. In order to evaluate pairing energies for the proton-neutron system, we first calculate the general expression for Racah's fractional parentage coefficients.

It has been pointed out by Racah [6]) and Teitelbaum [7]) that the general formula for the fractional parentage coefficient can be obtained algebraically for states with seniority quantum number $\mathscr{S} = 1$. By applying their method, therefore, a general expression for the pairing energy can be obtained for states with seniority quantum number $\mathscr{S} = 1$. To illustrate this we shall show the procedure in the j–j representation.

First we wish to show the procedure used in calculating fractional parentage coefficients which are related to the evaluation of the pairing force.

In the following, we use only $(\mathscr{S}, t)$, T and if necessary J or L and S among all the quantum numbers in schemes 3 and 4.

In order to obtain the fractional parentage coefficients $[j^n(0, 0)T\{j^{n-2}(00)T_1, j^2(00)1]$ we first calculate the fractional parentage coefficient $[j^n(00)T\{j^{n-1}(1, \tfrac{1}{2})T \pm \tfrac{1}{2}, j^1]$.

First let us recapitulate the procedure used by Racah and Teitelbaum. By using the normalization condition and also the equation $\sum_i t_{\zeta i} = T_\zeta = T$, we obtain the following equations:

$$[j^n(0, 0)T\{j^{n-1}(1, \tfrac{1}{2})T+\tfrac{1}{2}, j^1]^2+[j^n(0, 0)T\{j^{n-1}(1, \tfrac{1}{2})T-\tfrac{1}{2}, j^1]^2 = 1, \tag{9}$$

$$[j^n(0,0)T\{j^{n-1}(1,\tfrac{1}{2})T+\tfrac{1}{2},j^1]^2\frac{-T}{2T+2}$$

$$+[j^n(0,0)T\{j^{n-1}(1,\tfrac{1}{2})T-\tfrac{1}{2},j^1]^2\times\tfrac{1}{2}=\frac{T}{n}. \tag{10}$$

Hence it follows that

$$[j^n(0,0)T\{j^{n-1}(1,\tfrac{1}{2})T+\tfrac{1}{2},j^1]^2=\frac{(n-2T)(T+1)}{n(2T+1)}, \tag{11}$$

$$[j^n(0,0)T\{j^{n-1}(1,\tfrac{1}{2})T-\tfrac{1}{2},j^1]^2=\frac{(n+2T+2)(T)}{n(2T+1)}. \tag{12}$$

Thus $[j^n(0,0)T\{j^{n-2}(0,0)T\pm1,j^2(0,0)1]^2$ can be expressed as

$$[j^n(0,0)T\{j^{n-2}(0,0)T\pm1,j^2(0,0)1]^2$$
$$=[j^n(0,0)T\{j^{n-1}(1,\tfrac{1}{2})T\pm\tfrac{1}{2},j^1]^2[j^{n-1}(1,\tfrac{1}{2})T\pm\tfrac{1}{2}\{j^{n-2}(0,0)T\pm1,j^1]^2[j]^2[\tau]^2, \tag{13}$$

where $[j]$ and $[\tau]$ are recoupling coefficients on the space-spin function and the isobaric function respectively. In the above special case these are clearly equal to 1.

The quantity $[j^{n-1}(1,\frac{1}{2})T+\frac{1}{2}\{j^{n-2}(0,0)T+1,j^1]^2$ can be easily calculated by using the well known relation

$$[j^{n-1}(1,\tfrac{1}{2})T+\tfrac{1}{2}\{j^{n-2}(0,0)T+1,j^1]^2 \tag{14}$$
$$=\frac{\{4j+2-(n-2)\}\{2(T+1)+1\}}{(n-1)\{2(T+\frac{1}{2})+1\}(2j+1)}[j^{4j+2-(n-2)}(0,0)T+1\{j^{4j+2-(n-2)-1}(1,\tfrac{1}{2})T+\tfrac{1}{2},j^1]^2.$$

Using eq. (12) we obtain for this expression

$$\frac{(4j+8-n+2T)}{2(n-1)(2j+1)}. \tag{15}$$

Thus eq. (13) is reduced to the following form:

$$[j^n(0,0)T\{j^{n-2}(0,0)T+1,j^2(0,0)1]^2=\frac{n-2T}{n}\,\frac{T+1}{2T+1}\,\frac{4j+8-n+2T}{2(n-1)(2j+1)}. \tag{15'}$$

In the same way, it follows that

$$[j^n(0,0)T\{j^{n-2}(0,0)T-1,j^2(0,0)1]$$
$$=[j^n(0,0)T\{j^{n-1}(1,\tfrac{1}{2})T-\tfrac{1}{2},j^1]^2[j^n(1,\tfrac{1}{2})T-\tfrac{1}{2}\{j^{n-1}(0,0)T-1,j^1]^2[j]^2[\tau]^2$$
$$=\frac{n+2T+2}{n}\,\frac{T}{2T+1}\,\frac{4j+6-n-2T}{2(n-1)(2j+1)}. \tag{16}$$

Thus the pairing energy can be obtained as follows:

$$\begin{aligned}(j^n(0,0)T|Q|j^n(0,0)T) &= \tfrac{1}{2}n(n-1)(j^n(0,0)T|q_{12}|j^n(0,0)T) \\ &= \tfrac{1}{2}n(n-1)\{[j^n(0,0)T\{j^{n-2}(0,0)T+1, j^2(0,0)1]^2 \\ &\quad +[j^n(0,0)T\{j^{n-2}(0,0)T-1, j^2(0,0)1]^2\}(j^2(0,0)1|q_{12}|j^2(0,0)1) \\ &= \tfrac{1}{2}n(2j+1-n+2)+\tfrac{1}{4}[n(n+2)-4T(T+1)].\end{aligned} \tag{17}$$

It is clear that eq. (17) is reduced to a special case of eq. (8) when $T = \frac{1}{2}n$.

The same procedure can be applied to the L–S representation and the pairing energy in the L–S representation is

$$(l^n(0,0)T|Q|l^n(0,0)T) = \tfrac{1}{2}n[2(2l+1)-n+2]+\tfrac{1}{4}[n(n+2)-4T(T+1)]. \tag{18}$$

3.3. ODD MASS NUCLEI

Let us proceed to estimate the pairing energy of odd mass nuclei. In order to do this, we need to calculate the fractional parentage coefficients

$$[j^n(1,\tfrac{1}{2})T\{j^{n-2}(1,\tfrac{1}{2})T_1, j^2(0,0)1]. \tag{19}$$

To obtain these we first calculate the following quantities related to the above coefficient:

$$\begin{aligned}&[j^n(1,\tfrac{1}{2})T\{j^{n-1}(0,0)T\pm\tfrac{1}{2}, j^1]^2, \\ &\sum_J [j^n(1,\tfrac{1}{2})T\{j^{n-1}(\mathscr{S},t)JT+\tfrac{1}{2}, j^1]^2_{\mathscr{S},t\neq 0},\end{aligned} \tag{19'}$$

and

$$\sum_J [j^n(1,\tfrac{1}{2})T\{j^{n-1}(\mathscr{S},t)JT-\tfrac{1}{2}, j^1]^2_{\mathscr{S},t\neq 0}.$$

We shall denote these quantities as $C(00\pm)$, $C(\mathscr{S}t+)$, $C(\mathscr{S}t-)$ respectively.

To calculate these we make use of the relations $\sum \mathbf{j}_i = \mathbf{j}$ and $\sum_i \boldsymbol{\tau}_i = \mathbf{T}$ in addition to the normalization condition. Rewriting these equations into a clearer form, we obtain the following equations:

$$C(00+)+C(21+)+C(20+) = \frac{(n-2T)(T+1)}{n(2T+1)}, \tag{20}$$

$$C(00-)+C(21-)+C(20-) = \frac{(n+2T+2)T}{n(2T+1)}, \tag{21}$$

$$\begin{aligned}&(2j+2)C(00+)+C(21+)-C(20+) \\ &\qquad +(2j+2)C(00-)+C(21-)-C(20-) = \frac{2j+2}{n}.\end{aligned} \tag{22}$$

The following subsidiary equations simplify the above equations [7]):

$$\begin{aligned} &C(00+)=0, \quad C(20-)=0, \quad \text{for} \quad N_o>N_e, \\ &C(00-)=0, \quad C(20+)=0, \quad \text{for} \quad N_e>N_o. \end{aligned} \tag{23}$$

Further simplification of eqs. (18)–(20) can be achieved by using the well known reciprocity relation

$$\begin{aligned} C(00+) &= [j^n(1,\tfrac{1}{2})T\{j^{n-1}(0,0)T_1, j^1]^2 \\ &= \frac{(4j+3-n)(2T_1+1)}{n(2T+1)(2j+1)}[j^{4j+3-n}(0,0)T_1\{j^{4j+2-n}(1,\tfrac{1}{2})T, j^1]^2. \end{aligned} \tag{24}$$

The quantity $[j^{4j+3-n}(0,0)T_1\{j^{4j+2-n}(1,\frac{1}{2})T, j^1]^2$ has been obtained in eqs. (11) and (12) and

$$[j^n(1,\tfrac{1}{2})T\{j^{n-1}(0,0)T-\tfrac{1}{2}, j^1]^2 = \frac{(4j+4-n-2T)}{2n(2j+1)} \quad \text{for} \quad N_o>N_e, \tag{25}$$

$$[j^n(1,\tfrac{1}{2})T\{j^{n-1}(0,0)T+\tfrac{1}{2}, j']^2 = \frac{(4j+6-n+2T)}{2n(2j+1)} \quad \text{for} \quad N_e>N_o. \tag{26}$$

Using eqs. 23, 25 and 26, we obtain, in the case of $N_o > N_e$ [7]),

$$\begin{aligned} C(21+) &= \frac{(n-2T)(2T+3)}{4n(2T+1)}, \\ C(21-) &= \frac{(n+2T+2)T}{n(2T+1)} - \frac{4j+4-n-2T}{2n(2j+1)}, \\ C(20+) &= \frac{n-2T}{4n}, \quad C(20-)=0. \end{aligned} \tag{27}$$

In order to obtain (19), we further need to calculate the quantities

$$\begin{aligned} &[j^{n-1}(0,0)T\pm\tfrac{1}{2}\{j^{n-2}(1,\tfrac{1}{2})T\pm 1, j^1]^2, \\ &[j^{n-1}(0,0)T\pm\tfrac{1}{2}\{j^{n-2}(1,\tfrac{1}{2})T, j^1]^2, \\ &\sum_J [j^{n-1}(\mathscr{S},t)T+\tfrac{1}{2}\{j^{n-2}(1,\tfrac{1}{2})JT', j^1]^2_{\mathscr{S},t\neq 0}, \\ &\sum_J [j^{n-1}(\mathscr{S}t)T-\tfrac{1}{2}\{j^{n-2}(1\tfrac{1}{2})JT'', j^1]^2_{\mathscr{S},t\neq 0}, \end{aligned}$$

(where $T'=T+1$ or T and $T''=T-1$ or T), which we shall refer to as

$$\begin{aligned} &\bar{C}(00,\mp\mp), \quad \bar{C}(00\mp), \quad \bar{C}(\mathscr{S},t--) \text{ (in the case } T'=T+1), \\ &\bar{C}(\mathscr{S},t+) \quad \text{(in the case } T'=T), \\ &\bar{C}(\mathscr{S},t++) \text{ (in the case } T''=T-1), \\ &\bar{C}(\mathscr{S},t-) \quad \text{(in the case } T''=T). \end{aligned} \tag{28}$$

These can be calculated by using the reciprocal equations

$$[j^m(\mathscr{S},t)JT\{j^{m-1}(1,\tfrac{1}{2})T_1,j^1]^2$$
$$=\frac{(4j+4-m)(2T_1+1)(2j+1)}{m(2T+1)(2J+1)}\,(j^{4j+4-m}(1,\tfrac{1}{2})T_1\{j^{4j+3-m}(\mathscr{S},t)JT_1,j^1]^2.$$

Thus (19) can be obtained by using (28) together with recoupling coefficients $[j_{12}j_3|j_1j_{23}]^j$ and $[\tau_{12}\tau_3|\tau_1\tau_{23}]^\tau$, where $j_1=j_2=j_3=j$, $j_{12}=J$ and $j_{23}=0$. Further we have $\tau_1=\tau_2=\tau_3=\frac{1}{2}$, $\tau=T$, and $\tau_{23}=1$.

By using eq. (11.8) in ref. [8]), we obtain

$$[j_{12}j_3|j_1j_{23}]^j=\varepsilon\frac{\sqrt{2J+1}}{2j+1}, \tag{30}$$

$$(\tau_{12}\tau_3|\tau_1\tau_{23})^T=\begin{cases}1 & \text{for}\quad \tau_1=T+1\\ \varepsilon\sqrt{\dfrac{T}{2T+1}} & \text{for}\quad \tau_1=T\end{cases}\Bigg\}\ \tau_{12}=T+\tfrac{1}{2},$$
$$\begin{cases}1 & \text{for}\quad \tau_1=T-1\\ \varepsilon\sqrt{\dfrac{T+1}{2T+1}} & \text{for}\quad \tau_1=T\end{cases}\Bigg\}\ \tau_{12}=T-\tfrac{1}{2}. \tag{30'}$$

In the following we refer to them as simply $[j]$ and $[\tau]$.

From the special relation

$$[j^n(1,\tfrac{1}{2})T\{j^{n-1}T\pm\tfrac{1}{2}(\mathscr{S},t)J,j^1]^2=\begin{cases}\dfrac{2J+1}{(2j-1)(j+1)}\,C(\mathscr{S}t\pm) & \text{for}\quad (\mathscr{S}t)=(21),\\ \dfrac{2J+1}{(2j+1)(j+1)}\,C(\mathscr{S}t\pm) & \text{for}\quad (\mathscr{S}t)=(20),\end{cases} \tag{31}$$

it follows that

$$[j^n(1,\tfrac{1}{2})T\{j^{n-2}(1,\tfrac{1}{2})T+1,j^2(0,0)1]$$
$$=\varepsilon_1\sum_J\sqrt{\frac{C(21+)(2J+1)\bar{C}(21--)}{(2j-1)(j+1)\frac{1}{2}(2j-1)}}\,[j]^2[\tau]^2$$
$$+\varepsilon_2\sum_J\sqrt{\frac{C(20+)(2J+1)\bar{C}(20--)}{(2j+1)(j+1)\frac{1}{2}(2j-1)}}\,[j]^2[\tau]^2. \tag{32}$$

Using eq. (30), eq. (32) becomes

$$\varepsilon_1\frac{\sqrt{2(j+1)C(20+)\bar{C}(20--)[\tau]^2}}{2j+1}+\varepsilon_2\frac{\sqrt{2(j+1)C(20+)\bar{C}(20--)[\tau]^2}}{2j+1}. \tag{33}$$

In a similar way it follows that

$$[j^n(1,\tfrac{1}{2})T\{j^{n-2}(1,\tfrac{1}{2})T-1, j^2(0,0)1] \tag{34}$$
$$= \varepsilon_3 \frac{\sqrt{2(2j+1)C(00-)\bar{C}(00++)[\tau]^2}}{2j+1} + \varepsilon_4 \frac{\sqrt{2(2j+1)C(21-)\bar{C}(21++)[\tau]^2}}{2j+1},$$

$$[j^n(1,\tfrac{1}{2})T\{j^{n-2}(1,\tfrac{1}{2})T, j^2(0,0)1]$$
$$= \frac{\sqrt{2(j+1)}}{2j+1}\{\varepsilon^5\sqrt{C(00-)\bar{C}(00-)[\tau]^2} + \varepsilon_6\sqrt{C(21-)\bar{C}(21-)[\tau]^2} \tag{35}$$
$$+\varepsilon_7\sqrt{C(21+)\bar{C}(21+)[\tau]^2} + \varepsilon_8\sqrt{C(20+)\bar{C}(20+)[\tau]^2}.$$

Here, the quantities ε_i are left unknown.

Thus the pairing energies can be calculated as follows:

$$(j^n(1,\tfrac{1}{2})T|Q|j^n(1,\tfrac{1}{2})T)$$
$$= \tfrac{1}{2}n(n-1)\sum_{T_1}[j^n(1,\tfrac{1}{2})Tj^{n-2}(1,\tfrac{1}{2})T_1, j^2(0,0)1]^2\times(2j+1). \tag{36}$$

The ambiguity caused by the unknown signs ε_i can be solved very easily. They can be fixed by calculating pairing energies of some specific configurations, However, the following two conditions seem particularly useful in solving the ambituity.

Firstly, at the limit $j\to\infty$, the pairing energies Q satisfy

$$\frac{Q}{2j+1}\to\tfrac{1}{2}n. \tag{37}$$

Secondly, the pairing energies of two conjugate configurations $Q(j^n)$ and $Q(j^{4j+2-n})$ are connected to each other by the following relation:

$$Q(j^{4j+2-n}) = Q(j^n)+3(2j+1-n). \tag{38}$$

Eq. (38) corresponds to eq. (41) in ref. [4]), which is deduced by Racah for systems of one kind of particle.

As an example of the results obtained above, we shall give the pairing energy of the state $(\mathscr{S}, t) = (1, \frac{1}{2})$, $T = \frac{1}{2}$ in the j^n configuration:

$$[j^n(1,\tfrac{1}{2})T = \tfrac{1}{2}|Q|j^n(1,\tfrac{1}{2})T = \tfrac{1}{2}) = \tfrac{1}{4}(n-1)(n'+3), \tag{39}$$

where

$$n' = 4j+4-n. \tag{39'}$$

All the results obtained above are checked by calculating the pairing energies of some states, using the wave function constructed by the method used in ref. [3]). Also, results for a few particles are checked by using some of the tables of fractional parentage coefficients by Jahn and some of those by Edmond and Flowers for the j–j limit.

Pairing energies of nuclei with $N_e > N_o$ can be calculated by the same method. However, these are directly derived by using the relation (38) and it was found that eq. (39) represents the pairing energy for $N_e > N_o$ as well.

The same method can be applied to the L–S representation. The corresponding equation to (39) in the L–S representation is

$$(l^n(1, \tfrac{1}{2})T = \tfrac{1}{2}|Q|l^n(1, \tfrac{1}{2})T = \tfrac{1}{2}) = \tfrac{1}{4}(n-1)(n'+3), \tag{40}$$

where

$$n' = 4(2l+1)-n+2. \tag{40'}$$

4. The Pairing Energy in Intermediate Coupling Near the *j*–*j* Limit

In this section we deal with the case when the spin-orbit force is so strong that the j–j limit gives a first approximation. In this case an even better result is obtained by taking into account the mixing of the $(j_+)^{n-2}(j_-)^2$ configuration, and excitation of more than four nucleons from the j_+ to the j_- orbit is less important.

Let us assume $\psi^J(j_+{}^{n-2}) = \psi_m{}^J(j_+{}^{n-2}(\mathscr{S}, t)T_1)$ and $\psi^0(j_-{}^2) = \psi_0{}^0(j_-{}^2(0, 0)1)$ to be the normalized eigenfunctions of $n-2$ nucleons in the j_+ orbit and of two nucleons in the j_- orbit respectively. Then the eigenfunction $\Psi = \Psi(j_+{}^{n-2}\, j_-{}^2 (\mathscr{S}, t)T\{j_+{}^{n-2}(\mathscr{S}, t)T_1, j_-{}^2(0, 0)1)$ of n nucleons is written as

$$\Psi = \sqrt{\frac{2}{n(n-1)}} \sum_p \varepsilon_p PC\psi^J(j_+{}^{n-2})\psi^0(j_-{}^2), \tag{41}$$

where C is a Wigner coefficient for isobaric spin to form total isobaric spin T.

From this it can be easily derived that

$$\begin{aligned}(\Psi|Q|\Psi) &= (\psi^J(j_+{}^{n-2})|\sum_{ij>n-1} q_{ij}|\psi^J(j_+{}^{n-2}))+(\psi^0(j_-{}^2)|q(n-1, n)|\psi^0(j_-{}^2)) \\ &= Q(j_+{}^{n-2}(\mathscr{S}, t)T_1)+Q(j_-{}^2(0, 0)1).\end{aligned} \tag{42}$$

In the particular case when $(\mathscr{S}, t) = (1, \frac{1}{2})$ and $T = \frac{1}{2}$, eq. (42) becomes

$$\tfrac{1}{4}((n-2)-1)(4j_+ +4-(n-2)+3)+(2j_-+1). \tag{43}$$

It is quite evident that

$$(\Psi|Q|\Psi') = 0,$$

where

$$\Psi' = \sqrt{\frac{2}{n(n-1)}} \sum_p \varepsilon_p PC\Psi_m{}^{J'}(j_+{}^{n-2}\mathscr{S}' t' T'_1)\psi_0{}^0(j_-{}^2) \tag{44}$$

and

$$(\mathscr{S}', t', T') \neq (\mathscr{S}, t, T).$$

Let us calculate non-diagonal matrix elements of the pairing force between the pure j–j component $\Psi(j_+^n(1,\frac{1}{2})T=\frac{1}{2})$ and the component (41).

In contrast to the expression (41), the pure j–j component can be written in the following form:

$$\begin{aligned}\Psi(j_+^n(1,\tfrac{1}{2})T=\tfrac{1}{2}) &= f\psi(j_+^{n-2}(3,t)T_1)\psi(j_+^2(1t')) \\ &+[j_+^n(1,\tfrac{1}{2})\tfrac{1}{2}\{j_+^{n-2}(1,\tfrac{1}{2})\tfrac{1}{2},\, j_+^2(0,0)1]C\psi(j_+^{n-2}(1,\tfrac{1}{2})\tfrac{1}{2})\psi_0{}^0(j_+^2(0,0) \\ &+[j_+^n(1,\tfrac{1}{2})\tfrac{1}{2}\{j_+^{n-2}(1,\tfrac{1}{2})\tfrac{3}{2},\, j_+^2(0,0)1]C\psi(j_+^{n-2}(1,\tfrac{1}{2})\tfrac{3}{2})\psi^0(j_+^2(0,0)1), \quad (45)\end{aligned}$$

where the quantities C are Wigner coefficients to form the $T=\frac{1}{2}$ total isobaric function.

Thus it easily follows that

$$\begin{aligned}&(\Psi(j_+^n(1,\tfrac{1}{2})\tfrac{1}{2})|Q|\Psi(j_+^{n-2}j_-^2(1,\tfrac{1}{2})\tfrac{1}{2})\{j_+^{n-2}(1,\tfrac{1}{2})\tfrac{1}{2},\, j_-^2(0,0)1\}) \\ &\quad=\sqrt{\tfrac{1}{2}n(n-1)}[j_+^n(1,\tfrac{1}{2})\tfrac{3}{2}\{j_+^{n-2}(1,\tfrac{1}{2})\tfrac{1}{2}, \quad j_+^2(0,0)1]\sqrt{(2j_++1)(2j_-+1)}, \quad (46)\\ &(\Psi(j_+^n(1,\tfrac{1}{2})\tfrac{1}{2})|Q|\Psi(j_+^{n-2}j_-^2(1,\tfrac{1}{2})\tfrac{1}{2}\{j_+^{n-2}(1,\tfrac{1}{2})\tfrac{1}{2},\, j_-^2(0,0)1)) \\ &\quad=\sqrt{\tfrac{1}{2}n(n-1)}[j_+^n(1,\tfrac{1}{2})\tfrac{1}{2}\{j_+^{n-2}(1,\tfrac{1}{2})\tfrac{3}{2},\, j_+^2(0,0)1]\sqrt{(2j_++1)(2j_-+1)}. \quad (47)\end{aligned}$$

Thus the eigenfunction of the Hamiltonian which consists of a strong one body spin orbit force and the pairing energy can be obtained by diagonalizing the following matrix:

$$\begin{pmatrix} \tfrac{1}{4}(n-1)(n'+3) & \sqrt{\tfrac{1}{2}n(n-1)(2j_++1)(2j_-+1)} \times[j_+^n(1,\tfrac{1}{2})\tfrac{1}{2}\{j_+^{n-2}(1,\tfrac{1}{2})\tfrac{1}{2}, j_+^2(0,0)1] & \sqrt{\tfrac{1}{2}n(n-1)(2j_++1)(2j_-+1)} \times[j_+^n(1,\tfrac{1}{2})\tfrac{1}{2}\{j_+^{n-2}(1,\tfrac{1}{2})\tfrac{3}{2}, j_+^2(0,0)1] \\ \sqrt{\tfrac{1}{2}n(n-1)(2j_++1)(2j_-+1)} \times[j_+^n(1,\tfrac{1}{2})\tfrac{1}{2}\{j_+^{n-2}(1,\tfrac{1}{2})\tfrac{1}{2}, j_+^2(0,0)1] & Q(j_+^{n-2}(1,\tfrac{1}{2})T=\tfrac{1}{2})+Q(j_-^2(0,0))-k & 0 \\ \sqrt{\tfrac{1}{2}n(n-1)(2j_++1)(2j_-+1)} \times[j_+^n(1,\tfrac{1}{2})\tfrac{1}{2}\{j_+^{n-2}(1,\tfrac{1}{2})\tfrac{3}{2}, j_+(0,0)1] & 0 & Q(j_+^{n-2}(1,\tfrac{1}{2})T=\tfrac{3}{2})+Q(j_-^2(0,0))-k \end{pmatrix}$$

where $k=(2l+1)V_{ol}/V^0$.

The mixing of the component (43) is particularly appreciable when n approaches $4j_++1$, because the pairing energy (40) at the j–j limit becomes smaller than the pairing energy (43) of the state (41); the difference between the pairing energies (43) and (40) then compensates for the loss in spin orbit energy at a certain value of the ratio V_{ol}/V^0. In this particular case, the matrix (48) is

$$\sqrt{\tfrac{2}{3}j_+}\sqrt{(2j_-+1)}\begin{pmatrix} 0 & 1 & \sqrt{8} \\ 1 & \dfrac{(2j_++2j_--3-k)}{\sqrt{\frac{2}{3}j_+(2j_-+1)}} & 0 \\ \sqrt{8} & 0 & \dfrac{2j_++2j_--5-k}{\sqrt{\frac{2}{3}j_+(2j_-+1)}} \end{pmatrix}+\tfrac{1}{4}(n-1)(n'+3). \quad (49$$

5. Magnetic Moments of Ground States of B^{11}, Al^{27} and V^{51}

It should be mentioned that the magnetic moments of light nuclei deviate from values calculated for both the j–j and L–S limits at and near $n = 4j_+ + 1$. We apply the result obtained in the previous section to nuclei with $n = 4j_+ + 1$, i.e. B^{11} and Al^{27}, and show the calculated magnetic moments as functions of the parameter $V^0/V_{\sigma l}$.

Inserting $\frac{5}{3}$, $\frac{3}{2}$ and $\frac{3}{2}$, $\frac{1}{2}$ for j_+ and j_- in (49), and diagonalizing it, we obtain eigenfunctions for B^{11} and Al^{27}. Magnetic moments of each component of the eigenfunctions thus obtained can be easily calculated by the method used in (I) and ref. [3]) or the method used by Racah [6]) and Teitelbaum [7]).

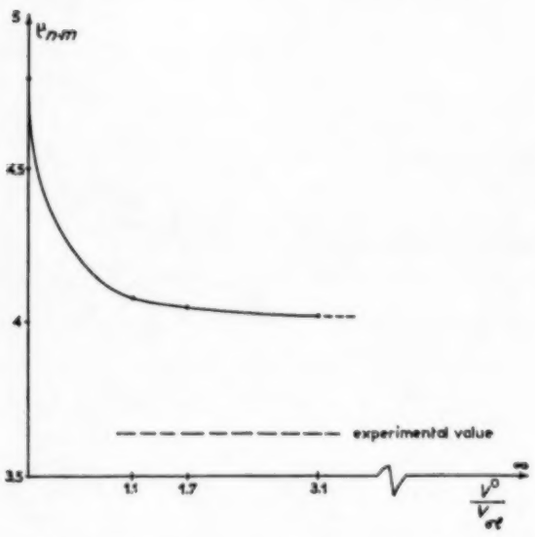

Fig. 1. The magnetic moment of Al^{27} for five values of the ratio $V^0/V_{\sigma l}$.

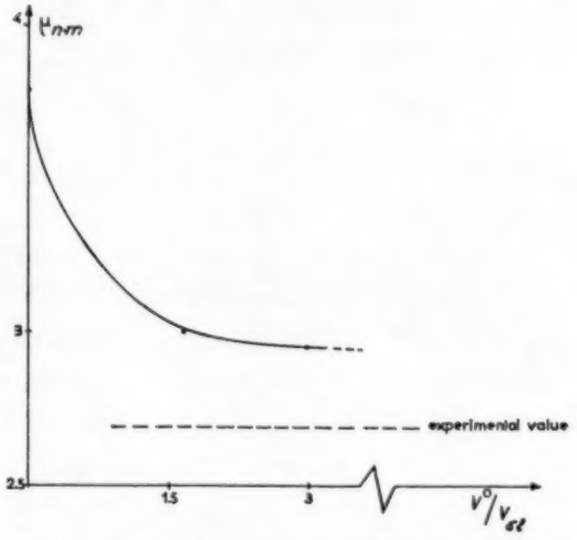

Fig. 2. The magnetic moment of B^{11} for four values of the ratio $V^0/V_{\sigma l}$.

The final values calculated for the magnetic moments are shown in figs. 1 and 2. In both cases, pure j–j components are about 50 % at $V_{\sigma l}/V^0 = \frac{3}{5}$ and $\frac{1}{3}$ for Al^{27} and B^{11} respectively.

In both cases, the magnetic moments obtained are very much nearer to the experimental value than those calculated at the j–j limit. Remaining deviations from experimental values at $V_{\sigma l}/V^0 = \frac{3}{5}$, $\frac{1}{3}$ for Al^{27} and B^{11} may be accounted for by taking into account the excitation of more than two particles into the j_- orbit.

The magnetic moment is also calculated for V^{51} as a function of the parameter $V_{\sigma l}/V^0$. The result is found not to be very different from the result obtained in ref. [5]). To avoid further complication we shall make use of the result obtained in ref. [5]). There, the pure j–j component was found to be 50 % at $V_{\sigma l}/V^0 = \frac{10}{7}$.

For a two-particle system in the f orbit, the pure j–j component is found to be the overwhelming part of the eigenfunction at $V_{\sigma l}/V^0 = \frac{10}{7}$. However, in the d orbit, the pure j–j component is larger at $V_{\sigma l}/V^0 = \frac{3}{5}$ but not overwhelmingly

predominant. For a two particle system in the p orbit, the pure j–j component is no longer particularly large at $V_{\sigma l}/V^0 = \frac{1}{3}$. This may give an interesting insight into the effectiveness of the j–j coupling scheme for light nuclei.

Judging from the values $\frac{10}{7}$, $\frac{5}{3}$ and $\frac{1}{3}$ at V^{51}, Al^{27} and B^{11}, $V_{\sigma l}/V^0$, may not be constant and the pure j–j coupling scheme may be applied only for relatively heavier nuclei. However, the above calculations fix the lowest necessary values of $V_{\sigma l}/V^0$ to explain the magnetic moments of nuclei. Therefore it is not possible to deduce decisive conclusions regarding the dependency of the ratio $V_{\sigma l}/V^0$ on orbital angular momentum l. We hope to be able to limit the value of this ratio further by calculating intermediate cases near the L–S limit.

However, it is quite evident that the extreme short range force represented by $\delta(\mathbf{r}_i - \mathbf{r}_j)(\frac{1}{2} - 2(\boldsymbol{\sigma}_i \cdot \boldsymbol{\sigma}_j))$ is not suitable, since this force gives a factor $(-1)^l$ to the pairing energy of a configuration $(l)^n$.

6. Concluding Remarks

In sect. 4 it was shown that, in intermediate coupling near the j–j limit, the configuration mixing is most significant near closure of a j–j subshell. Results are applied to the magnetic moments of B^{11}, Al^{27} and V^{51} and considerable improvement is achieved of the agreement with the experimental moments. However, the effect of a quadrupole force has not yet been estimated. We hope to estimate it in a future paper.

Lastly, we wish to give a very brief account of the relation between the Bogoliubov treatment [11]) and ours.

In case of a singlet nuclear potential without spin orbit force, the pairing energy will be derived separately for protons and neutrons by the Bogoliubov-Valatin transformation

$$C_\alpha = U_a a_\alpha + S_\alpha V_a a_\alpha^* \quad \text{and its conjugate,} \tag{50}$$

where

$$\alpha = (l_z, \sigma_z).$$

The notations used in eq. (50) are those used in ref. [11]).

It should be mentioned that this transformation ignores the interaction between proton and neutron and loses some parts of the pairing energy in (40).

With a strong spin orbit force in addition to the nuclear potential, we have to use the following transformations:

$$\begin{aligned} C_\xi &= U_a a_\xi + S_\xi V_a a_{-\xi}^* \quad \text{and its conjugate,} \\ C_\eta &= U'_a a_\eta + S_\eta V'_a a_{-\eta}^* \quad \text{and its conjugate,} \end{aligned} \tag{51}$$

where $\xi = j_{+_a}$ and $\eta = j_{-_a}$.

For the pure j–j limit, U, V are chosen so that

$$\sum C_\xi^* C_\xi = n. \tag{52}$$

For intermediate coupling near the j–j limit, corresponding to eq. (41), U, V, U' and V' are chosen so that

$$\sum_\xi C_\xi^* C_\xi = n-2, \quad \sum_\eta C_\eta^* C_\eta = 2. \tag{53}$$

Because of the presence of the spin-orbit force, the pairing force accompanying the singlet nuclear potential is not diagonal in these representations. Therefore, Bogoliubov's vacuum states which satisfy (52) and (53) respectively interact strongly with each other.

A full explanation of the relation between the Bogoliubov treatment and our treatment will be given in a future paper. Also the competition between spin-orbit force and the general type of nuclear force will be dealt with in a future paper.

The author wishes to express his deep gratitude to Prof. Gorodetzky who made it possible for him to carry out this work at the Centre de Recherches Nucléaires in Strasbourg. The author also would like to thank Prof. Gallmann and Dr. Knipper for kindly letting me use their facilities. Deep thanks are also due to Dr. Ullmann who has kindly read this paper and made it presentable.

References

1) V. G. Soloviev, Nuclear Physics **9** (1958) 655
1a) M. G. Mayer, Phys. Rev. **78** (1950) 16
2) M. Umezawa, Proc. Roy. Soc. A **232** (1955) 88 (referred to as (I))
3) M. Umezawa, Progr. Theor. Phys. **8** (1952) 509
4) G. Racah, Phys. Rev. **63** (1943) 367
5) M. Umezawa, Nuclear Physics, to be published
6) G. Racah, Birmingham Conference of 1953
7) P. Teitelbaum, Bulletin Research Council Israel **3** (1954) 299
8) U. Fano and G. Racah, Irreducible Tensorial Sets (Academic Press, New York)
9) H. A. Jahn and H. van Wieringen, Proc. Roy. Soc. A **209** (1951) 502
10) B. H. Flowers and A. R. Edmonds, Proc. Roy. Soc. A **214** (1952) 515
11) M. Baranger, Phys. Rev., to be published

1.D.3 *Nuclear Physics* **25** (1961) 674—686; © *North-Holland Publishing Co., Amsterdam*

Not to be reproduced by photoprint or microfilm without written permission from the publisher

PAIRING PLUS QUADRUPOLE FORCE MODEL FOR ODD-MASS SINGLE CLOSED SHELL NUCLEI

RAYMOND A. SORENSEN

Department of Physics, Columbia University, New York, New York †

Received 27 January 1961

Abstract: An intermediate coupling calculation is performed for odd-mass nuclei with the neutrons or protons at a closed shell. The Hamiltonian, an adiabatic approximation to the pairing force plus quadrupole Hamiltonian, is diagonalized to include all states containing up to two phonons of quadrupole vibration. The validity of the approximations is discussed. The level energies and wave functions resulting from the calculation are compared with experimental results and with the results of ref. [1]).

1. Introduction

It has been shown by detailed calculations [1]) that many of the low energy properties of spherical nuclei can be understood on the basis of a nuclear model first studied in detail by Belyaev [2]). This was an interacting shell model in which the particles moving in the single particle levels interact with a two body force of two components, a pairing force and a quadrupole force. In refs. [1, 2]) the pairing force was treated in the quasi-particle approximation [3]), while for the quadrupole force, adiabatic perturbation theory was used with the cranking model expression for the inertial parameter. For even spherical nuclei this led to a simple collective Hamiltonian for quadrupole vibrations. For the odd-mass isotopes, a collective Hamiltonian was suggested in which the quasi-particles are coupled to the quadrupole vibrations. In the calculations of ref. [1]), this coupling was taken only to lowest order.

The degree of success of this simple nuclear model suggested that it might be of value to improve some of the approximations which have been used. It is the purpose of this paper to present an improved calculation of the effect of the quadrupole interaction on those odd-mass nuclei with the even number of protons or neutrons completely filling a major shell. The validity of the improved approximation is also investigated.

2. The Calculation

An intermediate coupling calculation is made with the collective Hamiltonian of ref. [1])

$$H_{\mathrm{col}} = \tfrac{1}{2}C\sum_{\mu}|Q_{\mu}|^2+\tfrac{1}{2}B\sum_{\mu}|\dot{Q}_{\mu}|^2+\sum_{\nu}E_{\nu}(\alpha_{\nu}^{+}\alpha_{\nu}^{+}+\beta_{\nu}\beta_{\nu}) + \chi\sum_{\nu\nu'\mu}(-1)^{\mu}q_{\nu\nu'}^{-\mu}(U_{\nu}U_{\nu'}-V_{\nu}V_{\nu'})(\alpha_{\nu}^{+}\alpha_{\nu'}+\beta_{\nu'}^{+}\beta_{\nu})Q_{\mu}. \tag{1}$$

† This work was supported in part by the U. S. Atomic Energy Commission.

Here Q_μ is the nuclear quadrupole moment operator and α_ν, β_ν and E_ν are the quasi-particle annihilation operators and energy. C and B are the restoring force and inertial parameters for the collective quadrupole vibration and χ is the coupling parameter of the interaction term. The U, V factor, which comes from the quasi-particle transformation, is a measure of the separation of the quasi-particle energy E_ν from the Fermi energy. Finally $q^\mu_{\nu\nu'} = \langle \nu | r^2 Y_\mu{}^2 | \nu' \rangle$ with $\nu \equiv j$, m is the single particle quadrupole moment. The values of all of these quantities are taken from ref. [1]).

The Hamiltonian (1) is diagonalized including, with the quasi-particles, all admixed states containing up to two phonons of collective vibration. The matrix elements for this calculation aside from the U, V factor are just those given by Chaudhury [4]). In terms of the quantities evaluated in ref. [1]), the no-phonon to one-phonon matrix elements of the interaction are

$$\langle j | (2j')_J \rangle = -\chi \sqrt{\frac{1}{2B\omega}} \sqrt{\frac{5}{4\pi}} \langle j | r^2 | j' \rangle \times C^{2jj'}_{0\frac{1}{2}\frac{1}{2}} (-1)^{j-j'} (U_j U_{j'} - V_j V_{j'}), \tag{2a}$$

while the one-phonon to two-phonon elements are

$$\begin{aligned} \langle (2j)_J | (Ij')_J \rangle = &-\sqrt{2}\chi \sqrt{\frac{1}{2B\omega}} \sqrt{\frac{5}{4\pi}} \langle j | r^2 | j' \rangle C^{2jj'}_{0\frac{1}{2}\frac{1}{2}} \\ &\times (-1)^{j-j'} \sqrt{(2I+1)(2j+1)}\, W(22Jj'; Ij)(U_j U_{j'} - V_j V_{j'}). \end{aligned} \tag{2b}$$

The C and W symbols are Clebsch-Gordan and Racah coefficients and the j, j' are the quasi-particle angular momenta. The 2 is the angular momentum of one phonon while two phonons can couple to $I = 0$, 2, 4. The quantities χ, ω and B are the coupling constant, phonon energy and inertial parameter listed in ref. [1]). Owing to the large number (4 or 5) of near lying quasi-particle levels, the two phonon calculation involves the diagonalization of matrices as large as 14×14. The matrices were generated and diagonalized on the I.B.M. 650 electronic computer furnished by I.B.M. Watson Laboratories in New York. The matrix diagonalization program was kindly furnished by Dr. K. King.

3. The Validity of the Approximation

The validity of the two-phonon cut off may be investigated by examining the no-, one- and two-phonon amplitudes of the low energy states resulting from the diagonalization. The result is that although the one-phonon amplitudes of the lowest state of a given spin are often large (in some cases greater than 0.5) the two-phonon amplitudes are always quite small. In nearly all cases they are less than 0.1.

To investigate the validity of the Hamiltonian (1), the Sawada [5]) approxima-

tion, recently applied to the nuclear problem [6]) †, may be considered. In the quasi-particle approximation, the pairing plus quadrupole Hamiltonian may be written

$$H = \sum_{\nu} E_{\nu}(\alpha_{\nu}^{+}\alpha_{\nu} + \beta_{\nu}^{+}\beta_{\nu}) - \tfrac{1}{2}\chi \sum_{\mu} |\hat{Q}_{\mu}|^2, \tag{3}$$

where

$$\begin{aligned}\hat{Q}_{\mu} = &\sum_{\nu\nu'} q_{\nu\nu'}^{\mu}(U_{\nu}U_{\nu'} - V_{\nu}V_{\nu'})(\alpha_{\nu}^{+}\alpha_{\nu'} + \beta_{\nu'}^{+}\beta_{\nu}) \\ &+ \sum_{\nu\nu'} q_{\nu\nu'}^{\mu}(U_{\nu}V_{\nu'} + V_{\nu}U_{\nu'})(\alpha_{\nu}^{+}\beta_{\nu'}^{+} + \beta_{\nu}\alpha_{\nu'}).\end{aligned} \tag{4}$$

The validity of the quasi-particle approximation will not be discussed here. The Sawada approximation is to drop the first sum of eq. (4). The justification for this is that matrix elements of the first sum will be of single particle magnitude multiplied by the number of quasi-particles, which we expect to be low for the low energy states; while the second sum will have matrix elements proportional to the number of shell model particles filling the associated quasi-particle levels contributing to the low energy states [7]). Thus, for the approximation to be valid, the quadrupole force should be strong enough to mix several quasi-particle pairs into the lowest two quasi-particle state, but not so strong as to put many quasi-particles into the low energy states. Eq. (3) may be solved with this approximation and the resulting wave functions examined to estimate the validity of the approximation.

Consistent with this approximation, the Hamiltonian (3) may be written, for even nuclei, focusing on the $\mu = 0$ degrees of freedom, in the form [8])

$$H = \sum_{i} O_i^{+} O_i \mathscr{E}_i - \tfrac{1}{2}\chi |\sum_{i} Q_i (O_i^{+} + O_{\tilde{i}})|^2, \tag{5}$$

where $\mathscr{E}_i = E_{\nu} + E_{\nu'}$, $i = \nu, \nu'$, $\tilde{i} = \nu', \nu$, $Q_i = q_{\nu\nu'}^{0}(U_{\nu}V_{\nu'} + V_{\nu}U_{\nu'})$ and $O_i = \alpha_{\nu}\beta_{\nu'}$. From the form of the interaction term in (5) and the definition of $q_{\nu\nu'}^{\mu}$, it is clear, after summing on m values, that the quasi-particle states are altered only for pairs of quasi-particles coupled to spin 2+. For these degrees of freedom, the normal mode energies ω of (5) may be obtained as the solutions to [6])

$$\sum_{i} \frac{|Q_i|^2 \mathscr{E}_i}{\mathscr{E}_i^{\,2} - \omega^2} = \frac{1}{2\chi}, \tag{6}$$

where the sum is over all pairs of quasi-particles which can couple to 2+. Eq. (6) depends on treating the O_i as Bose destruction operators with commutation relations $[O_i, O_j^{+}] = \delta_{ij}$. This commutator will be approximately correct for those linear combinations of O_i corresponding to 2+ states, but will generally be most accurately satisfied for the linear combination corresponding to the

† In ref. [6]) further references are given.

lowest normal mode of the Hamiltonian (5). Observe that if for the lowest mode, $\omega \ll \mathscr{E}_i$,

$$\omega^2 \approx \frac{\sum_i \frac{|Q_i|^2}{\mathscr{E}_i}}{\sum_i \frac{|Q_i|^2}{\mathscr{E}_i^3}} \left(1 - 2\chi \sum_i \frac{|Q_i|^2}{\mathscr{E}_i}\right), \tag{7}$$

which agrees with the result of adiabatic perturbation theory [1]). The adiabatic result, eq. (7), is compared to eq. (6) for a typical case in figure 1.

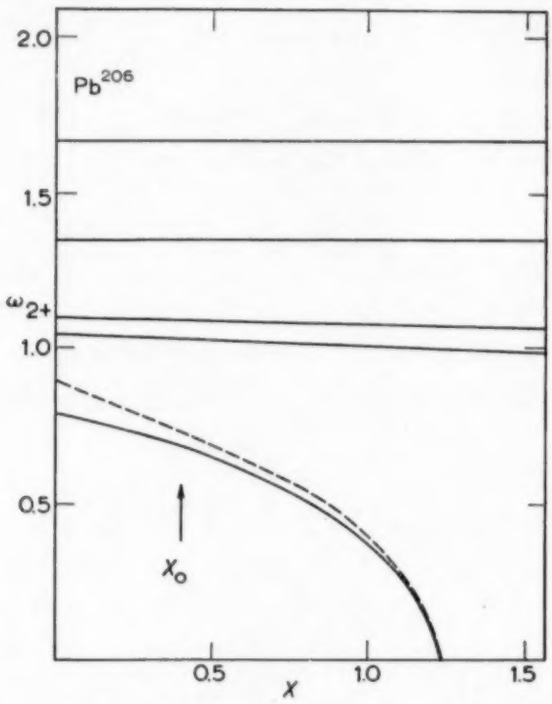

Fig. 1. Energies of typical 2+ levels as a function of the coupling parameter χ. The solid curves represent the 2+ energies ω determined from eq. (6). The dashed curve represents the adiabatic approximation eq. ((7)) used for the lowest 2+ state in ref. [1]). The isotope pictured is Pb^{206}, and X_0 is the coupling parameter actually used for these isotopes here and in ref. [1]). For the other isotopes, see fig. 2.

The Hamiltonian (5) may be written in terms of the normal modes,

$$H = \sum_i O^+_{\omega_i} O_{\omega_i} \omega_i, \tag{8}$$

where the ω_i are the solutions of eq. (6) and

$$O_{\omega_j} = \left(\sum_i \frac{|Q_i|^2 \mathscr{E}_i}{(\mathscr{E}_i^2 - \omega_j^2)^2}\right)^{-\frac{1}{2}} \sum_i \frac{Q_i \sqrt{\mathscr{E}_i}}{\mathscr{E}_i^2 - \omega_j^2}$$
$$\times \tfrac{1}{2} \left\{ O_i \left(\sqrt{\frac{\mathscr{E}_i}{\omega_j}} + \sqrt{\frac{\omega_j}{\mathscr{E}_i}} \right) - O_{\tilde{i}}^+ \left(\sqrt{\frac{\mathscr{E}_i}{\omega_j}} - \sqrt{\frac{\omega_j}{\mathscr{E}_i}} \right) \right\} = \sum_i a_{ji} O_i + \sum_i b_{ji} O_i^+. \tag{9}$$

To calculate the number of quasi-particles in the ground state, the following wave function, obtained by requiring $O_{\omega_i}\Psi_0 = 0$, may be used:

$$\Psi_0 = \exp\{-\tfrac{1}{2}\sum_{ij} O_i^+ c_{ij} O_j^+\}|0\rangle, \tag{10}$$

where $c = a^{-1}b$, matrix multiplication being indicated and $|0\rangle$ is the original quasi-particle vacuum. The low excited states are

$$\Psi_\omega = O_\omega^+ \Psi_0. \tag{11}$$

Sample calculations show that when the lowest ω is about half the energy gap, as seems to be the case with most single closed shell nuclei with the exception perhaps of the lead isotopes, the agreement with adiabatic perturbation theory is quite good. At the same time, the number of quasi-particles in the ground state is quite small (≈ 0) even though there are several different quasi-particle pairs contributing to the lowest 2+ state. The reduced transition rate given by[6])

$$B(\mathrm{E2}) = \left(\sum_i \frac{|Q_i|^2 \mathscr{E}_i}{\mathscr{E}_i^2 - \omega^2}\right)^2 \left[\omega \sum_i \frac{|Q_i|^2 \mathscr{E}_i}{(\mathscr{E}_i^2 - \omega^2)^2}\right]^{-1}, \tag{12}$$

corresponds, under these conditions, to an enhancement of about ten times the single particle value, and is seen to be well approximated by the adiabatic expression [1])

$$B(\mathrm{E2})_{\text{adiabatic}} = \left(\sum_i \frac{|Q_i|^2}{\mathscr{E}_i}\right)^2 \left[\omega \sum_i \frac{|Q_i|^2}{\mathscr{E}_i^3}\right]^{-1}. \tag{13}$$

In fig. 2, eqs. (6), (7) and eqs. (12), (13) are compared for all the nuclei to be considered. Thus, if only those degrees of freedom are considered which correspond to levels lying within the pairing energy gap, the Hamiltonian (8), in general, is well represented by the first two terms of the approximate Hamiltonian (1).

In the quasi-particle approximation for odd-mass nuclei, the low lying states are one-quasi-particle states. The first sum of eq. (4) can scatter these quasi-particles. Thus the cross term in $|\hat{Q}_\mu|^2$ should be included in eq. (3) even though the only quasi-particle pair excitations considered are those due to the second sum of eq. (4). The approximate Hamiltonian for odd-mass nuclei corresponding to eq. (5) may then be written as

$$\begin{aligned} H = &\sum_i O_i^\dagger O_i \mathscr{E}_i - \tfrac{1}{2}\chi \sum_\mu |\sum_i Q^\mu (O_i^\dagger + O_i)|^2 \\ &+ \sum_\nu (\alpha_\nu^+ \alpha_\nu + \beta_\nu^+ \beta_\nu) E_\nu - \chi \sum_\mu [\sum_{\nu\nu'} (-1)^\mu \mathbf{q}_{\nu\nu'}^{-\mu} (\alpha_\nu^+ \alpha_{\nu'} + \beta_{\nu'}^+ \beta_\nu) \sum_i Q_i^\mu (O_i^\dagger + O_i)], \end{aligned} \tag{14}$$

where $\mathbf{q}_{\nu\nu'}^\mu = q_{\nu\nu'}^\mu (U_\nu U_{\nu'} - V_\nu V_{\nu'})$. Eq. (14) depends for its validity not only on the approximate Bose commutation relations for O_i but also on the independence of

the O_i and α_ν, i.e. $[O_i, \alpha_\nu^+] = 0$. This relation will be approximately satisfied for that linear combination O_{ω_j} of eq. (9) corresponding to the lowest ω_j. Eq. (14) may then be written in terms of these degrees of freedom as

$$H = \sum_i O^+_{\omega_i} O_{\omega_i} \omega_i + \sum_\nu (\alpha^+_\nu \alpha_\nu + \beta^+_\nu \beta_\nu) E_\nu$$

$$-\chi \sum_\mu \left[\sum_{\nu\nu'} (-1)^\mu \mathbf{q}^{-\mu}_{\nu\nu'} (\alpha^+_\nu \alpha_{\nu'} + \beta^+_\nu \beta_{\nu'}) \frac{\sum_{ij} \frac{|Q_i|^2 \mathscr{E}_i}{\mathscr{E}_i^2 - \omega_j^2}}{\left(\sum_k \frac{|Q_k|^2 \mathscr{E}_k}{(\mathscr{E}_k^2 - \omega_j^2)^2} \right)^{\frac{1}{2}}} \frac{(O^+_{\omega_j} + O_{\omega_j^-})_\mu}{\sqrt{\omega}} \right], \qquad (15)$$

as can be seen from the inverse transformation to eq. (9). Finally, the approximate Hamiltonian (1) with matrix elements given by eq. (2) is obtained from eq. (15) when only the lowest energy ω_i is included and when the approximation $\omega^2 \ll \mathscr{E}_i$ is made in the sums involving $|Q_i|^2$ in eq. (15).

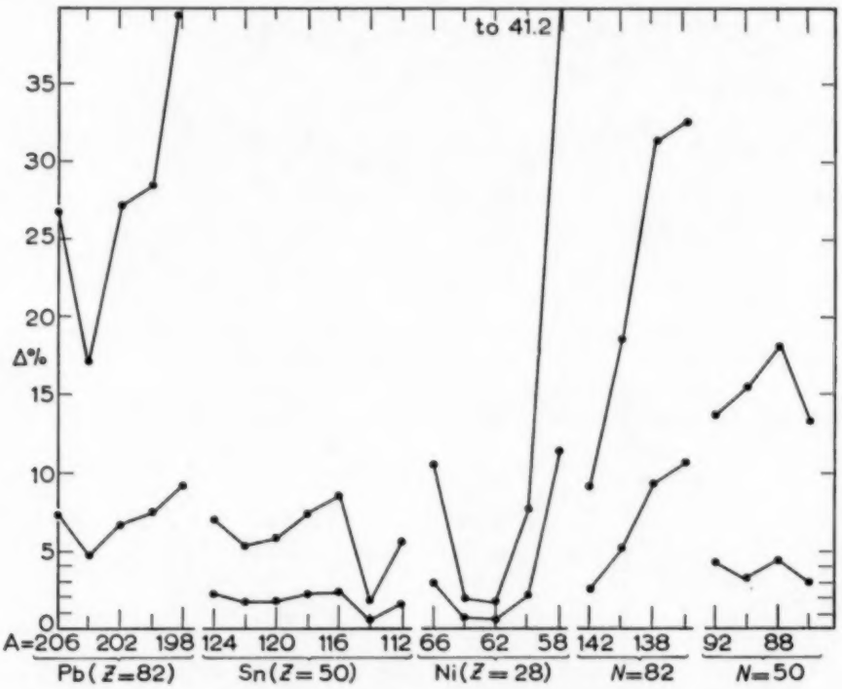

Fig. 2. Fractional difference between the Sawada and adiabatic approximations to the energy and reduced transition rate of lowest 2+ states. The upper curve is $\Delta B(\mathrm{E2})/B(\mathrm{E2})$ adiabatic in %, and the lower curve is $\Delta\omega/\omega$ adiabatic in %, where Δ is the difference between the theoretical results for the first 2+ levels as calculated by the adiabatic approximation (eqs. (7) and (13)) and by the Sawada method (eqs. (6) and (12)). The parameters of ref. [1]) are used in both cases.

4. The Results of the Calculation

The low energy states resulting from this calculation correspond predominantly to mixtures of generalized seniority one (one quasi-particle), and certain seniority three (three quasi-particle) states. The broken pair of the seniority three state is just that combination corresponding to the 2+ phonon to which

the additional odd particle is coupled. At higher energies, $E > 2\Delta$, other three quasi-particle states will enter, but these states are not included in the discussion except in the cases of Ni^{59} and Ni^{61}.

For each isotope all the level energies, spins and parities are listed up to some energy cut off determined mainly by the availability of experimental data. The wave functions are a linear combination of pure quasi-particle (no phonon), of quasi-particle plus one phonon and (with small amplitudes) of quasi-particle plus two phonon. For each nuclear state there is only one pure quasi-particle amplitude, but several different amplitudes for the various one and two phonon parts of the wave function. For simplicity, then, and because it is of particular interest, only the magnitude of the pure quasi-particle amplitude is listed with each state. The complete wave functions of these states and those of higher energy have been computed and may be obtained from the author.

The isotopes of each nuclear region will be discussed separately and compared with the results of ref. [1]) and with experimental data.

4.1. THE Pb ISOTOPES

The results of the calculation for the Pb isotopes, shown in table 1, should not be taken too seriously as far as the effect of the $P^{(2)}$ force is concerned. Firstly, it can be seen from fig. 2 that the adiabatic approximation is quite poor.

TABLE 1

Energies, spins, parities and pure quasi-particle amplitude calculated for the low-lying states of the odd-mass Pb isotopes

	E	$J\pi$	Ampl.
Pb^{197}	0.00	$\frac{3}{2}-$	0.99
	0.10	$\frac{5}{2}-$	0.99
	0.27	$\frac{13}{2}+$	0.99
	0.45	$\frac{1}{2}-$	0.96
Pb^{199}	0.00	$\frac{3}{2}-$	0.99
	0.03	$\frac{5}{2}-$	0.99
	0.34	$\frac{1}{2}-$	0.97
	0.42	$\frac{13}{2}+$	0.99
Pb^{201}	0.00	$\frac{5}{2}-$	0.99
	0.06	$\frac{3}{2}-$	0.99
	0.25	$\frac{1}{2}-$	0.98
	0.58	$\frac{13}{2}+$	0.98

	E	$J\pi$	Ampl.
Pb^{203}	0.00	$\frac{5}{2}-$	0.99
	0.14	$\frac{1}{2}-$	0.99
	0.15	$\frac{3}{2}-$	0.98
	0.77	$\frac{13}{2}+$	0.98
	0.90	$\frac{1}{2}-$	0.07
	0.90	$\frac{5}{2}-$	0.05
	0.90	$\frac{7}{2}-$	0.07
	0.90	$\frac{9}{2}-$	0.00
	0.91	$\frac{3}{2}-$	0.06
	1.00	$\frac{7}{2}-$	0.30
	1.03	$\frac{1}{2}-$	0.00
	1.04	$\frac{3}{2}-$	0.00
	1.04	$\frac{5}{2}-$	0.03
	1.04	$\frac{9}{2}-$	0.04
	1.06	$\frac{9}{2}-$	0.13

	E	$J\pi$	Ampl.
Pb^{205}	0.00	$\frac{1}{2}-$	0.99
	0.03	$\frac{5}{2}-$	0.99
	0.27	$\frac{5}{2}-$	0.98
	0.80	$\frac{3}{2}-$	0.06
	0.80	$\frac{5}{2}-$	0.00
	0.82	$\frac{1}{2}-$	0.00
	0.82	$\frac{7}{2}-$	0.05
	0.82	$\frac{9}{2}-$	0.00
	0.84	$\frac{3}{2}-$	0.10
	0.84	$\frac{9}{2}-$	0.12
	0.97	$\frac{13}{2}+$	0.98
	1.03	$\frac{7}{2}-$	0.20
	1.05	$\frac{1}{2}-$	0.04
	1.06	$\frac{9}{2}-$	0.05
	1.09	$\frac{9}{2}-$	0.14

In the first column, the energies are listed in MeV, with the ground state taken as 0.0 MeV. The second column lists the spin and parity of the level. The third column contains the amplitude of the pure quasi-particle (of the spin and parity of column two) component of the normalized wave function of the corresponding state. The complete wave functions may be obtained from the author.

Secondly, for Pb^{205}, a three neutron hole system, the two-phonon states, corresponding to seniority five, are non-existent in fact.

In any case, table 1 shows that the effect of quadrupole coupling is small. The quasi-particle states remain very nearly pure, the smallest amplitude being 0.96, and furthermore the energy shifts of these states are given quite accurately by the perturbation treatment of ref. [1]). Thus the agreement with experiment evident in ref. [1]) particularly with respect to the M4 transition energy and rate is maintained.

Now, however, we have also the energies of the one-phonon states. Note that for Pb^{205} there are one-phonon states below as well as above the $i_{\frac{13}{2}}$ quasi-particle level. This in agreement with Alburger [9]) and Stockendal [10]) who find a $\frac{7}{2}-(\frac{9}{2}-)$ at 0.703, a $\frac{9}{2}-$ at 0.988 and $\frac{13}{2}+$at 1.014. The other predicted low energy phonon states are not seen experimentally. For Pb^{203} and the lighter odd Pb isotopes, the phonon states are all higher in energy than the $i_{\frac{13}{2}}$ state. This is consistent (except for Pb^{203} which has a $\frac{7}{2}$, $\frac{9}{2}-$ at 0.820 and the $\frac{13}{2}+$ at 0.825 MeV) with the non-observation of the phonon states and with the isomerism of the $\frac{13}{2}$ level.

4.2. THE Sn ISOTOPES

The Sn results are shown in table 2. It may be seen from fig. 2 that the adiabatic approximation is quite good for these isotopes. Also, the neutron numbers are not too near the major shell closings at $N = 50$ and $N = 82$. Thus, the calculation may be reasonably valid for these isotopes. The lowest two or three states of each of the odd-mass Sn isotopes have a large (> 0.90) pure quasi-particle amplitude. The energies of these levels are in good agreement with the available experimental information as was already noted in ref. [1]). Owing to lack of experimental information, only the lowest states are listed in table 2 for Sn^{109}—Sn^{115}.

For the higher excited states, the perturbation approximation of ref. [1]) is entirely inadequate. Two important effects occur. Firstly, there are large energy shifts which lower, considerably, the energy of the first excited $\frac{5}{2}+$ and $\frac{7}{2}+$ levels with respect to the ground states of the heavy Sn isotopes. Secondly, the wave functions of most states become complicated mixtures of the no-phonon and one-phonon amplitudes so that three or four different levels in one isotope may have an appreciable amplitude for a particular pure quasi-particle. For example, in Sn^{125}, there is a pure $\frac{5}{2}+$ quasi-particle amplitude of greater than 0.28 in the four levels at 1.07, 2.08, 2.68 and 2.75 MeV. As examples of the computed wave functions consider the two lowest $\frac{5}{2}+$ levels of Sn^{125} at 1.07 and 1.38 MeV. The 1.07 MeV wave function is $0.47\,|\frac{5}{2}\rangle + 0.65\,|(2_{\frac{1}{2}}^{1})_{\frac{5}{2}}\rangle - 0.47\,|(2_{\frac{3}{2}}^{3})_{\frac{5}{2}}\rangle +$ smaller contributions. The 1.38 MeV wave function is $0.50\,|(2_{\frac{1}{2}}^{1})_{\frac{5}{2}}\rangle + 0.80\,|(2_{\frac{3}{2}}^{3})_{\frac{5}{2}}\rangle +$ smaller contributions. The $|\frac{5}{2}\rangle$ is the pure $\frac{5}{2}+$ quasi-particle state while

TABLE 2

The Sn isotopes (see the caption of table 1)

	E	$J\pi$	Ampl.
Sn^{109}	0.00	$\frac{7}{2}+$	0.99
	0.02	$\frac{5}{2}+$	0.98
Sn^{111}	0.00	$\frac{7}{2}+$	0.98
	0.06	$\frac{5}{2}+$	0.96
Sn^{113}	0.00	$\frac{7}{2}+$	0.96
	0.02	$\frac{1}{2}+$	0.93
	0.12	$\frac{5}{2}+$	0.94
	0.18	$\frac{3}{2}+$	0.91
	0.66	$\frac{11}{2}-$	0.89
Sn^{115}	0.00	$\frac{1}{2}+$	0.95
	0.14	$\frac{3}{2}+$	0.94
	0.44	$\frac{7}{2}+$	0.93
	0.47	$\frac{11}{2}-$	0.90
	0.57	$\frac{5}{2}+$	0.91
Sn^{117}	0.00	$\frac{1}{2}+$	0.96
	0.11	$\frac{3}{2}+$	0.97
	0.28	$\frac{11}{2}-$	0.91
	0.70	$\frac{7}{2}+$	0.89
	0.76	$\frac{5}{2}+$	0.81
	1.31	$\frac{3}{2}+$	0.10
	1.41	$\frac{5}{2}+$	0.18
	1.44	$\frac{1}{2}+$	0.12
	1.45	$\frac{7}{2}+$	0.16
	1.45	$\frac{9}{2}-$	0.00
	1.46	$\frac{5}{2}+$	0.30
	1.48	$\frac{3}{2}+$	0.16
	1.57	$\frac{13}{2}-$	0.00
	1.63	$\frac{7}{2}-$	0.00
	1.64	$\frac{15}{2}-$	0.00
	1.74	$\frac{11}{2}-$	0.41
	1.97	$\frac{9}{2}+$	0.00
	2.00	$\frac{11}{2}+$	0.00
	2.01	$\frac{9}{2}+$	0.00
	2.03	$\frac{3}{2}+$	0.14
	2.09	$\frac{7}{2}+$	0.09
	2.14	$\frac{1}{2}+$	0.21
	2.25	$\frac{5}{2}+$	0.14
	2.25	$\frac{7}{2}+$	0.40
	2.32	$\frac{5}{2}+$	0.39
	2.33	$\frac{3}{2}+$	0.02
	2.84	$\frac{7}{2}+$	0.01

	E	$J\pi$	Ampl.
Sn^{119}	0.00	$\frac{1}{2}+$	0.96
	0.08	$\frac{3}{2}+$	0.98
	0.19	$\frac{11}{2}-$	0.94
	0.80	$\frac{5}{2}+$	0.69
	0.83	$\frac{7}{2}+$	0.80
	1.20	$\frac{3}{2}+$	0.04
	1.31	$\frac{1}{2}+$	0.06
	1.31	$\frac{5}{2}+$	0.11
	1.32	$\frac{3}{2}+$	0.03
	1.41	$\frac{13}{2}-$	0.00
	1.46	$\frac{7}{2}+$	0.35
	1.46	$\frac{7}{2}-$	0.00
	1.46	$\frac{15}{2}-$	0.00
	1.53	$\frac{11}{2}-$	0.34
	1.54	$\frac{9}{2}-$	0.00
	1.58	$\frac{5}{2}+$	0.47
	1.97	$\frac{9}{2}+$	0.00
	2.03	$\frac{11}{2}+$	0.00
	2.10	$\frac{9}{2}+$	0.00
	2.15	$\frac{3}{2}+$	0.17
	2.21	$\frac{1}{2}+$	0.23
	2.21	$\frac{7}{2}+$	0.03
	2.31	$\frac{3}{2}+$	0.03
	2.31	$\frac{5}{2}+$	0.15
	2.31	$\frac{7}{2}+$	0.42
	2.32	$\frac{5}{2}+$	0.43
	2.69	$\frac{9}{2}+$	0.01
	2.70	$\frac{1}{2}+$	0.00
	2.70	$\frac{3}{2}+$	0.00
	2.70	$\frac{7}{2}+$	0.00
	2.73	$\frac{9}{2}+$	0.00
	2.77	$\frac{7}{2}+$	0.04
	2.80	$\frac{5}{2}+$	0.05
Sn^{121}	0.00	$\frac{1}{2}+$	0.94
	0.03	$\frac{3}{2}+$	0.96
	0.17	$\frac{11}{2}-$	0.97
	0.86	$\frac{5}{2}+$	0.60
	0.91	$\frac{7}{2}+$	0.68
	1.23	$\frac{3}{2}+$	0.20
	1.27	$\frac{3}{2}+$	0.02
	1.28	$\frac{5}{2}+$	0.03
	1.31	$\frac{1}{2}+$	0.21
	1.40	$\frac{13}{2}-$	0.00
	1.42	$\frac{7}{2}-$	0.00
	1.42	$\frac{15}{2}-$	0.00
	1.45	$\frac{11}{2}-$	0.23
	1.46	$\frac{9}{2}-$	0.00
	1.54	$\frac{7}{2}+$	0.55
	1.73	$\frac{5}{2}+$	0.57
	2.05	$\frac{9}{2}+$	0.00
	2.11	$\frac{11}{2}+$	0.00
	2.29	$\frac{9}{2}+$	0.00
	2.30	$\frac{3}{2}+$	0.16
	2.35	$\frac{1}{2}+$	0.22
	2.36	$\frac{7}{2}+$	0.20
	2.39	$\frac{3}{2}+$	0.04
	2.39	$\frac{5}{2}+$	0.15
	2.39	$\frac{7}{2}+$	0.36
	2.41	$\frac{5}{2}+$	0.45
	2.70	$\frac{1}{2}+$	0.02
	2.78	$\frac{9}{2}+$	0.00

	E	$J\pi$	Ampl.
Sn^{123}	0.00	$\frac{3}{2}+$	0.94
	0.03	$\frac{1}{2}+$	0.91
	0.14	$\frac{11}{2}-$	0.99
	0.95	$\frac{5}{2}+$	0.52
	0.98	$\frac{7}{2}+$	0.55
	1.30	$\frac{3}{2}+$	0.17
	1.30	$\frac{9}{2}+$	0.01
	1.33	$\frac{3}{2}+$	0.23
	1.37	$\frac{1}{2}+$	0.31
	1.38	$\frac{7}{2}-$	0.00
	1.38	$\frac{9}{2}-$	0.00
	1.38	$\frac{13}{2}-$	0.00
	1.38	$\frac{15}{2}-$	0.00
	1.40	$\frac{11}{2}-$	0.08
	1.68	$\frac{7}{2}+$	0.68
	1.90	$\frac{5}{2}+$	0.64
	2.21	$\frac{9}{2}+$	0.00
	2.25	$\frac{11}{2}+$	0.00
	2.46	$\frac{3}{2}+$	0.14
	2.48	$\frac{7}{2}+$	0.37
	2.50	$\frac{9}{2}+$	0.00
	2.51	$\frac{5}{2}+$	0.17
	2.53	$\frac{1}{2}+$	0.18
	2.53	$\frac{3}{2}+$	0.02
	2.55	$\frac{5}{2}+$	0.42
	2.55	$\frac{7}{2}+$	0.10
	2.67	$\frac{11}{2}-$	0.00
	2.68	$\frac{11}{2}-$	0.00
Sn^{125}	0.00	$\frac{3}{2}+$	0.93
	0.06	$\frac{11}{2}-$	0.99
	0.08	$\frac{1}{2}+$	0.90
	1.07	$\frac{5}{2}+$	0.47
	1.07	$\frac{7}{2}+$	0.50
	1.36	$\frac{7}{2}-$	0.00
	1.36	$\frac{9}{2}-$	0.00
	1.36	$\frac{13}{2}-$	0.00
	1.36	$\frac{15}{2}-$	0.00
	1.37	$\frac{11}{2}-$	0.00
	1.38	$\frac{3}{2}+$	0.17
	1.38	$\frac{5}{2}+$	0.07
	1.46	$\frac{1}{2}+$	0.35
	1.47	$\frac{3}{2}+$	0.27
	1.85	$\frac{7}{2}+$	0.75
	2.08	$\frac{5}{2}+$	0.71
	2.26	$\frac{9}{2}+$	0.00
	2.43	$\frac{11}{2}+$	0.00
	2.46	$\frac{9}{2}+$	0.00
	2.63	$\frac{7}{2}+$	0.34
	2.65	$\frac{3}{2}+$	0.11
	2.68	$\frac{11}{2}-$	0.00
	2.68	$\frac{5}{2}+$	0.31
	2.69	$\frac{11}{2}-$	0.00
	2.73	$\frac{3}{2}+$	0.01
	2.75	$\frac{1}{2}+$	0.15
	2.75	$\frac{5}{2}+$	0.28
	2.75	$\frac{7}{2}+$	0.05

$|(2\frac{1}{2})_{\frac{5}{2}}\rangle$ means a $\frac{1}{2}+$ quasi-particle is coupled to a spin 2 phonon to make a total angular momentum $J = \frac{5}{2}$.

These results are of particular interest in connection with data recently obtained by Cohen and Price [11]) on (d, p) and (d, t) reactions in the Sn region. On the basis of a direct interaction interpretation of these experiments, the l value of the stripped (or picked up) neutron may be inferred from the angular distribution of the outgoing proton or triton. In the case of even Sn targets, $J = 0+$ and all the angular momentum of the resulting odd nucleus comes from the stripped (or picked up) neutron so that strong statements may be made concerning the spins and parities of the nuclear levels of the odd Sn isotopes.

Also, the rate at which the reaction proceeds to a particular odd Sn level should depend on the overlap between the wave function for that level, and the wave function obtained by simply adding the neutron (or hole) to the target wave function.

Cohen and Price [11]) and Yoshida [12]) have analyzed the Sn data including the effect of the pairing correlations on the overlap mentioned above. They conclude that there is good agreement, for the level energies and overlaps, between the experiments and the quasi-particle approximation to a pairing force with the parameters of ref. [1]). The exception to this generally good agreement is the $\frac{5}{2}+$ level for which the quasi-particle energy is too high in the heavy isotopes by 0.7—0.8 MeV. The agreement and the exception are both just as expected on the basis of the calculation described here. Table 2 shows that the $\frac{1}{2}+$, $\frac{3}{2}+$ and $\frac{11}{2}-$ levels are in fact fairly pure quasi-particles, while the $\frac{5}{2}+$ level (and the $\frac{7}{2}+$ for which there is little experimental data) are strongly mixed and shifted. Associating the lowest theoretical $\frac{5}{2}+$ levels with the lowest $d\frac{5}{2}$ levels labelled by Cohen one sees that the theoretical level is not too high, but rather too low, but only by about 0.2 MeV for the heavy isotopes. This association is reasonable since the lowest theoretical $\frac{5}{2}+$ level always has a sizable pure $\frac{5}{2}+$ quasi-particle amplitude.

The assignment of spins to higher levels on this basis would seem to be a dubious procedure. For example, the 1.51 MeV state in Sn^{125} labelled $d\frac{5}{2}$ by Cohen and Price might not be $\frac{5}{2}+$. Only the l value can be determined from the angular distributions, the J must come from some model. On the basis of the pairing plus quadrupole model described here, the theoretical $\frac{3}{2}+$ level at 1.47 MeV seems a more likely candidate for this state than the nearest $\frac{5}{2}+$ level with an appreciable pure quasi-particle amplitude, which lies at 2.08 MeV.

That not all the theoretical levels are seen is not surprising since the weakly excited phonon levels could easily be hidden under stronger levels obtainable by a direct interaction on the no-phonon even-mass target. For a more detailed comparison with the data the probability of exciting these phonon levels in (d, p) and (d, t) should be computed and the resulting angular distributions for the various states compared with the experiments.

4.3. THE Ni ISOTOPES

The Ni results for three odd-mass isotopes are listed in table 3. From fig. 2 it is clear that the adiabatic approximation is good for Ni^{63} and Ni^{61}, but not as good for Ni^{59}, a three neutron system.

TABLE 3

The Ni isotopes (see the caption of table 1)

	E	$J\pi$	Ampl.
Ni^{59}	0.00	$\frac{3}{2}-$	0.99
	0.19	$\frac{5}{2}-$	0.94
	0.44	$\frac{1}{2}-$	0.82
	1.53	$\frac{7}{2}-$	0.00
	1.55	$\frac{3}{2}-$	0.05
	1.60	$\frac{5}{2}-$	0.07
	1.69	$\frac{1}{2}-$	0.11
	1.69	$\frac{9}{2}+$	0.00
	1.77	$\frac{7}{2}-$	0.00
	1.85	$\frac{9}{2}-$	0.24
	1.88	$\frac{3}{2}-$	0.10
	2.05	$\frac{5}{2}-$	0.10
	2.06	$\frac{5}{2}-$	0.20
	2.15	$\frac{1}{2}-$	0.55

	E	$J\pi$	Ampl.
Ni^{61}	0.00	$\frac{3}{2}-$	0.95
	0.07	$\frac{5}{2}-$	0.98
	0.17	$\frac{1}{2}-$	0.86
	1.28	$\frac{9}{2}+$	0.00
	1.35	$\frac{5}{2}-$	0.15
	1.35	$\frac{7}{2}-$	0.00
	1.36	$\frac{9}{2}-$	0.01
	1.40	$\frac{1}{2}-$	0.02
	1.40	$\frac{7}{2}-$	0.00
	1.42	$\frac{9}{2}-$	0.13
	1.49	$\frac{3}{2}-$	0.20
	1.51	$\frac{5}{2}-$	0.09
	1.58	$\frac{5}{2}-$	0.20
	1.69	$\frac{1}{2}-$	0.51

	E	$J\pi$	Ampl.
Ni^{63}	0.00	$\frac{3}{2}-$	0.99
	0.09	$\frac{5}{2}-$	0.93
	0.15	$\frac{1}{2}-$	0.96
	1.19	$\frac{9}{2}+$	0.00
	1.22	$\frac{5}{2}-$	0.04
	1.22	$\frac{7}{2}-$	0.00
	1.24	$\frac{1}{2}-$	0.13
	1.24	$\frac{3}{2}-$	0.08
	1.26	$\frac{5}{2}-$	0.06
	1.27	$\frac{7}{2}-$	0.00
	1.33	$\frac{3}{2}-$	0.03
	1.35	$\frac{1}{2}-$	0.25
	1.39	$\frac{5}{2}-$	0.14
	1.61	$\frac{3}{2}-$	0.36
	1.86	$\frac{9}{2}+$	0.76

The calculated levels agree well as observed in ref. [1]) with the few experimental levels with assigned spins. A comparison may also be made with higher excited states. Many, if not all, energy levels of Ni^{59} and Ni^{61} up to about 4 MeV are known from high resolution reaction experiments [13]). These may be compared to the theory simply by counting levels. In Ni^{59} below 2.15 MeV there are 13 predicted levels and 12 experimental levels. In Ni^{61} below 1.69 MeV there are 13 predicted levels and 10 experimental levels. At higher energies, the other three quasi-particle states will enter. If one simply counts all the three quasi-particle and one quasi-particle levels of the pairing force calculation, the following results are obtained. In Ni^{59} below 4.0 MeV, there are 46 predicted levels and 47 experimental levels. In Ni^{61} below 3.4 MeV, there are 47 predicted levels and 36 experimental levels.

4.4. THE ISOTOPES WITH $N = 82$

The adiabatic approximation is not too good in this case. Owing to the scarcity of experimental information, only the lowest levels of La^{139} and Pr^{141}

TABLE 4

The isotopes with 82 neutrons (see the caption of table 1)

	E	$J\pi$	Ampl.
La^{139}	0.00	$\frac{7}{2}+$	0.99
	0.16	$\frac{5}{2}+$	0.97

	E	$J\pi$	Ampl.
Pr^{141}	0.00	$\frac{5}{2}+$	0.97
	0.07	$\frac{7}{2}+$	0.99

are included in table 4. The results are very similar to those of ref. [1]) and agree with the experiments.

4.5. THE ISOTOPES WITH $N = 50$

The results for four of the isotopes are shown in table 5. The adiabatic approximation is seen from fig. 2 to be better than with Pb, but not as good as with the Sn isotopes. The results are quite similar to those of ref. [1]) in agreement with the lowest experimental energy levels, and the predominantly phonon states are higher in energy than most of the experimental data.

TABLE 5

The isotopes with 50 neutrons (see the caption of table 1)

	E	$J\pi$	Ampl.
Rb^{87}	0.00	$\frac{3}{2}-$	0.99
	0.14	$\frac{1}{2}-$	0.99
	0.33	$\frac{5}{2}-$	0.98
	1.29	$\frac{9}{2}+$	0.95
	1.72	$\frac{7}{2}-$	0.00
	1.73	$\frac{1}{2}-$	0.02
	1.73	$\frac{5}{2}-$	0.06
	1.77	$\frac{3}{2}-$	0.12
	1.88	$\frac{3}{2}-$	0.02
	1.88	$\frac{5}{2}-$	0.03
Y^{89}	0.00	$\frac{1}{2}-$	0.99
	0.63	$\frac{3}{2}-$	0.98
	0.91	$\frac{9}{2}+$	0.98
	1.13	$\frac{5}{2}-$	0.97
	2.24	$\frac{5}{2}-$	0.15

	E	$J\pi$	Ampl.
Nb^{91}	0.00	$\frac{1}{2}-$	0.99
	0.06	$\frac{9}{2}+$	0.99
	0.96	$\frac{3}{2}-$	0.97
	1.49	$\frac{5}{2}-$	0.95
	2.31	$\frac{11}{2}+$	0.00
	2.32	$\frac{3}{2}-$	0.19
	2.32	$\frac{5}{2}-$	0.28
	2.33	$\frac{9}{2}+$	0.00
	2.33	$\frac{13}{2}+$	0.00
	2.34	$\frac{9}{2}+$	0.13
	2.35	$\frac{7}{2}+$	0.00
Tc^{93}	0.00	$\frac{9}{2}+$	0.99
	0.45	$\frac{1}{2}-$	0.98
	1.44	$\frac{3}{2}-$	0.94
	1.94	$\frac{5}{2}-$	0.84
	1.95	$\frac{11}{2}+$	0.00
	1.96	$\frac{5}{2}+$	0.00
	1.96	$\frac{7}{2}+$	0.00
	1.96	$\frac{9}{2}+$	0.07
	1.96	$\frac{13}{2}+$	0.00

The result of the calculation for the $N = 28$ isotopes is not shown since the approximations used here are quite poor in those cases.

5. Conclusions

As the wave function of the ground state is always reasonably pure, the considerations of this paper will not affect the perturbation results of ref. [1]) concerning the static moments of the nuclear ground states.

Thus it is seen that the improved treatment of the Hamiltonian, eq. (1), maintains the agreement (or disagreement) with experiment concerning the low-lying levels of the odd-mass spherical nuclei investigated in ref. [1]). At the same time definite predictions are made concerning the energies and wave

functions of the somewhat higher levels. Where experimental data is available, no obvious gross discrepancies with these predictions occur. While the observed agreement with experiment is suggestive, it certainly does not prove the existence of wave functions of the type described here for excited states of odd-mass spherical nuclei. Such a proof must be based on more detailed calculations of the behaviour of the levels described here and a more detailed experimental investigation of the levels in question.

Thanks are due to Ken King and the I.B.M. Watson Computing Center for making their facilities available, and to Dr. M. Baranger, Dr. B. Cohen and Dr. L. S. Kisslinger for valuable discussions.

References

1) L. S. Kisslinger and R. A. Sorensen, Mat. Fys. Medd. Dan. Vid. Selsk. **32**, No. 9 (1960)
2) S. T. Belyaev, Mat. Fys. Medd. Dan. Vid. Selsk. **31**, No. 11 (1959)
3) J. Bardeen, L. N. Cooper and J. R. Schrieffer, Phys. Rev. **108** (1957) 1175;
N. N. Bogolyubov, JETP (USSR) **34** (1958) 58, 73, Nuovo Cim. **7** (1958) 794;
J. G. Valatin, Nuovo Cim. **7** (1958) 843
4) D. C. Chaudhury, Mat. Fys. Medd. Dan. Vid. Selsk. **28**, No. 4 (1954)
5) K. Sawada, Phys. Rev. **106** (1956) 372
6) M. Baranger, Phys. Rev. **120** (1960) 957
7) B. R. Mottelson, Nuclear structure, Cours de l'Ecole d'Eté de Physique Théorique des Houches, 1958 (Dunod Paris, 1959) pp. 297—299
8) G. Wentzel, Phys. Rev. **108** (1957) 1593
9) D. R. Alburger, Phys. Rev. **118** (1960) 1076
10) R. Stockendal, Phys. Rev. **118** (1960) 1074
11) B. L. Cohen and R. E. Price, Phys. Rev. **121** (1961) 1441
12) S. Yoshida, to be published
13) Massachusetts Institute of Technology Laboratory for Nuclear Science progress reports. (1957—1958)

1.E.1:
2.L

Nuclear Physics **25** (1961) 687—697; © *North-Holland Publishing Co., Amsterdam*
Not to be reproduced by photoprint or microfilm without written permission from the publisher

INELASTIC SCATTERING OF HIGH ENERGY PROTONS AND LEVELS OF NUCLEI

YOSHIYUKI SAKAMOTO

Yoshida College, University of Kyoto, Kyoto, Japan

Received 13 February 1961

Abstract: The high energy protons scattered from some levels of nuclei are accounted for by means of the radiative widths or lifetimes of the levels without using the wave functions of the ground and excited states of nuclei. The inelastically scattered protons at high energies give information on the spin, parity and isobaric spin values for the levels. Some levels of C^{12} are considered as examples.

1. Introduction

Amplitudes of high energy nucleons scattered from nuclei are treated as a superposition of those resulting from the interaction between the impinging nucleon and the individual nucleons in the target nucleus. The high energy nucleons elastically scattered from nuclei provide additional information about the two-nucleon interaction, and the nucleons quasi-elastically scattered from a nucleus give information about the structure of the nucleus, especially the momentum distribution of the nucleons in the nucleus. Also, the nucleons inelastically scattered from an excited level of the nucleus are helpful in obtaining information about the level.

Tyrén and Maris [1]) have measured the protons inelastically scattered from levels of various nuclei. Especially, they have measured the differential cross sections and polarizations of the protons scattered from some levels of C^{12} and O^{16}. In particular, the protons scattered from the levels of about 20 MeV excitation, i.e. the levels of dipole γ-resonance regions, have been investigated as functions of the cross sections for dipole γ-absorption and the ratios of spin-flip to no-spin-flip reduced matrix elements of the nucleus [2]). The fair agreement between the experimental data and the calculated results suggested that the investigation of the protons scattered from the levels of the dipole γ-resonance regions would give information on the dipole γ-absorptions and the reduced nuclear matrix elements [2]).

In the present paper, in a similar way as the protons scattered from the levels of dipole γ-resonance regions, the protons scattered from some other levels are explained by making use of the experimental data regarding the nuclear matrix elements, without any other information referring to the wave functions

for the ground and excited states of the nucleus. And it is shown that the investigation of the protons gives information about the excited levels of the nucleus and the nuclear matrix elements between the ground and excited states.

2. Protons Scattered from Levels of Magnetic Dipole Excitation

In this section †, we investigate the protons inelastically scattered from levels of magnetic dipole excitation, and suggest that the measurement of such protons gives a possibility of assigning isobaric spin values to the levels.

Within the framework of the impulse approximation, the amplitude for the scattering of an impinging proton from some initial momentum and spin state into another final state, exciting the nucleus into a certain state, is a superposition of the nucleon-nucleon scattering amplitudes, multiplied by a nuclear factor which depends on the initial and final nuclear states. Thus, the amplitude of the scattered proton is expressed as

$$T = [\tfrac{1}{4}\{3t_1(\boldsymbol{\sigma}_1)+t_0(\boldsymbol{\sigma}_1)\}+\tfrac{1}{4}\{t_1(\boldsymbol{\sigma}_1)-t_0(\boldsymbol{\sigma}_1)\}\boldsymbol{\tau}_1]F_{t,1}(\boldsymbol{\sigma}_j, \boldsymbol{\tau}_j), \tag{2.1}$$

where t_1 and t_0 are the scattering spin matrices with $T = 1$ and 0 for the two-nucleon scattering, $\boldsymbol{\sigma}_1$ and $\boldsymbol{\sigma}_j$ are the spin operators and $\boldsymbol{\tau}_1$ and $\boldsymbol{\tau}_j$ are the isobaric spin operators of the incident and target nucleons, respectively. The nuclear factor $F_{t,1}$ is of the form

$$F_{t,1}(\boldsymbol{\sigma}_j, \boldsymbol{\tau}_j) = \langle \Psi_t\{s_t(j)t_t(j)\}|\sum_j^A \exp[-\mathrm{i}(\mathbf{k}_t-\mathbf{k}_1)\cdot\mathbf{r}_j]\boldsymbol{\sigma}_j\cdot\boldsymbol{\tau}_j|\Phi_1\{s_1(j)t_1(j)\}\rangle \tag{2.2}$$

The symbols have the following meaning: i and f refer to the initial and final states of the system, s and t are the spin and isobaric spin eigenfunctions, $\mathbf{k}_1$ and $\mathbf{k}_t$ are the wave numbers for incident and scattered nucleons and Φ and Ψ are the nuclear wave functions for initial and final states.

After some calculations, similar to those given in ref [2]), the differential cross section for the protons scattered from the level of magnetic dipole excitation of the nucleus with $J = 0$ in the ground state is approximated as

$$\frac{\mathrm{d}\sigma}{\mathrm{d}\Omega}(\theta) = 4\frac{k_1}{k_t}[(1-\rho)(|\beta|^2+|\gamma|^2+|\varepsilon|^2)+2\rho|\delta|^2]|F_{t,1}|^2, \tag{2.3}$$

where ρ is the ratio between the reduced nuclear matrix elements of the target nucleus, whose value [4]) is restricted to lie between 0 and 1. The meaning of the coefficients of the scattering spin matrix α, β, γ, δ and ε is given in ref. [2]).

When the ground and excited states are $T = 0$ and 1, respectively, the nuclear factor is expressed as

$$F_{t,1} = \langle \Psi_t\{s_t(j)t(j)\}|\sum^A \boldsymbol{\sigma}_j\boldsymbol{\tau}_j|\Phi_1\{s_1(j)t_1(j)\}\rangle, \tag{2.4}$$

† Some results of this section were reported in ref. [3]).

at very small scattering angles. If the distributions of the neutrons and protons in the nucleus are assumed to be the same, eq. (2.4) may be approximated as

$$\langle \Psi_f | \sum^{A} \boldsymbol{\sigma}_j \boldsymbol{\tau}_j | \Phi_1 \rangle = 2 \langle \Psi_f | \sum^{Z} \boldsymbol{\sigma}_j \boldsymbol{\tau}_j | \Phi_1 \rangle. \tag{2.5}$$

Meanwhile, the transition matrix element [5]) for the magnetic dipole excitation is given by

$$M_1 = \frac{e\hbar}{2Mc} \left(\frac{3}{4\pi} \right)^{\frac{1}{2}} \langle \Psi_f | \sum^{A} \mu_j \boldsymbol{\sigma}_j \boldsymbol{\tau}_j | \Phi_1 \rangle, \tag{2.6}$$

where μ_j is the magnetic moment of the j-th nucleon in the nucleus. Then, eq. (2.6) is rewritten as

$$\langle \Psi_f | \sum^{A} \boldsymbol{\sigma}_j \boldsymbol{\tau}_j | \Phi_1 \rangle = \frac{2}{\mu_-} M_1 \frac{2Mc}{e\hbar} (\tfrac{4}{3}\pi)^{\frac{1}{2}}, \tag{2.7}$$

where $\mu_- = \mu_p - \mu_n$. Here μ_p and μ_n are the magnetic moments of proton and neutron, respectively.

The radiative width for the level Γ_1, is connected with M_1 by

$$|M_1|^2 = \frac{\Gamma_1}{\kappa^3} \frac{3!!^2}{2 \times 8\pi}, \tag{2.8}$$

where κ is the wave number for emitted photon.

By using eqs. (2.4), (2.7) and (2.8), the differential cross section for the scattered proton is derived from eq. (2.3) as

$$\frac{d\sigma}{d\Omega}(\theta) = 4 \frac{k_f}{k_1} [(1-\rho)(|\beta|^2 + |\gamma|^2 + |\varepsilon|^2) + 2\rho|\delta|^2] \frac{12}{\mu_-{}^2} \frac{\Gamma_1}{\kappa^3} \left(\frac{Mc}{e\hbar} \right)^2. \tag{2.9}$$

Here, β, γ, δ and ε are given by

$$\begin{aligned} \beta &= \tfrac{1}{2}(\beta_{pp} - \beta_{pn}), & \gamma &= \tfrac{1}{2}(\gamma_{pp} - \gamma_{pn}), \\ \delta &= \tfrac{1}{2}(\delta_{pp} - \delta_{pn}), & \varepsilon &= \tfrac{1}{2}(\varepsilon_{pp} - \varepsilon_{pn}), \end{aligned} \tag{2.10}$$

where the subscripts pp and pn indicate the coefficients of the proton-proton and proton-neutron scattering spin matrices, respectively.

When both the ground and magnetic-dipole excited states of the nucleus have $T = 0$, the nuclear factor is given by

$$F_{f,1} = \langle \Psi_f \{ s_f(j) \} | \sum^{A} \boldsymbol{\sigma}_j | \Phi \{ s_1(j) \} \rangle \tag{2.11}$$

instead of by eq. (2.4). The coefficients of the scattering matrix are then expressed as

$$\begin{aligned} \beta &= \tfrac{1}{2}(\beta_{pp} + \beta_{pn}), & \gamma &= \tfrac{1}{2}(\gamma_{pp} + \gamma_{pn}), \\ \delta &= \tfrac{1}{2}(\delta_{pp} + \delta_{pn}), & \varepsilon &= \tfrac{1}{2}(\varepsilon_{pp} + \varepsilon_{pn}), \end{aligned} \tag{2.12}$$

instead of by eq. (2.10).

The polarization of the protons scattered from the level of magnetic dipole excitation is expressed as

$$P(\theta) = \frac{2(1-\rho)\mathrm{Re}\,\gamma^*\beta}{(1-\rho)(|\beta|^2+|\gamma|^2+|\varepsilon|^2)+2\rho|\delta|^2}. \tag{2.13}$$

Now, since the 15.11 MeV level of C^{12} has $T = 1$ and $J = 1^+$, the differential cross section and polarization of the protons scattered from this level are evaluated by setting eq. (2.10) into eqs. (2.9) and (2.13), without any need of using the wave functions for the ground and excited states of the nucleus. Fig. 1

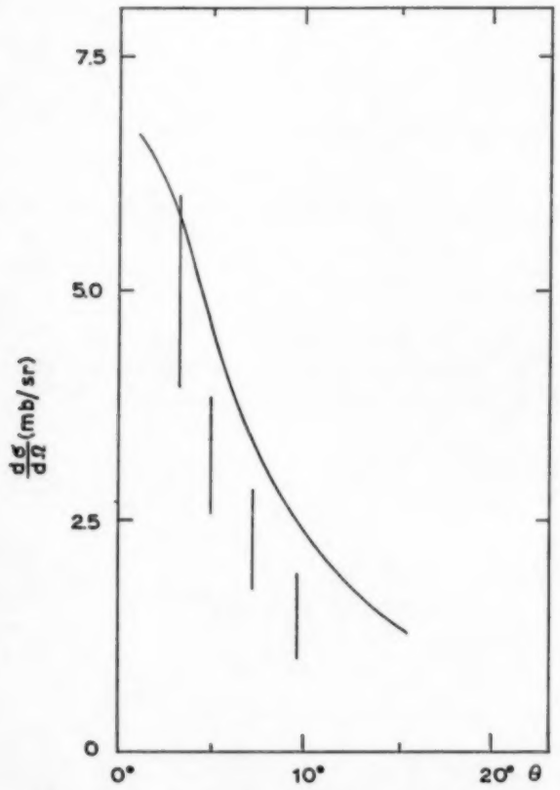

Fig. 1. The experimental and calculated differential cross sections of 180 MeV protons scattered from the 15.11 MeV level of C^{12}. The solid curve indicates the calculated result.

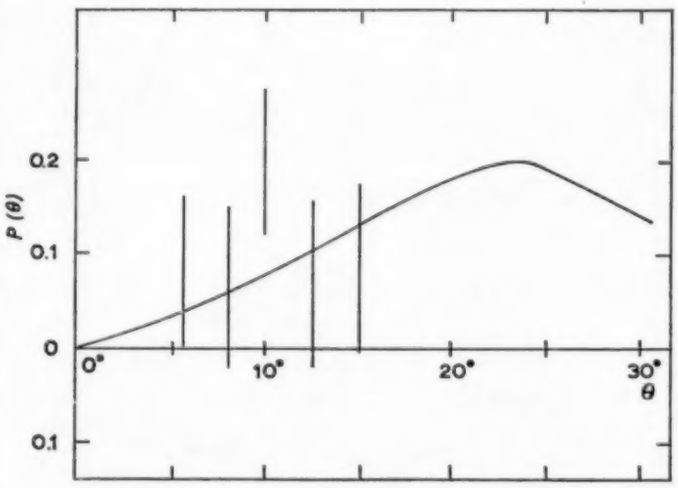

Fig. 2. The experimental and calculated polarizations of 180 MeV protons scattered from the 15.11 MeV level of C^{12}. The solid curve indicates the calculated result.

shows the differential cross section of the protons scattered from the 15.11 MeV level of C^{12}. The agreement with the experimental points measured by Tyrén and Maris [1]) is fairly good. Here we use the value of Γ_1 measured by Garwin [6]) and 0.5 for the value of ρ, which may be treated as a parameter to fix the polarization of the protons scattered from the level of magnetic dipole excitation of the nucleus, without referring to the reduced nuclear matrix elements. The coefficients of the scattering matrix are calculated by using the Gammel-Thaler phase shifts [7]) at 180 MeV.

The polarization of the protons scattered from the level in question is shown in fig. 2: the experimental points have been measured by Hillman *et al.* [8]), the curve is calculated by using $\rho = 0.5$.

The 12.73 MeV level of C^{12} has $T = 0$ and $J = 1^+$. The cross section and polarization ot the scattered protons are evaluated in this case by setting eq. (2.12) in eqs. (2.9) and (2.13), respectively. Fig. 3 shows the differential cross

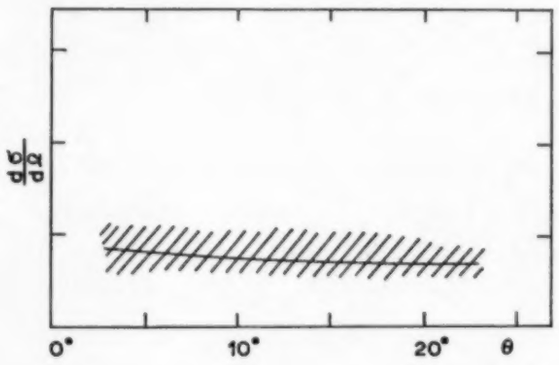

Fig. 3. The experimental and calculated differential cross sections of 180 MeV protons scattered from the 12.73 MeV level of C^{12}. The solid curve indicates the calculated result.

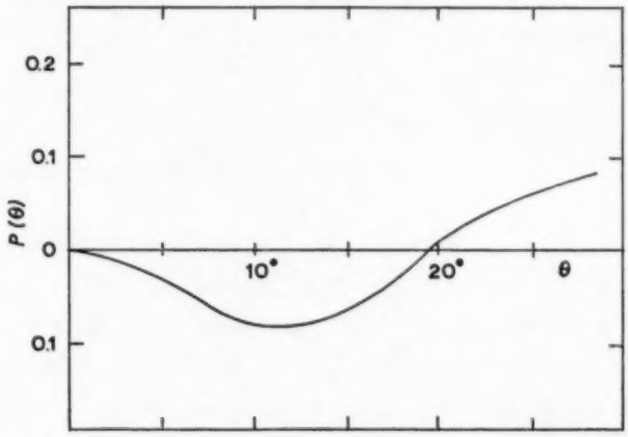

Fig. 4. The calculated polarization of 180 MeV protons scattered from the 12.73 MeV level of C^{12}.

section of the protons scattered from this level. The experimental data have been measured by Tyrén and Maris [1]). Since we have no observed radiative width corresponding to the nuclear matrix element, we cannot test the agreement between the evaluated result and the experimental data in absolute value. However, the pattern of the angular distribution for the calculated curve agrees with the data. If the polarization of the scattered protons were measured, we could fix the value of ρ, and furthermore might conjecture the magnitude of the radiative width or the nuclear matrix element. Fig. 4 shows the calculated polarization for $\rho = 0.5$. A rough estimation gives about 8 eV to the radiative width of the level.

At small forward scattering angles, the differential cross section of the scattered protons, taking into account the isobaric spin flip of the residual nucleus, is more peaked than without this spin flip: compare the curves of fig. 1 and fig. 3. Thus, it seems certainly that the measurement of the protons scattered from the levels of magnetic dipole excitation are helpful in the assigning the isobaric spin values to the levels on the basis of the angular distributions of the scattered protons with or without isobaric spin flip of the residual nucleus [3]).

Here, it is important to note that the effects of the Coulomb interactions

between the incident proton and protons in the target nucleus are very small. The coefficients of the scattering spin matrix β, γ, δ and ε do not contain terms proportional to $1/\sin^2\frac{1}{2}\theta$ included in the Coulomb amplitude of the proton-proton scattering: such a term is contained in the coefficient α. Thus, the amplitude of the proton is mainly contributed by the nuclear interactions between the proton and the nucleons in the nucleus. The forward-peaked angular distribution of the protons scattered from the level of magnetic dipole excitation is not caused by the Coulomb interactions but by the nuclear interactions.

3. Scattered Proton and Spin-Parity of Level

In this section, we show an example of how the high energy protons scattered from a certain level are of service in assigning the spin and parity values to the excited state of the nucleus. Let us consider the 9.63 MeV level of C^{12}. Experimental data from the deuteron stripping reaction and the electron and α-particle scattering assign 1^-, 2^+ or 3^- values to this level [9, 10]). Now, we investigate which assignment the experimental data of Tyrén and Maris support.

The differential cross section of the protons scattered from the level in question is expressed as

$$\frac{\mathrm{d}\sigma}{\mathrm{d}\Omega}(\theta) = 4\frac{k_f}{k_i}[|\alpha|^2+|\gamma|^2+\lambda(|\gamma|^2+|\beta|^2+|\varepsilon|^2)]|F_{f,i}|^2, \tag{3.1}$$

where λ is the ratio of spin-flip to no-spin-flip reduced nuclear matrix elements [2]). The nuclear factor is approximated as

$$F_{f,i} = \langle \Psi_f\{s_f(j)\}| \sum_j \sum_l \sqrt{4\pi}\sqrt{2l+1}\, i^l j_l(Kr_j) Y_{l,0}(\theta_j, \varphi_j)\Phi_i\{s_i(j)\}\rangle, \tag{3.2}$$

where

$$\mathbf{k}_f - \mathbf{k}_i = \mathbf{K}, \qquad |\mathbf{K}| = K.$$

If the level is assigned $J = l$ and parity $(-1)^l$, the non-vanishing nuclear factor is proportional to

$$K^l \langle \Psi_f\{s_f(j)\}| \sum_j r_j^l Y_{l,0}(\theta_j, \varphi_j)|\Phi_i\{s_i(j)\}\rangle. \tag{3.3}$$

Then, the angular distribution for the protons scattered at small forward angles is proportional to K^{2l}, accordingly as the level is assigned $J = l$.

In order to reproduce the angular distribution of the protons, we approximate † the nuclear factor as

$$\langle \Psi_f| \sum_j j_l(Kr_j) Y_{l,0}(\theta_j, \varphi_j)|\Phi_i\rangle \approx \sum (\text{angular part}) \times \int R_f^*(r) j_l(Kr) R_i(r) r^2 \mathrm{d}r, \tag{3.4}$$

† This approximation was derived by Y. Nishida in the analysis of the high energy protons scattered from the 4.43 MeV level of C^{12} (unpublished).

and we define the correction factor $C(\theta)$, which depends on the scattering angles only, as follows:

$$\int R_f^*(r) j_l(Kr) R_i(r) r^2 \mathrm{d}r = C_l(\theta) \int R_f^*(r) \frac{(Kr)^l}{(2l+1)!!} R_i(r) r^2 \mathrm{d}r. \qquad (3.5)$$

This correction factor is given by

$$C_l(\theta) = \frac{(2l+1)!!(l+3)}{K^l R^{l+3}} \int_0^R j_l(Kr) r^2 \mathrm{d}r, \qquad (3.6)$$

when one assumes that $R_i(r)$ and $R_f(r)$ are constant inside the nucleus.

By using this correction factor, the differential cross section of the protons scattered from the level considered is expressed as

$$\frac{\mathrm{d}\sigma}{\mathrm{d}\Omega}(\theta) = 4\frac{k_f}{k_i}[|\alpha|^2+|\gamma|^2+\lambda(|\beta|^2+|\gamma|^2+|\varepsilon|^2)]C_l^2(\theta)4K^{2l}\frac{4\pi(2l+1)}{(2l+1)!!^2}$$
$$\times|\langle\Psi_f|\sum^{Z} r^l Y_{l,0}(\theta,\varphi)|\Phi_i\rangle|^2, \qquad (3.7)$$

where $\alpha = \frac{1}{2}(\alpha_{pp}+\alpha_{pn})$ etc., since there is no isobaric spin change between the excited and ground states. In the derivation of eq. (3.7), it is assumed that the distribution of the neutrons is the same as that of the protons in the nucleus. Eq. (3.7) reproduces the experimental differential cross section of the protons scattered from the level without referring to the wave functions for the ground and excited states of the nucleus, when the nuclear matrix elements are determined by other experiments such as electron scattering by the nucleus.

Without an explicit evaluation of the nuclear matrix element, we do not obtain agreement between the experimental data and the calculated results in absolute value. We can, however, suggest spin and parity values for the level on the basis of the patterns of the calculated angular distributions of the scattered protons. Calculated results for the protons are compared with the data of Tyrén and Maris [1]) in fig. 5. The curve of the scattered protons calculated by assigning 2^+ to the level fits the experimental data better than the

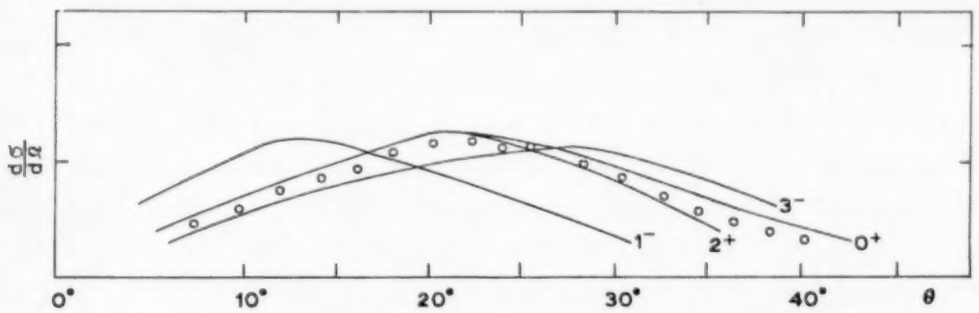

Fig. 5. The experimental and calculated differential cross sections of 180 MeV protons scattered from the 9.63 MeV level of C^{12}. The curves marked 0^+, 1^-, 2^+ and 3^- indicate the results for the level assignments 0^+, 1^-, 2^+ and 3^-.

curves calculated by assuming 1^- and 3^-. Thus, the experimental data of Tyrén and Maris seem to support a 2^+ value for the level. In the calculations of the curves in fig. 5, the ratio of spin-flip to no-spin-flip nuclear matrix elements λ is assumed to be equal to zero, since the polarization of the protons scattered from the level is very similar to the elastic polarization of the nucleus [8]).

It should be noted that the experimental data [9,10]) for the electron and α-particle scattering by the 9.63 MeV level also indicate a 0^+ value. When the level is assigned to be 0^+, the nuclear matrix element is given by

$$\langle \Psi_f | \sum^{A} e^{-i\mathbf{K}\cdot\mathbf{r}_j} | \Phi_1 \rangle = \langle \Psi_f | \sum^{A} \frac{K^2 r_j^2}{3!} | \Phi_1 \rangle, \tag{3.8}$$

and the correction factor $C_0(\theta)$ is expressed as

$$C_0(\theta) = \frac{3!}{K^2} \frac{5}{R^5} \int_0^R \{j_0(Kr) - 1\} r^2 \mathrm{d}r. \tag{3.9}$$

The differential cross section of the scattering to the level assigned the 0^+ value is approximated as

$$\frac{\mathrm{d}\sigma}{\mathrm{d}\Omega}(\theta) = 4 \frac{k_f}{k_i} (|\alpha|^2 + |\gamma|^2) C_0^2(\theta) \frac{1}{3!^2} K^4 |\langle \Psi_f | \sum^{A} r_j^2 | \Phi_1 \rangle|^2. \tag{3.10}$$

The nuclear matrix element for inelastic scattering by the level is proportional to K^2 at small scattering angles with the 0^+ as well as the 2^+ value. Comparing the results with the experimental data of Tyrén and Maris[1]), we find agreement for the level assignment 0^+ as well as 2^+. Thus, we conclude that the level may be assigned a 2^+ or 0^+ value.

4. The 6 MeV Level Group of O^{16}

In this section, we apply the method developed in the preceding sections to the scattering of protons by the 6 MeV level group of O^{16}, in order to establish the validity of the method on the basis of the agreement between the calculated result and experimental data.

There are 0^+ (6.056 MeV), 3^- (6.135 MeV), 2^+ (6.923 MeV) and 1^- (7.12 MeV) levels [9]) in the neighbourhood of the 6 MeV excitation of O^{16}. From the point of view of single particle excitation, it seems that the protons scattered from the 1^- level might be observed as well as those from the 3^- level. Experimentally, the protons from the 7.0 ± 0.2 MeV levels are not observed, while the protons from the 6.1 ± 0.2 MeV levels are clearly visible [1]). This fact is easily understood when the cross sections of the protons scattered from these levels are expressed in terms of the lifetimes or the radiative widths of the levels. The γ-radiation for the 3^- level is expected to be larger than those for the 1^- and 2^+ levels.

The protons scattered from the 6.1 ± 0.2 MeV levels were measured by Tyrén and Maris [1]). We first treat the protons scattered from the 3^- level. By using the method developed in the preceding sections, the differential cross section for these protons is given by

$$\frac{d\sigma}{d\Omega}(\theta) = 4\frac{k_f}{k_i}(|\alpha|^2+|\gamma|^2)C_3^2(\theta)\frac{4K^6}{7!!^2}28\pi|\langle\Psi_f|\sum^Z r_j^3 Y_{3,0}(\theta_j,\varphi_j)|\Phi_i\rangle|^2. \quad (4.1)$$

Here, it is assumed that the distribution of the neutrons is the same as that of the protons in the nucleus. The nuclear matrix element $\langle\Psi_f|\sum^Z r^3 Y_{3,0}|\Phi_i\rangle$ is evaluated by means of the lifetime for the 3^- level, since the inverse of the lifetime is expressed [5]) in terms of the nuclear matrix element as follows:

$$\frac{32\pi}{3\times7!!^2}|e\sum^Z\langle\Psi_f|r_j^3 Y_{3,0}(\theta_j,\varphi_j)|\Phi_i\rangle|^2\kappa^7. \quad (4.2)$$

For the scattered protons from the 0^+ level, the nuclear matrix element is given by eq. (3.8), and the pair emission proceeds at the rate [11])

$$\frac{1}{135\pi}\left(\frac{e^2}{\hbar c}\right)^2\frac{\omega^5}{\hbar^5c^4}|\langle\Psi_f|\sum_j^Z r_j^2|\Phi_i\rangle|^2, \quad (4.3)$$

where ω is the energy emitted in the transition. The lifetime [9]) for the 0^+ level, $7.2\pm0.7\times10^{-11}$ sec, gives 3.7×10^{-26} cm^2 for the nuclear matrix element $\langle\Psi_f|\sum^Z r^2|\Phi_i\rangle$. If the distribution of the neutrons is assumed to be the same as that of the protons in the nucleus, the cross section for the scattering to the 0^+ level is approximated as

$$\frac{d\sigma}{d\Omega}(\theta) = 4\frac{k_f}{k_i}(|\alpha|^2+|\gamma|^2)\frac{4K^4}{3!^2}C_0^2(\theta)\times(3.7\times10^{-26}\text{ cm}^2)^2. \quad (4.4)$$

Before comparing with the experimental data, we must add the differential cross sections associated with the 3^- and 0^+ levels. The ratio of the cross section of the protons scattered from the 3^- level to that for scattering from the 0^+ level is about 0.8 at $\theta = 20°$. Fig 6 shows the asymmetric cross section for the inelastic scattering of the polarized protons exciting the 6 MeV level group. The asymmetric cross section contains the same information as the cross section and polarization for the scattering of an unpolarized incident beam, since no asymmetry-polarization difference is indicated by the experimental data [1, 8]). The fair agreement between the calculated result and the experimental data for the protons scattered from the 6 MeV level group seems to support the validity of the above-developed method to calculate the high energy nucleons scattered from levels of nuclei and to investigate the spin, parity and isobaric spin values of the levels and the properties of nuclear matrix elements.

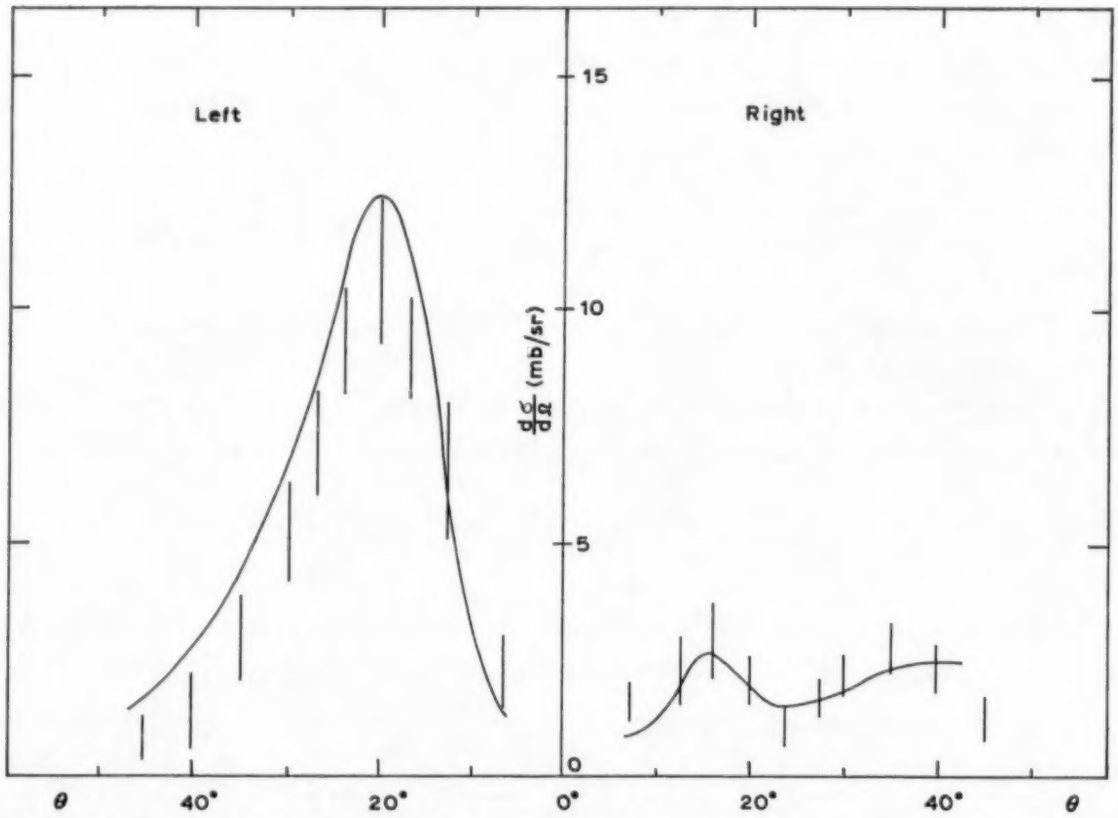

Fig. 6. The experimental and calculated asymmetric cross sections for the inelastic scattering of 180 MeV polarized protons exciting the 6.1 ± 0.2 MeV level of O^{16}. The solid curve indicates the calculated result.

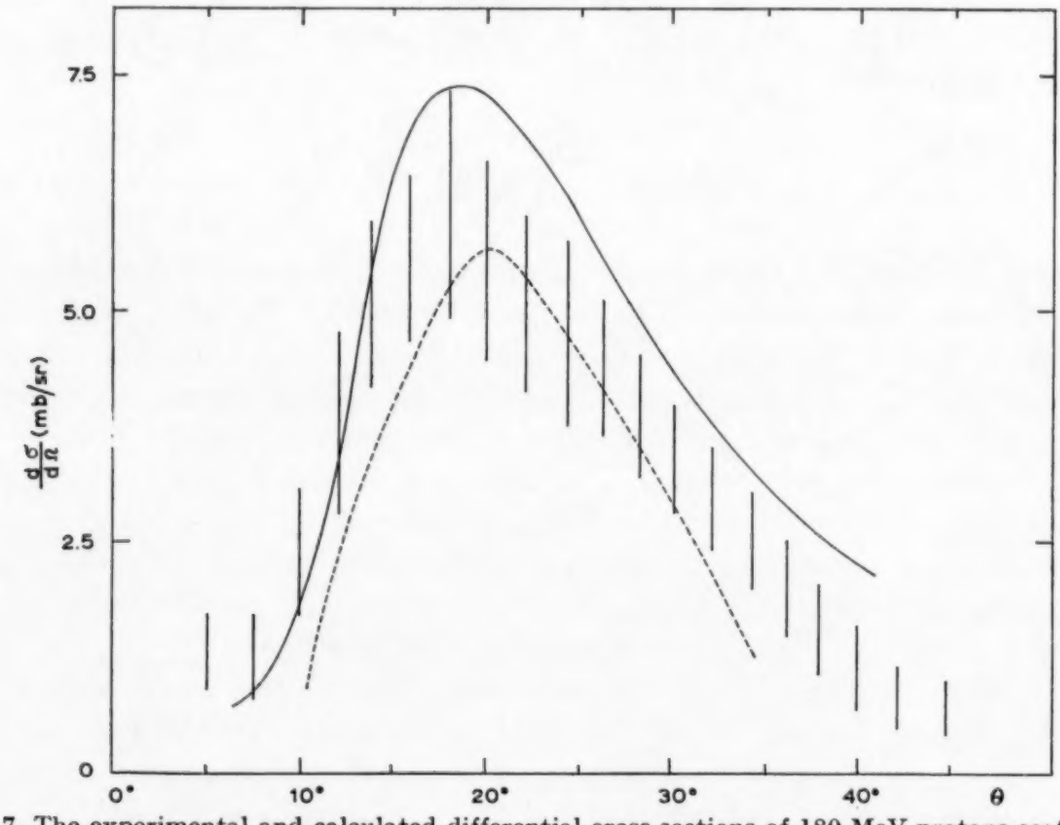

Fig. 7. The experimental and calculated differential cross sections of 180 MeV protons scattered from the 6.1 ± 0.2 MeV levels of O^{16}. The solid curve indicates the result calculated by using the method developed in the present paper and the dashed curve represents the result of Egardt. Both curves are calculated by using the Gammel-Thaler phase shifts at 180 MeV.

5. Concluding Remarks

A serious error is caused probably by neglecting the elastic and inelastic scattering of the incident and scattered protons before and after the excitation. This may be corrected by taking into account the distortion of the plane ingoing and outgoing waves by a complex optical potential [12]). A rough estimate by the WKB-method shows that at small scattering angles the effects of the distortion give angular distributions more isotropic than the present results, but indicate that our conclusions obtained by making use of the method developed in the present paper still hold.

Egardt calculated the protons scattered from the 6 MeV level group of O^{16} using the extreme $L-S$ coupling shell model wave functions [13]). He took into account the effects of distortion due to the optical potential for the incident and scattered waves. Fig. 7 shows that his result agrees with ours. The validity of the method developed in the present paper to deal with the high energy nucleons scattered from levels is also established by this agreement.

The author would like to thank Dr. Y. Nishida for his many suggestions and continued discussion.

References

1) H. Tyrén and Th. A. Maris, Nuclear Physics **3** (1957) 52, **4** (1957) 277, 637, **6** (1958) 82, 446, **7** (1958) 24, 281;
Th. A. Maris and H. Tyrén, Nuclear Physics **4** (1958) 662
2) Y. Sakamoto, Prog. Theor. Phys. **24** (1960) 81
3) Y. Sakamoto, Prog. Theor. Phys. **23** (1960) 1205
4) A. K. Kerman, H. McManus and R. M. Thaler, Ann. Phys. **8** (1959) 551
5) J. Blatt and V. Weisskopf, Theoretical nuclear physics (Wiley, New York, 1952)
6) E. L. Garwin, Phys. Rev. **114** (1959) 143
7) J. L. Gammel and R. M. Thaler, Phys. Rev. **107** (1957) 219, 1337
8) P. Hillman, A. Johansson and H. Tyrén, Nuclear Physics **4** (1957) 648
9) F. Ajzenberg-Selove and T. Lauritsen, Nuclear Physics **11** (1959) 1
10) F. C. Barker, E. Bradford and L. J. Tassie, Nuclear Physics **19** (1960) 101;
J. H. Fregeau, Phys. Rev. **104** (1956) 225;
A. I. Yavin and G. W. Farwell, Nuclear Physics **12** (1959) 1
11) J. R. Oppenheimer and J. S. Schwinger, Phys. Rev. **56** (1939) 1066
12) E. J. Squires, Nuclear Physics **6** (1958) 504;
G. P. McCauley, Proc. Phys. Soc. **73** (1959) 309
13) L. Egardt, Nuclear Physics **11** (1959) 349

10.D *Nuclear Physics* **25** (1961) 698—700; © *North-Holland Publishing Co., Amsterdam*

BOOK REVIEWS

H. G. JERRARD and D. B. MCNEILL, *Theoretical and Experimental Physics* (Chapman and Hall, London, 1960. v—611 p. 75 s.)

Under a rather misleading title, this very useful textbook presents, in a series of chapters surveying the various branches of classical physics, a theoretical and practical discussion of basic experimental techniques. The level of treatment is adapted to the needs of students, who are helped to further reading by extended lists of original papers and books appended to each chapter. A commendable feature of these lists is that they include references of great historical interest to the earliest literature of the topics treated.

L. R.

M. CALVIN, *Origin of life on earth and elsewhere* (UCRL—9005, Office of technical services, U. S. Department of Commerce, Washington 25, D.C. $ 1.25)

This report from the E. O. Lawrence Radiation Laboratory of the University of California dates from December 1959 and has deservedly reached the standard of best-seller as the copy received for review is a 15th edition. It is not too late to call attention to this stimulating lecture on a fascinating topic: it presents in a nut-shell the various elements of a vast problem, in a very clear and sober way. Most informative respecting the chemical aspects, the author touches perhaps too cursorily upon other questions, such as the possibility of other forms of organic development than the one we known on earth. The list of references is also too summary to be more than a help to general orientation: it would be useful to have a more complete compilation of papers, both biophysical and astronomical, containing detailed and quantitative discussions of special points; one would think there are not so many of them yet.

L. R.

JEAN ROSSEL, *Physique générale* (Dunod, Paris, 1960. xii—481 p.)

Il s'agit ici d'un aperçu très condensé de ce qui constitue la charpente de la physique moderne, basé sur la conception atomique de la matière. Le livre s'adresse aux étudiants arrivés à un stade intermédiaire de leur initiation à la physique, et il les aidera certainement à mettre de l'ordre dans les idées qu'ils ont pu tant bien que mal (et souvent plutôt mal que bien) acquérir dans les cours dits de propédeutique. On peut ne pas toujours être d'accord avec le point de vue de l'auteur, mais il faut reconnaître qu'il a abordé la tâche fort ingrate et difficile qu'il s'est donnée avec beaucoup de vigueur d'esprit et d'originalité.

L. R.

I. W. BUSBRIDGE, *The Mathematics of Radiative Transfer* (Cambridge University Press, Cambridge, 1960. xii—143 p. 30 s)

This "Cambridge tract" is intended to replace the well-known one by E. Hopf, which is out-of-print; the author has incorporated in his account, with some parts of Hopf's treatise, the results of more recent work. As the title indicates, the treatment is strictly mathematical, although it uses the physical terminology appropriate to electromagnetic radiation. In the domain of nuclear physics, it may be useful to people occupied with neutron diffusion.

L. R.

JOSEF SCHNITLMEISTER, (Herausgeber) *Der Isospin von Atomkernen* (Akademie-Verlag, Berlin, 1960. ix—156 p. DM 28.)

German translation of three Russian articles surveying the relationship of the isobaric spin with the stationary states of nuclei and the charge independence of nuclear forces. Although these articles date from 1954 and 1955, they are still very valuable as clear and comprehensive expositions of the many aspects of the subject.

L. R.

Proceedings of the International Conference on Nuclear Structure, Kingston, Canada, August 29—September 3, 1960, edited by D. A. BROMLEY and E. W. VOGT (North-Holland Publishing Co., Amsterdam, 1960. 990 p. 66 gl.)

Proceedings of the 1960 Annual International Conference on High Energy Physics at Rochester. edited by E. C. G. SUDARSHAN, J. H. TINLOT and A. C. MELISSINOS (Interscience Publishers, New York, 1960, xxv—890 p. $ 13.50)

Two books of a type becoming usual, both of them excellently edited and produced. Opinions differ about this new — alarmingly growing — branch of literature. An obvious advantage of such collections of papers is that they provide the latest detailed information on a rather precisely limited field in an easily accessible form, without the need of scanning and sifting the journals. The danger is that information not contained in the collection may be altogether lost. One may think that a better mode of publication would be the usual one in the specialized journals (as for instance, *Nuclear Physics*, *Nuclear Instruments* and a few others) that are international and of suitably limited scope.

There is another aspect of the problem to be considered. The proceedings of the large conferences, besides the confrontation of new information on points of detail, contain general surveys whose appeal is not limited to specialists. Would this laudable endeavour at synthesis not find easier diffusion and thereby better fulfil its purpose if such surveys and reports of progress were published and sold separately? Why not issue such conference proceedings in two parts: a general part, which would be comparatively thin and thus reasonably accessible to individual purchasers belonging to a much wider group than the specialists, and a bulkier special part, which would contain the detailed papers. This suggestion may be illustrated by the Comptes-Rendus of the 1958 Paris Conference on nuclear physics, in which this division into two parts is carried out — only the two are bound in a single, very bulky volume.

L. R.

T. A. BRODY and M. MOSHINSKY, *Tables of Transformation Brackets* (Monografias del Instituto de Fisica, Mexico City, 1960. LXXIII—175 p. $ 6.00)

These tables concern coefficients occurring in the transformation of wave-functions for a system of two harmonic oscillators into a representation in which the relative and barycentric motions are separated: see this journal **16** (1959) 104; **17** (1960) 16. They are available, for the price indicated (which includes postage), on application to Instituto de Fisica, Universidad de México, Apdo. Postal 31364, México 20, D. F. This Institute may be congratulated for the excellent production of tables which will doubtless prove very helpful in shell model calculations.

L. R.

Directory of Nuclear Reactors. Vol. III. Research, Test and Experimental Reactors (International Atomic Energy Agency, Vienna, 1960. 354 p. $ 4.00.)

The previous volumes of this Directory have been reviewed in this journal **14** (1959) 176; **16** (1960) 698. The present one is a continuation of vol. II. It is now planned to issue supplements to keep the Directory up to date.

The preface ends with an invitation for comments and suggestions of improvement. No notice has been taken, however, of the criticism formulated in the review of vol. II concerning the use of incorrect unit symbols.

L. R.

MAX VON LAUE, *Röntgenstrahl-Interferenzen* (Akademische Verlags-Gesellschaft, Frankfurt-am-Main, 1960. x—476 p. DM 75).

This is the third edition of a treatise which ranks as a classic. It is therefore quite right that it has retained the original set up and style, and only incorporated a few additions about recent progress. The masterly exposition of the theoretical argument , which leaves no detail in the dark, is illustrated by remarkably neat diagrams and beautiful photographs, thus conveying in words and pictures the fascinating beauty of the domain of atomic physics it describes. Together with the companion book on electron interference, this work will remain a worthy monument to the memory of a great pioneer.

L. R.

D. KASTLER, *Introduction à l'électrodynamique quantique* (Dunod, Paris, 1961. xiii—368 p. 68 NF)

In the preface of the book to be reviewed here the author states that he wants to present the physical theory of field quantization but using the language of modern mathematics and thus try to make an exposition which is acceptable both to physicists and to mathematicians. Of course, this is the kind of foreword which will stop most physicists from reading the book. However, the reviewer thinks that that would would be a pity. The book by Kastler makes a real effort to conform to the language of physics. For instance, it is refreshing in a book of this kind to find that no undue fuss is made about delta-functions and that the author does not even apologize for using them. Nevertheless, the correct interpretation of a field operator in terms of smoothed out averages over space and time is given at the appropriate place. This is something which has been well-known to physicists since the early nineteen-thirties after the pioneer work by Bohr and Rosenfeld while the mathematicians have come round to this idea only more recently. Further, the author does not despise the canonical quantization method but presents it in a way which most physicists will find reasonable. From the more mathematical side the author puts heavy emphasis on the theory of linear vector spaces, Grassmann algebra etc. and develops the theory of state vectors from this basis.

The book is mainly about free fields but some remarks about interacting fields are made on the last 80 pages of the book. A few elementary applications like Møller-scattering, the Klein-Nishina-formula and electron pair annihilation are given. In appendices the reader gets some technical advice about how to calculate traces of γ-matrices and about how to obtain a scattering cross section from an S-matrix element. More intricate applications which require renormalization and higher order perturbation theory are not given.

The notation in the book confirms in most cases to standard notations in physics. One notable exception is the author's somewhat unconventional disposal of an i in the definition of the singular functions.

In spite of what has been said above the reviewer hesitates to recommend the book as a first introduction to the subject. Someone who has never studied field theory before will most probably have difficulties to look through the rather heavy mathematical apparatus and find the physical significance of what is done. However, a student who has already some basic knowledge of the subject and who wants to get an idea about how the standard concepts in the theory of quantized fields can be presented from a more rigorous mathematical point of view is likely to find this book a stimulating and entertaining reading.

G. Källén

AUTHOR INDEX

AGUILAR, J., A. GARCÍA, J. B. A. ENGLAND, P. E. HODGSON and W. T. TONER, The elastic scattering of 29 MeV ^{3}He-particles by Cl, Kr and Xe 259

BALIAN, ROGER, CLAUDE BLOCH et CYRANO DE DOMINICIS, Formulation de la mécanique statistique en termes de nombres d'occupation (I) 529

BLOCH, CLAUDE, see BALIAN

BROWN, D., A. T. G. FERGUSON and R. E. WHITE, Polarization of 0.3 to 1.4 MeV neutrons scattered by copper, zinc, molybdenum and cadmium 604

CHAUDHRY, R., *see* RAMANNA

COOK, J. L., Photoproduction of neutral mesons in helium 421

DAY, P., *see* KLEMA

DE DOMINICIS, CYRANO, *see* BALIAN

DIAMOND, R. M., J. M. HOLLANDER, D. J. HOREN and R. A. NAUMANN, The neutron deficient iridium istopes Ir^{182}, Ir^{183} and Ir^{184} 248

ELBEK, B., *see* HANSEN

ENGLAND, J. B. A., *see* AGUILAR

EVERLING, F., L. A. KÖNIG, J. H. E. MATTAUCH and A. H. WAPSTRA, Adjustment of relative nuclidic masses (I) $A \leqq 70$ 177

FERGUSON, A. T. G., *see* BROWN

FERGUSON, A. T. G., *see* JAMES

FREED, N. and L. S. KISSLINGER, Magnetic dipole moments of odd-mass nuclei in the spherical region 611

FREUND, P. G. O., A. M. LONGONI and E. PREDAZZI, About the pion-hyperon resonance 656

GARCÍA, A., *see* AGUILAR

GAUDIN, MICHEL, Sur la loi limite de l'espacement des valeurs propres d'une matrice aléatoire 447

GOLDHABER, G., S. GOLDHABER and B. PETERS, Separation of high energy particles by means of strong interactions 502

GOLDHABER, S., *see* GOLDHABER

GREEN, L. L., J. C. WILLMOTT and G. KAYE, The comparison of d-shell nuclei with the Nilsson model 278

HANSEN, O., M. C. OLESEN, O. SKILBREID and B. ELBEK, Inelastic scattering from hafnium and wolfram isotopes 634

HARA, OSAMU, Collective correlation between vacuum nucleons in ps—ps meson theory 472

HAZEWINDUS, N., *see* VAN OOSTRUM

HODGSON, P. E., *see* AGUILAR
HOLLANDER, J. M., *see* DIAMOND
HOREN, D. J., *see* DIAMOND
HUIZENGA, J. R., *see* VANDENBOSCH
JAMES, A. N., A. T. G. FERGUSON and C. M. P. JOHNSON, The B^{10} (d, n) C^{11} reaction 282
JANOUCH, F., Internal bremsstrahlung in $0^- \rightarrow 0^+$ beta-transitions 328
JARMIE, NELSON, M. G. SILBERT and DARRYL B. SMITH, The two-stage nuclear reaction N^{14} (t, n) O^{16*} (p) N^{15} 443
JARMIE, NELSON, *see* SILBERT,
JOACHAIN, C., Polarisation nucléaire dans les atomes mésiques de tritium, d'hélium 3 et d'hélium 4 317
JOHNSON, C. M. P., *see* JAMES
JOHNSON, KENNETH, Current-charge density commutation relations 431
JOHNSON, KENNETH, Relation between the bare and physical masses of vector mesons 435
KÄLLÉN, GUNNAR, The analyticity domain of the four point function 568
KAPOOR, S. S., *see* RAMANNA
KARLSSON, E., C.–A. LERJEFORS and E. MATTHIAS, The gyromagnetic ratio of the 155 keV-rotational level in Os^{188} 385
KARLSSON, E., *see* LERJEFORS
KAYE, G., *see* GREEN
KEBERLE, E. M., *see* VANDENBOSCH
KISSLINGER, L. S., *see* FREED
KLEMA, E. D., C. A. MALLMANN and P. DAY, Energy levels of even nuclei on the hydrodynamical model with vibration-rotation interaction 266
KÖNIG, L. A., *see* EVERLING
LEFORT, M., G. N. SIMONOFF et X. TARRAGO, Réactions nucléaires de spallation induites sur le thorium par des protons de 150 et 82 MeV 216
LEMMER, RICHARD H. and VICTOR F. WEISSKOPF, On the preponderance of prolate deformations in nuclei 624
LERJEFORS, C.–A., E. MATTHIAS and E. KARLSSON, The gyromagnetic ratio of the 137 keV rotational level in Os^{186} 404
LERJEFORS, C.–A., *see* KARLSSON
LONGONI, A. M., *see* FREUND
MALLMANN, C. A., *see* KLEMA
MATTAUCH, J. H. E., *see* EVERLING
MATTHIAS, E., *see* KARLSSON
MATTHIAS, E., *see* LERJEFORS
MIKKE, K., *see* RAMANNA
MILLER, W. F., *see* VANDENBOSCH
MITRA, A. N. and J. H. NAQVI, A separable potential for the two-nucleon

($T = 1$) interaction 307
MITTELSTAEDT, P., On the degeneracy of the superconductive state . . 522
MONNAND, E. et A. MOUSSA, Étude des transitions gamma et des électrons Auger de ^{153}Eu 292
MOUSSA, A., *see* MONNAND
MURTHY, S. R. S., *see* RAMANNA
NAKAI, S. and M. SASAKI, On the theory of collective rotations 333
NAQVI, J. H., *see* MITRA
NAUMANN, R. A., *see* DIAMOND
OLESEN, M. C., *see* HANSEN
OLNESS, J. W., *see* VAN OOSTRUM
PARKER, J. L., *see* VAN OOSTRUM
PETERS, B., *see* GOLDHABER
PHILLIPS, R. J. N., Antinucleon-nucleon annihilation to two mesons . . 348
PREDAZZI, E., *see* FREUND
RAMAKRISHNAN, A. and S. K. SRINIVASAN, A note on electron photon showers 152
RAMANNA, R., R. CHAUDHRY, S. S. KAPOOR, K. MIKKE, S. R. S. MURTHY and P. N. R. RAO, The angular correlation of prompt neutrons and fission fragments in thermal neutron fission of U^{235} 136
RAO, P. N. R., *see* RAMANNA
RIDLEY, B. W., The electron-neutrino angular correlation in beta decay of helium 6 483
ROBINSON, D. W., Multipole Coulomb excitations of vibrational nuclei 459
RUSTGI, M. L., Note on the two-nucleon stripping process 169
SAKAMOTO, YOSHIYUKI, Inelastic scattering of high energy protons and levels of nuclei 687
SASAKI, M., *see* NAKAI
SEEGER, P. A., Semiempirical atomic mass law 1
SHARMA, B. L., Beta decay of Tm^{171} 175
SILBERT, M. G., NELSON JARMIE and DARRYL B. SMITH, Nuclear energy levels of N^{16} 438
SILBERT, M. G., *see* JARMIE
SIMONOFF, G. N., *see* LEFORT
SKILBREID, O., *see* HANSEN
SMITH, DARRYL B., *see* JARMIE
SMITH, DARRYL B., *see* SILBERT
SORENSEN, RAYMOND A., Pairing plus quadrupole force model for odd-mass single closed shell nuclei 674
SRINIVASAN, S. K., *see* RAMAKRISHNAN
TARRAGO, X., *see* LEFORT
TAYLOR, A. E. and E. WOOD, Proton scattering from light elements at

142 MeV 642
TER-MARTIROSYAN, K., On a symmetrical scheme of integral equations for spectral functions 353
TER-MARTIROSYAN, K., Equations for spectral functions in the simplest cases 368
TONER, W. T., *see* AGUILAR
TRUE, W. W., Shell model theory of Pb^{205} 155
UMEZAWA, MINORU, Pairings in the shell model (II) 661
VANDENBOSCH, R., J. R. HUIZENGA, W. F. MILLER and E. M. KEBERLE, Monte Carlo calculation of neutron evaporation; excitation energy dependence of nuclear level density 511
VAN OOSTRUM, K. J., N. HAZEWINDUS, A. H. WAPSTRA, J. W. OLNESS and J. L. PARKER, The reaction ^{28}Si (p, γ)^{29} P 409
WAPSTRA, A. H., *see* EVERLING
WAPSTRA, A. H., *see* VAN OOSTRUM
WEISSKOPF, VICTOR F., *see* LEMMER
WHITE, R. E., *see* BROWN
WILLMOTT, J. C., *see* GREEN
WOOD, E., *see* TAYLOR

SUBJECT INDEX

1. Nuclear Structure

1.B *Two-and three-body problems*

A separable potential for the two-nucleon (T = 1) interaction, A. N. Mitra and J. H. Naqvi 307
Polarisation nucléaire dans les atomes mésiques de tritium, d'hélium 3 et d'hélium 4, C. Joachain 317

1.C *Many-particle systems*

On the degeneracy of the superconductive state, P. Mittelstaedt 522
Formulation de la mécanique statistique en termes de nombres d'occupation (I), R. Balian, C. Bloch et C. de Dominicis 529

1.D *Nuclear models*

1.D.1. *Shell model*

Shell model theory of Pb^{205}, W. W. True 155
Magnetic dipole moments of odd-mass nuclei in the spherical region, N. Freed and L. S. Kisslinger 611

1.D.2 *Collective model*

The comparison of d-shell nuclei with the Nilsson model, L. L. Green, J. C. Willmott and G. Kaye 278
On the theory of collective rotations, S. Nakai and M. Sasaki 333
The gyromagnetic ratio of the 155 keV-rotational level in Os^{188}, E. Karlsson, C.-A. Lerjefors and E. Matthias, ... 385
The reaction ^{28}Si (p, γ)^{29}P, K. V. Van Oostrum, N. Hazewindus, A. H. Wapstra, J. W. Olness and J. L. Parker 409
Multiple Coulomb excitations of vibrational nuclei, D. W. Robinson . . 459
On the preponderance of prolate deformations in nuclei, R. H. Lemmer and V. F. Weisskopf 624
Inelastic scattering from hafnium and wolfram isotopes, O. Hansen, M. C. Olesen, O. Skilbreid and B. Elbek 634

1.D.3 *Other models*

Energy levels of even nuclei on the hydrodynamical model with vibration-rotation interaction, E. D. Klema, C. A. Mallmann and P. Day 266
Pairing plus quadrupole force model for odd-mass single closed shell nuclei, Raymond A. Sorensen 674

1.E *Properties of nuclei*

1.E.1 *Energy levels*

Beta decay of Tm^{171}, B. L. Sharma 175
The B^{10} (d, n) C^{11} reaction, A. N. James, A. T. G. Ferguson and C. M. P. Johnson. 282

The reaction ^{28}Si (p, γ) ^{29}P, K. V. Van Oostrum, N. Hazewindus, A. H. Wapstra, J. W. Olness and J. L. Parker 409
Nuclear energy levels of N^{16}, M. G. Silbert, Nelson Jarmie and Darryl B. Smith 438
Inelastic scattering of high energy protons and levels of nuclei, Yoshiyuki Sakamoto 687

1.E.2 *Binding energies; masses*

Adjustment of relative nuclidic masses (I) $A \leqq 70$, F. Everling, L. A. König, J. H. E. Mattauch and A. H. Wapstra 177

1.E.3 *Electric and magnetic moments*

Semiempirical atomic mass law, P. A. Seeger 1
The gyromagnetic ratio of the 155 keV-rotational level in Os^{188}, E. Karlsson, C.–A. Lerjefors and E. Matthias 385
The gyromagnetic ratio in the 137 keV rotational level in Os^{186}, C.–A. Lerjefors, E. Matthias and E. Karlsson 404

1.E.4 *Transition probabilities; Cross sections*

Inelastic scattering from hafnium and wolfram isotopes, O. Hansen, M. C. Olesen, O. Skilbreid and B. Elbek 634

1.E.6 *Nuclear moments of inertia*

On the theory of collective rotations, S. Nakai and M. Sasaki 333

2. Nuclear Reactions

2.B *Angular distributions, Correlations; Polarization*

Polarization of 0.3 to 1.4 MeV neutrons scattered by copper, zinc, molybdenum and cadmium, D. Brown, A. T. G. Ferguson and R. E. White 604

2.C *Resonance reactions; R-matrix theory*

The reaction ^{28}Si (p, γ) ^{29}P, K. V. Van Oostrum, N. Hazewindus, A. H. Wapstra, J. W. Olness and J. L. Parker 409

2.D *Statistical model*

Sur la loi limite de l'espacement des valeurs propres d'une matrice aléatoire Michel Gaudin 447
Monte Carlo calculation of neutron evaporation; excitation energy dependence of nuclear level density, R. Vandenbosch, J. R. Huizenga, W. F. Miller and E. M. Keberle 511

2.E *Optical model*

The elastic scattering of 29 MeV ^{3}He-particles by Cl, Kr and Xe, J. Aguilar, A. García, J. B. A. England, P. E. Hodgson and W. T. Toner 259
Proton scattering from light elements at 142 MeV, A. E. Taylor and E. Wood 642

2.G *Stripping and pick-up*

Note on the two-nucleon stripping process, M. L. Rustgi 169
The B^{10} (d, n) C^{11} reaction, A. N. James, A. T. G. Ferguson and C. M. P. Johnson 282
Nuclear energy levels of N^{16}, M. G. Silbert, Nelson Jarmie and Darryl B. Smith 438

2.H *Coulomb excitation*

Multiple Coulomb excitations of vibrational nuclei, D. W. Robinson 459
Inelastic scattering from hafnium and wolfram isotopes, O. Hansen, M. C. Olesen, O. Skilbreid and B. Elbek 634

2.J *Fission and spallation*

The angular correlation of prompt neutrons and fission fragments in thermal neutron fission of U^{235}, R. Ramanna, R. Chaudhry, S. S. Kapoor, K. Mikke, S. R. S. Murthy and P. N. Rama Rao 136
Réactions nucléaires de spallation induites sur le thorium par des protons de 150 et 82 MeV, M. Lefort, G. N. Simonoff et X. Tarrago 216
The neutron deficient iridium isotopes Ir^{182}, Ir^{183} and Ir^{184}, R. M. Diamond, J. M. Hollander, D. J. Horen and R. A. Naumann 248
The two-stage nuclear reaction N^{14} (t, n) O^{16*} (p)N^{15}, Nelson Jarmie, M. G. Silbert and Darryl B. Smith 443

2.L *Scattering processes (except two-nucleon system and meson scattering)*

The elastic scattering of 29 MeV ^{3}He-particles by Cl, Kr and Xe, J. Aguilar, A. García, J. B. A. England, P. E. Hodgson and W. T. Toner 259
Polarization of 0.3 to 1.4 MeV neutrons scattered by copper, zinc, molybdenum and cadmium, D. Brown, A. T. G. Ferguson and R. E. White 604
Proton scattering from light elements at 142 MeV, A. E. Taylor and E. Wood 642

3. Electromagnetic Radiation

3.B *Internal conversion*

Étude des transitions gamma et des électrons Auger de ^{153}Eu, E. Monnand et A. Moussa. 292

3.C *Extranuclear effects*

Étude des transitions gamma et des électrons Auger de ^{153}Eu, E. Monnand et A. Moussa 292
Polarisation nucléaire dans les atomes mésiques de tritium, d'hélium 3 et d'hélium 4, C. Joachain 317

4. Beta decay; Parity

4.A *General theory*

The electron-neutrino angular correlation in beta decay of helium 6, B. W. Ridley 483

4.B *Formulation of Fermi theory*

Internal bremsstrahlung in $0^- \rightarrow 0^+$ beta-transitions, F. Janouch 328

4.E *Analysis of data*

Beta decay of Tm^{171}, B. L. Scharma 175

6. Methods and Instruments

6.A *Experimental*

Separation of high energy particles by means of strong interactions, G. Goldhaber, S. Goldhaber and B. Peters 502

6.D *Tables and computational aids*

Semiempirical atomic mass law, P. A. Seeger 1

7. Quantum Field Theory

7.A *General*

On a symmetrical scheme of integral equations for spectral functions, K. Ter-Martirosyan 353
Equations for spectral functions in the simplest cases, K. Ter-Martirosyan . . 368
The analyticity domain of the four point function, G. Källén 568

7.B *Quantum electrodynamics*

Current-charge density commutation relations, Kenneth Johnson 431
Relation between the bare and physical masses of vector mesons, Kenneth Johnson. 435

7.C *π-meson field (scattering and nuclear forces)*

Antinucleon-nucleon annihilation to two mesons, R. J. N. Phillips 348
Photoproduction of neutral mesons in helium, J. L. Cook 421
Collective correlation between vacuum nucleons in ps-ps meson theory, Osamu Hara. 472

8. Elementary Particles

8.A *Experimental*

The electron-neutrino angular correlation in beta decay of helium 6, B. W. Ridley 483
Separation of high energy particles by means of strong interactions, G. Goldhaber, S. Goldhaber and B. Peters 502

8.B *Theory: interactions, transformation properties*

About the pion-hyperon resonance, P. G. O. Freund, A. M. Longoni and Predazzi. 656

9. Cosmic Radiation

9.B *Passage of particles through matter*

A note on electron photon showers, A. Ramakrishnan and S. K. Srinivasan . . 152

10. News Items

10.D *Book Reviews*

H. G. Jerrard and D. B. McNeill, Theoretical and experimental physics (L. R.) 698
M. Calvin, Origin of life on earth and elsewhere (L. R.) 698
Jean Rossel, Physique générale (L.R.) 698
I. W. Busbridge, The Mathematics of Radiative Transfer (L. R.) 698
Josef Schnitlmeister, Der Isospin von Atomkernen (L. R.) 699
Proceedings of the International Conference on Nuclear Structure, Kingston, Canada, August 29-September 3, 1960, edited by D. A. Bromley and E. W. Vogt (L. R.) 699
Proceedings of the 1960 annual International Conference on High Energy Physics at Rochester, edited by E. C. G. Sudarskan, J. H. Tinlot and A. C. Melissinos (L. R.). 699
T. A. Brody and M. Moshinsky, Tables of Transformation Brackets (L. R). 699
Directory of Nuclear Reactors, Vol. III. Research, Test and Experimental Reactors (L.R.) 699
Mac von Laue, Röntgenstrahl-Interferenzen (L. R). 700
D. Kastler, Introduction à l'électrodynamique quantique (G. Källén) . . . 700